

# INDIAN JOURNAL OF PHYSICS

VOL XXVI

AND

PROCEEDINGS

OF THE

*Indian Association for the Cultivation of Science XXXV*

*(Published in Collaboration with the Indian Physical Society)*

( With Forty Plates )

Printed by Sibendranath Kanjilal, Superintendent, Calcutta University Press,  
48, Hazra Road, Ballygunge, Calcutta and published by the Registrar,  
Indian Association for the Cultivation of Science.

Jadavpur, Calcutta 32.

1952

Price Rs. 20 or £ 2

	PAGE
1. High Frequency Measurements—By August Hund ...	159
2. Understanding Radio—By Watson, Welch and Eby ...	160

## No. 4

18. Experiments on the Internal Dispersion of Supersonic Waves in Liquids—By A. K. Dutta and S. K. Mukherjee ...	161
19. Heat Losses and their Dependence on Air Velocity—By D. G. Kapadnis and D. V. Gogate ...	171
20. $^5\text{II}-^5\Sigma$ Electronic Transition in Cobalt Chloride—By V. G. Krishnamurty ...	177
21. On the New Theory of Alpha-decay—By M. L. Chaudhury ...	186
22. On the Distribution of Stress in a Deep Beam Containing two Equal Circular Holes—By B. Karunes ...	197
23. On the Ultraviolet Absorption Spectra of Organic Substances in the Liquid and Solid States. Part III. Ethyl benzene and Isopropyl benzene—By A. R. Deb ...	201

## No. 5

24. The Complex Band Spectrum of Nickel Chloride—By V. G. Krishnamurty ...	207
25. Raman Spectra of Organic Crystals at low Temperatures. III. Orthoxylene and Benzyl bromide—By A. K. Ray ...	226
26. Absorption Spectra of Organic Substances in the Liquid and Solid States. III. Some Substituted Benzene Compounds—By H. N. Swamy ...	233
27. Associated Pairs of Penetrating Particles and other Events observed at Mountain Altitudes with Photographic Emulsions—By K. R. Dixit ...	243
28. High Multiplicity States in Diatomic Molecules—By K. Suryanarayana Rao ...	254

## No. 6

29. Absorption Spectrum of <i>p</i> -Chlorotoluene—By G. Viswanath ...	263
30. Pseudoscalar Meson Field and the Scattering of Fast Neutrons by Protons—By N. C. Sil ...	269
31. On the Raman Spectrum of Thianthrene in the Molten State—By S. K. Mukerji and Banarsi Lal ...	276
32. Ultrasonic Absorption and Relaxation Mechanism—By A. K. Dutta ...	279
33. A Comparative Study of the Different Methods of Heat-run Tests on Electrical Machines. II. Three-phase Transformers—By H. K. Basu ...	283
34. Pseudoscalar Meson Field and Relativistic Scattering of Neutrons by Protons—By D. Basu ...	291



	PAGE
55. Effect of Magnetic Field in Oblique Propagation over Equatorial Region—By B. Chatterjee ... ..	297
36. Detonation of Proton Gas—By M. P. Murgai ... ..	313

## No. 7

37. On the Distribution of Initial Stress due to Dislocation in an Infinite Plate containing two Unequal Circular Holes—By B. Karunes ... ..	317
38. A Thermionic Meter for Measuring Rectification Ratio of Current in Discharge Tubes—By V. L. Talekar ... ..	329
39. Neutron-Proton Scattering—By H. N. Yadav ... ..	337
40. The Ultraviolet Absorption Spectra and the Intensity of the Fluorescence Band at $4156 \text{ \AA}$ of Diamond—By B. M. Bishui ... ..	347
41. On the Distribution of Weather over Bengal on any Day During the Pre-monsoon Season as Related to the Position and Movement of a Barometric Trough—By K. R. Saha ... ..	357
42. Study of Diffuse X-ray Reflection by a Single Crystal of Meta aminophenol—By M. N. Datta ... ..	371

## No. 8

43. Current Division in a Plane Positive Grid Triode—By S. Deh ... ..	377
44. The Comparative Influence of Short and Long Range Crystalline Electric Fields on the Magnetic Behaviour of the Paramagnetic Salts of the Iron Group of Elements. Part I—By A. Bose and S. C. Mitra ... ..	393
45. Term Values of $f^4$ Electron Configuration. A Correction—By K. Suryanarayana Rao ... ..	427

## No. 9

46. The Complex Band Spectrum of Nickel Bromide—By V. G. Krishnamurty ... ..	429
47. A Note on the Problem of Dislocation in a Semi-infinite Plate containing a Circular Hole—By B. Karunes ... ..	442
48. The Ultraviolet Absorption Spectra of Organic Substances in the Liquid and Solid States. IV. Chlorotoluenes—By H. N. Swamy ... ..	445
49. Studies on the Sharp Extra Reflections from Phloroglucine Dihydrate Crystals—By M. N. Datta ... ..	452
50. Seat of Joshi effect in A. C. Silent Discharges—By P. S. V. Setty, Miss K. Kulkarni and C. M. Srivastava ... ..	455
51. Dynamics of the Elastic Vibration in a Bar Excited by Longitudinal Impact. Part II. Study of the time of Collision—By M. Ghosh and S. K. Ghosh ... ..	463

## No. 10

52. A High Precision Ionospheric Sounding Equipment—By B. M. Banerjee and R. Roy ... 473
53. Study of the Ionosphere by Extraterrestrial Radio Waves—By A. P. Mitra ... 495
54. Spectroscopic studies of Ozoniser Discharges. Part III. Effect of Irradiation on the Intensity Distribution of the Second Positive Nitrogen Bands—By N. Appalanarasimham ... 512
- Review :
3. Einführung in die Theoretische Physik—By Cl. Schaefer ... 519

## No. 11

55. Observations at Calcutta of Pulses transmitted from Delhi—By S. S. Baral and A. K. Saha ... 521
56. An X-ray Study of Andrographis Crystal—By B. S. Basak and D. R. Dasgupta ... 539
57. The comparative Influence of Short and Long Range Crystalline Electric Fields on the Magnetic Behaviour of the Paramagnetic Salts of the Iron Group of Elements. Part II—By A. Bose and S. C. Mitra ... 543
58. Admittance and Transfer Function of a Multimesh Resistance-Capacitance Filter Net-work—By Bimal Krishna Bhattacharyya ... 563
- Review :
- 4 An International Bibliography on Atomic Energy. Volume 2 —Dept. of Security Council Affairs, United Nations, New York ... 574

## No. 12

59. Investigation on the Bowed String with an Electrically driven Bow (Part II),—By N. K. Datta ... 577
60. Studies on the Ionospheric Absorption—By B. Chatterjee ... 585
61. A Study on the Triggering of a Plate-coupled Multivibrator by Negative Pulses—By Sunil Kumar Sen and Bimal Krishna Bhattacharyya ... 597
62. Influence of Radiation Damping on the Scattering of Pseudoscalar Charged Mesons by Nucleons—By S. N. Biswas ... 617
63. Some General Relations on the Viscosity of Homologous Liquids —By Santi R. Palit ... 627

PROCEEDINGS OF THE INDIAN ASSOCIATION FOR THE  
CULTIVATION OF SCIENCE

- Diffraction Effects in the Scattering of Neutrons,  $\mu$ -Mesons and Electrons by Nuclei—By E. Amaldi ... 1

# SUBJECT INDEX

SUBJECT	AUTHOR	PAGE
Absorption Spectra of Organic Substances in the Liquid and Solid States. II. Cresols	H. N. Swamy	119
Absorption Spectra of Organic Substances in the Liquid and Solid States. III. Some Substituted Benzene Compounds	H. N. Swamy	233
Absorption Spectrum of PbBr Molecule in the Ultraviolet Region	P. K. Sur and K. Majumder	111
Absorption Spectrum of <i>p</i> -Chlorotoluene	G. Viswanath	263
Admittance and Transfer Function of a Multimesh Resistance-Capacitance Filter Network	Bimal Krishna Bhattacharyya	563
Alpha-decay Energies. On the Calculation of	S. Jha and G. P. Dube	15
Alpha-decay. On the New Theory of	M. L. Chaudhury	186
Amethyst Quartz in the Visible Region. Spectroscopic Study of	M. K. Vainu Bappu	1
Associated Pairs of Penetrating Particles and other Events Observed at Mountain Altitudes with Photographic Emulsions	K. R. Dixit	243
Born Approximations in Potential Scattering of Fast Electrons by Atomic Nuclei in a Static Field. On Higher	S. N. Biswas	38
Bowed String with an Electrically driven Bow. Investigation on the (Part II)	N. K. Datta	577
Complex Band Spectrum of Nickel Bromide. The	V.G. Krishnamurty	429
Complex Band Spectrum of Nickel Chloride. The	V.G. Krishnamurty	207
Current Division in a Plane Positive Grid Triode	S. Deb	377
Detonation of Proton Gas	M. P. Murgai	313
Diatomic Molecules. High Multiplicity States in	K. Suryanarayana Rao	254
Dislocation in a Semi-infinite Plate Containing a Circular Hole. A Note on the Problem of	B. Karunes	442
Distribution of Initial Stress due to Dislocation in an Infinite Plate Containing two Unequal Circular Holes. On the	B. Karunes	317
Distribution of Stress in a Deep Beam Containing two Equal Circular Holes. On the	B. Karunes	197

SUBJECT	AUTHOR	PAGE
Distribution of Weather Over Bengal on any Day During the Premonsoon Season as Related to the Movement of a Barometric Trough. On the	K. R. Saha	357
Diffuse X-ray Reflection by a Single Crystal of Metaminophenol. Study of	M. N. Datta	371
Elastic Vibration in a Bar Excited by Longi- tudinal Impact. Dynamics of The. Part II. Study of the Time of Collision	M. Ghosh and S. K. Ghosh	463
$\Pi - \Sigma$ Electronic Transition in Cobalt Chloride .	V. G. Krishnamurty	177
Heat Losses and Their Dependence on Air Velocity	D. G. Kapadnis and D. V. Gogate	171
Heat-run Tests on Electrical Machines. A . Comparative Study of the Different Methods of. II. Three-phase Transformers	H. K. Basu	283
Internal Dispersion of Optical Waves .. Experiments on the	S. K. Mukherjee	154
Internal Dispersion of Supersonic Waves in . Liquids. Experiments on the	A. K. Dutta and S. K. Mukherjee	161
Ionosphere by Extraterrestrial Radio Waves. . Study of the	A. P. Mitra	495
Ionospheric Absorption. Studies on the .	B. Chatterjee	585
Ionospheric Echo. On the Origin of the Third ..	R. B. Banerji	28
Ionospheric Sounding Equipment. A High . Precision	B. M. Banerjee and R. Roy	473
Joshi Effect in A. C. Silent Discharges. Seat of .	P. S. V. Setty, Miss K. Kulkarni and C. M. Srivastava	455
Molecular Conductivity of Dyestuffs in Solution .. and the Influence of Foreign Substance on the same	K. D. Chaudhuri and D. R. Dasgupta	67
Molecular Motion in Fluids and Internal .. Dispersion and Absorption of Elastic and Optical Waves	A. K. Dutta	142
Neutron-Proton Scattering ..	H. N. Yadav	337
Oblique Propagation Over Equatorial Region. Effect of Magnetic Field in	B. Chatterjee	297
Observations at Calcutta of Pulses Transmitted from Delhi	S. S. Baral and A. K. Saha	521
Osmotic Coefficients. Determination of. I. Cons- truction and Calibration of the Thermistor Bridge	C. G. McGee and B. R. Y. Iyengar	

# Subject Index

ix

SUBJECT	AUTHOR	PAGE
Ozonizer Discharges. Spectroscopic Studies of. Part III. Effect of Irradiation on the Inten- sity Distribution of the Second Positive Nitrogen Bands	N. Appalanara- simham	512
Paramagnetic Salts of the Iron Group of .. Elements. The Comparative Influence of Short and Long Range Crystalline Electric Fields on the Magnetic Behaviour of the. Part I Do ... Part II	A. Bose and S. C. 393 Mitra  A. Bose and S. C. 543 Mitra	    452
Phloroglucine Dihydrate Crystals. Studies on the Sharp Extra Reflections from Pressure in a Liquid	M. N. Datta	452
Pseudoscalar Meson Field and Relativistic . Scattering of Neutrons by Protons	M. G. Bhatawdekar D. Basu	54 291
Pseudoscalar Meson Field and the Scattering of .. Fast Neutrons by Protons	N. C. Sil	269
Pulse Width Measurements in Radar	A. Sundara Babu	56
Raman Spectra of Organic Crystals at Low . Temperatures. III. Orthoxylene and Benzyl- bromide	A. K. Ray	226
Raman Spectrum of Solution of Benzoyl Chloride . in Benzene. On the	T. A. Hariharan	115
Raman Spectrum of Thianthrene in the Molten . State. On the	S. K. Mukerji and Banarsi Lal	276
Recombination Coefficient and Scale Height on the . Structure of the Ionized Region. Effect of Variation of	A. P. Mitra	79
Resonator Absorbers in Broadcast Studios	Ram K. Vepa	126
Scattering of Pseudoscalar Charged Mesons by . Nucleons. Influence of Radiation Damping on the	S. N. Biswas	617
Spin Splitting of $^3\Sigma$ and $^6\Sigma$ Electronic States	K. Surya- narayana Rao	47
Term Values of $f^4$ Electron Configuration. A Correction	K. Surya- narayana Rao	427
Thermionic Meter for Measuring Rectification Ratio of Current in Discharge Tubes. A	V. L. Taleker	329
Triggering of a Plate-coupled Multivibrator by Negative Pulses. A Study on the	Sunil Kumar Sen and Bimal Krishna Bhattacharyya	585

## *Subject Index*

SUBJECT	AUTHOR	PAGE
U. H. F. Radio Waves in Solutions of Cresols in ... Benzene. On the Absorption of	G. S. Kastha	103
Ultrasonic Absorption and Relaxation Mechanism ...	A. K. Dutta	279
Ultraviolet Absorption Spectra and the Intensity ... of the Fluorescence Band at $4156 \text{ \AA}$ of Diamond	B. M. Bishui	347
Ultraviolet Absorption Spectra of Organic Subs- ... tances in the Liquid and Solid States. On the. Part III. Ethyl benzene and Isopropyl Benzene	A. R. Deb	201
Ultraviolet Absorption Spectra of Organic Subs- ... tances in the Liquid and Solid States. IV. Chlorotoluenes	H. N. Swamy	445
Viscosity of Homogeneous Liquids. Some General ... Relations on the	Santi R. Palit	627
X-ray Study of Andrographis Crystal. An ...	B. S. Basak and D. R. Dasgupta	539

### PROCEEDINGS OF THE INDIAN ASSOCIATION OF THE CULTIVATION OF SCIENCE

Diffraction Effects in the Scattering of Neutrons, ... $\mu$ -Mesons and Electrons by Nuclei.	E. Amaldi	1
--	-----------	---

### R E V I E W S

1. High Frequency Measurements ...	August Hund	159
2. Understanding Radio ...	Watson, Welch and Eby	160
3. Einführung in die Theoretische Physik ...	Cl Schaefer	519
4. An International Bibliography on Atomic ... Energy, Vol. 2.	Dept. of Security Council Affairs, United Nations, New York.	574

# AUTHOR INDEX

AUTHOR	SUBJECT	PAGE
Appalanarasimham, N., ...	Spectroscopic studies of Ozoniser Discharges. Part III. Effect of Irradiation on the Second Positive Nitrogen Bands	512
Babu, A. Sundara ...	Pulse Width Measurements in Radar	56
Banerjee, B. M. and Roy, R. ...	A High Precision Ionospheric sounding Equipment	473
Banerjee, R. B. ...	On the Origin of the Third Ionospheric Echo	28
Banarsi Lal ...	(See Mukerji S. K. and...)	276
Bappu, M. K. Vainu ...	Spectroscopic Study of Amethyst Quartz in the Visible Region	1
Baral, S. S. and Saha, A. K. ...	Observations at Calcutta of Pulses Transmitted from Delhi	521
Basak, B. S. and Dasgupta, D. R. ...	An X-ray Study of Andrographis Crystal	539
Basu, D. ...	Pseudoscalar Meson Field and Relativistic Scattering of Neutrons by Protons	291
Basu, H. K. ...	A Comparative Study of the Different Methods of Heat run Tests on Electrical Machines. II. Three-phase Transformers	283
Bhatawdekar, M. G. ...	Pressure in a Liquid	54
Bhattacharyya, Bimal Krishna ...	Admittance and Transfer Function of a Multimesh Resistance Capacitance Filter Net-work	563
Bhattacharyya, Bimal Krishna ..	(See Sen Sunil Kumar and...)	597
Bishui, B. M. ...	The Ultraviolet Absorption Spectra and the Intensity of the Fluorescence Band of $4156 \text{ \AA}$ of Diamend	347
Biswas, S. N. ...	On Higher Born Approximations in Potential Scattering of Fast Electrons by Atomic Nuclei in a Static Field	38
„ ...	Influence of Radiation Damping on the Scattering of Pseudoscalar charged Mesons	617
Bose, A. and Mitra, S. C. ...	The Comparative Influence of Short and Long Range Crystalline Electric Fields on the Magnetic Behaviour of the Paramagnetic Salts of the Iron Group of Elements. Part I	363

AUTHOR	SUBJECT	PAGE
	Part II	543
Chatterjee, B.	Effect of Magnetic Field in Oblique Propagation over Equatorial Region	297
	Studies on Ionospheric Absorption	585
Chaudhuri, K. D. and Dasgupta, D. R.	On the Molecular conductivity of Dyestuffs in Solution and the Influence of Foreign Substance on the same	67
Chaudhury, M. L.	On the New Theory of Alpha-decay	186
Dasgupta, D. R.	(See Chaudhuri K. D. and...)	67
	(See Basak B. S. and...)	539
Datta, M. N.	Study of Diffuse X-ray Reflection by a Single Crystal of Metaaminophenol	371
	Studies on Sharp Extra Reflections from Phloroglucine dihydrate Crystals	452
Datta, N. K.	Investigation on the Bowed String with an Electrically Driven Bow. Part II	577
Deb, A. R.	On the Ultraviolet Absorption Spectra of Organic Substances in the Liquid and Solid States. Part III. Ethylbenzene and Isopropylbenzene	201
Deb, S.	Current Division in a Plane Positive Grid Triode	377
Dixit, K. R.	Associated Pairs of Penetrating Particles and other Events Observed at Mountain Altitudes with Photographic Emulsions	243
Dube, G. P.	(See Jha, S. and...)	15
Dutta, A. K.	Molecular Motion in Fluids and Internal Dispersion and Absorption of Elastic and Optical Waves	142
	Ultrasonic Absorption and Relaxation Mechanism	279
Dutta, A. K. and Mukherjee, S. K.	Experiments on the Internal Dispersion of Supersonic Waves in Liquids	161
Ghosh, M. and Ghosh, S. K.	Dynamics of the Elastic Vibration in a Bar Excited by Longitudinal Impact. Part II. Study of the Time of Collision	463
Ghosh, S. K.	(See Ghosh, M. and...)	463
Gogate, D. V.	(See Kapadnis D. G. and...)	171
Hariharan, T. A.	On the Raman Spectrum of solution of Benzoyal chloride in Benzene	115



AUTHOR	SUBJECT	PAGE
Iyengar, B. R. Y. ...	(See McGee, C. G. and...)	61
Jha, S. and Dube, G. P. ...	On the Calculation of Alpha-decay Energies	15
Kapadnis, D. G. and Gogate, D. V. ...	Heat Losses and their Dependence on Air Velocity	171
Karunes, B. ...	On the Distribution of stress in a Deep Beam containing two Equal Circular Holes	197
„ ...	On the Distribution of Initial Stress due to Dislocation in an Infinite Plate Containing two Unequal circular Holes	317
„ ...	A Note on the Problem of Dislocation in a Semi-infinite Plate Containing a Circulr Hole	442
Kastha, G. S. ..	On the Absorption of U. H. F. Radio in Solutions of Cresols in Benzene	103
Krishnamurty, V. G., ...	" $\Pi$ --" $\Sigma$ Electronic Transition in Cobalt-chloride	177
„ ...	The Complex Band Spectrum of Nickel-chloride	207
„ ...	The Complex Band Spectrum of Nickel bromide	429
Kulkarni (Miss), K. ...	(See Setty, P. S. V. and)	455
Majumdar, K. ...	(See Sur P. K. and)	111
McGee, C. G. and Iyengar B. R. Y. ...	Determination of Osmotic Coefficients. I. Construction and Calibration of the Thermistor Bridge	61
Mitra, A. P. ...	Effect of Variation of Recombination Coefficient and Scale Height on the Structure of the Ionized Region	79
„ ...	Study of the Ionosphere by Extraterrestrial Radio Waves	495
Mitra, S. C. ...	(See Bose, A. and)	393
„ ...		543
Mukerji, S. K. and Banarsi Lal ...	On the Raman Spectrum of Thianthrene in the Molten state	276
Mukherjee, S. K. ...	Experiments on the Internal Dispersion of Optical Waves	154
„ ...	(See Dutta, A. K. and)	161
Murgai, M. P. ...	Detonation of Proton Gas	313
Palit, S. R. ...	Some General Relations on the Viscosity of Homologous Liquids	627

AUTHOR	SUBJECT	PAGE
Rao, K. Suryanarayana ...	Spin Splitting of $^5\Sigma$ and $^6\Sigma$ Electronic States	47
,,	High Multiplicity States in Diatomic Molecules	254
,,	Term Values of $f^4$ Electron Configuration	427
Ray, A. K. ...	Raman Spectra of Organic Crystals at Low Temperatures. III. Orthoxylene and Benzylbromide	226
Roy, R. ...	(See Banerjee, B. M. and)	473
Saha, A. K. ...	(See Baral, S. S. and)	521
Saha, K. R. ...	On the Distribution of Weather Over Bengal on any Day During the Premonsoon Season as Related to the Movement of a Barometric Trough	357
Sen, S. K. and Bhattacharyya, B. K. ...	A study on the Triggering of a Plate-coupled Multivibrator by Negative Pulses	597
Setty, P. S. V., Kulkarni... (Miss), K. and Srivastava, C. M.	Scat of Joshi effect in A. C. Silent Discharges	455
Sil, N. C. ...	Pseudoscalar Meson Field and the Scattering of Fast Neutrons by Protons	269
Srivastava, C. M. ...	(See Setty, P. S. V. Kulkarni (Miss)K., and)	455
Sur, P. K. and Majumdar, K. ...	The Absorption Spectrum of PbBr Molecule in the Ultraviolet Region	111
Swamy, H. N. ...	Absorption Spectra of Organic Substances in the Liquid and Solid States. II. Cresols	119
,,	Absorption Spectra of Organic Substances in the Liquid and Solid States. III. Some Substituted Benzene Compounds	233
,,	The Ultraviolet Absorption Spectra of Organic Substances in the Liquid and Solid States. IV. Chlorotoluenes	445
Talekar, V. L. ...	A Thermionic Meter for Measuring Rectification Ratio of Current in Discharge Tubes	329
Vepa, Ram K., Viswanath, G. ...	Resonator Absorbers in Broadcast Studios	126
Yadav, H. N. ...	Absorption Spectrum of <i>p</i> -chlorotoluene	263
	Neutron Proton Scattering	337

## E R R A T A

1. In page 154, equation (1) should be as :

$$n^2 - k^2 \simeq n^2 = \frac{c^2}{v^2} = 1 + \frac{4\pi \sum N_K (e^2/m) (f_K^2 - \omega^2)}{(f_K^2 - \omega^2) + \omega^2 g^2}$$

2. In page 157, 9th line, read "...mean value" in the place of "...mean velocity".
3. In page 158, the first two references should be as :

Dutta, A. K., 1952, *Ind. J. Phys.*, **26**, 142.

Pinkerton, J. M. M., 1940, *Proc. Phys. Soc.*, B. **62**, 129.



# SPECTROSCOPIC STUDY OF AMETHYST QUARTZ IN THE VISIBLE REGION\*

By M. K. VAINU BAPPU

PHYSICAL LABORATORY, NIZAM COLLEGE HYDARABAD (DECCAN)

(Received for publication, June 16, 1951; received after revision, November, 30, 1951)

## Plate 1

**ABSTRACT.** In this paper a detailed study is made of the absorption of light in the visible region by amethyst quartz. It is found that in the visible region, an absorption band, the so called F-band appears, which decreases in intensity at high temperature the maximum also shifts towards longer wavelengths, but the number of colour centres remain constant till about 200°C. At higher temperatures these centres, which are responsible for the absorption, are destroyed by heat. When the crystal is exposed to radiation absorbed by the F band, a new F'-band appears. The facts reveal that the coloration is due to exposure to some penetrating radiations.

## INTRODUCTION

It has long been known that certain crystals, which are normally transparent, are found coloured in nature, and it has been found that these colours can also be produced artificially by physical means and by the addition of chemical impurities. Well known examples are those of the alkali halides which were thoroughly studied by Pohl and his collaborators. A good account of this work done by Pohl is found in two survey articles by Pohl (1937, 1938) and the more recent work can be found in a survey article by Seitz (1946).

The agencies which cause coloration of crystals may be broadly divided into two categories, chemical and physical. In the former may be included pigments, inclusion of foreign substances or even a small stoichiometric excess of one of the elements and in the latter purely physical processes are responsible for the coloration, the crystal remaining chemically pure. This discoloration may be due to exposure to ionizing radiations such as ultraviolet rays, X-rays and gamma rays or even cathode rays.

The coloured varieties of quartz have of late been investigated with a view to elucidating the cause of the coloration. It has been found that even the natural transparent crystals can be coloured. But so far no final solution has been obtained. In this paper a detailed study of the physical properties

\* Part of the thesis accepted for the M. Sc. research degree of the Madras University.

of the violet variety of quartz-amethyst quartz- is made in order to understand the nature of the coloration.

*Coloured alkali halides and F bands.* A systematic study of these crystals was carried out by Pohl and his collaborators. They found that when these crystals are exposed to ultraviolet or heated in alkali metal vapour they become coloured. This coloration is due to the presence of characteristic absorption band which lies in the visible region. Pohl has called this absorption band the F-band, and the absorption centres F-centres (Farbzentren).

*Coloured quartz.* In addition to the transparent variety, quartz is also found coloured. We have the violet blue, yellow or citrine, rose and smoky varieties found in widely scattered countries and in the same area several other mixed varieties can be seen. Amethyst quartz is found in abundance in certain quartz reefs of the Deccan. The crystals are well formed and are usually violet, but some of them are translucent and appear to be similar to amethyst crystals bleached by heat. Sometimes crystals, which are partly violet and partly smoky, are found and this suggests a common origin of the two varieties.

*Discoloration by X-rays and radium rays.* Discoloration of transparent quartz, especially by X-rays was studied recently. The earliest to investigate the effect of radium rays seems to be Bensaude and Costanzo (1922), Lind and Bradwell (1923) and Hoffmann (1931). The results obtained by different investigators appear to be conflicting. Apparently, the colour developed depends on the impurities and the initial colour of the specimen. Futtagami (1938) obtained a smoky colour when the transparent crystal was exposed to X-rays, while Laemmlein (1944) got a violet colour. He found that some specimens remained colourless. While glass prepared from smoky quartz acquired an intense violet colour, pale amethyst quartz acquired only an additional faint smoky colour. A systematic study of the coloration produced by radium rays in different varieties of quartz was made by Choong (1945). His conclusions are the following :

1. All coloured crystals acquire a smoky colour when exposed to radium rays.
2. The same rays render vitreous quartz violet in colour instead of smoky.
3. The natural colours and those produced by radium rays in the quartz, both crystalline and vitreous can be eliminated by heating. The artificial smoky and violet tints fade with perceptible rapidity at 190°C and 300°C respectively. After heating, the specimens regain their original transparency and they can be coloured again. The time required for the decoloration depends greatly on the temperature and also on the nature of the colour.

*Previous explanations of colour in coloured quartz.* Several attempts have been made to explain the colour of amethyst quartz and other varieties. Holden (1925) is of the view that the colour of the smoky quartz is due to

the atoms of silicon liberated by the action of rays of the radioactive substances during the long geological epoch. Mohler (1936) comes to the same conclusion in the case of smoky quartz. In a detailed investigation on the case of colour in blue quartz made by Jayaraman (1939) the conclusion reached is that the element responsible for the colour is titanium.

He suggests that the colour is only an opalescent colloidal one produced by colloidal particles of the size of 0.2 to 0.5 microns in diameter, modified by the absorption of titanium. Vedeneva (1940), who studied absorption spectra for the ordinary and extra-ordinary rays in amethyst quartz, found a maximum at  $5400 \text{ \AA}$  and deduced that the colour may be due to highly dispersed inclusions, perhaps of ferric ions. Recently another attempt was made by Narayana Rao (1947) to find the cause of the coloration of amethyst. With that view he found its dielectric constant.

In the present investigation a detailed spectroscopic study of amethyst quartz in the visible region is made in order to find the cause of coloration.

## PART I

### ABSORPTION COEFFICIENTS AT DIFFERENT TEMPERATURES

*Experimental study.* After careful examination, one plate 2.3 millimetres thick was cut off from one of the faces. There was no sign of the presence of any streaks of colour or cracks, the specimen being uniformly coloured and free from inclusions. Another plate of amethyst quartz was obtained from a crystalline specimen picked up from an entirely different quartz reef. This plate was also cut in such a way that its plane made an angle of 33 degrees with optic axis of the crystal. The coloration for all practical purposes could be taken as uniform. This specimen was used for the study of the effect of heat on specimens of crystalline amethyst quartz in order to understand clearly how thermal treatment removes the coloration. In future, this specimen of the amethyst quartz shall be called  $A_2$  and the former  $A_1$  for the sake of convenience.

Amethyst quartz, by transmitted light has a reddish violet colour, and this shows that by a process of selective absorption, the other components of the electromagnetic spectrum between the red and violet region are absent (see Plate I,) partially or completely in the light after transmission. A spectrogram of the transmitted light was taken. Exposure of the order of ten minutes were given on Kodak panchromatic plates. The spectrum of the mercury arc was photographed above and below each spectrogram for purposes of comparison. All the spectrograms indicated an absorption band from the blue to the orange region near about the mercury line  $5461 \text{ \AA}$ . There were no other bands in the visible region.

QUANTITATIVE EVALUATION OF THE ABSORPTION  
COEFFICIENT AT LIQUID AIR, ROOM AND HIGH  
TEMPERATURES

The evaluation of the absorption co-efficient for different wavelengths were made visually by means of spectro-photometer of the Marten's type made by Bausch and Lomb. The source of light was a powerful 250-watt lamp. To enable limited regions of definite width into the field of view, a slit was placed in the eye-piece. This was of sufficient width to let in 20 Angstroms in the violet region of the spectrum.

The study of the absorption of amethyst quartz in the visible region was made also at both high and low temperatures using the spectro-photometer. For high temperature work the specimen was placed in a specially designed heater constructed in this laboratory. The heater consisted of a cylindrical block of brass with an internal bore of diameter 2.5 cm. In this another hollow cylinder, with a rectangular enclosure in the centre for holding the specimen, fitted exactly. The specimen could be held firmly in the holder by means of a sliding tube, the axis of which was in coincidence with that of the external cylinder. This was arranged in such a way that the crystal would not experience any undue pressure. At right angles to the axis of the system, an aperture was made for holding the thermometer. This thermometer was used only in the temperature range  $0^{\circ}\text{C} - 350^{\circ}\text{C}$  when it was placed in position it would always be in actual contact with the specimen under study. The surface of the entire cylinder was first covered with a thin layer of asbestos over which was wound nichrome wire, and finally set in a mixture of plaster of paris asbestos flakes. The resistance coils were fed by A. C. from a variac 0-270 volts.

In making absorption measurements at room temperature, the crystal was mounted against an aperture in a cardboard in such a way that stray light would not pass through the sides. This mounting was then held against one of the rhomboid prisms and readings were taken.

For the purpose of making observations at the temperature of liquid air, a three walled Dewar flask was placed in position before the rhomboid prisms and liquid air was poured into it. The solid specimen was fixed in one of the two apertures of a brass rod provided for the entrance and exit of the two light beams. Enough liquid air had to be poured into the Dewar flask so that the surface of the liquid may be well above the two apertures. With this type of arrangement the specimen attained the temperature of liquid air within a few minutes.

## RESULTS

The respective calculated absorption co-efficients of the specimen at different temperatures for different wavelengths (given in electron volts)



in the visible region are diagrammatically represented in figure 1.

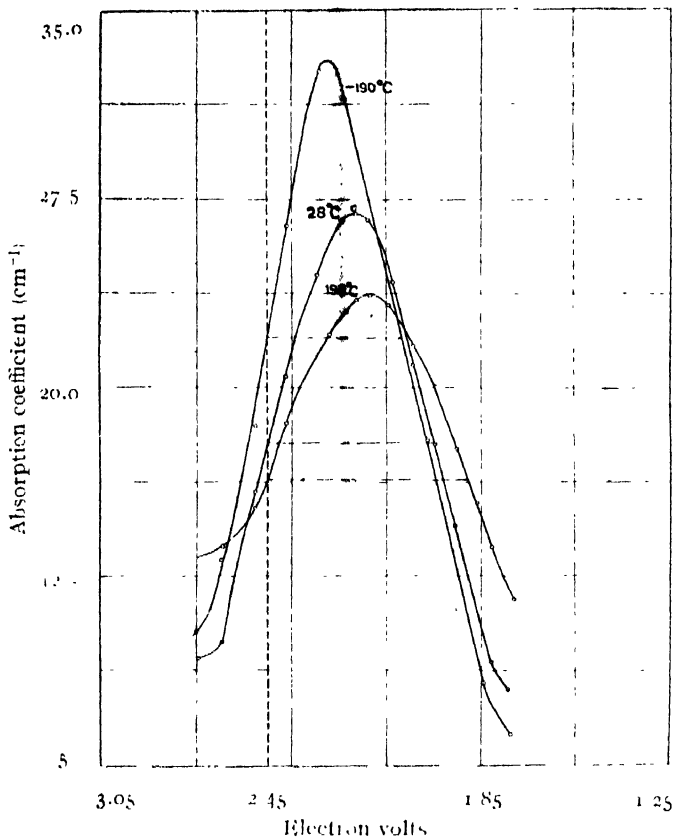


FIG. 1

Variation of the structure the of F-band with temperature

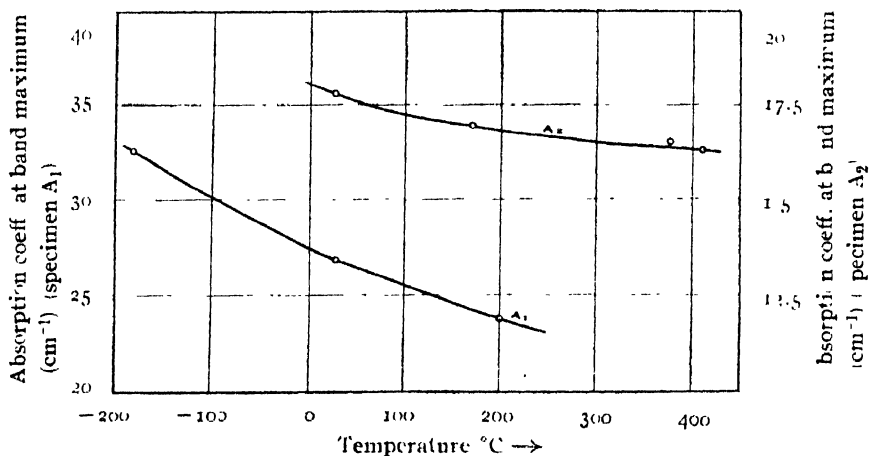


FIG. 2

Variation of absorption coefficient at band maximum in amethyst quartz with temperature

In confirmation of the results obtained from a study of absorption spectra by photographic methods, the spectro-photometric results revealed

a single bell shaped band with a maximum at 5500 Å. As the temperature of the specimen decreases it will be observed that the band narrows down, the width of the band at half maximum having shortened considerably.

The band maximum shifts towards shorter wavelengths with decreasing temperature. The long wavelength foot also simultaneously drops down in absorption values. As seen later, this process of cooling to low temperatures may not be capable of converting this absorption band into a narrow line or increase its absorption co-efficient to infinite values when brought near  $-273^{\circ}\text{C}$ . This is shown diagrammatically in figure 2, where the absorption co-efficients of the band maxima for the two specimens of amethyst quartz ( $A_1$ ) and ( $A_2$ ) are plotted for different temperatures.

It will be seen that the graph becomes asymptotic only at high temperatures and that low temperatures do not effectively increase the absorption values.

TABLE I

Structural details of F-bands for different temperatures

Temp. $^{\circ}\text{C}$	Band maximum in Å. U.	Absorption co-efficient of band max	λ in Å. U.		Width at half maximum in electron volt
			vio.	red.	
-193	5270	33.00	4900	5890	0.424
+28	5500	26.92	4900	6130	0.530
+198	5600	23.87	4900	6542	0.634

Table I summarises the behaviour of the various structural details of the single band with temperature. Further, as we proceed from the short wavelength foot of the band towards the band maximum, the points on the short wavelengths slope having values of absorption co-efficient equal to half values of those in the absorption maximum, can be seen to arrange themselves in a line indicating that they are always at the same wavelength. (4900 Å), shown by the dotted line in the figure 1, no matter what the temperature is. A similar result was obtained by Mollow (1933) in the case of potassium bromide. This is ascribed to a transition between two undisturbed energy levels of the crystal.

## PART II

### OPTICAL EXCITATION OF AMETHYST QUARTZ

*Experimental technique.* To study in detail the absorption curve of amethyst quartz when excited, we must have the absorption curve of the specimen when excited so that a proper comparison can be made. As the absorption at room temperature has already been studied the data can be

taken as that of the unexcited absorption curve, but there is a remote possibility that the green light of the incoming radiation may excite the F-centres a little without much interference from the red and infra-red passing through simultaneously. As such, it was considered worth while to take fresh readings of the absorption curves, taking care to quench the excitation if any such thing exists.

For this study the spectro-photometer was used again. The specimen was held in an aperture made in a card board and placed before a rhomboid prism of the photometer. A circular coil of thin constantan wire was placed in front of the crystal in such a way that it allowed light to traverse the specimen without any obstruction. This was made to glow appreciably by passing a strong current from a set of accumulators. The crystal was thus given a constant irradiation of infra-red light.

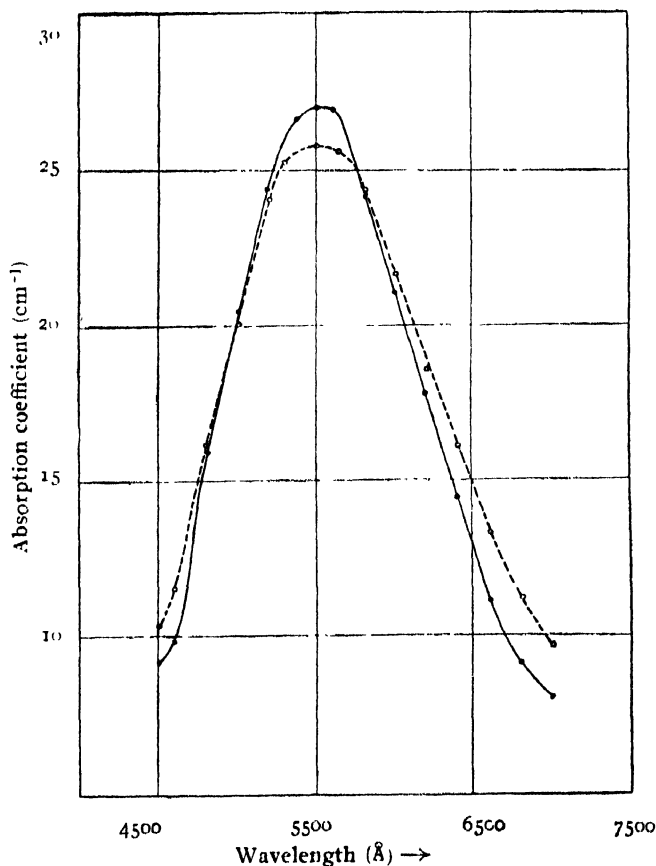


FIG. 3  
Excitation of the Farbenzentren in amethyst quartz  
—○— unexcited  
--○-- excited

To produce excitation, it is necessary to irradiate the specimen with light in the short wavelength foot of the absorption band, or in the band

a single bell shaped band with a maximum at 5500 Å. As the temperature of the specimen decreases it will be observed that the band narrows down, the width of the band at half maximum having shortened considerably.

The band maximum shifts towards shorter wavelengths with decreasing temperature. The long wavelength foot also simultaneously drops down in absorption values. As seen later, this process of cooling to low temperatures may not be capable of converting this absorption band into a narrow line or increase its absorption co-efficient to infinite values when brought near  $-273^{\circ}\text{C}$ . This is shown diagrammatically in figure 2, where the absorption co-efficients of the band maxima for the two specimens of amethyst quartz ( $A_1$ ) and ( $A_2$ ) are plotted for different temperatures.

It will be seen that the graph becomes asymptotic only at high temperatures and that low temperatures do not effectively increase the absorption values.

TABLE I

Structural details of F-bands for different temperatures

Temp. °C	Band maximum in Å. U.	Absorption co-efficient of band max	λ in Å. U vio.      red.	Width at half maximum in electron volt
-193	5270	33.00	4900   5890	0.424
+28	5500	26.92	4900   6130	0.530
+198	5600	23.87	4900   6542	0.634

Table I summarises the behaviour of the various structural details of the single band with temperature. Further, as we proceed from the short wavelength foot of the band towards the band maximum, the points on the short wavelengths slope having values of absorption co-efficient equal to half values of those in the absorption maximum, can be seen to arrange themselves in a line indicating that they are always at the same wavelength. (4900 Å), shown by the dotted line in the figure 1, no matter what the temperature is. A similar result was obtained by Mollow (1933) in the case of potassium bromide. This is ascribed to a transition between two undisturbed energy levels of the crystal.

## PART II

### OPTICAL EXCITATION OF AMETHYST QUARTZ

*Experimental technique.* To study in detail the absorption curve of amethyst quartz when excited, we must have the absorption curve of the specimen when excited so that a proper comparison can be made. As the absorption at room temperature has already been studied the data can be

taken as that of the unexcited absorption curve, but there is a remote possibility that the green light of the incoming radiation may excite the F-centres a little without much interference from the red and infra-red passing through simultaneously. As such, it was considered worth while to take fresh readings of the absorption curves, taking care to quench the excitation if any such thing exists.

For this study the spectro-photometer was used again. The specimen was held in an aperture made in a card board and placed before a rhomboid prism of the photometer. A circular coil of thin constantan wire was placed in front of the crystal in such a way that it allowed light to traverse the specimen without any obstruction. This was made to glow appreciably by passing a strong current from a set of accumulators. The crystal was thus given a constant irradiation of infra-red light.

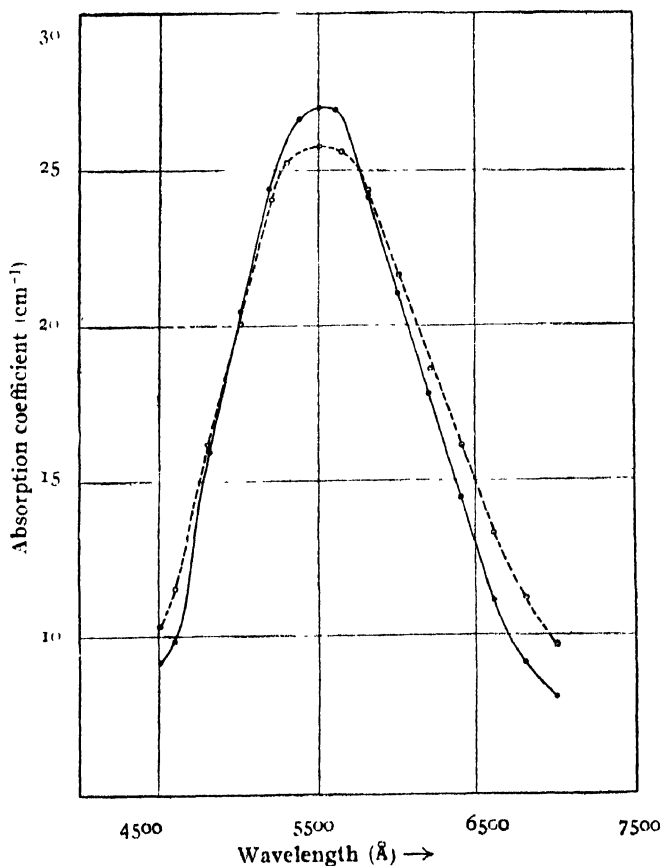


FIG. 3  
Excitation of the Farbenzentren in amethyst quartz  
—○—○— unexcited  
- - ○ - - ○ - - excited

To produce excitation, it is necessary to irradiate the specimen with light in the short wavelength foot of the absorption band, or in the band

maximum. In the case of amethyst quartz, a filter was used to transmit light of range between  $4300 \text{ \AA}$  and  $5200 \text{ \AA}$ . Intense white light from a 250-watt lamp was allowed to pass through a water cell in order to absorb completely the infra-red and then condensed on the crystal after passing through the blue filter. This flooding with blue light was the source of excitation and this was done between every two readings.

### RESULTS

In figure 3, the corresponding absorption co-efficients calculated from these data are plotted against the wavelengths recorded in A. U. From the figure we see that the main features of excitation *viz.* the decrease in value of absorption co-efficient of band maximum and the increase in absorption of the long wavelength foot of the absorption band, are found in this case. The new absorption band has an absorption co-efficient of  $25.68 \text{ cm}^{-1}$  in the band maximum as compared with  $26.92 \text{ cm}^{-1}$  in the unexcited F-band. The unexcited band had values of absorption co-efficient the same as those for absorption at room temperature. Also at  $7000 \text{ \AA}$ , the F-band has value of  $8.09 \text{ cm}^{-1}$  while the F'-band has one at  $9.73 \text{ cm}^{-1}$ . An increase in value of absorption co-efficient in the short wave-length foot is also seen.

*Refractive index of amethyst quartz.* The measurements of refractive index of the specimen of amethyst quartz ( $A_1$ ) were carried out using a Pulfrich refractometer. With the mercury arc in position the angles of emergence were measured for  $4358 \text{ \AA}$ , as well as for the  $D_1 D_2$  lines of sodium, for which purpose a sodium lamp is used. The calculated values of the refractive indices are given in Table II, and values of crystalline quartz being given for the sake of comparison. It will be seen that the results reveal the presence of slight anomalous dispersion in the region of the band.

TABLE II

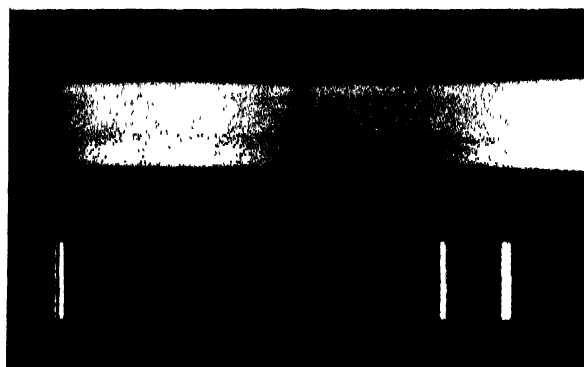
Wavelength in A. U.	Refractive index of amethyst quartz	Refractive index of crystalline quartz
5893	1.54924	1.5443
5461	1.54382	1.5462
4358	1.53858	1.5538

#### *Number of centres.*

The theory of dispersion by Smakula (1930) can be applied to F-centre bands in order to determine the density of these centres. It may be recalled that these bands probably arise from the excitation of electrons in vacant sites in crystals. As the electrons are coupled to the lattice the observed bands are much wider than lines of free atoms at room temperature.

According to Smakula

$$N_0 = \frac{18m}{\pi e^2 h} \cdot \frac{1}{(n_0 + 2)^2} \cdot K_{max} W.$$



The F band in amethyst quartz

- (a) Absorption spectrum of amethyst quartz (specimen  $A_3$ )
- (b) Comparison spectrum of the mercury arc.





where  $N_0$  is the number of absorbing centres,  $c$ ,  $h$  and  $m$  are the usual atomic constants,  $n_0$  the refractive index in the centre of the band,  $K_{max}$ , the absorption co-efficient of the band maximum and  $W$  the width of the absorption band at half maximum expressed in electron volts. Substituting the following values

$$\begin{aligned}c &= 4.803 \times 10^{-10} \text{ e. s. u.} \\m &= 0.910 \times 10^{-27} \text{ grams.} \\h &= 6.55 \times 10^{-27} \text{ erg. sec.} \\n_0 &= 1.5438. \\K_{max} &= 26.92 \text{ cm}^{-1}. \\W &= 0.53 \text{ electron volts.}\end{aligned}$$

we get  $N_0 = 6.05 \times 10^{15}$ . It will be noted that the value given for  $n_0$  is the value of the refractive index at the mercury wavelength 5461 Å.

The values of  $N_0$  for the three different temperatures  $+198^\circ\text{C}$ ,  $+29^\circ\text{C}$  and  $-190^\circ\text{C}$  are given in Table III and the respective deviations of the number of F centres at  $-190^\circ\text{C}$  and those at  $+198^\circ\text{C}$ , from the number of centres at room temperature are also entered.

It will be found that the deviation at  $-190^\circ\text{C}$  is of the order of 3.2% from the value at  $28^\circ\text{C}$  while that at  $198^\circ\text{C}$  is of the order of 6.8%. In calculating the values of  $N_0$  the refractive index of the band maximum was assumed to be the same as that at the wavelength 5461 Å, at room temperature.

Number of F-centres for different temperatures at which colour is stable.

TABLE III

Temperature.	No. of centres.	Deviation in $n_0$ from $28^\circ\text{C}$ .	Per cent deviation.
$-190^\circ\text{C}$	$5866 \times 10^{15}$	$190 \times 10^{15}$	3.2.
$+28$	$6056 \times 10^{15}$	$0.0 \times 10^{15}$	0.0.
$+198$	$6421 \times 10^{15}$	$368 \times 10^{15}$	6.0.

The deviations increase slightly with temperature showing thereby that by change of temperature, within limited ranges, a slight change is brought about in the number of F-centres. This can be taken as a further indication that the electron distribution confirms to classical statistics.

*Decolorisation of amethyst by heat.* The removal of F-centres has been made in various ways. The common way of removing these is by thermal treatment. When the crystal containing F-centres is heated at very high temperature the colour fades away. The speed of this process, *viz.* the loss in colour, depends essentially upon the temperature of the surroundings. The temperature at which all traces of colour vanish varies with the substance

under consideration. Amethyst quartz loses colour slowly at  $300^{\circ}\text{C}$  and quickly at temperature between  $400^{\circ}\text{C}$  and  $450^{\circ}\text{C}$ . The removal of colour in amethyst quartz was done by heating the specimen at high temperatures and the shape or the structure of the F-band observed at different stages.

The spectrophotometer was used again for determining the structure of the F-band when the specimen (A2) was maintained at different temperatures for different intervals of time. After obtaining the absorption curve at room temperature, the absorption curve was obtained after tempering the specimen in the heater described before at a constant temperature of  $380^{\circ}\text{C}$ . Later, the specimen was placed in a sand bath and heated to  $450^{\circ}\text{C}$  and then brought down to room temperature and the absorption curve was determined. It was again maintained at  $450^{\circ}\text{C}$  for some time and brought back to room temperature. The temperature in this case was measured by a calibrated copper-constantan thermocouple. In this way a spectroscopic analysis was made of the loss of colour in amethyst quartz due to heating.

## RESULTS

The spectrophotometric results are shown in figure 4. When maintain

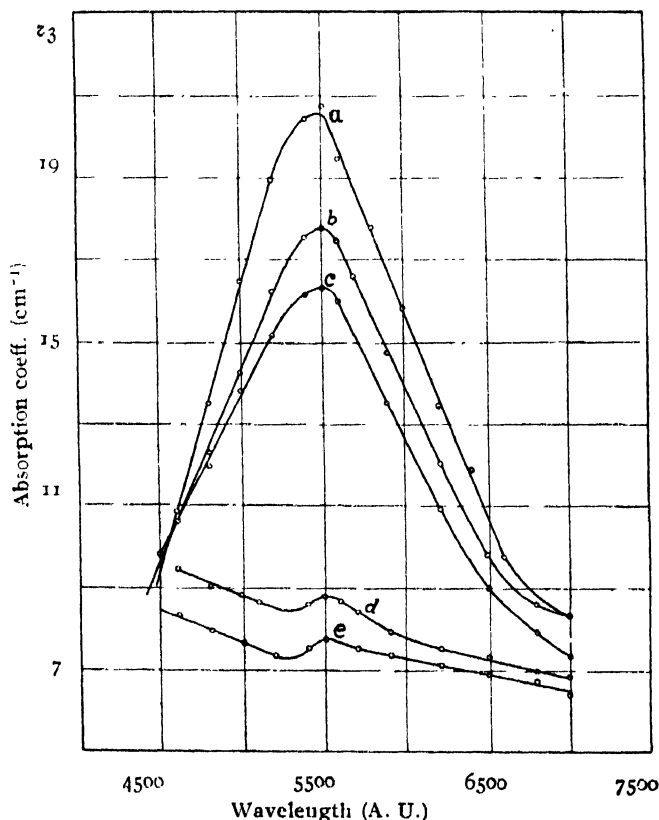


FIG. 4

Effect of tempering on the F band

at constant temperature of  $380^{\circ}\text{C}$ , a slow drop in absorption was noted.

The maximum of the absorption band had an absorption co-efficient of  $20.68 \text{ cm}^{-1}$  at  $380^\circ\text{C}$  (curve *a*). Fifteen minutes after this reading was noted, the new value of the absorption co-efficient was  $19.33 \text{ cm}^{-1}$ . After another fifteen minutes the new value of the band maximum was  $18.88 \text{ cm}^{-1}$ . It will be seen from this that when maintained at  $380^\circ\text{C}$  for a period of a number of hours, the process of the dropping of absorption value might continue until the specimen loses its colour completely. Curves (*b*) and (*c*) in figure 4, were obtained when the specimen was maintained at temperature of  $380^\circ\text{C}$  for one and two hours respectively.

Curve (*d*) was obtained when the temperature was raised to  $450^\circ\text{C}$  and maintained for 30 minutes, while curve (*e*) is the result of heating at  $450^\circ\text{C}$  for 20 minutes after curve (*d*) was obtained. No trace of any colour could be seen when readings on curve (*d*) were being taken. Table IV summarises the structural details of the F-bands after tempering. It is interesting to note that even when no trace of colour was found in the specimen when curves (*d*) and (*e*) were taken, there are a few F-centres still existing, as evidenced by the humps in the respective curves.

TABLE IV  
Structural details of the F-band after tempering

Curve No	Temp. of tempering $^\circ\text{C}$	Time of tempering	$\lambda$ of band max.	$K$ of band max.	$\lambda_F$	$\lambda_r$	Width at half max.	No of centres $\times 10^{15}$
<i>a</i>	28	0 mins	5480	20.6	4875	6100	0.510	44.0
<i>b</i>	380	60 "	5500	17.60	4875	6050	0.540	4054
<i>c</i>	380	120 "	5500	16.25	4850	6000	0.493	3399
<i>d</i>	450	30 "	5500	8.75	5400	5700	0.120	455.7
<i>e</i>	450	50 "	5525	7.75	5400	5630	0.100	319.0

When the crystal containing F-centres is heated the centres acquire thermal energy as a result of which they move back to their former places and recombine. This recombination depends upon the amount of thermal energy acquired which in turn depends on the temperature at which the specimen is maintained. This is why the colour vanishes quickly at high temperatures than at lower temperatures.

#### DISCUSSIONS

In the case of the ionic crystals the discoloration could be produced by ultraviolet light or X-rays. But in the case of quartz, which at ordinary temperatures cannot be considered ionic to the same extent as potassium chloride, a more penetrating radiation is required to produce an

F-band. This is shown by the work of Choong (1945). That the intensity of coloration is greater in the case of fused quartz may mean that in this case there may be a slight stoichiometric excess of one of the elements, or an impurity present may also induce the formation of F-centres. This can be decided by the study of the other coloured varieties of quartz. In amethyst quartz studied here, it is found from a chemical analysis that iron is found in the ferric form. It was also found that the coloration of quartz takes place when the crystal is exposed to ultraviolet radiation coming from the flourite window of hydrogen discharge lamp.

Mott and Gurney (1940) have shown that from the theoretical point of view, a broadening  $h\Delta\nu = \sqrt{h\nu_0 kT}$  is to be expected *i.e.* the breadth of the band at half maximum is proportional to the square root of the absolute temperature. This relation has been found to be valid approximately in the case of amethyst quartz. Table I leads to a similar conclusion.

It is known from the crystal structure of quartz (Mekeenan, 1923) that a silicon atom is surrounded by four oxygen atoms and each oxygen atom by two silicon atoms. But oxygen atom instead of having electrons for binding, actually lacks two electrons from a complete *p*-shell. These holes may be treated like positively charged electrons. Hence we say that the silicon oxygen bond occurs between a directed valence electron of silicon and a directed hole of oxygen. We should expect these bonds to be polar, because holes behave like positive charges. Hence photo-electric emission in the case of quartz can be considered to be similar to that in alkali halide crystal.

One is inclined to believe that the arrangement of the half values of the absorption co-efficient on the short wavelength side for different temperatures at the same wavelength (4900 Å) as well as the fact that the band maxima shift towards longer wavelength are sufficient indication that the coloration arises from a number of identical absorption centres which have the same absorption peaks (Seitz, 1946).

*Excitation.* The salient features of excitation are the broadening of the absorption band, the decrease in the value of the absorption co-efficient in the band maximum, and the shifting of the band maximum towards longer wavelengths, which phenomenon is markedly found at low temperatures. On the basis of origin of the F-band explained by Gyulai (1925) and Hilch and Pohl (1931), we shall discuss the explanation given regarding this phenomenon. Excitation, according to Gudden and Pohl (1926), is supposed to arise from ejection of electrons by absorbed light. The ejected electron moves through some distance in crystal lattice from the active centre by virtue of the energy received from the absorbed photon. The centres do not remain positively charged on this account. If they were all to become charged, their absorption spectrum would be shifted a considerable distance in the ultraviolet. That such a thing does not happen shows that the centres

become neutral by taking electrons from the surroundings. This process continues until the centre finds itself strongly influenced by the positive charges in its immediate neighbourhood and is thus capable of absorbing light of longer wavelength than was hitherto possible. This would account for the extension and increase of the absorption in the long-wavelength side of the absorption band. Seitz considered the striking differences of F' band from the F-band. One important fact is that the width of the F' band is relatively insensitive to temperature. He took into consideration the later work of Pick (1938) and of Glaser (1937) regarding the dependence of the displacement range of the photo-electrons on concentration of F centres. He then comes to the conclusion that the F'-band arises from a transition between two discrete levels because the F'-band represents a transition from a single discrete level to an ionization continuum, on account of the fact that the F-centres can be ionised with all the wavelengths lying in the F' band at all temperatures.

From the nature of the F-and F'-bands it appears that in the case of the F-band, the electrons are attached to the lattices, while in the case of the F'-band the electrons are free to move from lattice to lattice and thus behave like electrons in a conductor, This is all that can be said at present.

#### ACKNOWLEDGMENT

In conclusion the author has great pleasure in expressing his deep gratitude to Dr. J. C. Kamesvara Rav, Professor of Physics Nizam college, Hyderabad (Du) for his helpful guidance and keen interest in the investigation of this problem.

#### REFERENCES

- Bensaude, A. and Costanzo, G., 1922, *J. Phys. Chem.*, **3**, 384.  
 Choong, S. P. 1945, *Proc. Phys. Soc.*, **57**, 49.  
 Glaser, 1937, *Gottingen Nachrichten*, **3**, 11.  
 Futagami, 1938, *Proc. Phys. Math. Soc. Japan.*, **20**, 458.  
 Gudden and Pohl, 1925, *Z. f. Phys.* **34**, 249  
 „ „ 1926, *ibid.*, **37**, 881.  
 Gyulai, 1925, *ibid.*, **33**, 251.  
 Hilsch and Pohl, 1931, *ibid.*, **68**, 721.  
 Hoffman, 1931, *Z. Anorg. Chem.*, **197**, 29.  
 Holden, E. F. 1925, *Amer. Min.* **10**, 293  
 Jayaraman, 1939, *Proc. Ind. Acad. Sci.* **9**, 265.  
 Lind and Bardwell, 1923, *J. Frank Inst.*, **196**, 381.  
 Laemmlein, 1944, *C. R. Acad. Sc. U. R. S. S.*, **43**, 234  
 Mohler, N. M. 1936, *Amer. Min.*, **21**, 258.  
 Mollowoe, 1933, *Z. f. Phys.*, **85**, 56.

- Mott and Gurney 1940, *Electronic Processes in Ionic crystals* pp. 116.  
Narayan Rao D. A. A. S. 1947, *Proc. Ind. Acad. Sci.*, **25**, 488.  
Pick, 1938, *Ann d. Physik*, **31**, 365.  
Pohl R. W., 1937, *Proc. Phys. Soc.*, **49**, extra para  
„ „ 1938, *Physik. Zeit.*, **39**, 30.  
Seitz F. 1946, *Rev. Mod. Phys.*, **18**, 384.  
Smakula, 1930, *Z. f. Phys.*, **59**, 603.  
Vedeneeva, 1940, *Trans. Lab. Christ. Acad. Sc. U. S. S. R.* page 107.

## ON THE CALCULATION OF ALPHA-DECAY ENERGIES\*

BY S. JHA AND G. P. DUBE

[PHYSICS DEPARTMENT SCIENCE COLLEGE, PATNA]

(Received for publication, December 12, 1951)

**ABSTRACT.** The alpha-disintegration energy has been calculated for some isotopes near  $N=82$  and  $N=126$ , by using the Fermi-Weizsäcker formula; and its inadequacies have been discussed. As an alternative, the neutron and the proton binding energies have been used for this calculation, and this approach has been shown to be more satisfactory.  $B_N$  and  $B_p$  values in some isotopes from  $Z=59$  to  $Z=62$  have been estimated.

## INTRODUCTION

The importance of a reliable determination of the alpha-decay energies has greatly increased since the discovery of new elements, berkelium and californium (Thompson, *et. al.* 1950). One of the causes of the failure to detect these elements prior to December, 1949 was that "the methods of predicting the properties of radioactive nuclei were undeveloped. A very important contribution has been the further development of the systematics of radioactivity in the region of heavy elements" (Thompson *et. al.* 1950.)

For the understanding of the decay and disintegration properties of light elements, the exact knowledge of atomic masses has been extremely useful. It would have been fortunate if such knowledge were available in the region of the heavy and medium-heavy elements also. But, while the alpha-disintegration energies range from about 2 to 10 Mev and beta-decay energies from a few Kev to about 7 Mev ( $^{138}\text{I}$ ) amongst the heavy and medium-heavy elements, the mass spectroscopic measurements are accurate by not more than 5 in  $10^5$  and there is an error of about 100 mass-units or 10 Mev in the determination of the masses of the heavy elements. Naturally, these data are of no help in the understanding of the decay of the heavy and medium-heavy elements.

During the last decade or so, attempts have been made to set up a suitable semi-empirical mass-formula. It may be stated that in understanding the general trends of the mass-defect curve, the problems of nuclear fission, and the decay properties of the neutron-deficient and proton-deficient isotopes, the semi-empirical formula, at the hands of Feenberg (1947), and Bohr and Wheeler (1939), has been of immense help. But for the calculation of  $E_\alpha$ , even the Fermi-Weizsäcker formula, with the empirical correction term added by Stern (1949), is inadequate. Thompson, (1950) preferred to use the radioactive decay cycles, and their  $E_\alpha$  vs. mass-number curves for different elements (Perlman, *et. al.*, 1950; Meinke, *et. al.*, 1951) in their search for new isotopes and new elements.

\* Communicated by Prof. M. N. Saha, F.R.S.

Of late, an interest has arisen in the alpha activity of the rare-earth elements through the discovery of short half-life alpha emitters amongst them (Thompson *et. al.*, 1949). One would like to estimate in advance the energy and the half-life of the possible alphas.

In what follows we have shown that the semi-empirical formula, in its most accurate form given by Stern, fails to give correct  $E_\alpha$  in exactly the regions where one is most interested. In the region of the rare-earths, the empirical methods of decay cycles, and  $E_\alpha$  vs. mass-number curves are of no avail for the obvious reason that the available data are very meagre. An alternative method of calculating  $E_\alpha$ , which throws interesting light on nuclear shell structure theory, has been proposed, where one can make use of  $B_N$ ,  $B_P$ , i.e., the neutron and the proton binding energy values in the isotopes. Wherever these values are correctly known,  $E_\alpha$  can be calculated very correctly. Elsewhere, one can make reasonable guesses of these values on the basis of the nuclear shell structure theory.

#### THE SEMI-EMPIRICAL MASS-FORMULAE

Of the semi-empirical mass formulae, the one given by Bethe and Weizsäcker (1936) is of the form

$$\text{Mass defect } \Delta M(Z, A) = \alpha A - \beta \frac{(A - 2Z)^2}{A} - \gamma A^{\frac{2}{3}} - \frac{3}{5} \frac{e^2}{r_0} \frac{Z^2}{A^{\frac{1}{3}}} \quad (1)$$

where the constants are given (in Mev) by

$$\alpha = 14.01 \quad \beta = 18.90 \quad \gamma = 13.68; \quad \frac{3}{5} \frac{e^2}{r_0} = .58$$

The inadequacies of this formula are well-known and several attempts have been made to modify it. For convenience of calculation, Bohr and Wheeler recast this formula in the form :

$$M(Z, A) = A + D_A + \frac{1}{2} B_A (Z - Z_A)^2 \pm \frac{1}{2} \delta_A \quad \dots (2)$$

where  $D_A = A f_A$ , and  $f_A$  = packing fraction

They gave expressions for  $D_A$ ,  $B_A$ ,  $Z_A$  in terms of  $\alpha$ ,  $\beta$ ,  $\gamma$  and  $\delta$ , and gave tables of values of these quantities. They, however, added a new term  $\pm \frac{1}{2} \delta_A$  (the magnitude of which has to be empirically estimated) which is 0 for the isotopes with odd  $A$ , positive for  $A$  even and  $Z$  even, negative for  $A$  even and  $Z$  odd.

Thus, while Bethe and Weizsäcker deduced their formula strictly for even-even nuclei, Bohr and Wheeler held it to be true for nuclei with odd  $A$ . Kohman (1949) has used this formula for the calculation of the alpha-disintegration energies in the medium heavy nuclei. The general trend of the increase in the alpha energies with the decrease in the mass number of the parent nuclei can be explained by this formula. It fails to explain the peculiar behaviour observed in the alpha-active isotopes of bismuth, polonium, and astatine, where after a certain mass number, there is a sudden decrease



in the alpha energies followed by a slow increase in still lower mass numbers (Perlman, *et. al.*, 1950; Meinke, *et. al.*, 1951).

Saha and Saha (1946) tried to explain the general trends of energy-release in  $\beta^-$  and  $\beta^+$ -emissions, and in K-capture by the use of the Bethe-Weizsäcker formula. They found that in place of Bohr and Wheeler's  $\delta_A$ -term it were better to introduce a term  $\chi(Z, A)$  which had the properties

$$\begin{aligned} \chi(Z, A) &= 0, & \text{when } Z &= \text{even}, \quad N = \text{even} \\ &= +ve & \text{,, } Z &= \text{odd}, \quad N = \text{odd} \\ &= \text{indefinite}, & \text{,, } Z + N &= A = \text{odd}. \end{aligned}$$

This assumption explains the trend of the values of energy-release in  $\beta^+$  and  $\beta^-$ -emissions in the case of nuclei with even  $A$ , but is not so successful with nuclei for odd  $A$ . They interpret  $\chi(Z, A)$  as a spin-dependent term.

Das (1950), and Pryce (1950) have tried to utilize the Bethe-Weizsäcker formula to calculate the energy-release of  $\alpha$ -emission in heavy radioactive nuclei. Das found that, though there is numerical disagreement with experimentally determined values, the calculations show that with decrease of mass-number, there is an increase in the decay energies of the isotopes treated, as is actually found to be the case.

It may be remarked that in  $E_\alpha$  calculation, the extra term in the mass formula, added by both Bohr and Wheeler, and Saha and Saha, makes no significant contribution.

Another semi-empirical formula for the estimation of the atomic masses has been given by Fermi and Weizsäcker (Stern, 1949), which is of the form

$$M = 1.01464A + .014A^{\frac{2}{3}} + \frac{.041905}{Z_A} (Z - Z_A)^2 - .041905Z_A + \delta \quad (3)$$

$$\text{where } Z_A = \frac{A}{1.981 + .01498A^{\frac{2}{3}}}$$

$$\begin{aligned} \text{and } \delta &= 0, \text{ for } A \text{ odd} \\ &= +.036A^{-\frac{3}{4}}, \text{ for } A \text{ even}, Z \text{ odd} \\ &= -.036A^{-\frac{3}{4}}, \text{ for } A \text{ even}, Z \text{ even} \end{aligned}$$

Stern (1949) has tested the correctness of this formula in the region of heavy elements. He estimated the masses of these elements from the masses of  $\text{Pb}^{206}$ ,  $\text{Pb}^{207}$ ,  $\text{Pb}^{208}$ ,  $\text{Pb}^{209}$ , and from the radioactive decay data. It is claimed that formula (3) is adequate also for the light and medium heavy isotopes; but, for the heavy nuclei, a correction term

$$+ 0.01270 - 0.02340 \exp(-18x) \text{ has to be added to (3). Here } x = \frac{A - 208}{208}$$

and the exponential is to be applied only where  $A \geq 208$ .<sup>1</sup> With this correction term applied, the maximum discrepancy is claimed to be 1.5 Mev.

# CALCULATION OF $E_\alpha$ WITH THE FERMI-WEIZSACKER FORMULA

It should be interesting to calculate the alpha energy with a formula for which such a wide validity is claimed. Let us consider an alpha-emitter of the atomic mass  $M(Z, A)$ , and the daughter atom of mass  $M(Z-2, A-4)$ . The alpha-disintegration energy  $E_\alpha$  is given by

$$E_\alpha = M(Z, A) - M(Z-2, A-4) - M(2, 4).$$

Taking  $M(2, 4) = 4.00391$  mass units and using the equation (3), this gives

$$E_\alpha(mMU) = 54.65 + 14.4 \left[ A^{\frac{2}{3}} - (A-4)^{\frac{2}{3}} \right] + 41.905 \left[ \frac{(Z-Z_A)^2}{Z_A} - \frac{(Z-2-Z_{A-4})^2}{Z_{A-4}} \right] - 41.905 [Z_A - Z_{A-4}] \pm 36.0 \left[ (A-4)^{-\frac{3}{4}} - A^{-\frac{3}{4}} \right] + [\phi(A-4) - \phi(A)] \dots \quad (4)$$

in which the fifth term is to be retained only when  $A$  is even, and the + ve sign is to be taken for  $Z$  even and the - ve sign for  $Z$  odd; and the sixth term is to be retained only when  $A \geq 208$

where 
$$\phi(A) = 23.40 \exp\left(-18 \frac{A-208}{208}\right)$$

Taking  $1 mMU = 0.9311$  Mev, the  $E_\alpha$  in Mev is given by the relation

$$E(\text{Mev}) = 50.885 + 13.035 \left[ A^{\frac{2}{3}} - (A-4)^{\frac{2}{3}} \right] + 39.013 \left[ \frac{(Z-Z_A)^2}{Z_A} - \frac{(Z-2-Z_{A-4})^2}{Z_{A-4}} \right] - 39.018 [Z_A - Z_{A-4}] \pm 33.52 \left[ (A-4)^{-\frac{3}{4}} - A^{-\frac{3}{4}} \right] + .9311 [\phi(A-4) - \phi(A)] \dots \quad (5)$$

With the help of formula (5), we have calculated the alpha-disintegration energies in some of the isotopes of the elements  $Z=83, 84, 85$ ; and also in the isotopes containing  $N=83, 84, 85$  of elements from  $Z=60$  to  $Z=70$ . The values are given in Tables I and II; the observed values are taken from Seaborg, (1948).

TABLE I

Z		Mass number								
		210	211	212	213	214	215	216	217	218
83	Bi $E_\alpha$ cal. $E_\alpha$ obs.	4.77	6.619	8.67 6.081	7.99 5.86	6.39 5.50				
84	Po $E_\alpha$ cal. $E_\alpha$ obs.	5.3	7.43	9.29 8.77	8.6 8.33	6.72 7.68	6.76 7.36	6.97 6.77	6.25	5.44 5.99
85	At $E_\alpha$ cal. $E_\alpha$ obs.		5.94	9.86	9.21	7.61 8.78	7.36 8.00	7.50 7.79	6.86 7.02	6.43 6.72

TABLE II

Calculated values of  $E_\alpha$  in Mev for the rare-earth elements :

Z		Neutron number				
		83	84	85	86	90
60	Nd ...	-0.451	-0.638	-0.856		
61	Pm ...	0.003	0.17	0.38		
62	Sm ...	0.484	0.320	0.119		
63	Eu ...	0.890	0.660	0.560	-0.057	-0.826
64	Gd ...	1.37	1.24	1.04		
65	Tb ...	1.78	1.64	1.42		
66	Dy ...	2.21	2.10	1.9		
67	Ho ...	2.58	2.47	2.30		
68	Er ...	3.00	2.88	2.73		
69	Tm ...	3.32	3.26	3.05		
70	Yb ...	3.75	3.56	3.49		

A few points emerge from the examination of the calculated values. One will notice that in the region of the heavy elements, the agreement between the calculated and observed values is not bad ; and, also the general trend, that the alpha decay energy should increase with the decrease in the mass number of the decaying nucleus, is reproduced. In this connection it may be pointed out that the numerical agreement is brought about by the empirical correction term added by Stern : and also that the feature of the increase in  $E_\alpha$  with the decrease in the mass number is shown by the Bethe-Weizsäcker formula and the Bohr-Wheeler formula even without the  $\delta$  term. The real test of any empirical formula and the correction terms proposed lies in its ability to show the great drop in  $E_\alpha$  on the lower side of  $A$  containing less than 126 neutrons. Obviously, the correction term given by Stern cannot be applied for  $A$  less than 208 ; the formula, therefore, is not of much use, because in all the cases  $Z=83, 84, 85$ , the isotopes containing less than 128 neutrons have daughter products that have  $A$  less than 208 and the correction term cannot be applied.

In the case of the rare-earths, as Table II shows, the agreement between the observed and the calculated values is far from satisfactory, although the general trend of the increase in  $E_\alpha$  with the decrease in the mass number, is reproduced here also. The failure of the Fermi-Weizsäcker formula, in this region, unlike the region of heavy elements, is to be attributed solely to the absence of a correction term similar to the one proposed by Stern for the heavy elements. One cannot have the advantage of a correction term in this region for the simple reason that the radio-active decay data are very meagre. Bereft of a correction term like that, the semi-empirical formula is not of much use for the calculation of the alpha-energies.

The island of alpha-activity among the rare-earths is attributed to the completion of the neutron shell at  $N=82$ , and that in the immediate vicinity

of lead to the completion of the neutron shell at  $N=126$  and the proton shell at  $Z=82$ . The nucleons are relatively loosely bound immediately after the completion of the shell; and, therefore, facilitate the alpha-emission. Pryce (1950), who has studied the alpha-disintegration energies with the help of Bethe-Weizsäcker formula, which does not have a  $\delta$ -term to take account of the even-odd differences, has also tried to calculate  $(M-M)_{\text{calc}} c^2$  in terms of the looseness of the bindings of the nucleons just outside the shell and has estimated the value of the constants involved from the curve  $(E_{\text{obs}} - E_{\text{calc}})$  vs. mass number. The agreement in the region of the polonium and the astatine isotopes is very poor, and that is attributed to "crudities of the assumptions". Even that method cannot be applied to the region of the rare-earths for want of experimental data on the radioactive decay.

*Calculation of  $E_\alpha$  in terms of neutron and proton binding energies :*

We shall now use the binding energies of the last neutron, the last proton in a nucleus  $M(Z, A)$ , where  $A=Z+N$ , denoted respectively by  $B_N^\pi(Z, A)$  and  $B_P(Z, A)$  for the calculation of  $E_\alpha$ . We first explain the symbols.

Let  $M(Z, A)$  denote the mass of the atom,  ${}_ZM^A$  the mass of the bare nucleus, so that  $M(Z, A) = {}_ZM^A + Zm$ . Let  $M_N$  and  $M_P$  denote the masses of the neutron and the proton (bare), and  $m$  = mass of the electron. Then we have, according to definition.

$${}_ZM^A = {}_ZM^{A-1} + M_N - B_N(Z, A) \quad \dots (4.1)$$

or, using atomic masses, we have,

$$\begin{aligned} M(Z, A) &= M(Z, A-1) + M_N - B_N(Z, A) \\ B_N(Z, A) &= M(Z, A-1) + M_N - M(Z, A) \end{aligned} \quad \dots (4.2)$$

$$\text{or, } B_P(Z, A) \text{ is given by } {}_ZM^A = {}_ZM^{A-1} + M_P - B_P(Z, A) \quad \dots (4.3)$$

using atomic masses,

$$\begin{aligned} M(Z, A) &= M(Z-1, A-1) + M_H - B_P(Z, A) \\ \text{or, } B_P(Z, A) &= M(Z-1, A-1) + M_H - M(Z, A) \end{aligned} \quad \dots (4.4)$$

Now it has been shown (Saha and Saha, 1946) that

$E^-$  = total energy release in the emission of  $\beta^-$  particle by the nucleus  $M(Z, A)$  is given by

$$E^- = M(Z, A) - M(Z+1, A)$$

and  $E^+$  = total energy-release in a  $\beta^+$  emission by  $M(Z, A)$  is given by

$$E^+ = M(Z, A) - M(Z-1, A) - 2m$$

$E^K$  = total energy release in a  $K$ -capture by  $M(Z, A) = M(Z, A) - M(Z-1, A)$ .

From (4.2) and, (4.4) we easily calculate that for a nucleus  $M(Z, A)$

$$\begin{aligned} E^- &= M_N - M_H + B_P(Z+1, A) - B_N(Z, A) \\ &= .766 + B_P(Z+1, A) - B_N(Z, A) \end{aligned} \quad \dots (4.5)$$

$$\begin{aligned} E^+ &= M_N + M_P - m + B_N(Z-1, A) - B_P(Z, A) \\ &= -1.788 + B_N(Z-1, A) - B_P(Z, A) \end{aligned} \quad \dots (4.6)$$

$$\begin{aligned} E^K &= M(Z, A) - M(Z-1, A) \\ &= -M_N + M_H + B_N(Z-1, A) - B_P(Z, A) \\ &= -.766 + B_N(Z-1, A) - B_P(Z, A) \end{aligned} \quad \dots (4.7)$$

Relations (4.5) and (4.6) were deduced by one of us in his doctorate

dissertation. (Jha, 1950).

Then for  $E_\alpha$  from an atom  $M(Z, A)$ , we have the following expressions (Jha, 1950).

$$\left. \begin{aligned} E_\alpha &= D_\alpha - [B_N(Z, A) + B_N(Z, A-1) + B_P(Z, A-2) + B_P(Z-1, A-2)] \\ &= D_\alpha - [B_N(Z, A) + B_P(Z, A-1) + B_P(Z-1, A-1) + B_N(Z-2, A-1)] \\ &= D_\alpha - [B_N(Z, A) + B_P(Z, A-1) + B_N(Z-1, A-1) + B_P(Z-1, A-2)] \\ &= D_\alpha - [B_P(Z, A) + B_P(Z-1, A) + B_N(Z-2, A) + B_N(Z-2, A-1)] \\ &= D_\alpha - [B_P(Z, A) + B_N(Z-1, A) + B_P(Z-1, A-1) + B_N(Z-2, A-1)] \\ &= D_\alpha - [B_P(Z, A) + B_N(Z-1, A) + B_N(Z-1, A-1) + B_P(Z-1, A-2)] \end{aligned} \right\} \dots (4.8)$$

where,  $D_\alpha$  = the binding energy of the alpha-particle.

We have given the above six expressions for  $E_\alpha$ , because there are six ways of choosing two protons and two neutrons from the top shells in a nucleus; this has to be so, particularly because, due to the even-odd differences, the  $B_N$  and  $B_P$ -values in the different nuclei are different.

In Table III are given the  $B_N(Z, A)$  values obtained by Kinsey *et al*, (1950, 1951), and by Harvey *et al*, (1951). The figures of Kinsey are given within parenthesis.

TABLE III  
 $B_N(Z, A)$  values

$N \backslash Z$	81	82	83	84	85
123	6.54 (6.57)	6.49 (6.49)			
124	7.48 (7.48)	8.15 (8.15)			
125	6.23 (6.21)	6.74 (6.68)		6.71 (6.71)	
126	6.97 (6.88)	7.38 (7.37)	7.44 (7.45)	7.77 (7.77)	
127	3.86 (3.87)	3.87 (4.35)	4.17 (4.17)	4.56 (4.5)	
128	5.08 (5.7)	5.20 (4.81)	5.09 (5.12)	6.01 (6.0)	
129	3.00 (3.2)	3.75 (3.79)	4.41 (4.31)	4.32 (4.81)	
130		5.31 (5.13)	5.31 (5.72)	5.87 (5.48)	5.89
131		3.36 (4.04)	4.08 (3.63)	4.57 (4.11)	4.7

Note.—Harvey has obtained  $B_N$ -values from the measured  $Q$ -values in  $(d, p)$ ,  $(d, t)$ , and  $(\gamma, n)$ -reactions. Kinsey has obtained  $B_N$ -values from the measurements of  $\gamma$ -energies in the  $(n, \gamma)$  reaction in Pb and Bi and then with the help of  $\alpha$  and  $\beta$ -decay data, has been able to calculate the  $B_N$  and  $B_P$  in Ti, Po and At.

As one scans Table III, it is seen that immediately after the 126-neutron shell is completed (marked by dotted horizontal line), there is a sudden drop in  $B_N$  ( $Z, A$ )-values. If we take  $B_N$  ( $Z, A$ ) values under the same  $Z$ , we find that  $B_N$  ( $Z, A$ )-values for even  $N$ -values are larger than for  $N$  odd.

The  $B_P$  ( $Z, A$ )-values, estimated by Kinsey (Private communication to Prof. Feather) are given in Table IV.

TABLE IV  
 $B_P$  ( $Z, A$ ) values.

$Z \backslash N$	122	123	124	125	126	127	128	129	130	131
80										
81				7.04						
82			7.13	7.58	8.09	8.57	7.6	8.38		
83				4.2	4.28	4.09	4.4	4.9	5.5	5.1
84					4.57	4.9	5.86	6.28	6.0	6.48
85										

Note:—It is found that after the proton shell with 82 protons has been completed (marked by the horizontal line), there is a sudden drop in the  $B_P$ -values. Also it is found that the  $B_P(Z, A)$  values are greater for even  $Z$ -values than for odd ones.

The values of  $E_\alpha$ , as calculated from the formula (4.9) and as observed, are given in Table V. The agreement is as good as can be desired.

TABLE V

Parent nucleus	Po <sup>215</sup>	Po <sup>214</sup>	Po <sup>213</sup>	Po <sup>212</sup>	Po <sup>211</sup>	Po <sup>210</sup>
$E$ cal.	7.41	7.65	8.4	8.85	7.22	5.1
$E$ obs.	7.36	7.68	8.33	8.77	7.43	5.4
Parent nucleus	Bi <sup>214</sup>	Bi <sup>213</sup>	Bi <sup>212</sup>	Bi <sup>211</sup>	Bi <sup>210</sup>	Bi <sup>209</sup>
$E$ cal.	5.57	6.19	6.02	6.05	4.8	2.74
$E$ obs.	5.5	5.86	6.08	6.6	4.77	

$B_N$  and  $B_P$ -Values in rare-earth elements :

The neutron binding energies for some of the isotopes in the region of the rare-earths, measured in some recent experiments, are given in Table VI.

TABLE VI

57 La <sup>139</sup>	7.5	— 8 Mev	Hamermesh (1950)
59 Pr <sup>141</sup>	9.4	„	Hanson, <i>et al</i> (1949)
60 Nd <sup>140</sup>	7.4	„	„
62 Sm <sup>150</sup>	6.6	„	Kubitschek, <i>et al</i> (1949)

In order to be able to calculate  $E_\alpha$  in this region, one needs to know the  $B_N$  and  $B_P$  values for other isotopes also. But the experimental data are not available; therefore, they have to be estimated.  $B_P$  values can be found out from  $(\gamma, p)$ ,  $(d, n)$  and other reactions; but no attempt seems to have been made to determine them in this region. In the following an attempt has been made to calculate or guess, on the basis of the meagre data, the  $B_N$  and  $B_P$  values with the help of the formula (4.5, 4.6, and 4.7).

$\text{Nd}^{141}$  decays by K-capture (about 97%) emitting  $\gamma$ -rays of energy 1.05 Mev (Kurbatov; 1942; Wilkinson, 1949).  $B_N$  in  $\text{Pr}^{141}$  being 9.4 Mev,  $B_P$  in  $\text{Nd}^{141}$  is equal to 7.6 Mev (Eqn. 7). Since one would expect the proton-binding energy to increase with the increase in the number of neutrons in the isotopes of the same element, also, because the neutron binding energy in the completed neutron shell at  $N=82$  is 9.4 Mev, one can assume with reasonable confidence that  $B_P$  in the heavier isotopes of Nd would lie between 7.6 and 9.4 Mev., thus lending support to Feenberg's suggestion (Feenberg, 1919), based on the non-existence of stable isotopes with  $Z=61$  or  $N=61$ , that there is a completed  $4d$  sub-shell at  $Z=60$ . One can roughly assume  $B_P$  in  $\text{Nd}^{142}$ ,  $\text{Nd}^{144}$  to be 8 Mev. This is in agreement with the estimates of Elsassner (1934), referred to by Mayer (1948). From this one can calculate  $B_N$  in  $\text{Pr}^{142}$  ( $N=82+1$ ), which decays by  $\beta^-$ -emission,  $E_{\text{max}}$  of  $\beta$ -being 2.5 Mev.  $B_N$  in  $\text{Pr}^{142}$  comes out to be 4.5 Mev, which is very satisfactory. From the experimental value of  $B_N$  in  $\text{Nd}^{150}=7.4$  Mev, one can infer that the lower mass-number even isotopes of Nd will have  $B_N > 7.4$  Mev. There is no knowing if  $\text{Nd}^{142}$ ,  $\text{Nd}^{144}$  will have  $B_N$  as high as 9.4 Mev; that is because it is difficult to guess how the binding energy of the 82nd neutron will change with the change in the proton number. The neutron shell at  $N=82$  occurs in stable isotopes only between  $Z=56$  and  $Z=62$ ; and one would suppose that the binding energy of the 82nd neutron will increase from  $Z=56$ , and, after reaching a maximum, would diminish as one approaches  $Z=62$ . If that view be correct, one can take  $B_N$  in  $\text{Nd}^{142}$ ,  $\text{Nd}^{144}$  roughly equal to 8 Mev. On a similar consideration, one can take  $B_N$  of the 83rd and the 85th neutrons in  $\text{Nd}^{148}$ ,  $\text{Nd}^{150}$  equal to 6 and 5 Mev respectively.

Again,  $B_N$  in  $\text{Nd}^{150}=7.4$  Mev leads to  $B_P$  in  $\text{Pm}^{150} < 7.15$  Mev or equal to 6.6 Mev, depending on whether we take  $\text{Nd}^{150}$  to be  $\beta^-$ -stable or the emitter of the 11 Kev  $\beta^-$ 's (Jha, 1950; Ballou, 1948). The lower isotopes of Pm should be expected to have smaller  $B_P$  values i.e.,  $B_P$  in  $\text{Pm}^{142}$ ,  $\text{Pm}^{143}$ ,  $\text{Pm}^{144}$ ,  $\text{Pm}^{145} \approx 5$  Mev, and  $B_P$  in  $\text{Pm}^{146}$ ,  $\text{Pm}^{147}$ ,  $\text{Pm}^{148}$ ,  $\text{Pm}^{149} \approx 6$  Mev. The most stable isotope of Pm is the one for which the isotopic number  $I=N-Z=23$  or 25.  $\text{Pm}^{147}$  is a  $\beta^-$ -emitter, the half-life being 3.7 years; therefore  $\text{Pm}^{148}$  should be the most stable isotope, and one may assign a value of 8 Mev to  $B_N$  in  $\text{Pm}^{148}$  and  $\text{Pm}^{149}$  (this is perhaps an overestimate) and a value of 5 Mev to  $B_N$  in  $\text{Pm}^{146}$ ,  $\text{Pm}^{147}$ .

In the case of the samarium isotopes,  $B_N$  in  $\text{Sm}^{180}$  is 6.6 Mev. The neutron binding energy of the lower even mass isotopes will be for the above-mentioned reasons, larger. One can, therefore, assume  $B_N$  in  $\text{Sm}^{144}$  to be 8 Mev,  $B_N$  in  $\text{Sm}^{145} \approx 6$  Mev and in  $\text{Sm}^{146}$ ,  $\text{Sm}^{147}$ ,  $\text{Sm}^{148}$ , 7 Mev. Considering the  $\beta^-$ -stability of  $\text{Sm}^{144}$ , one can take its  $B_P$  to be 5 Mev, and  $B_P$  in  $\text{Sm}^{145}$ ,  $\text{Sm}^{146}$ ,  $\text{Sm}^{147}$  (i.e., the isotopes with a larger neutron number) 6 Mev. These  $B_N$  and  $B_P$  values are given in Table VII.

TABLE VII

mass	$^{59}\text{Pr}$		$^{60}\text{Nd}$		$^{61}\text{Pm}$		$^{62}\text{Sm}$	
	$B_P$	$B_N$	$B_P$	$B_N$	$B_P$	$B_N$	$B_P$	$B_N$
141		9.4*	7.6†					
142		5	8	8	5			
143		6	6	6	5	8		
144			8	8	5	5	5	8
145			5	5	5	8	6	6
146					6	5	6	7
147					6		6	7
148					6			7
149					6			6
150				7.4*	6.6-7.15†			6.6*

\*Observed values ; † calculated values ; the rest are guesses.

#### CALCULATION OF $E_\alpha$ IN RARE-EARTHS WITH $B_N$ AND $B_P$

The well-known 1.1 cm-range samarium alphas have now been finally assigned to  $\text{Sm}^{147}$  (Weaver, 1950, Rasmussen, *et al.*, 1950). There are reasons to believe that  $\text{Sm}^{146}$  is a short half-life alpha emitter (Rasmussen, *et al.*, 1950). There are evidences to show that the emitter of the 2 cm-range alphas found in the pleochroic haloes in mica and in the zinc residues of brass in  $\text{Pm}^{145}$ , the daughter product of the 11 Kev  $\beta^-$ -active  $\text{Nd}^{145}$  (Jha, 1950). Besides these,  $\text{Ho}^{151}$ ,  $\text{Dy}^{150}$ ,  $\text{Tb}^{149}$ ,  $\text{Gd}^{148}$ ,  $\text{Gd}^{149}$ ,  $\text{Eu}^{147}$  are alpha emitters (Thompson, *et al.*, 1949, Rasmussen, *et al.*, 1950; Hoff *et al.*, 1950).

With the help of the  $B_N$  and  $B_P$  values given in Table VII, one can estimate the energy of the emitted alphas from formula (4.8). As stated above, there are six ways in which two protons and two neutrons can group together to form an alpha particle; and in the case of the



disintegration  $\text{Sm}^{147} \rightarrow \text{Nd}^{143}$ , the mean energy required to free them can be seen to be 24.8 Mev., giving the energy of the emitted alphas =  $(28.2 \text{ Mev} - 24.8 \text{ Mev}) = 3.4 \text{ Mev}$ , the observed energy being 2.1 Mev, corresponding to the range in air equal to 1.1 cm. Similarly in the case of the disintegration  $\text{Sm}^{146} \rightarrow \text{Nd}^{142}$ , the mean energy of the emitted alphas, calculated as above, is 4.2 Mev, which is consistent with the non-occurrence of  $\text{Sm}^{146}$  in nature. Again, in the case of  $\text{Pm}^{145} \rightarrow \text{Pr}^{141}$ , the mean  $E_\alpha$  calculated = 2.9 Mev, the energy in Mev of alphas of range about 2 cm in air is  $\approx 3 \text{ Mev}$ .

The six other cases of the alpha emitting isotopes  $\text{Ho}^{151}$ ,  $\text{Dy}^{150}$ ,  $\text{Tb}^{149}$ ,  $\text{Gd}^{148}$ ,  $\text{Gd}^{149}$ , and  $\text{Eu}^{147}$  can be considered only qualitatively. In Ho, the stable isotope has mass number 165, whereas, the alpha-emitter has the mass number only 151, i.e. it is neutron-deficient by 14 neutrons;  $\text{Dy}^{150}$  is neutron-deficient by 12 to 14 neutrons;  $\text{Tb}^{149}$  is neutron-deficient by 10 neutrons;  $\text{Gd}^{148, 149}$  by 8 to 12 neutrons and  $\text{Eu}^{147}$  by 4. There are only two clues in making a guess of the neutron and proton binding energies in these isotopes, i.e. first, all these isotopes have only two neutrons more than 82 neutrons; secondly, these isotopes being proton-rich, the proton-binding energy would be very low, and the neutron binding energy high. But because the neutron number is approaching 82, the  $B_N$  vs.  $Z$  curve, which perhaps has a maximum at  $Z=58$ , is likely to flatten out at about  $Z=65$ ; in other words, the neutron binding energy does not perhaps increase in the same proportion in which the proton binding energy diminishes. One is not likely to be far from right if one takes  $B_N$  of the 83rd and the 84th neutron in this region to be  $\approx 10 \text{ Mev}$ ; and  $B_P$  of the last two protons  $\approx 2 \text{ Mev}$ . In that case, the calculated  $E_\alpha$  will be of the order  $28.2 - 2(10 + 2) \text{ Mev}$  i.e. 4 Mev. The observed alpha energy ranges from 4.2 to 3.1 Mev in  $\text{Gd}^{148}$ ,  $\text{Tb}^{149}$ ,  $\text{Dy}^{150}$ , and  $\text{Ho}^{151}$ , 3.0 Mev in  $\text{Gd}^{149}$  and 2.88 Mev in  $\text{Eu}^{147}$ .

#### DISCUSSION

It should thus be abundantly clear that, so far as alpha-decay properties are concerned, the semi-empirical mass formula cannot be regarded as a reliable guide even in the region of the heavy elements, far less so in the region of the rare-earths. A far more helpful way of looking at the problem is through the neutron and proton binding energies. If one knew the  $B_N$  and  $B_P$  values in all the isotopes, that would obviate altogether, at least for the radioactive decay studies, the need of the accurate knowledge of the atomic masses. Unfortunately, very few  $B_N$  and  $B_P$  values are experimentally known. Now that large-flux slow-neutron sources, betatrons producing constant energy electrons, and mono-energetic beams of deuterons and tritons are available, it should be possible to measure the  $B_N$  and  $B_P$  in most isotopes. The only other way of attacking this problem seems to be through the empirical determination of  $Z_A$ ,  $B_A$  and  $\delta_A$  in the Bohr-Wheeler formulae, as has been

attempted by Madame Curie (1946) ; for that method to be successful, very precise and extensive knowledge of  $E_{max}$  and the decay schemes, in the beta-decay of the isotopes is necessary. In the situation as it exists to-day, this knowledge is far from satisfactory. It must be admitted that even for  $B_N$  and  $B_P$  values, as must be clear from the above, the precise beta-decay data are necessary. Our method of calculating  $E_\alpha$  is important and superior to other methods for a different reason also. The study of alpha-systematics has brought out one point very clearly which is that, contrary to what is assumed in the Gamow derivation of the Geiger-Nuttall law, the alpha particles do not exist as separate entities in the nuclei, the probability of their emission is governed not only by their probability to leak through the potential barrier, but that there is a finite probability of the assembly of alpha-particles inside the nuclei ; and this probability is smaller for the odd-odd, odd-even and even-odd nuclei than for the even-even nuclei (Perlman, *et al*, 1950, Feather, 1951). The method of calculating  $E_\alpha$  with  $B_N$  and  $B_P$ , as described above, postulates a mechanism of the assembly of alpha particles out of the four constituent neutrons and protons. Basing on this mechanism, it has been possible to explain qualitatively, the degree of forbiddenness of alpha emission in the four classes of the nucle, (Jha, 1951),

#### ACKNOWLEDGMENTS

In conclusion, our thanks are due to Dr A. K. Saha of the Institute of Nuclear Physics, Calcutta, for many helpful discussions. We express our indebtedness to Prof. M. N. Saha, F. R. S. for his interest in this work and the great encouragement he gave us. One of us (S. J.) expresses his gratefulness to Prof. N. Feather, F. R. S. of Edinburgh, who introduced him to the problems of radioactivity amongst the rare-earths.

#### REFERENCES

- Ballou, 1948, *Phys. Rev.*, **73**, 630.  
 Bethe and Bacher, 1936, *Rev. Mod. Phys.*, **8**, 82.  
 Bohr and Wheeler, 1939, *Phys. Rev.*, **86**, 426.  
 Das, 1950, *Ind. J. Phys.*, **24**, 523.  
 Elsassner, 1934, *Jde. Phys. et Rad.*, **8**, 625.  
 Feather, 1951, *Phil. Mag.*, **42**, 568.  
 Feenberg, 1947, *Rev. Mod. Phys.*, **19**, 239.  
 Feenberg, *et al*, 1949, *Phys. Rev.*, **78**, 1877.  
 Hammermesh, 1950, *Phys. Rev.*, **80**, 415.  
 " " " " " " **81**, 412, **82**, 67.  
 Hanson, *et al.*, 1949, *Phys. Rev.*, **76**, 578,  
 Harvey, 1951, *Phys. Rev.*, **81**, 353.  
 Hoff, *et al*, 1951, *Phys. Rev.*, **83**, 1058.  
 Jha, 1950, Thesis, Edinburgh University,  
 Jha, 1951, In course of publication.  
 Kinsey, 1950, *Phys. Rev.*, **78**, 77.  
 Kinsey, 1951, *Phys. Rev.*, **82**, 388.

- Kohman, 1949, *Phys. Rev.*, **76**, 448.
- Kubitshek and Dankoff, 1949, *Phys. Rev.*, **70**, 531.
- Kurbatov, 1942, *Phys. Rev.*, **61**, 106
- Mayer, 1948, *Phys. Rev.*, **74**, 235
- Madame Curie-Joliot, 1945, *J. de Phys et Rad*, (8) **6**, 209.
- Meinke. *et al.*, 1951, *Phys Rev.*, **81**, 782,
- Perlman, *et al.*, 1950, *Phys Rev*, **77**, 26.
- Precy, 1950, *Pro. Phys Soc*, **A**, **63**, 692.
- Rasmussen, *et al.*, 1950, *Phys. Rev.*, **80**, 475,
- Saha and Saha, 1946, *Trans, Nat. Inst. of Sci Ind*, **2**, 193
- Seaborg, *et al.*, 1948, *Rev. Mod Phys.*, **20**, 585.
- Stern, 1949, *Rev. Mod. Phys.*, **21**, 376.
- Thompson, *et al.*, 1949, *Phys. Rev.*, **76**, 1406
- Thompson, *et al*, 1950, *Phys. Rev.*, **80**, 781, 790
- Way, 1949, *Phys. Rev.*, **76**, 1449
- Weaver, 1950, *Phys. Rev.*, **80**, 301.
- Wilkinson, 1930, *Phys. Rev.*, **76**, 1687

## ON THE ORIGIN OF THE THIRD IONOSPHERIC ECHO\*

BY R. B. BANERJI

[INSTITUTE OF RADIO PHYSICS AND ELECTRONICS, UNIVERSITY OF CALCUTTA]

*(Received for publication, November 29, 1951)*

**ABSTRACT.** There is still some difference of opinion regarding the ray, ordinary or extraordinary, to which the so-called third or Z-component of the ionospheric echoes correspond. It is pointed out in the paper that there need be no controversy on the subject because, as first clearly shown by Bhar, the branch of the dispersion curve which passes through the "point" of reflection of the Z-component is really an ordinary branch. Calculations are further carried out to determine the retardation that the extraordinary ray would suffer, if it were able to partially penetrate its first point of reflection, in its passage into regions of higher electronic densities. It is found that the retardation on reaching the asymptote of the dispersion curve would become infinite, so that, the extraordinary ray, under no circumstances, is able to penetrate the barrier. One is thus forced to the alternative that it is the ordinary ray which provides the Z-component in the ionospheric echo pattern.

## INTRODUCTION

In the usual C. R. tube displays of ionospheric echoes, split echoes are of common occurrence. Generally, two split echoes are observed due to the breaking up of the incident ray into two component rays—ordinary and extraordinary—by the anisotropy introduced by the earth's magnetic field. According to the ray theory (based on the Appleton-Hartree magneto-ionic theory) these echoes are due to reflections of the extraordinary ray at the level where the electron concentration is that represented at  $\delta E_1$  (figure 1) and of the ordinary ray the same as at  $O$ . The conditions of reflection at these points are  $\frac{Ne^2}{\pi m} = f^2 - ff_H$  and  $\frac{Ne^2}{\pi m} = f^2$  respectively, where  $N$  is the number density of the electrons,  $f$  the sounding frequency and  $e$  and  $m$  have their usual significance. Occasionally, however, three split echoes are observed. The third, the so-called Z component, is assumed to be due to the reflection of a ray which has partially penetrated its usual reflection level (at  $E_1$  or  $O$ ) and has suffered reflection from the level of electron concentration as at the point  $E_2$ . The reflection condition at this point is given by  $\frac{Ne^2}{\pi m} = f^2 + ff_H$ .

On rare occasions echoes are obtained which cannot be identified with any of the three echoes described above. This echo is sometimes described as an extraordinary echo due to a fourth reflection condition (Pant and Bajpai, 1936-7) corresponding to the level where the electron concentration

\* Communicated by Prof S. K. Mitra, D. Sc., F. N. I.

is as represented at  $D$ . The reflection condition is given by

$$\frac{Ne^2}{\pi m} = f^2 \frac{f^2 - f_H^2}{f^2 - f_L^2}.$$

Now, regarding the  $Z$ -component there is some controversy as to which of the two rays—ordinary or extraordinary—this component corresponds. For example, while according to Seaton (1948), the  $Z$ -component corresponds to the extraordinary ray, according to Scott (1950) and others, it belongs to the ordinary ray. But there need be no confusion if it be remembered that the so-called third point of reflection ( $E_2$ ) really belongs to the ordinary ray. Considering figure 1 it will be noticed that the portion  $FE_2$  of the

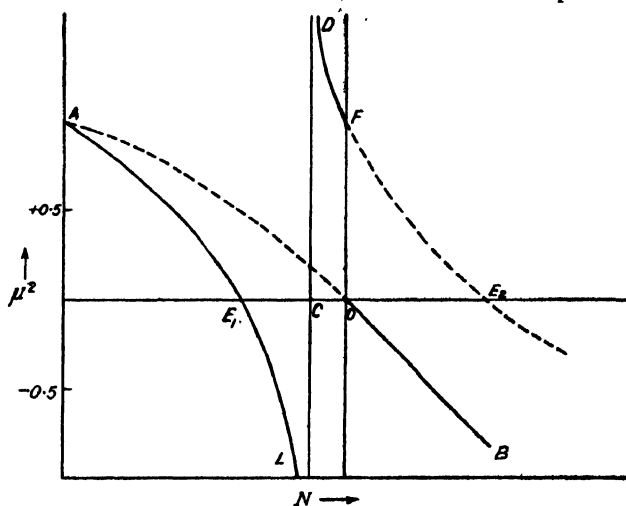


FIG. 1

dispersion curve which meets the  $N$ -axis at the point  $L_2$  is continuous with the portion  $DF$ . It has, however, been pointed out by Bhai (1936-7) that while the portion  $DF$  belongs to the extraordinary branch, the portion  $FE_2$  really belongs to the ordinary branch. In fact, it has been shown that the ordinary branch  $AO$  gives a discontinuous jump at  $O$  and proceeds along  $FE_2$  instead of along  $OB$  while the latter is really a portion of the extraordinary branch.

It is the purpose of the present work to provide further evidence in corroboration of the above. By actually calculating the retardation suffered by the extraordinary ray before it reaches the third point of reflection, it is found that the ray suffers infinite retardation at the asymptote long before it can reach the point  $E_2$ .

Incidentally, the fact that the extraordinary ray suffers infinite retardation in reaching the asymptote shows that the fourth reflection condition  $\frac{Ne^2}{\pi m} = f^2 \frac{f^2 - f_H^2}{f^2 - f_L^2}$  is inoperative. It is, however, occasionally reported that evidence of a "fourth" echo has been obtained (Martyn and Munroe, 1938; Pant and Bajpai, 1936-7). This can only be explained as due to some ionospheric conditions in which, on account of increased

collision frequency, the infinities in dispersion curve are substantially reduced.

The calculations of retardation that are to follow are all based on the ray theory. This is not strictly justified, because, according to the ray theory, there is no room for partial reflection and penetration. However, it is found that the results of retardation according to the ray theory differ only by a few per cent from those calculated from the wave theory (Poeyerlein, 1951). It is to be noted that a parabolic gradient of ionisation has been assumed. But results obtained in respect of infinite retardation do not depend to any marked extent on the shape of the rising ionisation gradient.

#### GROUP RETARDATION IN A PARABOLIC LAYER

In carrying out the calculation for retardation for any ray beyond the point of reflection, one has to use the portion of the dispersion curve below the  $N$  axis. The expression for  $\mu$  for this portion of the curve, however, is purely imaginary and as such has no physical significance. It is also simply understood from the ray theory that for such cases the ray cannot penetrate beyond the reflection point and the portion of the curve below the  $N$  axis loses its meaning. However, if effect of collision is taken into account, the refractive index becomes, complex. The real part of this complex expression is everywhere positive and the numerical value of  $\mu$ , as obtained from this positive part, is not greatly different from the modulus of  $\mu$  in the collision-free case. Hence, the branch  $E_1 D$  of the dispersion curve (figure 2) may be considered as the mirror image of the part below the  $N$  axis in figure 1. The correctness of this qualitative approach is corroborated by Booker (1935) and also by the similarity with the dispersion curves (Ghosh, 1938; Taylor, 1933) calculated by taking collision into account. The analysis that is to follow is based on the first order correctness of figure 2. In all other respects the propagation properties are assumed to be the same as that given by or derived from the Appleton-Hartree formula for the collision-free case.

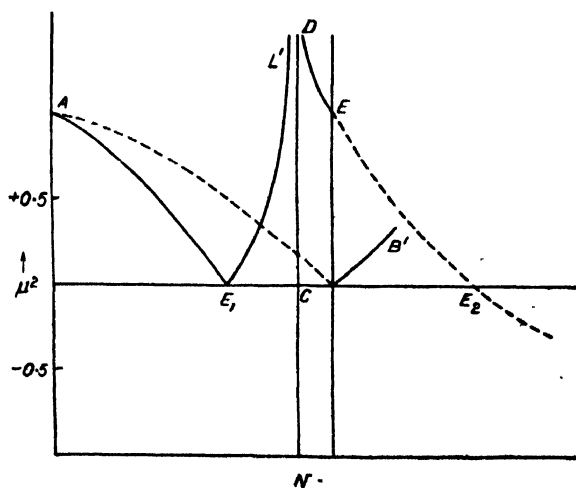


FIG. 2

For the group velocity  $U$ , we use the expression deduced by Rai (1937):

$$\begin{aligned}
 \frac{c}{U} = & \frac{\left\{ \left( \frac{f^2}{f_0^2} - 1 - \frac{f_T^2}{2f_0^2} \pm \sqrt{\left( \frac{f}{f_0} - \frac{f_0}{f} \right) \left( \frac{f_T^4}{f_0^4} + \frac{f_T^2}{4f_0^2} \right)} \right) \left( \frac{f}{f_0} - \frac{f_0}{f} \right) - \frac{f_T^2}{2f_0^2} \pm \sqrt{\left( \frac{f}{f_0} - \frac{f_0}{f} \right) \left( \frac{f_T^4}{f_0^4} + \frac{f_T^2}{4f_0^2} \right)} \right\}^{1/2}}{\left\{ \left( \frac{f}{f_0} - \frac{f_0}{f} \right)^2 - \frac{f_T^2}{2f_0^2} \pm \sqrt{\left( \frac{f}{f_0} - \frac{f_0}{f} \right) \left( \frac{f_T^4}{f_0^4} + \frac{f_T^2}{4f_0^2} \right)} \right\}^{1/2}} \\
 & \left( \frac{f}{f_0} - \frac{f_0}{f} \right)^2 + \frac{f_T^2}{2f_0^2} \mp \frac{f_0^2}{8f_0^2} \sqrt{\left( \frac{f}{f_0} - \frac{f_0}{f} \right) \left( \frac{f_T^4}{f_0^4} + \frac{f_T^2}{4f_0^2} \right)} \\
 + & \frac{\left[ \frac{f^2}{f_0^2} - 1 - \frac{f_T^2}{2f_0^2} \pm \sqrt{\left( \frac{f}{f_0} - \frac{f_0}{f} \right) \left( \frac{f_T^4}{f_0^4} + \frac{f_T^2}{4f_0^2} \right)} \right]^{1/2}}{\left\{ \left( \frac{f}{f_0} - \frac{f_0}{f} \right)^2 - \frac{f_T^2}{2f_0^2} \pm \sqrt{\left( \frac{f}{f_0} - \frac{f_0}{f} \right) \left( \frac{f_T^4}{f_0^4} + \frac{f_T^2}{4f_0^2} \right)} \right\}^{1/2}} \\
 & \left( \frac{f}{f_0} - \frac{f_0}{f} \right)^2 \left( 1 + \frac{f_0^2}{f^2} \right) \frac{f_L^2}{f_0^2} \\
 \pm & \frac{2 \sqrt{\left( \frac{f}{f_0} - \frac{f_0}{f} \right) \left( \frac{f_T^4}{f_0^4} + \frac{f_T^2}{4f_0^2} \right)} \left( \frac{f^2}{f_0^2} - 1 - \frac{f_T^2}{4f_0^2} \pm \sqrt{\left( \frac{f}{f_0} - \frac{f_0}{f} \right) \left( \frac{f_T^4}{f_0^4} + \frac{f_T^2}{4f_0^2} \right)} \right)^{3/2}}{\left\{ \left( \frac{f}{f_0} - \frac{f_0}{f} \right)^2 - \frac{f_T^2}{2f_0^2} \pm \sqrt{\left( \frac{f}{f_0} - \frac{f_0}{f} \right) \left( \frac{f_T^4}{f_0^4} + \frac{f_T^2}{4f_0^2} \right)} \right\}^{3/2}}
 \end{aligned}$$

in which

$f \equiv$  the sounding frequency

$f_0 \equiv$  the penetration frequency of the ordinary ray

$f_T = f_H \sin \theta$

$f_L = f_H \cos \theta$

where  $f_H$  is the gyro-frequency, and  $\theta$  is the angle of inclination of the direction of propagation to the magnetic field.

For convenience we can re-write the above as

$$\begin{aligned}
 \frac{c}{U} = & \frac{\left( 1 - \frac{f_0^2}{f^2} - \frac{f_T^2}{2f^2} \pm \sqrt{\left( 1 - \frac{f_0^2}{f^2} \right) \left( \frac{f_T^4}{f^4} + \frac{f_T^2}{4f^2} \right)} \right) \left( 1 - \frac{f_0^2}{f^2} \right) - \frac{f_T^2}{2f^2} \pm \sqrt{\left( 1 - \frac{f_0^2}{f^2} \right) \left( \frac{f_T^4}{f^4} + \frac{f_T^2}{4f^2} \right)} \right\}^{1/2}}{\left( 1 - \frac{f_0^2}{f^2} - \frac{f_T^2}{2f^2} \pm \sqrt{\left( 1 - \frac{f_0^2}{f^2} \right) \left( \frac{f_T^4}{f^4} + \frac{f_T^2}{4f^2} \right)} \right)^{1/2}} \\
 & \left( 1 - \frac{f_0^2}{f^2} \right)^2 + \frac{f_T^2}{2f^2} \mp \frac{f_0^2}{8f^2} \sqrt{\left( 1 - \frac{f_0^2}{f^2} \right) \left( \frac{f_T^4}{f^4} + \frac{f_T^2}{4f^2} \right)}
 \end{aligned}$$

$$\begin{aligned}
& + \frac{f_0^2}{f^2} \cdot \frac{\left(1 - \frac{f_0^2}{f^2}\right) + \frac{1}{2} \cdot \frac{f_T^2}{f^2} \mp \sqrt{\left(1 - \frac{f_0^2}{f^2}\right)^2 \frac{f_L^2}{f^2} + \frac{f_T^4}{4f^4}}}{\left(1 - \frac{f_0^2}{f^2} - \frac{f_T^2}{2f^2} \pm \sqrt{\left(1 - \frac{f_0^2}{f^2}\right)^2 \frac{f_L^2}{f^2} + \frac{f_T^4}{4f^4}}\right)^{3/2} \left\{\left(1 - \frac{f_0^2}{f^2}\right)^2 - \frac{f_T^2}{2f^2} \pm \sqrt{\left(1 - \frac{f_0^2}{f^2}\right)^2 \frac{f_L^2}{f^2} + \frac{f_T^4}{4f^4}}\right\}^{1/2}} \\
& \pm \frac{f_0^2}{f^2} \cdot \frac{\left(1 - \frac{f_0^2}{f^2}\right)^2 \left(1 + \frac{f_0^2}{f^2}\right)}{2 \sqrt{\left(1 - \frac{f_0^2}{f^2}\right)^2 \frac{f_L^2}{f^2} + \frac{f_T^4}{4f^4}} \left(1 - \frac{f_0^2}{f^2} - \frac{f_T^2}{2f^2} \pm \sqrt{\left(1 - \frac{f_0^2}{f^2}\right)^2 \frac{f_L^2}{f^2} + \frac{f_T^4}{4f^4}}\right)^{3/2} \left\{\left(1 - \frac{f_0^2}{f^2}\right)^2 - \frac{f_T^2}{2f^2} \pm \sqrt{\left(1 - \frac{f_0^2}{f^2}\right)^2 \frac{f_L^2}{f^2} + \frac{f_T^4}{4f^4}}\right\}^{1/2}}
\end{aligned}$$

Now in a parabolic layer of semi-thickness  $y_m$ , the ionic density can be represented by

$$f_0^2 = f_c^2 \left(2 \frac{y}{y_m} - \frac{y^2}{y_m^2}\right)$$

or, putting

$$\xi = 1 - \frac{y}{y_m}$$

$$f_0^2 = f_c^2 (1 - \xi^2).$$

so that, representing  $c/U$ , the retardation per unit path as a function of  $y$  or, of  $\xi$  we have, putting

$$\frac{f_c^2}{f^2} = \theta_c; \quad \frac{f_T^2}{f^2} = \theta_T; \quad \frac{f_L^2}{f^2} = \theta_L$$

$$\begin{aligned}
& \left\{ 1 - \theta_c (1 - \xi^2) - \frac{\theta_T}{2} \pm \sqrt{\{1 - \theta_c (1 - \xi^2)\}^2 \theta_L + \frac{\theta_T^2}{4}} \right\} \left\{ \{1 - \theta_c (1 - \xi^2)\}^2 - \frac{\theta_T}{2} \pm \sqrt{\{1 - \theta_c (1 - \xi^2)\}^2 \theta_L + \frac{\theta_T^2}{4}} \right\} \\
& \frac{c}{U} = \frac{\left\{ 1 - \theta_c (1 - \xi^2) - \frac{\theta_T}{2} \pm \sqrt{\{1 - \theta_c (1 - \xi^2)\}^2 \theta_L + \frac{\theta_T^2}{4}} \right\}^{3/2} \left[ \{1 - \theta_c (1 - \xi^2)\}^2 \theta_L + \frac{\theta_T^2}{4} \right]^{1/2}}{2}
\end{aligned}$$



$$\begin{aligned}
 & + \frac{\theta_c(I - \xi^2)\{I - \theta_c(I - \xi^2)\}^2 + \theta_c(I - \xi^2) \pm \theta_c(I - \xi^2)^2 \sqrt{\{I - \theta_c(I - \xi^2)\}^2 \theta_L + \frac{\theta_T^2}{4}}}{\left\{I - \theta_c(I - \xi^2) - \frac{\theta_T}{2} \pm \sqrt{\{I - \theta_c(I - \xi^2)\}^2 \theta_L + \frac{\theta_T^2}{4}}\right\}^{3/2} \left[\{I - \theta_c(I - \xi^2)\}^2 - \frac{\theta_T}{2} \pm \sqrt{\{I - \theta_c(I - \xi^2)\}^2 \theta_L + \frac{\theta_T^2}{4}}\right]^{1/2}} \\
 & \pm \frac{\theta_c(I - \xi^2)\{I - \theta_c(I - \xi^2)\}^2 \{I + \theta_c(I - \xi^2)\} \theta_L}{2 \left\{I - \theta_c(I - \xi^2) - \frac{\theta_T}{2} \pm \sqrt{\{I - \theta_c(I - \xi^2)\}^2 \theta_L + \frac{\theta_T^2}{4}}\right\}^{3/2} \left[\{I - \theta_c(I - \xi^2)\}^2 - \frac{\theta_T}{2} \pm \sqrt{\{I - \theta_c(I - \xi^2)\}^2 \theta_L + \frac{\theta_T^2}{4}}\right]^{1/2}} \\
 & + \frac{\theta_T^2}{4} \}^{1/2}
 \end{aligned}$$

If we now put  $I - \theta_c(I - \xi^2) = \zeta$ , the above equation reduces to

$$\begin{aligned}
 \frac{c}{U} &= \frac{\left[\zeta - \frac{\theta_T}{2} \pm \sqrt{\zeta^2 \theta_L + \frac{\theta_T^2}{4}}\right] \left[\zeta - \frac{\theta_T}{2} \pm \sqrt{\zeta^2 \theta_L + \frac{\theta_T^2}{4}}\right]}{\left[\zeta - \frac{\theta_T}{2} \pm \sqrt{\zeta^2 \theta_L + \frac{\theta_T^2}{4}}\right]^{3/2} \left[\zeta - \frac{\theta_T}{2} \pm \sqrt{\zeta^2 \theta_L + \frac{\theta_T^2}{4}}\right]^{1/2} + \frac{\theta_T^2}{4} \left[\zeta - \frac{\theta_T}{2} \pm \sqrt{\zeta^2 \theta_L + \frac{\theta_T^2}{4}}\right]^{2/2}} \\
 & \pm \frac{\theta_L(I - \zeta)(\zeta - \zeta)^2}{2 \sqrt{\zeta^2 \theta_L + \frac{\theta_T^2}{4}} \left[\zeta - \frac{\theta_T}{2} \pm \sqrt{\zeta^2 \theta_L + \frac{\theta_T^2}{4}}\right]^{3/2} \left[\zeta - \frac{\theta_T}{2} \pm \sqrt{\zeta^2 \theta_L + \frac{\theta_T^2}{4}}\right]^{1/2}}
 \end{aligned}$$

Reflection occurs from points where the group-velocity vanishes, i.e. retardation becomes infinite. The above expression becomes infinite for the extraordinary wave when (with the lower signs) :

$$(a) \quad \zeta - \frac{\theta_T}{2} - \sqrt{\zeta^2 \theta_L + \frac{\theta_T^2}{4}} = 0$$

$$\text{or} \quad \zeta = \frac{\theta_T}{1 - \theta_L} \text{ i.e. } f_0^2 = f^2 \frac{f^2 - f_H^2}{f^2 - f_L^2}$$

$$(b) \quad \zeta^2 - \frac{\theta_T}{2} - \sqrt{\zeta^2 \theta_L + \frac{\theta_T^2}{4}} = 0$$

$$\text{or} \quad \zeta = \pm \sqrt{\theta_H} \text{ where } \theta_H = \theta_T + \theta_L$$

$$\text{i.e.} \quad (bi) \quad f_0^2 = f^2 - ff_H \text{ and } (bii) \quad f_0^2 = f^2 + ff_H$$

We have to integrate the above expression over  $y$  from  $y=0$  to values of  $\zeta$  given by the above expressions.

Now, from our previous work (Banerji, 1951)

$$f^2 + ff_H > f^2 \frac{f^2 - f_H^2}{f^2 - f_L^2} > f^2 - ff_H$$

When  $y=0$ ,  $\zeta=1$  giving us the starting point of integration. We have to carry out the integration from  $\zeta=1$  to  $\zeta=\sqrt{\theta_H}$  for first reflection and from  $\zeta=1$  to  $\zeta=-\sqrt{\theta_H}$  for second reflection. We will first concentrate upon the first part.

$$\text{Since} \quad dy = -y_m d\zeta$$

$$\text{and} \quad d\zeta = -2\theta_c \xi d\xi$$

$$\text{i.e.} \quad d\xi = -\frac{d\zeta}{2\theta_c \sqrt{1 - \frac{1-\zeta}{\theta_c}}} = -\frac{d\zeta}{2\theta_c^{1/2} \sqrt{\theta_c - 1 + \zeta}}$$

we have

$$\begin{aligned} \int_0^y \frac{c}{U} dy &= -\frac{y_m}{2\theta_c^{1/2}} \int_1^\zeta \frac{\left[ \zeta^2 - \frac{\theta_T}{2} - \sqrt{\zeta^2 \theta_L + \frac{\theta_T^2}{4}} \right]^{1/2}}{\left[ \zeta - \frac{\theta_T}{2} - \sqrt{\zeta^2 \theta_L + \frac{\theta_T^2}{4}} \right]^{1/2}} \frac{d\zeta}{\sqrt{\zeta - (1 - \theta_c)}} \\ &= -\frac{y_m}{2\theta_c^{1/2}} \int_1^\zeta \frac{\left\{ (1-\zeta)\zeta^2 + (1-\zeta_c)\frac{\theta_T}{2} + (1-\zeta)^2 \sqrt{\zeta^2 \theta_L + \frac{\theta_T^2}{4}} \right\}^{1/2}}{\left[ \zeta - \frac{\theta_T}{2} - \sqrt{\zeta^2 \theta_L + \frac{\theta_T^2}{4}} \right]^{3/2} \left[ \zeta^2 - \frac{\theta_T}{2} - \sqrt{\zeta^2 \theta_L + \frac{\theta_T^2}{4}} \right]^{1/2}} \\ &\quad \times \frac{d\zeta}{\sqrt{\zeta - (1 - \theta_c)}} \end{aligned}$$

$$+ \frac{\gamma_m}{4\theta_e^{1/2}} \int_1^{\zeta} \frac{\theta_L(1-\zeta)(2-\zeta)\zeta^2}{\left[\zeta - \frac{\theta_T}{2} - \sqrt{\zeta^2\theta_L + \frac{\theta_T^2}{4}}\right]^{3/2} \left[\zeta^2 - \frac{\theta_T}{2} - \sqrt{\zeta^2\theta_L + \frac{\theta_T^2}{4}}\right]^{1/2} \sqrt{\zeta^2\theta_L + \frac{\theta_T^2}{4}}} \times \frac{d\zeta}{\sqrt{\zeta - (1-\theta_e)}}$$

For the first reflection we integrate from 1 to  $\sqrt{\theta_H}$ . In this range, the only discontinuity occurs when  $\zeta = \sqrt{\theta_H}$ . But, at this point the integral has the same order of infinity as  $\frac{1}{\sqrt{\zeta^2 - \theta_H}}$  and hence the integral converges and the retardation is finite. This, however, does not hold if  $\sqrt{\theta_H} = 1 - \theta_e$ , when the integral, due to two vanishing terms of order in the  $\frac{1}{2}$  denominator, diverges. This is clearly in accordance with the shape of the  $P'-f$  curve observed.

Integrating for the second reflection we note that the part of the expression under the radical changes sign beyond the point  $\zeta = \sqrt{\theta_H}$  and this continues till  $\zeta = -\frac{\theta_T}{1-\theta_L}$  when the expression having exponent  $3/2$  changes sign again,

the condition continuing till  $\zeta = -\sqrt{\theta_H}$ . The remarks made below are with this reservation that these changes of sign are to be avoided by considering the mirror images of the parts below the  $N$  axis as mentioned above.

In this range of integration it is to be noted that a discontinuity occurs at the point  $\zeta = -\frac{\theta_T}{1-\theta_L}$  in addition to that at the end point  $\zeta = -\sqrt{\theta_H}$ . At the

former discontinuity the expression is of same order of infinity as

$1/\left(\zeta - \frac{\theta_T}{1-\theta_L}\right)^{3/2}$ , and hence diverges, giving infinite retardation. This

happens at all frequencies, i.e. irrespective of the value of  $\theta_e$ . The  $P'-f$  curve, however, indicates that the  $Z$ -component is not retarded any further than the other two traces, retardation setting in only near the penetration frequency, i.e. when  $1 - \theta_e = -\sqrt{\theta_H}$  as above. This absence of retardation definitely indicates that the mode of propagation of the  $Z$ -component is not extraordinary.

From the above it seems reasonable to conclude that, as far as the ray theory holds valid, the ordinary, rather than the extraordinary ray would give rise to the  $Z$ -component.

#### CONCLUDING REMARKS

The above analysis shows that the possibility of the extraordinary ray being reflected from the third level (point  $E_3$ , figure 1) after partial reflection

at the first reflection level (point  $E_1$ , figure 1) is completely ruled out. The only other possibility, therefore, is that the ordinary ray is responsible for the production of the  $Z$ -component. This latter possibility is corroborated by the recent polarisation measurements (Hogarth, 1951) which shew that the sense of rotation of the  $Z$ -component is the same as that of the ordinary ray. Regarding the manner in which the  $Z$ -splitting occurs, Eckersely (1950) suggests that at the stage of transition from one mode of propagation to the other there is a "coupling" between the ordinary and the extraordinary rays near the point of reflection of the ordinary ray. A part of the energy of the ordinary ray thereby follows the path of the extraordinary ray and goes up to the third point of reflection. Scott (1950), however, favours the view that the  $Z$ -component is due to rays which are inclined slightly to the vertical and which, thus, following a longitudinal path, penetrate into the region of third reflection and are scattered back obliquely. This hypothesis presupposes the presence of scattering irregularities in the ionosphere. Rivault's (1950) observations corroborate this supposition. According to him the incidence of the  $Z$ -component generally coincides with the presence of a large amount of scattering in the ionosphere.

Both the above points of view consider the  $Z$ -component possible only at high latitudes. The observation of triple splitting at Allahabad (Toshniwall, 1950) and at Calcutta (Banerji, 1951, appears to be in direct contradiction to this. However, it is to be pointed out that, if the angle of scattering is large, then the explanation, as suggested by Scott, may be operative. It may be recalled in this connection that scattering being of frequent occurrence in the tropical latitudes, the occasional incidence of large angles is understood.

It is, however, more natural to consider the  $Z$ -component as reflection of the ordinary ray, which has partially penetrated the point  $O$  from  $E_2$  (figure 1). Because, as mentioned in the introduction, the portion of the curve  $FE_2$  is really a portion of the ordinary branch of the dispersion curve, as has been pointed out by Bhar (1936-7). It may be pointed out that Pöeverlein (1949) has recently mentioned the possibility of the ordinary ray going over to the branch  $EF_2$  at the point  $O$  though only for a certain oblique angle of incidence.

#### ACKNOWLEDGMENTS

The author's grateful thanks are due to Prof. S. K. Mitra, D. Sc., for his encouragement and helpful guidance. Thanks are also due to the Government of India for providing him with a research training scholarship which enabled him carry out the work.

REFERENCES

- Banerji, R. B., 1951, *Proceedings of the 38th Indian Science Congress*  
 Bhar, J. N., 1936-7, *Sci. and Cult.*, **2**, 322.  
 Booker, H. G., 1935, *Proc. Roy. Soc.*, **150**, 267.  
 Eckerseley, T. L., 1950, *Proc. Phys. Soc.*, **163B**, 49.  
 Ghosh, S. P., 1938, *Ind. Jour. Phys.*, **12**, 341.  
 Hogarth, J. E., 1951, *Nature*, **167**, 943.  
 Martyn, D. F. and Munroe, G. H., 1938, *Nature*, **141**, 159.  
 Pant, B. D. and Bajpai, R. R., 1936-7, *Sci. and Cult.*, **2**, 409.  
 Poeverlein, H., 1949, *Zeits. fur Angew. Phys.*, **1**, 517.  
 Poeverlein, H., 1951, *Zeits. fur Angew. Phys.*, **3**, 135.  
 Rai, R. N., 1937, *Proc. Nat. Ints. Sci.*, **3**, 307.  
 Rivault, E., 1950, *Proc. Phys. Soc.*, **163B**, 120.  
 Scott, J. C. W., 1950, *Jour. Geophys. Res.*, **55**, 65.  
 Scaton, S. L., 1948, *Proc. I. R. E.*, **35**, 450.  
 Taylor, M., 1933, *Proc. Phys. Soc.*, **160**, 257.  
 Toshniwall, G. R., 1935, *Nature*, **138**, 471.

# ON HIGHER BORN APPROXIMATIONS IN POTENTIAL SCATTERING OF FAST ELECTRONS BY ATOMIC NUCLEI IN A STATIC FIELD

By S. N. BISWAS

DEPARTMENT OF THEORETICAL PHYSICS,  
INDIAN ASSOCIATION FOR THE CULTIVATION OF SCIENCE, CALCUTTA.

(Received for publication, December 17, 1951)

**ABSTRACT.** Some of the conclusions on higher Born approximation following the works of Sauter, Sexl and Distel as presented in the literature are incorrect. Mott, using the Dirac's second-order relativistic equation and taking the exact solution, has obtained a second-order correction term, which is different from the result of Urban. Urban's result is the same as that of Sexl. Both results are incorrect as they are not consistent expansions in powers of  $\alpha Z$ , where  $\alpha$  and  $Z$  are the fine-structure constant and the atomic number respectively. Using the matrix-formalism Dalitz has recently obtained a 2nd order term in the scattering cross section for the Dirac particle, pointing out the errors in the development of the former writers. In this paper, the second-order approximation in the elastic scattering of fast electrons by atom has been carried out using the hypercomplex notation. The first approximation has been checked by this method by Sauter. The method used here, is based on a consistent expansion in powers of  $\alpha Z$ . The series actually obtained for the cross section is given by,

$$(1 - \beta^2 \sin^2 \theta/2) + \pi \alpha Z \beta \sin^2 \theta/2 \left( \frac{2}{3} - 2 \sin^2 \theta/2 \right) + \dots$$

multiplied by the Rutherford scattering formula.

## INTRODUCTION

The method of higher Born approximation in the discussion of the scattering problems consists in the calculation of the series-expansion of the scattering-amplitudes in powers of the interaction potential. The Born approximation has been developed in a variety of forms and has been applied to different types of problems. But the calculations have not been carried out correctly beyond the first approximation. Sauter (1933b), using the time-dependent perturbation method has obtained the second-order correction which contains an error in the development (Dalitz 1951). Urban, (1943) following him proceeded to calculate the third approximation, but was unable to calculate all the terms of the series and his method is wrong. The method of Sommerfeld and Mao (1935) gives an unsurmountable difficulty in finding out the higher-order terms. Dalitz (1951) has found the second-order correction term, using the matrix-formalism of Dyson and Feynman. Sauter, (1933a) using the hypercomplex notation has correctly formulated the first Born approximation. In this paper, this formalism has been extended to calculate the second-order correction term in the scattering of fast Dirac

electron by the potential,  $V(r) = Ze \cdot e^{-r/a} / r$ , which is of some interest as a representation of the screened atomic field.

The wave function  $\Psi$  of a particle in a static field  $V(r)$  is expanded in a series  $\Psi = \psi_0 + \psi_1 + \psi_2 + \dots$ ; where  $\psi_0$  represents the incident wave undisturbed by the field, and  $\psi_1, \psi_2, \dots$  consist only of outgoing waves at infinity. The latter functions are to be found from a recurrence formula.

In this paper, actually the function  $\psi_2$  has been calculated. It is seen that the evaluation of  $\psi_2$  depends on the evaluation of the integrals (see Eq (9))  $L_1, L_2, L_3, L_4$  of which  $L_1 \rightarrow \infty$  in the limit  $a \rightarrow \infty$ . Others are finite. It can be easily observed from the wellknown formula of the current density, that the contribution to the scattering cross section is only due to the imaginary part of the integral,  $L_1$ . Thus the difficulty in handling with  $L_1$  due to its infinite-character has been avoided.

#### THE SCATTERING OF A DIRAC PARTICLE

The relativistic Dirac's equation may be written as

$$\left[ \sum_{\nu=1}^3 \gamma_{\nu} \frac{\partial}{\partial x_{\nu}} - \gamma_4 \frac{E - V}{\hbar c} + \frac{mc}{\hbar} \right] \Psi = 0 \quad (1)$$

where  $V$  is the general potential function and  $\gamma_K = i\beta\alpha_K$ ;  $\gamma_4 = \beta$  and  $\hbar = \frac{h}{2\pi}$

Now let  $\Psi$  be expanded as  $\Psi = \psi_0 + \psi_1 + \psi_2 + \dots$  (2)

where  $\psi_0 = a e^{\frac{2\pi i}{\hbar}(\vec{r} \cdot \vec{p})}$ , the incident undisturbed wave, ... (3)

and  $\psi_1, \psi_2, \dots$  are outgoing waves at infinity. Putting the value of  $\Psi$  from (2) in (1) and collecting the terms of the same order one gets the recurrence relation,

$$\left( \sum_{\nu} \gamma_{\nu} \frac{\partial}{\partial x_{\nu}} - \gamma_4 \frac{E}{\hbar c} + \frac{mc}{\hbar} \right) \psi_n = -\gamma_4 \frac{V}{\hbar c} \psi_{n-1} \quad (4)$$

Operating the equation (4) from the left by

$$\left( \sum_{\nu} \gamma_{\nu} \frac{\partial}{\partial x_{\nu}} - \gamma_4 \frac{E}{\hbar c} - \frac{mc}{\hbar} \right)$$

one gets,

$$\left[ \Delta + \frac{r^2}{\hbar^2} \right] \psi_n = - \left( \sum_{\nu} \gamma_{\nu} \frac{\partial}{\partial x_{\nu}} - \gamma_4 \frac{E}{\hbar c} - \frac{mc}{\hbar} \right) \gamma_4 \frac{V}{\hbar c} \psi_{n-1} \quad (4n)$$

where  $\Delta$  is the Laplacian operator.

The solution of this is given by

$$\psi_n(\vec{R}) = \frac{1}{4\pi\hbar c} \int \frac{e^{i\frac{2\pi p}{\hbar}(\vec{R}-\vec{r})}}{|\vec{R}-\vec{r}|} \cdot \left\{ \sum_{\nu} \gamma_{\nu} \frac{\partial}{\partial x_{\nu}} - \gamma_4 \frac{E}{\hbar c} - \frac{mc}{\hbar} \right\} \gamma_4 V(r) \cdot \psi_{n-1}(r) d\tau_r \dots (5)$$

where  $\vec{R}$  stands for the vector  $OP$  and  $\vec{r}$  for  $OP'$ . The point  $P$  has the coordi-

nate  $(X_1, X_2, X_3)$  and  $P'$  has  $(x_1, x_2, x_3)$ .  $OP$  is along the direction of observation, and  $P'$  the integration point (figure 1).  $O$  is the position of the

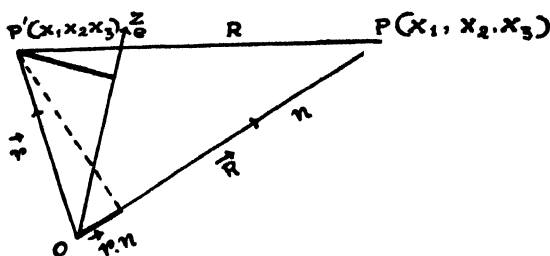


FIG. 1

scatterer. The distance between  $P$  and  $P'$  is denoted by  $R$ .

With regard to the source and sink point, one can write,  $\frac{\partial}{\partial x_v} f(\vec{R} - \vec{r}) =$

$-\frac{\partial}{\partial X_v} f(\vec{R} - \vec{r})$ , and with the help of this, the equation (5) may be written as

$$\psi_n(\vec{R}) = \frac{1}{4\pi\hbar c} \left\{ \sum_v \gamma_v \frac{\partial}{\partial X_v} - \gamma_4 \frac{E}{\hbar c} - \frac{mc}{\hbar} \right\} \int \frac{e^{i \frac{2\pi\nu}{\hbar} (\vec{R} - \vec{r})}}{|\vec{R} - \vec{r}|} \cdot V(\gamma) \psi_{n-1}(r) dr_r \quad \dots (6)$$

We have from (figure 1),  $|\vec{R} - \vec{r}| = R - \vec{r} \cdot \vec{n}$  where  $\vec{n}$  is the unit vector in the direction of observation, and replace  $|\vec{R} - \vec{r}|$  by  $R$  since  $R$  is very large.

Sauter (1933) has calculated the value of  $\psi_1$  and he has found,  $\psi_1 \rightarrow$

$$\frac{1}{4\pi\hbar^2 c^2} \cdot \frac{e^{2\pi i p/h}}{R} \left\{ -2E + icp(n - e, \vec{\gamma}) \cdot \gamma_4 \right\} a \cdot \int V \cdot e^{2\pi i p/h} (e - n_1 \vec{\gamma}) d\tau_r \quad \dots (7)$$

where  $e$  is the unit vector along the direction of the incident wave.

Noting that the amplitude  $a$  of equation (3) satisfies the following equation,

$$\left\{ icp(e \cdot \vec{\gamma}) - \gamma_4 E + mc^2 \right\} a = 0$$

we can turn the above equation (6) in the form (7). Now let us calculate  $\psi_2$  from the recurrence relation (6). Thus

$$\psi_2(\vec{R}) = \frac{1}{4\pi\hbar c} \left\{ \sum_v \gamma_v \frac{\partial}{\partial X_v} - \gamma_4 \frac{E}{\hbar c} - \frac{mc}{\hbar} \right\} \gamma_4 \cdot \int \frac{e^{2\pi i p/h} (\vec{R} - \vec{r})}}{|\vec{R} - \vec{r}|} \cdot V(r) \cdot \psi_1(r) dr_r$$

Substituting the value of  $\psi_1(r)$  from equation (7) we have

$$\psi_2(\vec{R}) = \frac{1}{\hbar^4 \pi c} \left\{ \sum_v \gamma_v \frac{\partial}{\partial X_v} - \gamma_4 \frac{E}{\hbar c} - \frac{mc}{\hbar} \right\} \cdot \frac{1}{4\pi\hbar^2 c^2} \int \frac{e^{2\pi i p/h} (\vec{R} - \vec{r})}}{|\vec{R} - \vec{r}|} \cdot V(r) \left[ \frac{e^{2\pi i p/h}}{r} \left\{ -2E + icp(n_1 - e, \vec{\gamma}) \cdot \gamma_4 \right\} a \int V(r') e^{2\pi i p/h} (e - n_1 \vec{r}') d\tau_r' \right] dr_r$$



where,  $e$ ,  $n$ , and  $n_1$  are the unit vectors in the direction of the vector  $\vec{r}$  (the direction of which has been taken as the  $Z$ -axis), in the direction of the vector  $\vec{R}$  (the direction of observation) and, in the direction of the vector  $\vec{r}$  (a variable vector), respectively (vide figure 2). The angles  $\theta$ ,  $\theta'$  and  $\omega$  are

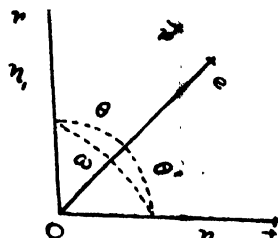


FIG. 2

respectively. the angles between the vectors  $(e, n_1)$ ,  $(e, n)$  and  $(n, n_1)$ , also we replace  $\cos \omega$  by  $\cos \theta \cos \theta' + \sin \theta \sin \theta' \cos \phi$  where  $\phi$  is the angle between the planes containing  $(e, n)$  and  $(e, n_1)$  vectors.

We set further the following abbreviations :

$$k = p/\hbar ;$$

$$V(r) = \frac{ZeE'}{r} \cdot e^{-r/a} ; \text{ and } b = 1 + \frac{1}{2a^2k^2}$$

Using the above abbreviations, we proceed to calculate  $\psi_2$ . Thus performing the  $r'$ -integration in the square bracket of the last expression, and changing the vector  $(n_1 - e)$  into its polar forms, we can write,

$$\psi_2(\vec{R}) = \left( \frac{1}{4\pi\hbar^2c^2} \right)^2 \frac{4\pi ZeE'}{R} \cdot e^{2\pi i p/\hbar R} \left( icp(n, \vec{\gamma}) - \gamma_1 E - mc^2 \right) \gamma_1 \left\{ L_1 + icp(L_2 + L_3 - L_4) \right\}$$

where,

$$\begin{aligned} L_1 &= \int \frac{e}{r} e^{ik(1-\cos \omega)r} V(r) \frac{1}{4k^2 \sin^2 \theta/2 + 1/a^2} (-2E) a \cdot d\tau_r \\ L_2 &= \int \frac{e}{r} e^{ik(1-\cos \omega)r} V(r) \frac{\sin \theta \cos \phi}{4k^2 \sin^2 \theta/2 + 1/a^2} \cdot \gamma_1 \gamma_4 \cdot a \cdot d\tau_r \\ L_3 &= \int \frac{e}{r} e^{ik(1-\cos \omega)r} V(r) \frac{\sin \theta \cdot \sin \phi}{4k^2 \sin^2 \theta/2 + 1/a^2} \gamma_2 \gamma_4 \cdot a \cdot d\tau_r \\ L_4 &= \int \frac{e}{r} e^{ik(1-\cos \omega)r} V(r) \frac{(1 - \cos \theta)}{4k^2 \sin^2 \theta/2 + 1/a^2} \cdot \gamma_3 \gamma_4 \cdot a \cdot d\tau_r \end{aligned} \quad \dots (9)$$

Now if by  $J$  we denote the number of particles scattered through unit solid angle per unit time, then  $J$  is given by a well known formula,

$$J = ic \{ \Psi^* \gamma_4(n, \vec{\gamma}) \Psi \} \\ = ic \{ \psi_1^* \gamma_1(n, \vec{\gamma}) \psi_1 \} + ic [ \{ (\psi_1^* \gamma_1(n, \vec{\gamma}) \cdot \psi_2) - \text{its conjugate complex} \} ] \text{ which is upto second-order terms.} \quad \dots (10)$$

$$J = J_1 + J_2 = J_1 + J_2^{(1)} + J_2^{(2)}$$

Now

$$J_2^{(1)} = ic \left\{ \psi_1^* \gamma_1(n, \vec{\gamma}) \psi_2 \right\} \\ = ic \frac{1}{4\pi\hbar^2 c^2} \cdot \frac{e^{-2\pi i p \cdot h \cdot R}}{R} \cdot a^* \left\{ -2E + icp(n - e, \vec{\gamma}) \gamma_4 \right\} \cdot \frac{4\pi Z e E'}{2k^2(b - \cos \theta')} \cdot \gamma_1(n, \vec{\gamma}) \\ \cdot \left( \frac{1}{4\pi\hbar^2 c^2} \right)^2 \cdot \frac{4\pi Z e E'}{R} \cdot e^{2\pi i p \cdot h \cdot R} \left( icp(n, \vec{\gamma}) - \gamma_1 E - mc^2 \right) \gamma_1 \cdot \left[ L_1 + icp(L_2 + L_3 - L_4) \right] \\ = ic \cdot \frac{1}{(4\pi\hbar^2 c^2)^3} \cdot \frac{(4\pi Z e E')^2}{R^2 \cdot 2k^2} \cdot \frac{1}{(b - \cos \theta')} \cdot a^* \left\{ -2E + icp(n - e, \vec{\gamma}) \cdot \gamma_1 \right\} \cdot \gamma_4(n, \vec{\gamma}) \\ \times \left( icp(n, \vec{\gamma}) - \gamma_1 E - mc^2 \right) \cdot \gamma_4 \left\{ L_1 + icp(L_2 + L_3 - L_4) \right\} \dots (11)$$

The differential cross section, after averaging over the initial electron states and the summing over the final states, is obtained from the expression

$$\frac{1}{2} \text{spur} \left[ \frac{ic}{(4\pi\hbar^2 c^2)^2} \cdot \frac{(4\pi Z e E')^2}{R^2 \cdot 2k^2} \cdot \frac{1}{(b - \cos \theta')} \cdot a^* \left\{ -2E + icp(n - e, \vec{\gamma}) \gamma_4 \right\} \gamma_1(n, \vec{\gamma}) \right. \\ \left. \cdot \left( icp(n, \vec{\gamma}) - \gamma_1 E - mc^2 \right) \cdot \gamma_1 \left\{ L_1 + icp(L_2 + L_3 - L_4) \right\} \right],$$

where the values of the integrals  $L_1$ ,  $L_2$ ,  $L_3$ , and  $L_4$  are evaluated in the appendix. It is easy to see that the contribution to the scattering cross section is due to the integral term  $L_1$ . Hence in calculating the spur value, of the above expression due to the term  $L_1$  we need only consider the following,

$$\frac{1}{2} \text{spur} \cdot a^* a \left\{ -2E + icp(n - e, \vec{\gamma}) \gamma_4 \right\} \gamma_4(n, \vec{\gamma}) \left\{ icp(n, \vec{\gamma}) - \gamma_1 E - mc^2 \right\} (-\gamma_3) \cdot \frac{|E| + H_0}{2E}$$

where  $H_0 = (\alpha p_0) + \beta \cdot mc$ ,  $\vec{p}_0$  is the momentum vector in the initial direction, which gives,

$$J_0 \cdot E \cdot c^2 p^2 \quad \dots (12)$$

where  $J_0^* \rightarrow v(\vec{a} \cdot \gamma_4 a)$

Now, utilising the values obtained in equations (11) and (12) the resultant cross section becomes the following (in this  $\theta'$  has been changed to  $\theta$  as usual :

$$J_2 = 2 \left( \frac{1}{4\pi\hbar^2 c^2} \right)^2 \cdot \frac{1}{R^2} \cdot \frac{(4\pi Z e E')^2}{2k^2 (b - \frac{1}{\cos \theta})} \cdot J_0 \cdot \frac{E'}{c^2} \cdot \frac{1}{1 - \cos \theta} \cdot \frac{2\pi^2}{2k^3}$$

Changing  $E'$  by  $-e$  for electron, and when  $b \rightarrow 1$  for the bare nucleus

$$J_2 = \frac{J_0}{R^2} \left( \frac{Z e^2}{2m v^2} \right)^2 (1 - \beta^2) \left[ \pi \frac{Z e^2}{\hbar c} \cdot \beta \frac{1 - 2 \cos \theta}{1 - \cos \theta} \right]$$

where  $\beta = v/c$

The value of  $J_1$ , has been checked by this method by Sauter (1933a) and has been found to be

$$J_1 = \frac{J_0}{R^2} \left( \frac{Z e^2}{2m v^2} \right)^2 (1 - \beta^2) \operatorname{cosec}^4 \theta/2 (1 - \beta^2 \sin^2 \theta/2)$$

Thus upto the second-order correction term, we get

$$J = \frac{J_0}{R^2} \left( \frac{Z e^2}{2m v^2} \right)^2 (1 - \beta^2) \operatorname{cosec}^4 \theta/2 \left[ 1 - \beta^2 \sin^2 \theta/2 + \pi \cdot \alpha \cdot \beta \cdot \sin^2 \theta/2 \left( \frac{1 - 2 \cos \theta}{2} \right) + \dots \right]$$

where  $\alpha = Z e^2 / \hbar c$

If  $R$  stands for the ratio of the scattering to the Rutherford scattering, then upto second-order approximation,  $R$  becomes

$$R = (1 - \beta^2 \sin^2 \theta/2) - \pi Z \cdot \alpha \cdot \beta \sin^2 \theta/2 \left( \frac{3}{2} - 2 \sin^2 \theta/2 \right)$$

where  $\alpha$ , stands for the fine-structure constant.

When still higher terms are calculated, this is consistent expansion in powers of  $Z \cdot \alpha$ .

#### CONCLUSION

The correction term of order  $Z e^2$  (relative to the first order) found here is

$\pi \cdot \frac{Z e^2}{\hbar c} \cdot \beta \cdot \sin^2 \theta/2 \left( \frac{3}{2} - 2 \sin^2 \theta/2 \right)$  which is not in agreement with that obtained

by Mott (1929). His correction term is  $\pi \cdot \frac{Z e^2}{\hbar c} \sin \frac{\theta}{2} \cos \frac{\theta}{2}$ . Urban (1942) obtained

the correction terms as  $\pi \cdot \frac{Z e^2}{\hbar c} \sin \frac{\theta}{2}$  as that of Sexl's (1933). But their

results originate from errors pointed out by Dalitz (1951). Dalitz's correction

term comes out to be  $\pi \cdot \frac{Z e^2}{c \hbar} \cdot \sin \frac{\theta}{2} (1 - \sin \theta/2)$ , which is at variance form the

result obtained here. The advantage of the method used here is that it is quite elegant and lucid.

#### ACKNOWLEDGMENT

The author's sincerest thanks are due to Dr. D. Basu for suggesting this problem as a research topic and for his constant help and invaluable counsel at every stage of the investigation.

#### APPENDIX

*The evaluation of the integrals occurring in (a)*

In evaluating the integrals in equation (a), we first consider the integral  $L_1$  which after the completion of  $\tau$ -integration gives the  $\phi$ -integration in the form,

$$\int_0^{2\pi} \frac{d\phi}{a - b \cos \phi}; \quad a > b$$

in which  $a = \lambda - \cos \theta \cos \theta'$ ,  $b = \sin \theta \sin \theta'$ ;  $\lambda \rightarrow 1$ ; the  $\theta$ -integration may be effected by transforming the integral by the substitution  $b - \cos \theta = Z$  to the wellknown form

$$\int \frac{dZ}{Z \sqrt{AZ^2 + BZ + C}}$$

the values of  $A$ ,  $B$ ,  $C$  can be easily found out. Thus,

$$L_1 = \frac{2\pi}{ik} \frac{E}{k^2} \frac{1}{b - \cos \theta'} \left\{ \frac{M}{2L} - \frac{1}{1+b} \right\} + \sqrt{\left( \frac{M}{2L} - \frac{1}{1+b} \right)^2 + \frac{1}{L} - \frac{M^2}{4L^2}} \\ \left\{ \frac{M}{2L} + \frac{1}{1-b} \right\} + \sqrt{\left( \frac{M}{2L} + \frac{1}{1-b} \right)^2 + \frac{1}{L} - \frac{M^2}{4L^2}}$$

where,

$$L = b^2 - 2\lambda b \cos \theta' + (\lambda^2 + \cos^2 \theta' - 1)$$

$$M = 2b - 2\lambda \cos \theta'$$

$$\lambda = 1 - \frac{1}{iak}; \quad b = 1 + \frac{1}{2a^2 k^2}$$

For the integrals  $L_2$  and  $L_3$  we see it convenient to take help of the contour integration. Combining  $L_2$  and  $L_3$  we have for the  $\phi$ -integration,

$$\int_0^{2\pi} \frac{e^{i\phi}}{a - b \cos \phi} d\phi; \quad a > b$$

and  $a$ ,  $b$  stand for the same values as in  $L_1$  by changing  $Z = e^{i\phi}$  this reduces to

$$\frac{2}{i} \int_{\Gamma} \frac{Z dZ}{2aZ - b - bZ^2} = \frac{2}{i} \cdot 2\pi i \text{ (sum of the residues at the poles) where } \Gamma \text{ is}$$

the unit-circle. The evaluation of  $L_1$  may be performed in the like manner. In this evaluation we have neglected the variation of the quantity

$$\left\{ \frac{1}{a^2 k^2} + \frac{2}{iak} (\cos \theta \cos \theta' - 1) \right\} \text{ in } \sqrt{[(\cos \theta - \cos \theta')^2 - \left\{ \frac{1}{a^2 k^2} + \frac{2}{iak} (\cos \theta \cos \theta' - 1) \right\}]}$$

in the limit  $a \rightarrow \infty$ . Thus we have

$$\lim_{a \rightarrow \infty} L_1 = L_3 = \frac{\pi i}{3} \{ \pi i + 2 \log \tan \theta/2 \}$$

#### REFERENCES

- Dalitz R. H., *Proc. Roy. Soc.*, **A 226**, 509.  
 Distel, F., 1932, *Z. f. Phys.*, **74**, 785.  
 Mott, N. F., 1929, *Proc. Roy. Soc.*, **A 124**, 425.  
 Mott, N. F., 1932, *Proc. Roy. Soc.*, **A 135**, 429.  
 Sauter, F., 1933 a, *Z. f. Phys.*, **36**, 118.  
 Sauter F., 1933, b. *Ann. Phys. LPZ.*, **5F, 18**, 61.  
 Seel, T., 1933, *Z. f. Phys.*, **81**, 178.  
 Sommerfeld and Mao, 1935, *Ann. Phys. LPZ.*, **8**, **228**, 629.  
 Urban, P., 1942, *Z. f. Phys.*, **119**, 67.  
 Urban, P., 1943, *Ann. Phys. LPZ.*, **5F. 43**, 557.



# SPIN SPLITTING OF $^5\Sigma$ AND $^6\Sigma$ ELECTRONIC STATES

By K. SURYANARAYANA RAO

Department of Physics, Andhra University, Waltair

(Received for publication, October 27, 1951)

**ABSTRACT :** Expressions are derived for the rotational energy levels of  $^5\Sigma$  and  $^6\Sigma$  states adopting methods due to Van Vleck and Kramers.

## INTRODUCTION

While investigating the rotational structure of band systems due to the oxides of the elements of the transition groups like columbium, manganese and chromium, it has become necessary to derive the rotational energies of terms of high multiplicity like  $^5\Sigma$ ,  $^6\Sigma$ ,  $^5\Pi$ ,  $^6\Pi$  etc., as such terms are expected to be involved in the electronic transitions giving rise to these bands.

Van Vleck (1929) has given a general method for the calculation of the rotational energy levels of a  $\Sigma$  state and has dealt with a  $^2\Sigma$  state. The rotational fine structure of the  $^3\Sigma$  state has been treated by Kramers (1929) who has taken into account the interaction of the individual electron spins. The method has been extended by Budo (1937) to the calculation of the rotational energy levels of a  $^4\Sigma$  state. It may be pointed out that, as the multiplicity of the state increases the mathematical difficulties increase. The spin component levels of  $^7\Sigma$  state have been worked out by Nevin (1945) using the same method, for the confirmation of his rotational analysis of the MnH bands.

As regards  $\Pi$  states, a method has been given by Hill and Van Vleck (1928) for the general intermediate case which they applied to doublets; but  $\Pi$  states, with multiplicity higher than four, have not been treated so far.

In this investigation Van Vleck's method for  $\Sigma$  states has been used to calculate and study the rotational fine structure of  $^5\Sigma$  and  $^6\Sigma$  states which have not been dealt with so far.

## THEORY

A  $\Sigma$  state belongs to Hund's case (b) where the magnetic interaction between  $\Lambda$  and  $S$  is negligible. In a state pertaining to case (b), the energy levels will be split up, in general, into  $2S + 1$  components which is called the case (b) spin splitting. If there were no case (b) spin splitting, the rotational energy levels are given by the expression

$$F_r(K) = B_v K(K+1) + D_v K^2(K+1)^2 + H_v K^3(K+1)^3 + \dots$$

To account for the spin component levels a small additional term  $f_r(K, J-K)$  is added to the above expression, which assumes different values for the different values of  $J$ .

Considering first the effect of the molecular rotation on the spin, the energies are, according to Van Vleck, given by the eigen-values of the perturbation matrix

$$H_1(\Sigma, \Sigma \pm 1) = B [J(J+1) - (\Lambda + \Sigma)(\Lambda + \Sigma \pm 1)]^{\frac{1}{2}} [S(S+1) - \Sigma(\Sigma \pm 1)]^{\frac{1}{2}}$$

The diagonal elements of the magnetic plus rotational energy are

$$H_1(\Sigma, \Sigma) = f(\Sigma) + B[J(J+1) - (\Lambda + \Sigma)^2] + B[S(S+1) - \Sigma^2]$$

where  $f(\Sigma)$  is the ordinary so-called 'magnetic energy' of the interaction between the spin and the orbital angular momentum and equal to  $A\Lambda\Sigma$  which is zero in a  $\Sigma$  state (as  $\Lambda = 0$  for a  $\Sigma$  state). The other matrix elements are zero according to equation (28)

$$H_1(n'\sigma'Vj'; n\sigma Vj) = 0 \quad \text{unless } \sigma' = \sigma \pm 1, j' = j$$

of Van Vleck's paper (page 480). Superposed on the above interaction is the magnetic interaction of the individual electron spins, the energy contribution from which has been shown by Kramers to be proportional to  $3 \cos^2\theta - 1$  where  $\theta$  is the angle between the direction of the resultant spin and the axis of the figure. This causes the diagonal elements of the perturbation matrix to be increased by the term

$$H_2(\Sigma, \Sigma) = \epsilon [3\Sigma^2 - S(S+1)]$$

where  $\epsilon$  is a small numerical factor. Standard matrix transformation theory shows that the energy levels are the roots of the secular determinant

$$H(\Sigma, \Sigma') - \delta(\Sigma, \Sigma')W = 0, \quad \Sigma, \Sigma' = -S, \dots, S,$$

where  $\delta$  equals unity if its arguments are equal and zero otherwise. This determinantal equation yields an algebraic equation for  $W$  of order  $2S+1$ . In the case of  $^5\Sigma$  and  $^6\Sigma$  therefore the determinantal equations of order five and six respectively are obtained. To the roots of the secular determinantal equation must be added the terms due to the interaction between the vectors  $\vec{K}$  and  $\vec{S}$  which is given (for values of  $K$  which are not too large) by the formula

$$\phi(K) = \frac{1}{2} [J(J+1) - K(K+1) - S(S+1)]$$

Then the complete expressions of the rotational levels are obtained by adding to the above two expressions the terms

$$DK^2(K+1)^2 + HK^3(K+1)^3 + \dots$$

which take account of the expansion of the molecule under the centrifugal force and the consequent variation of  $B$ .

## CALCULATIONS AND RESULTS

$^5\Sigma$ : The resulting secular determinantal equation is of order five and is of the form

$$\begin{array}{ccccc|l} & W & a_1 & 0 & 0 & 0 & \text{For } ^5\Sigma, S=2 \\ & & b-W & b_1 & 0 & 0 & \therefore \Sigma = 2, 1, 0, -1, -2 \\ a_1 & & b_1 & c-W & b_1 & 0 & \\ 0 & & 0 & b_1 & b-W & a_1 & \\ 0 & & 0 & 0 & a_1 & a-W & \\ 0 & & 0 & 0 & a_1 & a-W & \end{array} \quad \begin{array}{l} \\ \\ \\ \\ \\ \end{array} = 0$$



where  $a$ ,  $b$ ,  $c$ ,  $a_1$  and  $b_1$  are calculated from the formulae given above for the matrix elements by putting  $\Lambda = 0$  in them since for  $\Sigma$  states  $\Lambda = 0$ , and are given under :  
 $a = B[J(J+1) - 2] + 6\epsilon$ ;  $b = B[J(J+1) + 4] - 3\epsilon$ ;  $c = B[J(J+1) + 6] - 6\epsilon$   
 $a_1 = 2B[J(J+1) - 2]^{\frac{1}{2}}$ ;  $b_1 = B[6J(J+1)]^{\frac{1}{2}}$

These factors into a quadratic equation

$$(a - W)(b - W) - a^2_1 = 0$$

and into a cubic equation

$$(a - W)(b - W)(c - W) - a^2_1(c - W) - 2b^2_1(a - W) = 0$$

Neglecting terms involving powers of  $\epsilon$  higher than one, the roots of the quadratic equation are

$$B(J+1)(J+2) + 3\epsilon \frac{J-4}{2J+1} \quad \text{and} \quad BJ(J-1) + 3\epsilon \frac{J+5}{2J+1}$$

and those of the cubic equation are

$$BJ(J+1) + 3\epsilon \left[ 1 - \frac{12}{4J(J+1) - 3} \right]; \quad B(J-1)(J-2) - 6\epsilon \frac{J-2}{2J-1}$$

$$\text{and} \quad B(J+2)(J+3) - 6\epsilon \frac{J+3}{2J+3}$$

(The method of obtaining these is shown in detail in the appendix). If, as usual, the levels are numbered by the rotational quantum number  $K$ ,  $K = J-2, J-1, J, J+1, J+2$ , and following the usual notation the expressions for the quintet components take the simple forms :

$$F_1(K) = BK(K+1) - 6\epsilon \frac{K}{2K+3}$$

$$F_2(K) = BK(K+1) + 3\epsilon \frac{K+6}{2K+3}$$

$$F_3(K) = BK(K+1) + 3\epsilon \left[ 1 + \frac{3}{2K+3} - \frac{3}{2K-1} \right]$$

$$F_4(K) = BK(K+1) + 3\epsilon \frac{K-5}{2K-1}$$

$$F_5(K) = BK(K+1) - 6\epsilon \frac{K+1}{2K-1}$$

It remains now to add to the above expressions the contribution due to the interaction between  $K$  and  $S$  which we may designate as  $\phi_i(K)$  the values of which are :

$$\phi_1(K) = 2\gamma K; \quad \phi_2(K) = \gamma(K-2); \quad \phi_3(K) = -3\gamma K;$$

$$\phi_4(K) = -\gamma(K+3); \quad \phi_5(K) = -2\gamma(K+1)$$

Adding finally the terms

$$DK^2(K+1)^2 + HK^3(K+1)^3 + \dots$$

we get the complete expressions for the components of the rotational levels of a  ${}^5\Sigma$  state.

${}^6\Sigma$  : In this case the secular determinant is of the sixth degree and of the form :

$$\begin{vmatrix} a-W & a_1 & 0 & 0 & 0 & 0 \\ a_1 & b-W & b_1 & 0 & 0 & 0 \\ 0 & b_1 & c-W & c_1 & 0 & 0 \\ 0 & 0 & c_1 & c-W & b_1 & 0 \\ 0 & 0 & 0 & b_1 & b-W & a_1 \\ 0 & 0 & 0 & 0 & a_1 & a-W \end{vmatrix} \begin{array}{l} \text{For } {}^6\Sigma, S = 5/2 \\ \therefore \Sigma = 5/2, 3/2, 1/2, \\ -1/2, -3/2, -5/2 \\ \\ \\ \\ \\ = 0 \end{array}$$

where

$$a = B \left[ J(J+1) - \frac{15}{4} \right] + 10\epsilon; \quad b = B \left[ J(J+1) + \frac{17}{4} \right] - 2\epsilon;$$

$$c = B \left[ J(J+1) + \frac{33}{4} \right] - 8\epsilon$$

$$a_1 = \sqrt{5} B \left[ J(J+1) - \frac{15}{4} \right]^{\frac{1}{2}}; \quad b = 2\sqrt{2} B \left[ J(J+1) - \frac{3}{4} \right]^{\frac{1}{2}}; \quad c_1 = 3B \left( J + \frac{1}{2} \right)$$

This reduces to two cubic equations which are

$$(a-W)(b-W)(c-W) - a^2_1(c-W) - b^2_1(a-W) + c_1[(a-W)(b-W) - a^2_1] = 0 \dots (a)$$

$$(a-W)(b-W)(c-W) - a^2_1(c-W) - b^2_1(a-W) - c_1[(a-W)(b-W) - a^2_1] = 0 \dots (b)$$

The roots of equation (a) are

$$B \left( J - 3/2 \right) \left( J - \frac{1}{2} \right) + \epsilon \left( 1 + \frac{27}{2J} \right); \quad B \left( J + \frac{1}{2} \right) \left( J + 3/2 \right) + 4\epsilon \left( 1 - \frac{6J+27}{4J(J+2)} \right)$$

$$\text{and } B \left( J + 5/2 \right) \left( J + 7/2 \right) - 10\epsilon \frac{J+7/2}{2J+4}$$

and those of (b) are

$$B \left( J - 5/2 \right) \left( J - 3/2 \right) - 10\epsilon \frac{J-5/2}{2J-2}; \quad B \left( J - \frac{1}{2} \right) \left( J - 3/2 \right) + 4\epsilon \left( 1 + \frac{6J-21}{(J+1)(J-1)} \right)$$

$$\text{and } B \left( J + 3/2 \right) \left( J + 5/2 \right) + \epsilon \left( 1 - \frac{27}{2J+2} \right)$$

As before, numbering the levels by  $K$  and writing

$K = J - 5/2, J - 3/2, J - 1/2, J + 1/2, J + 3/2, J + 5/2$  we get

$$F_1(K) = BK(K+1) - 10\epsilon \frac{K}{2K+3}$$

$$F_2(K) = BK(K+1) + \epsilon \left( 1 + \frac{27}{2K+3} \right)$$

$$F_3(K) = BK(K+1) + \epsilon \left( 4 + \frac{27}{2K+3} - \frac{15}{2K-1} \right)$$

$$F_4(K) = BK(K+1) + \epsilon \left( 4 - \frac{15}{2K+3} - \frac{27}{2K-1} \right)$$

$$F_5(K) = BK(K+1) - \epsilon \left( 1 - \frac{27}{2K-1} \right)$$

$$F_6(K) = BK(K+1) - 10\epsilon \frac{K+1}{2K-1}$$

to which must be added the  $\phi_i(K)$  values which are

$$\phi_1(K) = 3\gamma K; \quad \phi_2(K) = \frac{\gamma}{2}(3K-5); \quad \phi_3(K) = \frac{\gamma}{2}(K-8)$$

$$\phi_4(K) = \frac{\gamma}{2}(K+9); \quad \phi_5(K) = \frac{\gamma}{2}(3K+8); \quad \phi_6(K) = \frac{5\gamma}{2}(K+1)$$

and also

$$DK^2(K+1)^2 + HK^3(K+1)^3 + \dots$$

to get the complete expressions for the rotational energy levels.

The theoretical curves showing the variation with  $K$  of the splitting caused

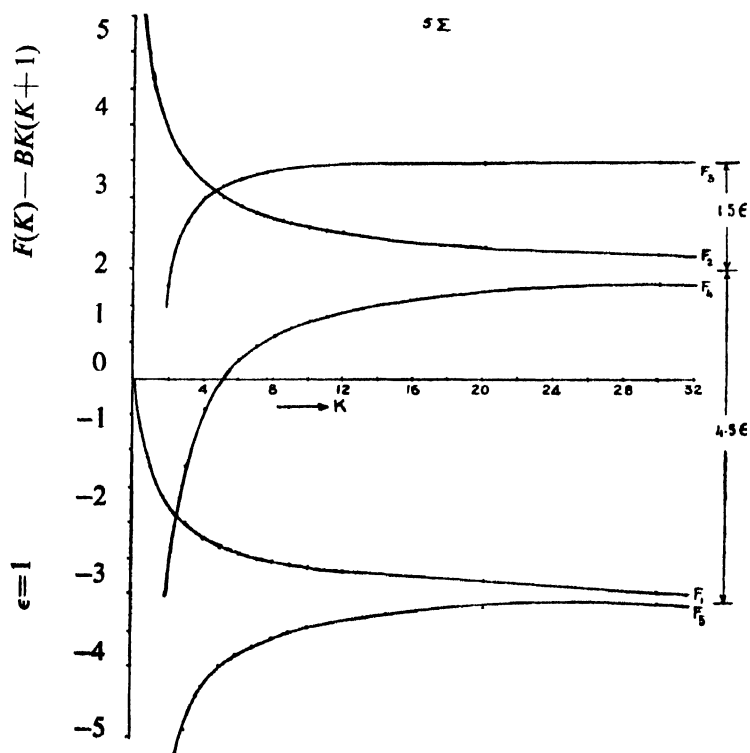


FIG. 1

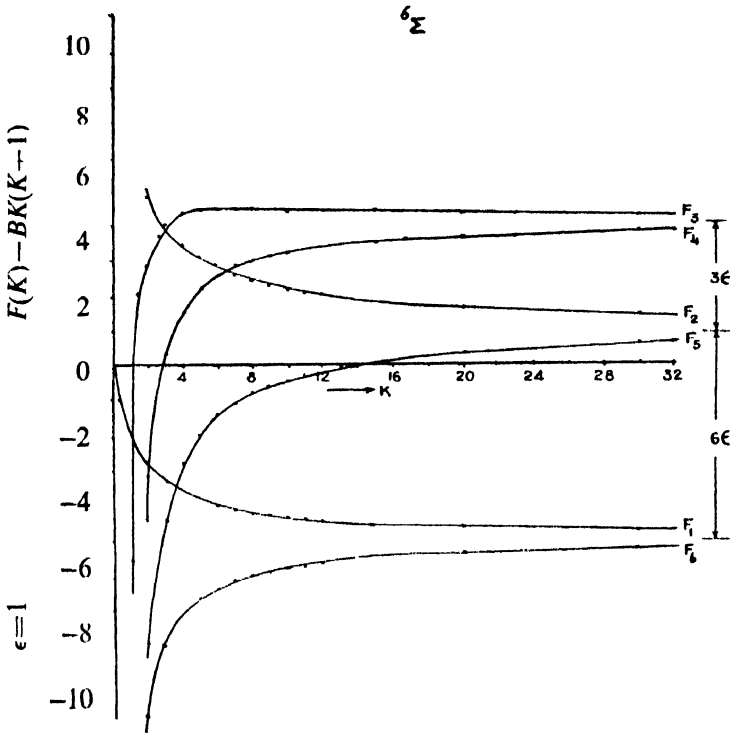


FIG. 2

by the magnetic interaction of the individual electron spins for  $\epsilon = 1$  are given in figures 1 and 2.

APPENDIX

The equations that are obtained in these calculations have been solved by a method which is applicable to an equation of any degree that we may come across in the derivation of the energy levels of states with the approximation that terms involving powers of  $\epsilon$  higher than one can be neglected. The method is as follows:

Let the equation of the  $n$ th degree in  $W$  be

$$W^n + a_1 W^{n-1} + a_2 W^{n-2} + \dots + a_{n-1} W + a_n = 0 \tag{1}$$

where the coefficients  $a_1, a_2, \dots, a_n$  are of the form

$$a_1 = a'_1 + \epsilon a''_1; a_2 = a'_2 + \epsilon a''_2; \dots \dots \dots a_n = a'_n + \epsilon a''_n$$

and let  $\alpha, \beta, \gamma, \dots$  be the known roots of the equation

$$W^n + a'_1 W^{n-1} + a'_2 W^{n-2} + \dots + a'_{n-1} W + a'_n = 0 \dots \dots \tag{2}$$

so that 
$$\left. \begin{aligned} \alpha^n + a'_1 \alpha^{n-1} + a'_2 \alpha^{n-2} + \dots + a'_{n-1} \alpha + a'_n &= 0 \\ \beta^n + a'_1 \beta^{n-1} + a'_2 \beta^{n-2} + \dots + a'_{n-1} \beta + a'_n &= 0 \end{aligned} \right\} \dots \dots \tag{3}$$

We may assume that a root of equation (1) is of the form  $(Z + \mu\epsilon)$  if we neglect higher powers of  $\epsilon$ , where  $Z$  takes the values  $\alpha, \beta, \gamma, \dots$  and where  $\mu$  is to be determined. Therefore

$$(Z + \mu\epsilon)^n + a_1(Z + \mu\epsilon)^{n-1} + a_2(Z + \mu\epsilon)^{n-2} + \dots + a_{n-1}(Z + \mu\epsilon) + a_n = 0 \dots \tag{4}$$

Simplifying (4) and neglecting higher powers of  $\epsilon$  than one, we get an equation where the term without  $\epsilon$  will be one of the expressions on the left of (3) which

is zero and the coefficient of  $\epsilon$  will be linear in  $\mu$ . This coefficient equated to zero gives the value of  $\mu$  which assumes different values as  $Z$  takes the different values

The method is illustrated by considering a  $^6\Sigma$  state. We get a determinantal equation of sixth degree which splits into two cubic equations and they are :

$$(a-W)(b-W)(c-W) - a^2_1(c-W) - b^2_1(a-W) + c^2_1 \{(a-W)(b-W) - a^2_1\} = 0 \quad (i)$$

$$(a-W)(b-W)(c-W) - a^2_1(c-W) - b^2_1(a-W) + c^2_1 \{(a-W)(b-W) - a^2_1\} = 0 \quad (ii)$$

The six roots of the determinantal equation without the term in  $\epsilon$  can be guessed in the following way. The six values of  $K$  are

$$J-5/2, J-3/2, J-1/2, J+1/2, J+3/2 \text{ and } J+5/2$$

so that the roots must be

$$B(J-5/2)(J-3/2); B(J-3/2)(J-1/2); B(J-1/2)(J+1/2)$$

$$B(J+1/2)(J+3/2); B(J+3/2)(J+5/2); B(J+5/2)(J+7/2)$$

as all of these must reduce to the form  $BK(K+1)$  when the levels are numbered by  $K$ . Which three of these belong to (i) and which three, to (ii) is decided by the properties of the roots, namely that the sums of the products of  $\alpha, \beta, \gamma, \dots$  taken one, two, .....  $n$  at a time are respectively equal to

$$-a'_1, a'_2, a'_3, \dots, (-1)^n a'_n \quad \text{in equation (2)}$$

Also it has been found, on comparing the levels of the various  $\Sigma$  states investigated, that in *all* these the roots belong alternately to the two equations into which the determinantal equation may generally split. Thus the roots

$$B(J-3/2)(J-1/2), B(J+1/2)(J+3/2) \text{ and } B(J+5/2)(J+7/2)$$

are found to belong to (i) while the remaining three belong to (ii). Now the coefficient  $\mu$  is determined as indicated above, leading to the roots given above. A similar procedure is adopted for  $^5\Sigma$  as well.

#### ACKNOWLEDGMENTS

The author is deeply indebted to Prof. K. R. Rao for his valuable guidance during the course of this investigation. He also wishes to express his grateful thanks to Prof. S. Minakshisundaram for his kind help in this work.

#### REFERENCES

- Budo, A., 1937, *Zeits. f. Phys.*, **105**, 73.  
 Hill, E. L. and VanVleck, J. K., 1928, *Phys. Rev.* **32**, 250.  
 Nevin, T. E., 1945, *Proc. Roy. Irish Acad.*, **50A7**, 123.  
 Kramers, H. A., 1929, *Zeits. f. Phys.*, **53**, 422.  
 Van Vleck, J. H., 1929, *Phys. Rev.*, **33**, 467.

## PRESSURE IN A LIQUID

BY M. G. BHATAWDEKAR

DEPARTMENT OF PHYSICS, MAHARAJA'S COLLEGE, JAIPUR, (RAJPUTANA).

(Received for publication, September 24, 1951)

**ABSTRACT.** Knowing the potential energy of a liquid, an idea is gained about the intermolecular forces. The pressure within the liquid at different temperatures is calculated by an application of the virial theorem. The virial function is seen to be a function of the volume of the liquid at that temperature; and hence an equation of state for the liquid is derived.

This paper is in continuation of a previous one by the author, (Bhatawdekar, 1951). From the virial theorem we know that

$$PV = RT + \frac{1}{3} \sum r \cdot f(r).$$

where  $f(r)$  is the intermolecular force at the average intermolecular distance  $r$ . Thus the total pressure in a fluid is due partly to molecular agitation and partly to intermolecular forces, which may be attractive or repulsive. In the deduction of the above expression, the force of repulsion is considered to be positive (Jeans, 1921). If  $f(r)$  is known for any liquid at any temperature, the calculation of pressure is possible. When the molecules of a liquid are very close to each other there exists a force of repulsion between them which goes on decreasing as the average distance between two molecules goes on increasing; i.e., as the temperature increases. Beyond a certain limit the force of repulsion gives way to one of cohesion which also decreases with increase of temperature. If  $\xi$  denotes the potential energy of a liquid,  $-d\xi/dr = f(r)$  will denote the force of attraction or repulsion between the molecules according to its sign.

In the previous paper (Bhatawdekar, 1951), the potential energy  $\xi = \phi/2k$  for  $\text{CCl}_4$  and  $\text{NH}_3$  has already been calculated. If  $d$  denotes the density of the liquid, its specific volume will be  $1/d$ , and if  $N$  denotes the number of molecules in one

TABLE I

Substance	Temperature °C	$r \times N^{\frac{1}{3}}$	$\xi \times 10^{13}$ ergs	$\frac{d\xi}{dr} \times N^{-\frac{1}{3}}$ $\times 10^{12}$	$\sum r f(r)$ $\times 10^{-10}$	$RT \times 10^{-8}$	$V$ Atm $\times 10^{-4}$	$P$
$\text{CCl}_4$	80	0.8780	3.16	12.0	4.12	1.91	0.6770	-1.98
	140	0.9059	5.93	10.0	3.54	2.23	0.7435	-1.54
	200	0.9439	8.96	6.0	2.22	2.56	0.8409	-0.837
	240	0.9858	11.39	4.0	1.54	2.78	0.9579	-0.398
	283	1.2140	17.55	2.0	0.95	3.01	1.739	-0.158
$\text{NH}_3$	-45	1.1280	0.582	6.0	23.9	11.1	1.4367	-5.39
	-20	1.1460	1.55	6.0	26.7	12.4	1.537	-5.77
	0	1.1610	2.37	5.5	22.6	13.3	1.5660	-4.66
	20	1.1790	3.26	5.0	20.8	14.3	1.6383	-4.01
	50	1.2120	4.68	3.0	8.60	15.8	1.7766	-1.44
	132.5	1.6240	12.1	1.0	5.74	19.8	4.2830	-0.418

gram of the liquid,  $1/dN$  will be the volume per molecule. Hence,  $r$  can be taken to be equal to  $(1/dN)^{1/3}$  to a first approximation. When a graph is plotted between  $\xi$  and  $r$  at various temperatures we get a continuous curve, the tangent at any point of which gives us the value of  $d\xi/dr = f(r)$  for that value of  $r$  and the corresponding value of the temperature. Thus  $N.r.d\xi/dr$  is calculated and this is taken to be equal to  $\Sigma r.f(r)$ . Knowing the temperature, the pressure is calculated. The results for  $\text{CCl}_4$  and  $\text{NH}_3$  are given in Table I. If the calculated pressure is negative, it is an indication that at that intermolecular distance the pressure due to the cohesion between the molecules preponderates over the pressure due to the random motion of the molecules. Water tends to show an anomalous behaviour, the potential energy diminishing with temperature upto  $70^\circ\text{C}$ .

It is found that the virial function  $N.r.d\xi/dr = \Sigma r.f(r)$  is a function of the volume of the liquid. From the graph it is seen that  $N.r.d\xi/dr = K/V^{2.66}$  where  $K$  is a constant for the liquid. This relation fails near the critical temperature as then the molecules are under no attracting forces. Thus, an equation of state is obtained of the form

$$PV = RT - K/V^{2.66}$$

$$K = 4.5 \times 10^9 \text{ for } \text{CCl}_4 \text{ and } 3.8 \times 10^{11} \text{ for } \text{NH}_3$$

#### ACKNOWLEDGMENT

The author wishes to express his thanks to Professor M.F. Soonawala for his help and guidance.

#### REFERENCES

- Bhatawdekar, M. G., 1951, *University of Rajputana Studies*, 1, 42.  
 Jeans, J. H., 1921, *Dynamical Theory of Gases*, 3rd edition p. 131.  
 Soonawala, M. F., *Ind. J. Phys.*, 10, 353. 1936.

# PULSE WIDTH MEASUREMENTS IN RADAR

BY A. SUNDARA BABU

PHYSICS DEPARTMENT, PRESIDENCY COLLEGE, MADRAS.

*(Received for publication, November 12, 1951)*

## Plate II

**ABSTRACT.** A very simple method of measuring short duration radar pulses, positive or negative has been developed. The theory of calculation of pulse duration after taking a photograph of the pulse superposed on an elliptical time base on an oscilloscope screen is completely given. The method is not only very accurate but also less costly than the existing elaborate method. Range marker units in radar equipments can also be calibrated easily using this method.

There are at present only a few accurate methods of measuring short duration pulses. The duration of the pulse used in radar transmission must be determined accurately so that not only the range of a target but also the peak power and the minimum detectable distance of the radar unit can be determined accurately.

Ludman (1945) uses a high speed linear time-base of duration 3 or 4 microseconds. The pulse, whose width is to be determined, is applied to the vertical deflection plates of a cathode-ray tube. Accurate measurements of pulse width can be made with this method provided the time rate of change per unit of deflection is known. To determine this, a damped sine-wave calibrating signal from a shock excited oscillator synchronised with the time-base is fed to the vertical deflection plates. The time interval between successive peaks depends upon the resonant frequency. The constancy of the frequency of the resonant circuit under continuous wave condition as well as under shock excitation is doubtful. Further, the time interval between any two successive cycles for damped waves is not the same. To overcome some of these disadvantages Ludman later on used a 5 megacycle crystal oscillator for calibration. Even then there are some disadvantages in this method. The sweep position on the oscilloscope screen should be kept the same for all measurements. Measurements as well as calibration are to be done near the centre of the screen in the same portion of the sweep.

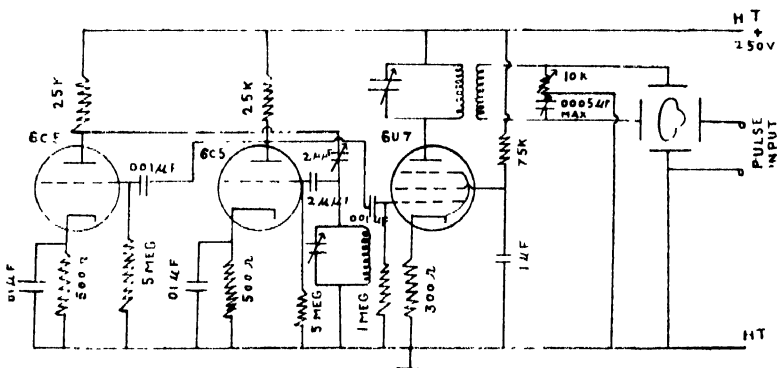
Neglecting the above method of measuring pulse width using a linear saw-tooth sweep, Allan Easton (1946) uses a circular sweep with the pulse superposed on it. The frequency of the oscillator producing the sweep is continuously varied until a stationary pattern results on the screen of the oscilloscope. He also measured the pulse width by superposing on a circular sweep, the differentiated pulses obtained as a result of passing the pulse, whose width is to be measured, through a short CR circuit. The spacing between the differentiated pulses on the circular sweep gives an idea of the duration of the pulse. An elliptical time-base has also been used with considerable accuracy. But the method has got several inherent disadvantages. The resolution of the coincidence sets the maximum accuracy of measurements. In this method it is absolutely essential to have the pulse on the maximum



velocity portion of the sweep and it is assumed that two-thirds of the horizontal deflection on the elliptical sweep corresponds to the maximum velocity portion.

The following method eliminates almost all the above restrictions. The calculations are simple and easy. The resolution error can be reduced to zero by taking the corresponding points at the feet of each pulse and thereby the pulse width can be calculated twice for the same pulse. The pulse may be displayed on any part of the elliptical sweep and yet its duration can be evaluated easily. The equipment is simple and easily operated.

The whole equipment consists of a Franklin oscillator whose frequency can be varied. The output of this is amplified by means of a tuned R.F. amplifier having a tuned circuit on the plate of the valve. The use of the amplifier suppresses any harmonic present. The amplified output is phase-shifted through  $90^\circ$  by means of a suitable condenser, and a potentiometer and the R.f. across the condenser and the potentiometer are applied to one horizontal and one vertical deflection plate, the junction of the condenser and the potentiometer which is earthed, is connected to another vertical deflection plate. The pulse output from the range calibrator unit TS-102/AP obtained from Army disposals is fed between the other horizontal deflection plate and earth. By varying the frequency of the oscillator a steady picture is obtained. To make the frequency of the oscillator and the R.F. amplifier steady without any variation due to voltage fluctuations of the high tension, a specially constructed voltage-stabilised power pack, giving less than 1% variation in the output voltage even if there is a change of 20 volts on either side



FIG

of the 110 volts input to the primary of the power transformer is used. The circuit diagram with the values of components is given in figure 1.

#### THEORY OF CALCULATIONS

Let us consider an ellipse (figure 2) of major axis  $2a$ , minor axis  $2b$  and having a pulse superposed on it. The ellipse is the resultant of two simple harmonic motions at right angles of same frequency but of different amplitudes. The

co-ordinates of any point on the ellipse with respect to the centre of the ellipse as the origin can be represented as

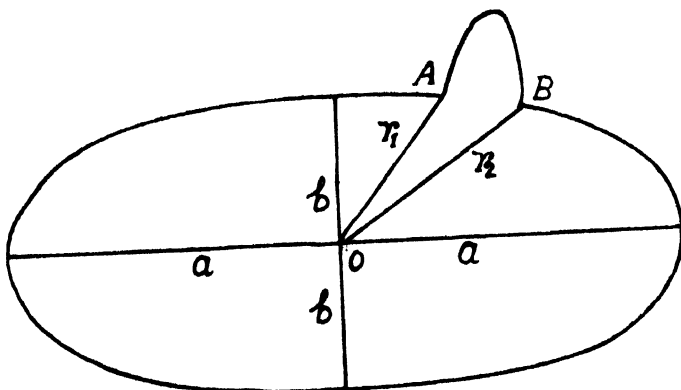


FIG 2

$$X = a \cos \omega t$$

and

$$Y = b \sin \omega t$$

Let  $x_1$  and  $y_1$  be the co-ordinates of  $A$ , the foot of the leading edge of the pulse on the ellipse.

$$\text{Then } x_1 = a \cos \omega t_1 \quad \dots (1)$$

$$\text{and } y_1 = b \sin \omega t_1 \quad \dots (2)$$

But the polar co-ordinates of the same point can be represented by  $r_1 \cos \theta_1$  and  $r_1 \sin \theta_1$  where  $r_1$  is the radius vector at  $A$  and  $\theta$  the angle which it makes with the  $X$ -axis.

$$\text{Then } r_1 \cos \theta_1 = a \cos \omega t_1 \quad (3)$$

$$r_1 \sin \theta_1 = b \sin \omega t_1 \quad (4)$$

Similarly for the point  $B$ , the foot of the trailing edge of the pulse, the co-ordinates are

$$r_2 \cos \theta_2 = a \cos \omega t_2 \quad (5)$$

$$r_2 \sin \theta_2 = b \sin \omega t_2 \quad (6)$$

Taking equation (3), the time  $t_1$  taken to describe that arc of the ellipse between the point  $A$  and the perihelion is given by

$$t_1 = 1/\omega \left[ \cos^{-1} \frac{r_1}{a} \cos \theta_1 \right] \quad \dots (7)$$

Taking the corresponding equation (5) for  $B$

$$\text{we have } t_2 = 1/\omega \left[ \cos^{-1} \frac{r_2}{a} \cos \theta_2 \right] \quad \dots (8)$$



Fig. a.



Fig. b.

Oscillograms of pulses superposed on  
elliptical time base.



The actual pulse duration, which is equal to  $t_2 - t_1$ , is given as

$$t_2 - t_1 = \frac{1}{\omega} \left[ \cos^{-1} \frac{r_2}{a} \cos \theta_2 - \cos^{-1} \frac{r_1}{a} \cos \theta_1 \right] \\ = \frac{1}{2\pi f} \left[ \cos^{-1} \frac{r_2}{a} \cos \theta_2 - \cos^{-1} \frac{r_1}{a} \cos \theta_1 \right] \quad \dots (9)$$

where  $f$  is the frequency of the elliptical sweep.

Similarly the pulse duration can be determined taking into consideration the  $Y$  co-ordinates of the points  $A$  and  $B$  on the ellipse.

$$\therefore t_2 - t_1 = \frac{1}{2\pi f} \left[ \sin^{-1} \frac{r_2}{b} \sin \theta_2 - \sin^{-1} \frac{r_1}{b} \sin \theta_1 \right] \quad \dots (10)$$

These formulae can further be simplified by substituting the values of  $\cos \theta$  and  $\sin \theta$  in terms of  $a$ ,  $b$  and  $r$ .

The polar equation to the ellipse is

$$\frac{r^2 \cos^2 \theta}{a^2} + \frac{r^2 \sin^2 \theta}{b^2} = 1 \quad \dots (11)$$

$$\frac{r^2}{a^2} \cos^2 \theta + \frac{r^2}{b^2} (1 - \cos^2 \theta) = 1$$

$$r^2 \frac{(b^2 - a^2)}{a^2 b^2} \cos^2 \theta = \frac{b^2 - r^2}{b^2}$$

$$\cos \theta = \frac{a}{r} \sqrt{\frac{b^2 - r^2}{b^2 - a^2}} \quad \dots (12)$$

$$\text{similarly} \quad \sin \theta = \frac{b}{r} \sqrt{\frac{r^2 - a^2}{b^2 - a^2}} \quad \dots (13)$$

Equation (9) becomes

$$t_2 - t_1 = \frac{1}{2\pi f} \left[ \cos^{-1} \sqrt{\frac{b^2 - r_2^2}{b^2 - a^2}} - \cos^{-1} \sqrt{\frac{b^2 - r_1^2}{b^2 - a^2}} \right] \quad \dots (14)$$

Equation (10) becomes

$$t_2 - t_1 = \frac{1}{2\pi f} \left[ \sin^{-1} \sqrt{\frac{r_2^2 - a^2}{b^2 - a^2}} - \sin^{-1} \sqrt{\frac{r_1^2 - a^2}{b^2 - a^2}} \right] \quad (15)$$

Thus for the same pulse the duration can be calculated twice. One important precaution to be observed here is that when  $A$  and  $B$  are on either side of the centre of the ellipse, the supplement of the angle which the first factor gives or the complement of the angle given by the second factor in the above equations will have to be considered for proper signs for the displacements.

Measurements were taken on the enlargement of the photograph of the trace shown in Plate II for the two resolved pulses.

TABLE I

Frequency 329.4 kilocycles per second

Pulse	$2a$	$2b$	$r_1$	$r_2$	$\cos^{-1} \sqrt{\frac{b^2 - r^2}{b^2 - a^2}} \sin^{-1} \sqrt{\frac{r^2 - a^2}{b^2 - a^2}}$	$t_2 - t_1$ in $\mu$ second
I	29.2 cm	5.0 cm	10.9 cm	2.6 cm	$42^\circ 29'$ $87^\circ 9'$	— .38
I	29.2 "	5.0 "	10.9 "	2.6 "	—	$42^\circ 28'$ $87^\circ 12'$ .38
II	29.2 "	5.0 "	9.5 "	2.8 "	$50^\circ 25'$ $95^\circ 2'$	— .38
II	29.2 "	5.0 "	9.5 "	2.8 "	—	$50^\circ 25'$ $95^\circ 5'$ .38
Fig b, Plate II	28.7 "	10.0 "	8.6 "	5.9 "	$58^\circ 9'$ $103^\circ 28'$	— .38
	28.7 "	10.0 "	8.6 "	5.9 "	—	$58^\circ 39'$ $103^\circ 28'$ .38

This method can also be used for calibrating range marker units employed in the radar equipments. When a nearly steady pattern of the ellipse having the pulse superposed on it is obtained by controlling the frequency of the oscillator, the duration of the sweep, which is equal to the pulse spacing, is obtained by finding the reciprocal of the frequency. This gives the total time taken by the electro-magnetic waves to travel from the radar unit to the target and from the target to the unit. Knowing the velocity of the electro-magnetic waves to be 984 ft. per microsecond, the range between two successive pulses can be calculated. In the present experiment the frequency of the sweep as measured by a precision GE wavemeter is obtained as 329.4 Kc/s. Therefore the duration is 3.042 micro-seconds. The distance travelled by electro-magnetic waves through half this time is equal to 1496 ft. But the actual spacing between the consecutive range marker pulses for the unit TS-102/AP is equal to 1500 ft. The error of calibration is less than .3% which is very small. The method therefore offers solution not only for measuring small duration pulses but also for calibrating range marker units.

## ACKNOWLEDGMENT

In conclusion the author wishes to thank Prof. T. Krishnamoorthy, Professor of Physics, Presidency College, Madras, for his guidance through this work and encouragement to do further work in the field.

## REFERENCES

- Allam Easton, 1946, *Electronics*, 13, 150.  
Ludman, W. W. 1945, *Electronics*, 18, 117.

# DETERMINATION OF OSMOTIC COEFFICIENTS

## I. CONSTRUCTION AND CALIBRATION OF THE THERMISTOR BRIDGE

BY C. G. MCGEE AND B. R. Y. IYENGAR

NATIONAL CHEMICAL LABORATORY, POONA

(Received for publication, December 3, 1951)

**ABSTRACT.** The apparatus and technique for measuring small vapour pressure differences of solutions are described. The method is based on the fact that the equilibrium temperature difference developed between a drop of solution and a drop of solvent, or reference solution, in an atmosphere saturated with solvent vapour is directly proportional to vapour pressure lowering. From this, osmotic coefficients are calculable. The advantages and the limitations of the method are discussed.

### INTRODUCTION

Osmotic coefficients have been evaluated from vapour pressure data by a variety of methods, such as, the direct measurement of vapour pressure difference, the 'dynamic' vapour pressure method, depression of freezing point, elevation of boiling point, dew-point, and the comparatively recent isopiestic method (Sinclair, 1933). While these methods are capable of giving results of considerable precision, they have some limitations and drawbacks, such as, the elaborateness of technique and experimental procedure or the incapability of being extended to temperatures and solution concentrations desired.

An entirely new technique was put forward by Hill (1930) who measured the vapour pressure difference between two solutions, or between a solution and the solvent, in terms of the equilibrium temperature difference between the faces of a thermopile exposed to the systems under investigation. Since the temperature difference is measured electrically, this method is often referred to as the 'thermo-electric' method (Roepke, 1942). Baldes (1934) modified Hill's method by using thermocouples in place of thermopile, and also by having the solution or solvent in the form of a drop on the thermo-junctions, which were constructed in the form of small loops. In an extensive investigation, Roepke and Baldes (1938) clearly demonstrated that under suitably controlled experimental conditions, the method gives reliable results which are unaffected by factors, such as, surface films, coefficient of diffusion of water in the droplets, non-solvent volume, shapes of drops, etc. This method has already found application in osmotic studies on biological fluids (Roepke, 1942) and colloidal electrolytes (Fineman and McBain, 1948).

Recently Brady, Huff, and McBain (1951) described a technique of measuring vapour pressure difference by means of matched thermistors incorporated suitably in an A.C. bridge circuit, thus replacing the thermocouples and galvanometer used by Baldes and others. The thermistor method is extremely sensitive and has

the further advantages of being rapid in its operation and free from the spurious electrical effects that might be encountered with the D.C. method of Baldes.

The present paper deals with the construction and operation of an apparatus, essentially similar to the one described by Brady, *et al*, but having some additional refinements. The limitations involved in work with thermistors are also briefly discussed.

#### APPARATUS AND TECHNIQUE

The thermistors (Stranetel, Type F 2311/300, Standard Telephones and Cables Ltd.) are contained in a thermostat especially designed to minimize sudden changes of temperature, even within the working temperature tolerance of  $0.02^{\circ}\text{C}$ . This thermostat (figure 1) consists of three concentric pyrex beakers (*A*, *B* and *C* of 100, 250 and 1000 ml capacity respectively) held in place by accurately cut cork

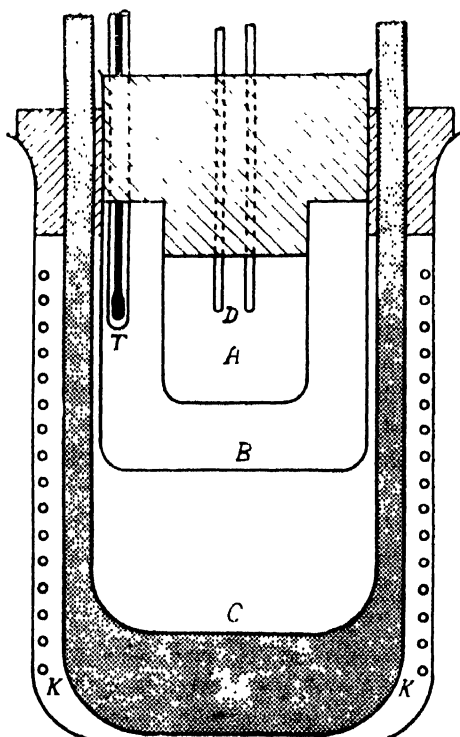


FIG. 1  
The thermostat

cylinders and rings. The thermistors themselves (*D*) pass through and are held firmly by the inner cork cylinder, with the active elements being in the small chamber formed by beaker *A*. This chamber also contains 10 to 15 ml. of the solvent; it is covered on the outside by a layer of aluminium foil having a small window for viewing the thermistor elements. There is also a hole through the cork top by means of which solutions can be placed on the thermistor tips with a



syringe having a 4 needle. This hole (not shown) is normally covered with a small cork block. The annular space between beakers *A* and *B* serves merely as a temperature lag. It also contains the thermometer *T*.

The outermost vessel contains both the mercury thermo-regulator (shaded portion of figure 1) *M* of circular cross-section and the electrical heater *K*. The latter consists of coils of nichrome wire mounted on the mica strips and having spacers of asbestos cord. Just within the heating coil is mounted a cylinder of copper foil (not shown) to distribute the heat more uniformly and to eliminate direct radiation to the innermost chamber.

The temperature control is quite satisfactory in view of the fact that it is only the difference ( $r_1 - r_2$ ) in resistance that is measured. With water on both the

thermistors, it was found that  $\frac{d(r_1 - r_2)}{dT} = 0.25$  ohms per degree Centigrade. Since the temperature control was  $\pm 0.02^\circ\text{C}$ , the limit of accuracy of measuring ( $r_1 - r_2$ ) is  $\pm (0.25 \times 0.02) = \pm 0.005$  ohms, corresponding to about 0.0006 molar. Thus, for a fully dissociated 0.03m solution of a uni-univalent electrolyte, the results may be accurate to within 1%.

The present set-up is strikingly compact and completely eliminates the necessity of having a manipulating chamber, as designed by Brady, *et al* (1951).

The resistance differential was measured by means of an A.C. bridge (figure 2) in terms of a variable linear resistor (*R*, of range 24 ohms) capable of recording a

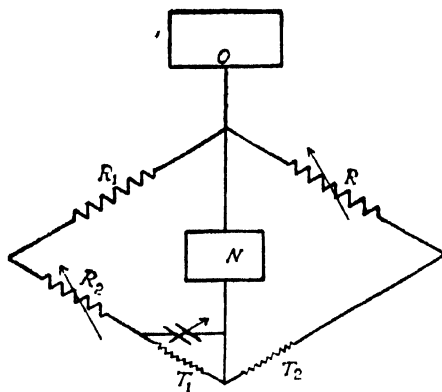


FIG. 2

The thermistor bridge  
 $R = 25$  ohms ;  $R_1 = 25$  ohms ;  
 $R_2 = 100$  ohms ;  $T_1, T_2$  thermistors  
*O* — Oscillator (1000c/s)  
*N* — Null detector

minimum change of resistance of 0.024 ohms and corresponding to a temperature difference of about  $0.0005^\circ\text{C}$ . An audiofrequency oscillator (Hewlett—Packard model 200°C.) supplied the bridge with 1000 c.p.s. while a standing wavemeter (Hewlett-Packard model 415 A) having input impedance of 75000 ohms was used as null detector. The operating technique is very simple. When the thermostat

has attained the desired temperature, an initial reading is obtained by placing drops of water on both the thermistors; another reading ( $r_s$ ) is obtained by replacing one of the water drops by a solution drop, taking sufficient precaution to see that the tip of the thermistor is rinsed with a few drops of solution before the drop is deposited. Thus ( $r_s - r_w$ ) is the difference in resistance due to the temperature difference between the drops arising out of their inequality of vapour pressure. From this, the osmotic coefficient is calculated as follows :

Define osmotic coefficient (Guggenheim, 1950)  $g$  by the equation :

$$\ln \frac{p}{p_0} = -g \ln(1 - x) \quad \dots (1)$$

where  $p$  and  $p_0$  are the vapour pressures of the solution and solvent, respectively and  $x$  is the mole fraction of the solute.

For dilute solutions,

$$\ln \frac{p}{p_0} = \ln \left( 1 - \frac{\Delta p}{p_0} \right) \approx - \frac{\Delta p}{p_0}$$

where  $\Delta p = (p_0 - p)$  is the vapour pressure lowering, and also  $x \ll 1$ , so that,  $\ln(1 - x) \approx -x$ . Then equation (1) becomes,

$$\Delta p = p_0 x g \quad \dots (2)$$

Since,

$$x = \frac{n_1}{n_0 + n_1} \approx \frac{n_1}{n_0} = \frac{M_0 m_1}{1000}$$

where  $n_1$  and  $n_0$  are the number of moles of solute and solvent, respectively,  $m_1$  is the molality of the solute and  $M_0$  is the molecular weight of the solvent, then equation (2) may be written as

$$\Delta p = \frac{p_0 m_1 M_0 g}{1000} = k g m_1 \quad (3)$$

$k$  being a constant for a fixed solvent.

Since  $\Delta p$ , the vapour pressure lowering, is proportional to the equilibrium temperature difference  $\Delta t$ , between drops (Hill, 1930),

$$\Delta p = k_1 \Delta t, \quad \dots (4)$$

and also,

$$\Delta t = k_2 \Delta r \quad \dots (5)$$

where  $\Delta r = (r_s - r_w)$  is observed experimentally, as will be shown later. From (4) and (5)

$$\Delta p = k_3 \Delta r \quad \dots (6)$$

$k_3$  being another constant. Comparing (6) and (3) we get

$$\Delta r = K g m \quad \dots (7)$$

for an electrolyte,

$$\Delta r = K V g m_1 \quad \dots (8)$$

where  $V$  is the number of ions.

The constant  $K$  is determined by calibration with standard solution (e.g. aqueous KCl) whose variation of  $g$  with concentration has been accurately established. Having once determined the value of  $K$ , the unknown osmotic coefficient of any solution may be computed from (7) or (8), once the resistance differential,

after the attainment of equilibrium between the drop of solution and the reference standard, has been measured. Experiments with solutions of potassium chloride ( $V = 2$ ) gave for  $K$  a value of 8.50 ohms per unit molality, with a mean average deviation of  $\pm 0.05$  in the concentration range studied (0.04m to 0.5m).

The result of runs on other electrolytes, non-electrolytes and colloidal electrolytes will be submitted shortly.

## DISCUSSION

It is worthwhile to explore the limitations of the thermistor method for measurement of vapour pressure differences. These limitations are governed by the conditions under which equation (7) is precisely true.

The first assumption in the derivation of (7) was that  $x \ll 1$ . For a unit molal solution of a uni-univalent electrolyte ( $V = 2$ ), this assumption introduces an error of about 2 per cent.

The other assumption made, viz, that  $\Delta r = k' \Delta t$  is valid only under certain conditions, as shown below :

If  $x$ , and  $y$  are the resistance differentials recorded with water on both the thermistors and water on thermistor (1) and solution on thermistor (2), respectively, then,  $x \sim y = \Delta r = r_2 - r_1$ ; where  $r_2$  and  $r_1$  are the resistances of the thermistor (2) with water and solution, respectively.

Over small ranges of temperature the variation of the resistance ( $r$ ) of a thermistor with temperature, is given by,

$$\Delta r = A \exp. \frac{B}{T},$$

where  $A$  and  $B$  are constants. Then

$$\begin{aligned} \Delta r = r_2 - r_1 &= A \exp. \frac{B}{T_2} - A \exp. \frac{B}{T_1} \\ &= r_2 \left( 1 - \exp. \frac{-B \cdot \Delta t}{T_2 T_1} \right) \quad \dots (9) \end{aligned}$$

where  $\Delta t = T_1 - T_2$  is a positive quantity, since the temperature of the solution drop  $T_1$  is higher than that of water drop  $T_2$ . If,

$$\frac{B \cdot \Delta t}{T_2 T_1} \ll 1,$$

then (9) approximates to

$$\Delta r = \frac{r_2 \cdot B}{T_2 T_1} \cdot \Delta t \approx \frac{r_2 B}{T_2^2} \cdot \Delta t$$

or

$$\Delta r = K' \cdot \Delta t$$

since  $r_2$ ,  $B$ , and  $T_2$  are constants.

Substituting  $r_2 = 1500$ ,  $T_2 = 303^\circ\text{K}$  and  $\Delta r = 20$  (one molal KCl solution),

$$\frac{B \cdot \Delta t}{T_2 T_1} = -\ln \left( 1 - \frac{\Delta r}{r_2} \right) = 0.013$$

whence the assumption of the approximation

$$\exp. \left( - \frac{B. \Delta t}{T_2 T_1} \right) = 1 - \frac{B. \Delta t}{T_2 T_1}$$

introduces an error of about 0.7 per cent which is less than that arising out of the approximation,

$$\ln (1 - x) \approx -x,$$

originally made in deriving the working equation

$$\Delta r = Kgm_1$$

Thus, the limitations imposed by the deviation from linearity of the resistance differential with respect to difference in temperature is comparatively less than that imposed by the algebraic approximation made in the original equation (1) defining the osmotic coefficient. Even though the 'practical' osmotic coefficient defined by

$$\ln \frac{p}{p_0} = \ln \left( 1 - \frac{\Delta p}{p_0} \right) \quad \frac{M_0 m_1}{1000}$$

is used in place of the rational osmotic coefficient  $g$  as defined in (1), it is seen that  $\Delta p$ , and hence  $\Delta r$ , is not proportional to molality  $m_1$  except at extreme dilutions.

#### ACKNOWLEDGMENTS

Thanks of the authors are due to Professor J. W. McBain for his keen interest in this work, and also to Dr. S. S. Marsden for helpful suggestions and valuable discussions.

#### REFERENCES

- Baldes, E.J. 1934; *J. Sci. Instr.*, **11**, 223.  
 Brady, A.P. and Huff, H., and McBain, J. W., 1951; *J. Phys. Coll. Chem.*, **55**, 304.  
 Fineman, M. N. and McBain, J. W., 1948, *J. Phys. Coll. Chem.*, **52**, 881.  
 Guggenheim, E.A., 1950; "Thermodynamics", North Holland Publishing Co., Amsterdam, p.p. 200.  
 Hill, A.V., 1930; *Proc. Roy. Soc., A* **127**, 9.  
 Roepke, R.R., 1942; *J. Phys. Chem.*, **46**, 359.  
 Roepke, R.R., and Baldes, E. J., 1938, *J. Biol. Chem.*, **126**, 349.  
 Sinclair, D.A., 1933; *J. Phys. Chem.*, **37**, 495

# ON THE MOLECULAR CONDUCTIVITY OF DYESTUFFS IN SOLUTION AND THE INFLUENCE OF FOREIGN SUBSTANCE ON THE SAME\*

BY K. D. CHAUDHURI AND D. R. DAS GUPTA

PHYSICS DEPARTMENT, DACC'A UNIVERSITY

(Received for publication, December 14, 1951)

**ABSTRACT.** The paper describes the results of the measurements of the molecular conductivities of dyestuffs in solution. It has been found that in most of the cases the molecular conductivities of dyestuffs in solution do not have linear relations with square root of concentration. The departure of the conductivity curve from the perfect straight line has been explained as due to the formation of ionic micelles. The influence of foreign molecule or ions on the conductivity of the fluorescent dyestuffs in solution has been investigated as well.

## INTRODUCTION

The quenching of fluorescence of dyestuffs with increase in concentrations or by addition of salts has been explained by various workers as due to two causes : (1) quenching by deactivating collisions of the second kind, (2) the formation of associated molecules which themselves are non-fluorescent and have a somewhat modified absorption spectrum.

The diminished fluorescence in concentrated dye solutions is largely due to aggregate formation as shown by the fact that they do not obey Beer's law (1935) as well as by other observations on mean life and depolarisation (Banow, 1929, 1930, 1933). Mitra, (1938) observed a close parallel between the change of molar absorption co-efficients with concentrations and the change of fluorescence yields. It is interesting to note that in very dilute solutions where Beer's law seems to hold, the fluorescence yield remains constant. Further increase in concentration diminishes the yield as well as absorption capacity per molecule. It is difficult to explain on purely collisional hypothesis the change of the absorption co-efficients to the extent observed by Mitra. Lewschin (1927) found modified absorption spectra of dyestuffs. He studied the effect of temperature on specific fluorescent capacity in concentrated solutions. Though temperature increases the number of collisions, the fluorescence yield increases at the same rate. Boucard (1936) has confirmed the above observations which go against the collision of the second kind as means of quenching. Banow (1933) has further shown that increase of temperature has, sometimes, a decreasing effect on the quenching of fluorescence by salts. All these go against the theory of the collision of the second kind and we are thus inclined to look for the explanation in the micelle formation of the ions of the dyestuffs to which the greater part of the effect may be due. The present investigation has been carried out to gain some insight as to the mechanism of micelle formation and to the ionic states of the dyemolecules.

\*Communicated by Prof. K. Banerjee.

The mechanism of micelle formation can be best studied from measurements on conductivity of dyestuffs. It is a well known fact that the equivalent conductivity of an electrolyte generally increases with dilution and tends to a limiting value at infinite dilution. It was pointed out by McBain (1913) that the equivalent conductivity of an electrolyte would be increased by the aggregations of ions of one kind to form ionic micelles and the remarkable increase of equivalent conductivity with increasing concentration has been attributed to association of solute molecules. Robinson (1934) and his co-workers determined the transport number as well as the equivalent conductivities of some of the rigorously purified dyestuffs. The equivalent conductivities of dye solutions, when plotted against square root of concentrations, give curves similar in nature to those obtained by Howell and Robinson (1933). The departure of the conductivity curve from the perfect straight line can only be explained on the assumption that ionic micelles are formed with increase in concentration.

The measurement of conductivity of dyes is, however, beset with difficulties. The Kohlrausch method of determining resistances of electrolytes is generally employed using electrodes coated with platinum black. The platinum black coating eliminates the disturbing effect of polarisation but it has certain inherent disadvantages. It adsorbs the solute molecules and acts as catalyst in the oxidation of certain substances, particularly dyestuffs. In our observations the coating has, therefore, been avoided altogether and a method devised by the senior author (Chaudhuri, 1948) to measure electrolytic resistance using bright platinum electrodes has been used. The method gives quite satisfactory results.

#### EXPERIMENTAL

The arrangement of apparatus is shown in figure 1. It is the usual Wheatstone's bridge arrangement in which an amplifier is used in the galvanometer or telephone arm. The detecting instrument is the vertical wattmeter devised by Mukherjee (1930, 1938). This instrument is composed of two systems of coils of which the fixed system produces the magnetic field and the moving system is deflected by the field. The former is put in the battery arm of the

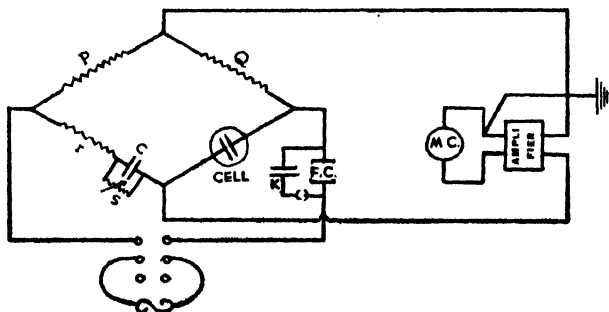


FIG. 1

bridge and the latter in the out-put side of the amplifier. The ratio arms are of equal resistances so that their inductances are

also the same. In the third arm, there is, in series with a resistance  $r$ , a condenser  $C$  shunted by a variable resistance  $S$ . The effective resistance and reactance of the system composed of the condenser and the shunt are respectively

$$\frac{S}{1 + S^2 C^2 p^2} \text{ and } \frac{S^2 C p}{1 + S^2 C^2 p^2}, \text{ where } p = 2\pi \text{ times the frequency of the source.}$$

In the fourth arm is placed the electrolytic cell which can be regarded as consisting of electrolytic resistance, polarisation capacitance and polarisation resistance. The polarisation capacitance is due to the reversible transformation of electrical energy into chemical energy and which is equivalent to an electrostatic condenser. The polarisation resistance is, according to Wien, due to irreversible process at the electrode. Perhaps much of the electrode loss is due to the employment of voltage higher than the decomposition voltage of the solution and was not appreciable in the work of the author. The peak voltage across the electrodes was less than the decomposition voltage of the solution. The electrode resistance  $\Delta R$ , can, therefore, be made to play insignificant part on the resistance of the solution. The polarisation capacitance can be compensated by introducing a capacitive reactance in the adjacent arm of the bridge. Therefore, when the true balance is obtained with the detecting instrument, the resistance of the third arm, namely,

$$r + \frac{S}{1 + S^2 C^2 p^2}$$

becomes equal to the resistance of the solution and the reactance  $-\frac{S^2 C p}{1 + S^2 C^2 p^2}$

balances the polarisation reactance of the solution as well as the residual inductive reactance of the third arm.

#### METHOD OF FINDING THE BALANCE POINT

In detecting instruments of the wattmeter or dynamometer type, the deflection is given by

$$\delta = A I_f I_m \cos \psi$$

where  $I_f$ ,  $I_m$  are the r.m.s currents in the fixed coils and moving coils respectively and  $\psi$ , the phase-difference between them. The deflection is, therefore, zero when

$$(1) \quad I_f \text{ or } I_m = 0$$

$$\text{or} \quad (2) \quad \cos \psi = 0 \text{ i.e., } \psi = \pi/2$$

The balance corresponding to condition (1) is called the true balance. In practice, the null point corresponding to condition (2) is easily obtained. If, however, the phase of the current through the fixed coil with respect to the current through the moving coil is altered by introducing a condenser,  $K$ , in parallel with the fixed coil, the null point is disturbed and there is deflection one way or the other according as  $I_f$  is in advance of, or behind,  $I_m$ .

The procedure for finding true balance, is as follows : keeping  $s = 0$ , a null point is obtained by adjusting  $r$ , when the condenser  $K$  is off the circuit. Then the direction and extent of deflection are observed when  $K$  is introduced. The shunt is then given an arbitrary value and after obtaining the null-point by adjusting  $r$  with  $K$  off, the direction and extent of deflection are again observed with  $K$  on. Proceeding in this manner a condition is attained when null point will not be disturbed by introducing  $K$ . This condition corresponds to true balance.

**Determination of  $Cp$ :** Since the resistance of the solution is equal to  $r + \frac{S}{1 + S^2 C^2 p^2}$  it is necessary to find the value of  $Cp$ . A method for determining  $Cp$  has been described by Mukherjee (1938). In it the moving coil of the wattmeter is made non-inductive by Sumpner's compensation method and from the null-point corresponding to  $\psi = \pi/2$ , the value of  $Cp$  is found with the aid of the formula :

$$\frac{1}{C^2 p^2} = \frac{Q}{P} R \left\{ R + \frac{(P + Q)G}{P + Q + G} \right\}$$

Figure 2 shows the arrangement of apparatus.

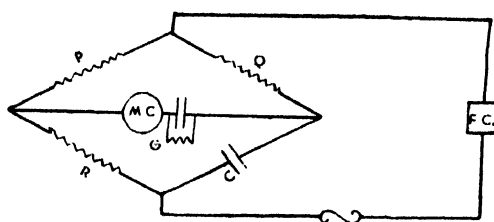


FIG. 2

## EXPERIMENTAL RESULTS

In the actual experiment the temperature was kept constant within 1/500th of a degree with a specially designed thermostat and a source producing high audio-frequency alternating current was employed to reduce polarisation effects to a minimum. The amplifier used was a simple resistance-capacity coupled one in which anode resistances attached to the valves were much larger than the valve resistances, thus ensuring the straight line character of the characteristic curves within a long range of grid voltages and eliminating the possibility of a feed-back effect. The output current from the amplifier was obtained through a  $4\mu F$  condenser. The amplification was such as to give one ampere (output) current per volt (input).



It took the cell about 2 to 3 hours to come to a steady temperature. The conductivities of different dyestuffs in water and alcoholic solutions at different concentrations were measured at constant temperature. The results of our measurements are given in the accompanying tables and graphs.

TABLE I  
Eosine in water

Molecular concentration $C$	$\sqrt{C}$	Sp. conductivity	Molecular conductivity
.02792	.167	.007244	259.4
.01396	.117	.003286	235.0
.00698	.0835	.001442	201.6
.00349	.0590	.0006709	192.0
.001745	.0417	.0003432	196.3
.000872	.0290	.0001751	200.6
.000436	.0208	.00009107	208.7
.000218	.0147	.00004968	231.4
.000109	.0104	.00002800	256.7
.0000545	.0074	.00001646	301.8

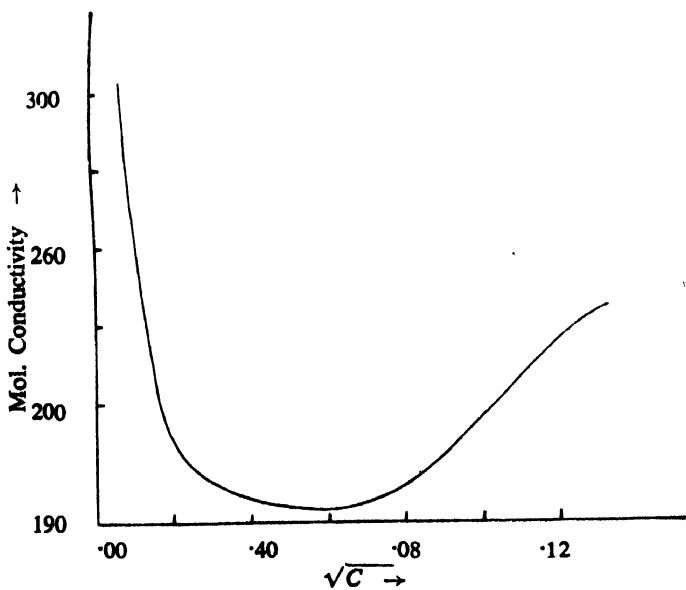


FIG. 3  
Eosine in water

TABLE II  
Erythrosine in water

Molecular concentration $C$	$\sqrt{C}$	Sp. conductivity	Molecular conductivity
.005308	.07285	.0006710	126.4
.002654	.05152	.0003375	127.2
.001062	.03259	.0001389	130.8
.0005308	.02304	.00007389	139.2
.0002654	.01629	.00003970	149.6
.0001327	.01152	.00002040	153.7
.00006635	.008145	.00001042	157.0

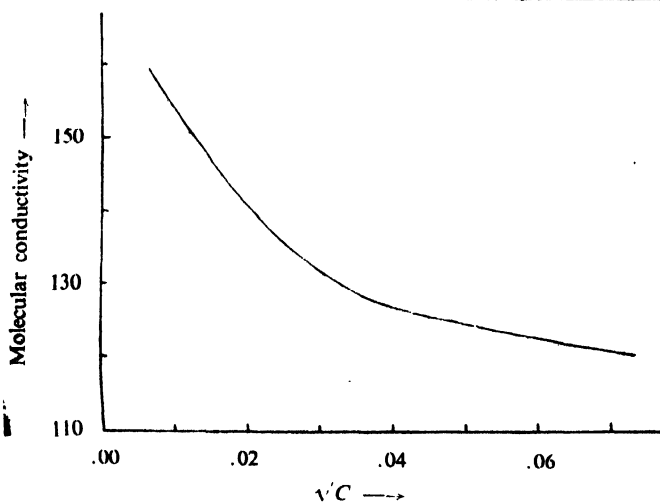


FIG. 4

Erythrosine in water

TABLE III  
Methyl violet in water

Molecular concentration $C$	$\sqrt{C}$	Sp. conductivity	Molecular conductivity
.001271	.0356	.0001021	80.35
.000635	.0252	.00005526	86.98
.0001271	.01127	.00001604	126.20
.0000635	.00797	.00001225	192.80
.00003175	.00563	.00001041	327.30

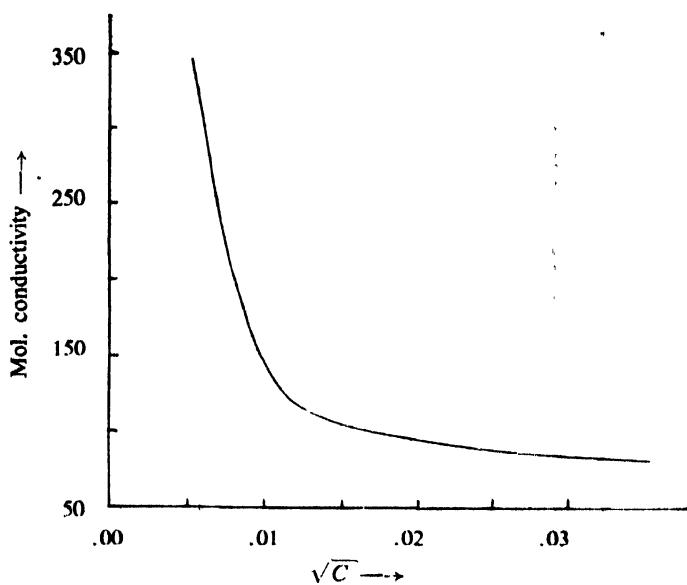


FIG. 5  
Methyl violet in water

TABLE IV  
Cyanine in water

Molecular concentration $C$	$\sqrt{C}$	Sp. conductivity	Molecular conductivity
.0001859	.0137	.00002653	142.7
.0000465	.0068	.00001128	201.8
.00002325	.0048	.000008680	386.7
.00001162	.0034	.000007773	693.7
.00000581	.0024	.000007031	1227.0

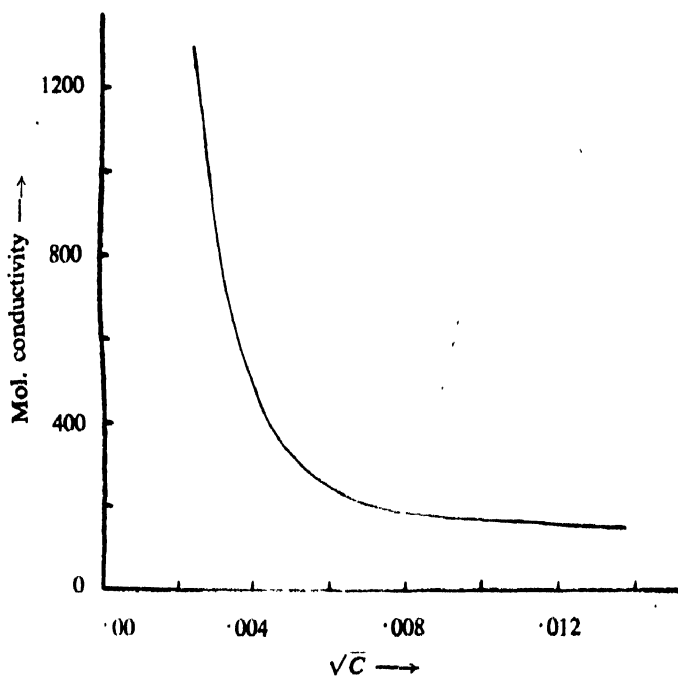


FIG. 6  
Cyanine in water

TABLE V  
Erythrosine in alcohol

Molecular concentration $C$	$\sqrt{C}$	Sp. conductivity	Molecular conductivity
.01752	.1324	.00008843	5.048
.008760	.09359	.00005048	5.762
.003480	.06618	.00003027	6.910
.001752	.04185	.00001499	8.557
.000584	.02417	.00000633	10.840
.000292	.01709	.00000395	13.530

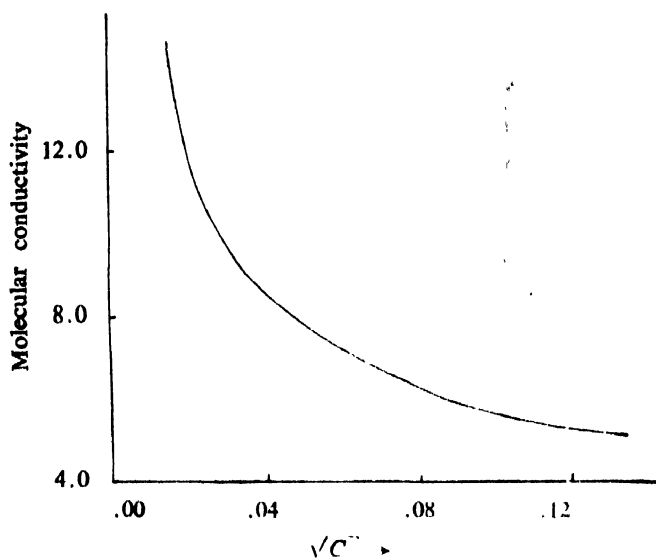


FIG. 7

Erythrosine in alcohol

TABLE VI

Cyanine in alcohol

Molecular concentration $C$	$\sqrt{C}$	Sp. conductivity	Molecular conductivity
.02324	.152	.0003845	165.5
.00581	.076	.0001236	211.7
.002905	.054	.00007532	259.2
.001452	.038	.00004055	278.9
.000242	.016	.000009406	388.6

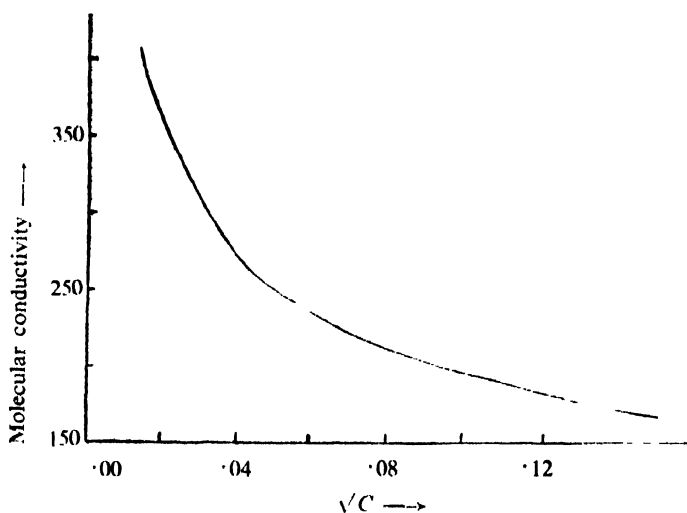


FIG. 8  
Cyanine in alcohol

## DISCUSSION OF THE RESULTS

It appears from the tables and graphs that the molecular conductivities of dyestuffs in aqueous solution do not have linear relation with square root of concentration. The molecular conductivities, when plotted against square root of concentration, give curves in most of the cases similar to those obtained by Howell and Robinson (1936). Howell and Robinson have worked on the electrical conductivities of aqueous solutions of sodium dodecyl sulphate and sodium hexadecyl sulphate and have found that the curves of the electrical conductivity against the square root of the concentration consist of three well defined sections. Over the first range the fall in conductivity is linear as for a simple electrolyte and is of the same order of magnitude. At the point where the first range is abruptly succeeded by the second it is shown that the mean free path of the anion is proportional to its rotational volume. Over the second range the fall in conductivity is extremely rapid. The anionic network postulated offers a satisfactory explanation and is in accordance with other properties observed over this range. At the point where the second range is succeeded by the third it is shown that the distance between the anions in the network is proportional to their length. In any homologous series the tendency to form micelle is proportional to the length of the anion. This is the point, therefore, at which the network falls into micelle formation. In our observations the curves that have been drawn are similar to the second and third regions of the curves found by Howell and Robinson. In most of the cases the fall in conductivity is extremely rapid and is followed by a region where the conductivity either rises to maximum or remains practically constant. At the point where the second range is succeeded by the third the network falls into micelle formation.

In the alcoholic solution also there is no perfect linear relationship between the molecular conductivity and square root of concentration and the conductivity-

concentration curves are similar to those for aqueous solution. The difference in the behaviour of dyestuffs in these two solvents may be due to different degree of aggregation of ions. It has been shown by Mitra that quenching co-efficients of dyestuffs in alcoholic solution are distinctly less than in aqueous solution which also supplies evidence as to the low association in alcoholic-solution.

It is interesting to note that the critical concentration at which the network falls into ionic micelles fairly coincides with the concentration after which rapid quenching of fluorescence begins. It, therefore, supports the view that the quenching of fluorescence is due to the formation of ionic micelles.

*Influence of foreign substances on the conductivity of the dyestuffs:* It is well known that the addition of small quantities of a foreign substance to a fluorescent solution causes a quenching of its fluorescent radiation with a simultaneous diminution of its efficiency. This phenomenon of the quenching of the fluorescence of the dye solution has been investigated by a number of workers and some of them are at present inclined to the view that the quenching effect is due to the deactivation of the excited molecule with a molecule of the foreign substance through collision of the second kind. The principal argument in the favour of this physical interpretation of the quenching effect is the increase of polarisation by quenching, which was first observed by Mitra in the case of dyestuffs.

In our present investigations we have also investigated the influence of the foreign molecule or ions on the conductivity of the fluorescent compounds in solution. The results of our measurements are shown in the following tables.

TABLE VII

Eosin and Potassium Iodide

0.1597 gms of eosin was taken in 35 c.c. of water and that corresponds to 1/4 C solution. 30 c.c. of the solution was taken in the conductivity cell.

Vol. in cc. of N-KI soln. added	Strength of KI solution in the mixt.	Sp. conduct. of the KI solution $K_1$	Strength of eosin soln. in the mixt.	Sp. cond. of the eosin soln. $K_2$	$K_1 \mid K_2$	Observed sp. conductivity.
0	0	0	C	.001444	.001444	.001444
.5	1/61 N	.002611	1/4.075C	.001440	.004051	.004084
1.0	1/31 N	.005021	1/4.12C	.001396	.006417	.006542
2.0	1/16 N	.009376	1/4.26C	.001350	.010726	.01062
4.0	1/8.5 N	.01713	1/4.53C	.001265	.018395	.01847
8.0	1/4.75 N	.02989	1/5.07C	.001119	.031009	.03028
12.0	1/3.5 N	.03868	1/5.6C	.001000	.03968	.04055

TABLE VIII

## Erythrosin and Potassium iodide

.3499 gms. of erythrosin was taken in 50 c.c. of water and that corresponds to 1/16C solution. 30 c.c. of the solution was taken in the conductivity cell.

Volume in c.c. of N-KI soln. added	Strength of KI solution in the mixt.	Sp. conduct. of KI soln. $K_1$	Strength of erythrosin soln. in the mixture	Sp. conduct. of erythrosin soln. $K_2$	$K_1 : K_2$	Observed sp. conductivity
0	0	0	C/16	.005540	.005540	.005540
.5	1/61 N	.002611	C/16.3	.005461	.008072	.008035
1.0	1/31 N	.005021	C/16.48	.005406	.01043	.01026
2.0	1/16 N	.009376	C/17.04	.005226	.01460	.01423
4.0	1/8.5 N	.01713	C/18.12	.004639	.02176	.02047
8.0	1/4.75 N	.02989	C/20.28	.004072	.03396	.03160
12.0	1/3.5 N	.03868	C/22.4	.003658	.04233	.04083

It will be seen from the tables that the conductivity of the solution is very nearly equal to the sum of the individual conductivities of the dyes and potassium iodide in solution. This shows that no new molecules are formed due to the gradual addition of potassium iodide and that the collision of the second kind is the major cause of quenching by foreign neutral salts. Our measurements are in agreement with those of Mitra and others.

## ACKNOWLEDGMENTS

In conclusion the authors express their gratitude to Dr. S. M. Mitra for his kind guidance and to Prof. H. P. Mukherjee for his kind interest in the work.

## REFERENCES

- Banow, 1929, *Zeit. f. Phys.*, **58**, 811.  
 " , 1930, *Zeit. f. Phys.*, **64**, 121.  
 " , 1933, *Zeit. Phys. Chem.*, **153A**, 172.  
 Bouchard, 1936, *J. d. Chim. Phys.* **33**, 50 and 232.  
 Chaudhuri, K. D., 1948, *Ind. J. Phys.*, **22**, 1.  
 Howell and Robinson, 1936, *Proc. Roy. Soc.* **155**, 386.  
 Lewschin, 1927, *Zeit. f. Phys.*, **43**, 230.  
 McBain, 1913, *Trans. Farad. Soc.*, **9**, 99.  
 Mitra, S. M., 1938, Dissertation for D. Sc. degree of the Dacca University  
 Mukherji, H., 1930, *Zeit. f. Phys.*, **64**, 286.  
 " , 1931, *Zeit. f. Phys.*, **67**, 702.  
 " , 1938, *Ind. J. Phys.*, **12**, 195.  
 Robinson and Molliet, 1934, *Proc. Roy. Soc.*, **143A**, 630.  
 Svesnikov, 1935, *Acta Phys Chim, U.R.S.S.*, **3**, 257.  
 " , 1936, *Acta Phys Chim, U.R.S.S.*, **4**, 453.  
 " , 1937, *Acta Phys Chim, U.R.S.S.*, **7**, 755.  
 Wawilow and Frank, 1931, *Zeit. f. Phys.* **60**, 100.



# EFFECTS OF THE VARIATIONS OF RECOMBINATION COEFFICIENT AND SCALE HEIGHT ON THE STRUCTURES OF THE IONIZED REGIONS

BY A. P. MITRA

INSTITUTE OF RADIO PHYSICS AND ELECTRONICS, CALCUTTA UNIVERSITY

( Received for publication, November, 29, 1951 )

**ABSTRACT.** The paper considers in detail the effects of the height gradient of the recombination coefficient and of scale height on the altitude-distribution of ionization for the ionospheric regions, D, E,  $F_1$  and  $F_2$ . The characteristics of the gradients are estimated from experimental data. General equations are derived for calculations of height distributions of electrons, taking into account the gradients of recombination coefficient and scale height. (For deriving the formulae for the D region the results of electron and ion distributions as already calculated by the author (Mitra, 1951*b*) have been utilised. For the E region the calculated distribution shows that it is not markedly different from the Chapman type of distribution. For the F-region, the gradients as noted above are found to have profound effects. It is found that a simple Chapman layer (which may be identified with the  $F_1$  region) 'bifurcates,' as it were, into two regions— $F_1$  and  $F_2$ , mainly as a result of the height gradient of the recombination coefficient. This lends support to the contemporary suggestion that the  $F_2$  region is not formed by an ionization process distinct from that for the  $F_1$  region. The effect of the scale height gradient is also estimated. While not affecting markedly the shape of the distribution curve, it makes significant contribution to the value of the ionization density. It is further found that the bifurcation effect is more pronounced under summer than under winter conditions. However, for a full explanation of the anomalous behaviour of the  $F_2$  region one has to take into account the effect of tidal motions under the influence of the geomagnetic field.

## I. INTRODUCTION

The assumption of a simple Chapman layer formed by absorption of monochromatic solar radiation in an isothermal atmosphere of constant composition has been of great help in the theoretical study of the characteristics of the ionized regions of the upper atmosphere. However, the assumption has got its limitations which make it unsuited for accurate predictions of the behaviours of the ionospheric regions. The limitations are due to the highly idealised nature of the assumptions made, namely, that (i) the absorbed radiation is monochromatic and (ii) that the temperature, the molecular weight (that is, the scale height  $H$ ) and the recombination coefficient  $\alpha$  remains constant with height. None of these assumptions holds strictly. In fact, there are regions of the ionosphere in which one or more of the above parameters diverge widely from the ideal assumption. Consider first the assumption regarding the monochromatic nature of the ionizing radiation. It is well known that the absorbed radiation is never monochromatic. However, one may reasonably assume that the band of wavelength which is absorbed for a particular process of ionization is narrow and as such may be approximately regarded as monochromatic. The assumptions regarding the constancy of temperature and recombination coefficient are, however, quite at variance with observed facts. Various indirect upper atmospheric observations, as also direct measure-

ments by high-flying rockets show that there are large temperature gradients in the upper atmosphere at the heights where the ionospheric regions are formed. Again, the ionospheric region E is formed round the height where  $O_2$  concentration changes rapidly with height due to dissociation. As such, calculations on the altitude distributions of ionization for the E layer is hardly justifiable without taking these factors into account. Further, it is known that the value of the recombination coefficient  $\alpha$  depends strongly on temperature and pressure. It is thus imperative to take account of these factors in estimating the height-ionization distributions of the ionized regions.

Amongst the attempts made in recent years to calculate the height-ionization distributions by taking account of the variabilities of the parameters listed above the following may be mentioned. Mitra (1951*b*) has considered the variations of temperature and recombination coefficient with height for the D layer, Pfister (1950) for the E layer, and Bates and Massey (1946) and later Bates (1949) have considered the effect of a variable recombination coefficient on the F-layers. Mention may also be made of the work of Gledhill and Szendrei (1950) who considered mathematically the effect of a linear temperature gradient on an otherwise Chapman layer and of Nicolet (1950) who considered the effects of both recombination coefficient and temperature on a layer produced by a band of solar ultraviolet radiation. These works have materially advanced our concept of the ionospheric layers; but in most cases they are not satisfactorily complete. In the present paper an attempt has, therefore, been made, firstly, to derive general formulae for calculating the height distribution of ionization taking into account the possible variabilities of  $H$  (that is, temperature and molecular composition) and of  $\alpha$ . Secondly, the available experimental data regarding the nature of variations of the above parameters with height are collected and scanned. Finally, with the help of the formulae and the collected data, the height-ionization distributions of the D, E,  $F_1$  and  $F_2$  regions are calculated.

## 2. BASIC FORMULAE

Before deriving the equations to be used in the calculation, it will be convenient to list the formation characteristics of the Chapman layer.

(i) *Chapman layer— $H$  and  $\alpha$  constant* (Chapman, 1931): We consider an isothermal atmosphere traversed by monochromatic solar radiation. The particle concentration is given by the exponential law:  $n = n_0 \exp(-h/H)$ , where  $h$  is the height measured from a datum level, and  $H$  is the scale height. The rate of electron production is given by

$$q = An_0Q \exp(-n_0AH_0 \sec \chi e^{-h/H}), \quad \dots (1)$$

where  $A$  = absorption cross-section of the active atmospheric constituent,

$$H_0 = \frac{kT}{mg} = \text{scale height,}$$

$\chi$  = solar zenith angle,

$h$  = height measured from a datum level where the particle concentration is  $n_0$ .  $q$  has a maximum  $q_m$  given by

$$q_m = q_0 \cos \chi, \quad \dots (2)$$

at the height  $h_m$  or  $z_m$  [ $= (h_m - h_o)/H_o$ ] given respectively by

$$h_m = H \log n_o A H_o \sec \chi, \quad \dots (3)$$

$$z_m = \log \sec \chi. \quad \dots (4)$$

It is to be noted that the height ( $h_m$ ) at which the rate of ion production is maximum is also the same at which the electron or ion concentration is maximum.

Another important quantity is  $n(h_m)$  the particle concentration at the height of maximum ion production and is given by

$$n(h_m) = \cos \chi / (A H_o). \quad \dots (5)$$

(ii)  $H$  (scale height) varying with height : We consider how the Chapman formulae will be modified if  $H$  varies linearly with altitude, i.e.,

$$H = H_o + ah,$$

where  $H_o$  is the value of the scale height at the datum level, and  $a$  is the gradient of scale height. For such an atmosphere the height variation of particle concentration  $n$  is no longer given by the exponential law, but by

$$n = n_o (1 + Bh)^{-(1+1/a)}$$

where

$$B = a/H_o$$

Eqns. (1), (2), (3) and (5) are now replaced by

$$q = A n_o Q (1 + Bh)^{-(1+1/a)} \exp [ n_o A H_o \sec \chi (1 + Bh)^{1/a} ] \quad \dots (6)$$

$$q_m = q_o (\cos \chi)^{1+a} \quad \dots (7)$$

$$h_m = H_o \left[ -\frac{1}{a} + \frac{1}{a} (A n_o H_o \sec \chi)^a \right] \quad \dots (8)$$

$$n(h_m) = \frac{\cos \chi (1+a)}{A H_o} \quad \dots (9)$$

where  $H_m$  is the value of scale height at the height  $h_m$ .

(iii)  $\alpha$  (recombination coefficient) varying with height : We next obtain formulae for the height of maximum ionization and the value of the maximum electron concentration, taking into account the variability of the recombination coefficient in addition to the variation of scale height just considered.

We note that unlike that in the Chapman layer, the height at which the rate of ion production is maximum is *not* the same as that at which the ionization density is maximum.

We have

$$\frac{dN}{dt} = q - \alpha N^2 \quad (10)$$

where  $N$ —number density of electrons/cm<sup>3</sup>,  $\alpha$ —coefficient of recombination.

For the regions where  $\alpha$  is large  $\frac{dN}{dt} = 0$ , throughout the day, specially during

noon. For the region where  $\alpha$  is small, such as the  $F_2$  region,  $\frac{dN}{dt}$  is usually much

different from zero. Sometime after noon, however, its value decreases to zero. We thus have

$$N = (q/z)^{\frac{1}{2}} \quad \text{when} \quad \frac{dN}{dt} = 0, \quad \dots (11)$$

$$N = \left\{ \left( q - \frac{dN}{dt} \right) / z \right\}^{\frac{1}{2}} \quad \text{when} \quad \frac{dN}{dt} \neq 0. \quad \dots (11a)$$

As  $z$  depends on temperature, pressure and electron concentration (depending on the region concerned), one may put

$$z = z_0 f(N, p, T), \quad \dots (12)$$

where  $z_0$  is a constant, and  $f$  is the function giving the variation of  $z$  with one or more of the parameters : temperature, height and electron concentration.

We thus have combining Eq. (6) and (11, 11a) with Eq. (12),

$$N^2 = \frac{An_0Q}{z_0} \left[ \frac{(1+Bh)^{-(1+a)} \exp \left\{ -\frac{n_0AH_0 \sec \chi (1+Bh)^{-a}}{f} \right\}}{f} \right] \quad \text{for} \quad \frac{dN}{dt} = 0, \quad (13a)$$

$$N^2 = \frac{An_0Q}{z_0} \left[ \frac{(1+Bh)^{-(1+a)} \exp \left\{ -\frac{n_0AH_0 \sec \chi (1+Bh)^{-a}}{f} \frac{dN}{dt} \right\}}{f} \right] \quad \text{for} \quad \frac{dN}{dt} \neq 0 \quad (13b)$$

### 3. SCALE HEIGHT AND RECOMBINATION COEFFICIENT VALUES

(a) *Scale height* : The scale height (that is, the temperature) of the atmosphere below 100 Km. is known with satisfactory precision from studies on abnormal sound propagation phenomena and from the luminosity of meteor trails as also from balloons and V-2 rocket flights. A standard temperature distribution, based on the above findings, has been tentatively assumed by the National Advisory Committee for Aeronautics (NACA) (figure 1). The distribution, of course, varies with the hour of the day, the season of the year and perhaps also with the solar cycle. Nevertheless, it may be expected that there will not be large deviations from the general shape of the NACA standard variation.

The scale height above 100 Km. is, however, not known with such precision. Evidence from auroral, ionospheric and other measurements all point to the existence of a rising scale height above 100 Km., reaching a value which may be as high as 70 Km. in the  $F_2$ -region heights.

*Scale height in region E* : The most accurate measurements of scale height for this region made so far are by Pfister (1950) who took account of the effect of the terrestrial magnetic field. The values obtained by him for Washington range from 5.5 to 12 Km. Pfister's report does not specifically state the amount of seasonal variation in  $H$ , but a ratio of about 1.5 or more between summer and winter values is likely.

The above values of  $H$  are obtained on the assumption of an isothermal atmosphere; we may, therefore, consider them as representing the actual values at the base of the layer ( $H_0$ ), say at 100 Km. height. The scale height at any altitude

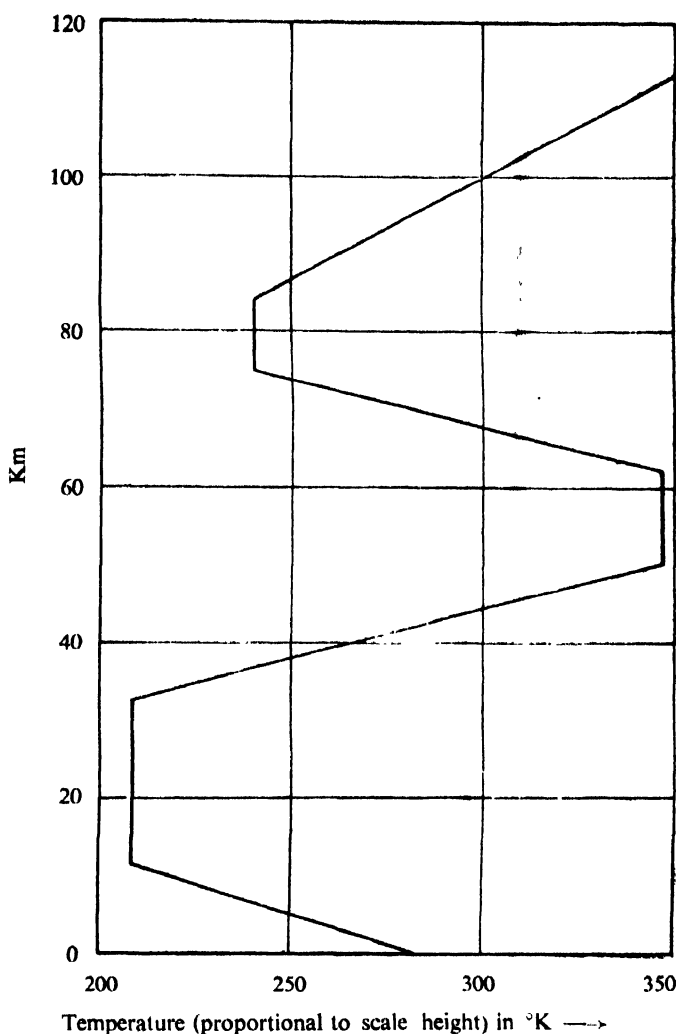


FIG. 1

Idealised temperature distribution (i.e., the scale height distribution) adopted by the National Advisory Committee for Aeronautics (NACA), U.S.A.

higher than this may be obtained if the scale height gradient  $a$  is known.  $a$  can be estimated from the diurnal variation curve for critical frequency. Thus, for an atmosphere in which the scale height increases linearly with height, the variation of critical frequency is given by (see sec. 2)

$$f = f_o (\cos \chi)^{(1+a)/4} \quad \dots (14)$$

In Table I are given (i) the values of the exponent of  $\cos \chi$  as obtained from routine ionospheric data of Washington, Kochel, Huancayo, Watheroo (Harnischmacher, 1951) and Calcutta, and (ii) the values of the scale height gradient obtained by the help of Eq. (14).

It is obvious from the table that the scale height gradient is a function of geographical latitude. But values round 0.30 in summer and 0.15 in winter may be

TABLE I

Location	Latitude	Value of exponent $(1+a)/4$		Value of $a$	
		Summer	Winter	Summer	Winter
Kochel	47.7° N	0.350	0.270	0.40	0.10
Washington	38.7° N	0.320	0.270	0.30	0.10
Watheroo	30.3° S	0.310	0.260	0.24	0.04
Calcutta	22.5° N	0.300	0.265	0.20	0.05
Huancayo	12.0° S	0.350	0.310	0.40	0.24

taken as representative values. The value of  $H$  at any height below region  $F_1$  can be easily estimated now.

*Region  $F_1$*  : Nicolet (1947) has estimated the scale height of this region as 30 Km. Bates and Massey (1946) also favour a value of the same order. Values higher than this have also been reported. Thus, Appleton and Beynon (1947) have obtained a value as high as 55 Km, while Kellog (1950) reports a value 43 Km. for equatorial latitudes. No report regarding the seasonal variation of the quantity is available, but, a summer to winter ratio as calculated from E-region-ionospheric parameters seems not unlikely.

For evaluation of the scale height gradient for this region the same method, as used for region E, can be utilised. The value obtained for middle latitude is found to be about 0.3.

*Region  $F_2$*  : Estimation of scale height for the  $F_2$  region has been made by various authors either on the basis of a parabolic layer or of higher order approximations to the Chapman type of distribution. The values quoted range from one as low as 20 Km. (Pekeris, 1940) to one as high as 186 Km. (Grace, Kelso and Miller, 1949). The normal range of the scale height is, however, from 40 to 70 Km. (Appleton, 1939; Baral and Mitra, 1950; Gerson, 1951), with a seasonal variation from about 70 Km. in summer to about 50 Km. in winter. It is clear that the scale height for this region depends on various factors, such as solar zenith angle, latitude of the place and the atmospheric height concerned.

It is important to remember that the above values of scale height are only the higher limits of the same. This is because in all these measurements, variations of recombination coefficient and temperature with height have not been taken into account. The effects of both these gradients will be to increase the thickness of the layer, so that the values cited above are too high. The ratio of winter to summer temperatures, however, will not be so much in error as the absolute values of either of these quantities.

The gradient  $a$  of scale height for this region cannot be determined as above. It is, however, possible that the gradient for this region is the same as that for region E. We, therefore, assume  $a = 0.3$ .

(b) *Recombination coefficient* : It has been shown by Bates and Massey (1946) that the value of the effective recombination coefficient may be expressed as

$$\alpha = \alpha_e + \lambda \alpha_i + \frac{1}{NT} \frac{dT}{dt} + \frac{1}{N(1 + \lambda)} \frac{d\lambda}{dt} \quad \dots (15)$$

with

$$\lambda = \beta N_n / (KN_n + \rho N + \alpha_i N^2 + q + \alpha_e N^2) \quad \dots (16)$$

where

- $\alpha_e$  —electronic recombination coefficient,
- $\lambda$  —negative ion to electron ratio,
- $\beta$  —coefficient of attachment,
- $K$  —coefficient of collisional detachment,
- $\rho$  —coefficient of photo-detachment,
- $\alpha_i$  —coefficient of mutual neutralisation.

(i) *Region D* : For the D region the important operative processes are : attachment, photo-detachment, mutual neutralisation and collisional detachment. On account of the relatively high gas densities involved, it is probable that electrons become attached to oxygen molecules mainly through the Bloch-Bradbury process. The coefficient  $\beta$  associated with this is given by  $\beta = 10^{-14} + 1.5 \times 10^{-12} p$  ( $p$ —pressure in mm.). For mutual neutralisation, a value  $10^{-8}$  cm<sup>3</sup>/sec. may be assumed (Bates and Massey, 1946). For the coefficient of collisional detachment a reasonable value is  $5 \times 10^{-16}$  cm<sup>3</sup>/sec. The photo-detachment rate is assumed to be 0.35/negative ion/sec.

It is at once seen that  $\alpha$ , under such conditions, will be given by (see also Mitra, 1951 b)

$$\left. \begin{aligned} \alpha &= \beta n \alpha_i / (Kn + \rho) \\ &= \alpha_i [n (10^{-14} + 1.5 \times 10^{-12} p)] / (Kn + \rho) \\ &= \alpha_i \lambda (h) \end{aligned} \right\} \quad \dots (17)$$

$\lambda (h)$  as given by the author in a previous paper (1951 b) is illustrated in figure 2.

(ii) *Region E* : Until recently it was believed that the recombination coefficient for the E region is constant (Appleton, Naismith and Ingram, 1937; Bates and Massey, 1946). Recent measurements by Baral and Mitra (1950) have, however, shown that the coefficient for this region is variable, though by a small amount. This view has also been confirmed by other workers (Weekes, 1950; Pfister, 1950; Mcleish, 1948). The coefficient is, in general, smaller at day-time than at night-time. Further, for a chosen hour, the summer values are, in general smaller than the winter ones. It is possible that these variations are due to variations in atmospheric temperature at the heights concerned. This is because the temperature at E region height is known to be greater in summer than in winter and greater in day than at night. A quantitative expression for this relation may also be derived by application of Eqns. (15,16) (Baral and Mitra, 1950). It is known that  $\beta$  for

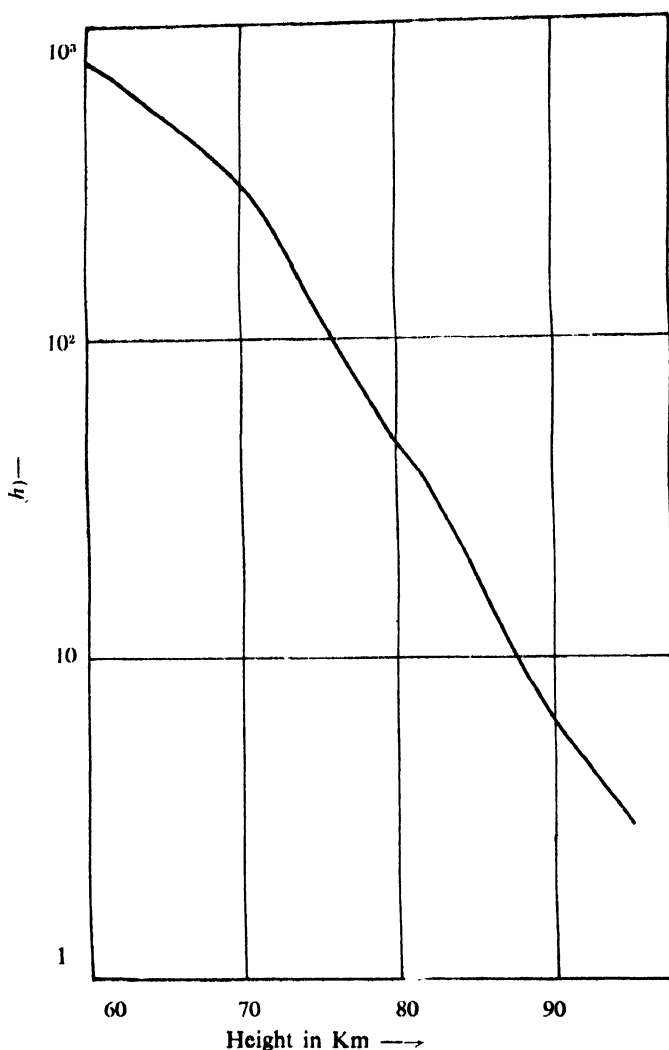


Fig. 2

The ion/electron number density ratio,  $\lambda$ , drawn as a function of height for the D-region. (After Mitra, 1951b.) The recombination coefficient  $\alpha$ , at any height is proportional to  $\lambda$ .

this region, is temperature-dependent, being  $6 \times 10^{-14}$  cm<sup>3</sup>/sec. at 250° K and  $1.5 \times 10^{-14}$  cm<sup>3</sup>/sec. at 1000° K, so that one may assume

$$\beta = \eta/T,$$

where

$$\eta = 1.5 \times 10^{-11} \text{ degree cm}^3/\text{sec.}$$

This gives from Eqn. (15),

$$\alpha_E = \eta \alpha_i / KT = \alpha_i (\eta/K) T^{-1}$$

In view of the uncertainties in the value of the exponent of  $T$ , one may write, in general,

$$\alpha_E = \alpha_i (\eta/K) T^{-r} \quad \dots (18)$$

Also since  $T_j / T_d = H_j / H_d$  ( $j$  - Northern solstice months and  $d$  - Southern solstice months) Eq. (18) may be written as



$$\frac{\alpha_j}{\alpha_d} = \left( \frac{H_d}{H_j} \right)^r \quad \dots (18a)$$

The variation of  $(H_j/H_d)$  for different values of  $r$  and for  $\alpha_d/\alpha_j = 1.5$  (as experimentally observed) is shown in Table II.

TABLE II

$r$	1	1.5	2.0
$H_j/H_d$	1.50	1.30	1.23

The actual variations of  $H_j/H_d$  observed is nearabout 1.5-2.0, so that  $r$  is in the neighbourhood of 1. Hence we can write

$$\alpha_E = \alpha_o (1 + Bh)^{-1} \quad \dots (18b)$$

(ii) *Region  $F_2$* : The variation in the value of  $\alpha$  in the  $F_1$  region is similar to that in the E region. An expression similar to that for the E region may, therefore, be assumed for the recombination coefficient:

$$\alpha_{F_1} = \alpha_o (1 + Bh)^{-1} \quad \dots (19)$$

(iv) *Region  $F_2$* : The recombination coefficients for this region are usually measured without taking account of tidal phenomena. Such measurements made at Calcutta (Baral and Mitra, 1950) showed large variations of the coefficient with height, with electron concentration and with the solar zenith angle. In view of the approximate nature of these values (due to the neglect of the tidal terms) new measurements have recently been made by Mitra (1951a) in which the tidal phenomena have been taken into account. The results obtained by him show that the values of the coefficient, even when tidal terms are considered, are subject to variations. The nature of these variations is similar to that obtained above. The values of  $\alpha$  are, however, lowered, as also the amplitude of the variations; the summer value being  $1.5 \times 10^{-11}$  cm<sup>3</sup>/sec, and the winter value  $3 \times 10^{-11}$  cm<sup>3</sup>/sec.

It is now necessary to have a quantitative expression for  $\alpha$  relating it to the different variable parameters. This can be obtained by utilising Eq. (15, 16). We readily get, when proper approximations are made,

$$\begin{aligned} \alpha_{F_2} = \eta n / TN &= \frac{\eta n_o}{T_o N_e} (1 + Bh)^{-\left(2 + \frac{1}{a}\right)} \\ &= \frac{\gamma_c}{N_e} (1 + Bh)^{-\left(2 + \frac{1}{a}\right)} \end{aligned} \quad (20)$$

It is probable that this equation is in error by a large amount; in particular the exponent of  $(1 + Bh)$  appears to be much too large. For instance, with  $\frac{1}{a} = 3$ , the

factor  $(1 + Bh)^{-\left(2 + \frac{1}{a}\right)}$  decreases to more than  $\frac{1}{10}$ -th of its value at 100 Km.

We therefore write

$$\alpha_{1/2} = \frac{\gamma_0}{N_0} (1+Bh)^{-g} \quad \dots (20a),$$

where the value of  $g$  is in the neighbourhood of 5 in order to make the variations in  $\gamma_0 (1+Bh)^{-g}$  conform to experimental observations.

#### 4. STRUCTURE OF THE D REGION

It is now generally accepted that D region is produced by ionization of  $O_2$  at the first ionization potential (12.2 eV) as first suggested by Mitra, Bhar and Ghosh (1938)\*. Calculations, based on this hypothesis, of the values of the electron concentration and of the scale height at various altitudes in this region have recently been made by the present author (Mitra, 1951b). The very close agreement between the calculated and the experimental values (Table III) provides convincing proof of the correctness of the hypothesis.

TABLE III

Electron concentrations (cm <sup>-3</sup> ) at				Scale height (Km) for					
60 Km		90 Km		16 Kc/s		43 Kc/s		113 Kc/s	
Exptl.	Theor.	Exptl.	Theor.	Exptl.	Theor.	Exptl.	Theor.	Exptl.	Theor.
$2.5 \times 10^3$	$2.6 \times 10^3$	$1.5 \times 10^4$	$2 \times 10^4$	$5.5 \pm .1$	5.5	$4.8 \pm .1$	4.6	$2.8 \pm .1$	2.6

It is to be noted that calculations for the height-ionization distribution are rendered difficult and laborious by the fact that the scale height  $H(=kT/mg)$  and the recombination coefficient ( $\alpha$ ) are not only *not* constant with height, but vary non-uniformly. However, one may assume that the D-ionization is comprised within the heights 30-100 Km. and divide up the region into five separate parts (Table IV) as per figure 1. The calculations may then be carried out separately for each of these five parts. This has been done by the author (and, with the assumption that the effective ionization process is photo-ionization of  $O_2$  at its first ionization potential) and the height-ionization distribution of electrons and ions for the entire D region obtained. The results are depicted in figures 3 and 4. The following points may be noted in the characteristics of the curves in this figure.

(i) As the ion-electron number density ratio is very high (about  $10^8$  times the number of electrons at a height of 60 Km.), the ions, notwithstanding their

\*The photo-ionization of sodium (Jouast and Vassy, 1941; Vassy and Vassy, 1942) is also sometimes suggested. It has a very low ionization rate, and, as will be shown by the present author in a later paper, is more likely to cause the irregularly occurring region called sporadic D rather than the regular D layer.

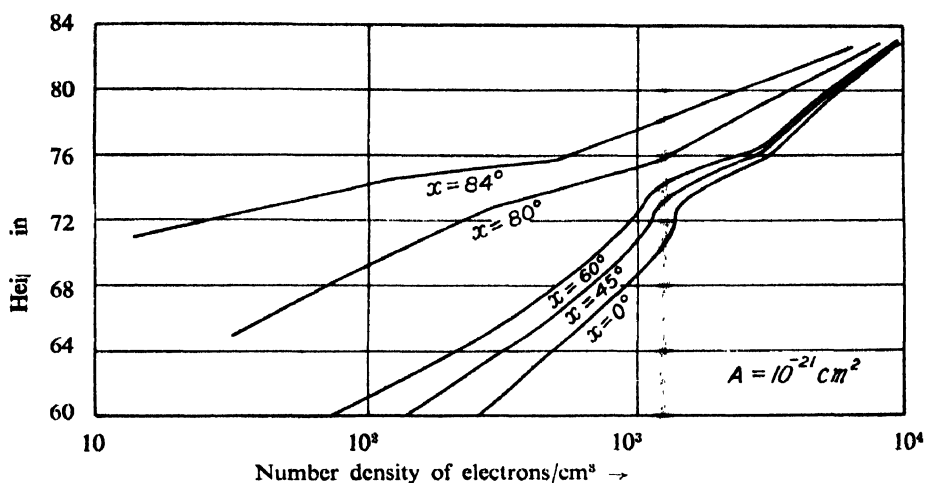


FIG. 3

Altitude distribution of electron concentration for the D region for  $A = 10^{-21} \text{ cm}^2$  on the assumption that the effective ionization process is the photo-ionization of  $\text{O}_2$  at the first ionization potential. The variation with solar zenith angle,  $\chi$ , is shown by drawing five separate distributions for five different values of  $\chi$ , namely  $\chi = 0^\circ$ ,  $45^\circ$ ,  $60^\circ$ ,  $80^\circ$ , and  $84^\circ$ .

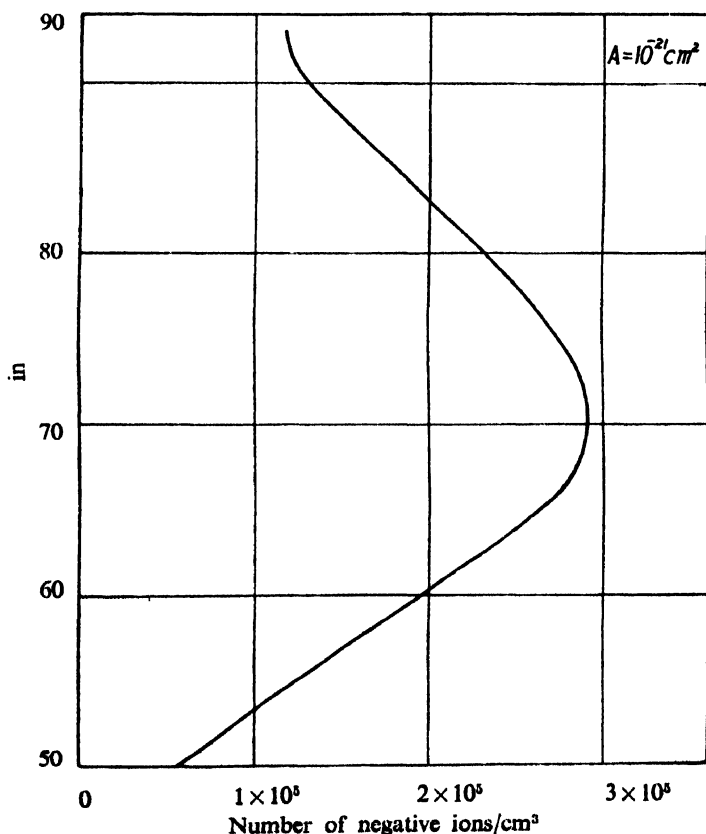


FIG. 4

Altitude distribution of negative ion concentration for the D region at the first ionization potential of  $\text{O}_2$  for  $A = 10^{-21} \text{ cm}^2$ .

low mobility, will play the dominating role (in contrast to that in the higher ionospheric regions) in radio wave propagation specially of long and very-long waves.

TABLE IV

Region	Range (Km)	Temperature ( $T_0$ ) at reference level ( $^{\circ}\text{K}$ )	Temperature gradient ( $\gamma$ ) ( $^{\circ}\text{K/Km}$ )	$n_0$ ( $\text{cm}^{-3}$ )
I	32-50	220 <sup>o</sup>	9.2	$5 \times 10^{18}$
II	50-63	350 <sup>o</sup>	0.0	$4 \times 10^{15}$
III	63-76	350 <sup>o</sup>	-10.4	$1.5 \times 10^{15}$
IV	76-83	240 <sup>o</sup>	0.0	$3.5 \times 10^{14}$
V	83-100	240 <sup>o</sup>	4.5	$1.4 \times 10^{14}$

(ii) The shape of the height-ionization distribution curves (specially for electrons) is totally different from that of the Chapman distribution. While the distribution for ions still maintains some similarity with the Chapman distribution, that for electrons is entirely different. The latter has no well-defined maximum but rises monotonously to a value of about  $10^4/\text{cm}^3$ , and merges with the tail of the E region. (If a very small value for  $A$  is assumed, then there is a slight dip in the distribution curve just below the E region.)

(iii) The changes in the distribution curve with the variation of  $\chi$  (solar zenith angle) is significant. With the decrease of  $\chi$ , the distribution curve as a whole moves up and undergoes changes in shape. A special feature, when the value assumed for  $A$  is very low, is the sudden increase of the ionization gradient from 73 to 76 Km. This occurs for all values of  $\chi$ , the gradient being sharpest for  $\chi = 0^{\circ}$ , and decreasing with the increase in the value of  $\chi$ .

It is possible to represent the above characteristics with simple equations, suitable for numerical calculations, if, as a first approximation, the small irregularities in the curves are ignored.

Taking first the case of electron distribution, we note from inspection of figures 3 and 4 that the distribution curve for a given value of  $\chi$  is composed of four distinct sections, each section being exponential in shape. These sections are : (1) 60\* to 71 Km., (2) 71 to 73 Km., (3) 73 to 76 Km., and (4) above 76 Km.

Now, let  $N_r$  represent the value of the electron concentration at any height  $h_r$  in the section  $r$ , and  $N_{r0}$  be the value of the same at the lower limit of the section concerned. Then for any of these sections we can write

$$N_r = N_{r0} (\cos \chi)^p \exp [a_{r0} (\sec \chi)^{nr} (h_r - x_r)] \quad \dots (21)$$

where  $r = 1, 2, 3, 4$  and  $x_1 = 60 \text{ Km.}$ ,  $x_2 = 71 \text{ Km.}$ ,  $x_3 = 73 \text{ Km.}$  and  $x_4 = 74 \text{ Km.}$

\*The base of the layer may lie even below 60 Km., specially for lower values of  $A$ ; but, for the present purpose we may neglect such ionizations at the very low levels.

The values of the parameters involved in the equations are given in Table V.

TABLE V

Region $r$	Range in Km.	$p$	$a_{r0}$	$n_r$
1	60-71 ( $h_1$ )	2	0.15	0.60
2	71-73 ( $h_2$ )	0	0.04	2.00
3	73-76 ( $h_3$ )	0	0.28	0.28
4	76- ( $h_4$ )	0	0.18	0.20

For the distribution of ions more exact expressions are possible, specially for the lower heights 60 to 80 Km. which are of importance to long wave propagation. Since the negative ion to electron number density ratio is  $\lambda$ , the concentration of negative ions is given by

$$N_i = \lambda \sqrt{q / [\alpha(1 + \lambda)]} \quad \dots (22)$$

At the lower heights (60-80 Km.),  $\lambda \gg 1$ . Hence

$$N_i = \left( \frac{q}{\alpha_i} \right)^{\frac{1}{2}}, \quad (23)$$

which is a very convenient expression.

The ionic distribution is thus not affected by variations of recombination coefficient, and is only sensitive to variations in temperature.

## 5. STRUCTURE OF THE E REGION

According to current ideas the E region is formed by ionization of  $O_2$  round the height of dissociation transition  $O_2 \rightarrow O + O$ . A strong point in favour of this hypothesis is that the measured heights of the E-peak ( $\approx 100$  Km.) lie close to the calculated height of the transition region. However, there has been some difference of opinion regarding the exact location of the E region with reference to the transition region.

According to Penndorf (1949) the E region is formed *above* the transition level. But recent work of Moses and Ta-You Wu (1951) seems to indicate that it may be *inside* the transition level. In the first case the concentration of  $O_2$  molecules drops with height more slowly than in the second case. However, we may write generally for the concentration ( $n$ ) of the active particles ( $O_2$ -molecules) at any height within the dissociation transition range as

$$n = n_0 (1 + Bh)^{-\left(1 + \frac{b}{a}\right)},$$

where the new term takes account of the effect of the additional drop in the number-density because of dissociation. Its value may be greater or less than 1.

For the region under consideration  $\alpha$  is a function only of temperature, and is given by  $(T/T_0)^{-1}$  where  $r$  is approximately equal to 1. Now  $T$ , is a function of height, so that, assuming the linear rise of  $T$  we write,

$$T = T_0 (1 + Bh).$$

Hence, combining Eqn. (13) of sec. (2) with the above relation, we have

$$N^2 = \frac{An_0 Q}{\alpha_n} (1 + Bh)^r \left(1 + \frac{b}{a}\right) \exp \left\{ \frac{-n_0 A H_0 \sec \chi}{r - (1 + b/a)} (1 + Bh)^{-\frac{b}{a}} \right\}$$

$$= N_0^2 (1 + P)^r \left(1 + \frac{b}{a}\right) \exp \left[ \left\{ 1 + \frac{a}{b} (1 - r) \right\} \left\{ 1 - (1 + P)^{-b/a} \sec \chi \right\} \right] \quad (24)$$

where we have put  $P = \frac{B(h - h_{mo})}{1 + Bh_{mo}}$ ,

$h_{mo}$  being the height at which the electron concentration is maximum, and is given by

$$(1 + Bh_{mo})^{-\frac{b}{a}} = [1 + \frac{a}{b} (1 - r)] / (n_0 A H_0 \sec \chi).$$

But as  $r \rightarrow 1$ , Eq. (24) may be written as

$$\frac{N}{N_0} = (1 + P)^{-\frac{b}{2a}} \exp \frac{1}{2} [1 - (1 + P)^{-\frac{b}{a}} \sec \chi] \quad (25)$$

The equation is further simplified if account is taken of the fact that for E region conditions  $a(h - h_{mo}) \ll H_0$ . Hence,

$$\frac{N}{N_0} = \left[ 1 - \frac{bz}{2R} \right] \exp \frac{1}{2} \left[ 1 - \left( 1 - \frac{bz}{R} \right) \sec \chi \right], \quad \dots \quad (25a)$$

where  $z = (h - h_{mo})/H$  and  $R = (1 + Bh_{mo})$ .

Figure 5 gives the distributions of electron concentration for the E region as deduced from Eq. (25a) for different values of  $b$ .

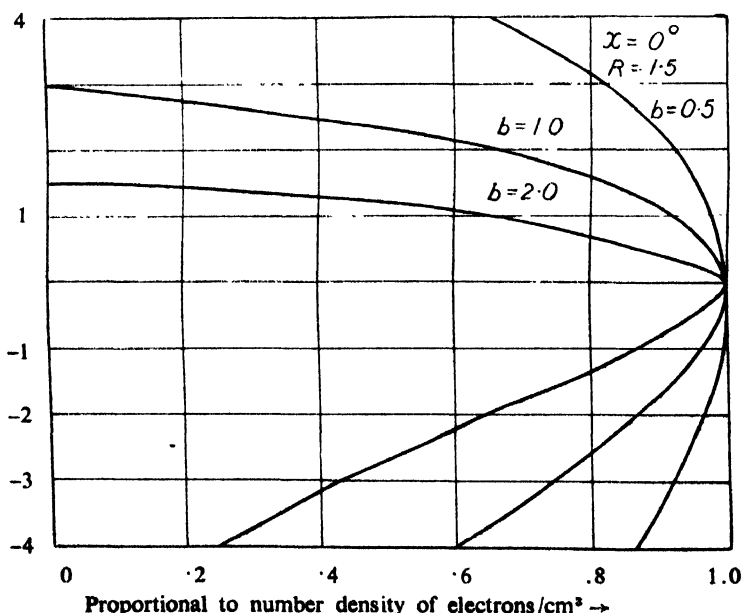


Fig. 5. Altitude distribution of electron concentration for the E-region for  $\chi = 0$  and  $R = 1.5$ .

## 6. STRUCTURES OF REGIONS $F_1$ AND $F_2$

According to earlier views, production of  $F_1$  and  $F_2$  regions was ascribed to photo-ionizations of two different atmospheric constituents at two different levels. For examples, Bhar(1938) postulated that  $F_1$  region is produced by ionization of  $N_2$  and  $F_2$  region by ionization of O. According to contemporary ideas (Bradbury, 1938; Bates 1949), however, the  $F_1$  and  $F_2$  regions form together, even in daytime, one single region produced by ionization of *only one* atmospheric constituent (atomic oxygen). This single region is "bifurcated," as it were, by the effect of the rapid decrease of the recombination coefficient with height, and thus appears as two separate regions of ionization. The quantitative analysis of the effects of decrease of recombination coefficient and of increase of scale height with height, and of the height distribution of electrons in the composite  $F_1$  and  $F_2$  regions that is to follow will show that the above hypothesis is fully justified. It is to be noted, however, that according to some authors (Martyn, 1948), the effect of tidal forces on the movement of electrons and ions in these regions (under the influence of the geomagnetic field) will also contribute to the bifurcation effects. This aspect of the problem has also been studied by the author of this note. Preliminary analyses show that the bifurcation effect, though present, is not large. The subject will be discussed fully in a separate communication.

We shall now, first consider the effect of the recombination coefficient decreasing with height regarding the scale height to remain constant. The more general case, where both the recombination coefficient and the scale height vary with altitude, will be considered next. This procedure will enable one to assess properly the relative contributions of the two variations to the bifurcating process.

(a) *Height distribution of electrons in the composite F-region when the recombination coefficient ( $\alpha$ ) decreases with altitude (scale height  $H$  is constant).*

For the isothermal atmosphere under consideration  $\alpha$  is sensibly constant in the  $F_1$  region. But, from a height  $z_0$  (which may be regarded as the boundary between the  $F_1$  and the  $F_2$  regions), above  $h_0$ , the recombination coefficient decreases rapidly with height. The actual value of  $z_0$  is a matter of guesswork. It cannot be very small (compared to the scale height)—for otherwise the  $F_1$ -peak would rise above  $z_0$  in winter months, and would consequently diverge widely from Chapman laws. This does not happen. The value of  $z_0$  cannot be very large either, for we know that the  $F_2$ -region conditions begin from only a little distance above  $h_0$ . The height  $z_0$  may thus be taken to be round 30 Km. ( $\approx H_0/2$ ).

We first consider the case of the steady state, that is, when  $\frac{dN}{dt} = 0$ . This is a highly idealized state, and exists only at height  $z_0$  and even then round noon-time only. Calculations of the altitude-distribution of the electrons ( $N/N_0$ ) will be carried out separately for the two regions, below  $z_0$  and above  $z_0$ , because, as already emphasised, the nature and magnitude of the recombination coefficient gradient are different for the two regions.

(i)  $(N/N_0)_0$  for heights below  $z_0$ :  $(N/N_0)_0$  for heights below  $z_0$  is given by Chapman's equation (Sec. 2), namely,

$$\left(\frac{N}{N_0}\right)_s = \exp \frac{1}{2} (1 - z - e^{-z} \sec \chi),$$

the height of maximum ionization being given by

$$z_m = \log \sec \chi$$

(The subscript  $s$  in the ratio of ionizations denotes the value for the steady state.)

(ii)  $(N/N_0)_s$  for heights above  $z_0$ : For heights above  $z_0$  one may write

$$\nu = \gamma/N_0$$

where  $\nu$  is a function of height. Let  $\nu = \nu_0 f(z)$ .

$$\text{Then } \left(\frac{N}{N_0}\right)_s = \frac{q_0}{\nu_0} f^{-1}(z) \cdot \exp [1 - z - e^{-z} \sec \chi]. \quad \dots (26)$$

The maximum electron concentration is

$$N_{mF_2} = \frac{q_0}{\gamma(z_{mF_2})} \exp [-z_{mF_2} - f'(z_{mF_2})/f(z_{mF_2})]. \quad \dots (27)$$

At the height  $z_m$  given by

$$e^{-z_{mF_2} \sec \chi} - 1 = f^{-1}(z_{mF_2})/f'(z_{mF_2}). \quad \dots (28)$$

Since  $H$  is constant,  $f(z)$  may be written as  $f(z) = \exp [-p(z - z_0)]$  (see Sec.3).

Further,  $\nu_0$  and  $\alpha$  are related by the equation

$$\alpha = \nu_0/N_{z_0}$$

We now have the following equations for the composite F-region consisting of  $F_1$  and  $F_2$  region:

$$\left(\frac{N}{N_0}\right)_s = \exp \frac{1}{2} (1 - z - e^{-z} \sec \chi) \text{ for } z < z_0$$

$$\left(\frac{N}{N_0}\right)_s = \left(\frac{N_0}{N_{z_0}}\right) e^{-pz_0} \exp [1 + (p-1)z - e^{-z} \sec \chi] \left. \vphantom{\left(\frac{N}{N_0}\right)_s} \right\} \text{ for } z > z_0 \quad (29)$$

In figure 6 the distributions of electrons, for a given ionization process, as calculated from the above two equations are plotted. Two values of  $p$  are chosen:  $p = 0.9$  and  $p = 1.5$ . For each of these values two separate curves are drawn representing the distributions for summer time and winter time conditions (i.e., for  $\chi = 0^\circ$  and  $\chi = 45^\circ$  respectively).

Even in this simple case, several interesting deviations from the Chapman distribution may be noticed. These are as follows:

(1) For values of  $p$  less than 1 the ionized region splits up at the top giving rise to a second maximum above the normal one. The lower normal maximum occurs, for the isothermal case considered, at exactly the same height as that of the maximum ion production rate, and is evidently the  $F_1$ -peak. The upper maximum, situated at a distance of  $z_{mF_2} = 2.3$  for  $\chi = 0^\circ$  and of  $z_{mF_2} = 2.6$  for  $\chi = 45^\circ$  is the peak of  $F_2$  region. A single ionization process has thus given rise to both the  $F_1$  and  $F_2$  regions. The splitting up of the region at its top portion we may call *bifurcation*.



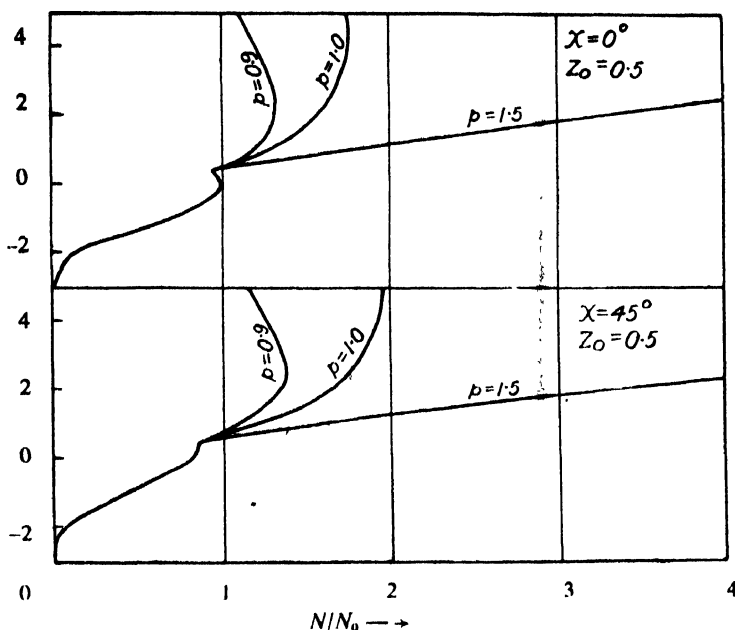


FIG. 6

Altitude distribution of electron concentration in the F-region on the assumption that  $dN/dt = 0$ , when the recombination coefficient decreases exponentially with height and scale height is constant. Both summer and winter time distributions are given, and  $z_0$  is assumed to be 0.5 in both seasons. For each season three different gradients of recombination coefficient (viz.,  $p = 0.9$ ,  $p = 1.0$  and  $p = 1.5$ ) are chosen.

(2) For values of  $p$  equal to or greater than 1, no well-defined second maximum exists. The electron concentration for such values of  $p$  decreases only slightly above the  $F_1$ -peak, and then increases monotonously upwards.

(3) The electron concentration at the second maximum (for the values of  $p$  for which it exists) increases as the value of  $p$  increases. For  $p$  equal to 0.9, the ratio ( $N_m F_2 / N_m F_1$ ) is 1.34 in summer and 1.39 in winter.

(4) The height of the second maximum is given by

$$Z_m F_2 = \log_e [\sec \chi / (1-p)] \quad \dots (30)$$

This gives for  $p = 0.9$ ,  $z_m F_2 = 2.3$  and 2.6, for  $\chi = 0^\circ$  and  $\chi = 45^\circ$  respectively. Remembering that the value of the scale height is 70 Km. in summer and 50 Km. in winter, we obtain

$$(h_m F_2 - h_0)_{\chi = 0^\circ} = 160 \text{ Km.}$$

$$(h_m F_2 - h_0)_{\chi = 45^\circ} = 130 \text{ Km.}$$

The  $F_1$ -peak is exactly at  $h_0$  for  $\chi = 0^\circ$  and 17 Km. above  $h_0$  for  $\chi = 45^\circ$ , so that the separation between the  $F_1$  maximum and the second, that is the  $F_2$  maximum is 160 Km. for  $\chi = 0^\circ$  and 113 Km. for  $\chi = 45^\circ$ .

The above calculations have all been made on the assumption of a steady state i.e.  $dN/dt = 0$ . Such an assumption is not strictly valid for the regions where the recombination coefficient is small, e.g. near the  $F_2$  region. Since  $dN/dt$  has the dimension of  $q$  and is subtracted from it, the actual value of  $(N/N_0)$  at heights where  $dN/dt \neq 0$  even during noontime, will be less than that obtained for the steady state.

It is thus generally seen that there will be well-defined upper maximum even for  $p > 1$ , contrary to the monotonous increase depicted in figure 6 for such cases.

Computation of the ionization distribution from Eq. (10) is necessarily elaborate and laborious. Such elaborate computations are not merited at this stage. We therefore use, instead, a very simple, albeit rough, method of evaluating  $(N/N_0)$ .

We have, combining Eqns. (10) and (29)

$$\frac{N}{N_0} = \left( \frac{N}{N_0} \right)_s - \left[ \left( \frac{dN}{dt} \right) / \gamma_0 N_0 \right] \exp [p(z - z_0)] \quad \dots (31)$$

$dN/dt$  will evidently be a function of height. If  $(N/N_0)$  were given by Eqn. (29) then, roughly,

$$\frac{dN}{dt} = lN,$$

where  $l$  is a constant. Eqn. (31) then becomes

$$N/N_0 = C \cdot (N/N_0)_s$$

where  $C$  is the correction term, being given by

$$C = [1 + l/\gamma_0 \cdot e^{p(z - z_0)}]^{-1}$$

For noon-time conditions the correction term  $C$  becomes unity at height  $z_0$  and below i.e. in the  $F_1$  region. This is possible only if  $(l/\gamma_0)$  is very small say, of the order  $10^{-2}$ .

The distribution curves of  $(N/N_0)$ , thus corrected by introduction of the factor  $C$  will represent more closely the actual distribution than only the  $(N/N_0)$  distribution. Figures 7 and 8 are drawn by assuming three different small values of  $l/\gamma_0$ , viz.,  $l/\gamma_0 = 0.05, 0.03$  and  $0.01$ . It will be noticed that a well-defined maximum now exists even for  $p > 1$ .

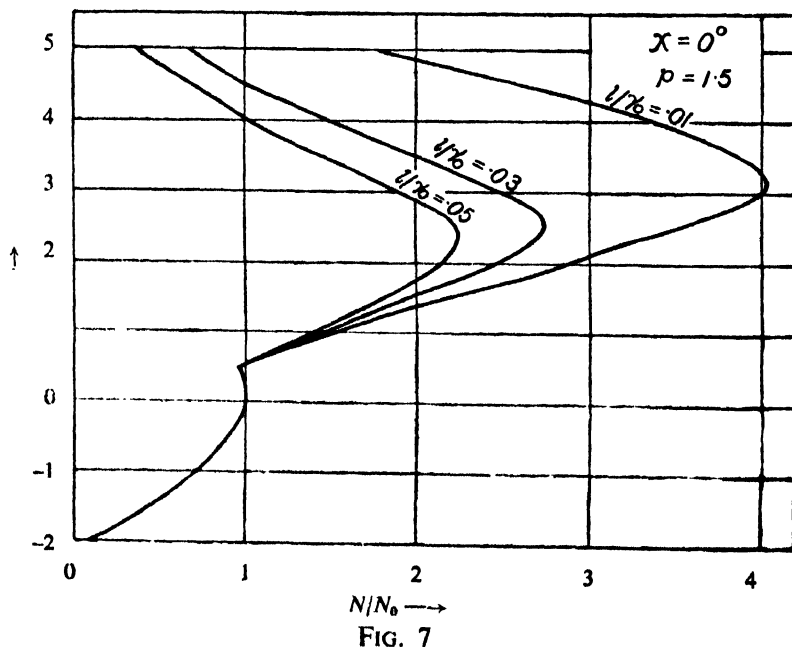


FIG. 7  
Approximate distributions of electron concentration for the F-region for  $\chi = 0^\circ$  and  $p = 1.5$  and  $dN/dt \neq 0$ , and for three different values of  $(l/\gamma_0)$ , viz., .05, .03 and .01. Compare these curves with the curve for  $\chi = 45^\circ$  in Fig. 8.

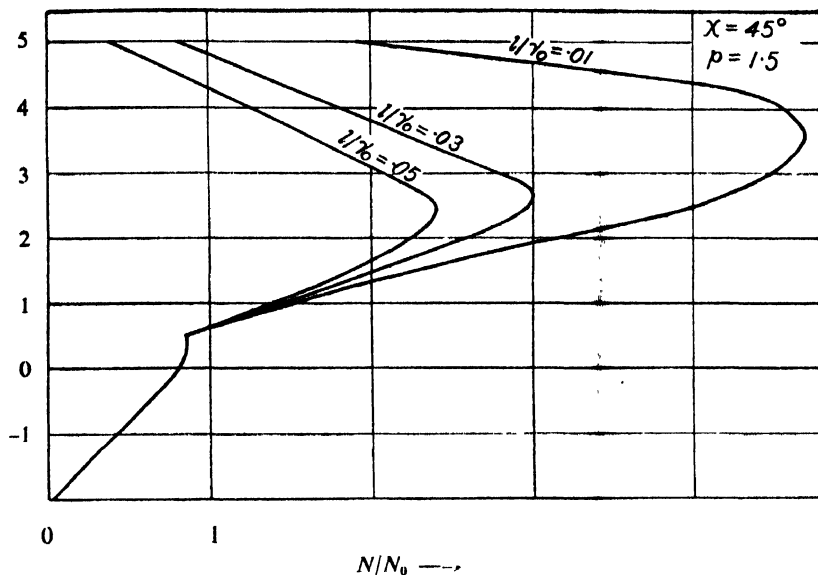


FIG. 8

Approximate distributions of electron concentration for the F-regions for  $\chi = 45^\circ$  and  $p = 1.5$  and  $dN/dt \neq 0$ , and for three different values of  $(1/\gamma_0)$ , viz., .05, .03 and .01.

(b) Height distribution of electrons in the composite F-region when the recombination coefficient ( $\alpha$ ) decreases and the scale height ( $H$ ) increases with altitude.

We now consider the more general case in which the recombination coefficient decreases with height according to Eqns. (19) and (20), and the scale height increases with altitude with a gradient of 0.3.

Let the boundary between the  $F_1$  and the  $F_2$  regions lie at a height  $b$  Km. (corresponding to the previously assumed value  $z_0$ ) above  $h_{m0}$ . In contradistinction to the isothermal case, the recombination coefficient is not constant below  $b$ , but varies slowly with height—so slowly in fact that within a height of 50 Km. the recombination coefficient falls only to 2/3 of its value. Above  $b$ , however, the coefficient decreases very rapidly. If we assume, as before, that  $b \approx 30$  Km., then  $P_b \approx 0.1$ .

We first consider the steady state, namely, when  $dN/dt = 0$ .

(i)  $(N/N_0)_s$  for heights  $h < b$ : The electron concentration for such heights is easily shown to be

$$\left(\frac{N}{N_0}\right)_s = (1+P)^{-\frac{1}{2a}} \exp. \frac{1}{2} [1 - (1+P)^{1/a} \sec \chi] \quad \dots (32)$$

(ii)  $(N/N_0)_s$  for heights  $h > b$ : As indicated in Sec. 3, the recombination coefficient for this region may be written as

$$\alpha = \frac{\gamma_0}{N_b} (1+Bh)^{-g}$$

Then, for the same ionization process as is operative for heights  $h < b$ , we have

$$N = \frac{A n_0 Q}{\gamma_0} (1+Bh)^{-(1+\frac{1}{a})} \exp [-(1+P)^{-1/a} \sec \chi].$$

Remembering that at  $h = b$ ,

$$\alpha_0(1+Bb)^{-1} = \frac{\gamma_0}{N_b} (1+Bh)^{-g},$$

we have

$$\left(\frac{N}{N_0}\right)_s = \left(\frac{N_0}{N_b}\right) \left(\frac{1+Bb}{1+Bh_{mo}}\right)^{1-g} (1+P)^{g-(1+1/a)} \times \exp [1 - (1+P)^{1/a} \sec \chi] \quad (33)$$

At  $P = P_b$ , this equation should give the same value for  $(N/N_0)_s$  as that given by Eqn. (32). Thus

$$\left(\frac{1+Bh}{1+Bh_{mo}}\right)^{1-g} = \left(\frac{N_b}{N_0}\right)^2 (1+P_b)^{1+1/a-g} \exp [(1+P)^{-1/a} \sec \chi - 1] = F(b).$$

Hence, 
$$\left(\frac{N}{N_0}\right)_s = \frac{N_0}{N_b} F(b) \cdot (1+P)^{g-(1+1/a)} \exp [1 - (1+P)^{-1/a} \sec \chi] \quad (34)$$

In figure 9 are given the height distributions of  $(N/N_0)_s$  for  $b = 0.1$  and  $g = 3.75, 4$  and  $5$ . For each case both the summer and winter time distributions ( $\chi = 0^\circ$  and  $\chi = 45^\circ$ ) are illustrated.

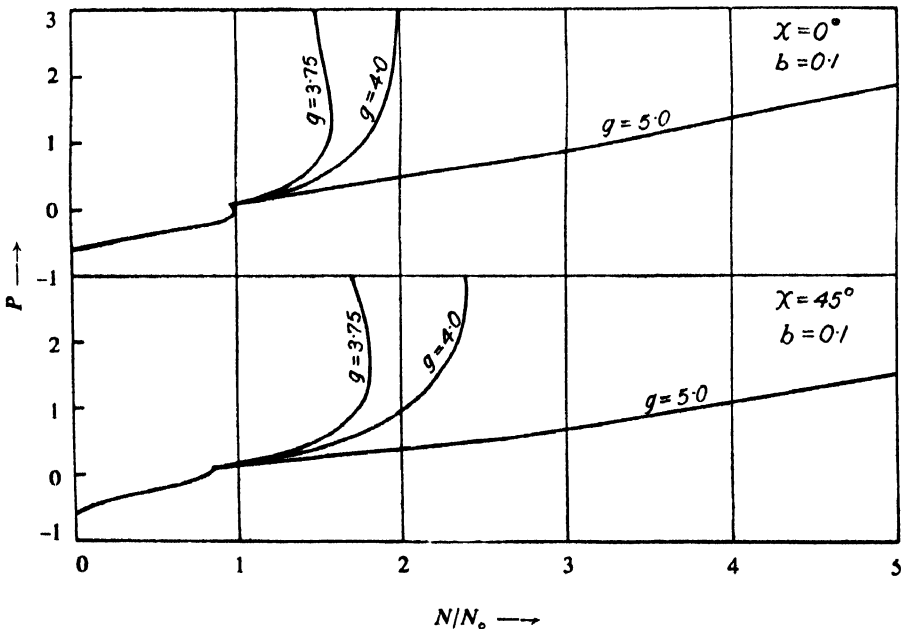


FIG. 9

Altitude distribution of electron concentration for the F-regions on the assumption that  $dN/dt = 0$ , when the recombination coefficient decreases exponentially and scale height increases linearly with height. Both winter and summer distributions are given and the boundary between the layers is assumed to be about 30 km. above  $h_0$ . For each season, three different gradients of recombination coefficient are chosen, namely,  $g = 3.75, 4.0$  and  $5.0$ .

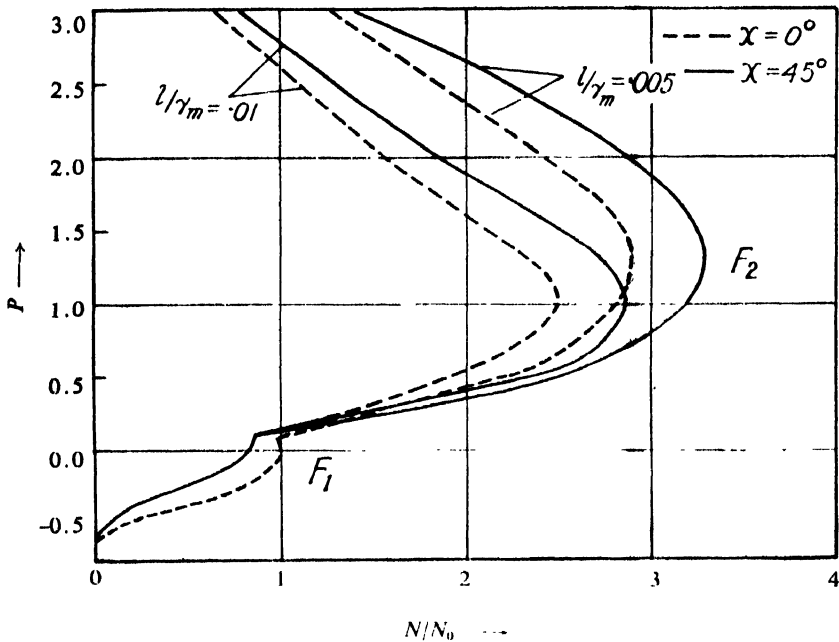


FIG. 10

Approximate distribution of the electron concentration for the F-regions when  $g = 5.0$  and  $dN/dt \neq 0$ . Curves for two different values of  $(l/\gamma_m)$ , namely, .01 and .005, and for both  $\chi = 0^\circ$  and  $\chi = 45^\circ$  are given.

We now apply corrections to take account of the fact that  $dN/dt$  is *not* zero. The procedure is similar to that before, the expression for the correction factor  $C$  being

$$C = 1 - \frac{l}{(1 + P)^g}$$

The corrected curves are given in figure 10.

It will be observed that the distribution curves for this case are of the same type as those for constant scale height. The main difference is in the ratio  $(N_{mF_2}/N_{mF_1})$  which, for similar conditions, is greater in this case than in case (i). It is concluded that the effect of a scale height gradient is only to increase the ionization of the upper maximum (i.e., the  $F_2$  layer).

(c) *Discussion of the results : The bifurcation phenomenon on :*

A glance at the curves in figures 6-10 shows that when the recombination coefficient is decreasing with height, or, when the recombination coefficient is decreasing and the scale height increasing with height, the  $F_1$  layer splits up at the top giving *two* distinct maxima, one at or near the level of maximum ion production and the other higher up. The lower region of ionization is the  $F_1$  region, the upper is the  $F_2$  region. This splitting up of the  $F_1$  region at the top is called *bifurcation*. Let us see how far the results obtained above agree with the observed facts of the bifurcation which are as follows :

(1) At night there is a single F-region. This is true for all localities. With the incidence of solar rays, the upper part of the region begins to separate out. As the solar zenith angle decreases, the lower part ( $F_1$ ) sinks downwards, while the upper part continues to move up. This results in increasing the separation

that the effect of the above mentioned gradients is least, and the distribution curve approximates to the Chapman layer. For the D region the effects of these gradients are so great that the electron distribution has no resemblance to the Chapman distribution. For the F<sub>1</sub> region the variation of recombination coefficient has this curious effect of splitting it up into two regions F<sub>1</sub> and F<sub>2</sub>. The effect of the height variation of scale height is mainly to increase the ionization of the F<sub>2</sub>-region. However, for a full explanation of the notoriously anomalous behaviour of the region effects of tidal motions under the influence of the geomagnetic field have to be considered.

#### ACKNOWLEDGMENTS

The present work forms part of the programme of the Radio Research Committee of the Council of Scientific and Industrial Research, Government of India, and the author wishes to express his thanks to the Council for financial assistance during the work.

It is a pleasure to acknowledge debts to Professor S. K. Mitra, under whose guidance the work was done, and whose kind help and attention enabled the author to finish the work within a very short time. Thanks are also due to colleague Mr. A. K. Saha who made the paper ready for the press.

#### REFERENCES

- Appleton, E. V. 1939, *Quar. Jour. Roy. Met. Soc.* **65**, 324.  
 Appleton, E. V. and Beynon, W. J. G., 1947, *Proc. Phys. Soc. B*, **59**, 58.  
 Appleton, E. V., Naismith, R., and Ingram, L. J. 1937, *Phil. Trans. Roy. Soc. A*, **236**, 191.  
 Baral, S. S. and Mitra, A. P., 1950, *J. Atmos. Terr. Phys.*, **1**, 95.  
 Bates, D. R. and Massey, H. S. W., 1946, *Proc. Roy. Soc. A*, **187**, 261.  
 Bates, D. R., 1949, *Proc. Roy. Soc. A*, **196**, 562.  
 Bhar, J. N., 1938, *Ind. J. Phys.*, **12**, 363.  
 Booker, H. G. and Seaton, S. L., 1939, *Int. Ass. Terr. Mag. Elec.*, Washington Assembly, Sept. 1939.  
 Bradbury, N. E., 1938, *Terr. Mag. Atmos. Elec.*, **43**, 55.  
 Gerson, N. C., 1951, *Rep. Prog. Phys.*, **14**, 316.  
 Gledhill, J. A. and Szendrei, M. E., 1950, *Proc. Phys. Soc.*, **63**, 427.  
 Grace, C. H., Kelso, J. M. and Miller, S. W., 1949, *Basic Ionospheric Research*, (Pennsylvania State College), No. 3.  
 Harnischmacher, E., 1951, *C. R. Acad. Sci., Paris*, **230**, 1301.  
 Jouast, R. and Vassy, E., 1941, *C. R. Acad. Sci., Paris*, **213**, 139.  
 Kellogg, W. W., 1950, *Upper Atmosphere*, (Los Angeles, California Institute of Geophysics, University of California).  
 Martyn, D. F., 1947a, *Proc. Roy. Soc. A*, **189**, 241.  
 Martyn, D. F., 1947b, *Proc. Roy. Soc. A*, **190**, 273.  
 Martyn, D. F., 1948, *Proc. Roy. Soc. A*, **194**, 429 and 445.  
 McLeish, C. W., 1948, *Canad. J. Res. A*, **26**, 3 and 137.  
 Mitra, A. P., 1950, *Ind. J. Phys.*, **24**, 387.  
 Mitra, A. P., 1951a, *J. Atmos. Terr. Phys.*, **1**, 286.  
 Mitra, A. P., 1951b, *J. Geophys. Res.*, **56**, 373.  
 Mitra, S. K., Bhar, J. N. and Ghosh, S. P., 1938, *Ind. J. Phys.*, **12**, 455.  
 Moses, H. E. and Ta-You Wu, 1951, *Phys. Rev.*, **83**, 109.  
 Nicolet, M., 1947, Relations entre les phenomenes solaires et Geophysiques, Colloques internationaux (Paris, Edit. Rev. d'opt. theor. instrum).  
 Nicolet, M., 1950, *Effect of the scale height gradient on the variation of ionization and short wave absorption*, Proceedings of the Conference on Ionospheric Physics, Pennsylvania State College, p. V1—10.  
 Pekeris, C. L., 1940, *Terr. Mag. Atmos. Elec.*, **45**, 205.  
 Penndorf, R., 1949, *J. Geophys. Res.*, **54**, 7.  
 Pfister, W., 1950, *Studies on Ionospheric Region E*, Proceeding of the Conference on Ionospheric Physics, Pennsylvania State College, p. T1—19.  
 Vassy, A. and Vassy, E., 1942, *Cahiers de Physique*, **9**, 28.  
 Weeks, K., *Proc. Phys. Soc. B*, **63**, 147.

# ON THE ABSORPTION OF U. H. F. RADIO WAVES IN SOLUTIONS OF CRESOLS IN BENZENE\*

By G. S. KASTHA

OPTICS DEPARTMENT, INDIAN ASSOCIATION FOR THE CULTIVATION OF SCIENCE, CALCUTTA

(Received for publication, February 12, 1951)

**ABSTRACT.** The absorption of U. H. F. radio waves of frequencies in the range 250–920 Mc/sec. in solutions of *o*-, *m*-, and *p*-cresol in benzene has been investigated, using G. R. oscillator 1205-A and the optical method. It has been observed that the pure liquids exhibit an absorption band near about 800 Mc/sec. and when they are dissolved in benzene the height of the absorption band increases in the case of meta and para-cresol and diminishes in the case of *o*-cresol. Also the position of the band shifts slightly towards higher frequencies. On heating the liquids to about 85°C, similar results are obtained. It is concluded from these results that the absorption observed in the case of *o*-cresol is due to a dimer, whereas, that observed in the case of the other two cresols is due to single molecules and that with a rise of temperature or with dissolution in solvents the number of single molecules increases and that of dimers diminishes. The values of  $a$ , the radius of the rotor calculated according to Debye's theory is about 3.2 Å in the case of *o*-cresol 2.7 Å in the case of *m*-cresol and 2.4 Å in the case of *p*-cresol. It is pointed out that the radius of the rotor also is larger in the case of *o*-cresol and this may indicate that the rotor is a dimer.

## INTRODUCTION

The absorption of U. H. F. radio waves in some aliphatic ketones dissolved in non-polar solvents was studied recently by Sen (1951 *b*) and it was observed by him that when acetone and methyl ethyl ketone were dissolved in benzene to make even 80% solutions of these substances, the absorption peak observed in the range 300–500 Mc/sec. shifted towards the higher frequencies and its height diminished greatly. In the case of other higher ketones the shift of the peak was in the same direction, but the height did not diminish so rapidly as in the two cases mentioned above. These results were interpreted by assuming that the absorption peak was due to dimers present in the liquid and that on dissolution the dimers split up into monomers having characteristic absorption bands at frequencies much higher than that mentioned above. Earlier investigations by Sen (1951 *a*) showed that when the temperature of these ketones is raised the absorption peaks observed in the region mentioned above, shift towards higher frequencies and also the height of the peak diminishes considerably. This

\* Communicated by Prof. S. C. Sirkar.

phenomenon also was explained on the same hypothesis as that mentioned above. In order to investigate whether polar molecules, having shapes different from those of the molecules mentioned above, behave also in the same way the absorption of the U. H. F. radio waves in a fairly large number of liquids is to be studied. The main difficulty in such an investigation, however, is the absence of any absorption band in the region 250–500 Mc/sec. in many such liquids. It was, therefore, thought worthwhile to investigate such an absorption in the region 250–920 Mc/sec. in the case of some aromatic compounds in the pure state as well as in solution in benzene and *o*-, *m*-, and *p*-cresol were chosen in the present investigation for this purpose.

#### EXPERIMENTAL

As mentioned above most of the liquids having benzene nucleus do not exhibit any absorption band in range 250–510 Mc/sec. which can be obtained from G. R. 857 U. H. F. oscillator. In order to investigate whether an absorption band is exhibited by these liquids in ranges above 550 Mc/sec. a G. R. 1209-A oscillator giving radiations in the range 250–920 Mc/sec. was used. This oscillator is shielded and the output can be taken by connecting the terminals of a loop floating inside the shield to a Lecher wire system. As it was intended to use the optical method attempt was made to detect the waves radiated by the loop, using the detector which was used previously by Sen (1950) and is suitable for the range 250–1250 Mc/sec. It was found that the radiated energy was too feeble to be detected in this way. The shield of the oscillator was next removed and the oscillating system was placed at the focus of a parabolic metallic reflector. It was observed that along directions in the plane of the ring constituting the inductance of the oscillating circuit, the intensity of radiation was maximum. By suitably adjusting the position of the parabolic reflector, it was possible to detect the radiations from a distance of about 80 cms from the oscillating loop with the detector. The liquids, *o*-, *m*-, and *p*-cresol, obtained from U. S. A. were distilled in vacuum and absorption cells similar to those used by Sen (1950) were used for studying the absorption of the radio waves in the pure liquids at different temperatures as well as in solutions in benzene by the optical method. In calculating the absorption coefficients in the case of solution, thicknesses proportional to concentrations were taken into account and the reading with a similar empty cell in the position of the absorption cell was taken as the reading in the detector for the incident radiation without any absorber. The apparatus was placed in the middle of a large hall so that interference of incident waves and those reflected at the walls could not interfere with the readings. Preliminary observations showed that in small rooms such an interference affected the readings in the detector. The temperatures of all the liquids were noted while the absorption was being studied. Similar observations were carried out with all the liquids at higher



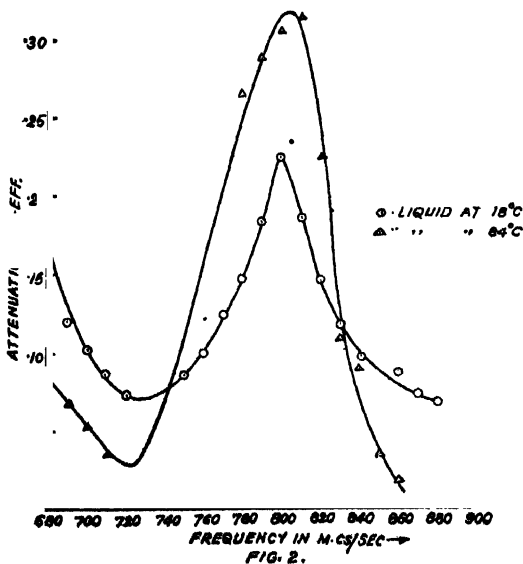
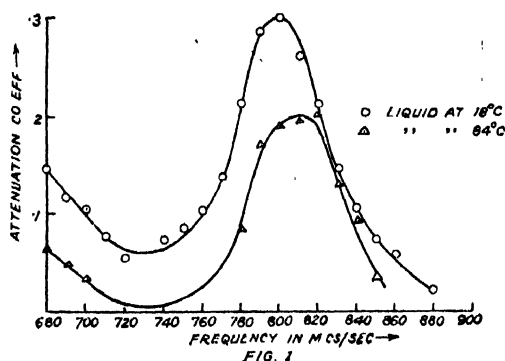
temperatures which was obtained in a water bath the temperature of which was kept constant. The absorption at high temperature was studied in the same way as that adopted by Sen (1950). The attenuation constant was calculated

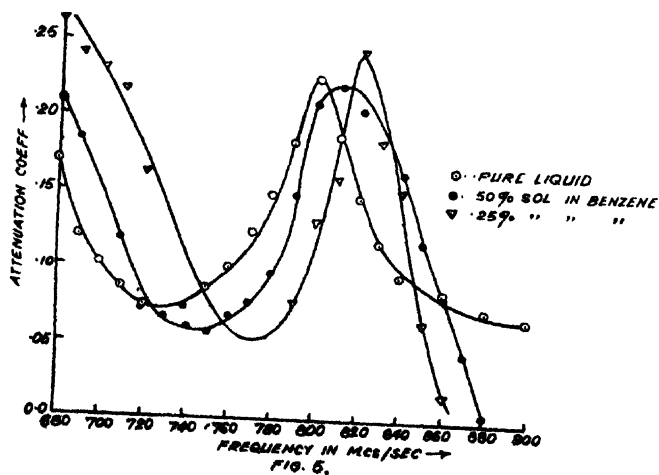
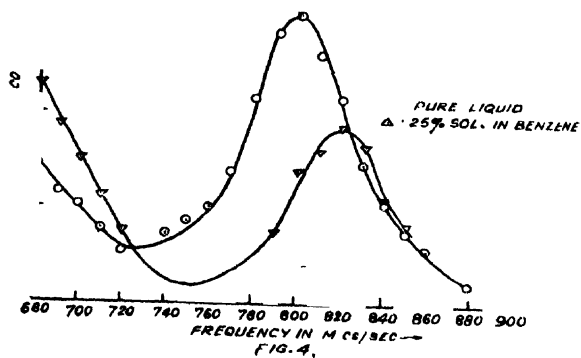
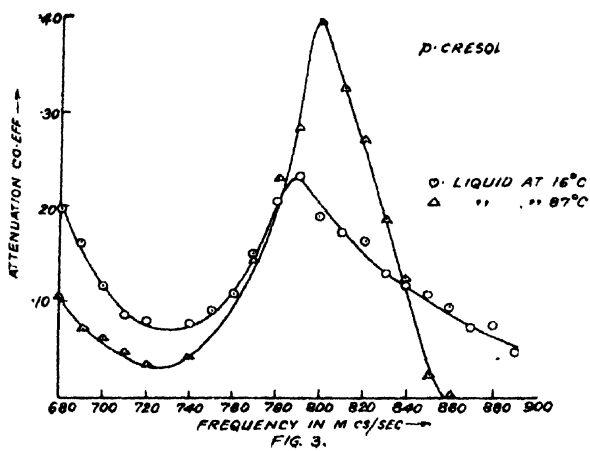
from the formula  $\mu = \frac{2.34}{t} \log_{10} \frac{I_0}{I}$  where  $t$  is the equivalent thickness of

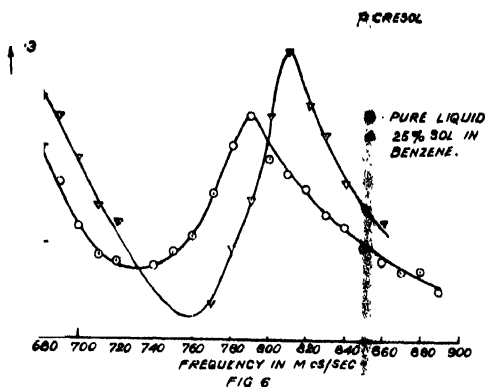
the experimental cell in cms, calculated from concentration,  $I_0$  the intensity of the incident beam with the empty glass cell in its path and  $I$ , the corresponding intensity with the glass cell filled with the liquid used as the absorber.

## RESULTS

The results obtained with *o*-, *m*-, and *p*-cresols are shown graphically in figures 1-6. Figures 1, 2 and 3 show the influence of temperature while those in 4, 5, 6 show the changes in the absorption with the concentration of the solution of these liquids in benzene.







## DISCUSSION

It can be seen from the curves that in case of *m*- and *p*-cresols the positions of the absorption peaks shift towards higher frequency with increase of temperature and also their heights increase, on the other hand, in the case of *o*-cresol, though the peak shifts towards higher frequency with rise of temperature, the height of the peak diminishes. As can be seen from figures 5 and 6, similar increase in the height of the peaks is observed when these two liquids are dissolved in benzene. The increase in the case of *p*-cresol is much larger than that in *m*-cresol. It can be seen from figure 5 that the position of the absorption peak in *m*-cresol shifts towards higher frequencies as the concentration diminishes. The shape of the absorption peak given by the 50% solution of *m*-cresol is different from that observed in case of the 25% solution. In the former case the height of the absorption peak is slightly smaller than that for the pure liquid but the integrated intensity is greater, whereas, in the latter case the peak is sharper and its height a little larger.

It can be seen from figure 4, however, that the height of the absorption peak as well as the integrated intensity observed in the case of the 25% solution of *o*-cresol in benzene are smaller than those for the pure liquid.

Thus it is evident that the changes observed in the case of *m*- and *p*-cresol are almost identical, while *o*-cresol behaves in a different manner. It is interesting to note that *o*-cresol shows peculiarities also in respect of other physical properties, *e.g.*, boiling point, density, refractive index, and viscosity. To illustrate this, the relevant data are given in Tables I and II.

It has been observed by Sen (1949, 50, 51) that the position of absorption peak of U. H. F. radio waves in several organic liquids shifts towards higher frequencies with the increase of temperature and the height of the absorption peak diminishes and also in most cases the peak becomes broader. He (Sen 1951 *b*) also observed that similar changes take place when some of the liquids are dissolved in non-polar solvents to make even an 80% solution.

TABLE I

	Boiling point °C	Density	Refractive index
<i>o</i> -cresol	190.8	1.051	1.547
<i>m</i> -cresol	202.8	1.035	1.540
<i>p</i> -cresol	201.1	1.039	1.540

TABLE II

Viscosity of *o*-, *m*- and *p*-cresol at different temperatures. Values of  $\eta \times 100$

t°C	<i>o</i> -cresol	<i>m</i> -cresol	<i>p</i> -cresol
10	17.9	34.6	39.6
20	9.56	16.9	18.9
30	6.12	9.47	10.5
40	4.10	5.92	6.54
60	2.24	2.99	3.28
80	1.43	1.80	1.93

These phenomena have been explained by him on the hypothesis that in pure liquids most of the molecules probably exist as dimers giving the absorption peaks observed in the range studied by him and with increase of temperature or increase of dilution these dimers break up into single molecules, thereby reducing greatly the population of dimers and consequently decreasing the height of the absorption peak. The peak due to the monomer is obviously far away from that due to the dimer. The results in fatty acids (Sen 1951 *c*) show that the calculated radius is twice as large as that of a single molecule.

It can be seen from figures 1 and 4 that *o*-cresol behaves in this respect in the same way as the other organic compounds investigated by Sen (1951 *a, b*) and therefore the absorption peak at about 800 Mc/sec is probably due to dimers.

The difference in the behaviour of *o*-cresol and that of meta and para cresol may be due to the fact that the peak observed in the latter cases at about 800 Mc/sec. and 790 Mc/sec. respectively may be due to single molecules the number of which increases with increase of temperature and also with dissolution in benzene. There is one difficulty, however, in such a hypothesis. It would appear that the dimers in *o*-cresol cannot show absorption peak almost at the same position at which monomers of *m*- and *p*-cresol show such peaks. The difficulty, however, disappears when the

viscosities of the liquids are taken into consideration. The radii of the rotors in all the three cases have been calculated from Debye's (1929) formula  $a^2 = \frac{\tau k T}{4\pi\eta}$  where  $a$  is the radius of the rotor,  $\tau$  the time of relaxation,  $k$  Boltzmann constant,  $T$  the absolute temperature and  $\eta$  the viscosity. The time of relaxation has been calculated from the equation  $\tau = \frac{\epsilon_0 + 2}{\epsilon_1 + 2} \sqrt{\frac{6}{\omega}}$  where  $\omega$ , is the angular frequency at which the absorption peak occurs,  $\epsilon_0$  the square of refractive index and  $\epsilon_1$ , the dielectric constant for static field. These values of  $\tau$  and  $a$  are given in Table III along with those for  $\eta$ .

TABLE III

	$\frac{\omega}{2\pi}$ in Mc/sec.	Temp °C	$\eta \times 100$	$\tau \times 10^{10}$	$a$ in Angstrom units
<i>o</i> -cresol	800	18°C	10.5	10.96	3.22
<i>m</i> -cresol	800	18°C	18.8	11.31	2.68
<i>p</i> -cresol	790	16°C	26	11.10	2.39

It can be seen from Table III that values of the radius of the Debye rotor in the case of *o*-cresol is higher than that for *m*- and *p*-cresol and the radius of *m*-cresol is slightly higher than that of *p*-cresol. This larger value in the case of *o*-cresol may indicate that the rotor in this case is a dimer. The actual radius of this rotor need not be double that of a monomer, because the radius depends on the position of the point of attachment of the two monomers in the dimer. It is, however, significant that the viscosity of *o*-cresol is only about half that of *m*-cresol, although the permanent electric moment of the single molecule is expected to be larger in the former case than in the latter case. Probably at room temperature the percentage of dimers in *o*-cresol is much higher than that in the other two liquids and that such an association of the molecules diminishes the viscosity. The fact that the dielectric constant increases rapidly with the increase of temperature in the case of all the three liquids also indicates that the molecules are associated in these liquids at room temperature. The values of the dielectric constants taken from International Critical Tables are given in Table IV to illustrate this point.

It can be seen from Table IV that the rate of increase of dielectric constant with increase of temperature is smaller in the case of *o*-cresol than that in other two cases although the value of permanent electric moment of the single *o*-cresol molecule is much larger than that of the other two isomers. This may be due to the fact that the virtual bond in dimers is stronger in *o*-cresol than in *m*- or *p*-cresol, so that in the former case the

TABLE IV

Values of  $\epsilon_1$ 

Temp	Liquid	<i>o</i> -cresol	<i>m</i> -cresol	<i>p</i> -cresol
24°C		5.8 ± .1	5.1 ± .1	5.6 ± .1
40°C		≈ 8	≈ 13	≈ 13

dimers break up only slowly with rise of temperature. The diminution of the height of the absorption peak in *o*-cresol with rise of temperature or with dissolution of the liquid in benzene is also small and this fact corroborates the hypothesis put forth above. Similar investigations with other liquids are in progress.

## ACKNOWLEDGMENT

The author's thanks are due to Prof. S. C. Sirkar for his kind interest and guidance throughout the progress of the work.

## REFERENCES

- Debye, P. 1929, *Polar Molecules*  
 Sen, S. N. 1949, *Ind. J. Phys.*, **23**, 495.  
 Sen, S. N. 1950, " " " **24**, 163.  
 Sen, S. N. 1951, *a*, " " **25**, 25.  
 Sen S. N. 1951 *b*, " " **25**, 187.  
 Sen, S. N. 1951, *c*, " " **25**, 237.

# THE ABSORPTION SPECTRUM OF $\text{PbBr}$ MOLECULE IN THE ULTRAVIOLET REGION\*

By P. K. SUR. AND K. MAJUMDAR  
DEPARTMENT OF PHYSICS, ALLAHABAD UNIVERSITY

(Received for publication, January 16, 1952)

**ABSTRACT.** A new system of bands comprising of about a dozen bands degraded to violet was observed in absorption in the ultraviolet region between  $\lambda\lambda$  2927–2701 Å. No splitting of the heads of the bands either due to structure or due to isotopic molecule  $\text{PbBr}^{210}$  was detected. The heads fit in the formula

$$\nu = 347(0.21 + 259(\nu' + \frac{1}{2}) - .5(\nu' + \frac{1}{2})^2 - 207.4(\nu'' + \frac{1}{2}) + .45(\nu'' + \frac{1}{2})^2$$

The ground state constants agree well with those determined by Frank and Morgan for the absorption of  $\text{PbBr}^{210}$  molecule in the visible region between  $\lambda\lambda$  4400 and 5400 Å.

## INTRODUCTION

Howell and Rochester (1934) have produced emission band spectra in  $\text{PbBr}$  molecule by the use of a high frequency electrical discharge but they did not make a vibrational analysis. Morgan (1936) obtained in absorption, using an open iron or graphite tube 30 cm long heated electrically to a temperature of 900°C, a single system of bands between  $\lambda\lambda$  4400 and 5400 Å. No other observations on the band spectra of  $\text{PbBr}$  seem to have been recorded. The present investigation was undertaken in the expectation that the  $\text{PbBr}$  molecule would give absorption system in the ultraviolet region like the  $\text{BiCl}$  molecule observed by one (Sur, 1950) of the authors. A short system of bands of the molecule was obtained in absorption between  $\lambda\lambda$  2927–2701 Å, using a graphite tube furnace heated to about 950°C.

## EXPERIMENTAL

The experimental arrangement was the same as that used by one of the authors in obtaining absorption spectrum of  $\text{BiCl}$  (Sur, 1950) and  $\text{BiS}$  (Sur, 1951) molecules. Lead bromide was introduced inside a vitreosil tube which was heated to 950°C within the graphite tube furnace used in the previous investigations. The substance is highly vaporisable and a very dense column of vapour is formed on heating it. Long exposures ranging from two and a half hours to three hours were needed to bring out these bands with measurable intensity on the photographic plates. As usual a water cooled hydrogen discharge tube was used to serve as the source of continuum. Observations were made on a medium quartz spectrograph. A copper arc was used for a standard comparison spectrum and the temperatures of the furnace were recorded in the usual way by an optical pyrometer.

\* Communicated by Prof. M. N. Saha, F.R.S.

## RESULTS AND DISCUSSION

Table I gives the wavelengths in Å., the observed wave numbers in  $\text{cm}^{-1}$ , the difference between the observed and calculated wave numbers, the relative intensities of the band heads on the scale of ten and vibrational analysis. Table II gives the Deslandres table of arrangement and figure 1 gives the intensity plots of the heads. Frank-Condon parabola cannot be accurately drawn on account of the very small number of band heads observed.

TABLE I

$\lambda(\text{Å})$	Int	$\nu$ in $\text{cm}^{-1}$ observed	$\nu$ in $\text{cm}^{-1}$ calculated	$\nu_{\text{obs}} - \nu_{\text{cal}}$ in $\text{cm}^{-1}$	$\nu', \nu''$
†2927.0	1	34155	34169	-14	0,3
2907.9	2	34379	34374	+5	0,2
2890.9	4	34581	34579.5	+1.5	0,1
2868.9	3	34846	34837.5	+8.5	1,1'
2852.7	7	35044	35044	0	1,0
2831.2	5	35310	35301	+9	2,0
2811.8	8	35554	35557	-3	3,0
2792.1	5	35805	35812	-7	4,0
2768.9	4	36105	36112.5	-7.5	6,1
2746.1	2	36405	36409.9	-4.9	8,2
†2723.3	0	36710	36704	+6	10,8
†2701.3	0	37008	36965	13	12,4
2832.9	atomic line due to Pb.				

† Not visible under comparatar, visually estimated.

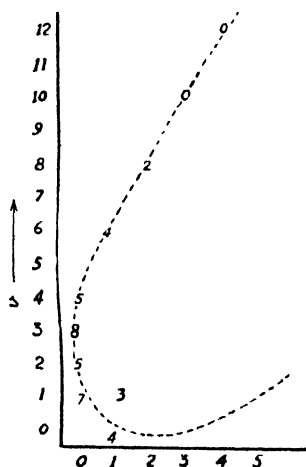


FIG. 1



TABLE II

12					37008	
11						
10				36701		
9				36405		
8						
7						
6		36105				
5						
4	3.805					
3	35554					
2	35310					
1	35044	34846				
0		34581	34379	34155		
$v' \quad v''$	0	1	2	3	4	5

All the band heads, with the exception of two which are very weak, closely fit in the formula

$$\nu = 34760.21 + 259(v' + \frac{1}{2}) - .50(v' + \frac{1}{2})^2 - 207.4(v'' + \frac{1}{2}) + .45(v'' + \frac{1}{2})^2$$

The ground state constants can be compared with those determined by Morgan for the system observed by him in the visible region, thus leaving no doubt that the present system of bands is due to PbBr molecule.

	Present authors	Morgan
	207.4	207.5
$x_e''w_e''$	.45	.50

As the number of electrons is odd for the halides of lead, the spin number must be half integral. Hence a doublet system of levels may be expected and from the electron configuration the halides of tin and lead might be expected to have a  $^2\Pi$  ground state. The heads of the bands observed in absorption are expected to be double with a constant separation. Morgan was able to obtain double heads quite distinctly in PbF bands and less so in PbCl bands. In the case of PbBr bands, only a few of the bands appeared to be double, which, however, could not be observed by him with any certainty. Morgan took all measurements from spectrograms taken on a 10 ft. concave grating in the second order. It is thus quite clear that for want of proper dispersion in the spectrograph employed the double heads could not be detected by the

authors. The band heads due to the isotopic molecule  $\text{PbBr}^{21}$  could not be observed as the isotopic shift is hardly  $12\text{ cm}^{-1}$  even for high  $v'$  value, say  $v'=12$ . The diffusiveness of the bands corresponding to high  $v'$  value, e.g. 12, in which case the discrepancy between the observed and calculated values is of the same order, suggests the presence of isotopic heads due to  $\text{PbBr}^{21}$  molecule.

Recently our attention has been drawn to a paper on the subject, by Newburg and Wieland (Helv. Phys. Acta. 22, 590, 1940) which has been referred to in Herzberg's Molecular Structure and Molecular Spectra, Diatomic Molecules, IIed (1950). The term value  $T_e$  reported by the workers do not agree with that obtained by us, though the constants for the upper and lower states of the molecule agree with our values. The original paper, however, is not available to us.

#### REFERENCES

- Howell and Rochester, 1934, *Univ. Durham Phil. Soc.*, **9**, 126  
Morgan, 1936, *Phys. Rev.*, **49**, 47.  
Sur, 1950, *Proc. Nat. Acad. Sci.*, **19**, 10.  
Sur, 1951, *Ind. J. Phys.*, **28**, 65.

# ON THE RAMAN SPECTRUM OF SOLUTION OF BENZOYL CHLORIDE IN BENZENE\*

By T. A. HARIHARAN

OPTICS DEPARTMENT, INDIAN ASSOCIATION FOR THE CULTIVATION OF SCIENCE, CALCUTTA

(Received for publication, February, 18, 1952)

## Plate III

**ABSTRACT.** The Raman spectra of solutions of benzoyl chloride in benzene of different concentrations have been investigated and the relative intensities of the lines  $162$  and  $316\text{ cm}^{-1}$  observed in the case of solutions have been compared with those for the pure liquid at room temperature. It is found that the ratio of the intensity of the line  $162\text{ cm}^{-1}$  to that of the line  $316\text{ cm}^{-1}$  diminishes gradually as the concentration of the solution decreases. It is concluded from these results that the line  $162\text{ cm}^{-1}$  may be due to inter-molecular vibration in a dimer and that in the pure liquid such dimers are predominant while in the solution some of them break up into monomers. The relative intensities of the two lines, however, are found to diminish very slightly even at  $150^{\circ}\text{C}$ .

## INTRODUCTION

It is wellknown that in the Raman spectra of some substituted benzene compounds in the liquid state there is a Raman line with frequency-shift having a value in the range,  $160-200\text{ cm}^{-1}$ . For instance, benzoyl chloride in the liquid state yields a line at  $161\text{ cm}^{-1}$  which is totally depolarised, as observed by previous workers (Sirkar and Bishui, 1946). This line is reported to be only slightly less intense than the line  $316\text{ cm}^{-1}$  when the intensity at the peak is concerned, but when the integrated intensity is taken into account the former line is more intense than the latter, because it is much wider than the line  $316\text{ cm}^{-1}$ . The origin of this line is not clearly understood. The deformation oscillation of the C-Cl group will be totally depolarised, but its frequency is expected to be a little higher. Also acetophenone, in which there is no C-Cl group, yields such a line. Hence it may be due to some other mode of oscillation. The line, however, may not be due to a monomer at all and in that case its intensity should alter with the rise of temperature of the liquid and also with the concentration of solution of this liquid in some suitable solvent. In order to find out actual origin of this line the Raman spectra of solutions of benzoyl chloride in benzene having concentrations of 1:3 and 1:5 by volume and also of the pure liquid at  $25^{\circ}\text{C}$  and  $150^{\circ}\text{C}$  have been studied in the present investigation.

\*Communicated by Prof. S. C. Sirkar

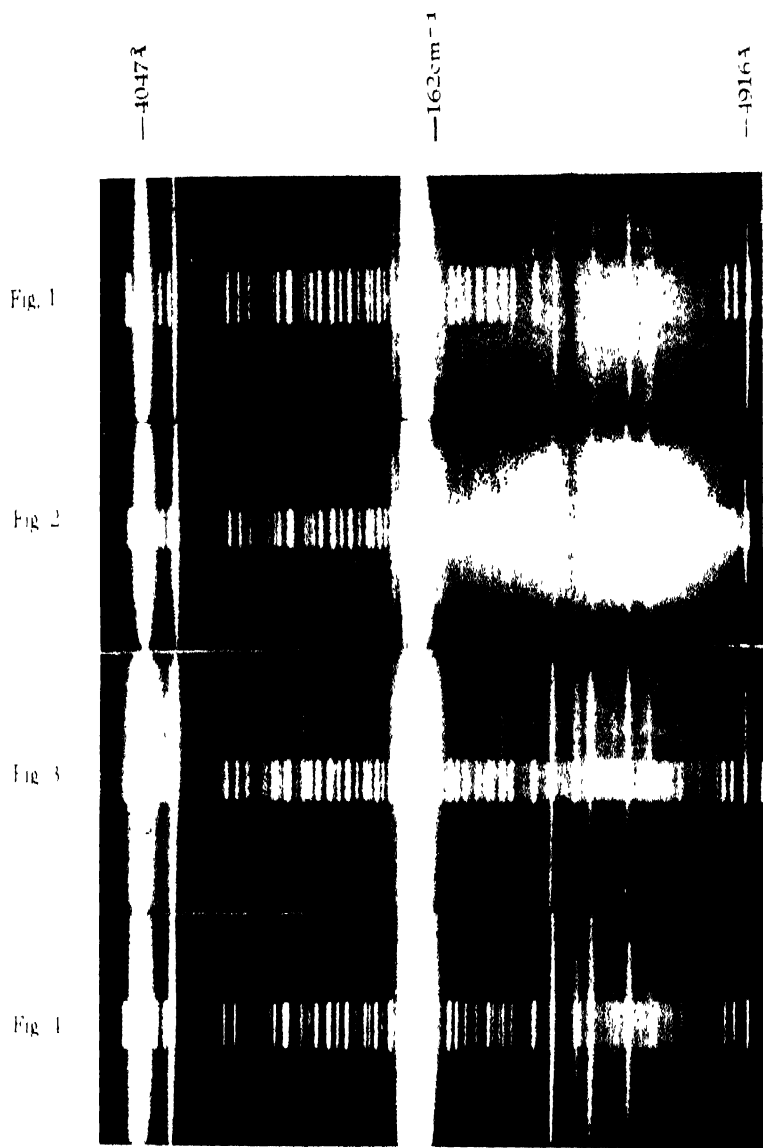
## EXPERIMENTAL

The liquid was obtained from the old stock and it was of Kahlbaum's chemically pure quality. It was distilled very carefully in an evacuated and sealed double bulb in order to get rid of fluorescence and continuous background. Chemically pure benzene was also distilled in the same way and when mixed with the liquid in the proportions mentioned above the solutions were found to be quite homogeneous without showing any trace of opalescence. A Fuess glass spectrograph having a dispersion about  $12 \text{ \AA}$  per mm. in the region of  $4046 \text{ \AA}$  was used to photograph the Raman spectra. Iron arc comparison spectrum was also photographed on each plate in order to find out whether any of the lines change their positions with the change of concentration of the solution. A very dilute solution of sodium nitrite in distilled water was used as a filter in order to cut off rays of wavelengths shorter than  $4000 \text{ \AA}$ , which were found to decompose the liquid and thereby to produce continuous background in the visible region of the Raman spectrum. Spectrograms with very clear backgrounds were obtained when the filter was used. Ilford special rapid plates were used for photographing the Raman spectra and plates from the same packet were used to photograph the Raman spectra of solutions of different concentrations and they were developed under identical conditions. The Raman spectrum of the liquid at  $150^\circ\text{C}$  was also photographed to see if any changes take place in the intensities or positions of the lines with rise of temperature of the liquid.

## RESULTS AND DISCUSSIONS

The spectrograms for the pure liquid at  $25^\circ\text{C}$  and  $150^\circ\text{C}$  and those for the solutions of benzoyl chloride in benzene of concentrations 1:3 and 1:5 (by volume) are reproduced in figures 1-4 in Plate III. The lines observed in the case of pure liquid and the solutions are listed in Table I.

It can be seen from Table I that the lines of benzoyl chloride do not shift appreciably from their original positions when the liquid is dissolved in benzene except the line  $1204 \text{ cm}^{-1}$ . There are, however, changes in the intensities of some of the lines. Most of such changes occur due to superposition of Raman lines of benzene on those of benzoyl chloride. Benzene, however, does not yield any Raman line below  $400 \text{ cm}^{-1}$ , and therefore, the change in the intensity of the line  $162 \text{ cm}^{-1}$  observed in the present case with dissolution of the substance in benzene is due to a different cause. It can be easily seen from Plate III and Table I that the line  $162 \text{ cm}^{-1}$  is much broader and slightly more intense than the line  $316$  or  $510 \text{ cm}^{-1}$  in the case of the pure liquid, but in the case of the solution of concentration 31% by weight the line  $162 \text{ cm}^{-1}$  is quite sharper and less intense than the line  $316 \text{ cm}^{-1}$  and in case of solution of concentration 22% by weight the line  $162 \text{ cm}^{-1}$  diminishes further in intensity. These facts definitely prove that this line, inspite of being totally depolarised, may not due to any mode of vibration of



Raman spectra of benzoyl chloride

Fig. 1 Pure liquid at 25 C

Fig. 2 „ „ at 150 C

Fig. 3 Solution in benzene, 1:3 by volume

Fig. 4 „ „ 1:5 „ „



# Raman Spectrum of Solution of Benzoyl Chloride in Benzene 117

TABLE I

## Benzoyl chloride

Pure liquid at 25°C	Solution in benzene (31% by wt)	Solution in benzene (22% by wt)
162(5b)	162(3)	162(2)
202(1)	202(1)	202(0)
316(5)	316(1)	318(4)
418(3b)	418(3b)	418(2b)
510(5)	510(4)	510(4)
618(5)	618(6)	618(6)
672(6)	672(5)	672(4)
774(1)	774(0)	
	855(4)	855(1)
1000(10)	995(20)	995(20)
1028(3)	1028(2)	1028(2)
1168(3)	1168(3)	1168(3)
1176(6)	1176(5)	1176(6)
1204(6)	1200(3)	1200(2)
1450(1)		
1480(0)		
1593(15)	1593(15)	1593(15)
1728(3)	1728(3)	1728(3)
1772(10)	1772(10)	1772(10)
3070(10)	3070(10)	3070(10)

the single molecule, because in that case its intensity with respect to that of any other line would not diminish with dissolution of the liquid in benzene. Hence it has to be concluded that in the liquid state some of the molecules form dimers without thereby changing the frequencies of the Raman lines of the monomer and in the solution the number of dimers diminish gradually as the concentration is diminished. It is not surprising that the formation of such dimers keeps the frequencies of other Raman lines unchanged, because it is known from the results obtained by Kojima (1949) that when methylmethacrylate is polymerised only the intensity of the line due to C=C vibration diminishes while the frequencies of the other lines remain unchanged. It is further seen from Table I that the intensity of the line  $1204\text{ cm}^{-1}$  relative

to that of the line  $1028\text{ cm}^{-1}$  is smaller in the case of the 22% solution than that in the case of the pure liquid. This may be due the superposition of the faint line  $1034\text{ cm}^{-1}$  of benzene on the  $1028\text{ cm}^{-1}$  line of benzoyl chloride. Similar superposition also affects the intensities of the lines 1000, 1176 and  $3070\text{ cm}^{-1}$ .

A comparison of the spectrograms for the pure liquid at  $25^{\circ}\text{C}$  and  $150^{\circ}\text{C}$  reproduced in Plate III shows that the intensities of the lines 162 and  $202\text{ cm}^{-1}$  with respect to those of the lines 316 or  $418\text{ cm}^{-1}$  diminish very slightly with the rise of temperature. This fact shows that the molecules in this liquid are too strongly associated to be affected by temperature. Only large change in the intermolecular field caused by non-polar molecules of the solvent breaks the dimers into monomers. The fact that the width of the lines 162 and  $202\text{ cm}^{-1}$  are not very large also indicates that the bond is fairly strong so that its strength is not affected appreciably during the modes of vibration giving these lines.

An attempt may be made to assign this line to a particular mode in a dimer. An examination of the published data shows that such a strong line occurs in the Raman spectra of acetophenone and other substances having the  $\text{C}=\text{O}$  group in the molecule. The mode in which the whole benzene nucleus executes bending oscillation against the remaining portion of a dimer may give rise to a line of frequency below  $200\text{ cm}^{-1}$  and such a line should be depolarised. Investigations undertaken with other similar liquids to test the correctness of the above hypothesis are in progress.

#### ACKNOWLEDGMENT

The author's thanks are due to Prof. S. C. Sirkar, D. Sc., F. N. I., for his kind interest and guidance throughout the progress of the work.

#### REFERENCES

- Sirkar, S. C. and Bishui, B. M., 1946, *Ind. J. Phys.* **20**, 111.  
Kojima, J. K. 1949, *J. Chem. Soc. Japan. Pure. Chem. Sec* **70**, 147.



# ABSORPTION SPECTRA OF ORGANIC SUBSTANCES IN THE LIQUID AND SOLID STATES—II. CRESOLS\*

By H. N. SWAMY

OPTICS DEPARTMENT, INDIAN ASSOCIATION FOR THE CULTIVATION OF SCIENCE, CALCUTTA

(Received for publication, January 16, 1951)

## Plate IV

**ABSTRACT.** The absorption spectra of extremely thin films of *o*-, *m*-, and *p*-cresols in the liquid state and in the solid state at low temperatures have been investigated, and bands have been observed. The results have been compared with those reported by previous workers for the vapour state of the substances and also for the solution of these substances in heptane. It has been observed that in all the three cases, the number of bands diminish with the liquefaction of the substance and further the  $\nu_0$ -band shifts towards the longer wavelength. It is pointed out that such a shift may be due to association of molecules in the liquid state and the diminution in the number of bands with liquefaction may be due to the influence of the impact of the surrounding molecules on the vibration of individual molecules in the liquid. It is further observed that the bands shift towards shorter wavelength when the liquids are solidified and in the case of *p*-cresol, the number of bands increases with solidification. The companions of the  $\nu_0$ -band in the case of *p*-cresol represent transitions to higher harmonics of the mode of frequency  $825\text{ cm}^{-1}$  of the benzene nucleus. It is pointed out that the increase in the electronic energy of the molecule with solidification may be due to contraction of the molecules which also increases the frequency of some of the modes of vibration of the molecule. Also, it is concluded that higher harmonics of some of the modes of vibration are allowed in the case of solid *p*-cresol probably because the pseudo-symmetry of the molecule in the crystal allows some space around the benzene nucleus of the molecule.

## INTRODUCTION

The ultraviolet absorption spectra of aromatic molecules in the vapour state have a number of characteristic features. Most aromatic compounds absorb light in the region  $2500-3000\text{ \AA}$  owing to an electronic transition involving the excitation of the  $\pi$ -electrons in the ring corresponding to the  $A_{1g} \rightarrow B_{2g}$  transition in benzene, the direct excitation from the ground state to higher state being forbidden. The ultraviolet absorption of aromatics in the liquid state has been widely used in analysis. The fine structure of the spectrum is largely wiped out in the liquid state, the bands being in general broad. Kronenberger (1926) has found that in the case of benzene, the broad bands in the liquid state become sharper at liquid oxygen tem-

\* Communicated by Prof. S. C. Sirkar.

perature. Recently, Broude *et al* (1950) have reported the results of investigations on the ultraviolet absorption spectra of a large number of substituted benzene compounds at low temperatures upto that of liquid hydrogen in some cases. The journal in which the results were published is in Russian and being not available to the author it could not be ascertained whether the authors mentioned above have studied the absorption spectra of cresols and whether they have actually compared the absorption spectra of the substances in the liquid state with those for the solid state in order to find out whether any significant changes occur with solidification of the substances. The present work is part of a programme aimed at studying the influence of change of state and lowering of temperature on the absorption spectra of organic substances and especially of substituted benzene compounds, and correlating the results with those observed in the investigations on the Raman spectra of those substances in different states. In the present investigation, the ultraviolet absorption spectra of *o*-, *m*-, and *p*-cresols have been investigated in the liquid and solid states at different temperatures.

#### EXPERIMENTAL

The experimental set up is that employed in an earlier investigation by the author (Swamy, 1951). The source of continuous spectrum used was a hydrogen discharge tube. Spectrograms were taken on Ilford HP3 films on a Hilger E<sub>1</sub> spectrograph having a dispersion of 3 Å. U. per mm. in the region 2600 Å°. Chemically pure BDH cresols distilled four times in vacuum were used in this investigation.

Previous workers (Purvis and McClelland, 1913), who investigated the absorption spectra of cresols in the liquid state, were not able to get bands probably because their films were too thick and produced continuous absorption over a wide range of wavelengths. It was found in the present investigation that a film of a thickness of a few microns produced the bands. Such a film was produced when a very small drop of the liquid was placed between two quartz plates and one of the quartz plates was slid till colours were produced by the thin film.

The study of the absorption spectra at low temperatures was carried out using the arrangement described by the author in a previous paper (Swamy, 1951). Copper plates were attached to the brass frame containing the cell and the plates were made to dip in liquid oxygen, while the brass frame was kept much above the level of liquid oxygen in order to keep the sample at  $-150^{\circ}\text{C}$ . To maintain the sample at  $-180^{\circ}\text{C}$ , the level of liquid oxygen was so adjusted that the lower part of the brass frame came in contact with the liquid oxygen. An exposure of 45 minutes was necessary to record the absorption spectrum for the solid state, while with proper alignment an exposure of 10 minutes was required to record the absorption spectra for the liquid state. For comparison, mercury arc spectrum was recorded with the help of Hartmann diaphragm on each spectrogram.

## RESULTS

Three sets of spectrograms for *o*-, *m*-, and *p*-cresol in the liquid and solid states are reproduced in Plate IV. The wave numbers of the bands observed are given in Tables I, II and III in which wave numbers of the bands observed in the vapour state and also in solution by previous workers are included for comparison.

TABLE I

Absorption bands of *o*-cresol.  $\nu$  in  $\text{cm}^{-1}$ 

Band No.	Purvis & McClelland (1913)	Robertson, Ginsberg and Matsen (1916) Prominent bands		Wolf and Herold (1931)		Present author		
						Liquid at 30°C	Solid at -180°C	Assignment
1	35387(w)							
2	Bet 36025 & 36260(w)	36247	$\nu_0$	35950(S)	$\nu_0$	35982 (Broad)	36109	$\nu_0$
3	37094(w)	36432	$\nu_0 + 185$	36881(m)	$\nu_0 + 931$	36789 (Broad)	36978	$\nu_0 + 869$
4	37219 (fst)	37108	$\nu_0 + 861$	37450(vw)	$\nu_0 + 1500$			
5	37400			38450(vw)	$\nu_0 + 931 + 1500$			

TABLE II

Absorption bands of *m*-cresol.  $\nu$  in  $\text{cm}^{-1}$ 

Band No.	Purvis and McClelland (1913)	Wolf and Herold (1931)		Present author			
				Liquid at 30°C	Solid at -150°C	Solid at -180°C	Assignment
	Vapour	Solution in heptane					
		35761(S)	$\nu_0$	35806(S) Broad	35831	38851	$\nu_0$
1	35986 f str						
2	36077 "						
3	36142 "			875			
4	36300 "						
5	Bet 36592 & 37149 vw diff	36740(m)	$\nu_0 + 979$	36661(S) (Broad)	36713	36774	$\nu_0 + 893$
6	37246 w	37302(vw)	$\nu_0 + 1541$				
7	37810 "						
8	37896 "						
9	37968 "						
10	38011 "						
11	38112 "						
12	38185 "						

TABLE III

Absorption bands of *p*-cresol.  $\nu$  in  $\text{cm}^{-1}$ 

Band No.	Robertson, Ginsberg and Matsen (1946). Prominent bands		Wolf and Herold (1931)	Present author			
	Vapour	Assignment	Solution in heptane	Liquid at $30^\circ\text{C}$	Solid at $-150^\circ\text{C}$	Solid at $-180^\circ\text{C}$	Assignment
1	35325(vs)	$\nu_0$	34960(s) 35430(w)	35044 (Broad)	35041(s)	35020(vs)	$\nu_0$
2	36116(s)	$\nu_0 + 791$	35810(s)				
3	36512(s)	$\nu_0 + 1187$	36220(s)	35957 (Broad)	35857(s) 36260(s)	35845(s) 36234(s)	$\nu_0 + 825$ $\nu_0 + 1211$
4	36916(s)	$\nu_0 + 2 \times 791$	36970(s)		37067(m)	36673(s)	$\nu_0 + 2 \times 825$
5	37302(m)	$\nu_0 + 1187$ $+ 791$	37440(m)			37056(m)	$\nu_0 + 825 + 1211$
6	37724(w)	$\nu_0 + 3 \times 791$	37720(m) 38120(w)				
7	38127(w)	$\nu_0 + 2 \times 791$ $+ 1187$					

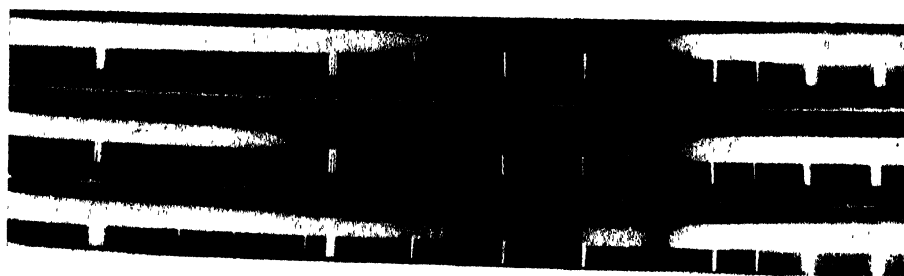
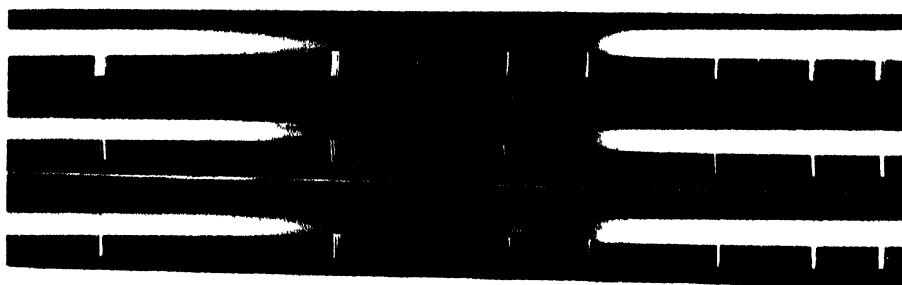
## DISCUSSION

The results given in Tables I, II, III show that there are some general features in the changes which take place in the absorption spectra with the change of state. First, the number of bands in the vapour state is much larger than that observed either in the liquid state or in the solid state. Secondly in all these three cases the principal absorption band due to transition from the ground state as well as its companions shift towards the longer wavelength side with the liquefaction of the vapour, and when the liquid is solidified these bands shift towards the shorter wavelength side. In the vapour state most of the bands are due to transitions of the electron to the higher energy state accompanied by transitions to vibrational energy states of different quantum numbers up to a large value of the latter. The diminution in the number of the bands in the liquid state may be due to the influence of translational motion of the molecules in the liquid in the state of aggregation. Probably, constant-impact of the neighbouring molecules hinders transitions to higher vibrational energy states. In the solid state the molecules are a little closer together and there is little room for much expansion of the molecule during different modes of oscillation. Hence such modes may be quenched in the solid state. There may be exceptions, however, in which case the regularity of the arrangement of the molecules together with peculiar

2537Å

2655Å

2891Å



Absorption spectra of cresols.

Fig. 1. *o*-cresol

(a) Liquid at 30°C

(b) Solid at -180°C

Fig. 2. *m*-cresol

(a) Liquid at 30°C

(b) Solid at -150°C

(c) Solid at -180°C

Fig. 3. *p*-cresol

(a) Liquid at 30°C

(b) Solid at 150°C

(c) Solid at -180°C



structure of the molecule may be responsible for peculiar type of packing in the solid state, in which the benzene ring may have some surrounding empty space to execute some modes of oscillation of higher quantum numbers. We shall now discuss the results for the three substances separately.

(a) *o*-Cresol. The results obtained by Robertson, Ginsberg, Matsen (1946) for the vapour state of *o*-cresol have been included in Table I. Tentative assignment has been made in column 4 of the frequencies observed. It is found that the vibrational frequencies 185 and 861  $\text{cm}^{-1}$  are represented in the bands. Probably the latter frequency represents the breathing vibration of the benzene nucleus in the excited state in the case of the vapour. On making an attempt to assign the frequencies observed in the case of solution of ortho-cresol in heptane by Wolf and Herold (1931) it is found that the frequencies deduced from these bands are 931 and 1500  $\text{cm}^{-1}$ , which are quite different from those observed in the case of the vapour. In the present investigation for the liquid and solid states much fewer bands are observed. The  $\nu_0$ -band seems to have shifted from 36247 to 35982  $\text{cm}^{-1}$  on liquefaction and only a companion representing the transition  $\nu_0 + 807 \text{ cm}^{-1}$  is present. Thus the bands shift towards longer wavelength. This may be due to the fact that in the liquid state molecules become associated with one another through virtual bonds and the electronic energy state is lowered during this process. The solid at  $-180^\circ\text{C}$  also exhibits two bands. The  $\nu_0$ -band eventually shifts again to shorter wavelength side and the companion represents the frequency  $\nu_0 + 869 \text{ cm}^{-1}$ . This increase in the value of the difference of energy between the two states is probably due to the contraction of the molecule itself in the solid at low temperature. The vibrational frequency of the ring also seems to increase a little in the solid state.

(b) *m*-Cresol. In this case the data reported by Purvis and McClelland (1913) showed that there are numerous bands besides the  $\nu_0$ -band. These companions of the  $\nu_0$ -band are due to the vibrational transitions as in the case of *o*-cresol. The data for solution in heptane reported by Wolf and Herold (1931) show vibrational frequencies 979, and 1541  $\text{cm}^{-1}$ . These frequencies can be reconciled only with those for the ground state of the molecule observed in the Raman spectra and not with those for the excited state. The frequencies observed in the Raman spectra for *o*-, *m*-, and *p*-cresol are quite different from each other. This shows that the relative positions of the substitution groups have much influence on the vibrational frequency of the benzene ring. In the case of *m*-cresol in the liquid state only two bands are observed in the present investigation. Both these are displaced towards longer wavelengths from the position of the corresponding bands in the vapour state. This again shows that there may be formation of virtual bonds among neighbouring molecules in this case also, as explained above. The second band represents the transition  $\nu_0 + 875 \text{ cm}^{-1}$  which shows that the vibrational frequencies of the excited state of the molecule in the liquid is 875  $\text{cm}^{-1}$ . In the solid state at  $-150^\circ\text{C}$ , both these bands shift towards shorter wave-

length by about  $25\text{ cm}^{-1}$ , but when further cooled down to  $-180^{\circ}\text{C}$ , the solid gives two bands shifted still further towards shorter wavelength and the vibrational frequency increases to  $893\text{ cm}^{-1}$ . This again may be due to contraction of the molecule in the solid state.

(c) *p*-Cresol. The results for *p*-cresol observed in the present investigation show some characteristics difference from those observed in the case of the other two cresols. The data for the vapour reported by Robertson, Ginsberg and Matsen (1946) are given in column (2) of Table III. Taking  $\nu_0$  to be  $35325\text{ cm}^{-1}$ , the assignment of other bands leads to vibrational frequencies  $791$  and  $1187\text{ cm}^{-1}$  are as shown in column 3 of the table. It is also found that transitions up to a value of the quantum number equal to 3 occurs in this case for the mode of frequency  $791\text{ cm}^{-1}$ . The data for the solution reported by Wolf and Herold (1931) cannot be classified satisfactorily according to such a scheme. Probably the intermolecular field of the solvent has influence on the electronic energy states of molecule. In the liquid state *p*-cresol yields only two bands, the second band representing the transition  $\nu_0 + 913\text{ cm}^{-1}$ . The solid at  $-150^{\circ}\text{C}$  yields 4 bands and this number increases to 5 when the solid is further cooled down to  $-180^{\circ}\text{C}$ . It is interesting to note that the vibrational frequencies deduced from these bands are  $825$  and  $1214\text{ cm}^{-1}$  in the solid state and that the transition  $\nu_0 + 2 \times 825\text{ cm}^{-1}$  as well as  $\nu_0 + 825 + 1214\text{ cm}^{-1}$  take place in this case at the low temperature. On comparing these results with those for the vapour, it is found that on liquefaction the principal band shifts towards longer wavelength by about  $300\text{ cm}^{-1}$  and on solidification the position remains almost the same as that in the liquid. Further, the vibrational frequency is about  $791\text{ cm}^{-1}$  for one of the modes and  $1187\text{ cm}^{-1}$  for the other mode in the case of the vapour, while these increase to  $825$  and  $1214\text{ cm}^{-1}$  respectively in the solid state.

When the two substitution groups are in the para position, there is some symmetry in the molecule and the permanent electric moment is much smaller than that of the molecule with the substitution groups either in ortho or meta position. The influence of intermolecular field is almost identical in the liquid and solid states of *p*-cresol, probably because the value of the permanent electric moment is small. The shift of the principal band towards longer wavelength side with the liquefaction of the vapour, however, shows that in the liquid state there may be formation of virtual bonds as in the other two cases. The pseudo-symmetry of the molecule may lead to such an arrangement of the molecules in the crystal as would leave some intervening space between the benzene rings, and therefore, vibrational transitions to higher quantum energy states may be possible in this case:

It is well known that according to Davydov's theory there may be splitting of the energy levels of the molecule in the crystal due to intermolecular forces. None of the three substances mentioned above shows such splitting and in the case of *p*-cresol the extra bands can be accounted for by assuming them to be due to excitation of harmonics of certain modes of



vibration of the benzene ring. This absence of Davydov's splitting in these three cases may be due to the fact that already in the liquid state the molecules get associated with each other and the association of molecules exhibits itself in the shifting of the bands towards longer wavelength side.

Investigations with other benzene compounds are in progress and the results will be reported later.

## ACKNOWLEDGMENTS

The author is indebted to Prof. S. C. Sirkar, D. Sc., F. N. I. for his kind interest and helpful guidance throughout the progress of the work and to the Government of India, Ministry of Scientific Research, for the award of a scholarship.

## REFERENCES

- Broude *et al* (1950), *Izvest. Akad. Nauk. Ser Fiz.* **14**, 487.  
Davydov, A. 1948, *J. Exptal. Theoret. Phys. (U. S. S. R.)* Vol. **18**, 210.  
Klingstedt, F. W. 1923, *Comp Rendus.* **176**, 674.  
Kronenberger, A. and Pringsheim P., 1926, *Z. f. Phys.* **40**, 75.  
Purvis, J. E., and McClelland, N. P., 1913, *J. Chem. Soc.* **103**, Pt. I, 1088.  
Robertson, W. W., Nathan Ginsberg, and Matsen, F. A., 1946, *Ind. Eng. Chem. Anal.* **18**, 746.  
Swamy, H. N., 1951, *Ind. J. Phys.*, **25**, 262.  
Wolf, K. L., and Herold, W., 1931, *Z. f. Phys. Chem.* **B 13**, 201

# RESONATOR ABSORBERS IN BROADCAST STUDIOS\*

BY RAM K. VEPA

RESEARCH DEPARTMENT, ALL INDIA RADIO, NEW DELHI

(Received for publication, October 27 1951)

## Plate V

**ABSTRACT.** Low-frequency absorption is often a matter of great difficulty in broadcast studios and different methods of providing it are discussed. It is shown that a perforated rigid sheet held at some distance from a non-yielding backing offers a convenient means of low-frequency absorption and expressions for the resonance frequency absorption coefficient, and  $Q$  value in terms of the physical parameters are derived. An experimental method is described both for the case of normal incidence (tube experiment) and random incidence (reverberation chamber). The effects of coupling and artificial damping of such structures are also studied. Finally some considerations for practical designs are outlined.

## INTRODUCTION

The frequency response of broadcast studios is increasingly recognized as an important factor in the quality of programmes that are generated in them and different optimum reverberation time-frequency curves have been postulated for most pleasing effect. However, one common difficulty in the proper acoustical design of most studios is the insufficient absorption that takes place at the lower frequencies. This is so because, while audience and most objects commonly found in studios show satisfactory absorption in the medium and higher frequency ranges, even commercial acoustical materials reveal a marked decline in their absorptive powers below 250 $\omega$ . This insufficient low frequency absorption introduces an unpleasant "boom" in the sound quality of the programmes. Besides, spurious frequencies sometimes appear in rooms producing undesirable effects in the programme. For instance, if the floor and ceiling are not treated adequately, standing waves are liable to be set up and these are usually in the frequency region below 100 $\omega$ .

## DIFFERENT METHODS FOR LOW FREQUENCY ABSORPTION

To correct these acoustical defects, various devices have been used in practice to provide considerable absorption at the lower frequencies. One

\* This investigation was carried out in the University of California, Los Angeles, as a part of the thesis for doctorate degree.

such is the membrane absorber consisting of an air-tight membrane, such as oil cloth, paper or plywood, placed at some distance from a rigid wall. However, for appreciable absorption, considerable quantities of such absorbers will have to be used and besides unwanted frequencies appear due to the membranes vibrating in different modes. Another device, used extensively in the main studios of the broadcasting house in this country, consists of wooden air-tight boxes ( $4' \times 2'$ ) broken up unsymmetrically by card board into 15 cells, to prevent any transverse standing waves being set up inside. A layer of glass silk is placed over the board, and over it is a perforated transite board. The depth of such an "impedance box" varies from 12" to 18" depending on the particular frequency range that is required to be absorbed.

#### RESONATOR ABSORBERS

A third device, becoming increasingly popular in western Europe and Scandinavia, utilises Helmholtz resonators, either singly or in groups to obtain high absorption over a narrow range in the low frequency end of the audio spectrum. Such an application is, however, not new as has been revealed by excavations of Greek open air theatres, where resonators were used both as absorbers and amplifiers. The use of such resonators in the form of vases in Scandinavian churches (of the 13th century) and the Byzantine cathedrals seems to have reduced the long reverberation times usually associated with such buildings.

More recently, an extensive use of such resonator absorbers has been made in the new Danish broadcasting house at Copenhagen (Jordan, 1947). The studio walls are made of wooden panels (16-23 mm in thickness) and a 10% perforation is employed for a broad absorption characteristic. The panels are divided into 12 sections (in one of the studios) which can be moved independently away from or towards the backing, thus varying the frequency absorption curve to the desired shape. The lower frequency limit in the dead room has been extended by the use of resonant structures of thickness 5.5 cms, with openings of  $3 \times 4$  cms and depth of 20 cms behind conventional porous material. Pronounced singularities in the concert studio (reverberation time of 10 secs at 63 c. s.) have been eliminated by the installation of resonators tuned to that frequency.

However, experimental data on the actual performance of such resonators is scanty, making design computations vague and unreliable. In the following pages, results of a complete and systematic investigation—both theoretically and experimentally on such resonator structures will be outlined, and some main design considerations set out.

#### THEORY OF SINGLE HELMHOLTZ RESONATOR

The theory of the single Helmholtz resonator (figure 1) which is a vibrating system consisting of a compressible fluid contained in an enclosure

communicating with an external medium through an opening of restricted area is dealt with in most text books (Rayleigh). The mass of the fluid in the neck can be considered as the inertance element in the analogous acoustical system ; inside the resonator, the fluid is alternately compressed and expanded by the motion of the fluid in the neck providing the stiffness element.

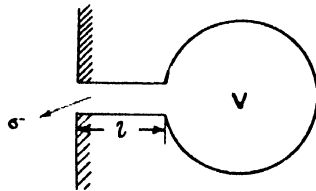


FIG. 1

The natural frequency of the resonator can at once be written down :

$$f_0 = \frac{c}{2\pi} \sqrt{\sigma / V l_e} \quad \dots \quad 4.1$$

where  $c$ =velocity of sound ;  $\sigma$ =area of the aperture ;  $V$ =volume of cavity ; and  $l_e$ =effective length of the neck.

A correction which Rayleigh computes relates to the length of the resonator neck. He finds that the edge effects can be accounted for by assuming an increase in the actual length ( $l$ ) to form the effective length of the neck,  $l_e$ . It can be shown from simple hydro-dynamical consideration of the air flow that for small values of  $l$ ,

$$l_e = l + \frac{\pi}{2} r \quad 4.2$$

where  $r$  is the radius of perforation.

However, Rayleigh's edge correction (4.2) for the case of wide apertures and small cavity depths comes out to be more than twice the depth of the cavity itself, which is obviously untenable. It can be seen that the presence of a rigid backing close to the aperture will modify the flow pattern and compress the stream lines nearer to the plane surface in which the aperture is situated (figure 2). An empirical estimate from an equation obtained by

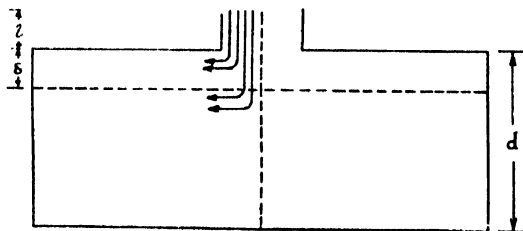


FIG. 2

considering the propagation of waves inside the resonator, shows that close correlation with measured values of resonance frequency is obtained when

the correction for the closed end,  $e = d/4.2$  where  $d$  = cavity depth (Vepa, 1950). There is not a marked dependence of  $e$  on aperture radius.

Hence for the case of small  $d$ , ( $d \ll 2r$ )

$$l_e = l + \frac{\pi r}{4} + \frac{d}{4.2} \quad 4.3$$

Such a resonator can either absorb energy by friction in the neck or else re-radiate the sound from the mouth, thus acting as a diffuser for the incident sound. Since the primary purpose here is to provide high absorption, attention will be focussed mostly on the former effect.

Though single resonators can be used effectively to eliminate any particular unwanted mode, it has been found more useful and economical in practice to employ a group of them. The study of such resonant group structures will form the bulk of this report.

#### PANEL RESONATORS

From figure 3, it can be seen that when rigid perforated sheets are placed at a convenient distance from a non-yielding backing, there is in effect

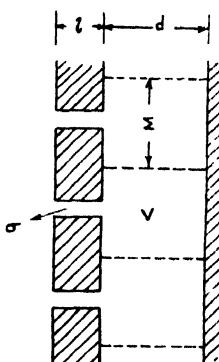


FIG. 3

formed a system of Helmholtz resonators each consisting of cavity  $V$ , a neck of length  $l$  (i.e. thickness of perforated sheet) and a sectional area  $\sigma$ , where the mouth is applied to an infinite flange.

To obtain expressions for the resonance frequency, absorption coefficient, and other characteristic quantities of the resonant group structure, the following assumptions are made:

- (i) That the resonators are distributed in a two dimensional lattice over a surface which is large compared to  $\lambda$ .
- (ii) That the perforation areas are equal to each other and small compared to the wavelength ( $\lambda$ ) of the incident sound.
- (iii) That distances between the perforations are equal to each other, are small compared to  $\lambda$  but are large compared to the perforations themselves; hence the resonators act individually with no interaction between them.
- (iv) That the impressed sound wave is plane and is incident normally.

(7) That the backing and the sheet in which perforations are made are both rigid.

For a normally incident sound, since the distances between the perforations are small compared to  $\lambda$ , nothing will be changed in the process of sound propagation if rigid tubes of section  $\Sigma$  in the centre of which apertures of area  $\sigma$  are to be introduced *i.e.*, the free surface of incident wave is equally divided between all apertures.\*

Isolating a layer of length  $z$  ( $\ll \lambda$ ), it can be assumed that on one side we have a plane incident and plane reflected wave, while on the other there is a quasi-stationary vibration process in the neck of the resonator (figure 4).

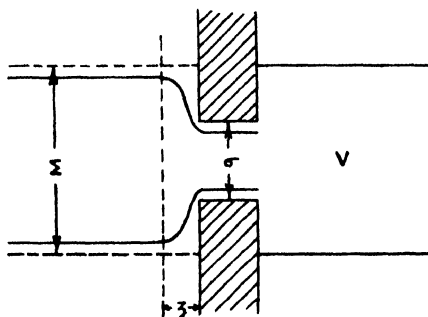


FIG. 4

The boundary conditions on either side of the transition layer can be expressed as :

$$\rho c(A_0 + A_1) = Z.A_2 \quad \dots \quad 5.1$$

$$\Sigma(A_0 - A_1) = \sigma A_2 \quad \dots \quad 5.2$$

where  $A_0$ ,  $A_1$ ,  $A_2$  are the amplitudes of the incident, reflected and transmitted waves respectively,  $Z$ , the input impedance in the resonator neck,  $\Sigma$  the area of the wavefront corresponding to a single perforation and  $\sigma$  the aperture area.

$$\frac{A_1}{A_0} = \frac{Z - \rho c/\epsilon}{Z + \rho c/\epsilon}$$

where  $\epsilon = \Sigma/\sigma$  = perforation coefficient or velocity amplification coefficient. For complete absorption *i.e.*, no reflection

$$Z = R + jX = \rho c/\epsilon$$

$$R = \rho c/\epsilon \quad \dots \quad 5.3$$

$$X = 0$$

$$\text{Absorption coefficient } (\alpha) = 1 - \left| \frac{A_1}{A_0} \right|^2 = \frac{4\alpha}{(\alpha + 1)^2 + \delta^2} \quad \dots \quad 5.4$$

\* This is not true in the case of oblique incidence.

where  $\alpha = \epsilon R / \rho c$  ;  $\delta = \frac{\epsilon \lambda}{\rho c}$

$$\left(\alpha - \frac{2-a}{a}\right)^2 + \delta^2 = \left(\frac{2\sqrt{1-a}}{a}\right)^2 \quad \dots \quad 5.5$$

where  $a$  is the absorption coeff. at any frequency.

Equation 5.5 is that of a circle in  $\alpha$  and  $\delta$  with centre at  $\left(\frac{2-a}{a}, 0\right)$

and radius  $\frac{2\sqrt{1-a}}{a}$

Specific acoustical impedance of the resonator opening

$$= \epsilon R + j\omega \epsilon \rho l_e - \frac{j\rho c^2}{\omega d} \quad \dots \quad 5.6$$

In the electrical analogue,

inductance

$$L = \epsilon \rho l_e$$

capacity

$$C = d / \rho c^2$$

writing

$$\beta = \frac{1}{\rho c} \sqrt{L/C} = \sqrt{\epsilon l_e / d}$$

$$\gamma = \omega \sqrt{LC} = \frac{\omega}{c} \sqrt{\epsilon l_e d}$$

It can be shown

$$\delta = \beta \left( \gamma - \frac{1}{\gamma} \right) \quad 5.7$$

$$\frac{4\alpha}{(\alpha+1)^2 + \beta^2 \left( \gamma - \frac{1}{\gamma} \right)^2} \quad \dots \quad 5.8$$

For resonance frequency, absorption coeff ;  $a_0 = \frac{4\alpha}{(\alpha+1)^2}$

$$\text{Frequency of resonance } f_0 = \frac{c}{2\pi} \sqrt{\sigma / V l_e} = \frac{c}{2\pi} \sqrt{\frac{\sigma}{l_e d}} = \frac{n}{S} \quad \dots \quad 5.9$$

where  $S$  = total area of the surface on which perforations are made.

$n$  = total number of perforations.

$$\text{Eq. 5.8 can be re-written as } a = \frac{4\alpha}{(\alpha+1)^2 + \beta^2 (f/f_0 - f_0/f)^2} \quad \dots \quad 5.10$$

For

$$f_1 = f_0 / \sqrt{1.5}$$

$$a_f = \frac{4\alpha}{(\alpha+1)^2 + \beta^2 / 6}$$

$$\beta^2 = 24\alpha \frac{a_0 - a_f}{a_0 + a_f} \quad \dots \quad 5.11$$

$\beta$  can be computed from equation 5.11 by taking the absorption coefficient values at two frequency points on the resonance curve.

Again 
$$\frac{\alpha f}{\sigma_0} = \frac{1}{1 + \beta^2 / (\alpha + 1)^2 (f/f_0 - f_0/f)^2} \quad 5.12$$

From equation 5.12, it can be seen that  $\beta^2 / (\alpha + 1)^2$  gives an indication of the sharpness of resonance of the absorption curve and can be considered as analogous to the  $Q$  values of the electrical resonance curves.

Measurements to check the equations obtained above, have been made on transite sheets of thickness varying from  $1/8''$  to  $1''$ , on which perforations (number ranging from 1 to 17) were made so that each perforation corresponds approximately to equal areas of sheet surface (and hence to equal volume of the cavity behind) figure a, Plate V). Distances between the sheet and the rigid backing are varied by using spacer rings of different depths ( $1/8'' - 4''$ ).

The impedance and absorption coefficient values are measured in a conventional manner by producing and exploring an interference pattern in front of the structure which closes one end of a long steel tube.

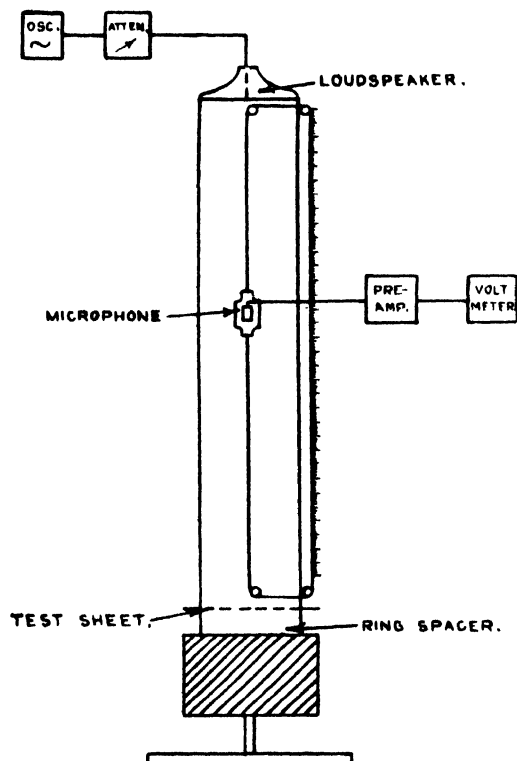


FIG. 5

Schematic of the tube assembly

Length of the tube 307.0 cm.

Inner dia ... 29.6 "

Thickness ... .6 "



Rayleigh's condition ensures that for the tube diameter employed, uniform plane waves are generated for frequencies less than 700.

Pressure amplitudes in the tube are measured with a tiny but sensitive Bi-morph crystal mike and this is capable of being moved along the axis of the tube by means of a graduated steel tape that runs round the tube (figure 5). The pressure maxima and minima after a 2-stage amplification are read on electronic voltmeter. By measuring also the distance of the first minimum with and without the test structure, the impedance ratios  $R/\rho c$  and  $X/\rho c$  can be read directly from the hyperbolic impedance charts (Beranek, 1947).

Since the pressure amplitudes can be measured accurately, a precision of 1-2% is attained in the measurement of the absorption coefficient. The determination of the impedances, however, presents greater difficulty particularly as the reactive part is sensitive to the position of pressure nodes and antinodes. The distances are measured on the tape to a millimeter and hence the accuracy of the impedance measurements does not seem to be greater than about 8-10%.

#### EXPERIMENTAL RESULTS OBTAINED

(i) The range of measured frequencies is between 150 $\sim$  and 400 $\sim$  and an agreement within 15% is obtained between computed and experimental values, the latter being usually the greater. The absorption coefficient—frequency characteristics are generally sharp curves with single peaks. In a few instances, minor peaks are obtained at neighbouring frequencies—not necessarily harmonics. These double humps are mostly in the low frequency region between 200 $\sim$  and 250 $\sim$  and with sheets of small thickness ( $\frac{1}{8}$ "'). It is possible that the natural vibration of the sheet, assumed in theory to be rigid, is responsible for the secondary peaks noted in some resonance characteristics.

(ii) *Variation of physical parameters* :—The dependence of the resonance frequency on the effective length of the resonator neck  $l_e$ , the depth of cavity  $d$ , the diameter  $2r$ , and number of perforations on the sheet  $n$ , is studied by varying each of the factors at a time. Equation 5.9 is followed to within 15%, except in the case of perforation diameter where some deviations are encountered due to the complex streaming phenomenon in the neck making it difficult to compute the effective sectional area. Some discrepancies are also noted for the case where  $n=17$ , when coupling effects, not taken into account in theory, might be expected to influence the result.

(iii) *Coupled resonators* :—The sharpness of resonance of the structure characteristics, however, precludes them from being used to absorb over a wide frequency band, which in most cases is only a few cycles wide. This can be extended by the use of complex resonating structures. Different sized perforations on the same sheet and the physical division of the cavity seem to aid greatly in the process. For instance, a band of 100 c/s, with a value

of a 0.7, is obtained when 3 sized perforations of diameters  $\frac{1}{4}$ ",  $\frac{9}{16}$ ",  $\frac{10}{16}$ " are made symmetrically on a sheet of thickness  $\frac{1}{4}$ ". The co rresponding band

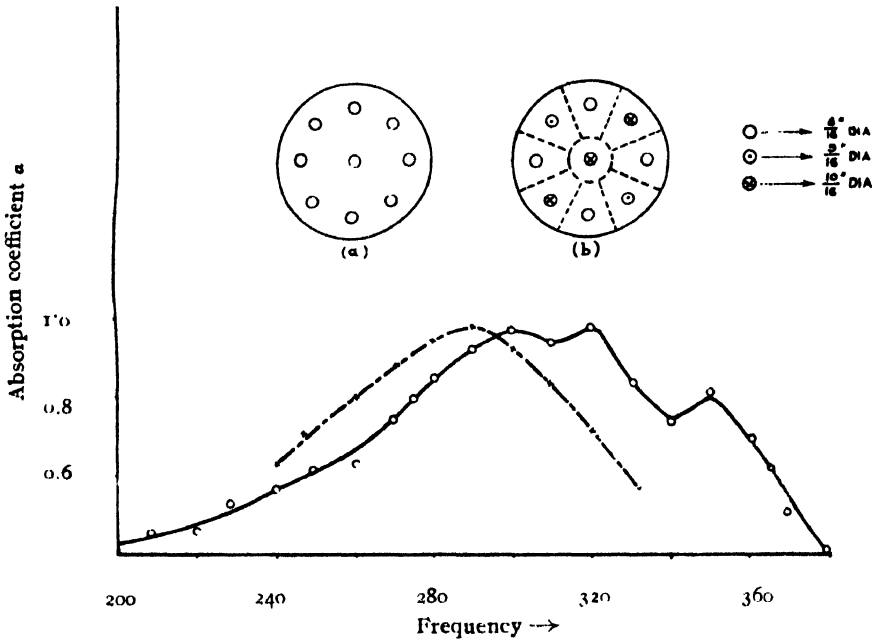


FIG. 6  
Coupled resonators

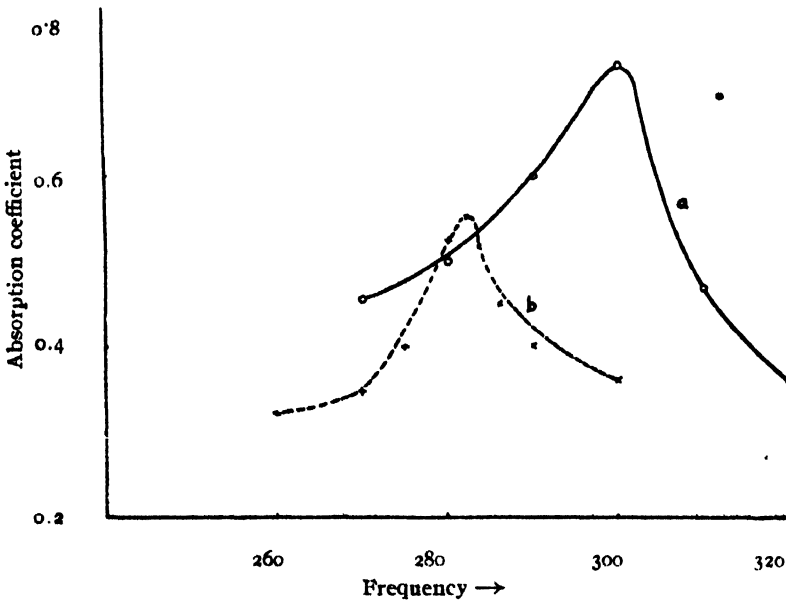


FIG. 7  
Damped resonator characteristics. (a) Structure alone,  
(b) With glass wool in the perforations.

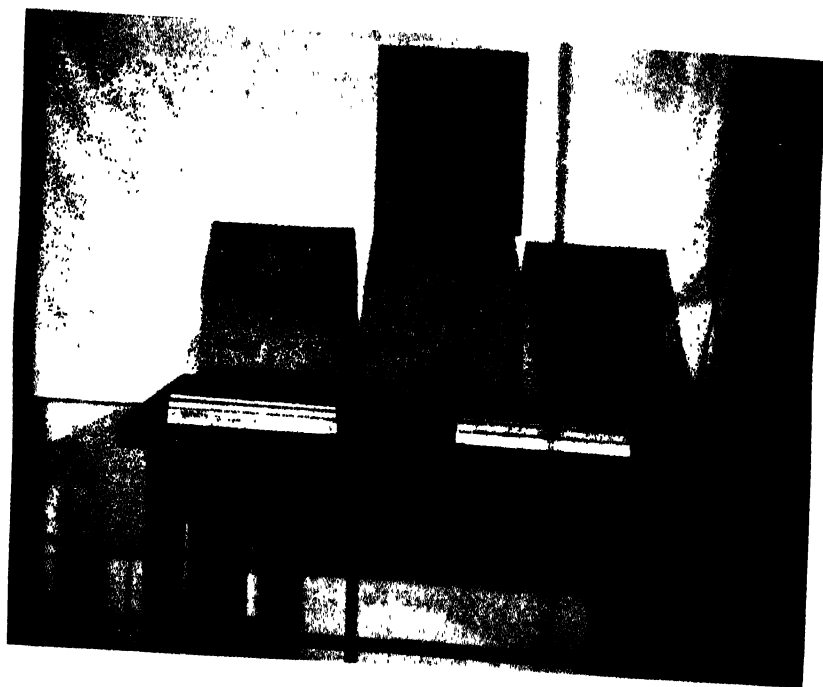


Fig. a

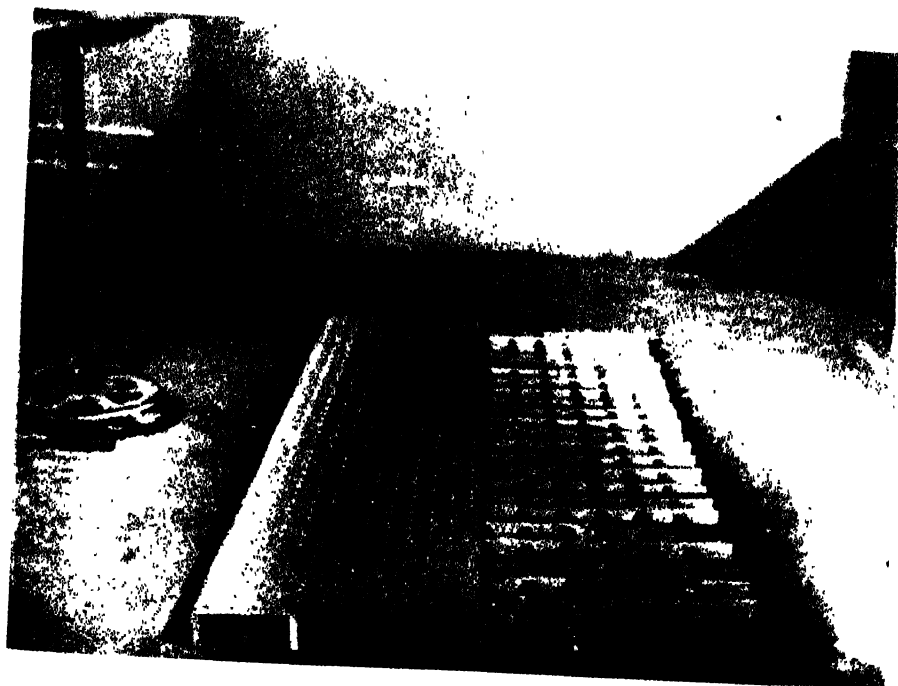


Fig. b



for uniform sized perforations of diameters  $\frac{1}{8}$ " is only 70% (figure 6). Little effect is noticed when 2 resonance structures are sought to be coupled by placing one above the other physically.

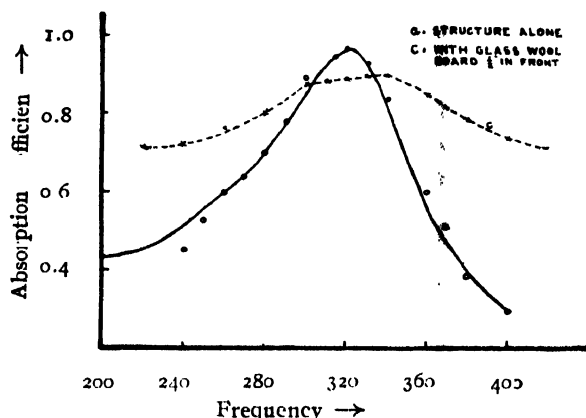


FIG. 8  
Damped resonator characteristic

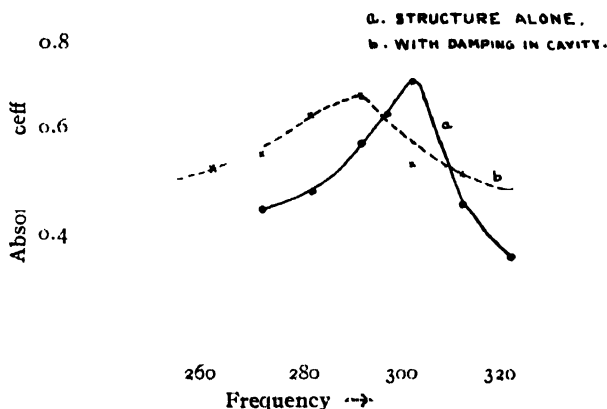


FIG. 9  
Damped resonator characteristics

(iv) *Artificially damped resonators*:—The artificial damping of resonators provides a convenient means to vary the resonance characteristics. With glass wool loosely packed in the perforations, there is an increase in the resistance and hence a decrease in  $a_{\max}$ . The sharpness of resonance remains substantially the same (figure 7). With a homogeneous glass wool board (of thickness 1") in front of the sheet, a considerable broadening of the curve is obtained (figure 8). If, however, the cavity is plugged with glass wool, there is a slight decrease in resonance frequency and absorption maximum together with a broadening of the curve (figure 9). Combinations of these damping methods indicate that an artificially damped structure is not much aided by further damping.

# REVERBERATION CHARACTERISTICS WITH RESONATORS

So far systems have been described where the sound is incident normally on the resonant structures. In actual use, however, sound is incident in all directions and it is interesting to investigate how these structures behave under conditions of random incidence.

The reverberation chamber of the acoustical laboratory, of the University of California, Los Angeles, is parallel-walled and of dimensions  $19' \times 20' \times 16'$ . Built of concrete, the chamber is separated from the earth by sand and corkstrips preventing any solid borne vibrations coming from below or other parts of the building. A motor driven paddle ensures a thorough mixing of the sound in the room.

The loudspeaker (dynamic)-Altec, with baffle for low frequency and horn for high frequency—is mounted at the corner of the chamber, since in this position the greatest number of room resonances are excited and the maximum energy is supplied to the room. The detector—dynamic microphone—is located at another corner of the room.

The schematic of the set-up is shown in figure 10.

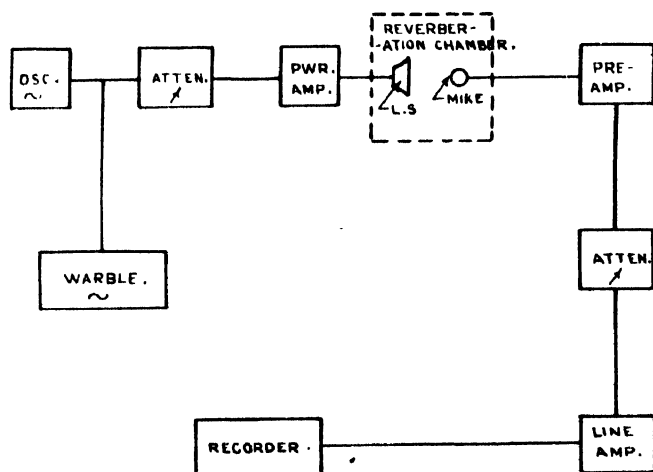


FIG. 10

Recorder:—High speed level recorder  
(sound apparatus—model HPL 17).

The resonator structures under test consist of four  $8' \times 2'$  transite board sheets of thickness ( $\frac{1}{8}$ " ) and having uniformly spaced perforations of 1 for 4 sq. inches. Two such structures were placed symmetrically on either side of the rotating paddle. The resonator depth was adjusted so that they tune to about 380 cs. (figure b, Plate V).

Since the dimensions of the structures here employed are comparable and larger than the wavelength of sound, the former assumption that the cavity behind is equally divided between the perforations is no longer valid. Further,

tangential waves are set up behind the sheet making the impedance more strongly dependent on the angle of incidence of the wave. The solution is to break-up the cavity by a honey-comb structure whose cells are small in dimension compared to  $\lambda$ . The cell structure eliminates the tangential modes and gives a normal particle velocity maximum at the resonator neck for all the modes present in a given frequency region (Bolt and Brown, 1940).

The experiment is conducted without any resonating structures and the warbled sound is fed into the chamber for some time to attain a steady level. The high speed level recorder is then switched on and a suitable paper speed actuated. The oscillator is turned off and the recorder inscribes the decay curve of the sound on a moving waxed paper.

The minimum value inscribed is determined by the noise level in the circuit. The experiment is repeated at different frequencies between 100 and 1500 *cs.* with and without the resonator structures.

A typical curve of the absorption coefficient-frequency characteristic is shown in figure 11. As can be seen, the values of absorption are generally lower than in the tube experiment. The structures are less selective than for normal incidence and hence can be used over a wider frequency range. A second harmonic effect is also noted.

When the structures are damped with glass wool in the perforations, the curves broadened considerably and the absorption maximum shifted to a slightly higher frequency (figure 12).

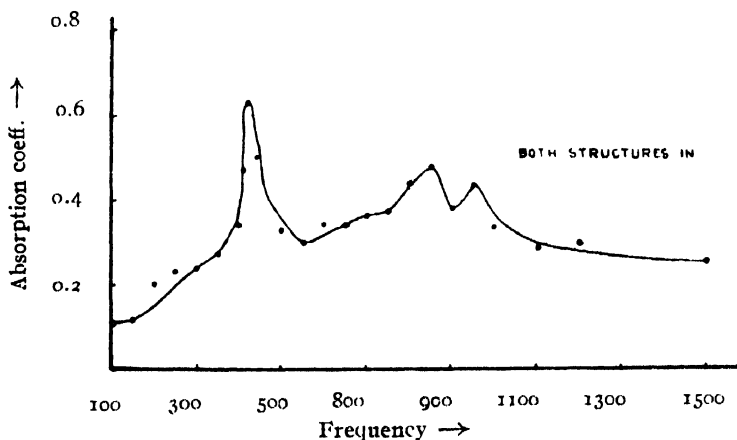


FIG. 11

Reverberation absorption coefficient of resonators

## SOME DESIGN CONSIDERATIONS

The actual design of resonators either single or in groups is a matter of choosing several physical parameters to give the best results for a specific purpose.

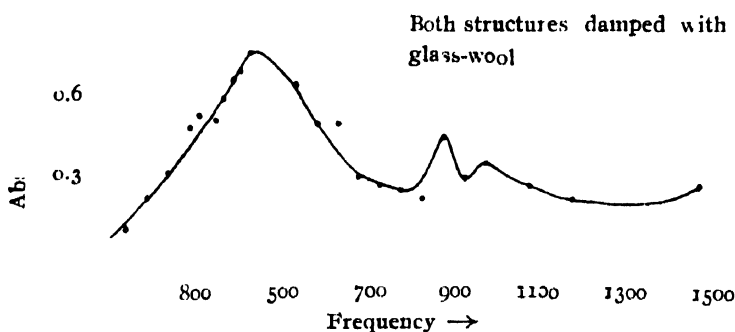


FIG. 12

\* Reverberation absorption coefficient of resonators

The choice of single resonator or group structure depends primarily on the type of absorption needed in the studio. If it is a matter of eliminating or reducing some undesirable modes at a single frequency or small range of frequency, single resonators are most effective. However, it turns out to be simpler and more economical in most cases to provide panel absorbers whose resonance characteristics are more flexible.

Data has indicated that equation 5.9, giving the frequency of resonance of the structure, holds to within 15% for small sized perforations and fewer number of them.

$$f_0 = \frac{c}{2\pi} \sqrt{\frac{\sigma}{l_e d}} \cdot n \cdot S$$

In many designs  $\sigma$ ,  $n$  and  $S$  may be determined by standard specifications and  $d$  by the physical factors of placement in the studio.

$$a_0 = \frac{4\alpha}{(\alpha + 1)^2}$$

$$\text{where } \frac{\epsilon R}{\rho c} \qquad \text{where } \qquad = S/n\sigma$$

$$a_0 = 1 \text{ where } R = \rho c / \epsilon$$

The theoretical evaluation of the resistance in the neck has been one of the most troublesome factors in correct design of resonators. Crandall's theoretical expression

$R = \frac{l\sigma}{r} \sqrt{2\rho\mu\omega}$  has in practice been found to be much lower than the measured value. Corrections have been applied to  $l$  taking the end correction into account and to  $\mu$ , taking the heat conductivity into consideration.

$$r = \frac{l_e \sigma}{\rho c}$$



Measured data Vepa, 1950 indicates that a close correlation with experimental values is obtained if

$$R = \frac{2l_e \sigma}{\tau} \sqrt{\frac{1}{2\rho\mu'\omega}}$$

$$l_e = l + \frac{\pi}{2}$$

The sharpness of resonance is dependent on the factor  $\beta^2/(\alpha+1)^2 = \frac{6l_e}{d(\alpha+1)^2}$ . This would mean that for small values of  $\sigma$  and of  $d$  and large values of  $l$ ,  $\beta$  becomes great, i.e. the curve becomes selective. However, changing  $l$  and  $\sigma$   $\beta$  changes and hence the equivalent  $Q$  value of the curve.

The design then resolves itself into choosing values of  $S$ ,  $l$ ,  $n$ ,  $r$ ,  $d$  and suitable damping to give the following equations best fit :

$$f = \frac{c}{2\pi} \sqrt{\frac{\sigma}{l_e d}} \cdot \frac{n}{S}$$

$$R = \rho c / e = \frac{2l_e \sigma}{\tau} \sqrt{\frac{1}{2\rho\mu'\omega}}$$

$$\frac{\beta^2}{(\alpha+1)^2} = \frac{e l}{d} \cdot \frac{1}{\left(\frac{eR}{\rho c} + 1\right)^2}$$

is small or great according as the characteristic is desired to be broad or sharp.

Obviously, a compromise will have to be effected between conflicting design parameters. Further refinement can be made by adding complications in the form of coupling and artificial damping.

Effective absorption introduced by one resonator =  $\Sigma \times a$

$$\text{No. of resonators required} = \frac{\text{No. of absorption units needed}}{\Sigma \times a}$$

The actual steps in the design may be outlined as follows :

$$f = \frac{c}{2\pi} \sqrt{\frac{1}{e l_e d}}$$

$$f^2 \times 4\pi^2 \times l_e \times d \quad \dots \quad 8.1$$

$$R = \frac{\rho c}{e} = \frac{2l_e \sigma}{\tau} \sqrt{\frac{1}{2\rho\mu'\omega}} \quad \rho c = 42 \text{ C.G.S. units.}$$

$$\frac{42\tau}{2l_e \sigma \sqrt{2\rho\mu'\omega}} \quad \dots \quad 8.2$$

Combining (1) and (2)

$$\frac{d}{r} = \frac{c^2 \times 2\pi \times \sqrt{2\rho\mu'\omega}}{42f^2 \times 4\pi^2} \quad 8.3$$

8.1 can be re-written as

$$\epsilon l_e d = \frac{S}{n\sigma} \quad l_e d = \frac{cr^2}{f^2 \times 4\pi^2} \quad 8.4$$

$$n = \text{no. of resonators} = \frac{\text{no. of absorption units}}{\Sigma \times \alpha}$$

$N$  is usually in sq. ft.

$$n = \frac{N \times 900}{\Sigma \times \alpha}$$

$$n\Sigma a = 900N$$

Taking  $a=1$ ,  $n\Sigma=S$ ,

$$S = N \times 900 \quad 8.5$$

Combining 8.4 and 8.5

$$\frac{n}{l_e} = \frac{f^2 \times 4\pi^2 \times d \times N}{1130 \times 1130 \times \pi r^2} \quad 8.6$$

(A) Evaluate  $\frac{d}{r}$  from equation 8.3; (B) evaluate  $\epsilon l_e d$  from equation 8.4; (C) evaluate  $n/l_e$  from equation 8.6 assuming either  $d$  or  $r$ ; (D) assuming  $l_e$  obtain  $n$ ; (E) correct the value of  $n$  to the nearest convenient figure; (F) obtain the characteristic quantities: frequency  $f$ , resistance  $R$ , absorption coefficient  $a$ , (since it would now vary from 1), sharpness of resonance coefficient,  $S$ ,  $\Sigma$ , and  $l$  (the actual length of the neck); (G) finalise the details of the design and the way in which the resonators are to be mounted and their location.

As can be seen, conflicting factors come in and one has to choose the most suitable compromise.

The choice of  $l$  and either  $d$  or  $r$  is usually determined by physical factors in the studio and the materials available.

If artificial damping or coupling is desired, the design becomes more complex but an approximate idea of the behaviour of such complex resonator systems can be had from the data already presented.

## CONCLUSIONS

(i) It is possible to design quite accurately groups of simple and cheap resonators to provide high absorption values in the low frequency region.

(ii) The range over which such absorption is obtained is generally restricted and hence such devices are most effective in eliminating single unwanted frequencies.

(iii) This range can be extended by choice of proper physical parameters. More effectively, this can be done by the use of resonators of different perforation diameters on the same sheet and breaking up the cavity behind physically.

(iv) Artificial damping in the resonators enables one to vary the resonance characteristic of the structures suitably.

(v) With large scale resonator structures in the reverberation chamber, lower values of absorption coefficients are obtained but over a wider range.

## ACKNOWLEDGMENT

This investigation was carried out in the University of California, Los Angeles, as part of the thesis work for the award of a Doctor's degree, under the direction of Dr. Robert W. Leonard and Dr. Vern O. Knudsen, to whom the author is indebted for much fruitful discussion and many helpful suggestions. Grateful thanks are also due to Mr. B. V. Baliga, Chief Engineer, All India Radio, for kindly according permission to publish this paper.

## REFERENCES

Jordan; 1947, *JASA*, **19**, 972.

Rayleigh; 1877, *Theory of Sound* (Dover; Vol. 2.), p. 170.

Vepa; 1950, Unpublished work.

Rayleigh; 1877, *Theory of Sound*, (Dover; Vol. 2), p. 159.

Beraneck, 1947, *JASA*, **19**, 420, 1947.

Bolt and Brown; 1940, *JASA*, **12**, 31.

Vepa; 1950, Unpublished work.

# MOLECULAR MOTION IN FLUIDS AND INTERNAL DISPERSION AND ABSORPTION OF ELASTIC AND OPTICAL WAVES

By A. K. DUTTA

DEPARTMENT OF PHYSICS, UTKAL UNIVERSITY, CUTTACK

(Received for publication, January 21, 1952)

**ABSTRACT.** A theory has been worked out on the basis of molecular motion to determine the absorption and internal dispersion of optical and elastic waves. The present available data on the supersonic absorption have been explained. A general broadening of the lines in the diffraction spectra obtained by the wave field grating has been noted and satisfactorily explained on the basis of a range of elastic wave velocity. The broadening of the spectral lines obtained with the help of a plane diffraction grating has also been noted and attributed to the effect of molecular motion in the liquids.

## INTRODUCTION

The velocity of the elastic waves is determined by the relation,

$$V^2 = d\rho/dp = \frac{1}{\rho\beta} \quad \dots (1)$$

where,  $\beta$  is the adiabatic compressibility. In the case of a gaseous medium, the relation works out in the simple, well known form,

$$V^2 = \gamma p / \rho \quad \dots (1a)$$

where,  $\gamma$  is the ratio of the specific heats. These relations bring out the important and verified characteristic property that the sound velocity is independent of the frequency of waves, unlike the optical waves. The above relations have been obtained without any associated relation for the absorption of the waves, as is usual for the optical case. A relation determining the absorption was given by Stokes (1845), on the basis of the equation of motion of a viscous medium, in the form,

$$\alpha/v^2 = \frac{8\pi^2\eta}{3\rho V^3} \quad \dots (2)$$

where,  $\alpha$  is the absorption coefficient per unit length,  $\eta$  the viscosity coefficient and  $v$  is the frequency of the wave motion. The method of procedure, however, does not give a corresponding relation for the velocity of the waves. The relation indicates that  $\alpha$  should be proportional to  $v^3$  or that  $\alpha/v^2$  should be a constant for different frequencies. The experimental findings are that  $\alpha/v^2$  is independent of frequency for a medium, but the magnitude of the constant is generally a multiple of the Stokes' constant. The experimental values of this Stokes' constant multiplier,  $M$ , varies from 1 to the

order of 1000 in the case of different substances. No justifiable explanation of this has been forthcoming, although attempts to explain it by the principle of relaxation mechanism have been made by different workers on the lines of Dutta and Ghose (1937-38, Kneser, 1938). Further, it has been experimentally observed (Rapuano, 1947; Biquard, 1935; Willard, 1941) that liquid carbon-bisulphide, which has the Stokes multiplier as 1500 in the region upto 1 megacycle per second has a drop in the amount of  $\alpha/v^2$  by 1/5th, in the region of 100 megacycles per second. In the case of acetic acid (Pikerton 1948), the value of  $\alpha/v^2$  shows a rapid increase with decreasing frequency, the magnitude being about  $3000 \times 10^{-17}$  c.g.s. units in the region of a few megacycles. The Stokes constant would be only of the order of a few units of  $10^{-17}$  c.g.s. units.

An important clue to the explanation of the whole phenomenon is the associated breadth of the spectral lines obtained by the method of Debye and Sears (1932), where diffraction spectrum is produced by the elastic wave field grating. It might have been noticed by all workers in the line that, whereas, water with the Stokes multiplier as 3, has very sharp spectral lines,  $\text{CS}_2$ , with the Stokes multiplier as 1500 has very diffuse and broad lines. Benzene, with a Stokes multiplier of about 100, has a breadth of the spectral lines in between them. One possible cause of this spreading of the spectral lines might be a range of variation of the velocity of the elastic waves and this would mean that a liquid with a large absorption coefficient or rather with a large Stokes multiplier has a large range of variation of the wave velocity. Such a varied range of velocities, in the case of substances, with different magnitudes of the Stokes multiplier has been obtained below on theoretical grounds. The spreading of the velocity may be termed as internal dispersion.

In order to substantiate internal dispersion and explain absorption, relations have been obtained for the elastic wave velocity and the absorption coefficient, on the basis of molecular motion, very similarly to the procedure adopted for the treatment of the optical wave velocity and absorption, on the basis of electronic motion.

#### THEORETICAL PROCEDURE FOR ELASTIC WAVES

The usual optical relation,

$$D = KE$$

where,  $D$ , is the electric displacement,  $E$  is the electric field, and  $K$ , the dielectric constant, is determined by the relation  $K = C^2/V^2$ , has a corresponding relation in elastic waves, when we set equation (1) in the form,

$$dp/\rho = K dp/\rho \quad \dots (3)$$

Here  $dp/\rho$  and  $dp/\rho$  denote the relative displacement and relative pressure change, and  $K = \frac{p/\rho}{V^2}$ , may be termed as the dielastic constant.

When  $K=1$ , we have  $V^2=p/\rho$ , in the ideal conditions when relative displacement would be equal to the relative pressure change. In optics under such ideal conditions, one has  $V^2=C^2$ , determining the velocity of the light in vacuum.

A convenient method of finding the velocity of light in ordinary matter is to consider the polarisation in the medium, due to electric field and set up an equation for the electric displacement in terms of the incident field and the polarisation. Thus, we take up the optical relation,

$$D=KE=E+4\pi P$$

such that  $E+4\pi P=KE$ , is the effective field in the medium to have an equivalent displacement. When we are able to express the polarisation in terms of the electric field, such that,  $D=E(1+\delta)$ , we have solved the optical problem, in as much as we have equated  $K$  to  $1+\delta$ , and the velocity of the light waves becomes determined.

In the relation (3), namely,  $d\rho/\rho=Kdp/p$

the quantity  $Kdp$  is the modified pressure change, which has an equivalent relative displacement. We may consider the nett effective  $dp$ , in producing an equivalent displacement, as the sum of the actual pressure change  $dp$  together with a polarisation pressure due to  $dp$ , similarly as in the case of light. This enables one to set,

$$Kdp=dp+\text{polarisation pressure due to } dp, \quad \dots (4)$$

The velocity of the elastic waves would be obtainable from the value of  $K$ , when the polarisation pressure due to  $dp$  could be explicitly expressed in terms of measurable quantities, with  $dp$  as a factor.

The polarisation pressure could be obtained, when we are able to write the complete equation of motion in terms of molecular motion. This would, naturally, involve the polarisation pressure as one of the terms in the equation of motion. In order to proceed to write the equation of motion, we consider a layer of the fluid with an area of unit cross section. We consider the extra force per unit area  $dp$ , acting on any surface inside the medium, as equivalent to the extra force on the  $N$  molecules attached per unit area, each with a mass ' $m$ ', together with a force of excitation of the molecules to different states, depending on the respective probability factors and some preventive or polarising force per unit area. The polarisation may be considered to be caused by the changes in the condition of stress of the medium with time. If we regard the displacement due to  $dp$ , in any direction, as  $\xi$ , we may set the equation of motion in the form,

$$dp - \text{polarisation pressure} - \text{excitation loss} = N.m. \ddot{\xi}, \quad \dots (5)$$

We have not considered, yet, the force of friction and the force of restitution acting on the molecules. When these are also taken into account, we obtain the complete equation of motion.

The extra force on unit area due to the polarisation, is produced by the time rate of change of stress at a point, and acts only during a change of the conditions of stress and vanishes when the change in the stress condition is made to disappear. As is well known, the stress components in a fluid medium is measured in terms of the time rate of change of displacements of the elements and not in terms of the displacements as for solids. This leads one to presume that the polarisation pressure contribution of  $dp$  should be considered as proportional to the impressed acceleration of the particles. Regarding the polarisation force, it is also evidently proportional to the total number of particles per c.c., and to a polarisation coefficient. One may thus set the polarisation force per unit area as  $P(Nm)\ddot{\xi}$ . Similarly, the loss of pressure due to excitation is expressible in the form  $- \alpha N.m\ddot{\xi}$ . We have here  $\alpha$  as the excitation coefficient and  $P(Nm)$  involves the polarisation coefficient and the number of molecules per c.c.. One has also to take into account the force of restitution and the force of resistance acting on the particle. These forces acting on the molecules are expected to have a large or small range of variation depending on the structural character of the molecules involved. These forces will act in a direction opposite to the direction of polarisation, helping the particles to return to the status quo, *i.e.*, of motion. Further, the force of restitution will involve the same function of  $\xi$  as the polarisation and the force of resistance will contain the time rate of change of the function of  $\xi$  involved in polarisation. One may, thus, set the complete equation of motion in the form,

$$\{dp - P(N, m)\ddot{\xi} - \alpha N.m\ddot{\xi}\} / N = m(\ddot{\xi} - f\dot{\xi} - g\frac{d}{dt}\dot{\xi})$$

$$\text{or } (dp + Nm f\ddot{\xi} + Nm g\frac{d}{dt}\dot{\xi}) - P(N, m)\ddot{\xi} = Nm\ddot{\xi}(1 + \alpha) \quad \dots (6)$$

where  $f$  and  $g$  are the coefficients of restitution and friction and will have a range. Since, further,  $P(N, m)$  is determined by the number of molecules per c.c. and by a polarisation coefficient, one may set

$$P(N, m) = N.m.q$$

for a gaseous medium and for any other medium, with a density ratio compared to the particular gaseous state as  $R$ , one has the general relation

$$P(N, m) = R.N.m.q. \quad \dots (7)$$

For a particular gaseous state  $q$  involves constants specifying the number of molecules and their masses and a polarisation constant. The polarisation constant is expected to be dependent upon the temperature and to fix upon  $R$ , one has to take the different states under similar conditions of temperature. The equation of motion (6) may, then, be expressed in the form,

$$(dp + Nm f \ddot{\xi} + Nm g \frac{d}{dt} \ddot{\xi}) - RqNm \ddot{\xi} = Nm \ddot{\xi} (1 + \alpha) \quad \dots (6a)$$

One may determine the unknown polarising coefficient  $q$  by studying the problem from another point of view. Let us consider the gaseous state, with  $R$  as unity. The total impressed energy will give rise to the energy of motion and excitation together with the energy of polarisation in the form of fluid strains. The polarisation part is a sort of conservation or storing up of energy that comes into existence only when there is a strain variation. When the energy is supplied at constant volume, the strain energy part remains unchanged and the polarisation term vanishes. The input energy,  $C_v dT$ , would be measured in terms of energy of motion and excitation only. Gradually, as the associated strain variation is established, the input energy,  $C_p dT$ , would be measured in terms of energy of motion and excitation, as also by the polarisation energy. Thus we have the right hand side of the above equation (6a), as a measure of  $C_v dT$ , the term in the parenthesis as a measure of  $C_p dT$ , and the polarisation term  $qNm \ddot{\xi}$  as a measure of  $(C_p - C_v) dT$ . This is in accordance with the accepted idea, that the specific heat at constant volume is a measure of the energy of motion  $C_v dT$ , together with the energy of excitation  $C_v dT$ . Indeed, it is the frequency dependence of  $C_v dT$ , that gives rise to the principle of relaxation phenomenon. For our present treatment, we disregard the consideration of the frequency dependence of the specific heat at constant volume, that is, we consider  $\alpha$  as frequency independent. Since  $qNm \ddot{\xi}$  is a measure of the energy difference  $(C_p - C_v) dT$ , the above relation immediately indicates that when  $q = 1 + \alpha$ , we would have,  $C_p = 2C_v$ . This gives us,

$$q = (1 + \alpha)(\gamma - 1),$$

where,  $\gamma$ , is the ratio of the specific heats. We have thus, determined the unknown polarising coefficient  $q$ , at any temperature, in terms of  $\gamma$ , the ratio of the specific heats of a particular gaseous state of the matter concerned, even when we are treating the case of a liquid state. We have, then, the polarising pressure in the form,

$$-P(N, m) \ddot{\xi} = -RNm(1 + \alpha)(\gamma - 1) \ddot{\xi},$$

and the equation of motion becomes,

$$dp = Nm(1 + \alpha) \{1 + R(\gamma - 1)\} \ddot{\xi} - Nm f \ddot{\xi} - Nm g \frac{d}{dt} \ddot{\xi}$$

With a periodic change of pressure  $dp = dp_0 e^{i\omega t}$ , and the associated displacement as  $\xi = ae^{i(\omega t - \tau)}$ , one obtains, immediately,

$$\xi = - \frac{dp / Nm}{(1 + \alpha) \{1 + R(\gamma - 1)\} \omega^2 - f \omega^2 - i g \omega^3}$$



and thus, one may set the polarisation pressure,

$$\begin{aligned} -P(N, m)\ddot{\xi} &= R(1+\alpha)(\gamma-1).N.m.\omega^2\xi. \\ &= -\frac{R(\gamma-1)(1+\alpha)d\rho}{(1+\alpha)\{1+R(\gamma-1)\}-f-ig\omega} \end{aligned} \quad \dots (8)$$

If we consider  $n$  as the elastic index of refraction and  $k$  as the coefficient of absorption per unit wavelength, we have, in view of relation (4), the di-elastic constant  $K$  as,

$$K = (n - ik)^2 = \left[ 1 - \frac{R(\gamma-1)(1+\alpha)}{(1+\alpha)\{1+R(\gamma-1)\}-f-ig\omega} \right] \quad \dots (9)$$

The real part of the di-elastic constant would be given by,

$$\begin{aligned} n^2 - k^2 \approx n^2 &= \frac{\rho}{V^2} = 1 - \frac{R(\gamma-1)(1+\alpha)[(1+\alpha)\{1+R(\gamma-1)\}-f]}{[(1+\alpha)\{1+R(\gamma-1)\}-f]^2 + g^2\omega^2} \\ &= 1 - \frac{R(\gamma-1)(1+\alpha)}{(1+\alpha)\{1+R(\gamma-1)\}-f+g'^2\omega^2} \end{aligned}$$

where,

$$g'^2 = g^2 / [(1+\alpha)\{1+R(\gamma-1)\}-f] \quad \dots (10)$$

For liquids, we would have the approximate relation,

$$g'^2 = g^2 / (1+\alpha)R(\gamma-1) \quad \dots (10a)$$

Thus, we have,

$$\frac{\rho}{V^2} = \frac{(1+\alpha)-f+g'^2\omega^2}{(1+\alpha)-f+g'^2\omega^2+(1+\alpha)R(\gamma-1)} \quad \dots (11a)$$

or

$$V^2 = \frac{\rho}{\rho} \left\{ 1 + \frac{R(\gamma-1)}{1-F+g'^2\omega^2} \right\} \quad \dots (11)$$

where,

$$\left. \begin{aligned} F &= f / (1+\alpha), \\ G^2 &= g'^2 / (1+\alpha) = g^2 / (1+\alpha)^2 R(\gamma-1) = g''^2 / R(\gamma-1) \end{aligned} \right\} \quad \dots (12)$$

with

$$G = g'' / (1+\alpha)$$

The imaginary part of the di-elastic constant  $K$  determines the absorption coefficient  $k$ . We have by equating the imaginary parts, in relation (9).

$$2nk = \frac{R(\gamma-1)(1+\alpha)g\omega}{[(1+\alpha)\{1+R(\gamma-1)\}-f]^2 + g^2\omega^2}$$

Utilising the relations (11a) and (10) we have

$$\begin{aligned} [(1+\alpha)\{1+R(\gamma-1)\}-f]^2 + g^2\omega^2 &= \rho \frac{V^2}{\rho} \left\{ (1+\alpha)-f+g'^2\omega^2 \right\} \\ &\quad \times [(1+\alpha)\{1+R(\gamma-1)\}-f] \end{aligned}$$

Thus, we obtain,

$$2nk = \frac{\rho R(\gamma-1)(1+\alpha)g\omega}{\rho V^2 \{ (1+\alpha)-f+g'^2\omega^2 \} [(1+\alpha)\{1+R(\gamma-1)\}-f]} \quad \dots (13)$$

For a liquid, neglecting  $\tau$  and  $f$ , compared to  $R(\gamma - 1)$ , the relation reduces to,

$$2nk = \frac{\hbar g \omega}{\rho V^2 \{ (1 + a) - f + g'^2 \omega^2 \}} \quad \dots (13a)$$

Thus the absorption coefficient  $k$  per unit wave length would be given by,

$$k = \frac{2\pi \hbar g'' v}{2n\rho V^2 (1 - F + G^2 \omega^2)} \quad \dots (14)$$

where the coefficients  $F$ ,  $G$ ,  $g''$ , etc., are defined by the relation (12). The absorption coefficient per unit distance, would be determinable from,

$$\alpha/v^2 = \frac{k}{Vv} = \frac{\pi \hbar g}{n\rho V^3 (1 - F + G^2 \omega^2)} \quad \dots (15)$$

#### ANALYSIS OF THE THEORY AND THE EXPERIMENTAL DATA

When we neglect the effect of the small quantities  $F$  and  $G$  the velocity equation (11), immediately reduces to the gas velocity equation (1a). It also gives us the so far undeterminable liquid pressure, by the approximate relation,

$$\hbar = \frac{\rho V^2}{R(\gamma - 1)}$$

In the case of liquids, with  $V^2$  of the order of  $10^{10}$ ,  $R(\gamma - 1)$  of the order of  $3 \cdot 10^2$ , the pressure comes out of the order of 30 atmospheres, and  $n$  the elastic index of refraction in liquids about  $5 \cdot 10^{-2}$ . For gases, the elastic index of refraction would be given by,

$$n = \left( \frac{\hbar}{\rho V^2} \right)^{1/2} = (1/\gamma)^{1/2} \approx 8 \times 10^{-1}$$

When we take the small quantities  $F$  and  $G$  into account and take note, that both of them are likely to have a large or small range of values, about the mean, depending upon the structure and constitution of the molecules, the Eq. (11) indicates that the velocity will have a range about its mean value, which may be termed as internal dispersion.

There is no sense, however, in absorption coefficient having a range of values. It will be experimentally determined by its maximum value only. The observed intensity will always be the lowest possible intensity, as reduced by the molecules moving under the largest value of the force of friction.

The absorption equation (15) is in complete accord with a constant value of  $\alpha/v^2$  for smaller values of  $\omega$ , and is very similar to the Stokes relation (2). On comparing these two equations, we may write,

$$\alpha/v^2 = \frac{8\pi^2 \eta}{3\rho V^3} = \frac{\pi \hbar g''}{n\rho V^3}$$

Thus the coefficient  $g''$  is determinable by the relation,

$$g'' = \frac{8\pi n}{3\dot{p}} \cdot \eta \quad \dots \quad (16)$$

As the viscosity coefficient,  $\eta$ , has only an average value, the value of  $g''$ , thus determined would give us only the average value. The experimental value of  $\alpha/\nu^2$  will, however, give us the maximum value of  $g''$ , and one may consider that the range of extension of  $g''$  from its mean value is given by the Stokes multiplier  $M$ . This would be more apparent when we consider the structure of different molecules and their  $M$  values, as discussed in detail in experimental paper on 'Internal dispersion', which follows.

It is possible, now, to calculate the mean value  $g''$ , from relation (16) above. For a liquid like  $\text{CS}_2$  the value of  $g''$  comes out about  $3 \cdot 10^{-11}$ . The value of  $g''_{\text{max}}$  would be fixed up by  $M \cdot g''$ , where  $M$  is the Stokes multiplier. With a Stokes multiplier of 1500 for  $\text{CS}_2$  (Pinkerton, 1949), one gets its  $g''_{\text{max}} = 4.5 \times 10^{-8}$ , and the corresponding value of  $G$  is given by the relation,

$$G_{\text{max}} = \frac{g''_{\text{max}}}{[R(\gamma - 1)]^{1/2}} = 3 \times 10^{-9}$$

The relation (15), with such a value of  $G$  gives the fall of  $\alpha/\nu^2$  to 1/5th its value, when the frequency changes from  $10^6$  to  $10^8$  c.p.s. It is, thus, in exact agreement with the experimental results of Rapuano, (1947) and others, that has been pointed out in the introduction.

Acetic acid would have a calculated mean  $g''$  value and the Stokes  $\alpha/\nu^2$  value, of the same order as that for  $\text{CS}_2$ . The experimental value (Pinkerton, 1948 and Bazulin, 1936) of  $\alpha/\nu^2$ , however, shows a very rapid increase with decreasing frequency, and at about  $10^6$  c.p.s., it becomes nearly 1000 times as large as Stokes' calculated value. It may be easily calculated with the help of relation (15), that with a Stokes multiplier of the order of  $10^4$ , which, from experimental data to date, is not at all an unlikely value, the characteristics of the  $\alpha/\nu^2$  variation with  $\nu$ , obtained experimentally, would, be fully explained. A small constant tail portion of the experimental results, however, remains unexplained. This may be reasonably attributed to the relaxation mechanism, having a maximum absorption, somewhere further up, in the high frequency region. Further, it gives one immediately that the usual character of the constant  $\alpha/\nu^2$  value, would be obtained, on the low frequency side, near about  $5 \cdot 10^4$  cycles per second. The experiment is worth trying.

The idea that the Stokes multiplier is to be regarded as giving the range of variability of  $g$  or  $G$  is nicely corroborated from the internal dispersion of spectral lines, obtained by the Debye and Sears (1932) diffraction method. A detail treatment of the subject is made in the experimental paper, that will follow. It is clear, however, from the velocity relation (11), that an internal dispersion or a broadening of the diffraction spectra lines, would be very large for a substance like  $\text{CS}_2$ , with an  $M$  value of 1500 and least for a liquid

like castor oil (Hunter, 1941, Pinkerton, 1949), with an  $M$  value of one only, although the magnitude of observed  $\alpha/\nu^2$  is nearly the same in the two cases. The experimental results on the width of the diffraction spectra lines, completely support this point of view, and one obtains the sharpest line with pure castor oil, whose breadth is actually fixed up by the Doppler broadening of the source only. With the other liquids, the Stokes multipliers and the spectral line widths are in good correspondence.

Further, even the large  $M$  value of  $\text{CS}_2$ , in association with the mean  $G$  would not give the observed internal dispersion, at low frequencies, of the order of one or two megacycles, when it is calculated by the velocity relation (11). One has to regard that  $F$  along with  $G$  would be of a variable character, determined by the Stokes multiplier  $M$ , and this is quite reasonable to expect.

It may be pointed out, however, that as the mean value of  $G$  is of the order of  $10^{-12}$ , the dispersion of the mean velocity would not be obtained until the frequency region of  $10^{10}$  to  $10^{11}$  c.p.s., is reached. The experimental results on mean dispersion, till now, is generally in agreement with this outcome of the theory.

#### INTERNAL DISPERSION OF OPTICAL WAVES

The molecular motion in a fluid medium, with its associated variable forces of restitution and friction would also give rise to an internal dispersion of optical waves and thus, also, the associated broadening of the spectral lines obtainable, say, by a plane glass diffraction grating. Such an effect, with greater broadening of spectral lines in liquids with large  $M$  values, have been observed and is being reported to in a separate paper. The basic relations, in consideration of the molecular motion, will be obtained in the following :

Any molecule, in view of its relative position with regard to its neighbours, will possess an instantaneous strong dipole moment  $p$ , say. The polarisation of the liquid, due to any further rotation of the dipole molecule, caused by any incident electric field, will give rise to a contribution in the dielectric constant and thus, will have an effect on the optical wave velocity. If we consider the electric field in the direction of  $x$ , the electrical polarisation in the same direction, caused by the rotation of the molecule, would be given by,

$$P_{m,x} = \Sigma N p_x' = \Sigma N p_y \varphi \quad \dots (17)$$

where,  $p_x'$  is the projection of the initial electric moment component  $p_y$  on the  $x$  axis, after it has been rotated by the electric field through any small angle  $\varphi$ .  $N$  here denotes the number of molecules per cubic centimetre. This gives us the additional polarisation, besides the usual electronic polarisation, which plays the major part.

The equation of motion of the molecule would be obtained by taking the  $z$ -component of the torque on the molecule. In accordance with the usual form of the torque relation, we may write,

$$\left[ \begin{matrix} \rightarrow \\ E', p. \end{matrix} \right]_x = I\ddot{\varphi} + IG\dot{\varphi} + IF_0^2\varphi \quad \dots (18)$$

Here  $\varphi$  is the angle of rotation,  $G$  and  $F_0^2$  determine the frictional force and the force of restitution,  $I$ , is the moment of inertia of the molecule, and  $E'$  is the total electric field acting on the molecule. The total electric field in the liquid would be given by the relation,

$$E_x' = E_x + \frac{4\pi}{3} P_e + \frac{4\pi}{3} P_m \quad \dots (19)$$

where  $P_e$  and  $P_m$  stand for the electronic and molecular polarisation parts. The electronic polarisation part in liquids is known and we may set, (Slater and Frank, 1933)

$$\frac{4\pi}{3} P_e = E_x \frac{4\pi}{3} \frac{\sum N_k l^2 / m}{f_k^2 - \omega^2 + 2\omega g} = E f(\epsilon) \quad \dots (20)$$

where  $\epsilon$  and  $m$  denote the electronic charge and the mass,  $\omega$  specifies the incident frequency.  $f_k^2 = f_k^2 - \frac{4\pi}{3} \sum N_k e^2 / m$ , with  $f_k^2$  giving the coefficient of restitution and  $g$  the coefficient of friction acting on the electron. Utilising the two polarisation expressions (17) and (20) and considering the incident electric field polarised in the  $x$  direction, we may put the equation of motion in the form,

$$E_x' p_y = I\ddot{\varphi} + IG\dot{\varphi} + IF_0^2\varphi.$$

$$\text{or} \quad \{E_x(1 + f(\epsilon)) + \frac{4\pi}{3} \sum N_k p_y \varphi\} p_y = I\ddot{\varphi} + IG\dot{\varphi} + IF_0^2\varphi \quad \dots (18a)$$

Taking  $\varphi$  to be periodic with  $E_x$ , we have,

$$\varphi = \frac{p_y E_x (1 + f(\epsilon)) / I}{F^2 - \omega^2 + i\omega G} \quad \dots (21)$$

$$\text{and, hence,} \quad P_m = \sum N p_y \varphi = \frac{\sum N p_y^2 E_x (1 + f(\epsilon)) / I}{F^2 - \omega^2 + i\omega G} \quad \dots (22)$$

$F^2$ , in these expressions, is given by,

$$F^2 = F_0^2 - \frac{4\pi}{3I} \sum N p_y^2.$$

The additional contribution to the dielectric constant would be  $4\pi P_m / E_x$  and thus, we may write for the molecular part of the dielectric constant as,

$$K_m = \frac{4\pi(1 + f(\epsilon)) \sum N_k p_y^2 / I}{F^2 - \omega^2 + i\omega g}$$

The numerator, which is a constant depending upon the substance, is smaller than the numerator of the electric part by a factor of the order of  $10^3$ , which is the approximate ratio of the molecular mass to the electronic mass. Thus the molecular polarisation will give rise to a small additional effect on the electronic effect and the calculated dielectric constant of a liquid medium,

on the basis of electronic polarisation only needs to be corrected by a very small amount. The form of the complete dielectric constant, would, thus, be given by,

$$K = 1 + 4\pi(P_e + P_m)/E_x$$

$$= 1 + \frac{4\pi \sum N_k \epsilon^2/m}{f_k^2 - \omega^2 + i\omega g} + \frac{4\pi \sum N_k \rho_n (1 + f(\epsilon))/I}{F^2 - \omega^2 + i\omega G} \quad \dots (23)$$

The real part of the dielectric constant determines the value of  $n^2 - k^2$ , where  $n$  is the refractive index and  $k$  is the absorption coefficient. When we neglect  $k^2$  compared to  $n^2$ , we may set,

$$n^2 = n_e^2 + \frac{4\pi C_m (F^2 - \omega^2)}{(F^2 - \omega^2)^2 + \omega^2 G^2}.$$

Here,  $n_e$  = the usual refractive index due to the electronic motion only, and

$$C_m = \sum N \rho_n^2 (1 + f(\epsilon))/I.$$

Considering the molecular contribution as the change in the usual value of  $n_e^2 \approx n^2$ , obtained under the consideration of the electronic motion only, we have,

$$d(n^2) = 2n dn = \frac{4\pi C_m (F^2 - \omega^2)}{(F^2 - \omega^2)^2 + \omega^2 G^2}.$$

or

$$\frac{dC}{V} = \frac{C dA}{V^2} = n \cdot \frac{dV}{V} = \frac{4\pi C_m / 2n}{(F^2 - \omega^2) + \omega^2 g'^2}$$

or,

$$\frac{dV}{V} = \frac{2\pi C_m / n^2}{F^2 - \omega^2 + \omega^2 g'^2} \quad \dots (24)$$

$c$ , in the above equations denote the velocity of light in vacuum, and we have,

$$g'^2 = G^2 / (F^2 - \omega^2).$$

The relation (24), above gives us the relative contribution of the molecular motion towards the optical wave velocity. When the coefficients  $F$  and  $G$  have a range and have a sufficiently large value to make its contribution effective in measurements of the velocity, we will have a broadening of the optical spectral lines due to internal dispersion. The broadening would be greater for substances with larger variability of the  $F$  and  $G$  values. In case, the  $F$  and  $G$  values are ineffective compared to  $\omega^2$ , no such broadening of the lines will be expected. Further, it is expected, that although the rotational coefficients, treated in the optical case, might be of a completely different order from the corresponding coefficients treated in the elastic case, as they would involve the elastic preventive or polarising force, the range of variability, which depends on the molecular structure, would have a correspondence in the two cases, and would be guided by the Stokes' multiplier,  $M$ . Experiments with a plane diffraction grating show a broadening of the spectral lines corresponding

with the Stokes' multiplier  $M$ . This indicates the effectiveness of the coefficients compared to the value of  $\omega^2$ . They are being reported in a separate paper (Mukherjee, 1952) in this issue (p. 154).

The imaginary part of the dielectric constant will give us the value of the absorption coefficient  $k$ , in two parts determined by the relation,

$$k = k\varepsilon + \frac{2\pi C_m \omega G}{n(F^2 - \omega^2)^2 + \omega^2 G^2}$$

From the experimental finding that there is an internal dispersion of the optical waves, it appears that the coefficients  $F$  and  $G$  are effective to some degree, and thus it is expected that there will be some measurable contributory part of the absorption coefficient due to molecular motion. A proper estimate of this, however, could not be made yet.

#### ACKNOWLEDGMENT

It is a pleasure to thank Dr. S. Ghose of the Applied Mathematics department for helpful discussions.

#### REFERENCES

- Bazulin, P., 1936, *C. R. Acad. Sci., U. R. S. S.*, **3**, 285  
 Biquard, P., 1935, These, Paris, also printed as 1936, *Ann. Phys. Paris.*, **6**, 195.  
 Debye, P., and Sears, F. W., 1932, *Proc. Nat. Acad. Sci.*, **18**, 410  
 Dutta, A. K., and Ghose, B. B., 1937-38, *Trans. Bose. Res. Inst.*, **13**, 31  
 Hunter, J. L., 1941, *J. Acoust. Soc. Amer.*, **13**, 36.  
 Kneser, H. O., 1938, *Ann. der. Phys.*, **32**, 281.  
 Pinkerton, J. M. M., 1948, *Nature*, 162, 106 ; 1949, *Proc. Phys. Soc.*, **62**, 129  
 Rapuano, R. A., 1947, *Phys. Rev.*, **72**, 78.  
 Slater, G. G., and Frank, N. H., 1933, *Theoretical Physics*, p. 280.  
 Stokes, G. G., 1845, *Trans. Camb. Phil. Soc.*, **8**, 287.  
 Willard, G. W., 1941, *J. Acoust. Soc. Amer.*, **12**, 438.

# EXPERIMENTS ON THE INTERNAL DISPERSION OF OPTICAL WAVES

By S. K. MUKHERJEE

DEPARTMENT OF PHYSICS PRESIDENCY COLLEGE, CALCUTTA

(Received for publication, Jan. 21, 1952)

**ABSTRACT.** It has been observed that the spectral lines obtained by passing monochromatic light through a plane grating, placed in different liquid media are broadened to different extents. This broadening effect is a particular characteristic of the liquid, and is determined by the discrepancy between the elastic wave absorption coefficient calculated by Stokes and the observed value. It has been considered that this discrepancy which is a measure of the range of variability of the molecular coefficients, is effective in producing a change in the optical wave velocity also.

## INTRODUCTION

The real part of the dielectric constant,  $K$ , in a medium, obtained from considerations of the electronic motion, determines the optical wave velocity. We have the standard relation for the dielectric constant (Slater and Frank, 1933) in the form,

$$K = 1 + \frac{4\pi \sum N_K e^2 / m}{f_K^2 - \omega^2 + i\omega g}$$

so that,

$$n^2 - k^2 \approx n^2 = \frac{C^2}{V^2} = 1 + \frac{4\pi \sum N_K e^2 / m (f_K^2 - \omega^2)}{(f_K^2 - \omega^2)^2 + \omega^2 g^2} \quad \dots \quad (1)$$

Here,  $C$ , and  $V$ , denote the optical wave velocity in vacuum and in the medium,  $n$ , the index of refraction and  $k$ , the coefficient of absorption,  $e$  and  $m$  denote the electronic charge and the mass,  $\omega = 2\pi\nu$  determines the frequency of the impressed waves,  $g$  is the coefficient of frictional force and  $f_K$  is the coefficient of the force of restitution, where

$$f_K^2 = f_{K0}^2 - \frac{4\pi}{3} N_K e^2 / m.$$

The relations give a dependence of ' $n$ ' or ' $V$ ' on  $\omega$  or  $\nu$  and hence a dispersion. When  $f_K^2$  and  $g$  are of definite magnitudes, we have, that for a particular frequency, the velocity in the medium  $V$  is fixed and thus  $\lambda$  determined by the relation  $V = \nu\lambda$ , is also fixed. We obtain a measure of  $\lambda$  from the plane grating relation,

$$(a + b) \sin \theta = N\lambda$$



where 'N' is the order number. For a monochromatic radiation, with a definite value of  $\nu$ , it should give us a geometrical line spectrum. In actual cases, however, the spectral lines have got a definite width, determined, mainly, by the Doppler broadening of the source of light.

It has, also, been shown by Dutta (1952) elsewhere in this number referred to as paper I that the molecular motion will set the dielectric constant  $K$ , modified by an additional amount in the form

$$K = 1 + \frac{4\pi \sum N_K e^2/m}{f_K^2 - \omega^2 + i\omega g} + \frac{4\pi \sum N_K p_v^2}{F^2 - \omega^2 + i\omega G} \left( 1 + \frac{f(\epsilon)}{3} \right) \cdot I. \quad \dots 2$$

where,  $I$  is the moment of inertia of the molecule,  $F$  and  $G$  denote the molecular coefficient of restitution and of friction, and

$$f(\epsilon) = \frac{4\pi}{3} \frac{\sum N_K e^2/m}{f_K^2 - \omega^2 + i\omega g}$$

If the  $F$  and  $G$  values were fixed quantities, like the electronic  $f$  and  $g$  values, we would have obtained a slightly modified value of  $V$  and thus also of  $\lambda$  and  $\theta$  of the diffraction spectra relation. When, however, a range of values of  $F$  and  $G$ , the molecular coefficients, are taken into account, the range of variability being determined by the Stokes multiplier  $M$ , as discussed by Dutta in paper I, we would obtain for a particular value of  $\nu$  a range of values of  $V$  and also of  $\lambda$ . This would give us a broadening of the spectral lines obtained by a diffraction grating, provided  $F$  and  $G$  have effective values in the equation (2). Such a range of values of  $V$  associated with a particular value of  $\nu$ , has been termed as 'internal dispersion' of optical waves. This will give a range of values of  $\lambda$  and hence a broadening of the spectral lines. According to the contention of Dutta, (paper I,) the spectral line breadth will be determined by the  $M$  values of the substance and will be different in the case of different liquids. The general character of the observed diffraction spectral lines show the effectiveness of the molecular forces of friction and restitution and the results are in complete accord with the point of view that the associated breadth of the spectral lines are determined by the values of  $M$ , the Stokes multiplier. This has been described in the following experiment.

#### EXPERIMENTAL

A plane ruled grating, with 250 lines per cm. was immersed in different liquids and the diffraction spectra were photographed at a constant room temperature. The spectroscope used was a Hilger constant deviation one, remodelled as a straight type spectroscope. The source of light was a powerful sodium lamp used with a bichromate filter. A critical study of the diffraction spectra relation makes it clear that the actual position of the grating in the liquid medium is immaterial in determining the width of the spectral lines. They will be determined by the molecular structure of the liquid and by the length of

the liquid column traversed by the light. In the present experiment, different liquids were tried in a vessel, with a light path of about 3 inches. The results recorded here, were obtained by placing the grating more or less centrally in the medium and in such a way that the spectra on the two sides of the central line were equally deviated.

It was observed, however, that the intensities of the spectral lines for different liquids were very different from each other. Indeed, in some of the liquids like benzene and xylene, the diffraction spectra lines with the plane grating could not be obtained at all. It may be pointed out, however, that one obtains the diffraction spectral lines of these liquids with a wave-field grating without any difficulty. This is perhaps due to the smaller angle of diffraction in the case of the wave field grating and also to the volume of grating effect. That the absorption was not in any way the determining factor of the width of the line was clear from the fact that carbon bi-sulphide liquid, with a Stokes multiplier of 1540 (Pinkerton, 1949) and carbon tetrachloride, with a Stokes multiplier of 27, both appear to have a stronger absorption than acetone with  $M=10$ . This was judged from the intensities of the spectra obtained with the same time of exposure, when the light was allowed to pass through these different liquids. The less intense  $\text{CS}_2$  spectral lines, however, record, with the same time of exposure, a larger width than the spectral lines through acetone, whereas, the less intense  $\text{CCl}_4$  lines have a smaller width in comparison with acetone lines. This, presumably, is due to the fact that  $\text{CS}_2$  has a very large value of the Stokes multiplier  $M$  and the associated spreading of the spectral lines is comparatively so large that even with weaker intensity, the lines appeared to be wider than the acetone lines, whereas,  $\text{CCl}_4$ , whose  $M$  value is not so markedly different from the  $M$  value for acetone, will have a comparatively smaller broadening effect and with a less intense line the broadening effect does not show up. In order to get a proper estimate of the broadening, however, the breadth of the spectral lines with equivalent intensities should be compared. It has been consistently observed that with equal intensities, the breadth of the spectral lines is greater in the case of liquids with a comparatively larger value of the Stokes multiplier  $M$ . A more systematic investigation of the subject would have been possible with gratings of different dispersive powers. It is, however, essentially necessary that for such a comparative study, the different gratings should have been drawn with the same ruling point. For such a systematic investigation, we have, accordingly, planned to have the necessary gratings and the work will be taken up in greater detail when the gratings will be available.

## RESULTS

It has been considered, consistently with the experimental results, and also in accordance with the theoretical expectation outlined by Dutta in paper I, that the breadth of the lines with equal intensities are determined

solely by the value of the Stokes multiplier  $M$ . On this contention we take up the breadth of the spectral lines of a liquid, with the Stokes multiplier as unity, as the standard liquid whose breadth is determined solely by the Doppler broadening of the source. On a measurement of the width of the spectral lines corresponding to other liquids as medium, we can easily determine the increase in width as compared to the standard. This helps us, immediately to obtain the percentage of internal dispersion, which determines for a particular frequency, the variation of the wave velocity or of the wavelength  $\lambda$ , about a mean velocity. In the case of the standard substance, it is implied that for a particular frequency the wave velocity or the wavelength has a unique value only. The method of calculating the percentage of 'internal dispersion' from a measurement of the increase in width of the spectral lines, compared to the spectral lines of the standard liquid, is very similar to the method of calculating the 'internal dispersion' of elastic waves and would be treated in detail in the paper on the subject, by Dutta and Mukherjee, referred to as paper II (in course of publication). The following table gives the results of measurements on internal dispersion of optical waves in the cases of some liquids. The values of the Stokes multiplier  $M$ , as also the logarithm of the Stokes multiplier have been tabulated for comparison. It will be observed from the table that there is a consistent increase of the internal dispersion with the increasing value of the Stokes multiplier. The magnitude of the internal dispersion is, however, less than the magnitude of the internal dispersion of the elastic waves for any particular liquid. This is evident on a comparative study of the results of paper II (in course of publication). It may, however, be noted that there is a close correspondence between the magnitudes of the internal dispersion and the logarithm of the Stokes multiplier, as in the case of the elastic waves also.

TABLE I

Liquid	Stokes multiplier 'M'	Logarithm of M (base 10)	Internal dispersion per thousand.
Castor oil	1	0	0
Water	3.1	0.47	0.8
Acetone	10.3	1.01	2.3
Carbon tetrachloride	27	1.43	4.0
Carbon bisulphide	1540	3.19	8.0

We remain content in showing in the above table, an effective broadening of the spectral lines obtained by passing light through a plane grating, placed

in a liquid medium. This broadening is completely unrelated to the absorption characteristics of the liquid and appears to be solely determined by the Stokes multiplier  $M$ . This is in accordance with the idea propounded by Dutta in paper I that the optical wave velocity will be affected by molecular motion in the liquid, and a broadening will be expected in accordance with the range of variation of the coefficients. A more detailed work will be undertaken.

#### ACKNOWLEDGMENT

The author's thanks are due to Dr. A. K. Dutta, for continuous help and guidance throughout the course of this work.

#### REFERENCES

- Dutta, A. K., 1952, *Ind. J. Phys.*, **28**.  
Pinkerton, J. M. M., 1949, *Proc. Phys. Soc. B*, **22**, 129  
Slater, J. C., and Frank, N. H., 1933, *Theoretical Physics*, p 280

# REVIEWS

## (1)

**High Frequency Measurements**—By August Hund. (International Series in Pure and Applied Physics), x + 676 pages, 417 figures, McGraw-Hill Book Co. Inc., 1951, Price \$ 10.

The volume under review is the second edition of the well known book on high frequency measurement by the author first published in 1933. Since the publication of the first edition, many new high frequency techniques have come into use. For example, we had no commercial FM in 1929 (when the first edition was prepared). But now FM and also PM are in wide use. The range of the frequencies to be measured has also extended enormously. The new edition, therefore, required a large amount of revision and several chapters had to be completely re-written.

The volume under reference deals with measurement procedures at low and medium radio frequencies and also at high, very high and ultra high frequencies. It is divided into seventeen chapters of which the first three are introductory dealing with fundamental relations, circuit properties and laboratory apparatus and system for h.f. measurements. The next eight chapters are devoted to the procedures for measuring voltage, frequency, capacitance, self-inductance, mutual inductance and coupling, effective resistance, h.f. power and losses and resonance. This is followed by three chapters on ferromagnetic measurements, tube measurements, modulation measurements and measurements on lines and aerial systems. Chapter XVI deals with wave propagation determinations and the last chapter describes some miscellaneous measurements, e.g., noise, electrical properties of piezo-electric crystals, gain determinations of microwave antennas and UHF admittance bridge. MKS units have been used throughout the book.

One or two criticisms may perhaps be made of this otherwise excellent and useful publication. It would have been better if SHF measurements were treated in a separate chapter instead of being distributed in several places as has been done. The modern UHF and microwave measurement procedures have been given only in broad outline. Further, the author's style of presentation is sometimes rather heavy. These are, however, only minor blemishes. The book, as a whole, is exhaustive and authoritative in its treatment. As such it should find a place on the table of every radio engineer and radio physicist. The printing, binding and get-up are of the McGraw-Hill standard.

(G. S. S.)

## (2)

**Understanding Radio**—By Watson, Welch and Eby, Second Edition, 716 pages, 522 figures, Mc-Graw-Hill Book Company, Inc., 1951, Price, \$ 5.50.

This is an elementary book written for "students who have little or no background in electricity or science." As is expected in such a book, the mathematics has been kept to a working minimum and the book is made as practical as possible. The book is divided into twenty-six chapters, each followed by a number of illustrative questions and list of technical terms used in the chapter. Some of the chapters headings are as follows: Radio Waves and Wave Travel (Chap. II), Ohm's Law by Simple Mathematics and Meters (Chap. V), Wave-form pictures (Chap. VIII), Dynamic Loud Speaker (Chap. XIII), Antennas (Chap. XXIII), The Very High Frequencies (Chap. XXIV), Frequency Modulation (Chap. XXV). The method adopted in preparing the text of each chapter is learn-by-doing. The book is profusely illustrated emphasising the visual-teaching approach. Towards the end, in the Appendix, a large number of data compiled from tube manuals, are given. These will be of great help to practical workers.

The book is eminently suited to those who want to learn the elements of practical radio and also to understand broadly why-it-works. Teachers in such elementary classes will find the book very useful. Undergraduate students in the colleges may also read the book with profit. We very heartily recommend the book to the large category of readers who are interested in radio as vocation or avocation, but are prevented from joining higher technical courses in the subject due to lack of systematic training in physics and mathematics.

(J. S. C.)

# EXPERIMENTS ON THE INTERNAL DISPERSION OF SUPERSONIC WAVES IN LIQUIDS

By A. K. DUTTA AND S. K. MUKHERJEE

UTKAL UNIVERSITY, CUTTACK, AND PRESIDENCY COLLEGE, CALCUTTA

(Received for publication, January, 21, 1952)

**ABSTRACT.** It has been observed that the spectral lines, formed by the elastic wave diffraction in various liquids, have various amounts of line widths. These line widths are determined by the discrepancy in the experimental values of  $\alpha/\nu^2$  as compared with the value calculated by the Stokes relation, and is not fixed up by the actual amount of absorption. It has been considered that when there is complete agreement between the experimental and the calculated values of  $\alpha/\nu^2$ , like that obtained for the case of castor oil, the line width is determined by the Doppler broadening of the source only and such a line width may be considered as a standard. Compared with such a standard, the broadening of the spectral lines of different liquids has been measured in terms of  $dV/V$ . This has been termed as internal dispersion and is tabulated for two different frequencies. The results are studied in the light of the theoretical expectations.

## INTRODUCTION

Various attempts have been made by different workers (Dutta, 1938; Hiedeman and others, 1936, Bér, 1938, Spakovskij, 1938, Zachoval, 1939, Schallamach, 1945) to find out if there is any change in the velocity of the supersonic waves in liquids with frequency. These investigators have generally found that the velocity remains unchanged with frequency, although dispersion effects of a very small order have been reported by some in the case of particular liquids. The usual and comparatively more accurate means for the determination of the supersonic wave velocity in liquids is to use the method of diffraction by supersonic wave field, suggested by Debye and Sears (1932). The supersonic velocity is determined by the diffraction spectra relation,

$$\Lambda \sin \theta = n\lambda \quad \dots (1)$$

where the usual grating constant has been replaced by the supersonic wavelength  $\Lambda$ . Having determined the wavelength and knowing the frequency of the waves, one can immediately calculate the velocity of the supersonic waves.

In studying the supersonic velocity with the help of this diffraction spectra, it might have been noticed by many workers that some of the diffraction pattern lines are much more broad and diffuse than the others. Indeed, it had long been noticed by one of us (Dutta, 1938), that  $\text{CS}_2$  had a very broad and diffuse lines, particularly at higher frequencies of the order of 5 megacycles, and measurements on dispersion could not be carried

out in this liquid just because of this difficulty. It has also been noticed for a long time that, compared to the spectra of the other liquids, water gave the sharpest spectra. No worker in the line has yet reported on these characteristic widths of the diffraction spectral lines, nor any attempt has yet been made to explain these very significant observations.

The breadth or diffuseness of the lines appeared initially to be somehow connected with the absorption characteristics of the substance. The most diffuse spectra of  $\text{CS}_2$  and the sharpest spectra of water seemed to be related in some way to the absorption constant  $\alpha/v^2$ , which is very large for  $\text{CS}_2$  and quite small for water. Looked upon from this point of view, it had also been noticed that other liquids with intermediate absorption, had the line widths between that of water and  $\text{CS}_2$ .

#### BASIC CONSIDERATIONS FOR INTERNAL DISPERSION OF ELASTIC WAVES

(i) *Theory.* A most reasonable cause for the appearance of the line width has been considered by one of us (Dutta, 1952), in a previous paper, referred to as paper I, to be a greater or less degree of the variation of the supersonic about velocity a mean value, thus giving rise to a range of  $\Delta$ , and hence, a larger or smaller broadening effect. The idea has been substantiated by a general type of relation giving the velocity of the elastic waves in the form,

$$V^2 = p/\rho \left[ 1 + \frac{R(\gamma - 1)}{1 - F + (\gamma^2 \omega^2)} \right] \quad \dots (2)$$

where,  $p$  = pressure in the medium.

$R$  = ratio of liquid density to vapour density under same conditions of temperature.

$\gamma$  = ratio of specific heats of the vapour under the conditions at which the density ratio is taken.

$F$  = coefficient of the force of restitution.

$G^2 = g'^2/R(\gamma - 1)$ . where  $g''$  = coefficient of the force of friction.

The coefficients of the force of friction and restitution are expected to have a range of values. The different liquid molecules in the whole assembly will be acted upon by different magnitudes of the frictional and restitutional forces, depending on the actual orientation of the particular molecule with regard to its neighbours. The range will evidently determine the variation of velocity about a mean value and this may be quite large or small depending on the molecular structure. It has been shown in paper I, that  $G$  and probably,  $F$ , also, will have a range of values about the mean value, determined by the Stokes' multiplier  $M$ . The Stokes' multiplier is given by the relation,

$$M = \frac{(\alpha/v^2) \text{ observed}}{(\alpha/v^2) \text{ Stokes}} \quad \dots (3)$$



where  $\alpha/v^2$  observed, denotes the maximum value of the quantity, as the observed value can only determine the absorption coefficient maximum and that calculated by the Stokes relation in terms of  $\eta$  determines only the mean value, as the viscosity coefficient  $\eta$  is only a measure of the average value. The theoretical relation for  $\alpha/v^2$  obtained in paper I, is of the form,

$$\alpha/v^2 = \frac{\pi \rho g'}{n \rho V^2 (1 - F + G^2 \omega^2)} \quad \dots (4)$$

where  $n$  is the elastic index of refraction and  $V$  is the velocity of the elastic waves.

Comparing with Stokes' absorption relationship, (Stokes, 1845)

$$\alpha/v^2 = \frac{8\pi^2 \eta}{3\rho V^3},$$

one has the approximate mean value of the frictional co-efficient  $g''$ , in the form,

$$g'' = \frac{8\pi n \eta}{3\rho}.$$

We would have, then, the maximum value of  $g''$ , which determines the limit of the range of its variation, given by,

$$g''_{\max} = M \cdot g''_{\text{average}}$$

The values of the Stokes multiplier  $M$  has been taken from Pinkerton, (1949) and is set up in the following Table I.

TABLE I

Liquid				( $\alpha/v^2$ ) Stokes $\times 10^{17}$ c.g.s.	( $\alpha/v^2$ ) observed $\times 10^{17}$ c.g.s.	Ratio- $M$
Carbon disulphide	...	...	...	1.8	7400	1540
Benzene	...	...	...	8.0	800	100
Carbon tetrachloride	...	...	...	19.7	533	27
Toluene	...	...	...	7.8	90	11.5
Acetone	...	...	...	6.2	64	10.3
m-xylene	...	...	...	8.0	78	9.6
Water	...	...	...	8.1	25.3	3.1
Methyl alcohol	..	...	...	14.0	37	2.64
Ethyl alcohol	...	...	...	25.0	52	2.68
Helium	...	...	...	27.3	430	1.1
Mercury	...	...	...	5.1	5.5	1.08
Glycerine	...	...	...	755	800	1.06
Castor oil	...	...	...	5000	5200	1.04

The values of  $\alpha/v^2$  recorded are not for the same temperature. As it is now established from experimental results (Pinkerton, 1949) that the ratio of the observed and the calculated values of  $\alpha/v^2$ , on the basis of Stokes' relation, is independent of temperature, one need not take note of the temperature at which the ratio has been taken. One needs only to be careful, that the calculated value of  $\alpha/v^2$  is for the same temperature at which the observations have been made. It may be particularly noticed from Table I, that the magnitude of the Stokes multiplier  $M$  is not in any way related to the amount of the absorption co-efficient  $\alpha$  or to the quantity  $\alpha/v^2$ . The observed values of  $\alpha/v^2$ , which in the tabulated units, are of the order of some thousands in the case of carbon disulphide and castor oil, give rise to the Stokes multiplier value  $M$ , as different as 1540 and 1.04. Whereas, mercury, with the observed value of  $\alpha/v^2$  as 5.5 only, has the Stokes multiplier  $M$  identical with that of castor oil.

According to the contention of paper I, the Stokes multiplier  $M$  determines the range of variability of the frictional and the restitutional co-efficients. Further, the relation (2) immediately tells us that the range of variability of the velocity square will be determined by the range of variability of  $G^2$  and also of  $F$ . When  $G^2$  and  $F$  will have a large range of values and will be effective by their magnitudes, we will have a large range of  $V^2$  values and thus also a large range of  $\Lambda$  values. This has been termed as internal dispersion and will give rise to a broadening of the diffraction spectral lines. On this basis, the spectral lines will be broadened in accordance with the magnitudes of the corresponding  $M$  values, and should be completely unrelated to the absorption co-efficient of the liquid. As will appear from the experimental results, set forth later on, this point of view is fully corroborated.

(ii). *Molecular structure and variability of the co-efficients of forces.*

A word about the structure of the molecules and the expected range of variation of the co-efficients of friction and restitution would be appropriate here. The co-efficients are likely to be least variable in the case of perfectly symmetrical molecules of the spherical type. The different molecules in the whole aggregate, will, during the course of their motion, be acted upon by the forces of friction and restitution which are approximately of the same magnitude. This is exemplified by the  $M$  values of unity in the case of molecules like helium and mercury. A large range of variation of the co-efficients is expected in the case of simple molecules when the symmetry of structure is restricted or when the range of extension of the molecular dimension is limited. In such a case the mode of approach to the neighbours may be of a widely different character. From this point of view, a linear molecule, with an extension in one dimension, is very much more unsymmetrical than a molecule with an extension in two dimension. The latter, again, is still unsymmetrical compared to molecules that have an extension in three dimensions. The observed largest value of  $M$  in the

case of  $\text{CS}_2$ , of a linear model type and the next largest value of  $M$  for benzene, with an extension in two dimensions only, is thus understandable. Molecules which have an extension in three dimensions, like  $\text{CCl}_4$ , xylene and water will have, naturally on this consideration, lower  $M$  values than that for the simple plane model type of benzene. Large molecules of the type of glycerine and castor oil, that have the Stokes multiplier as unity, behave, apparently like the completely symmetrical atoms of helium and mercury. The non-variability of the forces of friction and restitution implied by this value of the Stokes constant is, however, not due to the spherical, and symmetrical shape of the molecules, but due to the long chain character of the molecules, with a number of linking arms. This precludes different types of orientations of the moving molecule with regard to the surrounding molecules and as a result the forces of restriction obtain unique values only, determining the Stokes multiplier as unity.

This gives a clue to the understanding of the gradual decreasing values of the Stokes multiplier in the series, water, methyl alcohol, and ethyl alcohol, as shown in Table I. The replacement of a hydrogen atom in the water molecule by a  $\text{CH}_3$  radical in methyl alcohol or by a  $\text{C}_2\text{H}_5$  radical in ethyl alcohol gives rise to a gradually less freedom of approach to the neighbouring molecules and thus, a smaller range of variation of the restricting forces. This should give rise to a gradually smaller value of the Stokes multiplier  $M$ , as has been observed.

The peculiar behaviour of acetic acid, which seems to have a very large Stokes multiplier, is to be accounted for by the inherent dissymmetry of the  $\text{CHO}$  group. The approach towards the neighbours, with a  $\text{C}-\text{H}$  front or with a  $\text{C}=\text{O}$  front, will cause a large variation in the determining forces and thus a large value of the Stokes multiplier  $M$ .

The typical constitution of the molecules thus enables us to understand the discrepancy between the observed values of the absorption and that calculated by the Stokes relation. It follows from relation (2), that due to the large or small range of variation of the coefficients of friction and restitution, we would have a large or small amount of internal dispersion and hence a large or small amount of broadening of the spectral lines, which is observed by the wave field diffraction method. This broadening would be completely determined by the molecular structure like the discrepancy between the observed and the calculated values of  $\alpha/\nu^2$ .

#### EXPERIMENTAL METHOD AND RESULTS

(1) *Method.* The experiment on internal dispersion was carried out by a comparative study of the diffraction spectra obtained by the wave field grating produced in different liquids. A small Hilger constant-deviation spectrograph was adjusted as a straight type spectrograph, so that diffraction spectra photographs could be taken on photographic plates. The source of illumination was a powerful sodium lamp with a bichromate filter, placed at a distance

of about twenty inches from the collimator slit. The liquid container was a parallel plate glass vessel with sides of three and half inches and the piezo-electric quartz was used in a vertical position. In particular cases of liquids, like water, the quartz was placed in an inner metallic vessel with a mica window. The plane of the oscillating quartz surface was adjusted to the sharpest definition of the spectra.

The oscillator was made with a low power valve, running on 220 volts D.C., and the circuit employed was the Hartley circuit. With a variable coil and condenser system different frequencies in the range of megacycles have been tried, and the first set of photographs was taken with a three megacycle frequency system.

Plates were measured with a Hilger comparator, and readings for the spectral separation of the first order spectra and the line widths of the first order spectra were taken. It was observed that the spectral lines of the castor oil were sharpest and this was expected as the Stokes multiplier  $M$  was unity in this case. Moreover, according to our contention, this indicates that there is no broadening of the lines due to internal dispersion. We have taken the line width of castor oil as that determined by the Doppler broadening of the source, under the conditions of the experiment. As the line widths varied with the time of exposure, along with the intensity of the spectral lines, in accordance with the principle of Doppler broadening, several photographs were taken on a plate with different times of exposure. A comparative estimate of the line widths, in the case of other liquids was made with reference to the line widths of castor oil. The difference between the line widths of castor oil and that for any other liquid, with the same measure of the intensity of the lines, was taken to be due to the internal dispersion of the liquid considered, as this gives us the excess amount over the Doppler broadening, which must be identical in all cases when the recorded intensity remains the same and the working temperature of the liquid remains the same. Since the velocities of the liquids are measured in terms of the spectral line separations, we may have a measure of the percentage of dispersion by comparing the excess broadening of the lines, with regard to the castor oil lines, with the spectral line separations.

In order to estimate the line widths of any two liquids under the conditions of equal intensity, a rough visual estimate was made at first, such that the intensities of the spectral lines of the two liquids were of the same order. Generally, it becomes necessary to match two spectra of different liquids with different times of exposure, such that the intensities are of the same magnitude. The spectra of the two liquids, with a roughly matched intensities are then put together, face to face, under the comparator microscope. In this magnified image, any difference in intensity can be properly estimated. As the plates contain spectra with different times of exposure and hence with different intensities, any further adjustment of matching can be easily done by shifting one of the spectra with respect to

the other. This matching of intensity seems to be more accurate than the method of microphotometric study of the intensities, particularly so, when we are trying to find spectra of equal intensities and do not want to know the relative intensities. Having thus found out the spectra of equal intensities corresponding to two different liquids and placing both under the comparator microscope, one needs now only to record the widths of the respective spectral lines. Even in the case when the two liquids studied have each of them an internal dispersion, their Stokes multiplier being greater than unity, one may easily calculate the percentage dispersion of any of them referred to the ideal liquid, with a Stokes multiplier as unity, provided we have, for at least one of them, the excess of line width compared to the line width of castor oil, under the conditions of equal intensities. It is actually, thus that the amount of internal dispersion of a number of liquids has been calculated.

(ii) *Experimental results.* In the case of all the liquids studied, it has been observed that the line widths for equal intensities, are consistently broader in the case of liquids with greater values of the Stokes multiplier  $M$ , irrespective of the absorption coefficient of the medium. Typical examples to illustrate the method of calculations are the following cases :

(a) Internal dispersion in water :

Separation of the first order bands in water  $d_w = 1.2$  mm.

Width of first order spectral line, formed by 3 megacycles elastic waves in water, with an exposure time of 2 minutes, under the optical conditions of the experiment is given by,

$$D_w = 10.5 \times 10^{-2} \text{ mm.}$$

Width of first order spectral line, formed by 3 megacycles elastic waves in castor oil, with an exposure time of 30 secs. so as to give identical intensity with water lines, is given by,

$$D_c = 8.5 \times 10^{-2} \text{ mm.}$$

Hence, internal dispersion in water, with castor oil as standard would be,

$$(D_w - D_c)/d_w = 1.7 \text{ per cent.}$$

(b) Internal dispersion of carbon bisulphide :

Separation of the first order bands in  $\text{CS}_2$ , with 3 megacycles waves, is given by  $d_{\text{CS}_2} = 1.57$  mm.

Width of first order spectral line, formed by 3 megacycle elastic waves in  $\text{CS}_2$ , with an exposure time of 8 minutes, is given by

$$D_{\text{CS}_2} = 22.5 \times 10^{-2} \text{ mm.}$$

Width of first order spectral line, formed by 3 megacycles elastic waves in water, with an exposure time of 30 secs, is given by,

$$D_w = 7.1 \times 10^{-2} \text{ mm.}$$

This is equivalent to the castor oil width,

$$D_c = 5.10 \times 10^{-2} \text{ mm.}$$

Hence, the internal dispersion in carbon-bi-sulphide, with castor oil as standard, would be given by,

$$(D_2 - D_{CS_2})/d_{CS_2} = 11.1 \text{ per cent.}$$

Such measurements have been taken with various pairs of liquids and calculations of internal dispersion have been made with castor oil width as the standard. Internal dispersion of any particular liquid, calculated with the help of comparative measurements with a set of other liquids as intermediate steps give sufficiently consistent values, from which a mean value has been taken for a particular liquid. These have been tabulated in Table II.

TABLE II.

Liquid				Stokes multiplier $M$	Percentage of internal dispersion (mean value)
Castor oil ..	...	...	...	1	0
Water ...	...	...	...	3.1	1.7
Xylene ...	..	.	...	9.6	3.0
Benzene ...	...	.	.	100.0	6.5
Carbon bisulphide	...	...		1540.0	11.6

Table II above, shows that there is a consistently and increasing value of the internal dispersion of elastic waves, for increasing  $M$  values, as measured by the increasing width of the spectral lines of different liquids under the same optical conditions and having the same intensity. It has to be noted that the increase in the internal dispersion values is much more slow compared to the increase in the  $M$  values of the liquids.

Further, we have to critically study our results in the light of the theoretically expected result from considerations of the deduced relation (2). An internal dispersion would be expected, when the frictional coefficient  $G$  has a range of values and is of such magnitude that the term  $\omega^2 G^2$  has values to make an effective contribution in the denominator of the relation (2). In such a case the magnitude of the internal dispersion will be dependent upon the frequency of the waves and would rapidly increase with the frequency of the waves. An internal dispersion would also be expected when the restitutional coefficient  $F$  has a range of values, determined, presumably in some way by the Stokes multiplier  $M$ . It has to be noted, however, that whereas, the range of variation of  $G$  from its average value is determined directly by the Stokes multiplier  $M$ , such that  $M, G_{\text{aver.}}$  gives the maximum value of  $G$ , we do not expect such linear relationship with  $M$  to determine the range of variation of  $F$ . Further, it has to be noted that so far as the internal dispersion would be dependent upon the restitutional coefficient  $F$ , it would give us the internal dispersion as independent of the wave frequency. We would now proceed to discuss the observed amount of internal dispersion with a view to finding out its real cause,

For this purpose one needs to have a proper estimate of the average value of  $G$  for different liquids.

The average value of  $G$  may be estimated from the relations

$$G^2 = g''^2 / R(\gamma - 1)$$

$$g'' = \frac{8\pi n}{3\beta} \cdot \eta.$$

$$V^2 = p/\rho \left[ 1 + \frac{R(\gamma - 1)}{1 - F + G^2 \omega^2} \right] = \frac{p}{\rho} R(\gamma - 1)$$

approximately and the elastic index of refraction,

$$n^2 = \frac{p/\rho}{V^2}.$$

With the known values of  $V$ ,  $\rho$ ,  $R$ ,  $\gamma$ ,  $\eta$ , one may easily estimate the values of  $p$ ,  $n$ , and  $g''$  and thus also of  $G$ . The value so obtained would be the average value of  $G$ . As the order of values of the different quantities involved does not change for the different liquids, we can easily understand that the average value of  $G$  would be of the same order for different liquids. The calculated order of value of average  $G$  comes out to be  $10^{-12}$ . Hence the maximum value of  $G$ , even in the case of  $\text{CS}_2$ , with an  $M$  value of 1500, comes out of the order of  $10^{-9}$ . With an wave frequency of 3 megacycles the maximum value of  $G^2 \omega^2$ , in the case of  $\text{CS}_2$ , would come upto  $10^{-8}$  only. The effect of the variation of  $G$  on the wave velocity, with a frequency of the order of a few megacycles, would thus be not detectable, as it is vanishingly small compared to  $1 - F$ .

It thus appears that the observed dispersion of the wave velocity is not caused by the variation of  $G$ , and must have been caused by the variation of  $F$ . On this contention, as indicated before, the observed dispersion would be independent of the wave frequency. To check this point of view, measurements on internal dispersion were taken at the lower frequency of 1 megacycle. It has been observed that the magnitude of the internal dispersion remains about the same as for the case of the higher frequency waves. This confirms the idea that the variation of the coefficient of restitution  $F$  has been the source of internal dispersion of the comparatively lower frequency elastic waves. It has also to be noted that the amount of the observed internal dispersion varies more or less as the logarithm of the Stokes multiplier  $M$ . This will be apparent from Table III which follows. On a theoretical basis, proceeding from the velocity equation (2), we may proceed as follows, to find an expression for the internal dispersion  $dV/V$ . We have, neglecting  $G^2 \omega^2$ ,

$$V^2 = p/\rho \left[ \frac{R(\gamma - 1)}{1 - F} \right] = \frac{p}{\rho} R(\gamma - 1)(1 + F), \text{ for small } F,$$

$$dV^2 = 2VdV = \frac{p}{\rho} R(\gamma - 1)(F - F')$$

and thus,

$$2 \frac{dV}{V} = (F' - F).$$

Thus, when the internal dispersion is proportional to  $\log M$ , one may put,

$$F' = F + C \log M.$$

We are, however, not yet in a position to say whether the constant  $C$  is dependent on  $F$  or not. It is advisable to wait for more experimental results before one proceeds to say anything more on the point. To show the constancy of the internal dispersion at two different frequencies, as also the values of the Stokes multiplier  $M$  and of  $\log M$ , Table III is given below.

TABLE III.

Liquid			Stokes Multiplier $M$	$\log_{10} M$	% internal dispersion at 3 mega cycles	% internal dispersion at 1 mega cycle
Castor oil	...	...	1	0	0	0
Water	...	...	3	.17	1.7	1.5
Xylene	...	...	9.6	.98	3	not measured
Benzene	...	...	100	2.0	6.5	6.9
Carbon-bi-sulphide			15.10	3.19	12	12.5

The irregularities in the values of internal dispersion for two different frequencies are within the range of experimental error. It may be pointed out, however, that the actual widening of the spectral lines, as compared to any corresponding lines of another liquid, taken as a standard, appears to be much less for lower frequencies than for the higher ones. But as the spectral line separations measuring the velocity, is much narrower for lower frequencies, we expect, for about the same value of internal dispersion, measured by  $dV/V$ , a much smaller broadening of the spectral lines at lower frequencies. Indeed, this appears to be the reason for the vanishing of the diffraction spectral lines with carbon-bi-sulphide for higher frequencies of the order of 5 megacycles. With acetic acid even with 3 megacycle spectral lines could not be detected.

#### REFERENCES

- Bär, R., 1938, *Helv. Phys. Acta*, **11**, 472.  
 Debye, P., and Sears, F. W., 1932, *Proc. Nat. Acad. Sci.*, **18**, 410.  
 Dutta, A. K., 1938, *Phys. Zeits.*, **39**, 186.  
 " " 1952, *Ind. J. Phys.*, **28**, 142.  
 Hiedemann, E., Seifen, N., and Schreuer, E., 1936, *Naturwiss.*, **24**, 681.  
 Pinkerton, J. M. M., 1949, *Proc. Phys. Soc.*, B, **62**, 129.  
 Schallamach, A., 1949, *Proc. Phys. Soc.*, B, **62**, 70.  
 Spakovskij, G. B., 1938, *Compt. Rendus, U.S. S. R.*, **18**, 169.  
 Stokes, G. G., 1845, *Trans. Camb. Phil. Soc.*, **8**, 287.  
 Zachoval, L., 1939, *J. de Physique et le Radium*, **10**, 350.



# HEAT LOSSES AND THEIR DEPENDENCE ON AIR VELOCITY

By D. G. KAPADNIS AND D. V. GOGATE

PHYSICS DEPARTMENT, M. S. UNIVERSITY OF BARODA

(Received for publication, July 31, 1951)

**ABSTRACT.** In this investigation, the variation of convective heat losses with different air velocities, for vessels of different shapes and sizes, has been studied. The rate of heat loss is found to depend upon the shape of the vessel used and varies directly as the square-root of the air velocity

## INTRODUCTION

A vessel filled with a liquid at a temperature higher than its surroundings, loses heat by conduction, convection, radiation and also by evaporation of the liquid. With suitable arrangements it is easy to reduce considerably, losses by conduction, radiation and evaporation and under these conditions most of the heat loss will be due to convection alone. Now convection is partly natural and partly forced. The heating of a vessel by a current of hot air and the cooling of a surface with an electric fan are examples of forced convection, whereas, the streams of air rising about a warm surface, a hot metal cylinder etc., are examples of natural convection. Obviously the convection will be greater with greater velocity (and natural convection will be small compared to forced one) of the air stream and with greater difference of temperature between the surrounding air and the warm surface.

In the present paper we have investigated heat losses due to convection from different vessels. For this purpose the rate of heat loss from the surface of calorimeters of different shapes and sizes with air velocities above 250 cm/sec. (*i.e.*, 500 ft./min.) was measured and the relation between the heat losses and the air velocities was then studied.

## EXPERIMENTAL ARRANGEMENT

The experimental arrangement used in this investigation is as follows:

A calorimeter *A*, containing some warm water, was placed at a distance of about 70 cm from an electric fan *F* and a stream of air proceeding from the fan was directed on this calorimeter after allowing it to pass through a wire grid *G* situated at a distance of about 15 cm from the fan. The top of the calorimeter was closed by a lid having two holes in it. Through one

of the holes passed a sensitive thermometer and through the other a stirrer

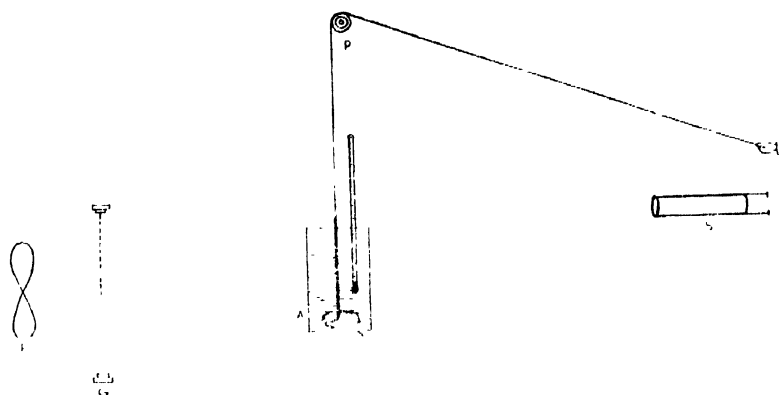


FIG. 1

was kept working so that a uniform temperature was maintained throughout the whole mass of water at any instant. Most of the evaporation was prevented in this way and in some cases a very thin layer of oil was spread on the surface of water inside the calorimeter to help in preventing the evaporation more effectively. The speed of the air stream issuing from the fan was varied by changing the strength of the current in the circuit of the fan and the air velocity was measured by means of a four-cup anemometer placed exactly in the place of the calorimeter *A* before and after the experiment. These values of air velocity were also checked by means of a silvered Kata thermometer (Bedford, 1946). The temperature of the water was measured by focusing a small telescope *S* on the vertical thermometer *T* passing through the lid of the calorimeter *A*. This procedure also eliminated the possibility of affecting the temperature of the calorimeter *A* by the breath of the observer. The stirrer was moved up and down in the calorimeter by connecting it to a string passing over a pulley *P* as shown in figure 1. The other end of the string was held by the observer who could move it to and fro, thus causing a vertical motion of the stirrer in the calorimeter. The temperature of the water was noted at intervals of half a minute and a graph of temperature against time was plotted. From this graph the value of the rate of fall of temperature per unit time, i.e.,  $\frac{d\theta}{dt}$ , for any mean temperature  $\theta$  could be calculated. The values of  $\frac{d\theta}{dt}$  were thus determined for different air velocities as measured by the anemometer and a graph of  $\frac{d\theta}{dt}$  against air velocity was plotted. In all the cases investigated, it is found that the rate of fall of temperature is governed by a relation of the type  $\frac{d\theta}{dt} = a + b\sqrt{v}$  where *a* and *b* are constants and *v* represents the velocity of the air stream.

Having obtained the values of  $\frac{d\theta}{dt}$ , the convective heat loss from the calorimeter was calculated by the relation

$$(M + M_0 S) \frac{d\theta}{dt} = H = C A \sqrt{v} \Delta\theta$$

where  $H$  = heat lost per hour ;

$A$  = area of the calorimeter surface exposed ;

$\Delta\theta$  = difference of temperature between the calorimeter and the surroundings ;

and  $C$  = a constant, which will be called the shape-constant hereafter, as it depends only on the shape of the calorimeter used.

It was found that when the calorimeter was subjected to forced convection, practically all the heat loss was due to convection alone. Care was, of course, taken to ensure that no appreciable heat was lost by conduction, radiation or evaporation. For avoiding conduction the base of the calorimeter was made to rest on three points of a tripod stand, small pieces of asbestos being fixed at those points. Radiation was avoided by polishing the calorimeter surface and evaporation was prevented by closing the top of the calorimeter by a lid and also by spreading a thin layer of oil on the surface of the water inside the calorimeter.

Vessels of different shapes and sizes were used as calorimeters in these experiments and the shape constant  $C$  was determined for each of them. As will be seen from the results discussed below the shape constant  $C$  is found to possess a remarkably constant value for vessels of different materials having different sizes provided their shape was the same. These determinations are expected to give some idea of the comparative efficiency of differently shaped vessels as containers of different fluids.

## RESULTS

Figure 2 shows how the convective heat losses vary with different air velocities in the case of vessels of different shapes and sizes, the actual observations being recorded in the Table I. The graphs also show that the convective heat loss decreases as the diameter of the vessel increases.

In figure 3, the heat loss is plotted against the square-root of air velocity and it is found that in every case the graph is a straight line, showing clearly that the relation between heat loss and square-root of air velocity is linear.\*

Vessels of copper and tinned iron were used as calorimeters in these experiments and different shapes like cylinders, spheres, rectangular parallelepipeds, etc., were used to find out whether the shape constant  $C$  defined

\* The exact nature of the graphs in figures 2 and 3 for velocities below 300 cm./sec. is not fully known as yet. Experiments are being carried out to investigate in this region and the results will be reported in due course.

TABLE I

Shape of the vessel.	Diameter in cm.	Area in sq. metres.	Air velocity in cm/sec	Square-root of air velocity	Heat losses in K cal/hr/m <sup>2</sup> /1°C	Shape constant
Cylindrical	15.0	0.1201	400	20.00	20.25	0.95 <sub>3</sub>
			445	21.10	21.75	
			540	23.24	23.56	
			624	24.98	25.47	
			694	26.34	26.59	
			761	27.58	27.75	
			811	28.48	28.48	
			877	29.62	29.61	
			913	30.23	30.27	
			952	30.86	30.75	
	21.8	0.1807	305	19.87	19.72	0.93 <sub>2</sub>
			445	21.10	20.04	
			505	22.47	22.32	
			580	24.27	23.88	
			667	25.83	25.46	
			735	27.11	26.50	
			795	28.19	27.32	
			854	29.20	28.47	
			913	30.23	29.49	
Rectangular	...	0.1417	328	18.10	22.79	1.07 <sub>1</sub>
			305	19.87	24.98	
			505	22.47	27.65	
			580	24.27	29.51	
			667	25.83	31.50	
			735	27.11	32.66	
			795	28.19	33.91	
			854	29.20	34.90	
			901	30.02	35.87	
	...	0.1952	376	19.40	23.70	1.05 <sub>9</sub>
			445	21.10	25.63	
			510	23.24	27.91	
			624	24.98	29.70	
			694	26.34	30.98	
			761	27.58	32.35	
			811	28.48	33.50	
			877	29.62	34.68	
			913	30.23	35.25	
Spherical	15.8	0.0784	956	30.92	35.87	1.62 <sub>9</sub>
			376	19.40	22.25	
			445	21.10	25.25	
			510	23.24	28.53	
			624	24.98	31.21	
			694	26.34	33.65	
			761	27.58	35.77	
			811	28.48	37.26	
			877	29.62	39.01	
	20.4	0.1307	913	30.23	39.79	1.56 <sub>8</sub>
			956	30.92	41.43	
			395	19.87	21.62	
			415	21.10	27.73	
			505	22.47	26.92	
			510	23.24	28.05	
			589	24.27	26.63	
			667	25.83	32.11	
			735	27.11	34.16	
			795	28.19	35.88	
			854	29.20	37.50	
			940	30.66	39.81	

by the relation

$$H = CA\sqrt{v} \Delta\theta$$

remains constant. Table I gives the results obtained with vessels of different shapes and different sizes. Following the practice adopted by other

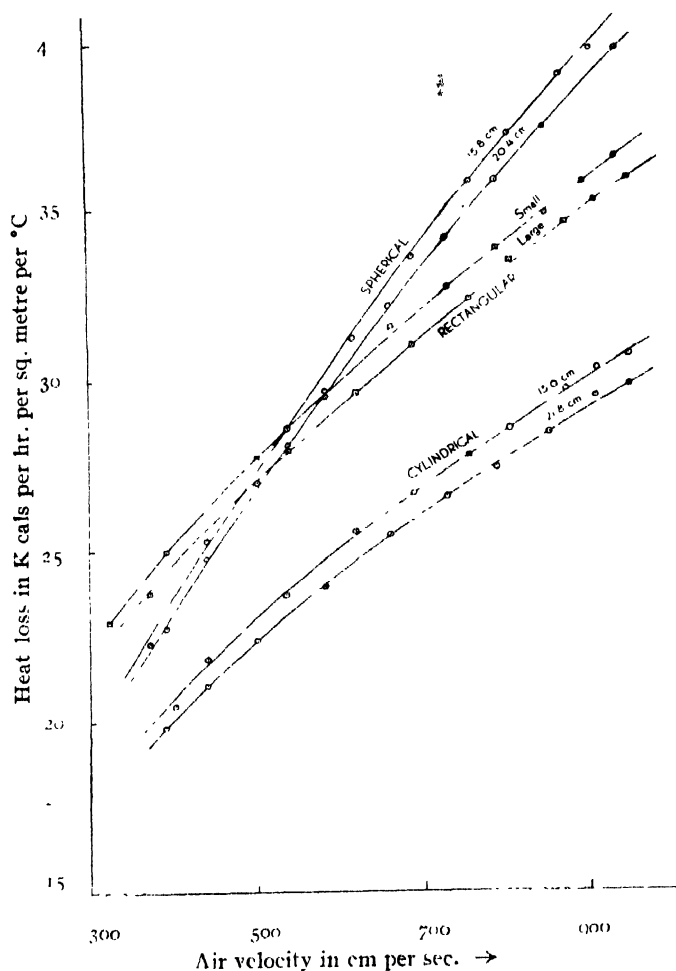


FIG. 2

workers, the heat loss was measured in terms of kilo-calories per hour per square metre per degree Centigrade and the air velocity in centimetres per second.

It will be seen from the table that amongst the different shapes of vessels employed in our experiments, the shape constant  $C$  has the lowest value for cylindrical vessels and hence the convective heat loss appears to be least in the case of vessels having a cylindrical shape.

This study is of interest in connection with the thermo-dynamics of heat interchange between the body and the surroundings under different

ambient conditions. Recently, a lot of work has been done in this field

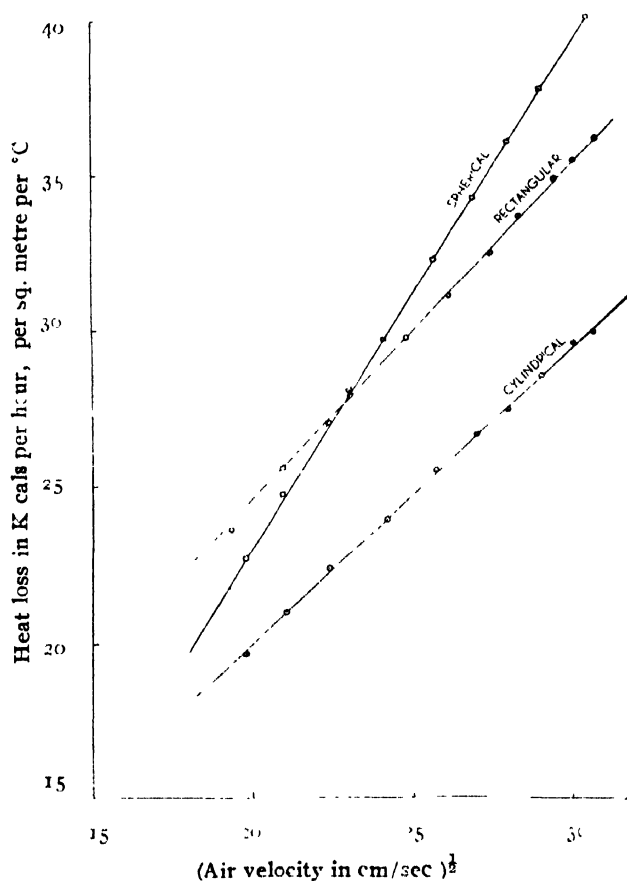


FIG.3

(Buttner, 1934 ; Winslow and others, 1937, 1939 ; Plummer, 1944 ; etc.) but as yet no satisfactory understanding has been obtained.

#### ACKNOWLEDGMENT

Our thanks are due to Dr. D. S. Kothari, Scientific Advisor to the Ministry of Defence, New Delhi, for his kind interest in this work. We are also grateful to the Defence Science Organization for the loan of a silvered Kata thermometer.

#### REFERENCES

- Bedford, T., 1916, *Med. Res. Council*, War Memorandum, **17**, 17  
 Buttner, K., 1934, *Publication of Prussian Met. Inst.*, **10**, 404.  
 Hill, L., 1919, *Sc. of Ventilation and Open Air Treatment*, Part I, *Med. Res. Council. Spec. Reports*, p. 32  
 Plummer, J. H., 1944, *Publication of the Climatology and Environmental Protection Branch, Office of the Quarter Master General*.  
 Soderstrom, G. F. and Du Bois, 1917, *E. F. Arch. Inst. Med.*, **19**, 931.  
 Winslow, C. E. A., Herrington, L. P. and Gagge, A. P., 1937, *Am. J. Physiol.*, **120**, 1.  
 1939, *Am. J. Physiol.*, **127**, 505.

# $\Pi - {}^5\Sigma$ ELECTRONIC TRANSITION IN COBALT CHLORIDE

By V. G. KRISHNAMURTY

DEPARTMENT OF PHYSICS, ANDHRA UNIVERSITY, WALTAIR

(Received for publication November 30, 1951)

## Plate VI

**ABSTRACT.** The band spectrum of the diatomic molecule CoCl has been obtained in emission using a heavy current discharge. The bands are slightly red degraded and occur in six groups extending from  $\lambda$  6000 to  $\lambda$  5350 Å. The bands are line like and are similar to the band systems obtained in the case of Mn and Cr halides. They are of complex structure and show an abnormal intensity distribution among the heads and are assigned to the transition  ${}^5\Pi - {}^5\Sigma$ , involving quintet electronic states.

The vibrational constants obtained are  $\omega_e' = 412.3$  and  $\omega_e'' = 416.0$ .

## INTRODUCTION

A study of the band systems of diatomic molecules of the transition group of elements has been the subject of several investigations in recent years. These elements contain incomplete  $d$  electron shell and form molecules which give rise to bands of a very complex structure. This complex structure is explained by the identification of high multiplicity terms among the electronic states for these molecules. The most complete analysis including the rotational structure is that of the  ${}^7\Pi - {}^7\Sigma$  system of MnH by Nevin (1942, 1945), Bacher (1948) and P. T. Rao (1949) have studied the band spectra of Mn halides and obtained similar transitions. V. R. Rao and K. R. Rao (1949) have analysed the band system of Cr Cl and ascribed it to the transition  ${}^6\Pi - {}^6\Sigma$ . Bands of Ti Cl in the 4200 Å region are ascribed by V. R. Rao (1949) to the transition  ${}^4\Pi - {}^4\Sigma$ . Miescher (1938) and Muller (1943) suggested  ${}^6\Pi - {}^6\Sigma$  and  ${}^4\Pi - {}^4\Sigma$  transitions respectively as giving rise to bands of the Fe Cl molecule.

Following the work in this laboratory referred to above, an extensive study of the band systems of the halides of Fe, Co, Ni and other similar elements has been undertaken by the author to examine the evidence of high multiplicity terms in these spectra. Results obtained in the case of CoCl are given in this paper.

Mesnage (1935, 1938) has studied the band systems of the chloride and bromide of cobalt in emission in a high frequency discharge with external electrodes. In the case of cobalt chloride, he has recorded two regions of emission bands, (1) a few bands in the 4300–4850 Å region and (2) a few other bands in the 5550–5850 Å region, but he did not give any analysis of these.

to the transition  ${}^5\Pi - {}^5\Sigma$  involving quintet terms in both the upper and lower electronic states of the molecule.\*

The possible rotational heads for  ${}^5\Pi - {}^5\Sigma$  transition can be formulated thus. The ground state  $\Sigma$  (with  $\lambda=0$ ) must correspond to coupling type, Hund's case (b). In a  ${}^5\Sigma$  state ( $\lambda=0$  and  $s=2$ ) there is a spin splitting of each rotational level. i.e., for each value of  $K$ , there will be five component levels with  $J$  lying between  $K-S$  and  $K+S$  which, following Muliken, may be designated as  $F_0, F_1, \dots, F_4$  respectively. These levels have small separations and ordinarily are not resolvable.

The upper  ${}^5\Pi$  state may approximate to case (a) or case (b) or may represent any state intermediate between the two. For higher values of  $K$  it approaches case (b) and for low values of  $K$ , case (a). The calculation can be made for higher values of  $K$  and reduced to the low values. Combining  $\Lambda$  and  $\Sigma$  we get 5 values giving  $\Pi_{-1}, \Pi, \dots, \Pi_4$  which we might denote as  $F_0, F_4 \dots F_1$  respectively. Whatever stage of coupling the state represents, the rotational energy term is given by equation (72) of Jevon's (1932) Report on Band Spectra, page 124.

A schematic diagram for the transition  ${}^5\Pi - {}^5\Sigma$  showing the various observable branches is represented in figure 1.

The form of the branches is indicated as  $T, S, R \dots N$  corresponding to the  $\Delta K$  values 3, 2, 1, ..., 3, changes of  $K$  by 0,  $\pm 1$  being permitted. The rotational lines would be represented by the formula

$$\nu = \nu_0 + F'(K') - F''(K'') = \nu_0 + B'K'(K'+1) - B''K''(K''+1)$$

where  $\nu_0$  represents the frequency of the nul-line of the band.

The formulae for the individual forms are

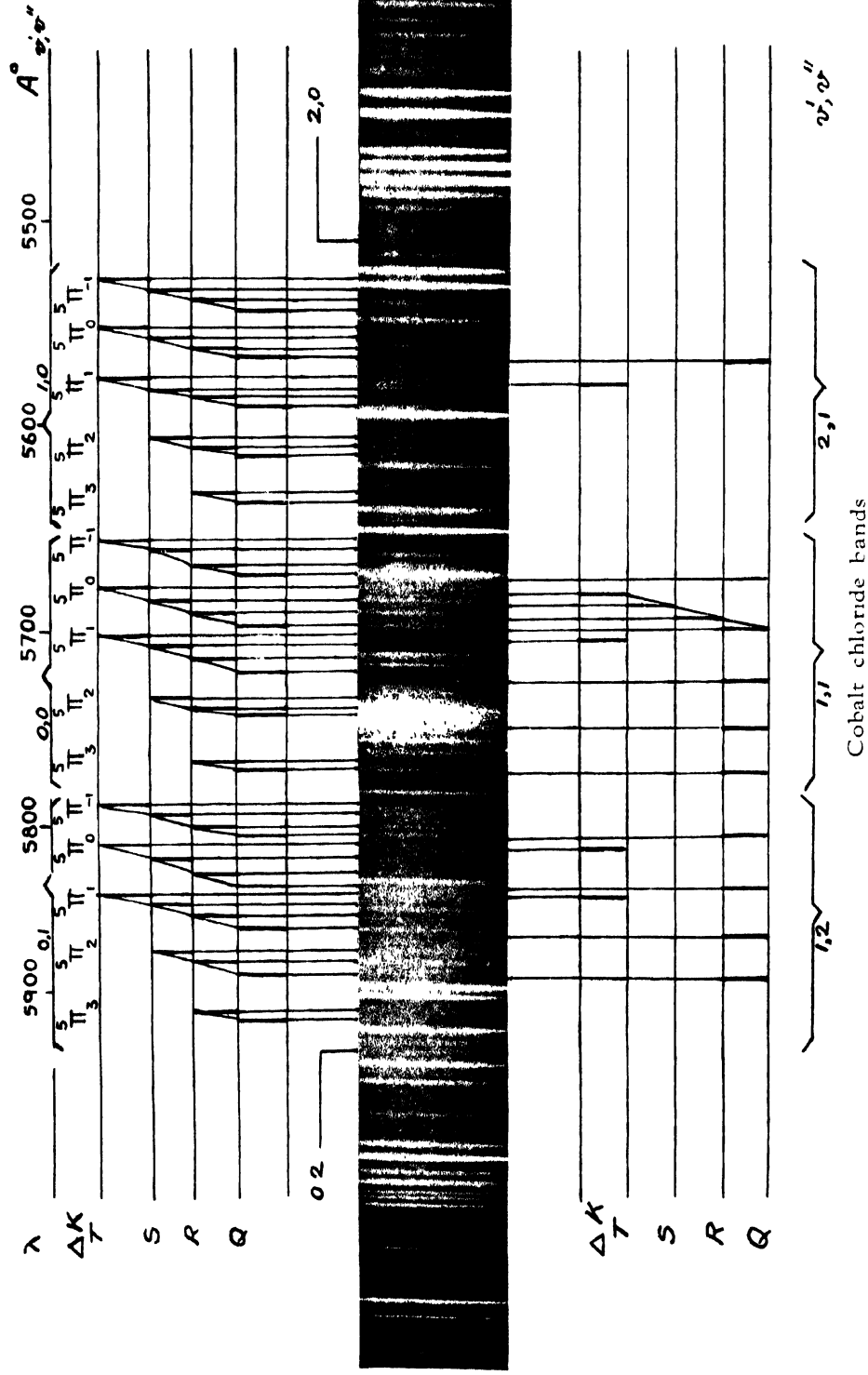
Form  $\Delta K$

$$\begin{array}{ll} T & +3 \quad \nu = \nu_0 + F'(K+3) - F''(K) \\ & \quad = \nu_0 + 12B' + (7B' - B'')K + (B' - B'')K^2 \\ S & +2 \quad \nu = \nu_0 + F'(K+2) - F''(K) \\ & \quad = \nu_0 + 6B' + (5B' - B'')K + (B' - B'')K^2 \\ R & +1 \quad \nu = \nu_0 + F'(K+1) - F''(K) \\ & \quad = \nu_0 + 2B' + (3B' - B'')K + (B' - B'')K^2 \\ Q & 0 \quad \nu = \nu_0 + F'(K) - F''(K) \\ & \quad = \nu_0 + (B' - B'')K + (B' - B'')K^2 \\ P & -1 \quad \nu = \nu_0 + F'(K-1) - F''(K) \\ & \quad = \nu_0 - (B' + B'')K + (B' - B'')K^2 \\ O & -2 \quad \nu = \nu_0 + F'(K-2) + F''(K) \\ & \quad = \nu_0 + 2B' - (3B' + B'')K + (B' - B'')K^2 \\ N & -3 \quad \nu = \nu_0 + F'(K-3) - F''(K) \\ & \quad = \nu_0 + 6B' - (5B' + B'')K + (B' - B'')K^2 \end{array}$$

\* More's system in the region  $\lambda$  4750 to  $\lambda$  4200 Å may be the  ${}^3\Pi - {}^3\Sigma$ , expected from the above states.







Differentiating the above expression with respect to  $K$  and equating to zero (the condition for head formation) we get the value of  $K$  at which the head is formed. For the case in which  $B'' > B'$  (red degraded bands),  $K_h$  is positive for  $T, S, R$  forms, 0 for  $Q$  forms and negative for  $P, O, N$  forms. The  $K_h$  values for  $T, S, R$  and  $Q$  forms are given below.

$\Delta K$	3	2	1	0
Form	$T$	$S$	$R$	$Q$
$K_h$	$-(7B' - B'') / 2(B' - B'')$	$-(5B' - B'') / 2(B' - B'')$	$-(3B' - B'') / 2(B' - B'')$	0

Hence in  $\text{CoCl}$  bands for which  $\omega_e' > \omega_e''$  we expect only the  $T, S, R$  and  $Q$  forms as head forming.

In Table I, a catalogue of the wavelengths together with the intensities and wavenumbers is given. The fourth column gives the vibrational assignment. The rotational designation of each head is given in the last column.

The wavenumbers of the  $Q$  heads as obtained in the  $(0,1), (0,0)$  and  $(1,0)$  sequences are given in Table II which also shows the values of the vibrational constants as calculated from the  $Q$  head separations.

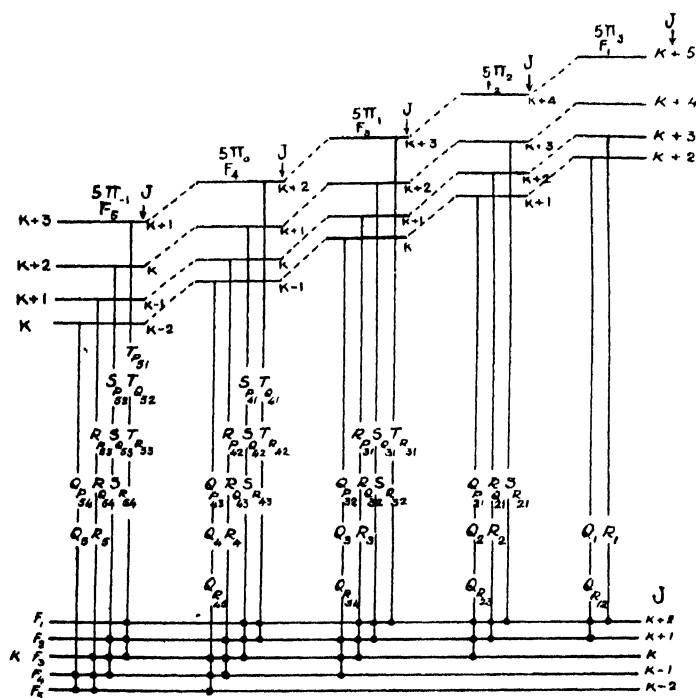


FIG. 1

Scheme of transitions in  ${}^5\Pi(a) - {}^5\Sigma$  for the cases  $B'' > B'$

TABLE I

Wavelength	Wavenumber	Int	$\nu', \nu''$	$\Delta J$		
				-1	0	+1
5977.5	16721.8	2	0,2	$\delta P_{43}$	$Q_4$	$QR_{45}$
71.2	16742.4	3	0,2	$RP_{42}$	$RQ_{12}$	$R_4$
65.1	16758.7	4	0,2	$SP_{41}$	$SQ_{42}$	$SR_{43}$
56.0	16783.7	3	0,2		$TQ_{41}$	$TR_{42}$
50.5	16802.1	3	0,2	$QP_{51}$	$Q_5$	
41.1	16827.2	4	0,2	$SP_{52}$	$SQ_{53}$	$SR_{54}$
31.2	16855.3	3	0,2	$TP_{51}$	$TQ_{52}$	$TR_{53}$
27.2	16866.7	2				
22.6	16879.8	3				$QR_{15}$
11.4	16911.8	3	0,1		$Q_1$	$R_1$
05.5	16928.7	3	0,1			
5693.4	16968.1	4				$QR_{22}$
86.0	16984.8	3	1,2	$QP_{21}$	$Q_2$	$QR_{23}$
83.0	16993.4	3	0,1	$QP_{21}$	$Q_2$	$R_2$
77.2	17010.2	5	0,1		$RQ_{21}$	$SR_{21}$
70.4	17029.9	4	0,1			
64.4	17047.3	3				$QR_{34}$
60.6	17058.4	3	1,2	$QP_{32}$	$Q_3$	$QR_{34}$
57.6	17067.1	5	0,1	$OP_{32}$	$Q_3$	$R_3$
50.7	17087.2	3	0,1	$RP_{31}$	$RQ_{32}$	$SR_{32}$
45.1	17103.6	5	0,1		$SQ_{31}$	$TR_{31}$
41.1	17115.3	4	1,2			$TR_{31}$
36.7	17128.2	4	0,1			$QR_{45}$
33.6	17137.3	4	1,2	$QP_{42}$	$Q_4$	$QR_{45}$
31.6	17143.2	5	0,1	$QP_{43}$	$Q_4$	$R_4$
26.1	17159.4	4	0,1	$RP_{42}$	$RQ_{43}$	$SR_{43}$
20.1	17177.1	3	0,1	$SP_{42}$	$SQ_{41}$	$TR_{42}$
16.7	17187.1	3	1,2		$TQ_{41}$	$TR_{42}$
13.4	17196.9	3	0,1		$TQ_{42}$	
10.5	17205.5	3	1,2	$QP_{54}$	$Q_5$	
04.8	17222.4	5	0,1	$QP_{54}$	$Q_5$	$R_5$
00.6	17234.8	3	0,1	$RP_{53}$	$RQ_{54}$	$SR_{54}$
5795.4	17250.3	3	0,1	$SP_{52}$	$SQ_{53}$	$TR_{53}$
90.2	17265.8	5	0,1	$TP_{51}$	$TQ_{52}$	
85.1	17281.0	3				
78.2	17301.6	4				$QR_{12}$
73.9	17314.5	5	1,1		$Q_1$	$QR_{12}$
69.4	17328.0	6	0,0		$Q_1$	$R_1$
65.7	17339.2	4	0,0			
60.2	17355.7	7				
58.8	17359.9	3				$QR_{23}$
46.1	17398.3	3	1,1	$QP_{21}$	$Q_2$	$QR_{23}$
41.9	17411.0	6	0,0	$QP_{22}$	$Q_2$	$R_2$
37.2	17425.3	7	0,0		$RQ_{21}$	$SR_{21}$
32.1	17440.8	5	0,0			
28.8	17450.8	5				
24.7	17463.3	5				
20.7	17475.5	3	1,1	$QP_{32}$	$Q_3$	$QR_{41}$
17.9	17484.1	3	0,0	$QP_{29}$	$Q_3$	$QR_{24}$
11.8	17502.8	4	0,0	$QP_{21}$	$RQ_{31}$	$R_3$
05.7	17521.5	3	0,0		$SQ_{31}$	$SR_{22}$
02.5	17531.3	3	1,1			$TR_{31}$
5699.7	17539.9	3	0,0			$TR_{31}$
90.0	17542.1	5	1,1	$QP_{43}$	$Q_4$	$QR_{45}$
94.5	17555.9	6	0,0	$QP_{43}$	$Q_4$	$QR_{45}$
91.2	17566.1	3	1,1	$RP_{42}$	$RQ_{43}$	$R_4$

TABLE I (contd.)

Wavelength	Wavenumber	Int.	$\nu', \nu''$	$\Delta I$		
				-1	0	+1
5688.0	17576.0	7	0,0	$RP_{42}$	$RQ_{43}$	$R_4$
85.3	17584.4	3	1,1	$SP_{41}$	$SQ_{42}$	$SR_{41}$
81.6	17595.8	6	0,0	$SP_{11}$	$SQ_{42}$	$SR_{43}$
79.0	17603.9	4	1,1		$TQ_{41}$	$TR_{42}$
75.3	17615.3	5	0,0		$TQ_{11}$	$TR_{42}$
71.9	17625.9	3	1,1	$QP_{34}$	$Q_5$	
67.8	17638.8	10	0,0	$QP_{54}$	$Q_5$	
63.7	17651.4	5	0,0	$RP_{53}$	$RQ_{54}$	$R_5$
55.7	17676.4	7	0,0	$SP_{52}$	$SQ_{53}$	$SR_{54}$
50.8	17691.7	3	0,0	$TP_{51}$	$TQ_{52}$	$TR_{53}$
34.5	17742.9	3	1,0		$Q_1$	$QR_{12}$
29.1	17759.9	3	1,0			$R_1$
24.5	17774.4	4				
20.4	17787.4	4				
15.7	17802.3	7				
9.4	17822.3	4	1,0	$QP_{21}$	$Q_2$	$QR_{21}$
66.2	17832.5	6	1,0		$RQ_{21}$	$R_2$
62.6	17843.9	5	1,0			$SR_{21}$
5599.2	17854.7	5				
87.0	17893.7	7	1,0	$QP_{22}$	$Q_3$	$QR_{31}$
83.0	17906.6	5	1,0	$QP_{21}$	$RQ_{21}$	$R_1$
77.8	17923.3	6	1,0		$SQ_{31}$	$SR_{32}$
75.4	17931.0	5	2,1			$TR_{31}$
72.3	17941.0	4	1,0			$TR_{31}$
69.1	17951.3	4				
65.2	17963.8	5	2,1	$QP_{43}$	$Q_4$	$QR_{45}$
63.3	17970.0	4	1,0	$QP_{42}$	$Q_4$	$QR_{46}$
58.7	17984.8	5	1,0	$RP_{42}$	$RQ_{43}$	$R_4$
53.8	18000.7	4	1,0	$SP_{41}$	$SQ_{42}$	$SR_{43}$
50.0	18013.0	3	1,0		$TQ_{41}$	$TR_{42}$
45.5	18027.6	8	2,1	$QP_{54}$	$Q_5$	
42.6	18037.1	5	1,0	$QP_{54}$	$Q_5$	
37.4	18054.0	6	1,0	$RP_{52}$	$RQ_{51}$	$R_5$
32.4	18070.3	3	1,0	$SP_{52}$	$TQ_{53}$	$SR_{54}$
25.1	18094.2	5	1,0	$TP_{51}$	$TQ_{52}$	$TR_{53}$
09.9	18144.1	5	2,0		$Q_1$	$QR_{12}$
05.0	18160.3	4	2,0			$R_1$
00.8	18174.1	4				
5487.8	18217.2	4	2,0	$QP_{21}$	$Q_2$	$QR_{21}$
80.1	18242.8	3	2,0		$RQ_{32}$	$R_2$
73.2	18265.8	3	2,0			$SR_{21}$
62.3	18322.2	5	2,0	$RP_{21}$	$RQ_{25}$	$R_3$
52.2	18336.2	5	2,0		$SQ_{21}$	$SR_{32}$
46.8	18354.3	4	2,0			$TR_{31}$
41.1	18373.5	3	3,1	$QP_{43}$	$Q_4$	$QR_{45}$
37.4	18386.0	4	2,0	$QP_{43}$	$Q_4$	$QR_{45}$
34.4	18396.2	4	2,0	$RP_{42}$	$RQ_{42}$	$R_4$
29.5	18412.8	4	2,0	$SP_{41}$	$SQ_{42}$	$SR_{43}$
27.3	18420.3	4	3,1		$TQ_{31}$	$TR_{42}$
24.4	18430.1	4	2,0		$TQ_{41}$	$TR_{42}$
17.6	18453.2	4	2,0	$QP_{51}$	$Q_5$	
10.1	18478.8	4	2,0	$SP_{52}$	$SQ_{22}$	$SR_{54}$
05.3	18495.2	4	2,0	$TP_{51}$	$TQ_{21}$	$TR_{53}$
00.3	18512.4	4				
5397.1	18523.3	4				
94.1	18533.6	4				
91.3	18433.8	4	3,0		$Q_1$	$QR_{13}$

TABLE II

$v^I, v^{II}$	$Q_5$	$Q_4$	$Q_3$	$Q_2$	$Q_1$
$0,0$	17538.8 81.0 70.1	17555.9 71.8 76.1	17484.1 73.1 73.7	17411.0 83.0 81.6	17328.0
$0,1$	17222.4 416.4	17113.2 412.7	17067.1 417.0	16903.4 417.6	16911.8 416.2
$1,0$	18037.1	17970.0	17803.7	17822.3	17742.9
$0,0$	17638.8 398.3	17555.9 414.1	17484.1 409.6	17411.0 411.3	17328.0 414.9

TABLE III

$\Delta K$	${}^5\Pi_{-1}$	${}^5\Pi_0$	${}^5\Pi_1$	${}^5\Pi_2$	${}^5\Pi_3$
$T$	68.9	68.7			
	15.5	10.8	24.6		
$S$	73.2	73.5	73.7		
$R$	15.5	18.7	16.4	19.7	
	75.4	72.2	77.0	81.5	
$Q$	12.4	16.2	20.1	16.8	16.9
	79.2	75.9	73.7	81.6	

The mean values of the vibrational constants are  $\omega_e' = 412.3$  and  $\omega_e'' = 416.0$ . The coupling constant as calculated from the  $Q$  heads has a value ranging from 67 to 83  $\text{cm}^{-1}$ . As the breadth of the multiplet which is about 310  $\text{cm}^{-1}$  is just smaller than the gross structure given by the vibrational intervals the different sequences do not overlap.

Table III gives the scheme of the intervals in the  $(0,1)$  group  $(\text{cm})^{-1}$

In order to bring out the rotational structure obtained in each sequence clearly, a reproduction with all the band heads marked in the  $\Delta v = 0, \pm 1$  sequences showing the rotational transition and the vibrational assignment of each band is shown in Plate VI

The rotational structure as depicted in Tables I, II and III is in complete accord with the predicted structure of  ${}^5\Pi - {}^5\Sigma$  transition.

#### ACKNOWLEDGMENT

The author wishes to express his indebtedness to Prof. K. R. Rao for his kind guidance and interest in the work. He is grateful to the Government of India, Ministry of Scientific Research for the award of a Senior Research Scholarship.

## REFERENCES

- Bacher, J., 1948, *Helv. Phys. Acta.*, **21**, 379.  
 Jevons, W., 1932, *Report on Band Spectra*.  
 Mesnage, P., 1935, *C. R. Acad. Sci., Paris.*, **201**, 389.  
 Mesnage, P., 1938, Thesis for doctorate, Paris.  
 Miescher, R., 1938, *Helv. Phys. Acta.*, **11**, 463.  
 More, K. R., 1938 *Phys. Rev.*, **54**, 122.  
 Muller, W., 1943, *Helv. Phys. Acta.*, **16**, 1.  
 Nevin, T. E., 1942, *Proc. Roy. Irish. Acad.*, **48**, 1.  
 Nevin, T. E., 1945, *Proc. Roy. Irish. Acad.*, **50**, 123.  
 Rao, P. T., 1949, *Ind. J. Phys.*, **23**, 517.  
 Rao, V. R. and Rao, K. R., 1949, *Ind. J. Phys.*, **23**, 508.  
 Rao, V. R., 1949, *Ind. J. Phys.*, **23**, 535.

## ON THE NEW THEORY OF ALPHA-DECAY\*

BY M. L. CHAUDHURY

PHYSICAL LABORATORY, PRESIDENCY COLLEGE, CALCUTTA

*(Received for publication, March 5, 1951; received after revision, July 21, 1951)*

**ABSTRACT** A detailed discussion of the implications of the recent theory of alpha-decay by Kar and Chaudhury is made on the following points.

1. A theoretical formula for the nuclear radius, *independent of  $\lambda$* , has been obtained. The values of nuclear radii calculated from this formula are discussed and compared with those assumed in the old theories of alpha-decay.

2. It is shown from the new theory that the spacing of the nuclear energy levels in the radioactive region is of the order of only several volts, instead of about  $10^5$  ev. as obtained from the previous theory of alpha-decay. The new values of level spacing is in agreement with those expected from the trend of the spacing observed in the experiments of resonance capture of neutrons by elements of atomic weight upto about 200.

3. The nature of variation of the ratio of anomalous scattering to normal scattering indicates the existence of the extra-nuclear potential of Yukawa type introduced in the new theory.

4. The experiments of Chang on the alpha ray spectra of  $\text{Po}^{210}$  and  $\text{Ra}^{226}$  which are reported to be "in serious disagreement" with the alpha-decay theory of Gamow and of others, have been discussed in the light of the new theory. The effect of the extra-nuclear field introduced has been useful in explaining the above disagreement in a qualitative way.

## INTRODUCTION

Recently, a theory of alpha-decay has been developed by Kar and the present author (Kar and Chaudhury, 1950) from a new standpoint. In the present paper it is intended to study some of the consequences of the theory.

The necessity of another theoretical attempt in this line arises from the discrepancy of the observations on the alpha ray spectra of  $\text{Po}^{210}$  and  $\text{Ra}^{226}$  by Chang (1946) with the alpha-decay theories of Gamow (1928) and of later authors. It is reported that the observed values of intensities of these low energy alpha groups of Po and Ra are larger than the theoretical values by a factor of the order of  $10^4$ . Several attempts, made to resolve this discrepancy between the theory and the experiment, have not been fruitful. The later form of Gamow's theory (1949) which takes into account of the azimuthal quantum number  $j$ , is shown by Chang to give unusually large values of spin changes for his data between the parent and the product nuclei. Similarly, Preston (1949) has found that the suggestion of non-central electric interaction between the alpha particle and the product nucleus is not of much use

\* Communicated by Prof. K. C. Kar, D. Sc.



in explaining the above disagreement. From the present discussion it will appear that the Gamow formula for  $\lambda$ , which is not satisfactory for many other elements as pointed out by Perlman and others (1950), requires to be modified in the exponential term which is the important part of the formula.

# SECTION I

It is wellknown that the previous theories of alpha decay are based on two principal hypotheses: (1) firstly, that the field outside the nucleus is purely Coulombian, (2) secondly, that the potential barrier around the nucleus is penetrable, i.e., the alpha particles can leak through the potential barrier by some unknown mechanism.

Now, regarding the first hypothesis it can be said that there is no reason why a nucleon, when well within the nucleus, would have a short range field all around it, while when at the surface would have such field not on all its sides but only in an arbitrary (hemi spherical) region cut off by the boundary of the nucleus. It is more reasonable to assume that when alpha disintegration has just occurred and the distance of separation between the nucleons in the outgoing alpha particle and those on the surface of the product nucleus is still small, being within the range, a field of Yukawa type would interact between them. It appears that this field will be more complicated than the simple neutron-proton or proton-proton field, because none of the interacting nucleons in the former case are completely free. From the above considerations it is assumed in the new theory that the resultant field outside the nucleus (beyond the nuclear radius,  $r_0$ ) is not purely Coulombian, but is the usual Coulomb field superposed by the extra nuclear field of Yukawa type,  $U(r)$ . Therefore the resultant potential barrier around a nucleus is  $\{2Z^*e^2/r_0 - U(r_0)\}$ , instead of  $2Z^*e^2/r_0$ , where  $Z^*$  is the charge number of the product nucleus. In support of the old model of field distribution, one might say that such Yukawa type field,  $U(r)$ , outside the nucleus will be small and negligible. This objection, however, is not supported from the magnitude of neutron-proton or proton-proton field obtained from the theory of scattering or from average binding energy per nucleon in a nucleus which gives a value of the order of several ( $\sim 8$ ) Mev. This being of the same order as the Coulomb field outside the heavy nucleus, the above hypothesis of extra-nuclear field,  $U(r)$ , seems to be not only plausible but necessary.

Now, regarding the second hypothesis of transparency of potential barrier, it may be said that from the classical point of view, this hypothesis is vague, as it requires the assumption of *negative* kinetic energy for the alpha particle going through the hypothetical tunnel in the barrier, or in other words, the penetration hypothesis requires that a *small* centrifugal force, corresponding to the energy of emission,  $E_\alpha$ , *overcomes a larger* centripetal binding represented by the peak of the barrier. That wave mechanics which

gives a solution for the wave equation with assumed negative kinetic energy for alpha particles, does not seem to be decisive, because wave mechanics would also give a solution for positive kinetic energy of the alpha particle if so assumed to retain the classical picture. On the other hand, in the classical picture of surmounting of the barrier, as used in the new theory, the positive kinetic energy of the alpha particle at every point of the field requires the range of the field  $U(r)$  to be of the order of  $10^{-12}$  cm. This is larger than the range of the nuclear field, as obtained from the theory of scattering. One may, however, distinguish between the emission range and the scattering range of the inter-nucleonic field  $U(r)$  in view of the other favourable results discussed below. It is also a matter for further study whether the results of the new theory in agreement with various facts as discussed in section II (i. e., regarding nuclear radius  $r_0$ , the spacing of the nuclear energy levels and the possibility of accommodating the observed variations from Gamow formula for  $\lambda_1$ ) can also be obtained by assuming the small range ( $\sim 2 \times 10^{-13}$  cm.) for the extra-nuclear field  $U(r)$  together with the consequent transparency of potential barrier.

From what has been stated above, the  $q$ -space for the alpha particle is divided into three regions and the regional distribution of the fields assumed in the new theory is given in figure 1 (P. 194).

*Region 1.*  $0 < r < r_0$ , i. e. the interior of the nucleus.

If  $M$  = mass of the alpha particle,  $E_1$  = total energy of the alpha particle in region 1, for spherically symmetrical emission of alpha particles,  $l=0$ , and the radial component  $R_1$  of the wave function satisfies

$$R_1 = R_1'/r; \quad d^2 R_1'/dr^2 + 8\pi^2 M E_1 (1 + b^2 h^2 / 16\pi^2 E_1^2) R_1'/h^2 = 0 \quad \dots (1)$$

where  $b$  is the damping coefficient (Kar, 1940) that causes disintegration.

*Region 2.*  $r_0 < r < r_1$ , i. e., the extent of the extra-nuclear field  $U(r)$ . We have taken mean potential  $U_0$  for simplicity in the wave equation, constant from  $r_0$  to  $r_1$ . Now corresponding to (1) since  $b$ , the cause of disintegration is zero outside the nucleus,

$$R_2 = R_2'/r; \quad d^2 R_2'/dr^2 + 8\pi^2 M (E_2 + U_0 - V(r)) R_2'/h^2 = 0 \quad \dots (2)$$

where  $E_2$  = total alpha-energy in region 2, and  $V(r) = 2Z^*e^2/r$ .

*Region 3.*  $r_1 < r < \infty$ , i. e., outside the influence of  $U(r)$ . In this region  $U_0 = 0$ , and corresponding to (2) we have

$$R_3 = R_3'/r; \quad d^2 R_3'/dr^2 + 8\pi^2 M (E_3 - V(r)) R_3'/h^2 = 0 \quad \dots (3)$$

$E_3$  = total alpha-energy in region 3, where  $E_1 = E_2 = E_3$ . Now since the minimum energy with which the alpha particle can leave the nucleus is equal to the peak value of the resultant potential barrier,  $\{2Z^*e^2/r_0 - U(r_0)\}$  the energy relation at  $r_0$  in region 2 in the general form is (if  $Z^* = Z - 2$ ),

$$(E_{Kin})_{r=r_0} = E_2 + [U(r_0)]_c - 2Z^*e^2/r_0 = \xi \quad \dots (4)$$

Subtracting from (4) the corresponding equation for  $(E_2)_{min}$  we get

$$E_2 = (E_2)_{min} + \xi + \beta \quad \dots (4.1)$$

where

$$\beta = [U(r_0)]_{\xi=0} - [U(r_0)]_{\xi} \quad \dots (4.2)$$

It has been shown that  $\beta$  is positive and hence from (4.2) the interaction potential  $U(r)$  decreases as the initial kinetic energy,  $\xi$ , increases. Now since  $U(r)$  is of Yukawa type, the mean value  $U_0$  must be less than the straight average  $U(r_0)/2$  (as  $U(r_1) = 0$ ).

Hence

$$[U_0]_{\xi} = [U(r_0)]_{\xi}/2s \quad \dots (5)$$

where

$$s > 1. \quad \dots (5.1)$$

Now using the proper solutions for regions 2 and 3 and using the boundary conditions at the second boundary  $r_1$ , we get the continuity equation from which a formula for nuclear radius,  $r_0$ , follows as

$$r_0 = (E_2)_{max} \times \left\{ (s+2)Z^*e^2 \tan \theta_0 - s\hbar v_{max} (1 - 3\eta_{max}/(E_2)_{max}) \right\} - L \quad \dots (6)$$

where

$$L = 2Z^*e^2 \tan \theta_0 \{ s\eta_{max} + (2s)/2(E_2)_{max} - (E_2)_{min} \} \quad \dots (6.1)$$

$$\tan \theta_0 = \tan \pi \left\{ \frac{Z^* \times 0.1303 (\sinh 2u_1 - 2u_1)}{v_{max} \times 10^{-19} \sqrt{5/4 - \eta_{max}/2(E_2)_{max}}} + 0.5 \right\} \quad \dots (6.2)$$

and  $\eta = (E_{kin})_r$ .

It has also been found that (Kar and Chaudhury, 1950)

$$\beta_{max} = \frac{s}{2} \{ (E_2)_{max} - (E_2)_{min} \} + \frac{\hbar s}{2Z^*e^2} \left\{ \frac{v_{max}(E_2)_{max}}{\tan \theta_0} - \frac{v_{min}(E_2)_{min}}{\tan \theta_{max}} \right\} \quad \dots (7)$$

$$\xi_{max} = \frac{2-s}{2} \{ (E_2)_{max} - (E_2)_{min} \} - \frac{\hbar s}{2Z^*e^2} \left\{ \frac{v_{max}(E_2)_{max}}{\tan \theta_0} - \frac{v_{min}(E_2)_{min}}{\tan \theta_{max}} \right\} \quad \dots (8)$$

and

$$\eta_{max} \approx \frac{1}{6}(E_2)_{max} + \frac{5}{6}\{ (E_2)_{max} - (E_2)_{min} \} \quad \dots (9)$$

Hence we can calculate  $r_0$  from (6) (*vide* Table I). For the disintegration constant  $\lambda$ , the new formula obtained is

$$\lambda = C \frac{\sqrt{2\delta - k_2 \{ 2 - \frac{n'}{2} \cdot (3 - 1/\sqrt{n'})^2 \}^{\frac{1}{2}}}}{\sqrt{(1 + \delta^2 \hbar^2 / M^2 v'^2 r_0^2)}} \cdot \frac{v'}{r_0} \cot u_0 \cdot e^{-2K_2(2u_0 - \sin 2u_0)} \quad \dots (10)$$

where  $C$  is a constant and

$$K_2 = 4\pi Z^*e^2 \sqrt{M}/h \sqrt{2(E_2 + U_0)} \quad \dots (10.1)$$

$$\cos u_0 = \sqrt{(E_2 + U_0)/(2Z^*e^2/r_0)} \quad \dots (10.2)$$

we shall now discuss the results formulated in the above equations.

## SECTION II

### (1) Nuclear radius :

The formula (6) for nuclear radius is independent of  $\lambda$ . Table I shows the calculated values of  $r_0$  of different alpha active nuclei.

TABLE I

Disintegrating nuclei Th-series	New nuclear radii $r_0 \times 10^{-12}$ cm. (Kar-Chaudhury)	Old nuclear radii (Bethe) $r_0 \times 10^{-12}$ cm.	Disintegrating nuclei U-series	New nuclear radii $r_0 \times 10^{-12}$ cm. (Kar-Chaudhury)	Old nuclear radii (Bethe) $r_0 \times 10^{-12}$ cm.	Disintegrating nuclei Ac-series	New nuclear radii $r_0 \times 10^{-12}$ cm. (Kar-Chaudhury)	Old nuclear radii (Bethe) $r_0 \times 10^{-12}$ cm.
$^{232}\text{Th}$	3.34	1.13	$^{238}\text{U}$	3.01	1.32	$^{235}\text{Ac-U}$	3.25	—
$^{228}\text{Th}$	2.78	1.23	$^{234}\text{U}$	3.14	1.30	$^{231}\text{Pa}$	3.01	1.16
$^{224}\text{Th}$	2.61	1.25	$^{230}\text{U}$	3.08	1.31	$^{227}\text{RdAc}$	2.26	1.14
$^{220}\text{Th}$	2.33	1.23	$^{226}\text{Ra}$	3.76	1.25	$^{223}\text{Ac}$	2.62	1.21
$^{216}\text{Th}$	2.15	1.27	$^{222}\text{Rn}$	2.64	1.26	$^{219}\text{Ac}$	2.22	1.20
$^{212}\text{Th}$	2.39	1.06	$^{218}\text{Ra}$	2.30	1.25	$^{216}\text{Ac}$	2.01	1.28
$^{212}\text{Th}$	1.45	1.30	$^{214}\text{Ra}$	2.56	1.09	$^{211}\text{Ac}$	2.21	1.06
			$^{214}\text{Ra}$	2.11	1.39	$^{211}\text{Ac}$	1.99	1.39
			$^{210}\text{Ra}$	2.95	1.15			

The values of  $r_0$  given by Bethe (1937) are also included for comparison in separate columns. It may be mentioned that the nuclear radius,  $r_0$ , involved in the formula for  $\lambda$  has hitherto been an unknown parameter. Because there is no direct method to find  $r_0$  experimentally. The semi-empirical  $A^{1/3}$  relation for  $r_0$  from the fast neutron capture experiments of Sherr (1945) is

$$r_0 = 1.22 \times A^{1/3} \times 10^{-13} \text{ cm.}$$

The values of  $r_0$  obtained from this formula are found to be too low to give any reasonable agreement of the theoretical formula for  $\lambda$  with experimental values. Hence it is suggested by Gamow that probably the nuclear radius  $r_0$  in the radioactive region is larger than those given by the above  $A^{1/3}$  relation due to formation of some new shells and also due to excitation. This seems to be plausible. Accordingly the previous authors assumed such values of  $r_0$  as would lead to a reasonable agreement of the theory with experiment, although with many deviations recently noted and no unique adjustment of  $r_0$  has been possible. It is an advantage of the present theory that  $r_0$  is

obtained independent of  $\lambda$  and the values are given in terms of charge number  $Z$ , electronic charge  $e$ ,  $(E_2)_{\max}$  and Planck's constant  $h$ , all of which being constant,  $r_0$  is fixed for an element.

The values of  $r_0$  given by Bethe are higher than those of Gamow and less than those obtained from Eq. (6). Neglecting the irregular elements, it can be seen from the Table I that for two of the three series the values of  $r_0$  by Bethe, in general, decreases with increasing atomic weight, while, the values of  $r_0$  from the new theory in general increases with increasing atomic weight as expected. As already mentioned, the  $r_0$  values from the previous alpha-decay theories depend on  $\lambda$  and  $E_\alpha$  (observed alpha-energy) being involved in the  $\lambda$  vs.  $E_\alpha$  relation. This leads to the difficulty that very large variation of  $r_0$  would come out for the same element if all the fine structure components of it are considered. Thus for the thirteen alpha groups emitted by the element  $\text{Po}^{210}$ , the previous method gives us many  $r_0$  values, which vary from  $0.58 \times 10^{-12}$  cm. to  $1.91 \times 10^{-12}$  cm. Such wide variations of nuclear size requires that the nuclear density for a state excited by 1.6 Mev over the ground state becomes about three times smaller than that for the normal state. Similar difficulty will arise for the other elements showing alpha-ray spectra. It has been shown [Chang (*loc. cit.*)] that attempts to remove this difficulty by distinguishing between the true radius  $r_0$  and the effective radius  $r_{\text{eff}}$  by a relation given by Gamow (1949) would lead to unusually large values of change of spin between the  $\text{Po}^{210}$ ,  $\text{Ra}^{226}$  nuclei and their products. On the other hand, the formula (6) gives unique value of  $r_0$  for the same element, as it comes out in terms of constant quantities.

Besides, the formula for the radius of cross-section as empirically given by Graham and Seaborg (1933) and Sheri (1945) from their measurements of the reduction in the intensity of fast neutron-beams observed in the direction of incidence on the target elements (assuming the cross-section of scattering to be equal to that for absorption) is

$$d_0 = [1.7 + 1.22\sqrt{A}] \times 10^{-13} \text{ cm.} \quad \dots (11)$$

The first part of (11) is constant, while the second part is dependent on the atomic weight  $A$  and represents the  $A^{1/2}$  -relation for the sizes of the nuclei. According to some authors, the first part represents the contribution of nuclear force. But if the nuclear force be not operative on an incident neutron unless it is within the actual nuclear volume ( $\pi r_0^2$  = cross section) it is difficult to think of any extra contribution to the total cross section by the internal nuclear forces. On the other hand, this additive contribution to the total cross section suggests the existence of the extra-nuclear attraction field  $U(r)$  assumed in the new theory of alpha-decay. The value of the range,  $1.7 \times 10^{-13}$  cm. given in Eq. (11) is sufficiently close to and less than (as expected) the value of  $(r_c - r_0)$  i.e.  $1.76 \times 10^{-13}$  cm. where  $r_c (= 3.2 \times 10^{-12}$  cm.), is the distance of critical approach of bombarding alpha particles to the centre of  $U_1$  nucleus (Rutherford, 1927) and  $r_0$  for  $U_1$  nucleus is

given in Table I from Eq. (6). (Cf. sub-section on the spacing of energy levels in radioactive nuclei).

(2) *Spacing of energy levels in radioactive nuclei :*

We shall now consider the average separation between the energy levels for the alpha particles in the radioactive nuclei from the new theory. It need be mentioned that we are here principally concerned in the spacing between the particle-states in the nuclei and not in the isomeric states of a nucleus as a whole, in which the product nucleus is left by different alpha-transformations.

According to the previous theories of  $\alpha$ -decay after the physical model of Gamow, the spacing of alpha-levels in a nucleus is exactly the same as that between the energies of the alpha groups in the observed spectrum. In this model any difference between the internal and observed level spacing is not accountable. Therefore, from the observed energies of the different alpha-groups in the spectrum of a radioactive element, one gets the average spacing in the internal energy level system of the order of 100 Kev.

On the other hand, from Eq. (4.1) it can be easily seen that the total range in the observed spectrum, i.e.,  $[(E_2)_{max} - (E_2)_{min}]$  is contributed partly by  $\xi_{max}$  and partly by  $\beta_{max}$ , where  $\xi$  is defined as the kinetic energy of the alpha particle at  $r_0$ . Since the lowest state capable of emitting an alpha particle is assumed to be equal to the peak of the resultant potential barrier, it corresponds to  $\xi=0$ . Hence  $\xi_{max}$ , as already mentioned, actually represents the energy difference between the highest and the lowest states (capable of alpha emission) in the nucleus. Or, in other words,  $\xi_{max}$  is the *total* internal spacing of the alpha level system. Again from Eq. (4.2)  $\beta_{max}$  is the decrease in the field  $U(r)$  corresponding to the increase  $\xi_{max}$  in the minimum energy of alpha-emission. Obviously  $\beta$  will also contribute to the observed range of alpha ray spectrum. From Eqs. (7) and (8) we can find the relative contributions of  $\xi_{max}$  and  $\beta_{max}$  to the observed range, provided the value of  $s$  is known. From (5.1) and (8) we have  $1 < s < 2$ . In the previous paper it was guessed that  $s$  is close to 2 as suggested from calculation of the numerical value of  $r_0$  for  $U_1$  nucleus which cannot exceed  $3.2 \times 10^{-12}$  cm, being the closest distance of approach of alpha particles to  $U_1$ -target in the classical experiments of Rutherford (1927). Now it will be shown that  $s$  should not differ from 2 by more than  $3 \times 10^{-3}$ . From Rutherford's experiment (1927) on alpha ray scattering in  $U_1$ -target pure Coulomb field is found to exist upto the critical distance  $r_c = 3.2 \times 10^{-12}$  cm. from the centre of the  $U_1$  nucleus. Now to fit this in the new conception of the extra-nuclear field the radius  $r_0$  of the  $U_1$  nucleus must be less than  $3.2 \times 10^{-12}$  cm., by at least the scattering range of the field  $U(r)$ . Therefore  $r_c - r_0$  is greater than or at least equal to the range of the nuclear field. Now from theoretical considerations of neutron-proton scattering, the range of nuclear field is  $0.173 \times 10^{-12}$  cm. as given by Rarita and Present (1937) and is considered to be more accurate than the older values of Feenberg and Share

(1936) or Bethe and Bacher (1936). So if we take this range for the scattering range of the field  $U(r)$ , we require that for  $U_1$  nucleus  $(r_c - r_0) \geq 0.173 \times 10^{-12}$  cm.

Now calculation with Eq. (6) shows that, if

$$(2-s) > 3 \times 10^{-3}$$

$$(r_c - r_0) < 0.173 \times 10^{-12} \text{ cm.},$$

which is impossible, because beyond  $r_c$  there is no perturbation other than the Coulombian. Hence

$$(2-s) \leq 3 \times 10^{-3} \quad \dots (13)$$

Therefore by taking  $3 \times 10^{-3}$  for  $(2-s)$  in (8) and remembering that the number of alpha groups in a spectrum to be about ten, one gets the average spacing in the internal alpha level system in the alpha active region to be of the order of about 100 volts as the maximum limit.

Thus the new theory gives the average spacing of energy level system in heavy nuclei to be about thousand times less than the value of about 100 Kev. given from the previous theory of alpha-decay. We shall presently see that of these two conclusions the experimental results are in favour of the small values for the level spacing of heavy nuclei.

From the experiments of proton capture,  $\gamma$ -ray spectra, resonance levels in alpha particle disintegration and slow neutron absorptions, it has been observed that the spacing of particle states in a nucleus decreases very rapidly with increasing mass number and also with increasing excitation energy of the particle. The experiments of Chadwick and Coustable (1932), Pose (1930), Duncanson and Miller (1934) and of others in the region of light elements, and from the slow neutron capture experiments of Fermi and Amaldi (1936) and others for heavy elements, it is found that the spacing of the particle states for light nuclei ( $A < 50$ ) is of the order of a hundred thousand volts and decreases very rapidly with increasing  $A$  and becomes only a few volts for  $100 < A < 200$ . Therefore in the radioactive region ( $206 \leq A \leq 238$ ) the value of the average spacing of energy levels, according to the trend observed, is expected to be of the order of only several volts in agreement with the new theory.

### (3). Anomalous Scattering :

According to the old model of field distribution, a particle can undergo anomalous scattering only when it penetrates through the barrier (or surmounts it) and enters into the actual nuclear region where Coulomb field is neglected compared to the nuclear field. Since anomaly appears at energy of the incident particle lower than the peak of the Coulomb potential barrier and since only Coulomb field exists outside the nucleus the old model might be regarded as plausible. But it becomes difficult to explain the general features of the variation of the ratio  $R$ , of anomalous scattering to the normal scattering in case of many elements

such as Be, B, C, Al etc. bombarded by alpha particles. It is found (Rasetti, 1937) that this ratio,  $R$ , increases with the velocity of the incident particle and indicates a sudden increase for a value of  $1.7 \times 10^9$  cm./sec. for boron. This characteristic is, however, general. Since the field inside a heavy nucleus is more or less constant it is difficult to see how the ratio  $R$  can be a function of the velocity of the incident particle and also how can have a steep rise at certain energy of the projectile. On the other hand, the field distribution according to the new theory (figure 1) can provide a qualitative explanation for this. The general feature of the variation of the ratio,  $R$ ,

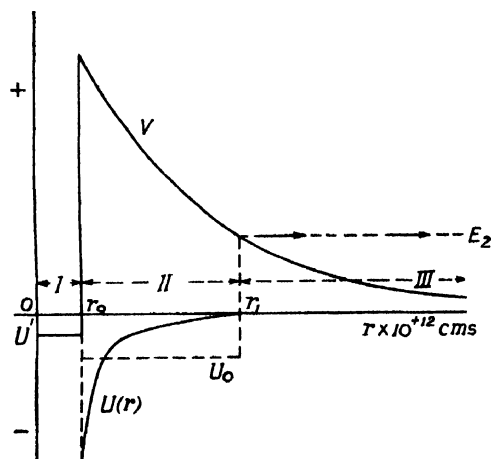


FIG. 1

→ arrow indicates  $\alpha$ -particle

$U''$  = Internal potential hole.

$r_0$  = Nuclear radius.

$U(r)$  = Yukawa-type potential outside the nucleus.

$U_0$  = Its mean constant value. I, II, III are the respective regions.

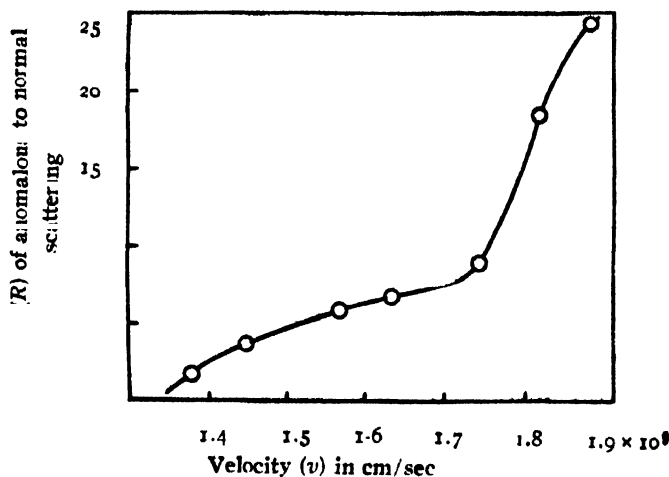


FIG. 2

Anomalous scattering of alpha particles in boron at  $160^\circ$



mentioned above, with the velocity of the incident particle is represented in figure 2 (Rasetti, 1937).

It is seen that the anomaly of scattering will start when the incident particle has entered into the range of the extra-nuclear field  $U(r)$  with energy corresponding to the point  $r_1$  (figure 1). Also since the field  $U(r)$  has a steep rise in magnitude at a point very near  $r_0$ , the ratio,  $R$ , (figure 2) will also show a steep rise for the energy of the incident particle corresponding to the point representing the steep gradient of  $U(r)$ .

(4) *Low energy alpha groups of  $Po^{210}$ -and  $Ra^{226}$ -spectra :*

We now conclude by discussing the new formula for  $\lambda$ . It is well-known that the  $\log \lambda$  vs.  $E$  curve obtained from the previous theories shows a steep positive gradient of  $\lambda$  with increasing alpha energy. Until recently, this was more or less satisfactory. Several of the spectral components were known to be well off the curve. The later modification of the theory by Gamow (1949) by assuming suitable values for the azimuthal quantum number  $l$  was able to accommodate some of these spectra while some were found to be anomalous. After the report of Chang about the low energy groups of  $RaF$  and  $Ra$  this spin theory of Gamow gave as high as 15 for the values of spin for the nuclei required to fit the theory with his observations. It may be mentioned that all the theories which lead to the same Gamow exponential term in the formula for  $\lambda$  will show more or less the same order of deviation. These formulae give  $\lambda$  as a function of  $Z$ ,  $r_0$ , and  $E_\alpha$  (observed alpha-energy). So for the same element  $RaF^{210}$  or  $Ra^{226}$ , with same  $Z$  and same  $r_0$ ,  $\lambda$  becomes unique function of the alpha energy  $E_\alpha$  and  $\lambda$  should increase monotonically with increasing  $E_\alpha$ . But from the observations of Chang (1946) we know that, say for  $RaF$ , there is no appreciable change in the  $\lambda$  value for a difference of about two Mev in the energy values between the minimum alpha energy group and the group corresponding to the next higher in excitation than the ground state transition (the group having maximum  $E_\alpha$  corresponding to the ground state transition, however, usually falling on the theoretical curve). In case of these two elements,  $RaF$  and  $Ra$ , the spectral components have nearly the same intensities (excepting the maximum energy groups) with increasing energy, and it indicates that the theoretical formula need include a compensating factor together with  $E_\alpha$ . Thus from empirical considerations  $\lambda$  depends on a fourth parameter besides the usual three variables, viz.,  $Z$ ,  $r_0$  and  $E_\alpha$  obtained previously, which adjusts the increasing effect of energy on  $\lambda$ -value. It is also suggested from the more or less constant character of the  $\log \lambda$  vs.  $E$  curve that this fourth parameter would decrease with increasing  $E$ . It is to be noted that in the new theory the potential term  $U(r)$  appears as a fourth parameter and has been introduced from physical considerations. It is worthwhile to find that the nature of variation of the field  $U(r)$  comes out as dependent indirectly on the velocity of the outgoing alpha particle through the different spins associated

with the corresponding internal energy levels which are responsible for  $\alpha$ -transformation and the subsequent emission. The dependence is of right sign. In Eq. (1.2)  $\beta$  has been shown to be positive which means that  $U(r)$  decreases with increasing alpha energy. It is not an assumption but comes out to be so from general treatment of the problem. Only thing assumed about  $U(r)$  is that it being of Yukawa type, is dependent on the spin values of the different isomeric states from which the  $\alpha$  particles are emitted. This dependence is represented by  $\beta$  whose sign was left to be inferred from the set of equations and the boundary conditions.

The new formula for  $\lambda$  may be symbolically written as (Eq. (10))

$$\lambda = \text{coeff.} \times \exp. (K_2, r_0, Z^*),$$

where

$$K_2 = f(E_2 + U_0), \text{ (vide Eq. (10.2))}$$

The formula involves  $K_2$  or  $(E_2 + U_0)$  as the variable instead of the observed alpha energy  $E_2$  ( $E_2 = E_\alpha$ ). As already discussed, if such values of  $U_0$  are obtained as would lead to a more or less constant value of  $E_2 + U_0$  for the spectral region then  $\log \lambda$  will remain nearly constant for that part of the energy spectrum as is required for the agreement with experiments of Chang.

The above discussion is qualitative and the problem has not been solved rigorously with the actual form of the extra-nuclear potential  $U(r)$ . However, the connection of the various aspects of the problem, as discussed above, with nuclear radius, nuclear energy levels, anomalous scattering etc., makes it interesting and further study will be desirable in this line.

#### ACKNOWLEDGMENT

The author wishes to acknowledge his indebtedness to Prof. K. C. Kar, D. Sc., for the keen interest he has taken during the progress of the work.

#### REFERENCES

- Bethe and Bacher, 1936, *Rev. Mod. Phys.*, **8**, 82.  
 Bethe, H., 1937, *Rev. Mod. Phys.*, **9**, 166.  
 Chadwick, J., and Constable, 1932, *Proc. Roy. Soc.*, **135**, 48.  
 Chang, W. Y., 1946, *Phys. Rev.*, **69**, 73.  
 „ „ „ *ibid.*, **70**, 632.  
 Duncanson and Miller, 1934, *Proc. Roy. Soc.*, **146**, 396.  
 Fermi and Amaldi, 1936, *Phys. Rev.*, **50**, 899.  
 Feenberg and Share, 1936, *Phys. Rev.*, **50**, 253.  
 Gamow, G., Critchfield, 1949, *Theory of atomic nucleus and nuclear energy sources*.  
 Grahame, D. C. and Seaborg, G. T., 1948, *Phys. Rev.*, **53**, 795.  
 Kar, K. C., and Chaudhury, M. L., 1950, *Ind. J. Phys.*, **24**, 545.  
 Posc, H., 1930, *Zeit. f. Phys.*, **64**, 1.  
 Preston, M. A., 1949, *Phys. Rev.*, **71**, 865.  
 Rarita, W., and Present, R. D., 1947, *Phys. Rev.*, **51**, 787.  
 Rasetti, 1937, *Elements of nuclear physics*.  
 Rutherford, E., 1927, *Phil Mag.*, **4**, 580.  
 Sherr, R., 1945, *Phys. Rev.* **64**, 240.

# ON THE DISTRIBUTION OF STRESS IN A DEEP BEAM CONTAINING TWO EQUAL CIRCULAR HOLES\*

By B. KARUNES

DEPARTMENT OF APPLIED PHYSICS, UNIVERSITY COLLEGE OF SCIENCE AND TECHNOLOGY,  
CALCUTTA.

(Received for publication, February 28, 1952)

**ABSTRACT.** The influence of two equal circular holes, placed symmetrically above and below the neutral axis of a deep plate beam on the distribution of stress in it, has been discussed. The values of the circumferential stress over the boundaries of the holes,  $\alpha=0.8$  and  $\alpha=-0.8$  are shown in a graph and discussed.

## INTRODUCTION

The solution to the problem of stress distribution in a deep plate beam containing two equal circular holes placed symmetrically above and below the neutral axis is here obtained in bipolar co-ordinates as introduced by Jeffery (1921). The corresponding problem, when the centres of the holes lie on the neutral axis, has been solved by Sengupta (1952). In this paper the notations of the co-ordinates etc. are kept the same as of Jeffery and the following equations, as given by him, are made use of.

$$h\chi = \{B_0\alpha + K \log(\cosh\alpha - \cos\beta)\}(\cosh\alpha - \cos\beta) + \sum_{n=1}^{\infty} \left\{ \phi_n(z) \cos n\beta + \psi_n(z) \sin n\beta \right\} \quad \dots \quad (1)$$

where

$$\begin{aligned} \phi_1(\alpha) &= A_1 \cosh 2\alpha + B_1 + C_1 \sinh 2\alpha \\ \psi_1(z) &= A_1' \cosh 2\alpha + C_1' \sinh 2\alpha \end{aligned} \quad \dots \quad (2)$$

and for  $n \geq 2$

$$\begin{aligned} \phi_n(\alpha) &= A_n \cosh(n+1)z + B_n \cosh(n-1)z \\ &\quad + C_n \sinh(n+1)z + D_n \sinh(n-1)z \\ \psi_n(z) &= A_n' \cosh(n+1)\alpha + B_n' \cosh(n-1)\alpha \\ &\quad + C_n' \sinh(n+1)\alpha + D_n' \sinh(n-1)\alpha \end{aligned} \quad \dots \quad (3)$$

$$a(\widehat{\alpha z} - \widehat{\beta\beta}) = (\cosh\alpha - \cos\beta) \left\{ \frac{\partial^2}{\partial \beta^2} - \frac{\partial^2}{\partial z^2} + 1 \right\} (h\chi) \quad \dots \quad (4)$$

\* Communicated by Prof. P. C. Mahanti.

## THE SOLUTION

Let  $2b$  be the depth of the beam and  $2c$  be its thickness. Using bipolar co-ordinates, let  $z=0$  i.e., the  $x$ -axis of the relevant Cartesian co-ordinates be the neutral axis and  $z=z_1$  and  $\alpha=-z_1$ , while  $z_1>0$ , be the boundaries of the two equal circular holes. If  $r$  be the radius and  $d$  be the distance of the centre of the holes from the neutral axis, we have,

$$r=a \operatorname{cosech} \alpha_1 \quad d/a = \cosh \alpha_1$$

Let  $M$  be the applied bending moment. Then at a great distance from the holes the stress function may be taken as

$$\chi_0 = Ay^3$$

where

$$A = \frac{M}{8b^3c}$$

Transforming in bipolar co-ordinates we obtain,

$$h\chi_0 = .1a^2 \frac{\sinh^3 z}{(\cosh z - \cos \beta)^2} \quad \dots \quad (5)$$

When  $z > 0$

$$h\chi_0 = .1a^2 \left\{ \cosh z + 2 \sum_{n=1}^{\infty} (n \sinh \alpha + \cosh z) e^{-n\alpha} \cos n\beta \right\} \quad \dots \quad (6)$$

and when  $z < 0$

$$h\chi_0 = .1a^2 \left\{ -\cosh z + 2 \sum_{n=1}^{\infty} (n \sinh z - \cosh \alpha) e^{-n\alpha} \cos n\beta \right\} \quad \dots \quad (7)$$

We have to add to  $h\chi_0$  another stress function  $h\chi_1$  such that  $h\chi_1$  gives no stress at infinity ( $z=0$ ,  $\beta=0$ ) and the complete stress function ( $h\chi_0 + h\chi_1$ ) gives no stress over the boundaries  $\alpha=z_1$  and  $z=-z_1$ .

Obviously the required stress function is odd in  $\alpha$  and even in  $\beta$ . Hence we may omit the terms in even functions of  $z$  and odd functions of  $\beta$  in the general solution of  $h\chi$  and choose

$$h\chi_1 = .1a^2 \left[ B_0 z (\cosh \alpha - \cos \beta) + C_1 \sinh 2\alpha \cos \beta \right. \\ \left. + \sum_{n=2}^{\infty} \left\{ C_n \sinh(n+1)z + D_n \sinh(n-1)z \right\} \cos n\beta \right] \quad \dots \quad (8)$$

It is clear that at infinity ( $z=0$ ,  $\beta=0$ )  $h\chi_1$  vanishes and  $h\chi_0$  becomes equal to the complete stress function.

Using the boundary conditions for no stress (Jeffery, 1921) over the boundaries  $z=z_1$  and  $z=-z_1$  separately, we obtain

$$B_0 = \frac{6 \cosh 2z_1}{\sinh 2\alpha_1 (\cosh 2z_1 - 1)}, \quad C_1 = \frac{3}{\sinh 2\alpha_1 (\cosh 2z_1 - 1)}$$

$$C_n = \frac{2(n-1)e^{-n\alpha_1} [n \sinh z_1 e^{(n-1)\alpha_1} + \cosh n\alpha_1]}{\sinh 2nz_1 - n \sinh 2z_1}$$

$$D_n = -\frac{2(n+1)e^{-n\alpha_1} [n \sinh \alpha_1 e^{(n+1)\alpha_1} + \cosh n\alpha_1]}{\sinh 2n\alpha_1 - n \sinh 2\alpha_1}$$

Substituting these values in (8), the stresses  $\beta\beta_1$  and  $\beta\beta_{-1}$  over the circular boundaries  $\alpha = \alpha_1$  and  $\alpha = -\alpha_1$  are calculated from the sum of the stress functions  $h\chi_1$  and the respective  $h\chi_0$  as

$$\widehat{\beta\beta}_1 = -\widehat{\beta\beta}_{-1} = Aa(\cosh\alpha_1 - \cos\beta) \times \left( \frac{6 \cosh 2\alpha_1}{\cosh \alpha_1 (\cosh 2\alpha_1 - 1)} + \frac{12 \cos\beta}{\cosh 2\alpha_1 - 1} + 8 \sum_{n=2}^{\infty} M_n \cos n\beta \right) \quad \dots (9)$$

where

$$M_n = \frac{n(n^2 - 1) \sinh \alpha_1 \cosh n\alpha_1}{\sinh 2n\alpha_1 - n \sinh 2\alpha_1} \quad (10)$$

The series in (9) converges only slowly, unless  $\alpha_1$  is large, so for convenience in numerical calculations the more slowly converging part in it is separated out by setting

$$M_n = n(n^2 - 1) \sinh \alpha_1 e^{-n\alpha_1} + N_n \quad \dots (11)$$

We can readily obtain

$$8 \sum_{n=2}^{\infty} n(n^2 - 1) \sinh \alpha_1 e^{-n\alpha_1} \cos n\beta = \frac{12 \{ (1 - \cosh \alpha_1 \cos \beta)^2 - \sinh^2 \alpha_1 \sin^2 \beta \} \sinh \alpha_1}{(\cosh \alpha_1 - \cos \beta)^4}$$

Substituting in (9) we have

$$\begin{aligned} \widehat{\beta\beta}_1 = -\widehat{\beta\beta}_{-1} = Aa \left[ \frac{12 \sinh \alpha_1}{(\cosh \alpha_1 - \cos \beta)^3} \left\{ (1 - \cosh \alpha_1 \cos \beta)^2 - \sinh^2 \alpha_1 \sin^2 \beta \right\} \right. \\ \left. + \frac{\cosh \alpha_1 - \cos \beta}{\cosh \alpha_1 (\cosh 2\alpha_1 - 1)} (6 \cosh 2\alpha_1 + 12 \cosh \alpha_1 \cos \beta) \right. \\ \left. + 8 \sum_{n=2}^{\infty} (\cosh \alpha_1 - \cos \beta) N_n \cos n\beta \right] \quad \dots (12) \end{aligned}$$

The numerical values of the coefficients  $N_n$  are given in Table I.

TABLE I

$\alpha_1$	0.6	0.8	1.0	1.2	1.4	1.6	1.8	2.0	2.2
$N_2$	1.677	0.755	0.370	0.188	0.099	0.053	0.028	0.015	0.001
$N_3$	0.021	0.274	0.082	0.020	0.008	0.002	0.001		
$N_4$	0.416	0.072	0.013	0.002	0.001				
$N_5$	0.159	0.016	0.001						
$N_6$	0.048	0.003							
$N_7$	0.015								
$N_8$	0.004								

The graphs of the stresses on the boundaries are plotted in figure 1 for a case in which the holes are fairly close to the neutral axis,  $\alpha = \pm 0.8$  for which the shortest distance between the boundaries of the holes and the neutral axis is approximately one-third of the radius of the circle. The maximum stresses are, as expected, on the points furthest from the neutral axis. But they quickly fall to zero at  $\beta = \pm 24^\circ$  and change sign there. They again change their signs at  $\beta = \pm 77^\circ$

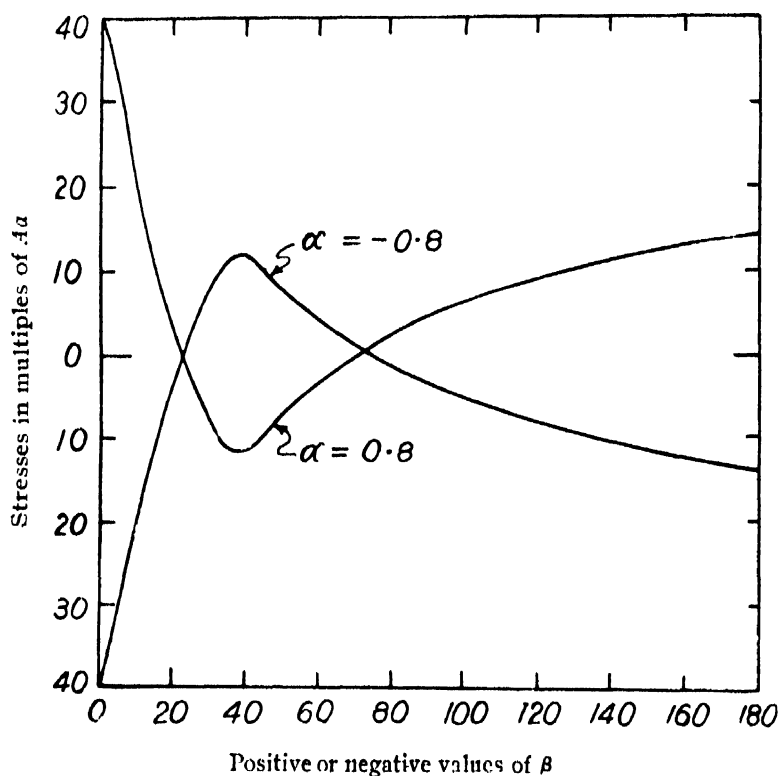


FIG. 1

## ACKNOWLEDGMENTS

The author wishes to express his respectful thanks to Dr. S. Ghose of the department of Applied Mathematics for his kind guidance during the preparation of the paper.

## REFERENCES

- Jeffery, G. B., 1921, *Phil Trans. Roy. Soc.*, A, **221**, 265.  
 Sengupta, A. M., 1952, *Proc 39th Ind. Sc. Cong.*, Part III, 11.

# ON THE ULTRAVIOLET ABSORPTION SPECTRA OF ORGANIC SUBSTANCES IN THE LIQUID AND SOLID STATES. PART III. ETHYLBENZENE AND ISOPROPYLBENZENE\*

By A. R. DIB

OPTICS DEPARTMENT, INDIAN ASSOCIATION FOR THE CULTIVATION OF SCIENCE,  
CALCUTTA.

(Received for publication March, 27, 1952)

## Plate VII

**ABSTRACT.** The absorption spectra of ethylbenzene and isopropyl benzene in the ultraviolet region ( $2440 \text{ \AA} - 2850 \text{ \AA}$ ) have been studied for the liquid and solid states at low temperatures. The results have been compared with those reported by previous authors for the vapour state and for solutions of these substances.

In the case of ethylbenzene 8 bands have been observed for the liquid state with the o-o band shifted by about  $335 \text{ cm}^{-1}$  towards longer wavelength side from its position in the vapour state. In the solid state three new bands, in addition to these, are observed in the shorter wavelength side and the whole spectrum is also shifted slightly towards the shorter wavelength side. In the case of isopropyl benzene only three broad bands have been observed in the liquid state with the o-o band considerably shifted towards the longer wavelength side. No appreciable shift of the band system towards the shorter wavelength side is observed when the liquid is solidified; but the third band extends more towards the shorter wavelength side, giving the appearance of new a band there.

These facts have been explained on the assumption that impacts of molecules in the liquid state quenches higher harmonics of vibration and that the nature of packing in the crystalline state determines the number of such modes allowed in the solid state. The shift taking place on liquefaction is attributable to formation of strongly associated groups in the liquid.

## INTRODUCTION

The study of ultraviolet absorption spectra of organic substances has gained much importance during recent years. The groups of compounds most widely studied are the mono-substituted benzene compounds (*e.g.* Spomer, and Teller, 1941; Ginsburg and Matsen, 1945; Matsen *et. al.*, 1945; Ginsburg *et. al.*, 1946) all of which give, in the region  $2400 \text{ \AA} - 2900 \text{ \AA}$ , definite

\* Communicated by Prof. S. C. Sirkar.

structures, which are composed of two subspectra (Sponer and Wollman, 1941), namely, (i) the  $A_{1g} - B_{2u}$  transition (normally forbidden in benzene) with  $e_g^+$  vibration superposed on one of the electronic levels and (ii) the transition which is made allowed by migration of electrons into the ring, thus allowing the o-o band to appear.

Most of the investigations made so far have been mainly directed towards the analysis of the bands in the vapour state. The usual procedure of study has been to compare the spectrograms of similar compounds in the vapour state and in solutions of different strengths in suitable solvents. Investigations with the substances in the pure liquid and solid states, made so far are, however, very few, probably because it is difficult to get bands with liquid films even of fairly small thickness. Such studies, however might be of great help in finding out whether the electronic energy levels in particular molecules are affected by intermolecular field in the state of aggregation and whether change of state brings about any fundamental change in the structure of absorption bands.

As mentioned earlier (Deb, 1951) in a programme of work undertaken with this end in view, the absorption spectra of a few aromatic compounds have been previously reported by the author. These results, as well as those reported by Kronenberger and Pringsheim (1926) show that the large number of bands in the vapour state are replaced by a few bands in the liquid state while in the solid state at low temperatures, some more vibration frequencies appear. Very recently, Swamy (1952) has observed such changes in the case of *o*-, *m*- and *p*-cresols and has explained the results on the hypothesis that in the liquid state transitions to harmonics of vibrational states are quenched by the constant impacts of molecules due to translatory movements and that in the case of many polar molecules, association of molecules takes place with liquefaction and consequently considerable shifts in the position of the bands take place with liquefaction.

In the present work, the absorption spectra of ethylbenzene and isopropyl benzene have been studied in the liquid and solid states and the results have been compared with those of previous authors in the vapour state and in solutions, in order to find out whether in these two cases also similar changes, as observed by Swamy (1952), take place.

#### EXPERIMENTAL

The experimental arrangement was the same as that used previously by the author (Deb, 1951). The liquids used were of chemically pure quality and were redistilled several times in vacuum before use. The thickness of the liquid film necessary to produce bands was not so small in the present case as that required in the case of anisole reported previously. For the



liquids in the present work, a film produced by placing a drop of the liquid between two quartz plates and slightly pressing them together, was of optimum thickness. The source of ultraviolet continuum was a hydrogen discharge tube run at about 3 K. V., as mentioned before.

Spectrograms were taken on Ilford H. P. 3 films with a Hilger E 1 spectrograph having a dispersion of about 3 Å. U. per mm. in the region of 2600 Å. Exposures of 8 to 10 minutes for liquids and about half an hour for solids were necessary. The width of the slit was .3 mm. For taking spectrograms at  $-180^{\circ}\text{C}$  the brass frame containing the cell with the substance was kept inside a transparent silica Dewar vessel with the lower end touching the liquid oxygen inside the Dewar vessel.

### RESULTS

The spectrograms obtained are reproduced in Plate VII, and the wave numbers of bands are given in Tables I and II. The results obtained for the vapour state and solutions by previous authors (Matsen, Robertson and Chuoke, 1947; Braude, 1949) are also included in the Tables. The frequencies at the centres of the absorption peaks have been determined from the curves reproduced by the authors and a tentative assignment of the frequencies have been made in column 3 of Tables I and II.

TABLE I  
Isopropyl benzene

Vapour (Matsen, et al, 1947)			Solution (Matsen et. al, 1947)		Pure liquid, room temp. (Present author)			Solid, $-180^{\circ}\text{C}$ (Present author)		
Band No.	$\nu\text{ cm}^{-1}$	Assign-ment.	$\nu\text{ cm}^{-1}$	Assign-ment	Band No & Int.	$\nu\text{ cm}^{-1}$	Assign-ment.	Band No. & Int.	$\nu\text{ cm}^{-1}$	Assignment.
1	37596	o-o	37472	o-o	1 w	35500	o-o	1 w	35500	o-o
2	38098	$\nu_0 + 532$			2 vst	36419	$\nu_0 + 919$	2 vst	36425	$\nu_0 + 925$
3	38553	$\nu_0 + 957$			3 st	37344	$\nu_0 + 2 \times 919$	3 st	37344	$\nu_0 + 2 \times 925$
4	38853	$\nu_0 + 1257$						4	37582	$\nu_0 + 925 + 1157$

TABLE II (Ethyl benzene)

Vapour (Matsen, et. al. 1947)			Solution (Matsen et. al, 1947)		Pure liquid-room temp. (Present author)		Solid, -180°C (Present author)	
Band No.	$\nu$ , cm <sup>-1</sup>	Assignment	Band No.	$\nu$ , cm <sup>-1</sup>	Assignment	Band No. & Int.	$\nu$ , cm <sup>-1</sup>	Assignment
1	37526	0-0	1	37193	0-0	1	37233	0-0
2	38050	$\nu_0 + 528$	2	37681	$\nu_0 + 488$	vst	37723	$\nu_0 + 490$
3	38494	$\nu_0 + 668$	3	38153	$\nu_0 + 660$	st	38167	$\nu_0 + 954$
4	38778	$\nu_0 + 1242$	vst	38420	$\nu_0 + 1204$	3	38167	$\nu_0 + 954$
5	39020	$\nu_0 + 528$ + 668	4	38650	$\nu_0 + 1260$	vst	38350	$\nu_0 + 1205$
6	39457	$\nu_0 + 2 \times 968$	5	39111	$\nu_0 + 1448$	4	38385	$\nu_0 + 1453$
7	39702	$\nu_0 + 968$	6	39404	$\nu_0 + 1465$	st	39112	$\nu_0 + 490 + 954$
8	39987	$\nu_0 + 2 \times 1242$	7	40196	$\nu_0 + 2 \times 960$	st	39413	$\nu_0 + 954$
9	40440	$\nu_0 + 3 \times 968$	8		$\nu_0 + 960$	7	39544	$\nu_0 + 1205$
10	40605	$\nu_0 + 3079$			$\nu_0 + 2 \times 1250$	8	40092	$\nu_0 + 2 \times 1205$
						9	40298	$\nu_0 + 3 \times 954$
						vw	41258	$\nu_0 + 3065$
						10		$\nu_0 + 954$
						w		+ 3065
						11		
						vw		
						(Broad)		

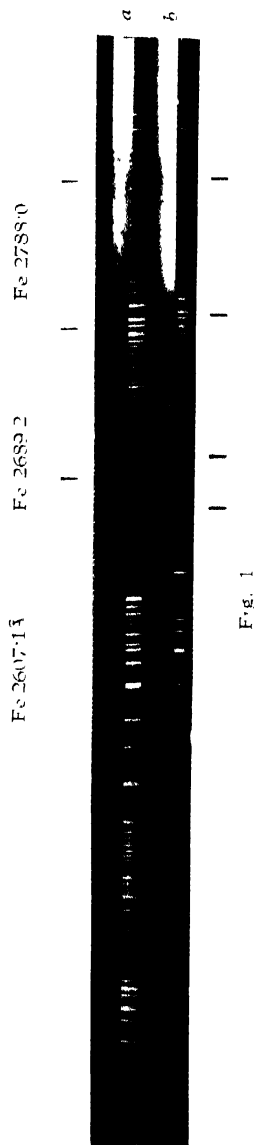


Fig. 1

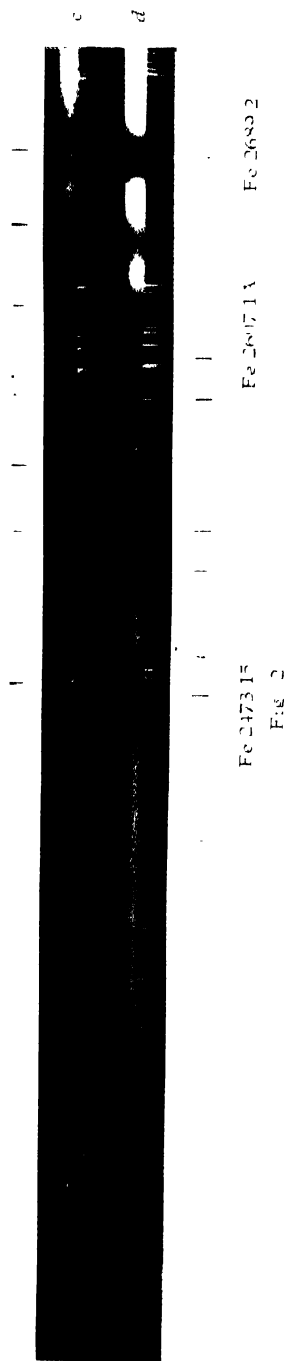


Fig. 2

### Ultraviolet absorption spectra

Fig. 1—Iso-propyl benzene

(a) Liquid at room temp., 26°C.

(b) Solid at -180°C.

Fig. 2—Ethyl benzene

(c) Liquid at room temp (26°C.)

(d) Solid at -180°C.



## DISCUSSIONS

(a) *Isopropylbenzene*. It is seen from figure 1, Plate VII, that there are only three bands of isopropylbenzene in the liquid state. The microphotometer curve reproduced by Matsen, et. al (1947), shows, however, a much greater number of bands with the o-o band at  $37596\text{ cm}^{-1}$ . In the liquid state, the second band at  $36419\text{ cm}^{-1}$ , which is the strongest of the three bands, cannot be taken as the o-o band, because, in that case the first band, which would be due to a transition from an excited vibrational state, would disappear at  $-180^{\circ}\text{C}$ . But actually, the positions and relative intensities of these three bands remain almost unchanged when the liquid is solidified at  $-180^{\circ}\text{C}$ . The first band is, therefore, taken as the o-o band. This shows a very large shift of the o-o band, by about  $1972\text{ cm}^{-1}$ , towards the longer wavelength side from its position in the vapour state. The third band, which is very broad in the liquid state with its centre at  $21919\text{ cm}^{-1}$  from the o-o band, is found to extend towards the shorter wavelength side and shows the appearance of a new band there in the solid state.

From this it is evident that the major change in the spectrum takes place on liquefaction, the subsequent change on solidification being smaller. These observations are in agreement with the results reported by Swamy (1952) in the case of the cresols, and lend support to the explanation offered by him, namely, that in the liquid state the transitions to higher harmonics of vibrational states are quenched in the state of aggregation by the constant collisions of molecules due to translational movements. It is also pointed out that the large shift of the band on liquefaction indicates a strong association of molecules in the liquid state, which lowers the electronic energy.

(b) *Ethylbenzene*. In this case, the results obtained are not exactly indetical with those observed in the previous case. Figure 2 of Plate VII, as well as Table II, show that, qualitatively the spectra of the two substances behave similarly with change of state as far as the decrease in the number of bands on liquefaction and the direction of shift of the o-o band on liquefaction are concerned.

In the previous case, practically no change of position of bands on change of state from liquid to solid was observed, but in the present case, very slight shift of the system towards shorter wavelength side has been observed. Again in the case of ethylbenzene, the shift of the  $\nu_0$  band towards longer wavelength side on liquefaction is much smaller, being  $335\text{ cm}^{-1}$ . This, on the hypothesis assumed, indicates that association of ethylbenzene molecule in the liquid state has much smaller influence on the electronic energy levels than in the case of isopropylbenzene. The number of bands (figure 2, Plate VII) is also comparatively large in the case of ethylbenzene, both for liquid and solid states. Again, in the liquid state the frequency differences of 488, 960 and  $1260\text{ cm}^{-1}$  with their first harmonics have been observed, while in the solid state, a few more bands appear on the shorter wavelength side. Probably,

the peculiarity of the shape of the group of strongly associated molecules present in isopropylbenzene in the solid state is responsible for a much closer packing than in the case of ethylbenzene.

#### ACKNOWLEDGMENT

It is a pleasure to thank Prof S. C. Sirkar, D.Sc., F.N.I. for his kind permission to work in the Laboratory of the Optics Department of the Association and for his guidance during the progress of the work.

#### REFERENCES

- Brande, E. A., 1949, *J. Chem. Soc.*, p. 1932  
 Deb, A. R., 1951, *Ind J Phys.*, **25**, 133, 133.  
 Ginsburg, N. and Matsen, F. A., 1945 *J. Chem. Phys.*, **13**, 157.  
 Ginsburg, N., Robertson, W. W. and Matsen, F. A., 1946, *J. Chem. Phys.*, **14**, 511.  
 Kronenherger, A. and Pringsheim, P., 1926, *Z. j. Phys.*, **40**, 75  
 Matsen, et. al., 1945, *J. Chem. Phys.*, **13**, 309.  
 Matsen, F. A., Robertson, W. W. and Chuoke, R. L., 1947, *Chem. Rev.*, **41**, 273.  
 Sponer, H. and Wollman, S. H., 1941, *J. Chem. Phys.*, **9**, 816.  
 Swamy, H. O., 1951, *Ind J. Phys.*, **25**, 162.  
 " " , 1952, *Ibid.*, **26**, 110.

# THE COMPLEX BAND SPECTRUM OF NICKEL CHLORIDE (NiCl)

By V. G. KRISHNAMURTY

DEPARTMENT OF PHYSICS, ANDHRA UNIVERSITY, WALTAIR

(Received for publication, January 28, 1952)

## Plates VIII A—D

**ABSTRACT.** The band spectrum of the diatomic molecule NiCl extending from  $\lambda 4900$  to  $\lambda 3800 \text{ \AA}$  has been obtained in emission using a heavy current discharge from a 2 K.W., D.C. generator. The bands are line-like and are slightly degraded to the red. The bands within many of the sequences show abnormalities in intensity and present on the whole a complex appearance. This peculiar structure is ascribed to be due to high multiplicity terms being involved in the electronic transitions and an overlapping of several band systems. The bands have been analysed into five systems designated as A, B, C, D, and E. The systems involve doublet and quartet terms.

The electronic transitions, the wavenumbers of the Q heads and the vibrational constants obtained in systems A, B, and E are given below:—

System	A	B	E
Electronic transition	$4\Pi-4\Sigma$	$4\Pi-4\Sigma$	$2\Pi-4\Sigma$
$Q_4$	$24305.7 \text{ cm}^{-1}$	$23547.1 \text{ cm}^{-1}$	
$Q_3$	$24185.6$	$23152.9$	
$Q_2$	$24064.1$	$23049.4$	$21688.2 \text{ cm}^{-2}$
$Q_1$	$23936.8$	$22946.7$	$21585.3$
$w'$	$400.9$	$398.0$	$400.1$
$w''$	$416.3$	$416.2$	$414.5$

Systems A, B and perhaps E have a common lower state.

The 0,0 sequence in system C presents double headed bands of equal intensity. The system is assigned to a  $2\Sigma-2\Sigma$  electronic transition, the band heads of which are represented by

$$\nu = 22749.2 \pm 398.9u' - 1.03u'^2 - 421.5u'' + 0.51u''^2.$$

The vibrational formula for the bands of the D system (also assigned as a  $2\Sigma-2\Sigma$  transition) is

$$\nu = 21920.5 + 404.4u' - 1.16u'^2 - 422.5u'' + 0.35u''^2.$$

Of the observed three different lower states, one  $4\Sigma$  and two  $2\Sigma$ 's the ground state of the NiCl molecule is  $4\Sigma$ .

## INTRODUCTION

Mesnage (1935 and 1938) has recorded some characteristic bands of the nickel chloride molecule in emission in a high frequency discharge with external electrodes and has suggested a provisional assignment of vibrational quantum numbers. As shown by More (1938), this quantum assignment is

untenable since a value of about  $1400\text{ cm}^{-1}$  is involved for the ground state vibrational frequency of NiCl molecule which is much too high.

More reinvestigated the spectrum and gave an analysis of most of the bands between  $\lambda_{4100}$  to  $4400\text{ \AA}$ .

An extensive study of the band systems of the halides of Fe, Co, Ni and other similar elements has been undertaken by the author to examine the evidence of high multiplicity terms in these spectra. In the case of cobalt chloride, a  ${}^3\Pi - {}^3\Sigma$  electronic transition has been established by him (1951). Results obtained in the case of NiCl are given in this paper.

#### EXPERIMENTAL

For the excitation of the bands, the method used for cobalt chloride has been employed. Different samples of anhydrous nickel chloride (B.D.H. and Merck reported to be of high degree of purity) are used in the investigation. A characteristic discharge of light blue colour is obtained at 1500 volts and 0.3 ampere. Photographs are taken on Ilford special rapid panchromatic plates with a Fuess spectrograph and Hilger  $\text{K}^2$  quartz Littrow spectrograph.

*Description of the bands.* The general appearance, as seen from the reproduction, is that of well separated close sequences extending from  $\lambda_{4900}$  to  $\lambda_{3800}\text{ \AA}$ . The bands occur in several groups. Each group gives the impression of a sequence with a particular  $\Delta v$  value. The intensity varies from group to group without evidence of any definite regularity. The intensity distribution among the bands within many of the sequences is also not regular. The bands show abnormalities in intensity and present on the whole a complex appearance. This peculiar structure is ascribed to be due to high multiplicity terms being involved in the electronic transitions and an overlapping of several band systems. The bands are slightly degraded to the red and are almost line like as in the case of MnCl and CoCl bands which are identified with  ${}^3\Pi - {}^3\Sigma$  and  ${}^5\Pi - {}^5\Sigma$  transitions respectively. In addition to the bands, several atomic lines are also excited in the source but they could be distinguished.

#### ANALYSIS

More identified four prominent groups of bands and arranged them into vibrational arrays with strong  $\Delta v = 0$  and weak  $\Delta v = \pm 1, \pm 2$  sequences. He reports the intensity distribution as conforming to narrow Condon parabolae. The following formulae were calculated representing the  $Q$  heads of the four systems analysed :—

$$v = 22747.6 + 400.2u' - 1.35u'^2 - 410.2u'' + 0.88u''^2 \quad \dots (1)$$

$$v = 23232.7 + 397.3u' - 1.18u'^2 - 417.2u'' + 0.35u''^2 \quad \dots (2)$$

$$v = 24138.5 + 401.3u' - 1.05u'^2 - 419.2u'' + 1.20u''^2 \quad \dots (3)$$

$$v = 24623.2 + 400.7u' - 1.58u'^2 - 416.6u'' + 0.55u''^2 \quad \dots (4)$$

$$\text{where } u = v + \frac{1}{2}$$



For  $\Delta v=0$  sequence, weak heads which may be *R* heads are observed by More in some cases but not recorded while for  $\Delta v=\pm 1, \pm 2$  sequences More could observe only *Q* heads. In a fifth system only one sequence consisting of double heads of about equal intensity was identified.

In addition to the above five systems, More recorded wavenumbers of other bands which were reported as single heads unrelated to the other observed bands.

An electronic interval of  $484\text{ cm}^{-1}$  occurring between More's systems 1 and 2 and also between his systems 3 and 4 led him to suggest that a common doublet term is involved in the transitions which probably is the ground state. He further suggested, on comparison of the intervals with the magnitude of multiplet splittings of the ground states of Ni I and Cl I, that the common doublet ground state may be a  $^2\text{II}$ . A  $^2\Delta$  or  $^2\phi$  was considered improbable for the ground state since the electronic interval  $484\text{ cm}^{-1}$  is a rather high value for either of these. No definite conclusions were made regarding the upper states of the four systems;  $^2\Sigma$  or  $^2\Delta$  was considered and  $^2\Delta$  was suggested as more probable although the evidence was not conclusive.

This analysis, as given by More, is represented schematically with reference to the spectrum itself in Plate VIII A which contains a reproduction of the overall band systems of nickel chloride as obtained in a heavy current discharge in the vapour.

A close examination of the analysis and a study of the head intensities within a group and in different groups have indicated what, at first sight, appeared to be inconsistencies in the analysis presented by More. In system 1, the 0, 0 sequence is no doubt the strongest. It is also the strongest in the entire spectrum. The 0, 1 sequence of the system falls off in intensity but in the region where 0, 2 sequence is expected, a very strong group of bands appears, as is evident from the reproduction, (from  $\nu=21911.2$  to  $\nu=21792.8$ ). If this strong group be taken as the 0, 2 sequence, anomalies in intensity arise making the entire system as intrinsically not genuine. Just two bands in this region are classified by More as part of the 0, 2 sequence leaving the entire group unclassified. Further, the bands in the 0, 0 sequence are distinctly double, consisting of components of nearly equal intensity—a feature which does not seem to have been noticed by More. This doublet character of each band is not distinct in the remaining sequences of More's system 1. More's observation of strong *Q* and very weak *R* heads is not noticed by us on our plates.

In More's system 2 in the region of  $\Delta v=0$  sequence, faint band heads have been observed in between the *Q* heads recorded by More. More's scheme for system 2 does not give an assignment of these. In fact these faint band heads have not been recorded by him.

More's system 3 is fragmentary.

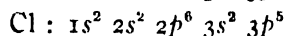
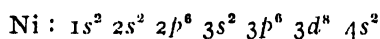
The sequence of doublets suggested by More as forming a fifth system remains unrelated to the other systems according to More's analysis.

The reproduction in Plate VIII A shows many more band heads which have not been recorded previously by More. The spectrum extends down to  $\lambda_{3800} \text{ \AA}$  while More's analysis is of bands mostly up to  $\lambda_{4000} \text{ \AA}$  only. Further in the spectra of the halides of Mn, Fe and Co, there is a definite evidence of complex electronic terms of high multiplicity giving rise to the bands and it may be expected that similar transitions do exist and account for the bands of Ni halides. The complex appearance of this spectrum reproduced in Plate VIII A justifies this assumption. Hence it is believed that a revision of More's analysis is necessary in order to assign all the band heads taking into account the intensity anomalies observed in More's scheme. This revision is attempted and described in succeeding sections.

#### ELECTRONIC STATES IN NiCl MOLECULE

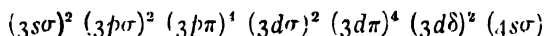
The total number of electrons in the nickel chloride molecule is odd being equal to 45; the multiplicity of the electronic term should therefore be even. The terms may be derived from the atomic configurations thus:

The electron configurations of nickel and Chlorine atoms are



giving rise to a  $^3F$  ground term in Nickel and a  $^2P$  ground term in chlorine.

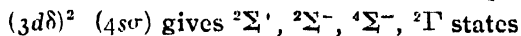
For the 17 outer electrons ( $d^8s^2$  of nickel and  $s^2p^5$  of chlorine) the following distribution among the possible molecular orbitals may be suggested as obtaining in the process of formation of the molecule:



The last 3 electrons ( $\delta^2, \sigma$ ) determine the nature and multiplicity of the electronic states.

Adopting the usual method for the derivation of the molecular states by writing down the  $m_l$  and  $m_s$  values,

(a) for the ground state of the molecule, the configuration



or  $(3d\delta) (4s\sigma)^2$  gives a  $^3\Delta$  state and

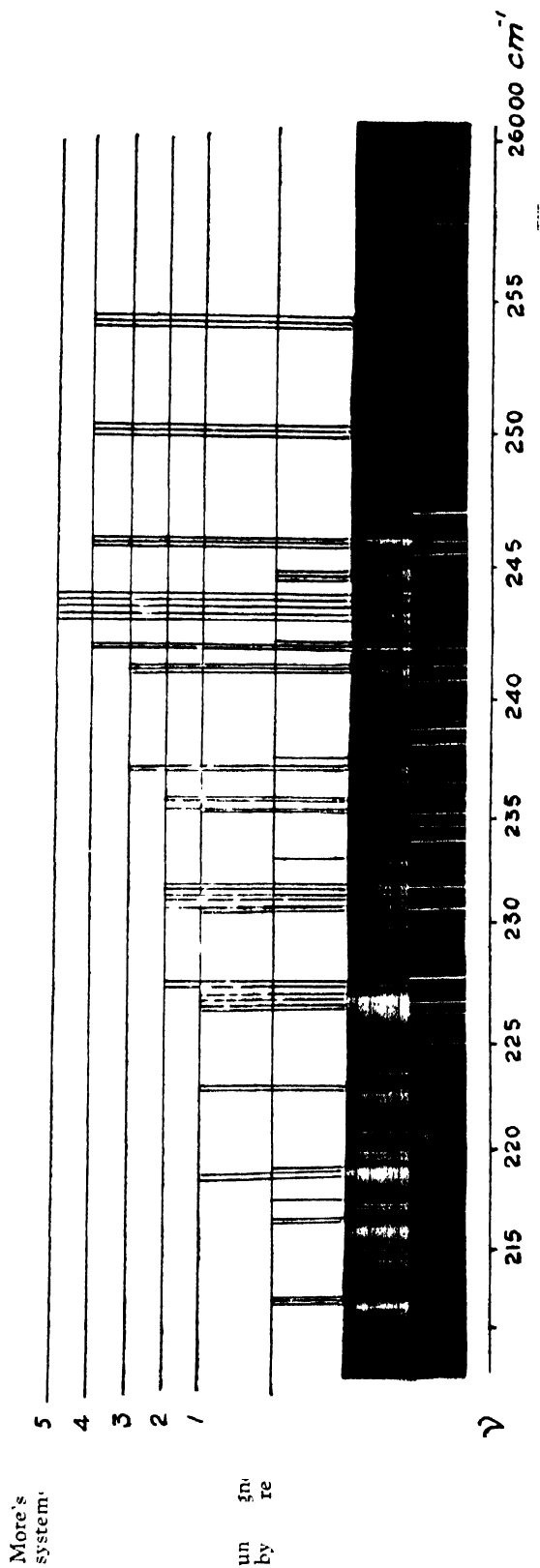
(b) for the upper state of the molecule, the different possible configurations give the respective molecular states shown below

- |     |                                    |       |  |
|-----|------------------------------------|-------|--|
| (1) | $(3d\delta)^2 (4p\sigma)$          | gives | $^2\Sigma^+, ^2\Sigma^-, ^4\Sigma^-, ^2\Gamma$ |
| (2) | $(3d\delta)^2 (4p\pi)$             |       | $^2\Pi, ^2\Pi, ^4\Pi, ^2\phi, ^2H$             |
| (3) | $(4s\sigma)^2 (4p\sigma)$          |       | $^2\Sigma^+$                                   |
| (4) | $(4s\sigma)^2 (4p\pi)$             |       | $^2\Pi$  |
| (5) | $(3d\delta) (4s\sigma) (4p\sigma)$ |       | $^2\Delta, ^2\Delta, ^4\Delta$                 |
| (6) | $(3d\delta) (4s\sigma) (4p\pi)$    |       | $^2\Pi, ^2\Pi, ^4\Pi, ^2\phi, ^2\phi, ^4\phi$  |

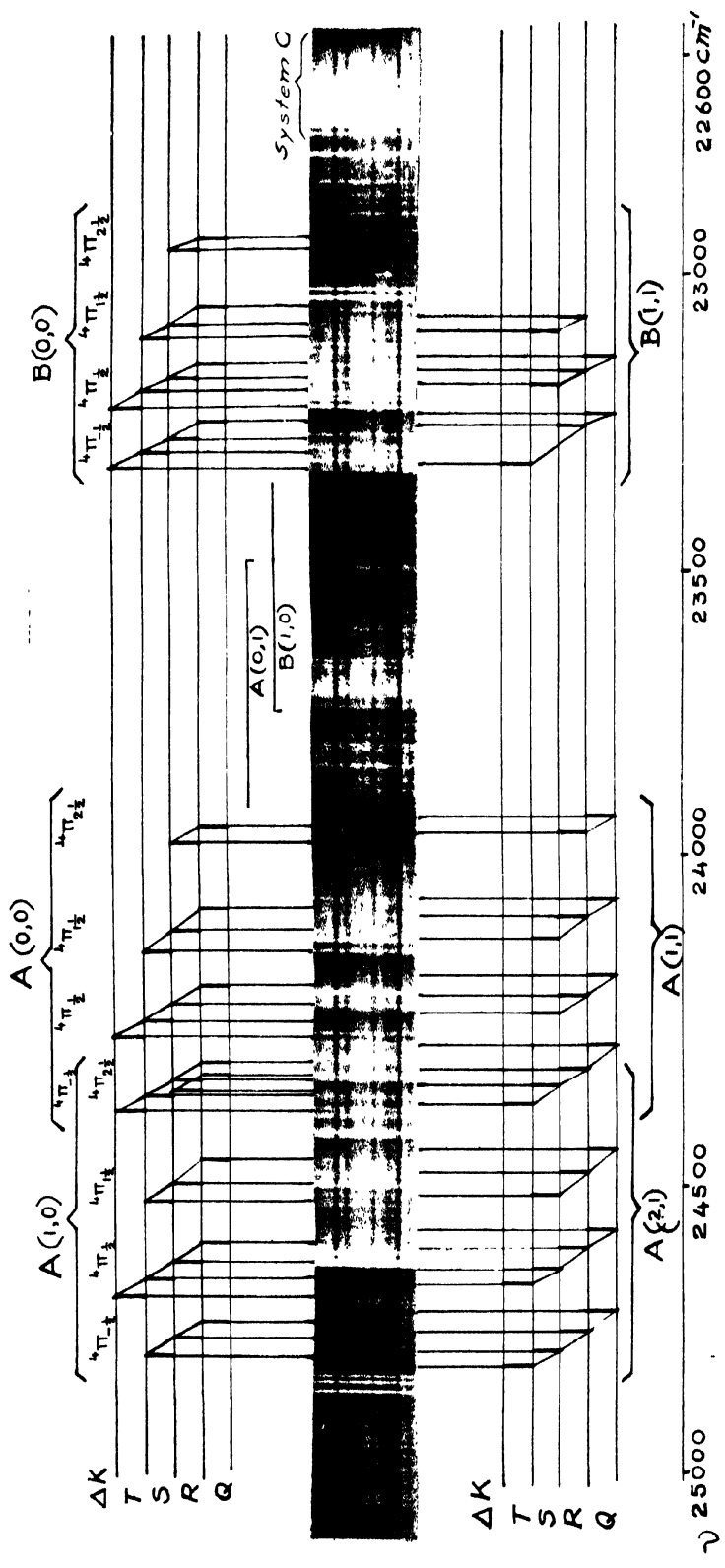
states.

The following electronic transitions may be expected among the band systems of nickel chloride molecule:—

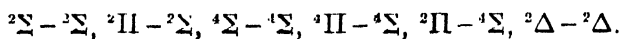
# KRISHNAMURTY



NiCl bands : More's analysis



NiCl bands : systems A and B



Examining the spectrum as a whole in the light of the above, possible electronic transitions, it seemed clear that all the bands in the region right from  $\lambda$  4900 Å to  $\lambda$  3500 Å cannot belong to a single electronic transition.

It is assumed that there is an overlapping of different systems and that some of these systems may be doublets and some, quartets, not excluding intercombination systems like  ${}^2\Pi - {}^4\Sigma$  since such intercombination systems have been established in molecules of the type  $\text{MnCl}$  and  $\text{MnBr}$ .

As a next stage in the interpretation of the spectrum, a start has been made on the assumption of quartet-quartet transitions,  ${}^4\Pi - {}^4\Sigma$  being considered more probable than  ${}^4\Sigma - {}^4\Sigma$ , as judged from the complexity of the system. The expected theoretical structure in a  ${}^4\Pi - {}^4\Sigma$  transition is calculated in the manner described for a  ${}^4\Pi - {}^2\Sigma$  transition identified by the writer in cobalt chloride.

The possible rotational heads for the transition  ${}^4\Pi - {}^4\Sigma$  can be formulated thus. The ground state  ${}^4\Sigma$  must correspond to the coupling type, Hund's case (b). In a  ${}^4\Sigma$  state ( $\Lambda=0$ ) and ( $s=1\frac{1}{2}$ ), there is a spin splitting of each rotational level, *i. e.*, for each value of  $K$ , there will be four component levels with  $J$  lying between  $K-S$  and  $K+S$ , which, following Mulliken, may be designated as  $F_4$ ,  $F_3$ ,  $F_2$  and  $F_1$  respectively. These levels have very small separations and ordinarily are not resolvable. The upper state  ${}^4\Pi$  may approximate to case (a) or case (b) or may represent any state intermediate between the two. The calculations can be made for higher values of  $K$  and reduced to the lower values. Combining  $\Lambda$  and  $\Sigma$ , we get four values giving  $\Pi_{-1}$ ,  $\Pi_1$ ,  $\Pi_{1\frac{1}{2}}$  and  $\Pi_{2\frac{1}{2}}$  which we may denote as  $F_4$ ,  $F_3$ ,  $F_2$ , and  $F_1$  respectively.

For red degraded bands ( $\omega'' > \omega'$ ), we expect only the  $T$ ,  $S$ ,  $R$  and  $Q$  forms as head forming. A schematic diagram for the transition  ${}^4\Pi - {}^4\Sigma$  representing the various observable branches (for red degraded bands) together with details of the expected rotational heads will be given in a subsequent communication dealing with the band systems of nickel bromide molecule in which also the author has succeeded in establishing the existence of an electronic transition  ${}^4\Pi - {}^4\Sigma$ . In general, this scheme is similar to that for a  ${}^5\Pi - {}^3\Sigma$  transition given in  $\text{CoCl}$  previously.

Two transitions of this type could be detected among the bands of  $\text{NiCl}$ : one in the region from  $\lambda$  3800 to  $\lambda$  4350 Å which is designated as system  $A$  and another in the region from  $\lambda$  3870 to  $\lambda$  1100 Å designated as system  $B$ , there being a certain region in which the two systems overlap. Of these, the system  $A$  is more extensively developed.

The analysis, including the wave number data and assignments of the bands ascribed to systems  $A$  and  $B$  is given in detail in Table VI at the end.

The main features of the rotational structure obtained in each sequence are shown in Plate VIII B. All the band heads, marked in the (o, o), (1, o) sequences of system  $A$  and (o, o) sequence of system  $B$ , with the respective

rotational transition and the vibrational assignment are indicated in the Plate. Similar bands, corresponding to the rotational transitions in the (1, 1) and (2, 1) sequences of system *A* and (1, 1) sequence of system *B*, are also indicated on the other side of the spectrum in the same figure.

The structure, as observed in each of the systems *A* and *B*, is found to agree very closely with the theoretical structure expected of the transition  ${}^4\Pi - {}^4\Sigma$ .

*System A.* The wavenumbers of the *Q* heads, as obtained in the (0, 1), (0, 0) and (1, 0) sequences of system *A* are given in Table I, which also shows the values of the vibrational constants as calculated from the *Q* head separations.

TABLE I

$v', v''$	$Q_4$	$Q_3$	$Q_2$	$Q_1$
0, 0	24305.7	120.1	24185.6	121.5
0, 1	23892.7	119.9	23772.8	120.3
$\omega_e''$	413.0	412.8	411.6	421.7
1, 0	24705.8	119.1	24585.7	124.6
0, 0	24305.7		24185.6	
$\omega_e'$	400.1	401.1	398.0	392.0

The mean values of the vibrational constants obtained for this electronic transition are  $\omega_e' = 400.9$  and  $\omega_e'' = 416.3$ .

Table II gives the scheme of intervals in the 0, 0 group.

TABLE II

$\Delta K$	${}^4\Pi - 1/2$	${}^4\Pi_{1/2}$	${}^4\Pi_{3/2}$	${}^4\Pi_{5/2}$
T	120.2			
	26.8	30.6		
S	114.0		118.2	
	26.7	30.0	29.7	
R	117.3		117.9	128.3
	28.4	31.2	34.8	33.8
Q	120.1		121.5	127.3

**System B.** The wavenumbers of the  $Q$  heads, as obtained in the (0,1), (0,0) and (1,0) sequences of system  $B$ , are given in Table III. The table also shows the values of the vibrational constants as calculated from the  $Q$  head separations.

TABLE III

$v', v''$	$Q_4$	$Q_3$	$Q_2$	$Q_1$
	91.2	103.5	102.7	
0,0	23247.1	23152.0	23049.4	22946.7
0,1	22833.5	22738.8	22632.4	22530.7
$\omega_e''$	413.6	414.1	417.0	416.0
	103.6	106.1	117.6	
1,0	23652.5	23548.0	23442.8	23325.2
0,0	23247.1	23152.9	23049.1	22946.7
$\omega_e'$	405.4	396.0	393.4	

The mean values of the vibrational constants obtained for this transition are  $\omega_e' = 398.0$  and  $\omega_e'' = 416.2$ .

Table IV gives the scheme of intervals in the 0,0 group

TABLE IV

$\Delta K$	${}^4\Pi_{-1/2}$	${}^4\Pi_{1/2}$	${}^4\Pi_{3/2}$	${}^4\Pi_{5/2}$
$T$		112.7		
$S$	27.2	23.3	105.0	
$R$	28.4	20.3	16.0	115.5
$Q$	31.8	24.8	27.6	14.8
	94.2	103.5	102.7	

Comparing the data of systems  $A$  and  $B$  with More's systems 2, 3, 4 and 5, it is seen that More's system 2 is comprised within system  $B$ . Systems 3 and 4 and the sequence of doublets in system 5 form part of the extensive system  $A$  designated as  ${}^4\Pi - {}^4\Sigma$ . All the wavenumber intervals established by More in building up the systems 2 to 5 proved in fact helpful in arriving at systems  $A$  and  $B$ . Most of the intervals are common in the two investigations.

The values of  $\omega_e''$  for the two systems *A* and *B* are identical, the upper state constants being different indicating a common ground state and different upper states. If the identification and assignments of these two systems prove correct, the common ground state of the molecule corresponds to the configuration  $(3d\delta)^2 (4s\sigma)$  which gives a  $^4\Sigma$ ; two other important electronic states which are both  $^2\Sigma$  also arise from this configuration and are expected to be low lying electronic levels of the molecule.

*Systems C and D.* The two systems described so far comprise of bands extending right from the extreme violet up to only  $\lambda 4400 \text{ \AA}$ . The spectrum, however, extends much further up. There are two very prominent groups in this region of longer wavelength: one at  $\nu 22738.6$  and another at  $\nu 21911.2$ . Closer scrutiny of the picture revealed these two prominent groups as very distinctive and different from each other as well as from the other groups. The first corresponds to the 0,0 sequence of More's system and the second falls in the region of the 0,2 sequence of the same system and is unclassified, as pointed out in an earlier paragraph. Several attempts have been made to analyse all the remaining bands right up to  $\lambda 4800$  either as one system or as just two systems with the two groups mentioned above as starting sequences. This was not possible; there are as many as at least ten groups of bands distinctly observable in this region from  $\nu 22738.6$  to  $20803.3$ . The intensities of these groups vary in such a manner that it was not possible to comprise all of these into one or two systems only. A clue to the interpretation is afforded by detection of a recurring frequency interval, of 422 units among some of these groups. On the basis of this frequency interval, two systems, designated here as *C* and *D*, have been isolated at first in this region. System *C* happened to be identical with system 1 of More. System *D* starts with the second prominent group mentioned above. These two systems are marked and indicated in Plate VIII D.

Details of the two systems and the band heads assigned under these are presented in Table VI at the end.

The vibrational formula obtained for the heads of system *C* is

$$\nu = 22749.2 + 398.9u' - 1.03u'^2 - 421.5u'' + 0.51u''^2$$

and that for system *D* is

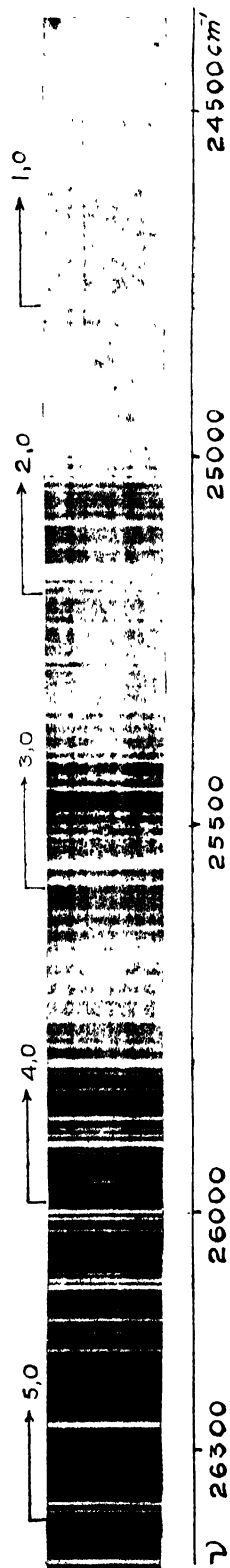
$$\nu = 21920.5 + 404.4u' - 1.16u'^2 - 422.5u'' + 0.25u''^2$$

where  $u = v + 1/2$ .

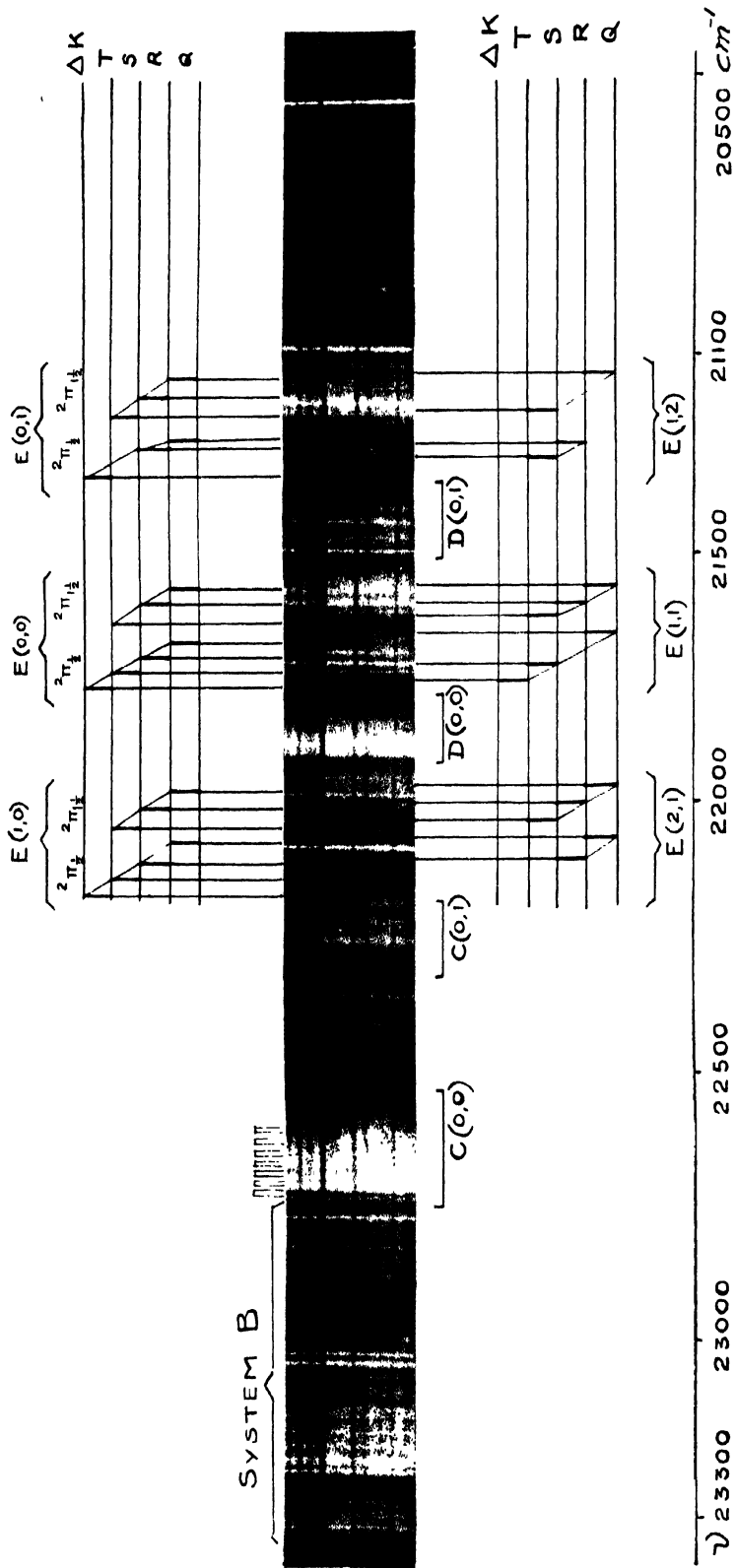
As mentioned previously, the members of the 0,0 sequence of system *C* are close doublets. In the 0,1 sequence, the doublet character is not very distinct but each member is slightly broad and has sharp edges on either side; perhaps each is a close unresolved doublet.

The electronic transitions for these systems are not definite. Since they have nearly equal lower state frequencies, one probability is to treat these as components of a  $^2\Pi - ^2\Sigma$  transition; the  $^2\Pi$  interval then is about





NiCl bands : system A



NiCl bands : systems C, D and E

827.4 units which is perhaps too large. Further the distinct doublet character of each band in the 0,0 sequence of system *C* with the two components of the doublet, equal in intensity, is suggestive of a transition  ${}^2\Sigma - {}^2\Sigma$ . System *D* may then be another  ${}^2\Sigma - {}^2\Sigma$  transition.

The molecular configuration giving rise to the two  ${}^2\Sigma$  ground states may be  $(3d\delta)^2 (4s\sigma)$ , same as that which gives the common lower  ${}^4\Sigma$  state of systems *A* and *B*.

*System E.* The interpretation of the remaining groups of bands in the region from  $\lambda 4430$  to  $\lambda 4800 \text{ \AA}$  after the elimination of those assigned to systems *C* and *D* is next considered. The classification of the systems already mentioned *i.e.*, *A*, *B*, *C* and *D* has established three low lying states. It appeared reasonable to assume that one of these states is the lower state of the system to which these unassigned bands may be expected to belong. If a  ${}^2\Sigma$  is the lower state, a transition  ${}^2\Pi - {}^2\Sigma$  may be expected; if a  ${}^4\Sigma$  is the lower state, the intercombination system  ${}^2\Pi - {}^4\Sigma$  may be expected rather than a  ${}^4\Pi - {}^4\Sigma$ , since it is difficult to derive a third  ${}^4\Pi$  upper state from the possible molecular electron configurations. Further, the region in which these unassigned bands occur is consistent with the former assignment.

In the halides of Mn, Bacher (1948) has suggested the existence of an intercombination system  ${}^3\Pi - {}^7\Sigma$  which has been established for MnCl in a communication from this laboratory to the Proceedings of the National Institute of Sciences of India (now in press).

On the above considerations, a search for the characteristic frequency difference corresponding to the states  ${}^2\Sigma$ ,  ${}^4\Sigma$  has been carried out in this region. The  ${}^2\Sigma$  intervals could not be detected. The grouping of the bands themselves is not found quite consistent with  ${}^2\Pi - {}^2\Sigma$ . Hence they are assumed to correspond to  ${}^2\Pi - {}^4\Sigma$ ; the ground state frequency 415 units corresponding to  ${}^4\Sigma$  has been observed between several bands. The detection of these and the variations in intensity among the band heads have confirmed the view regarding the assignments of the bands to the above mentioned intercombination system. The detailed structure is established in the manner adopted for quartet-quartet systems.

The predicted structure corresponding to this transition is presented schematically in figure 1 in which the various observable rotation heads (for red degraded bands) are indicated. This structure agrees very closely with the observed structure marked in the spectrogram in Plate VIII D. It shows the band heads for (0,1), (0,0) and (1,0) sequences and also the bands corresponding to (1,2) (1,1) and (2,1) sequences.

The wavenumber and intensity data of the heads together with their assignments are shown in Table VI at the end.

The values of the vibrational constants, as calculated from the *Q* head data, are shown in Table V.

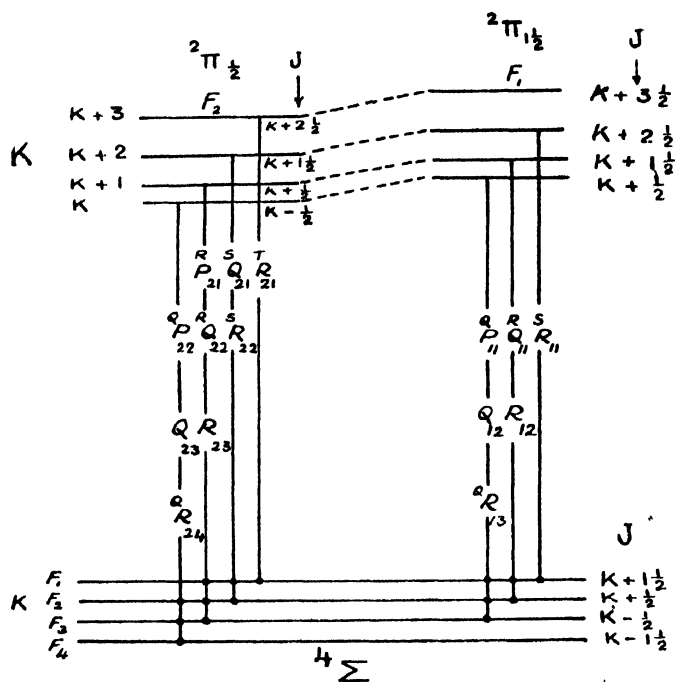


FIG. 1

Scheme of transition in a  ${}^2\Pi(u)-4\Sigma$  ( $B'' > B'$ )

TABLE V

$v', v''$	$Q_2$	$Q_1$
0, 0	21688.2	21585.3
0, 1	21272.9	21171.6
$\omega_e''$	415.3	413.7
1, 0	22086.4	21987.2
0, 0	21688.2	21585.3
$\omega_e'$	398.2	401.9

The mean values of the vibrational constants are  $\omega_e' = 400.1$  and  $\omega_e'' = 414.5$ . This lower state frequency is nearly equal to that of systems A and B for which the value of  $\omega_e'' = 416.3$ .

## ELECTRONIC TRANSITIONS

Examining the constants and other characteristics of the observed systems A, B, C, D and E and studying them in relation to the possible electron configurations and the corresponding molecular states in NiCl

molecule, the following energy level diagram (figure 2) is set up. It gives also tentatively the assignments of the levels to the possible electron

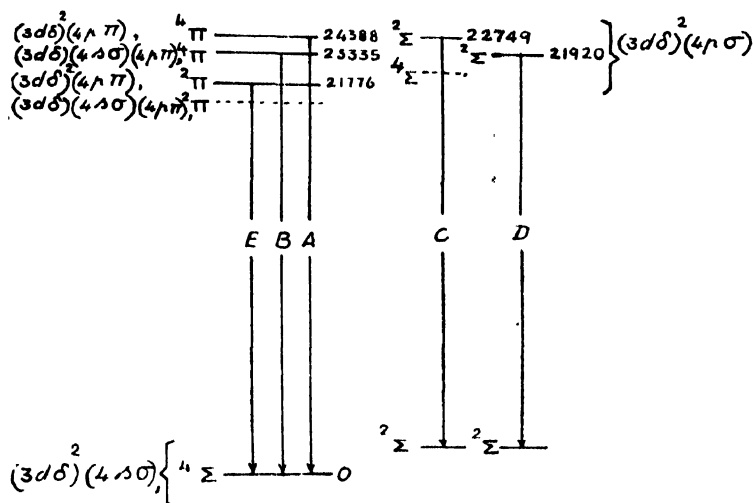
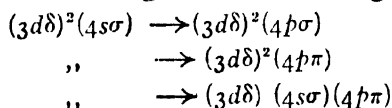


FIG. 2

Energy level diagram.

configurations. The transitions giving rise to the different observed systems are also shown. The following transitions are regarded as permissible:—



The relative magnitude of the doublets and their value with respect to the quartets are not correctly shown since they cannot be derived from the observed data. Two levels are shown dotted in the diagram, a  $^2\Pi$  and a  $^4\Sigma$ . The permitted transitions from these levels obviously occur further up in the region of longer wavelength, above  $\lambda 4800$ , the farthest wavelength to which the analysed systems are found to extend. Examination of the spectrum in this region does indicate the existence of band heads. They are, however, too faint and not conveniently measurable. Mesnage's data also reveal band heads in this region. As reported by Peaise and Gaydon (1950), two band heads, one at  $\lambda 5013.2$  and another at  $\lambda 5352.2$ , are recorded by Mesnage, the former is relatively strong. This region calls for further investigation which may lead to the determination of relative magnitudes between the quartet and the doublet systems.

The ground state of the NiCl molecule, as suggested by the results in this investigation, is a  $^4\Sigma$  state. It would be interesting to confirm this feature by a study of the absorption spectrum of NiCl in the visible region. Experiments in this direction are in progress.

In Table VI, the wavenumbers recorded by More are given in the first column. The wavenumbers obtained in the present investigation, their intensities and the designation of the systems are given in columns 2, 3 and 4.

The fifth column gives the vibrational assignment. The rotational assignments of the different heads are given in the last column.

TABLE VI (NiCl bands)

More Wavenumber	Author Wave-number	Int.	System	$v', v''$	$\Delta J$		
					-1	0	+1
	20803.3	3	E	1,3			$SR_{11}$
	813.7	3	E	0,2			$SR_{11}$
	822.8	3					
	836.2	3					
	916.9	3	E	1,3			$TR_{21}$
	931.4	3	E	0,2			$TR_{21}$
	951.9	3					
	21137.1	3					
	154.5	3	E	1,2	$QP_{11}$	$Q_{12}$	$QR_{13}$
	171.5	3	E	0,1	$QP_{11}$	$Q_{12}$	$QR_{13}$
	198.0	4	E	0,1		$RQ_{11}$	$R_{12}$
	214.7	3	E	1,2			$SR_{11}$
21230.1	227.3	5	E	0,1			$SR_{11}$
237.7							
246.1	215.8	4	E				
	272.9	2	E	0,1	$QP_{22}$	$Q_{23}$	$QR_{21}$
	287.4	2	E	1,2	$RP_{21}$	$RQ_{22}$	$R_{23}$
	296.0	3	E	0,1	$RP_{21}$	$RQ_{22}$	$R_{23}$
	313.3	3	E	1,2		$SQ_{21}$	$SR_{22}$
	350.6	3	E	0,1			$TR_{21}$
	360.3	3	D	7,8			
	383.0	3	D	6,7			
	402.3	3	D	5,6			
	417.9	3	D	4,5			
	438.1	3	D	3,4			
	450.2	1	D	2,3			
	460.8	1	D	1,2			
	489.2	5	D	0,1			
	517.1	3					
	557.3	3					
	572.7	3	E	1,1	$QP_{11}$	$Q_{12}$	$QR_{13}$
	585.3	3	E	0,0	$QP_{11}$	$Q_{12}$	$QR_{13}$
	592.7	4					
	603.4	4	E	1,1		$RQ_{11}$	$R_{12}$
	613.5	6	E	0,0		$RQ_{11}$	$R_{12}$
21627.1	638.0	6	E	1,1			$SR_{11}$
639.3	637.4	3					
	647.9	3	E	0,0			$SR_{11}$
	657.3	3					
	668.3	3	E	1,1	$QP_{22}$	$Q_{23}$	$QR_{21}$
	688.2	3	E	0,0	$QP_{22}$	$Q_{23}$	$QR_{21}$
	717.7	3	E	0,0	$RP_{21}$	$RQ_{22}$	$R_{23}$
	730.7	4	E	1,1		$SQ_{21}$	$SR_{22}$
747.4	747.7	4	E	0,0		$SQ_{21}$	$SR_{22}$
	757.2	3	E	1,1			$TR_{21}$
	775.5	3	E	0,0			$TR_{21}$
	792.8	3	D	6,6			
	806.1	3	D	5,5			
	827.4	3	D	4,4			
	843.9	3	D	3,3			
	865.5	3	D	2,2			
871.3							
888.2							
890.7	891.3	4	D	1,1			
911.0	911.2	5	D	0,0			
	922.0	2					
	940.3	2					

TABLE VI (contd.)

More Wavenumber	Author Wave-number	Int.	System	$v', v''$	$\Delta J$		
					-1	0	+1
	21953.5	3					
	966.1	3	E	2,1	$QP_{11}$	$Q_{12}$	$QR_{13}$
	978.9	4					
	987.2	3	E	1,0	$QP_{11}$	$Q_{12}$	$QR_{13}$
	22006.5	3	E	2,1		$RQ_{11}$	$R_{12}$
	022.2	3	E	1,0		$RQ_{11}$	$R_{12}$
	037.3	4	E	2,1			$SR_{11}$
	050.0	4	E	1,0			$SR_{11}$
	065.4	3	E	2,1	$QP_{22}$	$Q_{23}$	$QR_{24}$
	080.1	3					
	086.4	3	E	1,0	$QP_{22}$	$Q_{23}$	$QR_{24}$
	101.1	3	E	2,1	$RP_{21}$	$RQ_{22}$	$R_{23}$
	121.0	3	E	1,0	$RP_{21}$	$RQ_{22}$	$R_{23}$
	150.0	3	E	1,0		$SQ_{22}$	$SR_{22}$
	171.7	3	E	1,0			$TR_{21}$
	198.8	3	C	6,7			
	215.5	3	C	5,6			
	231.3	3	C	4,5			
	248.6	3					
	262.5	3	C	3,4			
	277.4	4	C	2,3			
22283.4							
289.8	290.8	4					
302.9	301.3	4	C	1,2			
	314.2	5	C	0,1			
	329.6	3					
	352.6	2					
	367.1	3	E	3,1	$QP_{11}$	$Q_{12}$	$QR_{13}$
	391.7	3	E	2,0	$QP_{11}$	$Q_{12}$	$QR_{13}$
	410.7	3	E	3,1		$RQ_{11}$	$R_{12}$
	429.4	3	E	2,0		$RQ_{11}$	$R_{12}$
	439.4	3	E	3,1			$SR_{11}$
	451.0	3	E	2,0			$SR_{11}$
	473.3	3	E	3,1	$QP_{22}$	$Q_{23}$	$QR_{24}$
	486.6	3	E	2,0	$QP_{22}$	$Q_{23}$	$QR_{24}$
	505.4	3	E	3,1	$RP_{21}$	$RQ_{22}$	$R_{23}$
	525.9	3	E	2,0	$RP_{21}$	$RQ_{22}$	$R_{23}$
	530.7	3	B	0,1		$Q_1$	$QR_{12}$
	549.7	3	E	2,0		$SQ_{21}$	$SR_{22}$
	602.8	3	C	0,0			
	614.5	3					
	625.8	3	C	5,5			
	632.4	3	B	0,1	$QP_{21}$	$Q_2$	$QR_{23}$
	647.8	3	C	1,4			
	653.0	3					
	670.9	3	C	3,3			
22676.3	675.0	3					
	686.9	3	C	2,2			
697.3	696.2	3					
	707.0	4	C	1,1			
718.2	719.4	4					
	726.1	6	C	0,0			
738.3	738.6	6	B	0,1	$QP_{32}$	$Q_3$	$QR_{34}$
	750.9	2	B	1,2	$RP_{31}$	$RQ_{32}$	$R_3$
	765.7	3	B	0,1	$RP_{31}$	$RQ_{32}$	$R_3$
762.8	785.1	3	B	0,1		$SQ_{31}$	$SR_{32}$
785.3	809.3	3	B	0,1			$TR_{31}$

TABLE VI (contd.)

More Wavenumber	Author Wave- number	Int.	System	$v', v''$	$\Delta J$		
					-1	0	+1
	22818.4	3	B	1,2	$QP_{43}$	$Q_4$	
	833.5	3	B	0,1	$QP_{43}$	$Q_4$	
	843.9	3	B	1,2	$RP_{42}$	$RQ_{43}$	$R_4$
	869.0	3	B	0,1	$RP_{42}$	$RQ_{43}$	$R_4$
	885.8	3	B	0,1	$SP_{41}$	$SQ_{42}$	$SR_{43}$
	903.1	3	B	1,2		$TQ_{41}$	$TR_{42}$
	921.5	3	B	0,1		$TQ_{41}$	$TR_{42}$
	946.7	3	B	0,0		$Q_1$	$QR_{12}$
	961.5	3	B	0,0			$R_1$
	976.3	3	A	0,3	$RP_{31}$	$RQ_{32}$	$R_3$
	988.4	3	A	1,4		$SQ_{31}$	$SR_{32}$
	23000.6	3	A	0,3		$SQ_{31}$	$SR_{32}$
	012.8	3	A	1,4			$TR_{31}$
	024.4	3	A	0,3			$TR_{31}$
	049.4	3	B	0,0	$QP_{21}$	$Q_2$	$QR_{23}$
	068.5	3	B	1,1		$RQ_{21}$	$R_2$
	077.0	3	B	0,0		$RQ_{21}$	$R_2$
	100.5	3	A	0,2		$Q_1$	$QR_{12}$
23112.8	113.8	4	A	1,3			$R_1$
125.9	124.5	4	A	0,2			$R_2$
	137.9	3	B	1,1	$QP_{32}$	$Q_3$	$QR_{34}$
152.7	152.9	5	B	0,0	$QP_{32}$	$Q_3$	$QR_{34}$
	162.6	3	B	1,1	$RP_{31}$	$RQ_{32}$	$R_3$
23177.7	180.3	5	B	0,0	$RP_{31}$	$RQ_{32}$	$R_3$
	187.3	3	B	1,1		$SQ_{31}$	$SR_{32}$
200.7	198.0	5	B	0,0		$SQ_{31}$	$SR_{32}$
222.7	221.8	7	B	0,0			$TR_{31}$
	238.5	3	B	1,1	$QP_{43}$	$Q_4$	
	247.1	3	B	0,0	$QP_{43}$	$Q_4$	
	258.5	3	A	0,2		$RQ_{41}$	$R_3$
	266.1	3	B	1,1	$RP_{42}$	$RQ_{43}$	$R_4$
	278.9	3	B	0,0	$RP_{42}$	$RQ_{43}$	$R_4$
	289.4	3	B	1,1	$SP_{41}$	$SQ_{42}$	$SR_{43}$
	307.3	4	B	0,0	$SP_{41}$	$SQ_{42}$	$SR_{43}$
	325.2	5	B	1,0		$Q_1$	$QR_{12}$
333.3	334.8	6	B	0,0		$TQ_{41}$	$TR_{42}$
	347.0	3	B	1,0			$R_1$
	355.2	3	A	1,3	$QP_{32}$	$Q_3$	$QR_{34}$
	363.4	3	A	0,2	$QP_{32}$	$Q_3$	$QR_{34}$
	372.11	3	A	1,3	$RP_{31}$	$RQ_{32}$	$R_3$
	382.0	3	A	0,2	$RP_{31}$	$RQ_{32}$	$R_3$
	395.7	3	A	1,3		$SQ_{31}$	$SR_{32}$
	410.4	3	A	0,2		$SQ_{31}$	$SR_{32}$
	429.6	3	B	2,1	$QP_{21}$	$Q_2$	$QR_{23}$
	442.8	3	B	1,0	$QP_{21}$	$Q_2$	$QR_{23}$
	453.3	3	B	2,1		$RQ_{21}$	$R_2$
	464.8	3	B	1,0		$RQ_{21}$	$R_2$
	473.7	3	B	2,1			$SR_{21}$
	488.0	4	B	1,0			$SR_{21}$
504.0			A	0,2	$QP_{43}$	$Q_4$	
511.6	515.1	4	A	0,1		$Q_1$	$QR_{12}$
	528.9	4	A	1,2			$R_1$
	548.9	3	A	0,1			$R_1$
557.6	556.6	3	A	0,2		$TQ_{41}$	$TR_{42}$
567.9	567.2	3	B	2,1	$RP_{31}$	$RQ_{32}$	$R_3$
	576.1	3	B	1,0	$RP_{31}$	$RQ_{32}$	$R_3$
23593.9	597.8	3	B	1,0		$SQ_{31}$	$SR_{32}$



TABLE VI (contd.)

More Wavenumber	Author Wave-number	Int.	System	$\nu', \nu''$	$\Delta J$		
					-1	0	+1
23697.6 712.8	23614.5	3	B	1,0			TR <sub>31</sub>
	635.1	3	B	2,1	QP <sub>43</sub>	Q <sub>4</sub>	
	643.0	3	B	1,0	QP <sub>43</sub>	Q <sub>4</sub>	
	652.5	3	A	0,1	QP <sub>21</sub>	Q <sub>2</sub>	QR <sub>23</sub>
	668.7	3	B	2,1	RP <sub>42</sub>	RQ <sub>43</sub>	R <sub>4</sub>
	677.1	3	B	1,0	RP <sub>42</sub>	RQ <sub>43</sub>	R <sub>4</sub>
	688.3	3	A	0,1		RQ <sub>21</sub>	R <sub>2</sub>
	698.5	4	A	1,2			SR <sub>21</sub>
	711.9	5	A	0,1			SR <sub>21</sub>
	735.3	5	B	1,0		TQ <sub>41</sub>	TR <sub>42</sub>
	752.5	3					
757.6	761.0	3	A	1,2	QP <sub>32</sub>	Q <sub>3</sub>	QR <sub>34</sub>
	772.8	3	A	0,1	QP <sub>32</sub>	Q <sub>3</sub>	QR <sub>34</sub>
	779.1	3					
	814.2	3	A	1,1		SQ <sub>31</sub>	SR <sub>32</sub>
	823.8	3	A	0,1		SQ <sub>31</sub>	SR <sub>32</sub>
	852.8	3	A	0,1			TR <sub>31</sub>
	867.1	3	B	2,0		RQ <sub>21</sub>	R <sub>2</sub>
	880.7	3	A	1,2	QP <sub>43</sub>	Q <sub>4</sub>	
	892.7	3	A	0,1	QP <sub>43</sub>	Q <sub>4</sub>	
	907.6	3	A	1,2	RP <sub>42</sub>	RQ <sub>41</sub>	R <sub>4</sub>
	915.6	3	A	0,1	RP <sub>42</sub>	RQ <sub>43</sub>	R <sub>4</sub>
	936.8	3	A	0,0		Q <sub>1</sub>	QR <sub>12</sub>
	948.8	3	A	0,1	SP <sub>41</sub>	SQ <sub>42</sub>	SR <sub>42</sub>
	956.8	3	A	1,1			R <sub>1</sub>
	970.6	3	A	0,0			R <sub>1</sub>
	982.1	3	B	3,1		SQ <sub>31</sub>	SR <sub>32</sub>
	995.9	3	B	2,0		SQ <sub>31</sub>	SR <sub>32</sub>
	24010.4	3	B	2,0			TR <sub>31</sub>
	024.8	3					
	031.7	3					
	042.7	3	B	3,1	QP <sub>43</sub>	Q <sub>4</sub>	
	051.9	3	B	2,0	QP <sub>43</sub>	Q <sub>4</sub>	
	064.1	3	A	0,0	QP <sub>21</sub>	Q <sub>2</sub>	QR <sub>23</sub>
	075.1	3	B	2,0	RP <sub>42</sub>	RQ <sub>43</sub>	R <sub>4</sub>
	085.0	3	A	1,1		RQ <sub>21</sub>	R <sub>2</sub>
24094.7	098.9	4	A	0,0		RQ <sub>21</sub>	R <sub>2</sub>
	112.0	4	A	1,1			SR <sub>21</sub>
	129.6	5	A	0,0			SR <sub>21</sub>
	143.7	2					
	160.6	3					
	172.3	3	A	1,1	QP <sub>32</sub>	Q <sub>3</sub>	QR <sub>34</sub>
	185.6	4	A	0,0	QP <sub>32</sub>	Q <sub>3</sub>	QR <sub>34</sub>
	201.9	5	A	1,1	RP <sub>31</sub>	RQ <sub>32</sub>	R <sub>3</sub>
	216.8	6	A	0,0	RP <sub>31</sub>	RQ <sub>32</sub>	R <sub>3</sub>
	233.3	3	A	1,1		SQ <sub>31</sub>	SR <sub>32</sub>
	246.8	3	A	0,0		SQ <sub>31</sub>	SR <sub>32</sub>
	267.4	3	A	0,0			TR <sub>31</sub>
	289.8	4	A	1,1	QP <sub>43</sub>	Q <sub>4</sub>	
	301.5						
305.4 327.8 331.9 354.9 359.1	305.7	5	A	0,0	QP <sub>43</sub>	Q <sub>4</sub>	
	328.8	5	A	1,0		Q <sub>1</sub>	QR <sub>12</sub>
	334.1	3	A	0,0	RP <sub>42</sub>	RQ <sub>43</sub>	R <sub>4</sub>
	355.5	3	A	1,0			R <sub>1</sub>
	359.1	3	A	0,0	SP <sub>11</sub>	SQ <sub>42</sub>	SR <sub>43</sub>
	360.8	3					

TABLE VI (contd.)

More Wavenumber	Author Wave-number	Int.	System	$v', v''$	$\Delta J$		
					-1	0	+1
	24373.9	3	A	1,1		$TQ_{41}$	$TR_{42}$
382.0	383.4	3	B	3,0		$SQ_{31}$	$SR_{32}$
387.6	387.6	3	A	0,0		$TQ_{41}$	$TR_{42}$
410.7	413.8	3	B	3,0			$TR_{31}$
417.7	420.9	3					
	428.7	3					
	434.0	3					
	436.4	3	B	4,1	$QP_{43}$	$Q_1$	
	447.2	3	B	3,0	$QP_{43}$	$Q_1$	
24460.0	462.1	3	A	1,0	$QP_{21}$	$Q_2$	$QR_{23}$
476.4	478.3	4	B	3,0	$RP_{42}$	$RQ_{43}$	$R_4$
494.5	496.3	5	A	1,0		$RQ_{21}$	$R_2$
	507.1	4	B	4,1	$SP_{41}$	$SQ_{42}$	$SR_{43}$
	515.7	4	B	3,0	$SP_{41}$	$SQ_{42}$	$SR_{43}$
	527.6	6	A	1,0			$SR_{21}$
	542.6	3	B	3,0		$Q_{41}$	$TR_{42}$
	553.5	3					
	572.2	3	A	2,1	$QP_{32}$	$Q_3$	$QR_{34}$
577.5	586.7	3	A	1,0	$QP_{32}$	$Q_3$	$QR_{34}$
596.7	600.6	4	A	2,1	$RP_{31}$	$RQ_{32}$	$R_1$
614.7	616.3	5	A	1,0	$RP_{31}$	$RQ_{32}$	$R_3$
	630.6	3	A	2,1		$SQ_{31}$	$SR_{32}$
	644.6	3	A	1,0		$SQ_{21}$	$TR_{31}$
	651.0	3	A	2,1			$TR_{31}$
	666.7	3	A	1,0			
	678.3	3					
	692.7	3	A	2,1	$QP_{43}$	$Q_4$	
	705.5	4	A	1,0	$QP_{43}$	$Q_4$	
	721.6	3	A	2,1	$RP_{42}$	$RQ_{43}$	$R_4$
	733.0	4	A	1,0	$RP_{42}$	$RQ_{43}$	$R_4$
	747.4	3	B	4,0	$RP_{41}$	$RQ_{32}$	$R_3$
	753.5	3	A	2,1	$SP_{41}$	$SQ_{42}$	$SR_{41}$
			A	3,1			$R_1$
	762.1	3	A	1,0	$SP_{41}$	$SQ_{42}$	$SR_{43}$
			A	2,0			$R_1$
	775.9	3	A	2,1		$TQ_{41}$	$TR_{42}$
	810.8	3	B	5,1			$TR_{31}$
	820.5	3	B	4,0			$TR_{31}$
	838.1	3	B	5,1		$Q_4$	
	846.1	3	B	4,0	$QP_{43}$	$Q_4$	
	856.9	3	A	3,1	$QP_{21}$	$Q_2$	$QR_{23}$
	864.9	3	A	2,0	$QP_{21}$	$Q_2$	$QR_{23}$
	877.0	4	B	4,0	$RP_{42}$	$RQ_{43}$	$R_4$
	892.2	3	A	3,1		$RQ_{21}$	$R_2$
	900.8	3	A	2,0		$RQ_{21}$	$R_2$
	917.9	3	A	3,1			$R_3$
	931.3	3	A	2,0			$SR_{21}$
	946.8	3	B	4,1		$TQ_{41}$	$SR_{31}$
	962.1	3					$TR_{42}$
24968.8	970.2	3	A	3,1	$QP_{32}$	$Q_3$	$QR_{34}$
991.3	981.1	4	A	2,0	$QP_{32}$	$Q_3$	$QR_{34}$
25012.5	25000.8	3	A	3,1	$RP_{31}$	$RQ_{32}$	$R_3$
	0.6.4	3	A	2,0	$RP_{31}$	$RQ_{32}$	$R_3$

TABLE VI (contd.)

More Wavenumber	Author Wavenumber	Int	System	$\tau'$ , $\tau''$	$\Delta I$		
					-1	0	+1
	25045.0	3	A	2,0		$SQ_{31}$	$SR_{32}$
	2555.0	4	A	3,1			$TR_{31}$
	2685.5	3	A	2,0			$TR_{31}$
	2681.7	3					
	2680.0	3	A	3,1	$QP_{11}$	$O_1$	
	2631.1	3	A	2,0	$QP_{43}$	$Q_1$	
	2113.8	1	B	5,0	$QP_{32}$	$Q_3$	$QR_{31}$
	2122.0	3	A	3,1	$RP_{42}$	$RO_{11}$	$R_1$
	2120.0	3	A	2,0	$RP_{12}$	$RQ_{43}$	$R_4$
	2137.2	3					
	2141.2	3	A	3,1	$SP_{11}$	$SO_{42}$	$SR_{43}$
	2186.9	3	A	2,0		$TO_{41}$	$TO_{42}$
	2192.6	3	B	5,0		$SQ_{31}$	$SR_{32}$
	2266.5	3	B	6,1			$TR_{31}$
	2221.2	3	B	5,0			$TR_{31}$
	2246.0	4	A	4,1	$QP_{21}$	$O_2$	$QR_{21}$
	2260.8	4	A	3,0	$QP_{21}$	$O_2$	$QR_{23}$
	2270.9	4	B	5,0	$RP_{12}$	$RQ_{43}$	$R_4$
	2280.2	3	A	4,1		$RQ_{21}$	$R_2$
	2291.7	3	A	3,0		$RO_{21}$	$R_2$
	2301.7	3	B	6,1	$SP_{41}$	$SO_{42}$	$SR_{43}$
	2312.5	3	B	5,0	$SP_{41}$	$SQ_{42}$	$SR_{43}$
	2324.4	3	A	1,1			$SR_{21}$
	2331.3	3	A	3,0			$SR_{21}$
	2342.0	3	B	5,0		$TO_{11}$	$TR_{42}$
	2355.0	3					
45382.2	2370.7	3	A	1,1	$QP_{12}$	$O_3$	$QR_{31}$
	2381.3	3	A	3,0	$QP_{12}$	$O_3$	$QR_{31}$
4665	2391.6	3	A	4,1	$RP_{11}$	$RO_2$	$R_3$
	2408.1	3	A	3,0	$RP_{31}$	$RQ_{32}$	$R_3$
	2423.2	3					
	2430.6	3	A	1,1		$SO_{31}$	$SR_{32}$
	2442.6	3	A	3,0		$SQ_{31}$	$SR_{32}$
	2460.8	3	A	1,1			$TR_{31}$
	2468.9	3	A	3,0			$TR_{31}$
	2479.0	3					
	2495.9	3	A	4,1	$QP_{43}$	$Q_4$	
	2501.7	3	A	3,0	$QP_{43}$	$O_4$	
	2508.3	3	A	1,1	$RP_{42}$	$RQ_{43}$	$R_4$
	2527.8	3	A	3,0	$RP_{42}$	$RQ_{43}$	$R_4$
	2544.5	5					
	2570.9	3	A	4,1		$TO_{11}$	$TR_{42}$
	2583.8	3	A	3,0		$TO_{41}$	$TR_{42}$
	2592.1	4	B	6,0		$SQ_{31}$	$SR_{32}$
	2609.8	3	B	7,1			$TR_{31}$
	2619.0	3	B	6,0			$TR_{31}$
	2627.9	3	B	7,1	$QP_{43}$	$Q_4$	
	2637.9	3	B	6,0	$QP_{43}$	$Q_4$	
	2646.0	3					
	2657.5	3	A	4,0	$QP_{21}$	$Q_2$	$QR_{21}$
	2663.4	3	B	7,1	$RP_{42}$	$RQ_{43}$	$R_4$
	2661.3	3	B	6,0	$RP_{42}$	$RQ_{43}$	$R_4$
	2679.2	3	A	5,1		$RO_{21}$	$R_2$
	2686.5	3	A	4,0		$RO_{21}$	$R_2$
	2695.1	3	B	7,1	$SP_{41}$	$SQ_{42}$	$SR_{43}$
	2710.6	3	A	5,1			$SR_{21}$
	2720.2	3	A	4,0			$SR_{21}$

TABLE VI (contd.)

More Wavenumber	Author Wave-number	Int.	System	$v, v''$	$\Delta J$		
					-1	0	+1
	25737.1	3	B	7,1		$TQ_{41}$	$TR_{42}$
	747.0	3	B	6,0		$TQ_{41}$	$TR_{42}$
	764.0	3	A	5,1	$QP_{32}$	$Q_3$	$QR_{34}$
	777.2	3	A	4,0	$QP_{32}$	$Q_3$	$QR_{31}$
	768.5	4	A	4,0	$RP_{31}$	$RQ_{32}$	$R_3$
	824.5	3	A	5,1		$SQ_{31}$	$SR_{32}$
	845.2	3	A	4,0		$SQ_{31}$	$SR_{32}$
	861.6	3	A	4,0		$SQ_{31}$	$SR_{32}$
	886.7	4	A	5,1	$QP_{43}$	$O_4$	$TR_{31}$
	804.7	4	A	4,0	$QP_{43}$	$Q_4$	
	926.3	4	A	4,0	$RP_{40}$	$RQ_{43}$	$R_4$
	935.0	3					
	945.1	2	A	5,1	$SP_{41}$	$SQ_{42}$	$SR_{43}$
	102.6	4	A	4,0	$SP_{41}$	$SQ_{42}$	$SR_{43}$
	970.7	3	A	5,1		$TQ_{41}$	$TR_{42}$
	980.2	3	A	1,0		$TQ_{41}$	$TR_{42}$
	990.3	3					
	26026.9	3					
	047.9	3	A	6,1	$QP_{31}$	$Q_2$	$QR_{22}$
	056.0	3	A	5,0	$QP_{21}$	$Q_2$	$QR_{23}$
	061.2	3	A	6,1		$RQ_{21}$	$R_2$
	100.2	2	A	6,1			$SR_{21}$
	108.4	3	A	5,0			$SR_{21}$
	124.8	2					
	148.7	2					
	159.7	2	A	6,1	$QP_{32}$	$Q_3$	$QR_{34}$
	184.3	4	A	5,0	$QP_{32}$	$O_3$	$QR_{34}$
	200.8	4	A	5,0	$RP_{31}$	$RQ_{32}$	$R_3$
	210.4	2					
	220.7	3	A	6,1		$SQ_{31}$	$SR_{32}$
	231.7	4	A	5,0		$SQ_{31}$	$SR_{32}$
	244.1	4	A	6,1			$TR_{31}$
	274.5	4					
	284.8	3	A	6,1	$QP_{43}$	$O_4$	
	293.1	3	A	5,0	$QP_{43}$	$O_4$	
	303.5	4	A	6,1	$RP_{42}$	$RQ_{43}$	$R_1$
	312.5	3					
	319.4	4	A	5,0	$RP_{42}$	$RQ_{43}$	$R_4$
	327.1	3					
	334.7	2	A	6,1	$SP_{41}$	$SQ_{42}$	$SR_{43}$
	345.1	3	A	5,0	$SP_{41}$	$SQ_{42}$	$SR_{43}$
	367.3	3	A	6,1		$TQ_{41}$	$TR_{42}$
	377.1	4	A	5,0		$TQ_{41}$	$TR_{42}$
	386.1	3					
	393.1	3					
	400.7	2					

## ACKNOWLEDGMENTS

The author wishes to express his grateful thanks to Prof. K. R. Rao for his kind guidance and interest in the work. He is grateful to the Government of India, Ministry of Scientific Research for the award of a Senior Research Scholarship.

## REFERENCES

- Bacher, J., 1948, *Helv. Phys. Acta.*, **21**, 379.
- Krishnamurty, V. G., 1951, *Cur. Sci.*, **20**, 323.
- Krishnamurty, V. G., 1952 *Ind. J Phys.*, **28**, 177.
- Mesnage, P., 1935, *C. R. Acad., Sci. Paris .*, **200**, 2072.
- Mesnage, P., 1938, Thesis for Doctorate, Paris;
- More, K. R , 1938, *Phys. Rev.*, **54**, 122.
- Pearse, R. W. Band Gaydon, A. G., 1950, *The Identification of Molecular Spectra*, page 191.
- Rao, P. T., 1949, *Ind. J. Phys.*, **23**, 517.
- Rao, P. T , *Proc. Nat. Inst. Sci. India.* (in Press).

# RAMAN SPECTRA OF ORGANIC CRYSTALS AT LOW TEMPERATURES. III. ORTHOXYLENE AND BENZYL BROMIDE\*

By A. K. RAY

OPTICS DEPARTMENT, INDIAN ASSOCIATION FOR THE CULTIVATION OF SCIENCE, CALCUTTA

(Received for publication March 28, 1952)

## Plate IX

**ABSTRACT** The Raman spectra of orthoxylene and benzyl bromide in the solid state at  $-180^{\circ}\text{C}$  have been photographed and new lines at 50, 88, 96,  $124\text{ cm}^{-1}$  in the former case and also the lines at 35, 51, 68, 88,  $96\text{ cm}^{-1}$  in the latter case have been observed. It is observed that in the former case the frequencies of the C-II deformation oscillations change slightly with the solidification and the line at  $1602\text{ cm}^{-1}$  due to C=C oscillation becomes appreciably weaker with the solidification of the substance. It is pointed out that such a change is also observed with the polymerization of methyl methacrylate and this weakening may be due to the formation of virtual bond at the expense of one of the C-C bonds in the C-C bond. In the case of benzyl bromide no such weakening of the corresponding line is observed, but the line  $3054\text{ cm}^{-1}$  due to C-II valence oscillation splits up into three lines. It is concluded that hydrogen atom may be responsible for the formation of virtual bonds in this case giving rise to the new lines in the low frequency region.

## INTRODUCTION

The Raman spectra of some substituted benzene compounds have been investigated recently by the present author (Ray, 1950, 1951) and from the study of the temperature dependence of the intensity and position of the low frequency Raman lines observed in the case of these substances in the solid state it has previously been concluded that the origin of such lines would be due to the formation of virtual bonds between neighbouring molecules in the solid state, because the frequencies of the lines cannot be correlated with moments of inertia of the molecules. For instance, the low-frequency lines at 47, 66, 86, 108,  $127\text{ cm}^{-1}$  are observed in the case of toluene in the solid state at  $-180^{\circ}\text{C}$  while ethyl benzene at  $-180^{\circ}\text{C}$  yields lines at 48, 63, 81, 100,  $130\text{ cm}^{-1}$ , and thus the frequency-shifts of some of the new lines in the latter case are not smaller than those of the corresponding lines observed in the case of toluene. It was, therefore, concluded that the frequency-shifts of these new lines were independent of the moment of inertia of the molecules. In order to investigate this question more thoroughly it was thought worth-while to study the Raman spectra of a few more

\* Communicated by Prof. S. C. Sirkar

substances of this type having heavier molecules. For this reason benzyl bromide and orthoxylene were chosen in the present investigation to compare the low-frequency Raman lines which may appear in the solid state in these cases with those observed earlier in the case of benzyl chloride and toluene respectively (Ray, 1950, 1951a).

#### EXPERIMENTAL

Orthoxylene used in the present investigation was obtained from the old stock of the laboratory and was of Merck's chemically pure variety. Liquid benzyl bromide was obtained from Kahlbaum's original sealed bottle. Both the liquids were further distilled in vacuum before use. The technique used for studying the Raman spectra of these substances in the solid state at low temperature was the same as that adopted in the previous investigations (Ray, 1950). In the case of benzyl bromide in the liquid state, the light from two horizontal Hg arcs was focused on the horizontal Wood's tube containing the liquid with the help of two condensers in order to prevent the sample from appreciable decomposition during the exposure to Hg lines in the near ultra violet region. These lines were absorbed by the condenser.

The purity of the sample of orthoxylene was tested by comparing the Raman spectra of the liquid with those observed by previous workers. No attempt was made in the present investigation to record the Raman spectra of the samples at temperature just below their melting points, as the interest lay only on the number and position of the low-frequency lines at  $-186^{\circ}\text{C}$ . Polarisation of the Raman lines of both the liquids was also studied by photographing the two components using a double image prism.

Iron arc spectrum was photographed in each plate in order to find out whether any of the lines shifts with the change of temperature and state.

#### RESULTS

The spectrograms are reproduced in Plate IX, figures 1 and 2. The low-frequency lines in the region  $4046.6\text{\AA}$ , enlarged about four times, are also shown in figures 3 and 4. The frequency-shifts of the Raman lines are given in Tables I and II. The data for orthoxylene in the liquid state, reported earlier by Wood (1931), are also included in Table I. The letters P and D denote polarised and totally depolarised, ( $\rho = \frac{1}{2}$ ), respectively. The Raman spectrum of benzyl bromide in the liquid state was previously studied by Reitz and Stockmair (1935) but as the literature was not available it was not possible to incorporate these data in Table II.

TABLE I

Orthoxylene ( $C_8H_{10}$ ) :  $\Delta\nu$  in  $cm^{-1}$ .

Wood (1931)	Magat (1934)	Present author	
		Liquid at 24°C	Solid at about -180°C.
			50(2b), e, k
			88(1), e, k
			95(2b), e, k
			124(6), e, k
177		176(2b), e, D	180(1b), e
256		255(2b), e, k, D	257(1), e, k
505		503(6d), e, k, P	500(1), e
580		580(2), e, k, D	577(1), e, k
732		731(5), e, k, P	733(6), e, k
860			
907		994(6), e, P	
1052		1050(4), e, k, P	1050(5), e, k
1161			
1221	1220(7)	1221(4), e, k, P	1225(2), e, k
	1287(6)	1292(6b) [e], k	1297(1) [e], k
1386	1381(4)	1384(2), e, P	1386(1), e
	1448(2)	1442(1d), e, P	1450(2), e
	1584(1)	1577(1), e, k, D	1581(6)
1602	1604(5)	1602(3), e, k, D	1606(1), e, k
	2574(6)		
	2855(2)		
	2880(3)	2863(1b), e, k	2860(1b), e, k
	2920(7)	2922(5), e, k, D	2920(2b), e, k
	2984(2)	2984(5), e, k, P	2980(2b), e, k
	3048(7)	3047(5b), e, k, P	3044(1), k
			3042(3), e, k

## DISCUSSION

Tables I and II show that in the case of orthoxylene in the liquid state there is a line at  $176\text{ cm}^{-1}$  and in the case of benzyl bromide the corresponding line is at  $103\text{ cm}^{-1}$ . Both these lines persist in the solid state with



16A

-4358A

Fig 1

Fig 2

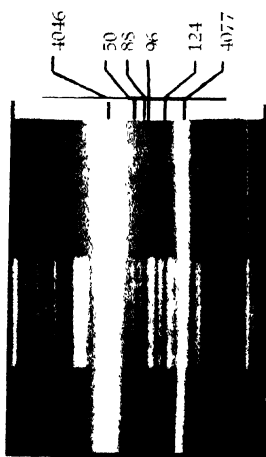


Fig 3

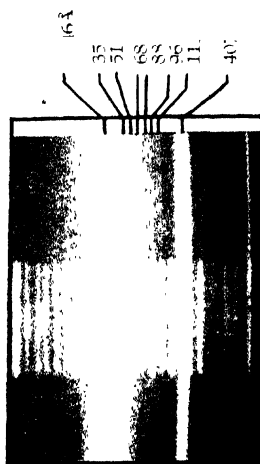


Fig 4

## Raman spectra

- Fig. 1. (a)  $C_8H_{10}$ —Liquid at about 24 C  
 (b) " —Solid " " —180°C  
 (c) " —Polarisation at room temp.  
 Fig. 2. (a)  $C_6H_5CH_2Br$ —Liquid about 24 C  
 (b) " —Solid at about —180°C  
 (c) " —Polarisation at room temp.  
 Fig. 3.  $C_8H_{10}$  —Solid at about —180°C  
 Fig. 4. " —Solid at about —180 C



TABLE II

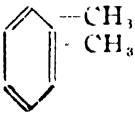
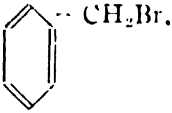
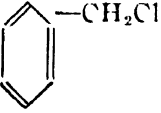
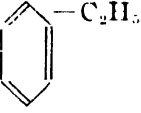
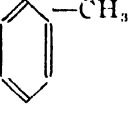
Benzyl bromide ( $\text{C}_6\text{H}_5\text{CH}_2\text{Br}$ ) :  $\Delta\nu$  in  $\text{cm}^{-1}$ .

Liquid at 24°C	Solid at about -180°C
	35(1b), k
	51(3), e, k
	68(2), e, k
	88(2), k
	96(1), e, k
103(4), e, $\pm$ k, D	113(5), e, k
239(2), e, $\pm$ k, P	242(1), e, k
448(5b), e, k, P	448(5s), e, k
544(2), e, k, D	541(2), e, k
601(7b), e, $\pm$ k, P	592(6), e, k
749(0), e, k, D	749(2s), e, k
803(1b), e, k, D	811(6), e, k
996(5), e, k, P	996(5), e, k
1015(0), e, P	1015(0), e,
1162(0), e, k, D	1162(0), e, k
1221(6b), e, k, P	1221(6s), e, k
1595(5b), e, k, D	1595(5s), e, k
2946(0), e, k, D	
2970(2), e, P	2966(1), e
	3010(0), e, k
3054(4b), k, P	3048(2s), e, k
	3067(1s), k

their frequencies increased slightly. These lines cannot be due to any mode of oscillation in the benzene ring because benzene does not yield a line of such low frequency. Probably this line is due to some mode of oscillation of the alkyl groups attached to the benzene ring. Since these lines do not disappear in the solid state they cannot be due to rotational oscillation of the  $\text{CH}_2\text{Br}$  or  $\text{CH}_3$  groups about C-C bond. The change in the frequency of these lines with the change of state shows that the intermolecular field has great influence on the frequency of the lines. The line  $103\text{ cm}^{-1}$  due to benzyl bromide is found to be totally depolarised, which suggests that these lines may be due to some deformation oscillation, and since the deformation oscillation of C-Br group in the case of bromo-benzene

probably yields a line at  $184\text{ cm}^{-1}$ , the line  $103\text{ cm}^{-1}$  may be due to deformation oscillation of the group  $\text{C}-\text{CH}_2\text{Br}$ . No such assignment is possible in the case of orthoxylene, because there is no heavy atom in the substitution groups in this case. However, in the case of the solid state all these substituted benzene compounds yield many new lines of low frequencies. These are shown in Table III for three such compounds along with those for orthoxylene and benzyl bromide observed in the present investigation.

TABLE III

Substance in the solid state at $-180^\circ\text{C}$			$\Delta\nu$ in $\text{cm}^{-1}$
Orthoxylene	...		50(b), 88, 96, 124
Benzyl bromide	...		35, 51, 68, 88, 96, 113
Benzyl chloride	...		46, 62, 82, 88, 119
Ethyl benzene	..		48, 63, 81, 100, 130
Toluene...	...		47, 66, 86, 108, 127

It is quite evident from Table III that inspite of wide variation in the mass of the substitution group two of the new lines, *e.g.*, those at about  $48\text{ cm}^{-1}$  and  $86\text{ cm}^{-1}$  are present in all the cases. It is also found that both orthoxylene and benzyl bromide yield two lines at 88 and  $96\text{ cm}^{-1}$ . If the lines were attributed to rotational oscillations of the molecule pivoted in the lattice about the axis of the molecules in their planes, as suggested by Kastler and Rousset (1941), the frequencies of some of the lines due to benzyl bromide would be much smaller than those of the corresponding lines due to orthoxylene, because the values of moments of inertia of the benzyl bromide molecule about an axis perpendicular to the plane of the molecule and also about another axis lying in the plane of the molecule are about

double the corresponding values for the orthoxylene molecule. It is, however, observed that the frequencies of three of the lines in the low frequency region are the same in both the cases. Hence it is evident that the modes of oscillation producing these lines are not dependent on the moments of inertia of the whole molecule about its axis. Probably the benzene ring itself oscillates against benzene rings of neighbouring molecules with which it is linked by virtual bonds and the frequencies are therefore only slightly affected by the mass of the substitution groups. It is, however, clearly seen from the spectrograms reproduced in Plate IX that when a halogen atom is present in the substitution group the new lines are sharp and very intense even at  $-180^{\circ}\text{C}$ . This shows that any angular oscillation cannot produce all these lines because the amplitude of such oscillation would diminish at lower temperatures and consequently the intensities of the lines would be small. All these facts thus lead to the conclusion that the lines are due to some modes of intermolecular oscillations in the lattice in which the molecules are linked to each other by virtual bonds of strength much larger than the ordinary Van der Waals forces, as suggested earlier by Sirkar (1936).

*Lines due to intramolecular oscillations.* Some of the Raman lines due to the single molecules in the liquid state undergo small changes in position and intensity in the case of orthoxylene. The lines  $1221$ ,  $1290$ ,  $1442$  and  $2863\text{ cm}^{-1}$  shift respectively to  $1225$ ,  $1297$ ,  $1450$  and  $2880\text{ cm}^{-1}$ . Three of these lines are due to C-H deformation oscillation and the fourth due to C-H valence oscillation. It seems therefore, that the hydrogen atom is responsible for the formation of the virtual bonds mentioned above. The line  $1602\text{ cm}^{-1}$  due to C=C oscillation on the other hand becomes appreciably weaker with the solidification of the substance. This was also observed in the case of para-dichloro-benzene and it was suggested (Ray, 1951*b*) that one of the two C-C bonds in some of the C=C groups might be involved in the formation of virtual bonds with neighbouring molecules. Similar results have been observed by Kojima (1949) in the case of polymerization of methyl methacrylate. It was concluded by him that the diminution of the intensity of the line at  $1602\text{ cm}^{-1}$  was due to diminution in the number of monomer molecules. It is also significant that the polymerization of methyl methacrylate does not alter appreciably the positions and intensities of the Raman lines due to the monomer. These results, therefore, support the view put forward above that the C=C bond diminishes in number with the solidification of orthoxylene owing to formation of virtual bonds among neighbouring molecules.

In the case of benzyl bromide also the lines  $601$  and  $803\text{ cm}^{-1}$  shift respectively to  $592$  and  $811\text{ cm}^{-1}$  and the line  $3054\text{ cm}^{-1}$  due to C-H valence oscillation splits up into three lines at  $3010$ ,  $3048$ , and  $3067\text{ cm}^{-1}$  when the liquid is solidified. In this case, however, the relative intensity of the lines  $996\text{ cm}^{-1}$  and  $1596\text{ cm}^{-1}$  due to C—C and C=C oscillations respectively remains unchanged with the solidification of the liquid. In this case probably

the hydrogen bonds are responsible for the association of the molecules in the solid state. Also the line  $239\text{ cm}^{-1}$  which is probably due to C-Br deformation oscillation diminishes in intensity with solidification and therefore the bromine atom also may take part in such association.

Examination of the spectrograms shows that in the case of both these compounds all the lines, excepting those due to C-H valence oscillations, become sharper with the solidification of the liquids. In the case of orthoxylene the broad line at  $3037\text{ cm}^{-1}$  splits up into two sharp lines at  $3034$  and  $3042\text{ cm}^{-1}$  and in the case of benzyl bromide also the broad line at  $3054\text{ cm}^{-1}$  splits up into three lines at  $3010$ ,  $3048$  and  $3067\text{ cm}^{-1}$ . As pointed out earlier this splitting may be due to association of the molecules in the lattice. The other lines do not show such splitting with the solidification. These results as well as those observed earlier (Ray, 1950, 1951) do not support the theory put forward by Bhagavantam (1941) that in the case of these crystals the Raman lines are due to simultaneous oscillations of the different molecules present in the unit cell either in the same phase or in opposite phases.

#### ACKNOWLEDGMENT

The author is indebted to Prof. S. C. Sirkar for his kind interest and guidance throughout the progress of the work.

#### REFERENCES

- Bhagavantam, S., 1941, *Proc. Ind. Acad. Sc., A*, **13**, 543.  
Kojima, K., 1949, *J. Chem. Soc., Japan, Pure Chem. Sect.*, **70**, 147.  
Kastler, A. and Rousset, A., 1941, *Compt. Rend.*, **212**, 645.  
Magat, 1936, *Annual Table of Constants*, p. 26-72.  
Reitz and Stockmain, 1935, *Wien, Ber.*, **144**, 665.  
Ray, A. K., 1950, *Ind. J. Phys.*, **24**, 111.  
,, 1951a, *Ind. J. Phys.*, **25**, 131.  
,, 1951b, *Ind. J. Phys.*, **25**, 459.  
Sirkar, S. C., 1936, *Ind. J. Phys.*, **10**, 109.  
Wood, R. W., 1931, *Phys. Rev.*, **38**, 2168.

# ABSORPTION SPECTRA OF ORGANIC SUBSTANCES IN THE LIQUID AND SOLID STATES. III. SOME SUBSTITUTED BENZENE COMPOUNDS\*

By H. N. SWAMY

OPTICS DEPT., INDIAN ASSOCIATION FOR THE CULTIVATION OF SCIENCE, CALCUTTA—32

(Received for publication, March 21, 1952)

## Plate X

**ABSTRACT.** The ultraviolet absorption spectra of thin films of *o*- and *p*-Xylene, benzyl alcohol and benzyl chloride in the liquid state at room temperature and in the solid state at low temperatures have been investigated. The results have been compared with those reported by previous workers for the vapour state of the substances and also for solution of these substances in various solvents. Discrete bands have been observed for the liquid state in all these substances. *o*-Xylene produces only three bands in the liquid state while on solidification and cooling to  $-180^{\circ}\text{C}$  six new bands appear. *p*-Xylene, on the other hand, produces six bands in the liquid state and at  $-180^{\circ}\text{C}$ , eleven bands are observed. Most of the frequencies observed in the solid state of *p*-Xylene can be attributed to the vibration of the benzene ring. It is pointed out that the symmetry of the molecule allows the benzene ring to execute vibrations probably because there is much space around the molecule even in the solid state. Five bands are observed in the case of benzyl alcohol both in the liquid and solid states. The bands become sharp and shift towards shorter wavelength with solidification. The bands in the liquid state shift considerably towards longer wavelength from their corresponding position in solution. It is concluded that the molecules in this case are already associated in the liquid state through virtual bonds and the association of molecules is not strengthened on solidification. In benzyl chloride also very little changes are observed on solidification of the substance and the main change occurs in the absorption spectrum with liquefaction of the vapour. It is concluded that the molecules in the liquid are strongly associated.

## INTRODUCTION

In a programme undertaken to study the ultraviolet absorption spectra of some organic compounds in liquid and solid states in order to find out whether the electronic energy levels undergo any remarkable changes with the change of state, interesting results were obtained in the case of the cresols (Swamy, 1952). It was found that while in the case of ortho and metacresol the  $\sigma, \sigma$  band shifts slightly towards shorter wavelengths with solidification, new bands appear when paracresol is solidified. In the present investigation the ultraviolet absorption spectra of ortho and para-

\* Communicated by Prof. S. C. Sirkar.

xylene, benzyl alcohol and benzyl chloride in the liquid and solid states have been studied. The results have been compared with those for the vapour state and discussed in the light of the hypothesis put forward in the previous paper (Swamy, 1952) regarding the quenching of vibrational transitions in the liquid and formation of associated groups in the solid state in some cases. The absorption spectra of xylenes in the solid state have been studied by Broude *et al* (1950) but as the paper is in Russian and was not available to the present author it was not known whether they have compared the spectra with those for the vapour state and whether they have tried to explain the changes which are observed to take place in the spectra with the change of state.

### EXPERIMENTAL

The experimental set up is that employed in an earlier investigation by the author (Swamy, 1951, 1952). Spectrograms were taken on Ilford IIP<sub>3</sub> films on a Hilger I<sub>51</sub> quartz spectrograph having a dispersion of 3 ÅU per mm in the region 2600 Å. Chemically pure substances supplied by BDH distilled four times in vacuum were used in this investigation.

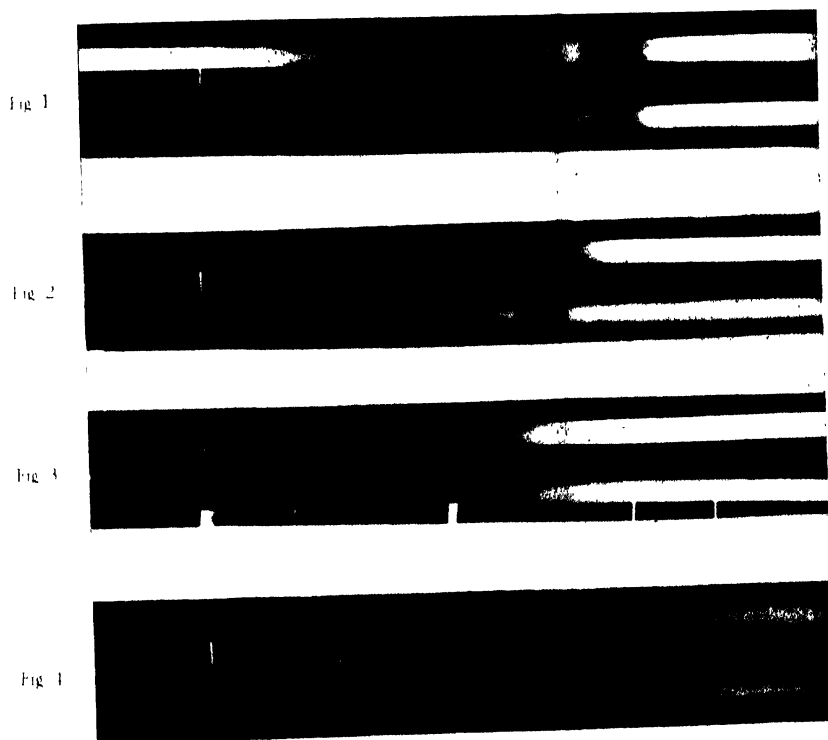
The film of benzyl chloride that produced bands in the ultraviolet absorption spectrum was extremely thin so that it showed interference fringes. The film was produced by taking a very small drop of the substance between quartz plates and sliding the latter till colours were produced by the thin film. In the case of *o*- and *p*-xylenes and benzyl alcohol, films having thicknesses of the order of 0.2 mm were required to produce the absorption bands.

To record the absorption spectra at low temperatures, the brass frame containing the cell was allowed to come in contact with liquid oxygen. The temperature of the cell was kept at  $-180^{\circ}\text{C}$  by replenishing oxygen from time to time. An exposure of 10 to 15 minutes was required to record the absorption spectra in the liquid state, while an exposure of 30 to 40 minutes recorded the spectra in the solid state at  $-180^{\circ}\text{C}$ . For comparison, mercury arc spectrum was recorded with the help of Hartmann diaphragm on each spectrogram.

### RESULTS

Spectrograms for *o*- and *p*-xylene, benzyl alcohol and benzyl chloride in the liquid and solid states are given in Plate X. The wave numbers of the bands observed in the liquid and solid state in each case are given in Tables I to IV in which wave numbers of the bands observed in solution by previous workers are included for comparison. The data for benzyl chloride in the vapour state reported recently (Kanda and Imanishi, 1949) are included in Table IV but similar data for the other three substances were





	Hg 2537Å	Hg 2652Å	Hg 2752.9Å
Fig. 1.	Absorption spectra of <i>p</i> -xylene--		(a) Liquid at 30°C (b) Solid at -180°C
Fig. 2.	"	"	<i>o</i> -xylene-- (a) Liquid at 30°C (b) Solid at -180°C
Fig. 3.	"	"	benzyl alcohol-- (a) Liquid at 30°C (b) Solid at -180°C
Fig. 4.	"	"	benzyl chloride (a) Liquid at 30°C (b) Solid at -180°C



not available. An attempt has been made to assign the bands to certain transitions and the assignments are given in the Tables.

TABLE I

Absorption bands of *o*-xylene;  $\nu$  in  $\text{cm}^{-1}$ .

Solution in heptane		Present author.				
(Wolf and Heiold)		Liquid 30°C	—	Band No.	Solid -180°C	Assignment
36850 (s)		36780 (V strong & broad)		1	36890 (vs)	$\nu_0$
				2	37411 (s)	$\nu_0 + 521$
		37318 (S)	5.9	3	37625 (m)	$\nu_0 + 735$
37360 (s)	1070			4	37822 (m)	$\nu_0 + 932$
				5	38026 (vs)	$\nu_0 + 1136$
		37930 (strong broad)	11.41	6	38206 (m)	$\nu_0 + 1376$
38900 (w)	2010			7	38597 (s)	$\nu_0 + 932 + 735$
				8	38800 (m)	$\nu_0 + 1136 + 735$
				9	39036 (w)	$\nu_0 + 1136 + 2 \times 521$
39850 (w)	2960					

TABLE II

Absorption bands of *p*-xylene;  $\nu$  in  $\text{cm}^{-1}$ .

Solution in hexane (Billroth)		Present author				
		Liquid 30°C	—	Band No.	Solid -180°C	Assignment
36500		36327 (vs)	$\nu_0$	1	36309 (vs)	$\nu_0$
				2	36767 (s)	$\nu_0 + 458$
	850	37117 (s)	$\nu_0 + 790$	3	37081 (s)	$\nu_0 + 772$
37350		37545 (s) (broad)	$\nu_0 + 1218$	4	37550 (vs) Broad	$\nu_0 + 1241$
37750	1250	37908 (w)	$\nu_0 + 2 \times 790$	5	37808 (s)	$\nu_0 + 2 \times 772$
				6	37977 (m)	$\nu_0 + 1241 + 458$
		38302 (s)	$\nu_0 + 790 + 1218$	7	38347 (s)	$\nu_0 + 1241 + 772$
38500	2000			8	38778 (m)	$\nu_0 + 2 \times 1241$
		38700 (m)	$\nu_0 + 2 \times 1218$	9	39150 (m)	$\nu_0 + 2 \times 772 + 1241$
39150	2650			10	39592 (m)	$\nu_0 + 2 \times 1241 + 772$
				11	39981 (w)	$\nu_0 + 2 \times 1241 + 772 + 458$
39800	3300					

TABLE III

Absorption bands of benzyl alcohol ;  $\nu$  in  $\text{cm}^{-1}$ .

Solution in ethyl alcohol, Campbell <i>et al</i> (1947)		Present author				
		Liquid 30°C		Solid -130°C		
37302	565	37164	$\nu_0$	37224		$\nu_0$
37867		37639	$\nu_0 + 475$			
		38048	$\nu_0 + 884$	37710	486	$\nu_0 + 486$
38673	1371	38548	$\nu_0 + 1384$	38113	889	$\nu_0 + 889$
	2200			38584	1360	$\nu_0 + 1360$
30592		39436	$\nu_0 + 1384 + 888$	39473	2249	$\nu_0 + 1360 + 889$
40310 (faint)	2998					

TABLE IV

Absorption bands of benzyl chloride ;  $\nu$  in  $\text{cm}^{-1}$ .

Vapour, Kanda and Imanishi (1949)		Solution in ethyl alcohol, Campbell <i>et al</i> (1949)	Present author			
			Liquid 30°C		Solid 180°C	
37098	$\nu_0 - 752$		36616	$\nu_0$	36526	$\nu_0$
37427	$\nu_0 - 424$		37372	$\nu_0 + 756$	37298	$\nu_0 + 772$
37640	$\nu_0 - 210$	37583	37408	$\nu_0 + 882$	37420	$\nu_0 + 891$
37850	$\nu_0$				38146	$\nu_0 + 1620$
38069	$\nu_0 + 210$	867	38222	$\nu_0 + 1606$		
38389	$\nu_0 + 530$		38369	$\nu_0 + 2 \times 882$	38304	$\nu_0 + 2 \times 894$
38601	$\nu_0 + 751$	38450				
38816	$\nu_0 + 966$					
39022	$\nu_0 + 1172$	1775			39198	$\nu_0 + 3 \times 894$
		39358	39266	$\nu_0 + 3 \times 882$		
39371	$\nu_0 + 966 + 539$					
39567	$\nu_0 + 966 + 751$					
39783	$\nu_0 + 2 \times 966$					

## DISCUSSION

As pointed out in a previous paper (Swamy, 1952), there are some general features in the changes which take place in the absorption spectra with change of state. The number of bands decreases when the vapour is liquefied. In some cases again, the solid at  $-180^{\circ}\text{C}$  gives larger number of bands than that in the liquid state. Also with liquefaction of the vapour in most cases, principal band and its companions shift towards longer wavelengths. The diminution in the number of bands in the liquid state has been ascribed previously (Swamy, 1952) to the influence of translational motion of the molecules in the liquid in the state of aggregation. It was assumed that constant impact of neighbouring molecules hinders transitions to higher vibrational energy states. The closeness of the molecules quench such modes of oscillation also in the solid state in the case of benzyl alcohol and benzyl chloride. Oscillations of higher quantum numbers, however, are found in the xylenes. The formation of a number of new bands cannot be attributed to splitting of the bands by the lattice field in the solid state. The pattern and arrangement of bands in the solid state are similar to those in the vapour state. The results will now be discussed for the four substances separately.

*o*-Xylene. The absorption spectra of *o*-xylene in the vapour and liquid states were studied previously by Grebe (1906a) and Mies (1909) and these authors reported that the bands shift towards longer wavelengths with liquefaction of the vapours. This may indicate formation of associated molecules in the liquid. As the data were reported in a journal which was not available to the present author these could not be given in Table I, but it was mentioned by Grebe (1906b) that attempts were made only to find out the changes in the absorption spectra with change in the substitution groups and also to discover any regularity which might be present in the arrangement of the bands. Hence the bands were not assigned properly by the author. In the present investigation only three broad bands are observed in the case of *o*-xylene in the liquid state, the frequency-difference being 529 and 1141  $\text{cm}^{-1}$ . The first of these two bands is at a distance of 100  $\text{cm}^{-1}$  on the longer wavelength side of the first band for the solution in heptane observed by Wolf and Herold (1930). When the liquid is solidified and cooled to  $-180^{\circ}\text{C}$  the first band shifts by about 101  $\text{cm}^{-1}$  towards shorter wavelengths and the three bands for the liquid are replaced by nine bands. Thus six new bands appear in the solid state. Some of the frequency-differences agree with the frequency-shifts observed in the Raman spectra of the substance in the solid state (Ray, 1952). It appears that only some of the modes of vibration of the ring and the deformation oscillations of the C-H bond appear in the absorption spectra of the crystal. It is, however, surprising that in the liquid state we get only three bands, two of them corresponding to the vibrational frequencies 529 and 1140  $\text{cm}^{-1}$ .

Probably, these are the only modes which are allowed inspite of continuous bombardment of the molecule by surrounding molecules in the liquid. Of course, all these frequencies observed in the absorption spectra relate to those of vibrations in the excited electronic state and therefore they are expected to be slightly lower than those observed in the Raman spectra, because the latter frequencies correspond to vibration in the ground state. The appearance of larger number of bands in the solid state may be due to the fact that the particular packing of the molecules in the crystals in this case is sufficiently loose to allow transitions to higher vibrational levels.

*p*-Xylene. A comparison of Tables I and II show that the two isomers *o*- and *p* xylene have distinctly different absorption spectra although the bands are in almost the same spectral region and their general behaviour with change of state is similar in the two cases. Such a conclusion was also drawn by Broude *et al* (1950) but a comparison of the results obtained by him with those obtained in the present investigation is not possible as the literature is not available to the present author. Paraxylene molecule belongs to the symmetry class  $A_{1g}$  and has no permanent electric moment. Orthoxylene molecule, on the other hand, has a large permanent electric moment. It is not surprising therefore that the structure of the spectra is different in the two cases. Some of the physical constants are also different in the two cases as shown in Table V.

TABLE V

Substance	Density gms/cc	Refractive index at 30°C	Viscosity at 30°C	Melting point	Boiling point	Vapour pressure at 25°C in mm. of mercury.
<i>o</i> -Xylene	0.88	1.503	0.00709	247.8°K	144°C	6.6
<i>p</i> -Xylene	0.86	1.493	0.00568	286.4°K	138.5°C	8.9

The absorption spectra of *p*-xylene in the vapour and liquid states were also studied previously by Grebe (1906a) and Mies (1909). The latter author has reported that the bands shift through 10 to 14 Å U. towards longer wavelengths on liquefaction of the vapour. Hence in this case also probably associated molecules are formed in the liquid state. The data for solution in hexane reported by Billroth (1935) given in column I, Table II show six bands which cannot be assigned satisfactorily. This may probably be due to the influence of inter-molecular field of the solvent on the electronic energy state of the molecule. There are, however, a large number of bands in the liquid state and they can be assigned to transitions  $\nu_0 + 790$ ,  $\nu_0 + 1218$ ,  $\nu_0 + 2 \times 790$ ,  $\nu_0 + 790 + 1218$ , and  $\nu_0 + 2 \times 1218$ . These frequencies in the excited state correspond to some of the frequencies observed in the Raman spectrum for the ground state. The principal band in the liquid state is at

a distance of  $170\text{ cm}^{-1}$  on the longer wavelength side of the first band for solution in hexane (Billroth, 1935). When the liquid is solidified and cooled to  $-180^{\circ}\text{C}$ , there is a very small shift of the first four bands towards longer wavelength side. The six bands in the liquid state are, however, replaced by 11 bands in the solid state. The bands are quite sharp. Vibrational frequencies deduced from these are 458, 774, 1241 and their harmonics. Besides the bands observed in the case of the liquid, there are five extra bands in the case of the solid and these can be assigned to combination frequencies shown in Table II. Some of the frequency-differences correspond to the frequency-shifts observed in the Raman spectra (Magat, 1936).

As the *p*-xylene molecule is non-polar, there is little chance for formation of associated groups of molecules in the liquid state. Freedom of rotation of the molecule is amply facilitated by the methyl radicals being in diametrically opposite positions in this case. *o*-Xylene molecule is unsymmetric and freedom of rotation of the molecules is less, being further hindered by a potential barrier to the value of 2000 cal/mole (Pitzer and Scott, 1943). The freedom of rotation is greater in the case of *p*-xylene than in *o*-xylene probably due to another reason also. The packing of molecules may be closer in the latter case than in the former. The density of *p*-xylene is smaller which lends additional support to the validity of such a hypothesis. This larger available space for rotation of the molecule and loose packing of molecules in *p*-xylene result in reducing the chances of quenching of vibrations by impact. Therefore transitions to higher harmonic states are made possible and a large number of bands are produced by *p*-xylene in the liquid state.

It is found from Table II that in the case of *p*-xylene the number of bands increases when the liquid is solidified. It appears therefore that even when the translational movement ceases there is enough intermolecular space to allow transitions to higher vibrational states. Most of the frequencies observed in this case in the solid state can be attributed to vibration of the benzene ring. The symmetry of the molecule allows the benzene ring to execute vibrations probably because there is much space around the molecules even in the solid state.

The validity of the hypothesis given above can be seen also from the results reported by Kronenberger (1930) in the case of *m*-xylene. He has shown that *m*-xylene in the crystalline state at  $-180^{\circ}\text{C}$  shows larger number of bands than the substance at  $-180^{\circ}\text{C}$  in the supercooled liquid state. In the solid state, translational motion ceases. It follows therefore that it is the change of state resulting in cessation of translational motion and not the temperature of the substance that is mainly responsible for increase in the number of bands in the case of *p*-xylene with solidification.

It is significant to note in this connection that both *o*- and *p*-xylene do not show any "Davydov splitting" (1948) at low temperatures. Even

though bands become sharp and additional bands are produced at low temperatures, they can be attributed to transitions to higher vibrational levels as mentioned above.

*Benzyl alcohol.* The results obtained by Campbell, *et al* (1947) for solution of benzyl alcohol in ethyl alcohol are included in Table III. Five bands are reported and the frequency-differences deduced from these bands are 565, 1371, 2290 and 2998  $\text{cm}^{-1}$  respectively. There has not been any satisfactory work on the absorption spectra of benzyl alcohol in the vapour state. The absorption spectra of benzyl alcohol vapour was studied by Hukumoto (1936) but he failed to observe any discrete bands. This may probably be due to the temperature and pressure of the absorbing cell being not proper and also due to his using a small dispersion spectrograph for photographing the spectrum. It is observed in the present investigation that in the liquid state, benzyl alcohol exhibits five bands, all the bands being considerably displaced towards longer wavelength side from the corresponding positions of bands in solution. The bands represent transitions  $\nu_0 + 475$ ,  $\nu_0 + 884$ ,  $\nu_0 + 1384$ ,  $\nu_0 + 1384 + 888$   $\text{cm}^{-1}$ . In the solid state at  $-180^\circ\text{C}$  also these five bands appear. The bands observed in the liquid state become sharp and prominent on solidification of the substance. All the bands also shift slightly towards shorter wavelengths with the solidification. The frequencies observed in the solid state represent transitions  $\nu_0 + 486$ ,  $\nu_0 + 889$ ,  $\nu_0 + 1360$  and  $\nu_0 + 1360 + 889$   $\text{cm}^{-1}$ . Of these the frequency 889  $\text{cm}^{-1}$  probably corresponds to that of the breathing vibration of the benzene ring in the excited state, the frequency for the ground state being 1092  $\text{cm}^{-1}$ , as observed in the Raman spectrum of the solid by Sirkar and Bishui (1946). Similarly the frequency 1360  $\text{cm}^{-1}$  may correspond to the frequency 1456  $\text{cm}^{-1}$  observed for the ground state in the Raman spectrum of the solid.

The large shifts of the bands in the liquid state from the corresponding positions in solution show that the molecules are already associated in the liquid state through virtual bonds. Also the absence of any considerable change in the position of bands and structure of the absorption spectra on solidification of benzyl alcohol show that the association of molecules is not strengthened on solidification. These results confirm the conclusion drawn from results of investigation of the Raman spectra by Sirkar and Bishui (1946) that in benzyl alcohol, the molecules are already strongly associated in the liquid state and the strength of the association does not further increase appreciably with solidification and lowering of temperature of the substance. It is also observed that in this case the number of bands exhibited by the liquid is fairly large and this number does not increase with solidification. Probably, the associated group is of such shape that some of the individual molecules are protected from the impact of neighbouring molecules so that the vibrational transitions are not quenched.



*Benzyl Chloride.* The results obtained by Kanda and Imanishi (1949) for benzyl chloride in the vapour state have been included in Table IV. According to the classification given by them, besides the frequency-differences 219, 539, 751, 966  $\text{cm}^{-1}$  and their harmonics in the excited state of the molecule, there appears to be bands produced in the ground state of the molecule corresponding to frequency-differences 210, 123 and 752  $\text{cm}^{-1}$ . The frequency-differences 966  $\text{cm}^{-1}$  in the excited state has been correlated by them with the totally symmetric vibration of benzene nucleus. On making an attempt to assign the frequencies observed in the case of solution of benzyl chloride in ethyl alcohol by Campbell *et al* (1917) it is found that the frequencies deduced from them are 867 and 1775  $\text{cm}^{-1}$  which are quite different from those observed in the case of vapour by Kanda and Imanishi (1949). In the present investigation it is observed that benzyl chloride produces six bands in the liquid state. The position of the  $\nu_0$ -band observed by Kanda and Imanishi (1949) does not agree with the  $\nu_0$ -band observed in the present investigation. The first band seems to have shifted towards longer wavelength side from 37008 to 36616  $\text{cm}^{-1}$  on liquefaction. The companions represent transition  $\nu_0 + 756$ ,  $\nu_0 + 882$ ,  $\nu_0 + 1606$ ,  $\nu_0 + 2 \times 882$ , and  $\nu_0 + 3 \times 882$   $\text{cm}^{-1}$ . All the bands are shifted towards longer wavelength side from their corresponding positions in the vapour state. The band  $\nu_0 + 756$  represents the strong C-Cl vibration and the band  $\nu_0 + 882$  represents the vibration of the benzene ring in the excited state. These two bands are superposed on each other so that the two together appear to be one broad band. Bands corresponding to frequencies  $\nu_0 + 1606$  and  $\nu_0 + 2 \times 882$   $\text{cm}^{-1}$  are also present. They are also superposed on each other so that the band becomes broad. These frequencies correspond to the frequencies 767 and 1608  $\text{cm}^{-1}$  observed in the Raman spectra (Magat, 1936). The band at 37640  $\text{cm}^{-1}$  representing  $\nu_0 - 210$   $\text{cm}^{-1}$  observed in the vapour state by Kanda and Imanishi (1949) is not observed in the case of the liquid. The large shift of the bands towards larger wavelength side on liquefaction may again indicate that in this case also the molecules become associated with one another through virtual bonds and the electronic energy state is lowered in this process.

There is very little change on solidification and lowering of temperature of the substance to  $-180^\circ\text{C}$ . All the bands observed in the liquid state are present in the solid state also and they do not become sharper. The shift of the bands with solidification is towards longer wavelengths and not towards shorter wavelengths as observed in the case of benzyl alcohol and many other benzene compounds. It has to be mentioned here that in the solid state there is a frequency 772  $\text{cm}^{-1}$  corresponding 756 and 751  $\text{cm}^{-1}$  respectively observed in the liquid and vapour states. This shows the presence of a strong C-Cl vibration and that the energy increases due to contraction of the molecule itself in the solid state at low temperature. The

frequency of the breathing vibration of the ring also seems to increase a little in the solid state but it is difficult to understand how in the case of the vapour Kanda and Imanishi observed the frequency  $751\text{ cm}^{-1}$  for this vibration both for the excited and ground states.

The investigations are being continued with other substances and the results will be reported shortly.

#### ACKNOWLEDGMENT

The author is indebted to Prof. S. C. Sirkar, D.Sc., F.N.I., for his kind interest and helpful guidance throughout the progress of the work and to the Government of India, Ministry of Scientific Research, for the award of a scholarship.

#### REFERENCES

- Billrath, H., 1935, *Z. f. Phys. Chem*, **29**, B, 170-177.  
 Broude *et al.*, 1950, *Izvest. Akad. Nauk. Ser. Fiz.*, **14**, 487.  
 Campbell *et al.*, 1947, *J. Am. Chem. Soc.*, **69**, 880.  
 Davydov, A., 1948, *J. Exptal. Theoret. Phys. (U.S.S.R.)*, **18**, 210.  
 Grebe, L., 1906a, *Zeit. Wiss. Photograph. Photophys. Photochem*, **3**, 376-394.  
 Grebe, L., 1906b, *J. Chem. Soc., Pt. II*, **90**, 410.  
 Hukamoto, Y., 1936, *Sc. Rep. Tohoku Imp. 'Varsity*, **28**, 1162.  
 Kanda and Imanishi, 1949, *J. Sc. Research, Inst.*, **43**, 1-16.  
 Kronenberger, A., 1930, *Z. f. Phys.*, **63**, 494.  
 Magat, M., 1936, Numerical data on Raman effect.  
 Mies, W., 1909A., *J. Chem. Soc., Pt. II*, **96**, 776.  
 Pitzer and Scott., 1943, *J. Am. Chem. Soc.*, **65**, 803.  
 Ray, A. K., 1952, *Ind. J. Phys.*, **28**, 226.  
 Sirkar, S. C., and Bishui, B. M., 1946, *Ind. J. Phys.*, **20**, 111.  
 Swamy, H. N., 1951, *Ind. J. Phys.*, **25**, 262.  
 Swamy, H. N., 1952, *Ibid.*, **28**, 119.  
 Wolf, K. L., and Herold, W., 1931, *Z. f. Phys. Chem*, B, **13**, 201.

# ASSOCIATED PAIRS OF PENETRATING PARTICLES AND OTHER EVENTS OBSERVED AT MOUNTAIN ALTITUDES WITH PHOTOGRAPHIC EMULSIONS

BY K. R. DIXIT

THE INSTITUTE OF SCIENCE, MAYO ROAD, BOMBAY

(Received for publication, March 17, 1952)

**ABSTRACT.** Ilford nuclear emulsions exposed at two places in the Himalayas at altitudes of 11,500 ft. and 14,300 ft. have been studied. All the events, singles  $> 100 \mu$  and stars which are not obviously radioactive are recorded. The singles appear to be produced by some radiation which is travelling in a direction which is almost vertical and which is twice as absorbable as the star-producing radiation. Observation of all stars leads us to expect that some stars which are normally excluded as of radioactive origin, on the criterion that a star smaller than sixfold is radioactive when all the six tracks are less than  $60 \mu$  could have been produced by the cosmic radiation. The cosmic ray stars appear to be produced in a cascaded process. Rare events like associated penetrating particles are observed. Four events are observed which are interpreted as those in which a  $\pi$  meson is produced by the interaction of  $V_0^1$  particle with a lithium nucleus. The value of the average mass of  $V_0^1$  calculated from these events comes out as 2166 times the electron mass.

Nuclear emulsion 100  $\mu$  Ilford C2 and G5 plates were exposed at two places in the Himalayas. The first place we shall designate as KL (altitude 11,500 ft.,  $77^\circ 30' E$  and  $34^\circ 00' N$ ) and the second we designate as SP (altitude 14,300 ft.,  $89^\circ 00' E$  and  $27^\circ 40' N$ ). The exposures were not made simultaneously but at different times. The plates at KL were 100  $\mu$  G5 and these were exposed during the months of March and April, 1951. The plates at SP were exposed in two lots; one lot was exposed in June, 1951 when they were all 110  $\mu$  G5 and the other lot was exposed in October and November, 1951 when they were 100  $\mu$  G2 and 100  $\mu$  G5. The plates at KL were placed in cardboard containers, surrounded by corrugated board in a light plywood box. The plates at SP were placed in airtight tin containers, the tin was then surrounded by corrugated board and finally placed in a light plywood box. With this packing the plates remain fixed in position, no light goes through the packing and at the same time the mass of material surrounding the plates is less than about 5 gm/cm<sup>2</sup>. During each exposure some plates were kept vertical, some horizontal and some inclined at an angle of  $60^\circ$  with the horizontal. The plates in each lot were manufactured at the same time and were processed together by a special technique developed in this laboratory (Dixit, 1952). They were scanned by the same scanner. This precaution enabled us to eliminate all personal differences. The differences observed by us in the different plates could, therefore, be attributed to their different dispositions.

The scanning was done with a binocular microscope using an objective 20X and eyepiece 8X. This objective gave a good depth of focus, and enabled us to note all the events and at the same time maintained a reasonable scanning speed. Details of events were then examined at higher magnifications including oil immersion, which was also used for estimating the nature and the energies of the particles by the standard method (Fowler, 1950). In the detailed scanning which has been carried out every possible event is noted. Thus all single tracks longer than 100 microns have been noted. Similarly all stars have been noted. Only those stars have been excluded which could obviously be regarded as radioactive. Stars with less than six prongs are definitely considered as due to cosmic rays when the star has at least one prong whose length is greater than 60 microns. Cosmic ray stars are noted as 2C, 3C, etc. The prefix 2 indicating the number of prongs. Stars with less than six prongs, when none of the prongs is longer than 60 microns, are classified as definitely radioactive when a short recoil track is visible in the neighbourhood of the star. Such stars are not noted. Stars with less than six prongs, which are not accompanied by recoils could be due either to radioactive impurities or cosmic rays. Such stars are noted as 3R, 4R, etc. The prefixes 3, 4, etc., indicate the number of prongs in any star.

The detailed scanning undertaken enabled us to detect in some plates pairs of parallel tracks. They are noted as parallel pairs (P.P). Statistics of the process compels us to regard these events as associated and a better nomenclature would be to call them associated particle pairs (A.P.P.).

Scanning of a reasonable amount of emulsion from each of the three batches mentioned above is completed and the results of the scanning are shown in Table I. The events given in Table I will be discussed separately as singles, parallel pairs, stars and rare star events.

#### SINGLES

In the group of plates SP1 which are all G5 and exposed at the same time the observed differences could reasonably be explained as due to their being exposed in different directions. The number of thin singles longer than 100 microns is almost identical for the vertical and the inclined plates. The difference is less than one per cent in 1774/ml. day, whereas in the horizontal plates this number is less by about 19%. The number of thick singles longer than 100 microns on the other hand is almost identical for the inclined and the horizontal plates. The difference here is also less than one per cent in 713/ml. day. The corresponding number of thick singles in the vertical direction is less by about 9%.

The tracks classified as 'thick' by us have a grain density greater than 160 grains per 100 microns and are similar to the 'Black' tracks of Camerini et al (1951). The nature of the majority of these tracks could not be identified. But where such an identification is possible, and this is the

TABLE I

	SP <sub>1</sub> , vertical, G <sub>5</sub>		SP <sub>1</sub> , inclined, G <sub>5</sub>		SP <sub>1</sub> , horizontal, G <sub>5</sub>		SP <sub>2</sub> , inclined C <sub>2</sub>		KL, horizontal G <sub>5</sub>	
	Number observed	Number in ml. per day	Number observed	Number in ml. per day	Number observed	Number in ml. per day	Number observed	Number in ml. per day	Number observed	Number in ml. per day
Singles > 100 $\mu$ (thin)	24, 615	1, 759	24, 626	1, 774	19, 791	1, 434	7, 539	479	4, 818	241
Singles > 100 $\mu$ (thick)	9, 009	644	9, 892	713	9, 811	710	979	56.7	2, 853	143
Singles > 3000 $\mu$	35	2.6	27	2	45	3.3	4	0.3	17	1
Parallel Pairs	15	1.1	37	2.7	nil	...	nil	...	1	...
3 R	163	12.0	110	8.0	253	19.0	132	8.4	291	14.5
4 R	175	12.1	127	9.1	225	15.3	276	17.2	236	11.8
5 R	38	2.7	63	4.5	45	3.3	20	1.3	75	3.7
6 R	2	..	1	..	2	...	nil	...	2	...
2 C	90	6.4	90	6.5	121	8.8	51	3.8	86	4.3
3 C	52	3.7	44	3.1	74	5.4	33	2.4	35	1.7
4 C	41	2.9	47	3.4	55	4.0	27	1.7	24	1.2
5 C	23	1.6	28	2.0	20	1.4	12	1.1	24	1.2
6 C	7	0.5	12	0.9	14	1.0	7	0.5	3	0.1
7 C	6	0.4	11	0.8	12	0.9	2	0.1	3	0.1
8 C to 12 C	17	1.2	15	1.1	20	1.4	7	0.5	10	0.5
> 12 C	5	0.4	4	0.3	10	0.7	3	0.2	2	0.1

case in about 5% of the observed number of tracks, it was found that half of them were protons of energy between 10 MeV and 20 MeV and the remaining mostly  $\alpha$ -particles of energy between 20 MeV and 37 MeV.

The majority of the tracks classified as 'thin' by us have a grain density between 60 and 160 grains per 100 microns; they are thus similar to the 'Grey' tracks of Camerini et al (1951). Here also the nature of the tracks could be identified for only about 5% of the particles. Out of these which could be identified about 80% were protons of energy between 50 MeV and 100 MeV; 5% were  $\pi$ -mesons of energy between 20 MeV and 30 MeV. The nature of the remaining 15% could not be identified either as a  $\pi$  or a P because their mean angle of scattering  $\alpha$  is  $< 0.024^\circ/100 \mu$ .

The number of thick and thin singles observed in the 2nd lot of plates SP<sub>2</sub> exposed at the same place, which in scanning has been chosen as C<sub>2</sub>, is considerably less. This happens because the high energy particles cannot be recorded by the C<sub>2</sub> plates. In general, it may be observed from the above description that the thin singles of the G<sub>5</sub> plates noted by us will not be recorded by the C<sub>2</sub> plates and thus the number of thick and thin singles longer than 100 microns recorded by the C<sub>2</sub> plates cannot be greater than the corresponding number of thick singles recorded on the G<sub>5</sub> plates. Table I will show that this is borne out by our observations.

A comparison of the number of these tracks observed in G<sub>5</sub> horizontal plates at SP and KL, shows that a difference of height of about 2800 ft or air thickness of about 70 gr/cm<sup>2</sup> reduces their numbers in the ratio of about 6:1 for thin singles and 5:1 for thick singles. The reduction for the C stars in the same plates is about 2.4:1.

These observations lead us to conclude that the majority of the long single tracks observed are high energy protons, some of them may be mesons. The number of these protons travelling in the vertical direction is slightly greater than those travelling in another (say horizontal) direction. These particles appear to be produced by some radiation which is about twice as absorbable as the star-producing radiation.

The nature of the extra long singles could be identified in almost all cases. About 50% of them were due to protons, about 20% due to mesons, and the rest could be either due to P or  $\Pi$ . It is difficult to say definitely for some of these tracks, specially those which did not end in emulsion, whether they are due to a  $\pi$ -meson or a  $\mu$ -meson. It is worthwhile noting that the energy of some of these protons corresponding to extra long tracks is greater than 100 MeV.

#### ASSOCIATED PARALLEL PAIRS

We have observed in all 53 pairs of parallel tracks. They consist of two thin (grey) single tracks parallel to one another. The length of the two parallel tracks, their distance apart and

their grain counts, differ for the different pairs (figure 1). In general, it can be said that their lengths vary between  $600\mu$  and  $1500\mu$  and their separation

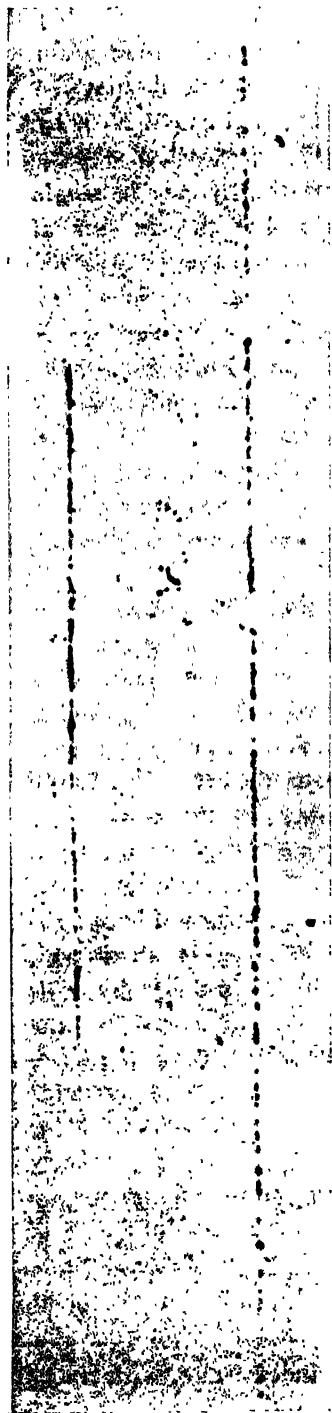


FIG 1

Two parallel tracks, 80 microns apart, with grain density of  $35 \pm 1$  per 100 microns. Each corresponds to a singly charged particle, a proton or a meson. Energy greater than 300 MeV or 60 MeV respectively.

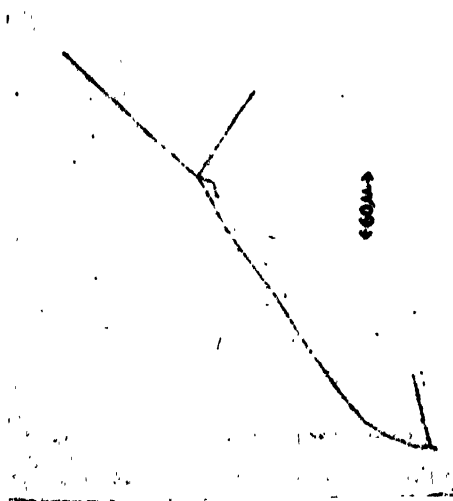


FIG 2

A negative  $\pi$ -meson produced in a nuclear fission, produces another fission.

from about  $5\mu$  to  $100\mu$ . These pairs are orientated in all directions, on the plate. The tracks are quite straight and parallel, their mean angle of scattering is less than  $0.02^\circ/100$  microns, and it is difficult to say whether they are produced by protons or mesons ( $\pi$  or  $\mu$ ). In general, their grain count is between 50 to 80 grains per 100 microns. The tracks thus may be produced either by protons of energy between 100 MeV and 200 MeV or by mesons ( $\pi$  or  $\mu$ ) of energy 30 MeV to 60 MeV.

These pairs of particles could either be associated or they may be single tracks which are accidentally parallel. Table I shows that the number of these parallel pairs does not depend on the total number of singles observed as would be the case if they are accidentally parallel. Their number is largest: being 37, for the inclined G5 plates at SP, but the inclined C2 plates at the same place do not show any such pair. Similarly the number of parallel pairs observed is 15 in the vertical plates and none in the horizontal plates; although the number of singles observed in the two cases is comparable and it is also comparable with the number of singles observed in the inclined plates. These observations and the statistics of the process lead us to assume that these pairs of parallel tracks are due to associated penetrating particles. (A.P.P.)

Associated pairs of penetrating particles have been observed before by Braddick and Hensby (1939) underground using a cloud chamber and by Braddick, Nash and Wolfendale (1951) in a cave with counter controlled cloud chamber. In an observation with a total sensitive time of 480 hours, and 2400 photographs, they observed 18 associated penetrating particles produced externally. They are inclined to attribute the events as due to pairs of mesons (probably  $\mu$ -mesons) produced in the rock of the cave. Our experiments were done neither underground nor in a cave, but on the top of a peak 14,300 ft. high in the Himalayas. But as it happens, towards the north of this peak (separated by a small gorge) at a distance of about 100 metres are still higher peaks. The magnetic dip at this place is about  $45^\circ$ . It is thus quite possible that the  $\mu$ -meson pairs produced in the rocky walls (as in Braddick's experiments) towards the north, are influenced by the magnetic field in their path and arrive as parallel penetrating particles. It is difficult to give a more definite interpretation from the data available to us at present, but we are also inclined to accept Braddick's view, 'It is likely that the production of a pair of A.P.P. is an event of more elementary type than the production of a penetrating shower.' More experiments are being carried out to ascertain the cause of the penetrating parallel pairs of particles.

#### STARS

As mentioned earlier, we have definitely excluded stars with tracks up to six as radioactive, when all of them are less than 60 microns and when a recoil track is seen in the neighbourhood. The recoil track is an alpha



track, which is probably emitted by the recoiled nucleus. But when only one of the criteria, namely, all the tracks up to six are less than 60 microns in length is satisfied and the other that a recoil is present in the neighbourhood is not satisfied, we have noted the number of such stars by the letter R, the prefix before R indicates the number of tracks in the star. The stars denoted by the letter C are such that at least one track is longer than  $60\mu$  and they are certainly due to cosmic radiation. The number before C indicates as usual the number of tracks in the star. Out of these genuine cosmic ray stars, specially those up to 6 C, a fairly large number is made up of stars where all tracks except one are very short, some of them as short as 10 or  $20\mu$ . In such a case it is quite likely that if this single long track had left the evaporating nucleus in some other direction only a part of it would have been recorded on the plate and the star would have been easily mistaken for a radioactive star and normally excluded. Such a star, not being really due to a radioactive inclusion, is not likely to show a recoil track in the neighbourhood. To avoid the possibility of the exclusion of such stars, we have included them in Table I, and have shown them as R. Thus it will be seen that some of the stars included as R may be really C while others may be really due to a radioactive inclusion. Having already excluded radioactive stars which showed a neighbouring recoil track, the

TABLE II

	Number in ml per day	
	R	C
SP <sub>1</sub> vertical G <sub>5</sub>	20.8	17.1
SP <sub>1</sub> inclined G <sub>5</sub>	21.6	18.1
SP <sub>1</sub> horizontal G <sub>5</sub>	38.6	23.6
SP <sub>2</sub> inclined C <sub>2</sub>	26.0	10.3
KL horizontal G <sub>5</sub>	30.0	9.2

number of radioactive stars included in R will be small. To ascertain the true fraction of the cosmic ray stars included in R, two methods of procedure are permissible. In the 1st one we could consider a disposition of plates as in SP<sub>1</sub>, vertical, inclined and horizontal. All the plates are manufactured from the same emulsion, and are otherwise treated identically. The number of true radioactive stars per ml. per day, which only depends on the radioactive impurities present, should, therefore, be identical for all the three dispositions of the plates. Table II clearly shows that neither the number of R stars nor the number of C stars is identical in the three divisions of the group SP<sub>1</sub>. This is probably due to our exclusion of some

genuine radioactive stars by the criterion of recoil tracks. This method, therefore, will not enable us to find out what fraction of R could be considered of cosmic ray origin.

To calculate the number of truly radioactive stars in ml. per day we must divide the total number of such stars by the total time from the date of manufacture to the date of processing. In Table I we have divided the total number of R-stars, by the time of exposure at high altitudes, to obtain the number in ml. per day. Such a procedure is reasonable for the cosmic ray stars but it will result in the number of radioactive stars appearing too large. We have, however, followed this procedure as it better enables us to estimate the order of magnitude of the C-star part included in R-stars.

The second method consists in assuming that the number of cosmic ray stars which should be observed per ml. per day at the height of KL (11,500 ft.) is about 17.0. This number is arrived at from the finding of Harding quoted by Thomson and Hodgson (1951), that the number of stars observed at Jungfrau is 16.2 per ml. per day. Thus we write that the true number of cosmic ray stars observed at KL is equal to  $17 \approx 9.2 + 30.0 \times f$ ; which gives  $f = \frac{1}{4}$  or about 25% of the R stars must be due to cosmic rays at this altitude for the particular plates employed. Assuming this number and an absorption length of about 120 gr./cm<sup>2</sup> for the star producing radiation, the number of cosmic ray stars which should be observed in similarly situated similar plates at SP should be about 30. This gives a value of  $\frac{1}{6}$  for the corresponding fraction for this set of plates and we write  $30 \approx 23.6 + 38.6/6$ . If we assume the same value of the fraction  $f$  for the inclined and vertical plates the number of C stars comes out as 21.6 for the vertical or the inclined plates. If we assume that the stars are produced by a cascade process by a vertical radiation, then the majority of the tracks of the stars will lie in a plane perpendicular to the direction of the radiation, namely, the horizontal direction. Thus if a cascade is assumed for the formation of stars, fewer stars are likely to be missed when the plates are horizontal than when they are vertical or inclined. The value of  $f$  therefore, will be larger for these two dispositions of the plates. Thus if we assume  $f = \frac{1}{2}$  for the inclined and vertical plates then C comes out as 28.9 and 30.5 respectively. These values are close enough to the value 30.0 obtained for the horizontal plates.

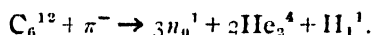
The probability of missing energetic particles is greater for the C<sub>2</sub> plates than for the G<sub>5</sub> plates. Thus it would be reasonable to expect that the values of  $f$  are larger for the C<sub>2</sub> plates than for the G<sub>5</sub> plates. This is also borne out by the observation. It will be seen that a value of 30.0 will be obtained for the SP<sub>2</sub> inclined C<sub>2</sub> plates by taking  $f = 2/3$ .

The calculations made above and the discussion will indicate that by adopting the normal criterion of excluding stars up to sixfold when none of the tracks is longer than 60μ, we are liable to exclude a fair number

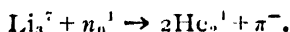
of stars which may be really due to cosmic rays. This fact must, therefore, always be kept in view, and the required corrections made while estimating the number of genuine cosmic ray stars. Further, in the light of this discussion it appears that the number of genuine cosmic stars which are likely to be excluded is least, when thick (15 emulsions are used in a horizontal direction.

#### RARE STAR EVENTS

Figure 2 shows a rare event, namely a meson ( $\pi$ ) produced in a nuclear fission, giving rise to another nuclear fission. The figure actually shows a threefold star and a fourfold star with a common track between them. At the fourfold the two long straight tracks are due to  $\alpha$  particles, the shorter one is due to  $H^1$  and the fourth one is due to a  $\pi$  meson. At the threefold the two straight tracks are also due to  $\alpha$ -particles, and the curved track is the same  $\pi$ -meson track. The  $\alpha$ -particle and the  $H^1$  tracks come to an end in the emulsion and their nature was identified by the grain count and their energies determined from their ranges. The  $\pi$  meson track was identified from the grain count and the Coulomb scatter. The fourfold thus corresponds to the fission of  $C_6^{12}$  according to the following scheme proposed by Perkins (1949).



It is, however, not possible to give definitely the fission reaction corresponding to the threefold, but it may be



For a reaction like this the kinetic energy of the neutron will have to be greater than 137 MeV. For all practical purposes then, such an equation indicates that almost the entire kinetic energy of the neutron is converted into the mass of a  $\pi$ -meson. Such a reaction where almost the entire kinetic energy of a very fast nucleon is converted into a particle by interaction with a light nucleus, has a very low probability. In view of this low probability we are compelled to consider an alternative process (Armenteros et al, 1951), namely,



In this reaction the  $V_0^1$  particle could be moving very slowly and interacting with the lithium nucleus. A knowledge of the mass of  $Li_3^7$  and the masses and the kinetic energies of the particles on the R.H.S. gives us the mass of  $V_0^1$  particle as 2120 electron masses. This is a reasonably good value for the mass of the  $V$  particle.

We have observed 3 more similar threefolds produced by cosmic rays. Each of these threefolds shows 2 straight dark tracks due to  $\alpha$ -particles and one curved track, showing Coulomb scatter, produced by a meson. In these three cases the meson does not produce a further nuclear disintegration

as mentioned above. In two cases, however, the  $\pi$  meson is able to produce short recoil tracks (Perkins, 1949; Harding, 1951) about  $5\mu$  and  $10\mu$  in length. The  $\alpha$ -particles in these two cases have a much longer range,  $590\mu$  and  $95\mu$  in the first case which gives for the mass of  $V_0^1$  a value 2185 electron masses, and  $480\mu$  and  $840\mu$  in the second case which gives the value of 2227 electron masses. In the third event we have two  $\alpha$ -particles of ranges  $40\mu$  and  $60\mu$  and a  $\pi$ -meson of range  $550\mu$ . But in this case the  $\pi$ -meson neither produces a star nor a recoil. Even in this case we have assumed that the reaction is produced by a  $V_0^1$  particle and calculated its mass which comes out as 2131 electron masses.

The four cases we have probably observed of a  $V$ -particle producing a disintegration of a lithium nucleus, giving us  $\alpha$ -particles and a meson, represent certainly a small number but it is comparable with the number observed by Armenteros, et al (1951) who observed only 12 events which permitted, accurate measurement. Our mean value of the mass of the  $V_0^1$  particle, 2166 electron masses, is also comparable with their value  $(2203 \pm 12) m_e$ .

Our interpretation of these rare events is based on two things; first is the observation of four  $^3\text{C}$  stars, each one with two tracks of  $\alpha$ -particles and one  $\pi$ -meson track. In one event the  $\pi$ -meson produces a further disintegration of a light nucleus; in two events the  $\pi$ -meson produces recoil tracks and in one event the  $\pi$ -meson does not produce any visible event. Four events is rather a small number for drawing statistical conclusions. But we should like to compare our findings with the following conclusion of Perkins (1949). "Most of the multi-prongstars due to  $\pi^-$ -mesons arise from the light nuclei. In about half the disintegrations following capture of a  $\pi^-$ -meson by a heavy nucleus, a single proton or alpha particle is emitted, and most of the remainder lead to ejection of neutrons only. Thus about one quarter of all the  $\pi$ -mesons do not produce a visible event on coming to rest in the emulsion". Our observation and inferences were based on the measurements of the grain count and the Coulomb scatter for the tracks of the threefolds, in addition, our observations with the four  $\pi^-$ -mesons agree in a general way with those of Perkins. This leads us to assume that the threefolds have been correctly interpreted by us. The second thing is to consider the plausible agent which could have produced the disintegration of lithium. The two agents are a very fast neutron whose kinetic energy is almost entirely converted into a  $\pi$ -meson and a slowly moving  $V_0^1$  particle whose mass is split up inside the compound nucleus into two parts—one part equal to the nucleonic mass and the other part equal to the mass of a  $\pi$ -meson. The probabilities of both processes are small, but that of the neutron process is smaller than the  $V$ -particle process by a factor which is at least equal to  $1/137$ , the fine structure constant which appears in the calculations of such probabilities.

We should like to point out that our observations are made at 14,300 ft, with plates exposed for about 30 days and in the light of the work done

by Armenteros, et al (1951), it would not be unreasonable to expect the detection of four  $V$  particles by photographic plates. Further, the two alternative modes suggested for the disintegration of the lithium nucleus lead us to believe that the  $V_0^1$  particle may be looked upon as the excited state of the neutron. Indeed it is interesting to note that such a conclusion has been arrived at by Sachs (1951) from purely theoretical considerations.

## REFERENCES

- Armenteros, R., Barker, K. H., Butler, C. C. and Cachon, A., 1951, *Phil. Mag.*, **42**, 1113.  
 Braddick, H. J. J., Nash, W. F. and Wolfendale, A. W., 1951, *Phil. Mag.*, **42**, 1277.  
 Braddick, H. J. J. and Hensby, G. S., 1939, *Nature (Lond)* **144**, 1612.  
 Camerini, V., Davies, H. J.; Fowler, P. H.; Franzinetti, C.; Muirhead, H.; Lock, W. O., Perkins, D. H. and Yekutieli, G., 1951 *Phil. Mag.*, **42**, 1241.  
 Dixit, K. R., 1952, (in course of publication)  
 Fowler, P. H., 1950, *Phil. Mag.*, **41**, 169.  
 Harding, J. B., 1951, *Phil. Mag.*, **42**, 651.  
 Perkins, D. H., 1949, *Phil. Mag.*, **40**, 651.  
 Sachs, R. G., 1951, *Phys. Rev.*, **84**, 305.  
 Thomson, G. P. and Hodgson, P. E., 1951, *Phil. Mag.*, **42**, 978.

## HIGH MULTIPLICITY STATES IN DIATOMIC MOLECULES

By K. SURYANARAYANA RAO

PHYSICS DEPARTMENT, ANDHRA UNIVERSITY, WALT AIR

*(Received for publication, December 3 (1951))*

**ABSTRACT.** Adopting Hill and Van Vleck's method, expressions for the energy levels of electronic states of higher multiplicities belonging to general intermediate case have been derived.

## INTRODUCTION

In a previous paper the author (1951) has calculated the rotational energy levels of  $^3\Sigma$  and  $^6\Sigma$  using the methods of Van Vleck and Kramers. This paper is a continuation of the work and gives the calculations carried out for the rotational energy levels of electronic states belonging to any general intermediate case of coupling with multiplicities ranging from five to seven. Hill and Van Vleck's (1928) procedure for general intermediate case has been used. This method has been applied by Budo (1935) to the calculations in the case of a  $^3\Pi$  state and the solutions are expressed as power series of certain parameter by a method applicable only to a cubic equation. The  $^1\Pi$  state has been treated by Brandt (1936) and the quartic equation obtained in  $^4\Pi$  has been solved by him by a general method which is applicable to an equation of any degree that may be encountered in general intermediate case states. As, however, the application of this method to states of higher multiplicities involves very cumbersome calculations, only approximate formulae have been worked out for states with multiplicity five, six and seven.

## THEORY

The method due to Hill and Van Vleck, which has been adopted in these calculations, can be briefly outlined as follows: Starting with case (b) we work back to case (a), that is, the interaction between the spin and electronic orbital angular momenta is first neglected, then the Hamiltonian function representing this interaction is set up, and the method of perturbations of the new quantum mechanics is taken recourse to to determine the eigenvalues of the energies in the general case. The particular form of the perturbing Hamiltonian function which is used is the ordinary 'cosine' expression.

$$H_p = A(\delta_k.S) = A(\sigma_{kx}S_x + \sigma_{ky}S_y + \sigma_{kz}S_z)$$

The matrix elements of  $H_p$  have been determined by Hill and Van Vleck by a method from the classical mechanics which is also valid in the new

quantum mechanics. It is to be noted that  $H_p$  can have elements involving transitions for which  $\Delta K = 0, \pm 1$ . The matrix elements have been derived to be :

$$H_p(n, \Lambda, K; n, \Lambda, K+1) = \frac{A\Lambda}{2} \left[ \frac{\{(K+1)^2 - \Lambda^2\}}{(K+1)^2(2K+1)(2K+3)} \right]^{\frac{1}{2}} \\ \times [\{J+K+1\}(J+K+2) - S(S+1)] \{S(S+1) - (J-K)(J-K-1)\}^{\frac{1}{2}}$$

and the diagonal elements are given by

$$H_p(n, \Lambda, K; n, \Lambda, K) = A\Lambda^2 [\{J(J+1) - K(K+1) - S(S+1)\} / 2K(K+1)]$$

To the above diagonal terms must be added diagonal terms concerned with the nuclear rotational energy. Thus  $H = H_r + H_p$ , where  $H_r$  is the diagonal matrix

$$H_r(n, \Lambda, K; n, \Lambda, K) = [K(K+1) - \Lambda^2] (h^2 / 8\pi^2 I)$$

The eigen values of the problem are given by the roots of the determinantal equation

$$\begin{vmatrix} H(K_1; K_1) - W & H(K_1; K_1-1) & \dots & \dots & \dots & \dots \\ H(K_1; K_1-1) & H(K_1-1; K_1-1) - W & \dots & \dots & \dots & \dots \\ \dots & \dots & \dots & \dots & \dots & \dots \\ \dots & \dots & \dots & \dots & \dots & \dots \\ \dots & \dots & \dots & \dots & \dots & H(K_2; K_2) - W \end{vmatrix} = 0$$

where  $K_1$  and  $K_2$  represent the largest and smallest values respectively of  $K$  corresponding to a given set of values for  $J$  and  $S$ , that is,  $K_1 = J+S$  and  $K_2 = |J-S|$ . The values of  $W$ , which satisfy the above determinant, give the energy levels for the complete transition stage from case (b) to case (a).

## CALCULATIONS AND RESULTS

*Quintet States.* For quintet states  $S=2$  and  $K_1 = J+2$ ;  $K_2 = J-2$ . The determinantal equation is of the form

$$\begin{vmatrix} a-W & a_1 & 0 & 0 & 0 \\ a_1 & b-W & b_1 & 0 & 0 \\ 0 & b_1 & c-W & c_1 & 0 \\ 0 & 0 & c_1 & d-W & d_1 \\ 0 & 0 & 0 & d_1 & e-W \end{vmatrix} = 0$$

where  $A/B=Y$ ,  $B=h^2/8\pi^2 l$  and

$$a=B\left[(J+2)(J+3)-\Lambda^2-\frac{2Y\Lambda^2}{J+2}\right]$$

$$b=B\left[(J+1)(J+2)-\Lambda^2-\frac{Y\Lambda^2(J+4)}{(J+1)(J+2)}\right]$$

$$c=B\left[(J+1)-\Lambda^2-\frac{3Y\Lambda^2}{J(J+1)}\right]$$

$$d=B\left[(J-1)J-\Lambda^2+\frac{Y\Lambda^2(J-3)}{(J-1)J}\right]$$

$$e=B\left[(J-2)(J-1)-\Lambda^2+\frac{2Y\Lambda^2}{(J-1)}\right]$$

and

$$a_1^2 = \frac{2A^2\Lambda^2J\{J+2\}^2-\Lambda^2\}}{(2J+3)(J+2)^2} ; b_1^2 = \frac{3A^2\Lambda^2(2J-1)(J+2)\{J+1\}^2-\Lambda^3\}}{(2J+1)(J+1)^2(2J+3)}$$

$$c_1^2 = \frac{3A^2\Lambda^2(J-1)(2J+3)\{J^2-\Lambda^2\}}{(2J-1)J^2(2J+1)} ; d_1^2 = \frac{2A^2\Lambda^2(J+1)\{(J-1)^2-\Lambda^2\}}{(2J-1)(J-1)^2}$$

The above determinantal equation yields the following fifth degree algebraic equation in  $W$

$$\begin{aligned} & (a-W)(b-W)(c-W)(d-W)(e-W) - a_1^2(c-W)(d-W)(e-W) \\ & - b_1^2(d-W)(e-W)(a-W) - c_1^2(e-W)(a-W)(b-W) - d_1^2(a-W)(b-W)(c-W) \\ & + a_1^2c_1^2(c-W) + a_1^2d_1^2(c-W) + b_1^2d_1^2(a-W) = 0. \end{aligned}$$

The roots of this equation, correct to a first order of approximation, are :

$$F_5(J) = a - \frac{a_1^2}{b-a} ; F_4(J) = b - \frac{a_1^2}{a-b} + \frac{b_1^2}{b-c} ; F_3(J) = c - \frac{b_1^2}{b-c} + \frac{c_1^2}{c-d}$$

$$F_2(J) = d - \frac{c_1^2}{c-d} + \frac{d_1^2}{d-e} ; F_1(J) = e - \frac{d_1^2}{d-e}$$

The approximation used in solving this equation is that  $a_1^2, b_1^2, \dots$  can be regarded as small compared to  $a, b, c, \dots$  because the highest power of  $J$  in both the numerator and the denominator of expressions for  $a_1^2, b_1^2, \dots$  is the same, so that they will be of the nature of a constant depending on  $A^2$ , whereas  $a, b, c, \dots$  are of the order of  $J^2$ . Therefore  $a_1, b_1, c, \dots$  can be regarded, to a first approximation, as the roots of the determinantal equation. The method of obtaining the above roots is given in the Appendix.



**Sextet States:** In the sextet states,  $S=5/2$  and  $K_1=J+5/2$  and  $K_2=J-5/2$  and the determinantal equation is

$$\begin{vmatrix} a-W & a_1 & 0 & 0 & 0 & 0 \\ a_1 & b-W & b_1 & 0 & 0 & 0 \\ 0 & b_1 & c-W & c_1 & 0 & 0 \\ 0 & 0 & c_1 & d-W & d_1 & 0 \\ 0 & 0 & 0 & d_1 & e-W & e_1 \\ 0 & 0 & 0 & 0 & e_1 & f-W \end{vmatrix} = 0$$

where

$$a = B \left[ (J+5/2)(J+7/2) - \Lambda^2 + \frac{5Y\Lambda^2}{2(J+5/2)} \right]$$

$$b = B \left[ (J+3/2)(J+5/2) - \Lambda^2 + \frac{Y\Lambda^2(3J+25/2)}{2(J+3/2)(J+5/2)} \right]$$

$$c = B \left[ (J+1/2)(J+3/2) - \Lambda^2 + \frac{Y\Lambda^2(J+19/2)}{2(J+1/2)(J+3/2)} \right]$$

$$d = B \left[ (J-1/2)(J+1/2) - \Lambda^2 + \frac{Y\Lambda^2(J-17/2)}{2(J-1/2)(J+1/2)} \right]$$

$$e = B \left[ (J-3/2)(J-1/2) - \Lambda^2 + \frac{Y\Lambda^2(3J+19/2)}{2(J-3/2)(J-1/2)} \right]$$

$$f = B \left[ (J-5/2)(J-3/2) - \Lambda^2 + \frac{5Y\Lambda^2}{2(J-2/2)} \right]$$

and

$$a_1^2 = \frac{5\Lambda^2 J \{ (J+5/2)^2 - \Lambda^2 \}}{4(J+2)(J+5/2)^2}; \quad b_1^2 = \frac{\Lambda^2 \Lambda^2 (2J-1)(2J+5) \{ (J+3/2)^2 - \Lambda^2 \}}{2(J+1)(J+3/2)^2(J+2)};$$

$$c_1^2 = \frac{9\Lambda^2 \Lambda^2 (J-1)(J+2) \{ (J+1/2)^2 - \Lambda^2 \}}{4J(J+1/2)^2(J+1)}; \quad d_1^2 = \frac{\Lambda^2 \Lambda^2 (2J-3)(2J+3) \{ (J-1/2)^2 - \Lambda^2 \}}{2(J-1)(J-1/2)^2 J}$$

$$e_1^2 = \frac{5\Lambda^2 \Lambda^2 (J+1) \{ (J-3/2)^2 - \Lambda^2 \}}{4(J-1)(J-3/2)^2}$$

and the approximate roots in this case are :

$$F_6(J) = a - \frac{a_1^2}{b-a}; \quad F_5(J) = b - \frac{a_1^2}{a-b} + \frac{b_1^2}{b-c}; \quad F_4(J) = c - \frac{b_1^2}{b-c} + \frac{c_1^2}{c-d};$$

$$F_3(J) = d - \frac{c_1^2}{c-d} + \frac{d_1^2}{d-e}; \quad F_2(J) = e - \frac{d_1^2}{d-e} + \frac{e_1^2}{e-f}; \quad F_1(J) = f - \frac{e_1^2}{e-f}$$

**Septet States:** In the septet states  $S=3$  so that  $K_1=J+3$  and  $K_2=J-3$  and the determinantal equation is of the form

$$\begin{vmatrix} a-W & e_1 & 0 & 0 & 0 & 0 & 0 \\ a_1 & b-W & b_1 & 0 & 0 & 0 & 0 \\ 0 & b_1 & c-W & c_1 & 0 & 0 & 0 \\ 0 & 0 & c_1 & d-W & d_1 & 0 & 0 \\ 0 & 0 & 0 & d_1 & e-W & e_1 & 0 \\ 0 & 0 & 0 & 0 & e_1 & f-W & f_1 \\ 0 & 0 & 0 & 0 & 0 & f_1 & f-W \end{vmatrix}$$

and those calculated according to this method is good for higher  $J$  values. For lower  $J$  values the differences are large.

#### APPENDIX

The approximate roots of the secular equations are calculated in the following manner. We illustrate the method adopted by taking the secular equation for quintet state. On expanding the determinant we get the following equation :

$$\begin{aligned} & (a-W)(b-W)(c-W)(d-W)(e-W) - a_1^2(c-W)(d-W)(e-W) - b_1^2(d-W) \\ & (e-W)(a-W) - c_1^2(c-W)(a-W)(b-W) - d_1^2(a-W)(b-W)(c-W) + a_1^2c_1^2 \\ & (c-W) - a_1^2d_1^2(c-W) + b_1^2d_1^2(a-W) = 0 \end{aligned} \quad \dots (1)$$

According to the approximation mentioned earlier  $a_1^2, b_1^2, c_1^2 \dots$  are assumed to be small compared to  $a, b, c \dots$  so that  $a, b, c \dots$  can be taken, as a first approximation, as the roots of the equation. Then we consider the equation

$$\begin{aligned} & (a-W)(b-W)(c-W)(d-W)(e-W) - \epsilon a_1^2(c-W)(d-W)(e-W) - \epsilon b_1^2(d-W) \\ & (e-W)(a-W) - \epsilon c_1^2(c-W)(a-W)(b-W) - \epsilon d_1^2(a-W)(b-W)(c-W) + \epsilon^2 a_1^2 c_1^2 \\ & (c-W) + \epsilon^2 a_1^2 d_1^2(c-W) + \epsilon^2 b_1^2 d_1^2(a-W) = 0 \end{aligned} \quad \dots (2)$$

where  $\epsilon$  is a parameter. We now assume a root of the equation in the form

$$W = \alpha_0 + \alpha_1 \epsilon + \alpha_2 \epsilon^2 + \dots$$

Substituting this value of  $W$  in equation (2) and equating to zero the constant term, the coefficient of  $\epsilon$ , the coefficient of  $\epsilon^2$ , ... we observe that

$$\alpha_0 = \begin{cases} a \\ b \\ c \\ d \\ e \end{cases} ; \quad \alpha_1 = \begin{cases} -\frac{a_1^2}{b-a} \\ -\frac{a_1^2}{a-b} + \frac{b_1^2}{b-c} \\ -\frac{b_1^2}{b-c} + \frac{c_1^2}{c-d} \\ -\frac{c_1^2}{c-d} + \frac{d_1^2}{d-e} \\ -\frac{d_1^2}{d-e} \end{cases} ; \quad \alpha_2 = \begin{cases} \dots\dots \\ \dots\dots \\ \dots\dots \text{ and so on.} \\ \dots\dots \\ \dots\dots \end{cases}$$

By putting  $\epsilon = 1$  we obtain the roots of equation (1). The same procedure is used for the other equations.

#### ACKNOWLEDGMENTS

The author is deeply indebted to Prof. K. R. Rao for his valuable guidance during this investigation. He also wishes to express his grateful

thanks to Prof. S. Minakshisundaram for his kind help in this work.

## REFERENCES

- Brandt, W. H., 1939, *Phys. Rev.*, **50**, 778.  
Budo, A., 1935, *Zetts. f. Phys*, **96**, 219.  
Hill, E. L. and Van Vleck, J. H., 1928, *Phys. Rev.*, **32**, 250.  
Nevin, T. E., 1938, *Phil. Trans. Roy. Soc*, **237**, 471.  
Rao Suryanarayana, K., 1952, *Ind. Jour. Phys.*, **26**, 17.



# ABSORPTION SPECTRUM OF *p*-CHLOROTOLUENE

By G. VISWANATH

DEPARTMENT OF PHYSICS, ANDHRA UNIVERSITY, WALT AIR

(Received for publication, February 15, 1952)

## Plates XI A-B

**ABSTRACT.** Ultraviolet absorption spectrum of *p*-chlorotoluene vapour has been photographed in the region 2818-2436Å. An interpretation for most of the observed band heads has been suggested. Excited state frequencies 796, 1044, 1068 and 1189 cm<sup>-1</sup> and difference frequencies 26, 57 and 100 cm<sup>-1</sup> have been newly proposed. A comparison of ground state frequencies with those of Raman shifts has also been made.

## INTRODUCTION

The spectra of vapours of mono-halogenated derivatives of toluene (*p*-chloro, *p*-fluoro and *p*-bromo) were first investigated by Tintea (1939). All the spectra were photographed on medium quartz spectrograph using under-water spark as continuous ultraviolet source. Following formulae were suggested by him for the absorption band heads of *p*-chlorotoluene.

$$\nu = 36297 + (p' - p_0) 1055 - 29 p_0 + (q' - q_0) 763 - 10q_0 + (r' - r_0) 215$$

$$\nu_0 - \nu'_0 = 89 \text{ cm}^{-1}$$

$$\nu' = 36208 + (p' - p_0) 1055 - 29 p_0 + (q' - q_0) 763 - 10q_0 + (r' - r_0) 215$$

The bands were divided into groups and families depending upon the values of  $(p' - p_0)$ ,  $(q' - q_0)$  and  $(r' - r_0)$ . The analysis of the spectrum was based on three frequencies 1055, 763 and 215 cm<sup>-1</sup> without distinguishing between ground and excited states. The distribution of the bands was interpreted on the basis of two different origins and no correlation with Raman frequencies was made. Intensity and wavelength data of all the bands that have been observed were also not given.

In this investigation the absorption spectrum of the substance in vapour phase was photographed under higher dispersion and an analysis of the bands is presented in the light of the recent theoretical advances made in the interpretation of the spectra of benzene and its derivatives.

The absorption of benzene vapour in the region 2600Å has been attributed to a forbidden transition  $A_{1g} - B_{2u}$  of  $D_{6h}$  symmetry class made allowed by the superposition of  $\nu_2^+$  vibration on one of the electronic levels. The reduction of symmetry of benzene molecules from  $D_{6h}$  to any lower symmetry by the substitution of one or more atoms or groups in the ring generally makes the forbidden transition an allowed one. A number

of mono-, di- and tri-substituted benzenes have been investigated by several workers, following the treatment of Sklar, Sponer and their collaborators in case of chloro and fluoro benzenes.

*p*-Chlorotoluene is a disubstituted benzene derivative. Substituents of the type Cl, Br, F, CH<sub>3</sub>, NH<sub>2</sub>, etc. possess an unshared pair of electrons in suitably oriented *p*-orbitals and the intense absorption spectra of substituted benzenes are attributed to the excitation of these electrons. In *p*-chlorotoluene one methyl group and one halogen atom are substituted in para positions of the benzene ring. The methyl group, though it has no unshared pair of electrons or the capacity to give rise to resonance effect by itself, can resonate with the ring due to the hyper conjugation creating the same effect on the ring as a Cl atom. Hence the spectrum can be understood as similar to that of *p*-dichlorobenzene, but as one characteristic of a different symmetry class.

#### EXPERIMENTAL

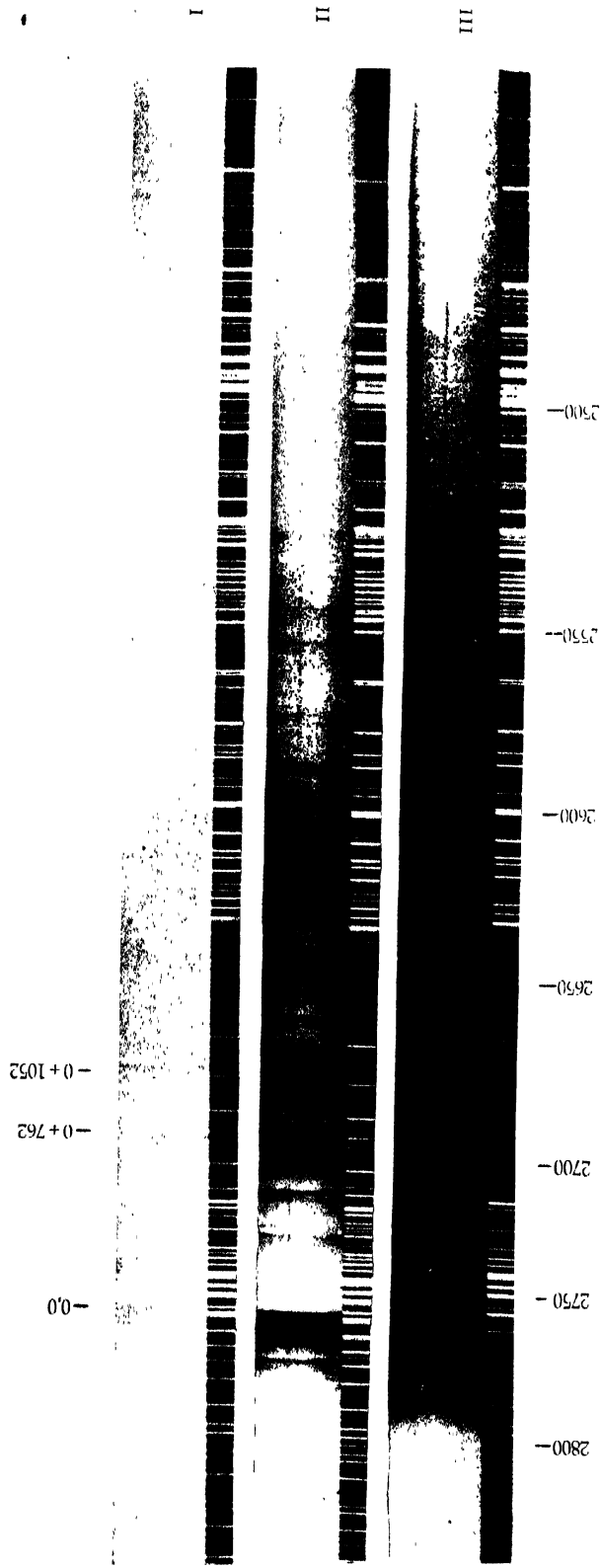
The experimental set-up is essentially the same as that used in the earlier investigations in this laboratory with similar spectra.

A pure sample of the substance was taken and subjected to fractional distillation. The fraction boiling between 160-161°C was used. Spectrograms were taken with the container of the liquid kept at the different temperatures ranging from -10° to 65°C and the path lengths varied from 5 cm to 50 cm. Low voltage Beckman hydrogen arc was the source of continuum. Hilger medium and Littrow quartz instruments were employed with the exposure times varying from 8 minutes to 4 hours. Photographs were taken under different conditions and reproduced in Plates XIA and B. No photo-decomposition was observed. The spectrum extends from 2800Å to 2436Å. All the bands are degraded towards the low frequency side of the spectrum and most of them possess a sharp violet edge. The spectrum is more similar to that of *p*-dichlorobenzene than either *p*-cresol or *p*-fluorotoluene and is much more complex than the spectra of other para-derivatives. About 100 bands have been measured.

#### ANALYSIS AND DISCUSSION

*p*-Chlorotoluene, which has the structure  $\text{H}_3\text{C}-\text{C}_6\text{H}_4-\text{Cl}$ , may be assigned to the symmetry class  $C_{2v}$ . (The symmetry types of this point group may be obtained from Herzberg, 1945).

The spectrum represents a transition from the totally symmetrical state  $A_1$  to a state antisymmetrical to the two-fold axis and symmetrical to the molecular plane  $B_1$ . This transition is an allowed one giving a strong 0-0 band; the spectrum, in general, should consist of a large number of bands arising from the excitation of totally symmetrical vibration. In addition to



Absorption spectrum of *p*-chlorotoluene (medium quartz spectrograms).

- I. 5 cm absorption column container at 0°C.
- II. 50 " " " at 5°C.
- III. 50 " " " at 55°C.

0 + 1189

0 + 1068

0 + 1052

0 + 1044

0 + 796

0 + 762

0 + 544

0 + 357

0.0.

0 - 380

2700

2750

2800

0 + 1190  
+ 1052

0 + 2 × 1052

0 + 762  
+ 11890 + 1052  
+ 762

2550—

2600—

2650—

Absorption spectrum of *p*-chlorotoluene ( Littrow spectrogram ).  
30 cm absorption column container at 26 C.



this allowed transition another forbidden transition made allowed by the excitation of the vibrations of the type  $\beta_1$  and  $\alpha_2$  may also give rise to a set of bands.

The intense band at  $36299\text{ cm}^{-1}$  which persists at the lowest vapour pressure conditions is taken as 0-0 band. To the less refrangible side of the 0-0 band the spectrum could be extended only up to  $2818\text{ \AA}$ . In this region bands corresponding to six ground state frequencies  $\nu''$  equal to 310 (w), 380 (w), 639 (vw), 700 (vw), 796 (vw) and 827 (vw) have been identified which agree closely with the known Raman shifts (Magat, 1936), 307 (8), 376 (12), 634 (5), 692 (1), 796 (12), 822 (2). These bands appear under different conditions on account of the difference in their Boltzman factors. Five other shifts are known from Raman effect data, namely, 1090 (12), 1177 (1), 1208 (7), 1303 (0), 1379 (4). These could not be observed as the spectrum did not extend far enough, in particular, the frequencies in the region of  $1000\text{ cm}^{-1}$  from 0-0 which may be expected to correspond to the carbon ring vibration.

The main part of the spectrum lying on the short wavelength side of the 0-0 band extends to  $2436\text{ \AA}$ . Bands in this region give vibrational levels associated with upper electronic states. The positions of all the observed bands together with the analysis suggested for each are given in Table I. An interpretation of most of the bands, with the exception of a few weaker ones, has been obtained with the following values of vibration frequencies of the upper state, namely,  $\nu' = 357$  (w), 544 (mst), 762 (mst), 796 (w), 1044 (mst), 1052 (mst), 1068 (w) and 1189. (mst). Strong and extensive progressions are absent in this spectrum; in this respect, the spectrum is more like that of *p*-dichlorobenzene than either of *p*-cresol or *p*-fluorotoluene. Combinations,  $0 + \nu'_1 + \nu'_2$  + etc., give the stronger bands rather than  $0 + n\nu'$ . The frequency 762 and the group in the vicinity of  $1000\text{ cm}^{-1}$  represent the most intense heads, the latter, in particular 1044 and 1052, may be mostly carbon vibrations corresponding to the strong Raman shifts 1090 and 1208. The frequencies 1189 and 1068 give rise to comparatively weaker bands, 1189 being stronger of the two. There was some doubt in considering the frequencies 1052 and 1044 as two independent frequencies since the spectrum reveals a number of doublets having an interval of about  $8\text{ cm}^{-1}$  units. But the existence of a number of combinations with 1044 and 1052 involving two quanta of these frequencies led to the consideration of these as independent frequencies.

Besides 762, another frequency of this order of magnitude, namely, 796 has been found to give rise to a number of combinations. It is difficult to interpret definitely the origin of these two frequencies. Since *p*-chlorotoluene may be expected to contain both C-CH<sub>3</sub> and C-Cl valence vibrations, 762 may represent one or the other of these. Tables II and III show the magnitudes of C-CH<sub>3</sub> and C-Cl vibrations in ground and excited states in different molecules.

TABLE I

Wavenumber and intensity	Assignment	Wavenumber and intensity	Assignment
35472 (vw)	0-827 (822R)	37725 (vw)	0+ 1068+327
495 (vvw)	0-2 × 380-57	756 (vw)	0+762+796-100
504 (vw)	0-795 (796R)	795 (w)	0+2 × 796-100
599 (vvw)	0-700 (692R)	809 (w)	0+2 × 357+796
647 (w)	0-2 × 310-27	818 (vw)	
660 (vw)	c-639 (634R)	855 (vw)	0+762+796
693 (vvw)	0-310-3 × 100	893 (w)	0+1052+544, (2 × 796)
750 (vvw)		907 (vw)	0+1068+544
816 (vvw)	0-380-100	38021 (vw)	0+2 × 1052-380
861 (vw)	0-380-57	083 (w)	0+1068+2 × 357
887 (vw)	0-310-100	114 (mst)	0+1052+762
919 (w)	0-380 (376R)	129 (w)	0+1068+762
958 (w)		150 (vw)	0+762+2 × 544
979 (w)		160 (w)	0+796+1068
989 (w)	0-310 (307R)	222 (w)	0+762+1189-26
36005 (mw)	0-3 × 100	251 (m)	0+762+1189
014 (w)	0-2 × 100-57-26		(2 × 796+357)
040 (mw)	0-2 × 100-57	295 (w)	0+1068+1052-100-26
070 (m)	0-2 × 100-26	383 (m)	0+2 × 1044
087 (mst)	0-100-2 × 57	399 (mst)	0+2 × 1052
104 (vw)	0-2 × 100	415 (vvw)	0+1068+1052,
115 (mw)	0-100-57-26		(1068+1044)
139 (m)	0-100-57	440 (vvw)	0+1052+2 × 544
172 (mst)	0-100-26	466 (vw)	
199 (mst)	0-100	529 (w)	0+1044+1189
212 (mst)	0-57-26	541 (mw)	0+1052+1189
242 (st)	0-57	572 (w)	
273 (st)	0-26	618 (vw)	0+2 × 762+796
286 (st)		39126 (vw)	0+2 × 1044+762-26
299 (vst)	0-0	172 (w)	0+2 × 1052+796-26
355 (vw)		184 (vvw)	0+1068+1052+762
418 (w)	0+762-639		(2 × 1044+796)
474 (vw)	0+544-310-57	299 (w)	0+1189+1052+762
627 (vw)		358 (vvw)	
648 (w)		379 (vvw)	
656 (w)	0+357	413 (vw)	
671 (vw)		561 (vvw)	
684 (vw)	0+762-380	40523 (vvw)	
718 (w)	0+796-380	41038 (vvw)	
758 (w)	0+544-57-26		
801 (mw)			
843 (mst)	0+544		
851 (vw)	0+1189-639		
972 (m)	0+1052-380		
37001 (mw)	0+762-57		
028 (mst)	0+762-26		
061 (mst)	0+762		
095 (w)	0+796		
106 (mw)	0+357+762-310		
134 (w)			
271 (w)			
340 (m)			
343 (mst)	0+1044		
351 (mst)	0+1052		
367 (w)	0+1068		
405 (vvw)	0+357+762,		
420 (vw)	(796+357-26)		
447 (w)	0+796+357		
488 (mst)	0+1189		
504 (w)	0+762+544-100		
540 (w)	0+796+544-100		
572 (w)	0+1044-357-100-26		
594 (mw)			
608 (mw)	0+762+544		

TABLE II

Frequencies assigned to C-CH<sub>3</sub> vibration

Molecule	$\nu''$	$\nu'$
Toluene	706 (st)	751 (m)
<i>o</i> -Xylene	740	
<i>m</i> -Xylene	744	
<i>p</i> -Xylene	750	708
1 : 2 : 4 trimethyl benzene	754	711
1 : 3 : 5 trimethyl benzene	575	555 (st)

TABLE III

Frequencies assigned to C-Cl vibration

Molecule	$\nu''$	$\nu'$
Chlorobenzene	702 (st)	665 or 726 (weak)
<i>o</i> -Dichlorobenzene	658	Could not be traced
<i>m</i> -Dichlorobenzene	666	Could not be traced
<i>p</i> -Dichlorobenzene	751 (st)	728 (st)
1 : 2 : 4 trichlorobenzene	676	629
1 : 3 : 5 trichlorobenzene	375	369

A comparison with the above data would indicate the probable assignment of 762 as C-Cl and 796 as C-CH<sub>3</sub> vibration.

The two other frequencies 544 and 357 may next be considered. 554 represents a much stronger head than 357. Previous work on substituted benzene spectra has well established the existence usually of two components from the degenerate 606  $\epsilon_g^+$  vibration of benzene, one totally symmetrical and the other nontotally symmetrical. The nontotally symmetrical vibration in most of the spectra due to  $\epsilon_g^+$  splitting in the ground state usually has a value close to 600 cm<sup>-1</sup>. The 634 vibration in Raman effect may represent the nontotally symmetrical component and it may be associated with frequency 544 cm<sup>-1</sup> in excited state.

Another feature of the spectra of benzene derivatives is the recurring pattern of small frequency differences consisting of groups of bands on the longer wavelength side of some of the main bands. Although a convincing explanation of these is not given, the bands are usually considered as  $\nu$ - $\nu$

transitions. In *p*-chloro toluene three such frequencies have been noticed, which are 26, 57 and 100. It may be of some significance to note that the differences between 1090 and 1068, 827 and 796, 795 and 762 and 380 and 357 are 22, 31, 33, and 23 respectively.

#### ACKNOWLEDGMENTS

The author is highly grateful to Prof. K. R. Rao for his kind guidance and interest in the work. The author acknowledges his thanks to the UNESCO for information regarding Tintea's data in the form of microfilm.

#### REFERENCES

- Herzberg, G , 1945, *Infra red and Raman spectra*, p. 106.  
Magat, M., 1936, *Numerical data on Raman effect*, p. 77.  
Tintea, H., 1939, *Bull. Sect. Sci. Acad. Roum.*, **21**, 219.

# PSEUDOSCALAR MESON FIELD AND THE SCATTERING OF FAST NEUTRONS BY PROTONS

By N. C. SIL

DEPT. OF THEORETICAL PHYSICS, INDIAN ASSOCIATION FOR THE CULTIVATION OF SCIENCE,  
CALCUTTA

(Received for publication, April 9, 1952)

**ABSTRACT.** In this paper the differential cross sections for the neutron-proton scattering as calculated on the basis of the symmetrical, Serber's and charged combinations of pseudoscalar meson field with pseudovector interaction have been compared with recent experimental findings. The effect of the elimination of the contact potential ( $\delta$ -function type) and the influence of the tensor force terms upon the differential scattering cross section have been investigated.

## INTRODUCTION

The trends of present experiments involving mesons in interaction with nucleon indicate that the  $\pi$ -meson which is responsible for the nuclear force, is to be described by the pseudoscalar theory. The comparison of the cross section for the production of  $\pi^+$ -meson by proton-proton collision with that for the inverse process of the absorption of  $\pi^+$ -meson in deuteron (Durbin, Loar and Steinberger, 1951 and Clark, Roberts and Wilson, 1951) supports the spin value of the  $\pi^+$ -meson to be zero. As predicted by Yang (1950) and experimentally corroborated by Steinberger, Panofsky and Steller (1950), the process of decay of the neutral  $\pi^0$ -meson into two  $\gamma$ -rays rules out the value 1 for its spin; the fact that the cross section for the production of  $\pi^0$ -meson is very small, as compared to that for the production of the  $\pi^+$ -meson, favours the pseudoscalar nature of the  $\pi^0$ -meson (Chew, Goldberger, Steinberger, and Yang, 1951 and Moyer, Madey *et al*, 1951). Comparing the various competitive reactions (Panofsky, Aamodt and Hadley, 1951) in the capture of the negative  $\pi^-$ -meson by deuteron, the scalar nature of the  $\pi^-$ -meson may be ruled out with good certainty (Marshak, 1951). On grounds of symmetry we are led to assume the same nature of theory for the three kinds of meson, it means that the  $\pi$ -meson is described by the pseudoscalar field.

Previously, the emphasis (Basu, 1951) was on the Möller-Rosenfeld interaction which succeeded in eliminating the tensor force in the non-relativistic approximation. Incidentally, it may be mentioned that the presence of the tensor force is necessitated to explain the quadrupole moment of the deuteron and the pseudoscalar theory gave qualitative agreement. But now

the pseudoscalar interaction appears to be the most plausible one, hence it may be worth while to study in details how far the differential cross section for the neutron-proton scattering, as calculated from the pseudoscalar theory, agrees with present experimental observations. It is our object in the present paper to bring into bold relief the influence that the tensor force, contact potential of the form of  $\delta$ -function and the different charge combinations have on the nature of the differential cross section of neutron-proton scattering. As will be seen later, the presence of the tensor force term profoundly changes the character of the differential cross section, as obtained from the simple Yukawa potential. The final interaction term, as derived from field-theoretical considerations, has to be free from any  $\delta$ -function term. The imposition of this condition has considerable influence on the differential cross section. It is found that experimental observation favours the Serber's combination of charged and neutral field in preference to the symmetrical combination of Kemmer.

#### PSEUDOSCALAR INTERACTION

The symmetrical pseudoscalar interaction between two nucleons in the non-relativistic approximation may be expressed in the momentum representation as follows :

$$\begin{aligned} \Lambda_{ps}^{1,2} = & -\frac{8\pi g^2}{\chi^2 V} \left[ \tau_{PN}^1 \tau_{NP}^2 \frac{(\boldsymbol{\sigma}^1 \mathbf{p})(\boldsymbol{\sigma}^2 \mathbf{p})}{\epsilon^2} e^{-\frac{2\pi i}{hc}(\mathbf{p} \cdot \mathbf{X}^1 - \mathbf{X}^2)} + \tau_{NP}^1 \tau_{PN}^2 \frac{(\boldsymbol{\sigma}^1 \mathbf{p})(\boldsymbol{\sigma}^2 \mathbf{p})}{\epsilon^2} \right. \\ & \times e^{+\frac{2\pi i}{hc}(\mathbf{p} \cdot \mathbf{X}^1 - \mathbf{X}^2)} \\ & + \frac{1}{2} \tau_s^1 \tau_s^2 \frac{(\boldsymbol{\sigma}^1 \mathbf{p})(\boldsymbol{\sigma}^2 \mathbf{p})}{\epsilon^2} e^{-\frac{2\pi i}{hc}(\mathbf{p} \cdot \mathbf{X}^1 - \mathbf{X}^2)} + \frac{1}{2} \tau_s^1 \tau_s^2 \frac{(\boldsymbol{\sigma}^1 \mathbf{p})(\boldsymbol{\sigma}^2 \mathbf{p})}{\epsilon^2} e^{+\frac{2\pi i}{hc}(\mathbf{p} \cdot \mathbf{X}^1 - \mathbf{X}^2)} \left. \right] \dots \quad (1) \end{aligned}$$

where  $g$  is the coupling constant having the dimension of electric charge.  $\tau_{NP}$  and  $\tau_{PN}$  denote the charge exchange operators  $\tau_s$  denotes the third component of the isotopic spin vector  $\boldsymbol{\tau}$ ,  $\boldsymbol{\sigma}$  is the spin operator,  $\mathbf{X}$  is the position of a nucleon. The superscript 1 or 2 refers to the particular nucleon.  $\epsilon$  and  $p$  denote the energy and momentum (expressed in energy unit) of the meson and  $\chi$  is  $2\pi\mu/hc$ ,  $\mu$  being the meson mass in energy unit and  $h$  and  $c$  having their usual meanings. The reciprocal of  $\chi$  has the dimension of length and its value for meson mass  $276 m_e$  is  $1.39 \times 10^{-13}$  cm.  $V$  denotes the volume in which the wave-functions are normalised.

This would yield the following static interaction between two nucleons :

$$\begin{aligned} W_{ps}^{1,2} = & \frac{g^2}{\chi^2} (\boldsymbol{\tau}^1 \boldsymbol{\tau}^2) (\boldsymbol{\sigma}^1 \nabla) (\boldsymbol{\sigma}^2 \nabla) [exp(-\chi|\mathbf{X}^1 - \mathbf{X}^2|)] / |\mathbf{X}^1 - \mathbf{X}^2| \\ = & g^2 (\boldsymbol{\tau}^1 \boldsymbol{\tau}^2) \left\{ \frac{1}{2} (\boldsymbol{\sigma}^1 \boldsymbol{\sigma}^2) + S_{12} \left( \frac{1}{2} + \frac{1}{\chi|\mathbf{X}^1 - \mathbf{X}^2|} + \frac{1}{\chi^2|\mathbf{X}^1 - \mathbf{X}^2|^2} \right) \right\} \\ & [exp(-\chi|\mathbf{X}^1 - \mathbf{X}^2|)] / |\mathbf{X}^1 - \mathbf{X}^2| \end{aligned}$$

$$-\frac{4\pi}{3} \frac{g^2}{\chi^2} (\boldsymbol{\tau}^1 \boldsymbol{\tau}^2) (\boldsymbol{\sigma}^1 \boldsymbol{\sigma}^2) \delta(\mathbf{X}^1 - \mathbf{X}^2) \quad \dots \quad (2)$$

where  $S_{12}$  denotes  $3(\boldsymbol{\sigma}^1 \mathbf{n})(\boldsymbol{\sigma}^2 \mathbf{n}) - (\boldsymbol{\sigma}^1 \boldsymbol{\sigma}^2)$ ,  $\mathbf{n}$  being a unit vector in the direction  $\mathbf{X}^1 - \mathbf{X}^2$ . The tensor force term involving  $S_{12}$  contains the undesirable  $1/r^3$  singularity.

The delta function term represents a point interaction between two different nucleons, such an interaction is not compatible with the finite binding energy of the deuteron and as such the final expression for the interaction should be free from  $\delta$  function. The elimination of the  $\delta$ -function can be achieved in a Lorentz invariant manner by adding to the original Lagrangian a suitable term involving  $\delta$ -function which would exactly cancel the  $\delta$ -function term mentioned above. This is possible because the  $\delta$ -function term is a relativistically invariant quantity and as such we are free to add it to the Lagrangian. This, however, introduces an additional term in the interaction  $\Lambda_{ps}^{1,2}$  leading to the corresponding static interaction  $W_{ps}^{1,2}$  which becomes free from any  $\delta$  function.

The final interaction in the momentum representation when properly corrected for the elimination of  $\delta$ -function is given by

$$\begin{aligned} \Lambda_{ps}^{1,2} = & -\frac{8\pi g^2}{\lambda^2} \left[ T \tau^1_{pN} \tau^2_{Np} \left\{ \frac{1}{1^2 e^2} (\boldsymbol{\sigma}^1 \mathbf{p})(\boldsymbol{\sigma}^2 \mathbf{p}) e^{-\frac{2\pi i}{\hbar c} (\mathbf{p} \cdot \mathbf{X}^1 - \mathbf{X}^2)} - \frac{1}{3} (\boldsymbol{\sigma}^1 \boldsymbol{\sigma}^2) \delta(\mathbf{X}^1 - \mathbf{X}^2) \right\} \right. \\ & + T \tau^1_{Np} \tau^2_{pN} \left\{ \frac{1}{1^2 e^2} (\boldsymbol{\sigma}^1 \mathbf{p})(\boldsymbol{\sigma}^2 \mathbf{p}) e^{+\frac{2\pi i}{\hbar c} (\mathbf{p} \cdot \mathbf{X}^1 - \mathbf{X}^2)} - \frac{1}{3} (\boldsymbol{\sigma}^1 \boldsymbol{\sigma}^2) \delta(\mathbf{X}^1 - \mathbf{X}^2) \right\} \\ & + \frac{1}{2} \tau^1_3 \tau^2_3 \left\{ \frac{1}{1^2 e^2} (\boldsymbol{\sigma}^1 \mathbf{p})(\boldsymbol{\sigma}^2 \mathbf{p}) e^{-\frac{2\pi i}{\hbar c} (\mathbf{p} \cdot \mathbf{X}^1 - \mathbf{X}^2)} - \frac{1}{3} (\boldsymbol{\sigma}^1 \boldsymbol{\sigma}^2) \delta(\mathbf{X}^1 - \mathbf{X}^2) \right\} \\ & \left. + \frac{1}{2} \tau^1_3 \tau^2_3 \left\{ \frac{1}{1^2 e^2} (\boldsymbol{\sigma}^1 \mathbf{p})(\boldsymbol{\sigma}^2 \mathbf{p}) e^{+\frac{2\pi i}{\hbar c} (\mathbf{p} \cdot \mathbf{X}^1 - \mathbf{X}^2)} - \frac{1}{3} (\boldsymbol{\sigma}^1 \boldsymbol{\sigma}^2) \delta(\mathbf{X}^1 - \mathbf{X}^2) \right\} \right] \quad \dots \quad (3) \end{aligned}$$

$T=1$  for symmetrical case  
 $T=\frac{1}{2}$  for Serber's case

#### N-P SCATTERING CROSS SECTION

The differential scattering cross section per steradian is given by

$$\begin{aligned} \sigma(\theta) &= \frac{1}{16\pi^2} \cdot \frac{E_0^2}{(\hbar c)^4} |V^2| \left| \sum_m (f^* | I | m) (m^* | I | i) \right|^2 \\ &= \frac{1}{16\pi^2} \cdot \frac{E_0^2 |V^2|}{(\hbar c)^4} \left| (f^* | \Lambda_{ps}^{1,2} | i) \right|^2 \quad \dots \quad (4) \end{aligned}$$

where  $f, m, i$  are the nucleon wavefunctions in the final, intermediate and initial states respectively,  $I$  being the interaction causing transitions,  $E_0 = (p_0^2 + M^2)^{1/2}$  denotes the initial energy of either of the nucleons,  $p_0$  and  $M$ , both expressed in energy units, being the momentum in the centre of mass system and the rest mass of the incident neutron or proton.

The matrix elements of the interaction term are given by

$$(f^* | \Lambda_{ps}^{1,2} | i) =$$

$$\frac{1}{2V} \int \left[ \phi_{S,p'}^{*1} \phi_{S,p'}^{*2} \psi_N^{*1} \psi_p^{*2} e^{-\frac{2\pi i}{\hbar c} (\mathbf{P}_0 \cdot \mathbf{X}' - \mathbf{X})} - \phi_{S,p'}^{*1} \phi_{S,p'}^{*2} \psi_p^{*1} \psi_N^{*2} e^{+\frac{2\pi i}{\hbar c} (\mathbf{P}_0 \cdot \mathbf{X}' - \mathbf{X})} \right] \\ \left[ \Lambda_{ps}^{1,2} \right] \left[ \phi_{S^*,p}^1 \phi_{S^*,p}^2 \psi_N^1 \psi_p^2 e^{-\frac{2\pi i}{\hbar c} (\mathbf{P}_0 \cdot \mathbf{X}' - \mathbf{X})} - \phi_{S^*,p}^1 \phi_{S^*,p}^2 \psi_p^1 \psi_N^2 e^{-\frac{2\pi i}{\hbar c} (\mathbf{P}_0 \cdot \mathbf{X}' - \mathbf{X})} \right] dV$$

where  $\phi$ 's are the normalised spin functions and  $\psi$ 's are the normalised charge functions for the nucleons.

Taking those terms only which are compatible with the conservation of momentum and noting that  $\int e^{i\mathbf{a} \cdot \mathbf{x}} \delta(\mathbf{x}) dV = 1$  we obtain

$$(f^* | \Lambda_{ps}^{1,2} | i) = \\ \frac{4\pi g^2}{\chi^2} \left[ T \phi_{S,p'}^{*1} \phi_{S,p'}^{*2} \Lambda(p') \phi_{S^*,p}^1 \phi_{S^*,p}^2 + T \phi_{S,p'}^{*1} \phi_{S,p'}^{*2} \Lambda(p') \phi_{S^*,p}^1 \phi_{S^*,p}^2 \right. \\ \left. + \frac{1}{2} \phi_{S,p'}^{*1} \phi_{S,p'}^{*2} \Lambda(p') \phi_{S^*,p}^1 \phi_{S^*,p}^2 + \frac{1}{2} \phi_{S,p'}^{*1} \phi_{S,p'}^{*2} \Lambda(p') \phi_{S^*,p}^1 \phi_{S^*,p}^2 \right] \dots \quad (5)$$

where

$$\Lambda(p) = \frac{(\boldsymbol{\sigma}^1 \mathbf{p})(\boldsymbol{\sigma}^2 \mathbf{p})}{\epsilon^2} - \frac{1}{3}(\boldsymbol{\sigma}^1 \boldsymbol{\sigma}^2)$$

$$\Lambda(p') = \frac{(\boldsymbol{\sigma}^1 \mathbf{p}')(\boldsymbol{\sigma}^2 \mathbf{p}')}{\epsilon'^2} - \frac{1}{3}(\boldsymbol{\sigma}^1 \boldsymbol{\sigma}^2)$$

$$p = 2p_0 \sin \theta/2$$

$$p' = 2p_0 \cos \theta/2$$

$$\epsilon^2 = \mu^2 + p^2$$

$$\epsilon'^2 = \mu^2 + p'^2$$

$\theta$  being the angle between the incident and scattered directions of the neutron.

Substituting the square of expression (5) in Eq. (4) we evaluate the differential cross section by averaging over the initial and summing over the final spin states of the nucleon, while taking spur one has to make use of the spin exchange operator  $\frac{1}{2}\{1 + (\boldsymbol{\sigma}^1 \boldsymbol{\sigma}^2)\}$  for reasons which were explained by Basu (1949).

We obtain finally the value of the differential cross section per steradian

$$\sigma'(\theta) = \frac{a^2(1+x^2)}{\chi^2} \cdot \left( \frac{g^2}{\hbar c} \right)^2 \left[ 4 \frac{p'^4}{\epsilon'^4} + \frac{p^4}{\epsilon^4} - 2 \frac{p'^2 p^2}{\epsilon'^2 \epsilon^2} - 2 \frac{p'^2}{\epsilon'^2} + 1 \right] \dots \quad (6)$$

... symmetrical combination

$$\sigma(\theta) = \frac{a^2(1+x^2)}{\chi^2} \cdot \left( \frac{g^2}{\hbar c} \right)^2 \left[ \frac{p'^4}{\epsilon'^4} + \frac{p^4}{\epsilon^4} - \frac{p'^2 p^2}{\epsilon'^2 \epsilon^2} - \frac{1}{3} \frac{p'^2}{\epsilon'^2} - \frac{1}{3} \frac{p^2}{\epsilon^2} + \frac{1}{3} \right] \dots \quad (7)$$

... Serber's combination



where  $a$  is the ratio of the nucleon mass to the meson mass and is 6.66 for the meson mass being  $276 m_e$ ;  $x$  is the ratio  $p_0/M$

The expression (6) may be written as sum of the contributions of the singlet and triplet states.

$$\sigma(\theta) = \frac{1}{4}\sigma_s(\theta) + \frac{3}{4}\sigma_t(\theta)$$

$$\text{where } \sigma_s(\theta) = \frac{E_0^2}{(\hbar c)^4} \cdot \frac{g^4}{\chi^4} \left( 2 \frac{\mu^2}{\epsilon'^2} - \frac{\mu^2}{\epsilon^2} \right)^2$$

$$\text{and } \sigma_t(\theta) = \frac{1}{4} \frac{E_0^2}{(\hbar c)^4} \cdot \frac{g^4}{\chi^4} \left( 2 \frac{\mu^2}{\epsilon'^2} - \frac{\mu^2}{\epsilon^2} \right)^2 + 32 \frac{b'^4}{\epsilon'^4} + 8 \frac{b^4}{\epsilon^4} - 16 \frac{b'^2 b}{\epsilon'^2 \epsilon^2}$$

The above expression agrees exactly with that derived by Hulthén (1944) from the interaction in co-ordinate representation. The agreement is due to the fact that Hulthén omitted *ad hoc* the naturally occurring  $\delta$ -function from his interaction term.

#### COMPARISON WITH EXPERIMENTAL RESULTS

Let us now compare the theoretical results with the recent experimental findings of Kelly and others (1950) for 90 Mev neutron energy. For this purpose we choose the coupling constant so as to normalise the total cross section  $Q = \int_0^\pi 2\pi\sigma(\theta) \sin \theta d\theta$  to the value  $7.8 \times 10^{-26} \text{ cm}^2$  as obtained by

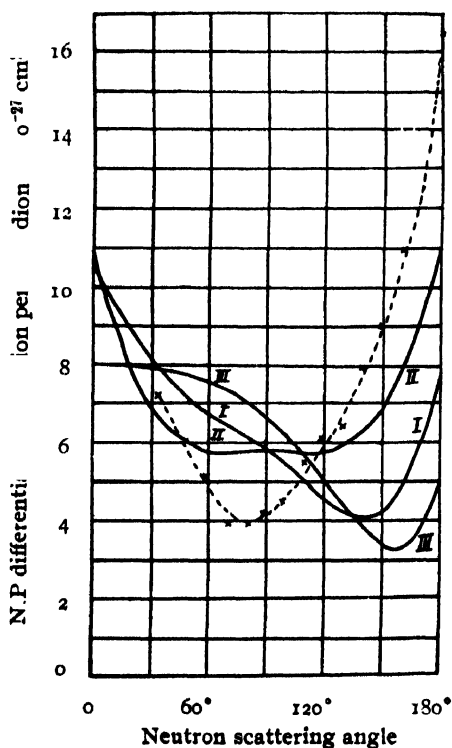


FIG. 1

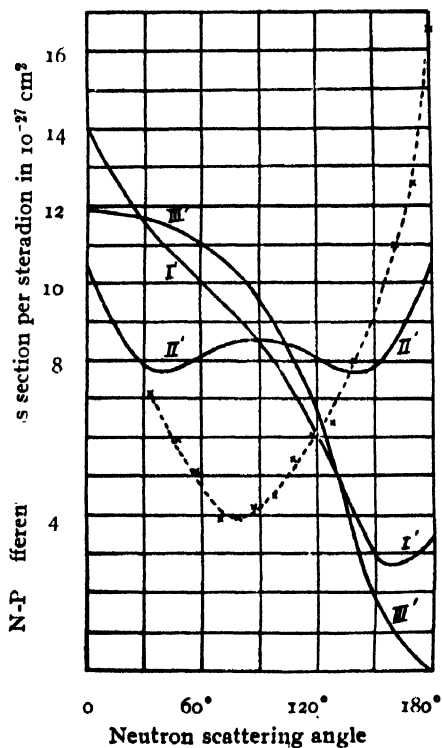


FIG. 2

experimental measurements for 90 Mev neutron energy (Fox and others, 1950, and Dejuren, 1950).

In figure 1, the curves marked as I, II and III represent respectively the theoretical results of the scattering cross sections calculated on the basis of the symmetrical, Serber's and charged combinations of pseudoscalar meson field with pseudovector interaction in which the  $\delta$ -functions have been corrected in such a way that the final potential is free from any  $\delta$ -function.

In figure 2, I', II' and III' represent the same as above with the difference that the interactions are the usual ones in which the  $\delta$ -functions have *not* been properly corrected.

The dotted curves in figures 1 and 2 give the experimental results.

### DISCUSSION

We notice from the curves given in figures 1 and 2 that the agreement of theoretical findings with the experimental results is not so good in either the symmetrical or Serber's combination. The experimental curve is steeper than either of the two theoretical curves. However, the Serber's combination showing symmetrical distribution about  $90^\circ$  is the nearest approach to the experimental curve; coming to details, the Serber's curve gives more scattering at  $90^\circ$  and less at  $180^\circ$  than the experimental findings.

The effect of the delta function is very pronounced in all the combinations. The curves properly corrected for the  $\delta$ -function agree certainly better with the experimental results than the uncorrected ones. In Serber's case, if the  $\delta$ -function is not eliminated, one gets a hump at  $90^\circ$ , which is at complete variance with the experimental curve, whereas, if the  $\delta$ -function is properly eliminated, the hump is reduced very nearly to a flat portion; however, the experiment indicates a trough at  $90^\circ$ .

The tensor force terms have grown much important at this energy. This is illustrated in all the curves. For example, in the symmetrical combination of ordinary Yukawa potential we should expect greater backward scattering due to the excess of the charged part of the meson field, but we notice here greater forward scattering. Thus the tensor force has a predominating influence over and gives an entirely different pattern of scattering from that due to the simple Yukawa potential.

We have used the Born approximation which is perhaps not so good for such low energy scattering. Further, in our calculations we have taken into account only the static interaction, neglecting those terms which depend upon the nucleon velocity.

### ACKNOWLEDGMENT

The author is indebted to Dr. D. Basu for suggesting the problem as a research topic and for his kind interest and guidance throughout the progress of the work.

REFERENCES

- Basu, 1949, *Proc. Roy. Ir. Acad.*, **52**, 127.  
 „ 1951, *Ind. J. Phys.*, **25**, 246.  
 Clark, Roberts and Wilson, 1951, *Phys. Rev.*, **83**, 649.  
 Chew, Goldberger, Steinberger and Yang, 1951, *Phys. Rev.*, **84**, 581.  
 Dejuren, 1950, *Phys. Rev.*, **80**, 27.  
 Durbin, Loar and Steinberger, 1951, *Phys. Rev.*, **83**, 646.  
 Fox, Leith, Wouters and Mac Kenzie, 1950, *Phys. Rev.*, **80**, 23.  
 Hulthén, 1944, *Arkiv. Mat. Astr. Fys.*, **31A**, No. 15.  
 Kelly, Leith, Segre and Wiegand, 1950, *Phys. Rev.*, **79**, 96.  
 Marshak, 1951, *Rev. Mod. Phys.*, **23**, 146.  
 Moyer, Madey, Hildebrand, Knable and Hales, 1951, *Phys. Rev.*, **83**, 206.  
 Panofsky, Aamodt and Hadley, 1951, *Phys. Rev.*, **81**, 365.  
 Steinberger, Panofsky and Steller, 1950, *Phys. Rev.*, **78**, 832.  
 Yang, 1950, *Phys. Rev.*, **77**, 242.

# ON THE RAMAN SPECTRUM OF THIANTHRENE IN THE MOLTEN STATE

BY S. K. MUKERJI AND BANARSI LAI,

DEPARTMENT OF PHYSICS, AGRA COLLEGE, AGRA

(Received for publication, November 10, 1951 ; received after revision, April 15, 1952)

## Plate XII

**ABSTRACT.** The Raman spectrum of thianthrene in the molten state has been studied for the first time by using special technique for its purification and to get rid of fluorescent background. The lines are at 3052(6), 2789(5), 1567(8), 1273(4), 1123(10), 1033(10), 768(2), 668(3), 305(4), 244(4) and 159(4)  $\text{cm}^{-1}$  respectively. An anti-Stokes line at 159  $\text{cm}^{-1}$  has also been recorded.

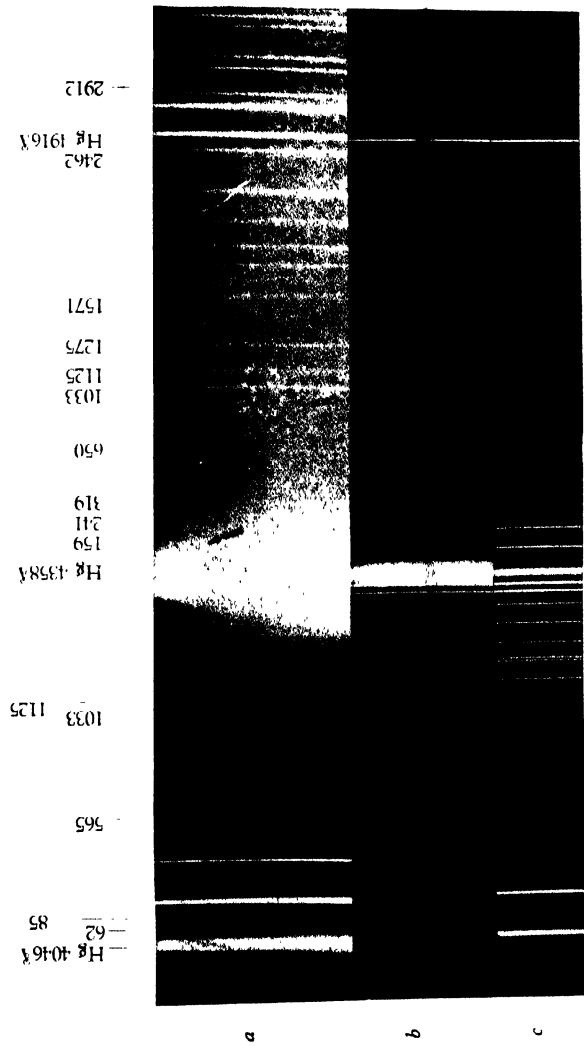
The Raman frequencies obtained in the molten state have been compared with those already obtained in the solid state. The lines of very low frequency which appeared in the solid state, have not appeared in the molten state, thus lending support to the view that these lines are characteristic of the solid state.

## INTRODUCTION

The only reference to the Raman spectra of linear tricyclic compounds appears in the work of Manzoni Ansidei (1936) who has studied some compounds of the anthracene series. The Raman spectrum of thianthrene in the solid state was first studied by us in this laboratory. We have now succeeded in obtaining its Raman spectrum in the molten state. This compound is highly fluorescent and begins to decompose if kept above its melting point for even a few hours. It was only after a laborious process of purification and using other technique that it could be kept in the molten state for more than forty hours which gave the Raman lines mentioned above.

## EXPERIMENTAL

Thianthrene, obtained from the Research Laboratory of Eastman Kodak Company, was purified by repeated crystallization with extra pure benzene till perfectly colourless and transparent crystals were obtained. These crystals were slowly melted in the Raman tube, and the tube itself was surrounded by an electric furnace in which the current was carefully regulated. When the molten mass was kept a little above its melting point, that is, 154°C, it was found to have been charred and rendered opaque after an exposure of only three or four hours. After several trials it was found that the substance could be supercooled to about 145°C. The current in the electric



Raman spectra of thianthrene

- (a) In the solid state
- (b) In the molten state
- (c) Standard iron arc spectrum for comparison



furnace was then carefully regulated to maintain this temperature. Under such circumstances the substance developed no opacity even after an exposure of over forty hours.

The spectra were taken with a Füess glass spectrograph, having a dispersion of about 21 Å. U. per mm in the 4358 Å region. Ilford selochrome plates were used for photographing the spectra, and exposures of about 40 hours were given. Concentrated solution of sodium nitrite was used as filter which reduced the fluorescent background and also cut down the intensity of  $\lambda$  4046 and 4077 Å. U. mercury lines. Thus only the  $\lambda$  4358 Å line of mercury was used as the exciting line. Spectrograms for solid state and molten state are reproduced in Plate XII.

The measurements were made with an accurate Zeiss Ikon comparator and the wavelengths were calculated in the usual manner.

TABLE I

Raman frequencies of thianthrene in wavenumbers

No.	Solid (Mukerji and Banarsi Lal, 1951)	Molten state present investigation
1	62(2)	
2	85(2)	
3	$\pm 159(4)$	$\pm 159(4)$
4	241(4)	244(4)
5	319(4)	305(4)
6	565(5)	
7	650(4)	
8		668(3)
9		768(2)
10	1033(10)	1033(10)
11	1125(10)	1123(10)
12	1275(4)	1273(4)
13	1571(4)	1567(8)
14	2462(2)	
15		2789(5)
16	2912(2)	
17	3044(6)	3052(6)

The numbers within brackets denote the intensity of the Raman lines.

## RESULTS AND DISCUSSIONS

It will be observed from Table I that a number of frequencies obtained in the solid state, that is, 2912(2), 2462(2), 650(4), 565(5), 85(2) and 62(2)  $\text{cm}^{-1}$  respectively, have not appeared in the molten state. A number of frequencies, i.e. 2789(5), 768(2), 668(3)  $\text{cm}^{-1}$  respectively, are observed only in the molten state and not in the solid state. As the table will show, there occurs a slight decrease in frequencies 1571(4), 1275(4), 1125(10), 319(4)  $\text{cm}^{-1}$  as the substance passes from the solid to the molten state. These frequencies in the molten state are observed at 1567(8), 1273(4), 1123(10) and 305(4)  $\text{cm}^{-1}$  respectively. Also the intensity of the line at 1567  $\text{cm}^{-1}$  remarkably increases as the substance passes on to the molten state.

By comparing the spectra in the solid and molten states, it appears that the lines obtained in the molten state are generally sharper and more intense than those already obtained in the solid state.

The wing of the exciting line 4358 Å is very narrow in the molten state. The frequencies 1275 and 1571  $\text{cm}^{-1}$  are characteristic of the benzenoid rings present in thianthrene. Higher frequencies of the order of 2789  $\text{cm}^{-1}$  etc. are due to C-H vibrations as no other frequency can be of this order. The frequencies 650, 1033 and 1125  $\text{cm}^{-1}$  are due to the C-S linkage present in thianthrene.

The frequencies 319, 241 and 159  $\text{cm}^{-1}$  respectively undergo a slight variation in passing from the solid to the molten state. They may be attributed to the intramolecular oscillations of the rings. Such low frequencies are not generally observed in compounds containing a single ring like benzene and its derivatives. It may also be argued that these low frequencies may be due to the intramolecular oscillations of the polymerised groups (Gupta, 1938).

The lines at 85 and 62  $\text{cm}^{-1}$  are of very low frequency, and it has been suggested by Sirkar (1936) that low frequencies of this order are due to a weak electronic binding between the molecules of a polymerised group. But the fact that these lines do not appear in the molten state tends to show that they are due to the lattice vibrations of the crystal. The Raman spectra of thianthrene in various solutions have also been studied by us but these lines of very low frequency have not appeared in any solution. This lends further support to the view that they are due to the lattice vibrations of the crystal.

## REFERENCES

- Donzelot and Chaix, 1935, *C. r. Acad. Sci. Paris*, **201**, 501.  
 Gupta, 1938, *Ind. J. Phys.*, **12**, 355.  
 „, 1936, *ibid.*, **10**, 117.  
 Manzoni Ansidei, 1936, *Atti. Acad. Lincei.*, **24**, 368.  
 „, „, 1936, *Ricerca. Sci.*, **7**(1), 314.  
 „, „, 1937, *Gazz. Chem. ital.*, **67**, 790.  
 Mukerji and B. Lal, 1951, *Ind. J. Phys.*, **28**, 309.  
 Sirkar, 1936, *Ind. J. Phys.*, **10**, 109.



# ULTRASONIC ABSORPTION AND RELAXATION MECHANISM

By A. K. DUTTA

DEPARTMENT OF PHYSICS, UTKAL UNIVERSITY, CUTTACK

(Received for publication, January 18, 1952; received after revision, April 15, 1952)

**ABSTRACT.** It is considered that absorption of elastic waves is always due to some sort of relaxation mechanism which may be of varied nature. The general relationship to express the co-efficient of absorption may, however, be put in the same form for different types of relaxation mechanism, with two constants which are determinable by the process of relaxation mechanism. As such, the absorption due to viscosity considered by Stokes, is also regarded as arising from a relaxation mechanism termed as frictional relaxation mechanism. On this basis the usual Stokes relation for absorption co-efficient requires modification. From a systematic correlation between the discrepancy in experimental and calculated values of  $\alpha/v^2$  on Stokes theory on the one hand and the broadening of elastic wave diffraction spectral lines on the other hand, for different liquids, it has been argued that the same relaxation mechanism should explain the discrepancy in different cases and this has been considered to be due to the necessary modification of the Stokes theory of absorption. Thus, it is considered that the absorption of elastic waves is mainly due to the frictional relaxation mechanism in different liquids.

The phenomenon of absorption of elastic waves, due to various causes can always be considered to be caused by a particular relaxation mechanism. In accordance with the different causes the relaxation mechanism would evidently be different. These are, however, always expressible in the general form,

$$\mu / Vv = \alpha / v^2 = \frac{A_1}{V \cdot v_m} \cdot \frac{1}{1 + (v/v_m)^2} \equiv \frac{A}{v_m} \cdot \frac{1}{1 + (v/v_m)^2} \quad \dots (1)$$

In the particular region, where  $v \ll v_m$ , one may write the absorption relation in the form,

$$\alpha / v^2 = A / v_m = \text{const.} \quad \dots (2)$$

Here,  $\mu$  and  $\alpha$  are the absorption co-efficients per unit wavelength and per unit distance, the constant  $A$  is a function of the wave velocity  $V$ , and may be considered as a measure of the absorption energy due to the particular cause considered. The quantity  $1/v_m$  is a measure of the relaxation time or the time required by a particle for the transfer of energy from the initial condition to the changed condition. In most of the cases, the constant  $A$ ,

to some extent, and the relaxation time  $1/\nu_m$ , are unknown quantities and require to be found by the experimental results. There appears, however, the apparent difficulty that when there are more than one plausible cause of relaxation, we do not know why we should choose one particular mechanism in preference to others, to explain the absorption. The difficulty, nevertheless, disappears when the constants are determinable.

The experimental results on the absorption of ultrasonic waves in liquids have been summarised in a paper by Pinkerton (1949). They are, in many cases, much larger than the absorption calculated on Stokes' theory (Stokes, 1845). It was suggested initially by Dutta and Ghose (1937-38) and also by Kneser (1938), that the excess absorption from Stokes' theory, in the case of liquids, might be due to a relaxation process associated with excitation to vibrational states.

The difficulties, with the excitation relaxation mechanism to explain the excess, have been many. It was pointed out (Dutta and Ghose, 1937-38; Herzfeld, 1941) that the irregular absorption in water could not be explained by the excitation to higher vibrational states, as the measure of absorption due to vibrational excitation becomes much too small in this case, to make any appreciable contribution to absorption.

A different process of relaxation mechanism, as that due to the changes in the molecular arrangements of the minutest particles, was put forth (Hall, 1947) to explain these cases. We are thus presented with an excitation relaxation mechanism to account for the excess absorption in non-associated molecules and a rearrangement relaxation mechanism to account for the excess of absorption in associated molecules. To fit in with the experimental results one has only to give suitable values to  $A$  and  $\nu_m$ .

In a recent note (Jamb and Andreae, 1951), attempt has been made to establish positively, the excitation relaxation mechanism as the cause of excess absorption, in the case of carbonbisulphide. To conform to the experimental results, they have obtained the values of  $A_1$  as 0.46 and  $\nu_m$  as 72 megacycles per second. The amount of unaccounted for absorption on this basis, has been calculated by them to be given by  $\alpha/\nu^2 = 428 \times 10^{-17}$ . This is much too large compared to the other main contributory part of absorption, namely, the Stokes' absorption, which gives a value of  $5 \times 10^{-17}$  units only. We are, thus, again confronted with an excess absorption which has to be explained anew.

Further, from a study of the excitation states in different molecules it has been considered by various workers (Pinkerton, 1949; Dutta and Ghose, 1937-38; Fricke, 1941) that the constant  $A_1$  would be of the order of 0.25 for benzene. To explain the experimental value of excess  $\alpha/\nu^2$ , this gives, on the basis of relaxation mechanism, the  $\nu_m$  value for benzene as  $3 \times 10^8$  cycles per second. Thus at an impressed frequency of the same

value, the measure of absorption co-efficient in benzene would drop down from the  $\alpha/\nu^2$  value of  $800 \times 10^{-17}$  to a value of  $400 \times 10^{-17}$ . The experimental results of Rapuano (1947) do not give this indication. A large variation of the  $\nu_m$  values of benzene and carbon bisulphide is, also, not understandable.

Besides, the experimental results of Pinkerton (1948) on acetic acid, so far as the downward trend of  $\alpha/\nu^2$  is concerned, are exactly of a similar type to the results of Rapuano (1950) on carbon bisulphide. There is only a shift in the frequency scale. No process of excitation mechanism would, however, explain the large excess absorption in the case of acetic acid, as this would require much too large value of  $A$ , or much too small value of  $\nu_m$ .

It, thus appears that the excitation relaxation mechanism is without positive support from any case of absorption in liquids. Even when we try the mechanism in the case of  $\text{CS}_2$ , we have to seek for another relaxation process to explain the absorption left over, and this is difficult to conjecture. We have, thus, to leave out the relaxation mechanism due to excitation as a major contributory cause of absorption.

From the consideration of the close relationship between the diffuseness and breadth of the lines of elastic wave diffraction spectra (Dutta, 1952), indicative of a range of velocity, and the departure of the  $\alpha/\nu^2$  values from the Stokes' values, irrespective of the amount of absorption and of the associated or the unassociated states of the medium, it requires to be considered that all the liquids have to be treated by an identical relaxation mechanism. For, the departure from the Stokes' absorption value has shown a uniformly varying property of the molecules in the form of spectral line widths, and this must have been impressed by any particular relaxation process.

It may be considered, that the Stokes' absorption relation,

$$\alpha/\nu^2 = 8\pi^2\eta/3\rho V^3 \quad \dots (3)$$

also corresponds to a particular relaxation mechanism, namely, the frictional relaxation mechanism. Thus, the absorption should have been properly represented by a relation of the type of equation (1). The constant  $A$  would have been a measure of the absorption of energy, due to the overcoming of the frictional force and  $\nu_m$  would have been a measure of the time required for the transfer of energy from the initial condition to the condition of motion after overcoming the frictional force. In the usual Stokes' relation, the frequency  $\nu$  has been considered to be much too small compared to the characteristic constant  $\nu_m$ , and thus, the second factor has not occurred in the Stokes' relation. On the basis of a justifiable, variable force of friction and restitution, however, acting on the molecules, the complete ultrasonic absorption data may be explained on the basis of a frictional relaxation mechanism, with the help of the necessary and implied modifications of the Stokes' theory. This has been shown in a recent paper (Dutta, 1952).

## REFERENCES

- Dutta, A. K., 1937-38, *Trans. Bose. Res. Inst.*, **13**, 31.  
Dutta, A. K., 1952, *Ind. J. Phys.*, **28**, 142, 161.  
Fricke, R. F., 1941, *J. Accous. Soc. Amer.*, **12**, 245.  
Hall, L., 1947, *Phys. Rev.*, **71**, 318.  
Herzfeld, K., 1941, *J. Accous. Soc. Amer.*, **13**, 32.  
Kneser, H. O., 1938, *Ann. der Phys.*, **32**, 281.  
Pinkerton, J. M. M., 1948, *Nature*, **162**, 106.  
Pinkerton, J. M. M., 1949, *Pro. Phys. Soc. B*, **62**, 129.  
Lamb, J., and Andreac, J. H., 1941. *Nature*, **167**, 898  
Rapuano, R. A., 1945, *Phys. Rev.*, **72**, 78.  
Rapuano, R. A., 1950, *Res. Lab. Electronics. Mass Inst. Tech. Report*, 151.  
Stokes, G. G., 1845, *Trans. Camb. Phil. Soc.*, **8**, 287.

# A COMPARATIVE STUDY OF THE DIFFERENT METHODS OF HEAT-RUN TESTS ON ELECTRICAL MACHINES

## II. THREE-PHASE TRANSFORMERS

By H. K. BASU

DEPARTMENT OF APPLIED PHYSICS, UNIVERSITY COLLEGE OF SCIENCE AND TECHNOLOGY,  
CALCUTTA

*(Received for publication, April 17, 1952)*

**ABSTRACT.** The paper makes a critical study of the different methods of heat-run tests on a three-phase transformer and of estimating its final temperature-rise when fully loaded. The results of tests show definitely that the secondary open-vee injection run may be used where it is not possible to carry out the direct loading method.

### INTRODUCTION

In a previous communication (Basu, 1950) it was reported that in the absence of facilities for carrying out a direct load test for determining the temperature-rise in a single-phase transformer one may employ the alternate open-circuit and short-circuit heat-run test for the purpose with a fair degree of accuracy. It was further noted that where the final temperature rise takes a considerable time to attain its steady value, one may estimate it with fair accuracy with the Cotton's graphical method. In the present paper are reported the results obtained from tests on a three-phase transformer.

### EXPERIMENTAL

In addition to the direct loading method, the following alternative methods have been suggested by several workers (Madden, 1913 ; Stigant and Lacey, 1941) for carrying out a heat-run test on a three-phase transformer without actually loading it :

- (a) Secondary open-vee injection run,
- (b) Equivalent short-circuit run,
- (c) Equivalent open-circuit run, and
- (d) Alternate open and short-circuit run.

With a view to comparing the results obtained by these different methods with those of the direct loading method, a fairly small three-phase

transformer provided with three windings and having the following specifications was chosen :

Type	...	...	...	AN-core type
Output	...	...	...	2 KVA.
Frequency	...	...	...	50 c/s.

It may be noted here that the innermost winding is rated at 133 volts per coil while the outermost one at 400 volts per coil and the intermediary one at 230 volts per coil.

The measuring instruments and the mercury-in-glass thermometers were all calibrated and checked from time to time during the investigation in comparison to the standards of the laboratory.

*Direct load test* : The 133-volt coils were used as primary and connected in delta across a 3-phase, 133-volt and 50 c/s source (figure 1).

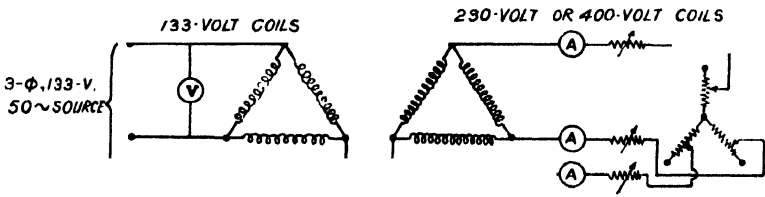


FIG. 1

The primary voltage was maintained constant at the rated value when the transformer was fully loaded on the secondary side. Under the full load conditions the secondary line current was 5 amps. when the 230-volt coils were used as secondary and 2.89 amps. with the 400-volt coils as secondary and was maintained constant throughout the test.

*Secondary open-vec test* : The connections were made as shown in figure 2.

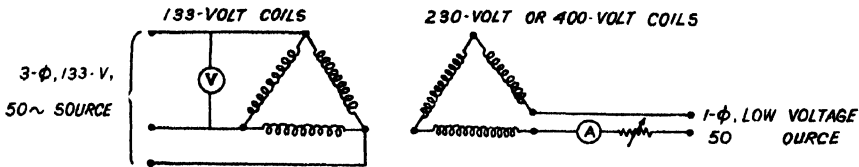


FIG. 2

The primary was connected as in the direct load test. One of the junctions of the delta connection of the secondary was opened and the two points were connected to a 1-phase 50 c/s source of low voltage through an ammeter and a rheostat. The secondary applied voltage was adjusted so as to send the full load phase current through the secondary windings. Since the applied voltage to the primary supplies the core loss and the injected current to the secondary necessary copper loss, the primary applied voltage and the secondary injected current were kept constant at their rated values throughout the test. It is thus evident that the transformer under test although

not directly loaded would develop maximum heating because of the presence of the full load losses.

Before carrying out the remaining heat-run tests, the full load losses of the test transformer were determined in the usual way and it was found that the ratio of core loss to copper loss was 3 : 4 when the 230-volt coils were used as secondary and 3 : 5 with the 400-volt coils as secondary.

*Equivalent short-circuit test :* A low voltage was applied to the primary of the test transformer with its secondary short-circuited and the applied voltage adjusted until the power input (in watts) into the transformer was equal to its normal full load losses. The electrical connections are shown in figure 3.

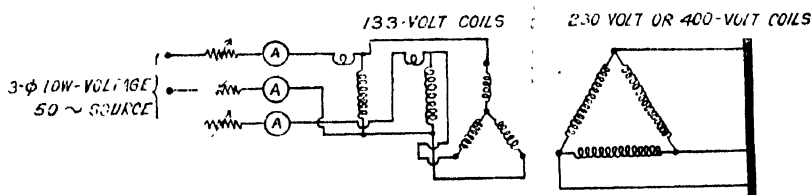


FIG. 3

*Equivalent open-circuit test :* This test was carried out by applying a high voltage to the primary, keeping the secondary open as shown in figure 4 and

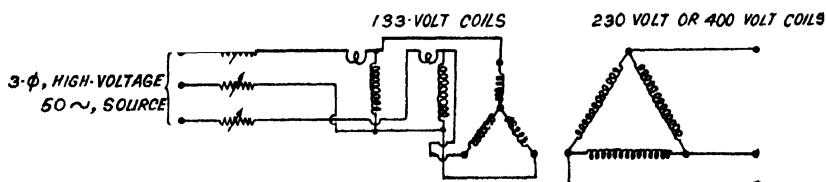


FIG. 4

adjusting the applied primary voltage until the input power (in watts) was equal to the total normal full load losses.

*Alternate open-circuit and short-circuit test :* For carrying out this test the transformer was connected as shown in figure 5. To begin with, a suitable

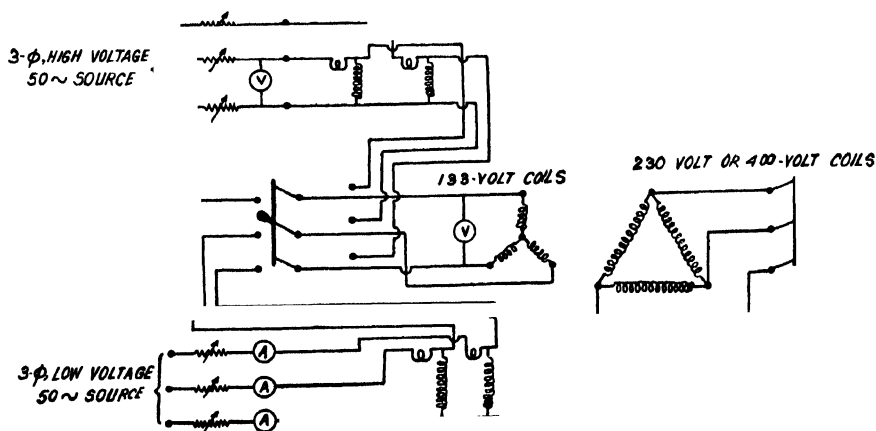


FIG. 5

voltage higher than the rated value was applied to the primary of the transformer with its secondary open and this voltage was gradually increased till the value of the core loss was equal to that of the total full load losses as previously determined. The transformer was run under this condition for 12 minutes and the primary was switched on to a low voltage source. Then with the secondary short-circuited this applied low voltage was adjusted till the copper loss was equal in value to that of the total full load losses. Under this condition the transformer was run for 16 minutes when the 230-volt coils were used as secondary and for 20 minutes when the other secondary was used. This cycle of operations was repeated till a steady hot temperature of the test transformer was reached. It may be noted here that as suggested by McConahey and Fortescue (1913) and also Madden (1913) the period of each run was so chosen that the ratio of the two periods of the two heat-run tests was equal to that of the core loss and the copper loss of the test transformer.

TABLE I  
Direct-loading heat-run test

Time		Temperature in °C			
		230-V. secondary		400-V. secondary	
Hour	Min.	Cold	Hot	Cold	Hot
0	0	30.40	30.40	30.70	30.70
0	15	30.40	32.70	30.75	34.00
0	30	30.40	37.20	30.75	39.90
0	45	30.40	41.30	30.75	44.50
1	0	30.50	44.70	30.75	48.50
1	15	30.50	47.50	30.75	51.70
1	30	30.50	49.80	30.75	54.20
1	45	30.50	51.70	30.85	56.20
2	0	30.50	53.30	30.85	57.90
3	0	30.55	57.35	30.85	62.00
4	0	30.70	59.60	30.95	64.50
5	0	30.70	60.90	31.00	65.70
6	0	30.80	61.80	31.05	66.60
7	0	30.90	62.20	31.05	67.10
8	0	30.90	62.40	31.05	67.30
9	0	30.90	62.40	31.05	67.30



TABLE II  
Secondary open-vee injection heat-run test

Time		Temperature in °C			
		230-V. secondary		400-V. secondary	
Hour	Min.	Cold	Hot	Cold	Hot
0	0	30.60	30.60	30.60	32.60
0	15	32.55	32.60	30.50	36.90
0	30	30.50	36.90	30.55	42.35
0	45	30.50	40.60	30.60	46.70
1	0	30.50	43.70	30.60	50.30
1	15	30.50	46.30	30.60	53.10
1	30	30.50	48.50	30.65	55.50
1	45	30.50	50.30	30.65	57.30
2	0	30.50	51.90	30.65	58.90
3	0	30.50	56.00	30.65	62.70
4	0	30.35	58.30	30.70	64.75
5	0	30.35	59.30	30.70	66.20
6	0	30.40	60.25	30.70	67.00
7	0	30.40	60.80	30.70	67.30
8	0	30.40	61.20	30.70	67.30
9	0	30.40	61.20	—	—

TABLE III  
Equivalent short-circuit-heat run test

Time		Temperature in °C			
		230-V. secondary		400-V. secondary	
Hour	Min	Cold	Hot	Cold	Hot
0	0	31.70	31.70	30.10	30.10
0	15	31.50	34.80	30.10	40.00
0	30	31.50	41.40	30.10	48.00
0	45	31.50	46.80	29.95	54.00
1	0	31.50	50.90	29.95	58.50
1	15	31.60	54.20	29.90	61.80
1	30	31.60	56.80	30.00	64.20
1	45	31.60	58.90	29.80	66.10
2	0	31.60	60.50	29.80	67.50
3	0	31.60	63.70	30.00	71.30
4	0	31.60	65.50	29.90	72.80
5	0	31.70	66.60	29.90	73.80
6	0	31.70	67.30	29.95	74.30
7	0	31.70	68.00	29.95	74.60
8	0	31.80	68.30	29.95	74.60
9	0	31.80	68.30	—	—

TABLE IV  
Equivalent open-circuit heat-run test

Time		Temperature in °C			
		230-V. secondary		400-V. secondary	
Hour	Min.	Cold	Hot	Cold	Hot
0	0	31.40	31.40	30.50	30.50
0	15	31.30	31.70	30.50	30.70
0	30	31.30	32.20	30.50	31.30
0	45	31.30	32.90	30.50	32.20
1	0	31.30	33.70	30.50	33.15
1	15	31.35	34.60	30.50	34.20
1	30	31.35	35.60	30.50	35.30
1	45	31.35	36.60	30.50	36.40
2	0	31.35	37.50	30.50	37.50
3	0	31.40	40.50	30.50	41.00
4	0	31.40	42.50	30.55	43.40
5	0	31.40	43.80	30.55	44.90
6	0	31.40	44.50	30.55	45.80
7	0	31.40	45.10	30.60	46.50
8	0	31.40	45.30	30.60	46.90
9	0	31.40	45.30	30.60	46.90

TABLE V  
Alternate open-circuit and short-circuit heat-run test

230-V. secondary				400-V. secondary			
Time		Temperature in °C		Time		Temperature in °C	
Hour	Min.	Cold	Hot	Hour	Min.	Cold	Hot
0	0	31.30	31.30	0	0	30.50	30.50
0	20	31.30	32.30	0	22	30.50	37.20
0	48	31.20	39.80	0	54	30.50	47.50
1	16	31.20	44.70	1	26	30.50	53.80
1	44	31.20	48.40	1	58	30.45	57.20
2	12	31.20	50.80	2	30	30.45	59.60
2	40	31.05	52.70	3	2	30.60	61.00
3	8	31.00	54.00	3	34	30.50	62.00
3	36	31.00	54.60	4	6	30.60	62.90
4	4	30.90	55.40	4	38	30.60	63.70
4	32	31.00	56.00	5	10	30.65	64.30
5	0	31.00	56.20	5	42	30.65	64.50
5	20	30.90	56.40	6	14	30.65	64.50
5	56	30.60	56.40	—	—	—	—

*Temperature measurement* : The temperature was measured, as described in the previous communication (Basu, 1950), except that the thermometer was placed in contact with the outermost winding. Since the estimation of temperature-rise by the measurement of hot resistance has no special advantage over the thermometric method, it was thought desirable to estimate the temperature-rise by the graphical methods in addition to the thermometric method. Tables VI and VII contain the data of temperature-rise as estimated by each of these three methods. In each table, the columns 2, 3, and 4 refer to data of temperature-rise as indicated below :

Column 2 :—As read by the thermometer placed in contact with the outermost winding.

Column 3 :—As found from the graph  $d\theta/dt$  vs.  $\theta$ .

Column 4 :—As found by Cotton's graphical method.

TABLE VI  
230-V. secondary

Methods of heat-run tests	Temperature-rise in °C		
1	2	3	4
Direct loading	31.50	30.10	31.00
Secondary open-vee-injection	30.80	30.00	32.00
Equivalent short-circuit	36.50	34.80	37.00
Equivalent open-circuit	13.90	14.10	20.00
Alternate open & short-circuit	25.50	—	33.00

TABLE VII  
400-V. secondary

Methods of heat run tests	Temperature-rise in °C		
1	2	3	4
Direct loading	36.25	34.30	34.00
Secondary open-vee injection	36.60	35.40	26.00
Equivalent short-circuit	44.65	41.40	41.00
Equivalent open-circuit	16.30	17.25	25.00
Alternate open & short-circuit	33.85	—	38.00

## DISCUSSIONS

From Tables VI and VII one may note the following :

(i) The transformer under test is well within the limit of temperature-rise as stipulated for an AN-type of transformer with class A insulation and running continuously under full load conditions.

(ii) Amongst the alternative methods the results obtained by the secondary open-vec injection heat-run test are in very close agreement with those obtained by direct loading method as can be easily seen from column 2 of each table.

(iii) The two graphical methods give fairly satisfactory results but in view of the uncertainty involved in the Cotton's graphical method, one is led to prefer the first graphical method.

## ACKNOWLEDGMENTS

The author desires to express his heartfelt thanks to Prof. P. C. Mahanti, Head of the Department and his colleague Mr. M. N. Roy for their helpful discussions and encouragement during the course of the investigation.

## REFERENCES

- Basu, H. K , 1950, *Ind. J. Phy.*, **24**, 171.  
Madden, J. J., 1913, *Proc. A. I. E. E.*, **32**, 325.  
McConahey, W. M. & Fortescue, C., 1913, *Proc. A. I. E. E.*, **32**, 507.  
Stigant, S. A , & Lacey, H. M., 1941. *The J. & P. Transformer Book*.

# PSEUDOSCALAR MESON FIELD AND RELATIVISTIC SCATTERING OF NEUTRONS BY PROTONS

By D. BASU

DEPARTMENT OF THEORETICAL PHYSICS, INDIAN ASSOCIATION FOR THE CULTIVATION OF SCIENCE, CALCUTTA

(Received for publication, May, 1952)

**ABSTRACT.** In view of the present trends that the meson responsible for the nuclear force is pseudoscalar in nature, the relativistic expression for the differential cross section of neutron-proton scattering is calculated for the pseudoscalar meson field with Serber charge combination and charge symmetrical theory. A comparison with the experimental results of n-p scattering at 90 and 260 Mev shows that Serber charge combination approaches the experimental curve nearer than the charge symmetrical theory and further the angular anisotropy of the n-p scattering decreases with increasing energy, whereas, experimentally the same quantity increases with increasing energy.

## 1. INTRODUCTION

During the last decade, the charge symmetrical Möller-Rosenfeld interaction has been preferred to other ones for the following reasons: In the non-relativistic approximation the interaction is free from the inadmissible  $1/r^3$ -singularity which renders the Schrödinger equation insoluble in the proper sense, the M.-R. interaction offers an easy explanation to the singlet and triplet states of the deuteron, on the other hand, because of the  $1/r^3$ -singularity involved in the tensor force term of the pure vector or pseudoscalar field, in calculations of physical processes recourse has to be taken of cut-off procedure which is not desirable from the point of view of relativistic invariance. The experimental investigations of the last year which have been briefly summarised in a preceding paper by Sil (1952), demand that the meson responsible for the nuclear force has spin value zero and most probably obeys pseudoscalar field equations\*. That being so, it is interesting to see to what extent the pure pseudoscalar field is capable of explaining the angular distribution of the neutrons scattered by protons at high energies. In the above-mentioned paper, Sil (1952) has compared the theoretical results as calculated in the non-relativistic approximation with the experimental values of neutron-proton scattering at 90 Mev energy, he has concluded that a nearest, though not quite satisfactory, approach to the experimental curve is obtained if Serber's charge combination is

\*This was pointed out to the author by Prof. W. Heitler almost a year ago in a private communication.

introduced in place of the charge symmetrical one and further, the interaction in the momentum representation is so chosen that the static potential in the co ordinate system is free from  $\delta$ -function. In the present paper the same problem is studied in the relativistic region by making exact calculations with second order matrix elements ; it may be mentioned here that matrix elements of fourth order may not affect appreciably the angular distribution of the n-p scattering as can be guessed from the work of Watson and Lepore (1949). A comparison of the theoretical values with the experimental findings at 260 Mev shows that even with Serber's charge combination and proper corrections for  $\delta$ -functions, the agreement is poor ; indeed there is complete disagreement round about  $90^\circ$  scattering angle. The experimental values of the differential cross sections at 40, 90 and 260 Mev show minima at  $90^\circ$  scattering angle and an approximate symmetry about the same angle. The angular distribution due to the charge symmetrical theory, while giving a minimum at  $150^\circ$  angle, shows an asymmetrical pattern not consistent with the experimental curve.

The pseudoscalar interaction is characterised by the prominence of the tensor force term ; it has been pointed by Sil (*loc.cit.*) that the nature of the angular distribution due to the tensor force term is opposite to that due to ordinary Yukawa force, *i. e.*, for neutral meson field the ordinary Yukawa force gives decreasing value of scattering cross section with increasing angle, whereas, the tensor force gives just the opposite. For low energy region the influence of the tensor force is not so appreciable but the influence increases sharply with increasing energy. The ratio of the differential cross section at  $180^\circ$  angle to that at  $90^\circ$ , which roughly measures the degree of steep rise of the scattering cross section from  $90^\circ$  to  $180^\circ$  angle, increases with increasing energy, the experimental values for 40, 90 and 260 Mev being respectively 1.6, 3.7 and 9.2 ; whereas, the theoretical values, as calculated from the pseudoscalar interaction with Serber charge combination, decreases with increasing energy, the values being 1.8 and 1.5 for 90 Mev and 260 Mev respectively. This observation seriously goes against the pseudoscalar interaction as being the proper one for n-p scattering (c.f. Hulthén, 1944). It has been shown by Christian and Hart (1950) that the ordinary Yukawa potential with the constants properly adjusted give good fit to the experimental values at 90 Mev, the M.-R. interaction is free from tensor force term in the low energy region, the tensor force term does not reappear till after 500 Mev (Hu, 1945; Basu, 1949), that being so the M.-R. interaction at low energy would correspond nearly to the ordinary Yukawa potential.

## 2. SCATTERING OF NEUTRONS BY PROTONS

For the evaluation of the matrix elements of the scattering cross section, we follow the notations of the previous paper (Basu, 1949). The scattering process is considered in the frame of reference in which the centre of gravity is at rest, the neutron and proton having momentum  $p_0$  and  $-p_0$ .

initially and  $p_0'$  and  $-p_0'$  after the scattering has taken place. The scattering takes place through an exchange of positive, negative and neutral meson. The scattering cross section is given by

$$dQ = \frac{1}{16\pi^2} \frac{E_0^2 V^2}{(\hbar c)^4} |(f^* | H | i)|^2 d\Omega \quad \dots (1)$$

where  $E_0$  is the energy of the nucleon,  $V$  is the quantisation volume and  $(f^* | H | i)$  denote the final result of the second order matrix element after summation over the intermediate states through which the final state  $(f)$  is reached from the initial one  $(i)$ . The expression for  $(f^* | H | i)$  is as follows.

$$(f^* | H | i) = -\frac{1}{2} \left[ T \phi_{s_{1p_0'}}^*(1) \phi_{s_{2-p_0'}}^*(2) \left\{ \Lambda^{1,2}(p') + \Delta^{1,2} \right\} \phi_{s_{s_2-p_0}}(1) \phi_{s_{s_1p_0}}(2) \right. \\ \left. + \phi_{s_{1p_0}}^*(1) \phi_{s_{2-p_0}}^*(2) \left\{ \Lambda^{1,2}(p) + \Delta^{1,2} \right\} \phi_{s_{s_1p_0}}(1) \phi_{s_{s_2-p_0}}(2) \right] \quad \dots (2)$$

where  $p' = p_0 + p_0'$ , and  $p = p_0 - p_0'$  (the quantities being vectors).

Here  $\phi_{s_{1p_0'}}(1)$  represents the Dirac spin function of particle (1) in the state typified by  $s_{1p_0'}$ .  $T$  has the value  $\frac{1}{2}$  for Serber charge combination and 1 for symmetrical charge theory. It is clear that the first part of (2) is due to an exchange of a charged meson and second due to that of a neutral meson.  $\Lambda^{1,2}$  is the usual relativistic pseudoscalar interaction and  $\Delta^{1,2}$  is the  $\delta$ -function correction term which when added to  $\Lambda^{1,2}$  makes the final static potential in the co-ordinate representation free from any  $\delta$ -function. The expressions in momentum representation for  $\Lambda$  and  $\Delta$  are as follows:

$$\Lambda^{1,2}(p) = -\frac{4\pi f^2}{\chi^2} \left[ \frac{(\sigma^1 p)(\sigma^2 p)}{\epsilon^2} + \rho_1^1 \rho_1^2 \right] \quad \dots (3)$$

$$\Delta^{1,2} = \frac{4\pi f^2}{\chi^2} \left[ \frac{1}{3}(\sigma^1 \sigma^2) + \frac{2}{3}\rho_1^1 \rho_1^2 \right] \quad \dots (4)$$

where  $\chi = \mu/\hbar c$ ,  $\mu$  and  $\epsilon$  are respectively the mass (in energy unit) and energy of the meson.  $\sigma$ 's (vector quantity) and  $\rho$ 's are the usual Dirac matrices. The superscripts 1 and 2 distinguish the two particles. The non-relativistic approximation of (3) in co-ordinate representation becomes

$$W = f^2 \left[ \frac{1}{3}(\sigma^1 \sigma^2) + S_{12} \left( \frac{1}{3} + \frac{1}{\chi r} + \frac{1}{\chi^2 r^3} \right) \right] \frac{e^{-\chi r}}{r} - \frac{4\pi f^2}{3\chi^2} (\sigma^1 \sigma^2) \delta(r)$$

$$\text{where } S_{12} = 3 \frac{(\sigma^1 r)(\sigma^2 r)}{r^2} - (\sigma^1 \sigma^2)$$

The last term involving the  $\delta$ -function is cancelled by the first term of (4).

The final result for the differential cross section is

$$\begin{aligned}
 d\varphi = & \frac{1}{4\lambda^2} \frac{f^4}{\hbar^2 c^2} \frac{M^2}{\mu^2} \frac{1}{1+\lambda^2} \left[ T^2 4 \left\{ \frac{2}{3} \lambda^4 (1 - \cos \theta)^2 + \frac{8}{9} (1 + \lambda^2)^2 + 4 \left[ \frac{1}{3} - \frac{p'^2}{\epsilon'^2} \right] \right\} \right. \\
 & + \left\{ \frac{2}{3} \lambda^4 (1 + \cos \theta)^2 + \frac{8}{9} (1 + \lambda^2)^2 + 4 \left[ \frac{1}{3} - \frac{p^2}{\epsilon^2} \right] \right\} \\
 & + T \left\{ \lambda^4 \left[ -\frac{28}{9} + \frac{1}{3} \frac{p^2}{\epsilon^2} + \frac{1}{3} \frac{p'^2}{\epsilon'^2} \right] \right. \\
 & + \lambda^4 \cos^2 \theta \left[ -\frac{4}{9} + \frac{1}{3} \frac{p^2}{\epsilon^2} + \frac{1}{3} \frac{p'^2}{\epsilon'^2} \right] \\
 & - 2 \lambda^4 \cos \theta \left[ \frac{1}{3} \frac{p'^2}{\epsilon'^2} - \frac{1}{3} \frac{p^2}{\epsilon^2} \right] - 4 \lambda^2 \left[ \frac{2}{3} + \frac{2}{3} \frac{p^2}{\epsilon^2} + \frac{2}{3} \frac{p'^2}{\epsilon'^2} \right] \\
 & \left. \left. - 4 \lambda^2 \cos \theta \left[ \frac{2}{3} \frac{p'^2}{\epsilon'^2} - \frac{2}{3} \frac{p^2}{\epsilon^2} \right] + 4 \left[ -\frac{2}{3} + \frac{2}{3} \frac{p'^2}{\epsilon'^2} + \frac{2}{3} \frac{p^2}{\epsilon^2} - \frac{2 p'^2 p^2}{\epsilon'^2 \epsilon^2} \right] \right\} 2\pi \sin \theta d\theta \right]
 \end{aligned}$$

In the above expression the third part which is multiplied by  $T$  is the term arising from interference between the charge and neutral meson

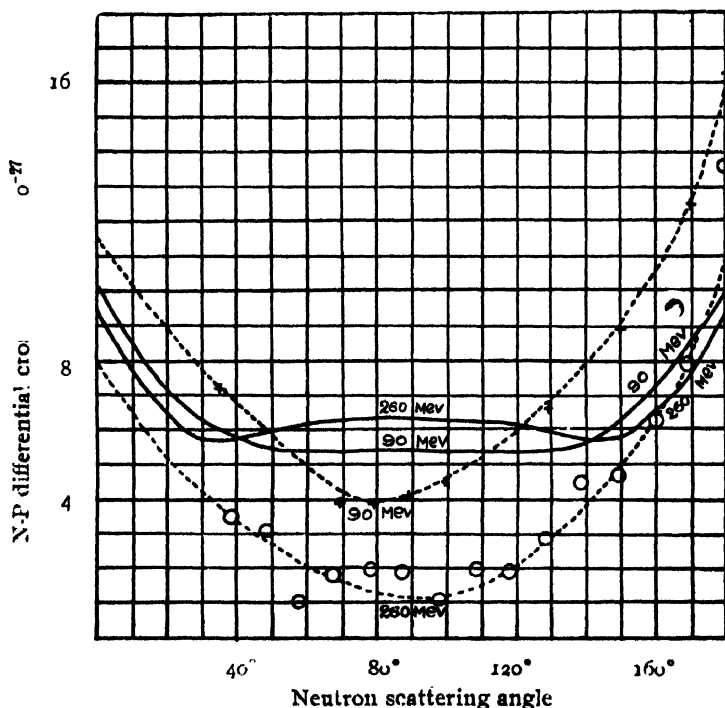


FIG. 1

Theoretical curve with Serber charge combination

... .. Experimental curve



fields. The numerical results of expression (6) are compared with the experimental findings of Kelly, Leith, Segre and Wiegand (1950). In figure 1, the theoretical curves are drawn with Serber's charge combination which give a symmetry about 90° scattering angle, while in figure 2 the

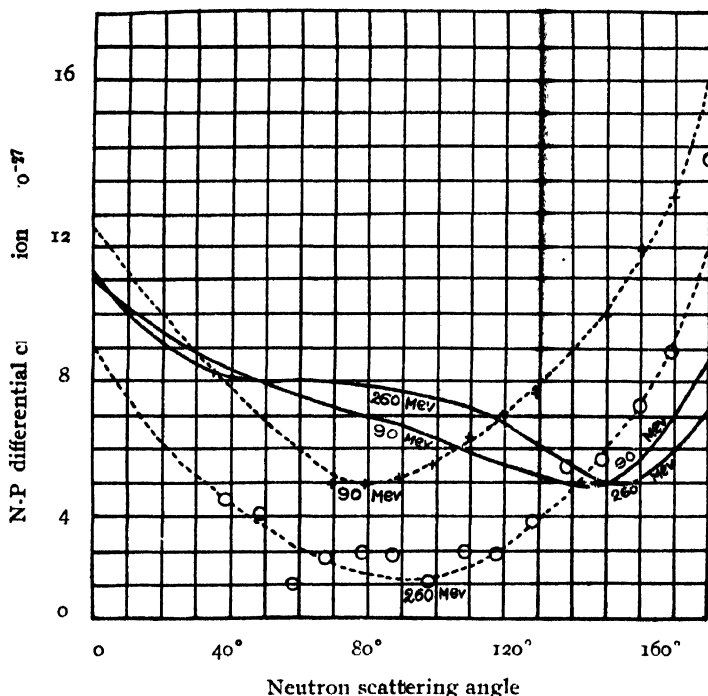


FIG. 2

—Theoretical curve with charge symmetrical combination  
 .....Experimental curve

theoretical curves represent the charge symmetrical theory which is at variance with the nature of the experimental curves. The values of the coupling constants are the same as evaluated by Sil (1952) by comparing the theoretical and experimental results of the total cross section for n-p scattering at 90 Mev energy. The value for the mass of meson is taken to be  $276 m_e$ ,

$$\frac{f^4}{\hbar^2 c^4} \equiv 0.0149 \text{ (Serber)} ; \frac{f^4}{\hbar^2 c^2} \equiv 0.00496 \text{ (symmetrical)}$$

$$1/\chi \equiv 1.39 \times 10^{-13} \text{ cm}$$

It is obvious that the presence of tensor force term tends to flatten the nature of the angular distribution curves with increasing energy, whereas, the experimental findings are just the contrary, the angular anisotropy of scattering increases with increasing energy. This contradiction of trends between the theoretical and experimental results constitutes a difficulty

for the pseudoscalar field. The total cross section of n-p scattering according to pseudoscalar theory has very nearly the same value for both 90 and 260 Mev energy. However, the experimental value at 260 Mev is about half of that at 90 Mev. It was found in a previous paper by the author (Basu, 1951) that the influence of radiation damping at 260 Mev is quite appreciable and reduces the ordinary value of the cross section by a factor 2 for this energy, the radiation damping can be neglected for 90 Mev; as far as the total cross section is concerned the drop of the value at 260 Mev as compared to that at 90 Mev is explained by the pseudoscalar theory provided the influence of radiation damping is taken into account. It may be mentioned here that interference part of expression (6) in effect reduces the value of the cross section to a considerable extent; it would not be proper to neglect it.

## REFERENCES

- Basu, D, 1949, *Proc. Roy. Ir. Acad.*, **52**, 127.  
Basu, D, 1951, *Ind. J. Phys.*, **28**, 246.  
Christian and Hart., 1950, *Phys. Rev.*, **77**, 441.  
Hu, 1945, *Phys. Rev.*, **67**, 339.  
Hulthén, 1944, *Arkiv. Mat. Astr. Fys.*, **31A**, No. 15.  
Kelly, Leith, Segre, and Wiegand, 1950, *Phys. Rev.*, **79**, 96.  
Sil, N.C., 1952, *Ind. J. Phys.*, **28**, 269.

# EFFECT OF MAGNETIC FIELD IN OBLIQUE PROPAGATION OVER EQUATORIAL REGION

By B. CHATTERJEE

INSTITUTE OF RADIO PHYSICS AND ELECTRONICS, CALCUTTA UNIVERSITY

(Received for publication, May 3, 1952)

**ABSTRACT.** The paper discusses in a simplified manner the effect of magnetic field in oblique propagation of radio waves, with special reference to propagation across equatorial region. A few sets of propagation curves have been drawn for transmission across equatorial region, after Booker. The phenomenon of lateral deviation has been discussed in a simple manner. Propagation curves for two special cases of transmission, Calcutta-Bandoeng and Calcutta-Bombay, are also delineated.

## I. INTRODUCTION

The study of the phenomenon of oblique propagation of electro-magnetic wave through the ionosphere under the influence of geomagnetic field is of great practical importance in radio communication. Though, since the earliest days of the deduction of Appleton-Hartree magneto-ionic formula, the case of vertical propagation has been worked out by many investigators (Mitra, 1952), unfortunately, that of oblique propagation has received comparatively little attention. This is perhaps due to the fact that the case of vertical incidence is relatively simple. In this case, the angle between the direction of the ray and the direction of the magnetic field remains unchanged during the propagation. For the case of oblique propagation, on the other hand, the angle between the two changes constantly as the ray proceeds into the ionosphere. This makes the analysis more complicated. The case of oblique propagation was first considered by Booker (1938), who showed that the treatment becomes simpler by the introduction of the so-called *propagation factor*  $q$  which is the vertical component of the phase propagation vector. The meaning of  $q$  will be clear from the consideration of figure 1.

The propagation of the phase of the wave at any point, in a direction making an angle  $\psi$  with the vertical, may be represented by a vector of length  $\mu_\psi$  as shown in the figure. The length of this vector is equal to the ratio of the velocity of phase propagation (in the direction  $\psi$ ) to that of light in vacuo, and its direction is the direction of phase propagation at the point. By Snell's law, the horizontal component,  $\mu_\psi \sin \psi$  is equal to  $\sin \theta$  and is thus a constant for the particular ray path.

The vertical component,  $\mu_\psi \cos \psi (=q)$ , however, varies with electron concentration and the propagation of the ray is completely described by the

variation of this single quantity  $q$ . Booker has further shown that  $q$ , for the general case, is given by a rather complicated quartic formula.

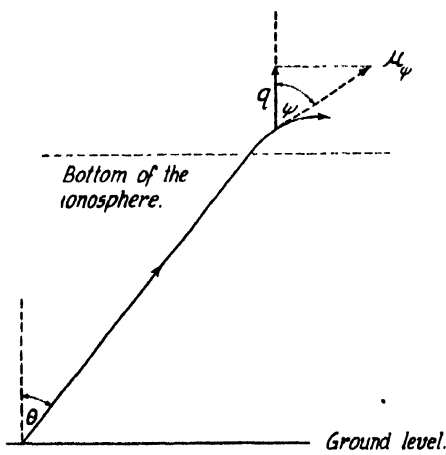


FIG. 1

Illustrating  $q$ , vertical component of the phase propagation vector

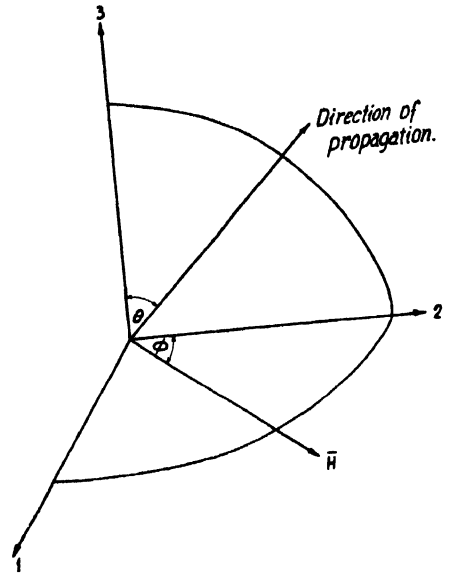


FIG. 2

Direction 3 is vertical, and 23 plane is the plane of incidence

But, for the simpler case of propagation across the equatorial region, *i.e.*, for the case when the ray is incident on the ionosphere in the region where the magnetic lines of force run horizontally, the quartic formula reduces to a simpler quadratic formula (Booker, 1938). Neglecting the damping due to collision (as  $\frac{\nu}{p} \ll 1$ ) in the deviating E or F region of the ionosphere, this simplified quadratic expression becomes :

$$q^2 = c^2 - \frac{x(1-x)}{(1-x) - \frac{1}{2}(y_1^2 + c^2 y_2^2) \pm \sqrt{\frac{1}{4}(y_1^2 + c^2 y_2^2)^2 + s^2 y_2^2(1-x)}} \quad (1)$$

where  $q = \mu_\psi \cos \psi$ ,

$$x = \frac{4\pi e^2}{m p^2} N, \quad N \text{ being the electron concentration,}$$

$$\bar{y}^* = \frac{e\bar{H}}{mc p} \quad \text{and} \quad p\bar{H} = 2\pi f\bar{H} = \frac{c\bar{H}}{mc},$$

where  $\bar{H}$  is earth's magnetic field ;

$$y = \left| \bar{y} \right| = \frac{f_H}{f} = \frac{p_H}{p}$$

\*The terms with bar represent vector quantities

where  $f_H$  is gyro-frequency and  $f$  is the wave frequency ;

$$c = \cos \theta \text{ and } s = \sin \theta.$$

$y_2$  and  $y_1$ , are the components of  $\bar{y}$  in the plane of incidence and in the perpendicular direction respectively.

This formula, simpler as it is, is specially helpful for the following reasons: Propagation curves, (*i.e.*, curves delineating the relation between  $q$  and  $x$ ) in order to be of practical use, have to be drawn for a large number of cases, for different values of wave frequency  $f$ , angle of incidence  $\theta$ , on the ionosphere, and azimuthal angles of propagation  $\varphi$ , *i.e.*, the plane of incidence making different angles with the magnetic meridian plane. Calculations with the general quartic equation is necessarily long and laborious. But Booker has shown that if, with the help of equation (1), the  $q$ - $x$  or  $q^2$ - $x$  curves are first drawn for the magnetic equatorial region (which it is possible to do on a mass production scale), the curves for other cases for which the magnetic field has a component in the vertical direction can be easily visualised from these curves.

The practical uses of these propagation curves are many, *e.g.*, for a given set of values of  $f$ ,  $\theta$ ,  $\varphi$  and  $x$ , one can find out if there will be reflection or penetration. Again, if it is found that the maximum value of  $x$  for a given ionized layer is less than that for which  $dq/dx$  is infinity in the corresponding propagation curve, then for particular case, the ray will penetrate that ionized layer. Reflection will take place from the point for which the value of  $x$  is such that  $dq/dx$  is infinity. Also, knowing the ionization gradient, one can determine the penetrations of the magneto-ionically split components of the ray. Attenuation, lateral deviation, equivalent path, etc., can also be calculated with their help. Booker, in the paper referred to above, has worked out, as an example, the case, where each of the components, angle of incidence  $\theta$ , angle between the plane of incidence and the magnetic meridian  $\varphi$ , and the magnetic dip  $\eta$ , are each of  $45^\circ$ . In this paper, we shall utilise equation (1) to draw the propagation curves for the equatorial region, for a number of typical cases.

## 2. PROPAGATION CURVES FOR THE EQUATORIAL REGION

Since the  $q$ - $x$  curves are symmetrical for the case of equatorial propagation, the curves have all been drawn to delineate the variation of  $q^2$  with  $x$ , rather than that of  $q$  with  $x$ . For such cases of propagation, the general condition of reflection *viz.*,  $\frac{dq}{dx} = \infty$  becomes identical with the condition  $q=0$ .

Since the condition of reflection *viz.*,  $\frac{dq}{dx} = \infty$  becomes identical with the condition  $q=0$ .

It is to be noted that for east-west propagation, the  $q^2$ - $x$  curves are

symmetrical not only for equatorial propagation but also for propagation in any other plane parallel to magnetic equator.

The nature of the propagation curves for the symmetrical and unsymmetrical cases is illustrated in figure 3. In these and all other curves to follow, the continuous lines represent ordinary and the discontinuous lines represent extraordinary components.

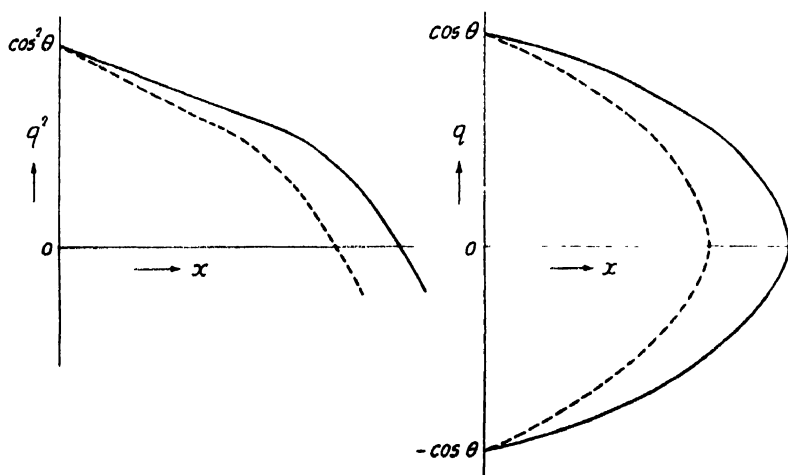


FIG. 3(a)

$q^2$ - $x$  and  $q$ - $x$  curves for the symmetrical cases

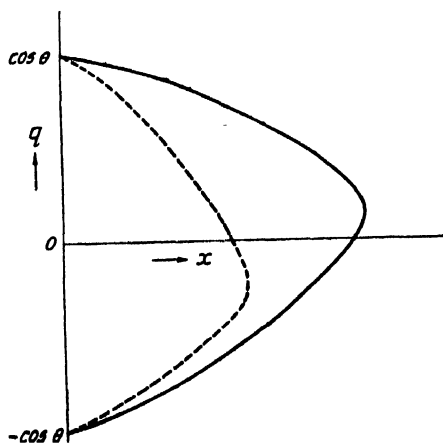


FIG. 3(b)

$q$ - $x$  curves for an unsymmetrical case

In this section we shall delineate the propagation curves for three values of wave frequencies, related to the gyro-frequency ( $f_H$ ) as follows :

- (i)  $f = \frac{1}{2}f_H$ , (ii)  $f = 2f_H$ , (iii)  $f = 5f_H$ .

For each frequency, curves are plotted for six azimuths of propagation, or, for eight values of  $\varphi$ , viz.,  $\varphi = 0^\circ$  or  $180^\circ$  (north-south),  $\varphi = \pm 30^\circ$ ,  $\varphi = \pm 60^\circ$  and  $\varphi = \pm 90^\circ$  (east-west).

(i)  $f = \frac{1}{2}f_H$  : figures 4(a), (b), (c) and (d).

The propagation curves are drawn for four angles of incidence, viz.,  $\theta = 10^\circ, 30^\circ, 45^\circ$  and  $60^\circ$ .

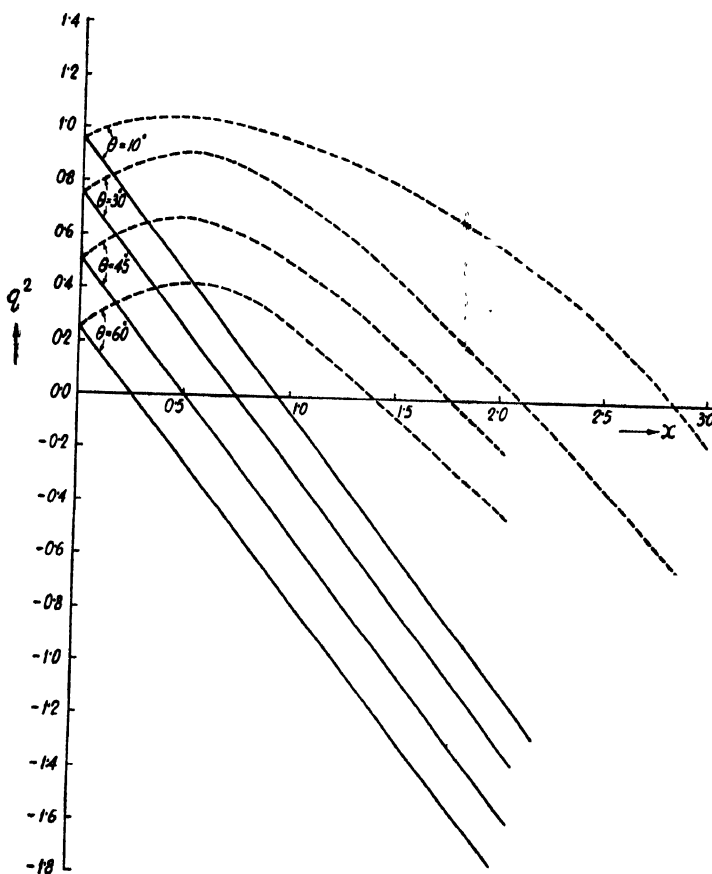


FIG. 4(a)

$q^2$ - $x$  curves in the equatorial region for  $f = \frac{1}{2}f_H$  and for  $\cos \phi = 0$ , i.e., for east-west propagation.

It will be seen from the curves that for all values of  $\varphi$ , the critical value of  $x$  for the ordinary component lies between  $x = c^2$  and  $x = 1$  when

$\theta < \tan^{-1} \sqrt{y}$  and between  $x = c^2$  and  $x = c^2(1 + y)$  where  $\theta > \tan^{-1} \sqrt{y}$ .

The critical values of  $x$  for the extraordinary component lies between  $x = c^2(1 + y)$  and  $x = \frac{1}{2}\{1 + c^2 + \sqrt{s^4 + 4y^2c^2}\}$  when  $\theta < \tan^{-1} \sqrt{y}$  and between  $x = 1$  and  $x = \frac{1}{2}\{1 + c^2 + \sqrt{s^4 + 4y^2c^2}\}$  when  $\theta > \tan^{-1} \sqrt{y}$

(ii)  $f = 2f_H$  : figures 5(a), (b), (c) and (d).

The propagation curves are drawn for five angles of incidence, viz.,  $\theta = 10^\circ, 30^\circ, 45^\circ, 60^\circ$  and  $90^\circ$ . It will be seen that the critical values of  $x$  for the ordinary component lies between the same limits as those for the case of  $f = \frac{1}{2}f_H$ . The critical value of  $x$  for the extraordinary component lies between

$$x = c^2(1 - y) \text{ and } x = \frac{1}{2}\{1 + c^2 - \sqrt{s^4 + 4y^2c^2}\}.$$

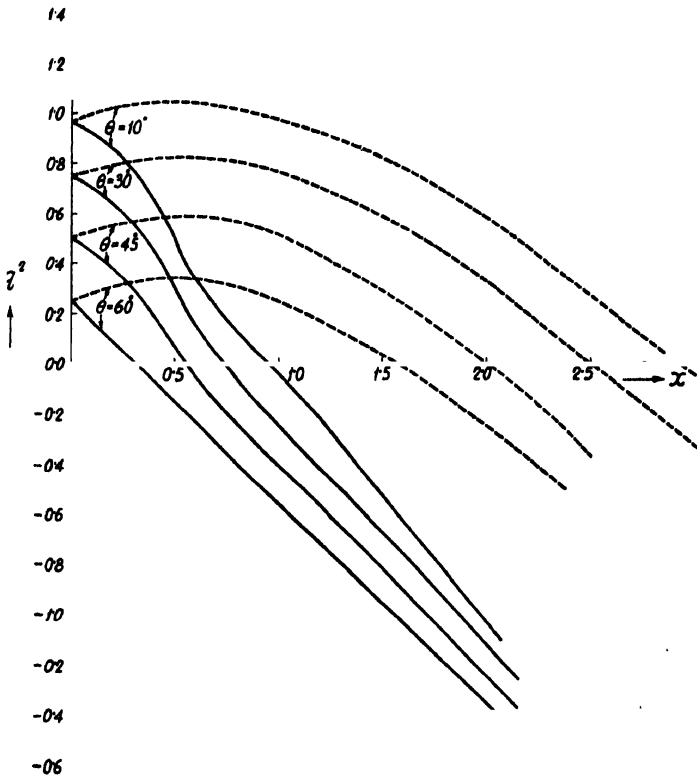


FIG. 4(b)

$q^2$ - $x$  curves in the equatorial region for  $f = \frac{1}{2}fH$  and for  $\cos \phi = \pm 0.5$ , i.e., the plane of incidence making an angle of  $\pm 60^\circ$  with the magnetic meridian.

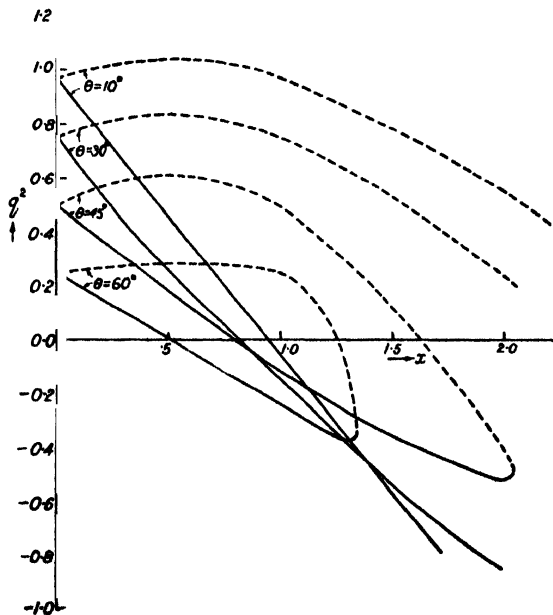


FIG. 4(c)

$q^2$ - $x$  curves in the equatorial region for  $f = \frac{1}{2}fH$  and for  $\cos \phi = \pm 0.866$ , i.e., the plane of incidence making an angle of  $\pm 30^\circ$  with the magnetic meridian.



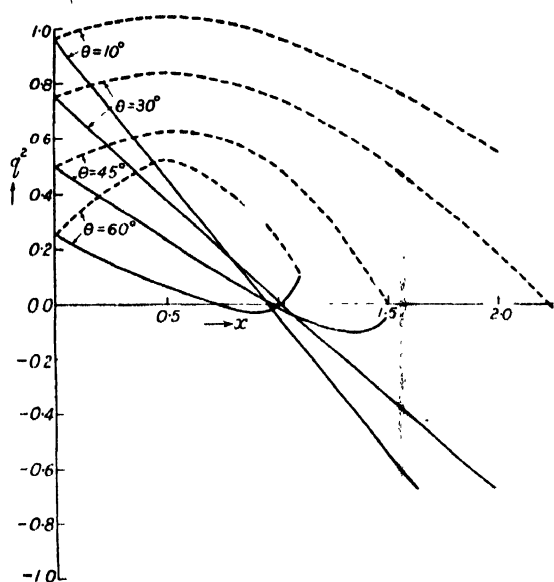


FIG. 4(d)

$q^2$ - $x$  curves in the equatorial region for  $f = \frac{1}{2}H$  and for  $\cos \phi = \pm 1.0$ , i.e., for north-south transmission.

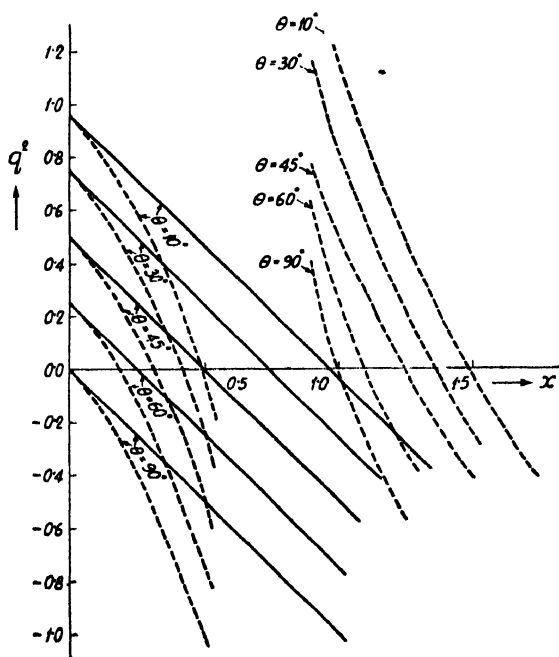


FIG. 5(a)

$q^2$ - $x$  curves in the equatorial region for  $f = 2H$  and for  $\cos \phi = 0$ , i.e., for east-west transmission.

(iii)  $f = 5H$  : figures 6(a), (b), (c) and (d).

The propagation curves are drawn for four angles of incidence, viz.,  $\theta = 30^\circ$ ,  $45^\circ$ ,  $60^\circ$  and  $90^\circ$ . Here again, it will be noticed that the ordinary component of the critical value of  $x$  lies between the same limits as those in the case

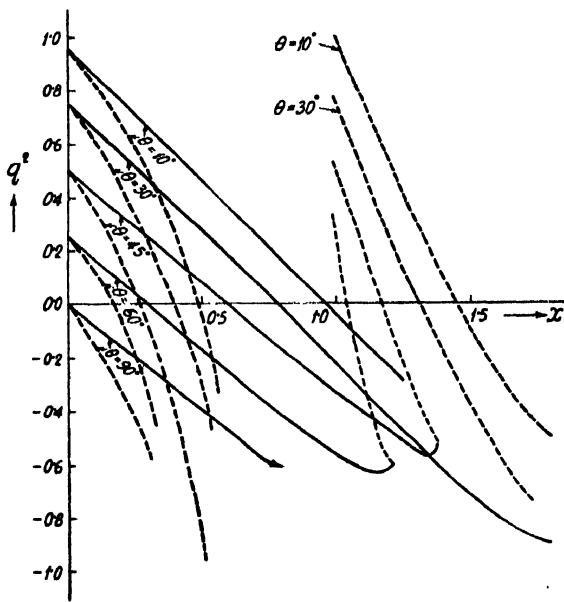


FIG. 5(b)

$q^2$ - $x$  curves in the equatorial region for  $f=2/H$  and for  $\cos \phi = \pm 0.5$ , i.e., the plane of incidence making an angle of  $\pm 60^\circ$  with the magnetic meridian.

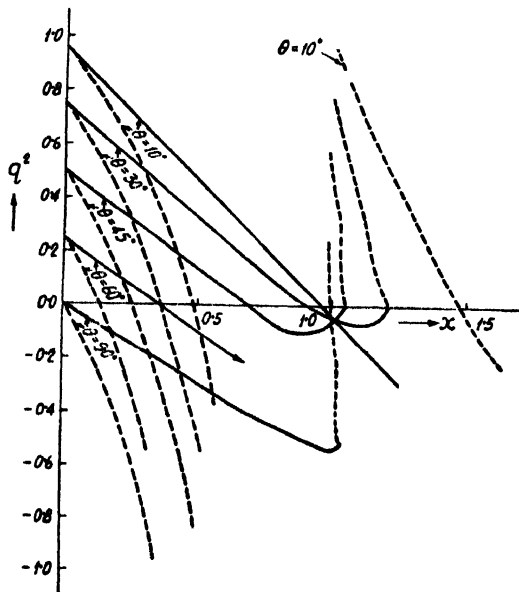


FIG. 5(c)

$q^2$ - $x$  curves in the equatorial region for  $f=2/H$  and for  $\cos \phi = \pm 0.866$ , i.e., the plane of incidence making an angle of  $\pm 30^\circ$  with the magnetic meridian

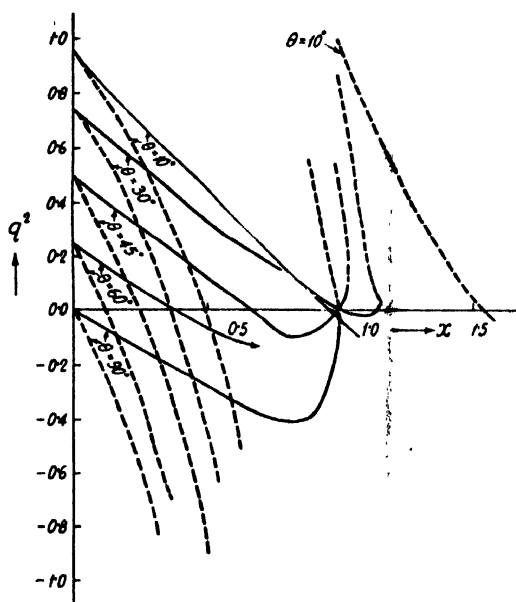


FIG. 5(d)

$q^2$ - $x$  curves in the equatorial region for  $f = 2/f_H$  and for  $\cos \phi = \pm 1.0$ , i.e., for north-south transmission.

$f = \frac{1}{2}f_H$ . It can be generally stated that for the ordinary ray, the critical value lies between the same limits as those given for  $f = \frac{1}{2}f_H$ , and is independent of the value of  $f$ , whether it is higher or lower than  $f_H$ .

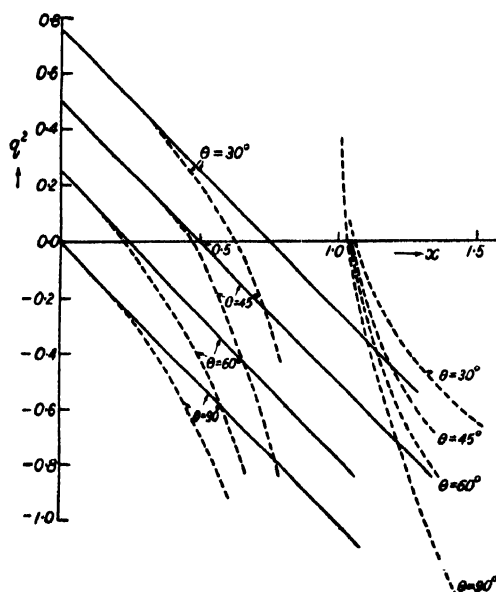


FIG. 6(a)

$q^2$ - $x$  curves in the equatorial region for  $f = 5/f_H$  and for  $\cos \phi = 0$ , i.e., for east-west transmission.

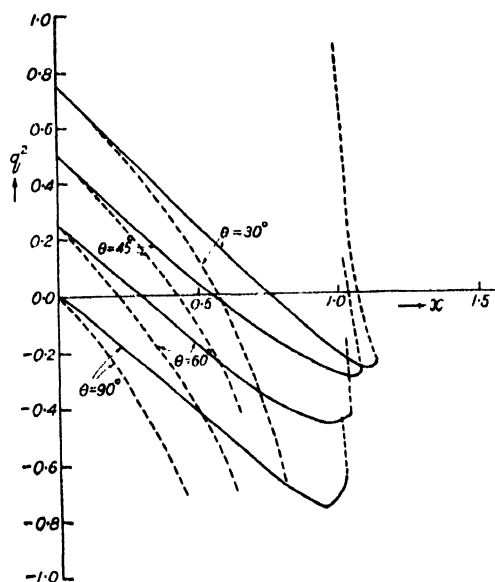


FIG. 6(b)

$q^2$ - $x$  curves in the equatorial region for  $f=5f_H$  and for  $\cos \phi = \pm 0.5$ , i.e., the plane of incidence making an angle of  $+60^\circ$  with the magnetic meridian.

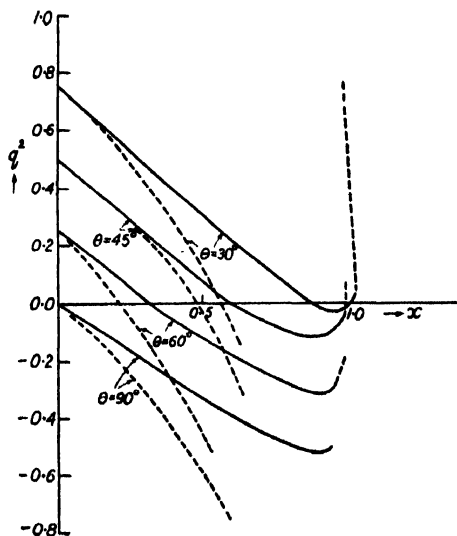


FIG. 6(c)

$q^2$ - $x$  curves in the equatorial region for  $f=5f_H$  and for  $\cos \phi = \pm 0.366$ , i.e., the plane of incidence making an angle of  $\pm 30^\circ$  with the magnetic meridian.

For the extraordinary component, the critical value of  $x$  lies between the same limits as for  $f=2f_H$ , which is generally valid for all values of  $f > f_H$ . From figures 5 and 6 (i.e. for  $f > f_H$ ) it will be noticed that for the case of equatorial propagation under consideration,  $q$  attains an infinite value when  $x = \frac{1-y^2}{1-y_s^2} = 1 - y^2$  (for the equatorial region). This value of  $x$

evidently corresponds to the so-called fourth condition of reflection found in the case of vertical propagation (Mitra, 1952).

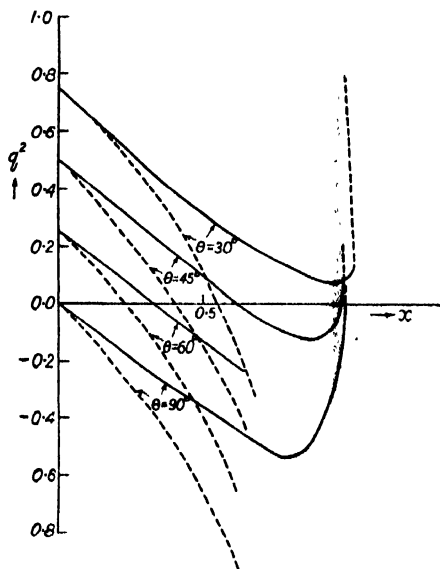


FIG. 6(d)

$q^2$ - $x$  curves in the equatorial region for  $f = 5f_H$  and for  $\cos \phi = \pm 1.0$ , i.e., for north-south transmission.

### 3. L A T E R A L D E V I A T I O N

Simple consideration of the magneto-ionic formula shows that as a result of the influence of the terrestrial magnetic field, there will, in general, be lateral deviation of the wave from the great circle path. As the ordinary and the extraordinary components are deviated to opposite sides of the great circle path, it follows that when the receiver receives the two components

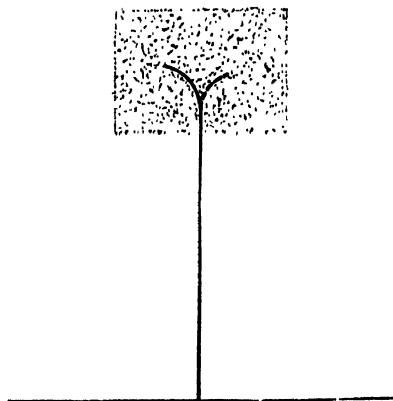


FIG. 7(a)

Lateral deviation for vertical incidence (not to the scale)

simultaneously, they must have come by reflection from different regions of the ionosphere separated not only vertically, but also horizontally [figure 7(b)], the

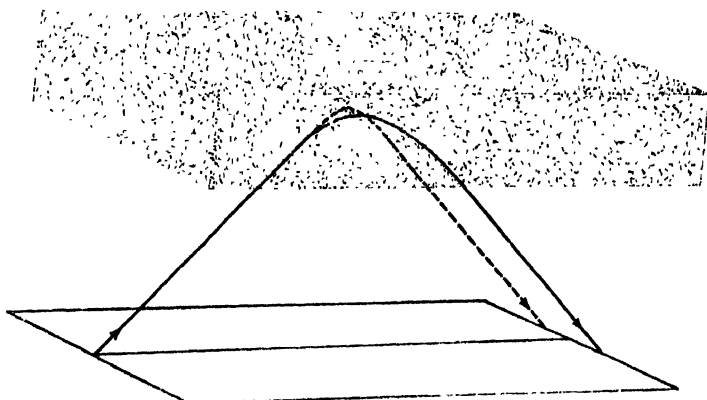


FIG. 7(b)

Lateral deviation for oblique incidence (not to the scale)

separation being of the order of a few kilometers. This explains the oft observed fact that the fadings of the two magneto-ionically split echoes are independent of each other. It is also to be noted that as for oblique propagation, the  $q$ - $x$  curves are in general, unsymmetrical about the  $x$ -axis the lateral deviations of the upgoing and the downcoming waves are also in general unequal. The lateral deviations for vertical and oblique incidences are roughly illustrated in figure 7.

It should be noted that when the propagation is in the magnetic meridian plane there is no lateral deviation. There is also no net lateral deviation in east-west transmission, *i.e.* in transmission in a magnetic latitudinal plane. In this case, though the wave is deviated in the ionosphere, the deviation of the upgoing and the downcoming waves are completely neutralized by each other.

To determine the lateral deviation for any given case, the curves showing the relation between  $dx_1/dh$  and  $x$ , as depicted in figure 8 after Booker, may be utilised. The lateral deviation per unit height is expressed as  $dx_1/dh$  (where  $x_1$  is the deviation from the great circle path).  $dx_1/dh$  tends to infinity as the reflection level is approached. This is because near the reflection level, change in  $h$  is very small, the group path becoming horizontal.

If the ionization gradient is assumed to be linear, then the total lateral deviation is simply calculated—being proportional to the area between the upgoing and downcoming branches of the appropriate curves. For parabolic or other types of gradient the calculation is somewhat more complicated, because the curves are to be replotted as appropriate functions of  $h$ . Results of calculation of total lateral deviation for two special cases of propagation, *viz.*, Calcutta-Bandoeng and Calcutta-Bombay on the assumption of linear gradient, are given in the next section.

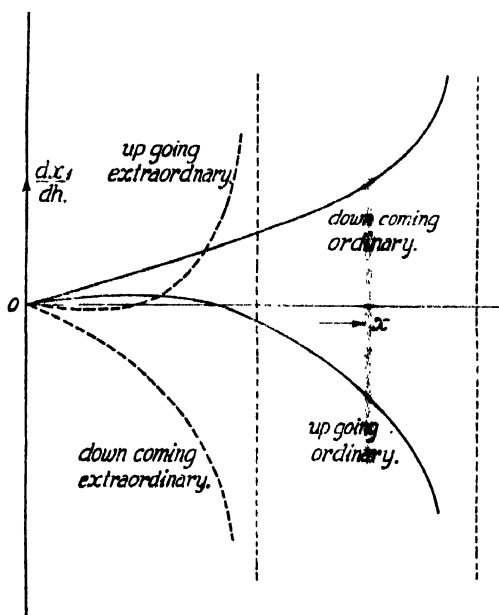


FIG. 8

Calculation of lateral deviation by the method of graphical integration

#### 4. TWO SPECIAL CASES OF RADIO PROPAGATION

(a) *Calcutta-Bandoeng*. The transmitted ray for propagation between Calcutta and Bandoeng (in Java) reaches the ionosphere at a point practically over the magnetic equator. Under such condition the formula for equatorial propagation, as discussed in Sec. 2, can be used. From the latitudes and longitudes of Calcutta and Bandoeng, and taking the ionospheric characteristics at the point of reflection to be the mean of these two stations, the angle of incidence for the single hop F-layer transmission was estimated by the method of Appleton and Beynon (1940) and found to be  $70^{\circ} 21'$ . From the value of the magnetic field at the F-layer, the gyro-frequency was found to be 1.001 Mc/s. The angle between the magnetic meridian and the plane of incidence is  $35^{\circ} 6'$  (Tuve and Fleming, 1946). Considering the 9.53 Mc/s transmission from the Calcutta Station of All India Radio, the  $q-x$  curve, as shown in figure 9, has been plotted. It is seen from the curve that the ordinary component is retarded more than the extraordinary, as is usual at such frequencies.

The total lateral deviation for the ordinary ray is found to be 3 Km. in a direction at right angles to the plane of incidence and towards the south pole. That for the extraordinary is about 2 Km. towards the north pole. Knowing the ionization gradient and the maximum ionization density at the point of reflection, the penetration of the ray within the ionosphere can be determined, and the retardation can be calculated.

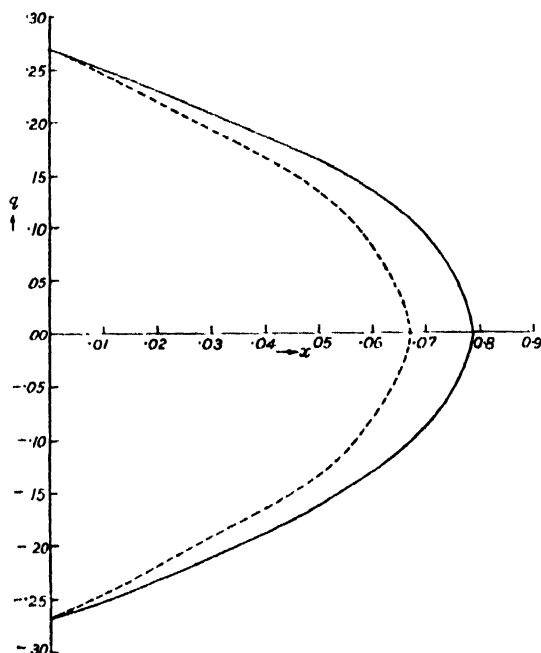
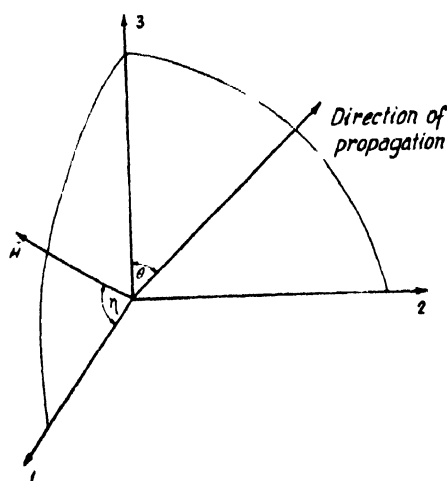


FIG. 9

$q$ - $x$  curves for propagation between Calcutta and Bandong

(b) *Calcutta-Bombay (east-west transmission)*. The case of Calcutta-Bombay transmission is of special interest as the ray path is practically coincident with a magnetic latitudinal plane. The case is thus of (magnetic) east-west transmission. For such case the general dispersion formula assumes



[ $\eta$  is the angle of dip at the point.]

FIG. 10

Co-ordinate axes as given in Eq. 2. The plane of incidence is given by the 23 plane, the direction 3 being the vertical  $\eta$  gives the angle of dip at the point.



a simpler form. The simplified formula as given by Booker (1938) is :

$$q^2 = c^2 - \frac{x(1-x)}{(1-x) - \frac{1}{2}(y_1^2 + s^2 y_s^2) \pm \sqrt{\frac{1}{4}(y_1^2 + s^2 y_s^2)^2 + y_s^2(c^2 - x)(1-x)}} \quad (2)$$

All the terms have got the same meaning as in equation (1).  $y_s$  and  $y_1$  are the components of  $\gamma$  in the vertical and horizontal directions, respectively. As the plane of incidence is at right angles to the magnetic meridian,  $y_1$  is perpendicular to the plane of incidence. [Here also, collisional damping has been neglected as in Sec. 2]

Knowing the latitudes and longitudes of Calcutta and Bombay and taking the ionosphere characteristics at the point of reflection to be the mean of these two stations, the angle of incidence as calculated by Appleton and Beynon's method is found to be  $65^\circ 48'$ . The magnetic dip at the point of reflection is  $30^\circ 10'$  and the gyro-frequency at the F-region was calculated to be 1.018 Mc/s. From these data the propagation curve for Calcutta-Bombay transmission at 9.53 Mc/s. has been drawn and is represented in figure 11.

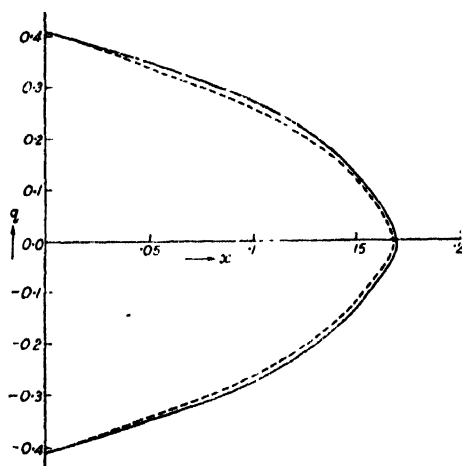


FIG. 11

$q$ - $x$  curves for propagation between Calcutta and Bombay

It is seen from the above figure that the retardation suffered by the two magneto-ionically split components are nearly equal. As it is a case of east-west propagation, the net lateral deviation for both the components is zero, though both the components suffer deviation within the ionized region, the ordinary being deviated towards south and the extraordinary towards north. The deviations suffered by the upgoing and downcoming waves are equal and opposite for both the components and neutralise each other. The maximum lateral deviation of the waves in their paths within the ionosphere is estimated to be about 2 Km. The penetration of the ray within the ionosphere can be determined as in the previous case.

## 52 CONCLUSION

The discussions as given above and the propagation curves for the ionospheric layers as have been plotted, are all for the case of a flat stratified ionospheric layer over a flat earth. The ionospheric layer is, however, curved, being concentric with the earth's curvature. The above calculations are, therefore, of limited accuracy and for more accurate results correction factors have to be introduced to take account of these curvatures. The correction factor is, however, in general not large. The expressions for the dispersion formula, attenuation, lateral deviation, etc. and the corresponding propagation curves from consideration of a curved ionosphere will be discussed in a future communication.

## ACKNOWLEDGMENTS

The author is indebted to Professor S. K. Mitra for his kind guidance and assistance, and to Mr. S. S. Baral for suggesting the work. Thanks are also due to the Scientific Man Power Committee, Government of India, for financial help.

## REFERENCES

- Mitra, S. K., 1952, *The Upper Atmosphere*, Second Edition, Asiatic Society, Calcutta.  
Booker, H. G., 1949, *J. Geo. Res.*, **54**, 243.  
Booker, H. G., 1938, *Phil. Trans. Roy. Soc.*, **A**, **237**, 411.  
Tuve, M. A. and Fleming, J. A., 1946, *The Geomagnetic Field, Its Description and Analysis*, Carnegie Institute of Washington Publication.  
Appleton, F. V. and Beynon, W. J. G., 1940, *Proc. Phys. Soc.*, **52**, 518.

# DETONATION OF PROTON GAS

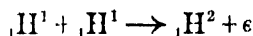
By M. P. MURGAI

DEFENCE SCIENCE LABORATORY, NEW DELHI

(Received for publication, March 7, 1952)

**ABSTRACT.** The hydrodynamic theory of detonation has been applied to proton gas. Due to the very high value of the energy released in the proton-proton reaction, the calculated values of detonation parameters are much greater than those for chemical explosives. Due account of radiation pressure and energy has been taken.

The Chapman-Jouguet theory of detonation, when applied to chemical explosives, enables the various parameters of detonation to be determined from purely initial and final states of the explosive, along with a suitable equation of state for the products, without the knowledge of the intermediate kinetics. This fact suggests the extension of the theory to the nuclear explosive phenomenon. The present work is an attempt at calculating such parameters for proton gas enclosed in a cylindrical tube of uniform cross section. The postulated reaction, when the non-reactive shock traverses the gas, is the formation of deuteron so that we have



Due to the high value of  $\epsilon$ , as compared to that for ordinary high explosives, the temperatures are extremely high ; so that due account of the pressure and the energy of radiation has to be taken in applying the conservation laws. In fact, due to the very rapid variation of radiation pressure with temperature, as compared to the kinetic pressure, both are important simultaneously only in a very narrow range and the former is important beyond, and the latter is so, before that range of temperature. The change in the kinetic pressure in this case is much more due to high temperature, than due to compression by the pressure behind the shock. Therefore, it is predicted fairly accurately by the perfect gas equation  $p_v = RT$ .

The radiation pressure  $p_r = \frac{a}{3} T^4$ ,  $a$  being the energy density constant.

By the application of the laws of conservation of mass, momentum, and energy, we have in this case,

$$D^2 \rho_0^2 = (p + p_r) \rho' \quad \dots (1)$$

$$W^2 = \left( \frac{p + p_r}{\rho'} \right) \quad \dots (2)$$

$$1/\rho' = 1/\rho_0 - 1/\rho$$

$$(E + E_r) - \alpha \epsilon = \frac{1}{2}(p + p_r)(v_0 - v) \quad \dots (3)$$

in which  $D$  and  $W$  are the detonation velocity and the particle velocity respectively,  $p$  and  $p_r$  are the kinetic pressure and the radiation pressure;  $E$ ,  $E_r$  are the thermal energy and the energy due to radiation;  $\epsilon$ , the heat of the reaction;  $\alpha$  is a parameter which takes account of the cross section of the reaction;  $v_0$ ,  $v$  are the specific volumes in the initial and the final states of the explosives.

From the relations  $E_r = 3p_r v \quad \dots (4)$

$$E = \bar{C}_v T \quad \dots (5)$$

$$T = \left(\frac{3}{a}\right)^{1/4} p_r^{1/4} \quad \dots (6)$$

$$p = \frac{R}{v} \left(\frac{3}{a}\right)^{1/4} p_r^{1/4} \quad \dots (7)$$

we have the Rankine-Hugoniot equation

$$\alpha_5 p_r^{1/4} + 3.5 p_r v - \alpha_4 p_r - \alpha_2 p_r^{1/4} / v - \alpha \epsilon = 0 \quad \dots (8)$$

where

$$\alpha_5 = \alpha_1 + \alpha_3 \quad \dots (8a)$$

$$\alpha_1 = \bar{C}_v \left(\frac{3}{a}\right)^{1/4} \quad \dots (8b)$$

$$\alpha_2 = \frac{R}{2} \left(\frac{3}{a}\right)^{1/4} v_0 \quad \dots (8c)$$

$$\alpha_3 = \frac{R}{2} \left(\frac{3}{a}\right)^{1/4} \quad \dots (8d)$$

$$\alpha_4 = 0.5 v_0 \quad \dots (8e)$$

The value of  $\epsilon$ , if 1 Kgm of the gas undergoes the reaction completely ( $\alpha=1$ ), is

$$1.05 \times 10^{10} \text{ Kc/Kgm.}$$

$\bar{C}_v$  can be taken to be the value of the specific heat for a perfect non-degenerate diatomic gas = 3.5 Kc/Kgm.

$$a = 1.81 \times 10^{-25} \text{ Kc/cc/T}^4$$

$$v_0 = 11.14 \times 10^6 \text{ cc/Kgm.}$$

Putting these values eqn. (8) becomes

$$8.07 \times 10^6 p_r^{1/4} + 3.5 p_r v - 5.57 \times 10^6 p_r - 1.13 \times 10^{13} p_r^{1/4} / v - 1.05 \times 10^{10} \alpha = 0$$

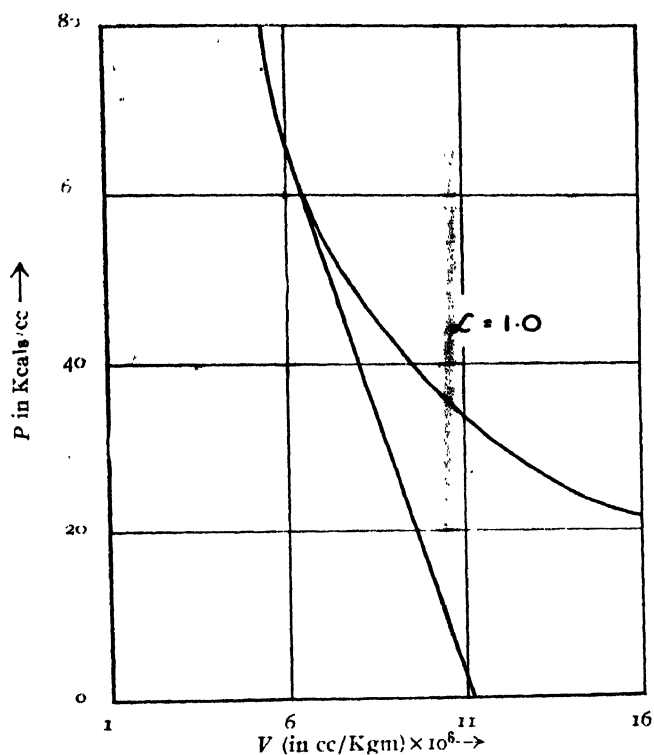


FIG. 1. R-H curves for proton gas

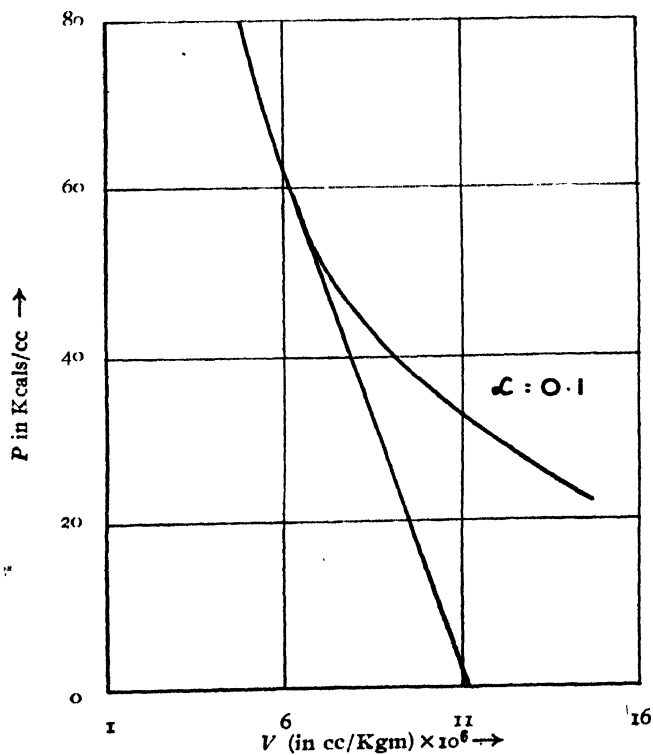


FIG. 2. R-H curves for proton gas

These curves have been drawn for  $\alpha = 1.0, 0.1$  and  $0.001$  (see figures 1—3). The Chapman-Jouguet points, which are the points at which tangents from  $(0, v_0)$  touch the curves provide the data to calculate the following :

$\alpha$	$P$ dynes/cm	$v$ cc/Kgm	$T^\circ K$	$D$ cm/sec	$W$ cm/sec
1.0	$2.51 \times 10^{13}$	$6.58 \times 10^6$	$1.0 \times 10^7$	$8.26 \times 10^8$	$3.39 \times 10^8$
0.1	$2.04 \times 10^{12}$	$5.80 \times 10^6$	$5.84 \times 10^6$	$2.64 \times 10^8$	$1.25 \times 10^8$
0.001	$3.09 \times 10^{10}$	$4.71 \times 10^6$	$1.62 \times 10^6$	$2.51 \times 10^7$	$1.19 \times 10^7$

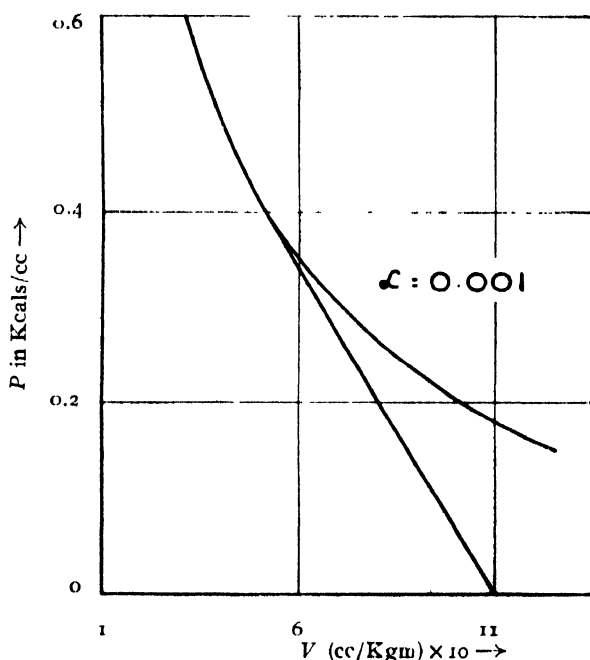


FIG. 3. R-H curves for proton gas

For the first two values of  $\alpha$ ,  $p_r \gg p$ , but for  $\alpha = 0.001$  both  $p_r$  and  $p$  are comparable. Figure 3 gives  $p_r$ ; then  $p$  is known from equation (7) whence by virtue of equations (1) and (2) various parameters are calculated. (cf.—Calculations made by Caldirola (1948) for uranium, who has taken account of  $p_r$  only, without introducing  $\alpha$ ).

#### ACKNOWLEDGMENT

The author is grateful to Dr. D. S. Kothari, Scientific Adviser to the Govt. of India, Ministry of Defence, for suggesting the problem and for his interest during the course of the work.

#### REFERENCE

Caldirola, 1948, *J. Chem. Phys.*, **16**, 846.

# ON THE DISTRIBUTION OF INITIAL STRESS DUE TO DISLOCATION IN AN INFINITE PLATE CONTAINING TWO UNEQUAL CIRCULAR HOLES\*

By B. KARUNES

DEPARTMENT OF APPLIED PHYSICS, UNIVERSITY COLLEGE OF SCIENCE AND TECHNOLOGY,  
CALCUTTA

(Received for publication, April 17, 1952)

**ABSTRACT.** Solutions are obtained for two problems on state of initial stress due to dislocation in an infinite plate containing two unstressed unequal circular holes. The dislocations are due to (1) a parallel fissure joining the two circular holes or joining each hole to infinity and (2) two opposite kinds of wedge shaped fissures of the same apex-angles, on two sides of the  $x$ -axis. Cases of equal holes in each of these problems are treated as particular examples and tables for numerical values of the constant coefficients when the hole boundaries are  $a=0.8$  and  $a=-0.8$  are given. Graphs showing the stresses are drawn and discussed.

## INTRODUCTION

Let an elastic body, occupying a multiply connected region, be cut along a system of barriers which would make the region occupied by the body simply connected and let the two faces of each barrier be rejoined after removal or insertion of thin slices of the same material. Then the state of initial stress of the body is given by a solution of equations of elastic equilibrium which gives rise to multiple valued displacements, the displacements on one side of the barrier relative to the other being possible in a rigid body. In the present paper solutions are given of two problems of dislocation in an infinite elastic plate containing two unequal circular holes. In the first, dislocation is due to a parallel fissure joining the two circular holes or joining each hole to infinity, while in the second, dislocation is due to a wedge shaped fissure on one side of the  $x$ -axis with its apex at the origin and insertion of a similar wedge shaped strip below the  $x$ -axis. The solutions are obtained in bipolar co-ordinates, defined by the substitution (Jeffery, 1921)

$$\alpha + i\beta = \log \frac{x + i(y+a)}{x + i(y-a)}$$

Here

$$x = \frac{a \sin \beta}{\cosh \alpha - \cos \beta}, \quad y = \frac{a \sinh \alpha}{\cosh \alpha - \cos \beta}$$

and

$$h = \frac{d(\alpha + i\beta)}{d(x + iy)} = \frac{1}{\cosh \alpha - \cos \beta}$$

\* Communicated by Prof. P. C. Mahanti

In terms of the stress function  $\chi$ , the displacements are given by

$$2\mu u = \frac{\mu}{\lambda + \mu} \cdot h \cdot \frac{\partial \chi}{\partial \alpha} - h \frac{\partial Q}{\partial \beta} \quad \dots (1)$$

$$2\mu v = \frac{\mu}{\lambda + \mu} h \frac{\partial \chi}{\partial \beta} + h \frac{\partial Q}{\partial \alpha}$$

where

$$hQ = \frac{\lambda + 2\mu}{2(\lambda + \mu)} \iint \left\{ \frac{\partial^2(h\chi)}{\partial \alpha^2} - \frac{\partial^2(h\chi)}{\partial \beta^2} - h\chi \right\} d\alpha \cdot d\beta \quad \dots (2)$$

and the stresses are given by

$$a\alpha\alpha = \left\{ (\cosh \alpha - \cos \beta) \frac{\partial^2}{\partial \beta^2} - \sinh \alpha \frac{\partial}{\partial \alpha} - \sin \beta \frac{\partial}{\partial \beta} + \cosh \alpha \right\} (h\chi)$$

$$\left\{ (\cosh \alpha - \cos \beta) \frac{\partial^2}{\partial \alpha^2} - \sinh \alpha \frac{\partial}{\partial \alpha} - \sin \beta \frac{\partial}{\partial \beta} + \cos \beta \right\} (h\chi) \quad \dots (3)$$

$$a\alpha\beta = -(\cosh \alpha - \cos \beta) \frac{\partial^2}{\partial \alpha \partial \beta} (h\chi)$$

#### DISLOCATION DUE TO A PARALLEL FISSURE

Let  $\alpha = \alpha_1$  and  $\alpha = -\alpha_2$  be the boundaries of the two unequal circular holes in an infinite plate.

To obtain many valued terms in expressions for displacements, let us choose a stress function

$$h\chi_0 = A\alpha \sinh \alpha \quad (4)$$

Writing only the many valued terms in the displacements, we have

$$u = \frac{\lambda + 2\mu}{2\mu(\lambda + \mu)} \cdot \frac{A\beta \sinh \alpha \sin \beta}{\cosh \alpha - \cos \beta}$$

$$v = \frac{\lambda + 2\mu}{2\mu(\lambda + \mu)} \cdot \frac{A\beta(1 - \cosh \alpha \cos \beta)}{\cosh \alpha - \cos \beta} \quad (5)$$

when  $\beta = \pi$

$$u_+ = 0; \quad v_+ = \frac{\lambda + 2\mu}{2\mu(\lambda + \mu)} \cdot \pi A \quad (6)$$

and when  $\beta = -\pi$

$$u_- = 0; \quad v_- = -\frac{\lambda + 2\mu}{2\mu(\lambda + \mu)} \cdot \pi A \quad (7)$$

Thus  $u$  remains continuous across the barrier  $\beta = \pm \pi$ , i.e., the  $y$ -axis and  $v$  suddenly decreases by the constant amount

$$\frac{\lambda + 2\mu}{\mu(\lambda + \mu)} \cdot \pi A$$

Therefore, the chosen stress function  $h\chi_0$  will suit the state of dislocation due to a parallel fissure of that thickness along the line joining the centres



of the two holes or any other line parallel to this line cutting both the circles  $\alpha = \alpha_1$  and  $\alpha = -\alpha_2$ .

The stress function  $h\lambda_0$  produces normal stresses over the circular boundaries  $\alpha = \alpha_1$  and  $\alpha = -\alpha_2$  and they are given by

$$a \widehat{\alpha\alpha}_1 = -A \sinh^2 \alpha_1; \quad a \widehat{\alpha\alpha}_{-2} = -A \sinh^2 \alpha_2 \quad (8)$$

To reduce these stresses to zero, for the case of stress-free boundaries, add a stress function  $h\chi_1$  to  $h\lambda_0$ , where

$$h\chi_1 = B_{01}\alpha(\cosh \alpha - \cos \beta) + (A_{11} \cosh 2\alpha + B_{11} + C_{11} \sinh 2\alpha) \cos \beta \quad \dots \quad (9)$$

and it gives stresses over the circular boundaries, equal and opposite to those given by  $h\lambda_0$ , i.e.

$$\widehat{\alpha\alpha}_1 = \frac{A}{a} \sinh^2 \alpha_1; \quad \widehat{\alpha\alpha}_{-2} = \sinh^2 \alpha_2 \quad (10)$$

From the solution given by Jeffery (1921) for an eccentrically bored pipe under constant pressure over its boundaries, where he used the same stress function as  $h\chi_1$ , we obtain by suitable substitutions

$$\begin{aligned} B_{01} &= 2AM(\sinh^2 \alpha_2 - \sinh^2 \alpha_1) \cosh(\alpha_1 + \alpha_2) \\ A_{11} &= -AM(\sinh^2 \alpha_2 - \sinh^2 \alpha_1) \sinh(\alpha_1 - \alpha_2) \\ C_{11} &= AM(\sinh^2 \alpha_2 - \sinh^2 \alpha_1) \cosh(\alpha_1 - \alpha_2) \\ B_{11} &= AM\{\sinh^2 \alpha_1 \cosh(\alpha_1 + \alpha_2) \sinh 2\alpha_2 \\ &\quad + \sinh^2 \alpha_2 \cosh(\alpha_1 + \alpha_2) \sinh 2\alpha_1 \\ &\quad - (\sinh^2 \alpha_2 + \sinh^2 \alpha_1) \sinh(\alpha_1 + \alpha_2)\} \end{aligned} \quad (11)$$

where

$$M = \frac{1}{2} \operatorname{cosech}(\alpha_1 + \alpha_2) \{\sinh^2 \alpha_2 + \sinh^2 \alpha_1\}^{-1} \quad (12)$$

From the sum of the stress functions  $h\lambda_0$  and  $h\chi_1$ , we get no stress over the boundaries  $\alpha = \alpha_1$  and  $\alpha = -\alpha_2$ , but a constant all round stress is obtained at infinity ( $\alpha = 0, \beta = 0$ ). The value of this stress is given by

$$\begin{aligned} a \widehat{\alpha\alpha} = a \widehat{\beta\beta} &= AM \sinh \alpha_1 \sinh \alpha_2 \{\sinh 2(\alpha_1 + \alpha_2) - \sinh 2\alpha_1 - \sinh 2\alpha_2\} \\ &= \text{constant} = S \text{ (say)} \end{aligned} \quad \dots \quad (13)$$

For the complete solution of the problem we must add to ( $h\lambda_0 + h\chi_1$ ) another stress function  $h\chi_2$  such that  $h\chi_2$  produces stresses equal and opposite to ( $S/a$ ) at infinity and no stress over the boundaries  $\alpha = \alpha_1$  and  $\alpha = -\alpha_2$ . To get the required all round constant stress at a great distance from the holes, we may choose

$$h\chi_{20} = -\frac{1}{2}S(\cosh \alpha + \cos \beta) \quad \dots \quad (14)$$

and add to it another stress function

$$h\chi_{21} = \frac{1}{2}S \left\{ B_0\alpha + K \log(\cosh \alpha - \cos \beta) \right\} (\cosh \alpha - \cos \beta) + \sum_{n=1}^{\infty} \phi_n(\alpha) \cos n\beta \quad (15)$$

where

$$\begin{aligned}\phi_n(\alpha) = & A_n \cosh (n+1)\alpha + B_n \cosh (n-1)\alpha \\ & + C_n \sinh (n+1)\alpha + D_n \sinh (n-1)\alpha\end{aligned}\quad \dots (16)$$

for  $n \geq 2$ , and

$$\phi_1(\alpha) = A_1 \cosh 2\alpha + B_1 + C_1 \sinh 2\alpha$$

$h\chi_{21}$  is such that it produces no stress at infinity and the sum ( $h\chi_{20} + h\chi_{21}$ ) =  $h\chi_2$  produces no stress over the holes  $\alpha = \alpha_1$  and  $\alpha = -\alpha_2$ .

We get, when  $\alpha > 0$ ,

$$\begin{aligned}h\chi_2 = & -\frac{1}{2}S \left[ \cosh \alpha + (B_0 + K)\alpha \cosh \alpha - K \log 2 \cosh \alpha + K e \right. \\ & + \left\{ 1 - (B_0 + K)\alpha + K \log 2 - 2K \cosh \alpha e^{-\alpha} + \frac{K}{2} e^{-2\alpha} + \phi_1(\alpha) \right\} \cos \beta \\ & + K \sum_{n=2}^{\infty} \frac{1}{n(n^2-1)} \left\{ (n+1)e^{-(n-1)\alpha} - (n-1)e^{-(n+1)\alpha} \right\} \cos n\beta \\ & \left. + \sum_{n=2}^{\infty} \phi_n(\alpha) \cos n\beta \right]\end{aligned}\quad (17)$$

and when  $\alpha < 0$ ,

$$\begin{aligned}h\chi_2 = & -\frac{1}{2}S \left[ \cosh \alpha + (B_0 - K)\alpha \cosh \alpha - K \log 2 \cosh \alpha + K e^{\alpha} \right. \\ & + \left\{ 1 - (B_0 - K)\alpha + K \log 2 - 2K \cosh \alpha e^{\alpha} + \frac{K}{2} e^{2\alpha} + \phi_1(\alpha) \right\} \cos \beta \\ & + K \sum_{n=2}^{\infty} \frac{1}{n(n^2-1)} \left\{ (n+1)e^{(n-1)\alpha} - (n-1)e^{(n+1)\alpha} \right\} \cos n\beta \\ & \left. + \sum_{n=2}^{\infty} \phi_n(\alpha) \cos n\beta \right]\end{aligned}\quad (18)$$

To calculate the values of the constant coefficients, the boundary conditions for no stress (Jeffery, 1921),

$$\begin{aligned}\text{and} \quad \frac{\sigma}{\partial \alpha}(h\chi) = \text{constant} = \rho \\ h\chi = \rho \tanh \alpha + \sigma (\cosh \alpha \cos \beta - 1) + \tau \sin \beta\end{aligned}\quad \dots (19)$$

are applied separately on equations (17) and (18) for the boundaries  $\alpha = \alpha_1$  and  $\alpha = -\alpha_2$  respectively. We obtain

$$\begin{aligned}B_0 = & KN_1 \{ \cosh 2(\alpha_1 + \alpha_2) - 1 \} (\cosh 2\alpha_2 - \cosh 2\alpha_1) \\ A_1 = & -KN_1 (\cosh 2\alpha_1 - 1) (\cosh 2\alpha_2 - 1) (\sinh 2\alpha_2 + \sinh 2\alpha_1) + K/2 \\ B_1 = & KN_1 (\cosh 2\alpha_1 - 1) (\cosh 2\alpha_2 - 1) \sinh 2(\alpha_1 + \alpha_2) - 2 \\ C_1 = & -\frac{1}{2}KN_1 [ (\cosh 2\alpha_2 - 1) (\cosh 2\alpha_1 - \cosh 2\alpha_2 - \sinh 2\alpha_1 \sinh 2\alpha_2 \\ & - \sinh^2 2\alpha_1) + (\cosh 2\alpha_1 - 1) (\cosh 2\alpha_1 - \cosh 2\alpha_2 \\ & + \sinh 2\alpha_1 \sinh 2\alpha_2 + \sinh^2 2\alpha_1) ]\end{aligned}\quad \dots (20)$$

where

$$N_1 = \{\cosh 2(\alpha_1 + \alpha_2) - 1\}^{-1} (\cosh 2\alpha_1 + \cosh 2\alpha_2 - 2)^{-1} \quad \dots \quad (21)$$

and for  $n \geq 2$ ,

$$\begin{aligned} A_n &= \frac{KN}{n(n+1)} \left[ (n \sinh 2\alpha_2 - \sinh 2n\alpha_2) \{-(n+1) + n \cosh 2\alpha_1 + \cosh 2n\alpha_1\} \right. \\ &\quad \left. + (n \sinh 2\alpha_1 - \sinh 2n\alpha_1) \{-(n+1) + n \cosh 2\alpha_2 + \cosh 2n\alpha_2\} + N^{-1} \right] \\ B_n &= -\frac{KN}{n(n-1)} \left[ (n \sinh 2\alpha_2 - \sinh 2n\alpha_2) \{(n-1) - n \cosh 2\alpha_1 + \cosh 2n\alpha_1\} \right. \\ &\quad \left. + (n \sinh 2\alpha_1 - \sinh 2n\alpha_1) \{(n-1) - n \cosh 2\alpha_2 + \cosh 2n\alpha_2\} + N^{-1} \right] \quad (22) \\ C_n &= \frac{KN}{n(n+1)} \left[ n \{\cosh 2(n\alpha_1 - \alpha_2) - \cosh 2(n\alpha_2 - \alpha_1)\} \right. \\ &\quad \left. + (n+1) \{n(\cosh 2\alpha_1 - \cosh 2\alpha_2) - (\cosh 2n\alpha_1 - \cosh 2n\alpha_2)\} \right] \\ D_n &= \frac{KN}{n(n-1)} \left[ n \{\cosh 2(n\alpha_1 + \alpha_2) - \cosh 2(n\alpha_2 + \alpha_1)\} \right. \\ &\quad \left. - (n-1) \{n(\cosh 2\alpha_1 - \cosh 2\alpha_2) + (\cosh 2n\alpha_1 - \cosh 2n\alpha_2)\} \right] \end{aligned}$$

where

$$N = \{\cosh 2n(\alpha_1 + \alpha_2) - n^2 \cosh 2(\alpha_1 + \alpha_2) + (n^2 - 1)\}^{-1} \quad \dots \quad (23)$$

To obtain the values of  $K$ , we have

$$\sum_{n=1}^{\infty} \phi_n(0) = 0 \quad \dots \quad (24)$$

as  $h\chi_1$  is to produce no stress at infinity ( $\alpha=0$ ,  $\beta=0$ ).

Putting

$$A_1 = K/2 + Ka_1 \quad B_1 = -2 + Kb_1$$

and for  $n \geq 2$

$$A_n = \frac{K}{n(n+1)} + Ka_n \quad B_n = -\frac{K}{n(n-1)} + Kb_n$$

we get from (24)

$$K(a_1 + b_1) + K \sum_{n=2}^{\infty} (a_n + b_n) = 2 \quad \dots \quad (25)$$

$a_1$ ,  $b_1$ ,  $a_n$ ,  $b_n$  being known from (22), the values of  $K$  can be calculated.

Therefore, the complete solution for the state of initial stress caused by dislocation due to a parallel fissure between the unequal circular holes is given by the stress function

$$\begin{aligned}
h\chi &= h\chi_0 + h\chi_1 + h\chi_2 \\
&= A\alpha \sinh \alpha + B_0\alpha(\cosh \alpha - \cos \beta) \\
&\quad + (A_{11} \cosh 2\alpha + B_{11} + C_{11} \sinh 2\alpha) \cos \beta \\
&\quad - \frac{1}{2}S \left[ \cosh \alpha + \cos \beta + \{B_0\alpha + K \log (\cosh \alpha - \cos \beta)\}(\cosh \alpha - \cos \beta \right. \\
&\quad \left. + \sum_{n=1}^{\infty} \phi_n(\alpha) \cos n\beta \right]
\end{aligned} \tag{26}$$

The circumferential stress  $\widehat{\beta\beta}$  over the hole boundaries  $\alpha = \alpha_1$  and  $\alpha = -\alpha_2$  are calculated from the complete stress function  $h\chi$  as

$$\begin{aligned}
a\widehat{\beta\beta}_1 &= 2A \cosh \alpha_1 (\cosh \alpha_1 - \cos \beta) \\
&\quad + JAM(\cosh \alpha_1 - \cos \beta)(\sinh^2 \alpha_2 - \sinh^2 \alpha_1) \\
&\quad \times \{\sinh (\alpha_1 + \alpha_1) \cos \beta + \sinh \alpha_1 \cosh (\alpha_1 + \alpha_2)\} \\
&\quad - \frac{1}{2}S(\cosh \alpha_1 - \cos \beta) \left[ 2K e^{-\alpha_1} + 2(B_0 + K) \sinh \alpha_1 \right. \\
&\quad + \phi_1''(\alpha_1) \cos \beta - 2K \sin^2 \beta (\cosh \alpha_1 - \cos \beta)^{-1} \\
&\quad \left. + \sum_{n=2}^{\infty} \{\phi_n''(\alpha_1) + n^2 \phi_n(\alpha_1) - \phi_n(\alpha_1)\} \cos n\beta \right]
\end{aligned} \tag{27}$$

and

$$\begin{aligned}
\widehat{\beta\beta}_2 &= 2A \cosh \alpha_2 (\cosh \alpha_2 - \cos \beta) \\
&\quad - JAM(\cosh \alpha_2 - \cos \beta)(\sinh^2 \alpha_2 - \sinh^2 \alpha_1) \\
&\quad \times \{\sinh (\alpha_1 + \alpha_2) \cos \beta + \sinh \alpha_2 \cosh (\alpha_1 + \alpha_2)\} \\
&\quad - \frac{1}{2}S(\cosh \alpha_1 - \cos \beta) \left[ 2K e^{-\alpha_2} - 2(B_0 - K) \sinh \alpha_2 \right. \\
&\quad + \phi_1''(-\alpha_2) \cos \beta - 2K \sin^2 \beta (\cosh \alpha_2 - \cos \beta)^{-1} \\
&\quad \left. + \sum_{n=2}^{\infty} \{\phi_n''(-\alpha_2) + n^2 \phi_n(-\alpha_2) - \phi_n(-\alpha_2)\} \cos n\beta \right]
\end{aligned} \tag{28}$$

If the two holes be equal, i.e.  $\alpha = \alpha_1$  and  $\alpha = -\alpha_1$ , we have

$$\begin{aligned}
h\chi &= A\alpha \sinh \alpha + B_{11} \cos \beta \\
&\quad - \frac{1}{2}S \left[ \cosh \alpha + \cos \beta + K(\cosh \alpha - \cos \beta) \log (\cosh \alpha - \cos \beta) \right. \\
&\quad \left. + \sum_{n=1}^{\infty} \phi_n(\alpha) \cos n\beta \right]
\end{aligned} \tag{29}$$

where

$$\phi_n(\alpha) = A_n \cosh (n+1)\alpha + B_n \cosh (n-1)\alpha$$

for  $n \geq 2$ , and

$$\phi_1(\alpha) = A_1 \cosh 2\alpha + B_1 \tag{30}$$

and

$$S = A \sinh^2 \alpha_1$$

The values of the constant coefficients are

$$\begin{aligned} B_{11} &= A \sinh^2 \alpha_1 \\ A_1 &= \frac{1}{2} K (1 - \tanh \alpha_1) \\ B_1 &= \frac{1}{2} K \tanh \alpha_1 \cosh 2\alpha_1 - 2 \end{aligned}$$

and for  $n \geq 2$ ,

$$\begin{aligned} A_n &= \frac{K}{n(n+1)} \left[ 1 - \frac{n \cosh 2\alpha_1 + \cosh 2n\alpha_1 - (n+1)}{\sinh 2n\alpha_1 + n \sinh 2\alpha_1} \right] \\ B_n &= \frac{-K}{n(n-1)} \left[ 1 + \frac{n \cosh 2\alpha_1 - \cosh 2n\alpha_1 - (n-1)}{\sinh 2n\alpha_1 + n \sinh 2\alpha_1} \right] \end{aligned} \quad (32)$$

while  $K$  is determined from the equation

$$K = 2 \left[ \frac{(\cosh 2\alpha_1 - 1)^2}{2 \sinh 2\alpha_1} + 2 \sum_{n=2}^{\infty} \frac{(\cosh 2n\alpha_1 - 1) - n^2 (\cosh 2\alpha_1 - 1)}{n(n^2 - 1)(\sinh 2n\alpha_1 + n \sinh 2\alpha_1)} \right] \quad (33)$$

The stresses over the circular boundaries  $\alpha = \alpha_1$  and  $\alpha = -\alpha_1$  are given by

$$\begin{aligned} a\widehat{\beta}\beta_1 &= a\widehat{\beta}\beta_{-1} \\ &= 2A \cosh \alpha_1 (\cosh \alpha_1 - \cos \beta) - \frac{1}{2} S (\cosh \alpha_1 - \cos \beta) \\ &\times [2K \cosh \alpha_1 + 4A_1 \cosh 2\alpha_1 \cos \beta - 2K \sin^2 \beta (\cosh \alpha_1 - \cos \beta)^{-1} \dots (34) \\ &+ \sum_{n=2}^{\infty} 2n \{ (n+1)A_n \cosh (n+1)\alpha_1 + (n-1)B_n \cosh (n-1)\alpha_1 \} \cos n\beta] \end{aligned}$$

The numerical values of the constants  $K$ ,  $A_n$  and  $B_n$  for several values of  $\alpha_1$  are given in the Tables I, II and III.

TABLE I

$\alpha_1$	0.6	0.8	1.0	1.2	1.4	1.6	1.8	2.0	2.2
$K$	8.356	2.655	1.485	0.889	0.555	0.355	0.231	0.152	0.101

TABLE II

$\alpha_1$	0.6	0.8	1.0	1.2	1.4	1.6	1.8	2.0	2.2
$A_1$	1.240	0.446	0.177	0.074	0.032	0.014	0.006	0.002	0.001
$A_2$	0.243	0.066	0.019	0.006	0.002	0.001			
$A_3$	0.065	0.011	0.002						
$A_4$	0.015	0.002							
$A_5$	0.004								
$A_6$	0.001								

TABLE III

$\alpha_1$	0.6	0.8	1.0	1.2	1.4	1.6	1.8	2.0	2.2
$B_1$	0.605	0.271	0.127	0.059	0.029	0.013	0.005	0.003	0.001
$-B_2$	1.783	0.692	0.296	0.131	0.058	0.026	0.012	0.005	0.001
$-B_3$	0.310	0.083	0.023	0.007	0.002	0.001			
$-B_4$	0.075	0.012	0.002						
$-B_5$	0.016	0.002							
$-B_6$	0.001								

Stresses over the circular boundaries  $\alpha=0.8$  and  $\alpha=-0.8$  are shown in figure 1, in multiples of  $A/a$ , between  $\beta=0^\circ$  and  $\beta=180^\circ$  only, because

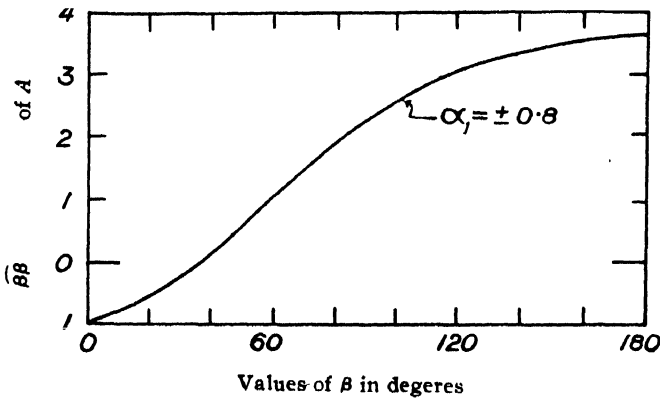


FIG. 1

the stress distribution is symmetrical about the  $y$ -axis. The maximum stresses are, as expected, at  $\beta = \pm 180^\circ$  i.e. at those points on the holes which are nearest to each other. The maximum stresses have the value  $3.63 A/a$ . At  $\beta=0$  the stresses are negative on both the circles. The stress change from negative to positive at  $\beta \approx \pm 37^\circ$ , i.e. at about the middle of the top quadrants of the holes.

#### DISLOCATION DUE TO WEDGE SHAPED FISSURE

To obtain such many valued terms in expressions for displacements so as to suit the case of wedge shaped fissure between two unequal circular holes in an infinite plate, choose

$$h\chi_0 = A\alpha \cosh \alpha$$

The many valued terms in the displacements are given by

$$\begin{aligned} u &= \frac{\lambda + 2\mu}{2\mu(\lambda + \mu)} \cdot A \cdot \frac{\beta \cosh \alpha \sin \beta}{\cosh \alpha - \cos \beta} \\ v &= -\frac{\lambda + 2\mu}{2\mu(\lambda + \mu)} \cdot A \cdot \frac{\beta \sinh \alpha \cos \beta}{\cosh \alpha - \cos \beta} \end{aligned} \quad (36)$$

If  $\alpha > 0$ , we have when  $\beta = \pi$

$$u_+ = 0; \quad v_+ = \frac{\lambda + 2\mu}{2\mu(\lambda + \mu)} \pi A \frac{\sinh \alpha}{\cosh \alpha + 1} \quad \dots (37)$$

and when  $\beta = -\pi$

$$u_- = 0; \quad v_- = -\frac{\lambda + 2\mu}{2\mu(\lambda + \mu)} \pi A \frac{\sinh \alpha}{\cosh \alpha + 1} \quad \dots (38)$$

The discontinuity over the barrier  $\beta = \pm \pi$  is

$$v_+ - v_- = \frac{\lambda + 2\mu}{\mu(\lambda + \mu)} \pi A \frac{\sinh \alpha}{\cosh \alpha + 1} = v_0 \text{ (say)}$$

we have, when  $\beta = \pm \pi$

$$y = y_0 = \frac{a \sinh \alpha}{\cosh \alpha + 1}$$

Therefore

$$v_0 = \frac{\lambda + 2\mu}{\mu(\lambda + \mu)} \cdot \frac{\pi A}{a} \cdot y_0 \quad \dots (39)$$

And if  $\alpha < 0$ , we get

$$v_0 = -\frac{\lambda + 2\mu}{\mu(\lambda + \mu)} \cdot \frac{\pi A}{a} \cdot y_0 \quad \dots (40)$$

So the chosen stress function  $h\chi_0$  will suit the state of dislocation due to the removal of a wedge shaped strip bounded by the planes

$$x = \pm \frac{\lambda + 2\mu}{\mu(\lambda + \mu)} \cdot \frac{\pi A}{a} \cdot y \quad \dots (41)$$

above the  $x$ -axis, and insertion of another wedge shaped strip of the same description below the  $x$ -axis, or *vice-versa*.

The normal stresses on the holes produced by  $h\chi_0$  are given by

$$a\widehat{\alpha\alpha_1} = A(\alpha_1 - \sinh \alpha_1 \cosh \alpha_1), \quad a\widehat{\alpha\alpha_{-2}} = -A(\alpha_2 - \sinh \alpha_2 \cosh \alpha_2) \quad \dots (42)$$

To reduce these stresses to zero, a stress function  $h\chi_1$  of the same form as in (9) is added to  $h\chi_0$ . In this case  $h\chi_1$  has to produce stresses over the circular boundaries as given by

$$a\widehat{\alpha\alpha_1} = -A(\alpha_1 - \sinh \alpha_1 \cosh \alpha_1), \quad a\widehat{\alpha\alpha_{-2}} = A(\alpha_2 - \sinh \alpha_2 \cosh \alpha_2) \quad \dots (43)$$

Adjusting the constant coefficients to suit this requirement, we get

$$\begin{aligned}
 B_{01} &= AM\{2(\alpha_1 + \alpha_2) - \sinh 2\alpha_1 - \sinh 2\alpha_2\} \cosh (\alpha_1 + \alpha_2) \\
 A_{11} &= -\frac{1}{2}AM\{2(\alpha_1 + \alpha_2) - \sinh 2\alpha_1 - \sinh 2\alpha_2\} \sinh (\alpha_1 - \alpha_2) \\
 C_{11} &= \frac{1}{2}AM\{2(\alpha_1 + \alpha_2) - \sinh 2\alpha_1 - \sinh 2\alpha_2\} \cosh (\alpha_1 - \alpha_2) \\
 B_{11} &= \frac{1}{2}AM[2(\alpha_2 \sinh 2\alpha_1 - \alpha_1 \sinh 2\alpha_2) \cosh (\alpha_1 + \alpha_2) \\
 &\quad + \{2(\alpha_1 - \alpha_2) - \sinh 2\alpha_1 + \sinh 2\alpha_2\} \sinh (\alpha_1 + \alpha_2)]
 \end{aligned} \quad \dots (44)$$

where

$$M = \frac{1}{2} \operatorname{cosech} (\alpha_1 + \alpha_2) (\sinh^2 \alpha_2 + \sinh^2 \alpha_1)^{-1} \quad \dots (45)$$

As in the previous case here too we get a constant uniform all round stress at infinity due to the stress function  $hX_1$ . The value of this stress is

$$\begin{aligned}
 &AM[(2\alpha_1 - \sinh 2\alpha_1) \cosh \alpha_1 \sinh \alpha_2 - (2\alpha_2 - \sinh 2\alpha_2) \sinh \alpha_1 \cosh \alpha_2 \\
 &\quad + (\alpha_2 \sinh 2\alpha_1 - \alpha_1 \sinh 2\alpha_2) \cosh \alpha_1 + \alpha_2] \quad \dots (46) \\
 &= a \widehat{\alpha\alpha} = a \widehat{\beta\beta} = S'(\text{say})
 \end{aligned}$$

To reduce this stress at infinity to zero, a stress function  $hX_2$  of the same form and nature as in (15), with the substitution of  $S'$  in place of  $S$ , is added to  $(hX_0 + hX_1)$ . The complete solution is therefore given by

$$\begin{aligned}
 hX &= hX_0 + hX_1 + hX_2 \\
 &= A\alpha \cosh \alpha + B_{01} \alpha (\cosh \alpha - \cos \beta) \\
 &\quad + \{A_{11} \cosh 2\alpha + B_{11} + C_{11} \sinh 2\alpha\} \cos \beta \\
 &\quad - \frac{1}{2}S'[\cosh \alpha + \cos \beta + \{B_0\alpha + K \log(\cosh \alpha - \cos \beta)\}(\cosh \alpha - \cos \beta) \\
 &\quad \quad \quad + \sum_{n=1}^{\infty} \phi_n(\alpha) \cos n\beta]
 \end{aligned} \quad \dots (47)$$

The circumferential stress  $\widehat{\beta\beta}$  over the circular boundaries are now easily calculated from (47) and (3) as follows.

over  $\alpha = \alpha_1$

$$\begin{aligned}
 a \widehat{\beta\beta}_1 &= 2(\cosh \alpha_1 - \cos \beta) \{ (A + B_{01}) \sinh \alpha_1 - (A_{11} \cosh 2\alpha_1 \\
 &\quad \quad \quad + C_{11} \sinh 2\alpha_1) \cos \beta \} \\
 &\quad - \frac{1}{2}S'(\cosh \alpha_1 - \cos \beta) [2Ke^{-\alpha_1} + 2(B_0 + K) \sinh \alpha_1 + \phi_1''(\alpha_1) \cos \beta] \\
 &\quad - 2K \sin^2 \beta (\cosh \alpha_1 - \cos \beta)^{-1} \\
 &\quad \quad \quad + \sum_{n=2}^{\infty} \{ \phi_n''(\alpha_1) + n^2 \phi_n(\alpha_1) - \phi_n(\alpha_1) \} \cos n\beta
 \end{aligned} \quad \dots (48)$$



**over  $\alpha = -\alpha_2$**

$$\begin{aligned} a\beta\widehat{\beta}_{-2} = & -2(\cosh \alpha_2 - \cos \beta)\{(A + B_{01})\sinh \alpha_2 + 2(A_{11} \cosh 2\alpha_2 \\ & - C_{11} \sinh 2\alpha_2) \cos \beta\} \\ & - \frac{1}{2}S'(\cosh \alpha_2 - \cos \beta)[2Ke^{-\alpha_2} - 2(B_0 - K)\sinh \alpha_2 + \phi_1''(-\alpha_2)\cos \beta] \\ & - 2K \sin^2 \beta (\cosh \alpha_2 - \cos \beta)^{-1} \\ & + \sum_{n=2}^{\infty} \{\phi_n''(-\alpha_2) + n^2 \phi_n(-\alpha_2) - \phi_n(-\alpha_2)\} \cos n\beta \end{aligned} \quad \dots \quad (49)$$

If the holes be equal, we have  $B_{11}=0$ ,  $A_{11}=0$  and  $S'=0$ . Therefore

$$h^{\chi} = A\alpha \cosh \alpha + B_{01}\alpha(\cosh \alpha - \cos \beta) + C_{11} \sinh 2\alpha \cos \beta \quad \dots \quad (50)$$

where

$$B_{01} = 2AM(2\alpha_1 - \sinh 2\alpha_1) \cosh 2\alpha_1, C_{11} = AM(2\alpha_1 - \sinh 2\alpha_1) \quad \dots \quad (51)$$

The stresses over the hole boundaries are now given by

$$a \widehat{\beta \beta}_1 = -a \widehat{\beta \beta}_{-1} = 2(\cosh \alpha_1 - \cos \beta) \{ (A + B_{01}) \sinh \alpha_1 - 2C_{11} \sinh 2\alpha_1 \cos \beta \} \dots \quad (52)$$

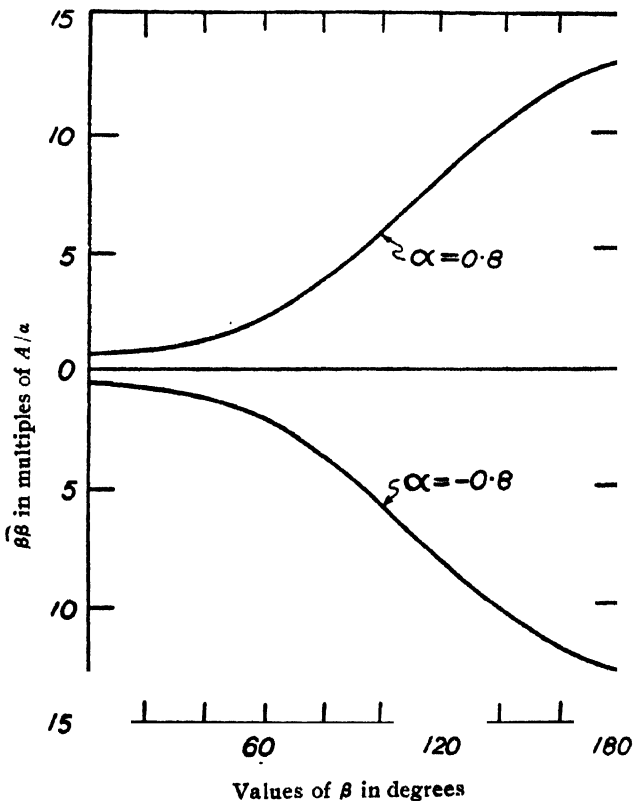


FIG. 2

In figure 2, the stresses in multiples  $A/a$  over the hole boundaries  $\alpha=0.8$  and  $\alpha=-0.8$  are shown in a graph. Here again the maximum stresses are

at  $\beta = \pm 180^\circ$  and the minima are at  $\beta = 0$ . The minimum and the maximum values are  $0.506A/a$  and  $12.59A/a$  and are of opposite signs on the two holes.

#### ACKNOWLEDGMENT

The author wishes to express his respectful thanks to Dr. S. Ghose of the Department of Applied Mathematics for suggesting the problems and for his constant guidance during the preparation of this paper.

#### REFERENCE

Jeffery, G. B., 1921, *Phil. Trans. Roy. Soc.*, **A221**, 265.

# A THERMIONIC METER FOR MEASURING RECTIFICATION RATIO OF CURRENT IN DISCHARGE TUBES

By V. L. TALEKAR

DEPARTMENT OF PHYSICS, DUNGOR COLLEGE, BIKANER

(Received for publication, February 1, 1952)

**ABSTRACT.** A new type of thermionic meter is developed for measuring rectification ratio of current in discharge tubes. Its operating conditions are investigated in some detail. Available range of the meter is also calculated from the operative characteristic of the same. Result of a test with the meter of commercial 220 volts 50 cycles supply is reported as a specimen of its use.

## INTRODUCTION

Right from earlier workers, like Townsend (1915), on rectification of current in discharge tubes the conventional method has been to connect an A. C. and D. C. meter in series in the earth circuit. The former reads the total current, whereas, the latter gives the rectified component. The ratio of the rectified to the total current is designated as rectification ratio, taken to be positive when the D. C. component flows into the earth and negative when the same flows from the earth. The rectification can also be detected qualitatively by visual analysis of the discharge current wave-form on a cathode ray oscillograph. But to determine the rectification ratio, the wave-form has to be photographed and the areas of the positive and the negative parts of a cycle have to be computed. The task often is not quite simple, as might be imagined, for various reasons, chief of which is the presence of high frequency components in the discharge current. Recently, Chiplonkar (1951) has used an arrangement with two diodes and two galvanometers (micro-ammeters) to determine the rectification ratio in discharge current through a photo cell. His arrangement consists in passing the discharge to earth through two diodes connected in opposition each being followed by a galvanometer. Thus one diode passes current during the positive part and the other during the negative part of a cycle, the rectification ratio being given by difference divided by the sum of the two meter readings. This calculation, therefore, embodies an implicit assumption that the current read by each of the two meters is the average discharge current during the corresponding part of a cycle, or is proportional to the average value in which case the constant of proportionality must be the same for both the diodes. Unless this condition is experimentally realised in the circuit employed the rectification calculated thereof will be subject to error.

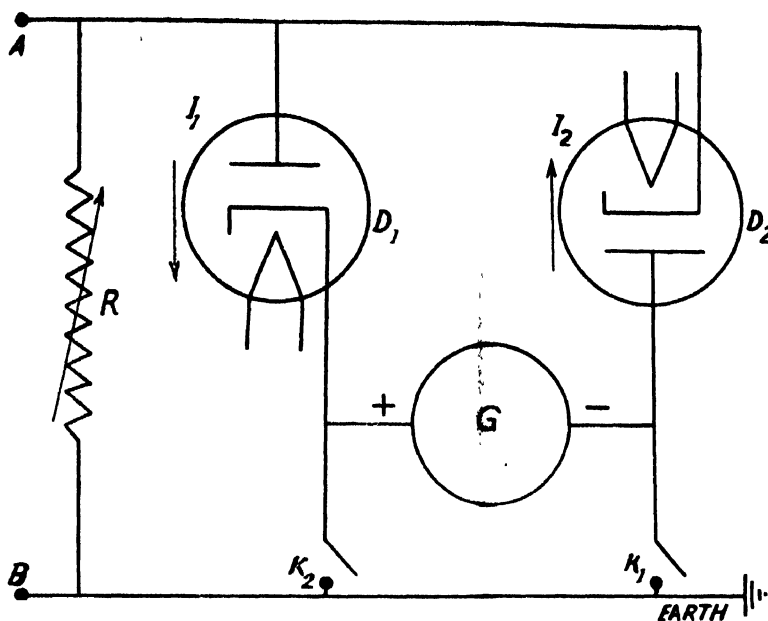
In the circuit under reference it may be noted that the readings recorded by either of the meters is not merely the average discharge current during the corresponding part of a cycle, but is the sum of this and the thermionic emission of the diode. Since the latter depends on the operating conditions, *e.g.* the filament current and the tube drop caused by the passage of discharge current through the diode, the same cannot be equal for both the tubes in view, specially, of the tube drop. Even if this adjustment be possible, the error being additive in the denominator, will still persist though get eliminated in the numerator of the rectification ratio. Thus the error on this account cannot be altogether avoided, though it can be reduced to a certain extent by keeping the emission current low.

There is another possible source of error which arises due to direct feeding of discharge current to the diode making it act as the input impedance. Since the impedance of a diode is not pure resistance, it leads to distortion of wave-form which might result in alteration of the rectification to be measured. This effect will be more pronounced if the discharge were to contain fair degree of relatively higher frequency components which are generally found to be present. In this connection some typical results by Joshi (1944 and 1945) may be pointed out, where a very large number of much higher frequency components have been observed oscillographically in the discharge current of a chlorine tube excited by 50 cycles frequency.

The object of the present paper is to report a modified circuit with its operating conditions, which obviates the difficulties mentioned above.

#### THERMIONIC RECTIFICATION METER

It is now clear from the foregoing remarks that if the rectification ratio is to be reliable, the discharge current should not be mixed with emission current and a pure resistance-coupling should be used. The voltage developed across such an input impedance, if analysed without distortion should then lead to faithful values of rectification. The process, therefore, involves the use of two thermionic voltmeters one for each part of a cycle. Terman (1943) has described diode vacuum tube voltmeters for peak voltages. Since our interest lies in average values of voltages developed during the positive and negative parts of a cycle rather than the peak values, the peak voltmeters are modified to suit the purpose. The output condenser across which the peak voltage develops together with the D. C. voltmeter to measure the same is removed, and a D. C. galvanometer is substituted to record the emission current. Two such modified circuits are then combined into one and only a single galvanometer used for both with suitable arrangement of keys. This evidently results in economy of one galvanometer and improves accuracy since both emission currents are read on the same instrument. The circuit is shown in figure 1.



Thermionic rectification meter

FIG. 1

$A, B$ . — Input terminals.

$R$  — Non-inductive non-capacitive resistance.

$D_1, D_2$  — Two sections of double diode 6H6 metal tube.

$G$  — D.C. micro-ammeter

$I_1$  — Average diode current in the positive part of a cycle measured by  $G$  when key  $K_1$  is closed.

$I_2$  — Average diode current in the negative part of a cycle measured by  $G$  when key  $K_2$  is closed.

### EXPERIMENTAL

It should be mentioned here that the two diodes used in the circuit must possess identical  $I_p-V_p$  characteristic and their operation must be restricted to only the straight portion of the same. Since the maximum value of rectification ratio that can be measured depends on the length of this straight portion, as shown later, it is desirable to have the same as extensive as possible.

The two diodes connected as in figure 1 will show current even in absence of any signal when the filaments are lighted with full rated voltage. It happens due to the circuit of each diode being closed through the other. This circulation current is reduced to zero by lowering the filament voltage and the critical value of the filament current  $I_f$  is noted. The diodes are then lighted with this critical filament current and their  $I_p-V_p$  characteristic determined.

For obvious reasons double diode 6H6 tube is used in the circuit. Before the right one could be selected some twentyone tubes were examined for

circulation current characteristic ( $I_c$ - $V_f$ ) as well as the ( $I_p$ - $V_p$ ) characteristic and very widely divergent results were obtained in almost all cases. The

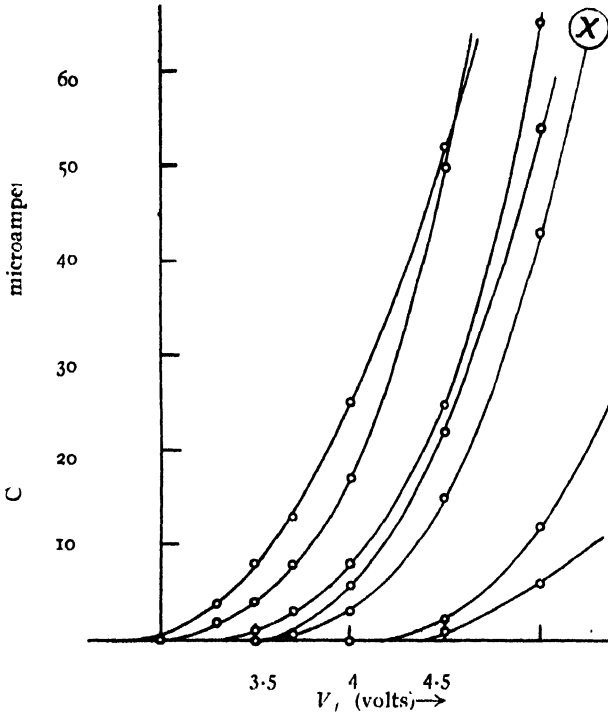


FIG. 2

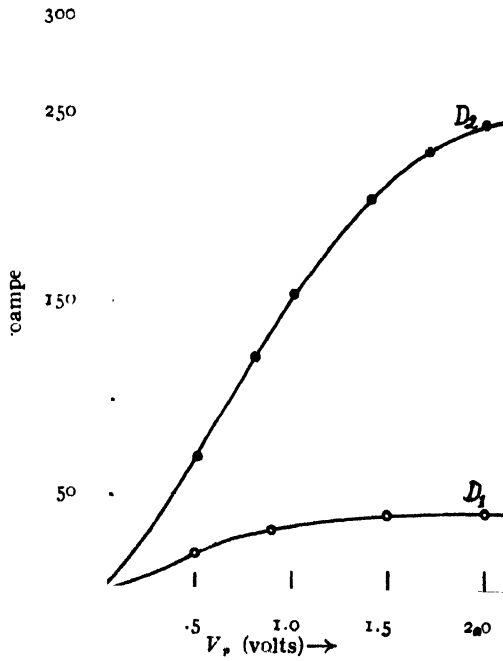


FIG. 3(a)

circulation current characteristic and the plate current-plate voltage characteristic for the finally selected tube (marked as  $X$ ) and also for some others, typically divergent, are shown in figures 2 and 3 respectively.

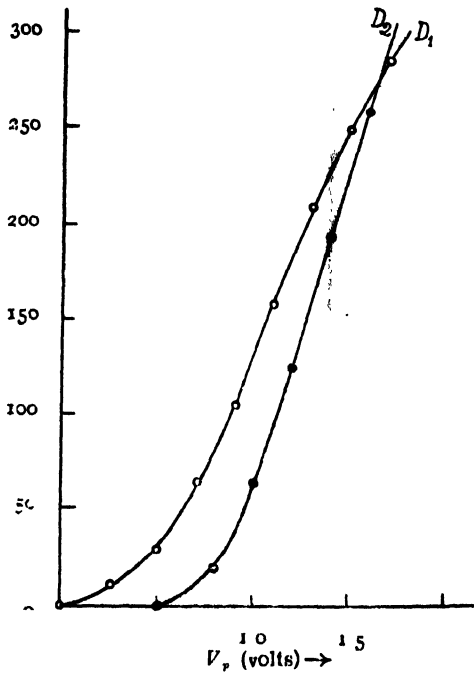


FIG. 3(b)

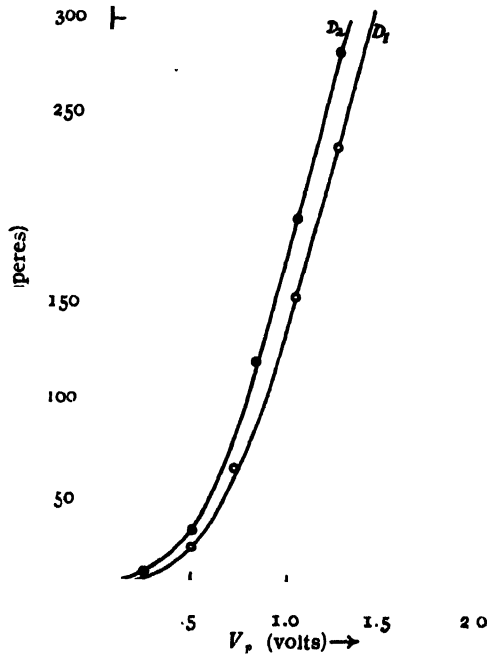


FIG. 3(c)

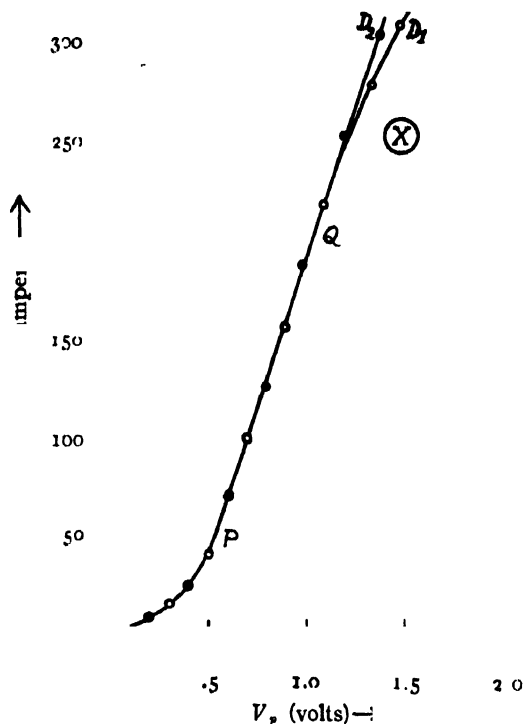


FIG. 3(d)

## DISCUSSION

As seen in figure 2, most of the tubes just start the circulation current for the filament voltage lying between 2.9 and 4.4 volts; the normal rating of all the tubes being 6.3 volts. The critical value of filament current varies between 170 and 230 milliamperes, whereas, the rated value is 0.3 ampere. Figure 3(d) shows the  $I_p$ - $V_p$  characteristics of two diodes  $D_1$  and  $D_2$  of the finally selected tube, whereas, figures 3(a), 3(b) and 3(c) show the same for three others which are typically in disagreement. In the case of the chosen tube, disagreement begins after the current of 225 microamperes is reached when  $D_1$  just shows the sign of tending towards saturation. However, the portion PQ between the current range 50 to 200 microamperes is quite straight and, therefore, is utilised for operation. If the current in one diode corresponds to the point P and that in the other to the point Q, then the maximum rectification ratio that can be measured with this characteristic is

$$\frac{I_1 + I_2}{I_1 - I_2}$$

$$= 60\%.$$



The length of straight portion of the  $I_p-V_p$  characteristic thus defines the range of the instrument. To get 100 % range the point  $P$  must coincide with origin  $O$ . In other words, the diode characteristic must be a straight line passing through  $O$ .

#### RECTIFICATION IN COMMERCIAL A.C. SUPPLY

The rectification meter has been tested and put to very useful purpose in the study of discharge currents in this laboratory. A typical result of a test as applied to commercial power supply is given here.

The phase terminal of 220 volts 50 cycles commercial power supply was connected to the rectification meter at  $A$  through a high non-inductive resistance. The voltage developed across  $R$  was then analysed. Several readings were taken by changing the value of  $R$ . Readings and the rectification obtained thereof are recorded in Table I.

TABLE I

Trial No.	$I_1$	$I_2$	Rectification	Mean
1	70	72	.0141	1.71%
2	82	85	.0179	
3	97	100	.0152	
4	108	112	.0182	
5	118	122	.0167	
6	127	132	.0193	
7	135	140	.0182	

As shown in the last column the rectification in the A.C. supply is 1.7 % This, being too small, could not be detected when the wave form was examined oscillographically. Such negligible rectification is to be expected from the fact that due to efficient designing of commercial alternators the wave form is almost free from even harmonics and they are the ones which are responsible for the rectification.

#### ACKNOWLEDGMENT

In conclusion, the author expresses his very grateful thanks to Shri A. S. Rao, E. E. Stanford, Reader, Tata Institute of Fundamental Research Bombay, for making a number of 6H6 tubes available for examination.

## REFERENCES

- Chiplonkar, V.T., 1951, *Ind. J Phys.*, **28**, 138.  
Joshi, S.S., 1944, *Curr. Sci.*, **13**, 253.  
" 1945, *Proc. Ind. Acad. Sci.*, **22**, 389.  
Terman, F.E., 1943, *Radio Engineers' Handbook* (Mc Graw-Hill), p-933.  
Townsend, J.S., 1915, *Electricity in Gases* (Oxford).

## NEUTRON-PROTON SCATTERING

BY H. N. YADAV

PHYSICS DEPARTMENT, SCIENCE COLLEGE, PATNA

*(Received for publication, February 23, 1952)*

**ABSTRACT.** The angular distribution and the total cross section have been calculated for incident neutrons of energy 83 Mev scattered by protons. Interactions considered are of symmetrical type and one with interaction in the even states only, for Yukawa potential with ranges:

$1.18 \times 10^{-13}$  cm for singlet states

$0.80 \times 10^{-13}$  cm for the central part in the triplet states

and  $1.60 \times 10^{-13}$  cm for the non-central part in the triplet states.

The constants for the singlet potential are taken to fit the proton proton scattering and the low-energy neutron-proton scattering. The constants for the triplet potential are determined by the interaction method to fit the binding energy, the electric quadrupole moment and the magnetic moment of the deuteron. The low energy scattering total cross sections obtained are in agreement with the experimental values. But the high energy (83Mev) total cross sections are large as usual, viz., for symmetrical interaction it is  $14.6 \times 10^{-26}$  cm<sup>2</sup> and for interaction in the even states only, it is  $12.1 \times 10^{-26}$  cm<sup>2</sup>.

## 1. INTRODUCTION

The theoretical investigations of high energy n-p scattering by several authors [Ashkin and Wu (1948), Massey, Burhop and Hu (1948), Hsu and Hu (1949), Rohrllich and Eisenstein (1949), Wu and Foley (1948), Burhop and Yadav (1948, 1949)] give values for the total cross section too large compared with the experimental results. The only investigation so far which gives results in agreement with the experiment is that of Camac and Bethe (1948) for the case of a spherical well potential consisting only of a central force of range  $2.0 \times 10^{-13}$  cm.

In the present calculation, a brief reference of which was made by the author (Yadav 1949), the non-central force has been retained in order to account for the electric quadrupole moment of the deuteron. Also, the singlet range has been taken different from the triplet ones, as is suggested by the analysis of the experiment of the scattering of thermal neutrons by the para-and ortho-hydrogen molecules (Sutton 1947). Moreover, for the triplet states the range for the central force has been taken different from that of non-central forces, as the same range for the central and non-central forces do not seem to be consistent with the requirement of the various experimental data. For, if we consider Yukawa potential of a single range for both the central and non-central forces, then in order to satisfy the scattering of

thermal neutrons by hydrogen molecules the range should be between  $0.75 \times 10^{-13}$  cm. and  $1.06 \times 10^{-13}$  cm. On the other hand, the electric quadrupole moment and the magnetic moment of the deuteron cannot both be fitted if equal range of value in the above interval be chosen for both the central and non-central forces. This requirement can, however, be fulfilled if a larger range of the non-central force is used. Besides, none of the attempts with equal range, as already mentioned, has yielded results in agreement with experiments on high energy scattering.

Castillejo and Richardson (1949) have carried out calculations for 83 Mev n-p scattering, with different central and non-central ranges for a spherical well interaction with ranges and constants given by Miss Padfield (1949). The values of the total cross section are again very large. Taking all these facts in view it was considered worthwhile to undertake the calculation with Yukawa potential with range  $1.18 \times 10^{-13}$  cm in the singlet states and  $0.8 \times 10^{-13}$  cm for the central triplet and  $1.6 \times 10^{-13}$  cm for the triplet non-central potential. All the constants were calculated to fit the low energy scattering and the properties of the deuteron. However, this new attempt has not been any more successful than the previous attempts with a single range for 83 Mev neutrons scattered by protons.

## 2. DETERMINATION OF CONSTANTS AND LOW ENERGY SCATTERING

(a) *Determination of constants in the expression for the interaction:*

(i) *Triplet states*—The potential assumed is of the form

$${}^3V = \frac{\hbar^2}{3M\tau_0^2} \left\{ a \frac{e^{-2r/r_0}}{r/r_0} + a\gamma S_{12} \frac{e^{-r/r_0}}{r/r_0} \right\}$$

which in the case of even states reduces to

$${}^3V_{\text{even}} = -\frac{\hbar^2}{M\tau_0^2} \left\{ a \frac{e^{-2r/r_0}}{r/r_0} + a\gamma S_{12} \frac{e^{-r/r_0}}{r/r_0} \right\}$$

where  $r_0 = 1.6 \times 10^{-13}$  cm is the range for the non-central force and  $r_0/2 = .8 \times 10^{-13}$  cm is that for the central force. Other symbols have their usual meaning.

Assuming the binding energy of deuteron, the wave equations for the ground state of deuteron are solved by the interaction method. The constants  $a$  and  $a\gamma$  are determined by making use of the expression and the experimental value of the electric quadrupole moment of the deuteron. The values obtained are as follows :

$$a = 2.662, a\gamma = 1.835, \text{ and } D\% = 3.78,$$

satisfying the requirement of the magnetic moment of the deuteron.

(ii) *Singlet states*:—The potential in this case is of the form

$${}^1V = - \frac{\hbar^2}{M\tau_1^2} \tau_1 \cdot \tau_2 g \frac{e^{-r/\tau_1}}{r/\tau_1},$$

which for the even states becomes

$${}^1V_{\text{even}} = - \frac{\hbar^2}{M\tau_1^2} g \frac{e^{-r/\tau_1}}{r/\tau_1}.$$

The range  $\tau_1 = 1.18 \times 10^{-13}$  cm. and the potential constant  $g = 1.575$ . These values were calculated by Hsu who determined them to give correctly the low-energy n-p scattering.

(b) *The scattering of low-energy neutrons by protons*

In calculating the total cross section for the scattering of low energy neutrons by protons the following approximate expressions (Wu and Foley 1949) have been used

$$k_1 \cot \delta_1 - k_2 \cot \delta_2 = (k_2^2 - k_1^2) \int_0^\infty (v_0^2 - u_0^2) dr. \quad \dots (1)$$

for the singlet scattering, where  $k_1 = \frac{ME_1}{\hbar^2}$  and  $\delta_1$  is the phase shift of the wave for incident neutron of energy  $E_1$ ;  $u_0/r$  is the radial part of the wave function for zero energy and tends asymptotically to  $v_0/r$ . For the triplet scattering,

$$k \cot \delta = -\alpha + (\alpha^2 + k^2) \int_0^\infty \{v_\alpha^2 - (u^2 + w^2)\} dr. \quad \dots (2)$$

where  $\alpha^2 = \frac{M|E_0|}{\hbar^2}$ ,  $E_0$  being the binding energy of the deuteron and  $\frac{u}{r}, \frac{w}{r}$

are respectively the radial parts of the *S* and *D* wave of the ground state of the deuteron and normalized such that  $u$  tends asymptotically to  $v_\alpha = e^{-\alpha r}$ .

Also  $k^2 = \frac{ME}{\hbar^2}$  and  $\delta$  is the phase shift of the wave for incident neutron of energy  $E$ .

The total cross sections calculated by using (1) and (2) are in good agreement with those calculated by the exact method. This has been verified for the case of a spherical well interaction up to 6 Mev. We expect that in the case of the Yukawa potential it will give results in agreement with exact calculations up to at least 3 Mev. The total cross sections obtained are given in the Table I. As seen from figure 1. they are in good agreement with experimental values obtained by various authors.

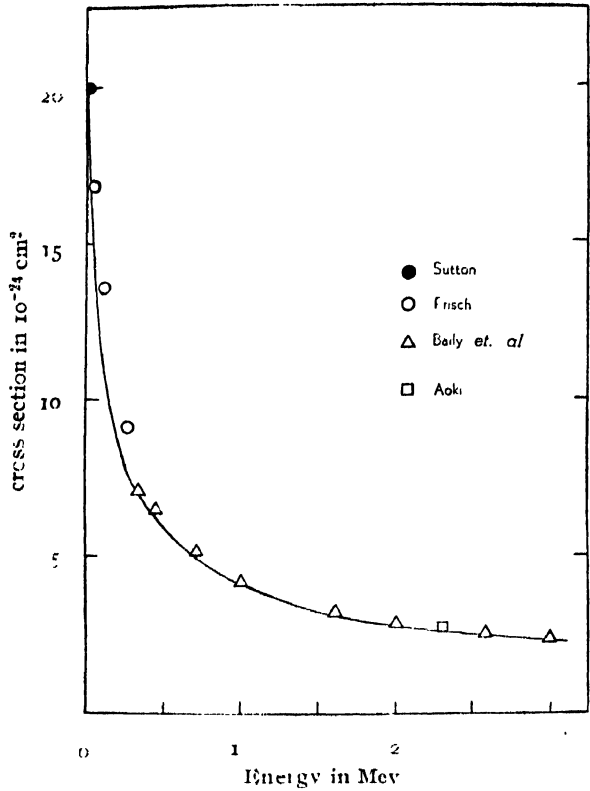


FIG. 1

TABLE I

Energy of incident neutron in Mev.	Total cross section in $10^{-24} \text{ cm}^2$ .
0	19.59
.1	12.35
.5	5.94
1.0	4.11
1.5	3.29
2.0	2.80
2.5	2.46
3.0	2.20

3. SCATTERING OF 83 MEV NEUTRONS BY PROTONS.

(i) *Triplet states* :—The phases for the coupled states  $^3S_1$  and  $^3D_1$  and for the uncoupled states  $^3P_0$ ,  $^3P_1$  and  $^3D_2$  were calculated from the solutions of the radial wave equations obtained exactly by numerical integration. All higher phases, being very small, are taken account of by Born's approximation. The procedure adopted is briefly outlined below.

For an incident plane wave  $e^{ikz}X_M$  the outgoing scattered spherical wave can be written as (Hu and Massey 1949)

$$\frac{\sqrt{\pi}}{ik} \frac{e^{ikr}}{r} \sum_{Jl} \sqrt{2l+1} C_{JlM_0} \left\{ e^{2i\eta_{JlM}} - 1 \right\} F_{JlM} \quad \dots (3)$$

where the notations are the same as in the paper referred to above. From (3) the scattering amplitude can at once be written down as

$$f(\theta)X_M = \frac{\sqrt{\pi}}{ik} \sum_{Jlm} \sqrt{2l+1} C_{JlM_0} C_{JlM-m} Y_{lm} X_{M-m} \left\{ e^{2i\eta_{JlM}} - 1 \right\} \quad \dots (4)$$

If we define the matrix element for the scattering amplitude by

$$f(\theta)_{M'M} = X_{M'} f(\theta) X_M$$

i.e. the probability amplitude of scattering of the incident wave with spin component  $M$  into a scattered wave with spin component  $M'$  then from (4)

$$f(\theta)_{M'M} = \frac{\sqrt{\pi}}{ik} \sum_{Jl} \sqrt{2l+1} C_{JlM_0} C_{JlM-M'} Y_{l,M-M'} \left\{ e^{2i\eta_{JlM}} - 1 \right\} \quad \dots (5)$$

Hence the  $\sigma(\theta)$  is given by

$$\sigma(\theta) = \frac{1}{4} \sum_{M'} \sum_M |f(\theta)_{M'M}|^2$$

where the summations indicate averaging over the initial spin states and summing over the final spin states.

In the case of Born's approximation (Ashkin and Wu 1948; Burhop and Yadav 1948, 1949) for the symmetrical interaction

$$f(\theta)_{M'M} = - \frac{1}{4\pi r_0^2} \int e^{-ik\vec{n} \cdot \vec{r}'} X_{M'} \frac{r_1^2}{3} (aV_c + a\gamma V_n S_{12}) e^{i\vec{k} \cdot \vec{r}} X_M d\vec{r} \quad \dots (6)$$

where  $V_c = \frac{e^{-2r'/r_0}}{r'/r_0}$ , the central potential

and  $V_n = \frac{e^{-r'/r_0}}{r'/r_0}$ , the non-central potential

The expression (6) can be integrated out explicitly in the form

$$f(\theta)_{M'M} = \frac{1}{2} a \delta_{M'M} [2F(\pi - \theta) + F(\theta)] + \frac{1}{2} a \gamma [2I_{M'M}(\pi - \theta, \pi + \varphi) c(\pi - \theta) + \Gamma_{M'M}(\theta, \varphi) c(\theta)] \quad \dots (7)$$

The various terms occurring here are explained and worked out in the papers referred to above.  $(\theta, \varphi)$  are the angular coordinates of  $\vec{n}$  referred to  $\vec{n}_0$ .

In the case of interactions in the even states only, as suggested by Serber,  $f(\theta)_{M'M}$  are obtained from (5) if the terms associated with odd  $l$ 's are omitted. And it can easily be shown that the Born amplitudes in this case are given by

$$f(\theta)_{M'M} = \frac{1}{2}a\delta_{M'M}[F(\pi-\theta) + F(\theta)] + \frac{1}{2}a\gamma[\Gamma'_{M'M}(\pi-\theta, \pi+\varphi)C(\pi-\theta) + \Gamma_{M'M}(\theta, \varphi)C(\theta)] \quad \dots (7a)$$

To take account, by Born's approximation, of the contribution from states of higher angular momenta, for which phases were not calculated by exact method, the following procedure was adopted. The amplitudes were calculated by Born's approximation using expressions (7) and (7a) which give contribution from all  $l$  values. To this is added the expression

$$f(\theta)_{M'M}(\text{exact}) - f(\theta)_{M'M}(\text{Born}) \quad \dots (8)$$

for the states  $^3S_1$ ,  $^3D_1$ ,  $^3P_0$ ,  $^3P_2$  and  $^3D_2$ . This has the effect of using the exact phases in place of Born ones for the states in question while retaining all the Born phases for higher states. In order to evaluate (8) the expression (6) for  $f(\theta)_{M'M}$  (Born) is to be cast in the form (5). The incident wave  $e^{ikz}\chi_M$  can be expanded in the form

$$e^{ikz}\chi_M = \sum_l \sqrt{4\pi(2l+1)} i^l C_{lM0} \frac{g_l(kr)}{kr} F_{JM}(\theta, \varphi) \quad \dots (9)$$

Following Mott and Massey (1950), the Born phases can easily be deduced in the form

$$\delta_{JM} = \frac{1}{kr^2_0} \int_0^\infty \sum_{l'} \sqrt{\frac{2l'+1}{2l+1}} \frac{C_{JM0}}{C_{JM0}} g_l(kr) g_{l'}(kr) i^{l-l'} \times (aV_c\delta_{ll'} + a\gamma V_n < l | S_{12} | l' >) dr \quad \dots (10)$$

where

$$< l | S_{12} | l' > = < F^*_{JM} | S_{12} | F_{JM} >$$

and has the following values :

$$< J-1 | S_{12} | J-1 > = - \frac{2(J-1)}{2J+1}$$

$$< J | S_{12} | J > = +2$$

$$< J+1 | S_{12} | J+1 > = - \frac{2(J+1)}{2J+1}$$

$$< J \mp 1 | S_{12} | J \pm 1 > = \frac{6\sqrt{J(J+1)}}{2J+1}$$

all other elements vanishing.

$$\text{Also } e^{-ik\mathbf{n}\cdot\mathbf{r}} = 4\pi \sum_l (-i)^l Y_{lm}(\theta, \varphi) Y_{lm}(\theta', \varphi') \frac{g_l(kr')}{kr'} \quad \dots (11)$$

where  $\theta, \varphi$  are the co-latitude and azimuth angles of  $\vec{n}$  referred to  $\vec{n}_0$  and  $\theta', \varphi'$  are those for  $\vec{r}'$  referred to  $\vec{n}_0$ . Substituting the expansions (9) and (11) in (6) and integrating over the spin and the angular coordinates we get



$$f(\theta)_{M'M}(\text{Born}) = \frac{1}{r_0^2} \int \sum_{Jl'} (i)^{l'-l} C_{JlM, M-M'} C_{Jl'M_0} Y_{l, M-M'} \\ \times \sqrt{4\pi(2l'+1)} (aV_c \delta_{ll'} + a\gamma V_n < l | S_{12} | l' >) \frac{g_l^{(kr)} g_{l'}^{(kr')}}{k^2} dl$$

which according to (10) gives

$$f(\theta)_{M'M}(\text{Born}) = \frac{\sqrt{\pi}}{ik} \sum_{Jl} \sqrt{(2l+1)} C_{JlM, M-M'} C_{JlM_0} Y_{l, M-M'}(\theta, \varphi) (2i\delta^{JlM}) \quad \dots (12)$$

(we use  $\delta^{JlM}$  for Born's phases and  $\eta^{JlM}$  for exact ones).

Hence

$$f_{M'M}(\theta)(\text{exact}) - f_{M'M}(\theta)(\text{Born}) \\ = \frac{\sqrt{\pi}}{ik} \sum_{Jl} \sqrt{(2l+1)} C_{JlM, M-M'} C_{JlM_0} Y_{l, M-M'} \{e^{2i\eta^{JlM}} - 1 - 2i\delta^{JlM}\} \quad \dots (13)$$

(ii) *Singlet states* : In the singlet states, there being only one spin function, the amplitude of scattering for Born's approximation is given by

$$f(\theta) = g[2F(\pi - \theta) - F(\theta)] \quad \text{for symmetrical interactions}$$

$$\text{and } f(\theta) = \frac{1}{2}g[F(\pi - \theta) + F(\theta)] \quad \text{for interaction in the even states only.}$$

Also the expression (8) for the singlet scattering can easily be shown to be

$$f(\theta)(\text{exact}) - f(\theta)(\text{Born}) = \frac{1}{2ik} \sum_l (2l+1) P_l(\cos \theta) \{e^{2i\eta^l} - 1 - 2i\delta^l\} \quad \dots (14)$$

The factor  $(e^{2i\eta} - 1 - 2i\delta)$  both in (13) and (14) is negligible if  $\eta$  is small. This is approximately true for the states for which exact phases are not calculated. Thus the Born's approximation for these states will give almost the same contribution as the exact calculation.

#### 4 RESULTS

The phases obtained are given in Table II and the angular distribution in Table III. Figure 2 represents the angular distribution graphically.

TABLE II  
(a) Triplet coupled phases

	${}^3S_1$		${}^3D_1$	
	$M = \pm 1$	$M = 0$	$M = \pm 1$	$M = 0$
Exact ( $e^{2i\eta} - 1$ )	$1.799 + .819i$	$-1.364 + .501i$	$-.413 - .197i$	$+.021 - .515i$
Born $2f\delta$	$+.777i$	$+.615i$	$-.952i$	$-.114i$

(b) Triplet uncoupled phases

	$^3P_0$	$^3P_1$	$^3D_2$	
$\eta(\text{Exact})$	+ 3 0	-.191	+.266	
$\delta(\text{Born})$	+.305	-.207	+.250	

(c) Singlet phases

(These phases are taken from Hsu's calculations)

	$S$	$P$	$D$
Exact $\eta$	+.571	-.565	+ .105
Born $\delta$	+.565	-.741	+.099

TABLE III

(a) Angular distribution (in  $10^{-26} \text{ cm}^2$ )

$\theta^\circ$	0	15	30	60	90	120	150	165	180
Sym. $\sigma(\theta)$	1.488	1.430	1.300	.968	.806	1.058	2.081	2.647	2.971
Serber $\sigma(\theta)$	1.303	1.302	1.268	.887	7.33	.887	1.268	1.302	1.303

(b) Total cross sections  $\sigma$  and ratio  $\frac{\sigma(180^\circ)}{\sigma(90^\circ)}$

Interaction		$\frac{\sigma(180^\circ)}{\sigma(90^\circ)}$
Symmetrical	$14.62 \times 10^{-26} \text{ cm}^2$	3.68
Serber	$12.07 \times 10^{-26} \text{ cm}^2$	1.78

As the Serber interaction gives a symmetrical scattering cross section about  $\theta=90^\circ$  in the centre of mass system it does not seem to be in agreement with the experimental results, though it reduces the total cross section to some extent.

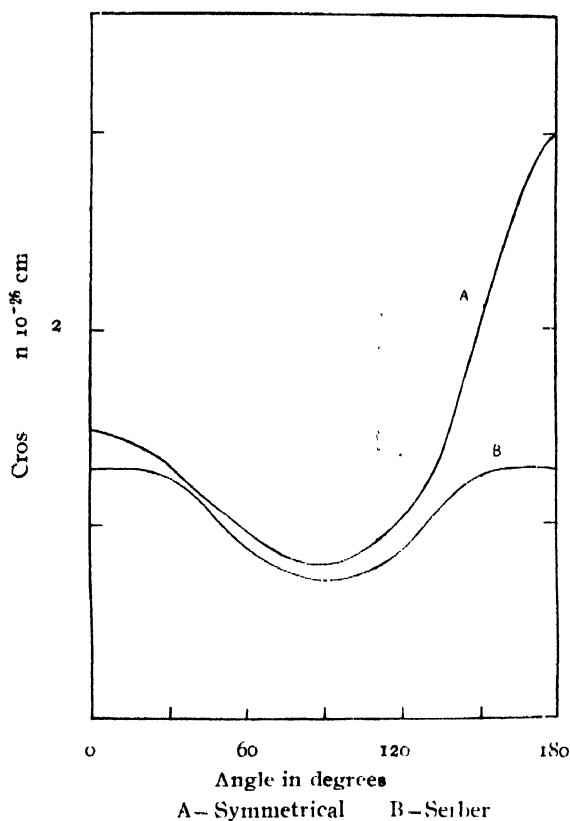


FIG. 2

Thus it hardly requires to be said that the Yukawa potential with different ranges, as attempted in the present calculations, does not give any better result for the high energy scattering than is obtainable with a single range of interactions.

#### INVESTIGATION OF BORN'S APPROXIMATION FOR SCATTERING IN THE TRIPLET STATES

It will not be out of place to record here the striking disagreement between the results obtained by using Born's approximation and the exact method for scattering in the triplet states.

Figure 3 shows a comparison of the triplet differential cross sections calculated by the exact method and by Born's approximation. While the angular distribution differs widely in the two cases, the cross section in the triplet states obtained by Born's approximation is only  $8.14 \times 10^{-26} \text{ cm}^2$  whereas, the exact calculation gives  $14.96 \times 10^{-26} \text{ cm}^2$ . The reason for the low value for this cross section is the shortness of the range. If the range is taken to be zero then the cross section for all forms of potentials (spherical well, exponential well, Yukawa potential and Gaussian potential) will be zero if Born's approximation is used, while the exact method gives a non-

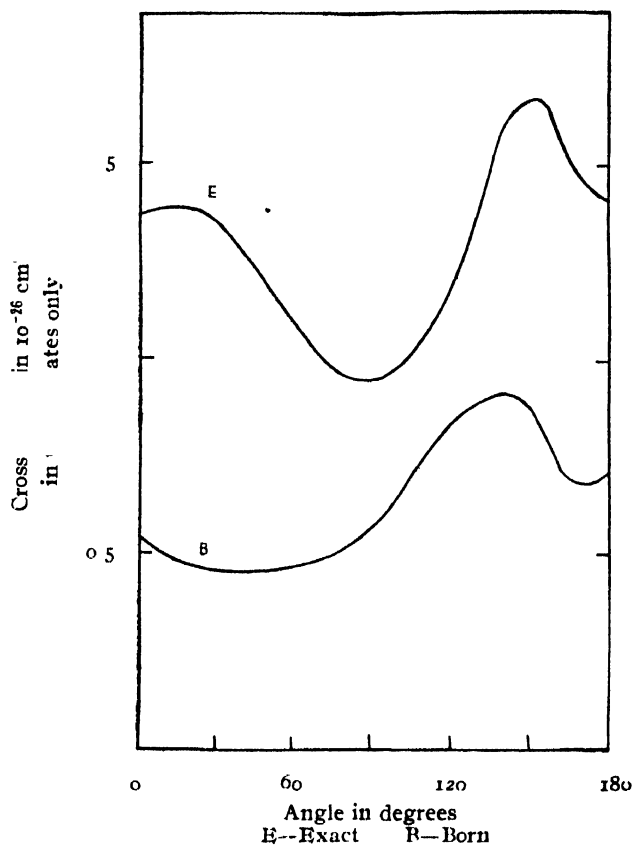


FIG. 3

vanishing finite value for the cross section. Thus it seems that unless the range is sufficiently large, Born's approximation will always yield too low a value.

#### ACKNOWLEDGMENTS

The author wishes to express his indebtedness to Prof. H. S. W. Massey, F.R.S. and Dr. E. H. S. Burhop for their keen interest in the calculation. Thanks are also due to Dr. T. M. Hu and Dr. K. N. Hsu for allowing the author to use their results of calculation for the singlet states and for many valuable discussions.

#### REFERENCES

- Ashkin, J., and Wu, T. Y., 1948, *Phys. Rev.*, **73**, 973.  
 Burhop, E. H. S., and Yadav H. N., 1948, *Nature*, **162**, 738,  
 1949, *Proc. Roy. Soc.*, **A 197**, 505.  
 Camac, M., and Bethe, H. A., 1948, *Phys. Rev.*, **73**, 191.  
 Castillejo, L., Richardson, H. T., 1949, *Phys. Rev.*, **76**, 1732.  
 Hsu, K. N. and Hu T. M., 1949, *Phys. Rev.*, **76**, 687.  
 Hu, T. M. and Massey, H. S. W., 1949, *Proc. Roy. Soc.*, **A 196**, 135.  
 Massey, H. S. W., Burhop, E. H. S. and Hu, T. M., 1948, *Phys. Rev.*, **73**, 1403.  
 Padfield, Miss D. G., 1949, *Nature*, **163**, 22.  
 Rohrlich, F., and Eisenstein, J., 1949, *Phys. Rev.*, **75**, 705.  
 Sutton, R. B., et al., 1947, *Phys. Rev.*, **70**, 1147.  
 Wu, T. Y. and Foley, H. M., 1949, *Phys. Rev.*, **75**, 1581.  
 Yadav, H. N., 1949, *Phys. Rev.*, **76**, 1720.

# THE ULTRAVIOLET ABSORPTION SPECTRA AND THE INTENSITY OF THE FLUORESCENCE BAND 4156 Å OF DIAMOND\*

By B. M. BISEUI

OPTICS DEPARTMENT, INDIAN ASSOCIATION FOR THE CULTIVATION  
OF SCIENCE, CALCUTTA-32

(Received for publication, May 21, 1952)

## Plates XIII A-B

**ABSTRACT.** The intensity of the fluorescence band 4156 Å of diamond with respect to that of the Raman line  $1332\text{ cm}^{-1}$  excited by the Hg line 4358 Å has been measured quantitatively in the case of eight specimens, using the method of heterochromatic photographic photometry. It has been observed that the transparency of the crystals for wavelengths shorter than 3000 Å cannot be correlated with the intensity of the fluorescence band. It is pointed out that these results do not support the conclusion arrived at by previous authors from visual observations that the intensity of the band increases with the increase of transparency of the crystal in the ultraviolet region. It is also observed that the intensity of the fluorescence band is large in the case of diamonds transparent only upto 2240 Å, when these show two absorption bands at 2360 Å and 2363.5 Å respectively and that the fluorescence band is much feeble in the case of crystals transparent upto 2240 Å and showing no absorption bands anywhere in the ultraviolet region. The intensity of the fluorescence band was not found to depend, however, on the amount of absorption in the absorption band at 4156 Å.

It is concluded from the results mentioned above that the fluorescence band 4156 Å is originated by some impurity which also produces the absorption bands at 2360 Å and 2363.5 Å, and that diamonds which may not possess this impurity in appreciable quantities, but possess some other impurities which produce absorption in the region 3000 Å, do not show the fluorescence band at 4156 Å with any appreciable intensity. It is further concluded that diamonds showing no absorption band anywhere in the spectrum upto 2240 Å are really diamonds of rare and the purest variety and only such diamonds should be classified under Type II, while the other diamonds showing absorption bands anywhere between 2240 Å and the red region should be classified under Type I.

## INTRODUCTION

It is well known that according to Robertson, Fox and Martin (1934) diamonds of Type I generally absorb strongly all the ultraviolet radiation of wavelengths shorter than about 3000 Å, while those of Type II are transparent upto 2250 Å. Nayar (1941) first observed that in the case of some specimens of diamond of Type I having different thicknesses the absorption limit in the ultraviolet region for the thinner specimen is at about 2700 Å, although that in the case of the thicker one is at about 3000 Å. He further

\* Communicated by Prof. S. C. Sirkar.

observed that a few diamonds showing weak blue fluorescence exhibit absorption bands in the region between  $3000 \text{ \AA}$  and  $3160 \text{ \AA}$ . These bands are absent in the case of diamonds showing strong blue fluorescence. Sunanda Bai (1944) repeated these investigations, using 47 specimens of diamond of different types. She confirmed the latter observation of Nayar, but she concluded from the facts observed by her that the ultraviolet transparency of diamonds increases with the intensity of fluorescence shown by them. Ramanathan (1946) investigated the same problem using 26 specimens of diamond and using different portions of a particular wedge-shaped specimen having thickness varying from .37 mm at one edge to .15 mm at the other edge. The ultraviolet absorption limits of the 26 specimens were studied, using long and short exposures and the intensity of fluorescence shown by these specimens was also studied qualitatively. It was observed that in the case of all non-luminescent or yellow-luminescent specimens the absorption limit was in the region of  $2240 \text{ \AA}$ - $2250 \text{ \AA}$ , but in the case of most of the specimens showing blue fluorescence the limit was not shorter than  $2380 \text{ \AA}$ . In the case of a specimen of thickness .12 mm showing blue fluorescence, however, the absorption limit was at  $2240 \text{ \AA}$ . Also in the case of the wedge-shaped diamond the absorption limit was at about  $2500 \text{ \AA}$  for the thickness equal to 0.37 mm and it moved to about  $2270 \text{ \AA}$  when the thickness was reduced to 0.15 mm. Further, besides the bands lying in the region between  $2360 \text{ \AA}$  and  $2296 \text{ \AA}$  observed by Sunanda Bai (1944) Ramanathan observed some new bands between  $2244 \text{ \AA}$  and  $2312 \text{ \AA}$  in the case of a thin blue-fluorescent diamond.

In the investigations mentioned above no attempt was made to measure quantitatively the intensity of the fluorescence band at  $4156 \text{ \AA}$  and to correlate the results with the absorption limit in the ultra-violet region. The conclusion drawn by Sunanda Bai (1944) that the ultraviolet transparency of diamonds increases with the intensity of fluorescence shown by them is also based on visual estimation in the case of a few specimens. Further, no attempt was made by any of the previous workers to investigate whether the intensity of any of the absorption bands lying between  $2240 \text{ \AA}$  and  $2360 \text{ \AA}$  can be correlated with the intensity of the fluorescence band at  $4156 \text{ \AA}$ .

It was concluded by the present author (Bishui, 1950) from results of quantitative measurement of the intensity of the fluorescence band at  $4156 \text{ \AA}$  that the intensity of the fluorescence band at  $4156 \text{ \AA}$  changes with temperature exactly in the same way as that of the fluorescence bands of phosphors activated by impurities. It was also pointed out that if the intensity of the Raman line  $1332 \text{ cm}^{-1}$  is not taken as the criterion in measuring the intensity of the fluorescence band the results obtained are very often misleading. The results of investigations of the fluorescence of a few specimens of diamond excited by X-rays (Bishui, 1951) also confirmed the conclusion that the fluorescence band at  $4156 \text{ \AA}$  is due to presence of some chemical impurity in diamond. It was not known definitely, however, whether this

impurity shows any characteristic absorption band of wavelength shorter than  $3000 \text{ \AA}$  in blue-fluorescent diamonds. In the present investigation the intensity of the fluorescence band at  $4156 \text{ \AA}$  relative to that of the Raman line  $1332 \text{ cm}^{-1}$  excited by  $4358 \text{ \AA}$  has been measured quantitatively in the case of eight chosen specimens of diamond and the ultraviolet absorption limits of those specimens have also been photographed in order to find out whether the impurity responsible for the origin of the fluorescence band at  $4156 \text{ \AA}$  shows any characteristic absorption band in the ultraviolet region. The absorption in the visible region was also studied in the case of all the specimens kept both at room temperature and at about  $-170^\circ\text{C}$  in order to find out whether the intensity of fluorescence can be correlated with the percentage of absorption.

### EXPERIMENTAL

The specimens of diamond were selected by trial from the stock of the local firm of Messrs. Benud Behari Dutt. The dimensions of these specimens studied in the present investigation are given in Table I.

TABLE I

Identification No.	Description	Thickness.
D 7	Rectangular plate, slightly pink 9 mm $\times$ 7.5 mm	1.353 mm
D 8	Rectangular plate, colourless, 9 mm $\times$ 5.5 mm	1.3 mm.
D 9	Low pyramid, slightly pink, base 30 sq. mm.	0.8 mm (max)
D 10	Plate, colourless, 7.5 mm $\times$ 5.5 mm.	1.092 mm.
D 11	Low pyramid, colourless, base 35 sq. mm.	0.952 mm. (max)
D 12	Triangular plate, colourless, area 28 sq. mm.	0.647 mm.
D 13	Very low pyramid, colourless, base 40 sq. mm.	0.838 mm.
D 14	Almost circular plate, colourless, area 25 sq. mm.	0.812 mm.

(a) *Study of the absorption spectra.* The ultraviolet absorption spectra of these specimens were photographed with a Hilger medium quartz spectrograph, using a slit about .2 mm wide. A hydrogen tube run at 3 K. V. was used as the source of continuum and Ilford Special Rapid plates were used to photograph the spectra. Iron arc comparison was photographed

in each spectrogram, as usual. The absorption spectra in the visible region were also studied with the specimens kept both at 30°C and at about -170°C. A tungsten filament lamp was used as the source of radiation and an Adam Hilger two-prism glass spectrograph was used to photograph the spectra.

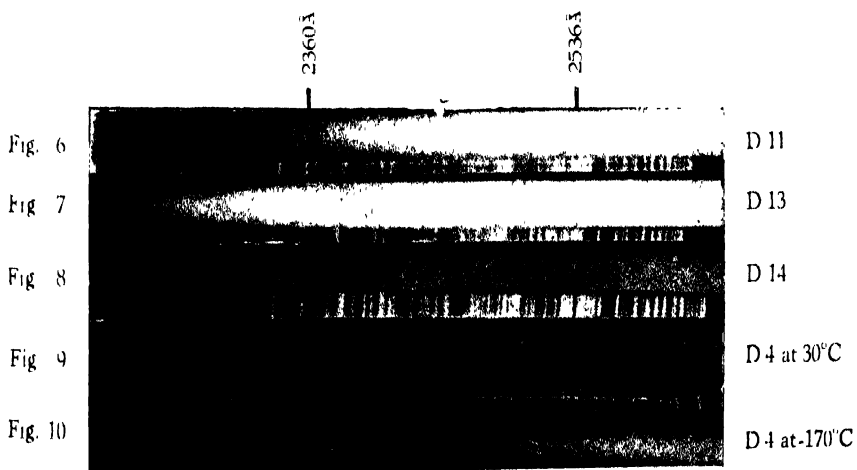
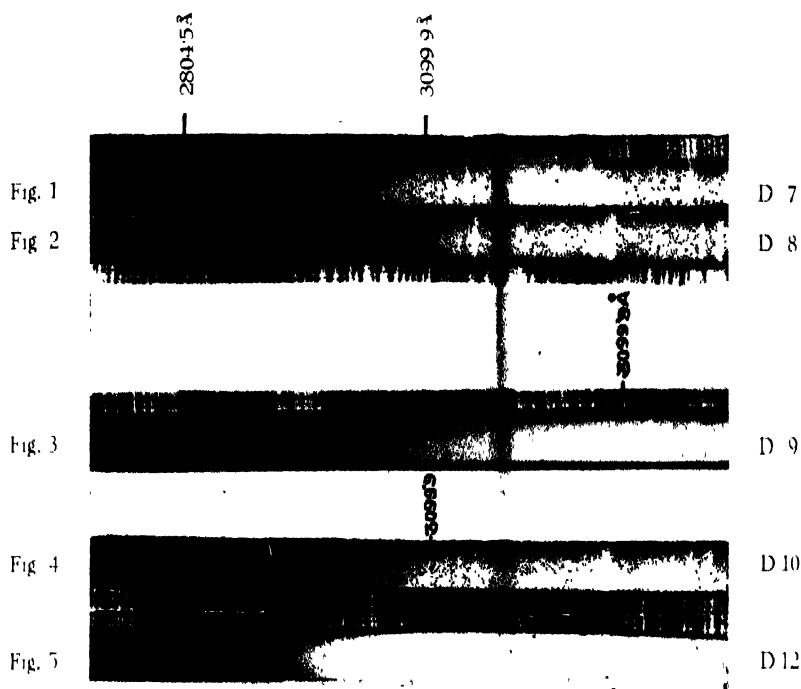
(b) *Study of the intensity of fluorescence.* The samples were so chosen that the fluorescence exhibited by them was not too intense to mask the Raman line  $1332\text{ cm}^{-1}$  excited by the Hg lines 4046 Å and 4358 Å. The spectra were photographed, using an Adam Hilger two-prism glass spectrograph having a dispersion of about 20 Å in the 4046 Å region. The width of the slit was about 0.5 mm. A vertical mercury arc in silica tube was used as the source of exciting radiation and the crystal was held obliquely and was illuminated from the front side. Gevaert Superchrome plates were used to photograph the fluorescence spectra. All the plates were developed under identical conditions, using developer of the same strength. On one of the plates taken from the same packet intensity marks were photographed for different known widths of the slit of the spectrograph, which was illuminated by the vertical glowing ribbon of a standard tungsten ribbon lamp placed at a large distance from the slit on the axis of the collimator. The colour temperatures of the lamp for different currents flowing through it were known.

Microphotometric records of the fluorescence band at 4156 Å and of the Raman line excited by the 4358 Å line of Hg were obtained with a Kipp & Zonen type self-recording Moll microphotometer. The densities for the corresponding wavelengths in the standard intensity marks were also measured with the help of the records obtained for these wavelengths and blackening-log-intensity curves were drawn. The curves for 4156 Å and 4627 Å were not exactly parallel, but the relative intensities of these wavelengths in the standard continuous spectrum were known from Wien's law. Assuming the maximum density for each of these two wavelengths to correspond to an intensity 100, the intensities of the fluorescence band at 4156 Å due to the different specimens and those of the Raman line excited by 4358 Å were determined. The intensity of the background was subtracted from the total intensity in each case to obtain the intensity of the band or the Raman line. These intensities were then multiplied by half the width of the line, or the band, as the case may be, to obtain the integrated intensity. In any particular case if  $I_1$  and  $I_2$  be the intensities of the fluorescence band 4156 Å and the Raman line respectively found in this way, the true ratio  $I_F/I_R$  is obtained from the relation

$$\frac{I_F}{I_R} = \frac{I_1}{I_2} \times \frac{I_0}{I'_0}$$

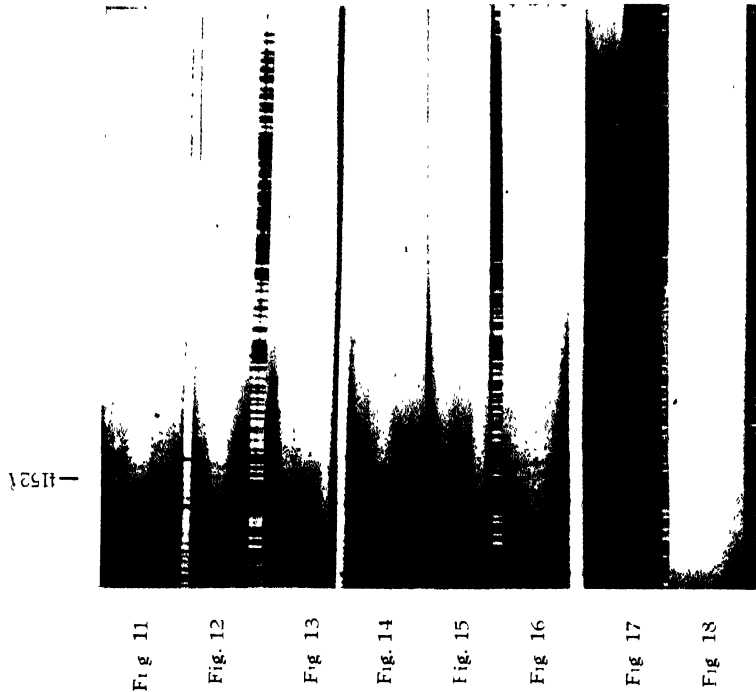
where  $I_0/I'_0$  is the ratio of the intensities for the lines 4156 Å and 4627 Å in the continuous spectrum due to the standard lamp.



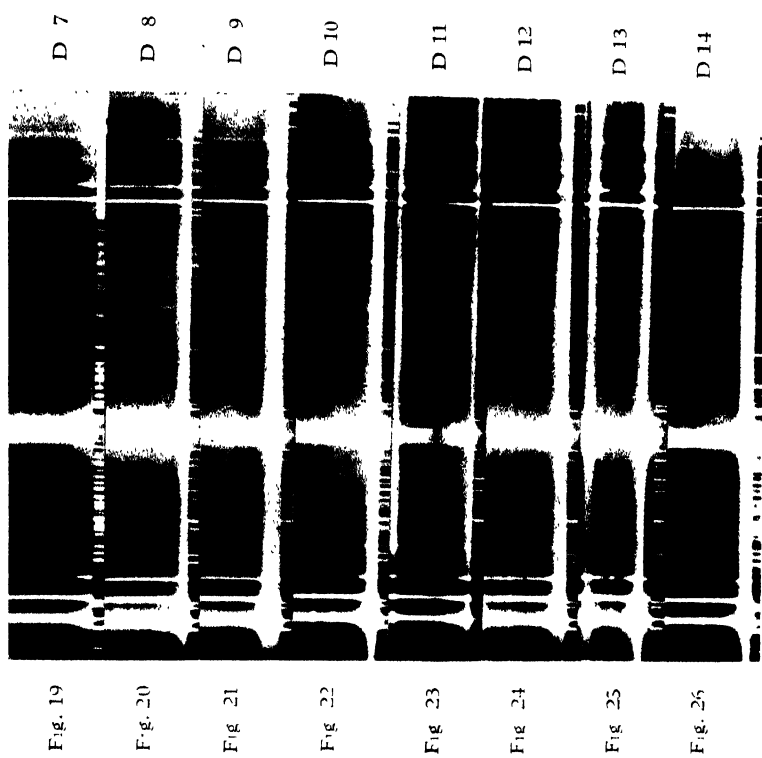


Absorption spectra of diamond in the ultraviolet regions





Absorption spectra of diamond at—170°C



Fluorescence spectra of diamond



## RESULTS

The absorption spectra in the ultraviolet region are reproduced in figures 1-10, Plate XIII A. Those for the visible region with the specimens at  $-170^{\circ}\text{C}$  are reproduced in figures 11-18 Plate XIII B. Figures 9 and 10 show the absorption spectra of D IV at about  $30^{\circ}\text{C}$  and  $-170^{\circ}\text{C}$  respectively. The absorption spectrum of this crystal at room temperature was studied previously but that at a temperature of about  $-170^{\circ}\text{C}$  was studied in the present investigation to find out whether along with the increase in the intensity of the fluorescence band at  $4156 \text{ \AA}$  with the lowering of temperature any new absorption band appears in the region between  $2250 \text{ \AA}$  and  $2400 \text{ \AA}$ .

The intensities of the fluorescence band at  $4156 \text{ \AA}$  relative to those of the Raman line at about  $4627 \text{ \AA}$  excited by  $4358 \text{ \AA}$  are given in Table II. As these values of the intensities have been obtained by the method of photographic photometry explained earlier, they are correct upto a maximum deviation of about  $\pm 10\%$ . These values also represent the relative fluorescence yields in the band  $4156 \text{ \AA}$  for the different specimens. The colour temperature of the standard lamp for the current used (14 amps) is  $2575^{\circ}\text{K}$ . This led to the value 0.437 for  $I_{4156} : I_{4625}$  according to Win's law for the continuous spectrum of the standard lamp. The absorption limits in the ultraviolet region shown by the absorption spectra reproduced in figures 1-10 are also given in the last column of Table II. The fluorescence spectra are reproduced in figures 19-26 Plate XIII B and some of the microphotometric records are reproduced in figure 27.

TABLE II

Description of the spec-	$I_F$ = Integrated intensity (peak) of the Raman line relative to standard radiation as 100	$I_R$ = Integrated intensity of the fluorescence band relative to standard radiation at $4156 \text{ \AA}$ as 100	True Ratio $I_F : I_R$	Absorption limit (Approx) in $\text{\AA}$
D 7	2.8	34.7	5.2	2560
D 8	5.7	21.3	1.5	3000
D 9	1.0	21.2	9.26	2550
D 10	2.7	51.8	8.4	2810
D 11	2.1	34.2	7.1	2270
				(bands at 2360 and 2363.3 $\text{\AA}$ )
D 12	2.8	24.5	3.8	2720
D 13	4.55	0	0	2240
D 14	1.4	12.0	6.0	2300 $\text{\AA}$
				(bands at 2360 $\text{\AA}$ and 2363.5 $\text{\AA}$ )

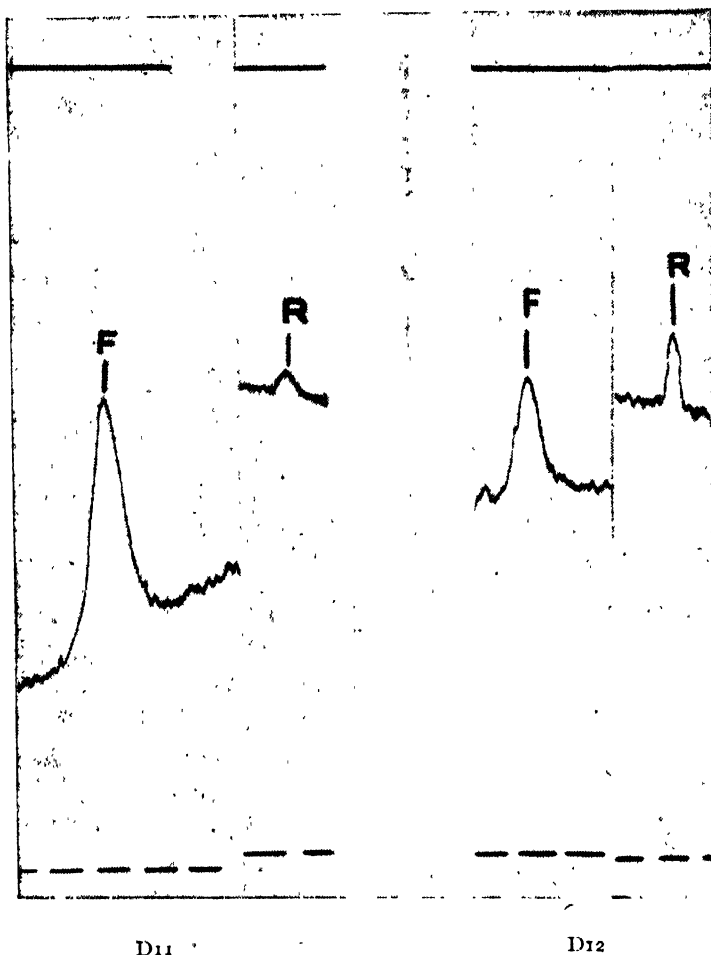


FIG. 27

Microphotometer records

## DISCUSSION

It can be seen from Table II that the intensity of the fluorescence band at  $4156 \text{ \AA}$  varies from 1.5 to 9.26 in the case of the seven of the eight specimens studied in the present investigation, while that in the case of D 13 is zero. It is evident from figure 7 in Plate XIII A that D 13 is transparent upto  $2240 \text{ \AA}$  and so it belongs to Type II. The results given in Table II show that the ultraviolet transparency of the crystal cannot be correlated with the intensity of the fluorescence band at  $4156 \text{ \AA}$ . For instance, D 10 transmits upto  $2810 \text{ \AA}$  only, while D 7 and D 11 transmit upto  $2560 \text{ \AA}$  and  $2270 \text{ \AA}$  respectively, but the fluorescence band due to D 10 is more intense than that due to either D 7 or D 11. Similarly D 14 transmits upto  $2300 \text{ \AA}$ , but the fluorescence band  $4156 \text{ \AA}$  due to this crystal is less intense than that due to D 10, which transmits only upto  $2810 \text{ \AA}$ .

Thus the general conclusion drawn by Sunanda Bai (1944) that diamonds having greater transparency in the ultraviolet region show fluorescence band at  $4156 \text{ \AA}$  of larger intensity is not correct. Of course, a comparison of the absorption limit and the intensity of the fluorescence band due to D 8 with those for any of the diamonds D 7, D 9, D 11, D 12 or D 14 would support the conclusion drawn by Sunanda Bai, but as shown above, the results obtained with the other specimens are contradictory to such a conclusion.

The intensity of the fluorescence band due to D 11 and D 14 is quite large, although the former crystal is transparent upto  $2270 \text{ \AA}$  and the latter upto  $2300 \text{ \AA}$ . Both the specimens show two absorption bands at  $2360 \text{ \AA}$  and  $2363.5 \text{ \AA}$  respectively. These two bands were also observed in the case of blue-fluorescent diamonds by Sunanda Bai (1944) and Ramanathan (1946). The latter author observed it in the case of his wedge-shaped specimen NC 78 for the thickness  $0.15 \text{ mm}$ . The portion having a thickness  $0.37 \text{ mm}$ , however, showed the absorption limit approximately at  $2520 \text{ \AA}$ . Sunanda Bai (1944) also observed these two bands along with other bands on both sides of it in the case of a large number of diamonds showing blue fluorescence. Ramanathan (1946), did not observe the other bands mentioned by Sunanda Bai in the case of NC 62 and NC 78 studied by him. The results obtained by the present author, however, lead to the conclusion that the presence of the absorption bands at  $2360 \text{ \AA}$  and  $2363.5 \text{ \AA}$  is responsible for the origin of the fluorescence band at  $4156 \text{ \AA}$ , but the other bands in the ultraviolet region have no connection with this fluorescence. Figure 9, Plate XIII A shows that D 4 does not show even any feeble absorption bands at  $2360 \text{ \AA}$  or  $2363.5 \text{ \AA}$ . It was reported earlier (Bishui, 1950) that the fluorescence band  $4156 \text{ \AA}$  due to D 4 is less intense than the Raman line excited by  $4358 \text{ \AA}$ . On the other hand, the fluorescence bands due to D 11 and D 14 are respectively about 7 and 6 times more intense than the Raman line excited by the Hg line  $4358 \text{ \AA}$ . D 13 does not show any absorption bands at  $2360 \text{ \AA}$  and  $2363.5 \text{ \AA}$  and the fluorescence band at  $4156 \text{ \AA}$  is absent in this case. These facts show that when the fluorescence band at  $4156 \text{ \AA}$  is more intense than the Raman line  $1332 \text{ cm}^{-1}$  excited by  $4358 \text{ \AA}$  line of mercury, the crystal invariably shows the absorption bands at  $2360 \text{ \AA}$  and  $2363.5 \text{ \AA}$ , but when these absorption bands are absent, the fluorescence band is either totally absent or it is less intense than the Raman line. These two absorption bands are evidently due to a particular impurity in the crystal which is also responsible for the origin of the fluorescence band at  $4156 \text{ \AA}$ . If the crystal possesses other impurities those may produce either continuous absorption or absorption bands in the region between  $2250 \text{ \AA}$  and  $3000 \text{ \AA}$ , but the intensity of the fluorescence band is determined solely by the amount of

the impurity which produces the absorption bands at  $2360 \text{ \AA}$  and  $2363.5 \text{ \AA}$  and not by the percentage of other impurities. This can be seen from the comparison of the absorption spectra and intensities of fluorescence observed in the case of D 12 or D 8 with those of D 11 and D 14. Although the former two crystals completely absorb all radiation of wavelengths shorter than  $3000 \text{ \AA}$ , the absorption is not due to the impurity which produces the fluorescence band, because the intensity of the fluorescence band due to these two crystals is smaller than that observed in the case of the crystals D 11 and D 14. On the other hand, the percentage of the impurity which produces the fluorescence band in D 9 is evidently higher than that in D 11, because the fluorescence band is more intense in the former case, but as D 9 also contains some other impurities which produce continuous absorption in the region on the shorter wavelength side of  $2550 \text{ \AA}$ , the amount of absorption at  $2360 \text{ \AA}$  and  $2363.5 \text{ \AA}$  cannot be determined in this case.

These results cannot be explained on the hypothesis that the absorption observed in the ultraviolet region is due to interpenetration of two particular types of diamond lattice and that it is not due to any impurity, because such an interpenetration would produce only a particular set of absorption bands. Actually, however, it is observed that the bands  $2360 \text{ \AA}$  and  $2363.5 \text{ \AA}$  have an origin different from that of the other bands or of the continuous absorption on the longer wavelength side observed in the case of different specimens. Such results can be explained only on the assumption that these bands are due to impurities of different types present in the diamond lattice. Pringsheim (1949) also came to such a conclusion from the results published by previous workers.

The larger number of bands observed in the ultraviolet absorption spectra of different specimens studied by Sunanda Bai (1944) and Ramanathan (1946) were not observed in the present investigation, although the crystals were sufficiently thick and some of them showed strong fluorescence band at  $4156 \text{ \AA}$ . These bands are thus not characteristic bands of the diamond lattice, but they are due to different types of impurities present in the different specimens. The facts mentioned above cannot be explained on the hypothesis that in blue-fluorescent diamonds there are no impurities and only there is a mixture of two types of lattice, because in that case such a mixture would produce only a particular set of absorption bands and these would be present with smaller or larger intensities in all blue-fluorescent diamonds. As most of the bands are present in some specimens of diamond showing blue fluorescence and are absent in other such specimens it is evident that these bands are due to different impurities present in the different specimens.

As regards the influence of thickness of the crystal on the absorption



in the ultraviolet region it can be seen from a comparison of the data given in Table I and Table II that the amount and the extent of absorption do not depend on the thickness at all. For instance, the thickness of D 12 is less than half that of D 7, but the latter transmits upto 2560 Å, while even with a long exposure no transmission at wavelengths shorter than 2720 Å was observed in the case of D 12. Similarly, D 10 has a thickness smaller than that of D 7, but the former crystal absorbs radiations of all wavelengths shorter than 2800 Å while the latter transmits upto 2560 Å. Again a comparison of the results obtained in the present investigation for D 11 with those for a similar diamond (N. C. 78) reported by Ramanathan (1946) shows that the bands at 2360 Å and 2363.5 Å appear in the case of D 11 even for a thickness of 0.95 mm while in the case of NC 78 the bands appear only when the thickness of the crystal is reduced to 0.15 mm. Hence the thickness of the crystal is not primarily responsible for the appearance of these bands. Probably, the impurity which produces these two bands is present in NC 78 in much larger percentage than in D 11. The gradual increase in the transparency of any particular specimen in the ultraviolet region with diminution of its thickness observed by Ramanathan (1946) can also be explained on the assumption that some impurities are responsible for continuous absorption in this region and they are uniformly dispersed in the matrix of the specimen. As the thickness of the crystal is diminished that of the absorbing layer also diminishes proportionately and the diminution in continuous absorption results in the shift of the absorption limit towards shorter wavelengths.

The absorption spectra in the visible region for the first eight specimens at room temperature did not show any absorption band at 4156 Å. The band appeared, however, except in the case of D 13 and D 14, when the crystals were kept at about  $-170^{\circ}\text{C}$  in a Dewar vessel containing liquid oxygen. It was shown earlier (Bishui, 1950) that the intensity of the fluorescence band increases greatly with lowering of temperature of the crystal to about  $-170^{\circ}\text{C}$ . Hence the increase in intensity of the fluorescence band at 4156 Å is intimately connected with the increase of absorption at almost the same wavelength. The absence of such absorption at the low temperature in the case of D 14 is, however, an exception, because the intensity of the fluorescence band of this crystal at room temperature is larger than that observed in the case of D 12 which shows strong absorption band at 4152 Å at  $-170^{\circ}\text{C}$ . This discrepancy cannot be due to self reversal of the fluorescence band due to D 12 at room temperature, because this crystal does not show the absorption band at room temperature even very faintly.

Finally, it has to be pointed out that the results reported in the present investigation indicate the necessity of revision of the criterion for the classification of diamonds. Robertson, Fox and Martin (1934) classified diamonds showing absorption of radiation of wavelength shorter than

3000 Å under Type I and those showing transparency even upto 2300 Å were classified under Type II. Some of the latter type showed absorption bands at 2351 Å and others at 2359 Å and 23635 Å respectively. Evidently, the latter are of the same type as D 11 or D 14 studied in the present investigation. As these crystals show the fluorescence band at 4156 Å with fairly large intensity just as the other crystals showing absorption in the region 3000 Å do, all these diamonds of fluorescent type should be placed under Type I, as they contain impruities of different types. The crystals showing no absorption band upto 2240 Å should be placed under Type II, because these diamonds contain no impurities and and do not show fluorescence band at 4156 Å with any appreciable intensity. Such diamonds are rare and they are of the purest variety. D 13 studied in the present investigation and D 4 studied earlier (Bishui, 1950) are examples of such diamonds of Type II.

#### ACKNOWLEDGMENT

The author is indebted to Prof. S. C. Sirkar for his keen interest and helpful suggestions during the progress of the work. Thanks are also due to Prof. M. N. Saha, F.R.S. for kindly lending the Adam Hilger two-prism spectrograph.

#### REFERENCES

- Bishui, B. M., 1950, *Ind. J. Phys.*, **24**, 441  
 Bishui, B. M., 1951, *Ind. J. Phys.*, **26**, 275.  
 Nayar, P. G. N., 1941, *Proc. Ind. Acad. Sc. A.*, **14**, 1.  
 Pringsheim, P., 1949, *Fluorescence and Phosphorescence*, (*Interscience Publications*), p. 648.  
 Ramanathan, K. G., 1946, *Proc. Ind. Acad. Sc. A.*, **24**, 137.  
 Robertson, Sir R., Fox, J. J. and Martin A. R., 1934, *Phil. Trans. Roy. Soc. A.*, **232**, 463.  
 Sunanda Bai, 1944, *Proc. Ind. Acad. Sc. A.*, **19**, 253.

# ON THE DISTRIBUTION OF WEATHER OVER BENGAL ON ANY DAY DURING THE PREMONSOON SEASON AS RELATED TO THE POSITION AND MOVEMENT OF A BAROMETRIC TROUGH\*

By K. R. SAHA

I. A. P. STATION, PALAMU, DELHI

(Received for publication March 7, 1952)

**ABSTRACT.** Synoptic evidence is brought forward in support of a view that a relatively high proportion of the total weather over Bengal on any day during the premonsoon season is to be related to the position and movement of a quasi-stationary barometric trough that lies over the region in an approximately W-E direction in this season. The results of a graphical representation of the weather at Calcutta and the daily position of the trough line are discussed. Some physical characteristics of the trough and its behaviour with regard to formation of weather are discussed with the aid of aerological data of two stations, viz., Lalmonirhat and Barrackpore. It is concluded that the trough in space probably behaves as a quasi-stationary frontal surface and that its movement causes the weather that is observed. Theoretical position is reviewed and a tentative explanation of the latitudinal movement of the trough is offered. The possibility of forecasting the movement of the trough and the associated weather is discussed.

## 1. INTRODUCTION

Norwesters or severe thundersqualls are important features of Bengal's weather during the premonsoon season from mid-March to May; besides, during this period, there is, occasionally, weather due to western disturbances which cross the area eastward and also weather due to local heat convection. But if one takes stock of the total weather that occurs over the region over a reasonably long period, say a month, one is impressed by an appreciably large proportion of weather in the form of rain and thunderstorms which cannot be said to fall in any of the categories already cited. It is also noticed that this latter weather is not haphazardly distributed but would appear to show some kind of association and alignment with the position and movement of a quasi-stationary barometric trough (shown by a double line in figure 1) which lies over Bengal during this period in an approximately W-E direction as part of the seasonal low pressure over north and central India. In the present paper this probable association is investigated. Synoptic data of weather at Calcutta and the corresponding position of the trough line from day to day

\*A summary of this paper was read before the Physics section of the 39th annual session of the Indian Science Congress in Calcutta on the 5th January, 1952.

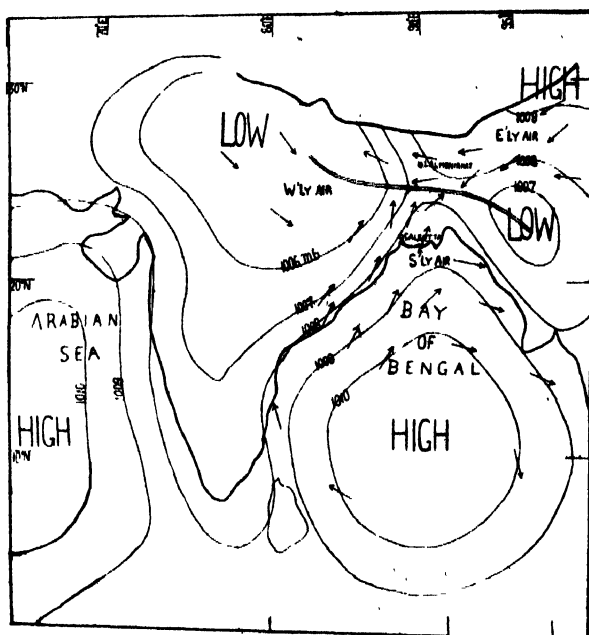


FIG. 1

Mean surface isobaric map, April. Arrows indicate mean wind directions. The double line represents the W-E barometric trough over Bengal.

during the months of April and May in four years 1942-43 and 1945-46 are presented in graphs and the results of this graphical representation are discussed in some detail. A high correlation being indicated, the properties and the role of the W-E barometric trough in the formation of the observed weather are discussed with the aid of synoptic and aerological data in sections 3 and 4. In section 5, the theory of movement of a barometric trough is briefly stated and a possible explanation is offered of the movement of the W-E trough line. In section 6, the possibility of forecasting the movement the trough line is discussed.

## 2. GRAPHICAL REPRESENTATION AND DISCUSSION OF SYNOPTIC DATA

To investigate a probable association of the weather of Bengal with the seasonal W-E trough line over the region in premonsoon season, synoptic data of weather at Calcutta and the position of the trough line at two main synoptic hours of 0230z (GMT) and 1130z (except in 1942 when the time of the morning data was 0800 hrs local mean time which corresponds to 0206z at Calcutta) on each day during the months of April and May of four years 1942-43 and 1945-46 were plotted in a series of graphs (figures 2-5). In these graphs a system of coordinates formed by Lat.  $22\frac{1}{2}$  degrees N (base line) and

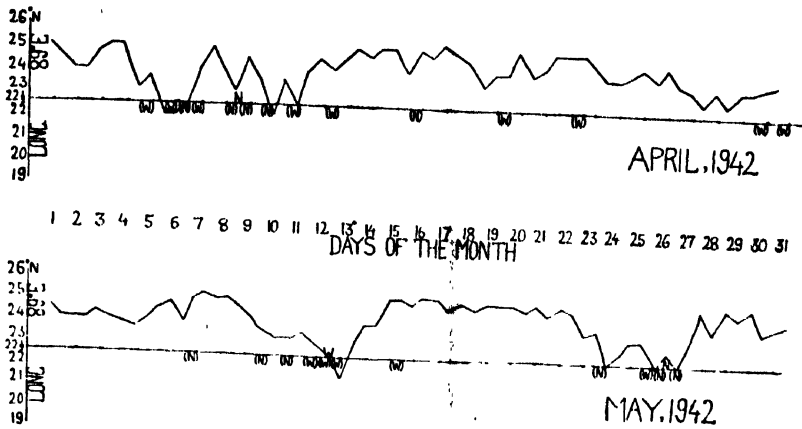


FIG. 2  
Latitudinal movement graphs, April and May, 1942.

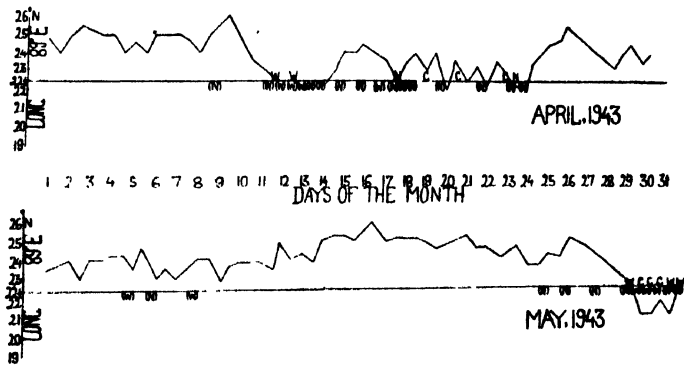


FIG. 3  
Latitudinal movement graphs, April and May, 1943.

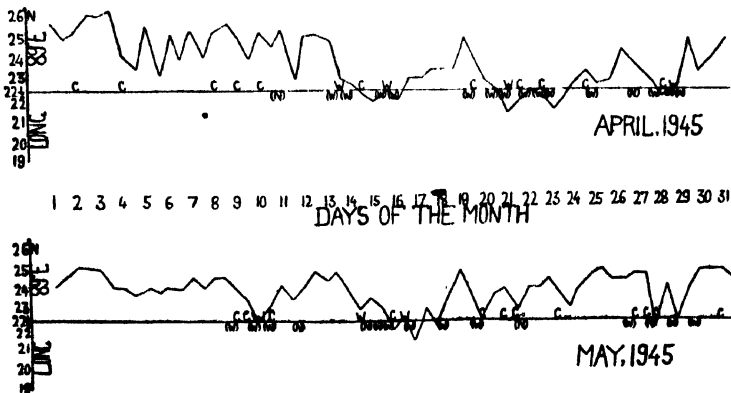


FIG. 4  
Latitudinal movement graphs, April and May, 1945.

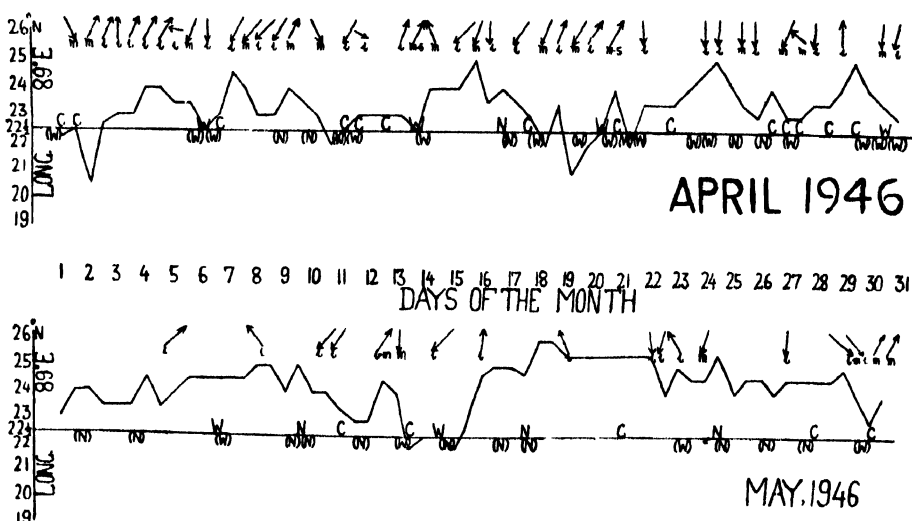


FIG. 5

Latitudinal movement graphs, April and May, 1946. The arrows at the top of each curve give direction of isallobaric winds (an arrow pointing downward indicates a N'y isallobaric wind), the speed being given as *l*, *m*, or *s* according as these winds are light, moderate, or strong.

long. 89 degrees E (ordinate) was used to plot the position of the trough line and the corresponding weather at Calcutta which lies close to origin of the chosen system of coordinates. The position of the trough line was located with the aid of surface synoptic charts as well as winds-aloft charts for levels up to a height of 3,000-5,000 ft above M. S. L. and the surface position was marked on the ordinate at both the main synoptic hours of each day. On the base line the weather at Calcutta was noted in letter symbols. The symbols used were: *f* for fine, fair and fair to cloudy weather; *c* for cloudy weather; *N* for Norwester; and *W* for rain or thunderstorm or both. For the sake of neatness, the symbol *f* was omitted from the graphs. The position on the base line immediately above or below a date-mark in the centre corresponds to 0230z, whereas, that halfway to the following date on its right corresponds to 1130z. The present weather was shown on the top of the base line, whereas, past weather was shown below it and in brackets. Past weather at 1130z was counted from 0230z of the same day but that at 0230z from 1130z of the previous day. Thus a thunderstorm at 1330z on a day would be taken as past weather at 0230z of the following day and placed symbolically below the base line between the present weather symbols of 1130z of the same day and that of 0230z of the following day and in brackets.

In figure 5 for the year 1946, the isallobaric components of surface winds as computed from the available 24-hours pressure-changes over the region were presented on the top of each curve. The significance of these

wind components would be discussed in a later section. In deciding between a Norwester and any other thunderstorm the very severe character of the thundersquall associated with the former was the guiding consideration.

#### DISCUSSION

*April, 1942 : figure 2.* (a) Apart from four Norwesters and four cases of weather from local heat convection, there appears to be a close correlation between the weather at Calcutta and the position of the trough line. There were four days on which weather occurred at Calcutta when the W-E trough line lay on or in the vicinity of the city. With the trough line lying far away the weather over the city was generally fair or fine, apart from the occasional visitation of Norwesters or sporadic local air mass showers or thunderstorms. During the month the trough line lay most of the time north of the base line and approached the city close enough only three or four times and crossed it only on two occasions.

(b) The movement of the trough line would appear to be somewhat oscillatory. The northward movement of the trough line was interrupted by two successive Norwesters on the 8th and the 9th. But for this interruption, it may be argued, the crest position would have been reached on either of these days which would have given the oscillation a period of about 8 days. The maximum amplitude of oscillation was  $3\frac{1}{2}$  degrees of latitude (approx). The oscillation appeared to be rapid and marked in the first half of the month but rather slow and feeble in the latter half.

*May, 1942 : figure 2.* The close association of weather at Calcutta and the position of the trough line on or in the vicinity of the city is again indicated in this month. Though in the main the trough line lay north of the base line, it approached or crossed over the city three or four times and on all these occasions there was weather over the city. Weather was fair or fine on days when the trough line lay far away from the city except for Norwesters and local airmass showers which appeared to have no connection with the W-E trough line.

The movement curve would appear to be oscillatory in this month, but the period is not clearly defined. The flat nature of the curve from the 15th to 22nd is not understood. It may be that the trough did move appreciably during this period but the movement was difficult to follow because of the very weak intensity of the trough. The maximum amplitude of the oscillation was 3 degrees of latitude.

*April, 1943 : figure 3.* During this month there were as many as 10 Norwesters of which 7 occurred between the 14th and 23rd. Outside this period, the correlation between the weather at Calcutta and the position of the trough line would appear to be high. The movement of the trough would appear to be oscillatory apart from the very marked distortion caused to it by the Norwesters over a fairly long spell. But for the effect of the Norwesters, a

period of about 8 or 9 days would appear to be justifiable. The maximum amplitude of oscillation was 4 degrees of latitude.

*May, 1943 : figure 3.* Unlike April, only 3 Norwesters affected the city in May. None of these appeared to affect the trough line seriously. There were two days of local airmass showers or thunderstorms. Towards the end of the month, a depression formed in the NW corner of the Bay of Bengal and the W-E trough line moved rapidly southward crossing Calcutta on the 29th. It remained south till the 31st when it recrossed the base line on the return journey. But for this depression the trough line lay north of the base line all the time. It is clear that in this month the axis of oscillation of the curve had moved somewhat northward.

*April, 1945 : figure 4.* During the first two weeks of this month a number of western disturbances in almost occluded states passed over north Bengal and in the course of the eastward passage of these depressions the W-E trough line, which in most cases behaved as an overtaken warm front, moved eastward followed by a weak cold front. The position of the curve on many days in this period refers to that of the cold front on the ordinate and not to the W-E trough line. There is, of course, little justification for this deviation from the set procedure but it was made with the sole object of recording the effect of the movement of any other type of front across the long. 89 degrees E on weather at Calcutta when the W-E trough line position was not available. Apart from minor disturbances referred to above, the movement curve would appear to be oscillatory with a period of about 7 or 8 days and an amplitude of  $3\frac{1}{2}$  degrees of latitude. During the month there were two days of Norwesters, one day of airmass thunderstorm, and eight or nine days of rain or thunderstorm which occurred when the W-E trough line lay on or near Calcutta. The passage of low pressure waves across north Bengal did not disturb the fair weather over the city apart from giving cloudiness on some days.

*May, 1945 : figure 4.* A very high correlation between the weather at Calcutta and the position of the W-E trough line is shown in this month. The extraneous influences were few, there being only four Norwesters of which only one affected the movement of the trough line appreciably on the 27th and four occasions of local airmass weather. In the first week of the month when the trough line lay far north of Calcutta, the weather over the city was uneventful but afterwards whenever it approached the city close enough or crossed it to the south, there was weather or appearance of thick massive clouds over the city. The oscillation of the trough movement appears to be fairly regular during this month and the period and amplitude of the oscillation would appear to be the same as in April.

*April, 1946 : figure 5.* The correlation of weather with the position of the trough line and the oscillation of the trough movement are very clearly evidenced in this month. There were five Norwesters, and eleven



occasions of rain or thunderstorms. Of the latter, most occurred when the W-E trough line lay on or in the proximity of Calcutta. With the trough line lying far away from the city, the weather was generally fair or fine apart from occasional visitation of Norwesters or local showers. On the occasions when Norwesters occurred, the trough line position was well away from the city. The oscillation of the trough movement would appear to have a period of 7 or 8 days and maximum amplitude of 4 degrees of latitude.

May, 1946 : figure 5. The curve shows almost the same characteristics as in April. The following differences are, however, noted :

There were nine days of Norwesters in May. The trough line approached or crossed over to the south or north of Calcutta on fewer days in May than in April. This would give a smaller frequency and hence a longer period in May. The axis of oscillation of the trough appeared to be further north in May than in the previous month. Rain or thunderstorms occurred in Calcutta on the few occasions when the W-E trough line crossed over or approached the city. Norwesters appeared to occur, as a rule, in complete disregard of the position of the trough line.

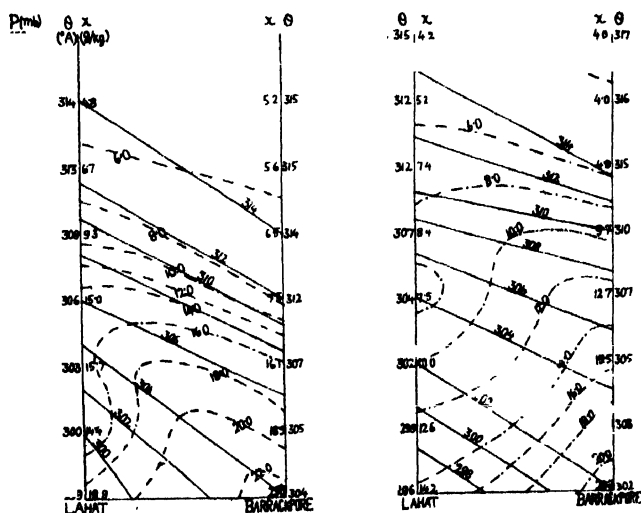


FIG. 6

Vertical distribution of potential temperatures ( $\theta$ ) and humidity mixing ratio ( $x$ ) over Lahat and Barrackpore at 1300 G.M.T. on 8-5-45 and 15-5-45. Continuous lines represent potential temperature and dotted lines humidity mixing ratio.

### 3. SOME STUDIES OF THE PHYSICAL CHARACTERISTICS OF THE TROUGH LINE

It would be evident from the previous section that a close association exists between the weather at Calcutta and the position of the W-E trough

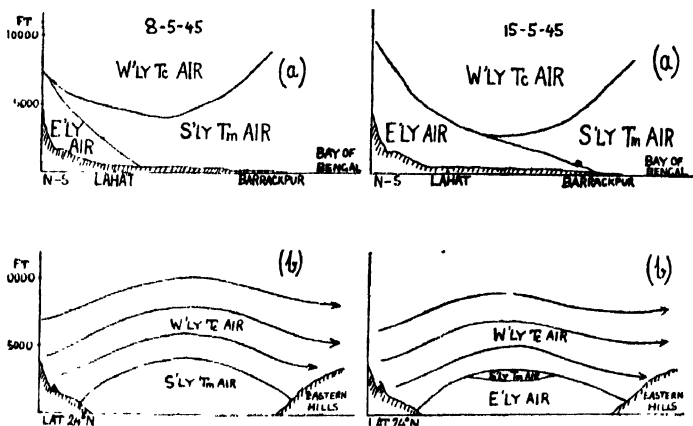
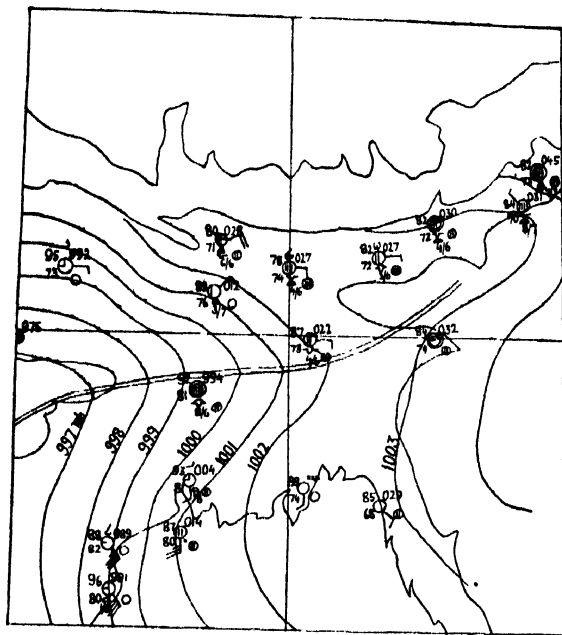


FIG. 7

Airmass crosssections (vertical). (a) N-S, along about long. 89°E; (b) E-W, along about 24°N.



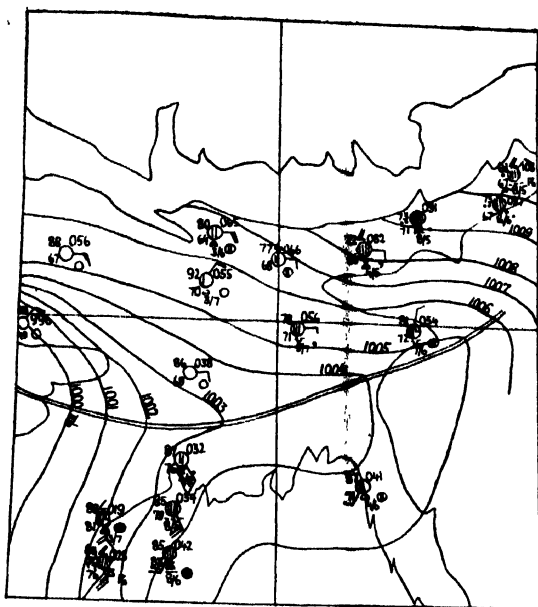


FIG. 9

Surface synoptic chart, 1130, G.M.T, 15-5-45.

perature and humidity, at least in the lower levels and in early summer months, to meet on the trough line. This means that both temperatures and dew points will be lower on the north of the trough line. This is exactly what is observed. During the months of March and April, the dew points on the north of the trough line are on an average 5-10°F lower than on the south. But surface observations may not always faithfully represent the airmass properties in space. Hence supplementary aerological data of two stations, Lalmonirhat (Lat. 25°55'N, long. 89°25'E) and Barrackpore (Lat. 22°34'N, long. 88°20'E) were computed and the results are presented in figure 6 which shows the upper-air distributions of potential temperature and humidity mixing ratio on two selected days, the 8th and the 15th May, 1945. The synoptic situations on these days are shown in figures 8 and 9. In Table I the equivalent potential temperatures on these days up to a level of 650 mbs are given for the two stations. It would seem to follow from these results that the airmass over Lahat (abbreviation of Lalmonirhat) which lies most often to the north of the trough line is definitely cooler and less humid than the airmass over Barrackpore. It would also seem to be established that the airmass contrast extends occasionally to a height of 3,000-5,000 feet above M.S.L. or even higher. With the overlying W'ly air which is warmer and drier than either of the lower airmasses, the special distribution of airmasses over Bengal during the months of April and May would look somewhat like that represented in figure 7 which gives (a) an approximately N-S vertical cross section

through Lahat and Barrackpore, and (b) a W-E vertical cross section along Lat.  $24^{\circ}\text{N}$  on the dates mentioned. The relative disposition of the airmasses as shown in this figure is, however, to be regarded as tentative in the absence of further substantiating data. Aerological data from a closer network of radio sonde stations (R.S. stations) would be required for a more thorough and critical study.

TABLE I

Equivalent potential temperatures ( $\theta_E$ ) over Lahat and Barrackpore  
(Mean time of ascent-1300 G.M.T.).

Date	Station	1000 mb	950	900	850	800	750	700
8/5/45	Lahat	356	345	352	354	340	337	332
"	Barrackpore	375	367	358	338	337	334	332
15/5/45	Lahat	339	338	333	328	334	336	327
"	Barrackpore	365	363	355	348	343	333	331

The contrast between the airmasses on either side of the trough line would, however, seem to be well-established by the present study. The relative properties would lead to the formation of a sloping surface of discontinuity with cooler and less humid air on the north underlying warmer and more humid air on the south. An idea regarding the mean slope of the surface can be had from the position of the trough line at different heights above M.S.L. as found in winds-aloft charts. It is, therefore, concluded that the W-E trough in space probably functions as a frontal surface and that any weather that may form as a result of its movement should be amenable to frontological interpretation. This aspect of the question is examined in the following section.

#### MECHANISM OF WEATHER FORMATION AS A RESULT OF MOVEMENT OF THE TROUGH

The incidence of weather at Calcutta whenever the W-E barometric trough approached or crossed over the city as presented in section 2 would suggest that the weather was formed by the action of the trough itself. The conclusions drawn in section 3 would seem to support this view. During the premonsoon season a marked degree of latent and convective instability exists in the air mass over Bengal. Almost superadiabatic lapse rate of temperature in the overlying dry W'y air is the chief cause of the instability of the season's atmosphere. When such a degree of instability occurs in the atmosphere, any agency which can lift the air sufficiently from the ground level may be instrumental in forming weather over Bengal.

The W-E barometric trough in space would seem to be capable of acting as such an agency. Its movement would lift the warm and moist air of the S lies to a higher level and cause cloud, rain and thunderstorms. The intensity of the weather to develop would depend on the strength and the degree of convergence of the interacting airstreams and hence may be different at different points along the trough line. Observations appear to show that the number of thunderstorms that are formed is somewhat greater when the trough moves southward than when it moves in the opposite direction. This is, of course, subject to further confirmation. It may be that the wedge action of the relatively cool and less humid air on the north is responsible for the apparent discrepancy but, in presenting this view it is considered necessary to stress that the weather that forms on the W-E trough seldom has the pattern and sequence of weather that is found on a pure frontal surface of the cold front or the warm front type connected with a travelling depression of the middle latitudes. In actual fact, it appears to conform more closely to the weather that is observed on a quasi-stationary frontal surface. We may, however, note here an important distinction between this weather and the Norwester of Bengal. Observations seem to indicate that apart from the greater severity of the Norwester as a thundersquall it has no genetical relation with the W-E trough. A Norwester may originate anywhere near the hills of Chotanagpur (Type-A Norwesters), southern slopes of the Himalayas (Type-B Norwesters), and the Khasi hills of Assam (Type-C Norwesters) (*vide* "Norwesters of Bengal," 1944) and move to some southerly direction. There is, however, an effect which is noticeable when the Norwester moves. It distorts and sometimes completely breaks through the W-E trough line but as would be evident from the data presented in section 2 this disturbance is only short-lived and the trough regains its normal position and characteristic as soon as the Norwester dies out.

It is interesting to observe on any day the movement of the W-E trough line over a station. A bank of thick cloud and rain and thunderstorm oriented more or less in a W-E direction approaches the station. Just when the cloud moves over, there is a wind-shift. This change is usually attended with gusts but light squall is not rare. The wind speed may reach 30/40 knots if the trough happens to be a deep one. If the trough is weak, there may be simply a bank of cloud that moves over. In any case, the cloudiness and weather that forms appear to move in a narrow latitudinal belt in alignment with the position of the trough line.

The position of the trough may, therefore, be regarded as a deciding factor in the distribution of weather over Bengal on any day. When it lies over extreme south Bengal, weather deteriorates over that region while it becomes fine and clear in the north and *vice versa*. Roy (1938), in a paper on the distribution of rainfall over south Bengal during the premonsoon season found a high correlation between the frequency of rainy days over the region

and the existence of a higher barometric pressure at Berhampore (Lat.  $24^{\circ} 05'N$ , long.  $88^{\circ} 15'E$ ) than at Calcutta. As a corollary to the same investigation he concluded that the favourable condition of higher barometric pressure at Berhampore than at Calcutta indicates the probable presence of dry and somewhat cooler air of land origin to the north of deltaic Bengal at some upper level, if not actually on the ground level, and perhaps also its movement towards deltaic Bengal. The present investigation would appear to lend support to the conclusion reached by Roy in that a higher barometric pressure at Berhampore than at Calcutta is only feasible when the W-E barometric trough line lies over extreme south Bengal. The probable presence and the southward movement of land air suspected by him also appear to be confirmed. But the evidence brought forward in the present study would seem to indicate that rainfall and weather over Bengal at any instant during the premonsoon season are not haphazardly distributed but occur in a narrow latitudinal belt somewhat in alignment with the W-E trough line. It is this regularity in the distribution of the observed weather that would appear to have been specially brought out by the present investigation.

#### 5. THEORY OF MOVEMENT OF A TROUGH AND A POSSIBLE EXPLANATION OF THE MOVEMENT OF THE W-E TROUGH

Petterssen (1940) gives for the movement of a trough line the following expressions :

$$C = - \frac{\partial^2 p / (\partial x \partial t)}{\partial^2 p / \partial x^2} \quad \dots (1)$$

$$A = \frac{\partial^3 p / (\partial x \partial t^2) + 2C \partial^3 p / (\partial x^2 \partial t)}{\partial^3 p / \partial x^3} \quad \dots (2)$$

where  $C$  denotes the velocity of the trough line along the  $x$ -axis drawn normal to the trough line in the horizontal plane;  $A$ , the acceleration along the  $x$ -axis, and

$\partial^2 p / (\partial x \partial t)$  = the increase in the barometric tendency  $\partial p / \partial t$  per unit length along the  $x$ -axis,

$\partial^2 p / \partial x^2$  = the increase in the pressure gradient  $\partial p / \partial x$  per unit length along the  $x$ -axis,

$\partial^3 p / (\partial t^2 \partial x)$  = the slope of the  $\partial^2 p / \partial t^2$  profile along the  $x$ -axis, and

$\partial^3 p / (\partial x^2 \partial t)$  = the curvature of the tendency profile along the  $x$ -axis.

The displacement,  $S$ , of the trough in time,  $t$ , is given by

$$S = Ct + \frac{1}{2}At^2 \quad \dots (3)$$

In equation (2), the terms in the numerator are usually small, whereas,  $\partial^3 p / \partial x^3$  may vary within wide limits. Hence in a rough qualitative estima-

tion of the displacement the factor .1 may be neglected. Writing equation (1) in the form

$$C = \frac{-I}{\partial^2 p / \partial x^2} \quad \dots (1)$$

where  $-I$  is the isallobaric gradient, we note that the movement of the trough line occurs along an isallobaric gradient, i.e., in the direction from the centre of an isallobaric 'high' to the centre of an isallobaric 'low' and that the rate of movement is directly proportional to the magnitude of this gradient.  $\partial^2 p / \partial x^2$  is always positive for a barometric trough and its value must be computed in a quantitative study of the speed of a trough line. In the present study the exact speed of the movement was not calculated. The direction of movement being always down the isallobaric gradient a qualitative estimate of the speed was made from an examination of the isallobaric distribution and intensity of the pressure trough over the region.

An analysis of the 24-hour pressure change charts at 0230z and 1130z during April and May in 1946 appeared to support the above theoretical expressions for the movement of the W-E trough line. Isallobaric wind components (Petterssen, 1940) were estimated from the charts and expressed as light, moderate, or strong according as the isallobaric gradient was weak, moderate, or steep. In figure 5 the isallobaric winds are presented at the tops of the movement curves, the direction of the wind being shown by the conventional arrow and the speed expressed as *l*, *m*, or *s* according as it was light, moderate, or strong. Estimation of the isallobaric wind in the case of weak isallobaric gradients was a difficult problem. A second difficulty arose when there were a number of isallobaric 'highs' and 'lows' on the chart. In the present investigation isallobaric winds were estimated in all cases of pronounced pressure tendency 'highs' and 'lows' and the resultant isallobaric winds were estimated in some cases. In the remaining cases in which the gradient was weak or there was an unduly large number of 'highs' and 'lows' the estimation was either dropped or the wind was expressed as light variable.

It would be seen from the foregoing analysis that the movement of the trough is vitally related to the pressure changes that occur on either side of the trough line. Figure 1 shows the normal position of the trough between the subtropical high pressure cell over north Assam and western China and the high pressure cell over the Bay of Bengal. It is plausible to hold that the pressure changes that occur on either side are vitally related to the growth or decay of these high pressure cells. However, it is the relative pressure change that moves the trough. In the course of the present investigation it was observed that the trough line moved southward whenever the northern high pressure cell intensified relative to the southern high pressure cell and vice versa for movement in the opposite direction.

## 6. POSSIBILITY OF FORECASTING THE MOVEMENT OF THE TROUGH AND ASSOCIATED WEATHER

Thus the history of the movement of the barometric trough is indissolubly bound up with that of the intensification or dissipation of one system of high pressure relative to the other. It is the relative change that matters and not the individual changes. This fact, coupled with probable existence of periodicity in the movement of the trough line, points to the possibility of forecasting its movement on any day. For this purpose the isallobaric gradient and the phase of the periodic movement will have to be determined with sufficient accuracy. It is also to be borne in mind that extraneous factors, such as the Norwester or the western disturbance, may interfere with the movement of the trough, although temporarily, and that these factors should be duly considered and their effects assessed in order to obtain the resultant movement of the trough. Another factor which must be taken into consideration in a full analysis is a diurnal oscillation of the trough brought about by temperature differences between land and sea. An examination of the movement curves presented in section 2 reveals a slight northward movement in most afternoons and southward movement in mornings. These small scale diurnal oscillations are superimposed on the main latitudinal oscillation of the trough line. The resultant movement of the trough at any instant, therefore, will depend upon the amplitude and phase relations of both these oscillations. But the effect of the diurnal oscillation is not sought to be discussed in any detail in the present paper. In the course of the investigation it was realised that pressure change charts for a period much shorter than 24 hours are necessary to reveal the micro-structure of the changes that occur in the isallobaric gradient over any period. This will involve predetermination of normal diurnal oscillation of pressure at a number of stations at intervals of, say, 3 or 6 hours.

## ACKNOWLEDGMENTS

The author is indebted to Mr. A. K. Roy, B.Sc., (Cal), B.A. (Oxon), Indian Meteorological Department, for having kindly gone through the paper and offered valuable criticism and suggestions. Acknowledgment is made to Air Headquarters, India, for permission to publish the paper.

## REFERENCES

- Indian Meteorological Department, 1944, Nor' westers of Bengal, Technical Note No. 10, p2.
- Petterssen, S., 1940, Weather analysis and forecasting, Mc Graw-Hill Book Co, London, pp 210-211 and 86-88.
- Roy, A.K., 1938, On the forecasting of rain over south Bengal during the Nor'wester season, mid-March to mid-May, Ind. Met. Dept. Scientific Note No. 83.



# STUDY OF DIFFUSE X-RAY REFLECTION BY A SINGLE CRYSTAL OF META AMINOPHENOL\*

BY M. N. DATTA

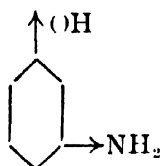
KHAIRA LABORATORY OF PHYSICS, CALCUTTA UNIVERSITY

(Received for publication, May 6, 1952)

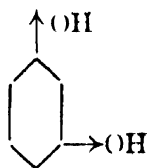
Plates XIV A-B

**ABSTRACT.** The refractive indices in different directions of the crystal were measured, the plane of molecule was taken to be in a perpendicular direction of least refractive index, namely in the *c*-direction. The axes of the crystal were found, by rotation photographs, to be :  $a=6.310$  A.U.,  $b=11.12$  A.U. and  $c=8.60$  A.U. Planes (211), (330), (213), (212), (340), (321) (350), and (333) show extra Laue reflections, of which the extra Laue reflections from (211) persist from  $18^\circ$  to  $6.8^\circ$  and yield an interesting result when plotted on reciprocal lattice, namely, the derangement waves pass strictly on *b* axis.)

Robertson has studied the structure of  $\alpha$ -resorcinol ortho- $C_6H_4(OH)_2$ . He has found that the structure of the crystal is fairly dense, since the hydrogen bonds draw the molecules closer together than the normal Van der Waals distance, and it is relatively isotropic. Lonsdale (1942) has found the most interesting results of diffuse X-ray reflection by resorcinol. The most noticeable features of the diffuse scattering are the dense halo surrounding the central spot, and the arrangement of diffuse spots on layer line. Since meta aminophenol has the similar structural formula as resorcinol, so it will be interesting to study X-ray properties as well as the optical properties of this crystal.



Meta aminophenol



Resorcinol

From early days of science the physicists and mineralogists have studied the optical properties of the crystals, because such studies gave some information about the structure of crystal. In the case of aromatic organic crystals, the refractive indices in different directions give the indications of the orientations of the benzene rings inside the crystals (Datta, 1947).

The crystal studied in the present investigation was meta aminophenol. The substance was crystallised by slow evaporation of alcohol solution. The face

\* Communicated by Prof. S. N. Bose

angles of the crystal were measured and the axes were determined. The crystal belongs to orthorhombic system, hence the crystallographic directions are also the principal directions. The crystal was mounted on Fedorov stage placed between the crossed nicols of a polarising microscope, and the crystal was rotated about the direction until the extinction was observed. For the determination of the principal refractive indices, the Becke method was used. The crystal was immersed in a drop of liquid whose refractive index was intermediate between two principal indices of the crystal. The crystal was illuminated by polarised light and was rotated about the axis of the optical system until the Becke line disappeared. This was repeated for another liquid of intermediate refractive index. The two principal refractive indices  $\alpha$  and  $\beta$  are given by the relations

$$\alpha^2 = \frac{n_1^2 n_2^2 \cos^2 \theta_2 \sin^2 \theta_1 - n_1^2 n_2^2 \sin^2 \theta_2 \cos^2 \theta_1}{n_1^2 \sin^2 \theta_1 - n_2^2 \sin^2 \theta_2} \quad \dots (1)$$

$$\beta^2 = \frac{n_1^2 n_2^2 \cos^2 \theta_1 \sin^2 \theta_2 - n_1^2 n_2^2 \sin^2 \theta_2 \cos^2 \theta_1}{n_1^2 \cos^2 \theta_1 - n_2^2 \cos^2 \theta_2} \quad \dots (2)$$

where  $n_1$  and  $n_2$  are the refractive indices of the liquids and  $\theta_1$  and  $\theta_2$  are the angles between the first principal axis and the directions of electric vectors for the disappearance of the Becke line.

The third refractive index  $\gamma$  is obtained from the relation

$$\frac{\gamma}{\alpha} \sqrt{\frac{\alpha^2 - \beta^2}{\beta^2 - \gamma^2}} = \tan V_a$$

where  $V_a$  is half the optic-axial angle. The optic-axial angle was measured by the following method :

Both the analyser and polariser were moved simultaneously through 45 degrees. The hemisphere on the Fedorov stage was rotated on the horizontal circle until the extinction was obtained. This is half optic-axial angle.

*Measurement on semi-optic-axial angle ( $V_a = 15.30'$ ).*—The measurement shows (010) plane to be optic-axial plane, with  $a$ -axis to be acute-bisectrix, so that the crystal shows negative birefringes.

*Measurement of  $\alpha$  and  $\gamma$ .*—The first liquid used has refractive index  $= 1.552$  and extinction angle  $= 53^\circ$ . The second liquid used has refractive index  $= 1.515$  and extinction angle  $= 74^\circ$ . Therefore, from

$$\alpha^2 = \frac{n_1^2 n_2^2 \cos^2 \theta_2 \sin^2 \theta_1 - n_1^2 n_2^2 \sin^2 \theta_2 \cos^2 \theta_1}{n_1^2 \sin^2 \theta_1 - n_2^2 \sin^2 \theta_2}$$

we get

$$\alpha = 1.638$$

and from

$$\gamma^2 = \frac{n_1^2 n_2^2 \cos^2 \theta_1 \sin^2 \theta_2 - n_1^2 n_2^2 \cos^2 \theta_2 \sin^2 \theta_1}{n_1^2 \cos^2 \theta_1 - n_2^2 \cos^2 \theta_2}$$

we get

$$\gamma = 1.505.$$

From

$$\tan V_a^2 = \frac{\gamma}{\alpha} \sqrt{\frac{\alpha^2 - \beta^2}{\beta^2 - \gamma^2}}$$

$$\beta = \frac{\gamma \alpha \sec V}{\sqrt{\gamma^2 + \alpha^2 \tan^2 V}} = 1.625.$$

Thus we have  $\alpha = 1.638$ ,  $\beta = 1.625$  and  $\gamma = 1.505$ .  $\alpha$ ,  $\beta$  and  $\gamma$  represent the refractive indices along  $a$ ,  $b$  and  $c$  axes respectively.

The results show that the plane of benzene ring is closer to  $\alpha$  and  $\beta$  directions than to  $\gamma$  direction.

$\alpha$ -resorcinol is relatively isotropic because OH bonds draw the molecules closer than the normal Van der Waals distance. In the case of meta aminophenol one of OH is replaced by  $\text{NH}_2$ , which causes the higher anisotropy property of the crystals (Lonsdale and Smith, 1942).

We have studied X-ray properties of the crystal. The crystal is of orthorhombic-pyramidal type of pronounced hemimorphism with axial data,  $a = 6.310$  A.U.,  $b = 11.12$  A.U.,  $c = 8.60$  A.U. The number of molecules per unit cell is four and space group is  $C_{2v}^4$  and simple lattice  $T_0$  (Caspari, 1926).

The crystal shows extra Laue reflection when exposed to Ni-radiations. The planes (211), (330), (212), (213), (340), (321) and (333) show extra spots. One of the extra spots (211) shows very interesting results when plotted on reciprocal lattice network with values of  $a^*$  and  $b^*$  where  $a^* = \lambda/a$  and  $b^* = \lambda/b$ . Let us consider a sphere that touches the origin of the lattice and that has a unit radius. Any crystal plane will be in reflecting condition if the corresponding reciprocal lattice point lies on the surface of this sphere provided that the direction of incident X-ray beam is along the diameter of the sphere (Banerjee, 1947).

Figure 1 represents a set of crystal planes having the reciprocal lattice point at  $P$  and incident beam along  $OQ$ . The sphere of reflection is drawn with  $QO$  as its diameter, the distance  $QO$  being twice the distance that has been chosen as the unit distance for plotting the reciprocal lattice. The point  $P$  will be on the sphere of reflection if  $\sin \theta = \rho/2$ .

On substituting the value of  $\rho$  it will be equivalent to Bragg's equation,  $\sin \theta = \lambda/2d$ . The reflected ray will emerge out from crystal at an angle  $2\theta$  from the incident beam (Banerjee and Bose, 1944).

For equatorial layer line, the sphere of reflection will cut the reciprocal lattice network in a circle of unit radius and if X-ray passes along  $b^*$  axis of the crystal, the circle of unit radius is to be so placed that the diameter of the circle will be on  $b^*$  axis of the network. Then with centre  $O$  (origin of net work) and radius  $= \xi$ , we draw an arc which will cut the circle ( $r_0 = 1$ ) at the point  $P$ , then co-ordinates of the point  $P$  will give the values of  $h$  and  $k$ . Now if the crystal is rotated through an angle  $\omega$  on reciprocal lattice network through the origin  $O$ , the point  $O$  will remain the same as before,

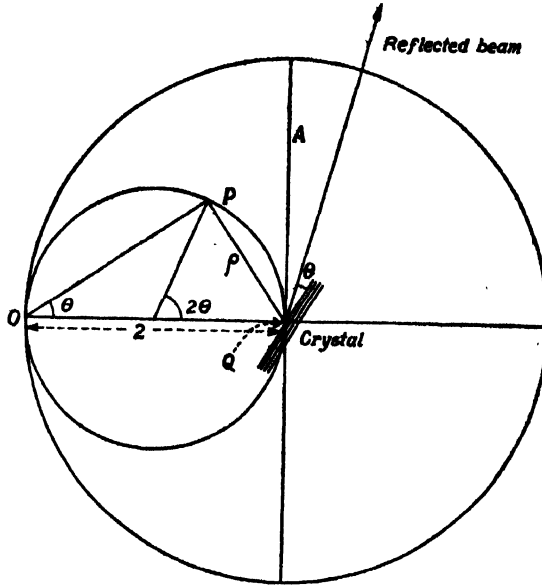


FIG- 1

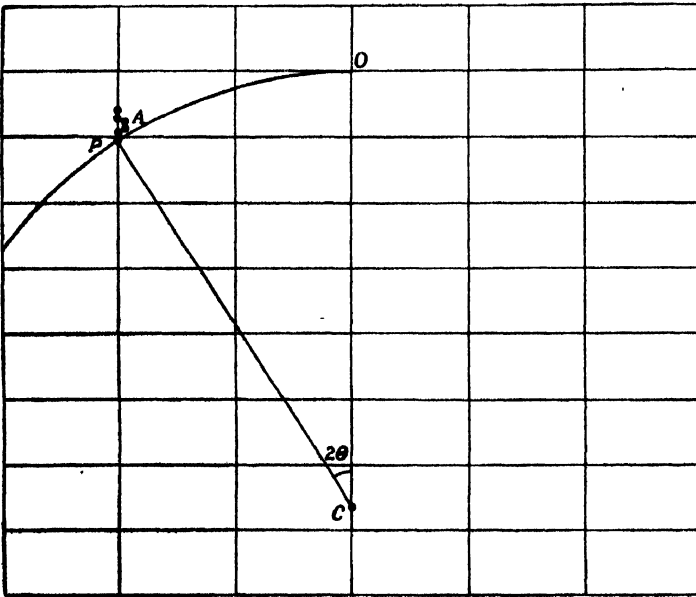


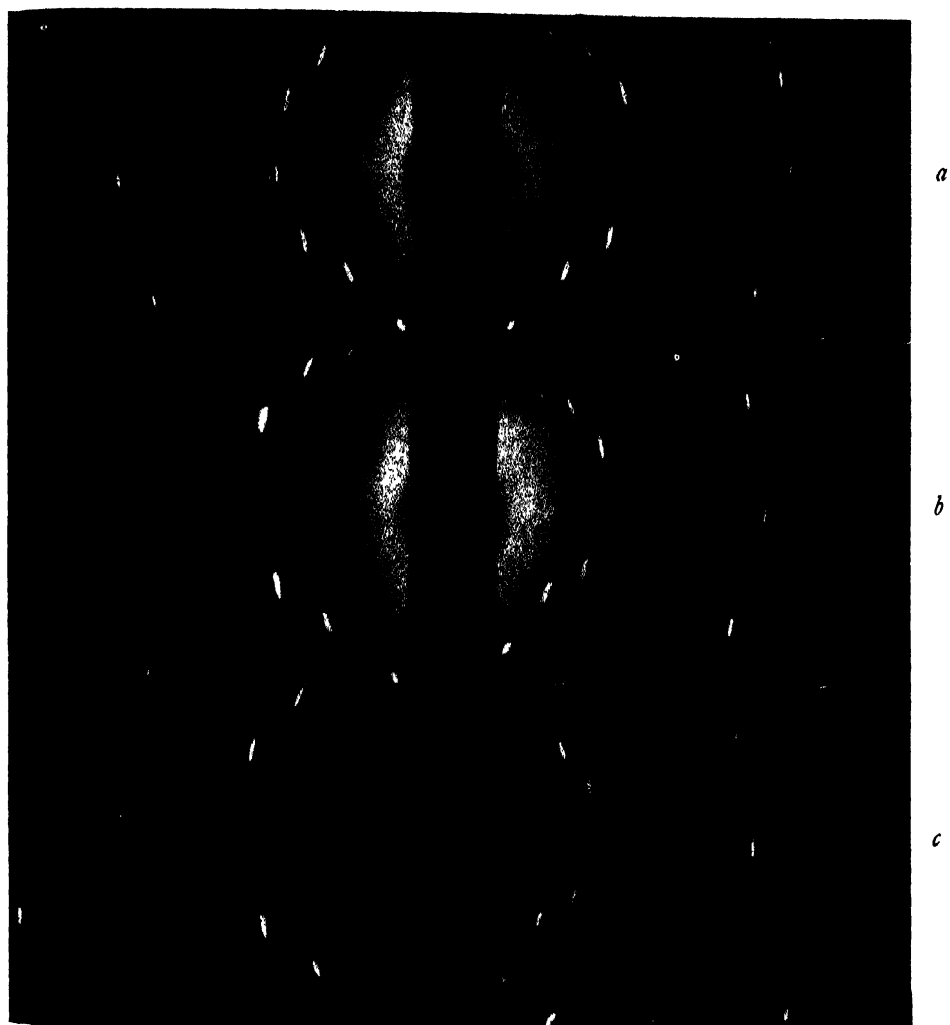
FIG. 2

Representation of extra spot (211) on a reciprocal lattice net work of  $a^*$  and  $b^*$ .

OC and CP are the directions of incident and scattered beam. A=positions of extra spots,  $2\theta$ =Bragg angle.

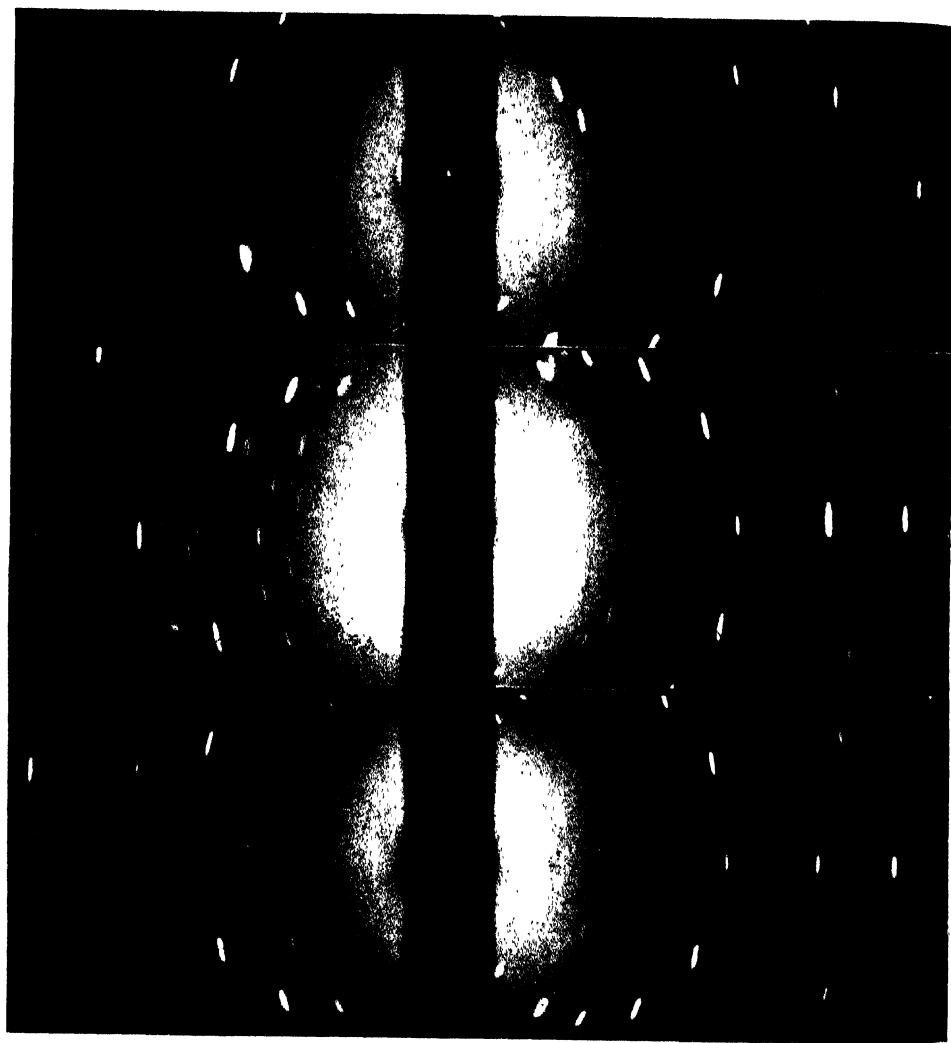
only the point Q will move to  $Q'$ , so that  $QQ' = \text{angle of rotation}$ . For any other layer  $n$  the sphere will cut the reciprocal lattice network in a smaller circle of radius  $r_n$  which is given by

$$r_n = \sqrt{r_0^2 - k_n^2 b^{*2}}$$



Laue photographs showing extra reflections from (211) plane

- (a) X-ray passes at  $18^\circ$  to the  $b$ -axis ;  $c$ -axis vertical
- (b) " " "  $1^\circ 50'$  " "  $b$ -axis ; " "
- (c) " " "  $2^\circ 50'$  " "  $b$ -axis ; " "



Laue photographs showing extra reflections from (211) plane

(*d*) Same setting as in (*a*) ; X-ray passes at  $3^{\circ}50'$  to the *b*-axis

(*e*) " " " " " ; " " "  $5^{\circ}5'$  " " "  
extra spot from (321) also appears

(*f*) Same setting as in (*a*) ; X-ray passes at  $6^{\circ}5'$  to the *b*-axis,  
extra spot from (340) $K\alpha$ , (340) $K\beta$  also appears.

## Anomalous spot (211) (see Plate XIV A-B)

No	Orientation	$x$	$y$	$h$	$k$	$l$
a	0°18'	3.15	1.2	2	1.014	1
b	1°50'	3.10	1.2	2	1.0	1
c	2°50'	3.08	1.2	1.95	.9	1
d	3°50'	3.06	1.2	1.95	.87	1
e	5°5'	3.17	1.2	2	.8	1
f	6°5'	3.20	1.2	2	.78	1

The representation of (112) on reciprocal lattice network shows that derangement waves are strictly confined to  $b$ -axis, such that the disturbance will be more on  $b$ -axis than on  $a$ -axis, which is shown on figure 2 (see Datta, 1947).

## ACKNOWLEDGMENT

The author wishes to express his grateful thanks to Prof. S. N. Bose for giving research facilities.

## REFERENCES

- Datta, M. N., 1947, *Ind. J. Phys.*, **21**, 303.  
 Banerjee, K., 1947, Proc. 34th Indian Science Congress, Part II Presidential Address of the Physics Section.  
 Banerjee, K. and Bose, C. R., 1944, *Nature*, **153**, 23.  
 Lonsdale, K. and Smith, H., 1942, *Proc. Roy. Soc. A.*, **179**, 8.  
 Datta, M. N., 1951, *Ind. J. Phys.*, **25**, 581.  
 Caspari, W. A., 1926, *Phil. Mag.*, **4**, 1276.





## CURRENT DIVISION IN PLANE POSITIVE GRID TRIODE\*

BY S. DEB

INSTITUTE OF RADIOPHYSICS AND ELECTRONICS, CALCUTTA UNIVERSITY

*(Received for publication, May 5, 1952)*

**ABSTRACT.** The paper presents a simple electron optical treatment of the problem of current division in a plane triode by assuming that the openings between the consecutive grid wires behave as thin cylindrical lenses free from spherical aberration. Both the cases of reflection and no reflection of electrons in front of the anode are considered. It is shown that for the latter the results obtained from the expressions for current division given earlier by Spangenberg and by Jonker and Tellegen follow as special cases of the same general equation obtained here (under all practical conditions of operation). For the former, the expression obtained is shown to be identical with the one given earlier by Jonker. Attempt has also been made to examine the applicability of the relation obtained to the case of valves using filamentary cathodes. It is found that the experimental results for such valves, as reported earlier by Hamaker, generally agree well with those given by the theory.

The assumptions underlying the treatment are discussed critically and are shown to be quite reasonable for all practical purposes.

## INTRODUCTION

The problem of the design of triodes as amplifier requires a knowledge of a number of tube constants, *viz.*, amplification factor ( $\mu$ ), transconductance ( $g_m$ ) and dynamic plate resistance ( $r_p$ ). For the problem of the design of high power amplifiers and oscillators it is also essential to know how the total current is divided between the grid and the anode. This division of the current has been found experimentally to depend on the tube geometry and on the ratio of the plate potential  $V_a$  and the grid potential  $V_g$  (Knoll and Schloemilch, 1934). Several attempts have been made to derive a theoretical expression for the ratio of the grid current  $I_g$  to the total current  $I_a$  in terms of the tube structure and electrode potentials. The methods of treatment are, however, difficult, involving a detailed consideration of the motions of the electrons within the inter-electrode space. Further, expressions thus derived are not in a form suitable for numerical calculations. It is the purpose of the present paper to show that quite satisfactory expressions for the current ratio can be obtained from simple electron optical considerations. Some of these expressions are also very convenient for numerical calculations.

## 2. EARLIER WORKS

For purposes of reference and comparison of results we first recall briefly the expressions for the current division, as obtained by earlier workers on the problem.

\* Communicated by Prof. S. K. Mitra, D.Sc.

Spangenberg (1940) considered the whole electronic path between the cathode and the anode without taking into account any possible strong variation of the field in the neighbourhood of the grid and obtained (for the case of no reflection of electrons in front of the cathode) the expression,

$$\frac{I_g}{I_c} = \frac{2r_g}{c} \left[ 1 + \frac{V_g - V_{eg}}{2V_{eg}} \frac{1 + \ln \left( \frac{4a}{r_g} \right)}{\ln \left( \frac{c}{2\pi r_g} \right)} \right] \quad (1)$$

where,

$r_g$  = the radius of the grid wire,

$c$  = the grid pitch,

$a$  = the distance between the grid and the cathode.

$V_{eg}$  = the equivalent grid plane potential (*vide* Sec. 3).

The effects of space charge, initial velocities of electrons and secondary emission are neglected.

Jonker and Tellegen (1945), following an earlier attempt by the latter, showed that a more satisfactory expression for the above case may be obtained by taking into account the possible strong deviation of electronic paths in the immediate vicinity of the grid wires. These authors carried out a detailed calculation of the extra moment gained by an electron in the above region and showed that,

$$\frac{I_g}{I_c} = \frac{2r_g}{c} \sqrt{\frac{V_g}{V_{eg}}} \left[ 1 + \frac{V_g - V_{eg}}{2V_{eg}} \ln \left( \frac{c}{2\pi r_g} \right) \right]. \quad \dots (2)$$

Jonker (1945) also considered the case when some of the electrons suffer reflection in front of the anode and are ultimately collected by the grid. The expression for this case was,

$$\frac{I_g}{I_c} = 1 - \frac{2}{\pi} \sqrt{\frac{V_{eg}}{V_g - V_{eg}}} \ln \left( \frac{c}{2\pi r_g} \right), \quad \dots (3)$$

the effects of space charge, initial velocities and secondary emission being neglected.

Eqns. (1), (2) and (3) are the commonly used expressions at present. We now proceed to derive the new expressions by electron optical method.

### 3. ELECTRON OPTICAL TREATMENT OF THE PROBLEM

To treat the problem theoretically by the electron optical method we start with the following assumptions:

- (i) Lateral deviations of the electrons from their paths perpendicular to the cathode plane are entirely due to electron optical effects of the grid.

- (ii) The openings between two consecutive grid wires behave as thin cylindrical lenses. The focal length  $f$  of such a lens, according to Davisson and Calbicks (1931, see also, Bull, 1945), is given by,

$$f = \frac{2V_{eg}}{E_2 - E_1}, \quad \dots (4)$$

where,

$V_{eg}$  = the equivalent grid potential

$$= \frac{V_g + V_a/\mu}{1 + \frac{1}{\mu} + \frac{1}{\mu} \frac{b}{a} - \frac{(\mu+2)}{2\pi\mu a} \frac{c}{\ln \cosh \left( \frac{2\pi r_g}{c} \right)}}, \quad \dots (5)$$

$b$  = the distance between the grid and the anode,

$E_2$  = the gradient of electrostatic potential on the anode side of the grid, and,

$E_1$  = the gradient of electrostatic potential on the cathode side of the grid.

- (iii) The lens action is confined to a very small region of width  $\pi r_g$  about the plane passing through the centre of the grid wires— $n$  being a numerical factor.

- (iv) The image due to the lens is free from spherical aberration. Thus, for a parallel beam of electrons incident along the lens-axis, the deviation of a ray striking the lens at a point distant  $y$  from the lens-centre is given by

$$\theta = \frac{y}{f}. \quad \dots (6)$$

- (v) The effects due to initial velocities of electrons, space charge and secondary emission are negligible.

The validities of some of the above assumptions will be discussed in Sec. 6.

We can put the expression for  $f$  in Eqn. (4) in a more practical form by noting that

$$E_2 = \frac{V_a - V_{eg}}{b}, \quad E_1 = \frac{V_{eg}}{a}.$$

Further, the term with  $\ln \cosh \frac{2\pi r_g}{c}$  in the expression for  $V_{eg}$  in Eqn. (5)

is generally very small compared to the other terms in the denominator. Hence we have,

$$V_{eg} \simeq \frac{V_g + V_a/\mu}{1 + \frac{1}{\mu} + \frac{1}{\mu} \frac{b}{a}}. \quad \dots (7)$$

Hence, from Eqn. (4),

$$\begin{aligned} &= -\frac{2(V_g + V_a/\mu)}{V_a\left(1 + \frac{1}{\mu} + \frac{1}{\mu} \frac{b}{a}\right) - (V_g + V_a/\mu) - \frac{V_g + V_a/\mu}{a}} \\ &= -\frac{2ab(V_g + V_a/\mu)}{a(V_g - V_a) + bV_g} \\ &= -\frac{2b(1 + \phi/\mu)}{(1 - \phi) + b/a} \tag{8} \end{aligned}$$

where,

$$\phi = \frac{V_a}{V_g} \tag{9}$$

We are now in a position to investigate the problem of current division in a plane positive grid triode with a plane equipotential cathode, a plane equipotential anode and a plane equipotential grid composed of straight, equally spaced wires of identical diameters. We shall consider two cases:

- (i) when there is no reflection of electrons in front of the anode, and
- (ii) when there is reflection of electrons in front of the anode.

*Case I: No reflection in front of the anode.*—If  $V_a > V_{ek}$  all the electrons emerging through the grid spaces are collected by the anode, there being no

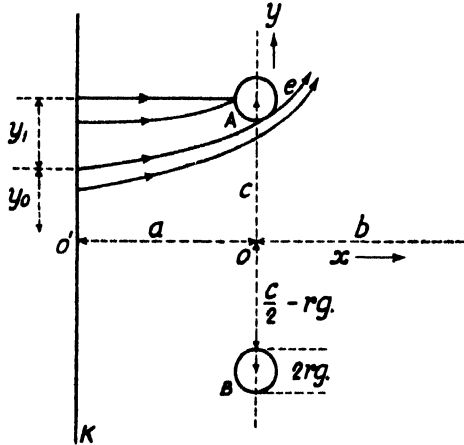


Fig. 1.

The nature of the trajectories of electrons in a plane positive grid triode when there is no reflection.

reflection of electrons in front of the same, and the grid current is composed only of the forward moving electrons. Consider now figure 1, where  $K$  is a section

of the cathode and  $A$  and  $B$  are sections of the grid wires (running perpendicular to the plane of the paper). The line  $OX$ , perpendicular to  $c$  and passing through the midpoint of  $AB$  is the axis of the electrostatic lens. An electron starting from  $O'$  on the cathode will not be deflected by the lens action. Those on either side will, however, be deflected—the deflection increasing from the axis  $O'$  outwards. Of particular interest is the electron which starts from a point on the cathode at a distance  $y_0$  from  $O'$  such that it just grazes the grid wire surface  $A$ . All the electrons starting from points beyond  $y_0$ , that is, from points within the length  $y_1 \left( = \frac{c}{2} - y_0 \right)$  will be captured by the grid wire  $A$ . And, those starting from within the length  $y_0$  will reach the anode.

Under such condition,

$$\frac{I_a}{I_g} = \frac{y_0}{y_1} = \frac{y_1 + y_0}{y_1} - 1 = \frac{c}{2y_1} - 1, \quad \dots (10)$$

$I_a$  being the anode current.

And, since

$$I_c = I_a + I_g,$$

$$\frac{I_g}{I_c} = \frac{2y_1}{c}. \quad \dots (11)$$

The value of  $y_1$  may be obtained as follows: If  $v_y$  be the lateral velocity of an electron on emergence from the grid and  $v_x$  its longitudinal velocity, then,

$$\theta = \frac{v_y}{v_x} = \frac{y}{f}. \quad \dots (12)$$

It may be noted that  $v_x$  remains practically unaffected by lens action, and hence the time during which the electron is subjected to lens action is  $\frac{n r_g}{v_x}$ , the numerical constant  $n$  taking account of the fact that the lens action is not confined to an ideally thin plane running through the centres of the grid wires, but extends a little to either sides of the plane. The average lateral velocity of the electron during the same time interval is  $\frac{v_y}{2}$ . Thus, the deviation of the electron from the path normal to the cathode plane is given by,

$$\begin{aligned} dy &= -\frac{v_y}{2} \cdot \frac{n r_g}{v_x} \\ &= -\frac{y}{2f} \cdot n r_g. \end{aligned} \quad \dots (13)$$

For the limiting electron the lateral displacement is  $y_1 - r_g = \frac{c}{2} - y_0 - r_g$ .

Thus, we obtain after writing  $y_0$  for  $y$ ,

$$dy = y_1 - r_g = -\frac{y_0}{2f} n r_g = \frac{c}{2} - y_0 - r_g.$$

This gives,

$$y_1 = -\frac{\frac{c}{2} n r_g - 2 r_g f}{n r_g - 2 f} \quad \dots (14)$$

Substituting (14) in (10) one obtains,

$$\frac{I_g}{I_c} = \frac{c}{2y_1} - 1 = \frac{c}{2r_g} \frac{1 - \frac{2r_g}{c}}{1 - \frac{cn}{4f}} \quad (15)$$

and substituting (14) in (11) one obtains,

$$\frac{I_g}{I_c} = \frac{1 - \frac{cn}{4f}}{\frac{c}{2r_g} - \frac{c}{4f}} \quad (16)$$

The value of  $n$  is not known; but, as the lens action can not extend beyond a region more than a few times the radius of the grid wire, we assume two values of  $n$ , namely 4 and 2. For  $n=4$ , we have

$$\frac{I_g}{I_c} = \frac{1 - \frac{c}{f}}{\frac{c}{2r_g} - \frac{c}{f}} \quad \dots (17)$$

For  $n=2$

$$\frac{I_g}{I_c} = \frac{1 - \frac{c}{2f}}{\frac{c}{2r_g} - \frac{c}{2f}} \quad \dots (18)$$

A useful parameter of a triode valve is the current division factor  $\delta$  defined as the ratio of plate current to grid current for the special case of  $V_a = V_g$  i.e.,  $\phi = 1$ .

Then, for  $n=4$  we have,

$$\delta = \frac{c}{2r_g} \frac{1 - \frac{2r_g}{c}}{1 - \frac{c}{f}} \quad \dots (19)$$

$$= \frac{c}{2r_g} \frac{1 - \frac{2r_g}{c}}{1 + \frac{c\mu}{2a(1+\mu)}} \quad \dots (20)$$

and, for  $n=2$ ,

$$\delta = \frac{c}{2r_g} \frac{1 - \frac{2r_g}{c}}{1 - \frac{c}{2f}} \quad \dots \quad (21)$$

$$= \frac{c}{2r_g} \frac{1 - \frac{2r_g}{c}}{1 + \frac{c\mu}{4a(1+\mu)}} \quad \dots (22)$$

*Case II: Electrons reflected from the front of the anode.* If  $V_a < V_{cg}$  some of the electrons which suffer lateral deviation will fail to reach the anode and turn back towards the grid, i.e., there will be reflection from the front of the anode. The grid current has now two components—one due to the forward moving electrons and the other due to those returning after reflection.

To investigate the above problem we adopt the same line of reasonings as that of Jonker (1945). We first note that an electron emerging through the grid opening into the grid anode space has a total velocity of magnitude  $v_x$  given by

$$v_x = \sqrt{\frac{2e}{m} V_{eg}}. \quad (23)$$

While the magnitude of this velocity changes with the motion of the electron, that of its component directed parallel to the anode remains constant. If  $V_a < V_{cr}$

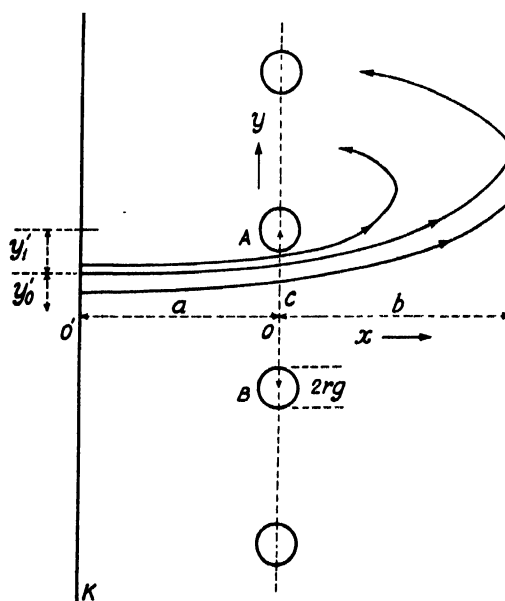


Fig. 2.

**The nature of the trajectories of electrons in a plane positive grid triode when there is reflection.**

the path within the grid-anode space will obviously be parabolic. The smaller the

value of  $v_y$  the nearer will be the vertex of the parabola to the anode. The limiting case occurs when the value of  $v_y$  is such that the vertex of the parabola touches the anode surface. Let us suppose that this occurs for an electron striking the lens at a point distant  $y_0$  from the lens centre (figure 2). Then, if we take

$$y_1' = -\frac{c}{2} - y_0', \quad \dots (24)$$

all electrons originating from a region  $2y_1'$  on the cathode, opposite the grid wires, will be collected by the grid, either, directly or after reflection. Thus, in this case,

$$\frac{I_g}{I_c} = \frac{2y_1'}{c}. \quad \dots (25)$$

If  $\theta_1$  be the angular deflection of the limiting electrons due to the lens action, then the part of the kinetic energy due to the component of the motion towards the anode is,

$$\frac{1}{2} m v_x^2 \cos^2 \theta_1.$$

Also, since the electron just fails to reach the anode, this energy must be used up entirely in gaining the potential energy  $c (V_{eg} - V_a)$  within the grid-anode space. Thus, we obtain after Jonker,

$$\theta = \sqrt{\frac{V_a}{V_{eg}}}$$

We now make use of Eqns. (12) and (8) to obtain the value of  $y_1'$  thus

$$\frac{c}{2} - y_0' = -\frac{c}{2} + f \sqrt{\frac{V_a}{V_{eg}}} \quad \dots (26)$$

Hence, from Eqn. (25),

$$\frac{I_g}{I_c} = 1 + \frac{2f}{c} \sqrt{\frac{V_a}{V_{eg}}}. \quad \dots (27)$$

This is expressible in the form

$$\frac{I_g}{I_c} = 1 - \frac{4ab(1+\phi/\mu)}{c[a(1-\phi)+b]} \sqrt{\frac{\phi \left( 1 + \frac{1}{\mu} + \frac{1}{\mu} \frac{b}{a} \right)}{1+\phi/\mu}}. \quad \dots (28)$$

#### 4. COMPARISON WITH OTHER EXPRESSIONS

The usefulness of Eqns. (17), (18), (20), and (22) can best be judged by comparing the results obtained from them with those obtained from Spangenberg's formula [Eqn. (1)] and from Jonker and Tellegen's formula [Eqn. (2)]. As an illustrative example we take the tube geometry as considered by Jonker and Tellegen, *viz.*,

$$a = b = c,$$

$$\text{and } \frac{2r_g}{c} = 0.064.$$



In figure 3(a) values of  $\frac{c}{2r_g} - \frac{I_g}{I_c}$  are plotted against  $\phi$ , for this tube geometry, as obtained from Eqn. (1). The points obtained from Eqn. (17) are shown by cross marks. These points fit remarkably well in the curve obtained from Eqn. (1). It thus appears that Eqn. (16) with  $n=4$  gives the same results

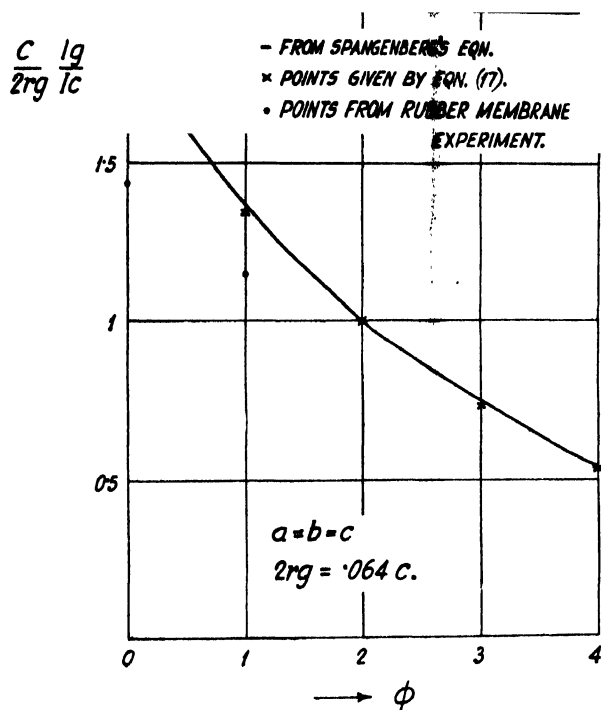


Fig. 3(a)

Comparison of results obtained from eqns. (1) and (17)

as those given by Eqn. (1). This conclusion is further substantiated by the results recorded in Table I where values of  $\delta$  for several valve geometries calculated from Spangenberg's relation and from Eqn. (20) are compared. The agreement between the two sets of values is surprisingly good.

TABLE I

$\frac{a}{r_g}$	$\frac{c}{r_g}$	$\mu$	$\delta$ From Spangenberg's relation Eqn. (1)	$\delta$ From Eqn. (20)
20	20	7.5	6.2	6.2
25	20	7.5	6.5	6.5
15	20	7.5	5.6	5.6
20	22	4	7	6.9
46	20	7.5	7.4	7.5
30	20	20	6.7	6.8

In figure 3 (b) values of  $\frac{c}{2rg} \frac{I_g}{I_c}$  are plotted against  $\phi$ , for the above tube geometry, as obtained from Eqn. (2). Points obtained for the same tube from Eqn. (18) are shown by cross marks, and those obtained from experiments with a rubber membrane model by Jonker and Tellegen (1945) are marked by circular

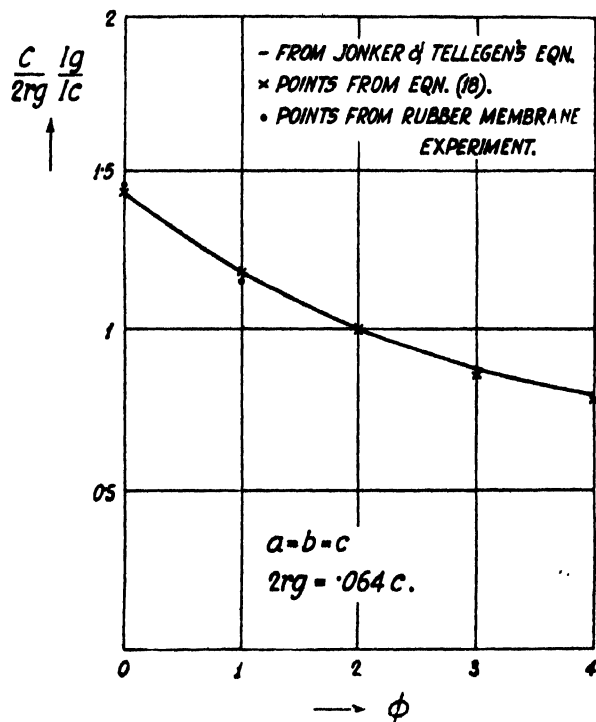


Fig. 3(b)

Comparison of results obtained from eqns. (2) and (18)

dots. It is seen that points given by Eqn. (18) lie closely on the curve and that Eqn. (16) with  $n=2$  gives, almost the same results as those given by Eqn. (2). Further, results obtained from experiments with rubber model agree more favourably with the values obtained with  $n=2$ . Thus in actual tube lateral deviation appears to occur sharply within a very small region.

It should, however, be noted that results obtained from Eqn. (2) are, in general, somewhat different from those obtained with Eqn. (18) when  $V_g$  is small compared to  $V_a$ . Thus, while Eqn. (2) requires that  $I_g$  should become zero when  $V_g=0$ , Eqn. (18) shows that this may be so even when  $V_g$  has a small positive value. To be precise, Eqn. (18) requires that

$$\text{for } I_g=0, \quad f=\frac{c}{2};$$

i.e., when the focal length of the grid aperture becomes equal to half its width. Under this condition  $y_1$  in Eqn. (11) becomes zero. If  $V_g$  is reduced further,

the value of  $c$  is effectively diminished in conformity with the relation  $f = \frac{c}{2}$  and hence the grid current remains nil. Only in case of valves having special geometry, conditions for  $I_g = 0$  as required by Eqns. (2) and (18) become identical.

It will be noted from Eqns. (8) and (10) that the focal length of the grid slot becomes infinity when  $\phi$  has the value,

$$\phi = 1 + \frac{b}{a}, \text{ i.e., } \frac{V_a}{V_g} = 1 + \frac{\text{grid-anode distance}}{\text{grid-cathode distance}}.$$

Under this condition,

$$-\frac{I_g}{I_c} = \frac{2r_g}{c} = \text{the screening constant of the valve.}$$

For smaller values of  $\phi$  the lens behaviour is diverging and

$$-\frac{I_g}{I_c} > \frac{2r_g}{c}.$$

For larger values of  $\phi$  the lens behaviour is converging and,

$$-\frac{I_g}{I_c} < \frac{2r_g}{c}.$$

For the tube considered above the critical value of  $\phi$  is 2 and is greater or less than the screening constant according as  $\phi$  is lesser or greater than 2. These facts are clearly understood from an inspection of figures 3 (a) and 3 (b).

It should be mentioned that the boundaries of the types of electrostatic lens, as constituted by the potential fields in the vicinity of two grid wires, are never well defined. In most cases the actual lens thickness may exceed the geometrical width  $2r_g$  of the grid openings. A thickness of  $4r_g$  as assumed in deduction of Eqns. (17) and (20) is, however, an over estimate for ordinary conditions of valve operation. Such large values may be approached only for low  $\mu$  valves when the electrostatic fields on the two sides of the grid are such that equipotential surfaces on one side penetrate the openings in the grid and bulge out appreciably on the other side. Therefore, it may be concluded that Eqns. (2), (18) and (22) are more reliable for practical purposes.

The usefulness of Eqn. (28) may be best judged by comparing it with Eqn. (3). It may be shown that the relations expressed by the two equations are, in fact, identical. For this, one may borrow the following relation from Jonker and Tellegen (1945):

$$[E_1 - E_2] \frac{c}{2\pi} \ln \frac{c}{2\pi r_g} = V_g - V_{eg},$$

$$\text{Or, } \frac{1}{E_2 - E_1} = -\frac{c}{2\pi} \frac{1}{V_g - V_{eg}} \ln \left( \frac{c}{2\pi r_g} \right). \quad \dots (29)$$

From Eqns. (4), (26), (28) and (29) one easily obtains Eqn. (3). It may be

noted that Eqn. (28) is true if  $\phi < 1$ . For the tube considered above this equation gives consistent results if  $\phi < 0.1$ . For higher values of  $\phi$  one must use Eqn. (18) or (22).

## 5. APPLICATION TO VALVES WITH FILAMENTARY CATHODES

In the present section we shall examine how far Eqn. (16), deduced for the ideal case of a plane, equipotential cathode, is applicable to filamentary cathodes of V or W shape as employed in practice.

It may appear at first sight that the ratios  $\frac{I_g}{I_c}$  for triodes with such cathodes would depart widely from those given by Eqn. (16). However, Kosunose (1929) has shown that under the usual conditions of operation (*viz.*  $V_g < V_a$ ) the plate current in such a triode is satisfactorily accounted for if it is assumed that the action of the filamentary cathode is equivalent to that of a plane equipotential strip of width twice the grid to cathode distance. Hence, it may be expected that Eqn. (16) would be applicable to such triodes, at least approximately, under the usual conditions of operation. To test this, we make use of the experimental results of Hamaker (1948) on the ratio of the grid current to the total current for four valve types with different valve parameters as shown in columns 1 and 2 of Table II. In column 4 of the same table are given the observed values of  $\frac{I_g}{I_c}$  for different values of  $\phi$  and in columns 5 and 6 the corresponding values as calculated from Eqn. (16) by putting  $n=2$  and  $n=4$  respectively.

A glance at the table shows that considering the very wide gulf between the idealised plane cathode and the actual filamentary cathode, the agreement in some of the cases is surprisingly good. Closer inspection shows that there is a regular trend in the closeness of the agreement. Thus, consider the figures in Table II enclosed between horizontal lines for each of the four types of valve.

It will be seen that for the case  $\phi \geq 1$ , the agreement between the observed and the calculated values of  $\frac{I_g}{I_c}$  is better when  $\phi$  is generally much larger than 1 and the value of  $n$  is taken as 2. For the rest of the cases agreement is better if  $n$  is taken as 4. The reason for this trend may be understood as follows: It will be recalled that for the plane cathode the field was uniform and its intensity on the cathode side of the grid was given by  $\frac{V_{eg}}{a}$ . For the case of filamentary cathode, however, the field is non-uniform and an expression like  $\frac{V_{eg}}{a}$  gives only the average value of the field. From the geometry of the filament and the grid it is evident that the field near the cathode is more intense and that near the grid less intense than the average value of the field  $\frac{V_{eg}}{a}$ . It, therefore, follows that if the focal length is calculated from Eqn. (4) using the average value of the

field, the true value of  $f$  is less than the calculated value. Hence, if the intensity of the field near the grid due to the grid potential is not much affected by anode potential, i.e., if  $V_a$  is not much larger than  $V_g$ , then the departures in the values of  $\frac{I_g}{I_c}$  from the case of the plane cathode (due to the actual focal length being smaller) may be compensated by taking a larger value of  $n$ . On the other hand, if  $V_a$  is much larger than  $V_g$ , then the field intensity near the grid is determined more by the anode potential which tends to make the field on the cathode side of grid uniform. Hence, calculated values of  $f$  agree better with the actual values and no compensation by taking a larger value of  $n$  is necessary. These considerations explain in a qualitative manner the trend of agreement between the observed and the calculated values.

TABLE II

Valve type	Valve parameter	$\phi = \frac{V_a}{V_g}$	Values of $I_g/I_c$		
			Experimental	From Eqn. (16) $n = 2$	From Eqn. (16) $n = 4$
(1)	(2)		(4)	(5)	(6)
KZ141	$a = 2.25$ mm $b = 2.5$ mm	0.5	.2	.11	.13
		1	.12	.1	.117
	$c = 2.1$ mm $2r_g = .18$ mm $\mu = 6$	2.5 5 10	.09 .06 .04	.085 .058 .034	.08 .03 0
KZ139	$a = 2.25$ mm $b = 2.5$ mm $c = 1.0$ mm	.5	.28	.203	.225
		1	.22	.2	.21
		2.5	.17	.175	.171
KZ104	$2r_g = .18$ mm $\mu = 24$	5	.13	.143	.104
		10	.1	.09	0
	$a = 2.25$ mm $b = 2.5$ mm $c = 1.4$ mm $2r_g = .18$ mm	.5 1 2.5 5	.25 .16 .1 .07	.15 .14 .118 .1	.173 .16 .108 .07
TC1/75	$a = 2.0$ mm $b = 8$ mm	.4	.219	.126	.15
		1	.15	.122	.14
	$c = 1.75$ mm $2r_g = .18$ mm $\mu = 24$	4 10 40	.105 .081 .033	.107 .085 .031	.112 .066 0

It will be seen from Table II that the theoretical values of  $\frac{I_g}{I_c}$  for  $\phi < 1$  are always smaller than the experimental values. This lack of agreement may be due to several reasons. Firstly, for such values of  $\phi$ , the grid potential plays a highly dominant rôle in controlling the valve action and the effect due to space charge becomes considerable on both sides of the grid. This makes the values of  $E_1$  and  $E_2$  uncertain—particularly that of the latter (Bull, 1945). Secondly, because of the excessive influence of grid potential the field distribution between the cathode and the grid may become so much different from that of a triode having plane equipotential cathode that Kosunose's approximation ceases to be applicable. Lastly, because of the predominant rôle of grid potential, the field  $E_1$  on the cathode side may become so much smaller than the average value  $\frac{V_{eg}}{a}$  that to compensate for this a value of  $n$  much larger than 4 has to be taken.

## 6. DISCUSSION ON THE ASSUMPTIONS MADE

We conclude the paper by checking how far the assumptions made in the above treatment are justified.

The assumption that the lateral deviation suffered by the electrons is due only to the electron optical action of the grid is approximately valid if, (i) the lateral component of the field in the cathode-grid space is a very small fraction of electron optical field and (ii) if the grid plane is a truly equipotential surface. Now, the lateral component of the field is given by (Spangenberg, 1948)

$$E'_y = \frac{2\pi q_g \sin \pi \left(1 - \frac{2y}{c}\right)}{c \left[ \cosh \left( \frac{2\pi x}{c} - \cos \pi \left(1 - \frac{2y}{c}\right) \right) \right]},$$

where  $q_g$  is the linear charge density of the grid wire given by

$$\frac{V_g c [a(1-\phi) + b]}{4ab \left[1 + \frac{1}{\mu} + \frac{1}{\mu} \frac{b}{a}\right]} = -\frac{c V_{eg}}{2\pi f} = -\frac{c [E_2 - E_1]}{4\pi},$$

$x$  is the axial distance and  $y$  the lateral distance measured in the manner as shewn in figures 1 and 2. It is evident that the value of  $E'_y$  remains extremely small for large values of  $x$  and small values of  $y$ . Now, for the cathode grid space bounded on one side by the grid openings, the smallest value that  $x$  can have is

$-r_g$  and the largest value that  $y$  can have is  $\frac{c}{2} - r_g$ . Thus, at the point

$\left(-r_g, \frac{c}{2} - r_g\right)$  the value of  $E'_y$  will be a maximum and will be given by

$$E'_y = \frac{c [E_2 - E_1]}{4\pi r_g}.$$

But, near this point the electron optical field is, to a first approximation, given by

$$E_y = y \frac{dE}{dx} = \left( \frac{c}{2} - r_g \right) \frac{E_2 - E_1}{2r_g}.$$

$$\therefore \frac{E'_y}{E_y} \simeq \frac{1}{\pi} < 1,$$

$$\text{Or, } E'_y < E_y.$$

Thus, even at the point where  $E'_y$  is strongest, electron optical field plays the dominant rôle.

The actual grid is, of course, not a truly equipotential surface; but, in making calculations use has been made of the equivalent grid potential which is based on the concept of a plane equipotential grid.

The assumption that the openings in the grid behave as thin lenses, not introducing spherical aberration, is true to a first approximation. This is seen as follows. Firstly, it has been found that satisfactory results are obtained if the lens action is assumed to extend over a thickness which is always much smaller than the focal length  $f$  and the aperture  $c$ . Secondly, although a single isolated cylindrical aperture gives rise to considerable spherical aberration, it is not so for the case of a set of such lenses placed side by side (as in a plane triode). This is because, the mutual influence of the adjacent apertures acts in such a manner as to reduce the effect of spherical aberration to a large extent. This has been verified by Jonker (1945) by experiments with rubber models. It has been found, in fact, that Eqn. (6) holds right up to the extremities of the grid opening in a plane triode.

The assumptions that there are no effects due to (i) space charge and (ii) to the initial velocity are not strictly correct. However, one may take account of these effects as follows: (i) Tellegen (1926) has advanced the view point that since for ordinary valves the effect of space charge is confined mostly within the cathode-grid space, its effect on off-cathode field would only cause an apparent reduction of  $a$ , say by 25%. Thus the equations developed in Sec. 3 may be applied to a space charge limited valve by substituting  $\frac{3}{4}a$  for  $a$ . (ii) The initial velocity components directed normal to the cathode surface have no doubt a Maxwellian distribution. Chaffe (1942) has, however, shown that in all cases where it plays significant rôle, the effect can be taken into account—to a reasonably good approximation—by adding a suitable small correlation  $V_m$  to  $V_a$ . Thus, the equations developed will hold for ordinary valves if  $V_a$  is replaced by  $V_a + V_m$ . However, it is easily seen that this correction does not alter the calculated values materially. It is to be noted that the electrons also possess a lateral velocity of the thermal agitational type. But, this does not affect the position, because, its effect will be merely to superpose a partition type of noise upon the steady electrode currents.

## CONCLUDING REMARKS

The proposed electron method of treatment of the problem of current division in a plane triode is found to give quite satisfactory results.

It is to be pointed out that the equations developed here give the current ratio in terms of a single pair of dimensionless quantities,  $\frac{2r_g}{g}$  and  $\frac{f}{c}$  both of which may be obtained readily. This makes the numerical calculations very easy. Further, since  $\frac{2r_g}{c}$  represents the screening constant and  $\frac{f}{c}$  the relative aperture of the lens the equations may easily be generalised so as to include the case of valves of any geometry and for plane valves having any form of grid. (This will form the subject matter of a future communication).

## ACKNOWLEDGMENT

Grateful thanks are due to Professor S. K. Mitra for his constant encouragement and helpful guidance in course of the work.

## REFERENCES

- Bull, C. S., 1945, *Jour. I.E.E.*, **92** (III), 86. (See also Klemperer, O., 1947, *Phys. Rev.*, **59**, 302).
- Chaffe, E. L., 1942, *Proc. I.R.E.*, **30**, 385.
- Davisson, C. J. and Calbicks, C. J., 1931, *Phys. Rev.*, **38**, 585.
- Hamaker, H. C., 1948, *App. Sci. Res.*, **B 1**, 77.
- Jonker, J.H.L., 1945, *Phil. Res. Rep.*, **1**, 13.
- Jonker, J. H. L. and Tellegen, B. D. H., 1945, *ibid*, **1**, 13.
- Knoll, M. and Schloemilch, 1, 1934, *Archiv. Electrotechnik.*, **28**, 507. (See also, *Wire. Eng.*, 1934, **11**, 618).
- Kosunose, Y., 1929, *Proc. I. R. E.*, **17**, 1706.
- Spangenberg, K. R., 1940, *Proc. I. R. E.*, **28**, 226.
- Spangenberg, K. R., 1948, *Vacuum tubes*, McGraw Hill Inc. New York.
- Tellegen, B. D. H., 1926, *Physica*, **6**, 113.



# THE COMPARATIVE INFLUENCE OF SHORT AND LONG RANGE CRYSTALLINE ELECTRIC FIELDS ON THE MAGNETIC BEHAVIOUR OF THE PARAMAGNETIC SALTS OF THE IRON GROUP OF ELEMENTS

## PART I

BY A. BOSE AND S. C. MITRA

DEPARTMENT OF X-RAYS AND MAGNETISM, INDIAN ASSOCIATION  
FOR THE CULTIVATION OF SCIENCE, CALCUTTA.

*(Received for publication, May 28, 1952)*

**ABSTRACT.** A critical discussion on the comparative influence of the various interactions, which arise in the solid or liquid states of the paramagnetic substances to cause the paramagnetic ions in them to deviate from the ideal gaseous behaviour has been presented. In the magnetically dilute solid salts the only interaction of importance is the crystalline electric field due to the diamagnetic ions and dipoles surrounding the paramagnetic ion. This consists of (a) the direct action of the diamagnetic atoms *immediately* surrounding the paramagnetic ion, (b) the direct action of those atoms lying outside this cluster and (c) the indirect action of these distant atoms. Van Vleck has theoretically shown that though (b) is comparatively small, (a) and (c) are of comparable magnitudes. According to his theory we should observe a large difference in the mean effective moment of these paramagnetic salts in the solid state and in solution as also an appreciable difference from salt to salt containing the same paramagnetic ion. In the iron group of salts, however, as is shown in the present review, this effect is observed definitely only in the  $\text{Co}^{++}$  salts. It is probable that the room temperature values of the mean moments are not sufficiently sensitive to the action of the distant atoms. In the next part it is intended to discuss the available data on the temperature variation of the mean moments and the anisotropies in single crystals.

## 1. INTRODUCTION

Of late the study of the magnetic anisotropies of crystals, in conjunction with their X-ray studies, has proved to be a powerful method for determining the detailed structure of crystals. An elegant method has been developed and widely employed by Krishnan and Banerjee (1933, 1935, 1938), Lonsdale (1936) and others, for the correct determination of the orientations of the molecules in the unit cell of the organic diamagnetic crystals, as also for the correlation between the crystalline and the molecular magnetic behaviours of these substances, in which the interactions between the molecules are not such as to modify their magnetic behaviours significantly.

In the paramagnetic crystals, however, the magnetic behaviour of the paramagnetic ions is profoundly influenced by the electric fields of the immediately surrounding diamagnetic ions and dipoles, and presumably also to some extent by those of the more distant ones, in addition to the exchange and magnetic dipole interactions between the paramagnetic ions themselves. It will be our task in the present paper to review the existing results and to estimate the magnitudes of these various types of interactions and their influences on the magnetic behaviours of the paramagnetic ions of the iron group of elements. This, together with a knowledge of the relative positions of the paramagnetic ions in the unit cell, as given by the X-ray methods, should enable us to correlate uniquely the ionic and the crystalline paramagnetic behaviours. Or, conversely, a study of the magnetic properties of the crystals should serve as a powerful adjunct to the X-ray method for predicting the fine structures of the crystals, as also for estimating the various fields of forces in a crystal, causing a departure from the normal behaviour of the "free" paramagnetic ions (Krishan and Mookherji, 1936, 1938; Mookherji, 1939, 1945; Bose, 1948).

## 2. THE NATURE OF THE INNER FIELDS ACTING ON THE PARAMAGNETIC IONS IN SINGLE CRYSTALS OF PARAMAGNETIC SALTS

As contemplated by Van Vleck (1937) the effect of the various interactions on the paramagnetic ions, mentioned in the previous section may be functionally represented by the Hamiltonian

$$H = \sum_i V_i + \sum_{j>i} w_{ij} \quad \dots \quad (1)$$

where  $V_i$  is the crystalline electric potential of Van Vleck (1932), Bethe (1929) and others, of the  $i$ th magnetic particle in the crystalline assembly, and  $w_{ij}$  is a function including within it the potentials due to the formally similar interactions, namely, the Heisenberg exchange interaction and the Lorentz magnetic dipole-dipole interaction, between the  $i$ th and  $j$ th magnetic particles. These two latter interactions, however, have quite different origins and whereas, the exchange interaction is capable of producing ferromagnetism, it is very doubtful whether the dipole-dipole interaction can do so in a true sense except an incipient type of it (Van Vleck, 1937; Simon, 1936, 1937; and others). On the other hand, unlike dipole-dipole interaction, the exchange coupling is not capable of giving rise to magnetic anisotropy, a salient feature of the paramagnetic crystals in general. However, except in substances in which the magnetic particles are packed together very densely, [vide 'Cryomagnetic anomalies', Stoner (1934) and "Metamagnetism", Starr, Bitter (1940) and others] both these interactions should be rather feeble; especially in the highly hydrated salts, such as the paramagnetic alums and the Tuttons salts, so much so that the corresponding Curie temperatures may be of the order of a few hundredths

of a degree Kelvin, (Van Vleck, 1937; Hebb and Purcell, 1937, Simon and others, 1936-37), and in consequence the effects of such interactions may not be appreciable above a few degrees Kelvin.

Quantitative results on these effects should not however, be expected owing firstly, to mathematical difficulties in formulating an exact theory and secondly, because even in the most simple cases of atoms having only spin moments, these effects are, in general, to a large extent masked by a much larger effect due to crystalline electric fields\*. It is only in the special case of an ion in the  $^2S$ -state† that the crystalline electric field is practically without any effect on the spin degeneracy (vide Kramers, 1929), and an accurate estimate of the other two interactions may be made; anisotropy of the dipole-dipole interaction in the crystal being made use of to distinguish it from the exchange interaction.

### 3. NATURE AND ORIGIN OF THE CRYSTALLINE ELECTRIC FIELDS ACTING ON THE PARAMAGNETIC IONS IN SOLIDS

It is now universally recognised that most of the generally observed magnetic behaviours of the paramagnetic substances may be explained to considerable minute details, on the assumption of interactions, between the paramagnetic ion and its surrounding charged atoms and dipoles, of the nature contemplated by Bethe (1929), Van Vleck (1932), Penney and Schlapp (1932) and others. These fields are mainly electrostatic in nature and their chief function, in modifying the "free ion" behaviour of the paramagnetic ions, appears through the removal of the degeneracy of the paramagnetic ion by them, partially or totally, depending upon their strength and asymmetry, thereby rendering ineffective or "quenching" more or less the magnetic moments of the particles.

A consideration of the origin of these fields has a peculiar interest from the point of view of the formation of associated groups of atoms surrounding a paramagnetic ion and in general, of the theory of crystal formation, in such substances. If we consider an assembly of atoms, each atom having an incomplete valency sub-shell and in general one or more completed inner shells of electrons, the system is degenerate, not only in so far as its chemical valency is not satisfied (*i.e.*, it is electrically degenerate), but also magnetically, since the unbalanced electrons in the outer shell will contribute to give a permanent magnetic moment to the atom. When by molecule formation its "chemical degeneracy" is completely

\* Splittings of the spin levels under the usual crystalline electric fields are of the order of about  $0.1 \text{ cm}^{-1}$  to a few units  $\text{cm}^{-1}$ .

† Such a ground state does not normally occur in the transition groups of elements, though a close approximation, as in  $\text{Ti}^{4+}$ , may be obtained. If, however, we could have a salt of singly ionised  $\text{Ca}^+$  then it would be in a  $^2S$ -ground state. Such a salt with high magnetic dilution, by the way, would be an ideal substance for producing extremely low temperature by the method of adiabatic demagnetisation.

removed, its "magnetic degeneracy" is at the same time removed and we have a chemically inert, diamagnetic molecule. It is as if each unsaturated atom draws about it a number of neighbours, and arranges them in such a manner as, by their mutual interaction, to neutralise the chemical as well as the magnetic instability of the central atom under the given conditions of equilibrium. This should apply not only to the nearest strongly bound primary group of atoms forming a molecule or complex, but presumably also to more loosely bound distant ones which go to build up the crystal unit, though as yet it is uncertain how far these latter can affect the residual magnetic instability, if any, of the central atom. Thus, the removal of chemical and magnetic instabilities are to a large extent concomitant effects of one another.

The above considerations are equally true for the transition groups of elements, where in addition to the valency shell, there are also other inner incomplete shells, so that in these cases the question of removal of magnetic degeneracy is brought more prominently to the forefront. It is not, therefore, surprising that in these elements in addition to normal valency bindings, a strong tendency for coordination linkage (more or less as strong as normal valency bonds) is found to exist, causing diamagnetic ions and dipoles to form clusters about the paramagnetic ion. These associated groups are to a large extent responsible for the partial or total quenching of the magnetic moments of the paramagnetic ions, not only in the solid states, but even in the state of solution, and what is more interesting, to about the same extent in these two states. This would point primarily towards a more or less simple yet constant type of interaction between the paramagnetic ion and a *closely bound* associated group of charged atoms and dipoles, persisting under a variety of physical conditions. In this connection it is of interest to remember the well known theorem of Jahn and Teller (1937, 1938), which tells us, that the distribution of the atoms immediately surrounding a given ion is conditioned by its quantum state in such a manner, that the intensity and asymmetry of the resulting electric field at the centre is sufficient to remove wholly the orbital part of the degeneracy of the energy levels of the central ion, consistent, of course, with the overall condition of stability of the given system. Apparently, when there is no orbital degeneracy to be removed, Jahn-Teller effect does not come into the picture (Van Vleck, 1939). But then, it is not quite clear why an atom with spin degeneracy alone can still gather round it asymmetrically and no less strongly other charged atoms, with the consequent removal more or less of that degeneracy. It seems that the significance of the above might be more far reaching than would appear at first sight and *the Jahn-Teller principle may have to be generalised further to conform with the demands of the spin degeneracy*.

We shall discuss the nature and the effect of the group formation on the paramagnetic ion, mentioned above, in the light of experimental facts, in a later section. Before proceeding further, it would be profitable to examine our reasons for believing in the existence of such group formation, on the basis of X-ray analysis of the fine structure of the crystals.

#### 4. X-RAY AND OTHER EVIDENCES FOR THE EXISTENCE OF ASSOCIATED GROUPS OF ATOMS ROUND THE PARAMAGNETIC ION IN THE SALTS OF THE IRON GROUP

The data on the X-ray analysis of the fine structure of the salts of the iron group of elements is rather meagre, unsystematic, and not always very reliable. Further, the actual analyses of structures in many cases refer to isomorphous diamagnetic salts from which the structures of the corresponding paramagnetic salts have to be inferred, which procedure though not of much structural significance may alter the magnetic behaviour profoundly (Van Vleck, 1939).

Some of the earliest measurements are on the alkali cupric chlorides by Hendricks and Dickinson (1927) refined later by Chrobak (1934). The salts belong to the space group  $D_{4h}^{14}$  of the tetragonal class with two molecules in the unit cell oriented parallel along  $c$  axis, but rotated at  $45^\circ$  to each other about this axis. Each  $\text{Cu}^{++}$  ion is here immediately surrounded by an octahedron, formed with two oxygens and four chlorines in pairs at opposite corners, the diagonals being all unequal, *e.g.*, for the potassium salt the interatomic distances are  $\text{Cu-O} = 1.97$  A.U.;  $\text{Cu-Cl} = 2.32$  A.U. and  $\text{Cu-Cl} = 2.95$  A.U. There are eight  $\text{K}^+$  ions, 8 other oxygens and 8 other chlorines between a distance of about 4 to 6 A.U. in the form of rhombic prisms. Other  $\text{Cu}^{++}$  ions are at larger distances and their effects may be neglected. For the three isomorphous salts the interatomic distances increase slightly in the order of  $\text{K}^+$ ,  $\text{NH}_4^+$  and  $\text{Rb}^+$  respectively.

Similarly, it is found that in the crystals  $\text{NiSO}_4 \cdot 6\text{H}_2\text{O}$  (tetragonal  $D_2^{14}$  Beever and Lipson 1932),  $\text{NiSO}_4 \cdot 7\text{H}_2\text{O}$  (orthorhombic  $D_2^{14}$ , Beever and Schwartz, 1935), the Tutton salts (monoclinic  $C_{2h}^{14}$ , Hoffmann 1931), and the alums of the iron group (cubic  $\text{Pa}3$  or  $T_h^{14}$  Beever and Lipson, 1935) and even the triclinic ( $C_1^{14}$  Beever and Lipson, 1934) salt  $\text{CuSO}_4 \cdot 5\text{H}_2\text{O}$ , the respective paramagnetic ions are each surrounded by an octahedron of water molecules (except in the last crystal where two sulphate ions are placed at the opposite vertices of the octahedron, shared by the two molecules in the unit cell). The octahedra are slightly distorted in all cases, the actual symmetry conforming to the minimum requirements of the space group to which a crystal belongs. The distances of the corners of the octahedra from the central paramagnetic ion, on the average, range between 1.95 A.U. and 2.2 A.U. There are also found other geometric arrangements of the distant atoms, such as other water molecules,  $\text{SO}_4^{--}$  ions, alkali ions, etc. about the central ion, lying at distances of not less than 4 A.U. and which need not be considered at all beyond about 6 A.U. In every case similar paramagnetic ions lie at a much greater distance and hence their effects are negligible. Each unit cell contains more than one molecule oriented with respect to each other so as to give the symmetry of the unit cell.

The few examples cited above are typical of the iron group of elements, and even for many anhydrous salts such as halides, sulphates, oxides, sulphides,

selenides, arsenides, etc., octahedral arrangements of diamagnetic ions and dipoles, around the paramagnetic ions, occur (Wyckoff, 1931, 1935). Of course, other types of arrangements such as tetrahedral, square or others do arise, but much less frequently and the octahedral arrangement appears to be the most preferred type in the iron group, quite strongly bound, so as to be stable under widely differing conditions, *e.g.*, even in liquid or solution state, over wide ranges of temperature and concentration, or even when some or all constituents of the group are replaced by others. Evidence on this behalf for the iron group of salts is overwhelming from chemical or physico-chemical considerations also, and the tightness of binding as obtained from such studies corresponds to the usual ionic, semipolar or covalent types\*.

It is very satisfactory that exactly the same type of asymmetric electric fields, as would arise from the above mentioned arrangements of the diamagnetic atoms closely about the paramagnetic ions, would explain, in general, the observed deviations from the "free ion" behaviour of these ions in the solid state as also in solution. Indeed, in the magnetically diluted salts of the iron group of elements it cannot be the exchange or the spin-spin interaction which is responsible for the large anisotropic quenching of the orbital moments or the deviations from the Curie law of temperature variation of the effective magnetic moments. Actually, such a mechanism should be capable of producing a Stark-separation of at least some of the orbital states of these paramagnetic ions, of the order of  $10^4 \text{ cm}^{-1}$ . This is directly observed from the evidence of absorption spectra of the crystals and solutions of the salts of the iron group. [Bose and Mukherjee, (1938, 1939); also refer absorption spectra of rare earth salts by Freed (1938), Spedding, (1937, 1938) and others]. The existence of such anisotropic groups in solutions of these salts is also proved by observations on their magnetic birefringence (Haenny, 1931, 1932; Chinchalkar, 1935).

##### 5. THE CHOICE OF THE MAGNITUDES AND ASYMMETRIES OF THE CRYSTALLINE ELECTRIC FIELDS AND THEIR EFFECTS ON THE DEGENERACY OF THE PARAMAGNETIC ION

From a consideration of the X-ray data on the relative interatomic distances, between the paramagnetic ion and its immediately neighbouring cluster of diamagnetic ions and dipoles on the one hand, and the more distant atoms on the other, in the salts of the iron group, it would appear that almost the entire crystalline electric field, acting on the paramagnetic ion, is due to the former group, and hence for most purposes, it would be sufficient to represent the potential of this field following Van Vleck (1932) and others (1932), by

$$V = Ax^2 + By^2 - (A + B)z^2 + D(x^4 + y^4 + z^4) \quad \dots (2)$$

\* For a good review of such chemical evidences refer to (1) L. Pauling: *Nature of Chemical Bonds* (Cornell Univ. Press, 1945). (2) O. K. Rice—*Electronic Structure and Chemical Binding* (McGraw Hill Book Company, 1940).

The fourth order terms represent a field of cubic symmetry which produces in general a large separation of the order of  $10^4 \text{ cm}^{-1}$ , of at least some of the orbital levels. It is of course assumed that in the ionic salts of the iron group, the electric fields are able only to break down the coupling between the resultant orbital angular momentum and spin angular momentum, but not the Russell-Saunders coupling. Thus, the spin-orbit coupling may be treated as a small perturbation potential of about the same order as a rhombic field represented by the second order terms in (2), which together would remove the remaining orbital degeneracy and even produce a small separation of the spin levels, separations being of the order of about  $10^2$  to  $10^3 \text{ cm}^{-1}$  and  $10$  to  $10^{-1} \text{ cm}^{-1}$ , respectively. Frequently it is sufficient to use an even simpler expression

$$A(x^2 + y^2 - 2z^2) + D(x^4 + y^4 + z^4) \quad \dots (3)$$

with an axial symmetry about the  $z$ -axis or similar other simple expressions. Of course, as has been recently asserted by Van Vleck (1939), the effect of the distant atoms on the paramagnetic ion may not be negligible in many cases, especially at low temperatures, and we may have to add not only the cross product terms but also odd order and sixth order terms in expression (2). We shall consider this fully in a later section.

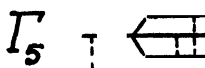
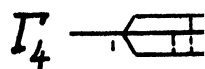
As regards the magnitudes of the fields as indicated by the values of the constants  $A$ ,  $B$ , and  $D$ , these will evidently depend in a complicated manner upon the charges on the ions and the distribution about the paramagnetic ion. For the iron group of salts the values, as estimated by Penney and Schlapp (1932) and others (1938), are:

$$D = 1000 \text{ cm}^{-1} - 1500 \text{ cm}^{-1}$$

$$A \sim B \sim C = \text{From } 0 \text{ to } 400 \text{ cm}^{-1}$$

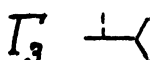
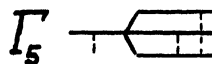
In the iron group of elements leaving aside the ions in an  ${}^6S_{5/2}$ -state, *i.e.*,  $\text{Mn}^{++}$  and  $\text{Fe}^{+++}$ , all other ions are either in a  $D$ -state or in an  $F$ -state, and under a crystalline electric field as contemplated above, the orbital levels are split up in the manner given in figures 1 and 2. In these Stark patterns  $\Gamma_2$  is orbitally non-degenerate and  $\Gamma_3$  though doubly degenerate is non-magnetic, while  $\Gamma_4$  and  $\Gamma_5$  are each triply degenerate. A uniaxial field such as tetragonal, trigonal or hexagonal will split the triplet levels  $\Gamma_4$  or  $\Gamma_5$  only partially, *i.e.*, into a singlet and a doubly degenerate one, full splitting being arrived at only with a field of orthorhombic or lesser symmetry. Each of these orbital levels again has a  $(2S + 1)$ -fold spin degeneracy which under the joint action of the rhombic field and the spin-orbit coupling, is removed to a very small extent, leaving alone a two-fold Kramers spin degeneracy, in the case of an ion with odd electrons, which a magnetic field alone can remove. Thus it will be seen from the above Stark patterns that if for any ion, even when the field is only cubic, either of the levels  $\Gamma_2$  or  $\Gamma_3$  lies lowest separated from the upper levels by intervals much larger than  $kT$  for ordinary temperatures, orbital contributions to the effective magnetic moment of the ion will be quenched except for a small amount, arising from high frequency matrix elements, proportional to  $T/D$ . In addition to this another orbital contribution will, in general, come

through the influence of the spin orbit coupling  $\lambda$ , causing a sharing of population between the upper and the lower cubic levels and will be proportional to



Cubic Rhombic  
(a) *F*-State

Fig. 1



Cubic Rhombic  
(b) *D*-State

Fig. 2

Stark-pattern for the ions of the iron group, for electric fields just sufficient to break down L-S coupling. Patterns erect for octahedrally coordinated ions having  $5-x$  and  $10-x$  electrons and inverted for  $x$  and  $5+x$  electrons in the  $3d$  sub-shell and *vice versa* for tetrahedral coordination.

$\lambda/D$ , but independent of  $T$ . The introduction of a rhombic field will in general make both these orbital contributions, anisotropic for different principal directions, in the ionic cluster, of the impressed magnetic field. In addition to this, small anisotropic spin contributions, involving  $\lambda$ ,  $1/T$  and the rhombic field constants, will arise.

On the other hand, if either of the levels  $\Gamma_4$  or  $\Gamma_5$  is the lowest in the Stark-pattern for any ion, since these states are degenerate in a cubic field, and even in a rhombic field of the type chosen the separations are comparable to  $kT$ , large anisotropic orbital contributions, depending in a complicated manner upon various factors, will arise even from these rhombic levels, in addition to those from the upper cubic states. The spins also will not be as free as in the previous cases and comparatively larger anisotropic spin quenching will occur.

The position in the iron group of elements has been clarified further by Van Vleck (1932), Gorter (1932) [cf. also Krishnan and Mookherji (1938); Bose (1948)], who prove that for electric field with a positive sign to its cubic constant  $D$ , as would occur with the usual type of octahedral co-ordination of the paramagnetic ion, the Stark-patterns for the reciprocally related ions, *i.e.*, ions having  $n$  or  $5+n$  and those having  $5-n$  or  $10-n$  electrons in the  $3d$  sub-shells respectively, are inverted with respect to each other. Actually, it has been shown that for this type of electric field, in the Stark-pattern for  $V^{++}$  and  $Cr^{+++}$  ions ( $3d^3$   ${}^4F_{3/2}$ -state) and  $Ni^{++}$  ( $3d^8$   ${}^3F_4$ -state) the singlet  $\Gamma_2$  is lowermost while the triplet  $\Gamma_4$  is lowermost for  $Ti^{++}$  and  $V^{+++}$  ( $3d^2$   ${}^3F_2$ -state) and also for  $Co^{++}$  ( $3d^7$  ( $F_8/2$ -state)). Similarly for  $Cr^{++}$  and  $Mn^{+++}$  ( $3d^4$   ${}^5D_0$ -state) and  $Cu^{++}$  ( $3d^9$   ${}^2D_{5/2}$ -state) the doublet  $\Gamma_3$  lies lowest, as against the triplet  $\Gamma_5$  at the bottom



for  $Ti^{+++}$  and  $V^{+4}$  ( $3d^1$   ${}^2D_{3/2}$ -state) and  $Fe^{++}$  ( $3d^6$   ${}^5D_4$ -state). For a crystalline field of the same type but with negative  $D$ , as happens in a tetrahedral or cubic coordination, the entire position is exactly reversed.

In the unit cell or in a single crystal of a salt, the principal moments will have to be calculated by taking into account the contributions of all the anisotropic ionic clusters in the unit cell which are in general inclined to each other\* (Krishnan and Mookherji, 1936, 1938; Mookherji, 1945, 1946; Bose, 1948). In the cases of a cubic crystal or a powdered salt or a salt in solution symmetry will preclude all anisotropy *en masse* \*\*. Under these latter conditions the anisotropic effects of the rhombic field upon the paramagnetic ion will be unobservable, but on the average a quenching effect will still introduce itself in the mean effective moment.

## 6. THE GENERAL MAGNETIC BEHAVIOUR OF THE PARAMAGNETIC SALTS OF THE IRON GROUP IN POWDERED SOLID STATE AND IN SOLUTIONS AT ROOM TEMPERATURES

The effects of the crystalline electric fields on the paramagnetic salts of the iron group as contemplated in the previous section may be then summed up as follows:

*In general* (1) the effective magnetic moment will deviate from the free ion value and may not even conform to the spin only value; (2) the deviations from the Curie law or even the Curie-Weiss law of the temperature dependence of the effective moment may occur; (3) magnetic anisotropy will arise in crystals of lower than cubic symmetry.

Our aim in the present paper and those following will be to see, how far the observed behaviour of the salts of the iron group of elements conform to above expectations in individual cases, as quantitatively predicted by the crystalline field theory. Any deviation from these in the actual cases would arise from our having neglected to include in the theory (1) the effect of strong covalency forces enough to break down Russel-Saunders coupling; (2) the effect of the interaction between the different quantum states of the same ion; (3) the effect of the relative orientation of the different ionic groups in the unit cell, (4) the effect of the exchange and the spin-spin interactions, (5) the effect of electric fields due to the distant atoms on the paramagnetic ion.

(1) This may be treated as an extreme case of the electric field theory (Van Vleck, 1936 and Howard, 1935). Such cases, where the spin moments are com-

\* In the papers of Penney and Schlapp (1932, Phys. Rev. **42**, 666) and most of the other authors (Jordahl, 1934, Van Vleck, 1932, 1939) the calculations of principal susceptibilities refer no doubt to a single ionic cluster, but the results are tacitly applied to a single crystal without any consideration of the relative orientations of different clusters in the unit cell.

\*\* The statement contained in a footnote of Penney and Schlapp's paper is rather obscure (*ibid*, footnote p. 679). Presumably it means that an individual  $Cr^{+++}$  ion, in a cubic crystal of the alum, may be anisotropic.

pletely balanced by pairing off of the spins in the non-bonding orbitals, so that diamagnetism or at most a temperature independent feeble paramagnetism can occur, may be easily recognized. Even when the spins are not all paired off it is possible in all cases to differentiate between an ionic and a covalent co-ordination (Pauling, Rice, *loc. cit.*), except when the spin moment is the same for the ionic and the covalent cases. But there are other intermediate cases in which Russel-Saunders coupling holds but as a rough approximation, which are, therefore, more difficult to tackle. For the ultimate object of our present paper we shall leave out all those cases where strong covalent bindings are found to occur, such that Russel-Saunders coupling fails.

(2) This has been considered by Van Vleck and Penney (1934) for the  $S$ -state ions  $Mn^{++}$  and  $Fe^{++}$ . Recently, this interaction has been calculated in some details by Abragam and Pryce (1951) for the other ions in connection with the ultra high frequency resonance of these substances. The effect is however, not always of much consequence.

(3) This effect can be neglected when all the ionic clusters in the unit cell are aligned parallel to each other or when there is only one such cluster in the unit cell. But this is not the case generally and the error in computing the electric fields from magnetic data on single crystals, neglecting the relative orientation of the ion may be considerable in many cases. However, in discussing the mean effective moment of the salts, as we shall be doing in the present paper, this consideration does not arise, unless we want to calculate the electric field constants from such data.

(4) In the anhydrous salts of the iron group the effects are often quite large and causes the salts to show an incipient ferro-magnetic, anti-ferromagnetic or metamagnetic behaviour. Even at room temperatures the mean effective moments of the salts deviate appreciably from the normal magnetically diluted salts and at low temperatures a Curie-Weiss law with very large values of  $\theta$ , and field dependence of susceptibilities may be observed (Starr, et al, 1940, de Haas et al, 1939). We shall try to estimate these interactions for such salts in a future paper. In the hydrated or otherwise diluted magnetic salts it has been said earlier that the exchange and the spin-spin interactions are negligibly small and in discussing purely the effects of crystalline electric fields our aim will be to consider only such salts and their solutions.

(5) The direct effect of the electric fields due to distant atoms, which are asymmetrically placed about the paramagnetic ion, bound in crystal lattice by Van der Waal forces or weak ionic bonds, is usually very small as calculated by Van Vleck (1939). But this asymmetric arrangement of the distant atoms in the lattice may perhaps be attributed primarily to the inherent tendency of the paramagnetic ion to form a closely bound asymmetric cluster about itself so as to remove the degeneracy of its energy levels. The repercussions of this dissymmetry of the distant atoms will cause added change in the position of the members of the ionic cluster until an equilibrium condition is attained. Such an indirect

effect of the distant atoms under certain circumstances may be about as large as that of the original electric fields due to the nearest neighbours, as has been shown by Van Vleck (1939).

In the state of solution of a given salt, the ionic clusters tend to retain their identities, (as is proved in an earlier section), whereas, the lattice structure breaks down completely, giving only an average spherical symmetry about the paramagnetic ion of the distant atoms, which are now even further removed from the paramagnetic ion than in the solid state. Hence, we should be able to observe an *appreciable* change in the mean effective moment, which may now be considered as being affected only by the nearest neighbours, rendered more symmetric than in the solid state, *if the effects of the distant atoms is as large as it claimed by Van Vleck*. The effect at room temperatures should be particularly noticeable in such substances in which the lowest orbital state, in the Stark-pattern of the paramagnetic ion caused by the cubic electric fields, is a degenerate one

Further, we should be able to observe systematic variations in the effective moments in a series of salts, of a given paramagnetic ion, *especially if they are isomorphous*, in which the members of the nearest groups are always the same, but the distant atoms are systematically different; or in different crystalline modifications of the same salt in which the parameters, connecting the different members of the clusters in the unit cell, are often changed considerably.

In this connection we should have to take care, that while studying the solutions or even the salts, the individual members of the ionic cluster are not replaced by others or the type of co-ordination does not change or the clusters are not dissociated themselves, since these would involve mainly changes in the crystalline fields due to the nearest neighbours.

We forthwith proceed to discuss the data on the mean effective moments of a large number of the magnetically diluted solid salts of the iron group and their solutions at room temperatures given in Table I, on the basis of the ideas presented just now. Unfortunately, quite often, data for the same salts by different observers differ considerably, no doubt owing to various experimental difficulties, and uncertain correction factors. Further, much of the data, especially those of the French, German, and Spanish schools, have been obtained to verify the existence of the imaginary 'Weiss magneton' or to fit the Weiss theory of 'inner fields'. The data for a series of similar salts and their solutions by a given author as is necessary from our present view point, is rarely available. In the following discussions we have taken only the average of the most probable values. On looking at experimental values for the mean effective moments given in the table several facts are immediately discernible.

(1) In the iso-electronic ions (a)  $Ti^{+++}$ ,  $V^{++++}$ , (b)  $Ti^{++}$ ,  $V^{+++}$ , (c)  $V^{++}$ ,  $Cr^{+++}$ , (d)  $Cr^{++}$ ,  $Mn^{+++}$ , or (e)  $Mn^{++}$ ,  $Fe^{+++}$ , the Stark-

patterns, under a given type of electric field, are the same. Hence they are expected to have the same effective moments, except for slightly different high frequency contributions, spin orbit coupling terms and spin quenchings. This expectation is fulfilled as far as the experimental results go.

(2) In the first half of the iron group all the salts of the ions are found to conform closely to the respective spin only values, even in the cases where an orbitally degenerate level lies lowest in the Stark-pattern for cubic field with positive  $D$ , *i.e.*, in the cases (a) and (b) of the previous paragraph. This is no doubt due to the fact that owing to comparatively small and positive values of the spin orbit couplings (Laporte, 1928) even the orbitally degenerate cubic levels are separated, by the rhombic fields, in general, to widths large compared to  $kT$  (Van Vleck, 1939) and hence the orbital contributions are comparable and opposite in sign to the high frequency contributions, thus more or less cancelling each other (*vide* Bose, 1948, case of  $\text{Cr}^{+++}$ ).

(3) This is not so in the latter half of the group where fairly large orbital contributions due to large and negative spin orbit coupling are observed even in the salts of  $\text{Ni}^{++}$  and  $\text{Cu}^{++}$  in which orbitally non-degenerate or non-magnetic levels lie lowest in the Stark-pattern under a cubic field with positive  $D$ .

(4) The rules of inversions of Stark-pattern between two halves of the group mentioned in the previous section, do not show themselves much prominently except in the cases of  $\text{Cr}^{+++}$  and  $\text{V}^{++}$  to  $\text{Co}^{++}$ , and of  $\text{Cr}^{++}$  and  $\text{Mn}^{+++}$  to  $\text{Fe}^{++}$  owing evidently to the same considerations as in (2) and (3) (Van Vleck, 1932). Of course, it might appear at first sight, that inversion comes all in the wrong place, due to other types of co-ordination than octahedral occurring in the observed salts. But this is not supported by the X-ray data as far as available. A surer test, however, of the validity of the rules of inversion would be the measurement of anisotropies of the crystals and their temperature variations\*. Experiments are in progress in this laboratory to add to the data available at present and the matter will be discussed in a future part of the paper.

\* A departure from the rules of inversion might occur also with odd or sixth order fields present (Van Vleck, 1932, *Phys. Rev.* 41, footnote p. 213).

TABLE I

Ground term —  $3d^1 {}^2D_{3/2}$ ; Ion —  $V^{+4}$ ; Theoretical  $\mu_{\text{eff}} - \Delta \nu \sim kT$   
 $= 1.78$ ; Spin only  $= 1.73$ .

Experimental $\mu_{\text{eff}}$ at 300°K				Author **
Salt studied	Powder	Solution or molten		
$\text{VOClO}_4$ soln.		1.74	Aq. soln.; Expt. done only at 20°C.; moment varies slightly with diff. conc.	Freed (1927)
$\text{V}_2\text{O}_5\text{Cl}_4 \cdot 5\text{H}_2\text{O}$		1.534— 1.503	Liquid at room temp.; moment varies with time; Temp. —79° to +53°C.	Perrakis (1927)
$\text{VO}(\text{SO}_4)_3 \cdot 3\frac{1}{2}\text{H}_2\text{O}$	1.709— 1.743		Moment varies with time; Temp. —79° to +100°C.	"

G.T. —  $3d^2 {}^3F_4$ ; Ion —  $V^{++}$ ; Th.  $\mu_{\text{eff}} - \Delta \nu \sim kT = 2.73$ ; Spin only  $= 2.83$ .

$(\text{VO})_2\text{SO}_4$ Soln.		2.827	Done only at 20°C with aqueous soln. (Brown) of low acid conc.; moment const. for diff. salt conc.	Freed (1927)
$\text{V}_2(\text{SO}_4)_3$ soln.		2.762	Done only at 20°C with aq. soln. (Green—high acid conc.); moment varies slightly with diff. salt conc.	"
$\text{VNH}_4(\text{SO}_4)_2 \cdot 12\text{H}_2\text{O}$	2.733		Temp. 297.—1.415°K. Follows Curie Law down to lowest temp.	Sigert and Vanden Handel Leiden Comm.

G.T. —  $3d^2 {}^4F_3/2$ ; Ion —  $V^{++}$ ; Th.  $\mu_{\text{eff}} - \Delta \nu \sim kT = 3.60$ ; Spin only  $= 3.87$ .

$\text{V}_2\text{SO}_4$ soln.	3.83	Done only at 20°C; moment varies slightly with diff. conc. Freed (1927) of aq. soln.
-------------------------------	------	--

\* Values of moment for free ions with  $\Delta \nu \sim kT$  and the spin only values given at the top of each table indicate the normal limits of quenching of the orbital moment.

\*\* For complete reference see the standard books by Stoner, Van Vleck, Bates and Selwood, and also Science Abstracts.

TABLE I. (contd.)

G.T. —  $3d^5 \text{ } ^4F_{5/2}$ ; Ion —  $\text{Cr}^{+++}$ ; Theo.  $\mu_{\text{eff}}$  —  $\Delta\nu \sim kT = 2.97$ ; Spin only = 3.87.

Experimental $\mu_{\text{eff}}$ at 300°K			Remarks	Author
Salt studied	Powder	Solution or Molten		
$\text{Cr}_2(\text{SO}_4)_3$		3.85	Violet soln; Conc. 1.2—10%, moment independent of conc.	Cabrera, Marquina (1917, 1919, and 1922).
		3.70	Green soln.; moment varies irregularly with conc.; add. acid raises moment to about 3.84.	Do.
$\text{CrCl}_3$		3.85	Conc. 1.3—19.81%.	Do.
$\text{Cr}(\text{NO}_3)_3$		3.80	Moment same for both violet and green solution; slight increase with acid.	Do.
$\text{CrCl}_3 \cdot 6\text{H}_2\text{O}$	3.821		Green. Temp. 290° — 14.28°K.	de Haas and Gorter. Leid. Comm.
$\text{CrK}(\text{SO}_4)_2 \cdot 12\text{H}_2\text{O}$	3.840		Temp. 290° — 14.33°K.	Do.
$\text{Cr}_2(\text{SO}_4)_3 \cdot (\text{OH})_2 \cdot 5\text{H}_2\text{O}$	3.498		Temp. 290° — 14.55°K.	Do.
$\text{CrK}(\text{SO}_4)_2 \cdot 12\text{H}_2\text{O}$	3.808	3.778	Melted in water of cryst.	Welo (1929)
$\text{Cr}(\text{NO}_3)_3 \cdot 3\frac{1}{2} \text{H}_2\text{O}$	3.454	3.506	Melted in water of cryst.	Do.
$\text{Cr}(\text{NO}_3)_3$		4.085—3.745	Aq. soln.; moment changes with conc. range 7.928 — .389%. Temp. 289° — 691°K.	Fahlenbranch (1932).
$\text{CrCl}_3 \cdot 6\text{H}_2\text{O}$	3.853		Green; Temp. 291.1-92.1°K.	Serres (1932).
$\text{Cr}_2(\text{SO}_4)_3 \cdot 16\text{H}_2\text{O}$	3.839		Violet; Temp. 91° — 295°K.	Do.
Do.	3.846	3.789	Melted in water of cryst. Temp. 273° — 356°K.	Do.
$\text{CrK}(\text{SO}_4)_2 \cdot 12\text{H}_2\text{O}$	3.881		Temp. 90° — 347°K.	Do.
Do.	3.877	3.959	Melted in water of cryst.	Do.
$\text{K}_2\text{Cr}(\text{SCN})_6 \cdot 4\text{H}_2\text{O}$	3.783		Temp. 295° — 82°K.	Janes (1945).

TABLE I. (contd.)

G.T. —  $3d^4 \ ^5D_0$ ; Ion —  $\text{Cr}^{++}$ ; Th.  $\mu_{\text{eff.}}$  —  $\Delta \nu \sim kT = 4.25$ ; Spin only = 4.90.

Experimental $\mu_{\text{eff.}}$ at 300°K			Remarks	Author
Salt studied	Powder	Solution or molten		
$\text{CrCl}_3$		4.81	Details not available.	Cabrera & Pina (1919)
$\text{CrSO}_4$		4.84	Do.	Do.
$\text{CrSO}_4 \cdot 6\text{H}_2\text{O}$	4.808		Temp. $54^\circ - 372^\circ \text{K.}$	Lips (1934).

G.T. —  $3d^5 \ ^6D_5$ ; Ion —  $\text{Mn}^{+++}$ ; Th.  $\mu_{\text{eff.}}$  —  $\Delta \nu \sim kT = 3.80$ ; Spin only = 4.90.

$\text{Mn}(\text{CH}_3\text{COCH} \cdot \text{COCH}_3)_3$	4.935		Temp. $292.2 - 16.95^\circ \text{K.}$	Jackson (1935).
$\text{Mn}(\text{C}_2\text{H}_3\text{O}_2) \cdot 2\text{H}_2\text{O}$	4.734		Temp. $293^\circ - 14.25^\circ \text{K.}$	de Haas and Schultz. Comm. Leid.

G.T. —  $3d^5 \ ^6S_{5/2}$ ; Ion —  $\text{Mn}^{++}$ ; Th.  $\mu_{\text{eff.}}$  —  $\Delta \nu \sim kT = 5.92$ ; Spin only = 5.92.

$\text{MnCl}_2$		5.443	Aq. soln.; moment independent of conc. over wide range = 22 to 28.	Cabrera and Duprier (1925).
$\text{Mn}(\text{NO}_3)_2$		5.443	Do.	Cabrera Moles and Marquina (1915).
$\text{MnSO}_4 \cdot 4\text{H}_2\text{O}$	5.859		Details not available.	Foex (1921)
Do.	5.864		Temp. $288.7^\circ - 14.4^\circ \text{K.}$	Onnes and Oosterhuis
$\text{Mn}_2\text{P}_2\text{O}_7$ anh.	5.846			Foex and Brunette (1927)
$\text{Mn}(\text{NH}_4)_2(\text{SO}_4)_2 \cdot 6\text{H}_2\text{O}$		* 5.672	Room temp. only. Mean value of single crystal.	Rabi (1927)
$\text{MnCl}_2$ $\text{MnSO}_4$ $\text{Mn}(\text{NO}_3)_2$		5.934	Temp. $25^\circ - 100^\circ \text{C}$ ; Moment independent of salts and concentration.	Bose (1935)

\* Measurement made with single crystal.

TABLE I (Contd.)

G.T. —  $3d^5 \ ^6S_{5/2}$ ; Ion —  $Mn^{++}$ ; Th.  $\mu_{eff}$  —  $\Delta\nu \sim kT = 5.92$ ; Spin only = 5.92.

Experimental $\mu_{eff}$ at 300°K			Remarks	Author
Salt studied	Powder	Solution or molten		
$Mn(NH_4)_2(SO_4)_2 \cdot 6H_2O$	5.896		Temp. 14.5 — 290°K	Jackson and Onnes (1923)
$Mn(NH_4)_2(SO_4)_2 \cdot 6H_2O$	*5.931		Temp. 227 — 287°K	Jackson (1927)
$Mn(NH_4)_2(SO_4)_2 \cdot 6H_2O$	*5.835		Temp. 79° — 293°K	Jackson (1933)
$MnSO_4 \cdot 4H_2O$	*5.835		Do.	Do.
$MnSO_4 \cdot 5H_2O$	*5.906		Do.	Do.
Mn. acetate	5.69		Temp. 32° — 122°C	Bhatnagar, Nevgi and Sarma (1946)
Mn. Formate	5.73		Do.	Do.
Mn. Lactate	5.71		Do.	Do.
Mn. Oxalate	5.70		Do.	Do.
$MnCl_2 \cdot 4H_2O$	5.884		Temp. 318° — 154°K	Lallemand (1935)
$MnCl_2$		5.888	Temp. 290 — 231°K	Do.
$MnSO_4 \cdot 5H_2O$	5.909		Temp. 294 — 148°K	Do.
$Mn_2P_2O_7$ anh.	5.846		Temp. 293 — 148°K	Do.

G.T. —  $3d^5 \ ^6S_{5/2}$ ; Ion —  $Fe^{+++}$ ; Th.  $\mu_{eff}$  —  $\Delta\nu \sim kT = 5.92$ ; Spin only = 5.92

$Fe(NH_4)(SO_4)_2 \cdot 12H_2O$	5.906	Temp. 14°K — 290°K	Onnes and Oosterhuis, Comm. Leid.
$FeCl_2 \cdot 2NH_4Cl \cdot H_2O$	5.590	Temp. 99° — 287°K	Honda and Ishiwara (1914)

\* Measurement made with single crystal.



TABLE I. (contd.)

G.T. —  $3d^5$   $S_{5/2}$ ; Ion —  $Fe^{+++}$ ; Th.  $\mu_{eff} - \Delta v \sim kT = 5.92$ ; Spin only = 5.92

Experimental $\mu_{eff}$ at 300°K			Remarks	Author
Salt studied	Powder	Solution or molten		
$FeCl_3$		5.45 — 5.98	Aq. soln.; moment increases with conc. and acid content to a limiting value.	Cabrera and Moles (1912)
$Fe_2(SO_4)_3$		5.25 — 5.86	Do.	Do.
$Fe(NO_3)_3$		5.45 — 5.98	Do.	Do.
$Fe_2(P_2O_7)_3$		5.05	Only one conc. done	Do.
$FeCl_3$		5.974 — 5.828	Aq. soln. conc. 6.6 to .348% moment decreases with conc.	Fahlenbrach (1932)
$FeNH(SO_4)_2 \cdot 12H_2O$	5.888	5.758	Melted in water of crystallization.	Welo (1929)
$FeCl_3 \cdot 6H_2O$	5.889	5.869	Do.	Do.
$Fe(NO_3)_3 \cdot 9H_2O$	5.853	5.626	Do.	Do.
$FeCl_3$		5.812 — 5.895	Aq. soln; Moment decreases with dilution, but increases to a limiting value with acid content; Temp. 25° — 100°C	Bose (1935)
$Fe_2(SO_4)_3$		5.365 — 5.798	Do.	Do.
$Fe(NO_3)_3$		5.599 — 5.902	Do.	Do.
$Fe(CH_3 \cdot COCH \cdot COCH_3)_3$	*5.936		Temp. 291.5 — 79.0°K	Jackson (1933)
$K_3 \cdot Fe(C_2O_4)_3 \cdot$	*5.924		Temp. 289.4 — 70.6°K	Do.
$FeCl_3 \cdot 6H_2O$	5.950		Temp. 140° — 290°K	Lallemand (1935)
$FeCl_3$		5.96	Aq. soln.; conc. .146 — .357; Temp. 286° — 370°K.	Do.
$FeCl_3$		5.914 — 5.870	Soln. in ethyl alcohol; conc. .403 to .0760; Temp. 2860 — 318°K.	Do.
$FeCl_3 \cdot 2NH_4Cl \cdot H_2O$	5.644		Temp. 143° — 290°K	Do.
do.		5.944	Aq. soln.; Temp. 288° — 330°K	Do.
$Fe(NO_3)_3 \cdot 9H_2O$	5.947		Temp. 149° — 293°K	

\* Measurement made with single crystal.

TABLE I. (contd.)

G.T. —  $3d^5 {}^5D_4$ ; Ion —  $\text{Fe}^{++}$ ; Th.  $\mu_{\text{eff.}} - \Delta\nu \sim kT = 6.54$ ; Spin only = 5.92.

Experimental $\mu_{\text{eff.}}$ at 300°K.			Remarks	Author
Salt studied	Powder	Solution or molten		
$\text{FeSO}_4 \cdot 7\text{H}_2\text{O}$	5.302			Omnes and Oosterhuis — Comm. Leid.
$\text{FeSO}_4$		5.330	Aq. soln.; details not available.	Cabrera, Moles, and Marquina (1915)
$\text{FeSO}_4$		5.352	Aq. soln.; conc. 0.48—20.7% Moment independent of conc.	Weiss and Frankkamp (1915)
$\text{Fe}(\text{NH}_4\text{SO}_4)_2$		5.348	Aq. soln. conc. 0.25—17.5% Moment independent of conc.	Do.
$\text{Fe}(\text{NH}_4\text{SO}_4)_2 \cdot 6\text{H}_2\text{O}$	5.659	5.322 — 5.725	Used both powder and soln. Details not available.	Foex (1924)
$\text{FeSO}_4 \cdot 7\text{H}_2\text{O}$	5.211		Temp. 14° — 290°K	Jackson (1924)
$\text{Fe}(\text{NH}_4\text{SO}_4)_2 \cdot 6\text{H}_2\text{O}$	5.505		Do.	Do.
$\text{Fe}(\text{NH}_4\text{SO}_4)_2 \cdot 6\text{H}_2\text{O}$	*5.252		Room temp. only	Rabi (1927)

G.T. —  $3d^7 {}^4F_{9/2}$ ; Ion —  $\text{Co}^{++}$ ; Th.  $\mu_{\text{eff.}} - \Delta\nu \sim kT = 6.56$ ; Spin only = 4.90.

$\text{CoCl}_2$		4.845 — 5.408	Aq. soln.; Data not available separately for different salts.	Cabrera, Jimmenez and Marquina (1916)
$\text{CoSO}_4$		Do.	Do.	Do.
$\text{Co}(\text{NO}_3)_2$		Do.	Do.	Do.
$\text{CoCl}_2$		4.96	Aq. soln.; Moment independent of conc.	Trumpler (1918)
$\text{CoSO}_4$		4.845 to 5.408	Aq. soln.; Moment varies with conc.; Data separately not available.	Do.
$\text{Co}(\text{NO}_3)_2$		Do.	Do.	Do.

\* Measurement made with single crystal.

TABLE I. (contd.)

G.T. —  $3d^7 \text{ } ^4F_{5/2}$ ; Ion —  $\text{Co}^{++}$ ; Th.  $\mu_{\text{eff.}} - \Delta \nu \sim kT = 6.56$  Spin only = 3.87.

Experimental $\mu_{\text{eff.}}$ at 300°K.			Remarks	Author
Salt studied	Powder	Solution or molten		
$\text{CoCl}_2$		4.946— 5.107	Aq. soln.; Moment varies with conc.	Quartoroli (1918)
$\text{CoCl}_2$		4.946	Done at 20°C. Aq. soln.; conc. 0.001018—2.0353 Mol./l.; Moment independent of conc.	Brant (1921)
$\text{Co}(\text{NO}_3)_2$		5.025	Aq. soln.; Moment const.	Foex (1921)
$\text{CoSO}_4 \cdot 7\text{H}_2\text{O}$	4.964 *4.870		Temp. 14°—290°K for all powder measurements, and ammon. salt single crystal.	Jackson (1924, 1927)
$\text{Co}(\text{NH}_4\text{SO}_4)_2 \cdot 6\text{H}_2\text{O}$	4.828 *4.803		Temp. 70°—290°K for heptahydrate single crystal.	Jackson and Onnes (1923)
$\text{Co}(\text{KSO}_4)_2 \cdot 6\text{H}_2\text{O}$	4.941 *5.110		Temp. 170°—290° for potassium salt single crystal.	
$\text{Co}(\text{RbSO}_4)_2 \cdot 6\text{H}_2\text{O}$	5.125		Do.	Do.
$\text{CoCl}_2 \cdot 6\text{H}_2\text{O}$	4.743	5.024	Melted in water of crystallization.	Welo (1929)
$\text{Co}(\text{NO}_3)_2 \cdot 6\text{H}_2\text{O}$	4.888	4.975	Do.	Do.
$\text{CoCl}_2 \cdot 6\text{H}_2\text{O}$	4.817— 4.943		Temp. 14°—288°K; second —79°C to +50°C and 110°—209°C.	Chatillon (1927)
$\text{CoCl}_2$		4.961	Aq. soln.; Independent of conc. and mode of treatment. Temp. 10°—140°C.	Do.
$\text{CoCl}_2$		4.955— 4.663	Aq. soln., acidified with HCl. Moment depends on conc. and acid content. Temp. 10°—140°C.	Do.
$\text{CoCl}_2$		4.754	Soln. in ethyl alcohol; Temp. 10°—140°C.	Do.
$\text{CoCl}_2$		4.647	Soln. in amyl alcohol; Temp. 10°—140°C.	Do.

\* Measurement made with single crystal.

TABLE I (Contd.)

G.T. —  $3d^7$   $^4F_{5/2}$ ; Ion —  $\text{Co}^{++}$ ; Th.  $\mu_{\text{eff.}} - \Delta \nu \sim kt = 6.56$ ; Spin only = 8.87

Experimental $\mu_{\text{eff.}}$ at 300°K			Remarks	Author
Salt studied	Powder	Solution or molten		
$\text{CoSO}_4$		4.961— 4.987	Dependent on time; Temp. 10°—140°C.	Chatillon (1927)
$\text{Co}(\text{NO}_3)_2$		5.016	Temp. 10°—140°C.	Do
$\text{CoCl}_2$		5.230— 4.829	Aq. soln. conc. 9.041—118%. Moment varies with conc., treatment and time. Temp. +60° to —60°C.	Fahlenbrach (1932)
$\text{CoCl}_2$		5.048— 3.836	In pyridine	Do
$\text{CoCl}_2$		Do.	In ethyl alcohol. Moment has two values in both cases, corresponding to colour of soln. blue at high and red at low temps. Temp. +60 to —60°C.	Do.
$\text{Co}(\text{NH}_4\text{SO}_4)_2 \cdot 6\text{H}_2\text{O}$	*4.928		Done only at room temp.	Rabi (1927)
$\text{Co}(\text{RbSO}_4)_2 \cdot 6\text{H}_2\text{O}$	*4.888 *4.946		Do.	Do
$\text{CoSO}_4 \cdot 7\text{H}_2\text{O}$	4.784		Temp. 284°—350°K.	Serres (1932)
$\text{CoCl}_2 \cdot 6\text{H}_2\text{O}$		4.82	Soln. in methanol. Temp. 293°—177°K.	Mercier (1935)
$\text{CoCl}_2$		4.891— 4.994	Aq. soln. of diff. conc. Moment varies with conc., mode of prep. and treatment. Temp. 290°—370°K.	Lallemand (1935)
$\text{CoCl}_2 \cdot 6\text{H}_2\text{O}$	4.922		Temp. 290°—370°K.	Do
$\text{CoSO}_4 \cdot 7\text{H}_2\text{O}$	4.779 *4.750		Measurements both on powder and single crystal. Temp. +65° to —45°C.	Bartlett (1932)
$\text{Co}(\text{NH}_4\text{SO}_4)_2 \cdot 6\text{H}_2\text{O}$	4.965 *4.991		Do.	Do
$\text{Co}(\text{KSO}_4)_2 \cdot 6\text{H}_2\text{O}$	4.976 *4.892		Do.	Do

\* Measurements made with single crystals.

TABLE I (Contd.)

G.T. —  $3d^7 \text{ } ^4F_3/2$ ; Ion —  $\text{Co}^{++}$ ; Th.  $\mu_{\text{eff.}} - \Delta v \sim kT = 6.56$ ; Spin only = 3.87.

Experimental $\mu_{\text{eff.}}$ at 300°K.			Remarks	Author
Salt studied	Powder	Solution or molten		
$\text{K}_2\text{Co}(\text{SCN})_4 \cdot 4\text{H}_2\text{O}$	4.974		Temp. 80°—300°K.	James (1935)
$\text{CoCl}_2 \cdot 6\text{NH}_3$	5.090		Do.	Do.
$\text{CoSO}_4 \cdot 6\text{NH}_3$	5.916		Do.	Do.
$\text{Co}(\text{CN})_2 \cdot 2\text{H}_2\text{O}$	3.225		Do.	Do.

G.T.— $3d^8 \text{ } ^3F_4$ ; Ion —  $\text{Ni}^{++}$ ; Th.  $\mu_{\text{eff.}} - \Delta v \sim kT = 5.56$ ; Spin only = 2.83.

$\text{NiCl}_2$		3.220	Aq. soln. of wide conc. range. Moment approximately constant for all salts and cons., done at room temperature only.	Cabrera and Dupe-rier (1925, 1927)
$\text{NiSO}_4$		Do.		Cabrera, Moles and Guzmán, (1914)
$\text{Ni}(\text{NO}_3)_2$		Do.		Do
$\text{NiK}(\text{CN})_6$		Do.		Do
$\text{NiSO}_4$		3.291	Aq. soln.; conc. .623—37.164%; Moment const. for all salts and concentrations.	Weiss and Bruins (1915)
$\text{NiCl}_2$		Do.		Do
$\text{Ni}(\text{NO}_3)_2$		Do.		Do
$\text{NiSO}_4$		3.196	Amm. soln. Addition of acids or $(\text{NH}_4)_2\text{SO}_4$ scarcely affects the value.	Do
$\text{NiCl}_2$		Do.		Do
$\text{Ni}(\text{NO}_3)_2$		Do.		Do
$\text{NiCl}_2$		3 3.229	Aq. soln. Conc. .00123 to 3.765 moles per litre; done at 20°C only; moment constant.	Brant (1921)
$\text{NiSO}_4 \cdot 7\text{H}_2\text{O}$	3.282 *3.308		Temp. 14.6°—292.2°K.	Jackson (1924, 1927)
$\text{Ni}(\text{NH}_4)_2 \cdot (\text{SO}_4)_2 \cdot 6\text{H}_2\text{O}$	3.188 *3.320		Temp. 14°—292°K for powder and 225°—287°K for single crystal.	Jackson and Onnes (1923)
$\text{NiCl}_2$		3.292	Aq. soln., moment independent of conc.	Schaffer and Taylor (1926)

\* Measurement made with single crystal.

TABLE I (Contd.)

G.T.— $3d^8$   $^3F_4$ ; Ion —  $Ni^{++}$ ; Th.  $\mu_{eff} - \Delta \nu \sim kT = 5.56$ ; Spin only = 2.83.

Experimental  $\mu_{eff}$  at 300°K

Salt studied	Powder	Solution or molten	Remarks	Author
NiCl <sub>2</sub>		3.233 to 3.185	Moment varies with added K <sub>2</sub> C <sub>2</sub> O <sub>4</sub> .	Schaffer and Taylor (1926)
Ditto		3.134—3.178	With added (NH <sub>4</sub> )OH	Do
		3.090	with CH <sub>3</sub> NH <sub>2</sub>	Do
		3.336	with KCl	Do
		1.773—2.967	with KCN & NH <sub>3</sub>	Do
NiBr <sub>2</sub>		3.250	Aq. soln.	Do
		3.289—3.240	with HBr	Do
NiSO <sub>4</sub> ·7H <sub>2</sub> O	3.217 and 3.234		Temp. 14°—288°K; 2nd value as corrected by Serres.	de Haas, Gorter and Handel, Comm. Leid.
NiCl <sub>2</sub>		3.218—3.281	Soln. in water and meth. alcohol; moment varies with conc., treatment and temp.	Foex and Kessler (1931)
Ni(NH <sub>4</sub> SO <sub>4</sub> ) <sub>2</sub> ·6H <sub>2</sub> O	*3.184		Done at room temperature only.	Rabi (1927)
Ni(KSO <sub>4</sub> ) <sub>2</sub> ·6H <sub>2</sub> O	*3.089		Do	Do
Ni(RbSO <sub>4</sub> ) <sub>2</sub> ·6H <sub>2</sub> O	*3.155		Do	Do
NiCl <sub>2</sub>		3.358—3.230	Aq. soln. conc. .429—4.271% moment varies with conc.	Fahlenbrach (1932)
Ni(NH <sub>4</sub> SO <sub>4</sub> ) <sub>2</sub> ·6H <sub>2</sub> O	3.196 *3.196		Temp. +55 to —45°C.	Bartlett (1932)
Ni(HCOO) <sub>2</sub> ·xH <sub>2</sub> O	3.258		Formulae uncertain in several cases. Temp. not stated. Nickel cyanide becomes diamagnetic progressively on dehydration.	Fereday (1932)
Ni(CN) <sub>2</sub> ·2H <sub>2</sub> O	2.714			Do
Ni <sub>2</sub> (C <sub>6</sub> H <sub>7</sub> O <sub>7</sub> ) <sub>2</sub> ·14H <sub>2</sub> O	3.333			Do
NiSO <sub>4</sub> ·7H <sub>2</sub> O	3.302			Do
Ni(NH <sub>4</sub> SO <sub>4</sub> ) <sub>2</sub> ·6H <sub>2</sub> O	3.268			Do

\* Measurement made with single crystal.

TABLE I (Contd.)

G.T.— $3d^8 \ ^3F_4$ ; Ion — Ni<sup>++</sup>; Th.  $\mu_{\text{eff}}$ — $\Delta\nu \sim kT = 5.56$ ; Spin only = 2.83.

Experimental $\mu_{\text{eff}}$ at 300°K			Remarks	Author
Salt studied	Powder	Solution or molten		
Ni(KSO <sub>4</sub> ) <sub>2</sub> ·7H <sub>2</sub> O	3.307		Formula uncertain in several cases. Temp. not stated. Nickel cyanide becomes diamagnetic progressively on dehydration.	Fereday (1932)
NiSO <sub>4</sub> ·4NH <sub>3</sub> ·2H <sub>2</sub> O	3.259		Do.	Do.
Ni(C <sub>6</sub> H <sub>5</sub> COO) <sub>2</sub> ·3H <sub>2</sub> O	3.302		Do.	Do.
Ni <sub>3</sub> (PO <sub>4</sub> ) <sub>2</sub> ·7H <sub>2</sub> O	3.325		Do.	Do.
Ni(C <sub>2</sub> H <sub>3</sub> O <sub>2</sub> ) <sub>2</sub> ·4H <sub>2</sub> O	3.235		Do.	Do.
NiCl <sub>2</sub> ·6H <sub>2</sub> O	3.218		Temp. 90°—313°K.	Serres (1933)
NiSO <sub>4</sub> ·1.12H <sub>2</sub> O	3.235		Temp. 91°—291°K.	Do,
NiSO <sub>4</sub> ·1.13H <sub>2</sub> O	3.255		Temp. 92°—293°K.	Do,
NiSO <sub>4</sub> ·4H <sub>2</sub> O	3.313— 3.253		Temp. 92°—294°K.	Do,
NiSO <sub>4</sub> ·6H <sub>2</sub> O	3.241		Temp. 92°—332°K.	Do,
NiSO <sub>4</sub> ·7H <sub>2</sub> O	3.296— 3.225		Temp. 91°—294°K. For diff. samples.	Do,
Ni(NH <sub>4</sub> SO <sub>4</sub> ) <sub>2</sub> ·6H <sub>2</sub> O	3.328		Temp. 91°—293°K.	Do,
Ni(CN) <sub>2</sub>	1.175— 1.340		Temp. 288°—528°K. Variation with progressive heating.	Do,
NiSO <sub>4</sub> ·6H <sub>2</sub> O	3.194		Temp. range 90°—300°K.	Janes (1925)
Ni(NO <sub>3</sub> ) <sub>2</sub> ·6H <sub>2</sub> O	3.199		Do.	Do.
NiNO <sub>3</sub> ·4NH <sub>3</sub>	3.123		Do.	Do.
Ni(CN) <sub>2</sub> ·C <sub>6</sub> H <sub>5</sub> ·NH <sub>3</sub>	2.278		Do.	Do.

TABLE I (Contd.)

G.T. —  $3d^9 D_2/s$ ; Ion —  $\text{Cu}^{++}$ ; Th.  $\mu_{\text{eff}} - \Delta\nu/kT = 3.53$ ; Spin only = 1.73.

Experimental $\mu_{\text{eff}}$ at 300°K			Remarks	Author
Salt studied	Powder	Solution or molten		
$\text{CuCl}_2$		1.998— 1.938	Aq. soln.; moment varies with conc.; detailed data not available.	Cabrera (1918)
$\text{CuSO}_4$		Do.		Cabrera and Moles (1914).
$\text{Cu}(\text{NO}_3)_2$		Do.		Do.
$\text{Cu}(\text{NO}_3)_2$		1.968	Aq. soln.; conc. varies from 52.5 to .0068%; details not available.	Cherbulicz Thesis. Piccard and Cherb. (1916)
$\text{CuCl}_2$		1.928	Aq. soln.; conc. 17.0.1%; details not available.	Jacobssohn (1916)
$\text{CuSO}_4$		Do.		Do.
$\text{Cu}(\text{NO}_3)_2$		Do.		Do.
$\text{CuSO}_4 \cdot 5\text{H}_2\text{O}$	1.918		Temp. 14.3—290°K.	de Haas and Gorter, Comm. Leid.
$\text{Cu}(\text{NO}_3)_2 \cdot 9\text{H}_2\text{O}$	1.922	1.955	Melted in water of crystallisation.	Welo (1929)
$\text{CuCl}_2 \cdot 2\text{H}_2\text{O}$	1.932		Temp. —78°C to +74°C.	Birch (1928)
$\text{CuCl}_2$		1.850— 1.827	Aq. soln.; Temp. 0—85°C.; moment varies with conc.	Do.
$\text{CuSO}_4 \cdot 5\text{H}_2\text{O}$	1.974— 1.952		Moment varies with temp. from —183°C to +155°C. probably due to change of water content.	Do.
$\text{CuSO}_4 \cdot 5\text{H}_2\text{O}$	1.943		Temp. —78°C to 0°C.	Do.
$\text{Cu}(\text{NH}_4\text{SO}_4)_2 \cdot 6\text{H}_2\text{O}$	*1.848		Done at room temp. only.	Rabi (1927)
$\text{Cu}(\text{KSO}_4)_2 \cdot 6\text{H}_2\text{O}$	*1.862		Do.	Do.
$\text{Cu}(\text{RbSO}_4)_2 \cdot 6\text{H}_2\text{O}$	*1.871		Do.	Do.
$\text{Cu}(\text{NO}_3)_2$		1.960	Aq. soln.; moment independent of conc. bet. 4.063—358%.	Schaffer and Taylor (1926)
Do.		1.963	With $\text{HNO}_3$ added.	Do.

\* Measurement made with single crystal.



TABLE I (Contd.)

G.T.— $3d^9 \ ^2D^{5/2}$ ; Ion— $\text{Cu}^{++}$ ; Th.  $\mu_{\text{eff}} - \Delta \nu \sim kT = 3.53$ ; Spin only = 1.73.

Experimental $\mu_{\text{eff}}$ at 300°K			Remarks	Author
Salt studied	Powder	Solution or molten		
$\text{CuBr}_2$		1.944— 1.987	Aq. soln.; moment varies with conc. bet. 2.91—0.738%.	Scaffer and Taylor (1926)
Do.		1.858— 1.965	Moment changes with diff. conc. of HBr.	Do.
Do.		1.956	With KCl added.	Do.
Do.		1.958	With KBr added.	Do.
Do.		1.945— 1.961	Moment varies with diff. conc. of $\text{CaBr}_2$ .	Do.
$\text{Cu}(\text{NH}_4\text{SO}_4)_2 \cdot 6\text{H}_2\text{O}$	1.900 *1.930		Temp. $-45^\circ\text{C}$ to $+55^\circ\text{C}$ .	Bartlett (1932)
$\text{Cu}(\text{KSO}_4)_2 \cdot 6\text{H}_2\text{O}$	1.882 *1.902		Do. Do.	Do.
$\text{Cu}(\text{NH}_4\text{SO}_4)_2 \cdot 6\text{H}_2\text{O}$	1.940		Temp. $80^\circ$ — $296^\circ\text{K}$ .	Janes (1935)
$\text{Cu}(\text{KSO}_4)_2 \cdot 6\text{H}_2\text{O}$	1.934		Do. Do.	Do.
$\text{CuSO}_4 \cdot 4\text{NH}_3 \cdot \text{H}_2\text{O}$	1.845		Do. Do.	Do.
$\text{CuSO}_4 \cdot 5\text{H}_2\text{O}$	1.911		Temp. $1.58^\circ$ — $293^\circ\text{K}$ .	Reekie (1939)
$\text{Cu}(\text{NH}_4\text{SO}_4)_2 \cdot 6\text{H}_2\text{O}$	1.929		Do. Do.	Do.
$\text{Cu}(\text{KSO}_4)_2 \cdot 6\text{H}_2\text{O}$	1.919		Do. Do.	Do.
$\text{Cu}(\text{KSO}_4)_2 \cdot 6\text{H}_2\text{O}$	1.942 *1.964		Temp. $1.627^\circ$ — $292.5^\circ\text{K}$ .	Hupse, Leid. Comm

\* Measurement made with single crystal.

## 7. THE EFFECT OF THE VARIATION OF LONG RANGE AND SHORT RANGE CRYSTALLINE FIELDS ON THE MAGNETIC BEHAVIOUR OF THE PARAMAGNETIC IONS OF THE IRON GROUP

We shall now consider in details whether the long range crystalline electric fields, arising from the atoms outside the closest bound ionic cluster, have any appreciable effect on mean effective moments. Let us consider one by one only those salts of the individual ions of the iron group, in which exchange and spin-spin action may be neglected.

(1)  $V^{+4}$ . For this ion the two salts,  $VOSO_4 \cdot 3\frac{1}{2}H_2O$  in the solid state and  $VOCIO_4$  in solutions have practically the same effective moment 1.74 not differing appreciably from the 'spin only' value, and hence presumably the same type of crystalline field independent of the state of aggregation and nature of the salt. It is difficult to say in the absence of X-ray data, whether the field is due to an octahedral or tetrahedral co-ordination of the  $V^{+4}$  ion since an inversion of the Stark-pattern here has very little effect owing to small and positive value of the spin-orbit coupling  $\lambda$ , as already discussed. The probability is, however, for an octahedral type for otherwise the value would have been somewhat higher than the 'spin only' value 1.73, owing to the spin-orbit and H.F. contributions being both positive. But it would be better to obtain fresh data, before deciding one way or the other.

A comparison, with the salt,  $V_2O_2ClO_4 \cdot 5H_2O$  (a liquid at room temperature) with a value of moment equal to 1.52, much lower than the theoretical spin only value of 1.73, evidently owing to the existence of appreciable negative spin-orbit contributions as also strong spin quenching, tends to show that here an octahedral co-ordination about the  $V^{+4}$  ion is also probably present, but with rhombic separation of the lowest lying triplet  $T_2$ , such that  $\lambda^2$  is comparable to  $h\Delta \nu \cdot kT$  unlike the previous two salts in which the fields must be comparatively stronger and asymmetric so as to separate the components of the triplet levels much more. Or again the fields might be uniaxial in this last salt such as to cause one of the levels of the triplet to remain doubly degenerate (Van Vleck, 1939, Siegert, 1936, 1937), so as to give a large negative orbital contribution which by far outweighs the positive high frequency contribution.

(2)  $Ti^{+++}$ ,  $Ti^{++}$ . No data on magnetically diluted salts or solutions available\*.

(3)  $V^{+++}$ . It is interesting to note that in the vanadium alum in which the co-ordination is certainly octahedral and consists of six water molecules, from X-ray data, and hence with triplet  $T_2$ , lowest in the Stark-pattern, the value of

\* Van Vleck mentions the behaviour of the titanium caesium alum in his paper (1939) but does not give any reference. Probably this refers to specific heat data by Simon and others (Hebb and Purcell, 1937) at low temperatures.

moment is 2.733, only a little lower than the spin only value 2.83, owing possibly to a slight preponderance of the negative upper level contribution over the high frequency ones. In  $V_2(SO_4)_3$  solutions the moment is 2.762 indicating the same type of co-ordination to exist here also, and further that the electric field in these two salts are practically independent of the effect of the distant atoms, the increase of about one per cent in the solution is rather dubious, being in the wrong direction. By the way, this strengthens our assumption of an octahedral co-ordination in the first two  $V^{+4}$  salts, and that a non-degenerate rhombic level lies lowest in those salts also, making the effective moments near about the spin only value. In this matter, the salt  $(VO)_2SO_4$  in solutions having a value of the moment 2.83 resembles the said two  $V^{+4}$  salts even more. This is no doubt due to the introduction of a closely bound oxygen into the cluster immediately surrounding vanadium ion, in all these cases, much closer than with any water molecule as in the case of vanadium alum or sulphate, rather than an effect of distant atoms being different.

(4)  $V^{++}$ ,  $Cr^{+++}$ . The only available data on the salt  $V_2SO_4$  in solution shows an actual value 3.83 compared to the spin only value of 3.87, which is not surprising considering that a non-degenerate  $\Gamma_2$ -state lies lowest in its Stark-pattern when the  $V^{++}$  ion is octahedrally co-ordinated in the salt.

Taking the iso-electronic ion  $Cr^{+++}$  in some details, we see that for  $CrCl_3 \cdot 6H_2O$  in solid state and in solution of both the violet and the green varieties, in which the  $Cr^{+++}$  is octahedrally coordinated with different number of chlorine ions and water molecules in the two cases, the moments are about 3.85 in all of them close to the spin only value. This would go to show that here neither a change of the near atoms nor of the distant ones is effective, which is not surprising in view of what has already been mentioned about its Stark-pattern. This is further supported by the fact that for violet  $Cr_2(SO_4)_3 \cdot 16H_2O$  in solid state or in solution and for  $CrK(SO_4)_2 \cdot 12H_2O$  solid, in both of which  $Cr^{+++}$  ion is surrounded by an octahedron of six water molecules, the moment is practically 3.85. In view of the above, much significance cannot be given to the fact that the green variety of the sulphate gives a somewhat lower value of the moment 3.70, or that the alum on melting (Welo, 1929) changes value from 3.959 to 3.778. The low values for the salt  $Cr(NO_3)_3 \cdot 3\frac{1}{2}H_2O$  in solid and molten states, namely, 3.454 and 3.506 (Welo, 1929) respectively, might be due to a change to tetrahedral coordination so that the Stark-pattern has the  $\Gamma_4$  level at the bottom, but these values need checking since the same salt, in solutions of both violet and green varieties, gives a moment of 3.80, by other observers. A small variation in the moment from 4.085 to 3.745 for the nitrate solution, by another observer, may be due to hydrolysis and uncertainties in the composition. Very low value of 3.498 in the basic sulphate  $Cr_2(SO_4)_2 \cdot (HO)_2 \cdot 5H_2O$  is also probably due to a tetrahedral coordination of the  $Cr^{+++}$  ion rather than to any changes in the distant atoms. It is in this connection very satisfactory that the salts  $K_3Cr(SCN)_6 \cdot 4H_2O$  having coordinated members quite different show nearly the same value of the moment 3.783, as the other salts.

(5)  $\text{Cr}^{++}$ ,  $\text{Mn}^{+++}$ . For the salt  $\text{CrCl}_2$  the data are on solution only but the value of the moment is in surprising agreement with that of  $\text{CrSO}_4$  in solution as also the solid salt  $\text{CrSO}_4 \cdot 6\text{H}_2\text{O}$ , the average value about 4.82 being a little lower than the spin only value. The indications in all these cases are for an octahedral coordination (as is borne out by X-ray studies) with little distortion from distant atoms. For the two  $\text{Mn}^{+++}$  salts studied the same type of coordination as above, and hence similar electric field is indicated, which is not apparent *a priori* from the complex nature of the salts. Somewhat lower value, 4.734, in the acetate cannot be explained on the line in which we have proceeded so far, since such a value would indicate larger contribution from upper levels and hence a narrower separation of the levels in the Stark-pattern, which is not in line with other similar acetates of the group (Mookherji, 1946). There is, however, strong reasons to believe that the coordination here tends towards covalency, with 4 and 2 unpaired electrons, respectively for the purely ionic and purely covalent octahedral hexacoordinations. This may lead certainly to a lower value of the moment. In other words, the fields in the acetate are sufficiently strong to affect even the spin moments appreciably, so as to cause a deviation from the 'spin only' value to obtain which orbital moments alone are supposed to be quenched. Apparently on this basis the acetyl acetonate should have mostly ionic bonds, which is perhaps surprising.

(6)  $\text{Mn}^{++}$ ,  $\text{Fe}^{+++}$ . These ions are in  ${}^6\text{S}_{5/2}$ -state so that no orbital contribution to the moments can arise and the mean effective moment should conform to the 'spin only' value to a high order of approximation (Van Vleck and Penny, 1934). This is supported by the general experimental results for the magnetically diluted salts of both  $\text{Mn}^{++}$  and  $\text{Fe}^{+++}$  ions.

In these two ions at ordinary temperature we should not expect the mean effective moment to change appreciably from salt to salt for the same type of coordination of the ion, nor with a change from octahedral to tetrahedral type. But in strong fields of the covalent type there may arise an anti-parallel coupling of some of the spins, leading to much lower values of the moment.

Taking the hydrated salts of  $\text{Mn}^{++}$  many of which are known to contain the  $\text{Mn}^{++}$  ion in an octahedral coordination, we find the mean effective moments for the solid salts  $\text{MnSO}_4 \cdot 4\text{H}_2\text{O}$ ,  $\text{MnSO}_4 \cdot 5\text{H}_2\text{O}$ ,  $\text{Mn}(\text{NH}_4\text{SO}_4)_2 \cdot 6\text{H}_2\text{O}$ ,  $\text{Mn}_2\text{P}_2\text{O}_7$ , and  $\text{MnSO}_4$ ,  $\text{MnCl}_2$  and  $\text{Mn}(\text{NO}_3)_2$  in aqueous solutions of different concentrations, have the values 5.859, 5.908, 5.905, 5.846, 5.934, 5.91 and 5.934 respectively. The maximum difference is about 1.3% and cannot mean much, though it is tempting to ascribe the closer agreement with 'spin only' value in all the solutions than in the solid salts, to a comparatively weaker and more symmetric field in solution than in the solid state. However, the systematically lower values in the solid salts are perhaps more an effect of changes in the constituents of the nearest cluster and their comparatively closer bonds and higher asymmetries, than an effect of the distant atoms. For the same reason in the organic salts of  $\text{Mn}^{++}$  such as the acetate, formate, lactate, and oxalate, the values of the moments (about 5.71 for all the compounds) are also somewhat lower even than the above-mentioned salts.

For the ferric salts, the data for the aqueous solutions are much complicated by their strong tendency for hydrolysis, and depend on concentration. But when this is avoided, say, by the addition of acid or taking an alcoholic solution, the moments for the different salts agree very closely with each other and the 'spin only' value. For example, the limiting values for the effective moments for the aqueous solution for  $\text{FeCl}_3$ ,  $\text{Fe}_2(\text{SO}_4)_3$ ,  $\text{Fe}(\text{NO}_3)_3$ , and  $\text{FeCl}_3 \cdot 2\text{NH}_4\text{Cl}$ ,  $\text{H}_2\text{O}$ , and  $\text{FeCl}_3$  in ethyl alcohol, are 5.952, 5.86, 5.941, 5.944, 5.914 respectively.  $\text{Fe}_2(\text{P}_2\text{O}_7)_3$  solution has the abnormally low value 5.05 no doubt due to hydrolysis. For the solid hydrated salts,  $\text{FeNH}_4(\text{SO}_4)_2 \cdot 12\text{H}_2\text{O}$ ,  $\text{FeCl}_3 \cdot 6\text{H}_2\text{O}$ ,  $\text{Fe}(\text{NO}_3)_3 \cdot 9\text{H}_2\text{O}$  and the organic salts ferric acetyl acetone and potassium ferric oxalate trihydrate the mean moments are 5.90, 5.92, 5.89, 5.936, 5.924 agreeing closely to the 'spin only' value and differing little amongst each other or the values in solution; indicating no changes in the electric fields either near or distant. The moments appear to be appreciably different, in the molten state of the three inorganic  $\text{Fe}^{+++}$  salts mentioned above, values being 5.758, 5.869 and 5.626 respectively. But the values are by Welo (loc. cit.) as in the previous case of some  $\text{Cr}^{+++}$  salts and too much significance need not be placed upon them. The solid salt  $\text{FeCl}_3 \cdot 2\text{NH}_4\text{Cl} \cdot \text{H}_2\text{O}$  contrasted with its solution presents a rather low value of 5.617 which cannot be explained except as due to an uncertainty in composition which is very probable.

(7) In the octahedrally coordinated salts of  $\text{Fe}^{++}$  large orbital contributions as well as spin quenchings are present since in the Stark-pattern the triplet  $T_2$  is the lowest and these ought to be largely affected by the long range fields. The two hydrated solid salts  $\text{FeSO}_4 \cdot 7\text{H}_2\text{O}$  and  $\text{Fe}(\text{NH}_4\text{SO}_4)_2 \cdot 6\text{H}_2\text{O}$  studied experimentally, have both an octahedral grouping of six water molecules about the  $\text{Fe}^{++}$  ion, though the distant neighbours of  $\text{Fe}^{++}$  are somewhat different in the two. The mean effective moments for the solid salts are 5.257 and 5.472 and their aqueous solutions in different concentration are 5.341 and 5.465 and are remarkably constant, considering the strong tendency of these salts and their solutions to oxidise in air. Thus, the effect of the long range fields direct or indirect (even if we take this as represented by the above small variation in the moments) are at any rate not comparable to the effect of the electric fields due to the nearest cluster as will be seen by a comparison of these values with the 'free ion' and the 'spin only' values. This is rather disappointing since  $\text{Fe}^{++}$  ion is certainly a good test case for verifying Van Vleck's (1939) estimation of the effect of long range fields, nearly as much as those of the short range ones.

(8)  $\text{Co}^{++}$ . The case of the cobalt salts is analogous to those of  $\text{Fe}^{++}$ , since here also a triplet  $T_4$  lies lowest in the Stark-pattern when the  $\text{Co}^{++}$  ion is octahedrally coordinated and hence the effective moments should be much affected by the long range fields. The case is a better test of the action of distant atoms than  $\text{Fe}^{++}$  since, though a two-fold Kramers' spin degeneracy in  $\text{Co}^{++}$  ion renders the spins more free than in  $\text{Fe}^{++}$  the orbital contributions are even higher. Also the salts of  $\text{Co}^{++}$  are some of the most investigated amongst the iron group of elements so that we can be more definite about our conclusions. However,

here a complication may arise, especially in the state of solution, due to a tendency of the  $\text{Co}^{++}$  ions to form tetrahedral complexes, the effects of the consequent inversion of the Stark-pattern being very marked.

Taking the series of hydrated sulphate and double sulphates of  $\text{Co}^{++}$  ion which is known to be surrounded by an octahedron of water molecules in all these salts, we find that the average value of the mean effective moments by different workers for the solid salts  $\text{CoSO}_4 \cdot 7\text{H}_2\text{O}$ ,  $\text{Co}(\text{NH}_4\text{SO}_4)_2 \cdot 6\text{H}_2\text{O}$ ,  $\text{Co}(\text{KSO}_4)_2 \cdot 6\text{H}_2\text{O}$ ,  $\text{Co}(\text{RbSO}_4)_2 \cdot 6\text{H}_2\text{O}$  are 4.829, 4.903, 4.961, 5.036 respectively, indicating an appreciable weakening tendency of the effects of the long range fields as we pass along the series, which may be expected in view of the increasing interatomic distances and symmetry in this series, though the exact sequence may not be very strictly valid. For  $\text{CoCl}_2 \cdot 6\text{H}_2\text{O}$  and  $\text{Co}(\text{NO}_3)_2 \cdot 6\text{H}_2\text{O}$  the mean moments are respectively 4.856 and 4.888, which means that  $\text{Co}^{++}$  being surrounded by six water molecules in both cases, the comparatively larger quenching effects here than in the double sulphates is due to the distant atoms but is somewhat less than in the heptahydrated sulphate. It is further found that the moments of the chloride and the nitrate on melting in their water of crystallisation rise to 5.024 and 4.975 respectively, evidently due to the breaking down of the lattice and consequent weakening of the effects of the distant atoms. This is further shown by the results on aqueous solutions of the sulphate, chloride and nitrate in all of which the moments, as observed by some workers, vary between 4.663—5.230 for the chloride and 4.845—5.048 for the sulphate and the nitrate. The higher limits are no doubt the correct values for the octahedrally coordinated red cobalt salts in solution, which tend to pass over to the tetrahedrally coordinated blue variety at higher dilutions and temperatures, with a moment much closer to the 'spin only' value as mentioned earlier. This fact is definitely indicated (1) in solutions of  $\text{CoCl}_2$  in ethyl alcohol, amyl alcohol or pyridine where the moments fall to 3.836 (spin only value = 3.37) at high temperatures and high dilutions while colour changes from wine red to sapphire blue, as also (2) by a constant high value of the moment of about 4.96 in aqueous solutions under certain circumstances\* observed by some workers. In methanol solution of  $\text{CoCl}_2$ , however, the variations are very little and the moment is approximately 4.82 much closer to the value in aqueous solutions.

It is very satisfactory that even for the complex salts  $\text{K}_2\text{Co}(\text{SCN})_4 \cdot 4\text{H}_2\text{O}$  and  $\text{CoCl}_2 \cdot 6\text{NH}_3$  the moments are respectively 4.974, and 5.090 which indicates the same type of octahedral coordination here as in the other cobalt salts. It is however, difficult to understand why  $\text{CoSO}_4 \cdot 6\text{NH}_3$  similarly composed as the aminochloride should have such a large value as 5.916, so much higher even than the normal salts of cobalt (unless the fields are very small). On the other hand, the abnormally low value even lower than the 'spin only' value of the moment, namely 3.225 for  $\text{Co}(\text{CN})_2 \cdot 2\text{H}_2\text{O}$  is evidently a result of very strong covalent type of field due to the nearest cluster, for which cyanides are noted, causing quenching of orbital moments as also some of the spins.

\* This depends apparently on mode of preparation, aging and previous treatment of the salt and its solution.

(9)  $\text{Ni}^{++}$ . Here as in the  $\text{Cr}^{+++}$  ion an orbitally non-degenerate level  $T_2$ , being the lowest in the Stark-pattern, under an electric field arising from an octahedrally coordinated  $\text{Ni}^{++}$  ion, we should have expected very little deviation from the spin only value of the moment, but owing to large spin-orbit coupling constant about  $-335 \text{ cm}^{-1}$ , unlike  $\text{Cr}^{+++}$  we have fairly large orbital contributions from the upper levels which should be affected by the distant atoms and their changes.

On a perusal of the data on effective moments of the salts of  $\text{Ni}^{++}$ , for example, the series  $\text{NiSO}_4 \cdot \text{H}_2\text{O}$ ,  $\text{NiSO}_4 \cdot 4\text{H}_2\text{O}$ ,  $\text{NiSO}_4 \cdot 6\text{H}_2\text{O}$ ,  $\text{NiSO}_4 \cdot 7\text{H}_2\text{O}$ ,  $\text{Ni}(\text{KSO}_4)_2 \cdot 6\text{H}_2\text{O}$ ,  $\text{Ni}(\text{NH}_4\text{SO}_4)_2 \cdot 6\text{H}_2\text{O}$ , and  $\text{Ni}(\text{RbSO}_4)_2 \cdot 6\text{H}_2\text{O}$  the moments are found to be 3.245, 3.283, 3.218, 3.266, 3.089, 3.240 and 3.115 respectively. The hexa- and hepta-hydrated sulphates as also the Tutton salts are known to have octahedral coordination of six water molecules with the  $\text{Ni}^{++}$  ion and the close agreement of their moments with those for the mono and tetra hydrated sulphates show that the coordination in these latter must also be the same except that in these latter some of the water molecules are most probably replaced by  $\text{SO}_4^{--}$  ions. Thus the short and long range fields in them should be more asymmetric than in the hexahydrated sulphate at least, where they have a tetragonal symmetry. The short and the long range fields are both more symmetric in  $\text{NiSO}_4 \cdot 6\text{H}_2\text{O}$  than in the Tutton salts. The long range fields should be weaker as we pass along the Tutton series. The variation in the moments from salt to salt are, however, not sufficiently pronounced or systematic to bring us to any definite conclusion and though a general tendency of the moment to rise with the increasing asymmetry or strength of the field is observed, this is contrary to our expectation in  $\text{Ni}^{++}$  and previous experience in  $\text{Co}^{++}$  salts, and cannot be explained except as being fortuitous.

The above conclusion is further supported by the salts  $\text{NiCl}_2 \cdot 6\text{H}_2\text{O}$ , and  $\text{Ni}(\text{NO}_3)_2 \cdot 6\text{H}_2\text{O}$ , both having octahedra of six water molecules about  $\text{Ni}^{++}$  ion but the distant atoms somewhat different, in which the moments are nearly the same namely, 3.218 and 3.192 and are also very close to the value for the hexahydrated sulphate. This indicates practically the same long range effect with  $\text{SO}_4^{--}$ ,  $\text{Cl}^-$ , and  $(\text{NO}_3)^-$  ions. The values of the moments in  $\text{Ni}(\text{KSO}_4)_2 \cdot 7\text{H}_2\text{O}$ ,  $\text{NiSO}_4 \cdot 4\text{NH}_3 \cdot 2\text{H}_2\text{O}$  and  $\text{NiNO}_2 \cdot 4\text{NH}_3$  are 3.307, 3.259 and 3.123 respectively supporting the same conclusions as before, the small changes being probably, more due to changes in the nearest cluster than the distant atoms.

The aqueous solutions of  $\text{NiCl}_2$ ,  $\text{NiBr}_2$ ,  $\text{NiSO}_4$ ,  $\text{Ni}(\text{NO}_3)_2$  and  $\text{Ni}(\text{KCN})_2$  all show more or less the same moment namely, 3.245, 3.250, 3.236, 3.236 and 3.220 respectively, remarkably independent of concentrations and temperatures, which shows a definite stabilisation of an octahedral coordination of the  $\text{Ni}^{++}$  ion with six water molecules in the solution state, giving an electric field of practically the same type and value as in the hexahydrated salts mentioned above and thus showing the absence of the effects of distant atoms on the  $\text{Ni}^{++}$  ion. It is particularly interesting to note this stabilisation effect even in the double cyanide

*solution* above, since in the *solid* cyanide salts  $\text{Ni}(\text{CN})_2 \cdot 2\text{H}_2\text{O}$  and  $\text{Ni}(\text{CN})_2 \cdot \text{C}_6\text{H}_6\text{NH}_3$ , the moments are 2.714 and 2.278 much lower even than the 'spin only value, owing to strong covalent type of fields, quenching partially even the spins. It is further interesting to note in this connection that the addition of substances such as  $\text{K}_2\text{C}_2\text{O}_4$ ,  $\text{NH}_4\text{OH}$ ,  $\text{CH}_3\text{NH}_2$  and even  $\text{KCN}$  to aqueous solutions of  $\text{NiCl}_2$  changes the moment but slightly (from 3.096 to 3.336), but the addition of  $\text{KCN}$  and  $\text{NH}_3$  causes a violent change in the value of the moment between 2.967 to 1.773 depending on concentration of the added substances. A large number of organic and other salts of  $\text{Ni}^{++}$  have been studied, the value of the moments showing the same type of electric fields in them as the sulphates and others, but it is not possible to draw conclusions from them regarding the variations in short and long range fields in the absence of structural data.

(10)  $\text{Cu}^{++}$ . The  $\text{Cu}^{++}$  ion behaves in some respects like the  $\text{Ni}^{++}$  ion, since here also, inspite of the non-magnetic doublet  $T_3$  lying lowest in the Stark-pattern for the usual type of electric fields, we have fairly large spin orbit contributions from the upper levels which might be affected by the long range fields. Here again the differences in the experimental results of different observers make it difficult to come to a definite conclusion. Taking for example Rabi's data on the Tutton salts we find that ammonium, potassium, and the rubidium salts give moments 1.848, 1.862 and 1.871 respectively, showing perhaps a slight increase in the right direction but the absolute values are certainly too low as shown by the data by other workers. For the series  $\text{CuSO}_4 \cdot \text{H}_2\text{O}$ ,  $\text{CuSO}_4 \cdot 5\text{H}_2\text{O}$ ,  $\text{Cu}(\text{NH}_4\text{SO}_4)_2 \cdot 6\text{H}_2\text{O}$  and  $\text{Cu}(\text{KSO}_4)_2 \cdot 6\text{H}_2\text{O}$ , (the values being the average of workers other than Rabi) the moments are 1.963, 1.924, 1.925, 1.924 respectively which are practically the same, except the first in which the water content is not certain. This shows that even in the triclinic crystal  $\text{CuSO}_4 \cdot 5\text{H}_2\text{O}$ , in which the octahedral cluster contains two  $\text{SO}_4^{--}$  ions unlike as in the Tutton salts, the electric field is the same as in the other salts. That the effect of changes either of the near or the distant atoms is negligible, is further shown by the value of the moment 1.921 for  $\text{CuSO}_4$  in aqueous solution, where most probably  $\text{Cu}^{++}$  is surrounded by an octahedron of water molecule alone.

The salt  $\text{Cu}(\text{NO}_3)_2 \cdot 9\text{H}_2\text{O}$  which has an water octahedron about its  $\text{Cu}^{++}$  ion gives a moment 1.922 in the solid state, the same as the previous salts and, shows but a slight increase to 1.955 when melted (Welo *loc. cit.*) and to 1.963 in solution, which much significance cannot be attached.

In  $\text{CuCl}_2 \cdot 2\text{H}_2\text{O}$  which is said to be a square quadricovalent compound of  $\text{Cu}^{++}$  ion with two  $\text{H}_2\text{O}$  and two  $\text{Cl}^-$  ions (Pauling, *loc. cit.*) the fields should be even more asymmetric and stronger than in the aforementioned salts, but the moment 1.932 does not bear any appreciable trace of such a different field. The aqueous solutions of the same salt in which  $\text{Cu}^{++}$  ion is no doubt surrounded by six water molecules give practically the same moment 1.921.

The solution of  $\text{CuBr}_2$  also gives nearly the same moment of about 1.961. In the salt  $\text{CuSO}_4 \cdot 4\text{NH}_3 \cdot \text{H}_2\text{O}$  the moment 1.845 is no doubt a little lower than



the others, but this is rather due to the more asymmetric and stronger type of binding between the  $\text{Cu}^{++}$  ion and its immediate neighbours, than a change in the distant atoms.

In conclusion, we may say that from the above discussions of the mean effective moments of the various salts and their solutions no reliable evidence is available for the existence at room temperatures, of any appreciable effect of the long range electric fields on the magnetic behaviour of the ions of the iron group except perhaps in such cases as  $\text{V}^{++}$  and  $\text{Fe}^{++}$  and more certainly in  $\text{Co}^{++}$ , in all of which the orbital contributions to the moments are large. In the cases where orbital contributions are small or negligible, the effect of the long range fields on the spin moments alone, need be considered. But then, even the short range field splitting of the spin levels is a very small effect and are scarcely observable, specially when mean moments are concerned at room temperatures. Probably the temperature variation values of mean moments would be more sensitive to variations of long range fields, which will be considered in the next two parts of the paper. No doubt for comparing the short and long range fields it would be even better to study the magnetic anisotropy and the temperature variations of the principal moments in crystalline salts, especially in the region of very low temperatures. This will be discussed in a future paper. For this reason we have intentionally refrained from giving the large amount of very systematic experimental results on the anisotropies of crystals done by Krishnam, *et al* (1932—1949), at this place.

#### ACKNOWLEDGMENTS

Our grateful thanks go to Prof. K. Banerjee, D.Sc., and Mr. R. K. Sen, M.Sc. in helping to elucidate the X-ray structural considerations of the crystalline electric fields, by frequent most valuable discussions and to Prof. A. Mookherji, D.Sc. for constructive criticism. One of us is thankful to the authorities, Indian Association for the Cultivation of Science for the grant of a scholarship during his work in this laboratory.

#### REFERENCES

- Abraham, A. and Pryce, M. H. L., 1951, *Proc. Roy. Soc.*, **206**, 164, 173.  
 Banerjee, S., 1938, *Zeits. f. Krist. (A)*, **100**, 316.  
 Beever, C. A. and Lipson, H. L., 1932, *Zeits. f. Krist.*, **38**, 123.  
 " " " " 1934, *Proc. Roy. Soc.*, **146**, 570.  
 " " " " 1935, *Ibid*, **148**, 664.  
 Beever, C. A. and Schwartz, 1935, *Zeit. f. Krist.*, **91**, 157.  
 Bethe, H., 1929, *Ann der Phys.*, **3**, 133.  
 Bose, A., 1948, *Ind. J. Phys.*, **22**, 74, 195, 226, 483.  
 Bose, D. M. and Mukherjee, P. C., 1938, *Phil. Mag.*, **26**, 757.  
 " " " " 1938, *Ind. Phys.*, **13**, 219.  
 Chinchalkar, S. W., 1935, *Phil. Mag.*, **20**, 856.  
 Chrobak, L., 1934, *Zeits. f. Phys.*, **88**, 35.

- Freed, S. and others, 1938, *J. Chem. Phys.* **6**, 297 and 654.  
 Gorter, C. J., 1932, *Phys. Rev.*, **42**, 437.  
 de Haas and Schultz, B. H., 1939, *Leid. Comm.* **256d**.  
 „ and Koolhaas, J., 1940, *Ibid.*, **259a**.  
 Haenny, C., 1931, *C. R.*, **193**, 931.  
 „ „ 1932, *Ibid.*, **195**, 219.  
 Hebb, M. H. and Purcell, E. M., 1937, *J. Chem. Phys.*, **5**, 338.  
 Hendricks, S. B. and Dickinsons, R. G., 1927, *J. Amer. Chem. Soc.*, **49**, 2149.  
 Hofmann, W., 1931, *Zeits. f. Krist.* **78**, 279.  
 Howard, J. B., 1935, *J. Chem. Phys.*, **3**, 813.  
 Jahn, H. A., 1938, *Proc. Roy. Soc.*, **164**, 117.  
 Jahn, H. A. and Teller, E., 1937, *Ibid.*, **161**, 220.  
 Jordahl, O. M., 1934, *Phys. Rev.*, **45**, 87.  
 Kramers, H., 1929, *Proc. Amst. Acad.*, **32**, 1176.  
 Krishnan, K. S. and Banerjee, S., 1933, *Phil. Trans. Roy. Soc.*, **231**, 235.  
 „ „ „ „ 1935, *Ibid.*, **234**, 265.  
 Krishnan, K. S. and Mookherji, A., 1936, *Phys. Rev.*, **50**, 860.  
 „ „ and „ 1938, *Ibid.* **54**, 533 and 841.  
 „ „ and „ 1938, *Phil. Trans. Roy. Soc.*, **237**, 135.  
 Laporte, O., 1928 *Zeits. f. Phys.* **47**, 761.  
 Lonsdale K. and Krishnan, K. S., 1936, *Proc. Roy. Soc.*, **156**, 597.  
 Mookherji, A., 1945 *Ind. Jour. Phys.* **19**, 63.  
 „ „ 1946, *Ibid.*, **20**, 9.  
 „ „ 1949, *Ibid.*, **23**, 217, 309, 410, 445.  
 Mookherji, A. and Tin, M. T., 1939, *Zeits. f. Krist. A*, **101**, 412.  
 Penney, W. G. and Schlapp, R., 1932, *Phys. Rev.* **41**, 194, **42**, 666.  
 Siegert, A., 1936, *Physica*, **3**, 85.  
 „ „ 1937, *Ibid.*, **4**, 138, 871.  
 Simon, F., 1936, 1937, *C. R.*, **202**, **204**, 1576, 675, 754.  
 Spedding, F. H. and others, 1937, *J. Chem. Phys.*, **5**, 191, 316, 416.  
 „ „ „ 1938, *Ibid.*, **6**, 297.  
 Starr, C., 1940, *Phys. Rev.*, **58**, 977 and 984.  
 Stoner, E. C., 1934, *Magnetism and Matter* (Methuen).  
 Van Vleck, J. H., 1932, *Theory of Electric and Magnetic Susceptibilities* (Oxford).  
 „ „ 1932, *Phys. Rev.* **41**, 208.  
 „ „ 1935, *J. Chem. Phys.* **3**, 803.  
 „ „ 1937, *Ibid.*, **5**, 320.  
 „ „ 1939, *Ibid.*, **7**, 61, 62.  
 Van Vleck, J. H. and Penney, W. G., 1934, *Phil. Mag.*, **17**, 961.  
 Welo, L. A., 1929, *Nature*, **124**, 575.  
 Wyckoff, W. C., 1931, *The Structure of Crystals*.  
 „ „ 1935, *Ibid.*

# TERM VALUES OF $f^4$ -ELECTRON CONFIGURATION A CORRECTION

By K. SURYANARAYANA RAO

PHYSICS DEPARTMENT, ANDHRA UNIVERSITY, WALT AIR

(Received for publication, April 27, 1952)

In our calculations (Rao, 1950) of the term values of the  $f^4$ -electron configuration by Slater's classical method, an error has crept in, in reading Condon's tables for  $a^k$ 's and  $b^k$ 's for  $f$  electrons. The denominator is used only for the particular combination against which it is given whereas it is common to all the others also. Since in these calculations Condon and Shortley's  $F_k$ 's are used instead of Slater's  $F^k$ 's where  $F_k = F^k/D_k$  this common denominator can be cancelled for convenience.

This error has been recently pointed out by Racah (1952); a recalculation of the values has been done with this correction and the corrected values are given in the following table. The correct values are obtained by merely cancelling the common denominator in our previous values.

TABLE I

Term	Value
$^6I$	$^6F_0 - 95F_2 - 240F_4 - 1079F_6$
$^6G$	$^6F_0 - 40F_2 - 174F_4 - 2080F_6$
$^6F$	$^6F_0 - 60F_2 - 198F_4 - 1716F_6$
$^5D$	$^6F_0 - 5F_2 - 132F_4 - 2717F_6$
$^5S$	$^6F_0 - 60F_2 - 198F_4 - 1716F_6$
$^3M$	$^6F_0 - 55F_2 - 150F_4 - 211F_6$
$^3L$	$^6F_0 - 70F_2 - 105F_4 - 316F_6$
$(^3K)$	$^6F_0 - 43F_2 - 119.5F_4 - 526F_6$
$(^3I)$	$^6F_0 - 15F_2 - 81F_4 - 1065F_6$
$(^3H)$	$^6F_0 - 11F_2 - 51F_4 - 711.5F_6$
$(^3G)$	$^6F_0 - 22F_2 - 69.33F_4 - 1058F_6$
$(^3F)$	$^6F_0 - 11F_2 - 70.25F_4 - 596F_6$
$(^3D)$	$^6F_0 - 3F_2 - 85.5F_4 - 1170F_6$
$(^3P)$	$^6F_0 + 6.33F_2 - 9.66F_4 - 957.66F_6$
$^1N$	$^6F_0 - 25F_2 - 86F_4 - F_6$
$(^1L)$	$^6F_0 - 43F_2 - 70.5F_4 + 104F_6$
$^1K$	$^6F_0 - 46F_2 - 23F_4 + 148F_6$
$(^1I)$	$^6F_0 + 0.33F_2 + 29F_4 - 192.33F_6$
$(^1H)$	$^6F_0 + 22F_2 - 83.5F_4 - 71F_6$
$(^1G)$	$^6F_0 + 5F_2 - 20.25F_4 - 379F_6$
$^1F$	$^6F_0 + 8F_2 + 74F_4 - 1324F_6$
$(^1D)$	$^6F_0 + 17F_2 + 22.5F_4 - 536.5F_6$
$(^1S)$	$^6F_0 + 110F_2 + 111F_4 + 104F_6$

## REFERENCES

- Racah, G., 1952, *Curr. Sci.*, **21**, 67.  
Rao, K. S., 1950, *Ind. J. Phys.*, **24**, 51.



# THE COMPLEX BAND SPECTRUM OF NICKEL BROMIDE (NiBr) \*

By V. G. KRISHNAMURTY

PHYSICS DEPARTMENT, ANDHRA UNIVERSITY, WALTAIR

(Received for Publication, April 16, 1952)

## Plates XV A-D

**ABSTRACT.** The band spectrum of the diatomic molecule NiBr extending from  $\lambda$  3900 to 5000 Å has been obtained in emission using a heavy current discharge from a 2 K.W., D.C. generator. The bands are line like and are slightly degraded to the red. As in NiCl, two electronic transitions of the type  ${}^4\Pi - {}^4\Sigma$  designated as  $\alpha$  and  $\beta$  have been identified with a common ground state of vibrational frequency  $\omega_e = 313$ . The wavenumbers of the  $Q$  heads  $\epsilon_s$  obtained in the (0,0) sequences of the two systems are:

System	$Q_4$	$Q_3$	$Q_2$	$Q_1$
$\alpha$	24017.9	23906.4	23789.2	23658.1
$\beta$	22688.6	22581.5	22461.6	22341.9

Another system is also identified and designated as  $\gamma$ . The vibrational formula for the heads of this system is

$$\nu = 21790.7 + 294.9 u' - 0.80 u'^2 - 317.2 u'' + 0.50 u''^2$$

Besides these three systems, some other systems have also been observed

In a previous paper, the structure of the band spectrum of the diatomic molecule NiCl extending from  $\lambda$  4900 to 3800 Å has been discussed. The analysis indicates division of the band groups into 5 systems designated as A, B, C, D, and E, involving doublet and quartet molecular electronic states. Systems A and B are shown as  ${}^1\Pi - {}^4\Sigma$  transitions with a common ground state while C and D are considered as corresponding to two different transitions of the type  ${}^2\Sigma - {}^2\Sigma$  and system E as an intercombination,  ${}^2\Pi - {}^4\Sigma$ .

Following the above investigation, the study of the band spectra of the other halides of nickel has been undertaken in order to establish similar quartet transitions, since these halides may be expected to emit spectra having identical structure and electronic transitions. The present paper describes the spectrum of nickel bromide.

The previous work on this spectrum consists of that published by Mesnage (1939) as part of his general study of the high frequency discharges through the vapours of the halides of a number of elements. In nickel bromide Mesnage reported altogether 36 bands in the region  $\lambda$  5000 to 3900 Å. The bands were divided into three systems named A, B, and C of which the system C was mentioned to be the strongest and most developed. For convenience of reference, Mesnage's classifications are given in Tables I(a, b and c).

\* Communicated by Prof. K. R. Rao.

TABLE I(a)  
System A

25438 (5)		
324		
25114 (2)	N	
319		
24795 (2), 273	25058 (4)	N
	307	
	24751 (5)	N
		N

TABLE I(b)  
System B

23952 (2)				
326				
23626 (4)	241	23867 (1)		
311		319		
23315 (2)	233	23548 (3)	239	23787 (3)
293		291		307
23022 (1)	235	23257 (3)	223	23480 (4)
		297		
		22960 (4)		
		277		
		22683 (c)		

TABLE I(c)  
System C

$v''$ ↓	$v' \rightarrow 0$	1	2	3	4
0	21779 (10)				
	324				
1	21455 (5)	286	21741 (7)	271	22012 (4)
		309			300
		21432 (1)	280	21712 (5)	
				300	
3				21412 (5)	
				286	
4				21126 (2)	257 21383 (2)
				285	285
5				20841 (2)	257 21098 (1)
6					21073 (4)

Eight other bands were left unassigned. From these three systems, Mesnage deduced a ground state frequency  $\omega'' = 334 \text{ cm}^{-1}$  and an anharmonic constant  $x''\omega'' = 5$ .

An overall reproduction of the bands, as obtained in the present work when the system is excited in emission in a heavy current D.C. discharge, is shown in Plate XV A; the method of excitation is described in detail elsewhere (Krishnamurty, 1952). It is at once obvious that the spectrum is very much richer than that described by Mesnage. About 245 band heads have been measured in this region from  $\lambda$  3800 to 5000 Å. The intensity distribution, the appearance, and the general structure of the bands are such that they cannot all be assumed to be those associated with the usual transitions between electronic states of low multiplicities. For clarity, the spectrum is reproduced in Plates XV B and C much enlarged and in three different strips named *a*, *b* and *c*. Strip *a* contains Mesnage's system *A* with its 5 band heads marked therein. In strip *b* all the heads of Mesnage's system *B* are indicated together with 3 bands in this region which are unassigned; similarly strip *c* shows Mesnage's system *C* and the remaining unassigned bands.

There is a clear indication that quite a large number of band heads lie unassigned in each of the regions of Mesnage's systems; several of these have not been measured by him. The analysis shown in Table I does not admit the inclusion of these new bands into the vibrational structure as represented by him. This is particularly evident from strip *b* showing Mesnage's system *B* where several distinct bands are left unassigned and unmeasured. The two bands at  $22960$  and  $22683 \text{ cm}^{-1}$  do not seem to be consistently included in the scheme. On the other hand, a comparison of

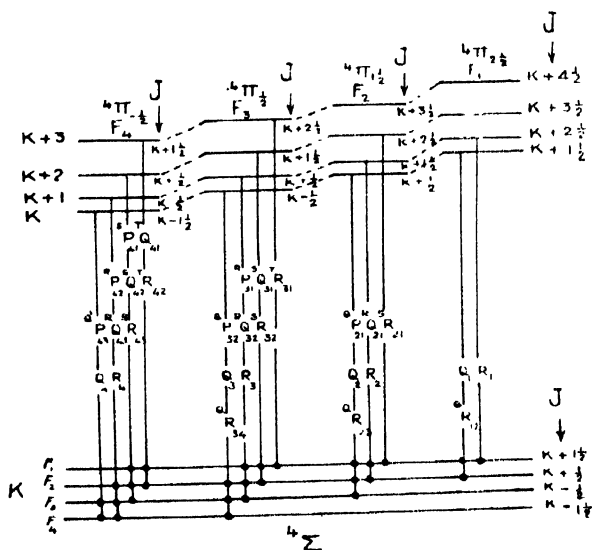


FIG. 1

Scheme of transitions in a  $4\Pi(a) - 4\Sigma(B' > B)$ .

the spectrum with that of nickel chloride reproduced in a previous paper (Krishnamurty, 1952a) shows a great resemblance in general appearance. Each consists of a large number of very close groups, each group giving the appearance of a close sequence. The intensity distribution among the groups in both the spectra is such that the groups cannot be considered as belonging to a single system. Different and probably overlapping systems must be assumed. Hence an analysis of the NiBr bands on the lines followed in the case of NiCl has been attempted. This has resulted in identifying among the stronger band groups, two systems designated as  $\alpha$  and  $\beta$  corresponding to the transition  ${}^4\Pi - {}^4\Sigma$ . The justification for the analysis is (1) the assignment of almost all the measured band heads, (2) in the close correspondence between the observed structure and that predictable in the case of  ${}^4\Pi - {}^4\Sigma$  transition and (3) its similarity with NiCl systems. The characteristics of transition  ${}^4\Pi - {}^4\Sigma$  are already indicated briefly in the author's previous paper. For red degraded bands ( $\omega_e'' > \omega_e'$ ), we expect only the T, S, R and Q forms as head forming. A schematic diagram for this transition representing the various observable branches is given in figure 1.

In figure 2 the expected heads in the (0,0) and (1,1) bands for this transition are shown compared to the observed structure in the  $\alpha$  system drawn on an arbitrary scale of frequencies. The correspondence between them is seen clearly.

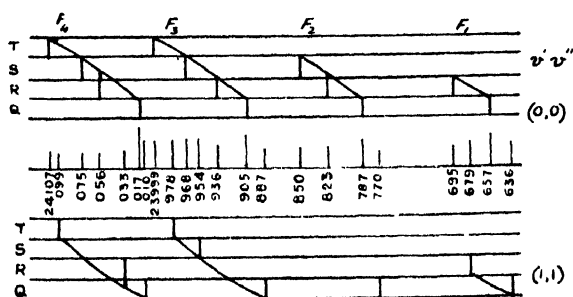


FIG. 2

Structure of (0, 0) and (0, 1) bands of  $\alpha$  system.

Band heads belonging to 1,1 group occur in the region of 0,0 group and many of these have been detected.

$\alpha$  System. This is found to extend from  $\nu$  24695 to 2 3020  $\text{cm}^{-1}$  which is partly the region of Mesnage's system B; five sequences (2,0), (1,0), (0,0), (0,1) and (0,2) have been detected. Details of the classification are given in Table VI at the end. The wavenumbers of the Q heads as obtained in the (0,1), (0,0) and (1,0) sequences of system  $\alpha$  are given in Table II which also shows the values of the vibrational constants as calculated from the Q head separations.



TABLE II

Vibrational differences in the  $Q$  heads

$v', v''$	$Q_1$	$Q_2$	$Q_2$	$Q_1$
$0, 0$	24017.9	111.5 23906.4	117.2 23789.2	131.1 23658.1
$0, 1$	23709.1	101.9 23607.2	130.4 23476.8	134.8 23242.0
$\omega_e''$	308.8		312.4	316.1
$1, 0$	24311.1	114.2 24196.9	121.8 24075.1	120.5 23954.6
$0, 0$	24017.9	23906.4	23789.2	23658.1
$\omega_e'$	293.2	290.5	285.9	296.5

The mean values of the vibrational constants obtained for this electronic transition are  $\omega_e' = 292$  and  $\omega_e'' = 312$ .

Table III gives the scheme of interval in the  $0,0$  group.

TABLE III

Differences between wavenumbers of  $(0,0)$  bands.

$\Delta K$	$^4\Pi_{1/2}$	$^4\Pi_{1/2}$	$^4\Pi_{1/2}$	$^4\Pi_{21/2}$
$T$		105.5		
$S$	19.1	25.4	108.4	
$R$	30.2	31.2	38.5	140.6
$Q$	35.5	36.9	43.0	22.9
	114.2	107.3	135.0	

**$\beta$  System.**—This system appears in continuation of system  $\alpha$  and extends from  $\nu$  23364 to 22029  $\text{cm}^{-1}$ . Four sequences are clearly observed,  $(0,0)$  being the most intense. Wavenumber data and analysis are contained in Table VI at the end.

The wavenumbers of the  $Q$  heads as obtained in the  $(0,1)$ ,  $(0,0)$  and  $(1,0)$  sequences of this system are given in Table IV which also shows the values of the vibrational constants as calculated from the  $Q$  head separations.

TABLE IV

Vibrational differences in the Q heads.

$\nu', \nu''$	$Q_1$	$Q_3$	$Q_2$	$Q_1$
$0, 0$	22688.6	107.1 22581.5	119.9 133.2	119.7 22341.9
$0, 1$	22374.1	97.2 22276.9	22461.6 22143.7	114.7 22020.0
$\omega_e''$	314.5	304.6	317.9	312.9
$1, 0$	22979.0	111.5 22867.5	110.3 22757.2	122.7 22634.5
$0, 0$	22688.6	22581.5	22461.6	22341.9
$\omega_e'$	290.4	286.0	285.6	292.6

The mean values of the vibrational constants obtained for this electronic transition are  $\omega_e' = 289$  and  $\omega_e'' = 313$ .

Table V gives the scheme of intervals in the  $0,0$  group.

TABLE V

Differences between wavenumbers of  $(0,0)$  bands.

$\Delta K$	${}^4\Pi_{-1/2}$	${}^4\Pi_{1/2}$	${}^4\Pi_{1/2}$	${}^4\Pi_{3/2}$
T				
S	19.5	117.3	14.0	128.0
R	30.1	111.8	30.4	114.3
Q	38.5	112.1	33.5	124.6
		107.1	119.9	119.7
				32.2

The lower state frequencies for the two systems  $\alpha$  and  $\beta$  may be regarded as equal, being 312 and 313 respectively but the upper state constants are different indicating a common ground state but different upper states.

Comparing the analysis obtained above of the  $\alpha$  and  $\beta$  systems with that given by Mesnage, it will be seen that instead of a single system which leaves out a number of bands unassigned, the complexity is interpreted in terms of two systems involving  ${}^4\Pi - {}^4\Sigma$  transitions and accounting for all the measured band heads.

The main features of this classification in the case of  $(0,0)$  groups in both the systems are marked in Plate XV D which may be compared with

Plate XV B (strip *b*) referred to above showing the fragmentary analysis reported by Mesnage.

*γ System.*—In the above sections, band heads from  $\nu$  24695 to 22029  $\text{cm}^{-1}$  have been considered. Reference to Plates XV B and C (strips *a* and *c*) shows that there are two regions in which important groups remain unclassified. In one of these regions (strip *c*) Mesnage's system *C* occurs. This contains some of the most intense bands characteristic of the spectrum. The analysis given by Mesnage accounts for most of the band heads in this region. The head at 21779  $\text{cm}^{-1}$  is the strongest and the bands associated with it must be considered as (0,0) sequence as given by Mesnage.

The remaining sequences have been slightly altered in order to include in the vibrational scheme some of the prominent heads which are omitted by Mesnage. The final scheme suggested by the author may be considered as a slight modification of Mesnage's analysis in order to include the band heads newly measured. The classifications are given in Table VI at the end. Some of the bands in this system are double consisting of components of nearly equal intensity. In this respect it is like the system *C* in NiCl which is suggested to be a  ${}^2\Sigma - {}^2\Sigma$  electronic transition. The vibrational formula obtained for the heads of this system is

$$\nu = 21790.7 + 294.9 u' - 0.80u'^2 - 317.2 u'' + 0.50 u''^2.$$

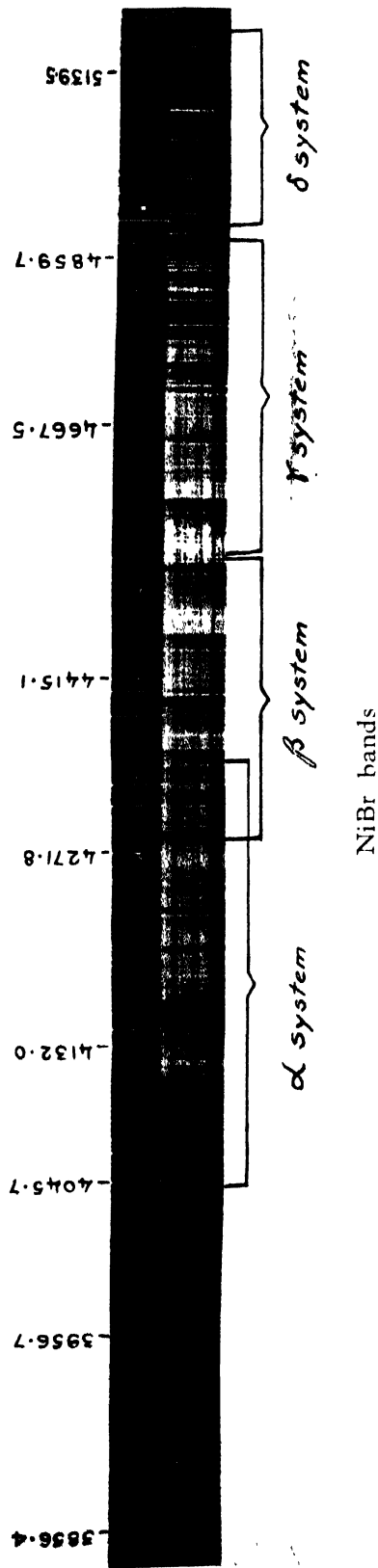
The value of  $x_e''\omega_e''$  according to this scheme is 0.5 and differs from the apparently large value of 5 derived by Mesnage. The value of  $\omega_e''$  may not be considered as identical with that for systems  $\alpha$  and  $\beta$  since a different ground state may be involved.

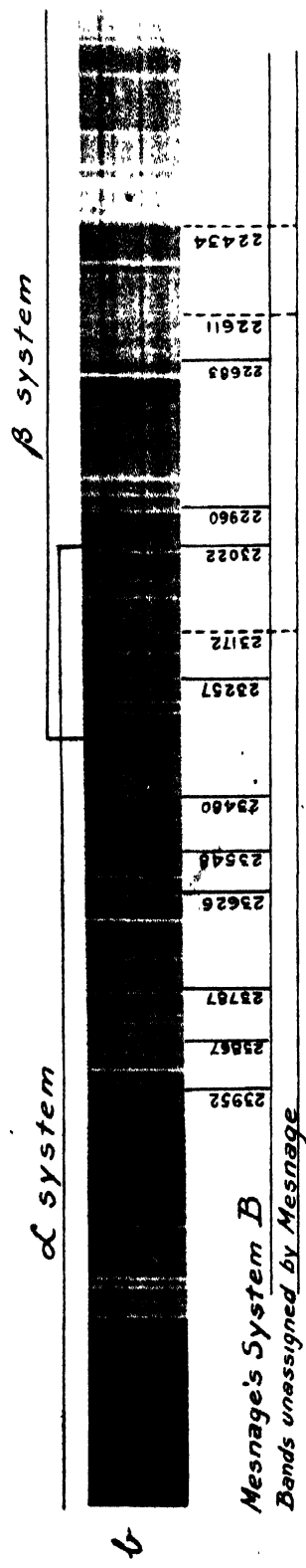
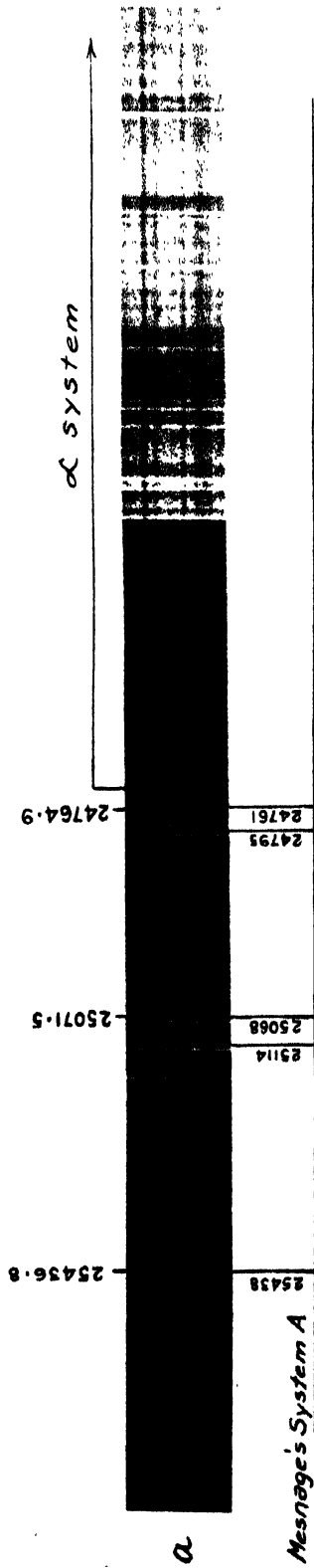
*Other systems.*—Further up on the less refrangible side of system  $\gamma$ , there is an indication of a few bands which are different in appearance and occur somewhat remote from the bands assigned to the  $\gamma$  system. These may probably constitute a different system provisionally designated as  $\delta$  system. The difference between the first members of two of the prominent groups is 302  $\text{cm}^{-1}$ . It may be of some significance to note that this difference is of the same order of magnitude as the common ground state interval 312  $\text{cm}^{-1}$  of the  $\alpha$  and  $\beta$  systems and also 317  $\text{cm}^{-1}$  which is the lower vibrational frequency of the  $\gamma$  system.

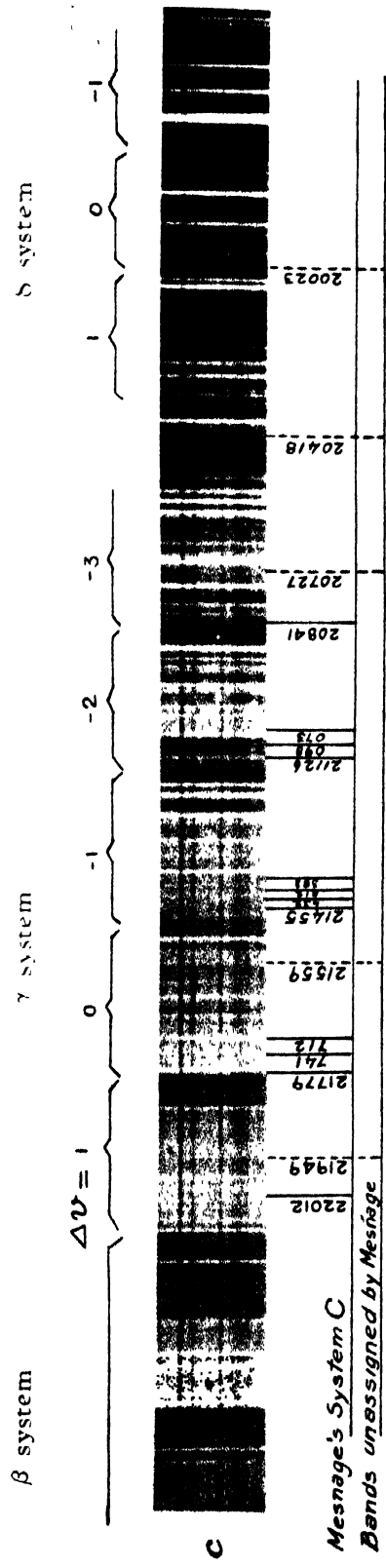
Another brief but prominent and somewhat complex system may also be referred to. This occurs beyond the  $\alpha$  system towards the more refrangible end of the spectrum. These groups are shown in Plate XV B, strip *a*. Three groups of bands are distinctly observable. It is the prominent members of these groups that constitute the fragmentary system *A* of Mesnage. Each of these groups consists of a number of band heads occurring in succession. Some of these bands show close doublet structure with components of nearly equal intensity. The band heads themselves appear to be more line like than the heads belonging to the other system such as  $\alpha$  or  $\beta$ . The direction of degradation is rather uncertain. The analysis

TABLE VI (NiB<sub>1</sub> bands)

Mesnage, wavenumber	Author, wavenumber	Int.	Svstem	$\nu', \nu''$			
	19690.0	3	$\delta$				
	704.4	3	$\delta$				
	719.9	3	$\delta$				
	976.1	4	$\delta$				
	20000.4	5					
	605.6	5	$\delta$				
20023.3	022.1	4	$\delta$				
	130.9	3	$\gamma$				
	296.9	4	$\delta$				
	343.1	3	$\gamma$	11, 15			
	353.5	3	$\gamma$	10, 14			
	372.1	3	$\gamma$	9, 13			
	393.7	3	$\gamma$	8, 12			
	406.6	3	$\gamma$	7, 11			
417.9	417.5	4	$\gamma$	6, 10			
	716.2	3	$\gamma$	6, 9			
72.9	725.6	3 }					
	738.5	4 }	$\gamma$	5, 8			
	748.0	3	$\gamma$	4, 7			
	776.9	4	$\gamma$	3, 6			
	789.3	3 }					
	803.3	3 }	$\gamma$	2, 5			
	819.3	3	$\gamma$	1, 4			
841.0	837.1	3	$\gamma$	0, 3			
	21000.8	3	$\gamma$	8, 10			
	008.7	3	$\gamma$	7, 9			
	022.9	3	$\gamma$	6, 8			
	046.8	3	$\gamma$	5, 7			
	059.2	4 }					
21073.4	070.7	4 }	$\gamma$	4, 6			
098.3	096.1	3	$\gamma$	3, 5			
	111.2	4	$\gamma$	2, 4			
126.8	127.7	5	$\gamma$	1, 3			
	145.6	4	$\gamma$	0, 2			
	172.0	3	$\gamma$	16, 17			
	219.2	3	$\gamma$	13, 14			
	238.1	3	$\gamma$	12, 13			
	278.2	3	$\gamma$	10, 11			
	290.7	3	$\gamma$	9, 10			
	320.4	3	$\gamma$	7, 8			
	347.7	3	$\gamma$	6, 7			
	356.8	4	$\gamma$	5, 6			
383.0	385.3	4	$\gamma$	4, 5			
411.9							
	421.8	4	$\gamma$	2, 3			
432.1	432.0	4 }					
	441.5	4 }	$\gamma$	1, 2			
455.1	452.8	6 }					
	463.4	6 }	$\gamma$	0, 1			
	473.3	3	$\gamma$	16, 16			
	484.4	3	$\gamma$	15, 15			
	497.8	3	$\gamma$	14, 14			
	527.2	4	$\gamma$	13, 13			
	537.1	4	$\gamma$	12, 12			
	549.4	4 }					
558.7	560.0	5 }	$\gamma$	11, 11			
	574.2	4	$\gamma$	10, 10			
	585.1	4 }					
	596.8	4 }	$\gamma$	9, 9			
	611.7	3	$\gamma$	8, 8			
	638.3	3	$\gamma$	7, 7			
	649.4	3	$\gamma$	6, 6			







Ni Br bands

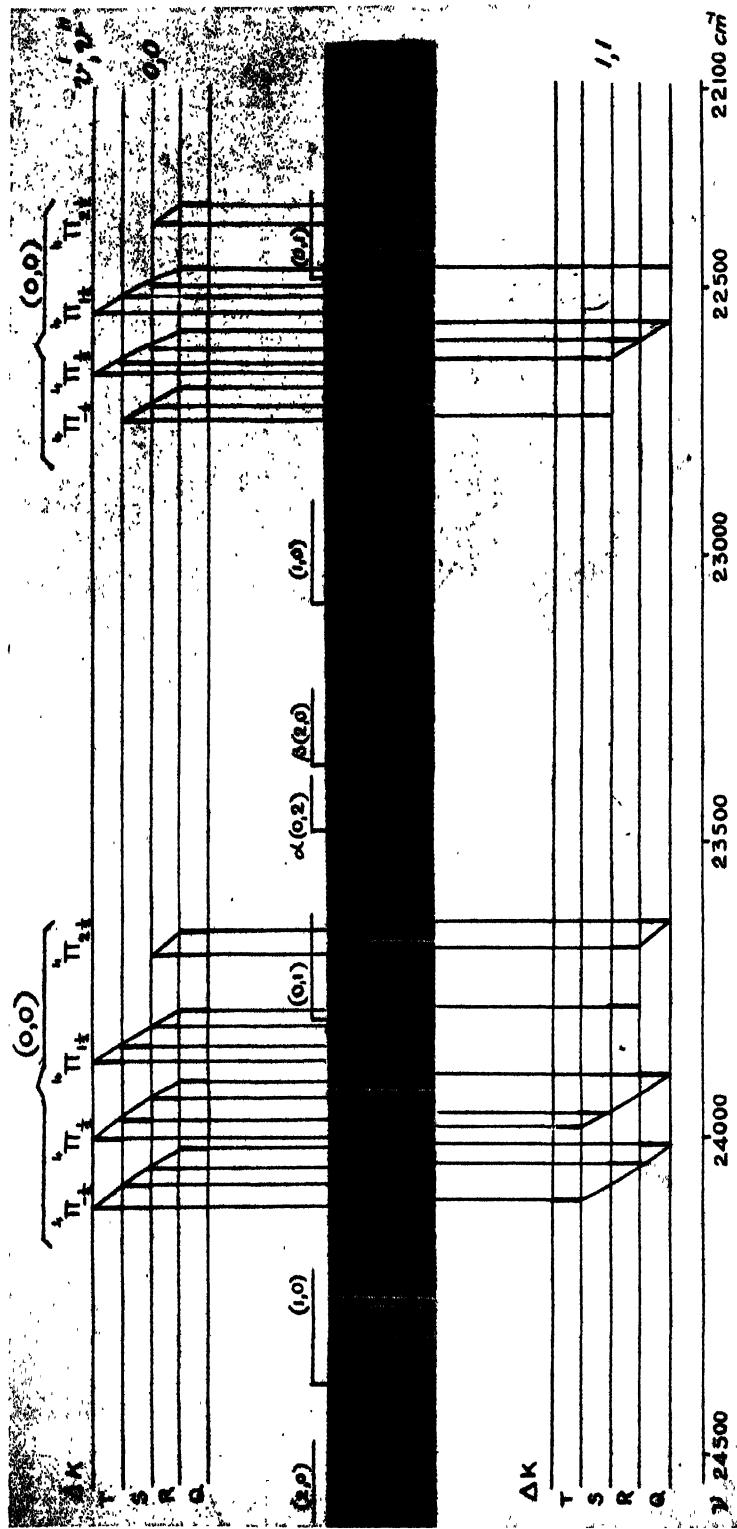
NiBr Bands  $\alpha$  and  $\beta$  systems



TABLE VI (contd.)

Mesnage, wavenumber	Author, wavenumber	Int.	System	$\nu', \nu''$	$\Delta J$		
					-1	0	+1
21711.8	21688.4	4	$\gamma$	4, 4			
	709.5	3	$\gamma$	3, 3			
740.6	733.2	5	$\gamma$	2, 8			
	740.3	4					
779.0	756.7	4	$\gamma$	1, 3			
	779.5	6	$\gamma$	0, 0			
	788.3	4	$\gamma$	15, 14			
	808.5	3	$\gamma$	14, 13			
	820.5	4	$\gamma$	13, 12			
	830.0	3					
	841.3	3	$\gamma$	12, 11			
	863.6	4	$\gamma$	11, 10			
	887.4	3	$\gamma$	10, 9			
	898.7	4	$\gamma$	9, 8			
	926.6	4	$\gamma$	8, 7			
	939.6	4	$\gamma$	7, 6			
948.7	949.2	5					
	966.1	3	$\gamma$	6, 5			
	977.0	3	$\gamma$	5, 4			
	996.7	3	$\gamma$	4, 3			
22012.5	22016.6	5	$\gamma$	3, 2			
	029.0	5	$\beta$	0, 1		$Q_1$	$QR_{12}$
	046.7	6	$\beta$	0, 1			$R_1$
			$\gamma$	2, 1			
	073.4	6	$\gamma$	1, 0			
	103.0	5	$\gamma$	14, 12			
	120.0	6	$\gamma$	13, 11			
	143.7	4	$\beta$	0, 1	$QP_{21}$	$Q_2$	$QR_{23}$
	172.2	4	$\beta$	0, 1		$RQ_{21}$	$R_2$
	191.2	4	$\beta$	1, 2			$SR_{31}$
	207.3	4	$\beta$	0, 1			$SR_{21}$
	234.0	4	$\gamma$	8, 6			
	276.9	3	$\beta$	0, 1	$QP_{32}$	$Q_3$	$QR_{31}$
	296.5	3	$\beta$	0, 1	$RP_{31}$	$RQ_{32}$	$R_1$
	314.3	5	$\gamma$	4, 2			
	341.9	2	$\beta$	0, 0		$Q_1$	$QR_{12}$
			$\beta$	0, 1		$SR_{31}$	$SR_{32}$
			$\beta$	0, 0			$R_1$
	374.1	3	$\beta$	0, 1	$QP_{43}$	$Q_4$	
			$\beta$	0, 1			
	384.4	5	$\gamma$	15, 12			
	393.5	4	$\beta$	1, 2	$RP_{42}$	$RQ_{43}$	$R_4$
	413.0	4	$\beta$	0, 1	$RP_{43}$	$RQ_{43}$	$R_4$
	433.4	6	$\gamma$	13, 10			
22433.9			$\beta$	1, 2	$SP_{41}$	$SR_{42}$	$SR_{43}$
	452.3	3	$\beta$	0, 1	$SP_{41}$	$SR_{42}$	$SR_{43}$
			$\beta$	1, 1	$QP_{91}$	$Q_2$	$QR_{23}$
	461.6	3	$\beta$	0, 0	$QP_{21}$	$Q_2$	$QR_{23}$
	471.9	3	$\beta$	0, 1		$TQ_{41}$	$TR_{42}$
	500.7	4	$\beta$	0, 0		$RQ_{21}$	$R_2$
	517.5	4	$\beta$	0, 0			$SR_{21}$

TABLE VI (contd.)

Mesnage, wavenumber	Author, wavenumber	Int.	System	$v', v''$	$\Delta J$		
					-1	0	+1
22610.9	72546.0	4	$\gamma$	8,5			
	565.0	4	$\beta$	1,1	$QP_{32}$	$Q_3$	$QR_{34}$
	581.5	4	$\beta$	0,0	$QP_{32}$	$Q_3$	$QR_{34}$
	593.6	3	$\gamma$	5,2			
	605.0	3	$\beta$	1,1	$RP_{31}$	$RQ_{32}$	$R_3$
	615.0	5	$\beta$	0,0	$RP_{31}$	$RQ_{32}$	$R_3$
	634.5	4	$\beta$	1,0		$Q_1$	$QR_{12}$
			$\beta$	1,1		$SQ_{31}$	$SR_{32}$
	645.4	3	$\beta$	0,0		$SQ_{31}$	$SR_{32}$
	659.4	5	$\beta$	0,0			$TR_{31}$
683.3			$\beta$	1,0			$R_1$
	688.6	7	$\beta$	0,0	$QP_{43}$	$Q_4$	
	727.1	4	$\beta$	0,0	$RP_{42}$	$RQ_{43}$	$R_4$
	738.3	3	$\beta$	1,1	$SP_{41}$	$SQ_{42}$	$SR_{43}$
			$\beta$	2,1	$QP_{21}$	$Q_2$	$QR_{23}$
	757.2	3	$\beta$	0,0	$SP_{41}$	$SQ_{42}$	$SR_{43}$
			$\beta$	1,0	$QP_{21}$	$Q_2$	$QR_{23}$
	776.7	4	$\beta$	0,0		$TQ_{41}$	$TR_{42}$
			$\beta$	1,0		$RQ_{21}$	$R_2$
	792.9	3	$\beta$	2,1			$SR_{21}$
959.4	809.9	4	$\beta$	1,0			$SR_{21}$
	830.2	5					
	856.0	3	$\beta$	2,1	$QP_{32}$	$Q_3$	$QR_{34}$
	867.5	3	$\beta$	1,0	$QP_{32}$	$Q_3$	$QR_{34}$
	879.9	4					
	887.9	4	$\beta$	2,1	$RP_{31}$	$RQ_{32}$	$R_3$
	895.4	4	$\beta$	1,0	$RP_{31}$	$RQ_{32}$	$R_3$
	917.3	5	$\beta$	1,0		$SQ_{31}$	$SR_{32}$
	932.7	6	$\beta$	2,0		$Q_1$	$QR_{12}$
	953.7	4	$\beta$	1,0			$TR_{31}$
23021.8	963.7	7	$\beta$	2,1	$QP_{43}$	$Q_4$	
	979.0	6	$\beta$	1,0	$QP_{43}$	$Q_4$	
	987.4	4	$\beta$	2,1	$RP_{42}$	$RQ_{43}$	$R_4$
	997.1	4					
	23007.2	4	$\beta$	1,0	$RP_{42}$	$RQ_{43}$	$R_4$
	020.2	3	$\alpha$	1,3		$Q_1$	$QR_{12}$
			$\beta$	2,1	$SP_{41}$	$SQ_{42}$	$SR_{43}$
	035.4	4	$\alpha$	0,2		$Q_1$	$QR_{12}$
			$\beta$	1,0	$SP_{41}$	$SQ_{42}$	$SR_{43}$
	049.9	4	$\alpha$	1,3			$R_1$
171.7	060.0	4	$\beta$	2,0	$QP_{21}$	$Q_2$	$QR_{23}$
	073.1	4	$\alpha$	0,1			$R_1$
	104.5	4	$\beta$	1,0		$TQ_{41}$	$TR_{42}$
	127.8	5					$SR_{21}$
	142.7	4	$\beta$	1,3	$QP_{32}$	$Q_3$	$QR_{34}$
	158.8	4	$\alpha$	1,3	$QP_{21}$	$Q_2$	$QR_{23}$
			$\beta$	0,2	$QP_{32}$	$Q_3$	$QR_{34}$
	173.3	5	$\alpha$	0,2	$QP_{21}$	$Q_2$	$QR_{23}$
	221.6	4	$\alpha$	0,2			$SR_{21}$
	230.4	4	$\beta$	3,1			$TR_{31}$
257.4	239.3	4	$\beta$	2,0			$TR_{31}$
	248.8	4					
	258.5	4					
	286.1	3	$\alpha$	0,2	$QP_{31}$	$Q_3$	$QR_{34}$
	306.8	5	$\alpha$	0,2	$RP_{31}$	$RQ_{32}$	$R_3$
			$\beta$	2,0	$RP_{42}$	$RQ_{43}$	$R_4$

TABLE VI (contd.)

Mesnage, wavenumber	Author, wavenumber	Int.	System	$\nu', \nu''$	$\Delta J$		
					-1	0	+1
23314.8	23334.5	5	$\alpha$	0,2		$SQ_{31}$	$SR_{32}$
			$\beta$	2,0	$SP_{41}$	$SQ_{42}$	$SR_{41}$
	342.0	3	$\alpha$	0,1		$Q_1$	$QR_{12}$
	352.8	3	$\alpha$	1,3			$TR_{31}$
	363.8	4	$\alpha$	0,2			$TR_{31}$
			$\beta$	2,0		$TQ_{41}$	$TR_{12}$
	373.8	3	$\alpha$	0,1			$R_1$
	389.1	5	$\alpha$	0,2	$QP_{43}$	$Q_1$	
	406.5	3	$\alpha$	1,3	$RP_{42}$	$RQ_{43}$	$R_4$
	419.2	4	$\alpha$	0,2	$RP_{42}$	$RQ_{43}$	$R_4$
	428.6	3	$\alpha$	1,3	$SP_{41}$	$SQ_{42}$	$SR_{43}$
	446.6	4	$\alpha$	0,2	$SP_{41}$	$SQ_{42}$	$SR_{42}$
	465.2	4	$\alpha$	1,2	$QP_{21}$	$Q_2$	$QR_{23}$
			$\alpha$	1,3		$TQ_{41}$	$TR_{42}$
			$\alpha$	0,1	$QP_{21}$	$Q_2$	$QR_{23}$
			$\alpha$	0,2		$TQ_{41}$	$TR_{42}$
480.3	475.8	5	$\alpha$	0,1		$RQ_{21}$	$R_2$
			$\alpha$	0,2		$RQ_{21}$	$R_2$
	488.3	3	$\alpha$	1,2			$SR_{21}$
	512.7	4	$\alpha$	0,1			
	527.0	3	$\alpha$	0,1			
548.3	553.3	5	$\beta$	3,0	$QP_{43}$	$Q_4$	$QR_{34}$
	582.2	5	$\alpha$	1,2	$QP_{32}$	$Q_3$	$QR_{34}$
	606.6	1	$\alpha$	0,1	$QP_{32}$	$Q_3$	$QR_{34}$
626.2	623.0	1	$\alpha$	0,1	$RP_{31}$	$RQ_{32}$	$R_3$
	636.3	5	$\alpha$	1,1		$Q_1$	$QR_{12}$
			$\alpha$	1,2		$SQ_{41}$	$SR_{32}$
			$\alpha$	0,0		$Q_1$	$QR_{12}$
	657.4	6	$\alpha$	0,1		$SQ_{31}$	$SR_{32}$
			$\alpha$	0,1			$TR_{31}$
	678.6	5	$\alpha$	1,1			
			$\alpha$	0,0			$R_1$
	695.3	4	$\alpha$	0,1	$QP_{43}$	$Q_4$	$R_4$
	709.1	4	$\alpha$	1,2	$RP_{42}$	$RQ_{43}$	$R_4$
787.5	723.2	4	$\alpha$	0,1	$RP_{42}$	$RQ_{43}$	$R_4$
	738.4	5	$\alpha$	1,2	$SP_{41}$	$SQ_{42}$	$SR_{43}$
	752.9	1	$\alpha$	0,1	$SP_{41}$	$SQ_{42}$	$SR_{43}$
	770.4	4	$\alpha$	1,1	$QP_{21}$	$Q_2$	$QR_{23}$
	778.3	4	$\alpha$	0,0	$QP_{21}$	$Q_2$	$QR_{23}$
	787.0	5	$\alpha$	0,1		$TQ_{41}$	$TR_{42}$
	796.6	5	$\alpha$	0,0		$RQ_{21}$	$R_2$
	822.5	5	$\alpha$	0,0			$SR_{21}$
	849.6	1	$\alpha$	0,0			
	856.8	4					
867.1	872.6	3					
	887.2	4	$\alpha$	1,1	$QP_{32}$	$Q_3$	$QR_{34}$
	905.0	6	$\alpha$	0,0	$QP_{32}$	$Q_3$	$QR_{34}$
	936.2	4	$\alpha$	0,0	$RP_{31}$	$RQ_{32}$	$R_3$
	944.5	5	$\alpha$	2,1		$Q_1$	$QR_{12}$
23952.3	954.2	6	$\alpha$	1,0		$Q_1$	$QR_{12}$
			$\alpha$	1,1		$SQ_{31}$	$SR_{32}$
	967.9	6	$\alpha$	0,0		$SQ_{31}$	$SR_{32}$
	978.3	6	$\alpha$	1,0			$R_1$
			$\alpha$	1,1			$TR_{11}$
	999.4	6	$\alpha$	0,0			$TR_{31}$

TABLE VI (contd.)

Mesnage, Wavenumber	Author, Wavenumber	Int.	System.	$v', v''$	$\Delta J$		
					-1	0	+1
	24009.5	5	$\alpha$	1,1	$QP_{43}$	$Q_4$	
	016.5	7	$\alpha$	0,0	$QP_{43}$	$Q_4$	
	032.9	3	$\alpha$	1,1	$RP_{42}$	$RQ_{43}$	$R_4$
	056.3	3	$\alpha$	0,0	$RP_{42}$	$RQ_{43}$	$R_4$
	075.1	3	$\alpha$	1,0	$QP_{41}$	$Q_2$	$QR_{43}$
			$\alpha$	0,0	$SP_{41}$	$SQ_{42}$	$SR_{43}$
	089.2	4					
	098.9	3	$\alpha$	2,1		$RQ_{21}$	$R_2$
			$\alpha$	1,1		$TQ_{41}$	$TR_{42}$
	107.0	3	$\alpha$	0,0		$TQ_{41}$	$TR_{42}$
	118.7	3	$\alpha$	1,0		$RQ_{21}$	$R_2$
	127.8	4					
	156.6	4	$\alpha$	1,0			$SR_{21}$
	165.3	3					
	195.6	1	$\alpha$	1,0	$QP_{32}$	$Q_3$	$QR_{34}$
	211.0	5	$\alpha$	2,1	$RP_{31}$	$RQ_{32}$	$R_3$
	234.1	6	$\alpha$	1,0	$RP_{31}$	$RQ_{32}$	$R_3$
	240.9	3	$\alpha$	2,1		$SQ_{31}$	$SR_{32}$
	249.7	3	$\alpha$	3,1		$Q_1$	$QR_{12}$
	265.3	4	$\alpha$	2,0		$Q_1$	$QR_{12}$
			$\alpha$	1,0		$SQ_{31}$	$SR_{32}$
	282.1	4	$\alpha$	2,0			$R_1$
	291.0	5	$\alpha$	1,0			$TR_{31}$
	301.0	6					
	312.0	4	$\alpha$	1,0	$QP_{43}$	$Q_4$	
	330.3	3	$\alpha$	2,1	$RP_{42}$	$RQ_{43}$	$R_4$
	347.5	3	$\alpha$	1,0	$RP_{42}$	$RQ_{43}$	$R_4$
	355.5	3	$\alpha$	3,1	$QP_{41}$	$Q_3$	$QR_{43}$
			$\alpha$	2,1	$SP_{41}$	$SQ_{42}$	$SR_{43}$
	376.0	3	$\alpha$	2,0	$QP_{41}$	$Q_2$	$QR_{23}$
			$\alpha$	1,0	$SP_{41}$	$SQ_{42}$	$SR_{43}$
	388.1	3	$\alpha$	3,1		$TQ_{41}$	$TR_{42}$
	395.9	3	$\alpha$	1,0		$TQ_{41}$	$TR_{42}$
	410.6	3	$\alpha$	2,0		$RQ_{21}$	$R_2$
	422.7	3					
	437.6	4	$\alpha$	3,1			$SR_{21}$
	449.0	5	$\alpha$	2,0			$SR_{21}$
	458.0	4					
	466.9	6					
	479.9	6		3,1	$QP_{32}$	$Q_3$	$QR_{34}$
	496.1	6	$\alpha$	2,0	$QP_{32}$	$Q_3$	$QR_{34}$
	515.5	3	$\alpha$	3,1	$RP_{31}$	$RQ_{32}$	$R_3$
	527.8	6	$\alpha$	2,0	$RP_{31}$	$RQ_{32}$	$R_3$
	540.2	3	$\alpha$	3,1		$SQ_{31}$	$SR_{32}$
	559.5	6	$\alpha$	2,0		$SQ_{31}$	$SR_{32}$
	567.9	4	$\alpha$	3,1			$TR_{31}$
	584.3	6	$\alpha$	2,0			$TR_{31}$
	598.8	4	$\alpha$	3,1	$QP_{43}$	$Q_4$	
	611.5	7	$\alpha$	2,0	$QP_{43}$	$Q_4$	
	631.8	3	$\alpha$	2,0	$RP_{42}$	$RQ_{43}$	$R_4$
	652.0	3	$\alpha$	3,1	$SP_{41}$	$SQ_{42}$	$SR_{43}$
	668.6	3	$\alpha$	2,0	$SP_{41}$	$SQ_{42}$	$SR_{43}$
	677.3	3	$\alpha$	3,1		$TQ_{41}$	$TR_{42}$
	695.2	4	$\alpha$	2,0		$TQ_{41}$	$TR_{42}$

suggested by Mesnage does not comprise or take into account all the heads that have been measured in this region. The interpretation of the structure

of these bands as well as of the few groups of bands on the least refrangible end of the spectrum (*i.e.*, the  $\delta$  system) is in progress.

In conclusion, a catalogue of the wavenumbers of all the band heads together with their intensities, is given in Table VI. The first column gives Mesnage's data also for comparison. The last columns describe the system to which the bands are assigned and their classifications. In this table the wavenumber and other data for bands occurring beyond the  $\alpha$  system *i.e.*, in the region of Mesnage's system  $\beta$  are not included. They will be published in a subsequent communication;

#### ACKNOWLEDGMENTS

The author wishes to express his grateful thanks to Prof. K. R. Rao for his kind guidance and interest in the work. He is grateful to the Government of India, Ministry of Scientific Research for the award of a Senior Research Scholarship.

#### REFERENCES

- Krishnamurty, V. G., 1952, *Ind. J. Phys.*, **26**, 177.  
Krishnamurty, V. G., 1952a, *Ind. J. Phys.*, **26**, 237.  
Mesnage, P., 1939, *Annales de Physique*, **12**, 5.

# A NOTE ON THE PROBLEM OF DISLOCATION IN A SEMI-INFINITE PLATE CONTAINING A CIRCULAR HOLE\*

By B. KARUNES

DEPARTMENT OF APPLIED PHYSICS, UNIVERSITY COLLEGE OF SCIENCE AND TECHNOLOGY, CALCUTTA

(Received for publication, April 23, 1952)

**ABSTRACT.** A stress function giving the stress distribution due to dislocation in a semi-infinite plate containing an unstressed circular hole near the straight edge of the plate is obtained in bipolar co-ordinates after the work of Ghosh on the problems of dislocation in a circular plate containing an eccentric hole. The circumferential stresses over the hole boundary and the straight edge are calculated.

## INTRODUCTION

Solutions to two problems of dislocation in a circular plate containing an eccentric circular hole are given by Ghosh (1926). The dislocations that he has considered are due to (1) a fissure of constant width joining the two boundaries and (2) a wedge shaped fissure with its wider end on the hole boundary. He has solved the problems in bipolar co-ordinates taking the apex of the wedge shaped fissure at the origin of the relevant Cartesian co-ordinates. It can be easily verified that his solutions hold good in cases of similar dislocations in a semi-infinite plate containing a circular hole near its straight edge, while the fissures are between the hole boundary and the straight edge or between the hole boundary and infinity, along the axis of symmetry of the hole. The apex of the wedge shaped fissure still remains at the origin of the Cartesian co-ordinates and the wider end of the wedge on the hole boundary. In the present paper a solution is given to the problem of dislocation due to a wedge shaped fissure in a semi-infinite plate containing a circular hole, where the apex of the wedge may be anywhere on the axis of symmetry. The solution is obtained by choosing a stress function equal to the sum of the stress functions required for the cases of a parallel fissure and a wedge shaped fissure with its apex at the origin.

## THE SOLUTION

In the solution we shall use bipolar co-ordinates in the same notations as those used by Jeffery (1921), so that  $\alpha=0$  represents the straight edge and  $\alpha=\alpha_1$  represents the hole boundary. Let us choose a stress function

$$h\chi_0 = A\alpha \sinh \alpha + B\alpha \cosh \alpha \quad \dots (1)$$

which gives the following multiple valued terms in the displacements.

\* Communicated by Prof. P. C. Mahanti.

$$\left. \begin{aligned} u &= \frac{\lambda + 2\mu}{2\mu(\lambda + \mu)} (A \sinh \alpha + B \cosh \alpha) \frac{\beta \sin \beta}{\cosh \alpha - \cos \beta} \\ v &= \frac{\lambda + 2\mu}{2\mu(\lambda + \mu)} \{ A(1 - \cosh \alpha \cos \beta) - B \sinh \alpha \cos \beta \} \frac{\beta}{\cosh \alpha - \cos \beta} \end{aligned} \right\} \dots (2)$$

Then at the barrier  $\beta = \pm \pi$ ,  $u$  is continuous and  $v$  has a discontinuity equal to

$$\begin{aligned} v_0 &= \frac{\lambda + 2\mu}{\mu(\lambda + \mu)} \left\{ A + B \frac{\sinh \alpha}{\cosh \alpha + 1} \right\} \pi \\ &= C + Dv_0 \end{aligned} \dots (3)$$

where

$$\left. \begin{aligned} v_0 &= y\text{-ordinate at } \beta = \pm \pi \\ C &= \frac{\lambda + 2\mu}{\mu(\lambda + \mu)} A \pi \\ D &= \frac{\lambda + 2\mu}{\mu(\lambda + \mu)} B \pi \end{aligned} \right\} \dots (4)$$

Therefore, the chosen stress function will suit the state of dislocation due to a fissure bounded by the planes

$$v = \pm (C + Dy) \dots (5)$$

By adjusting the values of  $C$  we shall be able to get point of intersection of these two planes at any desired point on the  $y$ -axis, and the value of  $D$  will determine the apex angle of the wedge. When  $C=0$  we get a wedge shaped fissure with its apex at the origin and when  $D=0$  we get a parallel fissure.

To obtain the complete solution to the problem we must add a stress function  $hX_1$  to  $hX_0$  such that  $hX_1$  produces no stress over the straight boundary ( $\alpha=0$ ) and at infinity ( $\alpha=0, \beta=0$ ), where no stresses are produced by  $hX_0$  either; and the sum ( $hX_0 + hX_1$ ) produces no stress over the boundary of the hole ( $\alpha=\alpha_1$ ). It can be verified that all these requirements are satisfied by the stress function

$$hX_1 = B_0 \alpha (\cosh \alpha - \cos \beta) + \{ A_1 (\cosh 2\alpha - 1) + C_1 \sinh 2\alpha \} \cos \beta \dots (6)$$

where

$$\left. \begin{aligned} B_0 &= 2C_1 \\ &= -\{ A + B(\cosh \alpha_1 \sinh \alpha_1 - \alpha_1) \operatorname{cosech}^2 \alpha_1 \} \coth \alpha_1 \\ A_1 &= \frac{1}{2} \{ A + B(\cosh \alpha_1 \sinh \alpha_1 - \alpha_1) \operatorname{cosech}^2 \alpha_1 \} \end{aligned} \right\} \dots (7)$$

Calculating the stresses  $\widehat{\beta\beta}$  over the boundaries from the complete stress function  $(h\chi_0 + h\chi_1)$ , we get over  $\alpha = \alpha_1$

$$a\widehat{\beta\beta}_1 = 2(\cosh \alpha_1 - \cos \beta) \operatorname{cosech}^2 \alpha_1 \quad \dots \quad (8)$$

$$\times [B(\alpha_1 \cosh \alpha_1 - \sinh \alpha_1) - \{A \sinh^2 \alpha_1 + B(\cosh \alpha_1 \sinh \alpha_1 - \alpha_1)\} \cos \beta]$$

and over  $\gamma = 0$

$$a\widehat{\beta\beta}_0 = 2(1 - \cos \beta) [A + \{A + B(\cosh \alpha_1 \sinh \alpha_1 - \alpha_1) \operatorname{cosech}^2 \alpha_1\} \cos \beta] \quad \dots \quad (9)$$

#### ACKNOWLEDGMENTS

The author wishes to express his respectful thanks to Dr. S. Ghose, under whose suggestion and guidance the note was prepared.

#### REFERENCES

- Ghosh, S., 1926, *Bul. Cal. Math. Soc.*, **17**, 4, 265.  
 Jeffery, G. B., 1921, *Phil. Trans. Roy. Soc.*, **A221**, 265.



# THE ULTRAVIOLET ABSORPTION SPECTRA OF ORGANIC SUBSTANCES IN THE LIQUID AND SOLID STATES. IV. CHLOROTOLUENES\*

By H. N. SWAMY

OPTICS DEPT., INDIAN ASSOCIATION FOR THE CULTIVATION OF SCIENCE, CALCUTTA 32

(Received for publication, June 6, 1952)

Plates XVI A, B

**ABSTRACT.** The ultraviolet absorption spectra of *o*- and *m*-chlorotoluene in the vapour, liquid and solid states and of *p*-chlorotoluene in the liquid and solid states have been investigated in order to find out the changes which may take place in the spectra with change of state. In all the cases the bands shift to longer wavelength side with liquefaction by more than  $250\text{ cm}^{-1}$  and in the case of both ortho- and metachlorotoluene the principal *o, o* band shifts by about  $700\text{ cm}^{-1}$  towards shorter wavelength side on solidification. In the case of these latter two compounds the principal band is accompanied by two fainter satellites. It is pointed out that these results may indicate formation of virtual bonds between neighbouring molecules in the solid state and that similar results reported by previous workers in the case of benzene may also indicate formation of such virtual bonds.

## INTRODUCTION

In a programme undertaken to study the ultraviolet absorption spectra of organic substances in the liquid and solid states in order to find out whether the electronic energy levels undergo any remarkable change with change of state, interesting results were observed in the case of the cresols and xylenes (Swamy, 1952*a*, 1952*b*). It was observed that the impact of neighbouring molecules hinders transitions to higher vibrational energy states in the liquid state. In the solid state, however, in some cases transitions to vibrational states of higher quantum numbers were observed. It was observed recently (Sirkar and Swamy, 1952) that besides the changes mentioned above, the solidification of orthodichlorobenzene at  $-180^{\circ}\text{C}$  brings about a splitting up of the electronic energy level into three components. These results were interpreted on the hypothesis that formation of virtual bonds between neighbouring molecules in the solid state is responsible for these changes in the absorption spectra. In order to find out whether the relative positions of substitution groups in other disubstituted benzene compounds have any influence on the changes in the absorption spectra which take place with the solidification of the substances, the absorption spectra of

\* Communicated by Prof. S. C. Sirkar.

*o*-, *m*- and *p*- chlorotoluenes in the vapour, liquid and solid states have been studied and discussed in the light of the hypothesis put forward in the previous papers (Swamy, 1952*a* 1952*b*) regarding the quenching of vibrational transitions in the liquid and formation of virtual bonds between neighbouring molecules in the solid state at low temperatures.

#### EXPERIMENTAL

The three chlorotoluenes were supplied by Eastman Kodak Company and they were distilled four times in vacuum before being used for the investigation. The absorption spectra of *o*- and *m*- chlorotoluene in the vapour state were photographed using absorption tubes of length 30 cm and of diameter 12 mm, quartz windows being fitted to the tube, using sodium silicate as cement. The liquid was contained in a small bulb attached to the tube and through another side tube the absorption tube was connected to a Cenco-Hyvac pump. After the tube had been evacuated, the stop-cock leading to the pump was closed and the vapour was allowed to fill up the tube with its saturation pressure at room temperature. An Adam Hilger E<sub>1</sub> quartz spectrograph having a dispersion of 3 Å. U. per mm in the region of 2600 Å was used and Ilford HP<sub>3</sub> films were used to photograph the spectra. On each spectrogram iron arc lines were photographed for comparison.

Films having thickness of the order of 0.2 mm were required to produce absorption bands in the liquid state. Absorption spectra in the solid state at  $-180^{\circ}\text{C}$  were photographed with the technique described previously (Swamy, 1951, 1952*a*). For comparison mercury arc spectrum was recorded with the help of a Hartmann diaphragm on each spectrogram.

#### RESULTS

Spectrograms for *o*-, *m*-, and *p*-chlorotoluene in the liquid state and for the solid state at  $-180^{\circ}\text{C}$  and those of *o*- and *m*- chlorotoluene in the vapour state are reproduced in Plate XVIA. The bands in the liquid and solid states being broad, microphotometer records were obtained to measure the frequencies accurately. These records are reproduced in figures 4, 5 and 6 of Plate XVIB. The Hg line 2537 Å included in the spectrograms served as the reference in the microphotometer records and measurements were made of the centre of the absorption peak. Only the prominent bands in the vapour state have been measured and assignments given. Measurements in this case were made of the edges of the bands. The wave numbers of the bands in the vapour, liquid and solid states are given in Tables I—III in which wave-numbers of bands observed in solution by previous workers are included for comparison. Assignments have been made in the case of bands of *o*- and *m*-chlorotoluene in the solid state at  $-180^{\circ}\text{C}$  on the assumption that the electronic energy level is split up into three components. Bands of *p*-chlorotoluene have been assigned to certain transitions and the assignments are given in the tables, the data for the vapour being those reported by Viswanath (1952).

TABLE I  
 Absorption bands of *o*-chlorotoluene.  $\nu$  in  $\text{cm}^{-1}$ 

Present author		Wolf and Herold (1931)	Purvis (1911)	Present author			
Vapour (Prominent bands)	Assignment	Solution in heptane	Liquid	Liquid 30°C	Assignment	Solid, -180°C	Assignment
36589 (ms)	$\nu_0 - 249$	36560 (s)	36340 (f st)	36381 (vs, broad)	$\nu_0$	36830 (m)	B <sub>0</sub> 290
36677 (s)	$\nu_0 - 161$						
36838 (vs)	$\nu_0$						
37206 (w)	$\nu_0 + 368$		1018			37122 (vs)	A <sub>0</sub> 590
37298 (m)	$\nu_0 + 460$		37358 (f st)	37396 (s, broad)	$\nu_0 + 1015$	37420 (m)	C <sub>0</sub>
37368 (msf)	$\nu_0 + 530$						
37463 (vw)	$\nu_0 + 625$						
37518 (w)	$\nu_0 + 680$	37550 (m)	2036				
37651 (m)	$\nu_0 + 813$		38376 (vw, wide)	38413 (weak)	$\nu_0 + 2 \times 1015$	37840 (vs)	B <sub>1</sub> B <sub>0</sub> + 1010
37753 (ms)	$\nu_0 + 915$					38130 (s)	A <sub>1</sub> A <sub>0</sub> + 1010
37843 (vs)	$\nu_0 + 1005$						
37922 (ms)	$\nu_0 + 1084$					38428 (msf)	C <sub>1</sub> C <sub>0</sub> + 1008
38030 (w)	$\nu_0 + 1192$						
38215 (s)	$\nu_0 + 915 + 460$						
38290 (ms)	$\nu_0 + 915 + 530$						
38364 (m)	$\nu_0 + 1005 + 530$						
38653 (m)	$\nu_0 + 1005 + 813$	38750 (s)					
38850 (mst)	$\nu_0 + 2 \times 1005$					38840 (m)	B <sub>2</sub> B <sub>0</sub> + 1010 X 2
39010 (w)	$\nu_0 + 2 \times 1084$						
39198 (w)	$\nu_0 + 2 \times 915 + 530$	3 500 (m)					
39250 (vw)	$\nu_0 + 1005 + 915 + 530$	40550 (w)					

 TABLE II  
 Absorption bands of a *m*-chlorotoluene.  $\nu$  in  $\text{cm}^{-1}$ 

Present author		Wolf and Herold (1931)		Purvis (1911)		Present author		
Vapour (Prominent bands)	Assignment	Solution in heptane	Assign- ment	Liquid	Liquid at 30°C	Assign- ment	Solid at -180°C	Assign- ment
36619 (vs)	$\nu_0$	36400 (s)	$\nu_0$	36287 (f st, wide)	36315 (vs, broad)	$\nu_0$	36120 (m)	C <sub>0</sub>
37037 (ms)	$\nu_0 + 418$						36630 (s)	B <sub>0</sub>
37095 (ms)	$\nu_0 + 476$							
37231 (w)	$\nu_0 + 612$							
37330 (m)	$\nu_0 + 711$							
37397 (msf)	$\nu_0 + 778$	37400 (s)	$\nu_0 + 1000$	37302 (f st, wide)	36742 (vw)	$\nu_0 + 427$	37015 (vs)	A <sub>0</sub>
37470 (m)	$\nu_0 + 851$							
37608 (s)	$\nu_0 + 981$							
37830 (ms)	$\nu_0 + 1211$							
38025 (m)	$\nu_0 + 981 + 418$							
38177 (m)	$\nu_0 + 2 \times 778$	38350 (m)	$\nu_0 + 1950$	38303 (vw wide)	38297 (m)	$\nu_0 + 2 \times 995$		
38580 (s)	$\nu_0 + 2 \times 981$							
38810 (s)	$\nu_0 + 1220 + 918$							
39036 (m)	$\nu_0 + 2 \times 1211$							
39194 (w)	$\nu_0 + 2 \times 981$ + 612							
39568 (m)	$\nu_0 + 3 \times 981$	39350 (w)	$\nu_0 + 1950$ + 1000				37656 (s)	B <sub>1</sub>
							38040 (s)	A <sub>1</sub> , A <sub>0</sub> + 1025
							38175 (m)	C <sub>1</sub>
							38680 (w)	B <sub>2</sub>
							39065 (s)	A <sub>2</sub> A <sub>0</sub> + 2 × 1025
							39200 (vw)	C <sub>2</sub>

TABLE III

Absorption bands of *p*-chlorotoluene.  $\nu$  in  $\text{cm}^{-1}$ 

Viswanath (1952)		Wolf and Herold (1931)	Present author			
Vapour (Prominent bands)	Assignment	Solution in heptane	Liquid, 30°C	Assignment	Solid, -180°C	Assignment
36299 (v st)	$\nu_0$	36030 (s)	36059 (vs, broad)	$\nu_0$	36224 (vs)	$\nu_0$
36843 (m st)	$\nu_0 + 544$				36992 (s)	$\nu_0 + 768$
37038 (m st)	$\nu_0 + 762 - 26$	36930 (s)	37071 (vs, broad)	$\nu_0 + 1012$	37282 (s)	$\nu_0 + 1058$
37061 (m st)	$\nu_0 + 762$				37756 (w)	$\nu_0 + 2 \times 768$
37343 (m st)	$\nu_0 + 1044$	37400 (w)				
37351 (m st)	$\nu_0 + 1052$	37990 (s)				
37488 (m st)	$\nu_0 + 1189$		38075 (m)	$\nu_0 + 2 \times 1008$	38048 (s)	$\nu_0 + 1058 + 768$
38114 (m st)	$\nu_0 + 1052 + 762$	38760 (s)			38341 (m)	$\nu_0 + 2 \times 1058$
38399 (m st)	$\nu_0 + 2 \times 1052$				39118 (m)	$\nu_0 + 2 \times 1058 + 768$
39172 (w)	$\nu_0 + 2 \times 1052 + 796 - 26$	39650 (w)				

## DISCUSSION

There are some general features in the changes which take place in the absorption spectra with change of state. Along the series *o*-, *m*-, and *p*-chlorotoluene, the position of the *o-o* transition moves towards lower frequencies. The number of bands diminishes when the vapour is liquefied and instead of sharp bands characteristic of vapour, only broad bands are observed in the liquid state. In the solid state at  $-180^\circ\text{C}$  more bands appear, and the bands become narrower, but the edges are not sharp, as can be seen from the microphotometric records. The principal band and its companions shift towards longer wavelengths on liquefaction of the vapour and they shift again to shorter wavelengths on solidification of the liquid. The formation of broad bands and the diminution in the number of bands with liquefaction were ascribed by the author (Swamy, 1952*a*) to the influence of translational motion of the molecules in the liquid in the state of aggregation. The constant impact of molecules hinders transitions to higher vibrational energy states. The considerable shift towards longer wavelengths may be due to the lowering of the electronic energy state due to the association of molecules through virtual bonds.

It is observed that in the case of both *o*- and *m*- chlorotoluene the electronic energy level is split up into three components in the solid state at  $-180^\circ\text{C}$ . In *o*-chlorotoluene, the components are on either side of the principal band, while in meta both the components are on the longer wavelength side. In *p*- chlorotoluene, the electronic energy level does not appear to be split up. It has to be concluded on the basis of these results that the splitting depends on the position of the substituent groups and that

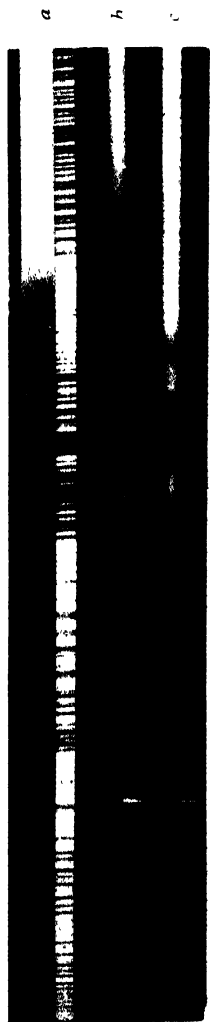


Fig. 1



Fig. 2



Fig. 3.

2537 Å                      2652 Å  
Ultraviolet absorption spectra

Fig. 1. Orthochlorotoluene

- (a) Vapour at 30°C
- (b) Liquid at 30°C
- (c) Solid at -180°C

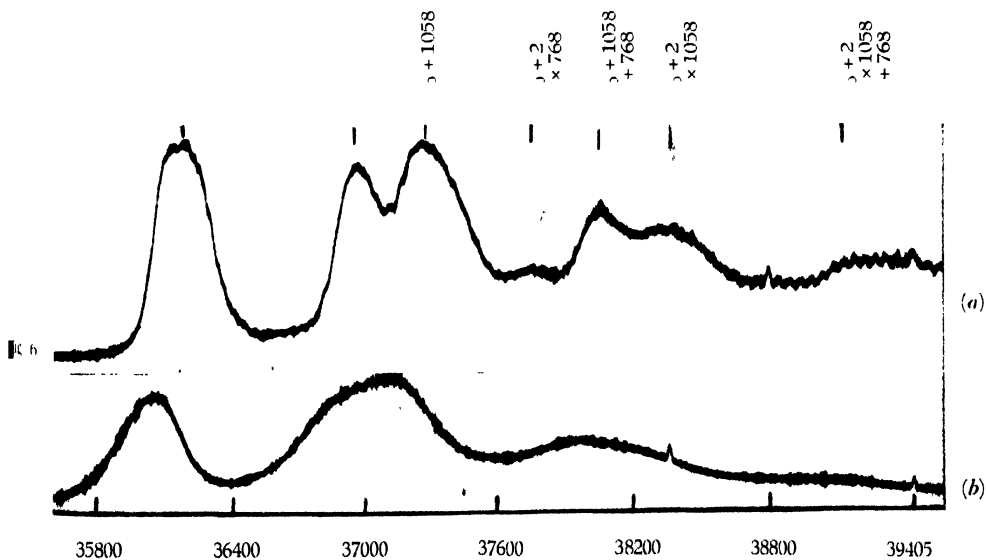
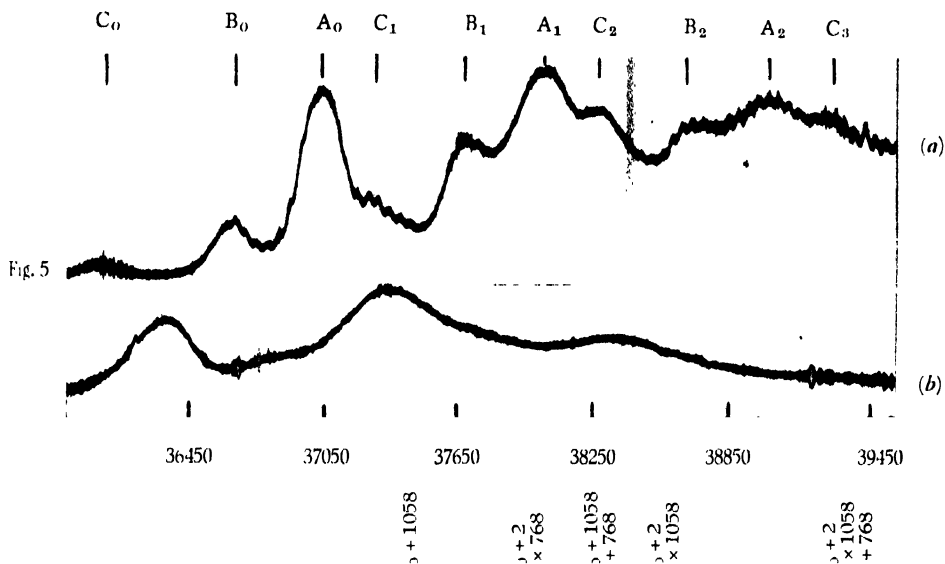
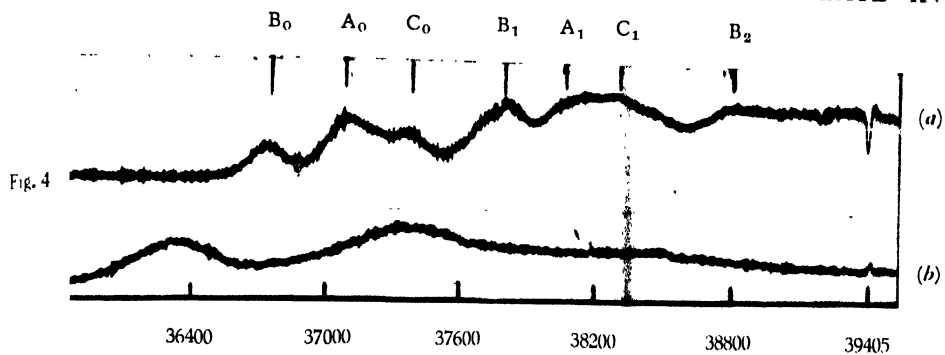
Fig. 2. Metachlorotoluene

- (a) Vapour at 30°C
- (b) Liquid at 30°C
- (c) Solid at -180°C

Fig. 3. Parachlorotoluene

- (a) Liquid at 30°C
- (b) Solid at -180°C





Microphotometer records of the absorption spectra of chlorotoluenes.

Fig. 4.	(a)	<i>o</i> -Chlorotoluene	solid at	-180°C
	(b)	"	liquid at	30°C
Fig. 5.	(a)	<i>m</i> -Chlorotoluene	solid at	-180°C
	(b)	"	liquid at	30°C
Fig. 6.	(a)	<i>p</i> -Chlorotoluene	solid at	-180°C
	(b)	"	liquid at	30°C





splitting of electronic energy levels does not take place when the permanent electric moment is small, as in the case of *p*-chlorotoluene. The results will now be discussed for the three substances separately.

(a) *o*-Chlorotoluene. The absorption spectra of *o*-chlorotoluene in the vapour state was studied previously by Purvis (1911) and Tintea (1939). The data reported by Purvis give only the positions of some of the bands without giving any assignments. The data reported by Tintea were not available to the author and hence the absorption spectra of *o*-chlorotoluene in the vapour state were photographed by the author. A large number of bands are observed, but measurements of only the principal bands produced in the excited state are made and assignments are given in column 2 of Table I. The vapour spectrum resembles that of *o*-fluorotoluene (Cave and Thompson, 1950). The  $\nu_0$  band is at  $36838\text{ cm}^{-1}$ . But just to the lower frequency side of this position there are several intense bands, the principal ones being at  $36677$  and  $36589\text{ cm}^{-1}$  respectively. These represent transitions  $0-161$  and  $0-249\text{ cm}^{-1}$  respectively and may be correlated with the strong Raman frequencies  $163$  and  $247\text{ cm}^{-1}$  (Magat, 1936). The principal frequencies are  $\nu_0 + 530$ ,  $\nu_0 + 813$ ,  $\nu_0 + 915$ ,  $\nu_0 + 1005$ ,  $\nu_0 + 1084$  and their harmonics and combinations. Strong bands seem to appear at intervals of about  $1000\text{ cm}^{-1}$ . The C-Cl vibration appears to be weak.

In the present investigation only three bands are observed in the case of *o*-chlorotoluene in the liquid state, the frequency difference being  $1015\text{ cm}^{-1}$ . The bands are broad and the  $\nu_0$  band is shifted by about  $450\text{ cm}^{-1}$  towards longer wavelength from its position in the vapour state probably due to formation of virtual bonds. The principal  $\nu_0$  band shifts from  $36381\text{ cm}^{-1}$  in the liquid state to  $37122\text{ cm}^{-1}$  in the solid state at  $-180^\circ\text{C}$  and splits up into three bands in the solid state. So, in place of the three bands in the liquid state there are altogether seven bands. The bands also become sharper in the solid state. There are two intense bands marked  $A_0$  and  $A_1$ , accompanied by less intense bands on either sides. The band on the longer wavelength side of the principal bands is at a distance of  $290\text{ cm}^{-1}$  and the distance on the shorter wavelength side is  $590\text{ cm}^{-1}$ . The former band cannot be due to a  $\nu \rightarrow 0$  transition, as the distance between the two bands is large enough to make the number of molecules present in the excited state of this mode of vibration negligible. There is no strong band even in the vapour state corresponding to this transition.

The feebleness of the two companions of the principal absorption band may be explained on the assumption that the virtual bond is formed only at some point in the molecule, the other carbon atoms remaining unaffected. The large shift of the principal band may be due to change of the energy of the whole molecule, i.e., of all the carbon atoms caused by the formation of the virtual bond.

(b) *m*-Chlorotoluene.—Column (2) of Table II shows the tentative assignments for the absorption bands of *m*-chlorotoluene in the vapour

state. Here again only the prominent bands have been measured. The spectrum is entirely different from that of *o*-chlorotoluene and resembles that of *m*-fluorotoluene reported by Cave and Thompson (1950). The  $\nu_0$  band is at  $36619\text{ cm}^{-1}$  and is at about  $220\text{ cm}^{-1}$  on the longer wavelength side of the  $\nu_0$  band for *o*-chlorotoluene. The principal frequencies are  $\nu_0 + 418$ ,  $\nu_0 + 476$ ,  $\nu_0 + 778$ ,  $\nu_0 + 981$ ,  $\nu_0 + 1211$  and their harmonics and combinations. The C-Cl vibration is more prominent in this isomer than in the ortho form. Strong bands appear at intervals of about  $980\text{ cm}^{-1}$ . In the liquid state the substance produces four bands, the frequencies being represented by  $\nu_0$ ,  $\nu_0 + 427$ ,  $\nu_0 + 995$  and  $\nu_0 + 2 \times 995$ . The bands are broad and the principal band is shifted by about  $300\text{ cm}^{-1}$  towards longer wavelengths from the corresponding position in vapour. This large shift of the  $\nu_0$  band towards longer wavelength in the liquid state may be again due to the association of molecules which lower the electronic energy state. In the case of the solid state at  $-180^\circ\text{ C}$ , the  $\nu_0$  band shifts to  $37015\text{ cm}^{-1}$  and the four bands in the liquid state are replaced by ten bands. The most intense band is at  $37015\text{ cm}^{-1}$  with two fainter companions at  $36630$  and  $36120\text{ cm}^{-1}$  marked  $B_0$  and  $C_0$  respectively. The principal bands are at a distance of about  $1025\text{ cm}^{-1}$  from one another and this is greater than the principal frequency  $981$  observed in the vapour state. It can, therefore, rightly be assumed that the electronic energy level in this case also splits up into three components, both the components lying on the longer wavelength side of the main band. This splitting is entirely different from Davydov splitting (1948) as the split components are far away from the principal band. On comparing the spectra of the two isomers *o*- and *m*-chlorotoluene in the solid state, it is observed that the nature of splitting of the electronic energy level depends on the position of the substituent groups.

It may be pointed out in this connection that even in the case of benzene in the solid state at  $-259^\circ\text{ C}$  Kronenberger (1930) observed new series of bands and also the forbidden *o, o* band was observed by him. This appearance of the *o, o* band may be due to the destruction of the six fold symmetry of the benzene molecule by the formation of virtual bonds among neighbouring molecules and the appearance of the new series of bands may be actually a case of splitting up of the energy level owing to the formation of the virtual bonds. These facts may lend additional support to such hypothesis put forward by Sirkar (1936) earlier and by Sirkar and Ray (1950) recently.

(c) *p*-Chlorotoluene.—The absorption spectra of *p*-chlorotoluene in the vapour state was studied very recently (Viswanath, 1952). The  $\nu_0$  band has been located at  $36299\text{ cm}^{-1}$ . The prominent bands represent frequencies,  $\nu_0$ ,  $\nu_0 + 762$ ,  $\nu_0 + 1044$ ,  $\nu_0 + 1052$ ,  $\nu_0 + 1189$  and their harmonics and combinations. The spectrum resembles that of *p*-dichlorobenzene, the main bands appearing at intervals of  $1052\text{ cm}^{-1}$ . The band at  $37061$  representing  $\nu_0 + 762$  is strong, which indicates the presence of fairly strong C-Cl vibration. In the present investigation only three bands are observed in the liquid state of the subs-

tance, the frequency-difference being  $1012\text{ cm}^{-1}$ . The bands are broad and the  $\nu_0$  band is shifted by about  $240\text{ cm}^{-1}$  towards longer wavelengths from its position in the vapour state.

When the liquid is solidified and cooled to  $-180^\circ\text{C}$  the  $\nu_0$  band shifts by about  $165\text{ cm}^{-1}$  towards shorter wavelength and altogether seven bands are observed. They may represent frequencies  $\nu_0 + 768$ ,  $\nu_0 + 1058$  and their combinations and harmonics. The C-Cl vibration which is not prominent in the liquid state appears prominently at  $-180^\circ\text{C}$ . Assignments of the bands are given in terms of the vibrational frequencies observed. It is observed that the electronic energy level is not split up in this case. The molecule of *p*-chlorotoluene has a symmetric structure, the methyl and chlorine atoms being in diametrically opposite positions in the benzene ring. This makes the permanent electric moment almost zero. Freedom of rotation of the molecule is amply facilitated and the packing of the molecules may be loose in the para compound. This makes transitions to higher harmonic states possible.

The investigations are being continued with other substances and the results will be reported shortly.

#### ACKNOWLEDGMENTS

The author is indebted to Prof. S. C. Sirkar, D.Sc., F.N.I., for his kind interest and helpful guidance throughout the progress of the work and to the Government of India for the award of a scholarship.

#### REFERENCES

- Cave, W. T. and Thompson, H. W., 1950, *Discussions of Faraday Soc.*, **9**, 35.  
 Davydov, A., 1948, *J. Exptal. Theoret. Phys. (U.S.S.R.)* **18**, 210.  
 Kronenberger, A., 1930, *Z. f. Phys.*, **63**, 494.  
 Magat, M., 1930, Numerical data on Raman effect.  
 Purvis, T., 1911, *J. Chem. Soc.*, **99**, Pt. III, 1704.  
 Sirkar, S. C., 1936, *Ind. J. Phys.*, **10**, 110.  
 Sirkar, S. C., and Ray, A. K., 1950, *Ind. J. Phys.*, **24**, 189.  
 Sirkar, S. C., and Swamy, H. N., 1952, *J. Chem. Phys.* (in press).  
 Swamy H. N., 1951, *Ind. J. Phys.*, **25**, 262.  
 Swamy, H. N., 1952a, *Ibid*, **26**, 119,  
 Swamy, H. N., 1952b, *Ibid*, **26**, 233.  
 Tintea, H. 1939, *Bull. Sect. Sci. Acad. Roum*, **21**, 219.  
 Vi-wanath, G., 1952, *Ind. J. Phys*, **26**, 263.  
 Wolf K. L., and Herold, W., 1931, *Z. f. Phys. Chem.*, **B**, **13**, 201.

# STUDIES ON THE SHARP EXTRA REFLECTIONS FROM PHLOROGLUCINE DIHYDRATE CRYSTALS\*

## Part II—Effect of Temperature

By M. N. DATTA

INDIAN ASSOCIATION FOR THE CULTIVATION OF SCIENCE, CALCUTTA

(Received for publication, June 5, 1952)

### Plates XVII A-D

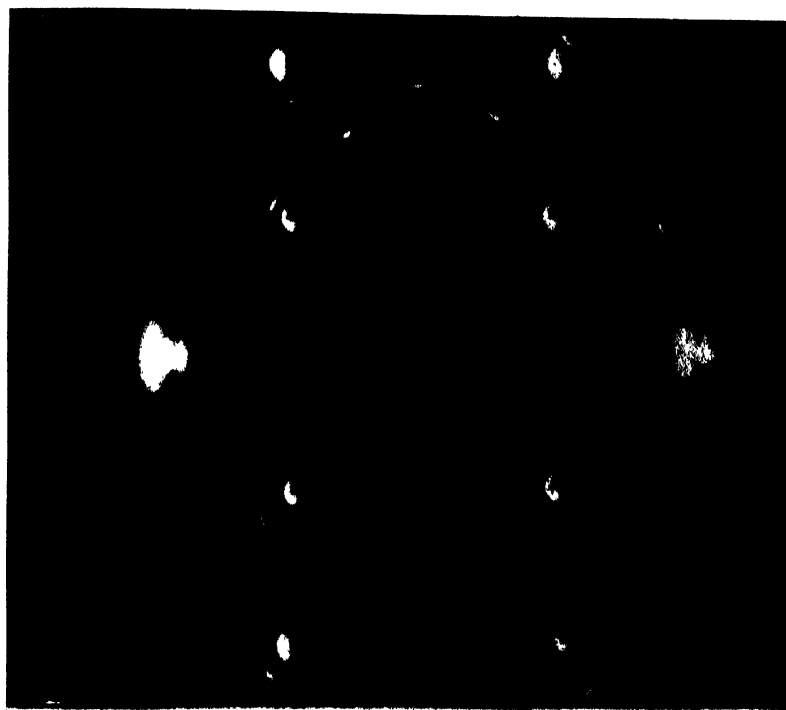
**ABSTRACT.** The intensities of the sharp extra spots in the Laue photograph of phloroglucine dihydrate were measured at different temperatures. It was found that intensities did not change appreciably with rise of temperature. It was also found that dehydration and breaking-up of the crystal into a microcrystalline aggregate began to take place at some temperature between 48°C and 58°C. Heating for different durations at 58°C showed that the breaking-up and dehydration took place gradually and was appreciable for heating for 45 minutes and complete for heating for about three hours. The nature of the sharp extra spots and their persistence with unchanged extension as long as Laue spots were present showed that the origin of these spots cannot be due to the defect structures originating from removal of  $H_2O$  molecules from lattice sites.

### INTRODUCTION

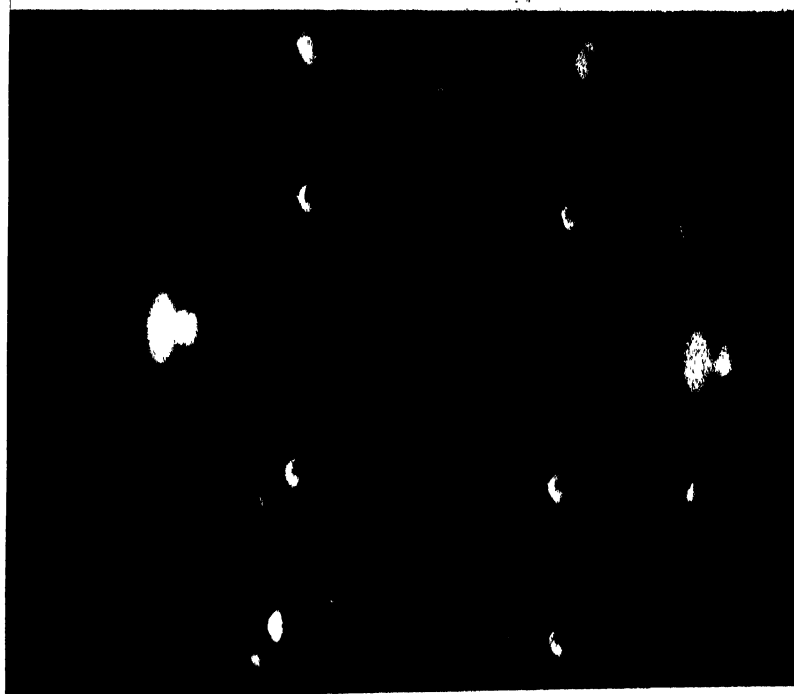
The sharp extra reflections on Laue photographs of phloroglucine dihydrate have been studied in a previous communication (Datta, 1951). The Fourier transforms for these reflections have been traced out by obtaining Laue photographs at various orientations of the crystal with respect to the incident X-ray beam and the conclusion of Banerjee and Bose (1944) that these spots are not of thermal origin has thus been confirmed.

Temperature variation of the intensities of diffuse spots was first measured by Laval (1939) for sylvine who found that the intensities and extensions of these extra spots increased rapidly with rise of temperature, particularly for low orders of reflections. Preston (1939) obtained the same results for NaCl, Al and Zn crystals. Lonsdale and Smith (1941) found that the diffuse spots of a large number of organic crystals vanish at liquid air temperatures. Near the melting point the intensity has been found to increase enormously for small rise of temperature. On the other hand, the sharp extra spots from diamond do not change appreciably in intensity even for a rise of temperature from liquid air temperature to 500°C. It is, therefore, interesting to see how the sharp extra spots of phloroglucine dihydrate behave with rise of temperature.

\* Communicated by Prof. K. Banerjee.

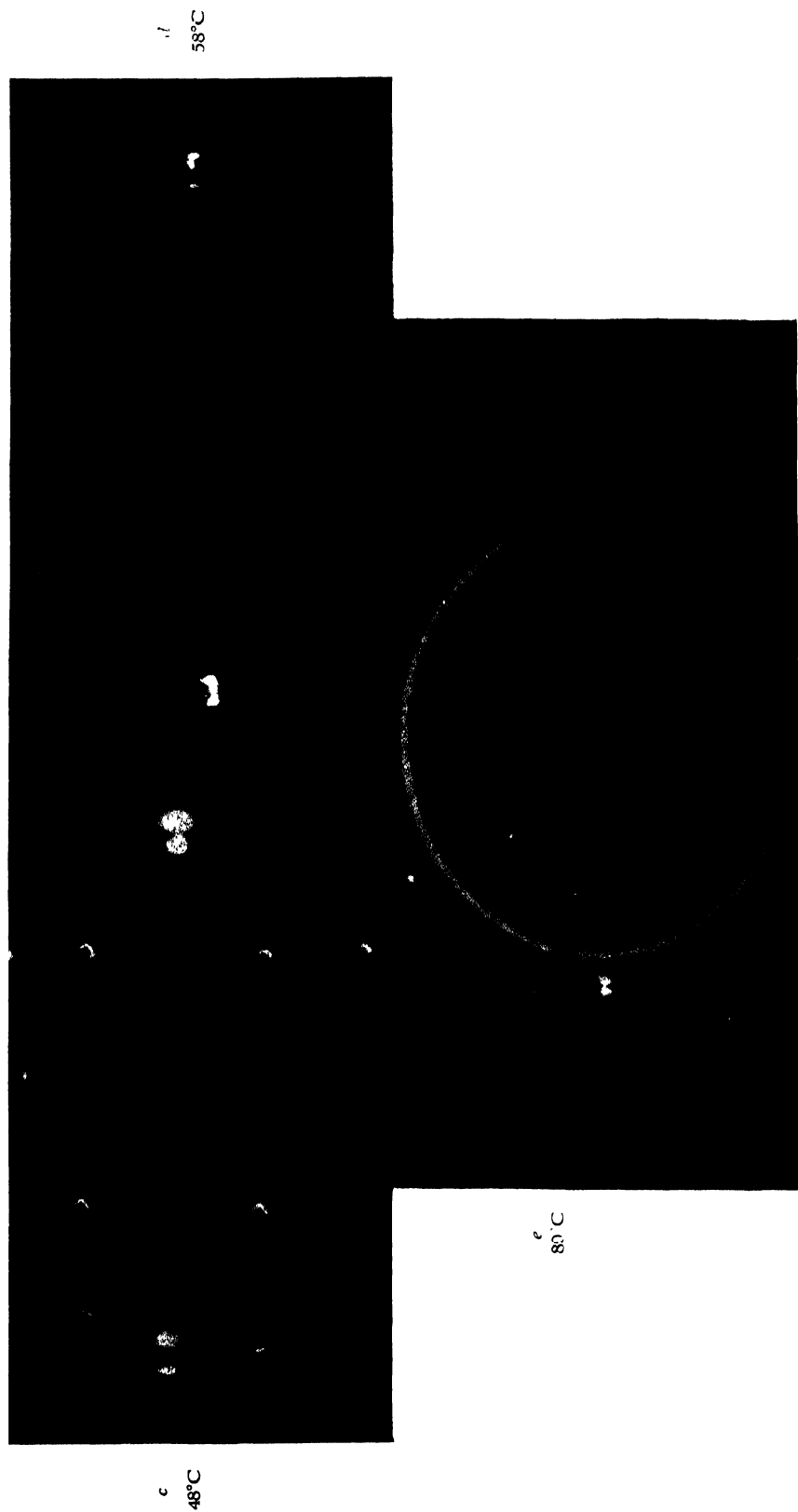


(a)  
27°C



(b)  
37°C

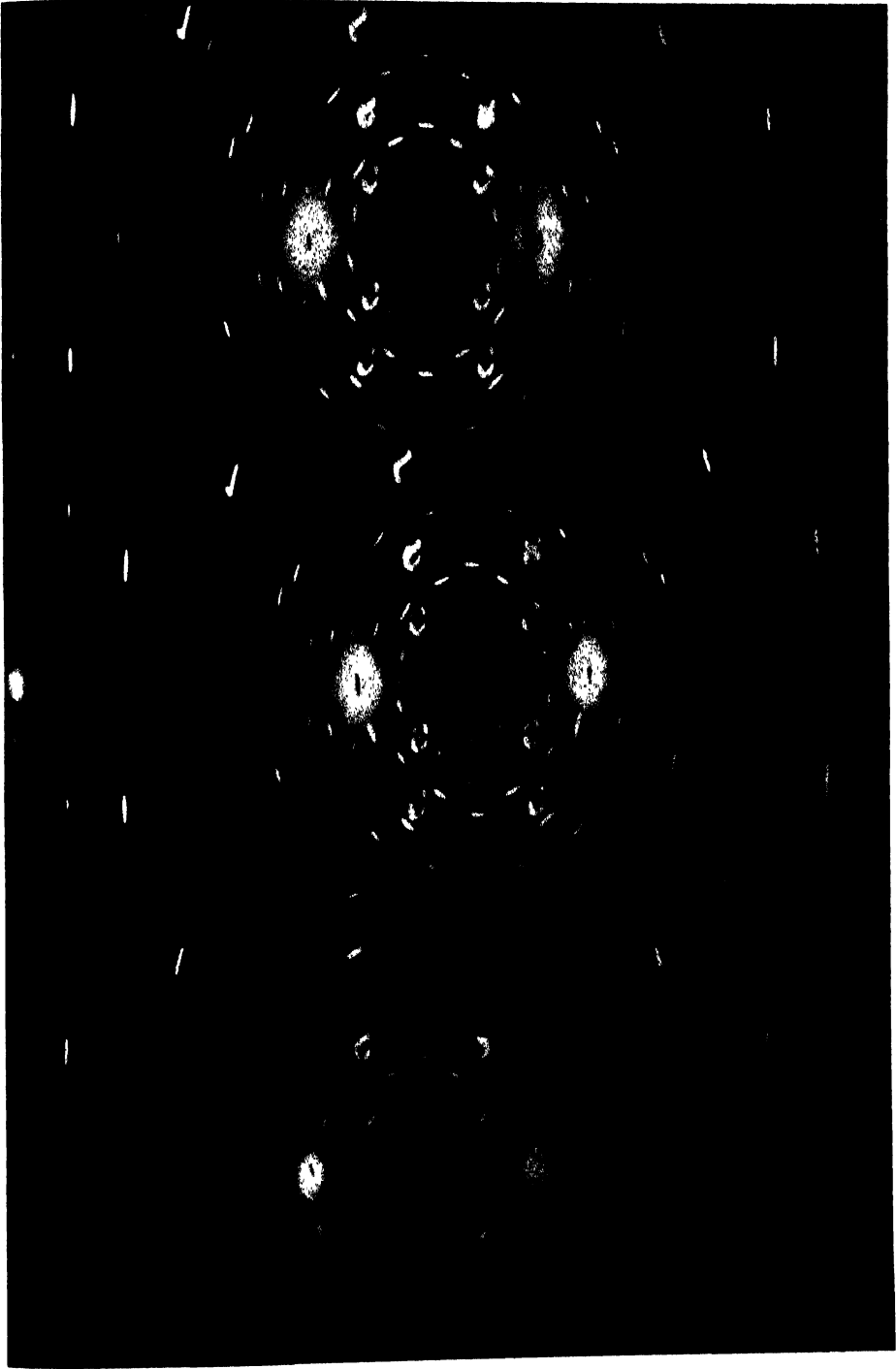
Laue photographs of phloroglucine dihydrate crystals



Figs. *c* and *d*—Laue photographs, Fig. *c*—powder photograph.  
Powder pattern also appears in *d*

20  
mm.

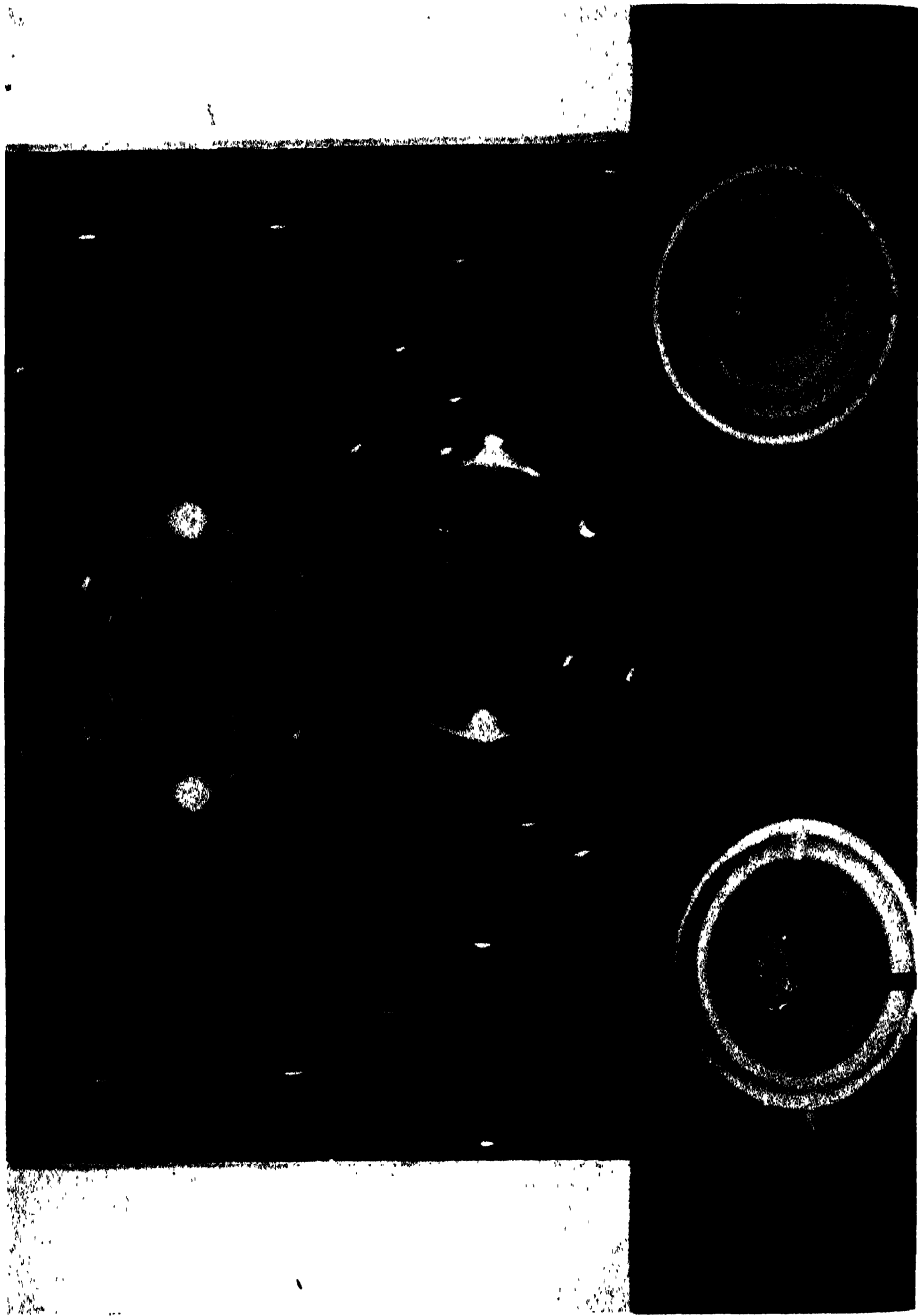
45  
mm.



Laue photographs of phloroglucine dihydrate crystals

DATTA

i  
h



7  
3 hrs.



## EXPERIMENTAL

The X-ray camera employed for studying the temperature variation of the extra spots is a cylindrical one. The cylinder has an outer jacket for circulating water in order to protect the photographic films from an electric heater. It is mounted by attaching it to a thin glass rod by dental cement, the glass rod being clamped on a goniometer head.

In order to have a standard for comparison of intensities of extra spots at different temperatures a small quantity of aluminium powder was dusted over the crystal. The variation of the intensities of aluminium lines over the small range of temperature studied was, however, neglected. The intensities were compared by means of a standard wedge prepared according to the method of Robinson. The ratio of the (111) aluminium line to the maximum intensities of the extra spots were found out by matching each of them against the standard wedge. The results are shown in Table I (see figures *a*, *b* in Plate XVII A and figure *c* in Plate XVII B).

TABLE I

Spot on left side					Spot on right side				
No.	<i>h</i>	<i>k</i>	<i>l</i>	Intensity in arbitrary unit	<i>h</i>	<i>k</i>	<i>l</i>	Intensity in arbitrary unit	
(1)	1	1	.51	27°C	1	1	.54	27°C	6.66
				37°C				37°C	6.73
				48°C				48°C	6.72
(2)	1	2	.909	27°C	1	2	1.09	27°C	5.54
				37°C				37°C	5.70
				48°C				48°C	5.71
(3)	2	1	1.05	27°C	2	1	1.63	27°C	.88
				37°C				37°C	.93
				48°C				48°C	.92
(4)	2	2	1.45	27°C	2	2	2.09	27°C	.45
				37°C				37°C	.48
				48°C				48°C	.46

From these experiments it is found that the intensities of extra spots remain the same within the limits of experimental errors, though, as has been mentioned before, diffuse extra spots show a large variation of intensity with temperature.

At higher temperatures the crystal becomes opaque and at 58°C (figure *d*, Plate XVII B) it gives rise to a powder pattern. This is identical with the powder pattern from dehydrated phloroglucine (figure *e*, Plate XVII B) but is different from the powder pattern that is obtained from phloroglucine dihydrate powder at room temperature. This shows that the dehydration process begins to take place at some temperature between 48°C and 58°C.

It was, however, found that at 58°C dehydration and consequent

breaking-up of the crystal lattice did not take place all at once. X-ray photographs were taken at room temperature after subjecting the crystal to  $58^{\circ}\text{C}$  for periods of 20, 30, 45, 60, 75 and 90 minutes and 3 hours. The results are shown (figures *f-l* in Plates XVII C-D). For heating periods of 20 minutes no change could be observed but for 30 minutes a slight change is discernable. After heating for 45 minutes, the intensities of the sharp extra spots diminished. The Laue spots also diminished in intensity and some disappeared showing that lattice of the crystal is now partially broken up. The photograph for the sample that has undergone one hour heating shows further diminution in intensity and Debye-Scherrer lines begin to appear. For the sample that has been heated for an hour and a half the powder diagram is obtained with slight traces of the sharp extra spots. The sample that has undergone 3 hours heating show a clear powder diagram without any trace of Laue or extra spot.

The defect structure originating from the partial removal of the water of crystallisation was considered to be one of the probable causes of the sharp extra spots. But the above observations are against such a theory, for the dehydration process does not increase the intensities of these spots nor does it diminish the extent of the blank spaces inside these spots.

#### ACKNOWLEDGMENTS

The author expresses his grateful thanks to Prof. K. Banerjee for suggesting the problem and interest in the work and to Sri R. K. Sen for constant advice. The work was carried out at the laboratories of the Indian Association for the Cultivation of Science, Calcutta, and the author wishes to thank the Authorities of the Association for facilities.

#### REFERENCES

- Datta, M. N., 1951, *Ind. J. Phys.*, **28**, 581.  
Banerjee, K., and Bose, C. R., 1944, *Nature*, **163**, 23.  
Laval, J., 1939, *Compt. Rend. Acad. Sci.*, **207**, 169; *Bull. Soc. Franc. Min.*, **62**, 137.  
Preston, C. D., 1939, *Proc. Roy. Soc. A.*, **172**, 116.  
Lonsdale, K., and Smith, H., 1941, *Proc. Roy. Soc. A.*, **179**, 8.

## SEAT OF THE JOSHI EFFECT IN A.C. SILENT DISCHARGES\*

By P. S. V. SETTY, (Miss) K. KULKARNI

AND

C. M. SRIVASTAVA

WIRELESS LABORATORY, PHYSICS DEPARTMENT, BANARAS HINDU UNIVERSITY.

*(Received for publication, April, 1952)*

**ABSTRACT.** Some experiments on the positive and negative Joshi effects in 'sleeve' discharge tubes containing iodine vapour and hydrogen gas have been performed to study the effect of illuminating the different parts of each discharge tube successively by a narrow beam of strong light. The results of these experiments are given in the paper with an account of the experimental arrangements. The results have shown that the Joshi effect (positive and negative) is associated predominantly with the regions of the electrodes. The role of the discharge column of the tube in the production of the Joshi effect, if any, is, however, regarded as uncertain.

The effect of stray light affecting the electrodes after being scattered from the illuminated part of the discharge tube is considered in discussing the experimental results of Agashe.

## 1. INTRODUCTION

There is now sufficient experimental evidence to show that the Joshi effect observed with an ozonizer or with an A.C. operated 'sleeve'-discharge tube is predominantly a surface phenomenon, located on the inner glass surface of either electrode of the ozonizer or round the inner glass surface opposite to either electrode in the case of a sleeve discharge tube. Nevertheless, the possibility of a volume effect is not altogether ruled out. The recent experimental results obtained by Agashe (1951) who used a short discharge tube with external electrodes and illuminated the different parts of the discharge tube by a narrow beam of light, indicated strongly that the positive column of the discharge has an important role in the production of the Joshi effect and that possibly the surface layer at the electrodes has little or no effect. In view of these striking experimental results, it was thought desirable to undertake an experimental study of the positive and negative Joshi effect by illuminating the different parts of the discharge tube successively by a narrow beam of strong light. The object of the present paper is to report the results of this experimental study with an account of the experimental arrangement and to make some general conclusions regarding the seat of the Joshi effect. We shall also indicate

\* Communicated by Prof. S. R. Khastgir.

the reason why little or no photo-reduction of discharge current was observed by Agashe when the regions near the electrodes were illuminated. The effect of light scattered from the illuminated part of the discharge tube is also considered.

## 2. EXPERIMENTAL ARRANGEMENT AND PROCEDURE

A 500-watt electric lamp was placed inside a wooden box lined inside with asbestos sheets. A narrow vertical slit backed by a sheet of glass was fitted up on one side of the box at the same level as the source of light. Another narrow vertical slit was mounted in front of the first slit in a wooden frame fixed to the side of the box. The second slit was also backed by a thick plate glass. In the space between the two vertical slits was inserted a suitable shutter which could be moved in and out by pulling or releasing a string attached to the shutter with the help of a suitable pulley. The discharge tube in question was suspended with the help of a string from a fixed support, and was held with its length horizontal and parallel to the plane of either slit at the same level as the source of light inside the box. A paper scale was attached lengthwise to the suspended discharge tube. Each 'sleeve'-electrode was made of a capillary glass tube bent into a circular form and fitted up tightly round the discharge tube at either end. Sodium chloride solution was introduced into each of these circular glass

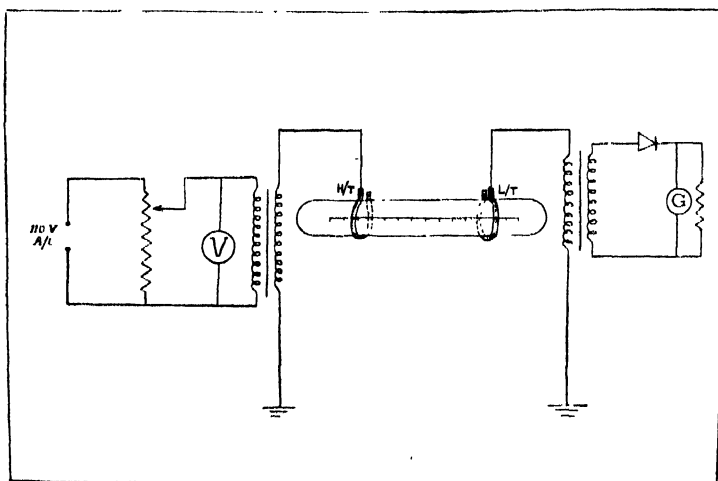


FIG. 1

tubes and connecting wires were taken from the conducting solution in the tubular glass electrodes. In some experiments, one-turn fine copper wire wound round the discharge tube was used as each electrode. The width of the beam obtained with the slit system was about 1.5 mm. The different parts of the discharge tube were illuminated successively by moving the box which was on wheels along with the slits and the shutter system, so that

the narrow beam of light was made to fall on the different parts of the discharge tube which was kept fixed.

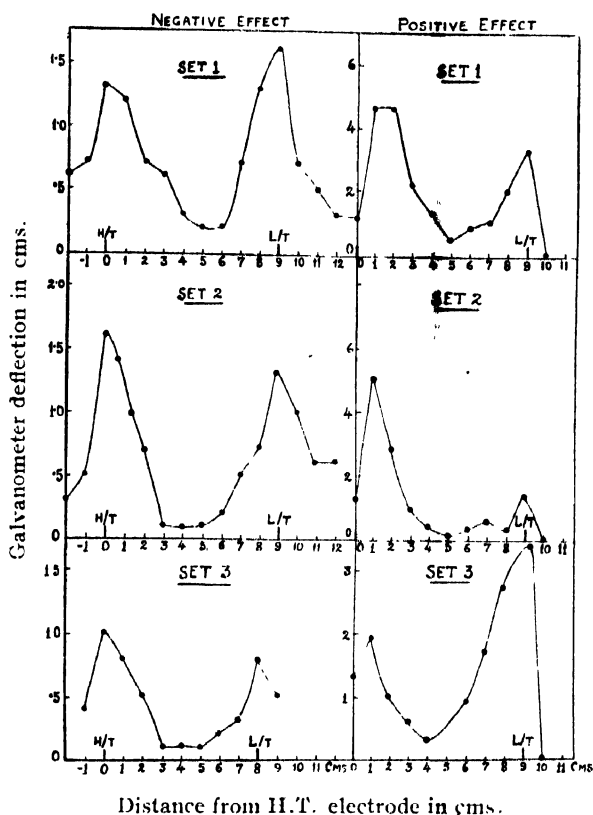


FIG. 2

Positive and negative Joshi effect in iodine vapour sleeve discharge tube. In set 3, the L.T. electrode was not earthed.

Employing 110 or 220 volts (50 cycles A.C.), a suitable step-up transformer and a 'variac' for obtaining a variable voltage for the primary, suitable high voltages were obtained from the secondary for the excitation of the discharge tubes. Usually one end of the transformer secondary was earthed and the other end was connected to one sleeve-electrode of the discharge tube, the other sleeve-electrode being earthed (see figure 1). We shall call the electrode which was earthed, the L.T. electrode and the one connected to that end of the transformer secondary which was not earthed as the H.T. electrode of the discharge tube. The discharge current was measured with a germanium crystal detector unit having a mirror galvanometer in series with the crystal circuit. Experiments were performed with (i) a sleeve discharge tube (length 15 cm., diameter 2 cm.) containing iodine vapour and (ii) a similar 'sleeve' tube (length 36 cm., diameter 1.7 cm.) containing hydrogen. With each tube, requisite voltages were applied to get the

negative and positive Joshi effects. Both the negative and positive Joshi effects, observed at suitable applied voltages, were measured by the increase and reduction of the discharge current when the different parts of the discharge tube were illuminated, part by part, by the narrow beam of light.

### 3. EXPERIMENTAL RESULTS

The results of a few typical experiments with the iodine tube, showing negative Joshi effect for different distances of the illuminated part as measured from one of the electrodes are shown in figure 2. Some typical

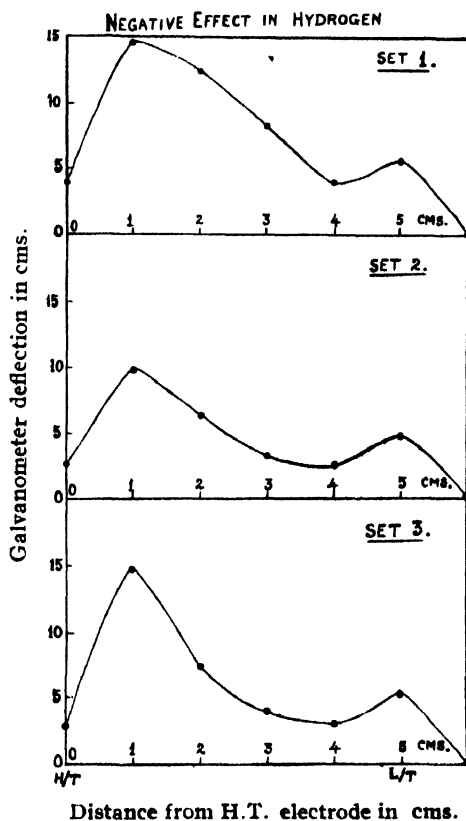


FIG. 3

Negative Joshi effect in hydrogen sleeve discharge tube. In set 3, the L.T. electrode was not earthed.

experimental results showing positive Joshi effect in the same tube for different positions of the illuminated part are also shown in the same figure. Similar experimental data for the hydrogen sleeve-discharge tube showing negative Joshi effect when the different parts of tube were successively illuminated are illustrated in figure 3. Some general features of these curves are enumerated below :

TABLE I  
Negative Joshi effect in iodine vapour

	Distance from HT electrode (cms.)	Galv. readings in cms.		
		Light off	Light on	Photo-reduction.
Set 1. Applied voltage = 1200 volts (50 cycles/sec.)	-2	46.1	45.5	0.6
	-1	46.3	45.6	0.7
	0(H.T.)	46.7	45.4	1.5
	1	46.4	45.2	1.2
	2	46.6	45.2	0.7
	3	46.5	45.9	0.5
	4	46.5	46.2	0.3
	5	46.5	46.3	0.2
	6	46.5	46.3	0.2
	7	46.8	46.1	0.7
	8	47.7	46.4	1.3
	9(L.T.)	50.5	48.9	1.6
	10	49.8	49.1	0.7
Set 2 Applied voltage = 1200 volts (50 cycles/sec.)	11	50.6	50.1	0.5
	12	50.8	50.5	0.3
	-2	48.1	47.8	0.3
	-1	48.1	47.6	0.5
	0(H.T.)	48.9	47.3	1.6
	1	48.0	46.6	1.4
	2	46.6	45.9	0.7
	3	46.7	46.6	0.1
	4	46.7	46.6	0.1
	5	46.7	46.6	0.1
	6	46.6	46.4	0.2
	7	47.1	46.6	0.5
	8	47.5	46.8	0.7
	9(L.T.)	48.8	47.5	1.3
Set 3. Applied voltage = 1820 volts (50 cycles/sec.)	10	48.8	47.8	1.0
	11	49.6	49.0	0.6
	12	50.2	49.6	0.6
	L.T. electrode not earthed			
	-1	56.6	56.2	0.4
	0(H.T.)	56.7	55.7	1.0
	1	56.6	55.8	0.8
	2	56.5	56.0	0.5
	3	56.3	56.2	0.1
	4	56.4	56.3	0.1
	5	56.5	56.4	0.1
	6	56.5	56.3	0.2
	7	56.4	56.1	0.3
	8(L.T.)	57.3	56.5	0.8
	9	57.6	57.1	0.5

TABLE II

Positive Joshi effect in iodine vapour

	Distance from H.T. electrode (cms)	Galv. readings in cms		
		Light off	Light on	Photo-increase
Set 1 Applied voltage = 700 volts (50 cycles/sec.)	0(H.T.)	9.7	10.8	1.1
	1	9.7	14.3	4.6
	2	9.7	14.3	4.6
	3	9.7	11.9	2.2
	4	9.7	11.0	1.3
	5	9.7	10.2	0.5
	6	9.7	10.5	0.8
	7	10.2	11.2	1.0
	8	10.2	12.2	2.0
	9(L.T.)	10.2	13.5	3.3
	10	10.2	10.2	0.0
Set 2 Applied voltage = 700 volts (50 cycles/sec.)	0(H.T.)	9.0	10.2	1.2
	1	9.0	14.0	5.0
	2	9.0	11.8	2.8
	3	9.0	9.9	0.9
	4	9.0	9.3	0.4
	5	9.0	9.1	0.1
	6	9.0	9.3	0.3
	7	9.0	9.5	0.5
	8	9.0	9.3	0.3
	9(L.T.)	9.0	10.3	1.3
	10	9.0	9.0	0.0
Set 3 Applied voltage = 800 volts (50 cycles/sec.)	L.T. electrode not earthed			
	0(H.T.)	14.3	15.6	1.3
	1	12.9	14.8	1.9
	2	13.0	14.0	1.0
	3	13.0	13.6	0.6
	4	13.0	13.3	0.3
	5	13.0	13.0	0.0
	6	13.0	13.9	0.9
	7	13.0	14.7	1.7
	8	13.0	15.7	2.7
	9(L.T.)	13.0	16.4	3.4
	10	13.0	13.0	0.0

(i) The amount of the Joshi effect (negative or positive) was found to have maximum values at (or very near) the two electrodes.

(ii) The effect showed an abrupt fall on either side of the region of each electrode.

(iii) The effect observed for the middle region was found to be minimum. The minimum value, in some cases, was not inappreciable.

(iv) The observed maximum effects in the electrode regions were not, in general, equal in value. In many cases, the effect, when the H.T. electrode was illuminated, was found to be greater than that when the other electrode was illuminated.



TABLE III

Negative Joshi effect in hydrogen. Applied voltage = 6800 volts, 50C/s

	Distance from H.T. electrode (cms)	Galv readings in cms.		
		Light off	Light on	Photo- reduction
Set 1	0(H.T.)	47.5	43.5	4.0
	1	47.5	33.0	14.5
	2	47.5	35.2	12.3
	3	46.5	38.3	8.2
	4	46.5	42.5	4.0
	5(L.T.)	46.5	41.3	5.2
	6	45.0	45.0	0.0
Set 2	0(H.T.)	45.5	43.0	2.5
	1	46.5	36.7	9.8
	2	46.5	40.1	6.4
	3	46.0	42.7	3.3
	4	47.0	44.5	2.5
	5(L.T.)	47.5	43.0	8.5
	6	46.5	46.5	0.0
Set 3 :	0(H.T.)	40.5	37.6	2.9
	1	41.5	26.8	14.7
	2	41.5	34.2	7.3
	3	41.0	37.0	4.0
	4	40.5	37.4	3.1
	5(L.T.)	40.5	35.3	5.2
	6	40.5	40.5	0.0

The experimental data for the iodine vapour discharge tube showing negative and positive Joshi effects are given in Tables I and II. In Table III are given the data for the hydrogen discharge tube showing negative Joshi effect.

#### 4. CONCLUSION AND DISCUSSION

It is abundantly clear from the experimental results that both the positive and negative Joshi effects should be associated *predominantly* with the regions of the electrodes. With regard to (iv), it can be said that the wall charges on the outer surface of the discharge tube were definitely different near the H.T. electrode from those near the electrode which was earthed. This would perhaps explain the difference in the effects observed at the two electrodes. When earth connections were removed and the secondary terminals were directly connected to the two electrodes of the discharge tube, the effects were, in general, found to be of about the same order for the two electrodes in the case of the negative Joshi effect. Further experiments on the effect of wall charges are in progress.

The small amount of photo effect observed when the middle region of the discharge tube was illuminated could be attributed to the stray light reaching the electrode regions after being scattered from the illuminated glass side of the discharge tube. Whether or not this should be regarded as a contribution of the discharge column is indeed difficult to say with any certainty. It is, however, definite that such contribution, if any, must be quite small.

With regard to the experimental results of Agashe, we shall now point out certain features in the lay-out of the experiments which must be taken into consideration in making any final conclusion. It should be noted that the electrodes in Agashe's experiments were plane metal electrodes fitted on to the flat ends of the discharge tube and that when either of the electrodes was illuminated by the beam of light, the latter grazed the surface of either electrode, the angle of incidence being  $90^\circ$ . Under such circumstances, according to the cosine-law of intensity variation, the intensity of light falling on either electrode should be minimum and there should be practically no Joshi effect. We are inclined to believe that little or no photo-reduction of discharge current observed by Agashe, when the electrode regions were illuminated, is to be attributed to this cause. It should also be noted that the length of the discharge tube in Agashe's experiments was as small as 4.5 cm. With such a short discharge tube, there must be some diffused or scattered light from the illuminated glass side of the discharge tube (and also from the attached paper scale) reaching either electrode and this should certainly contribute to some extent to the net photo-reduction of the discharge current. The light scattered from the gas or vapour at low pressure must, however, be too small to produce any appreciable effect. In view of the above considerations regarding the effect of light scattered from the illuminated glass side of the discharge tube to either electrode and in consideration of our experimental results with the sleeve-discharge tubes filled with iodine vapour and hydrogen, we can only say that the experimental evidence substantiating the role of the positive column in the production of Joshi effect should be considered inconclusive.

A short note on the subject has already been published elsewhere (Khastgir, 1952).

#### ACKNOWLEDGMENT

Our sincere thanks are due to Dr. S. R. Khastgir, D.Sc. (Edin.) F.N.I., under whose guidance the present experiments were carried out.

#### REFERENCES

- Agashe, V. V., 1951, *J. Chem. Phys.*, **19**, 8, 1002.  
Khastgir, S. R., 1952, *J. Chem. Phys.*, **20**, 1052.

# DYNAMICS OF THE ELASTIC VIBRATION IN A BAR EXCITED BY LONGITUDINAL IMPACT. PART II. STUDY OF THE TIME OF COLLISION.

By M. GHOSH AND S. K. GHOSH  
PHYSICAL LABORATORY, CITY COLLEGE, CALCUTTA

(Received for publication, May 23, 1952)

**ABSTRACT.** The complete dynamics of the elastic vibration of longitudinal character set up in a bar by the impact of an elastic load has been built up previously in Part I. In the present paper expressions for the time of collision using both hard and elastic load have been derived when the impact terminates during the first and second intervals and the possibility of deriving the same for higher interval has been discussed. The pressure fluctuation during the collision period has been studied and compared graphically for a fairly wide range of values of the elastic constant of the load. The variation of the time of collision with elasticity of the load has been thoroughly studied. It is found that with the increase of elasticity of the load the time of collision changes discontinuously until gradually the discontinuities become less and less pronounced as the hardness is reached.

It has also been observed that the time of collision in the case of a hard load changes discontinuously with the length of the bar, i.e., with the change of 'mass-ratio' of the bar and the load

## INTRODUCTION

The dynamics of the elastic vibration of a bar excited by the longitudinal impact of an elastic load has been worked out previously (Ghosh and Ghosh, 1951), applying the powerful operational method.

In developing the elastokinetics for the bar and the load system, the general expressions for the functions involved in calculation of displacement, as well as, pressure imparted during impact have been derived. Now in this paper we shall study the nature of the fluctuation of pressure during impact, as well as, the time of collision of the load, having different elasticity. The results obtained here will be of great industrial value in measuring the elastic properties of materials available in small lump and also claim to advance the theoretical knowledge of relation between molecular structure and mechanical properties of matter.

*Explanation of the symbols used.* The following symbols have been used throughout the paper.

$l$  = length of the bar ;  $t$  = variable time ;  $s$  = variable, measured along the length of the bar ;  $w$  = displacement at any section of the bar ;  $w_1$  = displacement at  $s=l$ , the struck point ;  $\rho$  = linear density of the bar ;  $\alpha$  = area of the

$$\phi = \frac{2l}{c} + \frac{\left( \frac{1}{A} e^{-\frac{2ql}{c}} + 2A \right) - \left( \frac{1}{A} e^{-\frac{2pl}{c}} + 2A \right) e^{(q-p)\frac{l}{c}}}{2(q+p)e^{(q-p)l/c}} \dots (4)$$

Table I shows the comparison between the values of  $c\phi$  obtained by the two methods just mentioned.

TABLE I

$E_2/E_1\alpha$	$c\phi$ from formula	$c\phi$ by graphical method
0.3	71	70
0.5	67.7	67
0.6	67.5	67
0.9	66	65.8
1.0	65.7	65.5
Hard	64.9	64.85

But we cannot but adopt the graphical method in order to find the time of collision when pressure terminates during  $5\theta_1 > t > 4\theta_1$  or higher intervals.

(C) *Light and soft load.* ( $p < q$ ) i.e. when  $\frac{E_2}{E_1\alpha} < \frac{4\rho}{m}$ .

In this case when the load is light and soft, the time of collision,  $\phi$  during the first interval is obtained by equating the pressure  $P_1=0$  and solving for  $t$ .

Thus, during the interval  $\theta_1 > t > 0$

$$P_1 = 2\rho v_0 c \frac{\mu}{v} e^{-\mu t} \sin vt.$$

and the time of collision is given by

$$\phi = \frac{\pi}{v} = \frac{2\pi}{\sqrt{4\frac{E_2}{m} - \left(\frac{E_2 c}{E_1 \alpha}\right)^2}} \text{ which is the same as given by Ghosh (1935).}$$

During the interval  $2\theta_1 > t > \theta_1$  the time of collision is obtained by equating the pressure equation

$$P_2 = P_1 + 4\rho v_0 c \frac{\mu^2}{v^3} e^{-\mu t_1} \left[ \sqrt{\mu^2 + v^2} vt_1 \cos \left( vt_1 - \tan^{-1} \frac{v}{\mu} \right) - \mu \sin vt_1 \right]$$

to zero and solving graphically for  $t$ .

(D) *Limiting case.* ( $q=p$ ) i.e. when  $\frac{E_2}{E_1\alpha} = \frac{4\rho}{m}$ . The pressures in the

different intervals are given by equations (15.4), (15.5), (15.6) and (15.7) as have been worked out earlier. Thus during  $\theta_1 > t > 0$  where  $\theta_1 = \frac{2l}{c}$  and

$q = \frac{1}{2} \frac{E_2 c}{E_1 \alpha}$ , pressure  $P_1 = 2\rho v_0 c e^{-qt} \cdot qt$ , and it does not terminate.

During  $2\theta_1 > t > \theta_1$ ,

$$P_2 = P_1 + 8\rho v_0 c e^{-qt_1} \left\{ \frac{(qt_1)^2}{2!} - \frac{(qt_1)^3}{3!} \right\}$$

and the time of collision  $\phi$  is given by

$$2e^{\frac{E_2 l}{E_1 \alpha}} \left( \frac{E_2 c}{2E_1 \alpha} \right)^2 (\phi - \theta_1)^3 - 6e^{\frac{E_2 l}{E_1 \alpha}} \left( \frac{E_2 c}{2E_1 \alpha} \right) (\phi - \theta_1)^2 - 3\phi = 0 \quad \dots (5)$$

provided the maximum value of  $\frac{E_2 l}{E_1 \alpha}$  is given by the equation

$$1 + \frac{E_2 l}{E_1 \alpha} \cdot e^{\frac{E_2 l}{E_1 \alpha}} \left( 1 - \frac{1}{3} \cdot \frac{E_2 l}{E_1 \alpha} \right) = 0 \quad \dots (5.1)$$

which has a root  $\frac{E_2 l}{E_1 \alpha} = 3.05$  (approximately)

So the pressure terminates during  $2\theta_1 > t > \theta_1$  i.e. during the second interval, so long as  $\frac{E_2 l}{E_1 \alpha} \nless 3.05$  and the maximum 'mass-ratio'

$m_1 \left( = \frac{m}{\rho l} \right) \nless 1.31$  as in this case particularly,

$$\frac{E_2 l}{E_1 \alpha} = \frac{4\rho l}{m} = 3.05 \quad \dots (5.2)$$

The general solution of equation (5) is well known in the theory of equation, but it may be solved numerically either by Newton's or Horner's method. Similarly, time of collision may be algebraically solved for higher intervals so long as  $\phi$  appears as a quartic, above which numerical or graphical solution has to be adopted.

It is interesting to note that the time of collision in the case of hard load, but of the above mass-ratio bears approximately a constant ratio,  $\frac{\sqrt{3}}{2}$  with the period of the fundamental which is evident from equation (2).

The nature of the pressure fluctuation with time, during collision, is shown graphically in figures 1-3 for different values of elastic constant the load.

In doing so, computation of the above pressure expressions is made

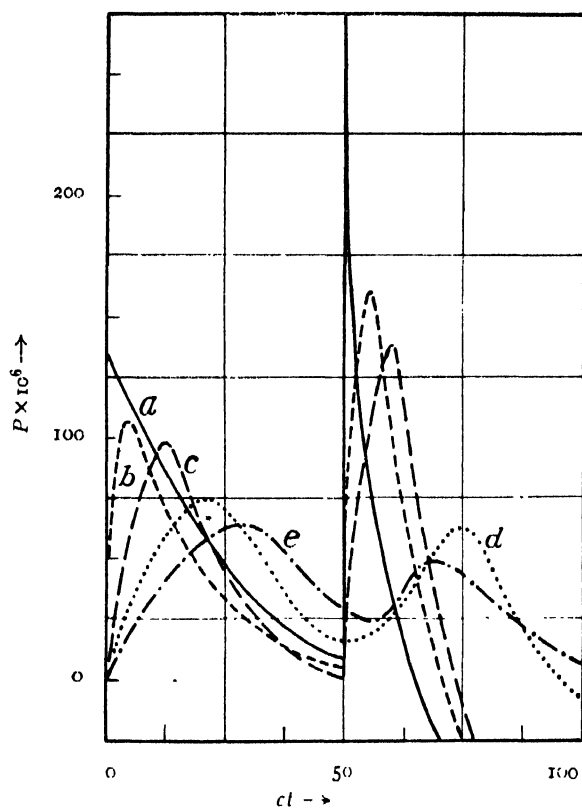


FIG. 1

with the help of some numerical data as :  $l = 25$  cm.,  $\rho = 7$  gm/cm.  $E_1 = 10^{12}$  dynes/cm<sup>2</sup>,  $E_2 = \tau E_1$  where  $\tau$  is a positive quantity integral or fractional and is of the dimension of length,  $m = 100$  gms.,  $m_1 = m/\rho = 0.573$ ,  $\alpha = 1$  cm<sup>2</sup>,

$v_0 = 50$  cm/sec and so  $c = \sqrt{\frac{E_1 \alpha}{\rho}} = \frac{10^6}{\sqrt{7}}$  cm/sec.

Now comparing the curves (a), (b), (c) and (d) in figure 1, we find that with the decrease of the elastic constant of the load, the discontinuous periodic rise of pressures loses its sharp angularities and well-rounded hump appears instead. Also the time of collision gradually increases as the hardness of the load gradually decreases, and after a certain limit,  $\phi$  changes enormously with slight change of the elastic constant of the load. This,

however, takes place when the load is light and soft (i.e. when  $\frac{E_2}{E_1 \alpha} < \frac{4\rho}{m}$ ).

But the time of collision is not much affected with the slight decrease of hardness, (in case when  $\frac{E_2}{E_1 \alpha} > \frac{4\rho}{m}$ ) and an appreciable change of hardness to a smaller value causes a sensible increase in the time of collision.

Curve (e) in figure 1 explains a typical ' $P-ct$ ' variation with a light and soft load for  $\frac{E_2}{E_1\alpha} = \frac{1}{2} \cdot \frac{\rho}{m}$ . Here, it is interesting to note that the pressure does not terminate even at the end of the second interval showing thereby an enormous increase in the value of  $\phi$ . This clearly indicates that with a light and soft load, apart from the consideration of mass-ratio, there is a limit to the reduction in the value of the elastic constant of the load that the pressure would terminate during the second interval ( $\phi = 2\theta_1$ ). A further reduction of the elastic constant of the load tends the pressure to terminate at intervals higher than the second.

Next we consider the effect of elasticity of the load on the time of collision in the present system. The result of the variation of  $E_2$  with  $c\phi$  is shown graphically in figure 2. It is found that with a hard load (i.e.,

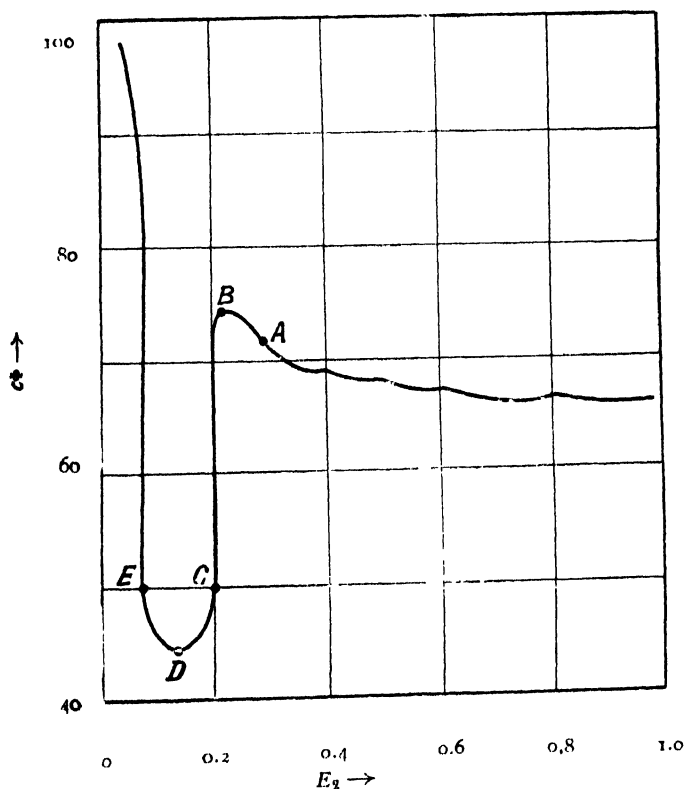


FIG. 2

when  $E_2 = \infty$ ), the time of collision has a minimum constant value ( $c\phi = 64.85$ ). As the hardness of the load decreases, the time of collision increases discontinuously till the point A is reached where  $\frac{E_2}{E_1\alpha} = \frac{4\rho}{m}$ . With further

decrease in hardness, the time of collision  $\phi$  still increases, reaches a maximum as at  $B$  and then abruptly falls to a very low value ( $\phi < 2l/c$ ) as indicated by  $C$  on the graph. After this,  $\phi$  decreases gradually with the decrease of

hardness of the load till it is minimum (when  $\frac{E_2}{E_1} = \frac{2\rho}{m}$ ) as denoted by the point  $D$ . The effect of further decrease of the elastic constant of the load gradually increases  $\phi$  which, however, is always less than  $\frac{2l}{c}$ , i.e., half the period

of the fundamental, until  $E$  is reached when  $\frac{E_2}{E_1} = \frac{\rho}{m}$ . Any further slight

decrease in the value of  $E_2$  causes  $\phi$  to increase abruptly to a high value which is evident from the asymptotic nature of the graph in this region.

We now study the variation of the time of collision using different lengths of the bar and a hard load. The time of collision during the second and third intervals has been computed from equations (2) and (3). The graph showing the variation of  $\phi$  with  $l$  is given in figure 3. The nature of the

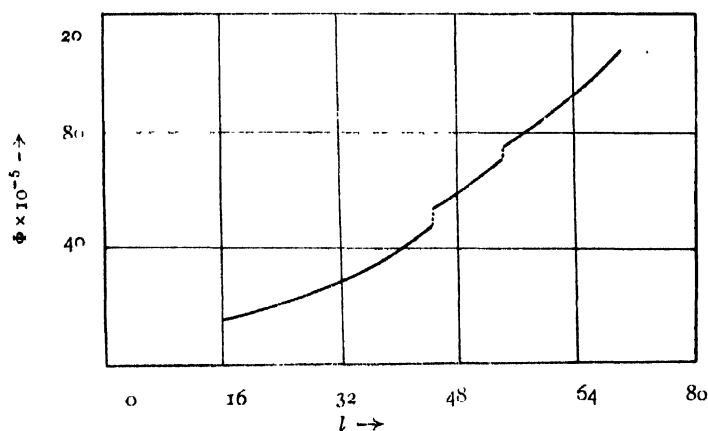


FIG. 3

curve shows that  $\phi$  varies discontinuously with  $l$  from epoch to epoch and for higher values of 'mass-ratio' the curve shifts towards greater value of the time of collision.

In Sec. II. of Part I we have also considered the collision of an elastic load striking the fixed end of the bar, other end being free. The expression for the pressure was obtained as

$$P = \frac{E_1 \alpha}{c} \left[ f_1'(t) - 2f_2'(t_1) + 4f_3'(t_2) - 2f_4'(t_2) + + \dots \right]$$

When  $E_2 = \infty$ , pressure is found to terminate at  $t = 2l/c$ . But with the



elasticity of the load  $\phi$  is not found to be a constant quantity but fluctuating.

Figure 4 shows the variation of  $\phi$  with  $E_2$ . The nature of variation is

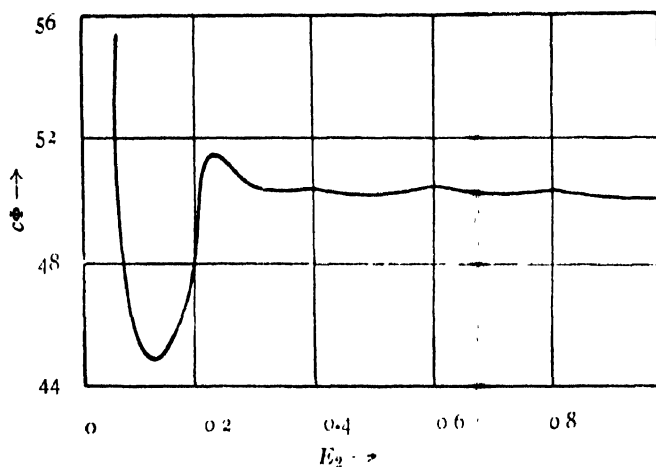


FIG. 4

similar to that obtained for the collision at the free end. But the value obtained in each case is much less pronounced.

The study of resonance vibration is in progress and will be published in due course.

#### REFERENCES

- Ghosh, M., 1935, *Bull. Cal. Math. Soc.*, **27**, 1.  
 Ghosh, M. and Ghosh, S. K., 1951, *Ind. J. Phys.*, **28**, 153.  
 Love, *The Mathematical Theory of Elasticity*, 4th Ed., p. 431.



# A HIGH PRECISION IONOSPHERIC SOUNDING EQUIPMENT\*

BY B. M. BANERJEE AND R. ROY

INSTITUTE OF NUCLEAR PHYSICS, CALCUTTA

(Received for publication, August 22, 1952)

Plates XVIII A—C

**ABSTRACT :** An ionospheric sounding apparatus of high resolving power and accuracy has been described. It utilizes a transmitter generating 50 K.W. sounding pulses of 6-30  $\mu$  seconds duration, interchangeable receivers of 50-200 Kc/s bandwidth and a twelve line raster time base to produce a greatly expanded presentation of the pulse echoes. A study of the height-measuring accuracy and resolving power of such instruments, in both ideal and practical conditions, that leads to interesting conclusions, has been appended.

## INTRODUCTION

The conventional ionospheric sounding equipments employ pulses of 100-200  $\mu$  seconds duration. This long duration pulse limits the resolution to 15 to 30 Km and the height measuring accuracy to about 5 to 10 Km. Investigations on (a) tides in the ionosphere, (b) gradient of ionisation density in the E layer, (c) magneto-ionic splitting, (d) reflections from a layer of patchy ionisation etc. demand a much better resolution and accuracy in height measurements. A ten-fold improvement in this direction would require the employment of pulses of 10-20  $\mu$  seconds duration. The oscilloscope time base must have also a sweep expanded at least ten times.

A short duration R.F. pulse necessarily contains sidebands scattered over a wide frequency range (Fink, 1947). For a pulse of duration  $d$ , these sidebands have appreciable intensity over a range of frequencies equal to  $1.2/d$ . The output of a receiver, having a bandwidth of this amount, would be a triangular pulse of half-width nearly equal to  $d$  (M.I.T. Staff, 1946). The output of a receiver of reduced bandwidth, would again be triangular but of a halfwidth that is proportionately greater. In order that a transmitter pulse of 10-20  $\mu$  seconds duration may not be unduly broadened, one must utilize receivers of 60 to 120 Kc/s bandwidth. Such a receiver would have its noise background† increased ten times, so that to obtain an equivalent signal to noise ratio in the echo reception, one would have to increase the transmitter power ten times. The larger bandwidth of the receiver would also cause objectionable interference due to heterodyning of adjacent broadcast stations, whenever sounding has to be made within such a band. These have actually been observed. It has been found that to obtain a readable pulse echo in this difficult case of broadcast interference, a peak pulse power in excess of that of the interfering stations is necessary. This puts the transmitter power requirement to a value in excess of ten kilowatts.

Besides the necessity of an increased power output in the transmitter, an ionospheric equipment that uses such short pulses is at a disadvantage as to its accuracy of frequency measurement. The wider side-band spread of the trans-

\*Communicated by Prof. M. N. Saha, F.R.S.

†Random noise—chiefly atmospheric—reduces the readability of a pulse echo most seriously. Random noise power is proportional to bandwidth.

mitter and the wider pass-band of the receiver, make the tuning of the receiver broader, so that the frequency measuring accuracy suffers in the same ratio by which the height measuring accuracy improves. Further, the different frequencies of the transmitted side-bands would require different ionisation densities to get 'reflected.' When the ionisation density in the ionospheric layer increases slowly with height, these side frequencies would be returned from sensibly different heights and would have correspondingly different time delays. Echo signals will, therefore, continue to be received by the receiver over a period of time appreciably greater than the original pulse duration. This would cause a broadening of the 'reflected' pulse which would seriously reduce the accuracy of height measurements.

To overcome these difficulties, we have used a frequency responsive detector (figure 9), such as is used in a frequency-modulation receiver. The response of a frequency-modulation detector to pulse signals, when properly tuned is a nearly symmetrical pulse with an up-and-down stroke (Plate XVIII A). To produce this symmetrical pattern, a critical positioning of the receiver frequency dial is needed. This greatly increases the accuracy of frequency determination. Besides, the central linear part (figures 15) of this pattern may be considered to represent the arrival of the different side frequencies at different times. In case when the ionosphere echo of a short duration pulse is broadened in the manner described in the last paragraph, this central part is also found to occupy a correspondingly greater duration. This makes it possible to assign different time delays to the different side frequencies that are identifiable from their output voltages\*. In any case the time delay of the centre frequency may be determined with high accuracy, being given by the time delay corresponding to the undeviated position of the spot at the centre of the output pulse.

#### GENERAL DESCRIPTION

The object of this communication is to describe the high precision sounding apparatus installed some time ago, (Banerjee and Roy, 1952), in the Institute of Nuclear Physics. The system is best described by the block diagram (figure 1). The sequence of operations are controlled by the timer incorporated in the raster time base. The timer actuates :

- (a) the sweep circuits of the cathode ray tube indicators delineating the pulse and ionosphere echoes,
- (b) the sweep circuit (figure 14) of the cathode ray tube monitoring the transmitted pulse,
- (c) the delay multivibrator in the transmitter assembly, almost synchronously.

The delay multivibrator, in its turn actuates the pulser (figure 2) after an adjustable time delay variable between 20-120  $\mu$  seconds. The pulser produces pulses of duration adjustable between 4-24  $\mu$  seconds, which operate on the cathodes of the pulsed oscillator (figure 3) generating R.F. pulses of 10-50 K.W.-peak power. This is delivered into the transmitting wide band delta aerial supported by a 75 foot mast. This delta aerial is normally terminated (figure 7) in its apex by a non-inductive resistance of 800 ohms. Relays in a box at the mast top, however, provide for other types of terminations, such as a 100 pf vacuum condenser, a short circuit and an open circuit.

The transmitter monitor delineates the envelope of the R.F. pulse by applying the rectified signal picked up by a diode to the vertical plate of the monitor oscilloscope (figure 14). The horizontal plates of the monitor scope is connected to the monitor sweep amplifier. The monitor time base produces a fast sweep of 150  $\mu$  sec. duration at the start of each sequence of operation. The cathode ray beam is blanked out automatically and instantaneously after the conclusion of

\*The F.M. detector produces an output which depends only on the frequency of the signal received, when the amplitude of the exciting signal is greater than a minimum level.

this fast sweep. The sweep normally occupies the entire face of the tube producing a satisfactory presentation of the pulse shape.

The pulse signals collected by the receiving delta aerial, are amplified by the tuned R.F. amplifiers in the receiver (figure 9). Then they are passed on to a balanced mixer, converted into intermediate frequency signals, amplified by the

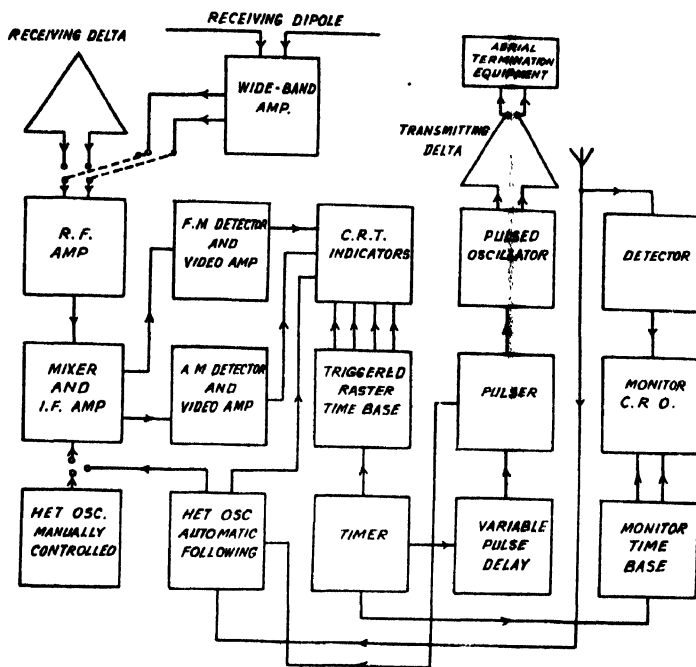


FIG. 1  
System block diagram

intermediate frequency amplifiers to be demodulated by the detectors. There are two detectors, the amplitude responsive (A.M.) detector and the frequency responsive (F.M.) detector. These are followed as usual by I.F. filters and are then passed on to direct coupled video amplifiers. The video amplifiers drive the cathode ray tubes. One of them is a double beam tube (figure 13).

The heterodyning oscillation is supplied by either (i) a manually controlled oscillator (figure 10) or (ii) an automatically following electronic servo controlled oscillator (figure 12). This controlled oscillator also delivers an output signal proportional to the frequency correction. This output may be used to deflect the C.R. tube beam in the vertical direction. With the A.M. output from the video-amplifier connected to the C.R. tube cathode, so that the normally blanked out beam is switched on during the pulse echoes, a sweep frequency presentation over a range of 600 to 800 Kc/s in frequency and 50 Km. in equivalent height is obtainable. This mode of presentation gives a greatly expanded sweep-frequency record and thus makes possible a very accurate study of a particular region of the ionosphere.

The receiving horizontal dipole on the mast top at 140 ft. above ground level and the wide band amplifier there (figure 8) make possible reception of pulse echoes under conditions of severe man-made interference and interference from the powerful local transmitters. This is due to the great reduction of pick-up of the vertically polarized radiation. The main receiver may be connected to the mast dipole (alternatively to the receiving delta aerial) and its amplifier through a readily interchangeable attachment. The wide-band amplifier receives its opera-



coil selector (figure 5) on pressing a push button. When in position, the five coil contacts mounted on the turret wheel, engage corresponding fixed contacts. This rotatable coil assembly not only keeps to a minimum the stray wiring capacity but simultaneously solves the rather formidable problem of the layout of wiring and its high voltage insulation.

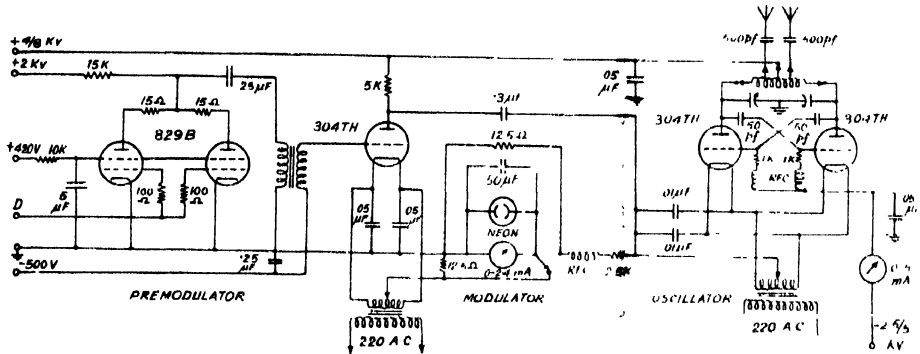
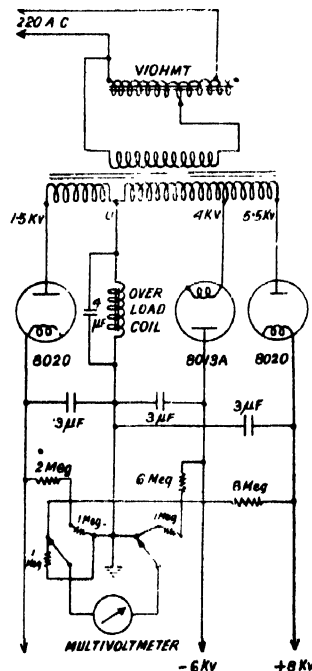


FIG. 3

### Pre-modulator, modulator and oscillator unit

The LC circuit at the anodes of the oscillator has been deliberately designed to work with a minimum of capacity so as to keep down the reactive energy stored in the tuned circuit. The build-up and decay time of the R.F. oscillations are



**FIG. 4**

### Transmitter power supply unit





circuit. It was felt that a reduction in the maximum value of the tuning capacity is desirable in view of the fact that it will be necessary to run the pulsed oscillator tubes at voltages far above their normal ratings—probably close to their break down limits—in the interests of high peak power output.

A small maximum capacity is also dictated by the size of the variable condenser which must have large spacings to withstand the high voltages. A reduction in spacings is possible if oil is used instead of air as the insulating medium. The entire resonant circuit assembly has, therefore, been designed to fit neatly within a rectangular tank of size 2'5"×10"×1'8". This could be filled up with oil, when high voltages may be applied safely. The motor driving the coil turret and the selsyn driving the condenser (figure 5) are coupled through vertical flexible shafts, and are situated above, as a separate unit, on the roof of the transmitter rack.

The dust cores in the coils secure a greater co-efficient of coupling between the aerial and the oscillator circuit. This helps materially in obtaining a high rate of power transfer to the aerial from the resonant circuit. Rapid decay of R.F. oscillations is thereby ensured.

The cathode pulsed oscillator has the following advantages :

1). It produces a pulse output corresponding to the sum of the H.T. and the negative pulse voltage at the cathode. As such, it would produce an output corresponding to 14 K.V. with only 8 K.V. as the maximum positive H.T.

2). The H.T. the oscillator tubes have to hold off after the pulse interval is only 8 K.V.

3). The capacity load to the pulser is small. Alternative schemes of pulsing—e.g. pulsing the plate through a pulse transformer would load up the modulator circuit with a capacity that may amount ten times as much.

4). The oscillator tubes are switched into the condition of complete conduction very rapidly, as the pulse voltage operates between grid cathode. The switch off is also very rapid, because as the pulser current shuts off, the large oscillator current rapidly charges up the cathode to ground stray capacity.

The 304 TH pulse modulator follows conventional practice, operates with an H.T. of 8 K.V. (figure 4) and is driven by an 829 B double pentode (figure 3) through a phase reversing pulse transformer. The 829 B operates with an H.T. of 2 K.V., a screen supply of 400 volts and is driven by a 6L6 (figure 2) through another pulse transformer. Two pulse transformer couplings were found essential as otherwise satisfactory drive for the final 304 TH could not be secured. Pulse transformer couplings enable a very straightforward and flexible design of the circuit, and reduce the H.T. drain and heat dissipation enormously.

The operation of the pulse generator (figure 2) is best explained by following the sequence from the start of the raster time base. This applies a positive spike that triggers the blocking oscillator in the time base chassis. The blocking oscillator delivers an output, a 3  $\mu$  seconds 70 volt square wave signal that is carried on through a shielded cable to the transmitter rack situated on the other side of the room. This pulse is applied through a diode (point A) to trigger the delay multivibrator of the pulse generator and, the fast time base of the transmitter monitor (figure 14).

The delay multivibrator generates a positive square-wave synchronous with the triggering signal. The duration of this square wave may be altered by the variable one megohm grid leak—a panel adjustable that forms the delay control. This pulse is inverted by a 6J5 amplifier and the differentiated output applied to the grid of the biased off 6SJ7 tube. The positive spike that gets applied to the 6SJ7 grid at trail of the delay multivibrator output, makes the 6SJ7 tube draw a burst of charge that triggers the 6SN7 multivibrator. The 6SN7 multivibrator which triggers at the trail of the delay multivibrator generates the pulse that goes on amplified by the transformer-coupled 6L6 and 829B tubes to the grid of the 304TH pulse modulator. Its duration may be controlled by the one megohm variable resistance that forms the panel mounted duration control.

The pulse transformers utilized in the pulser were constructed in the laboratory. They contain five layers of winding in the primary as well as in the secondary. The primary and secondary layers are interleaved. The layer insulation is empire cloth. The cores are collection from disposal junk—laminations of 3 and 5 mil. thickness. The performance of these transformers have been found to be surprisingly good—they will pass on pulses of 3-50  $\mu$  seconds duration practically undistorted. The rise and trailing times with resistance load is about a microsecond. The blocking oscillator transformer is wound on the 3 mil. core and contains single layer windings.

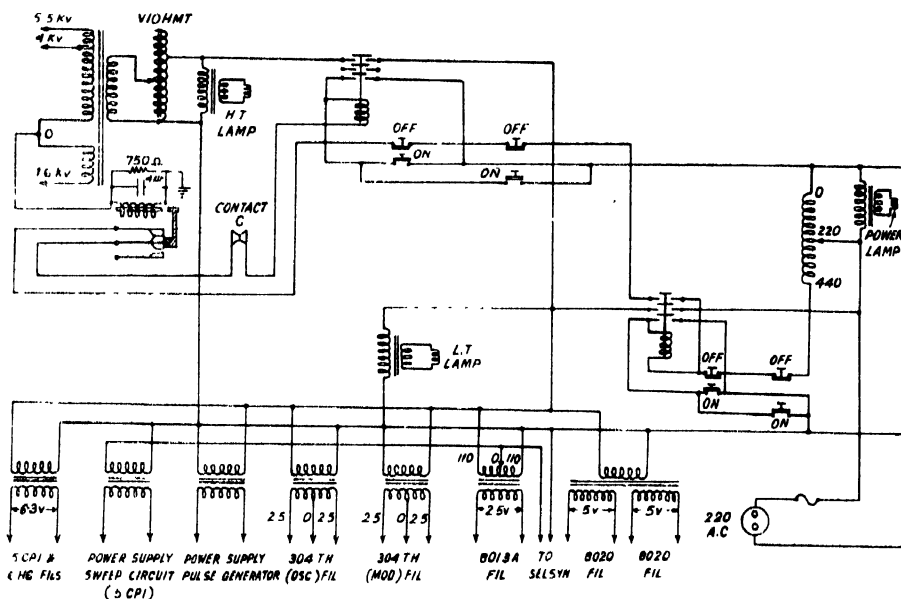


FIG. 6

Remote control and interlocking arrangement of the transmitter

**The Wide Band Aerials.** The transmitter feeds the wide band multiple wire delta aerial symmetrically at its base through a short length of high voltage cable. This triangular aerial has a base that is 150 ft. long and its apex is at a height of 75 feet from the base. It is supported by a multi-section plywood mast of 75 feet height. The mast base is at the central and the top-most point, 65 ft. above the ground level, of the building. The three aerial wires that run in parallel to reduce the characteristic impedance are spread to 1 ft. at the base. The sides converge at both ends and are spread out by a 3 ft. spreader at a distance of 22 ft. from the apex. The normal termination at the apex is a resistance of 800 ohms. This may be altered (figure 7) by a combination of two antenna relays—special high voltage contactors, for an open circuit, a short circuit and a vacuum condenser of 100 pf. The characteristics of an aerial of this type are very suitable for ionospheric work and has been studied in detail by Cones (1951). The radiation pattern has a maximum in the vertical direction and falls off rapidly as the angle to the vertical increases. Minor lobes, tipped at various angles to the vertical in the plane of the antenna, are no doubt found at the higher frequencies (above 12 Mc/s) but even then the vertical lobe takes the major fraction of the radiated power. The impedance characteristics are also very suitable, in as much as the impedance remains approximately constant over the major part of the frequency range, i.e. from 3 to 20 Mc/s and is chiefly resistive. The reactive component is small and vanishes periodically. At frequencies above 4 Mc/s, more than half

the power fed into the aerial gets radiated. However, at frequencies below 4 Mc/s, the radiated power diminishes rapidly and most of the power is wasted in the terminating resistance. As at these low frequencies, the vertical directivity is also very greatly lost, it was thought that an advantage may be secured if the system is operated like a resonant aerial, without the dissipative termination. The relays at the mast top that provide the alternative terminations, have actually been found helpful. They enable a much needed improvement in the echo signal strength at frequencies below 2.5 Mc/s.

A smaller single wire delta aerial, supported on the same mast, with its plane at right angles to the plane of the transmitting delta feeds the receiver. Its signal pick-up is adequate and impedance variation with frequency of little consequence in soundings.

It was well known that in the location where the apparatus was intended to be installed, noise from electrical machinery would constitute the most serious obstruction in the reception of pulse echoes. It was apparent that a drastic reduction in the interference pick-up would be needed, if soundings are to be made

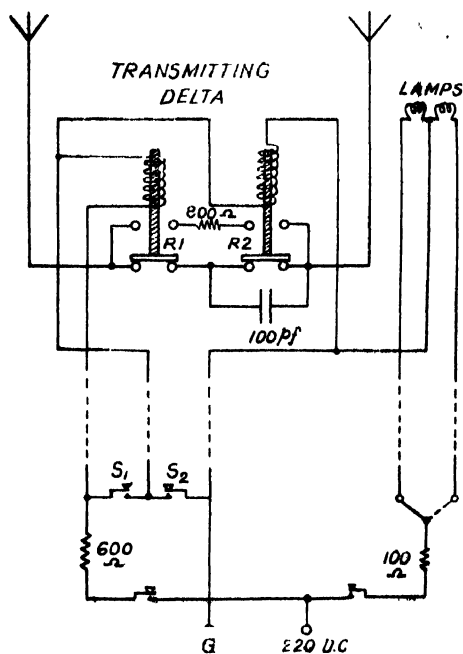


FIG. 7

- Termination assembly at mast top for the transmitting delta antenna

reliably at all times of the day and season. With this end in view, shielded polystyrene cables are utilized for the downloads from this delta to the receiver.

Experience with the equipment showed that although a great improvement in the S/N ratio is secured by the above means, nevertheless man-made interference was still responsible for the most serious limitation of the usefulness of the apparatus.

A further reduction in man-made interference was secured by an alternative aerial system (figure 8), that was erected later. It consists of two horizontal dipoles, fourteen feet aluminium pipes of one inch diameter, situated on the mast top, the highest point (140 ft. above ground) attainable. This effectively picks up the horizontally polarised echo signals and feeds them straight into a wide band amplifier, situated at the mast top. This transmits the signal, at a low impedance

level, down twin cables to the receiver. The field of the electrical noises at the location (140 ft. above ground) of the dipoles is much smaller. However as the signal must be carried down below, to the location of the receiver, wherein the noise field is very much greater, some pick-up takes place in the twin cable, so that some noise is still collected by the receiver. The wide band amplifier improves matters greatly by strengthening the echo signals when they pass down the twin cables through the noise field, to the receiver. The improvement in the  $S/N$  ratio would have been much smaller if the wide band amplifier were not used.

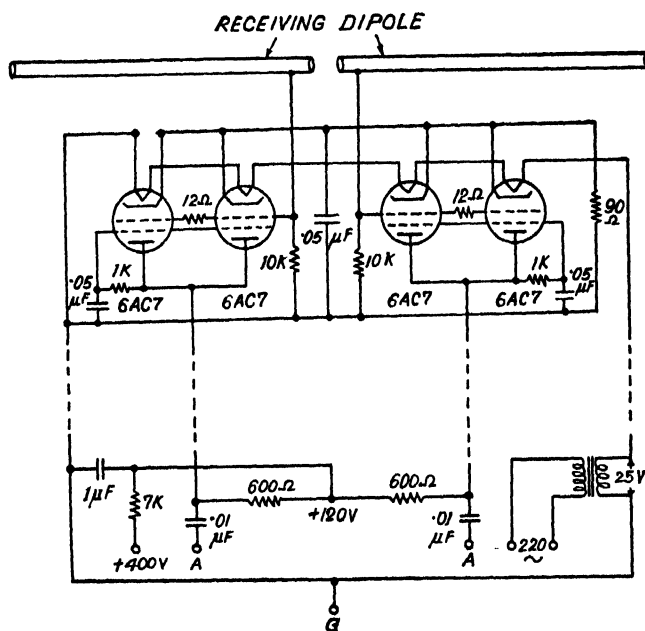


FIG. 8

#### Receiving dipole and wide band amplifier

The horizontal dipoles secure another advantage. It minimises the pick-up of the local stations. Effective soundings could be made right at the frequency of the local station, when the dipole is connected to the main receiver. With the receiving delta the heterodyne whistles with an adjacent powerful signal, obliterates completely the ionosphere echoes.

*The Receiver.* The receivers (figure 9) consist of a tuned R.F. amplifier, a balanced mixer, three or four low gain intermediate frequency-amplifier stages, a diode detector and a direct coupled video amplifier. Besides, they also contain a limiter, phase discriminator and a video amplifier, like a frequency-modulation receiver.

High intermediate frequencies (11.3 Mc/s and 25 Mc/s) are utilized. This choice became originally necessary to obtain the large bandwidths needed for handling short duration pulses. At present, it is also necessary for the sweep-frequency arrangement with the automatically controlled oscillator.

The local oscillators are separate units (figures 10 & 12). There is a manually controlled unit, with a dial calibrated over the whole frequency range, which is obtained in a single sweep, without coil changing. This is a great convenience and is obtainable only when high intermediate frequencies are utilized.

A balanced mixer is necessary, to prevent overloading of the first I.F. amplifier, with the oscillator signal when the tuning frequency is low. At low values of

tuning frequencies such as 1 Mc/s, the difference between the oscillator frequency and the resonant frequency of the I.F. circuits is small, so that large oscillator frequency voltages are developed across the I.F. circuits and applied to the first I.F. amplifier. As the oscillator frequency-currents in a balanced mixer cancel out at the output, this voltage is greatly reduced.

The R.F. coils utilize adjustable dust cores and the circuits are 'trimmed' with these inductance adjustments at the low frequency end of the band. In the case of the receiver that is intended for operation with the automatically following oscillator, the R.F. circuits are stagger tuned and heavily damped with 2.5 K $\Omega$  resistors across the variable capacitor. The R.F. amplifier, in that receiver is a 6AC7 tube.

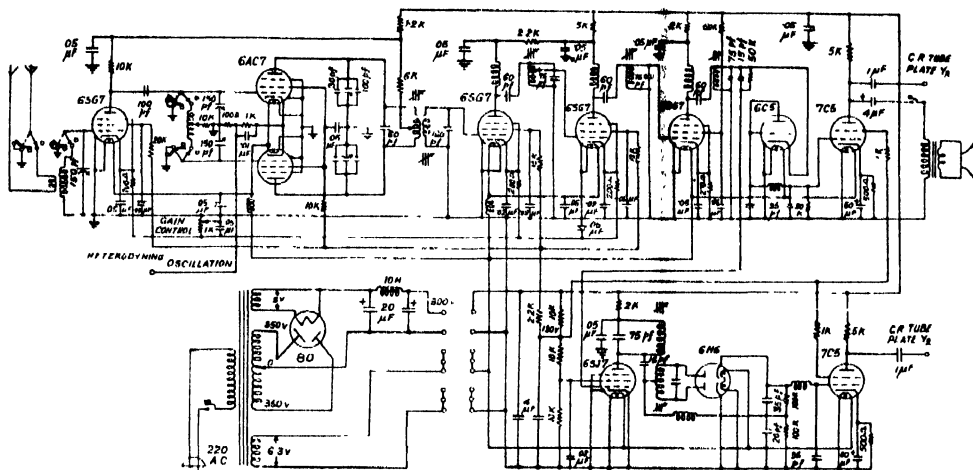


FIG. 9

Receiver circuit diagram

The single tuned circuits associated with the I.F. amplifier are easy to tune and provide a good pulse response. The iron core coils maintain their tuning very well. Besides, with single tuned circuits, small shifts in the tuning of the individual coils do not alter the bandwidth and pulse response adversely.

It will be noted that the low level stages have their heater lines filtered through chokes and condensers. This had been found necessary not only to suppress feedback and oscillation at the intermediate frequency, but also to eliminate

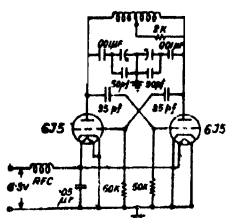


FIG. 10

Heterodyne oscillator, manually controlled

pick up of man-made interference. The receivers are well shielded in as much as pick up of man-made interference is not noticeable even at full gain. They have









The switching pulses needed are generated by a single shot cathode coupled multivibrator. This operates as a locked multivibrator generating pulses that have a duration equal to the pulser pulse, as it is triggered by a fraction of the positive pulse that is applied to the 829 B premodulator in the pulser circuit.

## RESULTS

The pulses will be found approximately triangular in shape, with a well defined tip. It has been our practice to use the tip\* (Whale, 1951) as the reference position in all measurements.

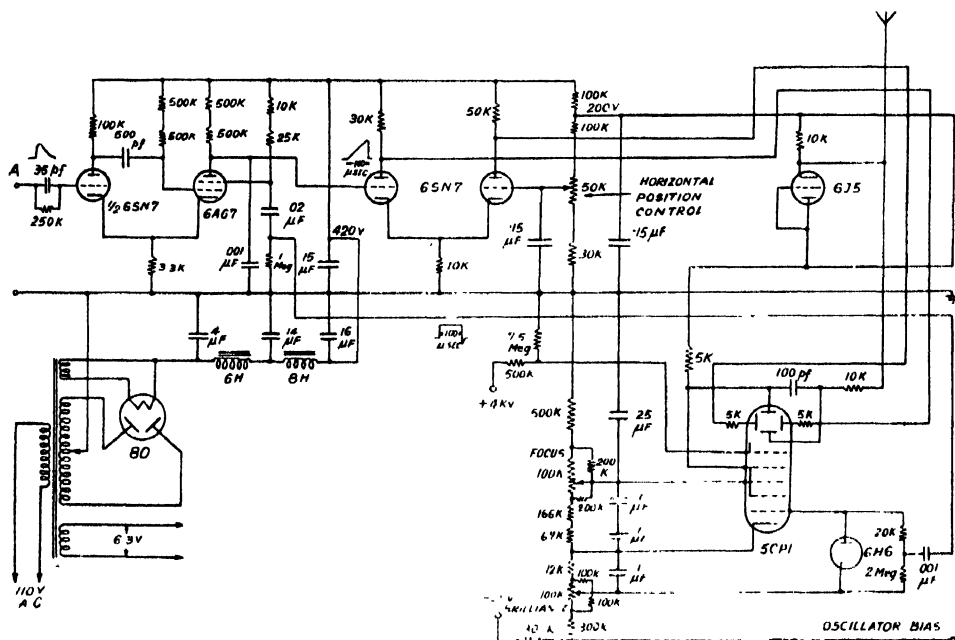


FIG. 14

### Monitor C. R. O. circuit

\* It is much more convenient to work with a triangular display on the oscilloscope than those which show a flat top. The well defined tip of a triangular display allows an easier and more accurate position fix of the pulse. It is more convenient to make measurements with reference to the tip as the tip position remains unaltered whatever be the amplitude. The minimum width of the triangular pulse greatly facilitates resolution of complex returns from the ionosphere.

## CONCLUSION

Ionospheric equipment of various types have been developed from time to time and are described in literature (Berkner, Wells and Seaton 1937, Gilliland and Taylor 1941, Thomas and Chalmers 1948). The chief concern of the designers of these equipments was to obtain a satisfactory tuning interlock between the receiver and the transmitter. The development of the beat-oscillator type sweep frequency apparatus (Gilliland 1934, Sulzer 1946 & 1949, Lindquist 1951) represents perhaps the last word in this direction. Tuning interlock in apparatus of this type is automatic, and they can sweep the entire frequency range of 1 to 24 Mc/s within fifteen to thirty seconds, and present the information in the desired form of a height vs. frequency curve traced out on the oscilloscope screen. The duration of the pulse utilized in these instruments is 50-200  $\mu$  seconds, and the resolution is correspondingly limited.

The development of the apparatus described in this paper is the outcome of a desire to obtain high resolution in ionospheric soundings. The need for high resolution in such apparatus cannot be overstressed. Although many (e.g., Appleton, 1933) have expressed their desire from time to time for improved performance in this direction, whatever efforts were made appeared to have met with discouragement and were not followed up.\*

The difficulties one has to face when shorter pulse durations are utilized are many and have clearly been outlined in the introduction. It has been shown there, that, a reduction in the pulse duration must be accompanied with a proportionate increase in the receiver bandwidth and the transmitter power. The transmitter power obtainable in most of the equipments developed for routine ionospheric sounding are small (a few kilowatts only). As a result, the pulse duration of 100-200  $\mu$  seconds, that is almost standard with such equipments, gives the most satisfactory allround performance.

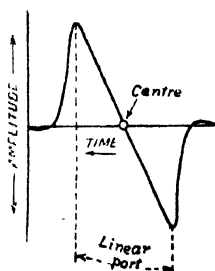


FIG. 15

The discussion in Appendix about the resolution and height measuring accuracy will make it clear that Type A presentation on an expanded sweep is essential to get the best resolving power and accuracy out of any sounding equipment. The intensity modulated presentation which simplifies the problem of a photographic record and economizes film length, loses much of the information of which the deflection modulated presentation is capable. The intensity modulated presentation reduces the resolution to barely the half-width, which may even be

\*In the search for low lying reflecting layers, various workers (e.g., Colwell and Friend 1937, Watson Watt, Wilkins and Bowen 1937) had used high resolution equipment. However, Appleton and Piddington (1938) disproved the existence of these low lying regions. Development of apparatus of really high resolution for sounding the wellknown ionised regions appear to have escaped attention. Recently, however, Helliwell (1949) reports a high power, high resolution low frequency sounding equipment and discovery of the complex structure of the E region.

Fig. a

The shape of the transmitter output of 20  $\mu$  sec duration.

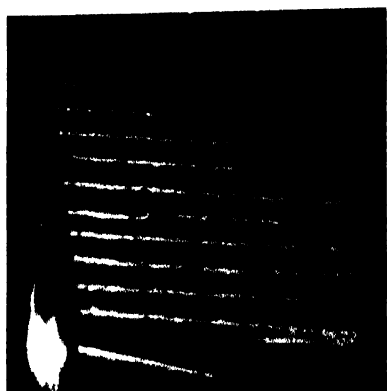
Fig. b

A broad echo due apparently to a slow gradient in the electron density of the F layer. The direct pulse, seen below in the first line, is of much smaller duration than the ionosphere echo (frequency 6.0 Mc/s, date 8.11.51, time 2150 hrs I.S.T.).

The response of an F M detector (upper) in comparison with the response of an A M detector (lower) when the receiver is properly tuned. It is quite apparent that the F M response allows a more accurate determination of height.

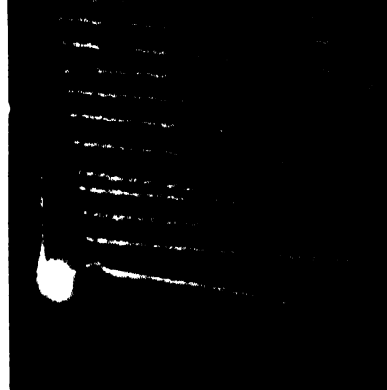
The light spot in these oscillograms move from right to left

Fig. d



Echoes due to first and second order reflection of the  $r$  and  $\phi$  waves that are obtained almost always from the F layer (5.95 Mc/s ; 14.11.51, 145 hrs I.S.T.)

Fig. e



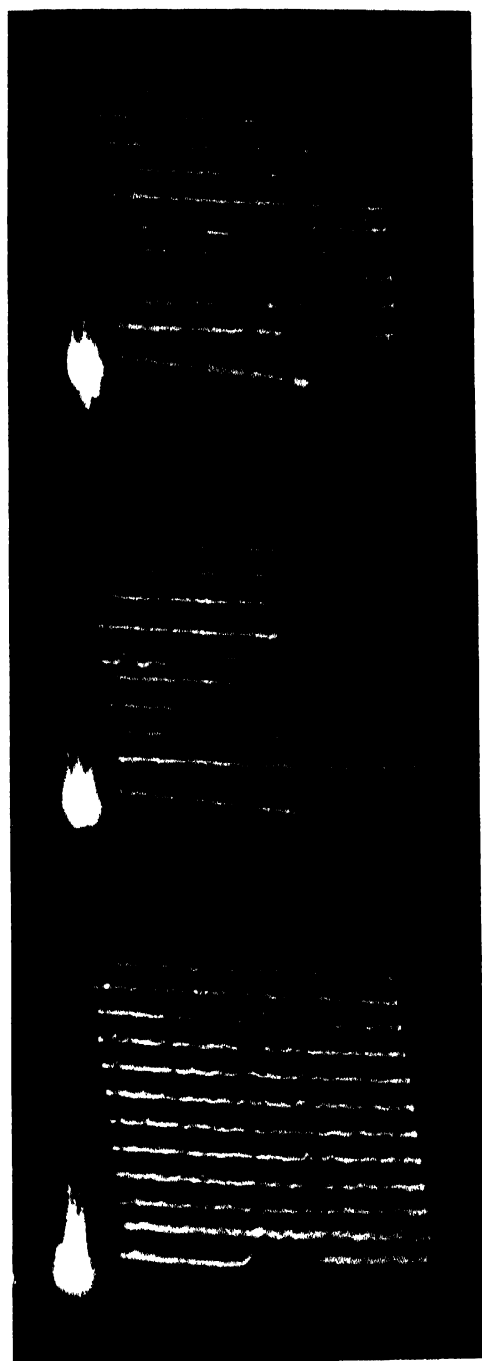
An unusual record in which multiples of the fourteenth and fifteenth order have come on the first and the sixth line, besides the first and second order on the fifth and the ninth line. The third and the other higher orders come at the position of the spot on the lower left. That these echoes have delays greater than twenty milliseconds was verified by changing the repetition period from twenty milliseconds to 6.6 milliseconds, when other orders appeared at different positions of the raster (c.f. Banerjee, 1945), the first and the second remaining unaltered. Changing repetition period from 6.6 milliseconds to 6.7 milliseconds altered the position of all orders having time delays greater than 6.7 milliseconds. The appearance of such high orders of reflection have also been reported by Toshniwal et al. (1935, 1936), and Mimno and Pierce (1930). (5.95 Mc/s, 13.11.51, 1715 hrs I.S.T.)

Fig. f



Twin echoes on the first order and a further splitting (3 Km separation) of the  $\phi$ -wave in the second order. The phenomenon is transitory, but occurs fairly frequently (9.95 Mc/s, 14.11.51, 1304 hrs I.S.T.)

e h



An unusual record in which there are four distinctly separate first order reflections from F (on the sixth line at 220, 225, 236 and 241 Km) and a complicated return in the second order on the twelfth line at 574 Km, and a single return at 563 Km (5.95 Mc/s; 11.11.51, 1304 hrs. I.S.T.)

Record of what was seen only four minutes later. There are seven distinctly separate echoes on the sixth line. The date of occurrence of this phenomenon was close to that of the Leonid shower and this peculiar phenomenon of the occurrence of more than three adjacent echoes persisted from 1230 hrs to 1322 hrs I.S.T.

A night time record obtained close to the penetration frequency. The four maxima of the broad wavy echo that is in the record, were rolling about - shifting their positions continuously (4.64 Mc/s, 9.11.51, 0120 hrs I.S.T.)



worse with a less careful adjustment of the apparatus and processing of the films.\*

The "anti-clutter" circuits, (such as a differentiating circuit before the oscilloscope, instantaneous automatic gain control in the receiver amplifiers) are frequently used now-a-days (Sulzer 1949, Lindquist 1951) to minimize broadcast station interference. These are considered to be great improvements and considerable effort has been directed towards their perfection. It is, however, not appreciated that they will reduce the resolution and height measuring accuracy of the sounding equipments to which they are fitted. I.A.G.C. would flatten out the top of the pulse and remove the amplitude variations that could have shown the presence of a twin. A differentiating circuit may mislead as to which one of the twin is the stronger when they are a close pair (figure 17.). In an instrument which aims at high resolution, I.A.G.C. should not be incorporated.\*\* However, a differentiating circuit is often necessary but one must be careful in interpretations regarding close twins. It is preferable to avoid these auxiliaries when complex echoes are observed.

The apparatus we have described contains a transmitter of 50 K.W. peak power. Its pulse duration may be varied from 6-30  $\mu$  seconds and interchangeable receivers of different bandwidths may be utilized. It is therefore possible to make the most as regards the resolving power, in any situation. One is not tied up to the unalterable instrumental characteristics.

The main short-coming of this apparatus is the limited range over which an automatically interlocked sweep is obtainable. This could have been avoided if the existing designs of the beat oscillator type sweep-frequency equipment could be modified to work with short duration pulses. So far as the pulser, transmitter circuits, receiver and time base are concerned, such modification is feasible. Attempt towards increasing the transmitter peak power beyond the values (10 kilowatts) at present realized would, however, meet with almost insurmountable difficulties. It must be appreciated that the final stages of the transmitter, in such a scheme, must operate as a Class A wide band amplifier and feed directly into the aerial, whose impedance, even when it is a properly designed wide band aerial may not be purely resistive. In such operating conditions, it is not possible to realise more than 10 K.W. from two 715 B tubes, although two such tubes may be capable of an output of 300 K.W. as a pulse modulator and a hundred kilowatts as pulsed R.F. oscillator (Sulzer 1948). The price of the mechanical simplicity of the newly introduced sweep-frequency equipment, that dispenses with tuned circuits in the high power stages, is a great reduction in the peak power output, besides the complication and cost of its many amplifier and pulser stages. The straight forward pulsed oscillator scheme that we have adopted in our transmitter, satisfies the most important requirement of a high power output, with the most simple arrangement. The drawback of a limited frequency range of automatically interlocked sweep may sometimes be of advantage in a research equipment that concerns itself chiefly with the studies of the fine structure of the ionosphere. For the routine work of drawing a complete height vs. frequency curve, the newly developed automatic sweep frequency equipments are admittedly more suitable. Greater time (ten minutes) and more effort are needed on the part of the human operator that operates this equipment to obtain a complete curve. The accuracy of the data obtained is, however, very much better. The improved resolution also makes observable many phenomena that would normally pass unnoticed in the conventional apparatus.

\*C.R. tube beam too strong and saturating the photographic emulsion; development to a high  $\gamma$ , and printing on hard paper, that gives a "clean" record.

\*\*It may be replaced by an A.V.C. system that comes into action when the echo amplitude exceeds a certain limit. Even then, this A.V.C. system should be gated to operate only on the ionosphere echoes, as otherwise background noise that are of high peak intensity, i.e., atmospheric and man made noise crashes may operate this A.V.C. to reduce the gain too much.

## ACKNOWLEDGEMENTS

The authors feel greatly indebted to Prof. M. N. Saha, for harnessing them into this project. The utility and urgency of the development of a high resolution ionospheric sounding apparatus was probably most acutely felt by Prof. Saha. The authors are grateful to him for his advice, inspiration, encouragement, guidance, his active help in procuring critical materials, in fact for an all out moral and material support. The authors are also grateful to Prof. S. K. Mitra for discussions that helped to clarify the basic difficulties expected in such an apparatus. In the early stage, the work was partly financed by the C.S.I.R. to which body, thanks are due.

## REFERENCES

- APPLETON, E. V., and BUILD, G., 1933, *Proc. Phys. Soc. B*, **45**, 208.  
 APPLETON, E. V., and PIDDINGTON, J. H., 1938, *Proc. Roy. Soc. A*, **164**, 467.  
 BANERJEE, B. M., 1945, *Ind. J. Phys.*, **19**, 75.  
 BANERJEE, B. M., and ROY, R., 1950, *Ind. J. Phys.*, **24**, 411.  
 BANERJEE, B. M., and ROY, R., 1952, *Sci. & Cult.*, **17**, 305.  
 BERKNER, L. V., WELLS, H. W., and SEATON, S. L., 1937, Contribution No. 15 from the Dept. of Terrestrial Magnetism, Carnegie Institute of Washington.  
 BRIGGS, B. H., 1951, *Proc. Phys. Soc. B*, **64**, 375-B, 255.  
 COLWELL, R. C., and FREUND, A. W., 1937, *Proc. I.R.E.*, **25**, 1531.  
 CONES, H. N., 1951, *J. Res. Nat. Bureau. Standards*, **46**, 113.  
 FINK, D. G., 1947, Radar Engineering, p. 99 and p. 55. Mc-Graw Hill.  
 GILLILAND, T. R., 1934, *Proc. I.R.E.*, **22**, 236.  
 GILLILAND, T. R., and TAYLOR, A. S., 1941, *J. Res. Nat. Bureau. Standards*, **26**, 377.  
 HELLIWELL, R. A., 1949, *Proc. I.R.E.*, **37**, 887.  
 LINDQUIST, R., 1951, *Chalmers Tekniska Hogskolas Handlingar*, Nr. 109.  
 M. I. T. RADAR SCHOOL STAFF, 1946, Principles of Radar, p. 4-13, & 4-17.  
 PIERCE, J. A., and MIMNO, H. R., 1940, *Phys. Rev.*, **57**, 95.  
 RAKSHIT, H., and CHATTERJEE, S. D., 1952, *Sci. & Cult.*, **17**, 520.  
 SULZER, P. G., 1946, *Electronics*, **19**, 137.  
 SULZER, P. G., 1948, *Proc. I.R.E.*, **36**, 389.  
 SULZER, P. G., 1949, *J. Appl. Phys.*, **20**, 187.  
 THOMAS, H. A., and CHALMERS, R. G., 1948, *J.I.E.E.*, **95**, III, 7.  
 TOSHNIWAL, G. R., and PANT, B. D., 1935, *Nat. Inst. Sci. Ind.*, **1**, 87.  
 TOSHNIWAL, G. R., PANT, B. D., BAJPAI, R. R., and VERMA, B. K., 1936, *Proc. Nat. Acad. Sci. Ind.*, **6**, 161.  
 WATSON WATT, R. A., WILKINS, A. F., and BOWEN, E. G., 1937, *Proc. Roy. Soc. A*, **161**, 181.  
 WHALE, H. A., 1951, *J. Atmos. Terr. Phys.*, **1**, 233.

## APPENDIX

*Resolution and height measuring accuracy.* There appears to be a good deal of confusion regarding the performance figures claimed as to the resolution and the height measuring accuracy of ionospheric sounding equipments. It must have been noticed that different workers put forward different figures for resolution and height measuring accuracy for equipment utilizing the same pulse duration and even for the same equipment. It is perhaps worthwhile to analyse the matter objectively, to understand the basic reason for such a diversity of opinion.

Figure 16 shows the most simple case, that of a single return from the ionosphere and typical displays produced on the oscillograph screen.

In case the reflected echo is displayed as a triangular one, it is preferable to make measurements in terms of the position of the tip. In case the pulse has a rectangular shape, it is convenient and common to take measurements from the "start" of the pulse. These positions *tip* and *start* should be defined a little more exactly.

The *start* of a rectangular pulse may well be defined as the intersection of the base line with the sloping line that passes through the 10% and 90% amplitude points. The *tip* position of the triangular pulse may be defined to be the projection on the base line of the intersection point of the sloping straight lines at the two sides of the triangular pulse that passes through the 10% and 90% amplitude points



(see figure 16). Defined in this manner the positions remain the same whatever be the amplitude of the pulse, so long as its shape remains unaltered. The output pulse of a receiver will retain its shape so long as it is not saturated.

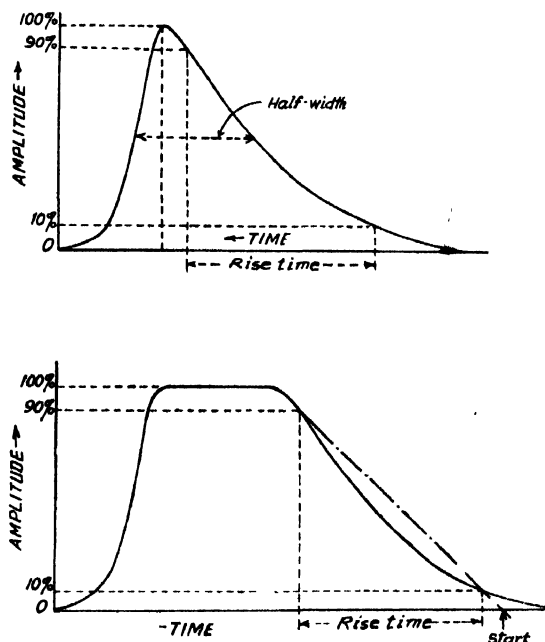


FIG. 16

While the positions of the pulses may thus be defined rigorously, in the actual case of the pulse echoes displayed on the receiver oscilloscope, that are unsteady because of interference with the background noise, and also because of fluctuations in amplitude, the operation outlined in the definition has to be performed mentally and would lead to a position fix that may be in error by varying amounts depending upon the conditions of operation. In the case of a triangular pulse, the accuracy with which the position of its tip may be fixed is much better than its half width when noise is negligible and the amplitudes are fairly steady. If the pulse echo is barely distinguishable in the background noise, the accuracy may not be better than the half width. With the pattern of echo display normally obtained in an ionospheric sounding apparatus, it is doubtful if an accuracy claim better than one tenth of the pulse half width is justified.

In the case of the so-called rectangular pulse, the accuracy with which its position may be determined depends upon the slope at the leading edge of the pulse. It is therefore logical to express accuracy obtainable in terms of the rise time. Background noise and amplitude fluctuations again determine the accuracy in a similar manner, which may be as good as one tenth of the rise time in a favourable case or as poor as barely the rise time in an unfavourable case.

When the amplitude of the pulses is perfectly steady and noise is absent, the accuracy may be greatly increased by suitable refinements in the measuring devices. This is because the pulse pattern is steady, so that the positions of the different amplitude points are fixed. The position of these fixed points may be determined with as great accuracy as needed by utilizing a sufficiently expanded sweep circuit (e.g., a raster time base). A particular amplitude point is determined with greater ease and accuracy if the pulse height is set to a standard value. This also requires adequate and controlled amplification in the pulse amplifier stages.

In a practical case, an ultimate accuracy of about one hundredth of the pulse rise time may be secured when the time base and the pulse amplitude are so expanded that the pattern occupies the entire area of the oscilloscope face. Suitable electronic circuits geared to the same basic functions may improve the accuracy still further. (Rakshit & Chatterjee, 1952).

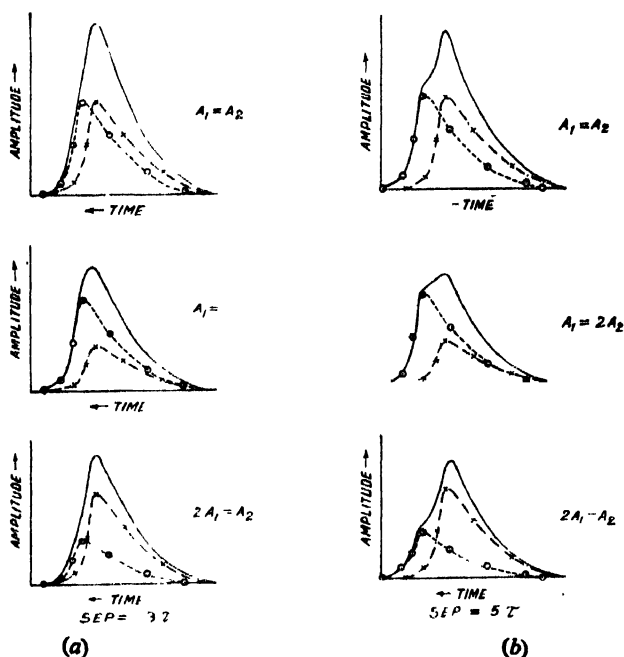


FIG. 17

**Resolution.** If an ionospheric sounding apparatus produces a pulse width of  $T$  microseconds as displayed on the oscilloscope, then it is quite evident from figures 17 *a-e*, that two close by echoes will be distinctly shown separate, if their spacing exceeds twice the half amplitude width. At this or greater spacing there would be no doubts about the *presence* of more than one echo, even though the second one is barely discernible above the noise level. If, however, the separation is smaller, it is possible to recognise easily the existence of the second echo, till their spacing shrinks to about the half amplitude width. If the second echo is of equal amplitude, recognition of its presence, is quite easy. It becomes more difficult when it is of smaller amplitude, much more so when this amplitude is only somewhat greater than the noise back-ground.

When the separation is greater than twice the half amplitude width, it is possible to *measure* this separation with great accuracy. The error may be no greater than the error in height measurement.

When the separation is less than the half width, its measurement ceases to be so precise. It may be difficult to say anything better than that the separation is somewhat less than a *half width*, from a visual inspection.

With no interfering noise and a perfectly steady amplitude, it is, however, possible to *compare* the ionospheric return, with the standard shape of the pulse, in a *greatly expanded presentation* over the oscilloscope face. Such a comparison may show up the existence of a second return (twin), and it is possible to calculate out its position and amplitude from the nature and position of the misfit with

reference to the standard shape. Theoretically, the presence of a second return may be deduced till it is almost coincident or of scarcely discernible amplitude.

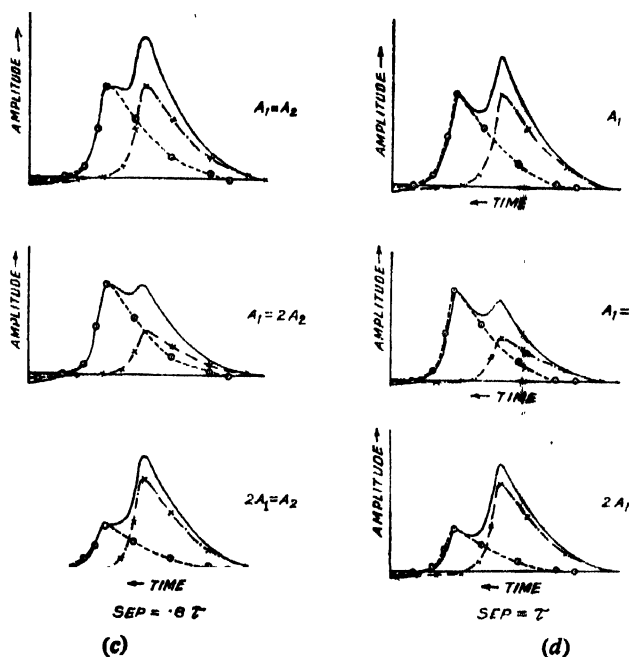


FIG. 17

A second return, that would otherwise pass unnoticed, may cause a rapid fluctuation in amplitude of the ionosphere echo. Fluctuation in amplitude may, however, be due to many other reasons, so that a fluctuation in amplitude does not necessarily indicate the presence of a second return.

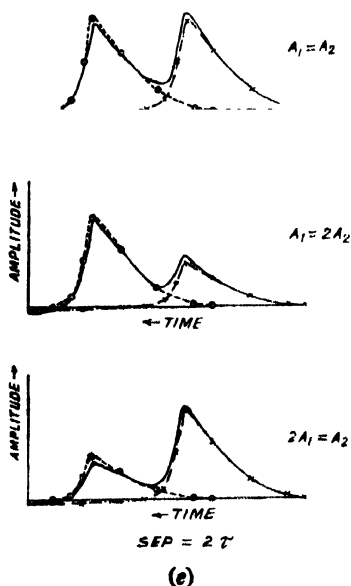


FIG. 17

From the above discussion, it is clear that the half amplitude width of the displayed echo is the measure of the resolution of an ionospheric apparatus. In a visual observation (practical case), it is seldom possible to predict with certainty and with an estimate of the separation, the existence of a second or third echo, unless the separation is of this order in magnitude. This is so chiefly because of interfering noise and the unsteadiness in the amplitudes of the ionosphere returns, that often render the effort of a comparison with a standard shape impractical. Such a comparison is, however, quite practical on a photographic record. In a photographic record, the amplitude gets steadied and the real shape of the pulse is indicated well, in spite of noise, so long as the S/N ratio is good.

# STUDY OF THE IONOSPHERE BY EXTRATERRESTRIAL RADIO WAVES\*

BY A. P. MITRA†

DIVISION OF RADIOPHYSICS, C.S.I.R.O., AUSTRALIA

(Received for publication, September 9, 1952)

**ABSTRACT.** The paper presents a connected account of a novel method of studying the ionosphere in which the radio-frequency radiations from extraterrestrial sources may be utilized. Four different types of measurements on such waves are discussed for this purpose, namely (i) ionospheric refraction, (ii) ionospheric attenuation, (iii) twinkling of "radio stars" and (iv) effects of sudden ionospheric disturbances (SID's). The available experimental results are compared with ionospheric theory and further lines of investigation which might profitably be followed are indicated.

## INTRODUCTION

The discovery by Jansky (1932) of the existence of galactic radio-frequency radiation opened up a new field—the field of radio astronomy. Since Jansky's pioneer discovery, a large amount of work has been done on galactic radiation, and on the later discovered solar radio-frequency radiation. Radiation from discrete sources, sometimes called "radio stars," has also been detected. In addition, waves transmitted from the Earth have been received again after reflection from the Moon.

Although, obviously, the immediate interest of such studies concerns the Sun, the Moon, the Galaxy and the "radio stars," there is another application of this science which has an important practical interest: the study of the ionosphere. It has frequently been emphasized that for satisfactory computation of the propagation characteristics of radio waves, it is important to know precisely the structure of the ionospheric regions and their varying characteristics. Since the extraterrestrial radio waves have to pass through the ionosphere, it is natural to expect that some of these will bear marks of such transmission, especially at frequencies near the critical frequency of the  $F_2$ -layer. Here, then, is a new tool for investigating the ionosphere. It is interesting to see how far the published observations in this field agree with those of the more conventional ionospheric techniques, and also whether they can supply information that is inaccessible to these techniques.

Until recently, information concerning the ionosphere was obtained almost exclusively from routine ionospheric soundings. A wave, usually transmitted almost vertically, is reflected by one of the ionospheric regions, depending on the wave frequency and the condition of the ionosphere. The highest frequency that can be reflected is equal to the critical frequency of the  $F_2$ -layer and so little information concerning the regions above the height of maximum ionization of the  $F_2$ -region may be obtained from this method.

In spite of this, occasional glimpses of ionization above the level of the  $F_2$ -peak have been obtained, mainly from the evidence of the "spread-F" echoes and the so-called G-echo. The former is believed to be caused by irregular regions of increased ionization density above the height of maximum  $F_2$ -ionization, and the latter by a regular layer above the  $F_2$ -layer under the rare condition when the

\*Communicated by Prof. S. K. Mitra, D.Sc., F. N. I.

†On leave from the Institute of Radiophysics and Electronics, University of Calcutta, and the Council of Scientific and Industrial Research, Government of India.

ionization density of the  $F_2$ -layer falls below that of the G-layer. This is largely speculative, and can only be considered with reserve, unless fresh evidence is available. It is here that measurements on extraterrestrial waves are of greatest interest. With such measurements the following ionospheric effects have been observed: (i) ionospheric refraction, (ii) ionospheric attenuation, (iii) "twinkling of radio stars," (iv) effects of sudden ionospheric disturbances (SID'S).

It is the purpose of the present paper to give a connected account of these different measurements, to compare the available experimental results with ionospheric theory, and to indicate further lines of investigation, which might profitably be followed.

## 2. IONOSPHERIC REFRACTION

(a) *Experimental results.* The apparent angle of elevation of a source, as measured at the ground, is the sum of the angle of elevation of the source that would be found if there were no atmosphere, and the refraction suffered by the radio waves in the ionosphere and in the lower atmosphere (troposphere). Measurement of ionospheric refraction involves the assumption that tropospheric refraction and the physical position of the source are both independent of the frequency or time of observation so that variations in angular position with frequency or time may be attributed to variation in ionospheric refraction. For frequencies many times the critical frequency of the  $F_2$ -layer, ionospheric refraction is very small.

Payne-Scott and McCready (1948) made refraction measurements on solar noise at sunrise from July 27 to August 7, 1946, simultaneously on 60 and 200 Mc/s. The difference in ionospheric refraction ( $R_{60} - R_{200}$ ), as obtained by them on one of these days, is shown in Table I. It may be remarked, however, that there is no certainty that the source of 60 Mc/s radiation is in the same position physically as the source of 200 Mc/s radiation. Further, these observations were made at sunrise, when the ionosphere is known to behave abnormally, and during times of solar disturbances. Hence they are probably not very accurate. However, the large refraction effects observed should be qualitatively true. Measurements on moon echoes at a frequency of about 20 Mc/s by Kerr and Shain (1951) have also revealed large refraction effects. These authors observed a vertical deviation of  $5^\circ$  for an altitude of  $5^\circ$ , decreasing to  $1^\circ$ — $2^\circ$  for an altitude of  $25^\circ$ .

TABLE I

Apparent angle of elevation in degrees	$\frac{1}{2}$	$2\frac{1}{2}$	$4\frac{1}{2}$	$6\frac{1}{2}$	$8\frac{1}{2}$
$(R_{60} - R_{200})$ for August 6 in minutes of arc. (Accuracy about 6')	55	37	29	26	14
Theoretical values for a symmetrical $F_2$ -layer calculated after Bailey in minutes of arc	13	12	11	$9\frac{1}{2}$	8

(b) *Theoretical studies.* Theoretical investigations of ionospheric refraction have been made by Bailey (1947) and later by Bremmer (1949) on the assumptions of parabolic distributions of the ionospheric layers and a flat earth. Recalculation for a curved earth utilizing the equivalence principle given by Appleton and Beynon (1947) has been done by Kerr and Shain.

The amount of refraction caused by any ionospheric layer depends on the variation with height of the refractive index  $\mu$ , and on the obliquity of the path. Considering a parabolic layer, which possesses only a normal ionization gradient and is locally spherical, Bailey obtained, for values of  $f$  at least one and one-half to two times larger than the maximum usable frequency (MUF) for the angle concerned,

$$R_f = 2d P(\xi, h_m) (f_0/f)^2 \quad \dots (1)$$

where  $R_f$  is the difference between the apparent and actual elevations of the source,  $d$ , the semi-thickness of the layer,  $f_0$  its critical frequency and  $P(\xi, h_m)$  is a function depending upon  $\xi$ , the angle of elevation of the received ray and on  $h_m$ , the height of maximum ionization.

Figure 1 shows, after Bailey, the magnitude of refraction  $R$  in minutes of arc calculated for different values of  $\xi$  and  $h_m$ . Obviously the lower the angle of elevation and the smaller the frequency of the incoming radiation the larger will be the refraction.

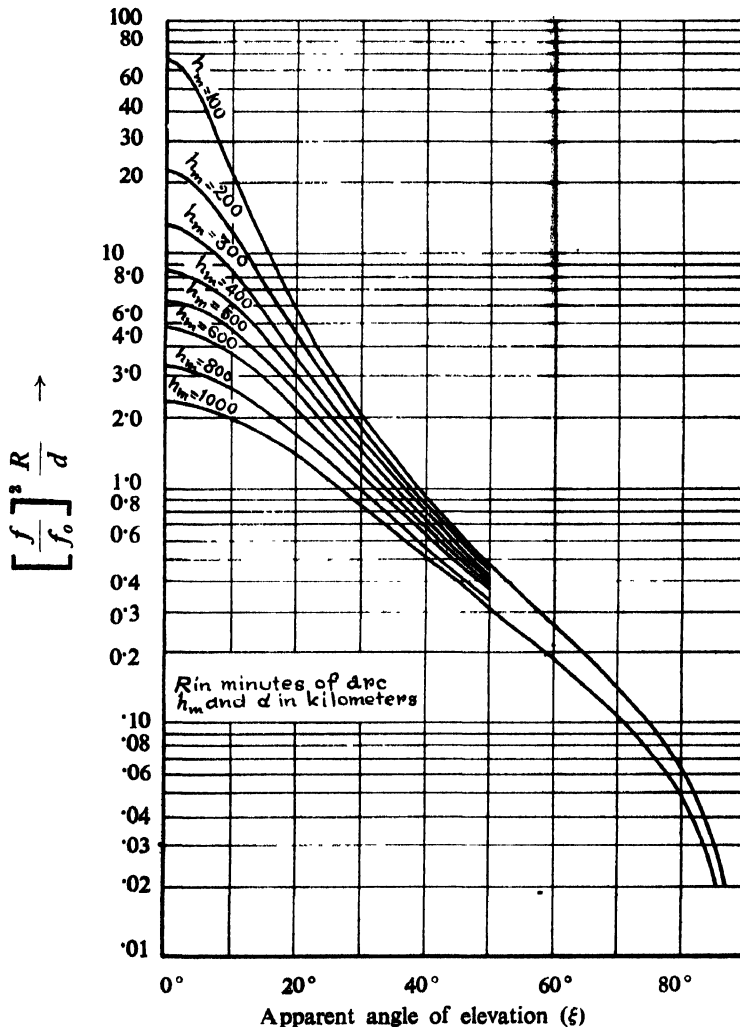


FIG. 1

$\left( \frac{f}{f_0} \right)^2 \frac{R}{d}$  plotted against  $\xi$ , the apparent angle of elevation of the received radiation, for different values of  $h_m$ , height of maximum ionization, for a parabolic layer of critical frequency  $f_0$  and semi-thickness  $d$ . (After Bailey).

For a non-symmetrical layer equation (1) does not hold. If, however, we assume that the upper part of the layer is also parabolic and has a semi-thickness  $d'$ , then, according to Bailey,

$$R \approx (d + d') P(\xi, h_m) (f_0/f)^2. \quad \dots (2)$$

(c) *Discussion.* Theoretical estimations of refraction on the basis of equation (1) have shown that the refraction observed by Payne-Scott and McCready is about three times as large as for a symmetrical  $F_2$ -layer (Table 1). A similar conclusion has been reached by Kerr and Shain.

Two possibilities immediately suggest themselves—the existence of a G-layer and a non-symmetrical  $F_2$ -layer. If the  $F_2$ -layer is symmetrical, any excess of refraction may be attributed to G-layer. In case of a non-symmetrical  $F_2$ -layer, however, the problem becomes more complicated. For this case both the  $d$  and G-parameters are unknown. Fortunately, however, the refraction produced by a non-symmetrical  $F_2$ -layer decreases far more rapidly than for a G-layer with symmetrical  $F_2$ -layer below. It should, therefore, be possible to distinguish between the two cases from an analysis of the observed nature of variation of  $R$  with  $\xi$ . Such analysis made by Payne-Scott and McCready (1948) (see also Table I) shows that the change of refraction is too rapid to be accounted for by a G-layer. The possibility of a G-layer has also been questioned by Kerr and Shain who concluded that a G-layer can account for the moon echo anomalies only if it were very thin, which is physically unlikely at such great heights. These authors have also discounted the possible effect of a non-symmetrical  $F_2$ -layer, mainly because they considered the refraction observed to be far too large even for such a layer. This conclusion will not, however, hold if the asymmetry of the  $F_2$ -layer is very pronounced (*vide infra*).

A model involving horizontal irregularities in the  $F_2$ -layer has been suggested (Kerr and Shain, 1951). It has been claimed that if the irregularities existing in the  $F_2$ -layer are of a serious nature, the secant law between vertical and oblique incidence critical frequency will not hold, and increased deviation would occur.

While effects of irregularities may actually make some contribution to these large refraction effects, the position should be reconsidered in the light of later theoretical work on the shape of the upper regions of the ionosphere. For example, ionospheric investigations have shown that while for region  $F_1$  the recombination coefficient is approximately constant, it decreases rapidly with height for region  $F_2$  (Bates and Massey, 1948; Seaton, 1948; Martyn, 1948, 1950; Mitra, 1952) and it is believed that regions  $F_1$  and  $F_2$  are produced by the same ionizing agency. On the assumption that the recombination coefficient above a certain level is a function of pressure as well as electron density, the form of the layer is as shown in figure 2. The large asymmetry in the  $F_2$ -region both in thickness and in shape will be noticed. Such an asymmetry may well explain the large refraction observed. It must be noted, however, that neither the lower nor the upper curve is really a parabola. When one considers, in addition to the effects of recombination coefficient, those of the variations with height of temperature and tidal velocity, the departure from the parabolic shape becomes much more pronounced. It has not yet been possible to arrive at a quantitative picture of the  $F_2$ -layer with all these factors taken into account: until this is done, and refraction calculated for the resultant distribution, it is not possible to draw any conclusion.\*

### 3. IONOSPHERIC ATTENUATION

Extraterrestrial radio waves at frequencies less than the critical frequency of the  $F_2$ -region cannot penetrate to earth. For frequencies higher than this, the waves will reach the earth, but will suffer attenuation by the ionosphere depending on the frequency of the waves and the obliquity of the path.

(a) *Experimental investigations.* Most of the reception of solar and galactic noise is made on high frequencies where ionospheric effects are small. For

\*It would appear from physical grounds that, for a layer non-symmetrical in shape as well as in thickness, refraction will increase with increase in gradient of ionization or with increase in thickness, and may be large when one or both is large.



studies of ionospheric absorption these are of little value. The first qualitative observations of ionospheric absorption of extraterrestrial radio waves were made by Jansky in 1936-37 at about the time of the sunspot maximum. He observed a decrease in the intensity of the 20 Mc/s radiation round noon which he rightly attributed to the ionosphere.

Quantitative measurements on ionospheric absorption have recently been made by Kerr and Shain (1951) using moon echoes at 20 Mc/s at low angles, and by Shain (1951) on 18.3 Mc/s galactic radiation at vertical incidence. The results obtained by them may be summarized as follows :

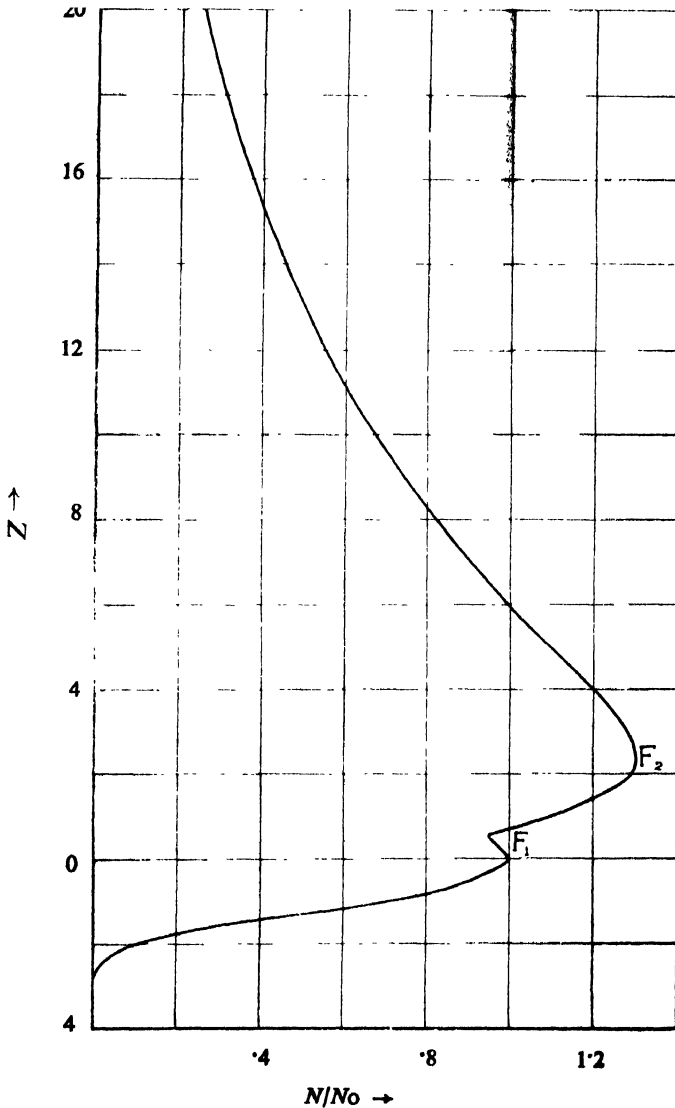


FIG. 2

Theoretical ionization distribution of the  $F_1$  and the  $F_2$ -layers for a common origin of both and for a recombination coefficient decreasing exponentially with height from a level slightly above the maximum ionization for region  $F_1$ .

(i) Attenuation at oblique incidence is larger than that for a parabolic layer (Kerr and Shain, 1951).

(ii) Attenuation increases more rapidly near the critical frequency of the  $F_2$ -layer than would occur for a Chapman layer (Shain, 1951).

(iii) Part at least of the observed attenuation is due to the  $F_2$ -layer (Kerr and Shain, 1951; Shain, 1951) (figure 3), there being little or no contribution by the E-layer (Shain, 1951).

(b) *Theoretical investigations.* In interpreting experimental results one should remember that for extraterrestrial radio waves reaching the earth, there are actually two kinds of attenuation—one is due to absorption caused by collisions between electrons, ions and neutral particles in the ionosphere, and the other is due simply to the divergence of energy because of ionospheric refraction.

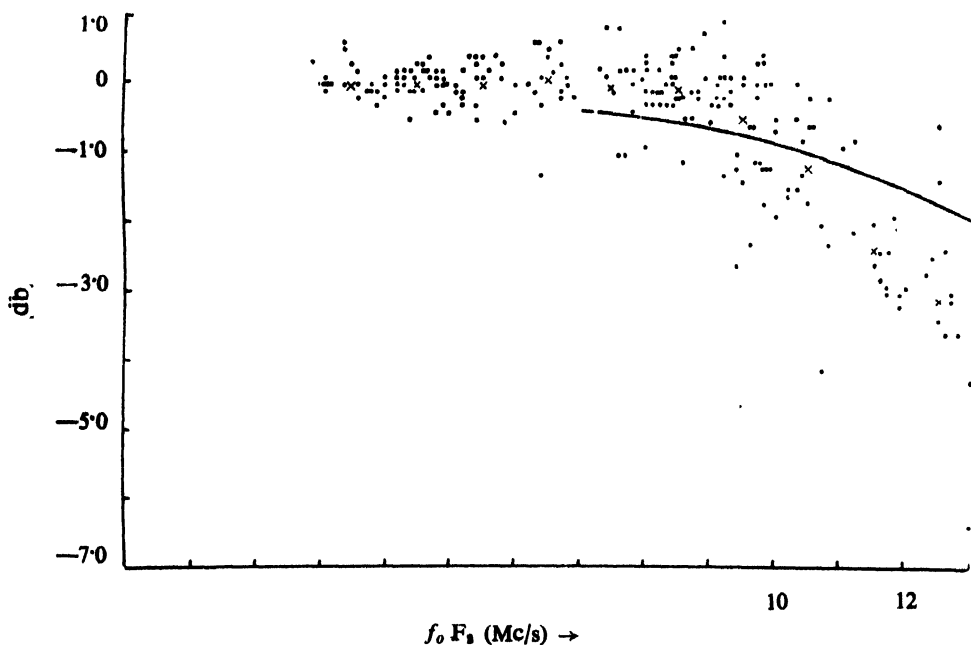


FIG. 3

Ratio of observed galactic intensities at 18.3 Mc/s to hourly average with  $f_o F_2 < 9.0$  Mc/s plotted against  $f_o F_2$ . The continuous curve represents theoretical absorption for a Chapman region. Crosses are average values for 1 Mc/s interval. (After Shain).

(i) *Attenuation due to absorption.* The problem of ionospheric absorption has been treated in detail by many authors, notably by Appleton (1937), Appleton and Beynon (1940, 1947) and Jaeger (1947, 1948). These investigations refer either to parabolic or Chapman type of electron distribution with or without correction for the curvature of the earth. Unfortunately, since, as we now know, none of the ionospheric regions (with the possible exceptions of regions E and  $F_1^*$ ) follows the parabolic or the Chapman distribution, the formulae as deduced by the above authors are of little value for accurate computation of ionospheric absorption.

\*Even regions E and  $F_1$  show deviations from the Chapman law, due possibly to the fact that the atmosphere at these heights is not isothermal. But these deviations are easily taken into account.

*Region D.* The electron distribution for region D is not conclusively known, but it has become increasingly apparent that what is known as the normal D-layer cannot show a Chapman-like structure because of the variations of recombination coefficient and temperature with height. Recent investigations by the author (Mitra, 1951), on the basis of temperature and pressure variations that occur at these heights, have yielded a roughly exponential structure of the electron distribution which increases gradually with height and merges into the tail of region E. For such a region the values of absorption are many times higher than those for a Chapman layer. In figure 4 are given curves illustrating absorption for such a layer for different values of the exponent.

The absorption problem for region D may actually be more complicated than this, because the above estimation neglects, for simplicity, the sudden bends in the electron distribution curves that would occur for a temperature distribution identical with or similar to that given by NACA (1947). Further, it should be remembered that recent long-wave work at Cambridge and Edinburgh (Bracewell and Bain, 1952) indicates the existence of two distinct layers, called  $D\alpha$  and  $D\beta$ . Finally, there is also the possibility of region D being predominantly an ion layer, though recent theoretical investigations seem to discourage such a possibility (Bates and Massey, 1951).

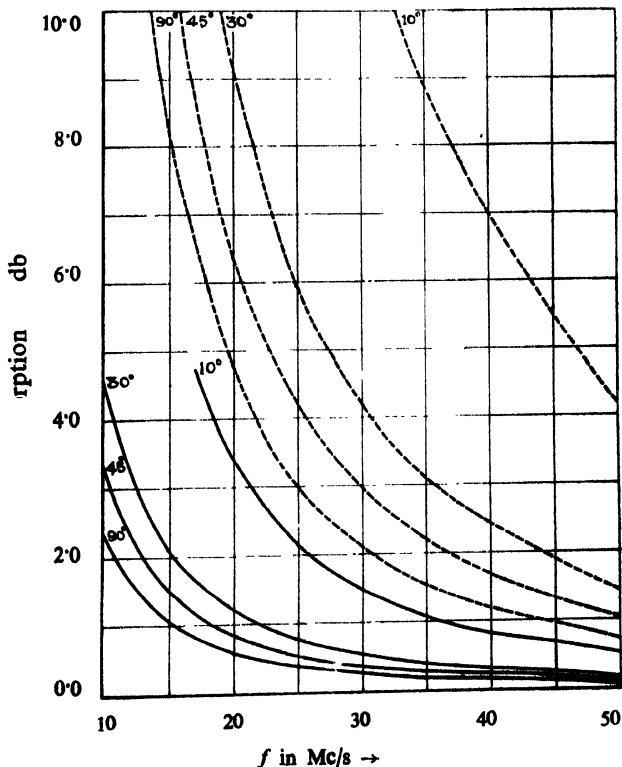


FIG. 4

Theoretical absorption curves for an exponential D-layer with electron concentration given by  $N=N_0 e^{H/h}$ , where the suffix  $o$  refers to a level of 70 Km. Curves for different values of  $\xi$  are shown. Assumed values of the parameters are  $\nu_0=10^8/s$ ,  $N_0=2 \times 10^3/cm^3$ , and  $H=8km$ . Continuous curves for  $g=3$  and dotted curves for  $g=4$ .

*Region E.* If the part of the region below 90 km. is included in the D region, then integration between limits 90 km. and infinity gives for absorption  $A$  at an angle of incidence  $\xi$ ,

$$A \approx 2 \times \frac{H\nu_m}{2c \sin \xi} (f_c/f)^2 \text{ nepers} \quad \dots (3)$$

where  $H$  is scale height,  $\nu_m$  the collisional frequency at the height of the maximum ionization and  $f_c$  the critical frequency. The factor 2 replaces the usual factor 4.13 which is obtained if the whole of the Chapman region is considered. For typical values of the constants it is found that absorption of extraterrestrial radio waves in the E region is usually small.

*Regions  $F_1$  and  $F_2$ .* In view of the common origin of the F layers and their possible lack of symmetry (section 2), it is necessary to recalculate absorption due to these layers under conditions indicated in section 2. It is certain that the results will disagree with those for a Chapman layer. In particular, the absorption for a layer of the type illustrated in figure 2 will be larger than for a Chapman layer.

(ii) *Attenuation due to refraction.* This kind of attenuation has been treated by Bremmer (1949) in some detail for the case of a parabolic layer. It has already been emphasized that excepting regions E and  $F_1$ , no other ionospheric region can be considered even approximately parabolic. This point is particularly important here as the  $F_2$  region is the one which causes most refraction. The theory has not yet been worked out for the layer shown in figure 2, but Bremmer has shown that for the case of a parabolic layer the attenuation due to refraction is comparable with that due to absorption only at very oblique incidence, and the result should be qualitatively correct for the new theory.

(c) *Discussion.* As a possible cause of the large absorption suffered by the transmitted pulse in moon echo experiments (and also of the large deviations that simultaneously occur (section 2), Kerr and Shain have suggested the irregularities existing in the  $F_2$ -region of the ionosphere. While some loss due to diffraction by such irregularities is expected, it is not likely to be large enough to explain the very large absorption observed. In view of the preceding discussion an obvious alternative will be a non-symmetrical  $F_2$ -layer. As already noted, even an asymmetry caused only by a variable recombination coefficient increases absorption of the incoming radiation. Still larger absorptions are expected for an asymmetry caused by gradients of both recombination coefficient and scale height.

It is certainly significant that the asymmetry provides a reasonable explanation for both large refraction and absorption effects and confirms Shain's view that the peculiar absorption result and refraction result are tied together. One should, however, bear in mind the anomalies in MUF which are associated with large refraction effects (Kerr and Shain 1951), and no explanation can be accepted which fails to explain the MUF anomalies as well.

From the theoretical results obtained in sub-section 3(b), one should expect that a large part of the ionospheric absorption will be due to the D-layer. It is difficult to assess this contribution. It is significant, however, that during SID when, as is believed, the ionization of the D-region is greatly enhanced with little or no change in  $F_2$  and E-region ionization (Berkner and Wells, 1937), there is increased absorption in cosmic noise (see also section 5). This increase in absorption must be due to the increased ionization in D-region.

#### 4. "TWINKLING OF RADIO STARS"—IONOSPHERIC IRREGULARITIES

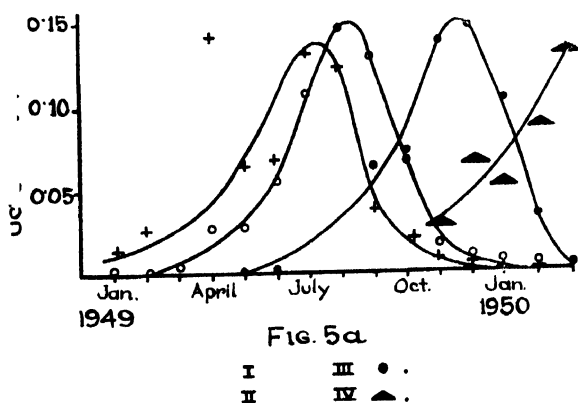
Observations on the radio waves from discrete sources of the galactic radiation reveal occasional fluctuations of intensity, known, because of the similarity with the optical phenomenon, as the "twinkling of radio stars." The

fluctuations were first discovered in 1946 by Hey, Parsons and Phillips who noticed, while making a survey of galactic noise at 64 Mc/s that the noise intensity from the constellation of Cygnus fluctuated by as much as 15 per cent. of the total power received by the aerial system, the average period of fluctuation being about 1 minute. Since then fluctuations of radiation from the Cygnus source and also on a number of other "radio stars" have been observed by many authors.

(a) *Evidence of terrestrial origin of the fluctuations.* Evidence of terrestrial origin of these fluctuations is supplied by the following observations : Spaced receiver measurements by Smith (1950) on 6.7 metre wavelength showed that the fluctuations were markedly different when the receivers were separated by 20 km., while for a separation of 170 km., no correlation existed. Similar results were obtained by Little and Lovell (1950) on 3.7 m. Mills and Thomas (1951), working in Australia, also found that for a distance of 300 m. the fluctuations were similar, but for a distance of 30 km., no correlation existed. An exhaustive series of measurements made recently in England (Little and Maxwell, 1951) has conclusively shown that correlation between fluctuations begins to disappear at a distance of about 5 km.

These results indicate that the fluctuations cannot be due to the diffraction in the interstellar medium, because then, for a duration of 30 sec. in the fluctuations a diffraction pattern of dimension as large as 900 km. will be required (the orbital velocity of the Earth being 30 km./sec.) Lack of correlation between records obtained with receivers at much smaller distances shows that the diffraction pattern is of much smaller dimensions. The observations can, therefore, be explained only if the diffraction pattern is moving with the Earth and is of terrestrial origin.

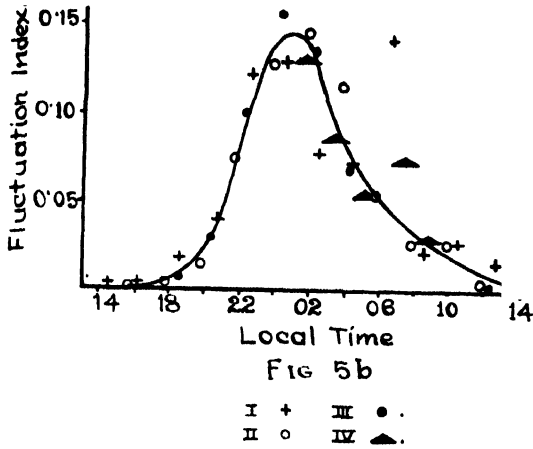
(b) *Variations of fluctuations.* For convenience in the study of such variations, a quantity known as the "fluctuation index" has been introduced. This represents the ratio of the mean deviation of the intensity to mean intensity. Ryle and Hewish (1950) have studied the indices at vertical incidence for four different "radio stars" on 3.7 m. It was found that an apparent annual variation of the indices existed and that the variations for the different sources were similar, although displaced in time in order of their respective right ascensions (figure 5(a)). It was suspected that the apparent annual variation was really diurnal



(Apparent) annual variation of the fluctuation index for four sources during December, 1948, to March 1950 observed in England. (After Ryle and Hewish).

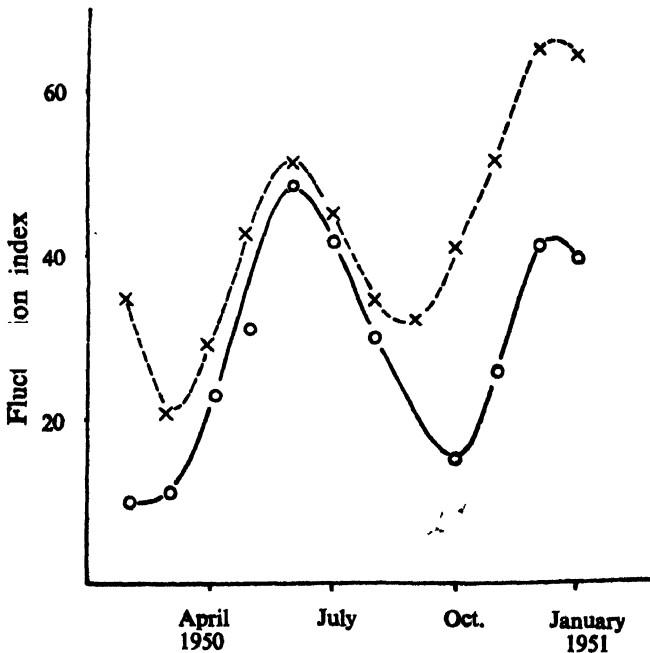
in nature, and was caused by the difference in local time at which the observations were made. When the curves were replotted with the local time of observations as abscissa, they were found to coincide (figure 5 (b)). The diurnal curve

now showed a rapid rise from 2000 hours to 2200 hours, a maximum at 0100 hours, and a subsequent decrease. It was concluded that the variation really is diurnal in nature, and that there is no comparable annual variation. Experiments on a wavelength of 6.7 m. in which the intense source in Cassiopeia was continuously observed, showed similar diurnal variation (Ryle and Hewish, 1950).



Variation of the fluctuation index for the above four sources during the same time replotted as a function of the time of observation. (After Ryle and Hewish).

Entirely different results have been obtained by Bolton (unpublished) observing at a different part of the world (Sydney) and at low angles of elevation.



Annual variation of the fluctuation index for Cygnus (x....x) and Virgo (o-o) observed at Sydney by Bolton. (After Bolton, unpublished).

The apparent annual variations of the fluctuation indices for the sources in Cygnus (Cygnus-A) and in Virgo (Virgo-A) for the year January 1950—January 1951 as obtained by Bolton are shown in figure 6. The observations are for an hour at the rising of the source. As there is a difference of nine hours between the local rising times of the two sources, a large diurnal variation is unlikely. Further, the predominant seasonal variation has two maxima instead of the one maximum obtained by Ryle and Hewish. Earlier measurements by Stanley and Slee (1950) also indicated a possible annual variation of the fluctuation index.

The variations of the nature of radio scintillations on different frequencies present some interesting features. It has been found that good correlation between fluctuations exists up to frequency difference of the order of 5 per cent. to 10 per cent. (Little, 1951; Stanley and Slee, 1950).

Another interesting result obtained is the frequent occurrence of deviations in the apparent position of the source during times of fluctuations. The observed close correlation between the two phenomena point to their common origin (Mills and Thomas, 1951).

(c) *Fluctuations and Ionosphere.* Since the fluctuations are of terrestrial origin, their probable source would seem to be the ionosphere. The close correlation observed between the fluctuation index and "spread-F" echoes (Ryle and Hewish, 1950; Little and Maxwell, 1951) shows that the source of the fluctuations lies in ionospheric irregularities and not the regular ultraviolet ionization. This conclusion has also been arrived at independently by Mills and Thomas (1951).

This discovery of ionospheric origin of fluctuations is of great importance for the present study. It means that interpretation of the fluctuations will yield valuable information regarding the physical and ionospheric condition at F-region heights, especially  $F_2$ -region irregularities. In what follows such information, based on the existing knowledge of radio scintillations, is presented.

(i) *Nature of the irregularities causing fluctuations.* It is believed that "twinkling of radio stars" is due to irregular refraction processes occurring in the outer region of the terrestrial ionosphere. The process involved is that of diffraction by an irregular screen. Since the frequencies at which the fluctuations have been observed so far are comparatively high, ionospheric absorption may be ignored. The effect of irregularities, under these conditions, will be to produce only irregular variations of phase across the emergent wavefront. This is analogous optically to that of a transparent plate of glass of irregular thickness. Such a diffraction process may conveniently be regarded as due to a "non-absorbing" phase screen discussed by Booker, Ratcliffe and Shinn (1950). Applications of such a diffraction process (Hewish 1951; Little 1951; Ryle and Hewish 1950) have shown that a satisfactory interpretation of the fluctuations is possible if the irregularities are simply regions of enhanced ionization density corresponding to an increase in thickness of the  $F_2$ -region of about 0.1 per cent. and have dimensions of the order of 5 km. (see also Table II). It will be noted that the size of the irregularities is larger than that observed at lower heights. The very large size (100-500km.) obtained by Munro or by Bramley at lower heights refers possibly to disturbances of a different kind.

(ii) *Diurnal variation of the incidence of irregularities—"spread-F" echoes.* Measurements on the occurrence of "spread-F" echoes by means of ordinary ionospheric equipment have shown that a diurnal variation of the occurrence of "spread-F" echoes exists. The echoes begin to appear between 1900 hours and 2000 hours local time. The frequency of occurrence of these echoes increases after this time, decreases during the latter half of the night and disappears rapidly near dawn (Booker and Wells, 1938). This curious variation was at one time considered to be only apparent and was attributed to the formation of a strong lower layer during dawn which would mask off the irregularities above even if they existed.

This conclusion has now to be revised in the light of the diurnal variation of fluctuation index obtained by Ryle and Hewish (see also figure 5 (b)). These observations have been made at frequencies which will not be appreciably affected by the production of a lower layer. *It seems therefore difficult to escape the conclusion that the curious diurnal variation of "spread-F" echoes is real and that the variation follows that of the fluctuation index* (figure 5(b)). It has not been possible to explain these peculiar variations in terms of solar emissions. It has been suggested that the variation is due to the interception of interstellar matter moving under the gravitational attraction of the Sun (Ryle and Hewish, 1950); but this hypothesis is too tentative at present to merit detailed discussion.

(iii) *Fluctuations and the angle of elevation of the source—influence of the effective ionospheric thickness—high latitude and auroral ionizations.* Little and Maxwell (1951) have made some interesting comparisons between the amplitudes of Cygnus fluctuations observed at different elevations at Jodrell Bank and the change in the effective thickness of the ionosphere in the line of sight. It was found that the effective thickness and amplitude curves follow each other closely for elevations greater than  $20^\circ$ , but below  $20^\circ$  the rate of increase in the amplitude of fluctuations is much greater than the corresponding rate of increase in effective thickness. It would therefore appear that fluctuations can be accounted for in terms of increased thickness of the disturbing region for large angles of elevation, but not for low angles of elevation. It is interesting to note that at Jodrell Bank, where the observations were made, the line of sight of the source at low angles of elevation crosses the F-region near the auroral zone. The ionosphere at these high latitudes is always disturbed, and it would appear that the disturbing nature of the ionosphere at these high magnetic latitudes is the main controlling factor in the fluctuations observed at low angles.

Increase in amplitude and occurrence of fluctuations of Cygnus with decrease in the angle of elevation have also been observed by Seeger (1951) at a higher frequency (205 Mc/s). As in the Jodrell Bank, observations there were considerable fluctuations below  $20^\circ$ .

It is interesting to note that a possible effect of aurora on fluctuation index has been noted by Bolton at Sydney, Australia (Bolton, unpublished) for the source in Cygnus observed at low angle of elevation. At a time when for some consecutive days the records were quiet, there were sudden high fluctuations in the records on the day when an aurora was reported to have been observed in south-eastern Australia. An aurora is a very rare occurrence in this region.

(iv) *Motion of irregularities—winds in the  $F_2$ -region.* It has become apparent in recent years that the whole of the atmospheric region from a height of about 90 km. to that of the lower  $F_2$ -region is traversed by high-velocity winds\*. There was, however, no available method to extend the investigations to the upper portion of the  $F_2$ -layer. Study of the motion of irregularities causing radio scintillations provides this much-needed method.

Estimates of motion by this method have been, made in recent years by Ryle (1951), Lovell (1951) and Maxwell and Little (1952). By correlation of the records of two receiving stations set up one km. apart in an E-W line, and working on a wavelength of 7 m., Ryle has determined the E-W component of the velocity of ionospheric "ripples" passing overhead. It was found to lie between 10 and 300 m/s and to go in either direction, sometimes reversing within an unexpectedly short period of about thirty minutes. More recent measurements by Maxwell and Little gave, for the horizontal component of motion, an average velocity of 100 m/s, the direction of motion being predominantly towards west.

\*Evidence of these "winds" has been obtained from sources of widely different nature, such as meteor trains, noctilucent clouds, luminous strips and radio measurements of moving irregularities. Though such evidence is fairly convincing, it is yet premature to state that the movements—especially those of irregularities—represent actual movements of winds rather than those of an ionospheric disturbance.



Lovell has estimated the velocity of the irregularities from the duration of fluctuations, taking proper account of the apparent movement of the "radio stars." Speeds of the order of 100 m/s have been inferred in this way.

A comparison between the motions in the upper part of the  $F_2$ -region and those observed at lower heights is presented in Table II.

## 5. EFFECTS OF SUDDEN IONOSPHERIC DISTURBANCES

There seems to have been little work regarding the effect of the ionosphere on extraterrestrial radio noise during sudden ionospheric disturbances (SID's). The only published information available is by Hey, Parsons and Phillips (1947) whose observations with a simple aerial on 25 Mc/s have revealed increased absorption of galactic radiation during fadeouts.

They observed that a burst of solar noise sometimes obscures the start of the fadeout.

An example of the fadeout effect from records taken by Shain (unpublished) with a narrow beam aerial is given in figure 7. A preliminary analysis has shown that a close correlation exists between the observed attenuation and  $f_{min}$  recorded by Canberra Ionospheric Station of the Ionospheric Prediction Service.

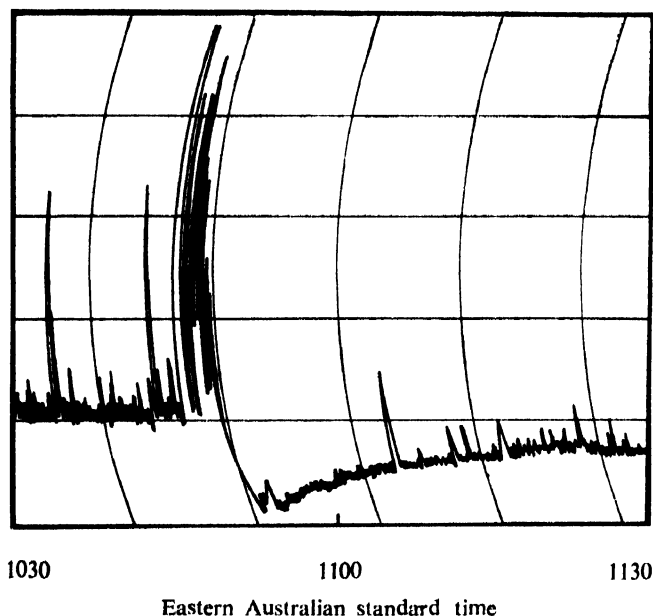


FIG. 7

Increase in absorption during fadeout starting at 1050 hours E.A.S.T. on April 20, 1951, observed at Hornsby, Australia, on galactic radiation at 18.3 Mc/s. Maximum increase in absorption during the fadeout was as high as 9 db.

In this connection we may mention a problem of considerable astrophysical interest. This is the comparison of the simultaneous activities of the Sun in the ultraviolet range (as measured from ionospheric abnormalities and increased absorption on extraterrestrial radiation during SID's) with those in the radio range (as measured by the solar radio emissions) during these times.

6. CONCLUDING REMARKS

In this section will be given first a tentative picture of the ionosphere as may be deduced from studies of extraterrestrial radio noise made so far, and then an account of future possibilities of such studies.

(a) *Ionospheric information as deduced from Radio Astronomy.*

(i) *D-layer.* There is an enhancement of D-region ionization during SID's. The magnitude of enhancement depends on the degree of radio fadeout and increases with the increase in the value of  $f_{min}$ .

(ii) *F-layers.* The behaviour of the F-layers cannot be adequately represented by the assumption of a Chapman distribution (section 2 and 3). It is possible that the  $F_2$ -layer is highly non-symmetrical, the portion above the maximum being many times as large as the portion below. If this is so, this would confirm the belief that the recombination coefficient which decreases from a level little above the  $F_1$ -maximum continues to do so to heights well above the  $F_2$ -maximum.

Ionospheric irregularities exist even above the height of maximum ionization of region  $F_2$ . It is possible that these irregularities are in the nature of ionization clouds of density greater than that of the  $F_2$ -maximum corresponding to a variation of the thickness of region  $F_2$  by only 0.1 per cent. The lateral sizes of these irregularities are about 5 km. and are much larger than those of the irregularities occurring at lower heights and lower frequencies (as obtained from spaced-receiver ionospheric measurements) (section 4).

The "spread-F" echoes frequently observed in ordinary ionospheric equipments are caused by these irregularities. The incidence of these ionizations has a curious diurnal variation attaining maximum at 0100 hours. Such a variation would possibly be due to interception of interstellar matter moving under the gravitational attraction of the Sun (section 4).

The incidence of irregularities appears to be greater at high latitudes (where the ionosphere is known to be always disturbed) than at low latitudes, and it is possible that some of the irregularities are formed by extraterrestrial corpuscles producing auroras (section 4).

TABLE II

Approximate height (km).	Method	Approximate size of irregularities	Drift velocity (m/s)	Author and remarks
300	Movement of irregularities causing fluctuations of radiations from "radio stars"	5 km	(i) 10-300	(i) Ryle (ii) Lovell (iii) Maxwell and Little. Irregularities are possibly identical with those causing "spread-F" echoes.
			(ii) 100	Sudden reversals of wind direction within one hour (Ryle ; Maxwell and Little).
			(iii) 100	
250	(a) Movement of ionospheric irregularities	(i) 500 km. (ii) 200 m.	(i) 100-200 (ii) 80	(i) Munro. No diurnal variation. Seasonal changes near the equinoxes. Movement predominantly towards the east.
	(b) Movement of ionospheric tilts	100-500 km.	35-350	(ii) Phillips. Bramley. Movement towards east.

100	(a) Movement of ionospheric irregularities	(i) > 200 m. (ii) 80 60-420	(i) Phillips (also S. N. Mitra, Ratcliffe and Pawsey). Also in America. Some rapid reversals. (ii) Reported by Dieminger. Gerson.
	(b) Movement of E <sub>s</sub> -clouds	60	
	(c) Luminous strips in the sky	50-90	Krautkramer
	(d) Luminous auroral clouds	50-100	Reported by Harang.
70-100	Meteor trains	(i) 50 (ii) 170 (iii) 80-100 (iv) 25	(i) Oliver. Drifting north with considerable E-W tendency. (ii) Fedynsky. (iii) Villard and Manning. (iv) Lovell.

Movements of irregularities with as high a velocity as 100 m/s have been detected. This velocity is of the same order as that of the irregularities at lower heights. There are occasional sudden reversals of the movements within a surprisingly small time of 30 minutes. It is not known whether these movements represent the movement of ionization or actual movements of air.

(iii) *G-layer*. There is no evidence for the existence of a G-layer.

(b) *Future possibilities*. The importance of extraterrestrial radio waves as an instrument for obtaining information on the ionosphere and for determining the radio propagation characteristics of the relevant regions cannot be doubted. Of the various available types of extraterrestrial sources, namely the Galaxy and the "radio stars," the Sun, and artificially stimulated reflections from the Moon, the former two appear to be the most suitable for ionospheric studies below 500 Mc/s.

The possible methods that may be employed for such studies and their applications are summarized in Table III. These studies have only just begun, and are far from complete. In some cases the results obtained have not been properly interpreted. We indicate below further lines of investigation that are likely to throw light on these results and may yield new information on the subject.

The most pressing need on the theoretical side is an estimation of ionospheric absorption and refraction of extraterrestrial radio waves on the basis of our present knowledge of ionospheric ionization, taking account of the variation of recombination coefficient and temperature at the heights concerned.

TABLE III

Method	Ionospheric applications	
1. Ionospheric refraction	(i) F <sub>2</sub> -region	Structure of the region especially above F <sub>2</sub> -maximum. Physics of the atmosphere at these heights.
	(ii) G-region	
2. Ionospheric absorption	(i) F <sub>2</sub> -region	Structure of the region. Physics of the atmosphere at F <sub>2</sub> -region heights.
	(ii) D-region	

## 3. Radio scintillations

F<sub>2</sub>-region

F<sub>2</sub>-irregularities and spread-F echoes.  
 Auroral ionization (?).  
 High latitude ionization (?).  
 Motion of irregularities at F<sub>2</sub>-heights.  
 Physics of the atmosphere at F<sub>2</sub>-region heights.

## 4. Measurements during SID's

- (i) Extra ionization in D region  
 (ii) Relation between solar radiations at radio and ultraviolet wavelengths (?).

Experimental work desirable includes (i) Extension of the observations of ionospheric refraction and absorption and of the scintillations of radio stars to include all possible angles of incidence and a range of frequencies down to frequencies near the critical frequency of the F-region. (ii) Simultaneous observations on radio scintillations by at least two, and preferably three, suitably separated stations (separated by a few km.) employing nearly identical receiving equipments to investigate motion of irregularities. (iii) Experiments to clarify the differences in results obtained for radio scintillations by Bolton in Sydney and Ryle and Hewish in Cambridge. (iv) Comparison of low angle fluctuations with vertical incidence ionospheric measurements of the ionosphere penetrated by the radiation, and (v) effects of SID's on the absorption of extraterrestrial radio waves at different frequencies.

Of immediate practical interest are studies on ionospheric absorption. Besides yielding information on ionospheric ionization, they give absorption characteristics of short radio waves important for radio communication.

## ACKNOWLEDGMENTS

The present work was done in the Radiophysics Laboratory, Sydney, of the Commonwealth Scientific and Industrial Research Organization, Australia during the tenure of a Fellowship awarded by the Australian Government under the Colombo plan.

The author acknowledges gratefully the very considerable help he received from various members of the Research Staff of the Radiophysics Laboratory C.S.I.R.O., Australia. In particular he would like to express his thanks to Dr. J. L. Pawsey, Assistant Chief of the Division of Radiophysics, for continued advice and guidance, to Mr. J. G. Bolton for permission to present his unpublished results, to Mr. F. J. Kerr for various discussions and suggestions, and finally to Mr. C. A. Shain for stimulating discussions, for considerable assistance in the preparation of the paper and for permission to present some of his unpublished records.

## REFERENCES

- APPLETON, E. V., 1937, *Proc. Roy. Soc. A*, **162**, 451.  
 APPLETON, E. V. and BEYNON, W. J. G., 1940, *Proc. Phys. Soc.*, **52**, 518; 1947, *Ibid*, **59**, 58.  
 BAILEY, D. K., 1948, *Terr. Mag. Atmos. Elec.*, **53**, 41.  
 BATES, D. R. and MASSEY, H. S. W., 1948, *Proc. Gen. Ass. U.R.S.I.*, Stockholm, p. 299.  
 BATES, D. R. and MASSEY, H. S. W., 1951, *J. Atmos. Terr. Phys.*, **2**, 1.  
 BERKNER, L. V. and WELLS, H. W., 1937, *Terr. Mag., Atmos. Elec.*, **42**, 183 and 301.  
 BOOKER, H. G., RATCLIFFE, J. A. and SHINN, D. H., 1950, *Phil. Trans. Roy. Soc.*, **242A**, 579.  
 BOOKER, H. G. and WELLS, H. W., 1938, *Terr. Mag., Atmos. Elec.*, **43**, 249.  
 BRACEWELL, R. N. and BAIN, W. C., 1952, *J. Atmos. Terr. Phys.*, **2**, 216.  
 BREMMER, H., 1949 *Terrestrial Radio Waves*, Elsevier Publishing Co, Inc., New York, pp. 271-277.  
 HEWISH, A., 1951, *Proc. Roy. Soc. A*, **209**, 81.  
 HEY, J. S., PHILLIPS, J. W. and PARSONS, S. J., 1946, *Nature*, **157**, 296.  
 HEY, J. S., PARSON, S. J. and PHILLIPS, J. W., 1947, *Nature*, **160**, 371.

## *Study of the Ionosphere by Extraterrestrial Radio Waves 511*

- JAEGER, J. C., 1947, *Proc. Phys. Soc.*, **59**, 87.  
JAEGER, J. C., 1948, *Proc. Phys. Soc.*, **61**, 78.  
JANSKY, K. G., 1932, *Proc. Inst. Radio Engrs.*, **20**, 1920.  
JANSKY, K. G., 1937, *Proc. I.R.E.*, **25**, 1517.  
KERR, F. J. and SHAIN, C. A., 1951, *Proc. I.R.E.*, **39**, 230.  
LITTLE, C. G. and LOVELL, A. C. B., 1950, *Nature*, **165**, 422.  
LITTLE, C. G. and MAXWELL, A., 1951, *Phil. Mag.*, **42**, 267.  
LITTLE, C. G., 1951, *Mon. Not. Roy. Ast. Soc.*, **111**, 289.  
LOVELL, A. C. B., 1951, See Geophysical Discussion of the Royal Astronomical Society, *Nature*, **167**, 626.  
MARTYN, D. F., 1948, *Proc. Roy. Soc. A*, **194**, 445.  
MARTYN, D. F., 1950, *Proc. Mixed Comm. Ionosphere, Brussels*.  
MAXWELL, A. and LITTLE, C. G., (In course of publication).  
MILLS, B. Y. and THOMAS, A. B., 1951, *Aust. J. Sci., Res. A4*, 158.  
MITRA, A. P., 1951, *J. Geophys. Res.*, **56**, 373.  
MITRA, A. P., 1952, *Ind. J. Phys.*, **26**, 79.  
NACA, See C. N. WARFIELD, 1947, NACA Technical Note No. 1200.  
PAYNE-SCOTT, R. and MCCREADY, L. L., 1948, *Terr. Mag. Atmos. Elec.*, **53**, 429.  
RYLE, M. and HEWISH, A., 1950, *Mon. Not. Roy. Ast. Soc.*, **110**, 381.  
RYLE, M., 1951, See Geophysical Discussion of the Royal Astronomical Society, *Nature*, **167**, 626.  
SEATON, S. L., 1948, *J. Met.*, **5**, 5.  
SEEGER, C. L., 1951, *J. Geophys. Res.*, **56**, 239.     *M*  
SHAIN, C. A., 1951, *Aust. J. Sci. Res.*, **A4**, 258.  
SMITH, F. G., 1950, *Nature*, **165**, 422.  
STANLEY, G. J. and STEE, O. B., 1950, *Aust. J. Sci., Res. A3*, 234.

# SPECTROSCOPIC STUDIES OF OZONISER DISCHARGES

## Part III

### Effect of Irradiation on the intensity distribution of the second positive nitrogen bands.

By N. APPALANARASIMHAM

SPECTROSCOPY LABORATORY, BANARAS HINDU UNIVERSITY.

(Received for publication, June 14, 1952)

#### PLATE XIX

**ABSTRACT.** The intensities of the second positive nitrogen bands obtained in an ozoniser discharge through nitrogen at different voltages of excitation with and without irradiation by 3650-60 Å.U. group of radiations of mercury, have been measured using photographic photometric method. It is found that the irradiation brings about a general decrease in the intensities of all the bands and further that a redistribution of the intensities of the bands occurs in such a way that the percentage decrease of the intensities has the following order :

$$(0,3) > (0,2) > (0,1).$$

Also the percentage decrease in the intensity of the (1,3) band is greater than that of (0,2) band.

While the general decrease in the intensities of all the bands is a consequence of the reduction in the number of collisions of the neutral nitrogen molecules with electrons and/or ions, the redistribution in intensity is to be attributed to the alteration of the velocities of ions and particles of atomic masses. The redistribution in the intensities of the bands (0,1), (0,2) and (0,3) and (1,3) and (1,4) of the  $v''$ -progressions of  $v'=0$  and 1 respectively, is suggested to be due to induced perturbation of the low  $v''$  levels e.g.,  $v''=2$ , brought about by irradiation.

A comparative study of the intensities of the second positive bands obtained in low pressure induction coil discharges through nitrogen and air with those obtained in the present experiments, shows that external irradiation alters the intensity distribution of the bands in just the same manner as the substitution of air for nitrogen does, the other conditions remaining the same.

#### INTRODUCTION

In an earlier paper, Part I (Appalanarasimham, 1950-51), a decrease in the optical densities of blackening of the bands of nitrogen second positive system on external irradiation has been reported. At a given voltage of excitation, it was found that the percentage decrease on irradiation, of the densities of blackening of the several bands is not constant but varies from band to band. In order to study this variation on a relatively absolute scale, the usual intensity technique of heterochromatic photographic microphotometry (Read and Johnson, 1931, Tawde and Patel, 1937) has been employed to determine the intensities of the bands. The results are reported and discussed in this paper.

#### EXPERIMENTAL

The experimental procedure adopted for exciting the ozoniser is the same as described in Part I. A step slit consisting of slits of widths 0.22, 0.27, 0.32, 0.47, 0.63, 0.83, 1.04, 1.24, 1.58, and 2.03 mm. is used to photograph the calibration density marks beside the spectra. A helical filament lamp (supplied by Kipp and Zonen, Holland) is used as a standard source of continuous radiation. This was the one already calibrated for the visible region of the spectrum and its colour temperature determined for the current intensity at which the lamp is run.

A Hilger E3 quartz spectrograph is used for recording the spectra. The

discharge tube is collimated on to the slit of the spectrograph and kept close to it. No auxiliary lens is used to focus the discharge on to the slit. The slit width of the spectrograph is adjusted to 0.1 mm, a value which makes the fine structure of the bands disappear while at the same time there is no intermixture of the bands with one another. This procedure also enabled to bring down the exposure time which would otherwise be inconveniently long in the case of the feeble intensity available in the discharge through the ozoniser which had to be worked at low voltages in order to get the maximum negative Joshi Effect (Joshi, 1939; 1943).

The spectrum of the discharge is photographed so as to get the bands in the violet and near ultra-violet regions within an exposure time not exceeding two hours. Next the spectrum of the discharge excited under the same voltage and irradiated by the 3650-60 Å. U. group of radiations of a filtered\* mercury arc run at a constant current, is photographed. Later, the usual slit of the collimator is replaced by the step slit and the radiation from the standard lamp, placed along the line of the collimating arm of the spectrograph, is photographed. The correct position of the step slit is found by a preliminary experiment to give a spectrum in best focus with the lens reading as that with the usual slit. The ten strips of slits give ten continuous spectra of optical densities of blackening varying from one strip to another at any desired wave length. These serve as the calibration marks for the spectrum of the discharge and are such that the spectrum blackenings are intermediate between the minimum and maximum blackenings of comparison marks.

A preliminary determination gave the time of exposure which is necessary to obtain the optical densities of the required bands within the straight line portion of the characteristic curve of photographic plate. For that time of exposure, the suitable distance of the standard lamp from the spectrograph is determined after a number of trial exposures so as to bring out the calibration marks from a region near above the under exposure part of the characteristic to one nearer the saturation density of blackening. The standard lamp is run at 6 volts with a constant current of 4 amperes supplied by a battery of large accumulators. Then, under the above conditions, the radiation of the standard lamp is photographed through the step slit for the same time as the discharge spectrum with and without irradiation. No lens is used to focus the light from the lamp on to the slit of the spectrograph.

The plates are developed immediately after the exposure according to specified conditions, with the developer recommended by the manufacturers of the photographic plates. The plates are then immersed and agitated for about a minute in water containing 2% acetic acid and later fixed in acid hardening fixing bath for twice the clearing time. The Kodak P 1200, Super Panchro Press, plates were found suitable and employed.

Adopting the above procedure, the following experiments were carried out. At graded voltages between 800 and 2800 volts, the spectra of the discharge with and without irradiation were photographed and on each plate calibration marks were also photographed. (The ozoniser used in these experiments is the same as that described in Part I). It is found with increasing voltage, that the same time of exposure for any sequence of bands tends to increase the optical density to saturation and consequently the spectral density gets beyond the calibration density mark. In order that the same set of calibration marks may serve for all the spectra at all voltages studied, it is found necessary to vary the distance of the spectrograph from the ozoniser suitably to keep the spectral density within the calibration marks.

The final plates selected for the study of the intensities are run under a

---

\*The filter used for the purpose gives 70% transmission which falls off rapidly on either side of the 3650-60 Å.U. group.

**Zeiss recording microphotometer\*** and the microphotometer curves of the bands and the calibration density marks are obtained in the usual manner. (e.g., Tawde and Patel, 1937). The microphotometer was checked for reproducibility and had no zero creep. The densities of blackening,  $D = \log_{10} (I_0/I)$ , are calculated and from these, the intensity values are computed as follows. For each wavelength, intensity and  $\log_{10} (I_0/I)$  curves are drawn. From these curves, the values corresponding to the densities of blackening of the bands are read off. The widths of the step slit are taken as proportional to the intensities of the radiations emitted by the standard lamp. In the present studies of the determination of the percentage decrease of intensity of any band, only the intensity values obtained from these curves are used. These are given in Tables I, II and III.

**TABLE I**

**Percentage decreases of optical densities of second positive bands excited at 800 volts.**  
**Percentage decrease of the discharge current on irradiation as recorded by a metal oxide**  
**rectifier type A.C. microammeter=75**

		3371	3577	3805	4059	3755	3998	2977
Figure 1	$v', v''$	0,0	0,1	0,2	0,3	1,3	1,4	2,0
	$D$	0.597	0.621	0.458	0.194	0.362	0.215	0.123
	$D'$	0.398	0.380	0.220	0.066	0.167	0.073	0.033
	$\% \Delta D$	33	39	52	67	54	70	74
Figure 2	$D$	..	0.569	0.436	0.219	0.378	0.240	..
	$D'$	..	0.371	0.235	0.071	0.174	0.066	..
	$\% \Delta D$	..	35	46	68	54	72	..

**$D$** =Density of blackening without irradiation

$D'$  = " " " on " "  
 $\% \Delta D$  = Percentage decrease of the optical density on irradiation.

Percentage decrease in intensity of bands at 4059Å (0,3) = 57 and at 3998Å (1,4) = 63

**TABLE II**  
**Percentage decrease of optical densities and intensities of the second positive bands**  
**excited at different voltages on irradiation**

Voltage of excitation	% $\Delta i$	% $\Delta D$			% decrease in intensity	
		0,1	0,2	1,3	0,2	1,3
1000	24	2	4	11	7	18
1200	33	9	23	24	24	20
1400	33	17	30	45	41	37
1600	27	15	18	19	21	18
2000	19	11	14	16	20	20
2400	12	17	33	43	33	32
2800	9	10	21	32	24	27

$\% \Delta I$  = Decrease in the discharge current on irradiation as recorded by the A.C. microammeter described in Table I.

$\% \Delta D$ —Percentage decrease of the optical density on irradiation.

\*We are thankful to Prof. L. M. Chatterjee, Science College, Patna, for permission and help in using the microphotometer.



TABLE III

Percentage decrease of optical densities and intensities of the second positive bands excited at different voltages on irradiation

In this case, a non-inductive resistance of 15,000 ohms is connected in series with the A.C. microammeter for the oscillographic studies made simultaneously.

Voltage of excitation	% $\Delta i$	% decrease of optical density			% decrease of intensity	
		0,1	0,2	1,3	0,2	1,3
1000	9	10	12	15	13	22
1200	21	12	19	22	40	31
1400	10	17	36	37	30	32
1600	15	..	19	22	21	20
2000	15	..	25	38	22	20
2400	12	16	30	32	30	30

All the leading bands of the sequences (0,1), (0,2) and (0,3) are completely free from superposition of any rotational structure of the preceding bands and all of them have nearly the same back-ground density (see figure 1, Plate XIX), subject to the small fluctuations due to the grain irregularity of the photographic plate. The measurements of the densities of blackening of these leading bands are therefore expected to be the most accurate. For the rest of the bands, a certain amount of overlapping of the preceding band exists and as such the back-ground density marks are generally higher. Hence a correction which takes into account the back-ground density of the previous band is necessary in computing the  $I_0$  value of the band in question. In the present experiments the exposure times were such that the density of blackening of only the leading band and the one after it, lie on the straight line portion of the characteristic curve of the plate. In the microphotometer curves, it was generally found that a mean value of the back-ground density of the leading band in a sequence and the position of the rise of intensity of the second band gave a value nearly equal to the true back-ground density of the second band. The point of intersection of the normal drawn from the peak of a band to the mean back-ground density and the tangent drawn from the declining curve of the previous band is also found to be not very different from the above value. This method avoids the ambiguity of the exact position wherefrom the tangent has to be drawn and also of the correct mean back-ground density line. The error in the evaluation of the optical densities is estimated to be less than 10% even for bands whose density is not very high relative to the back-ground density. For bands of higher relative density, the error will be very much less. Again, in the case of the measurement of the percentage decrease in density of bands on irradiation, this error gets further reduced.

#### OBSERVATIONS AND RESULTS

An examination of the tables show that at all voltages of excitation studied, the bands suffer a decrease in their intensities on irradiation. These decreases are not the same in a  $v''$  progression. The variations are more marked at 800 and 1000 volts of excitation which are just above the striking potential (viz., 780 volts). This observation is clearly borne out in the microphotogram reproduced figure 1, which is the one representative at 800 volts. In the  $\Delta v = -3$  sequence,

the peak of the band at 3998 A.U. (1,4) is greater in height than the 4059 A.U., (0,3) band without irradiation whereas, on irradiation both are almost of the same height. Similarly, while the peak of the 3755 A.U., (1,3) and without irradiation is above that of the 3805 A.U., (0,2), band, on irradiation it lies lower than that of the 3805 A.U., band. The 3577 A.U., and 3537 A.U., bands show a similar variation on irradiation.

From the values of the percentage decrease of intensities of the bands given in Tables I, II and III, we find that in the  $v''$  progression of  $v''=0$ , the decreases lie in the following order : (0,3) > (0,2) > (0,1); similarly for the  $v''$ -progression of  $v'=1$ , (1,4) is greater than that of (1,3). Also in the sequences  $\Delta v = -2$  and  $\Delta v = -3$ , the (1,3) and (1,4) bands suffer more decrease in intensity on irradiation than the (0,2) and (0,3) bands respectively,

Somewhat similar results were obtained by Tawde and Patankar (1944) in the course of their investigation of the intensity variations of the second positive nitrogen bands as obtained in pure nitrogen gas and air. In their experiments the conditions of excitation, namely pressure of the gas, voltage and source of excitation were identical for pure nitrogen gas and for dry air. Their values of  $I_A/I_N$  of the bands and the intensity ratio of the bands as obtained in the present experiments with and without irradiation are given in rows 1,2 and 3 of Table IV. On comparing, it is found, that in both cases, the variations of the intensity ratios of the higher members of the  $v''$  progressions of  $v''=0$  and 1 are greater than those of the preceding bands. This is analogous to what has been obtained in the present investigation and indicates that external irradiation alters the intensity distribution in just the same manner as the substitution of dry air for nitrogen does, the other conditions remaining the same.

TABLE IV

$I_A/I_N$  and  $I/I_{irr}$  values of the second positive nitrogen bands.

$v', v''$	0,1	0,2	0,3	1,3	1,4
$I_A/I_N$	0.86	0.61	0.40	0.67	0.49
$I/I_{irr}$ { figure 1	0.65	0.54	0.32	0.46	0.28
figure 2 (not reproduced)	0.61	0.48	0.33	0.46	0.30

$I_A$  and  $I_N$  are the intensity values obtained in a Geissler tube discharge (low voltage induction coil) in air and nitrogen by Tawde and Patankar (1944).

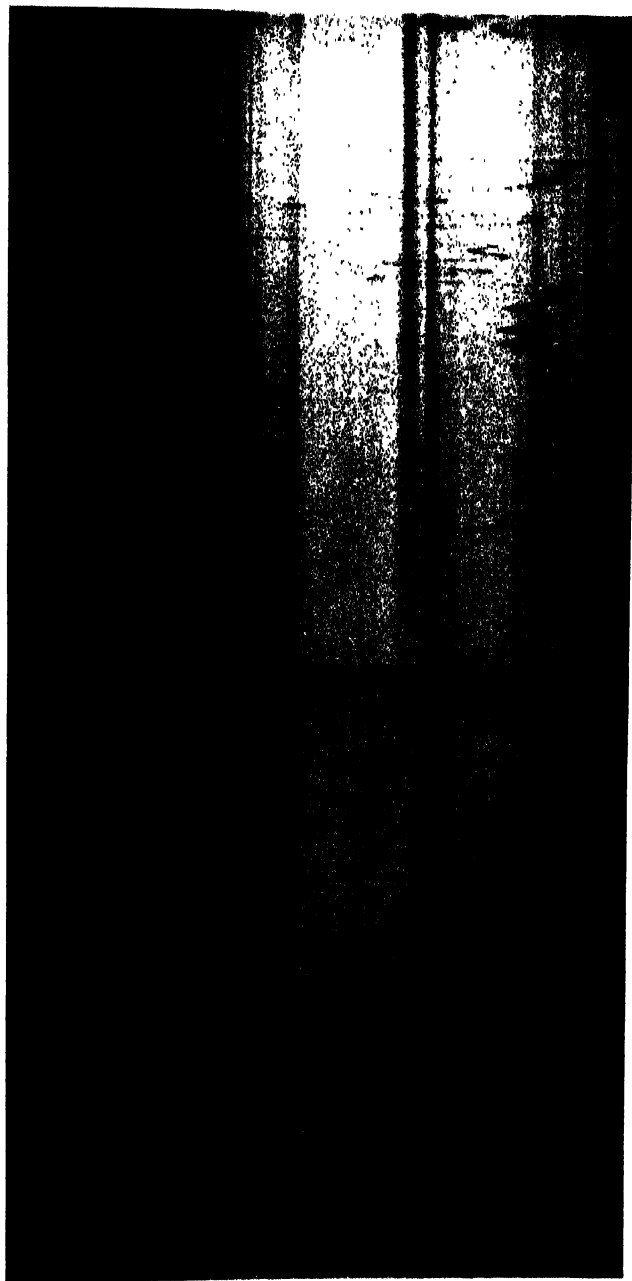
$I/I_{irr}$  = Ratio of the intensity values of the second positive bands without and with irradiation.

Tawde and Patankar (1944) have expressed the intensities of the individual bands of the second positive nitrogen system as obtained in discharges through nitrogen and air on a relative scale giving a value of 1000 for the (0,0) band in either sources. It is not known how the (0,0) band obtained in a discharge through nitrogen, for example, compares with the (0,0) band of the same system as obtained in a discharge through air. In such a case, though the relative intensity distribution of the bands in nitrogen discharge can be compared with that as obtained in the discharge through air, the intensities of the same band as produced in the two ways cannot be evaluated in the absence of a direct comparison of intensity of at least one identical band in the two methods of production. In spite of this, the variations of the intensity ratios of the bands can be compared amongst themselves for, all of them differ from the true intensity ratios by a constant factor.

4343.6 (0.4)  
4269.7  
4059.4 (0.3)  
3998.4  
3904.9 (0.2)  
3755.4  
3776.9 (0.2)  
3536.7

4269.7  
4059.4 (0.3)  
3998.4  
3804.9 (0.2)  
3755.4  
3650 Hg  
3576.9 (0.1)  
3536.7

-Limit of  
complete  
darkness



(a)

(b)

Fig. 1.

Microphotograms of the second positive nitrogen bands excited in a nitrogen ozoniser at 800 volts

(a) Without irradiation, (b) on irradiation with 3650 Hg are radiations.



## DISCUSSION

The results obtained in the present experiments are briefly as follows : On irradiation of the ozoniser, it is observed that,

- (1) the discharge current decreases;
- (2) there is a decrease in the intensities of all the bands and the nature of variation of this decrease is more or less *similar* to that of the variation of the %  $\Delta i$  in the range of voltages studied; (see Tables II and III) and
- (3) that the percentage decrease of the intensities of different bands is different.

The first observation indicates that there is an alteration in the number of charged particles (electrons and ions) and/or their velocities.

The second observation can be understood from the following. Excitation of the nitrogen molecules is brought about by collisions with electrons and/or ions. A reduction in the number of such collisions or in the velocities, within a particular range, of the colliding particles) decreases the population of the excited states of the molecules and consequently the intensities of bands involving such excited states show a decrease. The variation of the percentage decreases of the densities of blackening or the intensities of the bands is thus closely related to the alteration of the number of the charged particles and/or their velocities (that is, %  $\Delta i$ ). The present experiments, indeed, indicate a similarity in the two variations although the actual magnitudes of percentage  $\Delta i$  and percentage decrease of intensities at any particular voltage are not the same.

For the explanation of the third observation, we have to consider the possibility of an alteration in the velocities of the electrons and/or ions. Langstroth's (1935) experiments, however, indicate that the relative intensity of these bands in a  $v''$ -progression excited by electron collisions is independent of the velocities of the electrons for all accelerating voltages above 30. Hermann (1936) found from his measurements of the absolute intensities of the second positive nitrogen bands, that the intensity ratios of the individual bands are independent of electron velocity. These observations exclude the possibility of alteration of the velocities of the electrons being responsible for the change in the intensity distribution. The distribution of the relative intensities observed here on irradiation has, therefore, to be attributed to the alteration of the velocities of particles of atomic masses. That such an explanation seems to be the correct one is further shown by the fact observed elsewhere (Appalanarasimham, 1952) that along with electrons, also ions and particles of atomic masses play a significant role in the excitation of the nitrogen spectra in the ozoniser discharge. This mechanism, namely, an alteration in the velocities of ions and particles of atomic masses, also explains the fact that in sequences of bands the succeeding band involving, as it does, a higher initial vibrational level decreases to a greater extent than the leading band.

This, however, does not explain the redistribution of intensity in the  $v''$  progression ( $v''=0$ ) where the relative decreases are in the order  $(0,3) > (0,2) > (0,1)$ . According to Langstroth (1935) a similar effect recorded by Tawde (1934) under certain conditions of excitation, is brought about by a change in the transition probabilities caused by the occurrence of dissociation induced by external perturbations of the type examined theoretically by Zener (1933). Zener's treatment concerns the induced predissociation in the initial state of the bands brought by appropriate external fields or collisions. Thus Zener explained the magnetic quenching of the discrete bands of iodine above a certain initial vibrational level. A similar induced predissociation occurring in the final state of a band system will, however, lead only to a weakening of the bands having a certain  $v''$  levels (Johnson, 1949). In the case of the  $B^3\Pi_u$  state of the nitrogen molecule there is indeed observed a repulsive state (Okubo and Hamada, 1932; Kaplan, 1931) which intersects the stable state at  $v''=2$  but, under normal conditions, there is no interaction between the two curves. This appears to be brought about

by special conditions of excitation resulting in extraneous fields in the manner suggested by Langstroth and Zenner. The results of the present investigations show that a similar interaction is brought about by suitable irradiation of the ozoniser tube.

The present investigation, therefore, indicates that the effect of irradiation on an ozoniser discharge through pure nitrogen is two fold; first, there is an alteration of the velocities of the particles of atomic masses which play a significant role in such discharges; secondly, that it induces interaction of a repulsive curve with the  $B^3\Pi_g$  state at about  $V=2$ .

#### ACKNOWLEDGMENTS

The author takes this opportunity of according his grateful thanks to Dr. R. K. Asundi for suggesting the problem and for several discussions. He is also thankful to Dr. S. S. Joshi for his kind interest in the work.

#### REFERENCES

- APPALANARASIMHAM, N., 1950-51, *J. Sc. Res., B.H.U.*, **1**, 78.  
 " " 1951-52, *J. Sc. Res., B.H.U.*, **2**, 121.  
 ASUNDI AND APPALANARASIMHAM, 1952, *Curr. Sci.*, 240.  
 " " 1952, *Nature*, under publication.  
 HERMANN, 1936, *Ann. Phys., Lpz.*, **25**, 166.  
 JOHNSON, 1949, "An Introduction to Molecular Spectra," Methuen & Co., p. 41.  
 JOSHI, 1939, *Curr. Sci.*, **12**, 548.  
 —, 1943, Presidential address, Chemistry Section, Indian Science Congress.  
 KAPLAN, 1931, *Phys. Rev.*, **37**, 1409.  
 LANGSTROTH, 1935, *Proc. Roy. Soc.*, **150A**, 371.  
 OKUBO AND HAMADA, 1932, *Phys. Rev.*, **42**, 795.  
 READ AND JOHNSON, 1931, *Phil. Mag.*, **11**, 1152.  
 TAWDE, 1934, *Proc. Phys. Soc.*, **46**, 324.  
 " AND PATANKAR, 1944, *Phil. Mag., Ser. 7.*, **35**, 616.  
 " AND PATEL, 1937, *Bomb. Univ. Jour.*, 6 part II, 29.  
 ZENER, 1933, *Proc. Roy. Soc.*, **140A**, 660.

# REVIEW

(1)

## EINFÜHRUNG IN DIE THEORETISCHE PHYSIK,

Bd. III Teil 2. (1951)—By CL. SCHAEFER, publisher—Walter de Gruyter & Co., Berlin. Pp. vii + 510, Price DM 40

The book under review is very well-known throughout the world as a standard text book on the subject of the quantum theory and wave mechanics. Of this book, first five chapters deal with the ideas and the applications of quantum theory to atomic phenomena, the next four discuss among others, the same problems from the point of view of the non-relativistic wave mechanics and the last one is devoted to the relativistic wave mechanics—the Dirac electron theory. Usually in a book which covers such a wide field, selection of topics and relative length of exposition required to present each of them without obscurity is an exceedingly difficult task. It is here that the author has shown his remarkable skill. The subject matter beginning with Planck's radiation theory and ending up with the Dirac electron theory has been gradually and continuously built up, and appropriate experimental findings have been quoted to show how closely the theoretical formulae agree with them.

The introductory remarks deal with the significance of the Planck's radiation formula which is the starting point of quantum theory. Chapter I describes the Compton scattering of light by electron to show the corpuscular nature of electromagnetic radiation. Chapter II discusses the mathematical tools of the quantum theory and outlines the application to the Bohr-Rutherford model of the atom. Chapters III, IV and V deal with the elaboration of different quantum numbers in connection with Kepler problem together with the relativistic generalisation due to Sommerfeld, the characteristics of alkali spectra, Zeeman and Paschen-Back effect, the periodic classification and the Rontgen spectra. Chapter VI introduces wave mechanics from Hamilton's principle, and the applications of the Schrödinger equation to Kepler problem; oscillator and rotator cases are worked out in details in chapter VII which also includes both the theory and application of the perturbation theory (time-independent). Chapter VIII is devoted to the statistical interpretation of wave mechanics and the connection between statistical mechanics and wave mechanics is shown. Also a section deals with Heisenberg's matrix mechanics. Chapter IX discusses the wave mechanical interaction between electromagnetic radiation and charged particles. After giving a few definitions such as charge-current-density matrices and the dipole moments, the perturbation theory (time-dependent) is developed and applied to transition probabilities. The theory of dispersion and Raman-effect is also included in two sections of this chapter. Chapter X gives an account of the Dirac theory of electron and explains the solution of the equation for a free particle and for a particle subjected to electromagnetic field. The magnetic moment of the Dirac electron and the fine structure of the energy levels of the hydrogen atom have been fully worked out. Finally, a passing reference is made to the negative energy states and the theory of positrons.

In view of the considerable importance that has gathered round Tomonaga-Schwinger formalism of relativistic quantum electro-dynamics, one would have wished a short final chapter on the quantization of wave fields to make the book complete and up-to-date. There is no doubt that the present book, though in German language, will continue to prove itself extremely helpful to students doing final degree course and researches at the early stage.

D. B.





# OBSERVATIONS AT CALCUTTA OF PULSES TRANSMITTED FROM DELHI\*

BY S. S. BARAL AND A. K. SAHA

INSTITUTE OF RADIO PHYSICS AND ELECTRONICS, UNIVERSITY OF CALCUTTA

(Received for publication, July 21, 1952)

## Plate XX

**ABSTRACT.** The paper describes the results of observations made at Calcutta on pulses transmitted from Delhi during November, 1950 and May-June 1951 at frequencies of 17.74 Mc/sec and 21.70 Mc/sec. The various modes of propagation by which the echoes could be received have been critically examined. It has been concluded that the received echoes correspond only to single-hop  $F_2$ -layer reflection and not to multi-hop  $F_2$  layer or to single-hop E or  $F_1$  transmission. Absorption of the pulses in the Delhi-Calcutta transmission path has been estimated. From a statistical analysis of the fluctuations of the received echoes, it is concluded that the echo corresponding to the lower ordinary ray was more stable than that corresponding to the upper ordinary or the 'Pedersen' ray.

## 1. INTRODUCTION

In 1950 the Research Department of the All India Radio arranged, at the request of the Director of the Radio Research Board of Scientific and Industrial Research, England, a programme of pulse transmissions from Delhi in the European beam. The Research Department of the All India Radio requested the Ionospheric Research Station at Calcutta, working under the sponsorship of the Council of Scientific and Industrial Research, Government of India, to take observations on these pulses as may be possible.

The present note describes the results of observations made at Calcutta and discusses the possible modes of propagation by which the echoes were received, the total absorption suffered on the way and the fading characteristics of these echoes.

## 2. OBSERVATIONAL DATA

50 cycle pulses, each of 70 microseconds duration, were radiated in the European beam from the 100kW short wave station of the All India Radio, Delhi ( $28^{\circ}35'N$ ,  $77^{\circ}5'E$ ) using the antenna array H/4/4/1 (NN-SE). The zenithal and azimuthal distributions of radiations in and about the (NW-SE) plane and the zenithal distribution in the plane passing through Delhi and Calcutta are shown in figure 1. The midpoint of the transmission path is located at latitude  $25^{\circ}34'N$  and longitude  $82^{\circ}43'E$ , approximately above

\* Communicated by Prof S. K. Mitra, D. Sc.

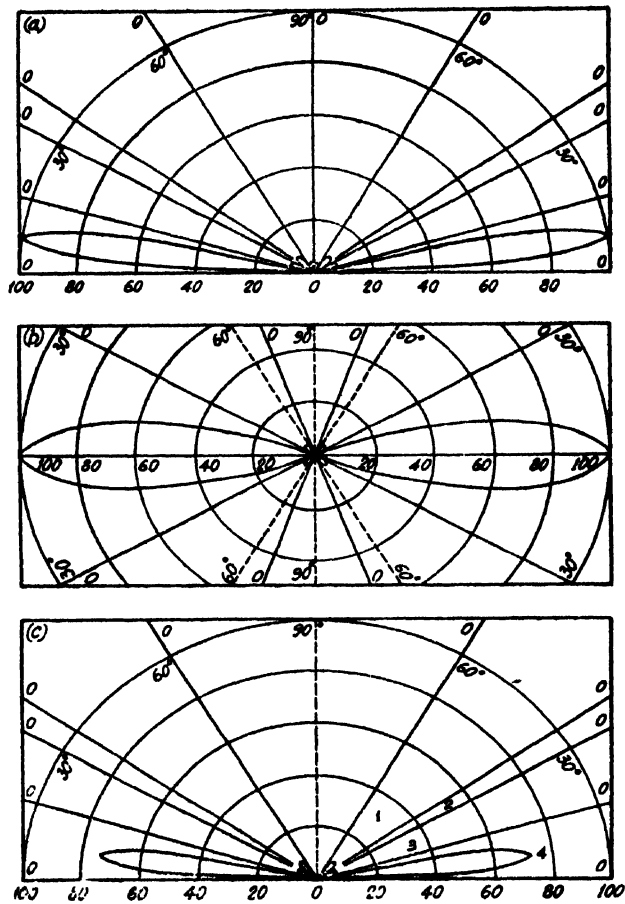


FIG. 1

Power distribution of the H/4/4/1 antenna array from which the pulses were transmitted from Delhi.

(a) and (b) Zenithal and azimuthal distribution in and around the NW-SH plane. (c) Zenithal distribution in Delhi-Calcutta great circle plane.

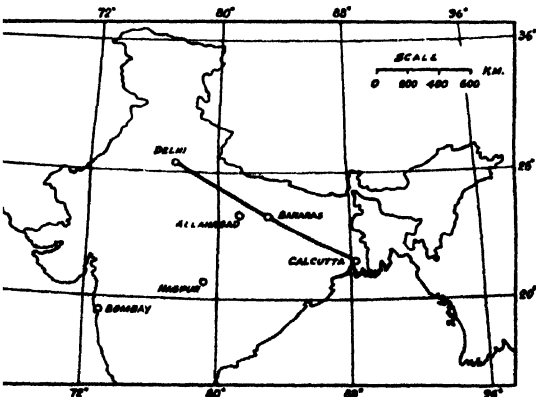


FIG. 2

Map showing the Delhi-Calcutta great circle distance. The mid-point is near Bazaras.

## *Observations at Calcutta of Pulses Transmitted from Delhi 523*

Banaras, geomagnetic latitude  $14^{\circ}30'N$  (figure 2). The pulses were received at the Ionospheric Research Station, Calcutta ( $22^{\circ}33'N$ ,  $88^{\circ}21'E$ ) at a great circle distance 1290 kms. in a direction  $25^{\circ}28'$  south of east from Delhi. A communication receiver of 20 kc/s bandwidth and sensitivity 1 microvolt for 7 volts across detector load was used. The receiving aerial was of the inverted L type. The observations were made with a cathode ray oscillograph connected across the detector load. The pulses were locked by controlling a phase shifting network in the A. C. supply used for synchronization.

The programme of transmissions was as follows :

Month	Date	Hour (L. S. T.)	Frequency (Mc/s)
November, 1950	13, 15, 17	1120-1230 and 1500-1600	21.70
	19, 21, 23	1120-1230 and 1500-1600	17.74
May, 1951	14, 16, 21, 23, 28, 30	1500-1615 and 0130-0300	21.70
	18, 25	1500-1615	21.70
June, 1951	1	1500-1615 and 0130-0300	21.70

Unfortunately, observations could not be made on all the transmissions. Those that were made are listed below :

November, 1950, on 15, 17, 21, 23.

May, 1951, on 14, 16, 18, 21, 25, 28, 30.

June, 1951, on 1.

The observations consisted in the measurement of the fluctuations in the amplitudes and the mutual separations of the echoes received. The measurements were made at intervals varying from one to two seconds. Simultaneous observations of the vertical incidence characteristics over Calcutta were also made. Table I gives the number of echoes received, the average values of the amplitudes of each of these echoes and their mutual separations during the periods of transmission. The mean values of the ionospheric characteristics over Calcutta and Delhi during the periods of transmission have also been included in this table. Sample records of the data for Nov. 1950, May 1951 and June 1951 are presented in figures 3-7.

### 3. INTERPRETATION OF THE OBSERVED RESULTS

In order to interpret the observed echo separations as given in Table I and also to explain the absence of the echoes during certain periods of transmission, it is necessary to know the equivalent paths of the rays reaching the receiver and the maximum usable frequencies (MUF's) for the particular distance of transmission at the hours of observations. This knowledge



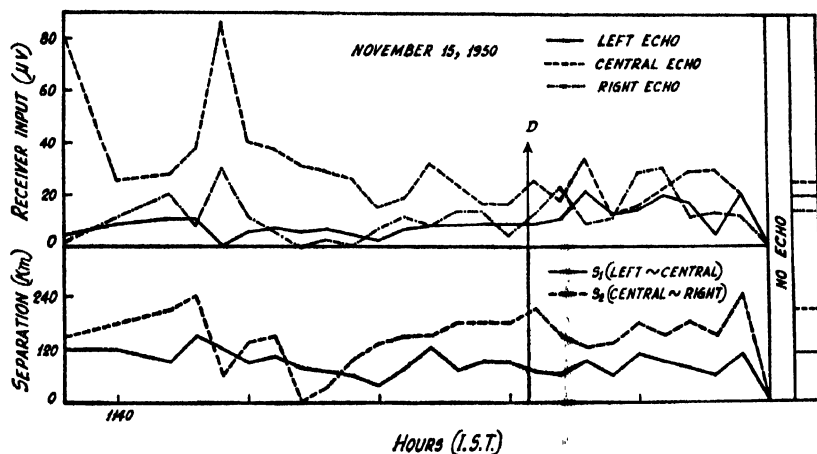


FIG. 3

Variations of (i) the amplitudes and (ii) the mutual separations of the echoes received from 1138 to 1207 hours on 15. 11. 50.

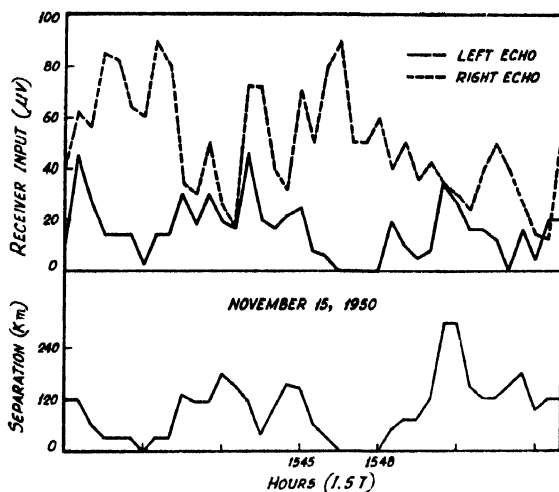


FIG. 4

Variations of (i) the amplitudes and (ii) the mutual separations of the echoes received from 1500 to 1601 hours on 13. 11. 50.

can be gained if we have information, at least approximate, of ionospheric conditions as existed at the hours of transmission over the midpoint of the path. This information may be deduced from the vertical incidence ionospheric data at the two points of the transmission path, Calcutta-Delhi.

(i) *Ionospheric conditions at the midpoint of the transmission path (Calcutta-Delhi).* The variations of the ionization densities of regions  $I_1$  and  $F_1$  with  $\chi$ , the zenith distance of the sun, are known to follow closely the  $\sqrt{\cos \chi}$  law. Hence the ionization values for these regions, over the midpoint,

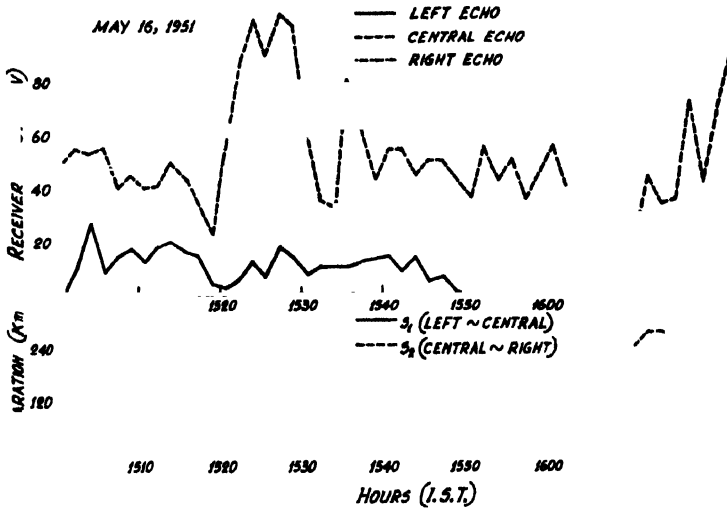


FIG. 5

Variations of (i) the amplitudes and (ii) the mutual separations of the echoes received from 1500 to 1626 hours on 16. 5. 51.

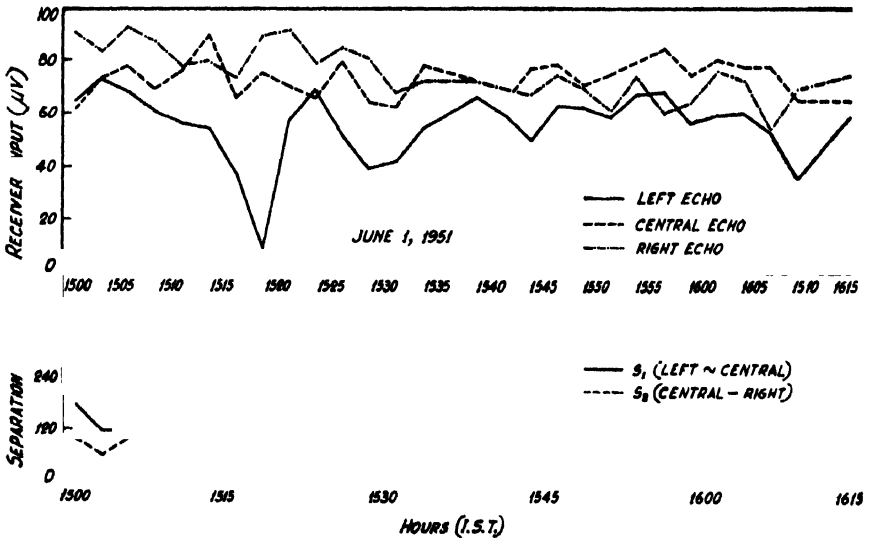


FIG. 6

Variations of (i) the amplitudes and (ii) the mutual separations of the echo received from 1500 to 1615 hours on 1. 6. 51.

may be deduced by applying the  $\sqrt{\cos \chi}$  law to the Calcutta or to the Delhi data. When the data for both the stations are available it is best to deduce the midpoint ionization values from both and take the mean of the two. However, as no relevant data for these regions were available from Delhi, the conditions at the midpoint were deduced by applying the  $\sqrt{\cos \chi}$  law to

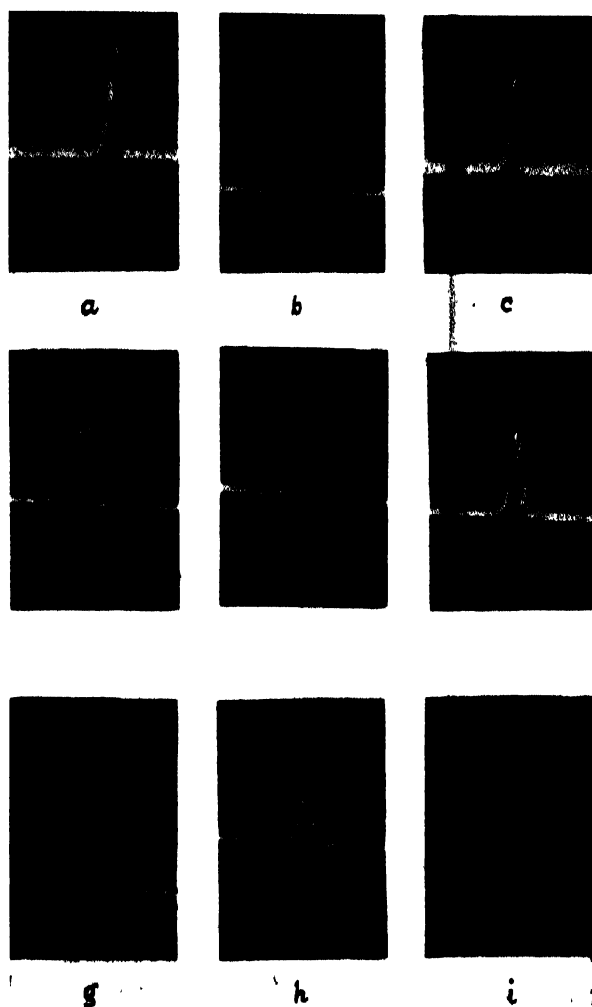


Fig. 7.

Sample records of observed echoes :

( *a* ), ( *b* ), ( *c* ). May 18, 1951 : 1500-1615 hrs.

( *d* ), ( *e* ), ( *f* ). May 28, 1951 : 1500-1615 hrs.

( *g* ), ( *h* ), ( *i* ). June 1, 1951 : 1500-1615 hrs.





TABLE II

Date	Hour I. S. T.	$f^{\circ}E$ at point of reflection Mc/s	$f^{\circ}F_1$ at point of reflection Mc/s	Maximum usable fre- quency (Mc/s) for Delhi- Calcutta		Frequency used in transmission (Mc/s)
				via region E	via region F <sub>2</sub>	
15.11.50	1120-1230	3.45	4.75	16.70	14.20	21.70
	1500-1600	3.08	4.25	15.90	12.75	21.70
17.11.50	1120-1230	3.56	4.30	16.35	12.90	21.70
	1500-1600	2.90	3.90	15.50	11.70	21.70
21.11.50	1120-1230	3.08	—	15.40	12.00	17.74
	1500-1600	2.70	3.00	13.50	17.74	17.74
23.11.50	112-1230	3.65	3.90	16.80	12.10	17.74
	1500-1600	2.78	3.45	14.90	11.20	17.74
14.5.51	1500-1615	3.20	5.00	16.10	15.10	21.70
	0130-0300	—	—	—	—	21.70
16.5.51	1500-1615	3.00	4.90	15.10	14.70	21.70
	0130-0300	—	—	—	—	21.70
18.5.51	1500-1615	3.50	4.75	17.50	14.25	21.70
21.5.51	1500-1615	3.28	5.20	16.40	15.60	21.70
	0130-0300	—	—	—	—	21.70
25.5.51	1500-1615	3.30	5.90	16.50	17.70	21.70
28.5.51	1500-1615	2.95	5.00	15.00	15.00	21.70
	0130-0300	—	—	—	—	21.70
30.5.51	1500-1615	3.55	5.50	17.55	16.80	21.70
	0130-0300	—	—	—	—	21.70
1.6.51	1500-1615	3.40	4.75	15.00	15.25	21.70
	0130-0300	—	—	—	—	21.70

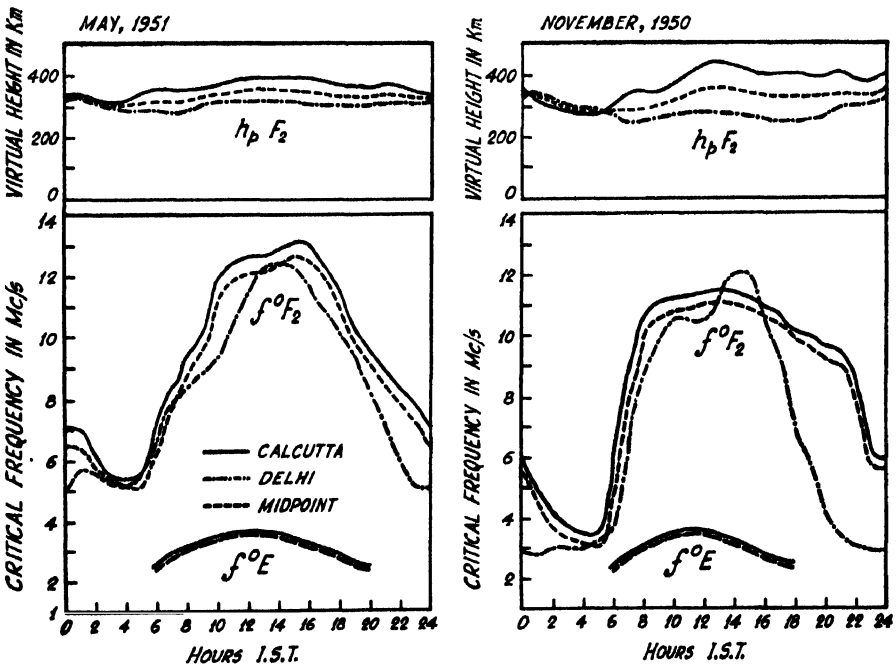


FIG. 8

Monthly average ionospheric characteristics estimated for the point of reflection :  
(1) November 1950 (winter month) (2) May 1951 (Summer month)

the Calcutta data only. Table II shows the values so deduced of  $f^\circ F_1$  and  $f^\circ F_2$  over the midpoint during the observed transmissions.

For the  $F_2$  region the deduction of the midpoint data is complicated by the fact that the ionization density of this region does not obey the  $\sqrt{\cos \chi}$  law. The geomagnetic control of the  $F_2$  region is also well known (Appleton, 1946). Hence, the midpoint data approaches closer to the data of the one of the two stations whose geomagnetic latitude is closer to that of the midpoint. Remembering this, the midpoint data for region  $F_2$  was determined from a study of the characteristics of this region over both Delhi and Calcutta. The monthly average  $F_2$  region characteristics at the midpoint for November 1950 and May 1951 deduced as above are shown in figure 8. From these monthly averages an estimate can be made of the corrections to be applied to the Calcutta data to obtain the probable  $F_2$ -region characteristics as existed at the hours of observation over the midpoint. For summer months (May) the corrections were found to be 0.65 Mc/s for  $f^\circ F_2$  and 40 km for  $h_p F_2$ . For winter months (November), -0.45 Mc/s for  $f^\circ F_2$  and -80 km for  $h_p F_2$ .

From the midpoint ionospheric characteristics determined as above it is now possible to calculate the equivalent paths and the MUF's for Delhi-Calcutta transmission (1290 kms) via the different ionospheric regions at the hours of observation.

(ii) *Propagation via regions E and F<sub>1</sub>*. For propagation via region E, we can consider the reflection to take place at a thin ionospheric layer at a height  $h=110$  km and can calculate geometrically the angle of incidence and equivalent path for a distance of transmission,  $D=1290$  km. The maximum usable frequency (corrected for earth's curvature) is obtained

by multiplying  $f^\circ E$  by the MUF factor  $\sqrt{\frac{4\left(h + \frac{D^2}{8R}\right)^2 + D^2}{4\left(h + \frac{D^2}{8R}\right)^2}}$ , where  $R$  is the radius of the earth.

For the  $F_1$  region we assume the semi-thickness  $y_m$  of the layer equal to 40 km. and height  $h_0$  of the lower edge above ground equal to 180 km. The angle of incidence and the equivalent path can be obtained from eq. (1) below and the MUF factor is obtained from figure 9 drawn after Appleton and Beynon (1940) for a transmission distance of 1290 km. Magneto-ionic splitting and propagation of high-angle ray (*vide infra*) are not considered. Table II summarizes the MUF values for propagation via regions E and  $F_1$  for ionospheric conditions as existed at the points of reflection during the hours of observation.

It will be seen from the table that the frequencies of transmission were in all cases greater than the E and  $F_1$  region MUF's. This means that the E and  $F_1$  region ionizations at the reflection point were too low to permit Delhi-Calcutta communication at the corresponding hours of transmission.

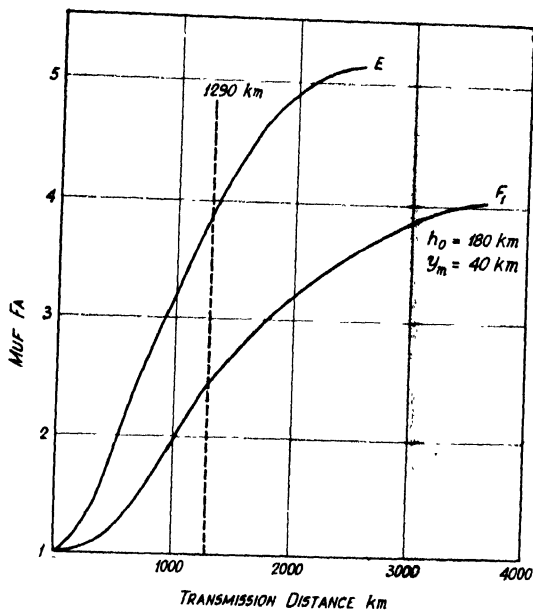


FIG. 9

MUF factor versus distance curves for transmission *via* regions E and F<sub>1</sub>. Factors for Delhi-Calcutta transmission distance (1290 km) are: 3.8 for transmission *via* region E and 2.45 for transmission *via* region F<sub>1</sub>.

We may also consider propagation *via* sporadic E. Calculations show that for Calcutta Delhi communication, the separation of the echo is about 100 km from the F<sub>1</sub> and about 240 km from the F<sub>2</sub> echo. As the frequencies used were greater than the MUF for region F<sub>1</sub> and the echo separation was much less than 240 km, it can be concluded that no E<sub>s</sub> echo was present, and that  $fE_s$  at the point of reflection was less than 3.80 Mc/s during the 17.74 Mc/s transmission and less than 4.5 Mc/s during the 21.70 Mc/s transmission.

(iii) *Propagation via region F<sub>2</sub>*: For studying propagation *via* F<sub>2</sub> region, the first step is to determine the angle at which the ray for a wave of given frequency must be incident on this region in order that it may reach the receiving point. If the ionization gradient is assumed to follow a parabolic law, then, for propagation *via* F<sub>2</sub>-layer, we can use the formula due to Appleton and Beynon (1940) (neglecting the magneto-ionic effect).

$$D = D_1 + D_2 \equiv \left| \frac{R}{R + h_0} \sin i_0 \chi Y_m \log_e \frac{1 - \chi^2 \frac{Y'_m}{R + h_0} \sin^2 i_0 + \chi \cos i_0}{1 - \chi^2 \frac{Y'_m}{R + h_0} \sin^2 i_0 - \chi \cos i_0} \right|$$

$$\cdot \left[ 2R \cot i_0 - 2R \sqrt{\cot^2 i_0 - \frac{2h_0}{R}} \right] \quad (1)$$

where,  $D$  = total transmission distance

$D_1$  = part range (ground distance corresponding to the horizontal range inside the ionosphere)

$D_2$  = range on ground corresponding to the ray path outside the ionosphere

$R$  = radius of the earth

$h_0$  = height of the lower edge of the ionosphere above ground

$i_0$  = angle of incidence on the ionosphere

$y_m$  = semi-thickness of the parabolic region

$\alpha$  = frequency at oblique incidence/critical frequency at vertical incidence

$$= f/f_0$$

For a given set of values of  $D$ ,  $h_0$  and  $y_m$ , eq. (1) gives two values of  $i_0$  if the wave frequency  $f$  lies in the range  $f_0 < f < \text{MUF}$ . There are thus two ray paths, leaving the transmitter at different angles of elevation by which communication between the two points is possible. These two rays are called the *high-angle* and the *low-angle* rays.

Taking, for example, the case of transmission on Nov. 15, 1950 at 1500 hours I. S. T., (winter afternoon transmission), we have  $f_0 = 10.85$  Mc/s,  $h_0 = 200$  km,  $f = 21.70$  Mc/s,  $y_m = 150$  km and  $\text{MUF} = 22.45$  Mc/s.

Hence we obtain,

	For the low-angle ray	For the high-angle ray
Angle of incidence	$56^\circ 37'$	$51^\circ 46'$
Angle of elevation	$31^\circ 0'$	$35^\circ 52'$
Part range $D_1$	325 km	260 km
Horizontal range inside the ionosphere	345 km	390 km
Ground distance corresponding to ray path outside the ionosphere, $D_2$	965 km	930 km

Similarly, taking the case of transmission on May 16, 1951, at 1500 hours, I. S. T. (Summer afternoon transmission), we have  $f_0 = 12.15$  Mc/s,  $h_0 = 180$  km,  $f = 21.70$  Mc/s,  $y_m = 160$  km and  $\text{MUF} = 23.50$  Mc/s.

Hence, we obtain,

	For the low-angle ray	for the high-angle ray
Angle of incidence	$52^\circ 15'$	$47^\circ 30'$
Angle of elevation	$35^\circ 15'$	$39^\circ 0'$
Part range $D_1$	415 km	465 km
Horizontal range inside the ionosphere	435 km	485 km
Ground distance corresponding to ray path outside the ionosphere, $D_2$	875 km	825 km

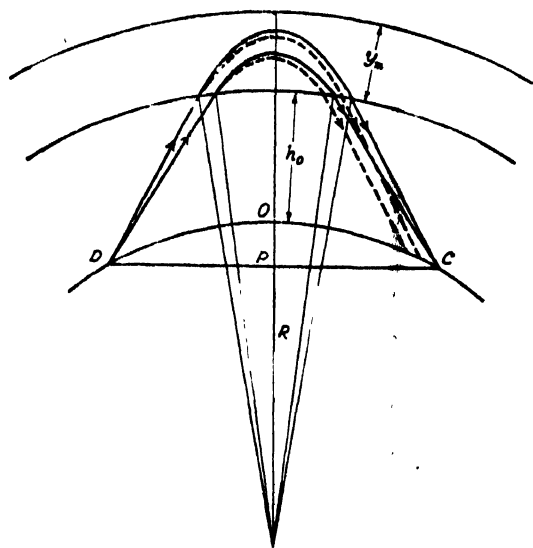


FIG. 10  
The paths of the "high-angle" and the "low-angle" rays for  
Delhi-Calcutta transmission via region-F<sub>2</sub>.

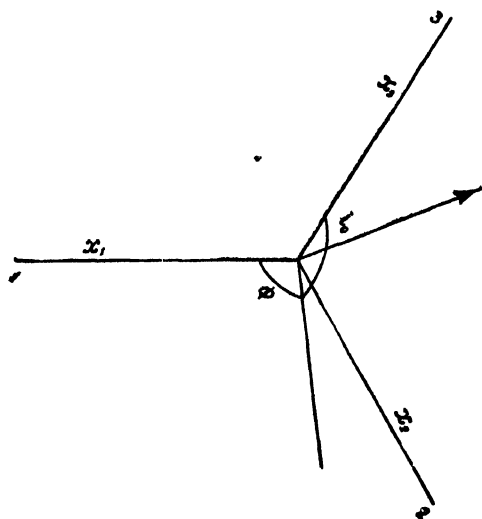


FIG. 11  
Co-ordinate axes showing the direction of incidence. Axis 1 points towards  
magnetic north and the 3-1 plane is in the magnetic meridian.

Similar calculations have been made for the other transmissions also. It has been found that in all cases the angles of incidence fall within the lobes (figure 1) marked 1 and 2 in the case of 17.74 Mc/s transmissions, and within only the lobe marked 2 in the base of the 21.70 Mc/s transmissions.

(iv) *Effect of the earth's magnetic field*: The effect of the earth's magnetic field on propagation within the ionosphere is to split each ray—

*high-angle* and *low-angle*—into two, giving rise to four rays—the upper ordinary (the so-called “Pedersen” ray), the upper extra-ordinary, the lower ordinary and the lower extra-ordinary. The approximate paths of each of the four rays are represented in figure 10.

It is of interest to know the following characteristics of the ray-paths shown in figure 10.

- (1) The total equivalent path of each ray.
- (2) The maximum height above the lower edge of the reflecting ionized layer, attained by each ray.
- (3) The horizontal range inside the ionosphere.
- (4) The lateral deviation, if any, of the rays from the plane of incidence.

Exact determination of the above quantities for spherical earth and concentric ionosphere is difficult. We may, however, consider the simpler case for flat earth and allow for the curvatures of the earth and the ionosphere by using the chord  $DPC$  instead of the arc  $DOC$  as the transmission distance (figure 10), and increasing the equivalent height of the ionosphere by an amount  $OP$ . With this approximation and neglecting collisions between electrons and air molecules, we can utilize Booker's analysis (Booker, 1940) to determine the above quantities for a flat earth and a horizontally stratified ionosphere.

Consider a Cartesian co-ordinate system  $x_1, x_2, x_3$  situated in free space below the ionosphere with axis 3 vertically upward and axis 1 pointing towards magnetic north, plane 3-1 being in the magnetic meridian (figure 11). Suppose a wave of frequency  $f$  is incident upon the ionosphere at an angle  $i_0$  to the vertical in the 2-3 plane and let  $\phi$  be the azimuth of the plane of incidence measured about the 3-1 plane. Then, following Booker,

we can graphically represent the variations of  $\frac{dx_1}{dh}$ ,  $\frac{dx_2}{dh}$  and  $\frac{d(ct)}{dh}$  [which are respectively the values per unit increase of  $h$  (height measured from the lower edge of the ionized layer), of the lateral deviation normal to the plane of incidence, the horizontal range inside the ionosphere in the plane of incidence, and the equivalent path] for a range of values of  $x$ , where

$x = \frac{Ne^2}{\pi mf^2}$ ,  $N$  = electron density,  $f$  = wave frequency,  $e$  and  $m$  are the charge and mass of the electron. For the case of Delhi-Calcutta transmission the data for the necessary calculations are as follows :

- (1) Angle between plane of propagation and plane of magnetic meridian =  $54^\circ 48'$ .
- (2) Magnetic dip value at the point of reflection =  $37^\circ 5' N$ .
- (3) Value of the earth's field at the point reflection = 0.36 Gauss.
- (4) Angle of incidence as obtained in Sec. 3(iii).

From the  $\frac{dx_1}{dh}$  vs.  $x$ ,  $\frac{dx_2}{dh}$  vs.  $x$  and  $\frac{d(ct)}{dh}$  vs.  $x$  curves we draw the

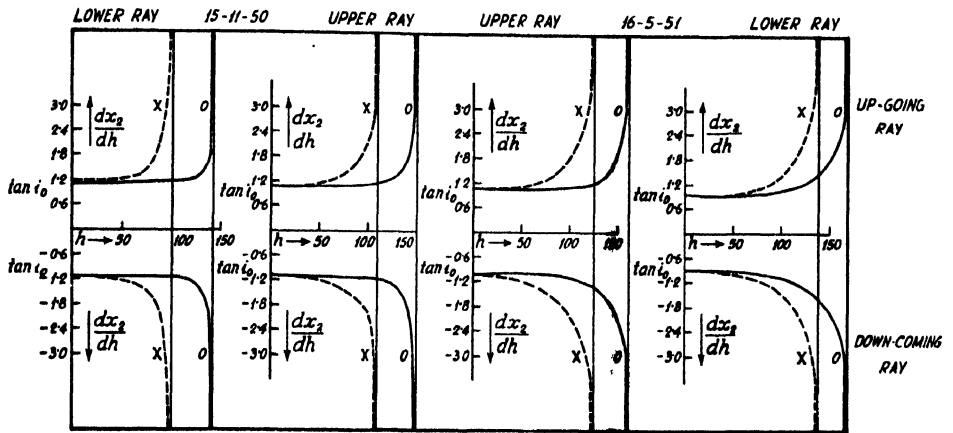


FIG. 12

The variation of  $\frac{dx_2}{dh}$  with  $h$ ;  $x_2$  is the horizontal range inside the ionosphere and  $h$  is the height inside the ionized region measured from its lower edge.

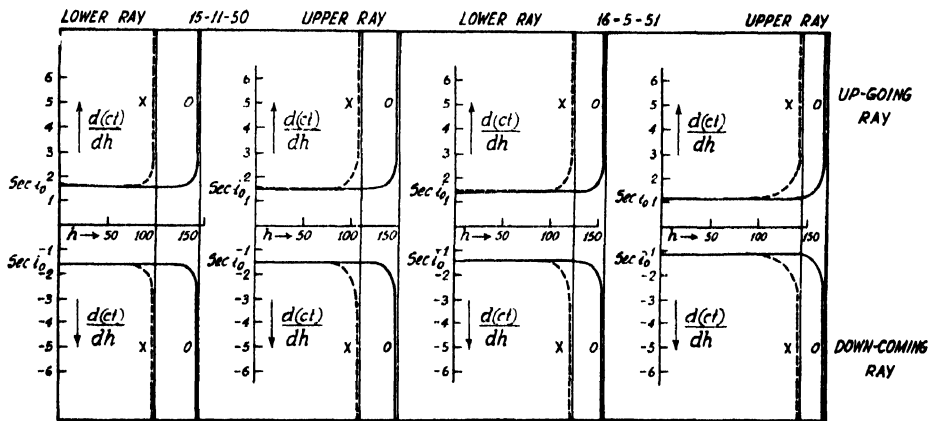


FIG. 13

The variation of  $\frac{d(ct)}{dh}$  with  $h$ ; ' $ct$ ' is the equivalent path inside the ionosphere and  $h$  is the height inside the ionized region measured from its lower edge.

$\frac{dx_1}{dh}$  vs.  $h$ ,  $\frac{dx_2}{dh}$  vs.  $h$  and  $\frac{d(ct)}{dh}$  vs.  $h$  curves assuming that the variation of  $N$  with  $h$  follows the parabolic law

$$N = N_{max} \left( 1 - \frac{h^2}{y_m^2} \right)$$

where  $y_m$  is the semi-thickness,  $N_{max}$  is the maximum electron concentration of the region and  $h$  is the height measured from the lower edge of the effective ionized layer. The total values of  $x_1$ ,  $x_2$  and  $ct$  (equivalent path), are now obtained by numerical integration from these graphs. The

$\frac{d\lambda_2}{dh}$  vs.  $h$  curves and the  $\frac{d'(cl)}{dh}$  vs.  $h$  curves for transmissions on Nov. 15, 1950, and May 16, 1951, are shown in figures 12 and 13 respectively. The total lateral deviation being small  $\frac{d\lambda_1}{dh}$  vs.  $h$  curves have not been drawn.

These curves also yield the following characteristics for the two transmissions considered above :

Transmission characteristics at 1500 hours I.S.T.	Date	High-angle ray		Low-angle ray	
		Ordinary	Extraordinary	Ordinary	Extraordinary
Horizontal range inside the ionosphere (in km).	15.11.50	375	360	345	315
	15.5.51	480	390	425	575
Height at which reflection occurs (in km) measured from the lower edge of the region	15.11.50	130	120	110	100
	16.5.51	160	125	160	140
Equivalent path inside the ionosphere (in km).	15.11.50	465	455	410	390
	16.5.51	535	470	410	400

The equivalent paths of the ordinary and extraordinary components for both the high-angle and low-angle rays during all the transmissions observed have also been calculated as above.

(v) *Interpretation of the echo separations.* We are now in a position to interpret the echo patterns observed. It is clear that at the hours when both the high and low-angle ray paths are possible, there may be four echoes that is, the upper ordinary and the upper extraordinary, the lower ordinary and the lower extraordinary. Since the equivalent path differences between the high-angle and the low-angle rays are of the same order as the path differences between the magneto-ionically split components, the interpretation of the origin of a particular echo is not always easy and requires careful consideration. However, calculations of the equivalent paths of all the rays, as made above, makes the interpretation possible. The origins of the observed echoes, as deduced from considerations of the path differences, are given in Table III. It will be seen that the observed echo-separations agree closely with those calculated. *It is therefore concluded that the echoes observed correspond to single-hop propagation of the high and the low-angle rays via region F<sub>2</sub>.*

(vi) *Absorption.* The transmission paths being ascertained as above it is easy to determine the unabsorbed field strength of the transmitted

pulses at the receiver from the formula  $\frac{ED}{\sqrt{k\omega}} = 1550 \sqrt{\frac{\rho_e}{100}} \frac{mV}{m} \times km,$

where  $E$  is the field,  $D$  the total path and  $\rho_e$ , is the radius vector in figure 1. The ratio of this calculated field and the average field estimated from the receiving aerial characteristics and the receiver sensitivity gives the total



TABLE III

Date	Hours I. S. T.	Frequency of transmission Mc/s	Maximum usable fre- quency Mc/s	Calculated echo separation kms				Observed echo separation kms				Interpretation of the echoes observed (single hop F <sub>2</sub> -layer transmission)			
				1-2	2-3	3-4	4	1-2	2-3	3-4	4	1	2	3	4
15.11.50	1120-1230	21.70	22.80	60	120	—	—	80	140	—	—	Lower ray unsplit	Upper extra- ordinary	Upper ordinary	—
	1500-1600	21.70	22.45	45	—	—	—	60	—	—	—	Lower ray unsplit	Upper ray unsplit	—	—
17.11.50	1120-1230	21.70	23.00	85	95	—	—	100	100	—	—	"	Upper extra- ordinary	Upper ordinary	—
	1500-1600	21.70	22.45	45	—	—	—	50	—	—	—	"	Upper ray unsplit	—	—
21.11.50	1120-1230	17.74	23.00	100	75	—	—	120	80	—	—	"	Upper extra- ordinary	Upper ordinary	—
	1500-1600	17.74	22.80	80	—	—	—	70	—	—	—	"	Upper ray unsplit	—	—
23.11.50	1120-1230	17.74	21.80	80	150	—	—	00	180	—	—	"	Upper extra- ordinary	Upper ordinary	—
	1500-1600	17.74	22.00	60	—	—	—	80	—	—	—	"	Upper ray unsplit	—	—
14.5.51	1500-1615	21.70	23.60	45	100	100	—	50	100	120	—	Lower extra- ordinary	Lower ordinary	Upper extra- ordinary	Upper ordinary
	0130-0300	"	11.20	—	—	—	—	—	—	—	—	—	—	—	—
16.5.51	1500-1615	"	23.30	60	65	—	—	75	70	—	—	Lower ray unsplit	Upper extra- ordinary	Upper ordinary	—
	0130-0300	21.70	10.70	—	—	—	—	—	—	—	—	—	—	—	—
18.5.51	1500-1615	21.70	23.00	45	55	—	—	60	80	—	—	Lower ray unsplit	Upper extra- ordinary	Upper ordinary	—



# Observations at Calcutta of Pulses Transmitted from Delhi 537

absorption of the rays *en route*. The absorption, calculated in decibels, is shown in Table IV for each of the observed transmissions.

(vii) *Fluctuations*. The fluctuations in amplitudes of the received echoes were statistically analysed. The analysis showed two interesting characteristics of the fluctuations. The upper ordinary ray mostly showed rapid fluctuations (of periods of a few seconds) and the lower ordinary ray mostly showed slow fluctuations (of periods ranging from a few minutes to about half an hour). It can thus be concluded that reception is more stable by way of the lower ray than by way of the upper ray.

TABLE IV

Date	Hours I. S. T.	Frequency Mc/s	Mean ordinary ray field strength at Receiver ( $\mu V/m$ )				Absorption of ordinary ray in db	
			Calculated		Observed		Upper	Lower
			Upper	Lower	Upper	Lower		
15.11.50	1120-1230	21.70	40	50	5	20	18	8
	1500-1600	"	60	50	5.5	20	8	8
17.11.50	1120-1230	"	48	65	6	10	18	16
	1500-1600	"	52	60	8	12	18	10
21.11.50	1120-1230	17.74	45	48	16	10	9	6
	1500-1600	"	60	70	11	20	15	10
23.11.50	1120-1230	"	63	75	12	18	11	12
	1500-1600	"	48	56	6	8	18	16
14.5.51	1500-1615	21.70	50	60	5	8	20	15
	"	"	52	68	9	12	15	12
16.5.51	1500-1615	"	45	48	12	12	12	6.8
18.5.51	1500-1615	"	42	45	12	20	11.8	7.2
21.5.51	1500-1615	"	38	46	18	20	6.4	7.8
25.5.51	1500-1615	"	42	52	16	25	8.2	6.4
28.5.51	1500-1615	"	40	46	18	28	7.2	4.6
30.5.51	1500-1615	"	55	65	15	18	10	6
1.6.51	1500-1615	"	50	60	20	20	10	8

## 4. CONCLUSION

The observations were made with a view to determining the possible paths of transmission between Delhi and Calcutta under transmission conditions as prevailed at the hours of observation. From the analysis made above it follows that under ionospheric conditions, as predicted at the midpoint, and on the same frequencies and the same aerial radiation pattern, only single-hop

transmission (Table V) is possible at 21.70 and 17.74 Mc/s. Multiple-hop  $F_2$  layer transmission, as also transmission *via* E and  $F_1$  regions are not possible.

TABLE V

Mode of propagation	Possibility	Remarks
<i>Via</i> region E	Nil	Electron concentration at the point of reflection insufficient at all the transmission hours to reflect wave on the frequency used.
<i>Via</i> $E_s$	Nil	Measured echo separation did not correspond to $E_s$ echo.
<i>Via</i> region $F_1$	Nil	Same as for propagation <i>via</i> region E.
<i>Via</i> region $F_2$ (single hop)	Maximum	Corroborated by experimental results: Propagation <i>via</i> 'high-angle' and 'low-angle' rays; magneto-ionic components observed: two only.
<i>Via</i> region $F_2$	Nil	Angle of incidence too steep to permit reflection.
<i>Via</i> regions $F_2$ and E, (M type reflection)	Nil	Same as for double hop $F_2$ region propagation.

Communication *via* sporadic ionization at region E level is, however, possible for the lowest radiation lobe (figure 1). Calculations also show that under such conditions  $fE_s$  should exceed 3.8 Mc/s for 17.74 Mc/s transmission and 4.5 Mc/s for 21.70 Mc/s transmission.

## ACKNOWLEDGMENTS

The work forms part of the programme of the Radio Research Committee of the Council of Scientific and Industrial Research, Government of India.

The authors are indebted to Prof. S. K. Mitra for constant guidance and advice in course of the work and to the Council for financial assistance.

The authors are thankful to the authorities of All India Radio for informing them about the schedules of transmission and also for checking figure 1 of the paper.

Grateful thanks are also due to Mr. A. P. Mitra, Mr. R. B. Banerjee and Mr. S. P. Chakrabarty for assistance in taking the observations.

## REFERENCES

- Appleton, E. V., 1946, *Nature*, **167**, 691.  
 Appleton, E. V., and Beynon, G. J. W., 1940, *Proc. Phys. Soc.*, **51**, 518.  
 Booker, H. G., 1949, *J. Geophys. Res.*, **54**, 243.

## AN X-RAY STUDY OF ANDROGRAPHIS CRYSTAL\*

BY B. S. BASAK AND D. R. DASGUPTA

DEPARTMENT OF X-RAYS AND MAGNETISM, INDIAN ASSOCIATION FOR THE CULTIVATION  
OF SCIENCE, CALCUTTA

(Received for publication, July 22, 1952)

## Plates XXI A-C

**ABSTRACT.** Andrographis, a crystalline bitter principle from *Andrographis Paniculata* (kalomegh) with molecular formula  $C_{20}H_{30}O_5$  has been studied both morphologically and by means of X-rays. Goniometric study, combined with rotation photographs and density measurements, showed that the crystal was monoclinic with the following axial lengths and angle,  $a = 5.537 \text{ \AA}$ ,  $b = 8.036 \text{ \AA}$ ,  $c = 19.53 \text{ \AA}$ ,  $\beta = 97^\circ 10'$ ,  $Z$  (=no. of molecules in the unit cell) = 2. Weissenberg photographs about the crystallographic axes showed that only the reflections ( $0k0$ ) are halved. So the space-group is either  $C_2^2 - P_2$  or  $C_{2h}^{2h} - P_{21}/m$ . But the fact that the number of molecules in the unit cell is only two, together with the steric and chemical considerations, excluded the possibility of the space-group  $C_{2h}^{2h} - P_{21}/m$  and the crystal is given the space-group  $C_2^2 - P_2$ .

Andrographis, a colourless crystalline bitter principle isolated from *Andrographis Paniculata* (kalomegh), has got the molecular formula  $C_{20}H_{30}O_5$  as determined from a study of chemical reactions and formations of various derivatives. This substance has previously been isolated and studied by Gorter (1911) and Bhaduri (1914) who gave it the formulae  $C_{20}H_{32}O_5$  and  $C_{19}H_{28}O_5$  respectively. Subsequently, Guha Sircar and Moktadar (1935) derived a purer form of it and from an elaborate chemical investigations ascribed the formula  $C_{20}H_{30}O_5$  to the compound which agrees completely with the present value given by Biswas, who very kindly supplied us the crystals for an X-ray examination.

On a morphological examination with the help of a two circle goniometer the crystal was found to be monoclinic with both  $a$  and  $c$  faces developing moderately well, but the  $b$  face being absent. Morphological study and rotation photographs about the three crystallographic axes gave the following values for the axial lengths and axial angle

$$a = 5.530 \text{ A.U.} \quad b = 8.036 \text{ A.U.} \quad c = 19.53 \text{ A.U.}$$

$$\beta = 97^\circ 10'$$

\* Communicated by Prof. K. Banerjee

The density of the crystal was determined by the floatation method as used by Mookherjee (1933). The density of the crystal came out to be  $1.21 \pm 0.01$ . On the basis of this value and those already obtained from the values of axial lengths and axial angle the number of molecules in the unit cell was calculated and found to be  $2.018 \approx 2$ .

Over-exposed oscillation photographs about the three crystallographic axes were taken in a Weissenberg goniometer using copper (K) radiations, giving (hko), (hol) and (okl) reflections. The spots were identified by drawing requisite Weissenberg charts by the method of Schneider (1928). The relative intensities, as determined by eye-estimation, were noted down against all the spots.

From the tables it was found that the only systematic extinctions present were that the odd orders of (oko) were absent. This leads to two possibilities. The space-group may be either  $C_{2h}^2 - P_{21}$  or  $C_{2h}^2 - P_{21}/m$ . In both, the *b* axis is a two-fold screw axis, but the latter has a plane of reflection coinciding with the (010) plane, while in the former case it is absent. X-ray diffraction cannot generally distinguish between these two alternatives. So this point is to be decided in the light of its physical and chemical properties. Fortunately, there are some features present in the present case by which an unambiguous conclusion can be arrived at and the space-group of the crystal can be determined.

Assuming that the space-group is  $C_{2h}^2 - P_{21}/m$ , let us see how far it can explain the existing facts. The number of equivalent points in this space-group is four, whereas, experimentally it has been found that there are only two molecules in the unit cell. Consequently, each of the molecules must have a centre of symmetry or a plane of symmetry normal to the *b*-axis. Existence of a molecular plane of symmetry is against all experiences about such complex organic molecules.

From a study of chemical reactions, Guha and Moktadar (*loc. cit.*) concluded the presence of only one double bond together with one methylenedioxy group and one OH group. These considerations preclude the existence of any plane or centre of symmetry in the molecule. The space-group thus cannot be  $C_{2h}^2 - P_{21}/m$ . This leads us to the conclusion that the space-group is  $C_{2h}^2 - P_{21}$ .

A look at the tables of reflections and their estimated intensities (Tables I, II and III) shows that the molecule does not lie in any simple crystallographic plane. This is only natural, as such a complicated molecule can hardly be expected to be planar and to lie entirely in any crystallographic plane.

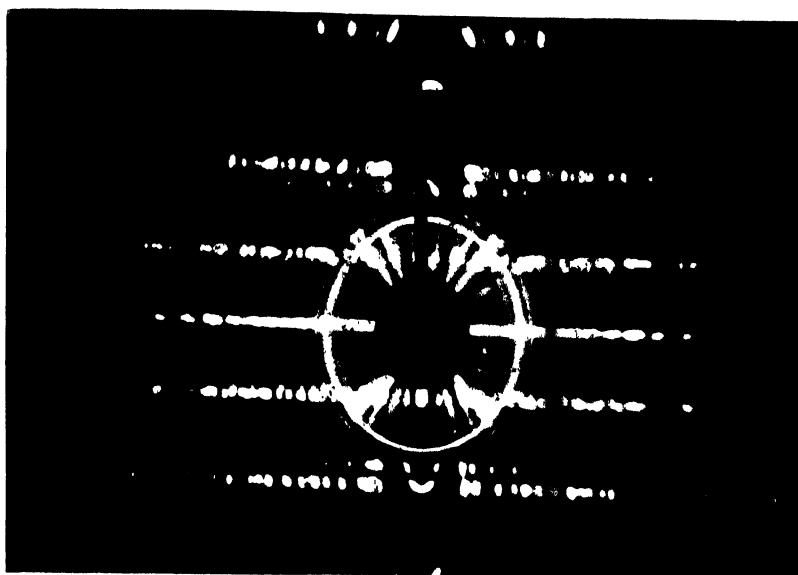


Fig. 1.  
Rotating crystal photograph taken about  $a$ -axis.



Fig. 2.  
Zero level Weissberg oscillation photographs taken about  $a$ -axis.

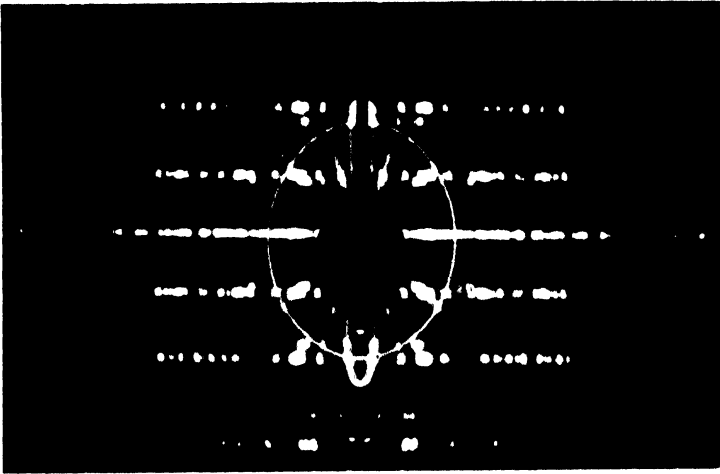


Fig 3.

Rotating crystal photograph taken about  $b$ -axis.

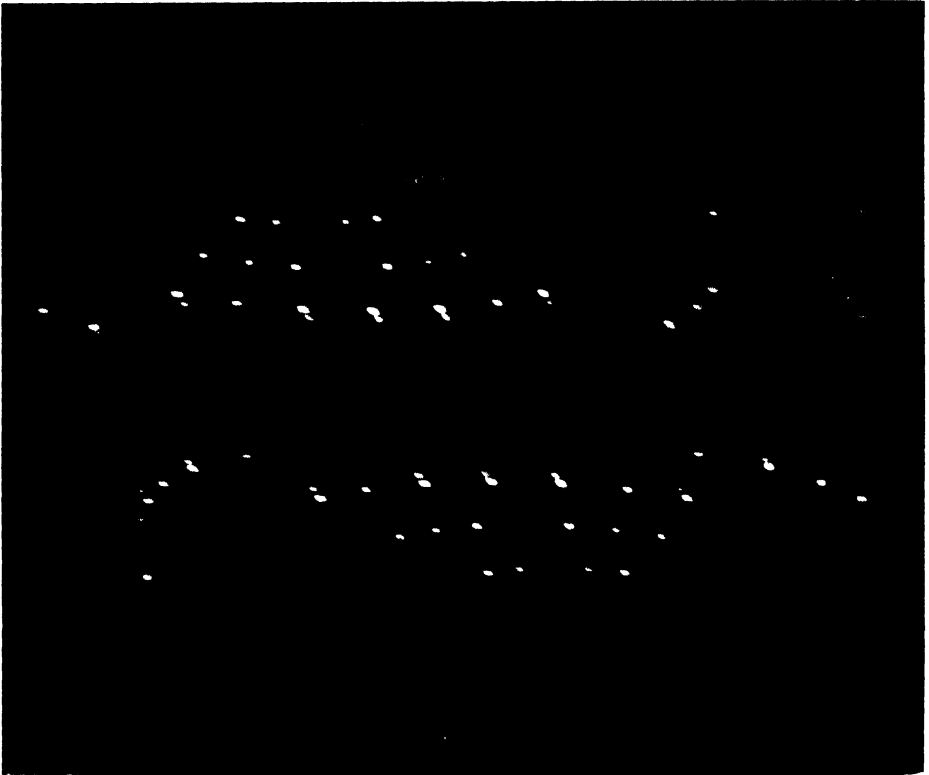


Fig 4.

Zero level Weissenberg oscillation photograph taken about  $b$ -axis.



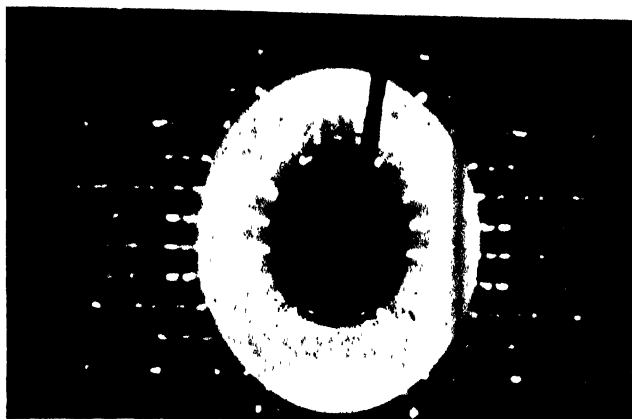


Fig. 5.

Rotating crystal photograph taken about  $c$ -axis.

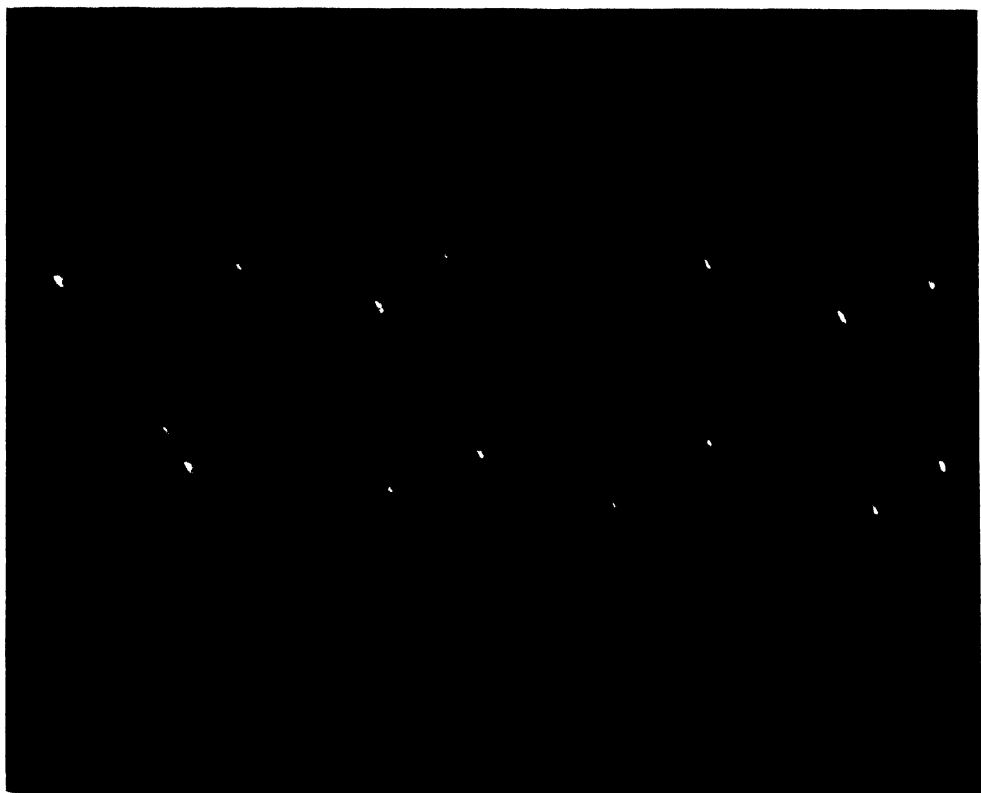


Fig. 6.

Zero level Weissberg oscillation photograph taken about  $c$ -axis.



TABLE I  
Indexing of spots and their estimated intensities  
(c-axis zero layer)

Index of spot	Intensity	Index of spot	Intensity
100	vs	110	s
200	s	120	s
300	m	130	m
400	s	140	m
500	vw	150	w
600	m	160	w
020	s	170	w
040	w	210	s
060	w	220	m
080	s	230	w
004	m	240	w
005	m	250	vw
006	m	260	w
007	w	270	vw
008	m	310	m
009	w	320	m
0011	w	330	m
0014	w	340	m
0015	vw	360	m
0016	vw	370	vw
0018	vw	380	w
		410	w
		420	w
		440	w
		450	w
		510	w
		540	w
		610	vw

\* cool planes observed in a and b axes zero layer photographs

TABLE II  
Indexing of spots and their estimated intensities  
(b-axis-zero layer)

Index of spot	Intensity	Index of spot	Intensity
101	vs	305	s
102	vs	306	s
103	vs	307	s
104	vs	308	m
105	vs	309	m
106	vs	310	w
107	vs	311	vw
108	vs	312	m
109	w	314	m
1010	s	315	w
1011	w	316	w
1012	w	401	vw
1013	vw	402	m
1014	w	405	m
1016	vw	406	w
201	s	407	w
202	s	408	vw
203	s	410	w
204	s	411	m
305	s	501	m
306	s	502	m
207	m	503	w
208	s	505	w
209	s	506	vw
2010	w	508	m
2011	m	5010	vw
2012	w	5011	w
2013	vw	5013	vw
2014	w	603	m
2015	w	604	m
2016	vw	605	m
301	m	608	vw
302	m	702	w
303	m		

TABLE III

Indexing of spots and their estimated intensities (*a*-axis zero layer)

Index of spot	Intensity	Index of spot	Intensity
013	s	038	w
014	s	039	w
015	s	0311	vw
016	111	0312	vw
017	111	041	m
018	111	042	s
019	s	043	m
0110	w	044	w
0111	vw	045	w
0113	w	046	w
0114	w	047	w
0115	w	049	w
0116	w	0410	w
0117	vw	0411	w
021	vs	0412	vw
022	s	051	w
023	vs	052	w
024	111	053	w
025	111	056	w
026	111	057	w
028	111	058	w
029	111	059	w
0210	w	0515	w
0213	w	0511	w
0214	w	0512	w
0215	w	0514	w
0216	w	0515	w
031	s	062	vw
032	m	063	vw
033	m	064	vw
034	w	066	vw
035	w	067	vw
036	m	0614	vw
037	vw	073	vw
		074	vw

## ACKNOWLEDGMENTS

We wish to express our sincerest gratitude to Prof. K. Banerjee, D.Sc., F.N.I., M. L. S. Professor of Physics, Indian Association for the Cultivation of Science, for his kind interest and valuable guidance. Thanks are also due to Dr. H. G. Biswas, D. Phil., for kindly supplying us the crystal of andrographis.

## REFERENCES

- Bhaduri, 1914, *Amer. J. Pharm.*, **86**, 349.  
 Gorter, 1911, *Rect. Trav. Chim.*, **30**, 151.  
 1914, *Rect. Trav. Chim.*, **33**, 239  
 Ghua Sircar, S. S. and Moktadar, A., 1935, *Sci. Cult.*, No. 6, 1, 300.  
 Mookherjee, A., 1933, *Ind. J. Phys.*, **8**, 147.  
 Schneider, W., 1928, *Z. Krist. (A)*, **69**, 41.

# THE COMPARATIVE INFLUENCE OF SHORT AND LONG RANGE CRYSTALLINE ELECTRIC FIELDS ON THE MAGNETIC BEHAVIOUR OF THE PARAMAGNETIC SALTS OF THE IRON GROUP OF ELEMENTS

## PART II

BY A. BOSE AND S. C. MITRA

DEPARTMENT OF X-RAYS & MAGNETISM, INDIAN ASSOCIATION FOR THE CULTIVATION OF SCIENCE, CALCUTTA

(Received for publication July 8, 1952)

**ABSTRACT.** In the first half of the iron group of elements between  $Ti^{+++}$  to  $Fe^{+++}$ , the orbital contributions to the magnetic moments are small or totally absent and the salts should approximately obey the Curie law. Effect of the long range fields, therefore, would be difficult to detect. When, however, a close investigation is made it is found that the moment-temperature curves even for these ions deviate from salt to salt, and from the Curie law appreciably, indicating the action of long range fields, as also the effect of the higher order terms usually neglected in discussions. The scope of the Jahn-Teller theorem, picturing the inherent mechanism for removal of degeneracy of the paramagnetic ion, is discussed and extended to the whole of the crystal lattice. It is pointed out that when so extended the Jahn-Teller mechanism is identified with the entire crystalline field effect, and no extra mechanism is necessary to explain the effect of the distant atoms on the paramagnetic ion.

## 1. INTRODUCTION

It is now well known that the magnetic behaviour of the paramagnetic ions in their solid salts and solutions may be explained to considerably minute details, on the basis of the existence in them, of strong and asymmetric electric fields, arising out of clusters of diamagnetic ions and dipoles, immediately surrounding the paramagnetic ions. The existence of such closely bonded asymmetric clusters is directly verified by the X-ray data on the fine structure of these salts in addition to other indirect methods such as absorption spectra, magnetic birefringence, etc. Especially, in the iron group of salts, such data, in a large majority of cases, point to an octahedral coordination of the paramagnetic ions, though other structures such as tetrahedral, square, etc., do also sometimes occur.

The effect of such electric fields in the paramagnetic salts is to split up the magnetically degenerate ground state of the paramagnetic ions into Stark-patterns. For the ionic salts of the iron group of elements, the fields are just sufficient to break down the L.S coupling and then the symmetric or

cubic part of the field partially removes the orbital degeneracy, thus quenching more or less the orbital contributions to the effective moments, whereas, the asymmetric (or rhombic) part removes the remaining orbital degeneracy, as also to some extent the spin degeneracy. The cubic and the rhombic splittings at ordinary temperatures are of the order of  $\hbar\Delta\nu_{\text{Cubic}} > kT$ , and  $\hbar\Delta\nu_{\text{Rhombic}} \sim kT$  for the orbital parts and  $\hbar\Delta\nu_{\text{Rhombic}} < kT$  for the spins. For both the *F*- and the *D*-state ions, containing  $x$  and  $5+x$  electrons in the  $3d$  subshell, when the coefficient of the cubic part of the electric field has a positive sign, as happens with an octahedral coordination of the paramagnetic ion, triply degenerate orbital levels lie lowest in the Stark-pattern; whereas, with  $5-x$  and  $10-x$  electrons a singlet is the lowest for the *F*-state and a doublet for the *D*-state. On the other hand, with a negative sign of the cubic field constant, as occurs with a tetrahedral coordination, the entire position is exactly reversed. It is very satisfactory that with highly hydrated ionic salts of the iron group, in which complications due to exchange forces, magnetic dipole-dipole interactions and strong covalent forces do not arise, the predictions of the above simple theory for the magnetic behaviours are surprisingly well fulfilled\*.

It is interesting to note that the necessity of postulating a mechanism such as above, for anisotropically quenching the magnetic moments of the paramagnetic ions in solid salts and solutions, follows as a natural consequence of the well known principle enunciated by Jahn and Teller (1937, 1938), which tells us that the underlying degeneracy of the ground state of the paramagnetic ion, associating with a closely bound cluster of other atoms, causes a distortion of the cluster such that the resulting asymmetry in the electric field due to the cluster is sufficient to remove the said degeneracy, consistent with the conditions of stability of the system. It is, however, to be remembered that during the formation of the lattice structure in crystalline substances, forces other than those arising from the members of the closest bound ionic clusters are brought to play upon the paramagnetic ion. Though the direct actions of such distant atoms may not be, in general, of much importance, their indirect influence by distorting the nearest cluster even slightly (of the order of about  $10^{-9}$  cm., Van Vleck, 1939) may be quite large, of the same order as the primary Jahn-Teller effect.

Theoretically, perhaps, we should not differentiate between the Jahn-Teller effect and the action of the distant atoms. For the Jahn-Teller effect need not confine itself to the nearest cluster alone, and also it is very probable that the distortions in the arrangements of the distant atoms and the consequent induced asymmetry in the nearest cluster are ultimately to a large extent the repercussions of the primary Jahn-Teller effect. Experimentally, however, it should be possible to distinguish between these two effects and to compare their magnitudes.

\* For full reference see Part I of the present paper

For example, if some, at least, of the asymmetry of the nearest ionic clusters in the solid salts were due to this distorting action of the distant atoms, then in the state of solution, where the distant atoms have on the average a spherical symmetry, and in any case are too far out to produce appreciable effect, we should observe a fairly large departure in the magnetic behaviour from the solid state. Further, in a series of salts of a given paramagnetic ion having the same ionic cluster but different distant atoms in the unit cell, we should observe small but appreciable differences in the effective magnetic moments (Bose 1948 ; Bose and Mitra 1952).

In view of the above, it has become necessary to examine afresh the available magnetic data on suitable salts and solutions of the iron group. Out of the vast array of rather haphazard experimental data, which are found in the literature, and from which at first sight it appears well nigh impossible to throw any light on the present problem, we have been able to gather the following informations for details of which reference may be made to the earlier part of this paper (*l.c.*)

(1) The values of the mean effective moments for the different salts and their solutions at room temperatures, of a given paramagnetic ion, are apparently remarkably constant for many of the iron group elements, which is not surprising since, in many of these the orbital moments are more or less completely quenched, by the electric fields and only the spins, very little so affected, remain.

(2) On a closer observation, however, a few cases will be found, in which orbital contributions are not so effectively quenched, showing, indeed, appreciable differences of the effective moments from salt to salt and from solid to solution and seeming to point to the existence of some effect of the long range fields, though not as much as predicted by a recent theory of Van Vleck (1939) and demanded by the paramagnetic absorption and resonance experiments\*.

It has been suggested in the earlier paper (*l.c.*) that the mean effective moments of the salts at room temperatures are not probably sufficiently sensitive to the changes in the long range fields, so as to make the consequent changes in the mean moments felt, over the rather large experimental uncertainties. It is, however, probable that, even allowing for the experimental errors, in many cases, it might be necessary to invoke some other mechanism which masks the rather large effect of the distance atoms postulated by Van Vleck and others (*loc. cit.*).

In the present paper we shall analyse the existing experimental results on the variations with temperature of the mean effective moments of the salts of the iron group of elements, with a view to clarifying the present unsatisfactory state of our knowledge regarding long range electric fields acting on the paramagnetic ions.

\* For a brief review of these results reference may be made to the masterly lecture by Van Vleck published in *Amer. Jour. Phys.* 1950.

## 2. THE SCOPE OF THE JAHN-TELLER MECHANISM IN QUENCHING THE ORBITAL MOMENTS OF THE PARAMAGNETIC IONS

From the discussions of the conditions of stability of paramagnetic ionic clusters as given by Jahn and Teller (1937, 1938) and Van Vleck (1939), it appears that in such a magnetically degenerate system, the symmetrical modes of vibrational displacements will be equivalent to several such nearly instantaneous distortional configurations of the cluster, amongst which the system will resonate, provided that the time average over the various configurations is consistent with the minimum symmetry requirements of the space group, which will amount to a coupling between the different members of the cluster sufficiently asymmetric and strong, so as to lift the degeneracy of the paramagnetic ion. For the above purpose a symmetric, degenerate, unstable structure is taken as a cube or a square, etc. A rectilinear structure is stable even if degenerate. Jahn and Teller find :

(1) That unless the coupling between the electrons in the underlying incomplete shell of the paramagnetic ion and the immediately surrounding atoms is strong, Jahn-Teller potential will be of the 2nd order instead of the first in terms of the displacement coordinates and hence negligible, as is shown to be the case in the rare earth salts (see Van Vleck, 1939).

(2) That the Jahn-Teller distortional effect on the degenerate orbital states is of the first order compared to the effect on the spin states though it is true that, a state degenerate in spin is as unstable as the other, the conditions for attaining stability being different ;

(3) It is further shown that the indirect effect on the spins through the spin-orbit coupling is so small as to be quite masked by the vibrations associated with the zero point energy ;

(4) Lastly, that the Jahn-Teller mechanism has no effect on the two-fold Kramer's spin degeneracy.

In the above conclusions the Jahn Teller distortions of the atoms outside the closest neighbours of the paramagnetic ion are not considered, presumably on the assumption that the bond between the distant atoms and the paramagnetic ion (usually at a distance of not less than about  $4 \text{ \AA}$ ) is very weak. But it might be argued : (1) that though these bonds are very much weaker compared to that in the nearest cluster, in the *stable solid state characterised by internal asymmetry*, they are much larger than the thermal energy  $kT$  tending to introduce a *spherical symmetry* in the whole system, in other words tending to break down the lattice ; (2) the outer configurations of the atoms are in close contact successively with each other and ultimately with the central cluster, which is always more or less distorted in the iron group of salts at least, owing to the primary Jahn-Teller effect ; (3) the weak binding amongst the distant atoms will actually help in giving a greater distortional displacement than occurring in the nearest



cluster, as is also evident from X-ray data of the iron group of salts; (4) thus, even if the *primary* Jahn-Teller distortion of the *distant atoms* may be smaller than that of the *nearest cluster*, the latter may cause a fairly large distortion of the distant configurations, the repercussions of which may lead to appreciable distortions in the nearest cluster, *consistent* with given conditions of equilibrium. Actually then, in considering the stabilising effect of the Jahn Teller mechanism, we should consider the entire unit cell as an asymmetric cluster about the paramagnetic ion. It will be seen that the above considerations are consistent with Van Vleck's postulate of a large indirect action of the distant atoms on the paramagnetic ion (Van Vleck *loc. cit.*), and in addition, the physical picture here lays more stress on the part played by the central paramagnetic ion in producing such action, whereas Van Vleck's picture considers the action of distant atoms as being an entirely static interaction between the atoms surrounding the paramagnetic ion.

Again, it will be seen that according to the fundamental postulates of Jahn and Teller, the self stabilising mechanism in the paramagnetic ionic cluster appears to be effective *only at short range* and appreciable only when the ground state of the ion is *orbitally degenerate*. Then, it remains to explain the following facts, namely :

(1) The appreciable Stark-splitting of the spin levels of the ground state (leaving aside the two-fold degenerate levels for odd number of electrons in the system which cannot be removed except by a magnetic field) ;

(2) The Stark-splitting of the upper degenerate orbital levels even though the lowest level in the Stark-pattern is non-degenerate.

(3) Even when the lowest level is degenerate the orbital splittings as well as the spin splittings are far too large compared to the theoretical Jahn-Teller splittings due to the distortion of the nearest cluster alone.

These indicate the obvious limitations of the original Jahn-Teller theorem and the explanations, at least qualitative, of the above follow immediately by extending the scope of the theorem to the whole crystal, as already pointed out. It has been found that for magnetically dilute solid salts containing an *S*-state ion or an ion, having an orbitally non-degenerate state lowest in the Stark-pattern already under a cubic field, the spin splittings, of the order of  $10^{-1}$  to  $10^{-2}$  cm (Van Vleck, Cr<sup>+++</sup> 1939, Mn<sup>++</sup> 1932, 1934), very much small compared to  $kT$  at ordinary temperatures, actually exist, which correspond to the influences of asymmetric electric fields of the nearest cluster as also the distant atoms. In other words, the Jahn-Teller *spin-distortion* is not confined to the nearest closely bound cluster alone but extends directly to the distant atoms, and perhaps to a greater extent indirectly through the intermediary of the nearest cluster. It is important to note that the above splittings are of the 2nd order compared to the spin-splittings if a primary Jahn-Teller orbital effect had

been present, *i.e.* if the lowest orbital state under a cubic field had been degenerate, *e.g.* such spin splittings would have been of the order of 1 to  $10\text{ cm}^{-1}$  (case of  $\text{V}^{+++}$ ,  $\text{Ti}^{+++}$ , etc. Van Vleck 1939) ; showing thereby that Jahn-Teller orbital effect can and does act upon the spin degeneracy through the spin-orbit coupling.

Again, if we consider the splittings of the upper orbitally degenerate levels due to asymmetric electric fields in a Stark-pattern which has a non-degenerate level lowest under the action of a cubic field, these may be attributed to Jahn-Teller effect of the nearest cluster as well as the distant atoms trying to stabilize the excited upper state. Primary Jahn-Teller splitting calculated for the upper cubic state of  $\text{Cr}^{+++}$  is of the order of  $10^2\text{ cm}^{-1}$  to  $10^3\text{ cm}^{-1}$  depending on the model of the field chosen (Van Vleck, 1939) though a few hundred  $\text{cm}^{-1}$  separation may also arise from the Jahn-Teller effect of the distant atoms both direct and indirect. It is noteworthy that these splittings further play an important part in deciding the resolution not only of their own spin components but of the lowest orbitally non-degenerate level, through the spin-orbit coupling (Penney and Schlapp, 1932). Again, under suitable circumstances even a small distortion of the normal spin-orbit coupling might occur causing an interaction between the excited and ground states, the so-called 'super-exchange coupling' (Van Vleck et al, 1934 ; Abragam and Pryce, 1951), which also would partially separate the spin levels, somewhat affecting the magnetic moments of the paramagnetic ion.

When, however, the case of a pattern with degenerate ground level is taken, it naturally becomes very much more complicated since the Jahn-Teller orbital distortions of the near as well as the distant atoms become very prominent and in considering the orbital and the spin splittings we have to give due consideration to all the interactions as already mentioned especially between the different orbital levels and between orbit and spin.

We shall conclude this section by making a few remarks regarding the short and the long range crystalline electric fields, rendered asymmetric by the Jahn-Teller effect as applied to the entire crystal. It is well-known that the crystalline electric fields can in general be represented by a predominant cubic part on which is superimposed a comparatively small rhombic component and by suitably adjusting the field parameters any type of symmetry may be built up. The cubic part of the field is mostly contributed by the nearest atomic cluster of paramagnetic ion and the distant atoms supply only a small part of it since this field falls off very rapidly with distance. Further, in case, the cubic field axes of the distant and the nearest groups are noncoincident, the field will only have a trigonal symmetry. The rhombic field axes of the nearest cluster, if its symmetry is purely due to *primary* Jahn-Teller distortion will coincide with those of the cubic field, and any lower symmetry than rhombic introduced either in the nearest cluster or in the unit cell as a whole must be an effect

of the *primary* Jahn-Teller distortions of the *distant atoms* and their *indirect secondary* influence on the closest cluster. In addition to this, a departure from centrosymmetry in the closest cluster might also arise owing to a mixing up of the excited and the ground states of the paramagnetic ion or from a lack of centrosymmetry in the distant atoms also. It will be seen that the fourth order rhombic fields may not always be negligible in comparison to the second order ones (Siegert, 1936, 1937 ; Van Vleck, 1930).

It is interesting to note in this connection that a purely cubic field, though sometimes postulated as a convenience (Penney and Schlapp, 1932), never arises in the solid paramagnetic salts so far studied. This would point to the fact that the removal of degeneracy of the paramagnetic ion whether in the ground state or excited state, by even a cubic field, is ultimately inseparably linked with the Jahn-Teller effect, representing the asymmetric part of the field. The separation into cubic and rhombic parts is to a large extent a mathematical convenience, which has little significance in the view of the degenerate ion, whose degeneracy is removed as a whole.

### 3. THE VALUE OF THE STUDY OF THE TEMPERATURE VARIATION OF THE MEAN EFFECTIVE MOMENTS OF PARAMAGNETIC SALTS TO FIND THE EFFECT OF THE DISTANT ATOMS

We have mentioned earlier the results obtained in Part I of this paper that at room temperatures for most of the magnetically dilute salts of a given paramagnetic ion except one or two, in solid state as also in solution, seem to give practically the same magnetic moments, thereby belying our expectations of getting the effect of the long range fields on the paramagnetic ion. There may be several reasons for this.

(1) Near about room temperature and higher, the mean effective moments of different salts have a greater tendency to obey the Curie law, and are less sensitive to changes of temperature. This is due to the fact that the orbital moments being largely quenched in many cases, only the spin moments are effective of which the Stark-splitting is very much smaller than  $kT$ . Hence the moments in such cases tend towards a limiting value equal to the spin only value, plus the high frequency contributions.

(2) As we have seen the contribution of the distant atoms to the cubic part of the field is much smaller than that of the nearest cluster. The major effect of the distant atoms lies in adding to the asymmetric field and in considering the mean effective moments of different salts the asymmetric effect of the field is wiped out ; only the absolute value of the cubic field and hence the moment is somewhat affected through averaged out rhombic terms.

(3) Within certain limits the Jahn-Teller effect might be a self-adjusting mechanism, and hence in passing from salt to salt, distant atoms as, also the

nearest cluster might readjust themselves such that the removal of degeneracy and hence the quenching of the moment tends to remain the same, provided the conditions of equilibrium are not exceeded. This may be particularly true for a series of solid salts of similar structure where systematic changes in the inter-atomic distances have been definitely established from X-ray data. In passing from solid to solution state, where we should expect to detect a large difference, owing to the action of the distant atoms vanishing practically altogether, and also because the self-adjusting mechanism might not be able to cope with the largely changed conditions of equilibrium, we again meet with new complications inasmuch as even the nearest cluster of atoms is in danger of being radically changed, leading to altogether different magnetic behaviours. It is therefore, frequently difficult to interpret the results in the absence of information of such structural changes.

It is evident that a study of temperature variation of the mean effective moments would lead to a much better elucidation of the Jahn-Teller mechanism as applied to the crystal as a whole, than room temperature studies, since the positions of the distant atoms and hence conditions of equilibrium would depend largely on the temperature. This we propose to discuss in the next section on the basis of the existing results.

#### 4. DISCUSSIONS OF THE RESULTS

In the present part of the paper we shall consider the magnetic measurements of the salts of the first half of the iron group, *i.e.*, from  $Ti^{+++}$  to  $Fe^{+++}$  in which the tendency for the orbital quenching is greater owing to the comparatively smaller spin-orbit coupling.  $Fe^{+2}$  to  $Cu^{+2}$  will be treated in the next part.

The results of the experiments are given for the different salts in the form of graphs of the squares of the mean effective moments  $\bar{\mu}_{eff}^2$ , against absolute temperature  $T$ . In many cases graphs had to be derived from a Curie-Weiss type of relation given by the original author, so that the values plotted are already smoothed out to some extent, whereas, in several instances, such as the Leiden data and those by Jackson, it was possible to use the original experimental values which show occasional kinks and inflexions, which may not be always real. The values even of the same salt differ much from author to author so that it is always better for comparison between different salts, to take the results by the same observer wherever possible. The dearth of such data will be immediately apparent. For a full reference of the data used here Part I of this paper may be consulted (*loc. cit.*).

(1)  $V^{+4}$  ion. In the two salts of  $V^{+4}$  ion measured by Perrakis (1927) namely,  $V_2O_2Cl_4 \cdot 5H_2O$  and  $VO SO_4 \cdot 3\frac{1}{2}H_2O$  the mean effective moments at any temperature change slightly with time, decreasing for the first and increasing for the second salt. But the temperature variation curve (figure 2) of the freshly prepared salt in either case is parallel to that after aging,

which indicates an uncertain change in the composition or structure without, however, much change in the electric fields. Both the salts obey the Curie law approximately, apparently showing that an orbitally non-degenerate level lies lowest in the Stark-pattern of both these salts. This might be the case if the coordination of  $V^{+4}$  ion in both are tetrahedral so that the non degenerate  $\Gamma_1$  level (Bose and Mitra, *l.c.*) is at the bottom. But then small positive spin-orbit contributions from the upper triplet  $\Gamma_1$  and high frequency terms arise causing a slight variation from the Curie law with the value of the moment somewhat above the 'spin only' value. However, since the spin-orbit coupling constant  $\lambda$  is small in the first half of the iron group, even if the coordination of  $V^{+4}$  is octahedral so that the triply degenerate  $\Gamma_1$  lies lowest, the triplet separation by the rhombic field being large compared to  $kT$ , virtually only the lowest level of the triplet contributes to the moment. Small negative spin-orbit contributions from the upper levels will be partially compensated by the high frequency terms and the Curie law will be better obeyed than in the previous case. The absolute values of the moments, however, are very different for the two salts. While the second salt has a moment close to the 'spin only' value of 3, the first salt has a much lower value even at room temperature. The difference in the moments observed might be due to  $SO_4$  and  $Cl$ -ions respectively as also different number of water molecules either within or outside the closest cluster. In the absence of detailed X-ray data, it is difficult to say much about this with certainty. We have tried to fit the time-mean curves in the two cases with a formula of the type :

$$\mu_{eff}^2 - 3 = A + BT + \frac{C}{T} \quad \dots (1)$$

where  $A$  is the temperature independent spin-orbit coupling contribution from upper levels, 2nd term is the high frequency contribution and 3rd term represents mainly the spin quenching through rhombic field and spin-orbit coupling. It is found that the above constants for the two salts are respectively,

	$A$	$B$	$C$
$V_2O_2Cl_4 \cdot 5H_2O$	-0.552	0.0001411	-62.16
$VO SO_4 \cdot 3\frac{1}{2}H_2O$	-0.561	0.001585	+11.13

Though much significance cannot be given to the absolute values of the above constants owing to the restricted range of temperature over which the data have been taken, it will be immediately seen from the negative and nearly equal value of the spin-orbit coupling contribution from upper levels that the crystalline fields in both the salts are nearly the same and arise from octahedral coordination of the  $V^{+4}$  ion. The high frequency terms are very small and the difference in order of magnitude is most probably owing to uncertain diamagnetic corrections applied. The real difference between the salts lies in the term  $C$ , the large negative value

in the first salt indicating a large spin quenching, which cannot be due to the crystalline electric field in  $V^{+4}$ , since the spin level has only a two fold Kramers' degeneracy. Hence, this may be due to exchange interaction leading to antiferro-magnetic quenching of the spins of the different  $V^{+4}$  ions in the unit cell. It is to be noted that the lowest spin state becomes non-degenerate due to this action and the moment of the salt tends to vanish somewhere about  $25^\circ\text{K}$  and it would be interesting to follow the behaviour of salt in this region. On the other hand, such a behaviour might also arise from a large negative orbital contribution, varying as inverse of  $T$ , which is possible if the field has an approximately uniaxial symmetry (Van Vleck, 1939) so that the lowest state  $\Gamma'_5$ , is only separated partially (figure 1).

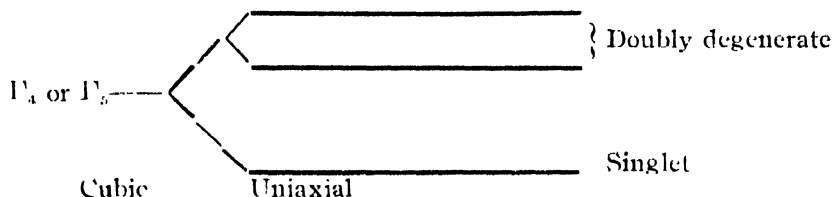


FIG. 1

Due to differences in the distant atoms in the two salts the 2nd and 4th order rhombic fields might be of comparable order and such that in one of the salts the singlet lies lowest and in the other the doublet, so that the orbital contributions of the order  $1/T$  from rhombic levels are quite different. It is to be noted that in the 1st salt the curve will fall to a minimum nearabout  $20^\circ\text{K}$  and then rise again. The difference in the action of the crystalline electric fields, either short range or long range, is difficult to estimate in the two salts of  $V^{+4}$ . In the first of the two cases discussed above, the electric fields are not very different, whereas, in the 2nd the fields are quite different. We are studying a large number of  $V^{+4}$  salts to clarify the position.

(2)  $V^{+3}$ . The only salt for which temperature variation of the moment has been studied is the alum  $\text{VNH}_4(\text{SO}_4)_2 \cdot 12\text{H}_2\text{O}$  (Van den Handel Comm. Leid 249e), and it obeys Curie law fairly well down to about  $14^\circ\text{K}$  (figure 2). From the structure of the alums (Beever and Lipson, 1935) it is well-known that the  $V^{+3}$  ion has six water molecules immediately surrounding it in the form of an octahedron which is so distorted as to give a trigonal field not only within the octahedron but all over the other atoms or ions in the unit cell. This would make the lowest triplet  $\Gamma'_4$  in its Stark pattern to lose only a part of its degeneracy, i.e., it will split into a singlet and a doublet (figure 1). The square of the mean effective moment being not very different from the 'spin only' value of 8, throughout the temperature range studied, it appears that in this salt the 2nd order and 4th order noncubic field constants are such as to make the singlet level lowest (Van Vleck, 1939), as shown in figure 1.

This points to a special arrangement of the distant atoms and hence is an evidence for the existence of a fairly large action of long range fields in this salt. In the absence of the data on other salts of  $V^{+3}$  it is not possible to estimate the changes in the long range fields from salt to salt.

Representing the variations of  $\mu_{eff}^2$  with  $T$  by a series expansion like (1) as before, we find the relation :

$$\mu_{eff}^2 = 8 - 1.130 + 0.00109T + \frac{0.001472}{T} \dots \quad (2)$$

to hold good down to about  $14^\circ K$ , showing only a fair negative contribution from the upper levels through spin orbit coupling. The two other terms are just perceptible and gives the small inclination to the straight portion of the curve seen in the graph. Below  $14^\circ K$ , however, the curve drops down steeply tending to zero moment at absolute zero. This occurs no doubt when the spin separation becomes comparable to  $kT$  and the lowest spin level is rendered non-degenerate.

It is not profitable to try to fit the curve below  $14^\circ K$  with the formula by introducing higher order terms. Without going into such complications it will be, however, seen that this steep fall in the curve would require a rather large overall separation of the spin levels of the upper limit of about  $10 \text{ cm}^{-1}$ , which is consistent with the theoretical calculations of Van Vleck (*l.c.* 1930) and of which about half is due to the action of long range fields.

(3)  $Cr^{+++}$ . Temperature variations of the salts of  $Cr^{+++}$  have been done by three schools of workers who differ amongst one another even for the same salt (figure 3). Taking first the measurements by Mlle. Serres (1932) for the salts  $CrK(SO_4)_2 \cdot 12H_2O$  (violet),  $CrCl_3 \cdot 6H_2O$  (green) and  $Cr_2(SO_4)_3 \cdot 16H_2O$  (violet) in the solid state, the mean effective moments are in the decreasing order and, within the moderate range of temperature studied, obey practically the Curie law. The small difference in the moments between the first and the third of the salts if real can be due only to differences in the distant atoms, since in both the salts the closest clusters of  $Cr^{+++}$  ions are octahedra of six water molecules. The fields are evidently stronger and more asymmetric in the first salt, orbital contributions being less. In the 2nd salt the nearest octahedron contains two chlorine ions in place of water molecules and hence both distant atoms as well as nearest atoms are different, and the asymmetry of the crystalline field is also presumably the largest, hence quenching of the moment should be the greatest, but the experimental value is actually between the two sulphates, which perhaps does not have much significance owing to the very small differences with which we are dealing. Over the entire range of temperatures down to  $80^\circ K$  the curves for the three salts are parallel to each other.

The Leiden measurements (208c, 222c) however, show little difference between the alum and the chloride at high temperatures, while at low temperatures below  $80^\circ K$  the curve for the alum tends to rise slightly whereas

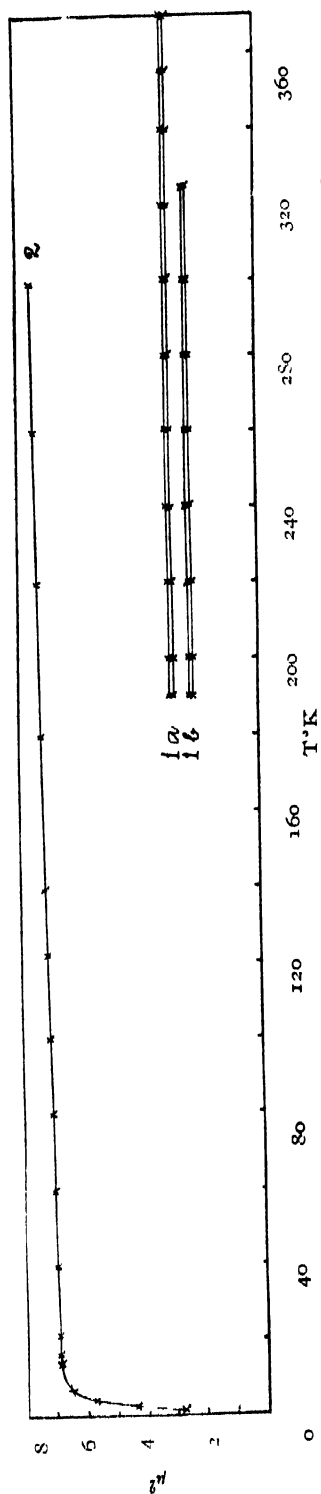


FIG. 2 (1). Perrakis (a)  $\text{VOSO}_4 \cdot 3\text{H}_2\text{O}$ , (b)  $\text{V}_2\text{O}_5 \cdot \text{Cl}_4 \cdot 5\text{H}_2\text{O}$  (2). Handel and Siebert— $\text{VNH}_4(\text{SO}_4)_2 \cdot 12\text{H}_2\text{O}$

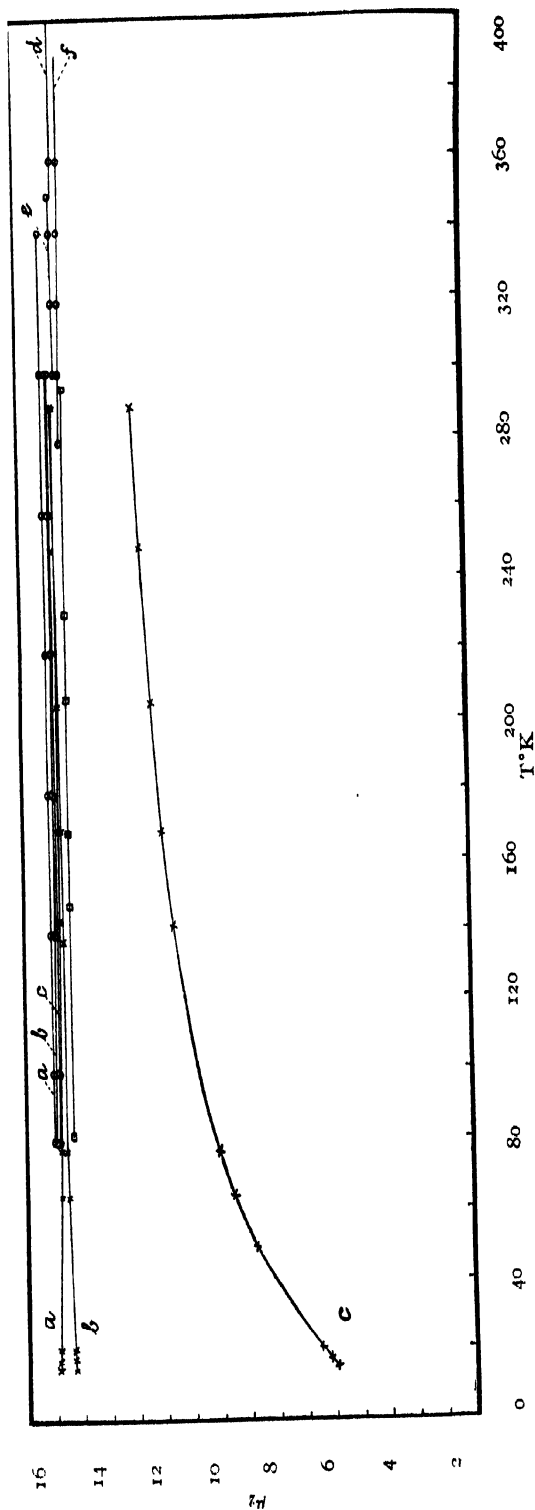


FIG. 3 (1). x—de Haas and Gorter, (a)  $\text{Cr K}(\text{SO}_4)_2 \cdot 12\text{H}_2\text{O}$  (violet); (b)  $\text{CrCl}_3 \cdot 6\text{H}_2\text{O}$  (green) (c)  $\text{Cr}_2(\text{SO}_4)_3 \cdot (\text{OH})_2 \cdot 5\text{H}_2\text{O}$ . (2). □—Janes  $\text{K}_2\text{Cr}(\text{SCN})_6 \cdot 4\text{H}_2\text{O}$  (3). O—Serres—(a)  $\text{Cr K}(\text{SO}_4)_2 \cdot 12\text{H}_2\text{O}$  (violet); (b)  $\text{CrCl}_3 \cdot 6\text{H}_2\text{O}$  (green); (c)  $\text{Cr}(\text{SO}_4)_3 \cdot 15.63\text{H}_2\text{O}$  (green); (d) (a) in molten state (green); (e) (a) revealed (violet); (f) (c) in molten state and revealed (green).



that for the chloride falls. The measurements of Serres for the molten sulphate (green) and the chloride (green) also obey Curie law approximately with a sharp decrease of the moment at the melting point which might be associated with the change in the nearest cluster as shown by the change of colour. This, however, is not supported by the further fact that on regelation the first salt retraces the same curve for the molten salt extrapolated backwards, though the colour returns to violet. The sharp change then is probably to be ascribed to the action of distant atoms becoming negligible as the lattice breaks down, since the decrease may be due to negative orbital contributions and is in the right direction. The slight difference in the slope of the curve for the green molten alum and the regealed salt has little significance as being over too restricted range of temperatures. The absolute values are all systematically higher for Serres' measurements than the Leiden workers who admit this as due to errors in their calibration.

From the above considerations it would thus appear that even in the  $\text{Cr}^{++}$  salts where orbital Jahn-Teller effect of the nearest atoms on the ground state is negligible, the orbital effect of the excited states and the spin effect through spin-orbit coupling due to nearest atoms and those due to distant atoms may be just appreciable above the experimental errors, especially at low temperatures.

Trying to fit the experimental values into an equation of type (1) with 'spin' only value of 15 for  $\text{Cr}^{++}$ , we find the following values for the coefficients  $A$ ,  $B$  and  $C$ .

TABLE I

Salt	Author	$A$	$B$	$C$
$\text{CrK}(\text{SO}_4)_2 \cdot 12\text{H}_2\text{O}$	Serres	- .0615	+ .0002693	--
$\text{CrCl}_3 \cdot 6\text{H}_2\text{O}$	do	-.0991	-.0001363	--
$\text{Cr}_2(\text{SO}_4)_3 \cdot 16\text{H}_2\text{O}$	do	-.2309	+ .0001363	--
$\text{CrK}(\text{SO}_4)_2 \cdot 12\text{H}_2\text{O}$	de Haas and Gorter	- .2595	-.0002693	1.867
$\text{CrCl}_3 \cdot 6\text{H}_2\text{O}$	do	.3711	+ .0001191	-4.767
$\text{Cr}_2(\text{SO}_4)_3 \cdot 16\text{H}_2\text{O}$	do	.48692	+ .000709	-77.38
$\text{K}_3\text{Cr}(\text{SCN})_6 \cdot 4\text{H}_2\text{O}$	Janes	-.6861	+ .00004650	

The high frequency terms for the normal sulphate, double sulphate and the chloride differ very much from each other. This has not much significance bearing in mind the very small magnitude of the terms and uncertain diamagnetic correction factors. The temperature independent terms are

more important, and are all negative as they should be, and definitely point to a variation in the splitting of the cubic and rhombic orbital levels from salt to salt due both to variation of short and long range fields.

The action on the spin degeneracy is further shown by the Leiden values for the chrome alum and the green chloride which extend to much lower temperatures to about 14°K and between this temperature and 80°K the divergence in the curves for the two salts is indicated by the opposite signs of the  $1/T$  dependent term. This gives us an idea of the different spin separations in the two salts originating from different short and long range fields.

The values of the salt  $K_3Cr(SCN)_6 \cdot 4H_2O$  (Janes 1935) follow the Curie law very well, indicating octahedral coordination of the  $Cr^{+++}$  ion, but the absolute value is much lower than the sulphates and the chlorides, showing a large negative orbital contribution coming from upper levels through the negative spin-orbit coupling term. This is evidently more an effect of the closely coordinated SCN radicals rather than of the distant atoms.

The most interesting result, however, is shown by the basic  $Cr_2(SO_4)_2(OH)_2 \cdot 5H_2O$ , measured in Leiden in which the moment even at room temperatures is very much below the spin only value and falls rapidly to even lower values at low temperatures. The crystalline field must be of an entirely different type here namely, due to a tetrahedral coordination of the  $Cr^{+++}$  ion, instead of octahedral as in the previous salts, so that an inversion of Stark-pattern is produced and the orbitally degenerate triplet  $\Gamma_4$  lies lowest. An X-ray investigation of the structure of the salt will be welcome.

The components of the triplet are only separated comparable to  $kT$ , so that contributions from the upper rhombic levels are no longer as small nor the spins as free as in the previous cases which is shown by the large negative  $A$  and  $C$  terms. In addition to these, higher order terms do also become important at low temperature regions, as shown by small misfit with the three constant formula. Here again we cannot compare the actions of the distant atoms with the previous salts as even the arrangement of the nearest atoms is radically different. The moment in this salt tends to become zero at about 7°K much above the region of spin levels for the normal  $Cr^{+++}$  salts (of the order of about  $0.1 \text{ cm}^{-1}$ ) which is perhaps justifiable in view of the stronger spin quenchings in this salt through spin orbit coupling.

In view of the fair magnetic dilution of the salt the exchange quenching of spins is not probably much important.

(4)  $Cr^{++}$  and  $Mn^{+++}$ . The salts of these two isoelectronic ions at room temperatures have nearly the same moment (Bose and Mitra, *l.c.*). But here the resemblance ceases and the detailed behaviour of the salts at low temperatures are very different (figure 4). The only  $Cr^{++}$  salt studied namely,  $CrSO_4 \cdot 6H_2O$  (Lips, 1934) with evidently an octahedral coordination about the  $Cr^{++}$  ion, obeys approximately the Curie law as is to be expected from its having the non-magnetic doublet  $1^1_2$  at the bottom of its Stark-pattern. There is,

however, on closer observation an appreciable deviation from the spin only value of 2.4, as shown by the term  $A$ , as also deviations from the Curie law especially at low temperatures, given by the term  $C$  in the equation.

$$\mu_{eff} = 2.4 = -0.004 + .00038T - \frac{28.60}{T} \quad \dots (3)$$

with which the experimental data fit well. These show the influence of the upper levels and also the degree of spin quenching.

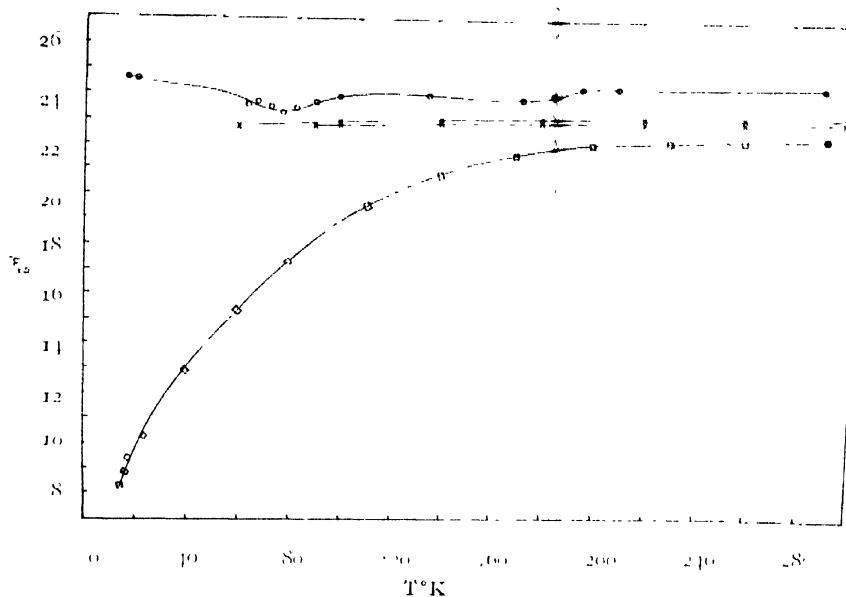


FIG. 1

1. x—Lips,  $\text{Cr SO}_4 \cdot 6\text{H}_2\text{O}$
2. □—de Haas and Schultz,  $\text{Mn}(\text{C}_2\text{H}_3\text{O}_2)_2 \cdot 2\text{H}_2\text{O}$
3. O—Jackson, Manganese acetyl acetate

The structure of the two  $\text{Mn}^{+++}$  salts studied are not known so that it is not possible to compare these with the  $\text{Cr}^{+++}$  sulphate even if we neglect the differences in their nuclear charges. The two salts  $\text{Mn}^{+++}$  acetyl acetate (Jackson, 1935) and dihydrated acetate (de Haas and Schultz, Leid. Comm. 256) cannot, as a matter of fact, be compared even amongst themselves. An attempt to fit the data with a three constant formula gives the following :

TABLE II

Salt	Author	A	B	C
$\text{Mn}^{+++}$ acetyl acetate	Jackson	- .9322	+ .00420	+ .24 .60
$\text{Mn}^{+++}$ acetate dihydrate	de Haas & Schultz	- 10.9571	+ .03055	- .83.51

Conformity with formula in either case is only approximate, indicating the necessity for introducing high order terms. However, without attempting this complication, we see that a large temperature independent term, about eleven times larger than in the acetyl acetonate, obtains in the acetate, no doubt due to much stronger fields in the latter. The *B* and *C* terms are also very much different the latter being even opposite in sign for the same reason. It is of course possible that the coordinations in the two salts might be octahedral and square respectively so that a much greater quenching without a change in the sign of either *A* or *B* terms, occurs in the latter salt. This is borne out further by the fact that the *A* term in acetyl acetonate has a comparable value to that of the  $\text{CrSO}_4 \cdot 6\text{H}_2\text{O}$ . That covalency plays a large part in quenching the spins in the case of the acetate is well known from the recent results on the other acetates of the iron group (Mookherji, 1945, Guha, 1951). Very recently, however, Bleaney and others (1952) have invoked "antiferromagnetism" in copper acetate, with orbital Stark pattern exactly similar to the  $\text{Mn}^{++}$  salt, but with only a twofold Kramer's spin degeneracy in the former, in order to explain its tendency to become nonmagnetic at liquid hydrogen temperatures. No doubt such a quenching effect of the exchange interaction would be adequate to explain the behaviour in copper acetate with the twofold Kramers degeneracy which crystalline fields cannot remove, and also presumably in the other acetates but then the large temperature variation of the moments and the strong anisotropy of the single crystals of the acetates (Mookherji *l.c.*) are difficult to understand.

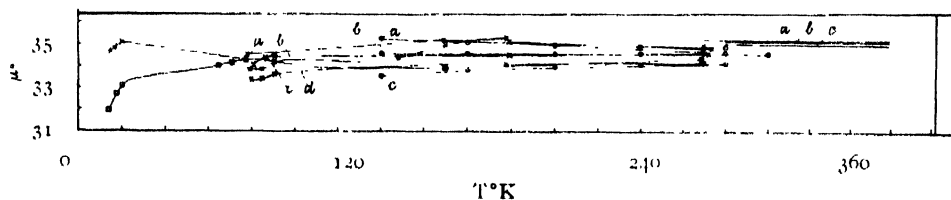


FIG. 5

1. × Jackson,  
(a)  $\text{Mn}(\text{NH}_4\text{SO}_4)_2 \cdot 6 \text{H}_2\text{O}$  (b)  $\text{Mn}(\text{NH}_4\text{SO}_4)_2 \cdot 6\text{H}_2\text{O}$ , (c)  $\text{MnSO}_4 \cdot 5\text{H}_2\text{O}$ ,  
(d)  $\text{MnSO}_4 \cdot 4\text{H}_2\text{O}$ .
2. □ Onnes & Oosterhuis,
3. ○ Lallmand  
(a)  $\text{MnCl}_2 \cdot 5 \text{H}_2\text{O}$ .  
(b)  $\text{MnCl}_2 \cdot 4 \text{H}_2\text{O}$  (solid) and aq solution  
(c)  $\text{Mn}_2 \text{P}_2\text{O}_7$
4. Bose, aqueous solutions (conc. in gms/gm. soln,  
(a)  $\text{MnSO}_4$ ,  $c = .2773$ ,  $.3755$ ,  $\text{Mn}(\text{NO}_3)_2$ ,  $c = .4334$ ,  $\text{MnCl}_2$ ,  
 $c = .2784$ . (b)  $\text{MnSO}_4$ ,  $c = .3241$ ,  $\text{Mn}(\text{NO}_3)_2$ ,  $c = .5690$ , (c)  $\text{Mn}(\text{NO}_3)_2$ ,  
 $c = .5948$ ,  $\text{MnCl}_2$ ,  $c = .3671$ .

It would appear from the results that the acetyl acetonate is not so covalent as the acetate, which is not surprising in view of the larger dimensions of the former molecule.

(5)  $\text{Mn}^{++}$  and  $\text{Fe}^{++}$  salts ; have been very widely studied for a large number of salts in solid and solution states (figures 5 and 6). In these two

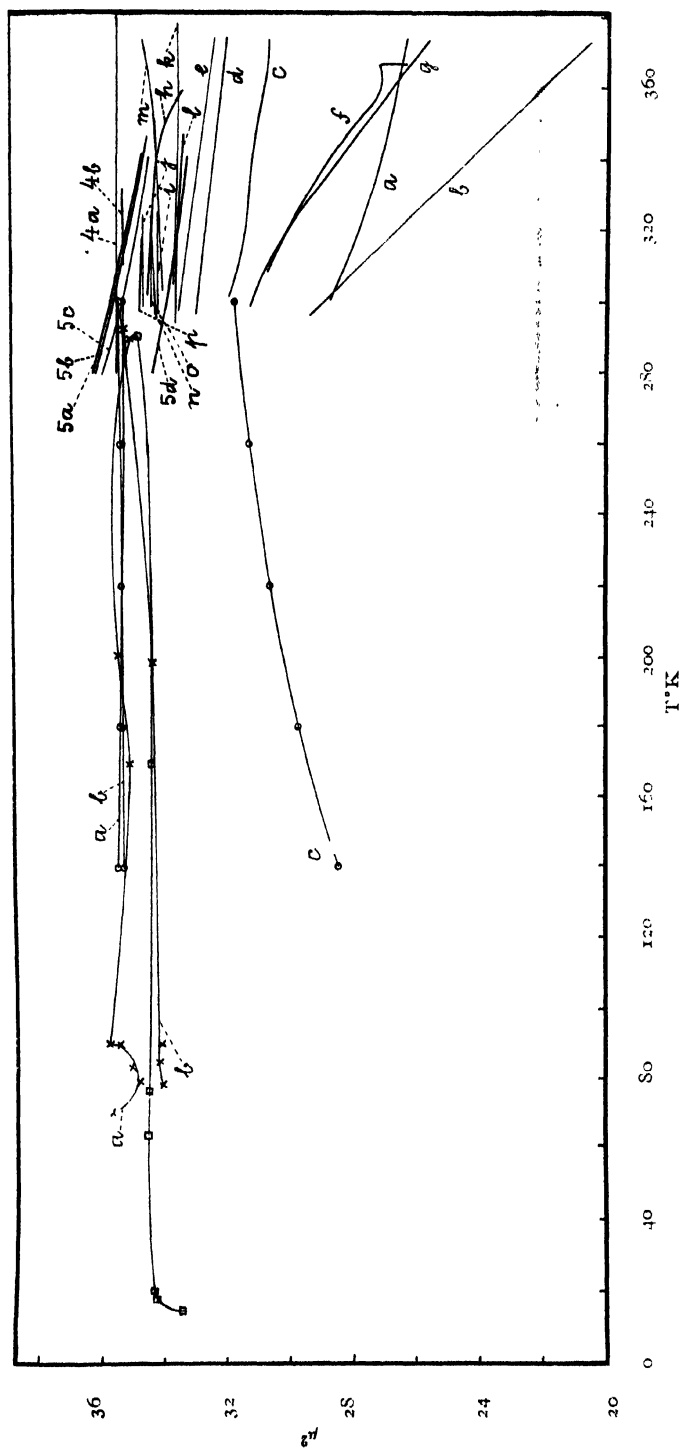


FIG. 6

1. x—Jackson. (a) Potassium ferri-oxalate (b) Ferric acetyl acetone.
2. □—Onnes & Oosterhuis.  $\text{Fe}(\text{NH}_4)(\text{SO}_4)_2 \cdot 12\text{H}_2\text{O}$ .
3. o—Lallemand. (a)  $\text{Fe}(\text{NO}_3)_3 \cdot 9\text{H}_2\text{O}$  (b)  $\text{FeCl}_3 \cdot 6\text{H}_2\text{O}$  (c)  $\text{FeCl}_3 \cdot 2\text{NH}_4\text{Cl} \cdot \text{H}_2\text{O}$  4 Lallemand, aqueous soln. (a)  $\text{FeCl}_3$  (b)  $\text{FeCl}_3 \cdot 2\text{NH}_4\text{Cl}$
5. Fahlenberach, aq. soln of  $\text{FeCl}_3$  (a)  $c = 5.60 \text{ gms}/100 \text{ c.c. soln.}$  (b)  $c = 1.98 \text{ gms}/100 \text{ c.c. soln.}$  (c)  $c = 0.829 \text{ gms}/100 \text{ c.c. soln.}$  (d)  $c = 0.348 \text{ gms}/100 \text{ c.c. soln.}$
6. Bose, aq. soln. conc.  $c$  in  $\text{gms}/\text{gm. soln.}$   $\text{Fe}_2(\text{SO}_4)_3$ . (a) .3292, (b) .2548, (c) .2694, (d) .1513, (e) .1103;  $\text{Fe}(\text{NO}_3)_3$ . (f) .3728, (g) .1832, (h) .3072, (i) .1807, (j) .0863;  $\text{FeCl}_3$ . (k) .4428, (l) .1985, (m) .3319 (n) .2503, (o) .1922, (p) .0937

ions where there are no orbital contributions to be considered, Van Vleck and Penney (1934) have shown that the mean moment should obey a Curie law up to and inclusive of the terms in  $1/T$ . The deviations from Curie law of a given salt, and from salt to salt, if existing should thus be of an even higher order. This is also as demanded by Jahn-Teller condition of stability as applied to spins, discussed in an earlier section.

Excepting  $\text{Mn}_2\text{P}_2\text{O}_7$ , of which the structure is not known, all the other salts studied namely,  $\text{Mn}(\text{NH}_4\text{SO}_4)_2 \cdot 6\text{H}_2\text{O}$ ,  $\text{MnSO}_4 \cdot 5\text{H}_2\text{O}$ ,  $\text{MnSO}_4 \cdot 4\text{H}_2\text{O}$ ,  $\text{MnCl}_2 \cdot 5\text{H}_2\text{O}$  and  $\text{MnCl}_2 \cdot 4\text{H}_2\text{O}$  have presumably similar octahedral coordination of the  $\text{Mn}^{++}$  ion. Taking the measurements of Jackson (1923, 1924, 1927) and Onnes and Oosterhuis (Leid. Comm. 132c) for the first three salts, peculiar kinks and bends in the curves appear at certain temperatures, possibly owing to some change in the composition of the salts. There is, however, no doubt that there are appreciable differences in the values especially at low temperatures in these salts, which are evidently partly due to changes in the long range fields, quenching of the moments being the least for the double sulphate and greatest for the tetrahydrate. At liquid hydrogen temperatures rapid fall in the moment is found to occur for the double sulphate as also the tetrahydrated sulphate, no doubt due to appreciable depopulation of the upper spin levels and exchange or super-exchange interactions might also become more important. Similar results are also obtained by Lallemand (1935) for the pentahydrated and tetrahydrated chlorides.

There is further evidence of an appreciable Jahn-Teller spin effect of the distant atoms from the measurements of the solutions of  $\text{MnSO}_4$ ,  $\text{MnCl}_2$  and  $\text{Mn}(\text{NO}_3)_2$  (Bose, 1935) which shows practically the same values of the moments at different temperatures and concentrations, very nearly equal to spin only value of 35 and *definitely above those of the solid salts*, as they should be, in the absence of long range fields in solution. When we consider the ferric salts, however, we find no appreciable difference between the salts  $\text{FeCl}_3 \cdot 6\text{H}_2\text{O}$  and  $\text{Fe}(\text{NO}_3)_3 \cdot 9\text{H}_2\text{O}$  done by Lallemand (1935), which obey practically the Curie law with spin only value of the moment. This might indicate a difference in structure in the two salts, compensating the difference in long range field actions from  $\text{Cl}^-$  and  $(\text{NO}_3)^-$  respectively. Same holds true also for the ferric alum done at Leiden (Onnes and Oosterhuis, Leid. Comm. 139e), only the absolute value of the moment is much lower, but it is not safe to draw any conclusions from these results in view of the smallness of the effect we are seeking. However, a steep fall in the Leiden curve at hydrogen temperatures reminds one of the similar behaviour in  $\text{Mn}^{++}$  salts. Ferric acetyl acetone (Jackson, 1933) shows a small deviation from Curie law at high temperatures and a downward bend at liquid oxygen temperature which perhaps is a precursor of a minimum in the curve in this region. This is actually shown quite clearly in the curve for ferric potassium oxalate (Jackson, 1933), which again has a larger absolute moment

than the previous salt all along its course and shows one more maximum and minimum in the higher temperature region. These facts are rather difficult to reconcile with the spin only ground state of the ferric ion unless we postulate some sort of violent changes in the crystalline fields.

Most surprising behaviour is, however, shown by Lallemant's (*l.c.*) data on  $\text{FeCl}_3 \cdot \text{NH}_4\text{Cl} \cdot \text{H}_2\text{O}$  which in the solid state has a very low moment and the moment falls fairly rapidly to even lower values, indicating strong anti-parallel coupling of at least some of the spins, either due to covalency or exchange interaction. It is very interesting to note that in the state of solutions the moment immediately goes back to normal spin only value and Curie law is followed. It is difficult to judge the action of distant atoms in ferric salts from a comparison of values in solid state and solutions since strong hydrolysis, with perhaps ferromagnetic group formations, sets in the aqueous solutions of these salts. But preventing hydrolysis by adding suitable acids Bose, (1935) and Lallemant (1935) have shown that the solutions of the sulphate, chloride and nitrate tend to approximate conformation of spin only limiting values and Curie law, as the action of the distant atoms vanish.

It appears that in  $\text{Fe}^{+++}$  and  $\text{Mn}^{++}$  salts, though here the ions are in a spin state, the effect of the distant atoms is more prominent than in the  $\text{Cr}^{+++}$  salts where orbital contributions are not negligible. This is evidently due to the much larger absolute moments in the former salts. It will be seen that in general, in all these cases the effect of the long range cubic fields are more important at higher temperatures and remain more or less constant down to the lowest temperatures, whereas, the asymmetric fields rise to importance only at sufficiently low temperatures.

#### CONCLUSIONS

From the foregoing discussions it appears that in the first half of the iron group the ions, irrespective of whether the lowest level in the Stark-pattern is orbitally degenerate or not, have at best only feeble orbital moments and hence their effective moments approximate to spin only values and obey nearly the Curie law. The differences in the action of short range and long range fields are, however, definitely noticeable, in the salts of most of the ions on proceeding to a higher order approximation of the behaviours of the different salts particularly at low temperature regions, wherever sufficient reliable data are available.

The latter half of the iron group with much greater orbital contributions to their moments would be more sensitive to changes in both short and long range fields and we proceed to discuss these in the next part of the paper.

## ACKNOWLEDGMENTS

Our sincere thanks are due to Dr. A. Mookherji, D.Sc. and Mr. R. K. Sen, M.Sc. for valuable discussions, while writing the paper. One of us is grateful to the Government of India for the grant of a senior scholarship in its 'Development Scheme'. We are grateful also to the authorities of the Indian Association for the Cultivation of Science for all laboratory facilities provided.

## REFERENCES

- Abraham, A. and Pryce, M. H. L., 1951, *Proc. Roy. Soc. A*, **239**, 164, 73.  
 Beevers, C. A. and Lipson, H., 1935, *Proc. Roy. Soc.*, **143**, 654.  
 Bose, A., 1935, *Ind. Acad. Sci.*, **1**, 605, 751.  
 Bose, A., 1948, *Ind. J. Phys.*, **22**, 195, 275, 483.  
 Bose, A. and Mitra, S. C., 1952, *Ind. J. Phys.*, **28**, 303.  
 Bleaney, B. and Bowers, K. D., 1952, *Phil. Mag.*, **43**, 372.  
 Guha, B. C., 1951, *Proc. Roy. Soc. A*, **206**, 353.  
 de Haas and Gorter, *Comm. Leid.*, 208c, 222c.  
 de Haas and Schultz, *Ibid.* 256d.  
 Jackson, L. C., 1924, *Phil. Trans. Roy. Soc.*, **224**, 1.  
 „ 1927, *Ibid.* **226**, 107.  
 „ 1933, *Proc. Phys. Soc. A*, **140**, 695.  
 „ 1935, *Proc. Phys. Soc.*, **47**, 1029.  
 Jackson, L. C. and Onnes K., 1923, *Proc. Roy. Soc. A*, **104**, 671.  
 Jahn, H. A., 1938, *Proc. Roy. Soc. A*, **164**, 117.  
 Jahn, H. A. and Teller, E., 1937, *Proc. Roy. Soc. A*, **161**, 220.  
 Kramers, H., 1929, *Proc. Amst. Acad.*, **32**, 1176.  
 Lallemand, A., 1935, *Ann. De. Phys.*, **3**, 97.  
 Lips, E., 1934, *Helv. Phys. Acta.*, **7**, 537.  
 Mookherji, A., 1945, *Ind. Jour. Phys.*, **19**, 63.  
 Onnes, K. and Oosterhuis, *Comm. Leid.*, 130c.  
 Perrakis, N., 1927, *Compt. Rend.*, **184**, 1430.  
 Penney, W. G. and Schlapp, R., 1932, *Phys. Rev.*, **41**, 1911.  
 „ 1932, *Ibid.*, **42**, 656.  
 Serres, Mlle., 1932, *Ann. der Phys.*  
 Siegert, A., 1936, *Physica*, **3**, 85.  
 „ 1937, „ **4**, 138, 71.  
 Van den Handel and Siegert A., *Comm. Leid.*, 249c.  
 Van Vleck, J. H., 1932, *Phys. Rev.*, **41**, 208.  
 „ 1935, *J. Chem. Phys.*, **3**, 803.  
 „ 1937, *Ibid.*, **5**, 320.  
 „ 1939, *Ibid.*, **7**, 61.  
 „ 1950, *Amer. J. Phys.*, **18**, 495.  
 Van Vleck, J. H. and Penney, W. G., 1934, *Phil. Mag.*, **17**, 961.



# ADMITTANCE AND TRANSFER FUNCTION OF A MULTIMESH RESISTANCE-CAPACITANCE FILTER NETWORK\*

By BIMAL KRISHNA BHATTACHARYYA  
INSTITUTE OF NUCLEAR PHYSICS, CALCUTTA UNIVERSITY

(Received for publication, July 5, 1952)

**ABSTRACT.** The impedance function of an  $n$ -mesh RC filter network is expressed in the form of a recurring continued fraction. Hindenburg's rule for writing a continuant of the  $n$ -th order as an integral function of the  $n$ -th degree of its constituents is adopted to express the above continued fraction as a quotient of two polynomials. The admittance function which is the reciprocal of the impedance function, is then expressed in a very elegant form. The transfer function of the network is then exactly evaluated. In a similar way, the admittance and transfer functions of an  $n$ -mesh CR filter network are derived.

## INTRODUCTION

Recently Tschudi (1950) has shown that for an  $n$ -mesh RC filter network (figure 1) the transfer and admittance functions are given by the expressions as follows :

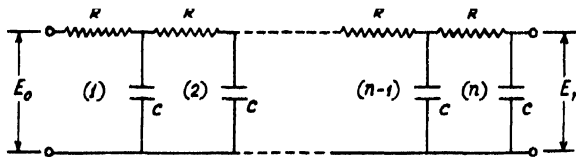


FIG. 1

Transfer function

$$F_n(p) = \left( \frac{E_n}{E_0} \right)_n$$

$$\frac{1}{1 + a_1 T p + a_2 T^2 p^2 + \dots + a_{n-1} T^{n-1} p^{n-1} + T^n p^n} \quad \dots \quad (1)$$

and

Admittance function

$$G_n(p) = \frac{C p [n + b_1 T p + b_2 T^2 p^2 + \dots + b_{n-1} T^{n-1} p^{n-1}]}{[1 + a_1 T p + a_2 T^2 p^2 + \dots + a_n T^n p^n]} \quad (2)$$

\* Communicated by Prof. M. N. Saha, F.R.S.

where  $T = RC$ ,  $p = j\omega$  and  $a_1, a_2, \dots, a_n$  and  $b_1, b_2, \dots, b_{n-1}$  are constants given by

$$a_m = \frac{(n+m)!}{(n-m)!(2m)!} \quad (3)$$

and

$$b_m = \frac{(n+m)!}{(n-m-1)!(2m+1)!} \quad (4)$$

Tschudi has, first of all, assumed the general values of the coefficients  $a_m$  and  $b_m$  and then proved by the method of induction that his assumptions are correct.

Storch (1951) has applied the junction law of currents to the above circuit (figure 1) to find out a recursion process which gives the complete solution. He has also obtained an alternate solution of the problem in terms of the image parameters  $\theta$  and  $Z_0$  of a single  $T$ -section with a resistor  $R/2$  in each series arm and a capacitor  $C$  in each shunt arm. The expressions obtained by him are

$$F_n(p) = \left( \frac{E_n}{E_0} \right)_n = \frac{\sinh(n+1)\theta}{\sinh \theta} - \frac{\sinh n\theta}{\sinh \theta} \quad \dots (5)$$

and

$$G_n(p) = \frac{Cp \sinh n\theta}{\sinh(n+1)\theta - \sinh n\theta} \quad \dots (6)$$

where

$$\cosh \theta = 1 + \frac{pT}{2} \quad \dots (7)$$

This paper deals with the problem with a direct mode of attack with the help of the theory of continued fractions. It will be shown that the admittance and transfer functions for an  $n$ -mesh RC filter network can be written in the form of recurring continued fractions. Hindenburg's rule can be applied to write a continuant of the  $n$ -th order as an integral function of the  $n$ -th degree of its constituents. This rule will be applied to express the recurring continued fractions that we shall obtain, in the form of a quotient of two power series.

The simple process of expressing a recurring continued fraction as a quotient of two polynomials can be applied to any multimesh two element network problem. As an example, the expressions for the admittance and transfer functions of an  $n$ -mesh CR network have been derived.

#### CONTINUED FRACTIONS AND HINDENBURG'S RULE

Let  $u_n = p_n/q_n$  be the  $n$ -th convergent of the continued fraction

$$P = a_1 + \cfrac{b_2}{a_2 + \cfrac{b_3}{a_3 + \cfrac{b_4}{\ddots}}} \quad \dots (8)$$

which is generally written as

$$P = a_1 + \frac{b_2}{a_2 +} \cdot \frac{b_3}{a_3 +} \cdot \frac{b_4}{a_4 +} \dots \quad (9)$$

$p_n$  and  $q_n$  are determined by the equations

$$\left. \begin{aligned} p_n &= a_n p_{n-1} + b_n p_{n-2} \\ q_n &= a_n q_{n-1} + b_n q_{n-2} \end{aligned} \right\} \dots \quad (10)$$

with the initial values

$$\begin{aligned} p_0 &= 1, \quad q_0 = 0 \\ p_1 &= a_1, \quad q_1 = 1 \end{aligned}$$

It is evident, therefore, that  $q_n$  is the same function of  $a_2, a_3, \dots, a_n; b_3, b_4, \dots, b_n$ , as  $p_n$  is of  $a_1, a_2, \dots, a_n; b_2, b_3, \dots, b_n$ .

The function  $p_n$  is denoted by

$$p_n = K \left( \begin{matrix} b_2, \dots, b_n \\ a_1, a_2, \dots, a_n \end{matrix} \right) \dots \quad (11)$$

and is called a continuant of the  $n$ -th order whose denominators are  $a_1, a_2, \dots, a_n$  and whose numerators are  $b_2, \dots, b_n$ .

So

$$q_n = K \left( \begin{matrix} b_3, \dots, b_n \\ a_2, a_3, \dots, a_n \end{matrix} \right) \dots \quad (12)$$

It is convenient to abbreviate both

$$K \left( \begin{matrix} b_2, \dots, b_n \\ a_1, a_2, \dots, a_n \end{matrix} \right)$$

and

$$K(a_1, a_2, \dots, a_n)$$

into  $K(r, n)$ . In this notation we have if  $r < s$ ,

$$K(r, s) = K \left( \begin{matrix} b_{r+1}, \dots, b_s \\ a_r, a_{r+1}, \dots, a_s \end{matrix} \right) \dots \quad (13)$$

and

$$K(s, r) = K \left( \begin{matrix} b_s, \dots, b_r \\ a_s, a_{s-1}, \dots, a_r \end{matrix} \right) \dots \quad (14)$$

In particular,

$$K(r, r) = a_r$$

and

$$p_1 = K(1, 1) = a_1$$

From equation (10), we have

$$\left. \begin{aligned} K(r, s) &= a_s K(r, s-1) + b_s K(r, s-2) \\ K(r, s-1) &= a_{s-1} K(r, s-2) + b_{s-1} K(r, s-3) \\ &\dots \dots \dots \\ K(r, r+1) &= a_{r+1} K(r, r) + b_{r+1} K(r, r-1) \\ K(r, r) &= a_r \\ K(r, r-1) &= 1 \end{aligned} \right\} \dots \quad (15)$$

where  $K( )$  stands either for unity or for a constituent of that continuant for which the system of numerators and denominators under consideration furnishes no constituents.

Hindenburg's rule is a convenient tool for writing down the terms of a series of continuants, say  $K(1, 1), K(1, 2), K(1, 3), \dots$ . This rule is given below

$a_1$	$a_2$	$a_3$	$a_4$	$a_5$
$b_2$		$a_3$	$a_4$	$a_5$
$a_2$	$b_3$	$a_4$	$a_5$	
$a_3$		$a_4$	$a_5$	
$b_2$		$b_4$	$a_5$	
$a_1$	$a_2$	$a_3$	$b_5$	
$b_2$		$a_3$	$b_5$	
$a_1$		$b_3$	$b_5$	

The rule for placing  $a_1, a_2, \dots$  and  $b_2, b_3, \dots$  in the separate rectangles is evident from the scheme given above.

The row in the rectangle 1,1 gives the first term  $K(1,1)=a_1$ . The rows in the rectangle 2,2 give the products in  $K(1,2)$  which is  $a_1a_2 + b_2$ . All the rows enclosed in 3,3 give the products in  $K(1,3)$  namely,  $a_1a_2a_3 + b_2a_3 + a_1b_3$ .

The process is thus continued. It is nothing but a graphic representation of the recurrence formula

$$K(1,n) = a_n K(1,n-1) + b_{n-1} K(1,n-2) \quad (16)$$

Hindenburg's scheme leads us to Euler's rule for writing down all the terms of a continuant of the  $n$ -th order :

The first term is  $a_1a_2a_3\dots a_{n-1}a_n$ . To get the rest, one or more pairs of consecutive  $a$ 's will be omitted from this product in every possible way ; the second  $a$  of each pair will be replaced by one  $b$  of the same order.

#### APPLICATION OF EULER'S RULE TO A SIMPLE CONTINUED FRACTION :

Let us consider the simple continued fraction

$$a_1 + \frac{1}{a_2 + \frac{1}{a_3 + \dots \frac{1}{a_n + \dots}}}$$

in which

$$a_1 = a_3 = a_5 = \dots = 1$$

and

$$a_2 = a_4 = a_6 = \dots = a$$

It will be assumed that the continued fraction is of  $2n$ -th order. So the continued fraction which we shall consider, is

$$1 + \frac{1}{a + \frac{1}{1 + \frac{1}{a + \dots \frac{1}{a}}}} \quad (17)$$

Now the problem is to find out  $K(1,2n)$ . The first term is

$$1.a.1.a.1.a.\dots\text{to } 2n \text{ factors} \\ = a^n \quad (18)$$

The pairs of consecutive  $a$ 's are formed and written below :

$$1a, a_1, 1a, \dots \text{to } (2n-1) \text{ terms.} \quad \dots (19)$$

Let us omit from the product (18) in every possible way  $r$  pairs of (19) and replace the second factor of each pair by one  $b$  of the same order.

$$\text{Since,} \quad b_2 = b_3 = \dots = b_{2n} = 1$$

the above replacement procedure will do nothing but multiply the remaining terms in (18) by unity.

So, if  $r$  pairs of (19) are removed from (18), the remaining factors in (18) will form a term  $a^{n-r}$ . The coefficient of  $a^{n-r}$  will be the number of the possible ways in which  $r$  pairs of (19) may be removed. Now it is evident from (18) and (19) that if  $1a$  is removed, the next term  $a_1$  cannot be taken, i.e., two consecutive pairs of (19) cannot be omitted simultaneously. So the coefficient of  $a^{n-r}$  is the total number of combination of  $(2n-1)$  terms in (19) taken  $r$  at a time so that no two consecutive terms are taken simultaneously. This number is equal to  ${}^{2n-1}C_r$ .

So, omitting  $r$  pairs of (19) from (18) in every possible way we obtain the term

$${}^{2n-r}C_r a^{n-r}. \quad \dots (20)$$

Substituting  $r=1, 2, \dots, n$  in (20) we get all the terms of the continuant  $K(1, 2n)$  of  $2n$ -th order as given below :

$$K(1, 2n) = a_n + t_1 a^{n-1} + \dots + t_r a^{n-r} + \dots + t_n \quad \dots (21)$$

where

$$\left. \begin{aligned} t_r &= {}^{2n-r}C_r \\ t_n &= 1 \end{aligned} \right\} \quad \dots (22)$$

Thus,  $p_{2n} = k(1, 2n)$  has been obtained. It is evident from equation (17) that  $q_{2n}$  is the  $(2n-1)$ -th partial numerator  $p'_{2n-1}$  of the continued fraction

$$a + \frac{1}{1 + \frac{1}{a + \dots \text{to } (2n-1) \text{ convergents.}}} \quad \dots (23)$$

In a similar way  $q_{2n}$  can now be found

$$q_{2n} = a[a^{n-1} + t'_2 a^{n-2} + \dots + t'_r a^{n-r} + \dots + t'_n] \quad \dots (24)$$

where

$$\left. \begin{aligned} t'_r &= {}^{2n-r}C_{r-1} \\ t'_n &= n \end{aligned} \right\} \quad \dots (25)$$

So equation (17) can be written in the form

$$\begin{aligned} 1 + \frac{1}{a + \frac{1}{1 + \frac{1}{a + \dots \frac{1}{a} \text{ (2n-th convergent)}}}} \\ = \frac{[a^n + t_1 a^{n-1} + \dots + t_r a^{n-r} + \dots + t_n]}{a[a^{n-1} + t'_2 a^{n-2} + \dots + t'_r a^{n-r} + \dots + t'_n]} \end{aligned} \quad \dots (26)$$

where

$$\left. \begin{aligned} t_r &= {}^{2n-r}C_r \\ t_r &= {}^{2n-r}C_{r-1} \end{aligned} \right\} \quad \dots (27)$$

and

## ADMITTANCE FUNCTION OF RC NETWORK

Consider an  $n$ -mesh RC filter network (figure 1). The input impedance function of this network is given by

$$Z_n = R + \frac{1}{Cp + \frac{1}{R + \frac{1}{Cp + \dots \text{to } 2n \text{ convergents}}}} \quad (28)$$

By means of equivalence transformation which consists in multiplying numerators and denominators of successive fractions by numbers different from zero, we can write equation (28) in the form

$$Z_n = R \left[ 1 + \frac{1}{Tp + \dots \text{to } 2n \text{ convergents}} \right] \quad (29)$$

where

$$\begin{cases} T = RC \\ p = j\omega \end{cases}$$

Equation (29) can be identified with equation (17) if we put  $Tp = a$ . So  $Z_n$  can be expressed as

$$Z_n = \frac{R}{Tp} \cdot \frac{[T^n p^n + t_1 T^{n-1} p^{n-1} + \dots + t_r T^{n-r} p^{n-r} + \dots + t_n]}{[T^{n-1} p^{n-1} + t'_1 T^{n-2} p^{n-2} + \dots + t'_r T^{n-r} p^{n-r} + \dots + n]} \quad (30)$$

where  $t_r$  and  $t'_r$  are given by equation (27).

Equation (30) can be simplified to

$$Z_n = \frac{1}{Cp} \cdot \frac{[T^n p^n + t_1 T^{n-1} p^{n-1} + \dots + t_r T^{n-r} p^{n-r} + \dots + t_n]}{[T^{n-1} p^{n-1} + t'_1 T^{n-2} p^{n-2} + \dots + t'_r T^{n-r} p^{n-r} + \dots + n]} \quad (31)$$

The admittance function  $G_n$  is the reciprocal of the impedance function  $Z_n$  and so

$$G_n = Cp \frac{[T^{n-1} p^{n-1} + t'_1 T^{n-2} p^{n-2} + \dots + t'_r T^{n-r} p^{n-r} + \dots + n]}{[T^n p^n + t_1 T^{n-1} p^{n-1} + \dots + t_r T^{n-r} p^{n-r} + \dots + t_n]} \quad (32)$$

Thus the expression for the admittance function  $G_n$  has been obtained by a direct method of converting a continued fraction in the form of a fraction in which both the numerator and the denominator are expressed as a power series in  $Tp$ .

Arranging the numerator and the denominator in an ascending series in  $Tp$ , it can be easily shown that this (equation 32) is identical with that (equation 2) given by Tschudi (1950).

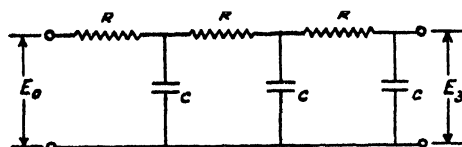


FIG. 2

Example :

Consider the 3-mesh network as shown in figure 2.

In this case  $n = 3$ ,

$$t_1 = {}^5C_1 = 5$$

$$t_2 = {}^4C_2 = 6$$

$$t_3 = {}^3C_3 = 1$$

$$t_1' = {}^5C_0 = 1$$

$$t_2' = {}^4C_1 = 4$$

$$t_3' = {}^3C_2 = 3$$

Substituting these values in equation (32), we have

$$G_3 = Cp \cdot \frac{T^2 p^2 + 4Tp + 3}{T^3 p^3 + 5T^2 p^2 + 6Tp + 1}.$$

# TRANSFER FUNCTION FOR AN $n$ -MESH RC NETWORK

Let the input voltage of an  $n$ -mesh RC filter network (figure 3) be denoted by  $E_0$  and the output voltage by  $E_n$ .

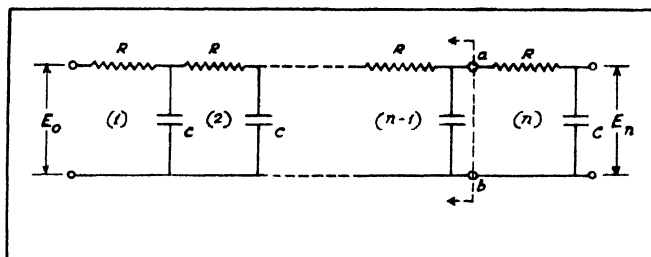


FIG. 3

This circuit is simplified by applying Thevenin's theorem to the portion of the system to the left of the points  $a, b$ . The equivalent circuit is as shown in figure 4.

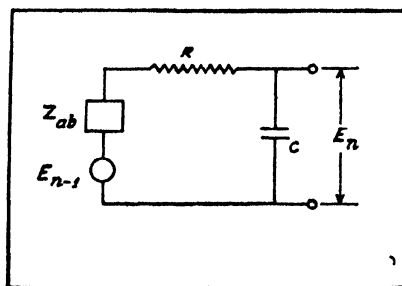


FIG. 4

$E_{n-1}$  = open-circuited voltage measured across  $a-b$  and  $Z_{ab}$  = impedance

of the network looking back into the terminals  $a-b$  with all generators replaced by impedances equal to their internal impedances.

Since the only generator present is  $E_0$  and its internal impedance is assumed to be zero,  $Z_{ab}$  is the impedance of the network looking back into the terminals  $a-b$ , when the far end is short-circuited.

From figure. 4,

$$\frac{E_n}{E_{n-1}} = \frac{1}{Cp[Z_{ab} + R + 1/Cp]} \quad \dots (33)$$

$$= \frac{Z_n'}{Z_{ab} + R} \quad (34)$$

where  $Z_n$  is the impedance of the  $n$ -mesh network looking back from the output when the input is short-circuited.

Now,

$$\begin{aligned} Z_n' &= \frac{1}{Cp + \frac{1}{R + \frac{1}{Cp + \dots \text{to } 2n \text{ convergents}}}} \\ &= \frac{1}{Cp} \left[ \frac{1}{1 + \frac{1}{a + \frac{1}{1 + \frac{1}{a + \dots \text{to } 2n \text{ convergents}}}}} \right] \dots (35) \end{aligned}$$

where  $a = RCp = Tp$

with the help of equations (21) and (26), we can write

$$Z_n' = \frac{Tp}{Cp} \left[ \frac{a^{n-1} + t_2' a^{n-2} + \dots + t_r' a^{n-r} + \dots + n}{a^n + t_1 a^{n-1} + \dots + t_r a^{n-r} + \dots + t_n} \right] \quad \dots (36)$$

where  $t_r$  and  $t_r'$  are given by equation (27).

Again,

$$\begin{aligned} R + Z_{ab} &= R + \left[ \frac{1}{Cp + \frac{1}{R + \frac{1}{Cp + \dots \text{to } (2n-2) \text{ convergents}}}} \right] \\ &= R \left[ 1 + \frac{1}{a + \frac{1}{1 + \frac{1}{a + \dots \text{to } (2n-1) \text{ convergents}}}} \right] \\ &= R \cdot \frac{[a^{n-1} + t_2' a^{n-2} + \dots + t_r' a^{n-r} + \dots + t_n]}{q_{2n-1}} \quad (37) \end{aligned}$$

where  $q_{2n-1}$  is the  $(2n-1)$ th partial denominator of (17).

From equations (34), (36) and (37), we have

$$\frac{E_n}{E_{n-1}} = \frac{q_{2n-1}}{a^n + t_1 a^{n-1} + \dots + t_r a^{n-r} + \dots + t_n} \quad (38)$$

$$= \frac{q_{2n-1}}{p_{2n}} \quad (39)$$



Substituting  $n = n-1, n-2, \dots, 1$ , we have,

$$\frac{E_{n-1}}{E_{n-2}} = \frac{q_{2n-3}}{p_{2n-2}}$$

$$\frac{E_1}{E_0} = \frac{q_1}{p_2}$$

From these equations we can easily show that

$$\begin{aligned} \frac{E_n}{E_0} &= \frac{q_{2n-1}}{p_{2n}} \cdot \frac{q_{2n-3}}{p_{2n-2}} \cdot \frac{q_{2n-5}}{p_{2n-4}} \dots \frac{q_1}{p_2} \\ &= \frac{q_1}{p_{2n}} \end{aligned} \quad \dots (40)$$

since for the continued fraction (17) the following identities hold good :

$$\begin{aligned} \text{and} \quad \frac{ap_{2n-1} + q_{2n}}{p_{2n-2} + q_{2n-1}} &= \left\{ \begin{array}{l} ap_{2n-1} + q_{2n} \\ p_{2n-2} + q_{2n-1} \end{array} \right\} \end{aligned} \quad \dots (41)$$

Remembering that  $q_1 = 1$ ,

Transfer function  $F_n(p) = E_n/E_0$

$$a^n + t_1 a^{n-1} + \dots + t_r a^{n-r} + \dots + t_n \quad \dots (42)$$

$$\begin{aligned} \text{where} \quad & t_r = 2^{n-r} C_r \\ \text{and} \quad & a = Tp \end{aligned} \quad \dots (43)$$

With the help of this equation we can at once find out the output voltage for an  $n$ -mesh network if the input voltage is known.

*Example :*

Let us calculate the transfer function for a 3-mesh RC filter network (figure 2) Applying equation (41) we can show that

$$\left( \frac{E_3}{E_0} \right) = \frac{1}{T^3 p^3 + 5T^2 p^2 + 6Tp + 1}$$

$n$ -MESH RC NETWORK



FIG. 5

The impedance function of an  $n$ -mesh CR network is given by

$$Z_n(CR) = \frac{1}{Cp} + \frac{1}{\frac{1}{R} + \frac{1}{Cp + \frac{1}{\frac{1}{R} + \frac{1}{Cp + \dots \text{to } 2n \text{ convergents}}}}} \quad (44)$$

By means of equivalence transformation we have

$$Z_n(CE) = \frac{1}{Cp} + \frac{1}{\frac{1}{RCp} + \frac{1}{RCp + \dots \text{to } 2n \text{ convergents}}} \quad (45)$$

Substituting

$$RCp = b,$$

$$Z_n(CR) = \frac{1}{Cp} + \frac{1}{b + \frac{1}{1 + \frac{1}{b + \dots \text{to } 2n \text{ convergents}}}} \quad (46)$$

The continued fraction within the brackets is the same as (17) and we can show with the help of equations (26) and (27),

$$Z_n(CR) = \frac{1}{Cp} \cdot \frac{[1 + t_1 Tp + \dots + t_r T^r p^r + \dots + t_n T^n p^n]}{[1 + t'_2 Tp + \dots + t'_r T^{r-1} p^{r-1} + \dots + t'_n T^{n-1} p^{n-1}]} \quad (47)$$

where  $t_r$  and  $t'_r$  are given by equations in (27).

So admittance function  $G_n(CR)$  is given by

$$G_n(CR) = Cp \cdot \frac{1 + t'_2 Tp + \dots + t'_n T^{n-1} p^{n-1}}{1 + t_1 Tp + \dots + t_n T^n p^n} \quad (48)$$

*Example :*

Let us find out the admittance function for a network in which  $n=3$  (figure 6).

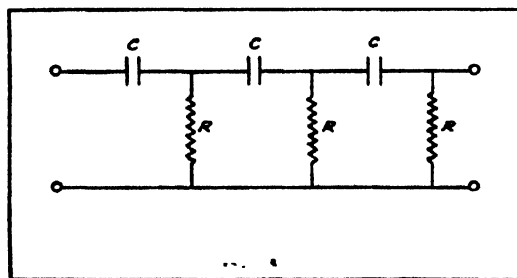


FIG. 6

In this case

$$t_1 = {}^5c_1 = 5$$

$$t_2 = {}^4c_2 = 6$$

$$t_3 = {}^3c_3 = 1$$

$$t'_1 = {}^5c_0 = 1$$

$$t'_2 = {}^4c_1 = 4$$

$$t'_3 = {}^3c_2 = 3$$

Substituting these values in equation (48) we have

$$G_s(CR) = Cp \cdot \frac{1 + 4Tp + 3T^2p^2}{1 + 5Tp + 6T^2p^2 + T^3p^3}$$

where

$$T = RC$$

and

$$p = j\omega$$

#### TRANSFER FUNCTION OF THE CR NETWORK

Following a procedure similar to that in the case of an  $n$ -mesh RC-network, we can show that the transfer function of an  $n$ -mesh CR network is given by

$$\left( \frac{E_n}{E_0} \right) = \frac{(Tp)^n}{[1 + t_1Tp + \dots + t_1T^1p^1 + \dots + t_nT^np^n]} \quad \dots (49)$$

This expression will be very useful in calculating the responses of the cascaded CR networks to specified signals.

*Example :*

For the network shown in figure. 6,

$$\left( \frac{E_3}{E_0} \right) = \frac{T^3p^3}{1 + 5Tp + 6T^2p^2 + T^3p^3}$$

#### CONCLUSION

The admittance function and transfer function are two very important parameters in network theory and design since they completely determine the response characteristic of a network. The problem to find out expressions for these functions has been tackled from a new and direct angle which will be useful to those who work with network synthesis and design.

The resistance-capacitance filter networks are of common use in electronic circuits. This is why several attempts have been recently made to develop the process of synthesis of RC networks with prescribed response characteristics. The results of this paper will be useful in dealing with such problems.

#### ACKNOWLEDGMENTS

It is a pleasure to record grateful thanks to Prof. M. N. Saha, F.R.S., for his kind interest in the work. The author is also indebted to Dr. A. K. Saha and Mr. P. K. Ghose for helpful discussions. Thanks are also due to Dr. B. D. Nag and Mr. B. M. Banerjee for their kind interest.

## REFERENCES

- Chrystal, 1952, A text book of Algebra, vol. II, p. 494.  
Storch, L , 1951, *Proc. I.R.E* , **39**, 1456  
Tschudi, E W , 1950, *Proc. I.R.E* , **38** 309.

## REVIEW

(4)

**An International Bibliography on Atomic Energy, Volume 2, Scientific Aspects.** Supplement No. 1, pp. 350 Atomic Energy Section ; Department of Security Council Affairs, United Nations, New York, 1952. Price \$ 3.50, 25/-Stg., 14.00 Swiss frs.

This volume is a supplement of an International Bibliography on Atomic Energy, Volume 2, Scientific Aspects, published in 1951. The volume under review contains a bibliography of the papers published during 1949 and 1950. The investigations have been classified under five broad lines, *viz.*, Fundamental Nuclear Science, Physics and Engineering of Nuclear Reactors, the Biological and Medical Effects of High Energy Radiations, Isotopes in Biology and Medicine and Applications of Radioactive Tracers in Non-biological Sciences and Technology. Each of these lines has been subdivided into different sections, the number of which is thirteen in the case of Fundamental Nuclear Science and smaller in the case of the other four lines. The thirteen sections in the line of Fundamental Nuclear Science are (A) The Stable Isotopes of the Elements, (B) The Spins, Magnetic Moments and Quadrupole Moments of the Nuclei, (C) The Acceleration of Charged Particles, (D) Detection of Nuclear Radiations, (E) Natural Radioactivity and Radioactivity Geochronology, (F) Artificial Disintegration of the Nucleus, (G) Artificial Radioactivity, (H) Interaction of Neutrons with Matter, (I) Fission of the Atomic Nucleus and Transuranic Elements, (J) Passage of Charged Particles or Photons through Matter, Scattering and Pair Production, (K) Cosmic Rays, Meson Physics and Astrophysics, (L) Theory of Nuclear Structure and (M) Books. Some of these sections are again subdivided into sub-sections. There are four sections under the headings, (A) Fissionable and Moderator Materials, (B) Nuclear Reactors, (C) Atomic Energy Establishments and (D) Health Protection in the line, The Physics and Engineering of Nuclear Reactors.

The investigations on the Biological and Medical Effects of High Energy Radiations are classified under twelve sections, *viz.*, (A) General, (B)-(I), Effects of High Energy Radiations on Micro-organisms, on Cells, Blood and Tissue, on Genetics and Mutations, on Growth and Development of Organisms, on Organ Systems, on Physiology and on Botany and Agriculture ; (J) Medical Aspects of High Energy Radiations, (K) Radiation Protection and Dosage Measurements and (L) Technical Aspects of Instrumentation.

There are six sections in each of the two lines, *Isotopes in Biology and Medicine*, and *Applications of Radioactive Tracers in Non-biological Sciences and Technology*. There are altogether 8,231 references and two Appendices, one being an author index and the other the list of abbreviated names of the journals quoted.

It is needless to mention that this supplementary volume along with the main volume published in 1951 will be immensely helpful to all research workers engaged in the lines of research mentioned above. If the number of pages and quality of the paper used are taken into consideration the price seems to be quite moderate.

S. C. S.

# STATISTICAL QUALITY CONTROL

## INDIAN STANDARD ISSUED

New Delhi, Oct. 27, 1952.

The Indian Standards Institution has issued the 'Indian Standard Method for Statistical Quality Control During Production by the Use of Control Chart'. It is recommended for use by operatives for maintaining a control procedure in the factory, as well as by teachers and students in any course of training in this field.

It will be recalled that Statistical Quality Control (SQC) Training Courses, arranged under an agreement between the Government of India and the U. N. Technical Assistance Administration, were recently inaugurated in Delhi. This standard has been welcomed both by the visiting professors conducting the course as well as by the trainees, and is being used in their training.

The standard contains two illustrative examples, collected from experience of Indian industry, but otherwise represents an adoption of the American Defence Emergency Standard Z1.3-1942. In its details, the standard describes, step by step, a procedure for setting up a control chart and using it during production to control quality of products.

The control of quality of products to maintain it at a given level reduces the rejection percentage and improves the quality of production without extra capital. The control chart method of controlling quality during production is meant to be an integral part of the production process. This technique, however, does not provide an automatic corrective action in the way mechanical or electrical control systems do. Instead, it gives a warning signal to the operative that he must take, here and now, corrective action on his machine or process to ensure maintenance of quality in further production. Its effectiveness, therefore, depends on the promptness with which the warning is heeded.

The practical value of control chart in SQC technique has been proved by extensive application made during years of actual manufacturing practice. Because of its particular success, its use spread rapidly during the last world war, and it is now being widely utilized in increasing productivity in the U. S. A., U. K., Canada, Australia, Japan, U. S. S. R. and other countries.

In India, attempts to introduce SQC started practically with the establishment in 1944 of a Committee on Statistics, Standards and Quality Control by the Council of Scientific and Industrial Research. On the recommendation of this Committee, courses in SQC began to be given in the Indian Statistical Institute from 1945-46. A big step was taken in 1947 when the Indian Statistical Institute, the Indian Standards Institution and

the Indian Science Congress Association invited Dr. Shewhart, the originator of the SQC technique, to visit this country and deliver lectures on the subject. He visited India for four months in 1947-48 and engaged himself in propagating knowledge of SQC through the available channels. At Ahmedabad, the Ahmedabad Textile Industry's Research Association embarked on a scheme to introduce statistical quality control methods in textile mills on a large scale. As a result of their efforts, a number of mills in Ahmedabad have established Statistical Departments.

It is hoped that the present intensive training courses which selected technicians from government departments and industries are undergoing, will lead to greater appreciation and wider application of SQC in India.

The standard is available on sale for Rs. 5/- per copy, and may be obtained from the Secretary (Administration), Indian Standards Institution, 19 University Road, Civil Lines, Delhi-8.

## GROWING RECOGNITION OF INDIAN STANDARDS A YEAR OF PROGRESS

*Fifth Annual Report of Indian Standards Institution*

New Delhi, October 27, 1952

Standardisation made further considerable progress in India during 1951-52. Growing recognition was accorded to Indian standards by industry and Government. The ISI (Certification Marks) Act was passed by Parliament during the year, the Central Government increased its grant to the Institution and well over a lakh of copies of Indian standards were sold and distributed, the sales revenue of nearly Rs. 30,000/- representing a 50 per cent increase over last year's figure.

The fifth Annual Report of the Indian Standards Institution, which has just been published, shows that the Institution completed another year of all-round progressive development in which it continued to receive good support both from industry and Government. The membership of the Institution rose from 684 in 1950 to 758 in 1951 with corresponding increase in the subscription collected from Rs. 1,86,500/- to Rs. 2,06,255/-. The number of sectional committees and subcommittees which held 142 meetings against last year's figure of 100, went up from 264 to 300. The membership of these committees is now about 2,700 and consists of experts drawn from the various technological and industrial spheres, and trade and government departments, spread all over the country. The number of new Indian Standards published by the Institution during 1951-52 was 112. Besides, there were over 500 subjects under study for standardisation, over 100 standards finalised and under print, and over 400 standards in circulation and other stages of preparation at the end of March 1952.

The list of Indian Standards published in the Report shows that nearly two-thirds of them have either been adopted by Government departments, such as the Directorate General of Supplies and Disposals and the Railway



Board, in place of their own specifications or referred to in their purchase specifications.

The important items of the Institution's activities and achievements which the Report records in detail, include the visit of the Prime Minister Shri Jawaharlal Nehru to the Institution in August 1951 and the presentation to him of a National Flag of India prepared in accordance with the Indian Standard. The ISI (Certification Marks) Act, intended to encourage effectively the production of goods in conformity with Indian Standards, was passed by Parliament in March last. The ISI convened a Conference of Directors of Industries of States which recommended to the Central and State Governments that all their purchases be made, as far as possible, according to Indian Standards. A Five-Year Plan for the development of ISI was drawn up and a substantial part of the plan relating to 1952-53 was approved by the Planning Commission, as a result of which the Government increased its grant to the Institution for 1952-53 from 2.2 lakhs to Rs. 4.2 lakhs. With the additional grant, the ISI General Council decided to embark on new projects of setting up the Building Division Council, a Steel Economy section, organising International Electrotechnical Commission work taken over from the Institution of Engineers and the work of laying standards relating to storage and handling of foodgrains.

#### *New Subjects for Standardisation*

The Division Councils considered 119 new subjects for standardisation during the year under review. Among those which were accepted are sanitary fittings and appliances, ball bearings, safes, fire fighting equipment, hurricane lanterns, bolts, nuts and other fasteners, sports goods, silk waste, towels, duries, blankets, handloom cloth, bone meal, ammonia, raw materials for ceramic industry, safety matches, cashew nut shell liquid and Turkey Red Oil.

For laboratory investigations required in the preparation of Indian Standards the Institution continued to receive active cooperation and assistance from all quarters in the country, and particularly from the laboratories of the Council of Scientific and Industrial Research, the Forest Research Institute, Dehra Dun, the Technical Development Establishment Laboratory (Stores), Kanpur, and the Government Test House, Alipore. The Report gives a list of 46 problems entrusted by the Institution to the organisations and laboratories.

In the international sphere, the ISI is an elected member of the Governing Council of the International Organisation for Standardisation (ISO), and Dr. Lal C. Verma, Director, Indian Standards Institution, is the elected Vice-President of ISO. The Report records the details of cooperation extended by the Indian Standards Institution in international standardisation work.



# INVESTIGATION ON THE BOWED STRING WITH AN ELECTRICALLY DRIVEN BOW (PART II)

By N. K. DATTA

PHYSICAL LABORATORY, PRESIDENCY COLLEGE, CALCUTTA

(Received for publication, May 23, 1952)

**ABSTRACT.** The paper verifies a part of the formula established in Part I. The values of  $\alpha\mu_d$ , where  $\mu_d$  is the dynamical coefficient of friction, during backward motion and  $\alpha$ , a constant factor, have been obtained with different specimens of metal wires and with different diameters of the same metal wire. The variation of  $\alpha\mu_d$  with bowing distance  $d$  for different diameters of the wires and for different materials has been studied. The paper indicates why gut and fine steel strings are generally used in violin. In all the different cases studied, it has been found that the zero-point is always at some distance from the mid-point of the bowed region. This explains (*vide* formula 1) why  $P_{min} \times d$  was found to be only approximately constant in Part I. For a given bowing velocity the distance ( $x$ ) of the zero-point from the mid-point of the bowed region has been calculated for all the wires and has been found to increase with bowing distance for metallic wires, but to decrease in the case of gut.

## INTRODUCTION

In our previous paper (Kar, Datta and Ghosh, 1951) the relation between the minimum bowing pressure ( $P_{min}$ ) required to elicit a steady fundamental tone and the bowing distance,  $d$ , for a given velocity,  $v$ , and that between  $P_{min}$  and bowing velocity keeping the bowing distance constant were studied. The effect of change of the vibrating length of the string on  $P_{min}$ - $V$  curves was also studied. A theoretical formula for minimum bowing pressure was derived. It was found that the formula was in good agreement with the experimental results.

The present paper records a detailed verification of the formula already established in part I.

It was shown in Part I that

$$P_{min} = \alpha\mu_d \left\{ \frac{l}{d} (V - V_0) + V_0 \right\} \quad \dots (1)$$

where  $P_{min}$ ,  $\mu_d$ ,  $\alpha$ ,  $V$ ,  $(V - V_0)$ ,  $l$  and  $d$  are respectively the minimum bowing pressure, dynamical coefficient of friction, a constant factor, the velocity of the bow or forward velocity of the zero-point of the string, the velocity of the mid-point, the vibrating length of the string and the bowing distance. Using the above formula the values of  $V_0$  for different bowing

distances are calculated for wires of different materials having different diameters and are given in column 5 of Tables I, II and III. The change in the values of  $V_0$  thus obtained indicates the change in the values of velocity of the mid-point.

It was already stated in part I that at high velocity when  $\mu_d$  is constant,  $P_{min}$ - $V$  curves should be straight; and tangents drawn at the straight portion of the curves cut the axes of velocity and pressure at  $A$  and  $B$  respectively. The length  $OA$  is obtained by putting  $P_{min}=0$  and  $OB$  by putting  $V=0$  in (eqn. 1). Thus we have as in Part I

$$OA = V_0 \left( 1 - \frac{d}{l} \right) \quad \dots (2)$$

$$\text{and} \quad OB = \alpha \mu_d \cdot V_0 \left( 1 - \frac{l}{d} \right) \quad \dots (2.1)$$

$$\text{and so} \quad \frac{OB}{OA} = -\alpha \mu_d \cdot \frac{l}{d} \quad \dots (2.2)$$

Thus for known values of  $OA$ ,  $OB$ ,  $l$  and  $d$ , the values of  $\alpha \mu_d$  are calculated from (2.2) for all the wires of different diameters and materials and given in column 2 of Tables I, II and III. The variation of  $\alpha \mu_d$  with different bowing distances is also studied.

It has been proved in (eqn. 3.2) Part I that the position of the zero-point is given by the formula

$$- \frac{V_0}{V - V_0} \cdot d \quad \dots (3)$$

where  $x$  is the distance of the zero-point from the mid-point of the bowed region. The values of  $x$  calculated from the above formula for a constant bowing velocity ( $V=22.5$  cms/sec) are given in column 6 of the tables. The change in the values of  $x$  is also studied.

#### EXPERIMENTAL

With the apparatus described in Part I the experiment is carried on with steel wires of different diameters, *i.e.*, of different linear densities. The vibrating length (32 cms) and frequency (256) are kept constant throughout the experiment.

The experiment is carried on with wires of different diameters but of same material (*viz.*, steel) and  $P_{min}$ - $V$  curves are obtained for different bowing distances. (*vide* figures 1 to 4).

The experiment is repeated with brass wire and gut and  $P_{min}$ - $V$  curves are obtained as shown in figures 5 and 6 for different bowing distances. The measurements of pressure and velocity are made as described in Part I. The radii of all the wires are given in the tables.

It should be mentioned here that the velocities are taken such that all the points obtained are on the straight portion of the  $P_{min}$ - $V$  curves where  $P_{min}$  varies as  $V$ .

## RESULTS

TABLE I (steel wires)

Distance $d$ from the bridge in cms.	Value of $a\mu_d$	Radius ( $r$ ) of wires in cms	$\frac{a\mu_d}{r}$	Value of $V_0$ from formula (1)	Value of $x$ from $x = \frac{V_0}{V - V_0} \cdot d$ for $V = 22.5$ cms/sec
2	.20	.015	13.47	15.4	4.33
2.5	.10	"	12.6	14.0	1.11
3	.17	"	11.33	13.0	4.10
4	.18	"	12.0	12.7	5.18
2	.30	.0198	15.1	14.3	3.18
3	.31	"	15.6	14.5	2.1
4	.32	"	16.1	14.5	7.25
2	.35	.0235	14.80	12.7	2.6
3	.33	"	14.01	11.2	2.8
4	.31	"	13.10	12.4	1.9
2	.49	.0275	17.82	14.5	3.62
2.5	.40	"	14.5	14.1	1.1
3	.35	"	12.7	13.7	4.66
3.5	.33	"	12.0	12.0	4.7

TABLE II (brass wire)

Distance $d$ from the bridge in cms.	Value of $a\mu_d$	Radius ( $r$ ) of wires in cms.	$\frac{a\mu_d}{r}$	Value of $V_0$ from formula (1)	Value of $x$ from $x = \frac{V_0}{V - V_0} \cdot d$ for $V = 22.5$ cms/sec.
2	.19	.027	7.0	5.0	.5
3	.20	"	7.1	4.1	.66
4	.187	"	6.5	5.7	1.30

TABLE III (gut)

Distance $d$ from the bridge in cms.	Value of $a\mu_d$	Radius ( $r$ ) of wires in cms	$\frac{a\mu_d}{r}$	Value of $V_0$ from formula (1)	Value of $x$ from $x = \frac{V_0}{V - V_0} \cdot d$ for $V = 22.5$ cms/sec.
2	.156	.0485	3.2	11.82	2.11
2.5	.156	"	3.2	9.7	1.8
	.14	"	2.8	7.0	1.35
4	.12	"	2.4	5.4	1.2
4.5	.112	"	2.3	3.1	.7

TABLE IV (variation of  $\alpha\mu_d$  with distance)

Distance $d$ from the bridge in cms.	$\alpha\mu_d$ for steel wire of radius $r$ =.015 cms	$\alpha\mu_d$ for steel wire of radius $r$ =.0198 cms.	$\alpha\mu_d$ for steel wire of radius $r$ =.235 cms	$\alpha\mu_d$ for steel wire of radius $r$ =.275 cms.	$\alpha\mu_d$ for brass wire of radius $r$ =.027 cms.	$\alpha\mu_d$ for gut string of radius $r$ = 0.485 cms.
2	.202	.3	.35	.49	.19	.156
3	.17	.31	.33	.35	.20	.14
4	.18	.32	.31	—	.187	.12

Table I contains the values of bowing distances,  $\alpha\mu_d$ , radii of wires,  $\alpha\mu_d/r$ ,  $V_0$  (calculated from eqn. 1), and  $x$  (calculated from eqn. 3) in columns 1 to 6 respectively which are values for steel wires of different diameters only. In Tables II and III, the corresponding values for brass and gut strings are given. Table IV shows comparative values of  $\alpha\mu_d$  for wires of different diameters of all the wires for three particular bowing distances.

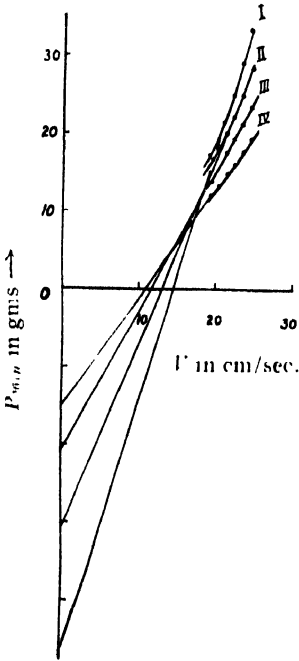


FIG. 1

$P_{min} - V$  curves for steel wire,  
I. for  $d = 2$  cms. } radius = .015 cms  
II. for  $d = 2.5$  ,, } frequency = 256.  
III. for  $d = 3$  ,, } (approx.)  
IV. for  $d = 4$  ,, } length = 32 cms.

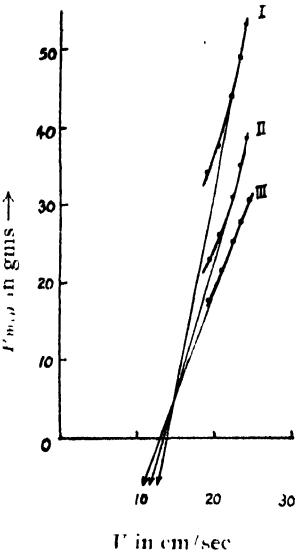


FIG. 2

$P_{min} - V$  curves for steel wire,  
I. for  $d = 2$  cms } radius = .0198 cms.  
II for  $d = 3$  ,, } frequency = 256 (approx.)  
III. for  $d = 4$  ,, } length = 32 cms.

Intercepts on ordinate  
I. 67.5 gms.  
II. 10.5 ,,  
III. 34 ,,

## DISCUSSION OF RESULTS

Different values of  $\alpha\mu_d$  are plotted against bowing distances  $d$ , for all the wires. Curves thus obtained (*vide* figure 7) show a slight decrease in all cases in general but it is very prominent in case of steel wire of large

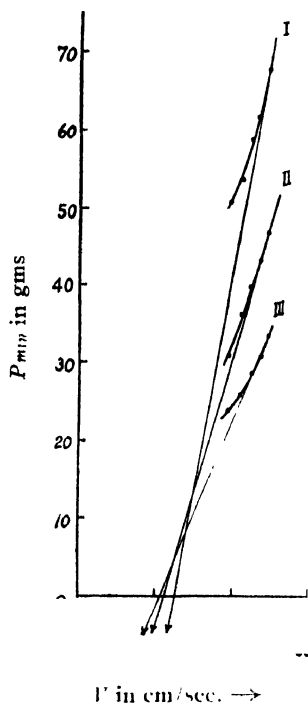


FIG. 3

$P_{min}$ — $V$  curve for steel wire

- |      |                 |  |
|------|-----------------|--|
| I.   | for $d = 1$ cms | } radius = .0235 cms<br>frequency = 256 (approx)<br>length = 32 cms. |
| II.  | for $d = 2$ "   |  |
| III. | for $d = 3$ "   |  |

Intercepts on ordinate.

- |      |        |
|------|--------|
| I.   | 51 gms |
| II.  | 40 "   |
| III. | 26 "   |

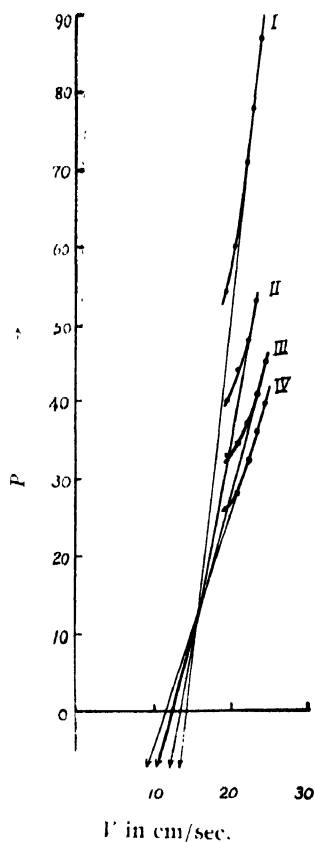


FIG. 4

$P_{min}$ — $V$  curves for steel wire.

- |      |                  |  |
|------|------------------|--|
| I.   | for $d = 2$ cms. | } radius = .0275 cms.<br>frequency = 265 (approx)<br>length = 32 cms |
| II.  | for $d = 2.5$ "  |  |
| III. | for $d = 3$ "    |  |
| IV.  | for $d = 3.5$ "  |  |

Intercepts on ordinate.

- |     |           |                  |
|-----|-----------|------------------|
| I.  | 107 gms   | } III. 47.5 gms. |
| II. | 72.5 gms. |                  |

diameter. Thus it may be inferred from the curves that  $\alpha\mu_d$  for metallic wires of fine diameters is nearly constant but decreases in the case of wires of large diameters. And also  $\alpha\mu_d$  for gut is lowest and decreases slightly with  $d$ .

Further the values of  $V_0$  obtained are found to be nearly constant for metallic wires but decrease rapidly with  $d$  in the case of gut. The numerical values of  $V_0$  for brass wire are far less than those for steel wires and the

corresponding values for gut are much smaller than those for steel and brass wires.

The values of  $\alpha$  for metal wires are found to increase with  $d$ . This means that the zero-point moves further away from the outer limit of the bowed region towards the further end of the string. But in the case of gut a

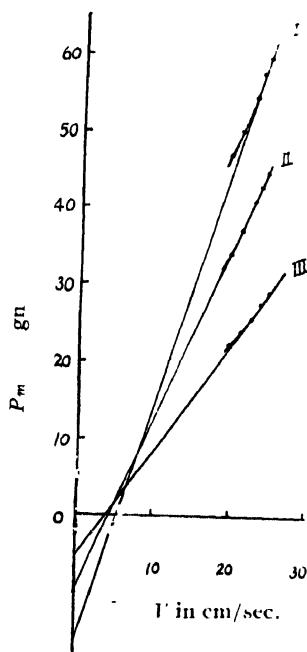


FIG. 5

$P_{min}-V$  curves for brass wire.

- |                  |   |
|------------------|---|
| I. for $d=2$ cms | } radius = .027 cms<br>frequency = 256 (approx.)<br>length = .32 cms. |
| II. for $d=3$ "  |   |
| III. for $d=4$ " |   |

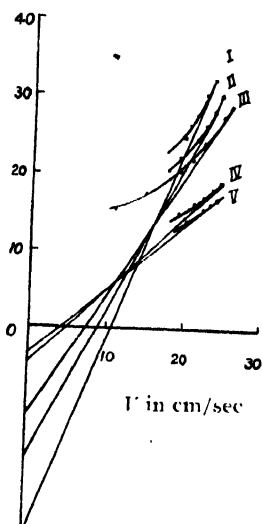


FIG. 6

$P_{min}-V$  curves for gut.

- |                   |   |
|-------------------|---|
| I. for $d=2$ cms. | } radius = .0485 cms.<br>frequency = 256 (approx.)<br>length = .32 cms. |
| II. for $d=2.5$ " |   |
| III. for $d=3$ "  |   |
| IV. for $d=4$ "   |   |
| V. for $d=4.5$ "  |   |

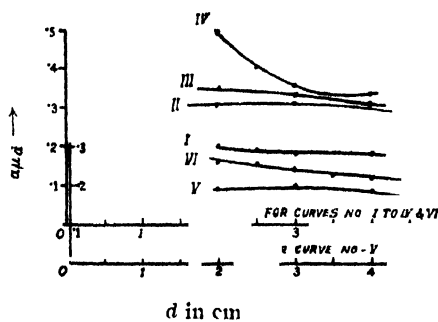


FIG. 7

- |  |  |
|--|--|
| I to IV.— $\alpha\mu_d-d$ Curves for steel wires       | } frequency = 256 (approx.)<br>length = .32 cms. |
| V & VI.— $\alpha\mu_d-d$ Curves for brass & gut wires. |  |

decreases with  $d$  which is just the opposite. This shows that the zero-point moves towards the mid-point.



The fact that  $\alpha\mu_d$  is lowest for gut indicates that for gut smallest pressure is required to elicit the fundamental tone.  $\alpha\mu_d$  for steel wire of fine diameter is slightly greater than that for gut. It is preferable that the exciting pressure should be as small as possible. So gut is used as G string of violin. The steel wire of fine diameter may also be used. But steel wire of large diameter should never be used as its exciting pressure is large.

The peculiarities shown in the case of gut may be due to its material property, stiffness, density, and elasticity which differ widely from those of metal wires.

It is evident from eqn. (1) that  $P_{min}$  is exactly proportional to  $1/d$  when  $V_0$  is zero i.e. when the zero point is exactly at the centre of the bowed region. But in Part 1 of this paper, the authors (Kar, *et al*, 1951), and also Sen (1949) established that  $P_{min}$  is approximately proportional to  $1/d$ . This shows that  $V_0$  is not zero. The validity of the fact that  $V_0$  is not zero is supported by finite and nearly constant values of  $V_0$  obtained in column 5 of the tables.

*Effect of radius.* When the bow makes contact with the string the string is slightly depressed at the surface of contact. The bending of the hairs of the bow obviously depends on the radius of the string used. As the hairs of the bow are spread over a finite breadth, there will be a rectangular curved area of the upper portion of the string in contact with the hairs of the bow (*vide* figure 8). Let  $\Delta_l$  and  $\Delta_b$  be the length and breadth of the hairs of the bow in contact with the string. Then the area of contact is  $\Delta_l \Delta_b$  which is the same as  $r\theta \Delta_b$  where  $r$  is the radius of the wire and  $\theta$  the angle between the two extreme tangents.

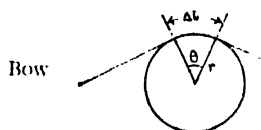


FIG. 8

It may be shown from eqn. (1) that

$$\alpha\mu_d = \frac{d}{l} \cdot \frac{dP_{min}}{dV} \quad \dots (4)$$

where  $\frac{dP_{min}}{dV}$  is the same as  $\frac{OB}{OA}$  in eqn. (2.2).

It is already seen that  $\alpha\mu_d$  is nearly constant for strings of fine diameters and varies slightly for strings of large diameters when the bowing distance is varied. This means that  $d \cdot \frac{dP_{min}}{dV}$  is constant in cases where  $\alpha\mu_d$  is constant and varies in cases where  $\alpha\mu_d$  varies.

Now, although  $P_{min}$  is said to be the minimum pressure exerted, actually it is the minimum force exerted by the bow. The force is obviously proportional to the area of contact which is  $\Delta_r \Delta_b$  or  $r \cdot \theta \cdot \Delta_b$ . Thus the slight variation for different wires having different radii may be explained as due to the slight variation in the area of contact  $r \cdot \theta \cdot \Delta_b$  i.e., due to a slight variation of both  $r$  and  $\theta$ .

As  $P_{min}$  is proportional to area of contact we may write eqn. (4) as

$$\alpha \mu_d = k \cdot r \cdot \theta \cdot \Delta_b \quad \dots (5)$$

$$\text{or} \quad \frac{\alpha \mu_d}{r} = k \cdot \theta \cdot \Delta_b \quad \dots (5.1)$$

where  $k$  is some constant.

Thus for the same wire the slight variation of  $\alpha \mu_d$  with bowing distances may be due to the slight variation in  $\theta$  since  $r$  is constant.

Lastly, it may be mentioned that in the present paper  $V_0$  has been calculated using eqn. (1) which should, however, be directly obtained by photographic method. Experiment in this direction is in progress.

#### ACKNOWLEDGMENT

The author is grateful to Dr. K. C. Kar, D.Sc., for suggesting the problem and for helpful criticism during the progress of work.

#### REFERENCES

- Kar, K. C., Datta N. K., and Ghosh, S. K., 1951, *Ind. J. Phys.*, **2**, 423.  
 Sen, B. K., 1949, *Ind. J. Phys.*, **23**, 7.

# STUDIES ON IONOSPHERIC ABSORPTION\*

By B. CHATTERJEE

INSTITUTE OF RADIOPHYSICS AND ELECTRONICS, CALCUTTA UNIVERSITY

(Received for publication, July 21, 1952)

**ABSTRACT** This paper discusses briefly the phenomenon of ionospheric absorption of radio waves in their passage through the ionospheric regions. Results of observations made at Calcutta on the variation of ionospheric absorption with that of wave frequency are described. The results show that in addition to the losses due to collisions there is a marked increase in attenuation near the critical frequencies of the layers due to partial penetration of the wave energy. Presence of sporadic E layers also causes increased attenuation of F echoes by partial reflection and scattering. When there is magneto-ionic splitting, the extraordinary component is always found to suffer higher attenuation as predicted by theory. On certain nights presence of sporadic D's was noticed. This caused high absorption on all frequencies in the short wave range. The sporadic D's are found to be associated with sporadic E and thunderstorms.

## 1. INTRODUCTION

Solution of practical problems of radio communication between distant points *via* ionosphere, necessitates a knowledge not only of the M. U. F.'s of the various ionospheric layers (which depend on the corresponding vertical incidence penetration frequencies) but also of the losses suffered by the radio wave in its passage through these layers. For example, a knowledge of the magnitude of the ionospheric loss is required for the determination of the power that must be used in a transmitter in order that the signals may reach a given distant station. Such knowledge is also required to estimate the maximum power on which a station may be allowed to work, in order that it may not interfere with the transmissions from other distant stations working on the same frequency.

Unfortunately, though observations on vertical incidence penetration frequencies are now made regularly on a fairly world wide scale, very little data are available for the absorption characteristics of the different ionospheric layers. Further, of the few experimental investigations on absorption that have been carried out so far, the majority are for the stations situated at higher latitudes only. There are very few experimental results for the equatorial regions. Since the latitude of Calcutta is low (geographical latitude  $22^{\circ}33'N$ ; magnetic latitude  $13^{\circ}N$ ), it was thought that observations on ionospheric absorption made here would fill the gap. A systematic programme of observation has, therefore, been arranged at the ionospheric

\*Communicated by Prof. S. K. Mitra, D.Sc.

station at Calcutta and the results will be published in due course. In the present communication results of some observations on the variation of reflection coefficient with frequency (for vertical incidence, white, *et. al.* 1930, 1936) for frequencies from two megacycles upwards, will be described and discussed.

It will be helpful, if we first briefly discuss the causes of attenuation of received radio waves in their passage through the ionospheric layers.

## 2. CAUSES OF ATTENUATION OF INDIRECTLY RECEIVED RADIO WAVES

The losses in energy leading to the attenuation of radio waves in their passage through the ionospheric layers may be listed as follows :

(1) *Loss due to collision.* The electrons in the ionosphere are set into oscillation by the incident radio wave. The energy of the oscillating electrons, which would otherwise have gone back to the wave field by re-radiation, is dissipated if there are collisions.

(2) *Loss due to partial reflection.* Sometimes partial reflection takes place from regions of large ionization density gradient or thin layers. The amplitude of the reflected wave is decreased, since a portion of the wave energy penetrates through the ionized region and is lost. Such partial penetration also takes place near the critical frequency of an ionized layer.

(3) *Losses due to irregularities.* Irregularities present in the ionosphere, *e.g.* ionospheric clouds, sporadic layers etc., scatter the incident radio wave and thus decrease the amplitude of the reflected wave. Further, the phases of the scattered waves change in a random manner and the waves scattered from different regions may reach the receiving point in phase or out of phase. Thus, the amplitude of the received signal changes rapidly with time, which causes fading. For the case in which there is an adding up in phase, the strength of the received signal may even sometimes be greater than that expected for propagation in free space (focusing effect, Rawer. *et al.*, 1951)

The losses due to all the above causes may be lumped together and may be regarded as loss by "absorption" in the ionosphere. We can thus speak of an effective "absorption coefficient",  $K$ , per unit length, so that the overall absorption suffered by the wave is given by  $\int K ds$ , where  $ds$  is an element of the ray path and the integration is carried out over the whole length of the path. The 'apparent reflection coefficient',  $\rho$ , which is defined as the ratio of the amplitudes of the reflected to incident field strength, is thus given by

$$-\log_e \rho = \int K ds \quad \dots (1)$$

As the loss due to (1) is the most important and is always present, let us consider it in some detail.

The wave in its passage through the ionosphere, suffers deviation before returning to earth. It is convenient to consider separately the losses suffered

(i) in the main deviating region and (ii) in the lower region where there is little deviation.

(i) *Deviative absorption.* The wave is deviated and gets reflected from this region. The refractive index in this region is less than unity, and, if there be collisions leading to absorption of energy, the refractive index becomes complex. Calculation of ionospheric absorption in a deviating region, considering the Chapman distribution of ionization density, is very involved. In practice, a parabolic approximation to the Chapman distribution is always used. Hacke (1948) and Hacke and Keiso (1948) have shown that a better result is obtained if the Chapman layer is represented by two parabolas—one representing the ionization density below the point of inflection in the Chapman distribution curve and the other giving the ionization above this point.

The deviative absorption is of special importance in the case of long and very long waves, as these are reflected from the lowermost ionized region, namely the D region, and suffer only this type of absorption. The absorption is generally high as the collisional frequency in this region is greater than the wave frequency. A peculiar feature of the attenuation of such waves is that as the frequency is lowered the attenuation at first increases being maximum at about 100 kc/s. (Best, *et al*, 1936). However, in the very long wave band (about 16 kc/s) there is strong reflection throughout day and night (Beynon, 1948). This shows that there is a transition in propagation properties between these two frequencies. The height of reflection of long waves generally lies between 60 and 80 kms. (Budden, 1951; Bracewell, 1948; Mitra, 1951). With decrease of sun's zenith angle, the longwave absorption increases, as the ionization of the D layer penetrates to lower levels where collisional frequency is high.

The deviative absorption is of less importance in the short wave range on which the long distance radio communication is generally carried out. At these frequencies, the reflection takes place from the E and the F layers where the collisional frequency is low. As such, most of the absorption takes place in the lower non-deviating D region.

(ii) *Non-deviative absorption (D region).* As mentioned above, short and medium waves reflected from the higher ionized regions (E or F layers) suffer non-deviative absorption in the lower D layer, through which the waves have to pass and repass. The D layer absorption for these waves is particularly effective during day time (excepting near the critical frequency of the reflecting E or F layer), as during day time, the ionization reaches low levels (even upto 60 km.) where the collisional frequency is high.

According to the magneto-ionic dispersion formula, the propagation through the ionosphere is said to be quasi-transverse or quasi-longitudinal according as (Mitra, 1952) :

$$\left| \frac{\gamma_T^4}{4(1 + \alpha + jB)^2} \right| > \text{or} < |\gamma^2 L|$$

It can be shown that for short waves, under collisional conditions in the D layer, the propagation is quasi-longitudinal. Hence, the non-deviative absorption in the region is proportional to

$$(f \pm f_H \cos \theta)^2$$

where  $f$  is the wave frequency,  $f_H$  is the gyrofrequency and  $\theta$  is the angle between the direction of propagation and the direction of the terrestrial magnetic field (+ sign refers to the ordinary component and - sign refers to the extraordinary component (Jaeger, 1947). For vertical incidence,  $\theta$  is the complement of the angle of magnetic dip  $\eta$  and hence the absorption is proportional to

$$(f \pm f_H \sin \eta)^2 \quad \dots (2)$$

This relation is approximately obeyed in the short wave range.

The supposition that the absorption of waves reflected during day time from the E or the F region is due to losses in the D region is supported by the fact that the diurnal and seasonal variations of waves so reflected, differ from those expected from a normal E region. Hence the absorption is ascribed to the D layer, where the distribution of ionization and the equilibrium processes differ from those in the E region (Mitra, 1951). Appleton (1938) has shown that for a Chapman layer, the variation of absorption with sun's zenith angle  $\chi$  when  $\chi < 85^\circ$  is proportional to  $\cos^n \chi$ . In general, the diurnal variation may be said to be proportional to  $\cos^n \chi$ . The reported experimental values of  $n$  vary between 0.5 and 2.0. A value of  $n=1$  (Rep. Rad. Res., 1950) represents the diurnal variation fairly well.

In addition to the diurnal and seasonal variations of ionospheric absorption with sun's zenith angle, the D region absorption has also been found to vary with the solar activity, (Benner, 1951) there being an increase by a factor of about 1.5 between sunspot numbers zero and hundred. Further, a 27-day cycle of variation of absorption, coinciding with the rotation period of the sun, has been reported.

*Abnormal absorption.* Besides regular absorption effects noted above, certain abnormal changes of ionospheric absorption are also observed. These include increased absorption associated with sudden outbursts of solar activity and of solar particle emanations, including the absorption effects manifest during ionospheric storms and sudden ionospheric disturbances, and also the absorption continually present in the auroral belts (Tyler, 1948).

*Absorption in oblique propagation.* The first author to make a detailed study of absorption in oblique propagation was Martyn (1951), who showed that for an angle of incidence  $i_0$ , the absorption is  $\sec i_0$  times greater than the vertical incidence case. His formula may be written as

$$[-\log \rho_e]_{f,i} = \cos i_0 [-\log \rho]_{f \cos i_0, 0}$$

The experimental values are generally greater than this. Booker (1940) made a more detailed study, taking into consideration the earth's magnetic field, but his calculations are laborious.

From their studies, Appleton, Beynon and Piggott (1948) have concluded that there is another factor besides collisional friction which is operative in causing the loss. This factor is scattering or partial reflection from the sporadic E layers, as stated earlier. When more than one reflection can be observed, the oblique incidence experiments give a simple method of separating frictional and scattering losses in the ionosphere.

### 3. OBSERVATIONS ON THE VARIATION OF ABSORPTION WITH FREQUENCY

*Method of measurement.* The measurement of the absorption was made by measuring the strength of the echoes of signals emitted from a Breit and Tuve type pulse transmitter, modulated with a pulse of repetition frequency 50 c/s and of duration 200 microseconds. The echoes were received in the same room by a communication type receiver. Both the transmitter and the receiver employed inverted L type aeri<sup>al</sup>s. The echoes received were displayed on the screen of the cathode ray oscillograph in the usual manner, the amplitude being visually measured by comparison with a scale on the screen of the oscillograph. With the emitting and receiving equipments in the same room, it was not possible to make use of the direct signal as the reference signal. When opportunity occurred, the electromotive forces due to the first and second order reflections were compared and these were used to calibrate the apparatus so as to give values of absorption even when only first order reflections were present. For this to be possible, the transmitting and receiving systems, including the aeri<sup>al</sup>s and aerial couplings, had to be maintained constant in every respect. The output of the transmitter was noted by readings of the transmitter plate current (which was kept constant), while the frequent recalibration of the receiver served as a check of it.

The amplitude of the echo is always subject to a random variation due to various causes. In order to find the average amplitude, each reading of absorption was based on eighteen readings taken at intervals of ten seconds. The arithmetic mean value was taken to be the average amplitude (Banerjee, 1951).

The reflection coefficient, as measured, is the so-called apparent reflection coefficient which takes into account the overall absorption by the wave in the deviating and the non-deviating regions, and the energy lost in scattering, if any. Further, remembering that the signal strength of the receiving aerial depends on the polarization of the receiving wave, it also includes the effect of changes in the polarization of the echo.

When both the first and the second order echoes are present, the apparent reflection coefficient is given by  $\rho = \frac{2F''}{F'}$ , where  $F'$  and  $F''$  are the amplitudes of the first and second order echoes, respectively and where the reflection coefficient of the ground has been taken to be unity. However, second order reflections are not always present. But even for such occasions, the reflection coefficient,  $\rho$ , may be measured by employing the following method: At some previous time, when second order echoes are present (on the same frequency) the reflection coefficient ( $\rho_0$ ), the amplitude of the first order echo ( $F'_0$ ) and the equivalent height ( $d_0$ ) of reflection are measured. With these data, the reflection coefficient at any subsequent time, when only the first order echo is present, can be determined, provided the receiving and the transmitting systems have been kept constant throughout. If  $F_1'$  be the amplitude of the first order echo and  $d_1$  be the corresponding equivalent height, then the reflection coefficient is given by

$$\rho = \frac{F_1' d_1}{F_0' d_0} \cdot \rho_0 \quad \dots (3)$$

As it takes an appreciable time to take one set of observations, the readings were not taken during sunrise and sunset hours; during these hours ionization changes considerably within the time taken for observations and thus vitiates the results. The observations were, therefore, made during midday and night hours only, when the ionospheric conditions were expected to remain sensibly constant within the time taken for the readings.

Figures 1 to 5 depict the variations of attenuation with frequency as were measured at Calcutta on a number of days in March, April and May, 1952. The attenuation is plotted in db (given by  $-20 \log_{10} \rho$ ) against frequency in Mc/s.

Figure 1 illustrates a typical case of variation of attenuation with frequency (and the corresponding  $P'-f$  curve) during midday hours. It will be noticed that for reflection from the E region, the attenuation has started increasing from well below the frequency (say about 4 Mc/s in the figure) at which the deviative absorption is expected to commence. This increase is due to the partial penetration of the wave through the E layer on account of its thinness. The attenuation rises more steeply as the E layer critical frequency is approached. For F layer reflections, the attenuation at first decreases with frequency due to decrease in non-deviative absorption. At points intermediate between E and F layer penetration frequencies, the decrease in non-deviative absorption seems to be completely balanced by the increase in the deviative absorption, and the attenuation remains more or less constant over a certain frequency range. Near the critical frequency the increase in deviative absorption is much greater and the overall attenuation increases. For frequencies very near the critical frequency of the layer, the increase in attenuation is much greater than that which can be accounted



for simply by increased penetration into the layer. This high attenuation is due, at least partly, to a partial transmission of wave energy through the layer. This large increase in attenuation is observed during all hours of the day, for frequencies very near the F layer critical frequency.

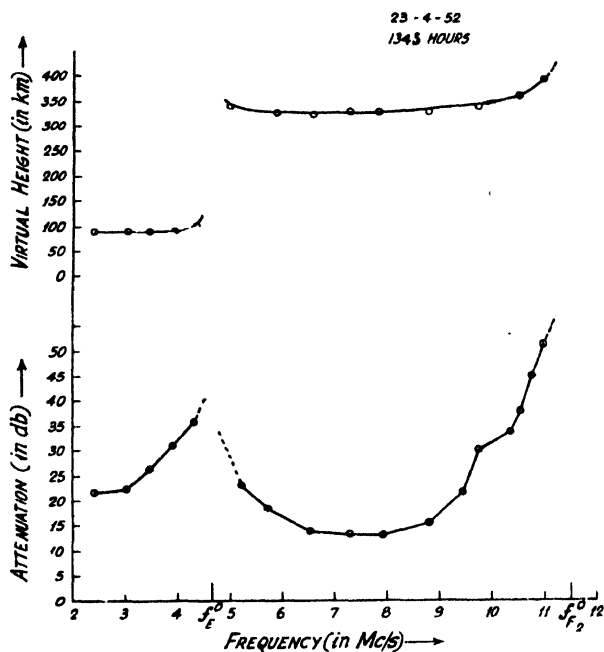


FIG. 1

Variation of absorption with frequency and the corresponding  $P$ - $f$  curve as observed on 23.4.52 at 13 hour 45 min. L. M. T.

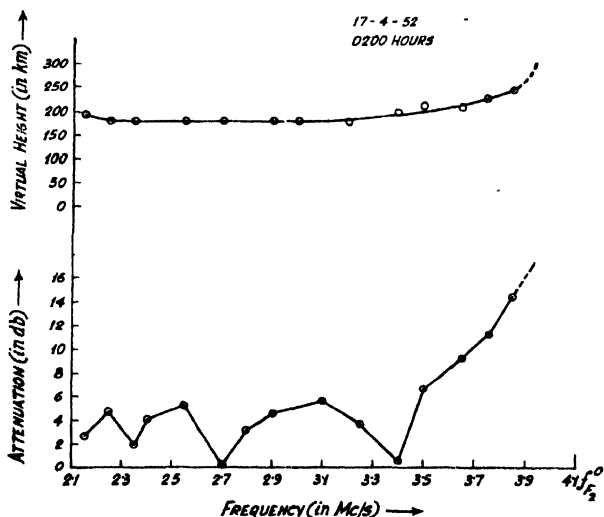


FIG. 2

Variation of absorption with frequency and the corresponding  $P$ - $f$  curve as observed at 02 hour 00 min. L. M. T. on 17.4.52.

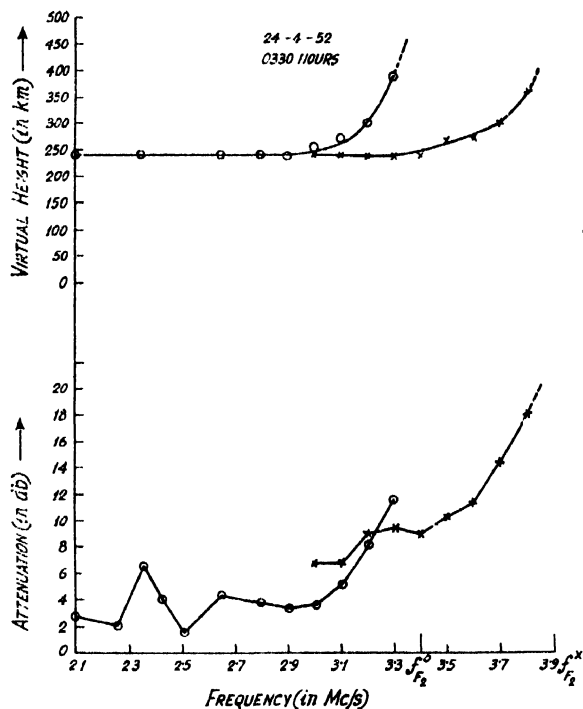


FIG. 3

Variation of attenuation with frequency and the corresponding  $P'-f$  curve as observed at 03 hour 30 min. L. M. T. on 24.4.52.

Figure 2 illustrates a typical night time absorption, during a quiet period and in the absence of  $E_s$ . Attenuation is very small (average of about 2 db compared to about 20 db, of figure 1), excepting near the critical frequency of the F layer. The random changes in the amplitudes of the echoes are however, much greater at lower frequencies: hence, the true attenuation at low frequencies is given rather by the mean curve and not by the point to point curve as drawn. Near the critical frequency, the echo amplitude becomes more or less steady, increasing the accuracy of observation.

Figure 3 depicts a typical night time absorption (also in absence of  $E_s$ ) but with magneto-ionic splitting. The attenuation of the extraordinary component is (and was always found to be) greater than that of the ordinary component (excepting at the critical frequency for the ordinary ray). This is in conformity with the theory. (Otherwise, the variations are as in figure 2 (Mitra, 1952).

Figure 4 illustrates a night time case when  $E_s$  was present. Up to the frequencies for which  $E_s$  echoes are present, there is increased attenuation of F echoes. As the collisional frequency in the E region is small, there is no appreciable absorption there. This increased attenuation appears to be due to partial penetration of wave energy and scattering at the sporadic

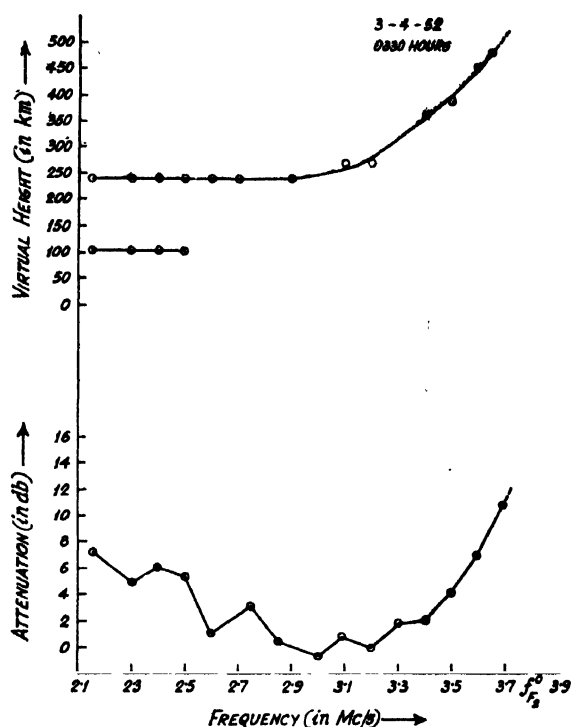


FIG. 4

Variation of absorption with frequency and the corresponding  $P'-f$  curve as observed at 03 hour 30 min. L. M. T. on 3.4.52.

E<sub>s</sub> layer. In other respects the results are as in figure 2. The apparent attenuation is found to be zero or even negative at some points. This is explained as due to the 'focusing effect'.

Figure 5 illustrates a typical case at night on the eve of the formation of an ionospheric disturbance—a blanketing E<sub>s</sub>. During the observation period there was only a transparent E<sub>s</sub> of low ionization density which gradually developed into a blanketing E<sub>s</sub> in about 15 minutes. The average absorption was much higher than in ordinary nights, being comparable to midday absorptions. The attenuation was extremely high below 2.3 Mc/s and above 3.5 Mc/s (near the penetration frequency of the F layer). The former attenuation may be explained as due to partial penetration and or scattering from the sporadic E<sub>s</sub> layer as in figure 4; the latter attenuation is due to partial penetration of the wave energy in the F region as in the previous cases. But, the unusually high average absorption in the range 2.4 to 3.5 Mc/s, which is below the frequency at which there is partial penetration in the F layer and is above the E<sub>s</sub> critical frequency (i.e. in the frequency range in which the wave completely penetrates the sporadic E<sub>s</sub> layer), cannot be so explained. From the observations it seems that there was, at the time, an appreciable ionization in the D region (where

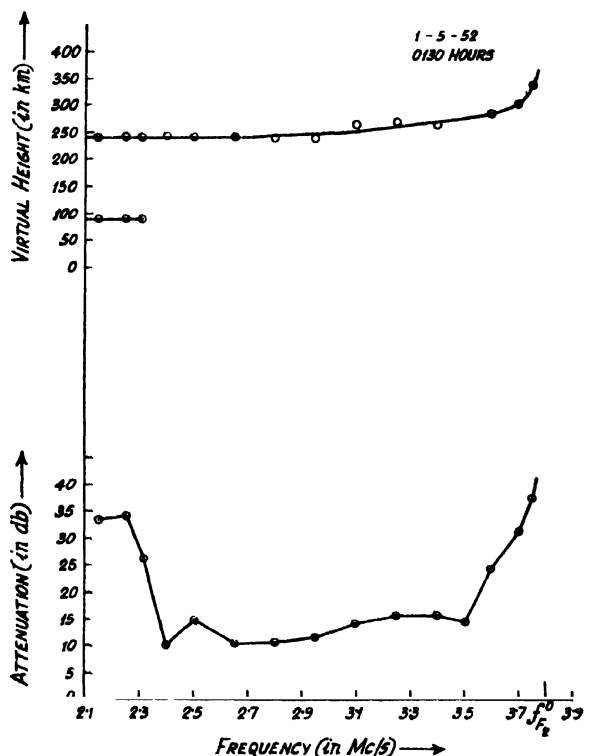


FIG. 5

Variation of absorption with frequency and the corresponding  $P'-f$  curve as observed at 01 hour 30 min. L. M. T. on 1.5.52.

the collisional frequency is high). This alone can explain such a large absorption at all frequencies. Such night time formation of sporadic D layers at low latitude stations have also been reported by Lillyett (1947) and others.

It thus seems that the occurrence of night time sporadic D is associated with the occurrence of sporadic E, which is often observed at Calcutta in premonsoon and monsoon months when thunderstorms are frequent. It is therefore not unreasonable to suppose that the thunderstorm mechanism which produces E, as suggested by Wilson (1925) (runway electrons and the strong field of the thundercloud-dipoles), may also be operative in producing increased D ionization. It may be mentioned in this connection that the observational data of Calcutta over a number of years show that there is definite correlation between the occurrence of E, and the occurrence of thunderstorm during the premonsoon and monsoon months (May to September). The problem of the production of sporadic D ionization at night, its correlation with night time E, and with the occurrence of thunderstorms forms a subject of further study.

#### 4. CONCLUSION

Results obtained in the previous sections show that there is partial penetration of the wave energy near the penetration frequencies of the E and F layers, there being more penetration *i.e.* less reflection for the former. Of the magneto-ionically splitted waves, the extraordinary component suffers higher absorption in conformity with theoretical calculations. The night time absorption is generally low as the normal D layer is absent at night. But the absorption becomes very high in certain nights and this has been explained as due to the formation of sporadic D's. The sporadic D's are found to be associated with E<sub>s</sub> and thunderstorms (as observed in premonsoon and monsoon months in Calcutta for a number of years) and their origin may be due to thunderclouds, in the same manner, as suggested by Wilson for the formation of E<sub>s</sub>.

#### ACKNOWLEDGMENT

The author's grateful thanks are due to Prof. S. K. Mitra for his kind guidance and help. The author is also indebted to the Scientific Man Power Committee, Government of India, for providing him with a scholarship.

#### REFERENCES

- Banerjee, R. B., 1951, *Ind J Phys*, **25**, 359.  
 Benner, A. H., 1951, *Proc. I. R. E.*, **39**, 186.  
 Best, J. F. and Ratcliffe, J. A., 1931, *Proc. Phys. Soc.*, **50**, 233.  
 Booker, H. G., 1949, *J. Geo. Res*, **54**, 243.  
 Beynon, W. J. G., 1948, *Jour. I. E. E.*, **95**, 325.  
 Best, J. F., Ratcliffe, J. A. and Wilkes, M. V., 1936, *Proc. Roy. Soc*, **156**, 614.  
 Bracewell R. N., 1948, *Jour. I. E. E.*, **95**, 326.  
 Budden, K. G., 1951, *Phil. Mag. Ser. 7*, **13**, 833.  
 Budden, K. G., Ratcliffe, J. A. and Wilkes, M. V., 1939, *Proc. Roy. Soc*, **171**, 186.  
 Appleton, E. V., and Piddington, J. H., 1938, *Proc. Roy. Soc.*, **164**, 467.  
 Appleton, E. V., Beynon W. J. G. and Piggot, W. R., 1948, *Nature*, **161** 967.  
 Ellyett, C. D., 1947, *Terr. Mag. and Atmos. Elec.*, **52**, 1.  
 Hacke, J. E. (Jr.), 1948, *Proc. I. R. E.*, **36**, 724.  
 Hacke, J. E. (Jr.) and Keiso, J. M., 1948, *Proc. I. R. E*, **36**, 1477.  
 Jaeger, J. C., 1947, *Proc. Phy. Soc.*, **59**, 87.  
 Mitra, A. P., 1951, *J. Geo. Res.*, **56**, 373.  
 Mitra, S. K., 1952, *The Upper Atmosphere*, Second Edition, Asiatic Soc. Cal. p. 186.

Martyn, D. F., 1953, *Proc. Phys. Soc.*, **47**, 323.

Rawer, K. and Bill. K., 1951, *J. Atmos and Terr. Phys.*, **2**, 51.

Report of the Radio Research Board, England, 1950.

Tayler, E. W., 1948, *Nat. Bureau, of Standards, U. S. Dept. Com.*, **41**, 575.

White, F. W. J. and Brown, L. W., 1936, *Proc. Roy. Soc* , **183**, 639.

White, F. W. J. and Straker, T. W., 1930, *Proc. Phys. Soc.*, **51**, 865.

# A STUDY ON THE TRIGGERING OF A PLATE-COUPLED MULTIVIBRATOR BY NEGATIVE PULSES\*

By SUNIL KUMAR SEN AND BIMAL KRISHNA BHATTACHARYYA

INSTITUTE OF NUCLEAR PHYSICS, CALCUTTA UNIVERSITY

(Received for publication, July 5, 1952)

## Plates XXII A-B

**ABSTRACT.** A study has been made on the triggering of the plate-coupled multivibrator by negative pulses. It has been observed that the voltage forms of different electrodes of such a multivibrator are markedly influenced by the form of the input pulses. In general, the triggering of such a multivibrator depends largely on the amplitude of the input pulse. It has been observed that triggering is more perfect by small amplitude pulses than by those of larger amplitudes, which is contrary to the general concept of triggering such a plate-coupled multivibrator. These are inherent characteristics of such a circuit, and the coupling valve is mainly responsible for it. Oscillograms of the voltage forms of different electrodes of the multivibrator have been presented.

A mathematical analysis of the transient characteristics of the multivibrator for different types of input pulses has been given. The theoretical curves have been plotted and it has been shown that these curves fit well with the oscillograms.

## INTRODUCTION

Multivibrator circuits now a days are used widely and mostly in timing circuits. There are different types of multivibrator circuits in use. The authors had the opportunity of closely studying the driven plate-coupled multivibrator which was utilised in producing delays between two signals from G-M counters to study the short-lived metastable states in titanium (46) (Nag, Sen and Chatterjee, 1949)

## EXPERIMENTS AND THE OBSERVATIONS

A detailed investigation has been made on the triggering of a plate-coupled multivibrator by negative pulses and the following observations were made therefrom.

(1) The different electrode voltage forms of the multivibrator are markedly influenced by the form of the input pulses.

(2) In general, the triggering of the multivibrator depends largely on the amplitude of the input pulse.

\*Communicated by Prof. M. N. Saha, F.R.S.

(3) The value of the coupling condenser  $C_2$  in figure 1 has much to alter the performance of the multivibrator.

(4) These are inherent characteristics of such a multivibrator circuit and the coupling valve is mainly responsible for it.

The experimental arrangement is shown in figure 1. A negative pulse from a pulse generator, (Banerjee, 1945) at the input of 6 AK 5 (coupling valve) is one stage amplified and applied to the grid of  $T_2$  through the

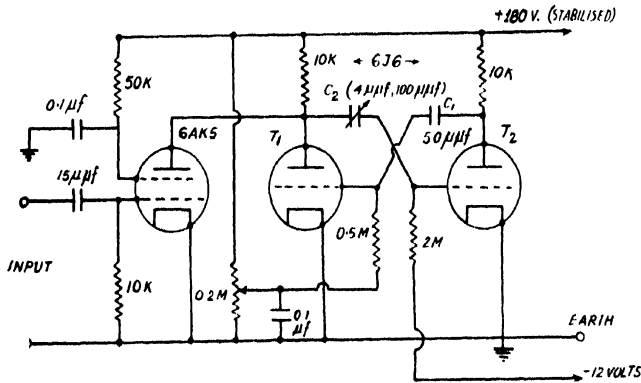


FIG. 1

Circuit diagram of the driven plate-coupled multivibrator.

condenser  $C_2$ . The grid of  $T_2$  is returned to a negative voltage ( $-12$  volts) so that initially  $T_1$  is non-conducting. With the arrival of a positive pulse at the grid of  $T_2$ ,  $T_2$  becomes conducting and its plate-point voltage decreases. This decrease of anode potential of  $T_2$  is transmitted through  $C_1$  to the grid of  $T_1$  (returned to positive voltage), whose anode potential then rises. The rise of  $T_1$  anode potential is again transmitted to the grid of  $T_2$  and the action is cumulative with the result that  $T_1$  becomes non-conducting and  $T_2$  fully conducting.

This cumulative or regenerative switching action, which ends with the plate current of  $T_1$  reduced to zero and that of  $T_2$  increased to a maximum, takes place extremely rapidly, in a small fraction of a microsecond in a well-designed multivibrator and in our theoretical discussion we shall assume this switching action to be instantaneous.

The positive pulse at the grid of  $T_2$  cannot cause the switching action to start if it is not large enough to raise the grid potential of  $T_2$  above cut-off and cause current to flow in the plate of  $T_2$ .

At the end of the switching action  $C_1$  will begin to discharge so that the grid voltage of  $T_1$  will begin to rise exponentially so much so that the cut-off bias voltage of  $T_1$  is reached,  $T_1$  begins to conduct and reverse regenerative switching process takes place by which  $T_1$  again becomes conducting and  $T_2$  non-conducting. This switching process is also extremely



rapid so that the process may also be assumed to be instantaneous for theoretical discussions.

Now, when  $T_1$  has again become conducting instantaneously, a high negative voltage is transferred to  $T_2$ -grid. Since the grid of  $T_2$  is returned to 12 volts negative, it cannot remain permanently at the high negative voltage and hence the condenser  $C_2$  will discharge to -12 volts exponentially. Thereafter the multivibrator tubes come to their original states and these states will continue to persist unless another negative pulse arrives at the input of 6 AK 5.

The grid of 6 AK 5 is normally at zero potential. The plate voltage of 6 AK 5, when both 6 AK 5 and  $T_1$  are conducting initially, is 75 volts. Now, as a negative pulse is applied to the grid of 6 AK 5, generally both 6 AK 5 and  $T_1$  are simultaneously made non-conducting and condenser  $C_2$  begins to charge. While the condenser is charging, the grid of 6 AK 5 falls to zero as the input pulse terminates. This makes 6 AK 5 conducting and the plate voltage of 6 AK 5 consequently comes down. Since  $T_1$  is still non-conducting, the plate voltage of 6 AK 5 which is also the plate voltage of  $T_1$ , finally comes down to a voltage higher than it was when both the tubes were conducting. Under this condition the condenser  $C_2$  will be experiencing simultaneously two changes of voltages, a growth of voltage due to charging as  $T_1$ -plate current is cut-off and a decay of voltage as 6 AK 5 is made conducting. Consequently, the actual voltage across the condenser will be the resultant of these two.

The plate current of 6 AK 5 may not always become zero when a negative pulse is applied at the grid of 6 AK 5. If the amplitude of the input pulse is big enough, then only 6 AK 5 will be non-conducting and the plate voltage of  $T_1$  may rise to its highest voltage. In all other cases, when the amplitude is small, there remains always in the plate of 6 AK 5 a current although  $T_1$  is non-conducting.

Oscillograms have been taken of the voltage forms of the different electrodes of the multivibrator with input pulses of various amplitudes and are represented in figures (i)-(iv) in Plates XXII A-B.

The photographs have been taken on a Cossor double beam oscilloscope (Model No. 1035). Input pulses have been applied to one beam and the electrode voltages of the multivibrator to the other. The multivibrator electrode voltages were not directly applied to the vertical plates of the oscilloscope but through a cathode follower circuit so that actual voltage forms are not changed during recording.

#### *Small Amplitude :*

Figures i (a), (b) and (c) [Plate XXII A] show the anode voltage of  $T_1$ , anode voltage of  $T_2$  and the grid voltage of  $T_1$ , respectively with  $C_2 = 4\mu\mu F$  and input pulses are shown in each photograph. In this case the input pulse

amplitude is not big enough to completely cut-off the plate current of 6 AK 5, though the  $T_1$ -plate current is zero. With  $C_2 = 4\mu F$ , the charging time is small so that very soon after  $T_1$  is made non-conducting  $C_2$  is fully charged and the anode voltage of  $T_1$  is raised to a high voltage near the supply voltage (not equal to the supply voltage because 6 AK 5 was not completely non-conducting ; it still had a plate current). Generally the anode voltage of  $T_1$  should remain constant at this value as long as  $T_1$  grid is held negative beyond its cut-off value. But although  $T_1$  is still non-conducting, 6 AK 5 is highly conducting because the grid of 6 AK 5 rises at the end of the input pulse, finally becoming zero. Consequently, the anode voltage of  $T_1$  will come down.

Figure *i* (b) shows the anode voltage form of  $T_2$  while figure *i* (c) that of  $T_1$ -grid voltage. It will be seen that the forms of these electrode voltages are similar.

Figures *ii* (a), (b) and (c) [Plate XXII A] show the  $T_1$ -anode voltage,  $T_2$ -anode voltage and  $T_1$ -grid voltage respectively with the same input pulse as before, but now  $C_2 = 100\mu F$ . In this case the charging time is very large so that long time after  $T_1$  is made non-conducting, the condenser  $C_2$  is charged to its full voltage. In the meantime since the grid of 6 AK 5 has been driven positive, the plate voltage of  $T_1$  has come down. This time it will be observed that the kink in the plate voltage of  $T_1$  is below the flat portion of the square top pulse and that the kink is less pronounced although the input pulse is the same as before. This can be explained as below.

Since  $C_2$  is large, the charging time is long so that long before the condenser has been charged to its full voltage, the grid of 6 AK 5 is driven positive and therefore the kink appears in the lower portion of the voltage form. Also when 6AK5 has been made less conducting by the negative drive of the grid of 6AK5, the plate voltage of  $T_1$  could not rise much from its initial value because of the large time constant and so the kink is not so pronounced as before. In the previous case,  $T_1$ -plate voltage reached the maximum value within a very short time and came down right from there when 6 AK 5 was again made conducting.

#### *Large amplitude :*

Figures *iii* (a), (b) and (c) [Plate XXII B] represent the anode voltage of  $T_1$ , anode voltage of  $T_2$  and the grid voltage of  $T_1$  respectively when the input pulse is very big and  $C_2 = 4\mu F$ . From the figures it will be observed that the output pulses are not like those from a multivibrator. Further, it was noted that changing the grid voltage of  $T_1$ , there was no appreciable change of the pulse width. At the first sight it will appear that the multivibrator did not trigger. But this is not so because the other electrode voltages have also been photographed under the same condition and shown in figures (iii)

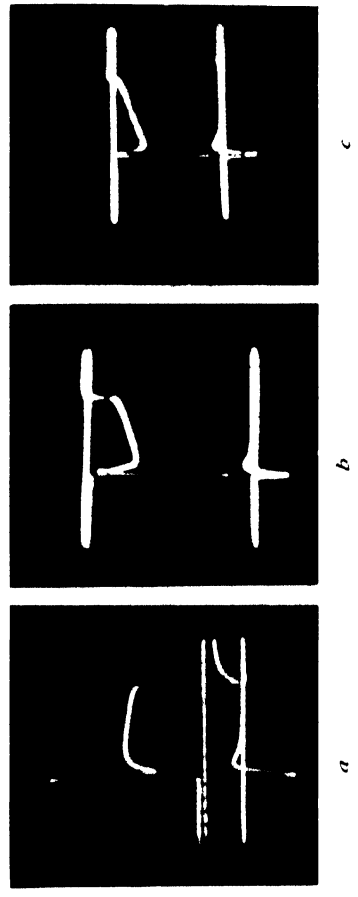


Fig. 1

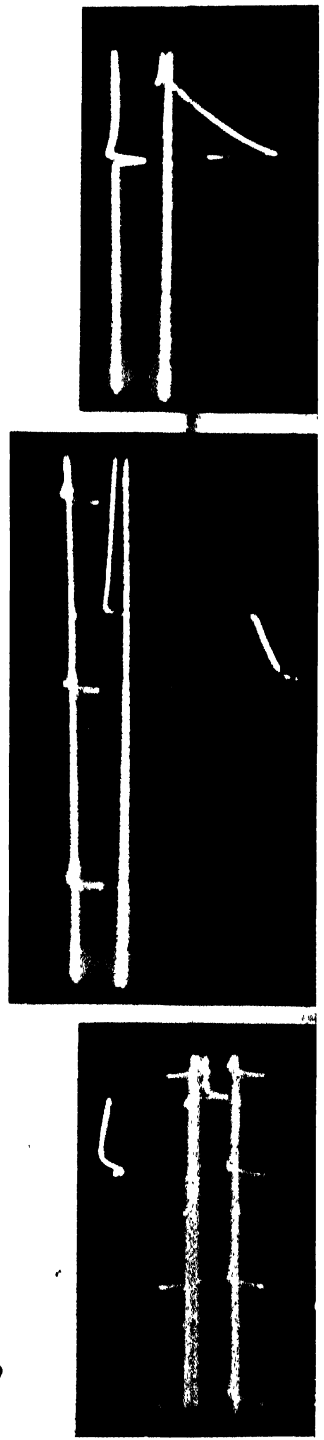


Fig. 2

a

Fig. 1:  $C_2 = 4\mu\mu F$

Input pulse—sharp and small amplitude shown at the bottom

- (a)  $T_1$  - plate voltage;
- (c)  $T_1$  - grid voltage

b

Voltage forms at different electrodes

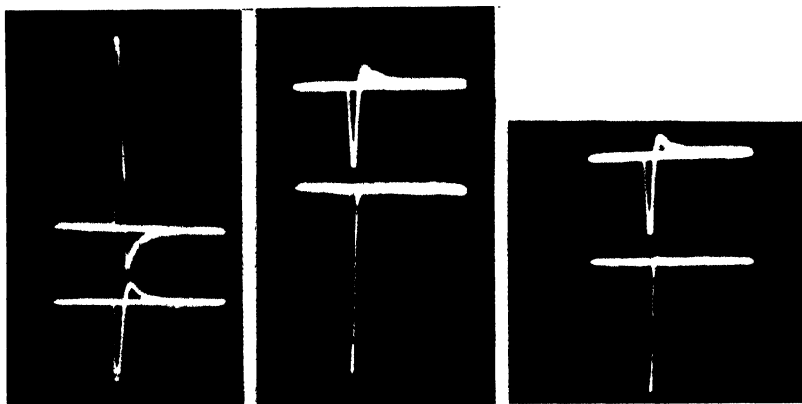
Fig. 2:  $C_2 = 100\mu\mu$

Input pulse—sharp and small amplitude shown at the bottom in (a) and at the top in (b) and (c).

- (a)  $T_1$  - plate voltage;
- (b)  $T_2$  - plate voltage
- (c)  $T_1$  - grid voltage

c

Fig. iii

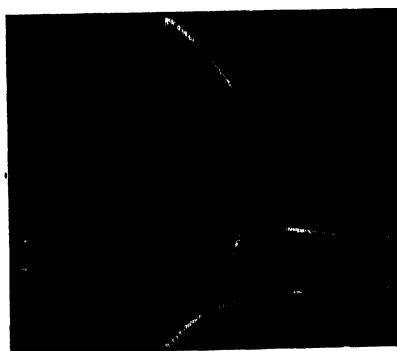


$$C_2 = 4\mu\mu\text{F}$$

Input pulse—sharp and big amplitude shown at the bottom in (a) and at the top in (b) and (c).

(a).  $T_1$  - plate voltage ; (b).  $T_2$  - plate voltage ; (c).  $T_1$  - grid voltage.

Fig. iv



$$C_2 = 4\mu\mu\text{F}$$

Input pulse - wide and big amplitude shown at the bottom.

$T_1$  - plate voltage.

(b) and (c) which suggests that with the arrival of a negative pulse at the input of 6AK5, both 6AK5 and  $T_1$  are made non-conducting as well as  $T_2$  conducting. This behaviour of the multivibrator circuit can be explained with the help of figure 1. As the input pulse amplitude is very big, the rise of anode voltage is also greater than before, because previously, the input pulse amplitude was not big enough to completely cut-off the plate current of 6AK5 and as such let  $T_1$ -anode voltage rise further. So the negative voltage transferred to  $T_2$  grid through  $C_2$ , when the plate of 6AK5 comes down at the end of the input pulse is also greater. The result is that  $T_2$ -anode voltage rises back too high to be transferred to  $T_1$ -grid through  $C_1$  to drive it towards zero voltage. Since this positive drive of  $T_1$ -grid is large enough to take the  $T_1$ -grid on the positive side of its cut-off bias value, this will result in changing from its non-conducting to conducting state and thus switching off the current from  $T_2$  to  $T_1$  rather abruptly. If we now compare figures ii (b) and (c) we find that positive drive of  $T_1$ -grid was not sufficient to take it beyond cut-off bias and that is why the states of  $T_1$  and  $T_2$  were not disturbed. It can also be observed from figure iii (a) that the output form of  $T_1$ -anode voltage is unlike that of the input pulse and it shows definite sign that the multivibrator becomes unstable abruptly.

Under the same condition (with big input pulse) triggering occurs when the condenser  $C_2$  of  $4pF$  is replaced by a large value condenser,  $C_2 = 100pF$ . This is due to the fact that when 6AK5 and  $T_1$  are made non-conducting, the plate voltage of  $T_1$  cannot rise faster, so that in the meantime, the grid of 6AK5 is driven positive making it conducting. The resultant negative pulse transmitted to grid of  $T_2$  is, therefore, not big enough to make it much negative.

Figure iv shows the anode voltage form of  $T_1$  when the input pulse is much broader and large in amplitude. It will be noticed that the widths of both the input pulse and the multivibrator output pulse are equal. Actually, the width of the multivibrator pulse ought to have been greater than this. But since the amplitude of the input pulse is large,  $T_1$  has been forcibly brought down to its original state by the positive drive of the input pulse proving that the output pulse is not at all independent of the input pulse.

#### SUMMARY AND DISCUSSION OF EXPERIMENTAL RESULTS

The output voltage forms of the multivibrator are not completely independent of the form of input pulses. As the coupling valve is conducting even when  $T_1$  is non-conducting, the plate voltage of  $T_1$  can never remain constant at the supply voltage. The quiescent voltage of the non-conducting tube ( $T_1$ ) is then equal to the voltage at which 6AK5 remains conducting. The use of pentode instead of a triode as the coupling valve ensures plate

current to be constant inspite of the plate voltage changing when  $T_1$  goes from conducting to non-conducting state.

In general, triggering of the multivibrator depends largely on the amplitude of the input pulse. If the initial plate current of 6AK5 is small, then with very small input pulse, it will be easily made non-conducting and very small pulses may not trigger the multivibrator at all. If, however, the screen voltage of 6AK5 is such that it initially draws a large plate current, the multivibrator may be easily triggered by very short pulses. But difficulties are being encountered when the input pulses are big. With big input pulses, the change of plate current is greater than that with the small pulses so that when 6AK5 grid is driven positive at the end of the input pulse, the output pulse amplitude of 6AK5 may be big enough to switch the current from  $T_2$  to  $T_1$ , bringing the multivibrator to its original state. These are all inherent characteristics of the plate-coupled multivibrator driven by negative pulses and the coupling valve is mainly responsible for them. The phenomena are pronounced when the coupling valve is sharing a large current although the multivibrator can be triggered by very small input pulses in this condition. When the plate current drawn by 6AK5 is very small, the phenomena are not so pronounced but at the same time it cannot be triggered by short amplitude pulses.

Thus, in general, when the input pulses have different amplitudes as those from a photomultiplier, one cannot be sure that the multivibrator is triggered by pulses of all amplitudes. In that case the pulses may have to be equalised before applying them to the input of 6AK5.

It has been observed that by making  $C_2$  larger, it may be possible to trigger the multivibrator with large amplitude pulses of very short duration when 6AK5 is drawing large plate current. Because, due to large charging time of  $C_2$  the plate voltage of 6AK5 may not rise much and in the meantime the grid of 6AK5 is already driven positive.

All these effects will not be observed in the case" of the plate-coupled multivibrator driven by positive pulse. Since in that case, normally the coupling valve and  $T_1$  are non-conducting while  $T_2$  is conducting. When a positive pulse is applied to 6AK5 input, it becomes conducting and by cumulative effect,  $T_1$  becomes conducting and  $T_2$  non-conducting simultaneously. At the first impulse, the grid of  $T_2$  is driven to a large negative voltage after which  $C_2$  begins to discharge. The tube  $T_2$  remains non-conducting so long the grid of  $T_2$  is beyond its cut-off bias voltage. Thus under this condition when 6AK5 is again non-conducting at the end of the input pulse (in this case the grid of 6AK5 is driven negative to its original voltage when the input pulse vanishes), the grid voltage of  $T_2$  is suddenly driven positive but not beyond its cut-off bias so that  $T_2$ -anode voltage is unaffected. As a result, the conditions of  $T_1$ -anode voltage,  $T_2$ -anode voltage as well as of the grid voltage of  $T_1$  remain unchanged.

# THEORETICAL ANALYSIS

It has been shown earlier that the height and width of the negative pulse at the input of 6AK5 have considerable effect on the triggering of the plate-coupled multivibrator.

We shall now proceed to consider the effect of the following negative pulses at the input of 6AK5 on the triggering of the multivibrator on theoretical basis :

- (i) Narrow and very short pulses that cannot make 6AK5 non-conducting.
- (ii) Narrow and short pulses that cannot make 6AK5 non-conducting but trigger the multivibrator.
- (iii) Narrow pulses of such height as to make 6AK5 non-conducting.
- (iv) Narrow and big pulses.

In group (i), pulses of such size come which cannot make the triggering possible. If the input negative pulse is very small, the plate current of 6AK5 will not very much diminish so as to increase the plate voltage of 6AK5 i.e. that of  $T_1$  and thus the grid voltage of  $T_2$  above its cut-off value. So  $T_2$  will not conduct and thus triggering is not possible.

If the pulses are so large as not to make 6AK5 non-conducting but to increase the plate voltage of 6AK5 to such a magnitude that causes the grid voltage of  $T_2$  to rise above its cut-off value, the triggering is possible. This type of pulse comes in group (ii).

In group (iii), lie those types of pulses which make 6AK5 non-conducting but the non-conducting period is very small compared to the actual time-period over which  $T_2$  remains conducting. We shall first of all, consider this type of pulse for our theoretical analysis.

To make the analysis clear and simple we consider first the effect of a negative pulse (figure 2) at the grid of 6AK5. During the time interval  $t=0$  and  $t=t_1$ , the plate current of 6AK5 is zero, assuming of course that the grid of 6AK5 is driven to maximum negative voltage instantaneously. In general, 6AK5 will be again conducting at  $t \geq t_1$  reaching the phase of full conduction at  $t=t_2$ .

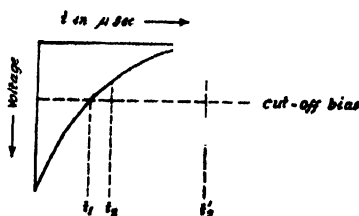


FIG. 2

Between time  $t=t_1$ , and  $t=t_2$ , however, the plate current of 6AK5 is very small so that for our theoretical analysis we shall consider the period

of actual conduction of 6AK5 to be between  $t=t_2$  to  $t=t_2'$ . Here  $t_1$  denotes the time at which the grid voltage of 6AK5 attains just the cut-off bias voltage while  $t_2$  denotes the time after which the grid attains such a value as to enable 6AK5 to draw appreciable current for its proper functioning.

(a) *Transient plate-point voltage of  $T_1$* : Now when considering the plate voltage of  $T_1$ , we shall assume that the plate currents of both 6AK5 and  $T_1$  are cut-off instantaneously, though actually a small fraction of a microsecond elapses during the process. As the plate currents are cut-off for the period  $0 < t < t_1$ , the equivalent circuit when considering the plate-voltage of  $T_1$  is given by figure 3. By applying Thevenin's theorem, figure 3 may be simplified to figure 4,

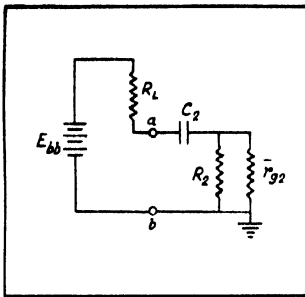


FIG. 3

$R_L$  = plate-load resistance.

$C_2$  = interstage coupling condenser.

$R_2$  = grid leak resistance of  $T_1$

$r_{g2}$  = conducting resistance between the cathode and grid of  $T_2$   
(when  $T_2$ -grid is driven positive).

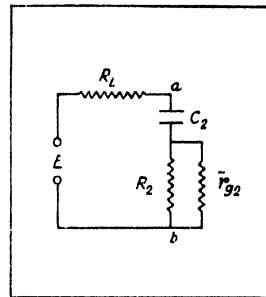


FIG. 4

The effect of inter-electrode capacitances and stray wiring capacitances at the output of  $T_1$  has been neglected in the above figures because the conducting resistance ( $r_{g2}$ ) between the grid and cathode of  $T_2$  is of very small value.

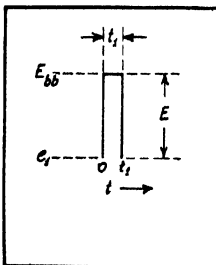


FIG. 5

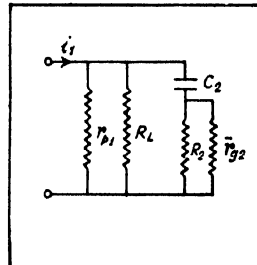


FIG. 6

Figure 5 represents the voltage step at the input of the circuit of figure 4 while the amplitude of the voltage step during  $0 < t < t_1$  is given by  $E = E_{b,b} - e_1$  where  $E_{b,b}$  = supply voltage and  $e_1$  is the plate-point voltage when both 6AK5 and  $T_1$  are conducting.



When 6AK5 begins to conduct between  $t=t_1$  to  $t=t_2'$  the equivalent circuit is as given in figure 6. The time period between  $t=t_1$  to  $t=t_2'$  may be again divided into two parts viz. (1)  $t=t_1$  to  $t=t_2$  when 6AK5 draws negligible current and (2)  $t > t_2$  when 6AK5 reaches gradually the phase of full conduction and the current of 6AK5 has reached a steady value.

For the first part i.e. during the period  $t_1 < t < t_2$ , the plate current of the pentode 6AK5 is negligible and the plate resistance  $r_{p1}$  is very large compared to  $R_L$  so that circuit of figure 6 is simplified to that in figure 7 where  $i_1=0$  and  $R_2$  has been omitted since the conducting resistance  $r_{o2}$  is very small compared to  $R_2$ .

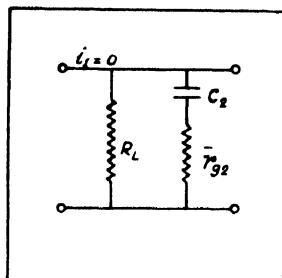


FIG. 7

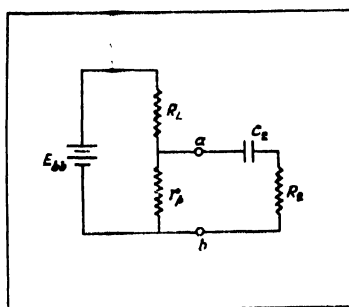


FIG. 8

The plate-voltage of  $T_1$  during the period  $t > t_2$  will be dependent on the change of  $T_1$ -plate voltage during  $t_1 < t < t_2$  and two cases may be considered here.

*Case (a):  $C_2$  of small value:* It will be shown later (eqn.2) that for small value of  $C_2$  (say,  $^{\circ}4$  pF), the  $T_1$ -plate voltage will diminish considerably in the time  $t_1 < t < t_2$  and as such the grid of  $T_2$  will be driven towards negative voltage not to draw any grid current.  $r_{o2}$  then may be taken open and thus the equivalent circuit for the period  $t > t_2$  becomes as shown in figure 8.

When  $C_2$  is big (say, 100 pF), the  $T_1$ -plate voltage will not change appreciably during time  $t_1 < t < t_2$  and consequently  $T_2$ -grid voltage will not come down to such an extent as to stop the grid current altogether; the grid current will, however, be decreased so that  $r_{o2}$  will be large. But  $r_{o2}$  will still be small compared to  $R_2$  and the equivalent circuit in this case for  $t < t_2$  will be as shown in figure 9.

The plate resistance  $r_p$  of 6AK5 which is a pentode, is very large compared to the load resistance  $R_L$  and assuming the internal resistance of the voltage supply to be zero, the impedances of the networks (figures 8 and 9) looking back into the terminals  $a-b$  are the same which may be taken to be  $R_L$ . When 6AK5 begins to conduct steadily during  $t > t_2$  the plate voltage of  $T_1$  will come down from the value  $E_{bb}$  to a lower value  $E_1$ , say, when the output  $a-b$  is open-circuited and the voltage across  $a-b$  is as shown

in figure 10 where  $e_1$  is the reference voltage equal to the plate-voltage of  $T_1$  when both 6AK5<sup>†</sup> and  $T_1$  are conducting. Norton's theorem is now

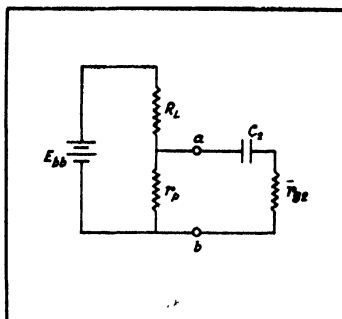


FIG. 9

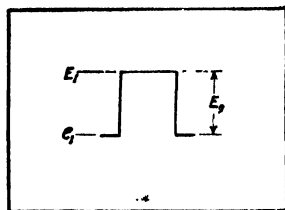


FIG. 10

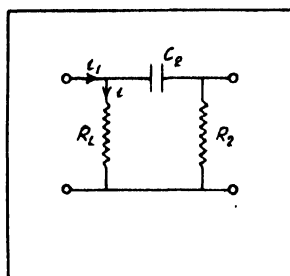


FIG. 11

applied to the circuits shown in figures 8 and 9 to obtain the simplified equivalent circuits as given in figures 11 and 12 respectively where  $i_1$  is the short circuited current at  $a-b$  (figure 13).

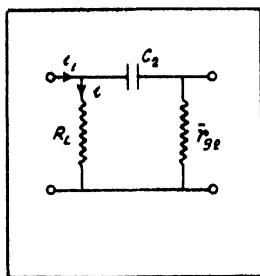


FIG. 12

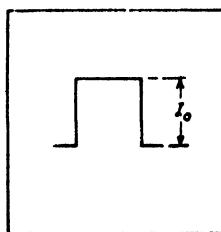


FIG. 13

The equivalent circuits (figures 11 and 12) are valid only for the time interval  $t_2 < t < t_3$ , where  $t = t_3$  reckons the time at which  $T_1$  again begins to conduct, or in other words, the plate current of  $T_1$ , remains cut-off from  $t = 0$  to  $t = t_3$ .  $i_1$  can also be analytically represented by

$$i_1 = I_0 U(t); [t_2 < t < t_3]$$

The plate point voltage of  $T_1$  is equal to the sum of the voltages across the coupling condenser  $C_2$  and the grid leak resistance  $R_2$ . This voltage may now be calculated by four distinct steps :

*Step 1 :* ( $0 < t < t_1$ ). The step voltage of figure 5 is applied to the input of figure 4. Taking  $R_2$  to be very large compared to  $r_{g2}$ , the output plate point voltage during the interval  $0 < t < t_1$  has been found out to be

$$e_0 = E[1 - R_L/(R_L + r_{g2})e^{-t/(R_L + r_{g2})C_2}] \quad \dots (1)$$

*Step 2 :* ( $t_1 < t < t_2$ ). The step voltage is terminated at  $t = t_1$  to form a rectangular pulse (figure 5) so that the response across  $C_2 - R_2$  combination i.e. across  $R_L$  is found, assuming no current flowing in the input of figure 7, as

$$e_0 = e_0(t_1)e^{-(t-t_1)/T} \quad \dots (2)$$

where,

$$e_0(t_1) = \text{plate point voltage at } t = t_1$$

and

$$T = C_2(R_L + r_{g2}) \quad \dots (3)$$

*Step 3 :* ( $t_2 < t < t_3$ ). (a) If the coupling condenser is of small magnitude, the response is obtained by assuming the small rectangular pulse (figure 13) at the input of figure 11. The plate point voltage is found out to be

$$e_0 = R_L I_0 + e_0(t_2)e^{-(t-t_2)/T}; (t_2 < t < t_3) \quad \dots (4)$$

where

$$T = C_2(R_L + R_2)$$

$$I_0 = \text{the amplitude of the current at the input of figure 11}$$

$$e_0(t_2) = \text{the plate-point voltage at } t = t_2.$$

(b) If the coupling condenser is of large value the response is obtained by assuming the small rectangular pulse (figure 10) applied to the input of figure 12. Since  $r_{g2}$  in this step is different from that in steps 1 and 2, it will be denoted by  $r'_{g2}$ . The plate point voltage is calculated to be

$$e_0 = R_L I_0 + e_0(t_2)e^{-(t-t_2)/T} \quad \dots (5)$$

where

$$T = C_2(R_L + r'_{g2})$$

and the other constants are the same as given in equation (4).

At time  $t = t_3$  the small rectangular pulse terminates and  $T_1$  begins to conduct. The equivalent circuit for coupling between the plate of  $T_1$  and the grid of  $T_2$  can now be drawn as given in figure 14 where

$$e_g = \text{grid voltage of } T_1 \text{ for } t \geq t_3$$

Since  $R_2$  is very large compared to  $R_L$ ,  $R_2$  may be taken as open and reactance of the coupling condenser is so small as to be the practical equivalent of short circuit, figure 14 can be simplified to figure 15 as shown below :

So the plate point voltage which is the voltage across  $R_L$  is

$$e_1 = - \frac{\mu R_L^2}{r_p + R_L} e_g \quad \dots (6)$$

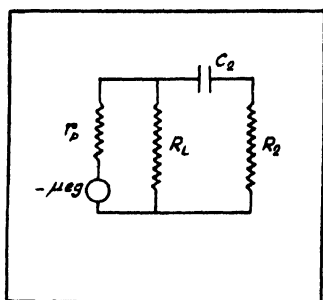


FIG. 14

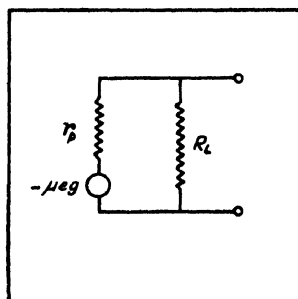


FIG. 15

We shall be able to show later that at  $t = t_3$

$$e_0 = \frac{R_1 R_2}{R_1 + R_2} I'_0 [e^{-t_3/T} - 1] \quad \dots (7)$$

Thus with the help of equations (7) and (8) we can find out the plate point voltage of  $T_1$  at  $t = t_3$  as

$$e_1 = -\frac{\mu R_L}{r_p + R_L} \cdot \frac{R_1 R_2}{R_1 + R_2} I'_0 [e^{-t_3/T} - 1] \quad \dots (8)$$

$(t > t_3)$

*Step 4 :* The voltage  $e_0(t_3)$  will begin to decrease with a time constant  $T_1$  which is equal to that with which the grid of  $T_1$  will begin to rise. The time constant, as will be shown later, is equal to  $C_1(R_L + r_{g1})$ . So the output voltage  $e_0$  is calculated to be

$$e_0 = e_0(t_3) e^{-\frac{t-t_3}{T}} \quad (t > t_3) \quad \dots (9)$$

The voltage waveform for the plate of the tube  $T_1$  is now drawn with the help of equations 1 to 9 (figure 23).

*Transient voltage in the plate of  $T_2$ .* To analyse the plate voltage of  $T_2$  we must form a clear picture about the current drawn by the plate of  $T_2$  at different times of the period during which  $T_2$  is conducting. Certain simplifying assumptions are to be made to have a not too complex analysis. First of all,  $R_2$  is taken to be grounded and not returned to H.T. Secondly the transition time which is necessary to make the plate current of  $T_2$  maximum is assumed to be instantaneous. Though this is not true, yet the time of switching over is very small compared to the actual time-period over which  $T_2$  remains conducting.

The current in the plate of  $T_2$  will remain maximum for a very short time  $t_1$  after which 6AK5 begins to conduct and the grid-voltage of  $T_2$  comes down.

During the interval  $t_1 < t < t_2$  the grid voltage of  $T_2$  will be reduced from its positive value and as a result the plate current of  $T_2$  will begin to diminish sharply and so the plate resistance ( $r_p$ ) of  $T_2$  will be taken to be very large during this interval.

The coupling condenser  $C_1$  which is moderately large, has little effect during the period between  $t=0$  and  $t=t_2$  when the rise and fall in the plate current of  $T_2$  are considerably steep. The effect of the inter-electrode and stray wiring capacitances cannot be neglected during this time; they really determine the times of rise and fall in plate point voltage of  $T_2$ .

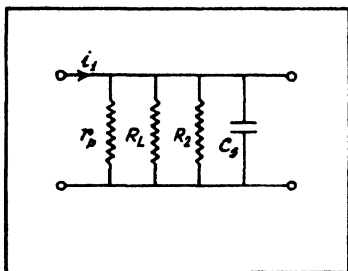


FIG. 16

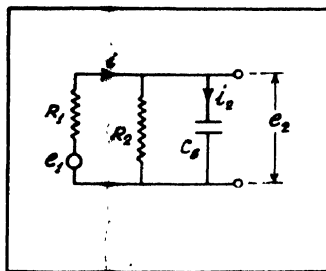


FIG. 17

The equivalent circuit during the time period  $0 < t < t_1$  for the tube  $T_2$  is as shown in (figure 16), where  $C_s$  takes into account of the stray wiring and inter-electrode capacitances. If Thevenin's theorem be applied and  $R_1$  be taken to be equivalent to the parallel combination of  $r_p$  and  $R_L$ , figure 16 can be simplified to the circuit as shown in figure 17 where  $e_1 = i_1 R_1$ . Since the coupling condenser has negligible effect on the output voltage  $e_2$  during this period the plate point voltage of  $T_1$  is the voltage across  $R_2$  or  $C_s$ . If the voltage  $e_1$  is taken to be a step function

$$e_1(t) = E_1 U(t) \quad (10)$$

the differential equation involving  $e_1(t)$  and  $e_2(t)$  is

$$e_1 \frac{R_1}{R_2} + C_s R_1 \frac{de_2}{dt} + e_2 = e_1 \quad (11)$$

Solving this equation, we have

$$e_2(t) = \frac{R_2}{R_1 + R_2} E_1 (1 - e^{-\gamma t}) \quad (12)$$

where

$$\gamma = \frac{R_1 R_2}{R_1 + R_2} \cdot \frac{1}{C_s} \quad (0 < t < t_1) \quad (13)$$

The equivalent circuit for the tube  $T_2$  during the period  $t=t_1$  and  $t=t_2$  is given in figure 18. Since in this interval  $r_p$  is very large and  $R_2$  is also very large compared to the reactance of  $C_s$ , a simplified equivalent circuit of figure 18 can be drawn (figure 19). The plate point voltage of  $T_2$  which is equal to  $e_2(t)$  is now found to be

$$e_2(t) = E_{bb} - [E_{bb} - e_2(t_1)] e^{-(t-t_1)/C_s R L} \quad \dots \quad (14)$$

where

$E_{bb}$  = plate-supply voltage

$e_2(t_1)$  = plate point voltage at  $t=t_1$ .

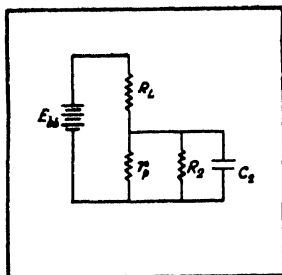


FIG. 18

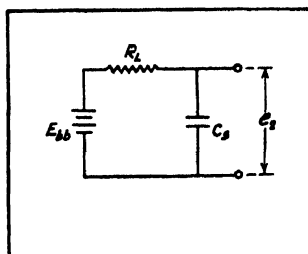


FIG. 19

After the time  $t=t_2$ , the plate current of  $T_2$  reaches a steady state. Since the plate current of  $T_2$  is then small,  $r_p$  is very large. In the reproduction of the flat top of the current pulse, which begins at time  $t=t_2$ , the coupling condenser  $C_1$  plays a major part while the shunting capacitance  $C_N$  is then practically open. So the equivalent circuit for coupling between the plate of  $T_2$  and grid of  $T_1$  becomes as drawn in figure 20 where  $R_1$  denotes the equivalent resistance for the parallel combination of  $r_p$  and  $R_L$  and  $R_2$  is the grid leak resistance of  $T_1$ .

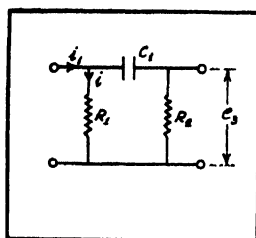


FIG. 20

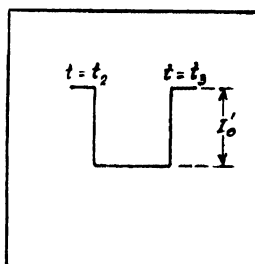


FIG. 21

The current drawn by the plate of the tube  $T_2$  remains steady at the small value in the interval between  $t=t_2$  and  $t=t_3$  after which the grid of the tube  $T_1$  rises so much as to enable  $T_1$  to conduct and following the cumulative switching action,  $T_2$  sharply regains its non-conducting state. So the current in the plate of  $T_2$  may well be represented by a rectangular pulse (figure 21) beginning at  $t=t_2$  and terminating at  $t=t_3$ , the amplitude of which is given by

$$I'_0 = -g_m e_g \quad \dots (15)$$

where  $g_m$  = mutual transconductance of tube which, for all purposes, may be assumed to be constant during the above mentioned period.

and

$e_g$  = grid voltage of  $T_2$

Now the current pulse may analytically be written as

$$i = I'_0 [U(t-t_2) - U(t-t_3)] \quad \dots (16)$$

where  $U(t-t_2)$  represents a unit step function beginning at  $t=t_2$ . If time is reckoned from  $t=t_2$ , equation (16) can conveniently be written as

$$i = I'_0 [U(t) - U(t-t_3)] \quad \dots (17)$$

The plate point voltage of  $T_2$  is the voltage across  $R_1$ . The differential equation involving the voltage  $e_2$  and current  $i_1$  in figure 20 is

$$\frac{de_2}{dt} + \frac{e_2}{T} = \frac{R_1 R_2}{R_1 + R_2} \frac{di_1}{dt} + \frac{R_1}{T} i_1 \quad (18)$$

where

$$T = C_1(R_1 + R_2)$$

Solving this equation with the help of equation (7) and with the initial condition that at  $t = t_2$ ,  $e_2(t) = e'_2(t_2)$ , we have

$$e_2(t) = R_1 I'_0 + e'_2(t_2) e^{-(t-t_2)/T} \quad (t_2 < t < t_3) \quad \dots (19)$$

At  $t = t_3$  the small current pulse is abruptly terminated. At that time the effect of the interstage coupling condenser is neglected due to the sharp change of current and so the plate voltage of  $T_2$  is equal to the voltage that is developed across  $R_2$  i.e. at  $t = t_3$ , the grid voltage of  $T_1$  and the plate voltage of  $T_2$  are exactly identical. The plate voltage of  $T_2$  is found to be

$$e_2(t_3) = \frac{R_1 R_2}{R_1 + R_2} I'_0 [e^{-t_3/T} - 1] \quad (20)$$

After time  $t = t_3$ , the tube  $T_2$  is non-conducting, whereas,  $T_1$  begins to conduct and so the equivalent circuit for  $t > t_3$  is changed to that shown in figure 22. The small conducting resistance  $r_{g1}$  between the grid and cathode of  $T_1$  is now put in parallel with  $R_2$ . Since  $R_2$  is very large compared to  $r_{g1}$ , it can be omitted from figure 22. Since  $T_2$  is non-conducting  $i_1 = 0$  and so, analysing the circuit of figure 22 we obtain,

$$\frac{de_2}{dt} + \frac{e_2}{T} = 0 \quad (21)$$

where

$$T = C_1(R_1 + r_{g1})$$

and

$$R_1 = R_L$$

Solving this equation we have

$$e_2(t) = e_2(t_3) e^{-(t-t_3)/T} \quad \dots (22)$$

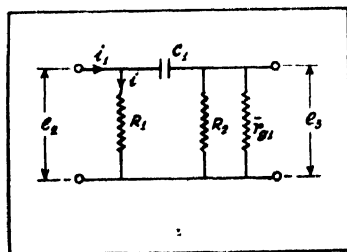


FIG. 22

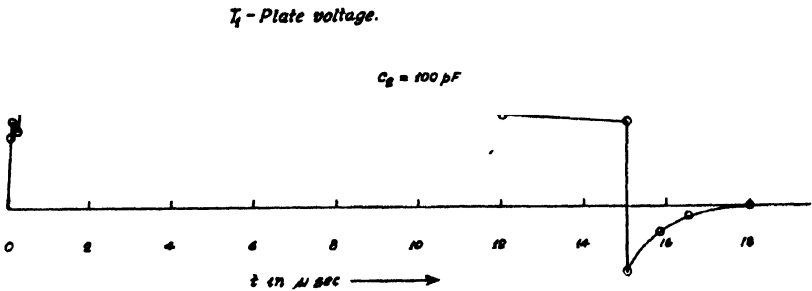
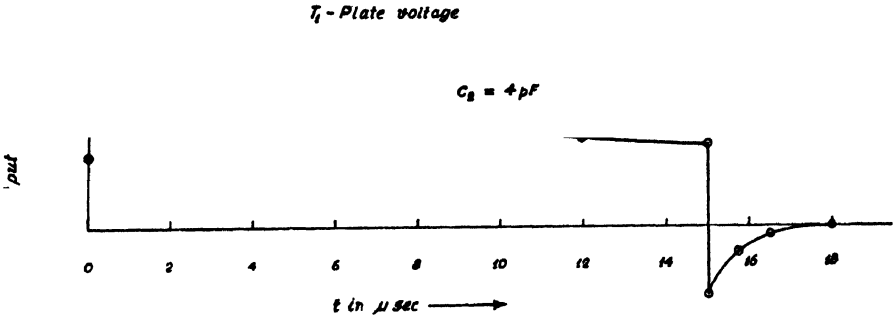


FIG. 23

The voltage waveform in the plate of  $T_2$  is now completely specified by equations (12), (14), (19), (20), (22) and plotted in figure (24).

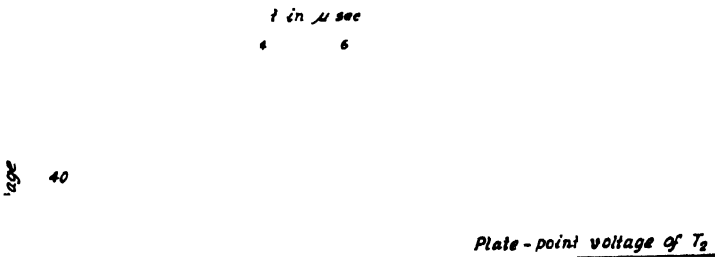


FIG. 24

*Transient Voltage in the Grid of  $T_1$ .* The grid voltage of  $T_1$  will show an almost identical nature as the plate voltage of  $T_2$  will do. The same equivalent circuits that were drawn to analyse the plate voltage of  $T_2$ , will explain the transient characteristics of the grid voltage in  $T_1$ .

Since the coupling condenser  $C_1$  has negligible effect on the different electrode voltage waveforms during the period  $t=0$  and  $t=t_2$ , the grid voltage of  $T_1$  which is the voltage across  $C_s$  (figures 17 and 19), is also the



voltage in the plate of  $T_2$ . So equations (12) and (14) will determine the transient voltage waveform in the grid of  $T_1$  during the two intervals between

$$(i) \ t=0 \text{ and } t=t_1$$

$$(ii) \ t=t_1 \text{ and } t=t_2$$

After time  $t=t_2$ , the voltage across  $R_2$  (figure 20) is the grid voltage of  $T_1$ . The differential equation for the circuit in figure 23 is

$$\frac{de_3}{dt} + \frac{e_3}{T} - \frac{R_1 R_2}{R_1 + R_2} \frac{di_1}{dt} \quad (23)$$

where  $i_1$  is given by equation (17). Solving this equation we have

$$e_3(t) = \frac{R_1 R_2}{R_1 + R_2} I'_0 \left| e^{-(t/T)} \right|; \quad (t > t_2) \quad (24)$$

$$e_3(t_3) = -\frac{R_1 R_2}{R_1 + R_2} I'_0 [e^{-t_3/T} - 1] \quad (t = t_3) \quad (25)$$

where

$$T = (R_1 + R_2)C_1$$

When  $t > t_3$ , the equivalent circuit shown in figure 22 is to be considered where  $i_1=0$  and  $R_2$  is very large compared to  $r_{o1}$ . So with the help of equation (23), the differential equation for the circuit in figure 22 can be written as

$$\frac{de_3}{dt} + \frac{e_3}{T} = 0 \quad (26)$$

Solving this, we have

$$e_3(t) = e_3(t_3)e^{-(t-t_3)/T} \quad \dots \quad (27)$$

So the grid voltage waveform can be drawn with the help of equations (12), (14), (24), (25) and (27) (figure 25).

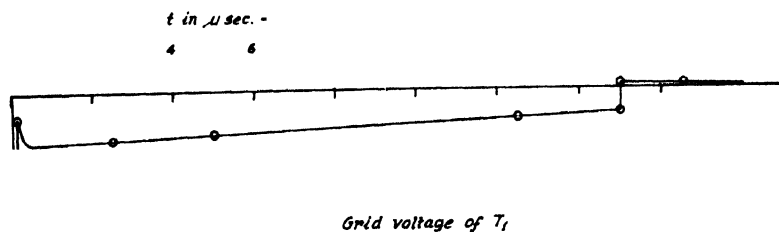


FIG. 25

The theoretical analysis has been made for the voltage waveforms at the different electrodes of the tubes of the multivibrator when the input pulse at the grid of  $T_2$  is of group (iii).

This analysis also holds good for the pulses of group (ii). This type of pulse can be represented by figure 26. Initially the plate current of 6AK5 is very small so that it can be regarded as virtually open for a very short time after the negative pulse has been applied to the grid of 6AK5. So the equivalent circuit for coupling between the plate of  $T_1$  and grid of  $T_2$  is given by figure 3 at that time and equation (1) then gives the plate-point voltage of  $T_2$ . Since the  $T_1$ -plate voltage does not rise so much as it would if 6AK5 becomes non-conducting, the transferred voltage in the grid of  $T_2$  is also less in this case and so  $r_{a2}$  is higher than it was when 6AK5 was non-conducting.

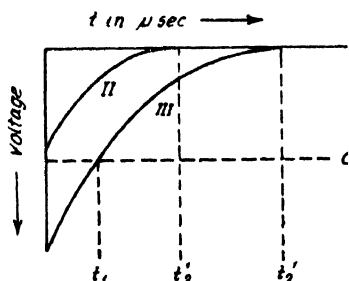


FIG. 26

Steps 2, 3 and 4 are evidently valid in this case also and this is why we can now conclude by saying that the voltage waveforms at the different electrodes of the multivibrator tubes which are obtained when triggering is done by a pulse of group (ii), are almost exactly identical with those found previously in our analysis for a negative pulse of group (iii) at the input.

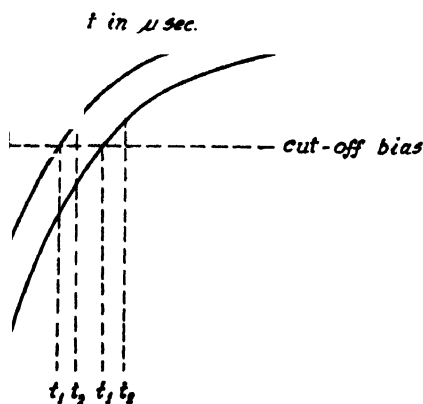


FIG. 27

*The effect of narrow and big pulses :* When the pulse is narrow and big (figure 27) the time  $t_1$  is slightly greater than that assumed for the pulses of group (iii). For the interval  $t_0 < t < t_1$  the voltage waveforms

at the plate of  $T_1$  and at the plate of  $T_2$  and grid of  $T_1$  are drawn with the help of equations (1) and (12) respectively.

During the period between  $t=t_1$ , and  $t=t_2$ , 6AK5 is gradually reaching the phase of full conduction and the grid voltage of  $T_2$  will begin to come down. Since the amplitude of the pulse is now big, this period ( $t_2-t_1$ ) is now greater than that in the case of pulses of group (iii). This is the interval when  $T_2$  -plate voltage and  $T_1$  -grid voltage will begin to rise (eqn. 14). Since ( $t_2-t_1$ ) is large in this case, the voltage in the grid of  $T_1$  will rise above its cut off value in the mean time making  $T_1$  conducting and simultaneously  $T_2$  non-conducting.

Thus the multivibrator waveforms at the different electrodes are altered markedly in this case.

The overshoot cannot rise too much since the grid voltage of  $T_1$  is increasing exponentially and as soon as the grid becomes positive, grid current is drawn and the overshoot is limited.

When  $t > t_2$ ,  $T_2$  -plate voltage and  $T_1$  -grid voltage will be given by equations (20) and (22). The  $T_2$  -plate voltage curve can then be plotted with the help of equations (8) and (9) respectively. Figures 28 and 29 show the theoretically plotted curves of  $T_1$  -plate voltage and  $T_2$  -grid voltage respectively.

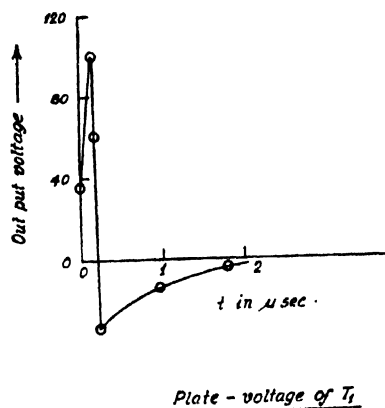


FIG. 28

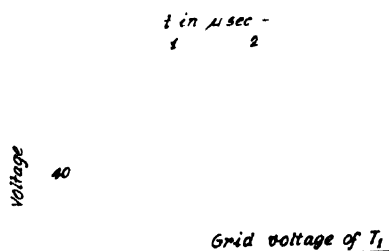


FIG. 29

## SUMMARY

The equivalent circuits have been considered and the expressions for the voltage waveforms of the different electrodes of the multivibrator have been deduced at three distinct time-intervals namely between (1)  $t=0$  to  $t=t_1$  when both 6AK5 and  $T_1$  are non-conducting, (2)  $t=t_1$  and  $t=t_2$  when only 6AK5 draws negligible current and (3)  $t=t_2$  and  $t=t_3$  when 6AK5 plate current is more or less steady,  $T_1$  being still non-conducting. These times have all been reckoned from the instant a negative pulse is

applied at the input of 6AK5 and so all the expressions could be related with the width of the input pulse.

Pulses of different amplitudes and widths have been considered. The experimental findings could well be explained by the theoretical analysis. The former conclusion that the triggering of such a multivibrator depends largely on amplitudes has been established as well by theoretical analysis. Theoretical curves for the voltage waveforms of the different electrodes of the multivibrator have been plotted with the equations derived and are found to fit well with the oscillograms.

#### ACKNOWLEDGMENTS

The authors' best thanks are due to Prof. M. N. Saha, F.R.S. and Dr. B. D. Nag for their keen interest in the work. They are grateful to Sri B. M. Banerjee for helpful discussions. The authors also wish to thank Sri A. P. Patro and Miss Sobhana Dhar for their help in taking photographs presented here.

#### REFERENCES

Banerjee, B. M., 1945, *Ind. J. Phys.*, **19**, 75,

Nag, B. D. Sen, S., and Chatterjee, S., 1950, *Ind. J. Phys.*, **24**, 479.

# INFLUENCE OF RADIATION DAMPING ON THE SCATTERING OF PSEUDOSCALAR CHARGED MESONS BY NUCLEONS

By S. N. BISWAS

DEPARTMENT OF THEORETICAL PHYSICS  
INDIAN ASSOCIATION FOR THE CULTIVATION OF SCIENCE, CALCUTTA

(Received for publication, August, 29, 1952)

**ABSTRACT.** In the present paper it is shown that the inclusion of the influence of radiation damping on the scattering of  $\pi^+$  meson by proton explains satisfactorily the variation of the total scattering cross section with energy of the incident  $\pi^+$  meson as experimentally observed by Anderson and by Sachs and Steinberger; for a proper fit to the experimental curve the value of the coupling constant  $g^2$  is 0.56. The well-known Heitler's integral equation for the above problem is, however, solved by the semi-variational method of Ma and Hsueh, because it is not possible to find an exact solution in this case. The corresponding integral equation for the scattering of  $\pi^-$  meson by proton has been exactly solved by Ma; a comparison of Ma's result with ours shows that experimentally observed ratio of the cross section of scattering by proton of  $\pi^+$  meson to that of  $\pi^-$  meson is explained by the weak coupling perturbation method which includes radiation reactions.

## 1. INTRODUCTION

It has been mentioned by Bhabha (1940) and Heitler (1941) that the theory of radiation damping plays a vital role in the meson theory. In fact, the wellknown discrepancy between the theoretical and the experimental results for the cross section of scattering of mesons by nucleons can be removed if we consider the effect of radiation damping. Attempts have been made by several authors (Heitler, Wilson, Peng and Gora) to take into account this field reaction. They have replaced the transition matrix element  $H_{fi}$  (in the Born approximation) by  $U_{fi}$ , where  $U_{fi}$  is the solution of the following integral equation:

$$U_{fi} = H_{fi} - i\pi \sum_f \int H_{ff'} \rho_{f'} U_{f'f} d\Omega_{f'}$$

Exact solutions of this integral equation have been obtained by Heitler (1941) in the non-relativistic approximation. Since the influence of radiation damping is important only at high energies, it is necessary to have an exact relativistic treatment of the problem. The solution of the integral equation in such cases is mathematically very complicated. Exact solutions of this integral equation can only be had in some particular cases when the kernel of this non-homogenous equation is degenerate. The formal method of solution of the integral equation with degenerate kernel is to transform

the equation to a system of algebraic equations by a suitable transformation. By this method, Ma (1943) and Hsueh and Ma (1944) have solved the integral equation for the scattering of a positive meson by neutron and that of a negative meson by proton.

Here we shall consider the scattering of a positive meson by a proton and that of a negative meson by neutron. In this case the kernel  $H_{ff}$  of the integral equation is non-degenerate. So the method of solving the integral equation by transforming it into a system of algebraic equations is not applicable here. Other methods, such as Fourier and Mellin transformations, are not applicable owing to the serious complicacy of the kernel.

The general series solution (Fredholm's series or Louville-Newman's method of iteration) does not always yield tenable results. The difficulty lies in the fact that the resulting iterated series cannot in all cases be summed and even in most relativistic cases, the calculations of higher order terms of the series are exceedingly involved due to spur calculations. It is seen that this particular method is only applicable in the case of non-relativistic treatment of scattering of light by electron (Thomson's formula). In this case the result agrees with the exact solution obtained by Heitler. In the relativistic scattering of the pseudoscalar charged positive meson by proton, this method is absolutely untenable.

In view of this difficulty, it is desirable to find approximate solutions of the problem. Of the approximate solutions proposed by Wilson and Hsueh and Ma, the semi-variational procedure of the latter is more reliable. By this approximate solution Basu (1949, 1951) in the scattering of neutron by proton at high energies has obtained a result which is in good agreement with the available experimental results. So we apply here this semi-variational procedure in the scattering of positive meson by proton and that of negative meson by neutron.

Recently, using pseudoscalar meson field, Corinaldesi and Field (1949, 1950) attempted to take into consideration this field reaction in the non-relativistic scattering of positive meson by proton. But they have not solved the integral equation rigorously. Only for qualitative analysis they have replaced the transition matrix element  $U_R$  in the damping term by an average over all angles. But this is not mathematically justifiable.

In this paper we shall assume the pseudoscalar meson field and our calculation has been performed in the case of pseudoscalar  $g_2$  coupling only. In the last section a comparison of the theoretical results with the experimental one obtained by Anderson and Steinberger (1951, 1951) has been made by means of a graph. The graph shows the energy dependence of the damped cross section. A higher value of  $g_2$  has been suggested in order that the theoretically obtained damped cross section to be in good agreement with the experimental one. Another feature of the curves drawn may be mentioned. It has been shown that the damped cross section of

the positive meson by proton is larger than that of the negative meson by proton. This is also an experimental fact.

For simplification, we have used throughout  $\hbar = c = 1$ .

#### METHOD AND SOLUTION

The matrix element  $U_{fi}$  which determines the transition from an initial state  $i$  to a final state  $f$ , in the theory of radiation damping is the solution of the following integral equation :

$$U_{fi} = H_{fi} - i\pi \sum_{f'} \int H_{ff'} U_{f'i} \rho_{f'} d\Omega_{f'} \quad \dots \quad (1)$$

Here  $\rho_{f'}$  denotes the density of the energy level corresponding to the state  $f'$ .  $H_{fi}$  is the scattering amplitude in the ordinary perturbation theory. The integration and summation are to be carried out over all directions and polarisations of the state  $f'$ .

As mentioned above, in this particular case of the scattering of a positive meson by a proton, the kernel  $H_{ff'}$  of the equation (1) is non-degenerate. So exact solutions cannot be had. We therefore look for an approximate solution of (1) by the semi-variational method proposed by Hscuh and Ma (1945).

An equivalent form of equation (1) is the following :

$$\sum_i \sum_j \int \delta U_{ij}^* \left[ U_{fi} - H_{fi} + i\pi \sum_{f'} \int H_{ff'} U_{f'i} \rho_{f'} d\Omega_{f'} \right] \rho_f d\Omega_f = 0 \quad \dots \quad (2)$$

where  $\delta U_{ij}^*$  is the arbitrary variation of the complex conjugate of  $U_{fi}$ . Equation (1) holds for all cases if (2) is satisfied for any arbitrary variation of  $\delta U_{ij}^*$ .

Let us assume a trial solution  $\lambda H_{fi}$  of  $U_{fi}$

$$i.e. \quad U_{fi} = \lambda H_{fi} \quad \dots \quad (3)$$

where  $\lambda$  is a parameter not depending on the final or initial state,  $f$  or  $i$ . Then equation (2) must hold good for the solution  $\lambda H_{fi}$  of  $U_{fi}$ .

Substituting (3) in (2) and varying  $\lambda$  we get

$$\delta \lambda^* \sum_i \sum_j \int H_{ij} \left[ H_{ij}(\lambda - 1) + i\pi \sum_{f'} \int H_{ff'} H_{f'i} \rho_{f'} d\Omega_{f'} \right] \rho_f d\Omega_f = 0 \quad \dots \quad (4)$$

On solving for  $\lambda$  we have

$$\lambda = \frac{a}{a + ib} \quad \dots \quad (5)$$

where

$$a = \sum_i \sum_j \int H_{ij} H_{ji} \rho_j d\Omega_j \quad (6a)$$

$$\text{and} \quad b = \pi \sum_i \sum_{f'} \int \int H_{if} H_{ff'} H_{f'f} \rho_f \rho_{f'} d\Omega_f d\Omega_{f'} \quad (6b)$$

where again each of these processes,  $H_i$ ,  $H_{ff'}$ , etc takes place in two successive stages through some intermediate states which we denote by  $n$ ,  $n'$  and  $n''$ . Hence from (6) we write

$$a = \sum_i \sum_{f'} \sum_{n, n'} \int \frac{H_{in} H_{nf'} H_{f'n'}}{(E_i - E_n)(E_{f'} - E_{n'})} \rho_f d\Omega_f \quad (7a)$$

and

$$b = \pi \sum_i \sum_{f'} \sum_{n'} \sum_{n''} \int \int \frac{H_{in} H_{nf'} H_{f'n''} H_{n''n'}}{(E_i - E_n)(E_{f'} - E_{n'}) (E_{n''} - E_{n'})} \rho_f \rho_{f'} d\Omega_f d\Omega_{f'} \quad \dots \quad (7b)$$

Now for the pseudoscalar charged meson field, the total Hamiltonian density is

$$H_1 = \pi^* \pi + (grad \psi^*, grad \psi) + \mu^2 \psi^* \psi \quad \dots \quad (8)$$

and for the nucleon field,

$$H_2 = \phi_i^* \left[ \frac{1}{i} \alpha_i grad + \beta M \right] \phi \quad \dots \quad (9)$$

where  $\alpha$  and  $\beta$  are the Dirac-matrices and the mass of the nucleon is  $M$ .  $\phi$  is an eight-component column matrix :

$$\phi = \begin{pmatrix} \phi_p \\ \phi_N \end{pmatrix} \text{ where } \phi_p = \begin{pmatrix} \phi_1 \\ \vdots \\ \phi_4 \end{pmatrix} \text{ and } \phi_N = \begin{pmatrix} \phi_5 \\ \vdots \\ \phi_8 \end{pmatrix} \quad \dots \quad (10)$$

The Hamiltonian density for the interaction field (in case of pseudoscalar  $g_2$ -coupling only) is given by

$$H_3 = - \sqrt{(4\pi)} g \{ (\psi^\dagger \gamma_5 \tau_{PV} \phi) \psi + (\psi^\dagger \gamma_5 \tau_{NV} \phi^*) \psi^* \} \quad \dots \quad (11)$$

where

$$\begin{aligned} \phi^\dagger &= i \phi^\dagger \beta \\ \gamma_5 &= \gamma_1 \gamma_2 \gamma_3 \gamma_4 \\ \tau_{PV} &= \begin{pmatrix} 0 & 1 \\ 1 & 0 \end{pmatrix} \text{ and } \tau_{NV} = \begin{pmatrix} 0 & 0 \\ 0 & 1 \end{pmatrix} \end{aligned} \quad \dots \quad (12)$$

Here we will discuss the process involving positive meson by proton. The second order process is schematically given by

$$\left. \begin{aligned} Y^*(\mathbf{p}) + P(-\mathbf{p}) + [N(-\mathbf{p} - \mathbf{p}')] \\ \rightarrow P(-\mathbf{p}') + P(-\mathbf{p}) \\ \rightarrow P(-\mathbf{p}') + Y^*(\mathbf{p}') + [N(-\mathbf{p} - \mathbf{p}')] \end{aligned} \right\} \quad \dots \quad (13)$$

where the frame of reference has been so chosen that the momenta of two particles are equal and opposite.

In the above scheme  $Y^*(\mathbf{p})$  represents a positive meson particle with momentum  $\mathbf{p}$ ;  $P(-\mathbf{p})$  represents a proton with momentum  $-\mathbf{p}$  and  $N(-\mathbf{p} - \mathbf{p}')$



in the square bracket stands for neutron with momentum  $(-\mathbf{p}-\mathbf{p}')$  in the negative energy state.

The second-order matrix element for the above process (13) is given by the theory of perturbation (Corinaldesi and Field).

$$H_{fi} = a_{fi}^* (\mathbf{P}_f) H' a_i (\mathbf{P}_i) \quad \dots (14)$$

where  $a(p)$  satisfies the Dirac equation for the nucleon

$$[(\boldsymbol{\alpha} \cdot \mathbf{P}) + \beta M] a(P) = E a(\mathbf{P})$$

$$\text{and} \quad H' = \frac{2\pi g^2}{V \sqrt{\epsilon_i \epsilon_f}} \left\{ \frac{\epsilon_i - E_i + \boldsymbol{\alpha} \cdot \mathbf{P} + M\beta}{(E_i - \epsilon_f)^2 + E^2} \right\} \quad \dots (15)$$

where  $V$  is the periodicity volume,  $\mathbf{P} = \mathbf{p}_i = -\mathbf{p}_f$ ,  $\epsilon_i = \sqrt{(\mathbf{p}_i)^2 + \mu^2}$ ,  $\epsilon_f = \sqrt{(\mathbf{p}_f)^2 + \mu^2}$ ,  $E_i = \sqrt{(P_i)^2 + M^2}$ ,  $E_f = \sqrt{(P_f)^2 + M^2}$ ,  $E = \sqrt{(P)^2 + M^2}$  and  $\mathbf{P}$  stands for the nucleon momentum and  $\mathbf{p}$  for the meson momentum.

In order to simplify calculations we take the reference system in which the centre of gravity of the proton and meson is at rest. So

$$\mathbf{P}_i = -\mathbf{p}_i; \quad \mathbf{p}_f = -\mathbf{p}_f$$

We shall also use the conservation of energy between the initial and the final states. Hence it follows that

$$|\mathbf{P}_i| = |\mathbf{p}_i| = |\mathbf{P}_f| = |\mathbf{p}_f| = p$$

and

$$\epsilon_i = \epsilon_f = \epsilon; \quad E_i = E_f = E$$

and the angle between the initial and the final directions of meson is  $\theta$  i.e.

$$(\mathbf{p}_i, \mathbf{p}_f) = p^2 \cos \theta$$

With these above simplifications, the matrix element for the process under investigation reduces to

$$i_{fi} = - \frac{2\pi g^2}{V \epsilon} a_{fi}^* \left\{ \frac{(\epsilon - E) - \boldsymbol{\alpha} \cdot (\mathbf{p}_i + \mathbf{p}_f) + M\beta}{(E - \epsilon)^2 + E^2} \right\} a_i$$

The evaluation of the expressions  $a$  and  $b$  given in (6a, 6b) with (16) as the matrix element is laborious but straightforward. We shall use the usual method of summing over the spin states. Thus

$$a = \frac{(2\pi g^2)^2}{2V^2 \epsilon^2 E^2} \rho_f \int \{A + B \cos \theta_{if}\} [X - 2p^2 \cos \theta_{if}]^2 d\Omega_f \quad \dots (17)$$

$$\text{where} \quad A = \mu^4 \left[ \frac{E^2}{\mu^2} \cdot \frac{(\epsilon - E)^2}{\mu^2} + \frac{M^2}{\mu^2} \cdot \frac{(\epsilon - E)^2}{\mu^2} + 2x^4 + \frac{M^4}{\mu^4} \right. \\ \left. + 2x^2 \frac{E^2}{\mu^2} - 4 \frac{E^3}{\mu^3} \frac{(E - \epsilon)}{\mu} \right]$$

$$B = \mu^4 \left[ x^2 (3x^2 + 1) + x^2 \cdot \frac{E \cdot \epsilon}{\mu^2} \right]$$

$$X = (E - \epsilon^2 - M^2 - 2p^2)$$

and  $x$  stands for the ratio  $p/\mu$ ,  $p$  is the meson momentum and  $\mu$  is the meson mass

and

$$b = - \left( \frac{2\pi g^2}{V \epsilon^2} \right) \rho_f \rho_f \pi \int \int_{-1}^1 E^3 (X - 2p^2 \cos \theta_{if}) (X - 2p^2 \cos \theta_{ir}) (X - 2p^2 \cos \theta_{fr}) (F_1 + F_2 + F_3 + F_4) d\Omega_f d\Omega_{f'} \quad \dots (18)$$

where

$$\begin{aligned} F_1 &= [3E^2(\epsilon - E)^3 + (\epsilon - E)^2 \{2M^2E^2 + M^2(2E\epsilon - p^2) + 2E^2p^2\} \\ &\quad + (2\epsilon - E)\{E^2(\epsilon - E)(E^2 + M^2) + 2M^2E^3\} \\ &\quad + (\epsilon - E)\{2M^2E(2E\epsilon - p^2) + 2M^2p^2E^2 + 3p^4E\} \\ &\quad + E^2\epsilon^2p^2 + M^2E^2(2E\epsilon - p^2) + 3E\epsilon p^4 + 2M^2p^2\epsilon^2 \\ &\quad + p^2(E\epsilon - p^2)^2 + M^2p^2E\epsilon + p^4E^2 + p^6] \\ F_2 &= p^2[(E\epsilon - E)^3 + (\epsilon - E)^2(4E^2 - M^2) + (\epsilon - E)\{2E^3 + E^2p^2 \\ &\quad + M^2E + (2E^3 + 3E^2p^2 - M^2E)\} + M^2E(E + \epsilon) \\ &\quad + E\epsilon(E\epsilon - p^2) - M^2(2E\epsilon - p^2) + 2p^2E\epsilon + 2M^2E\epsilon \\ &\quad + 4p^2E^2 - 2M^2\epsilon^2 + 2p^4] \cos \theta_{if} \\ F_3 &= p^2[(\epsilon - E)^2(E^2 + 3p^2) + (\epsilon - E)\{E^2\epsilon + 7E^2p^2 + 3EM^2\} \\ &\quad + M^2\epsilon(E + \epsilon) + p^2(E^2 + p^2) + 2p^2E^2 + 2p^2E\epsilon + 2p^4] \cos \theta_{ir} \\ F_4 &= p^2[\{3M^2E\epsilon + 3E^2(\epsilon - E)^2 + 4E^2p^2 + 2p^2E\epsilon + p^2(\epsilon - E)^2 + 2p^4\} \\ &\quad + (\epsilon - E)\{E^2\epsilon + M^2\epsilon + E(\epsilon - E)^2 + 2E^3 \\ &\quad + \epsilon p^2 + 6E^2p^2\}] \cos \theta_{fr} \end{aligned}$$

and  $X$  is the same as in eqn (17),

$\theta_{if}$ ,  $\theta_{ir}$  and  $\theta_{fr}$  are the angles through which the meson has been scattered.

If we denote by  $dQ_0$  the differential scattering cross section in which the radiation damping has been neglected and by  $dQ$ , the cross section including radiation damping, then from (5)

$$dQ = dQ_0 \left/ \left( 1 + \frac{b^2}{a^2} \right) \right. \quad \dots (19)$$

where  $b$  and  $a$  are given by (6a) and (6b)

$$\text{Now} \quad dQ_0 = \frac{\epsilon^2}{(2\pi)^2} |H_{if}|^2 d\Omega$$

Hence from (16)

$$dQ_0 = \frac{g^4}{2E^2} \left\{ \frac{A + B \cos \theta}{(X - 2p^2 \cos \theta)^2} \right\} d\Omega \quad \dots (20)$$

where  $A$ ,  $B$  and  $X$  are given by (17).

Integrating over the entire range of angles, we have from (17) and (18), for the expressions of  $a$  and  $b$ , the following results.

$$a = \pi^3 \rho_f g^4 \frac{1}{E^2 \epsilon^2 V^2 x^2} F_a(x) \quad \dots (20)$$

$$\begin{aligned} \text{where } F_a(x) = & \{ 2[(k^2 + x^2)\{(1 + x^2) + (k^2 + x^2) - 2(1 + x^2)^{1/2}(k^2 + x^2)^{1/2}\} \\ & + k^2\{(1 + x^2) + (k^2 + x^2) - 2(1 + x^2)^{1/2}(k^2 + x^2)^{1/2}\} + 2x^4 \\ & + k^4 + 2x^2(k^2 + x^2) - 4(k^2 + x^2)^2 + 4(k^2 + x^2)^{3/2}(1 + x^2)^{1/2} \\ & + 2x[(x^2\{3x^2 + (k^2 + x^2)^{1/2}(1 + x^2)^{1/2} + 1\})\{(1 + x^2)^{1/2} - 1\} \\ & - \left(\log \frac{x+1}{x-1}\right)[x^2\{3x^2 + (k^2 + x^2)^{1/2}(1 + x^2)^{1/2} + 1\}] \} \end{aligned}$$

where  $x$  stands for  $p/\mu$ ;  $k = M/\mu$  and  $z = \frac{(E - \epsilon)^2}{2p^2} - \frac{M^2}{2p^2} - 1$

$$\text{and } b = -\pi^2 \rho_f^2 \frac{g^4}{16 F_a^3 \epsilon^3} \frac{1}{x} \cdot F_b(x)$$

$$\begin{aligned} \text{where } F_b(x) = & \left( \log \frac{x+1}{x-1} \right)^2 \{ 3k^2(k^2 + x^2)^{1/2}(1 + x^2)^{1/2} + 3(k^2 + x^2) \\ & \{ (1 + x^2) + (k^2 + x^2) - 2(1 + x^2)^{1/2}(k^2 + x^2)^{1/2} \} \\ & + 4x^2(k^2 + x^2) + 2x^2(k^2 + x^2)^{1/2}(1 + x^2)^{1/2} + x^2\{(1 + x^2) \\ & + (k^2 + x^2) - 2(1 + x^2)^{1/2}(k^2 + x^2)^{1/2}\} + 2x^4 + \{(1 + x^2)^{1/2} \\ & - (k^2 + x^2)^{1/2}\}\{(1 + x^2)^{1/2}(k^2 + x^2)^{1/2} + k^2(1 + x^2)^{1/2} + (k^2 + x^2) \\ & [(k^2 + x^2) + (1 + x^2) - 2(1 + x^2)^{1/2}(k^2 + x^2)^{1/2}] + 2(k^2 + x^2)^{3/2} \\ & + x^2(1 + x^2)^{1/2} + 6x^2(k^2 + x^2)^{1/2} \} \} \end{aligned}$$

where again,  $k$ ,  $x$  and  $z$  represent the same values as in  $a$ .

From the values of  $b$  and  $a$  as calculated above, we have

$$\frac{b^2}{a^2} = \frac{1}{16(2\pi)^3} \frac{g^4}{(E + \epsilon)^2} \left\{ \frac{F_b(x)}{F_a(x)} \right\}^2 \quad (23)$$

It follows from (19) that the total cross section

$$Q = \frac{Q_0}{1 + b^2/a^2}$$

where  $Q_0$  can be evaluated from (20) and  $b^2/a^2$  has been given by (23).

Integrating over the entire range of angles, we have from (20)

$$Q_0 = \pi \frac{g^4}{4\mu^2(k^2 + x^2)} F_a(x)$$

Where  $\mu$  is the meson mass and  $p$ ,  $x$  and  $F_a'(x)$  are the same as given by (21) and (23).

## COMPARISON WITH EXPERIMENT

The energy dependence of the total cross section including radiation damping has been shown by means of the graph (Figure 1). We have taken

the mass of meson to be  $276.m_e$ , ( $m_e$  = mass of electron) hence the ratio  $M/\mu$  takes the value 6.67. In figure 1, the variation of cross sections with energy

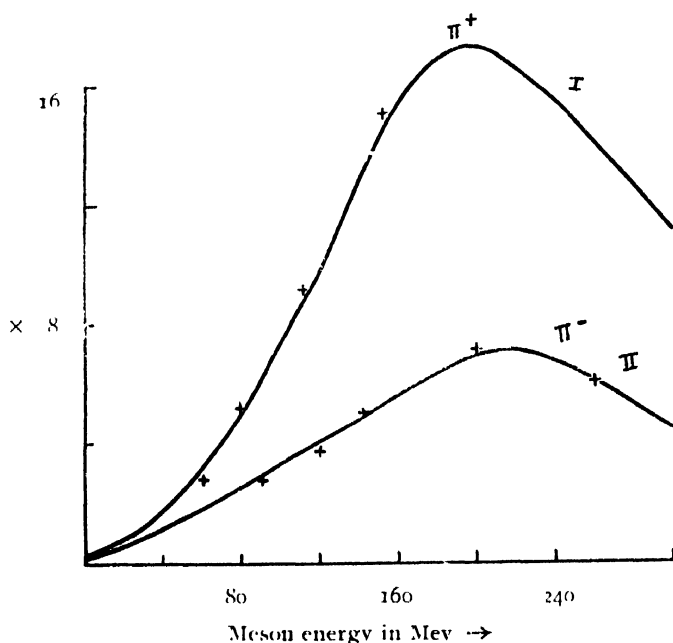


FIG. 1

has been studied in comparison with the experimental results. The general agreement of the theoretical results is fairly good. The effect of radiation damping is predominant at 180 Mev meson energy (kinetic energy). The curve rapidly rises from 2.7 to 15.5 at energies between 60 Mev to 135 Mev energy. The curve falls down from and after 180 Mev showing the non-divergency of the result. The cross points stand for the experimentally observed values. Except at 135 Mev, the curve is seen to be in good agreement with the experiment.

In order to fit the theoretical values in agreement with the experimental ones, a slightly higher value of  $g^2$  has been suggested. The value taken is 0.56. This value of  $g^2$  is reasonable since it will not disturb the convergency of the higher order cross section terms according to the perturbation theory.

Curve I (in figure 1) represents the total cross section of positive meson scattering by proton. Corresponding experimental values have been shown by cross points.

Curve II (in figure 2) represents the total cross section for the scattering

of negative meson by proton. The cross section has been evaluated from the following result of Heueh and Ma (1944).

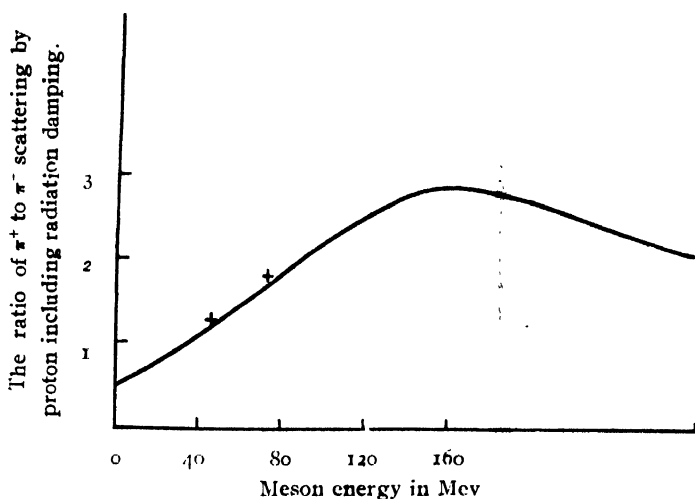


FIG. 2

The total cross section for this case according to the pseudoscalar theory using pseudoscalar coupling ( $g_2$  coupling) only.

$$\phi = \frac{8\pi}{3p^2} \frac{K_1^2 + K_2^2 + (K_1^2 - K_2^2)^2}{1 + 2(K_1^2 + K_2^2) + K_1^2 - K_2^2}$$

where

$$K_1 = \frac{p(A(E + \epsilon) + BM)}{2(E + \epsilon)\{(E + \epsilon)^2 - M^2\}}$$

$$K_2 = \frac{p(AM + B(E + \epsilon))}{2(E + \epsilon)\{(E + \epsilon)^2 - M^2\}}$$

with

$$A = -g_2^2 E$$

$$B = -g_2^2 M$$

$$C = -p \left[ \frac{g_2^2}{m^2} (\epsilon^2 + p^2 + 2E\epsilon) \right]$$

This cross section varies from 2.7 to 6 at energy 80 to 200 Mev with a highest peak of value 7 at 180 Mev energy. The values have been calculated taking  $g$  to be 0.56. This gives us an excellent agreement with the experimental result.

In figure 2, the ratio of positive meson scattering to negative meson scattering including radiation damping has been drawn. The values vary from 0.5 to 2.3 at energy 0 Mev to 200 Mev. The experimental point 1.8 at 72 Mev is slightly at variance with the theoretical result 1.8 at 80 Mev

energy. The experimental point shown by cross point is from the result of Steinberger (1951).

#### CONCLUSION

The present paper brings out two points: the influence of radiation reactions begins to assert itself from 200 Mev. The scattering by proton of  $\pi^+$  meson is greater than that of  $\pi^-$  meson, the difference in the two cases consists in two types of intermediate states, in the former the scattered meson is emitted before the incident meson is absorbed, so there are two mesons in the virtual state, whereas, in the latter case the incident meson is absorbed before the scattered meson is emitted. Because of this difference the matrix element for the former case has larger value than that for the latter. This result is in contradistinction to an observation made by Brueckner (1952) about the weak coupling theory.

#### ACKNOWLEDGMENT

The author is indebted to Dr. D. Basu for suggesting the problem as a research topic and for his continued interest and guidance in the problem.

#### REFERENCES

- Anderson, H. L., 1951, *Phys. Soc. Meeting (Am)*.  
 Basu, D., 1950, *Proc. Roy. Ir. Acad.*, **53**, 31.  
 Basu, D., 1951, *Ind. J. Phys.*, **28**, 246.  
 Bhabha, H. J., 1940, *Proc. Indian. Acad. Sci.*, **2**, 247.  
 Brueckner, A. K., 1952, *Phys. Rev.*, **86**, 106.  
 Corinaldesi, E. and Field, G., 1949, *Phil. Mag.*, **40**, 1150.  
 Corinaldesi, E. and Field, G., 1950, *Phil. Mag.*, **41**, 364.  
 Steinberger, Sachs, 1951, *Phys. Rev.*, **82**, 958.  
 Heitler, W. 1941, *Proc. Camb. Phil. Soc.*, **37**, 291.  
 Heitler, W. and Peng, H. W., 1942, *Proc. Camb. Phil. Soc.*, **38**, 296.  
 Hsueh and Ma, 1945, *Phys. Rev.*, **67**, 303.  
 Hsueh and Ma, 1944, *Proc. Comb. Phil. Soc.*, **40**, 167.  
 Ma S. T., 1943, *Proc. Camb. Phil. Soc.*, **39**, 168.  
 Wilson, A. H. 1941, *Proc. Camb. Phil. Soc.*, **37**, 1301.

# SOME GENERAL RELATIONS ON THE VISCOSITY OF HOMOLOGOUS LIQUIDS

BY SANTI R. PALIT

INDIAN ASSOCIATION FOR THE CULTIVATION OF SCIENCE, CALCUTTA-32

(Received for publication, November 8, 1952)

**ABSTRACT.** From recent theoretical developments in the field of viscosity of liquids as explained from the hole theory of liquid structure, the following relations have been deduced

(1) In any homologous series, at constant temperature, the logarithm of the molecular viscosity ( $\log \eta M$ ) is a linear function of the molar surface energy  $\gamma (Mv_{sp})^{2/3}$ . It is shown that the theoretical slope of this line is  $0.17 \times 10^{-2}$  and the observed slope for different homologous series is within a factor of two of this theoretical value.

(2) In any homologous series if the intercept of the Arrhenius plot (i.e.  $\log \eta$  vs  $1/T$ ) is  $A$ ,  $\log$  molecular weight is in linear relation with  $A$ , the slope of the line being negative of unity, i.e. (i)  $A = -\log M + \text{constant}$  or (ii)  $M = K\eta 10^{-A}$

It is pointed out that the experimental results with methyl esters confirm the above equation, the observed slope being  $-1.01$  and that the relation can evidently be utilised for determining molecular weight of liquids from viscosity measurements. There are too many exceptions to this equation which limits its utility but points to the soundness of the basic concept.

(3) In any homologous series,  $\frac{\ln \eta}{KE T_c}$  (where  $KE = \text{Eötvös constant} \approx 2.1$  and  $T_c = \text{critical temperature}$ ) plotted against  $1/T$  would produce a system of parallel straight lines with a slope of near about unity.

(4) In any homologous series  $\log$  molar viscosity plotted against reciprocal of absolute temperature would produce a system of straight lines which would all meet at near about the same point on the  $\log$  molar viscosity axis. The application of this relation to the establishment of chemical structure is obvious.

The above relations have been further simplified and applied in the case of high polymers.

All the above deductions have been found to be in conformity with the available experimental data.

Applying Eyring's rate theory considerations to the hole theory of liquid structure, Eyring *et al* (1941) gave the following equation for the viscosity of a liquid viz.,

$$\eta = \frac{(2\pi mkT)^{1/2} e^{\Delta E_f / kT}}{\lambda_1 \lambda_2} \quad \dots (1)$$

where  $\eta = \text{viscosity}$ ,  $\lambda_1 = \text{the distance between two layers of molecules in a liquid sliding past each other under the influence of an applied force}$ ,  $\lambda_2 = \text{the distance between two neighbouring molecules in the same direction}$ ,  $\lambda_3 = \text{the mean distance between two adjacent molecules in the moving layer}$

in the direction at right angles to the direction of motion,  $v_h$  = the volume of a single hole, or increase in volume per equilibrium position,  $v$  = the volume inhabited by a single molecule,  $v_s$  = the contribution of a single molecule to the volume of the unexpanded solid,  $m$  the mass of an individual molecule,  $k$  the Boltzmann constant,  $T$  the absolute temperature, and  $\Delta E_f$  the activation energy required for a single molecule to flow into a hole that is available in the absence of a shearing force.

Telang (1949) has taken an important step forward by identifying the activation energy required to move the liquid molecules from one position to the next, i.e., the activation energy for viscous flow as the free energy of formation of a surface (an idea which is somewhat similar to the concept of Frenkel (1946) that the activation energy required for the formation of a hole is proportional to the surface tension multiplied by the surface of the hole). From the above concept Telang has deduced the following equation (eqn. 2) for the viscosity of a liquid. This equation has the unique feature that it does not contain any arbitrary constant.

$$\eta = (hN/V^{2/3})(b/(v-b)^{1/3}) \exp(1.091N^{1/3}\gamma(M/D)^{2/3}/RT) \quad \dots (2)$$

where  $\eta$  = is viscosity,  $V$  is molar volume,  $\gamma$  is surface tension,  $T$  is the absolute temperature,  $h$  is Planck's constant,  $N$  is the Avogadro number,  $R$  is the gas constant and  $b$  is the volume occupied by the molecules in the liquid state per mole (van der Waals constant) and  $D$  is density.

In order to test the validity of the above equation Telang has made a few calculations with data on a number of liquids with, on the whole, satisfactory results. This equation, however, instead of being applied to one liquid can be suitably modified as to be applicable to a homologous series, and such extension of this equation has been found to lead to some highly interesting results, which we shall investigate in this paper.

*Viscosity of a homologous series.* If we put  $b_{sp}M$  and  $v_{sp}M$  for  $b$  and  $V$  respectively in eqn (2), the equation after taking logarithm becomes,

$$\ln \eta = \frac{1.091 N^{1/3}}{RT} \cdot \gamma v_{sp}^{2/3} M^{2/3} - \ln M + \ln \frac{hN b_{sp}}{v_{sp}^{2/3}(v_{sp} - b_{sp})^{4/3}} \quad \dots (3)$$

It can be safely assumed with a fair degree of approximation that though  $b$  and  $V$  will vary considerably with increase in molecular weight,  $b_{sp}$  and  $v_{sp}$  would vary only slightly from member to member in a homologous series; particularly, the last term in eqn (3), which involves log of ratio of these terms, would change very little from member to member. Hence, for the same homologous series at constant temperature we may write equation (3) in the following form,

$$\ln (\eta M) = \frac{1.091 N^{1/3}}{RT} \cdot \gamma v_{sp}^{2/3} M^{2/3} + k_2' \quad \dots (4)$$

$$\log (\eta M) = \frac{1.108}{2.303 T} \cdot \gamma v_{sp}^{2/3} M^{2/3} + k_2 \quad \dots (4a)$$



$$\log (\eta M) = k_1 \gamma v_{sp}^{2/3} M^{2/3} + k_2 \quad \dots (4b)$$

$$\text{At } 20^\circ \text{C } \ln (\eta M) = 0.38 \times 10^{-2} \gamma (M v_{sp})^{2/3} + k_2' \quad \dots (5)$$

$$\text{or, } \log (\eta M) = 0.165 \times 10^{-2} \gamma (M v_{sp})^{2/3} + k_2 \quad \dots (6)$$

Hence, we should expect that in a homologous series,  $\log (\eta M)$  when plotted against  $\gamma v_{sp}^{2/3} M^{2/3}$  would yield a straight line. Calling  $\eta M$  as molar viscosity we may say that in any homologous series the logarithm of the molar viscosity increases linearly with the molar surface energy, the relative rate of increase being roughly one sixth of one per cent at near about room temperature. It would be of interest to test the above relation with available experimental data.

In figure 1, we have made such plots for  $C_7$  to  $C_{12}$  straight chain alkanes, the alcohols, the four lowest methyl esters, and the four lowest ethyl esters. It is surprising, considering the assumptions involved in deriving the equation,

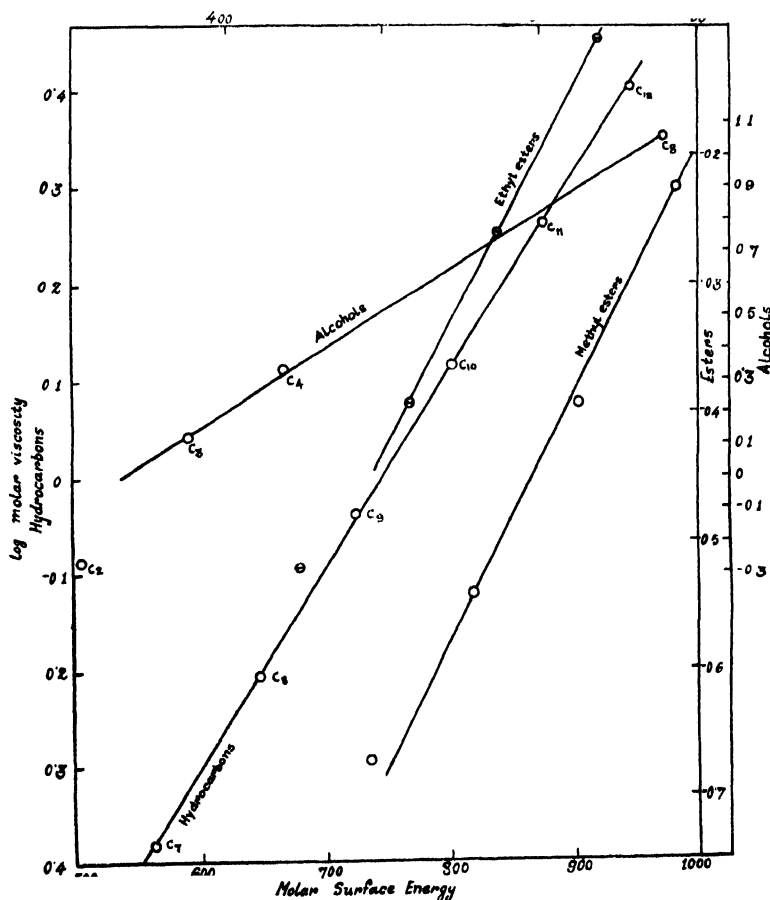


FIG. 1

Log molar. viscosity against molar surface energy of homologous liquids. Lower scales of abscissae for hydrocarbons, and alcohols, the scale for the alcohols having been displaced 170 units to the right. Top scale is for esters, the scale for methyl esters is displaced 100 units to the right.]

that the points (except for methyl alcohol, formates and ethyl alcohol) fall on excellent straight lines. This is more striking in consideration of the fact that the above plot is highly sensitive to slight errors in  $\gamma$  on which however, the published data are probably not of as high order of accuracy as those on the other quantities. So we conclude that the general features of equation (4), particularly the statement made in the previous para (in italics) are confirmed by experimental data.

The discrepancy in the case of methyl alcohol and formates is expected from the wellknown fact that the first member of a homologous series does not generally fall in line with the higher members in many properties and almost always behaves in an exceptional way. The case of ethyl alcohol, however is a real exception.

From equation (6) we should expect that the slope of the above plots should be  $0.16 \times 10^{-2}$ . Our observed slopes are  $0.21 \times 10^{-2}$ ,  $0.24 \times 10^{-2}$ ,  $0.23 \times 10^{-2}$  and  $0.24 \times 10^{-2}$  in the case of alkanes, the ethyl esters, the methyl esters and the alcohols respectively. It is gratifying to note that the observed slopes are of the right order and quite close to our expected value. We ascribe this slight numerical discrepancy to the assumptions made in the derivation of equation (2) that the molecules are spherical in shape and the activation energy of viscous flow is equal to the molar surface energy. The latter assumption cannot be entirely true as the potential inside a liquid is higher than that at the surface and so, the coefficient in eqn (4) should contain a parameter to take care of these factors and it appears from our calculations that this parameter generally lies within a factor of two or so. So we rewrite equation (4) as

$$\ln \eta M = \frac{1.108p}{T} \cdot \gamma(v_{sp}M)^{2/3} + k_2' \quad \dots (6)$$

$$\text{or, } \log \eta M = k_1[\gamma(v_{sp}M)^{2/3}] + k_2 \quad \dots (7)$$

where  $p$  is a parameter which generally lies between 1 and 2 and depends on the shape or packing possibility of the molecule and also on the strength of the field inside a liquid. It is of interest to note from figure 1 in this connection that the observed slope  $k_1$  is lowest for the hydrocarbons and increases in the order hydrocarbons < methyl esters < ethyl esters < alcohols. This may indicate that the more polar the liquid type is the higher will be the value of  $p$  i.e., higher will be  $k_1$ .

We have thus arrived at a method of calculating the molecular weight of any member of a homologous series from density, surface tension and viscosity data if  $k_1$  and  $k_2$  of eqn (7) are already known from experiments on a few other members of the same homologous series. Such calculations of molecular weight of substances represented in figure 1 are shown in Table I. It would be seen that the calculated molecular weights are in good agreement with the theoretical values.

TABLE I

Calculation of Molecular weight from viscosity, surface tension  
and density data (20° C)

Substance	$k_1 \times 10^2$	$k_2$	Molecular weight	
			Theoretical	Calculated from eqn (7)
<i>n-alkanes</i>				
(C <sub>7</sub> ) Heptane	0.2065	-1.5451	100.2	99.2
(C <sub>8</sub> ) Octane			114.2	113.7
(C <sub>9</sub> ) Nonane			128.2	129.3
(C <sub>10</sub> ) Decane			142.3	142.5
(C <sub>11</sub> ) Undecane			156.3	156.5
(C <sub>12</sub> ) Dodecane			170.3	169.5
<i>Ethyl esters</i>				
Acetate	0.2377	-1.6218	88.1	87.8
Propionate			102.1	102.0
Butyrate			116.1	116.0
<i>Methyl esters</i>				
Acetate	0.2431	-1.6575	74.1	75.1
Propionate			88.1	86.0
Butyrate			102.1	102.13
<i>Alcohols</i>				
<i>n</i> -Propyl alcohol	0.2436	-0.8883	60.1	58.1
<i>n</i> -Butyl alcohol			74.1	76.1
<i>n</i> -Octyl alcohol			130.2	130.0

*Effect of temperature.* By using Eötvös equation  $\gamma(M/D)^{2/3} = K_E(T_C - T)$  where  $K_E$  is the Eötvös constant and  $T_C$  is the critical temperature we can easily put equation (4) in the following form,

$$\ln \eta = \frac{1.11 K_E T_C}{T} - 1.11 K_E - \ln M + k_2' \quad \dots (8)$$

This equation, except for the  $\ln M$  term, has already been deduced by Telang combining his equation [Equation (2)] with Eötvös equation. This equation immediately leads to a number of very interesting conclusions when applied to a homologous series. It is thus apparent that if we plot  $\frac{2.303}{K_E T_C} \log \eta$  against  $1/T$  for members of the same homologous series, we shall get a system of parallel straight lines with a slope of the order 1.1. That this is true is shown in figure 2 for a number of esters. Conversely, by determining the slope of the  $\log \eta$  versus  $1/T$  plot (to be called Arrhenius plot in this paper) we can obtain the critical temperature of a liquid by dividing the slope by  $\frac{k_1 K_E}{2.303}$ . Thus, we have been able to obtain, theoretically

an expression for the slope of the Arrhenius plot. Thomas (1946), taking up a suggestion by Prasad (1933), has already shown that the Arrhenius slope of viscosity is proportional to critical temperature and equation (8) further shows that the slope is also proportional to  $K_E$  in any homologous series. The

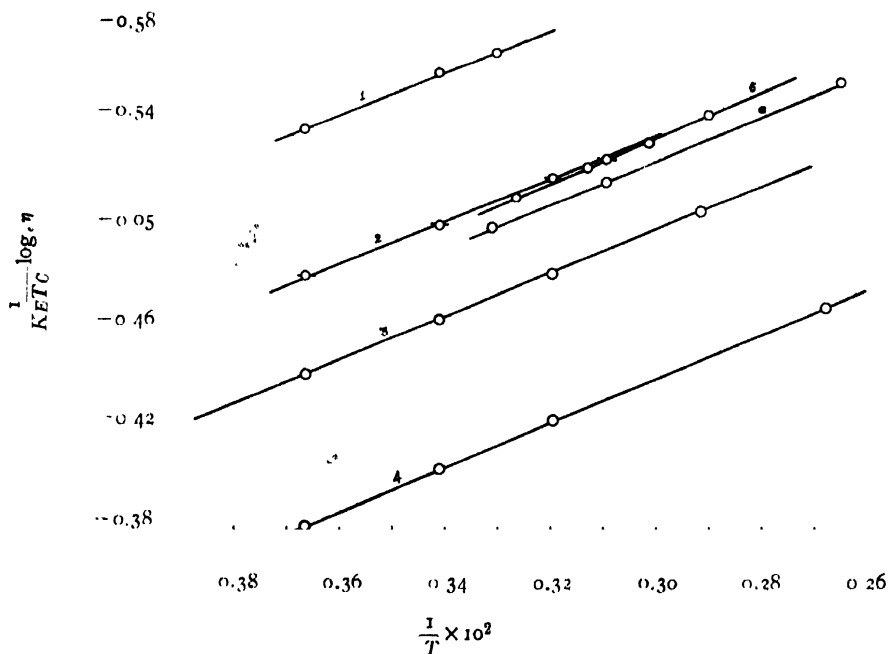


FIG. 2

$\frac{1}{KETC} \ln \eta$  against  $1/T$  for esters ; (1) methyl formate (2) methyl acetate (3) methyl propionate (4) methyl butyrate (5) ethyl acetate (6) ethyl propionate (for (5) and (6) the ordinates have been displaced upwards by 0.1 unit)

restriction to a homologous series comes from the fact that the slopes of the straight lines in figure 2 are not exactly equal to 1.11 but has been found to have nearly equal values for all members of a homologous series. Hence, it is advisable to write equation (8) in the following form where  $k_1$  is a constant whose value is of the order of unity.

$$\log \eta = -\frac{k_1 K_E T_c}{T} - k_1 K_E - \log M + k_2 \quad \dots (8a)$$

It should be remarked, however, that the slopes of the above straight lines (figure 2) are not exactly the same, the values being in the range  $0.82 \pm 0.02$ . It should also be noted that this value is somewhat lower than the theoretical slope 1.11. This discrepancy is partly due to causes as explained in the previous section and partly due to the approximate nature of Eötvös equation which we have taken help of in its derivation.

An interesting modification of equation (8) is to write it in the form

$$\log (\eta M)=k_1 K_E T_0 \cdot \frac{1}{T}+\left(k_1 K_E-k_2\right) \quad (9)$$

We should hence expect that if we plot  $\log (\eta M)$  against  $1/T$  we should obtain for all members of the same homologous series a system of straight lines which would meet at near about the same point on the  $\log \eta M$  axis. This is shown for a few typical homologues in figure 3. The application of

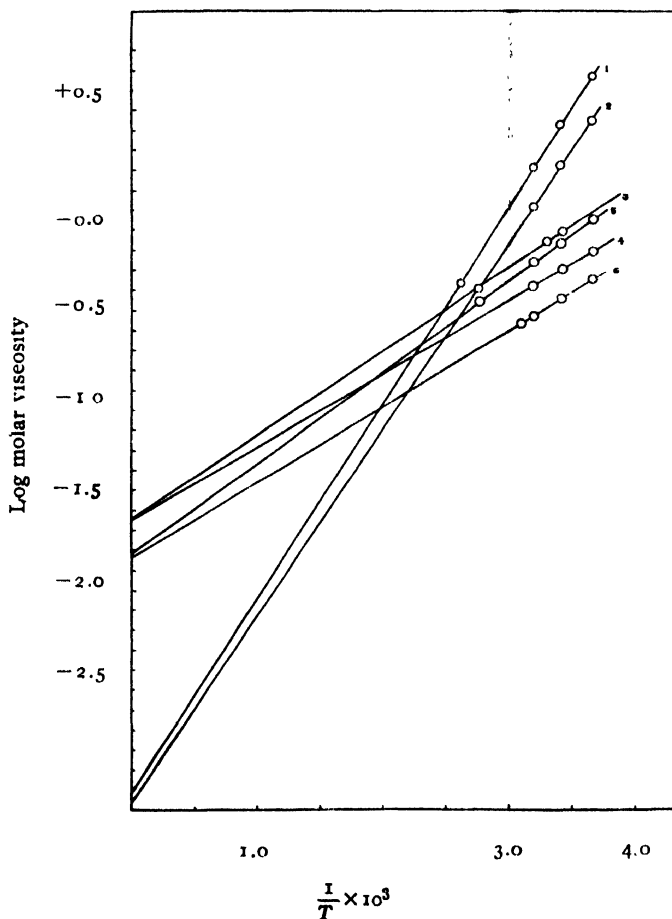


FIG. 3

Log molar viscosity against reciprocal of absolute temperature for various types of compounds. (1) Butyl alcohol (2) Propyl alcohol (3) Octane (4) Heptane (5) Ethyl propionate (6) Methyl acetate.

this relation for confirmation of the chemical structure of any unknown liquid is obvious. It is relevant to point out that instead of the usual plot of  $\log \eta$  against  $1/T$ , it is more convenient for comparative purpose to plot  $\log \eta M$  against  $1/T$  as almost all liquids can be easily accommodated on the same graph.

*Determination of molecular weight.* We have already pointed out in Table I how molecular weight can be calculated from viscosity, surface tension and density data at one temperature. Eqn (8) promises to provide another method from measurements of temperature variation of viscosity. It is easy to see that the intercept of the  $\log \eta$  versus  $1/T$  plot *i.e.* the intercept of the Arrhenius plot,  $A$  is given by the equation,

$$A = -1.11K_E - \log M + k_2 \quad \dots (10)$$

$$\text{or,} \quad A = -k_1 K_E - \log M + k_2 \quad \dots (11)$$

$$\text{or,} \quad M \approx K_{\eta} 10^A \quad \dots (12)$$

where  $k_1$  has a value near about unity and  $K_{\eta}$  is a constant for the same homologous series.

If the above equation is true we should expect that for any homologous series, the Arrhenius intercept,  $A$  would be a linear function of  $\log M$  and the slope of this straight line would be negative of unity. Figure 4

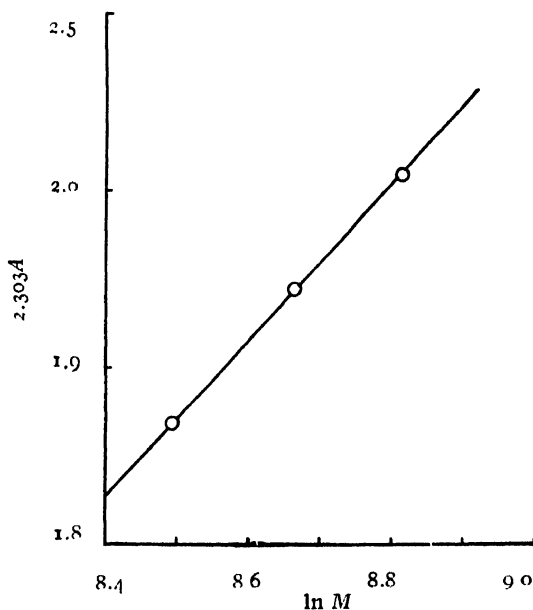


FIG. 4

$A$  versus  $\log M$  plot for methyl acetate, propionate and butyrate

Expected linear relationship between the Arrhenius intercept of viscosity and log molecular weight for members of the same homologous series (methyl acetate, propionate and butyrate).

illustrates the above relation for the methyl esters. The intercepts were obtained by the least square method. The points (except the first member) fall remarkably well on a straight line and its slope is  $-1.01$  *i.e.* practically the same as the theoretical slope of negative of unity.

This behaviour of methyl esters as shown in figure 4 is, however, exceptional rather than being the rule with any homologous series. Most series show quite irregular behaviour with the intercept  $A$  as already observed

by Andrade (1934), Thomas (1946) and others. Such failure of equation (10) or for that matter equation (8) is owing to the fact that Eötvös equation used in its derivation is only an approximate one and that  $k_2$  is not a strictly temperature independent constant. The agreement, however, is not fortuitous but shows the basic correctness of the underlying concept.

Equation (12) can be easily tested for ordinary liquids. Such a test is shown in Table II with data for methyl esters where equation (10) has been found to be valid. It would be seen that the calculated value of the constant  $K_\eta$  remains essentially constant as we go up the series and this establishes equation (12). This equation undoubtedly provides a simple method of determining molecular weight from viscosity data only, provided a table of  $K_\eta$  values is available.

TABLE II

Determination of molecular weight from Arrhenius intercept with the help of eqn. (12)

Substance	$A$	$\log M$	$\log K_\eta = -A + \log M$	$M = K_\eta 10^{-A}$	
				Calculated	Theoretical
Methyl acetate	-3.6880	1.8697	1.8183	74.08	74.08
Methyl propionate	-3.7607	1.9450	1.8157	87.84	88.10
Methyl butyrate	-3.8263	2.0092	1.8179	102.3	102.13

mean = 1.8170       $K_\eta = 10^{-1.8170}$

It should be pointed out, however, that equation (12) is only an approximate one and its validity depends on two assumptions *viz.*, (i)  $k_2$  is exactly the same for all members and (ii)  $K_E$  values are equal for all members of the homologous series. Even any slight deviation from the above conditions would produce large discrepancy in the calculated values of  $M$ . Hence, the equation is not very suitable for use with ordinary liquids and the case of methyl esters as given in Table II is rather exceptional than usual. Most probably nonpolar hydrocarbons and also high polymers would strictly conform to this equation and correct values of their molecular weights would be obtainable from temperature coefficient of viscosity. Only further work, now in progress in this laboratory, can decide the matter.

*Application to high polymers.* A series of high polymers of the same structure, for example, polystyrenes of different molecular weights, forms something akin to a homologous series where equation (3) finds an ideal application and admits of further simplification. This would be thoroughly discussed in a separate publication but we can write the final equation for such case forthwith as below

$$100\rho_0[\eta] = K_p M^{2/3} - \ln M + k_2 \quad \dots (13)$$

where  $\rho_0$  is the density of the solvent and  $[\eta]$  the intrinsic viscosity of the polymer. We have found that almost all published data show that  $\{100\rho_0[\eta]$

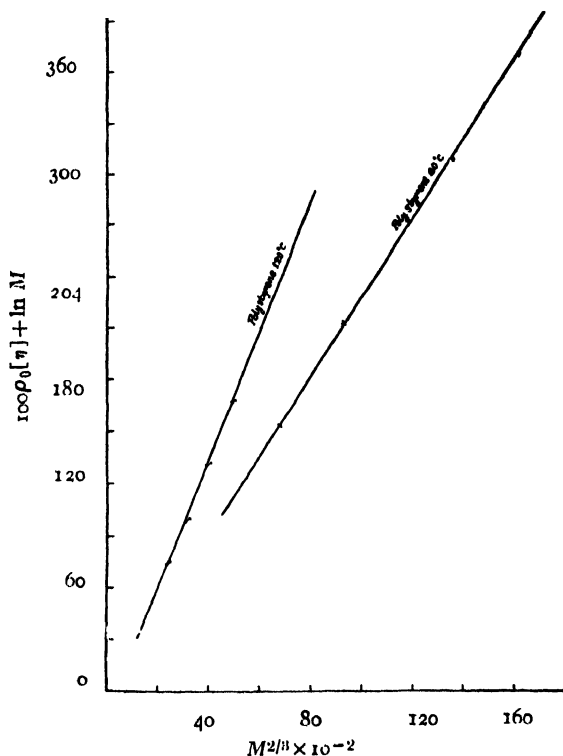


FIG. 5

A plot of  $100\rho_0[\eta] + \ln M$  versus  $M^{2/3}$  for fractions derived from two samples of polystyrenes prepared at  $60^\circ\text{C}$  and  $120^\circ\text{C}$  respectively (Data from T. Alfery, A. Bartovics, and H. Mark, *J. Amer. Chem. Soc.*, **16**, 2319 (1943))

$+\ln M\}$  when plotted against  $M^{2/3}$  give straight lines with a slope of the right order as expected from theory. figure 5 is a typical illustration for two samples of polystyrenes.

We, however, like to point here that though polymers being solids often of ill-defined melting points, have to be of necessity investigated in solution, we can probably apply equation (11) or (12) to their solutions and thus determine their molecular weight from temperature coefficient of the viscosity of their solutions in a suitable solvent. Experiments are in progress in this laboratory to investigate the possibility of such an application.

## REFERENCES

- Andrade, E. N. C., 1934, *Phil. Mag*, **17**, 698.  
 Frenkel, J., 1940, *Kinetic Theory of Liquids*, Oxford Press, p. 208.  
 Glasstone, S., Laidler, K. J., and Eyring, H., 1941, *The Theory of Rate Processes*, McGraw Hill Book Co., New York, p. 488.  
 Prasad, B., 1933, *J. Ind. Chem. Soc.*, **10**, 143.  
 Telang, M. S., 1949, *J. Chem. Phys.*, **17**, 556.  
 Thomas, L. H., 1946, *J. Chem. Soc. (London)*, 573.



*Ripon Professorship Lectures for 1951 delivered in the Indian Association  
for the Cultivation of Science, in January 1951*

DIFFRACTION EFFECTS IN THE SCATTERING  
OF NEUTRONS  $\mu$  MESONS AND  
ELECTRONS BY NUCLEI

BY

E. AMALDI

*Professor of Physics, University of Rome*

INDIAN ASSOCIATION FOR THE CULTIVATION OF SCIENCE  
JADAVPUR, CALCUTTA 32



# DIFFRACTION EFFECTS IN THE SCATTERING OF NEUTRONS, $\mu$ MESON AND ELECTRONS BY NUCLEI\*

By E. AMALDI

*Professor of Physics, University of Rome*

## INTRODUCTION

The investigation of the diffraction of X-rays and electrons has greatly contributed to our knowledge of the structures of crystals, molecules and atoms. From the detailed experimental determination of the corresponding diffraction patterns it has been possible to derive the interatomic distances, as well as the electron density distributions.

Now, one can ask what are the corresponding phenomena in nuclear physics and what information on nuclear structures can be derived today or will be derived in the future, from sufficiently precise determinations of the involved measurable physical quantities.

One could object that almost all problems of nuclear dynamics give rise to some diffraction effect simply as a consequence of the emission and propagation of the waves representing the incident and the outgoing particles.

However, among the great variety of nuclear processes there are a few which show a very striking similarity to the diffraction of electrons or X-rays by atoms. In the following we will limit our considerations to two phenomena of this type, the first one involving neutrons, *i.e.*, particles showing a very strong interaction with nucleons, the second one involving  $\mu$  mesons or electrons, *i.e.*, particles having a very weak specific interaction with nuclei.

In order to make clear from the beginning the similarities and differences existing between these nuclear phenomena and the diffraction of X-rays and electrons by atoms, we recall that both electrons and X-rays have a very weak interaction with the electron cloud surrounding the nucleus, so that the amplitude of the incident wave does not undergo an appreciable reduction going through the atom acting as scatterer. Therefore, each element of volume  $dv$  of the atom contributes to the scattered wave with a wavelet whose amplitude is proportional to the effective charge  $e|\psi|^2 dv$  contained in  $dv$ .

In the first part we will discuss the scattering and absorption processes by intermediate and heavy nuclei, of neutrons between 10 and 100 MeV kinetic energy because the corresponding wave lengths ( $1.5 - 0.4 \times 10^{-13}$  cm) are of the same order of magnitude or shorter than the nuclear dimensions and therefore, we have to expect diffraction effects.

\* Ripon Lectures delivered in the Indian Association for Cultivation of Science, Calcutta, on January 8 and 9, 1951.

We note that for such high energy neutrons, the special properties of the individual nuclei, such as the resonance levels distribution, are smoothed out and therefore, the cross sections exhibit very simple features which can be deduced by means of general theoretical considerations.

In the second part we note that fast  $\mu$  mesons have such a weak specific interaction with nucleons that they appear to be a tool for investigating the electromagnetic field at short distances, still better than fast electrons whose bremsstrahlung generates electron-showers.

In order to calculate the scattering of fast  $\mu$  mesons or electrons by nuclei we have to consider only the electromagnetic interaction. The result of such a calculation will depend on the used models for the nucleus and for the nucleons. Representing the nucleus with a "one particle model" it is shown that scattering experiments by hydrogen and light elements of  $\mu$  mesons or electrons, of total energy between 300 and 1,000 MeV, can give interesting informations on the law of distribution of the electric charge inside the nucleons as well as on the nuclear structures.

## 1. THE SCATTERING OF FAST NEUTRONS BY NUCLEI

### 1.1 *The Absorption and Scattering of Neutrons. The Optical Theorem*

The total cross section of neutrons with nuclei can be separated in two parts: the first, which we will call  $\sigma_{sc}$ , is the cross section for elastic scattering, the second one, which we will call  $\sigma_a$ , is the cross section for absorption, i.e., the cross section for all other processes different from elastic scattering:

$$\sigma_t = \sigma_{sc} + \sigma_a \quad \dots (1.1)$$

In order to make clear the general relations existing among  $\sigma_{sc}$  and  $\sigma_a$ , let us consider the plane wave representing (in the frame of reference of the centre of gravity of the neutron+nucleus system) the incident beam of mono-energetic neutrons, moving along the  $z$ -axis at great distance from the nucleus

$$\psi_i = \frac{1}{\sqrt{v}} e^{ikz} \quad \dots (1.2)$$

$v$  is the relative velocity,  $k = \frac{1}{\lambda^*} = \frac{mv}{\hbar}$  the corresponding propagation vector,  $m$  the reduced mass and  $\lambda^* = \lambda/2\pi$ . The factor  $\frac{1}{\sqrt{v}}$  has been introduced in order to get a wave function normalized to 1 incident neutron per  $\text{cm}^2$  and per sec.

It is well known that the plane wave (1.2) can be expanded into spherical harmonics (Mott and Massey,). The asymptotic form of such expansion is

$$\psi_i \rightarrow \sqrt{\frac{\pi}{v}} \frac{1}{kr} \sum_{l=0}^{\infty} (2l+1)^{1/2} l^{(l+1)} \left[ e^{-i(kr-l\pi/2)} - e^{+i(kr-l\pi/2)} \right] Y_l^{(0)}(\cos\theta) \quad \dots (1.3)$$

In this expression the incident plane wave has been separated in pairs of spherical waves ; each pair contains an incident as well an outgoing wave, both of angular momentum  $l\hbar$ .

The nucleus, that is supposed to be situated in the origin, will change the expression of the wave function with respect to the unperturbed wave (1.3) as a consequence of the fact that part of the incident neutrons will be scattered elastically, part will be absorbed while other particles,  $\gamma$  quanta or neutrons of lower energy, will be emitted.

Now we limit our considerations to the scattering and absorption processes of the incident neutrons, *i.e.*, we do not try to investigate the subsequent division of the cross section  $\sigma_a$  into the cross sections for the different reactions. From this point of view it is evident that the nuclear reactions will change only the outgoing wave with respect to the unperturbed expansion (1.3). Therefore, the asymptotic behaviour of the actual wave function  $\psi$  of the neutrons of velocity  $v$  will differ from (1.3) only in the coefficient of  $e^{ikr}$

$$\sqrt{\frac{\pi}{v}} \frac{1}{kr} \sum_l (2l+1)^{1/2} i^{l+1} \left[ e^{-i(kr-l\pi/2)} - \eta_l e^{i(kr-l\pi/2)} \right] Y_l^{(0)}(\cos\theta) \quad \dots \quad (1.4)$$

where the  $\eta_l$  are complex coefficients satisfying the condition

$$|\eta_l|^2 \leq 1 \quad \dots \quad (1.5)$$

as we will see in the following.

Equation (1.4) does not solve our problem but simply represents a convenient form under which our solution can be written.

In order to find the solution of our problem it would be necessary to calculate the factors  $\eta_l$  *i.e.* to solve the Schrödinger equation making use of a convenient model of the nucleus and of its interaction with the incident neutrons.

However, a few very general conclusions about the cross sections  $\sigma_{sc}$  and  $\sigma_a$  can be derived from equation (1.3) and (1.4) without detailed informations on the actual values of  $\eta_l$  (Blatt and Weisskopf, 1950).

In order to derive these general relations we note that the asymptotic form of the scattered wave  $\psi_{sc}$ , is simply given by the difference between (1.4) and (1.3), *i.e.*

$$\psi_{sc} = \psi - \psi_i \quad \dots \quad (1.6)$$

Our wave functions have been normalized to 1 incident neutron per  $\text{cm}^2$  and per second ; therefore the cross section  $\sigma_{sc}$  is simply given by the flux of the scattered particles through a great sphere of radius  $r$  surrounding the nucleus, *i.e.*, making use of the usual quantum mechanical expression of the density of current

$$\sigma_{sc} = \frac{\hbar}{2im} \int_{4\pi} \left\{ \frac{\delta\psi_{sc}}{\delta r} \psi_{sc}^* - \frac{\delta\psi_{sc}^*}{\delta r} \psi_{sc} \right\} r^2 \sin\theta d\theta d\phi \quad \dots \quad (1.7)$$

From (1.3), (1.4) and (1.7) one gets

$$: \sum_l \sigma_{sc}^{(l)} \quad \sigma_{sc}^{(l)} = \pi \lambda^2 (2l+1) |1 - \eta_l|^2 \quad (1.8)$$

In order to get  $\sigma_a$  we have to consider the net flux of neutrons into the sphere of radius  $r$  (very large) *i.e.*, the number of neutrons going into the sphere minus the number of neutrons coming out of it. Namely, we have to calculate the flux of neutrons going into the sphere of radius  $r$  making use of the wave function (1.4)

$$\frac{\hbar}{2im} \int_{4\pi} \left\{ \frac{\delta \psi}{\delta r} \psi^* - \frac{\delta \psi^*}{\delta r} \psi \right\} r^2 \sin \theta d\theta d\phi \quad (1.9)$$

From (1.4) and (1.9) one gets immediately

$$r_a = \sum_l \sigma_a^{(l)}, \quad r^{(l)} = \pi \lambda^2 (2l+1) (1 - \eta_l) \quad (1.10)$$

From this last equation we see that condition (1.5) is equivalent to the obvious condition  $\sigma_a \geq 0$ .

Let us now raise a few remarks about equations (1.8) and (1.10).

(a) First we note that, as a consequence of the orthogonality of the spherical harmonics, both cross sections  $\sigma_{sc}$  and  $\sigma_a$  can be expressed as sums of terms corresponding to different values of  $l$ . Such a separation will not be possible for the differential scattering cross section that we will consider in section 1.2.

(b) Using the inequality (1.5) in connection with the equations (1.8) and (1.10) we can derive the extreme values of  $\sigma_{sc}^{(l)}$  and  $\sigma_a^{(l)}$ . In Table 1.1 we give a few interesting examples:  $\eta_l = -1$  means that the nucleus does not produce a change of the amplitude but only a reverse of the phase of the outgoing wave; therefore, the nucleus does not absorb while  $\sigma_{sc}^{(l)}$  reaches its maximum value.  $\eta_l = +1$  means obviously that the nucleus does not affect at all the wave of angular momentum  $l$  and therefore,  $\sigma_{sc}^{(l)} = \sigma_a^{(l)} = 0$ . Finally,  $\eta_l = 0$  means that  $\psi$  does not contain an outgoing wave of angular momentum  $l$  and therefore  $\sigma_a^{(l)}$  reaches its maximum value and we have

(1)

TABLE 1.1

A few examples of the values of the cross sections  $\sigma_a^{(l)}$  and  $\sigma_{sc}^{(l)}$

$\eta_l$	$\sigma_a^{(l)}$	$\sigma_{sc}^{(l)}$
-1	0	$4\pi\lambda^2(2l+1)$
0	$\pi\lambda^2(2l+1)$	$\pi\lambda^2(2l+1)$
+1	0	0

(c) A very interesting case is that of a "very large black nucleus with sharp edge" i.e., a nucleus whose radius  $R$  is much larger than the wavelength  $\lambda^*$  and which absorbs completely the neutrons striking its surface while does not absorb at all the particles moving close to its surface. Owing to the condition

$$\lambda^* \ll R \quad \dots (1.11)$$

we can describe the collision process in classical terms, namely we can say that the impact parameter of a neutron of angular momentum  $\hbar l$  is given by  $\lambda^* = \frac{\hbar l}{p}$  so that the above mentioned conditions of a black body with sharp edge reduce to

$$\eta_l = 0 \quad \text{for } \lambda^* \leq R \quad \dots (1.11')$$

$$\eta_l = 1 \quad \text{for } \lambda^* > R$$

Introducing these values in (1.8) and (1.10) we get

$$\sigma_{sc} = \sigma_a = \sum_l \frac{R}{\lambda^*} (2l+1) \pi \lambda^{*2} = \pi (R + \lambda^*)^2 \approx \pi R^2 \quad \dots (1.12)$$

and therefore, from equation (1.1)

$$\sigma_t = \sigma_{sc} + \sigma_a = 2\pi R^2 \quad \dots (1.13)$$

Equations (1.12) and (1.13) are known as the optical theorem of Bohr, Peierls and Placzek (Bohr, Peierls and Placzek, 1939; Bethe, 1939).

## 1.2 The Shadow Diffraction

The result contained in equations (1.12) and (1.13) is a seeming paradox; a black sphere, whose radius  $R$  satisfies the condition (1.11) has a total cross section equal to twice the geometric cross section. The explanation of this difficulty lies in the fact that the incident plane wave plus the scattered wave must give account of the shadow behind the sphere. Therefore, the scattered wave has the function of extinguishing that part of the incident plane wave which lies behind the sphere. But the shadow cannot be sharp because of diffraction effects whose order of magnitude can be obtained in the following way: The angle of deflection of the incident neutrons of momentum  $p$ ,  $\theta = \Delta p/p$  corresponding to the diffraction, can be derived from the uncertainty relations  $\Delta p \Delta q \sim \hbar$  assuming  $\Delta q \sim R$  (figure 1.1):

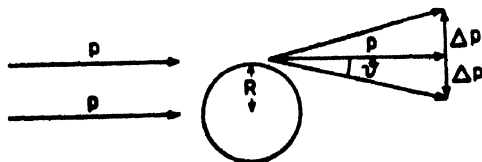


FIG. 1.1

$$\theta \sim \frac{\hbar}{R p} = \frac{\lambda^*}{R} \quad (1.14)$$

That means that the diffraction effect is concentrated in a forward cone of opening angle  $\vartheta$ , so that if we make an observation at such a great distance behind the black sphere that

$$L\vartheta > R \quad \dots \quad (1.15)$$

its shadow will be completely blurred over by the diffraction pattern.

In other words, we can say that if we make observations behind a black sphere at distances from it smaller than

$$L_c = \frac{R}{\vartheta} = \frac{R^2}{\lambda^*} \quad \dots \quad (1.16)$$

we will find the shadow, while if we make observations behind the same sphere at distances larger than  $L_c$  we will find a Fraunhofer diffraction pattern with a maximum of intensity for  $\vartheta=0$ . Such a diffraction pattern corresponds to the elastic scattering cross section  $\sigma_{sc}$  as we will see quantitatively in a short while. The seeming paradox contained in the optical theorem is due to the fact that for macroscopic black spheres the observations are usually performed at distances smaller than the critical distance  $L_c$ , while the contrary condition is satisfied in the scattering experiments of fast neutrons by nuclei.

That the elastic scattering cross section corresponds to a diffraction effect, can be easily recognized by calculating the corresponding differential expression.

This is immediately obtained by dropping the integration appearing in equation (1.7). One gets

$$\frac{d\sigma_{sc}}{d\omega} = \frac{\pi}{k^2} \left| \sum_l (2l+1)^{\frac{1}{2}} (1-\eta_l) Y_l^{(0)}(\cos \vartheta) \right|^2 \quad (1.17)$$

First we note that the remark (a) raised in section 1.1 about  $\sigma_{sc}$  does not hold for  $\frac{d\sigma_{sc}}{d\omega}$ : the waves corresponding to different angular momental interfere in equation (1.17), so that we cannot write it as a sum of contributions corresponding to different values of  $l$ . A detailed calculation of (1.17) needs the knowledge of  $\eta_l$ .

An interesting and simple case is again that considered at the end of the preceding section i.e. the case of a "very large black nucleus with sharp edge." Introducing the conditions (1.11) and (1.11') in (1.17) we get

$$\frac{d\sigma_{sc}}{d\omega} = \frac{\pi}{k^2} \left| \sum_l^{R/\lambda^*} (2l+1)^{1/2} Y_l^{(0)}(\cos \vartheta) \right|^2 \quad \dots \quad (1.18)$$



For small values of  $\vartheta$  this equation can be put in the form

$$\frac{d\sigma_{sc}}{d\omega} = R^2 \left| \frac{J_1\left(\frac{R\vartheta}{\lambda^*}\right)}{\vartheta} \right|^2 \quad \dots \quad (1.19)$$

where  $J_1(x)$  is a Bessel function of the first kind.\*

This expression gives simply the intensity distribution of the Fraunhofer diffraction pattern produced by a big black sphere. One can immediately recognize that in accordance with equation (1.12) we have

$$\sigma_{sc} = \int_0^\pi \frac{d\sigma_{sc}}{d\omega} 2\pi \sin \vartheta d\vartheta = \pi R^2$$

\* Equation (1.19) has been derived by Bethe and Placzek (1939) and Akhiezer and Pomeranchuk (1945). Its proof can be summarized as follows :

First we recall the well-known relations

$$Y_l^{(0)} = \frac{(2l+1)^{1/2}}{\sqrt{4\pi}} P_l ;$$

$$\lim_{l \rightarrow \infty} P_l \left( 1 - \frac{z^2}{2l^2} \right) = J_0(z)$$

which last, for  $z = 2l \sin \vartheta/2$ , gives

$$\lim_{l \rightarrow \infty} P_l (\cos \vartheta) = J_0(2l \sin \vartheta/2)$$

$$\vartheta \rightarrow 0$$

For very large  $\frac{R}{\lambda^*}$ , we can write

$$\begin{aligned} \sum_0^{R/\lambda^*} (2l+1)^{1/2} Y_l^{(0)} (\cos \vartheta) &= \sum_0^{R/\lambda^*} \frac{1}{\sqrt{4\pi}} (2l+1) P_l (\cos \vartheta) \simeq \\ &\simeq \frac{1}{2\sqrt{\pi}} \sum_0^{R/\lambda^*} 2l P_l (\cos \vartheta) \simeq \frac{1}{\sqrt{\pi}} \int_0^{R/\lambda^*} l P_l (\cos \vartheta) dl \simeq \\ &\simeq \frac{1}{\sqrt{\pi}} \frac{1}{(2 \sin \vartheta/2)^2} \int_0^{R/\lambda^*} J_0(2l \sin \vartheta/2) d(2l \sin \vartheta/2) = \frac{1}{\sqrt{\pi}} \frac{1}{(2 \sin \vartheta/2)^2} \int_0^{R/\lambda^* \sin \vartheta/2} J_0(x) x dx \\ &= \frac{d}{dx} [x J_1(x)] = x J_0(x) \end{aligned}$$

and introducing the factor  $\frac{\pi}{k^2} = \pi \lambda^{*2}$ ; give

$$\frac{d\sigma_{sc}}{d\omega} = R^2 \left[ \left( \frac{J_1\left(\frac{R}{\lambda^*} 2 \sin \vartheta/2\right)}{2 \sin \vartheta/2} \right)^2 \right] \text{ for } \vartheta \ll 1; R/\lambda^* \gg 1$$

Finally we note that in order to calculate  $\sigma_{sc}$  from the preceding equation we need the following integral

$$\int_0^{x \text{ large}} \left[ \frac{J_1(x)}{x} \right]^2 x dx = \pi/2$$

### 1.3 Experimental Result on $\sigma_t$ , $\sigma_a$ and $\sigma_{sc}$

In order to be able to compare the preceding theoretical considerations with some experimental results, we note that the de Broglie wave-length, divided by  $2\pi$ , of a neutron of kinetic energy  $E$ , is given by

$$\lambda_0^* = \frac{4.55 \cdot 10^{-10} \text{ cm}}{E_{\text{ev}}^{1/2}} \quad \dots \quad (1.20)$$

Two conditions must be satisfied for a correct use of (1.20): (1) the mass of the incident neutron must be so small with respect to the mass  $M$  of the target nucleus that the frame of reference of the centre of gravity can be identified with the laboratory frame of reference.

If such a condition is not satisfied, the correct value of  $\lambda^*$  is obviously given by

$$\lambda^* = \frac{m + M}{m} \lambda_0^* \quad \dots \quad (1.21)$$

(2) the velocity of the incident neutron must be so small with respect to the velocity of light that the relativistic corrections can be neglected. If this condition is not satisfied, we have to substitute (1.20) with

$$\lambda_n^* = \frac{4.55 \times 10^{-10} \text{ cm}}{\left[ E_{\text{ev}} \left( 1 + \frac{E_{\text{ev}}}{2mc^2} \right) \right]^{1/2}} \quad \dots \quad (1.22)$$

In the following we will discuss separately the measurements of the various quantities involved in the preceding considerations, namely  $\sigma_t$ ,  $\sigma_a$  and  $\sigma_{sc}$ .

Before doing that we note that most of the experiments, that will be described in the following, have been performed using the so-called threshold-detector technique which is based on the following principle. The neutrons emitted in a convenient reaction have a spectrum extending up to a maximum energy  $E_{\text{max}}$  and are detected by means of the activity produced in a convenient detector having a threshold energy  $E_{\text{th}}$ . The neutrons involved in an experiment of this type belong to the energy interval  $E_{\text{max}} - E_{\text{th}}$  and can be considered as almost monoenergetic provided the condition

$$E_{\text{max}} - E_{\text{th}} \ll E_{\text{max}} \quad \dots \quad (1.23)$$

is satisfied.

*A -Measurements of  $\sigma_t$ .* The total cross section is usually measured by means of a transmission experiment with a very good geometry. The existence of a shadow diffraction represented more or less correctly by equation (1.19), imposes that the solid angles, under which the scatterer is seen from the neutrons source and both the neutrons source and the detector are seen from the scatterer, have an opening angle  $\theta$  much smaller than  $\frac{\lambda^*}{R}$ . If this condition is not satisfied the experimental results need to be corrected for the so-called "scattering in" effects.

TABLE 1.2  
 $\sigma_t \times 10^{24} \text{cm}^2$ 

$E \text{ (MeV)}$ $\lambda^* \times 10^3 \text{cm}$	14 1, 21	25 0, 91	42 0, 60	90 0, 47	95 0, 45
Element					
1 H	$0.694 \pm 0.019$		$0.203 \pm 0.007$	$0.083 \pm 0.004$	$0.073 \pm 0.002$
2 D	$0.864 \pm 0.028$		$0.280 \pm 0.013$	$0.117 \pm 0.005$	$0.104 \pm 0.004$
3 Li			$0.684 \pm 0.011$	$0.314 \pm 0.006$	
4 Be	$0.65 \pm 0.04$		$0.853 \pm 0.010$	$0.431 \pm 0.008$	$0.396 \pm 0.004$
5 B	$1.16 \pm 0.13$		$0.985 \pm 0.020$		
6 C	$1.23 \pm 0.02$	1.29	$1.089 \pm 0.011$	$0.550 \pm 0.011$	$0.498 \pm 0.003$
7 N			$1.220 \pm 0.025$	$0.656 \pm 0.021$	$0.663 \pm 0.007$
8 O		1.60	$1.358 \pm 0.012$	$0.765 \pm 0.020$	
9 F			$1.603 \pm 0.030$		
11 Na			$1.67 \pm 0.060$		
12 Mg	$1.83 \pm 0.10$		$1.723 \pm 0.024$	$1.03 \pm 0.02$	
13 Al	$1.92 \pm 0.09$	1.85	$1.782 \pm 0.020$	$1.12 \pm 0.02$	$0.993 \pm 0.011$
16 S	$1.58 \pm 0.10$		$1.974 \pm 0.030$		
17 Cl		1.88	$2.11 \pm 0.040$	$1.38 \pm 0.03$	$1.28 \pm 0.02$
20 Ca			$2.210 \pm 0.026$		
26 Fe	$2.75 \pm 0.09$		$2.441 \pm 0.021$		
28 Ni	$2.62 \pm 0.09$		$2.510 \pm 0.034$		
29 Cu	$2.86 \pm 0.15$	2.50	$2.540 \pm 0.019$	$2.22 \pm 0.04$	$2.00 \pm 0.02$
30 Zn	$3.03 \pm 0.17$		$2.618 \pm 0.027$	$2.21 \pm 0.04$	
34 Se	$3.35 \pm 0.20$				
35 Br			$2.93 \pm 0.06$		
38 Sr			$2.99 \pm 0.12$		
42 Mo			$3.11 \pm 0.05$		
47 Ag	$3.82 \pm 0.13$	3.70	$3.229 \pm 0.034$		
48 Cd	$4.25 \pm 0.13$				
50 Sn	$4.52 \pm 0.14$		$3.251 \pm 0.023$	$3.28 \pm 0.06$	$3.18 \pm 0.03$
51 Sb	$4.35 \pm 0.15$				
53 I			$3.51 \pm 0.06$		
56 Ba			$3.57 \pm 0.12$		
73 Ta			$4.20 \pm 0.04$		
74 W			$4.31 \pm 0.06$		
79 Au	$4.68 \pm 0.9$				
80 Hg	$5.64 \pm 0.24$	5.25	$4.51 \pm 0.06$		
82 Pb	$5.05 \pm 0.15$		$4.44 \pm 0.05$	$4.53 \pm 0.09$	$4.48 \pm 0.03$
83 Bi	$5.17 \pm 0.17$		$4.58 \pm 0.06$		
90 Th			$5.03 \pm 0.07$		
92 U			$5.12 \pm 0.07$	$5.03 \pm 0.10$	$4.92 \pm 0.06$

The measurements of  $\sigma_t$  performed in the considered range of energy are collected in Table 1.2. For reason of completeness we give also the results obtained for very light elements although they will not be considered in the following.

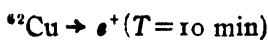
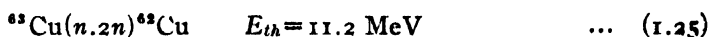
The experiments of column 2 (Amaldi, *et al.*, 1946, 1947; Ageno, *et al.*, 1943, 1947) and 3 (Sherr, 1945) have been performed making use of neutrons produced by means of the reaction

$$D + L_d \text{ (various } Q \text{ up to } Q = 15.03 \text{ MeV)} \quad \dots \quad (1.24)$$

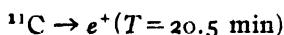
respectively for  $E_D = 0.9 \text{ MeV}$  and emission at  $90^\circ$ . ( $E_{max} \approx 14 \text{ MeV}$ ) and for  $E_D = 10.2 \text{ MeV}$  and emission in the forward direction with respect to the direction of motion of the deuterons ( $E_{max} = 25.4 \text{ MeV}$ ).

The experiments of column 4 (Hildebrand and Leith, 1950), 5 (Cook, *et al.*, 1949) and 6 (De Juren and Knable, 1950) have been performed with neutrons produced by "stripping" of deuterons (Helmholtz, *et al.* 1947) of respectively  $E_D \approx 80$  MeV, 190 MeV, colliding against a Be target.

In the experiment of column 2 as detector was used the reaction



while the experiments of columns 3, 4 and 5 have been performed using as detector the reaction



and that of column 6 a bismuth fission ionization chamber (Wiegand, 1948) which has a threshold of about 50 MeV.

Therefore, while the experiments at 14 MeV and 25 MeV refer to neutrons belonging to a rather narrow energy interval, at higher energy the neutrons spread extends over an interval which is not limited by the threshold of the detector: the neutrons spectrum is simply that produced in the stripping of the deuterons (Helmholtz, *et al.*, 1947), deformed by the excitation curve of the detector.

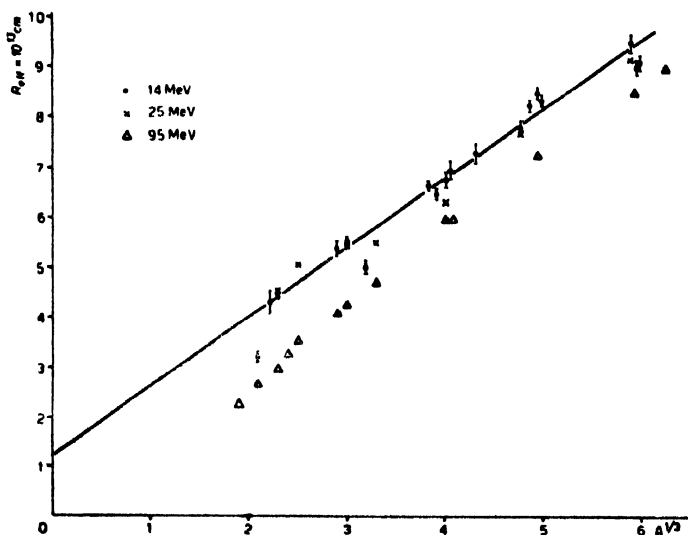


FIG. 1.2

Although the discussion of these results will be given in sections 1.4 and 1.5, we call attention to figure 1.2 where we plot, as function of  $A^{1/3}$

( $A$  = mass number)

$$R_{eff} = \left( \frac{\sigma_t}{2\pi} \right)^{1/2} \quad 1.27$$

for  $E = 14$  MeV, 25 MeV and 90 MeV.  $R_{eff}$  must be equal to the radius  $R$  of the nucleus only if the conditions for the applicability of the optical theorem are satisfied.

One recognizes immediately that the results obtained at 14 and 25 MeV can be roughly represented by a linear law

$$R_{eff} = b + r_0 A^{1/3} \quad 1.28$$

while that is not possible at higher energies: a systematic deviation of  $R_{eff}$  from equation (1.28) is evident already for  $E = 44$  MeV although for sake of simplicity the corresponding points have not been plotted in figure 1.2.

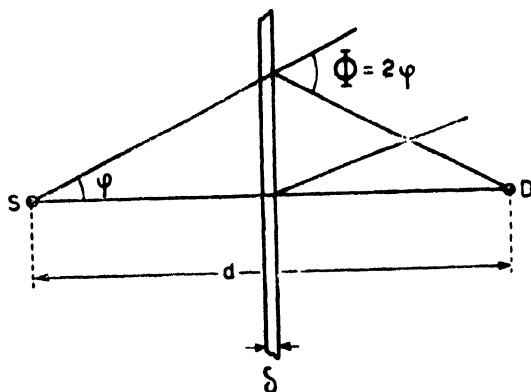


FIG. 1.3

From inspection of figure 1.3 one sees that while equation (1.28) represents rather well the general trend of the experimental results at low energy, on account of the deviations of the individual points, it is not possible to determine with precision the values of the constants  $b$  and  $r_0$ . The straight line drawn in Figure 1.2, corresponding to

$$b = 1.2 \times 10^{-13} \text{ cm}, \quad r_0 = 1.4 \times 10^{-13} \text{ cm}. \quad 1.29$$

has been obtained giving small weight to the values for  $\text{Be}^{(*)}$  and  $\text{S}$  which do not fit a smooth curve while, applying statistical methods (Amaldi, *et al.*, 1947) one obtains  $b = (0.696 \pm 0.082) \times 10^{-13}$ ;  $r_0 = (1.52 \pm 0.02) \times 10^{-13} \text{ cm}$ .

By comparing these last values with (1.29), we can conclude that although it is not possible to state the best values of  $b$  and  $r_0$ ,  $b$  is certainly different from zero and of the order of  $10^{-13} \text{ cm}$ . In the original papers (Amaldi, *et al.*, 1946, 1947; Sharr, 1945)  $b$ .

(\*) According to Lasdov (1951)  $\sigma_t$  for Be is much larger ( $\sigma_t = (1.41 \pm 0.11) \times 10^{-24} \text{ cm}^2$ ) than given in Table 1.2.

was interpreted as the surface effect of the nucleus or, using the term introduced by Bethe (1939), the "diffuseness of the nuclear surface" due, in part, to the range of the nuclear forces, and in part to the zero-point oscillation of the nuclear particles.

In section 1.4 we will come back to this point and we will see that a large part or perhaps all the constant intercept  $b$  can be interpreted in a different way.

Finally, we note that the deviations of the individual points for  $E=14$  MeV from the straight line (1.28) are much larger than expected according to their experimental errors. This fact suggests the existence of individual variations of the nuclear radii (Amaldi, et. al., 1947). Such a suspicion seems to have a confirmation in the recent measurements of Lasday (1951) who finds, for  $E=14$  MeV, an anomalously small value of  $\sigma$ , for Zr, whose more abundant isotope is  $^{90}_{40}\text{Zr}$  (48%) containing the magic number of neutrons  $N=50$ —

*B-Measurements of  $\sigma_a$ .* Also  $\sigma_a$  can be measured by means of a transmission experiment with a threshold detector, provided the two following conditions be satisfied :

(1) the threshold  $E_{th}$  of the detector is so close to the maximum energy  $E_{max}$  of the incident neutrons that all neutrons scattered inelastically have an energy smaller than  $E_{th}$ .

(2) the experimental set up is drawn in such a way as to eliminate completely the elastic scattering.

For a very thin absorber this last condition can be satisfied exactly(\*). However this case does not show much interest from the practical point of view

(\*) In figure 1.3,  $S$  is a point source and  $D$  a spherical detector of section  $A$  (very small) ; the absorber of thickness  $\delta$  (very small) containing  $N$  atoms per  $\text{cm}^3$  is an infinite plane placed midway between the source and the detector. The so called Christy argument runs as follows :

$$\begin{aligned} \text{Scattering in} &= N \int_0^{\pi/2} 2\pi \sin \phi d\phi \frac{\delta}{\cos \phi} \left( \frac{A}{2 \cos \phi} \right)^2 \frac{d\sigma_{sc}(2\phi)}{d\omega} \\ &= N \frac{A\delta}{d^2} 4 \int_0^{\pi/2} \frac{d\sigma_{sc}(2\phi)}{d\omega} 2\pi \cos \phi \sin \phi d\phi \\ &= N \frac{A\delta}{d^2} \int_0^\pi \frac{d\sigma_{sc}(\phi)}{d\omega} 2\pi \sin \phi d\phi \\ \text{Scattering out} &= N \frac{A\delta}{d^2} \int_0^\pi \frac{d\sigma_{sc}(\phi)}{d\omega} 2\pi \sin \phi d\phi \end{aligned}$$

These two expressions are equal to one another and therefore the transmission measured under these conditions is determined only by  $\sigma_a$ .

The preceding argument can be generalized as follows : if the absorber has the shape of a revolution surface of thickness  $\delta(\phi)$  (figure 1.4) we have immediately

$$\text{Scattering out} = N \frac{A\delta(0)}{d^2} \int_0^\pi \frac{d\sigma_{sc}(\phi)}{d\omega} 2\pi \sin \phi d\phi$$

and therefore the principle of an experiment devised to measure  $\sigma_a$  is usually the following : let us consider a sphere of radius  $Z_0$  having in the centre a monoenergetic point source of neutrons : one measures the flux of neutrons crossing the surface of the sphere, once with the sphere filled and once with the sphere evacuated of the element under investigation : the ratio  $T(Z_0)$  of these two quantities is simply given by

$$T(Z_0) = e^{-Z_0/\Lambda_a} f(Z_0) \quad \dots (1.30)$$

where  $\Lambda_a = \frac{1}{N\sigma_a}$  and  $N$  is the number of atoms per  $\text{cm}^3$ ,  $f(Z_0)$  is the correction factor (constant and equal to 1 in an ideal experiment) which is due to the fact that, as a consequence of the processes of scattering, the average distance crossed by the neutron through the absorber is larger than  $Z_0$ .

$f(Z_0)$  can be easily calculated if we know  $\frac{d\sigma_{sc}}{d\omega}$  through a direct experiment or a reasonable assumption about it (Amaldi, *et. al.*, 1946, 1947).

The first measurements of  $\sigma_a$  have been performed by Grahame and Seaborg (1938) detecting the neutrons emitted by a Ra + Be source by means of the activity induced according to the reaction  $^{235}\text{U}(n, p)^{235}\text{Mn}$ , which has

$$\text{Scattering in} = N \int 2\pi \sin \phi d\phi \delta(\phi) \frac{d\sigma_{sc}(\phi)}{d\omega} \frac{A}{\rho^2} = \frac{NA}{\delta(0)} \int 2\pi \sin \phi d\phi \frac{\delta(\phi)}{\delta(0)} \frac{d\sigma_{sc}(\phi)}{d\omega} \left( \frac{d}{\rho} \right)^2$$

In order to have that the scattering in compensates exactly the scattering out we have to impose

$$\int 2\pi \sin \phi d\phi \frac{\delta(\phi)}{\delta(0)} \frac{d^2}{\rho^2} \frac{d\sigma_{sc}(\phi)}{d\omega} = \int_0^\pi \frac{d\sigma_{sc}(\phi)}{d\omega} 2\pi \sin \phi d\phi$$

or

$$(I) \quad \sin \phi d\phi \frac{\delta(\phi)}{\delta(0)} \frac{d^2}{\rho^2} = \sin \phi d\phi$$

By inspection of Fig 1.4 we have

$$(II) \quad \frac{d}{\sin \phi} = \frac{r}{\sin(\phi - \phi)} ; \quad \frac{d}{\rho} = \frac{\sin \phi}{\sin \phi}$$

and, therefore,

$$\frac{\delta(\phi)}{\delta(0)} \frac{d\phi}{\sin \phi} = \frac{d\phi}{\sin \phi}$$

that, for  $\frac{\delta(\phi)}{\delta(0)} = 1$ , gives

$$\frac{d\phi}{\sin \phi} = \frac{d\phi}{\sin \phi}$$

(III)

$$\alpha \tan \phi / 2 = \tan \phi / 2$$

where  $\alpha$  is an arbitrary constant.

By combining (II) and (III) one gets immediately the equation  $r = r(\phi)$  which contains

the arbitrary constant  $r(0) = d \frac{\alpha - 1}{\alpha}$

an appreciable cross section only for neutrons of energy larger than 7 MeV. In this experiment conditions (1) and (2) are not satisfied and therefore the results of these authors will not be considered in the following :

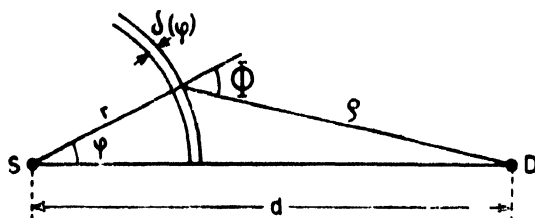


FIG. 1.4

The first experiment satisfying condition (1) has been done by Soltan (1938) who detected by means of reaction (1.25), the neutrons produced in reaction (1.24) by low energy deuterons. Although the geometry did not satisfy conditions (2) and the corresponding corrections had not been considered with the necessary care, the results of this author agree with that obtained, at a later time, by others (Amaldi, *et al.*, 1946) in the attempt to verify the optical theorem.

In these last experiments the conditions of production and detection of neutrons were exactly the same as that used in the measurements of  $\sigma_t$  at 14 MeV given in Table 1.2. The results are collected in Table 1.3 where we give also the correction factor  $f(Z_0)$  appearing in equation (1.30) whose values, very close to one, allow to recognize that the used geometry was rather satisfactory.

The result obtained for Pb has also been confirmed by other researchers (Gittings, *et al.*, 1949) who used the neutrons of  $14 \pm 0.5$  MeV produced by the D + T reaction.

In column 4 of Table 1.3 we give also the quantity

$$2\sigma_a$$

which according to the optical theorem (1.12) (1.13) is expected to be equal to 1.

TABLE 1.3

$\sigma_a$  at 14 MeV

Element	$f(Z_0)$	$\sigma_a \times 10^{24} \text{ cm}^2$	$\frac{2\sigma_a}{\sigma_t}$
Al	0.95	$0.99 \pm 0.04$	$1.03 \pm 0.05$
Fe	0.93	$1.43 \pm 0.05$	$1.04 \pm 0.04$
Hg	0.96	$2.47 \pm 0.12$	$0.88 \pm 0.06$
Pb	1.01	$2.22 \pm 0.05$	$0.88 \pm 0.03$



TABLE 1.4  
 $\sigma_a/\sigma_t$  at 95 MeV

Element	$\sigma_a/\sigma_t$
C	$0.45 \pm 0.015$
Al	$0.42 \pm 0.015$
Cu	$0.39 \pm 0.005$
Pb	$0.39 \pm 0.01$

From these experimental data we can conclude that the nuclei existing in nature satisfy, at least approximatively, the optical theorem. However, in section 1.4 we will come back to this point trying to discuss the properties of nuclei under assumptions not so extreme as that required for the validity of the optical theorem.

The only measurement of  $\sigma_a$  at higher energy is that of Dejuren and Knable (1950) who have used the same technique of production and detection of neutrons that they have employed in the measurements of  $\sigma_t$  given in column 6 of Table 1.2. In their experiment, condition (1) was not satisfied while probably the experimental set up was not very far from satisfying condition (2) on account of the fact that high energy neutrons scattered elastically move in a forward cone of small opening angle. Table 1.4 contains the ratio  $\sigma_a/\sigma_t$  as given by these authors for a few elements: owing to the fact that condition (1) was not satisfied, the data of Table 1.4 represent a lower limit of  $\sigma_a/\sigma_t$ , probably not to very far from the correct value.

From the inspection of these data we can conclude that although  $\sigma_t$  decreases appreciably going from 14 MeV to about 100 MeV, the ratio  $\sigma_a/\sigma_t$  remains roughly constant and is equal to  $1/2$ .

### C-Measurements of $\frac{d\sigma_{sc}}{d\omega}$ .

Aoki Kikuchi and Wakatuchi (1939) were the first to measure the angular distribution of neutrons scattered by Al, Fe and Pb using the neutrons of the D+D and D+Li reactions, detected with an ionization chamber filled with methane at high pressure, connected to an electrometer. These authors found a very strong scattering in the forward direction, which was soon confirmed by other authors, (Bacher, 1950) and they suggested, as an interpretation of the experimental results, the existence of diffraction effects of the incident neutrons by nuclei.

The conditions which have to be satisfied by an experimental set up drawn to measure  $d\sigma_{sc}/d\omega$  as a function of the angle of deflection  $\theta$ , are obviously the following :

(1) the spectrum of neutrons must extend over such a narrow energy interval that  $\frac{\Delta\lambda^*}{\lambda^*} < 1$

(2) the angular definition must be so good that  $\delta\vartheta < \frac{\lambda^*}{R}$

(3) the background due to neutrons scattered around from the floor, walls and so on and activating the detector, must be small with respect to the intensity of the diffraction pattern.

One could object that condition (3) is not peculiar to experiment on  $\frac{d\sigma_{sc}}{d\omega}$ ; however, in this case, condition (3) is a much more severe requirement than in the experiments on  $\sigma_i$  or  $\sigma_a$ .

The neutrons of 14 MeV produced by reaction (1.24) and detected by means of reaction (1.25) have  $\frac{\Delta\lambda^*}{\lambda^*} \sim \frac{1}{3}$  and therefore roughly satisfy condition (1).

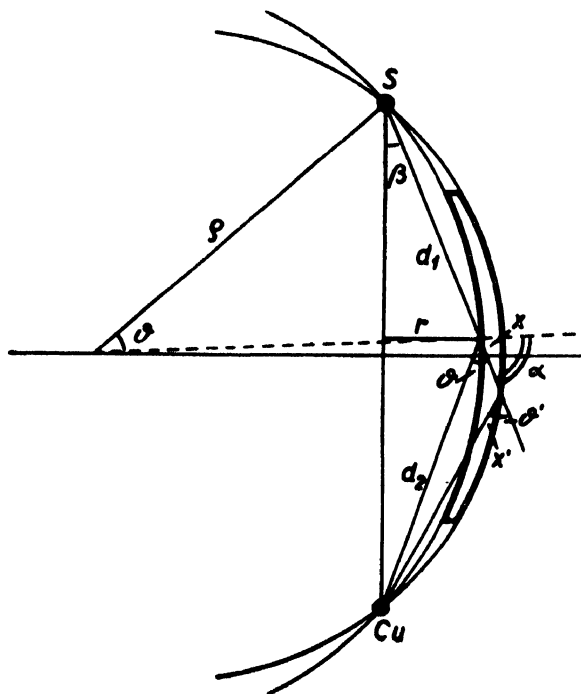


FIG. 1.5

A geometry which has been drawn in order to satisfy conditions (2) and (3) is reproduced in figure 1.5. S and Cu represent the neutron source and the detector. The scatterer is a revolution body, similar to a barrel obtained by rotating the thickly drawn lines around the line S-Cu. Such a scatterer has

the property that all neutrons emitted by S-and going, after a single collision in the scatterer, in the direction of Cu, have been scattered at an angle whose value is between  $\vartheta$  and  $\vartheta'$ .

If, by means of a convenient absorber, the neutrons going directly from S to Cu are cut away, the activity of the detector will give a measure of  $\frac{d\sigma_{sc}}{d\omega}$  integrated over the interval  $\vartheta - \vartheta'$  (Amaldi, *et al.*, 1946, 1947).

The results of figure 1.6 have been obtained using a series of  $\vartheta$  scatterer of Pb corresponding to  $\vartheta = 20^\circ, 25^\circ$  and so on, and  $\vartheta - \vartheta' \approx 2^\circ$ .

The large statistical errors are due to the background which was comparable with the intensity of the scattered neutrons and which has been subtracted from the actual measurements in order to get the results of figure 1.6.

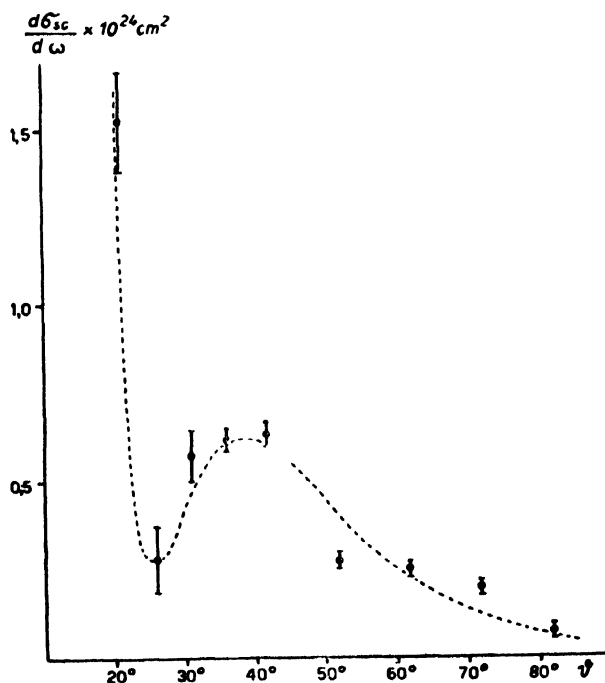


FIG. 1.6

This large background was due to the activation of  $^{63}\text{Cu}(n, \gamma)$  produced by low energy neutrons scattered from the floor, walls and so on.

In spite of that the results of figure 1.6 give some good indication of the existence of a minimum of  $\frac{d\sigma_{sc}}{d\omega}$  around  $\vartheta = 25^\circ$ . Assuming that  $\frac{d\sigma_{sc}}{d\omega}$  is given by equation (1.19) and using  $\lambda^* \approx 1.21 \times 10^{-13}$  one gets for Pb,  $R_{eff} \approx 9 - 10 \times 10^{-13}$  cm in reasonable agreement with the value  $R_{eff} = 9.10^{-13}$  that one gets by applying equation (1.27) to  $\sigma_t$ , i.e., making use of the optical theorem.

$\frac{d\sigma_{sc}}{d\omega}$  has been measured by a Berkeley group (Bratenahl, *et al.*, 1950) for neutrons of  $E = 84$  MeV ( $\lambda^* = 0.48 \times 10^{-13}$  cm), colliding against Al, Cu and Pb nuclei. The neutrons produced by stripping of D on Be were detected by means of reaction (1.26). The available intensity was sufficiently high to allow a very good angular definition with a simple geometry: a spherical scatterer of about 2.5 cm diameter was placed in the neutron beam emerging from a hole through the concrete walls surrounding the cyclotron: the detector was placed at a distance  $r$  from the scatterer in the desired direction (figure 1.7). The experimental results for Pb are reproduced in figure 1.8. The

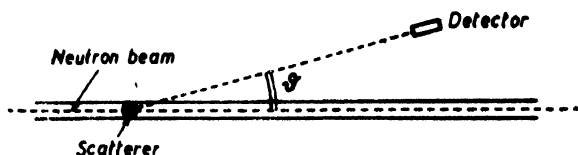


FIG. 1.7

velocity spread of the neutrons used in this experiment is too large to allow to make any statement about the existence of a minimum of  $d\sigma_{sc}$  at a convenient angle as one expects according to the theory of the shadow diffraction. We note that the curve drawn in figure 1.8 does not correspond to equation (1.19), *i.e.*, to the shadow diffraction of a black sphere but to the transparent model that we will discuss in section 1.5.

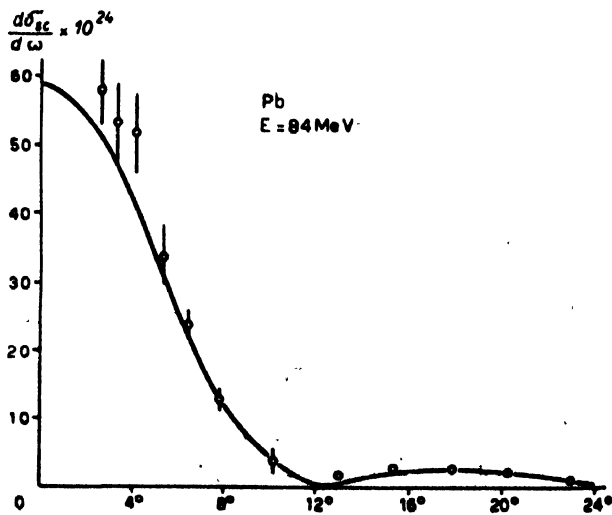


FIG. 1.8

It is perhaps interesting to note that while the transparent model curve fits the experimental results at large angles better than at small angles, the contrary happens with the black nucleus model discussed in sections 1.1 and 1.2.

#### 1.4 The Continuum Theory of the Nucleus

In section 1.3, and particularly in section 1.3 B, we have seen that the optical theorem is approximatively satisfied for neutrons of about 14 MeV. A better agreement between theory and experimental results cannot be expected because the conditions necessary for the validity of the optical theorem correspond to a limiting case which does not exist in nature.

First, we note that condition (1.11) i.e.,  $\lambda^* \ll R$  is not satisfied especially by neutrons of 14 MeV for which  $R/\lambda^*$  is, in the best case (heavy elements) about 7. Second, the assumption that the nucleus behaves as a "black body" up to its edge, is not satisfied at least for neutrons of about 100 MeV kinetic energy.

In this section we will discuss the consequences of the finite value of  $R/\lambda^*$ , while in section 1.5 we will discuss the transparency of the nuclei. Attention to the first point has been given by Feshbach and Weisskopf (1949) who have developed what they call a "continuum theory" of the nucleus. This theory is a great over-simplification of the actual situation which can be useful only as a first orientation of the orders of magnitude of the cross sections. The continuum theory is based on the three following assumptions regarding the structure of the nucleus :

(1) The nucleus has a well-defined surface which is a sphere of radius  $R'$ . The nuclear forces act on the neutron only if its distance from the centre of the nucleus is smaller than  $R'$ . We note that, according to this theory  $R'$  depends also on the type of the incident particle. For instance, in the case of neutrons, we must think  $R'$  as the sum of the radii of the incident neutron  $\rho$  and of the nucleus  $R$

$$R' = R + \rho \quad \dots (1.31)$$

(2) If the neutron penetrates the nuclear surface it moves with a kinetic energy  $E_{in}$  which is higher than its kinetic energy outside the nucleus  $E$ ,

$$E_{in} = E + V \quad \dots (1.32)$$

(3) Inside the nucleus the neutron interacts very strongly with the other nucleons so that it interchanges rapidly its energy with them.

We do not report the continuum theory in details for which we refer to the original paper (Feshbach and Weisskopf, 1949) but we simply raise a few remarks before giving the results of interest for our discussions.

In this theory, the properties of the nuclei are introduced by means of two constants : the radius  $R'$  and the mean potential energy  $V$  of the neutron inside the nucleus. For  $R'$ , Feshbach and Weisskopf assume

$$R' = r_0 A^{1/3} \quad \dots (1.33)$$

and choose that value of  $r_0$  which allows the best fit of all the experimental data collected in Tables 1.2 and 1.3 for  $E = 14$  and 25 MeV.

$V$  is usually taken equal to 28-30 MeV, as it is suggested by the following considerations based on the Fermi gas model (Feshbach, et.al, 1947). According to this model the nucleus, in its ground state, can be described as a completely degenerated Fermi gas contained in a sphere of radius  $R'$ . As a consequence of the fact that the nuclear matter has a constant density (i.e., a density independent of  $A$ ), one gets that the maximum kinetic energy of the Fermi gas is independent of  $A$  and of the order of magnitude of 20 MeV: its actual value depends on the value of the constant  $r_0$  appearing in (1.33): for  $r_0' = 1.5 \times 10^{-13}$  cm, one gets  $E_{max} = 21$  MeV. Making use of the empirical fact that the binding energy  $\epsilon_B$  of a nucleon in a nucleus is roughly constant and equal to 8 MeV, we find that

$$V = E_{max} + \epsilon_B = 21 + 8 = 29 \text{ MeV} \quad \dots (1.34)$$

The continuum theory goes along very simple lines: outside the nucleus the Schrödinger equation is that of a free neutron of propagation vector

$$k = \frac{\sqrt{2mE}}{\hbar}.$$

Inside the nucleus the wave function has roughly the form

of an ingoing wave only, because the chance that the neutron which has penetrated the surface of the nucleus leaves the nucleus with the same energy  $E$ , is extremely small according to assumption (3).

One has to impose the condition that for  $r=R'$ , the logarithmic derivatives of the wave functions outside and inside the nucleus are equal to one another. The logarithmic derivative of the wave function inside the nucleus is simply  $-iK$  where  $K$  is the propagation vector of the neutron inside the nucleus whose expression, according to (1.32) and (1.34), is

$$K = (k^2 + K^2)^{\frac{1}{2}} = k \left( 1 + \frac{V}{E} \right)^{\frac{1}{2}} \quad \dots (1.35)$$

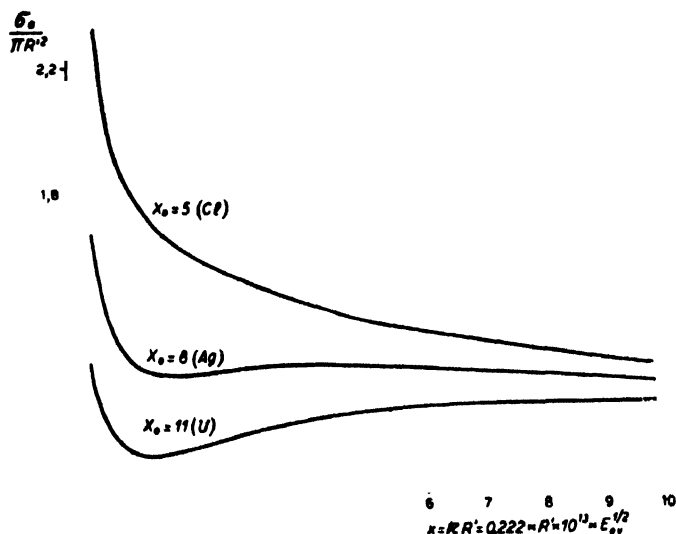


FIG. 1.9

TABLE 1.5

 $R'$  and  $r_0'$  according to the continuum theory

Element	$E$ (MeV)	$R' \times 10^{13}$ cm	$r_0' \times 10^{13}$ cm	Reference
Be	14	2.4	1.17	(Amaldi, <i>et al.</i> , 1946, 1947)
B	14	3.4	1.54	"
C	25	3.8	1.65	(Sherr, 1945)
O	25	4.3	1.71	"
Mg	14	4.5	1.57	(Amaldi, <i>et al.</i> , 1946, 1947)
Al	14	4.6	1.53	"
Al	25	4.6	1.52	(Sherr, 1945)
S	14	4.1	1.30	(Amaldi, <i>et al.</i> , 1946, 1947)
Cl	25	4.7	1.44	(Sherr, 1945)
Fe	14	5.6	1.46	(Amaldi, <i>et al.</i> , 1947, 1947)
Cu	25	5.5	1.38	(Sherr, 1945)
Zn	14	5.9	1.48	(Amaldi, <i>et al.</i> , 1946, 1947)
Sc	14	6.3	1.46	"
Ag	14	6.8	1.44	"
Ag	25	6.9	1.46	(Sherr, 1945)
Cd	14	7.2	1.48	(Amaldi, <i>et al.</i> , 1946, 1947)
Sn	14	7.4	1.52	"
Sb	14	7.3	1.46	"
Au	14	7.5	1.33	"
Hg	14	8.3	1.42	"
Hg	25	8.4	1.44	(Sherr, 1945)
Pb	14	7.8	1.32	(Amaldi, <i>et al.</i> , 1946, 1947)
Bi	14	7.9	1.34	"

We note that we make use of the fact that the wave function inside the nucleus is simply an ingoing wave of propagation vector (1.35), only for  $r=R'$ , while for  $r < R'$  we can think that the wave function is rapidly attenuated according to assumption (3).

In figures 1.9 and 1.10 we give the results of the continuum theory :  $\sigma_a$  and  $\sigma_i$  divided by  $\pi R'^2$  are plotted as a function of

$$x = kR^2 \quad (1.36)$$

for various values of  $X_0 = K_0 R'$ . In fig. 1.10 the curve marked  $\sigma_0$  represents the total cross section for an infinitely repulsive sphere of radius  $R'$ .

The graphs of these figures have been calculated assuming

$$K_0 = 1.0 \times 10^{+13} \text{ cm}^{-1} \quad \dots (1.37)$$

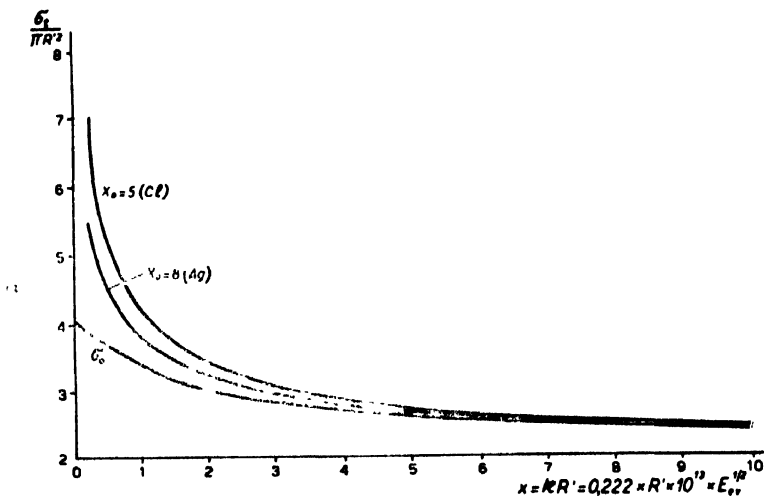


FIG. 1.10

Such a low value corresponds to taking  $\epsilon_H = 0$  in equation (1.34), which is justified, according to Feshbach and Weisskopf, by the fact that a considerable fraction of the binding energy is potential in virtue of the exchange forces between nucleons. The argument appears to be rather qualitative especially in consideration of the fact that the numerical values of  $R'$  and  $r_0$  deduced, applying the continuum theory to the experimental values of  $\sigma_t$  at  $E=14$  and  $25$  MeV (Table 1.5), depend on the chosen numerical value of  $K_0$ .

From figures 1.9 and 1.10 we see that for  $E=14$  or  $25$  MeV,  $\sigma_a$  and  $\sigma_t$  show appreciable deviations from the limit values deduced applying the optical theorem. The data of Table 1.5 show that a value of  $r_0$  close to  $1.4 \times 10^{-13}$  allows to represent fairly well, by means of equation (1.33), the experimental results in columns 2 and 3 of Table 1.2.

The fact that, according to the continuum theory, the radius  $R'$  is better represented by equation (1.33) than by an expression of the type of (1.28), is due to the fact that the asymptotic behaviour of the total cross section  $\sigma_t$ , at high energies, is given, according to equation (1.13), by the expression

$$\sigma_t = \pi(R' + \lambda^*)^2$$

as it is suggested by the semiclassical consideration that the position of the neutron is undefined within a wave length  $\lambda^*$  and by the fact that  $R'$  must not be much different from  $R$ ,



Therefore, the positive intercept  $b$  of equation (1.28) and figure 1.2 must correspond, at least in great part, to the de Broglie wave length  $\lambda^*$  of the incident neutrons. According to this point of view the straight line of figure 1.2 has been drawn taking

We can conclude that at low energies we have

$$R_{\text{eff}} \approx R' + \lambda^* \quad R' = R + \rho \approx R \approx r'_0 A^{\frac{1}{3}}$$

with

$$r'_0 = 1.4 \times 10^{-13} \text{ cm}$$

Here  $\rho$  represents the surface effect of the nucleus, considered at the end of section 1.3 A; such an effect is completely neglected in the continuum theory of Feshbach and Weisskopf which is based on assumption (1) of a well defined surface of the nucleus.

We are now facing a problem which is in great part a matter of definition: if we call  $R$  the radius of the region where the density of nuclear matter is constant, we must expect to have a surface effect (Present, 1941; Bethe, 1930). Therefore, the radius  $R'$  introduced by means of the continuum theory must be slightly larger than  $R$ . But it is evident that both, theoretical and experimental results, are too rough to allow to establish, by comparison, the value of the surface effect.

As a check of their continuum theory, Feshbach and Weisskopf compare the experimental data of Table 1.3 with the theoretical values of  $\sigma_a$  obtained making use of the numerical constants deduced from the empirical data on  $\sigma_i$  (Table. 2, columns 2 and 3). The satisfactory agreement proves that the continuum theory can be used, at least as a first rough approximation for the interpretation of the experimental data.

Finally, we like to call the attention on two aspects of the continuum theory applied to the problem of the elastic scattering. First, we recall that, according to assumption (3), the continuum theory excludes the possibility that the compound nucleus, once formed, emits a neutron of the same energy of the incident one. For  $E$  larger than 10 MeV, it is reasonable to expect that such a process has a rather small probability on account of the existence of many other competing processes, by which the compound nucleus may decay.

Second, the shadow diffraction is given again approximatively by equations (1.12) and (1.19), provided we write in these expressions  $R' + \lambda^*$  instead of  $R$ , but in addition to it, there is the reflection scattering from the side of the nucleus facing the incident beam whose cross section for high energy neutrons (namely  $x \gg X_0$ ) is given by (Feshbach and Hauser, 1950),

$$\sigma_{\text{reflection}} = \pi R'^2 \frac{1}{2} \left( \frac{X_0}{x} \right)^2 \ll \pi R'^2 \approx \sigma_a$$

while for low energy neutrons (namely  $x \ll X_0$ ) is given by

$$\sigma_{\text{reflection}} = \pi R'^2 \left( 1 - \frac{8}{3} \frac{x}{X_0} \right)$$

### 1.5 The Transparency of the Nucleus

Figure 1.11 shows, on a few examples taken from Table 1.2, that  $\sigma_i$  is a decreasing function of the energy  $E$ . By comparing Tables 1.3 and 1.4 we recognize that also  $\sigma_a$  shows a similar behaviour. Such a variation is not expected under the assumption of a "black nucleus" and finds its natural explanation in the transparency of nuclei which becomes quite appreciable at high energy.

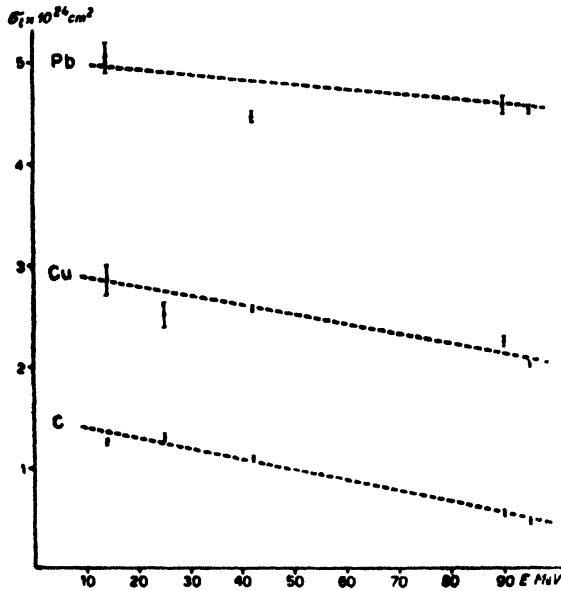


FIG. 1.11

The theory of this effect has been developed by Fernbach, Serber and Taylor (1949) who notice that in order to recognize whether the assumption of a black nucleus is correct or not, one has to consider the mean free path  $\Lambda$  of the incident neutron in the nuclear matter. Such a quantity will be given by the usual expression .

$$\Lambda = \frac{1}{n\sigma} \quad \dots (1.38)$$

where  $n$  is the number of nucleons per  $\text{cm}^3$  of nuclear matter

$$n = \frac{A}{\frac{4}{3}\pi R^3} = \frac{3}{4\pi} \frac{1}{r_0^3}, \quad \dots (1.39)$$

and  $\bar{\sigma}$  is the average scattering cross section of the incident neutron by the particles constituting the nucleus.

$$\sigma = \frac{Z\sigma_{np} + N\sigma_{nn}}{A} \quad \dots (1.40)$$

We note that in this equation  $\sigma_{np}$  and  $\sigma_{nn}$  refer to collisions of the incident neutron against nucleons, happening inside the nucleus. Therefore, the kinetic energy of the incident neutron is  $E_{in}$  given by equation (1.32). Furthermore, to account the effect of the Pauli principle, the cross section must be reduced with respect to the corresponding values for free nucleons. According to Goldberger (1948) the Pauli principle reduces the cross section by a factor  $\frac{2}{3}$ .

The cross section for collision of neutrons against free protons has been measured directly (Hadley, *et al.*, 1949) and, for energies not too different from 100 MeV, can be represented by

$$[\sigma_{np}(E)]_{free} = 8.3 \times 10^{-26} \times \frac{90}{E_{MeV}} \text{ cm}^2 \quad \dots (1.41)$$

$\sigma_{nn}$  is not known but it has been evaluated by Goldberger (1928) to be of the order

$$\sigma_{nn} \sim \frac{1}{4} \sigma_{np} \quad \dots (1.42)$$

Making use of equations (1.40), (1.41), (1.42) and of the reduction factor  $2/3$  due to the exclusion principle, we have

$$\Lambda_{cm} = \frac{8\pi}{5} r_0^3 \frac{A}{Z} \frac{1}{1 + \frac{A-2Z}{5Z}} \left[ \frac{1}{\sigma_{np}(E_{in})} \right]_{free} = 1.78 \times 10^{-15} \frac{A}{Z} \frac{1}{1 + \frac{A-2Z}{5Z}} (E_{in})_{MeV} \quad \dots (1.43)$$

From this formula we have, for  $Z=A/2$ , and  $E_{in}=90+30=120$  MeV,  $\Lambda=4$ ,  $27 \times 10^{-13}$  cm *i.e.* a value comparable with the radius  $R$  of light nuclei. That means that a neutron of  $E=90$  MeV kinetic energy, has an appreciable probability to cross the nucleus without colliding with anyone of the nucleons present in the nucleus.

For  $E=14$  MeV we have  $\Lambda=1$ ,  $56 \times 10^{-13}$  and therefore the probability that a neutron of this energy crosses a nucleus without colliding with its nucleons, is small also for light elements. The argument is quite satisfactory from a qualitative point of view, while the numerical values of the constants appearing in equation (1.43) are rather uncertain.

I will not reproduce the calculations of Serber and co-workers in all their details but I will simply recall a few points of their theory which appear to be of great interest.

Following the optical approach first given by Bethe (1939), the nuclear matter is treated as a medium characterized by an absorption coefficient

$\frac{1}{\Lambda}$  and a refraction index  $\frac{k}{K} = \frac{k}{k+k_1}$  where, according to equation (1.34)

$$k_1 = K - k = k[(1 + V/E)^{1/2} - 1] \quad \dots (1.44)$$

For example, for  $E=90$  MeV and  $V=30$  MeV we have

$$\begin{aligned} k &= 1/\lambda^* = 2.08 \times 10^{13} \text{ cm}^{-1} \\ k_1 &= 3.22 \times 10^{13} \text{ cm}^{-1} \\ 1/\Lambda &= 2.3 \times 10^{12} \text{ cm}^{-1} \end{aligned} \quad (1.45)$$

The surface effect is taken into account by Serber and co-workers in a qualitative way because in order to avoid reflection of the incident wave at the surface of the nucleus, they assume that  $k_1$  and  $1/\Lambda$  increase from zero, outside the nucleus, to their values inside the nucleus in a distance larger than  $\lambda^*$ . To illustrate the calculation, Serber derives the scattering and absorption cross section of a disk of nuclear matter of radius  $R$  and thickness  $T$  having the axis parallel to the velocity of the incident neutrons. If the incident wave has unit amplitude, the wave transmitted through the disk will have amplitude and relative phase given by

$$a = e^{-(1/2\Lambda + ik_1)T} \quad \dots (1.46)$$

and therefore the corresponding cross sections will be

$$\begin{aligned} \sigma_a &= \pi R^2 (1 - |a|^2) = \pi R^2 (1 - e^{-T/\Lambda}) \\ \sigma_{sc} &= \pi R^2 |1 - a|^2 = \pi R^2 \left( 1 - 2e^{-T/2\Lambda} \cos k_1 T + e^{-\frac{T}{\Lambda}} \right) \quad \dots (1.47) \\ \frac{d\sigma_{sc}}{d\omega} &= R^2 |1 - a|^2 \left[ \frac{J_1(kR_2 \sin \vartheta/2)}{2 \sin \vartheta/2} \right]^2 \end{aligned}$$

as one can easily recognize noting that the wave behind the disk is no longer plane, but differs from a plane wave by an amplitude  $1 - a$  in the shadow of the disk.

For  $T/\Lambda \gg 1$  the amplitude  $a$  of the transmitted wave turns out to be very small and the equations (1.47) reduce to the equations (1.12) expressing the optical theorem.

For  $T/\Lambda \ll 1$  and  $k_1 T \ll 1$  we have the opposite limiting case of a transparent nucleus with a refraction index close to 1. In this case we have

$$\begin{aligned} \sigma_a &= \pi R^2 \frac{T}{\Lambda} = \pi R^2 n \sigma T = A \sigma \\ \sigma_{sc} &= \pi R^2 \left( \frac{1}{4\Lambda^2} + k_1^2 \right) T^2 = \frac{1}{4} A \sigma \left[ 1 + 4(\Lambda k_1)^2 \right] \frac{T}{\Lambda} \quad \dots (1.48) \end{aligned}$$

i.e. the absorption cross section  $\sigma_a$  approaches the sum of the scattering cross sections of the separate nucleons, while  $\sigma_{sc}$  vanishes in the first approximation, being proportional to the probability of double scattering (terms of 2° order).

The case of a spherical nucleus is only slightly more complicated and can be derived from the case of the disk (figure 1.12) noting that the portion of the wave striking the surface of the nucleus at a distance between  $\rho$  and

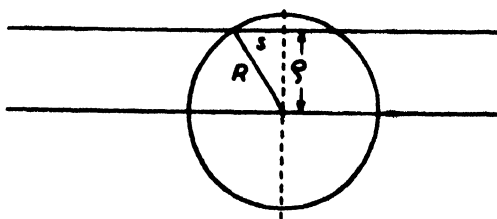


FIG. 1.12

$\rho + d\rho$  from the line going through the centre of the sphere, traverses a distance

$$2s = 2\sqrt{R^2 - \rho^2}$$

of nuclear matter, and therefore, its amplitude is

$$a = e^{-(1/\Lambda + 2ik_1)s}$$

For instance, we have

$$\sigma_a = 2\pi \int_0^R \left(1 - e^{-\frac{2s}{\Lambda}}\right) \rho d\rho = \pi R^2 \left\{1 - \left(1 + 2\frac{R}{\Lambda}\right)e^{-\frac{2R}{\Lambda}}\right\}$$

which, for  $\frac{\Lambda}{R} \ll 1$ , reduces again to the geometrical cross section. With the

same procedure  $\frac{d\sigma_{sc}}{d\omega}$  and  $\sigma_{sc}$  can be derived for a spherical nucleus.

In figure 1.13 we reproduce the results of Serber and coworkers as a function of  $\frac{R}{\Lambda}$ . It is to be noted that while  $\frac{\sigma_a}{\pi R^2}$  is a function of  $\frac{R}{\Lambda}$  only, the other two cross sections depend also on  $\Lambda k_1$ ; the corresponding curves, drawn in figure 1.13, have been calculated for

$$\Lambda k_1 = 1.5$$

which is very close to the value that one deduces for  $E = 90$  MeV (See. (1.45))

Serber and coworkers have shown that using  $\frac{1}{\Lambda} = 2.2 \times 10^{12} \text{cm}^{-1}$  the values of  $\sigma_i$  measured at 90 MeV (column 5 of Table 1.2) are very well represented by  $R = r_0 A^{1/3}$  taking

$$r_0 = 1.37 \times 10^{-13} \text{cm}.$$

The used value of  $\Lambda (4.55 \times 10^{13} \text{cm})$  corresponds to  $k_1 = 3.3 \times 10^{12} \text{cm}^{-1}$  and  $V = 30.8$  MeV.

From a detailed discussion they have also shown that a measurement of  $\sigma_i$  determines rather well  $k_1$  while it is rather insensitive to variations

of  $\Lambda$  with fixed  $k_1$ . Measurements of  $\sigma_a$  and  $\frac{d\sigma_{sc}}{dw}$  would be more appropriate

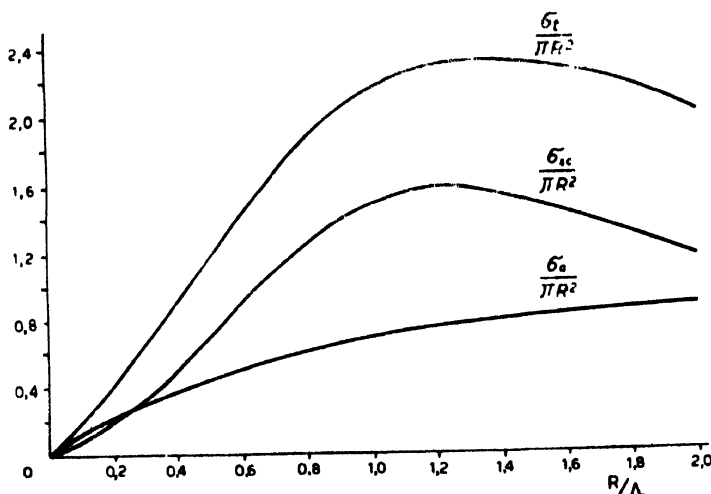


FIG. 1.13

for a determination of  $\Lambda$ . Furthermore in the deduction of the value of  $\Lambda$  from the value of  $k_1$ , the energy  $E$  of the incident neutrons is involved, which introduces an appreciable uncertainty as long as the used neutrons have such a wide spectrum as that produced by stripping the deuterons.

We can conclude that a refinement of the theories given in sections 1.4 and 1.5 will be necessary as soon as better measurements of  $\sigma_a$ ,  $\sigma_t$ , and  $\frac{d\sigma_{sc}}{dw}$  as a function of the energy, will be available.

Furthermore, let us consider again, as a final remark, the equations (1.48) valid in the limiting case of a transparent nucleus with a refractive index close to 1. We have already noted that under these conditions the cross section for shadow diffraction goes to zero while  $\sigma_a$  is equal to the sum of the cross sections of the separate nucleons.

But it is evident that in this limiting case, the representation of the properties of nuclear matter by means of a refractive index and an absorption coefficient is inadequate. Each one of the nucleons present in the nucleus, contributes to the scattering of the incident neutrons, and one has to distinguish a coherent scattering and an incoherent scattering according to the fact that the nucleus remains in its ground state or is excited: the coherent scattering is obviously the analogous effect of the diffraction of X-rays or electrons by atoms.

Therefore, in the limiting case of a completely transparent nucleus (for which  $\sigma_{sc}$  can be considered zero)  $\sigma_a$  separates into two parts: the first one

corresponds to the diffraction pattern, the second one to all other possible nuclear processes in which the nucleus is excited.

The treatment of this problem is rather complicated and needs the knowledge of the interaction among the incident neutron and the nucleons as well as of the wave functions of the nucleus in all its states.

We note that if the energy of the incident neutrons is large enough, ( $E \approx 200$  MeV), one has to consider also the process of production of  $\pi$  mesons, whose cross section increases by increasing the energy.

Therefore, heavy nuclei will satisfy the condition of complete transparency only approximatively in a very narrow energy interval, while light elements will approach this limiting case already at rather low energy.

#### REFERENCES

- Agno, M., Amaldi, E., Bocciarelli, D. and Trabacchi, G. C., 1943, *Naturwiss.*, **31**, 231; *N. Cim.* **1**, 253; 1947, *Phys. Rev.*, **71**, 20.
- Akhieser, A. and Pomeranchuk, I., 1945, *J. Phys. U. S. S. R.*, **9**, 471.
- Amaldi, E., Bocciarelli, D., Cacciapuoti, B. N. and Trabacchi, G. C., 1946, *Rend. Linc.*, **1**, 29; 1946, *N. Chim.*, **3**, 15; 1947, *Phys. Soc. Comb. Conf.* P. 97.
- Amaldi, E. and Cacciapuoti, B. N., 1947, *Phys. Rev.*, **71**, 739.
- Aoki, H., Kikuchi, S. and Wakatuchi, T., 1939, *Mat. Phys. Jap.*, **21**, 410.
- „ „ „ 1939, *Phys. Rev.*, **55**, 1264.
- Bacher, R. F., 1940, *Phys. Rev.*, **57**, 352.
- Bethe, H. A., 1939, *Phys. Rev.*, **57**, 1125.
- Bethe, H. A. and Placzek, G., 1939, *Phys. Rev.*, **57**, 1075.
- Blatt, J. M. and Weisskopf, V. F., 1950, *The theory of Nuclear Reactions*. Technical Report N. 42-1950 M. I. T. and Prentice Hall, New York in Press.
- Bohr, N., Peierls, R. and Placzek, G., 1939, *Nature*, **144**, 200.
- Bratenahl, A., Fernbach, S., Hildebrand, R. H., Leith, C. R. and Moyer, B. J., 1950, *Phys. Rev.*, **597**, 1950.
- Cook, L. J., Mc Millan, E. M., Peterson, J. M., and Sewell, D. C., 1949, *Phys. Rev.*, **75**, 7.
- De Juren, J. and Knable, N., 1950, *Phys. Rev.*, **77**, 606.
- Fernbach, S., Serber, R. and Taylor, T. B., 1949, *Phys. Rev.*, **75**, 1352.
- Feshbach and Hauser, 1950, Private Communications.
- Feshbach, H. and Weisskopf, V. F., 1949, *Phys. Rev.*, **76**, 1550.
- Feshbach, H., Peaslee, D. C. and Weisskopf, V. F., 1947, *Phys. Rev.*, **71**, 145.
- Gittings, H. T., Marshall, H. H. and Everhart, G. G., 1949, *Phys. Rev.*, **75**, 1610.
- Goldberger, M. L., 1948, *Phys. Rev.*, **74**, 1268.
- Graham, D. C. and Seaborg, G. T., 1938, *Phys. Rev.*, **53**, 795.
- Hadley, J., Kelly, E., Leith, C., Segre, E., Wiegand, C., and York, H., 1949, *Phys. Rev.*, **75**, 357.

Helmholz, A. C., Mc Millan, E. M. and Sewell, D. C., 1947, *Phys. Rev.*, **72**, 1003

Hildebrand, R. H., and Leith, C. E., 1950, *Phys. Rev.*, **80**, 842.

Lasday, A. H., 1951, *Phys. Rev.*, **81**, 139.

Mott, N. F. and Massey, H. S. W., *Theory of atomic Collisions*, Oxford, P. 22.

Present, R. D., 1941, *Phys. Rev.*, **60**, 28.

Serber, R., 1947, *Phys. Rev.*, **72**, 1008.

Sherr, R., 1945, *Phys. Rev.*, **68**, 240.

Soltan, A., 1938, *Nature*, **142**, 252, Trav. Inst. Phys. Exper. Univ. Varsoive n<sup>o</sup> 235

Weigand, C., 1948, *Rev. Sci. Inst.*, **19**, 790.

Note added in proof : For further developments of this subject see also the following papers:—

DeJuren, J., 1950, *Phys. Rev.*, **80**, 27.

DeJuren, J. and Moyer, B. J., 1951, *Phys. Rev.*, **81**, 919

Fox, R., Leith, C., Wouters, L. and MacKenzie, K. R., 1950, *Phys. Rev.*, **80**, 23.

Jarrows, R., 1961, *Phys. Rev.*, **82**, 261.



# DIFFRACTION EFFECTS IN THE SCATTERING OF NEUTRONS, $\mu$ MESONS AND ELECTRONS BY NUCLEI

## PART II

### 2 THE SCATTERING OF FAST $\mu$ MESONS AND ELECTRONS BY NUCLEI

#### 2.1-*Experimental Evidence on the Specific Interaction of $\mu$ Mesons with Nucleons*

The first informations about the specific interaction of  $\mu$  mesons with nucleons were obtained by different authors (Blackett and Wilson, 1938 ; Vargus, 1939 ; Wilson, 1940 ; Code, 1941, Shutt, 1942, 1946 ; Sinha, 1945 ; Scott and Snyder, 1948) who measured the anomalous scattering of  $\mu$  mesons by nuclei, *i.e.*, the scattering observed in addition to that to be expected from the purely electric forces. Most of these experiments that were performed with  $\mu$  mesons of kinetic energies of the order of 300 MeV, gave an upper limit of the cross section of about  $5 \times 10^{-24}$  cm.<sup>2</sup>/nucleon, *i.e.*, a value appreciably smaller than that expected under the assumption that the mesons observed in cosmic rays at sea-level can be identified with the particles responsible of the nuclear forces.

All the measurements in questions were based on very poor statistics and generally open to various criticisms that induced one to suspect that the scattering cross-section could be still smaller than the value quoted above.

A much lower upper limit can be deduced by the consideration of the experimental results of Conversi, Pancini and Piccioni (1945, 1946, 1947), on the behaviour of  $\mu$  mesons at the end of the range in materials of different atomic number. According to the discussions first given by Fermi, Teller and Weisskopf (1947) and detailed, later on, by other authors (Ferretti, 1948 ; Frölich and Wheeler, 1949), the above-mentioned effect shows that the interaction constant of low energy  $\mu$  mesons with nucleons, is  $10^6$  times smaller than that expected under the assumption that  $\mu$  mesons are the particles responsible of the nuclear forces.

In order to deduce from these data an upper limit of the scattering cross section we need to introduce some assumption about the mechanism of the processes of absorption and scattering of  $\mu$  mesons by nucleons. If, for instance, we assume that the absorption can be interpreted in terms of a charge-exchange reaction, as discussed by Tiomno and Wheeler (1949), and that the neutral particle emitted in such a process is comparable with the absorbed  $\mu$  meson, the scattering cross section turns out to be  $10^{10}$  times smaller than the upper limit set by the above-mentioned scattering

experiments. One arrives at similar conclusions also from other reasonable assumption about the mechanism of these processes (Wheeler, 1949; Tioinno and Wheeler, 1949).

It is to be noted, however, that these considerations contain the implicit assumption that conclusions drawn from experimental observations on the behaviour of  $\mu$  mesons almost at rest, can be extrapolated to the case of  $\mu$  mesons of some hundred MeV kinetic energy.

Therefore we thought worthwhile to carry on an experiment having the character of direct observation of large angle scattering of fast  $\mu$  mesons by nucleons.

The experimental set-up (Amaldi and Fidecaro, 1950, 1951) is shown schematically in figure 2.1.

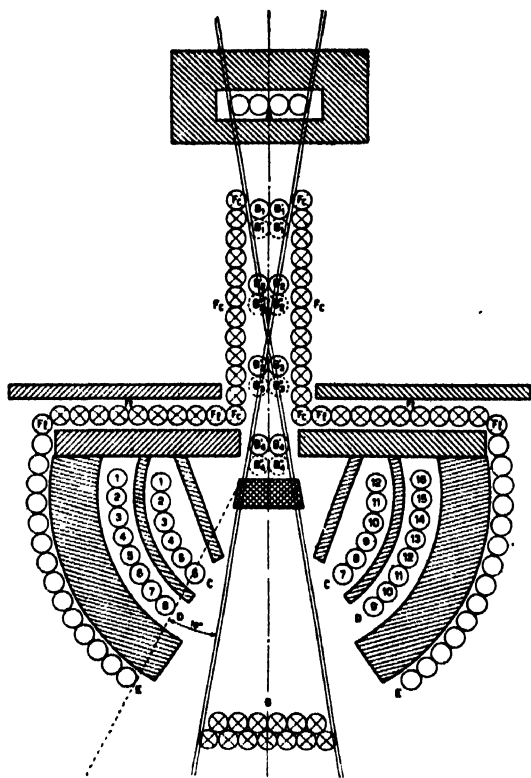


FIG. 2.1

While we refer to the original papers for details of the experimental set-up and of the discussion of the results of the measurements, we will recall the following main conclusions: in about 1,500 hours we recorded about  $0.5 \cdot 10^6$   $\mu$  mesons crossing the scatterer, and only 4 scattered particles in the low energy band and 3 particles in the high energy band.

Most of these particles are probably protons whose percentage in the cosmic radiation at sea-level is still rather uncertain. Making a rather conservative evaluation of the contribution given by protons to the observed

scattered particles, we could establish the following upper limits of the anomalous scattering cross-sections\* :

$$\text{for } 200 \leq T_{\mu} \leq 320 \text{ MeV} \quad \sigma \leq 4.5 \times 10^{-23} \text{ cm.}^2/\text{nucleon} \quad \dots (2.1)$$

$$\text{for } 320 \leq T_{\mu} \text{ MeV} \quad \sigma \leq 2.3 \times 10^{-10} \text{ cm.}^2/\text{nucleon} \quad \dots (2.2)$$

In the high energy band (corresponding to an average kinetic energy  $\bar{T}_{\mu}=900$  MeV) our upper limit is about 200 times smaller than that deduced by the preceding scattering experiments but still enormously larger than that deduced from the Conversi Pancini and Piccioni effect.

With the same experimental set-up we could establish an upper limit of about

$$10^{-30} \text{ cm.}^2/\text{nucleon} \quad \dots (2.3)$$

for the cross section for production of penetrating showers by  $\mu$  mesons at sea-level: this result refers to penetrating showers containing at last one particle emitted at an angle larger than  $18^{\circ}$ .

Two remarks about these values can be added. The first one is that although our upper limits are not extremely small, they are sufficiently small and refer to the right energy interval for the considerations that we are going to develop at a later time.

\* In order to visualize the specific interaction of  $\mu$  mesons and nucleons some authors (Wheeler, 1949; Tiomno and Wheeler, 1949; Fermi and Marshall, 1947, Havens, Rabi, Rainwater, 1947) represent the supplementary interaction with a potential well extending over a region that is small if compared with the meson's wavelength.

From the perturbation theory, one gets the following order of magnitude of the cross section

$$\sigma \sim \frac{2\pi}{\hbar} W^2 \frac{4\pi\hbar^2}{c^2\hbar^3} \quad \dots (I)$$

where  $W$  is the depth of the potential well multiplied by its volume. From equation (I) one gets

$$W \leq \frac{c^2\hbar^2}{2^{1/2}(2\pi)^{3/2}} \frac{\sigma^{1/2}}{c\hbar} \sim 3 \times 10^{27} \frac{\sigma^{1/2}(\text{cm}^2)}{(c\hbar)_{\text{ev}}} \times \frac{4\pi}{3} \left( \frac{e^2}{m_e c^2} \right)^3 \quad \dots (II)$$

where the classical radius of the electron has been introduced only to allow an easy evaluation of the orders of magnitude. Introducing in equation (II)  $\sigma \sim 2.3 \times 10^{-30}$  and  $c\hbar \sim 10^9 \text{ eV}$ , we get

$$W \leq 5,000 \text{ eV} \times \frac{4\pi}{3} \left( \frac{e^2}{m_e c^2} \right)^3$$

which is convenient for a comparison with the results obtained for the interaction among slow neutrons and electrons (Fermi and Marshall, 1947, Havens, Rabi and Rainwater, 1947).

We note that in the present case of the interaction among fast  $\mu$  mesons and nucleons, the wavelength  $\lambda^*$  of the incident particle is comparable with the classical radius of the electron and therefore the preceding considerations make sense only if the dimensions of the potential well were smaller than  $e^2/mc^2$  and its depth correspondingly larger.

undergo a transition from the ground state to an excited state. We note that we have to expect that the results obtained for the "one particle model" are better in the case of the coherent scattering, in which only the wave function of the ground state of the nucleus is involved, than in the case of the incoherent scattering (Weisskopf, 1950).

Most of the following considerations and conclusions are independent of the particular shape chosen for the potential well. Considering, however, that in order to be able to carry on the calculations in a simple form up to numerical results, we need, at a later time, to specify the potential well in a convenient way, we will choose from now the "parabolic well". With such an assumption, which gives satisfactory results only for light nuclei (Heisenberg, 1935; Bethe and Bacher, 1936), each nucleon will be represented by a three dimensional isotropic harmonic oscillator, whose energy interval  $W = h\nu$  is the only parameter that we have to adjust in such a way that our model reproduces correctly one conveniently chosen experimental feature of the nucleus. Considering the type of phenomena that we are investigating, we thought more convenient to adjust the length

$$a = \left( \frac{\hbar^2}{M_p w} \right)^{1/2} \quad \dots (2.4)$$

in such a way that our model has the experimental dimensions of the nucleus instead of the experimental binding energy (Wheeler, 1949; Tjonno and Wheeler, 1949), namely we have applied the Pauli principle to the nucleons, and we have imposed that the mean value of the square of the distance of the last nucleon is equal to the square of

$$R_0 = \frac{1}{2} \frac{e^2}{m_e c^2} A^{1/3}.$$

So we get

$$a = \frac{e^2}{m_e c^2} \frac{A^{1/3}}{\sqrt{2(2m+1)}}$$

where  $m$  is the quantum number of the last occupied level.

Going back to our scattering problem we note that if we neglect the spin of the particles, the electromagnetic interaction between the  $\mu$  meson and the nuclear protons reduces to the Coulomb interaction. Following an elementary analytical procedure similar to that given by Bethe (1930) in the discussion of the collision of electrons of a few keV against atoms, one gets the following equation for the total cross section

$$\frac{d\sigma}{d\omega} = R \left( F^2 + \frac{\pi}{Z} \right) \quad \dots (2.5)$$

$$\text{where} \quad R = \frac{1}{4} \left( \frac{e^2}{m_e c^2} \right)^2 \left[ \frac{m_e c^2 E_0}{(c p_0)^2} \right]^2 \frac{Z^2}{\sin^4 \frac{\theta}{2}} \quad \dots (2.6)$$

is the Rutherford cross section for particles of total energy  $E_0$  and momentum  $p_0$ , colliding against a point charge  $Ze$ .

The only remark that we like to make about the deduction of (2.5), is that, if we take, for sake of simplicity, one of the axis of the frame of reference, say the  $X_1$ -axis, in the direction of the vector

$$\vec{k} = \vec{K} - \vec{K}_0 \quad \dots \quad (2.7)$$

( $\vec{K}_0$  and  $\vec{K}$  are the wave vectors of the incident and of the scattered meson) the selection rules concerning our problem can be expressed in the following simple form

$$m_2 = n_2, \quad m_3 = n_3 \quad \dots \quad (2.8)$$

i.e. to the scattering of the incident particle contributes only the oscillation of the protons in the direction of the vector  $\vec{k}$ .

In (2.5) the term  $R F^2$  represents the coherent scattering ( $m_1 = n_1$ ).  $F$  is nuclear form factor that can be put in the form

$$F = \frac{1}{Z} \{z_1 f_1 + z_2 f_2 + z_3 f_3 + \dots\} \quad \dots \quad (2.9)$$

where  $z_i$  is the number of protons in the level  $i$  and the  $f_i$  are the following

functions of  $x = \frac{Q_0^2}{2}$

$$f_1 = e^{-x/2}; \quad f_2 = e^{-x/2}(1 - \frac{1}{3}x); \quad f_3 = e^{-x/2}(1 - \frac{2}{3}x + \frac{1}{12}x^2) \quad \dots \quad (2.10)$$

$$f_4 = e^{-x/2}(1 - x + \frac{1}{4}x^2 - \frac{1}{60}x^3); \dots$$

$$Q_0 = a k_0 = \frac{2a}{\lambda_0} \sin \frac{\vartheta}{2}. \quad \dots \quad (2.11)$$

If we neglect terms in  $x^2, x^3, \dots$  our  $F$  is identical with the  $F$  of Williams provided the length  $b$  representing, according to this author, the dimensions (not better defined) of the nucleus, is related to our  $a$  by the equation

$$b = a \sqrt{2 \left[ \frac{1}{2} + \frac{z_2 + 2z_3 + 3z_4}{3Z} \right]} \quad \dots \quad (2.12)$$

i.e.  $b$  must be, for light elements, about 30% smaller than the corresponding  $R_0$ .

The second term in (2.4), i.e.,  $R\pi/Z$ , corresponds to the incoherent scattering, namely the scattering accompanied by excitation of any one of the nuclear oscillations in the direction of  $\vec{k}$ , from its initial state  $n_1$  to any free final state  $m_1$ ,

$$\pi = \frac{1}{Z} \sum \sigma_{m_1, n_1} e^{-x} P_{m_1, n_1}(x) \quad \dots \quad (2.13)$$

where the sum has to be extended over all the free final states  $m_1$  and over all the occupied initial states  $n_1$  and

$$\sigma_{m_1, n_1} = 16 \sin^4 \frac{\vartheta}{2} \frac{\vartheta}{\{1 + \vartheta^2(y) - 2\varphi(y) \cos \vartheta\}^{1/2}} \quad \dots \quad (2.14)$$

$$\phi(y) = \left\{ 1 - \frac{1}{\beta_0^2} y(2-y) \right\}^{1/2} \quad y = (m_1 - n_1) \frac{W}{E_0}. \quad (2.15)$$

$P_{nm}$  are polynomials of the following type

$$P_{0m} = \frac{1}{m!} x^m; \quad P_{1m} = \frac{1}{m!} \{ x^{m+1} - 2mx^m + m^2 x^{m-1} \}; \quad (2.16)$$

$$x = \frac{Q^2}{2}; \quad Q = ak \frac{ap_0}{\hbar} \{ 1 + \phi^2(y) - 2\phi(y) \cos \vartheta \}^{1/2} \quad (2.17)$$

In figure 2.2, we give, as an example, the quantity  $F^2$  (marked C), the quantity  $\pi/Z$  (marked I), their sum (marked T) and the  $F^2$  according to Willams, taking, as it is usually done,  $b = R_0$ , for  $\mu$  mesons of  $E_0 = 200$  and  $E_0 = 600$  MeV, colliding against C.

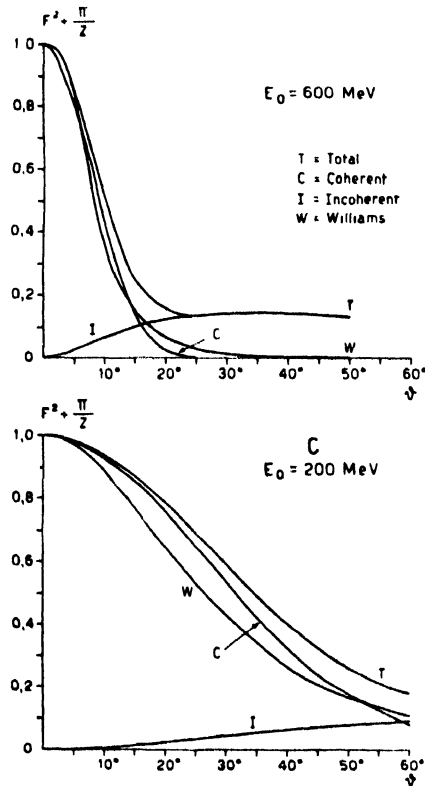


FIG. 2.2

The scattering of particles of spin  $1/2$  can be calculated following a procedure quite similar to that of Moller (1932), in which the spin-spin interaction and the retardation due to the finite value of the velocity of propagation of the electromagnetic field, are taken into account.

While for the incident and scattered meson we have used the Dirac wave functions of a free particle, for the nuclear protons we used the Darwin approximation according to which terms of the order of the square of

$$\frac{1}{K} = \frac{\hbar}{M_p c}$$

are neglected. Such an approximation, which is better satisfied in our case of nuclear protons than in the case of the atomic electrons allows one to specify the potential well as a parabolic one (i.e. a well of infinite depth which would give rise to complications if treated exactly in the Dirac theory).

A second consequence of such an approximation is that the Pauli additional term that can be introduced in the Lagrange function in order to take into account the anomalous magnetic moment of the protons  $\left(\mu_p = \gamma \frac{e\hbar}{M_p c} = \gamma \frac{e}{K}\right)$  can be neglected. In fact the corresponding term appearing in the current equation (the so called polarisation current) gives rise in the expression of the cross section only to terms of the order of  $\frac{1}{K^2}(\gamma - 1)^2$  as one can see from a direct calculation as well from the results of Corben and Schwinger (1940) on the collision between two free particles.

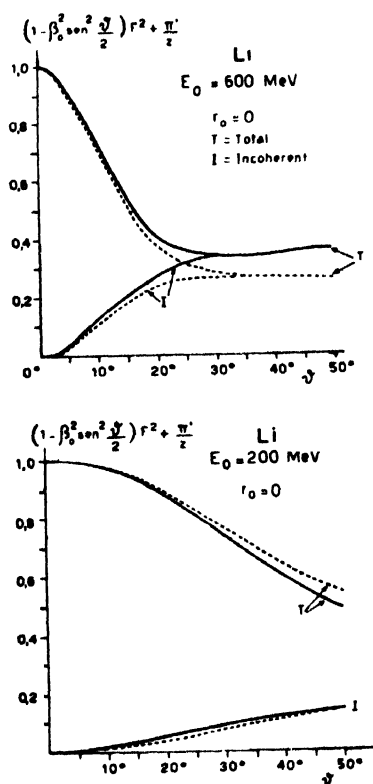


FIG. 2.3

By carrying on the calculations, one gets, the following in the first Born approximation (Amaldi, Fidecaro and Mariani, 1950) instead of (2.5)

$$\frac{d\sigma}{d\omega} = R \left\{ \left( 1 - \beta_0^2 \sin^2 \frac{\theta}{2} \right) F^2 + \frac{\pi'}{Z} \right\} \quad (2.18)$$

where  $F$  is still given by (2.9), while

$$\pi' = \frac{1}{Z} \sum \alpha'_{m_1-n_1} e^{-\kappa} P_{n_1, m_1}(\chi)$$

$$\alpha'_{m_1-n_1} = \frac{4\phi(y) \sin^4 \frac{\vartheta}{2}}{\left\{ 1 + \phi^2(y) - 2\phi(y) \cos \vartheta - \left( \frac{y}{\beta_0} \right)^2 \right\}^2} \left\{ (2-y)^2 - \beta_0^2 (1 + \phi^2(y) - 2\phi(y) \cos \vartheta) \right.$$

$$\left. - \frac{4\beta_0 p_0}{\hbar K} \frac{1 - \phi^2(y) - y [1 - \phi(y) \cos \vartheta]}{\{ 1 + \phi^2(y) - 2\phi(y) \cos \vartheta \}^{1/2}} \right\} 1 + \phi^2(y) - 2\phi(y) \cos \vartheta$$

$$p_0 a^{m_1} \frac{|I_{n_1, m_1-1}|}{|I_{n_1, m_1}|} + \frac{1}{2} \frac{|I_{n_1, m_1+1}|}{|I_{n_1, m_1}|}$$

$$I_{n_1, m_1} = a \int_{-\infty}^{+\infty} \phi_{n_1}(\xi) \phi_{m_1}(\xi) e^{iQ\xi} d\xi$$

$\phi_{n_1}$ ,  $\phi_{m_1}$  are the wave functions of a harmonic oscillator in state  $n_1$ ,  $m_1, \dots$

Figure. 2.3 shows a comparison between equation 2.10 (thickly drawn line) and 2.5 (broken line) for  $\mu$  mesons of  $E_0 = 100$  MeV, colliding against Li nuclei.

### 2.3—The Electromagnetic Dimensions of the Nucleons

In the preceding discussion we have tacitly assumed that each proton acts on the  $\mu$  meson as a point-charge. Now it is evident that such an assumption is not justified: on account of the nuclear forces the proton has radius of about  $1.4 \cdot 10^{-13}$  cm, but as long as we know, there is no definite experimental evidence in favour of or against the assumption that the electric charge (and eventually the magnetic moment) of the proton is spread on the same spatial dimensions covered by the nuclear forces. The problem is obviously connected with the nature of the nuclear forces and the existence of processes of emission and absorption of mesons ( $\pi$ ,  $\tau, \dots$ ) by a proton.

By the way it is to be noted that on account of these processes of emission and absorption of mesons by nucleons, one has to expect an electromagnetic interaction of  $\mu$  mesons also with neutrons similar to that of electrons with neutrons, in addition to the interaction due to the spins.

All these questions, however, are of a quite different type from those we have proposed to consider in the present discussion and have been mentioned only in order to show the "a priori" possibility that the electromagnetic radius of a proton is finite and different from its radius as determined by the nuclear forces.

It is also obvious that similar arguments can be applied to any other particle different from the nucleons, in particular to the  $\mu$  mesons.

In the present discussion we shall limit ourselves to discuss, in a pure phenomenological way, the influence of a finite electromagnetic radius of the



proton on the Coulomb scattering of  $\mu$  mesons by light nuclei (Amaldi, Fidecaro and Mariani, 1950).

As a first approach to this problem we have assumed that the charge  $e$  of the proton is distributed around its center according to a Gaussian law.

$$\rho(r) = e \frac{1}{\pi^{3/2} r_0^3} e^{-\left(\frac{r}{r_0}\right)^2} \quad \dots (2.19)$$

It is then immediately shown that the matrix element corresponding to a transition  $n \rightarrow m$  of the nucleus, induced by the incident point-charge  $\mu$  meson, calculated for a gaussian proton  $H_{nm}^{(g)}$  is connected to the corresponding matrix element  $H_{nm}$ , calculated for point-charge protons, by the simple relation,

$$H_{nm}^{(g)} = T H_{nm} \quad \dots (2.20)$$

with

$$T = e^{-q^2/4} ; \quad q = k_{10} = r_0 \left| \frac{\vec{p} - \vec{p}_0}{\hbar} \right| \quad \dots (2.21)$$

This result introduced in the expression of the cross section, allows one immediately to deduce the influence of a finite radius of the charge distribution of the proton on the Coulombian scattering of fast  $\mu$  meson.

In Figure 2.4 the quantity  $F^2 + \pi/Z$  is plotted as a function of the scattering angle for different values of  $r_0$  and for  $\mu$  meson of  $E_0 = 200$  and 600 MeV, colliding against C nuclei.

The used numerical values of  $r_0$  correspond to the Compton wave length of respectively nucleons and  $\pi$  mesons, which can be considered as a lower and an upper limit of the electromagnetic dimensions of the nucleons.

Figure 2.5 is a plot of the spectra of the inelastically scattered mesons by C for two values of  $r_0$  and  $E_0 = 600$  MeV ; from these figures we see that the electromagnetic scattering of  $\mu$  mesons by light nuclei is very sensitive to the electromagnetic dimensions of the nucleons.

#### 2.4—Discussion and Generalization of the Preceding Conclusions

The electromagnetic scattering has been calculated in sections 2.2 and 2.3 using very rough models for both the nucleus and the nucleons. Therefore, it seems of some interest to discuss how far do our numerical results depend on the particular models employed.

(a) *The model of the nucleus.* First we have changed the rule of filling the nuclear shells. In the calculations reported above the nucleons have been distributed uniformly in all the degenerate substates belonging to an unfilled shell.

We tried to put the nucleons in the degenerate substates according to the symmetries suggested by the one particle model developed mainly by Mayer (1948, 1949) and Haxel, Jensen and Suess (1948, 1950). No difference at all

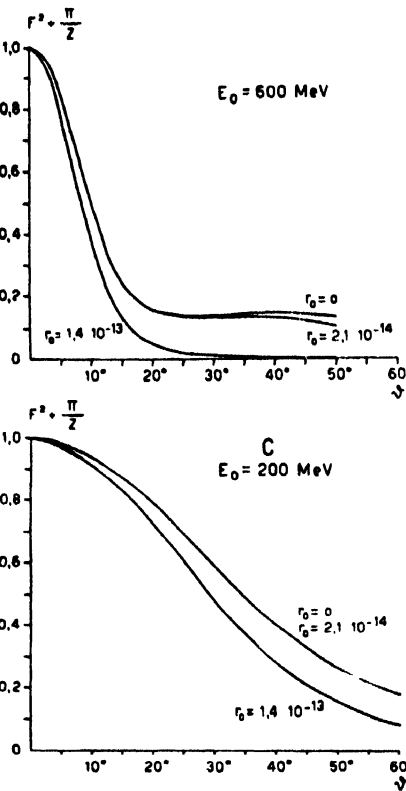


FIG. 2.4

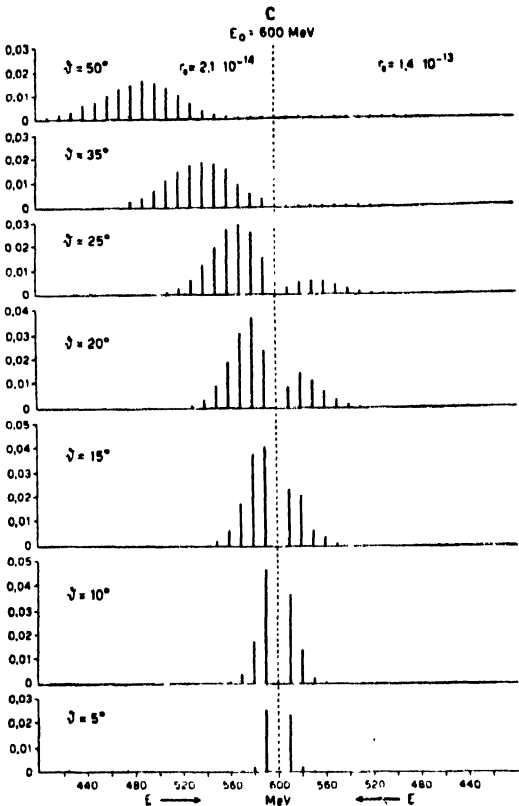


FIG. 2.5

exists for elements up to  $^{16} \text{O}$  (i.e. nuclei involving only the two first shells) and an almost negligible difference for heavier nuclei.

Then we tried to change the well by introducing a perturbation of the type  $V = Ae^{-\beta^2 r^2}$  whose effect is to flatten the bottom of the potential well (figure 2.6) making it a bit more similar to the square well. The calculations have been

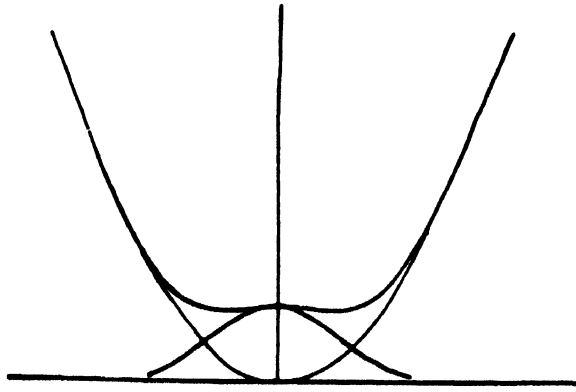


FIG. 2.6

completed for the two first shells. We found that the quantity  $\frac{d\sigma}{\sigma} : d\frac{A}{W}$  is rather small ( $\sim 4\%$ ) so that we can conclude that, at least for very light elements, the shape of the potential well is not of primary importance.

A third point that is now under consideration is to see what can be the influence of the coupling among different nucleons. The fact that the nucleons have been assumed completely independent of one another could be a too rough picture of the nucleus, especially for the calculation of the inelastic scattering.

(b) *The model of the nucleon.* The assumption of a Gaussian distribution of the charge of the proton has only the significance of simplest work assumption, which allows to see the influence of a spatial spread of the electric charge of the proton.

The question has been treated from a more general point of view by Corinaldesi (1951) who has given a purely phenomenological treatment assuming that both the proton and the incident meson have an extended distribution of charge as well as of magnetic moment. Furthermore, in order to preserve the covariance of the formalism, he has assumed that the charge and magnetic moment are spread in time as well as in space.

He has found that, provided the wave function of at least one of the two colliding particles is a plane wave, the relation (2.20) still holds in a generalized form, where four form-factors appear, two for each one of the particles, namely the first representing the charge distribution, the second representing the magnetic moment distribution.

Corinaldesi's result puts the phenomenological theory on sound basis: however its generality spoils in some way the advantages of a phenomenological theory whose main interest has to be looked for in the possibility of determining, by comparison with the results of some convenient scattering experiments, the minimum number of parameters characterising the structure of the considered particles.

A considerable simplification of Corinaldesi's formula can be obtained considering that the coupling between the  $\mu$  mesons and the fields of the  $\pi$  mesons and the electrons is so weak that in a first approximation we can try to assume the  $\mu$  as point-charged particles. If such a simplification is allowed, the generalized expression given by Corinaldesi would still contain two form-factors representing the structure of the nucleon: namely its charge distribution and its magnetic moment distribution.

A final remark still in the spirit of the phenomenological representation of the structure of the nucleons, is suggested by the consideration of the neutrons present in the nuclei. If the spread of the charge (and magnetic moment) of a nucleon is mainly due to processes of emission and absorption of mesons and if the coupling constant between the nucleon and the mesonic field is so weak that the only important states are those with 0 or 1 (Frölich, Heitler and Kemmer, 1938) emitted mesons, we can describe the charge density of a

nucleon surrounded by its mesonic field as the sum of charge densities (multiplied by convenient weights) of the "pure proton state" and of each one of the different types of emitted mesons.

For instance, if the emitted mesons are of a single type, say  $\pi$ , we have for a proton

$$\rho_p = t\rho_p + (1-t)\rho_\pi$$

and for a neutron

$$\rho_n = (1-t)(\rho_p - \rho_\pi)$$

where  $\rho_p$  is the charge distribution of the pure proton state,  $\rho_\pi$  the charge distribution of the emitted  $\pi$  meson, and  $t$  the fraction of time during which the proton is in the pure proton state and the neutron in the pure neutron state.

Considering that in the nuclear structure the protons and the neutrons are paired so that the two partners of each pair have almost exactly the same wave function, we must expect interference effects between the waves scattered by the two partners. One can easily recognize that in a case like that considered above, the coherent scattering due to an even-even nucleus is independent, in this approximation, from  $t$  and  $\rho_\pi$  and corresponds exactly to the

TABLE 2.2

$r_0$  as deduced by comparison with the results of mesonic theory

$$r_0 \times 10^{14} \text{ cm}$$

$$E = 300 \text{ MeV}; \quad \lambda^* = 6.57 \times 10^{-14} \text{ cm}$$

$\theta$	Scalar charged	Scalar neutral	Pseudoscalar charged	Pseudoscalar neutral
20°	10	3.8	3.8	3.8
40°	7.2	3.3	3.3	2.7
60°	6.9	3.0	3.2	2.7
$E = 600 \text{ MeV}; \quad \lambda^* = 3.28 \times 10^{-14} \text{ cm}$				
20°	7.6	3.2	3.8	2.7
40°	6.5	2.8	3.3	2.4
60°	5.4	2.7	2.9	2.3
$E = 940 \text{ MeV}; \quad \lambda^* = 2.1 \times 10^{-14} \text{ cm}$				
20°	6.9	3.2	3.2	2.7
40°	5.3	2.7	2.9	2.5
60°	4.2	2.5	2.6	2.1

scattering of  $Z$  protons existing during all the time in the "pure proton state".

Similar interference effects, although more complicated, can be expected also for the incoherent scattering.

If the coupling between the nucleons and the mesonic field is so strong that we can no more neglect the states in which 2 or more mesons are emitted, the total charge densities of a nucleon cannot be represented as a linear combination of the densities relative to each one of the corresponding partial states. A detailed discussion about what happens in this case needs a deeper insight into the nature of the mesonic field employed. The only qualitative consideration that we like to add, is that, if the coupling between nucleons and mesonic field is very strong, the exchange of mesons among the nucleons inside the nucleus can be so frequent that the charge distribution tends to spread over the whole volume of the nucleus itself.

#### *2.5—Comparison of the Phenomenological Theory with some Results obtained by Mesonic Field Theory*

Although the main advantage of the phenomenological point of view used above consists in its capacity to supply expressions of the cross section to be compared with experimental results, which are independent from the uncertainties of the mesonic field theory, it seems desirable to compare the results of the few calculations available today based on the mesonic theory, with some very simple phenomenological assumption, let us say for instance the Gaussian assumption.

The scattering of electrons of a few hundred MeV by protons has been calculated by Rosenbluth (1950); a similar calculation for  $\mu$  mesons has been performed by Corinaldesi (1951).

The first of these authors gives graphs of the effective proton charge as a function of the energy  $E$  and the scattering angle  $\vartheta$  of the incident electron for both charged and neutral meson theories of scalar and pseudoscalar type, with the coupling constant chosen to fit the magnitude of the observed proton anomalous magnetic moment.

By comparison of these graphs with the Gaussian assumption, one can derive the values of the phenomenological radius  $r_0$  of the proton as a function of  $E$  and  $\vartheta$ . Table 2.2 shows that  $r_0$  does not change very much by changing the angle of observation  $\vartheta$  and the energy of the impinging electrons. Therefore, considering the great uncertainties implicitly contained in perturbation theory calculations like that of Rosenbluth and Corinaldesi, it seems reasonable, at the moment to use the phenomenological theory with the Gaussian assumption for comparison with experimental results and try to derive from these last the quantity  $r_0$  as a function of  $E$  and  $\vartheta$ . At a later time these results could be compared with the provisions of the various mesonic theories.



- Heisenberg, W., 1935, *Z. f. Phys.*, **96**, 173.
- Mayer, M. G., 1948, *Phys. Rev.*, **74**, 235
- „ „ , 1949, *ibid*, **75**, 1969
- Moller, C., 1932, *Ann. d. Phys.*, **14**, 531
- Rosenbluth, M. N., 1950, *Phys. Rev.*, **79**, 615
- Scott, W. T., and Snyder, H. S., 1948, *Phys. Rev.*, **73**, 1260
- Shutt, R. P., 1942, *Phys. Rev.*, **61**, 6
- „ „ , 1946, *ibid*, **69**, 6.
- Sinha, M. S., 1945, *Phys. Rev.*, **63**, 153
- Stick, E., and Haar, D. Ter, 1950, *Phys. Rev.*, **78**, 68
- Vargus, J. A., 1939, *Phys. Rev.*, **50**, 480.
- Weisskopf, V., 1950, *Helv. Phys. Acta.*, **23**, 187
- Wheeler, J. A., 1949, *Rev. Mod. Phys.*, **21**, 133
- Tiomno, J. and Wheeler, J. A., 1949, *Rev. Mod. Phys.*, **21**, 153
- Williams, E. J., 1938, *Proc. Phys. Soc. A* **169**, 531
- 1802P—RI.





# STANDARD ON ALPHABETICAL ARRANGEMENT

New Delhi, October 31, 1952

The Indian Standards Institution has issued the 'Indian Standard Practice for Alphabetical Arrangement'--a standard of importance not only to documentalists, bibliographers and librarians, but also to users and producers of bibliographies, catalogues, indexes to books, directories, such as telephone directories and lists of a similar nature.

Alphabetical arrangement means arrangement of letters or their combinations according to the traditional values of letters which increase as we proceed from the first to the last letter of the alphabet. While usage fixes a unique arrangement among the letters of an alphabet, groups of letters with different spacings, punctuations and other marks, and the introduction of alien characters, which cannot be avoided in any collection of entries, give rise to the possibility of several alternative arrangements. This calls for standardization of alphabetical arrangement of entries.

The basis for alphabetical arrangement prescribed by the standard is all-through alphabetization, which ignores the presence of space, punctuation marks, apostrophies, brackets, etc, and also differences in the style of writing letters including capital and small letters. In one of the examples given in the standard to illustrate the rules, the terms 'Electrode-holder', 'Electrode, Metal', 'Electro-deposits', 'Electrodes' and 'Electrode (wire)', have been arranged in this order. The rule for numerals is that they shall precede letters of the alphabet. Thus the entries '6 books', '8 books', '100 books' shall be in this order. The unhelpful order to which the writing of numbers in letters instead of figures leads is illustrated by the example in the entries 'eight books', 'five books', 'one hundred book', 'seven books', 'six books', would appear in this order since the basis is all-through alphabetization.

Symbols, by which is meant non-alphabetical, non-numeral, internationally accepted characters, marks and signs, have been prescribed to precede numerals just as the latter are to precede letters of the alphabet. Mathematical symbols have been listed in an appendix according to the proposed order of arrangement for them. The standard prescribes that entries in different alphabets shall be arranged in separate sequences, and the letters of the Greek and Devnagri alphabets are listed in two separate appendices. Colon classification has been specified as the basis for the relative precedence between sets of symbols in different subjects as well as between alphabets of different languages.

The standard is available on sale for Rs. 1/8/- per copy, and may be obtained from the Secretary (Administration), Indian Standards Institution, 19 University Road, Civil Lines, Delhi-8.